

WAVES2019

14th International Conference on Mathematical and Numerical Aspects of Wave Propagation

Book of Abstracts

25. - 30. August 2019
Vienna, Austria



Editors:

Manfred Kaltenbacher

J. Markus Melenk

Lothar Nannen

Florian Toth

Published by:

Institute of Mechanics and Mechatronics, Faculty of Mechanical and Industrial Engineering

Institute of Analysis and Scientific Computing, Faculty of Mathematics and Geoinformation

TU Wien

Vienna, Austria

<https://www.waves2019.at>

ISBN:

978-3-200-06511-6

URN:

urn:nbn:at:at-ubtuw:3-5866

DOI:

10.34726/waves2019

Credits:

Cover design: Ruth K. Tscherne

LaTeX editors: F. Toth, S. Floss, S. Gombots, S. Schoder, J. Nowak, C. Freidhager, P. Seebacher

Contents

I Information	1
General Information	2
Committees	2
Plenary Speakers	4
Minisymposia	7
Sponsors	8
Practical Information	9
Conference Venue	9
Information for Presenters	11
Conference Office	11
Coffee & Lunch	12
WiFi at the Venue	12
Cloakroom	13
No Smoking Policy	13
Social Events	14
Welcome Reception	14
Mayor’s Reception	14
Conference Banquet	15
Scientific Program	17
Overview	17
Monday	22
Tuesday	29
Wednesday	36
Thursday	39
Friday	46

II Abstracts	49
Plenary Lectures	50
Minisymposia	78
Analysis and numerical methods for wave problems in heterogeneous media and complicated domains	78
Asymptotic models for the wave propagation in presence of periodic structures	108
Frames and PDEs	124
Modelling and numerical simulation of flow-acoustic interaction	138
Modern fast Boundary Element formulations for wave propagation problems	164
Nonlinear acoustics: analytical and numerical aspects	220
Resonant-state expansion of waves in the near- and far-field	230
Sweeping preconditioners and related iterative solvers for the Helmholtz equation	248
Tent-Pitching Space-Time Methods for Nonlinear Waves	266
Wave Phenomena: Analysis and Numerics	274
Wave propagation and imaging in complex media	308
Contributed Sessions	332
Analysis and Asymptotics	332
BEM and BIE	348
Domain Decomposition	366
Elastodynamics	378
High Frequency and Oscillatory Problems	384
Inverse Problems	396
Metamaterials	414
Method of Images and Green's Functions	420
Multiscale Problems	426
Numerical Methods	432
Optics	468
Optimization	474
Periodic Structures	482
Scattering	490
Seismic and Hydroacoustic Problems	496
Time Stepping	504
Transparent Boundary Conditions	514
Vibration	528
Waveguides	534

Welcome to WAVES 2019

A warm welcome to Austria, to Vienna, and to the WAVES 2019, the 14th International Conference on Mathematical and Numerical Aspects of Wave Propagation. The 2019 edition of the conference series takes place at TU Wien (Vienna University of Technology) and is jointly organized by the Institute of Mechanics and Mechatronics (Faculty of Mechanical and Industrial Engineering) and the Institute of Analysis and Scientific Computing (Faculty of Mathematics and Geoinformation).

With approximately 260 contributions, 8 plenary lectures, 11 minisymposia, and 20 contributed sessions, WAVES 2019 is a vivid forum for researchers from different areas of science to disseminate their latest advances in theoretical and computational modelling of wave phenomena, both in science and technology. The themes of the conference include: Analytical and Asymptotic Methods, Approximate Boundary Conditions, Domain Decomposition, Fast Computational Techniques, Flow-Acoustic Interaction, Forward and Inverse Scattering, Guided Waves and Random Media, Homogenization of Wave Problems, Mathematical Problems in Optics, Modelling Aspects in Photonics and Phononics, Nonlinear Wave Phenomena, and Numerical Analysis.

We would like to thank all our sponsors for their support and financial contributions: Austrian Acoustics Association, Acoustics Research Institute of the Austrian Academy of Sciences, City of Vienna, DS Simulia, Springer Verlag, TU Wien, Vienna Center for Partial Differential Equations, Special Research Programme „Taming Complexity in Partial Differential Systems“ (funded by FWF, the Austrian Science Fund), and Vienna Convention Bureau.

We are very pleased that WAVES 2019 could attract a large number of excellent presentations and we are particularly grateful to the mini-symposia organizers for contribution to this success. Finally, warm thanks to all members of the International Scientific Committee and Local Scientific Committee.

PART I

Information

General Information

Conference Chairmen

Manfred Kaltenbacher

Jens Markus Melenk

Technical Program Chairmen

Lothar Nannen

Florian Toth

International Scientific Committee

Xavier Antoine

Tilo Arens

Alex Barnett

Hélène Barucq

Eliane Bécache

Cédric Bellis

Abderrahmane Bendali

Marc Bonnet

Anne-Sophie Bonnet-BenDhia

Oscar Bruno

Annalisa Buffa

Fioralba Cakoni

Simon Chandler-Wilde

Lucas Chesnel

Xavier Claeys

Laurent Demanet

Julien Diaz

Rabia Djellouli

Björn Engquist

Sonia Fliss

Josselin Garnier

Dan Givoli

Marcus Grote

Housseem Haddar

Thomas Hagstrom

Laurence Halpern

Christophe Hazard

Jan Hesthaven

David Hewett

Ralf Hiptmair

Thorsten Hohage

Patrick Joly

Steven Johnson

Andreas Kirsch

Peijun Li

Robert Lipton

Eric Lunéville

Paul Martin

Hoài-Minh Nguyễn

Peter Monk

Vincent Pagneux

Jeffrey Rauch

Jerónimo Rodríguez García

Olof Runborg

Géza Seriani

Chrysoula Tsogka

Michael Weinstein

Local Scientific Committee

Piotr Borejko
Josef Eberhardsteiner
Manfred Kaltenbacher
Barbara Kaltenbacher
Alfred Kluwick
Wolfgang Kreuzer
Ulrich Langer
Markus Melenk
Lothar Nannen
Ilaria Perugia
Stefan Rotter
Martin Schanz
Joachim Schöberl
Olaf Steinbach
Florian Toth

Local Organizing Committee

Simon Brandstetter
Georg Canek
Manfred Kaltenbacher
Markus Melenk
Renate Mühlberger
Lothar Nannen
Florian Toth
Ruth K. Tscherne

Plenary Speakers

Assyr Abdulle (Ecole Polytechnique Fédérale de Lausanne, Switzerland) will lecture about *Numerical methods for wave propagation in heterogeneous media*.

Assyr Abdulle earned his Ph.D. in mathematics from the University of Geneva in 2001. He completed his first post-doctoral year at Princeton University in the Program in Applied and Computational Mathematics with successive positions at ETH Zurich, the University of Basel, and the University of Edinburgh. He was appointed full professor and chair of computational mathematics and numerical analysis at EPFL in 2009. He has been the director of the mathematics institute at EPFL since 2017. His awards include the SciCADE new talent prize (2005), an Advanced Research Fellowship by the UK Engineering and Physical Sciences Research Council (2007), the SIAM Wilkinson Prize in Numerical Analysis and Scientific Computing (2009), and the SIAM Germund Dahlquist Prize (2013). His research interests concern numerical methods for multiscale partial differential equations, numerical homogenization methods, Bayesian inverse problems as well as numerical methods for deterministic dynamical systems and stochastic differential equations.

Anne-Sophie Bonnet-Ben Dhia (French National Center for Scientific Research, France) will lecture about *Combining integral representations on infinite boundaries and complex scaling for time-harmonic scattering problems*.

Anne-Sophie Bonnet-Ben Dhia is a former student of the Ecole Normale Supérieure de Jeunes Filles. She received the PhD degree in Applied Mathematics in 1988 and the Habilitation à Diriger les Recherches in 1995 from the University Pierre et Marie Curie. She is presently Directeur de Recherche at CNRS. She is the leader of the research team POEMS (associated to CNRS, INRIA, and the Ecole Nationale Supérieure de Techniques Avancées) whose activities are devoted to the mathematical and numerical analysis of wave phenomena. She is a specialist of spectral theory and scattering theory, with a particular interest for waveguides configurations. Her theoretical and numerical contributions apply to various physical domains covering optics and electromagnetism, water waves, acoustics, aeroacoustics and ultrasonics.

Josselin Garnier (École Polytechnique, France) will lecture about *Wave propagation in randomly perturbed waveguides*.

Josselin Garnier has been a professor in applied mathematics since 2001, first in Toulouse, then in Paris at the University Paris Diderot, and at Ecole Polytechnique since 2016. His research interests concern various aspects of applied probability, including wave propagation in random media, imaging for waves in complex media, uncertainty quantification, and the design and analysis of stochastic algorithms.

Marlis Hochbruck (Karlsruhe Institute of Technology, Germany) will lecture about *Unified error analysis for certain full discretizations of wave-type problems*.

Marlis Hochbruck, born in 1964 in Germany, received her diploma degree in Technomathematics in 1989 and graduated in 1992 from the University of Karlsruhe. Her PhD studies included a research stay at the NASA Ames Research Center in California. Afterwards, she held postdoctoral positions at ETH Zürich, the University of Würzburg, and the University of Tübingen, where she completed her habilitation in 1997. In the winter semester 1997/98 she held a substitute professorship at the University of Kaiserslautern. In 1998 she became a full professor for applied mathematics at Heinrich-Heine University of Düsseldorf and in 2010 she moved to her current affiliation at Karlsruhe Institute of Technology (KIT) as a full professor of numerical analysis. Her research interests lie in various fields of numerical analysis, reaching from Krylov subspace methods for linear systems and matrix functions to the construction, analysis, and efficient implementation of time integrators for partial differential equations. Most recently, the focus was on time integration of wave type problems. Marlis Hochbruck is a member of several committees of the German Research Foundation (DFG), currently serving as one of its vice presidents. At KIT, she was the speaker of the DFG Research Training Group 1294 "Analysis, simulation and design of nanotechnology processes" from 2011-2015 and is now the speaker of the DFG Collaborative Research Center 1173 "Wave phenomena: analysis and numerics".

Andrii Khrabustovskyi (Graz University of Technology, Austria) will lecture about *Crushed ice problem revisited*.

Andrii Khrabustovskyi is a researcher working at Graz University of Technology, Austria. He works mainly at the intersection of spectral theory, asymptotic analysis, and homogenization for partial differential equations. Andrii Khrabustovskyi was born in 1984 in Kharkiv, Ukraine. He was graduated from Kharkiv National University in 2006. In 2010 he received his PhD from Institute for Low Temperature Physics and Engineering of the National Academy of Sciences of Ukraine. Since November 2012 he worked at Karlsruhe Institute of Technology, first as a postdoc at the Research Training Group "Analysis, Simulation and Design of Nanotechnological Processes" and then in the Collaborative Research Center "Wave phenomena: analysis and numerics". In January 2017 he completed his habilitation with a thesis entitled "Spectral and asymptotic properties of periodic media". In 2017 he received a Lise Meitner scholarship of the Austrian Science Fund (FWF). Since November 2017 he is a member of the Institute of Applied Mathematics at TU Graz.

Euan Spence (University of Bath, United Kingdom) will lecture about *For most frequencies, strong trapping has a weak effect in frequency-domain scattering*.

Euan Spence is a Reader in Mathematics at the University of Bath. His research interests lie at the interface between semiclassical analysis and numerical analysis of wave propagation problems, with this being the title of a 5-year EPSRC Early-Career Fellowship that he currently holds. Euan has been at Bath since 2009, first as a postdoc on the EPSRC-funded project "Boundary Integral Equation Methods for High Frequency Scattering Problems" (a joint project between Bath and Reading), then as an EPSRC Postdoctoral Fellow (2011-2014), then as a Lecturer (2014-2017). Before coming to Bath he did his undergraduate, masters, and PhD at the University of Cambridge.

Beth Wingate (University of Exeter, United Kingdom) will lecture about *Non-linear resonance and finite time-scale separation in highly oscillatory PDEs: examples in geophysical fluid dynamics and numerical analysis*.

Professor Beth Wingate's main research interest is the study of oscillations in fluid mechanics, mathematics, and numerics related to high performance computing. Her recent research is focused on physics of the Arctic Ocean, direct numerical simulations, and time-stepping methods for HPC and climate modeling, and the fluid mechanics of the slow/fast manifolds. She did her PhD work at the University of Michigan studying numerics, waves and ocean fluid dynamics. Other interests include spectral element methods, in particular the investigation of near optimal interpolation on triangles. She spent many years at the Los Alamos National Laboratory in New Mexico, USA before moving to the University of Exeter in Devon, UK in 2013.

Lexing Ying (Stanford University, USA) will lecture about *Building neural networks for wave-based inverse problems*.

Lexing Ying has been Professor of Mathematics at Stanford University since 2012. Prior to that, he was a professor at the University of Texas at Austin from 2006 to 2012. His research focuses on computational mathematics and scientific computing. He received his Ph.D. from New York University and was a postdoctoral scholar at California Institute of Technology from 2004 to 2006. He is a recipient of the Sloan Research Fellowship (2007), the National Science Foundation CAREER Award (2009), the Feng Kang Prize of Scientific Computing (2011), the James H. Wilkinson Prize in Numerical Analysis and Scientific Computing from SIAM (2013), and the Silver Morningside Medal in Applied Mathematics (2016).

Minisymposia

Analysis and numerical methods for wave problems in heterogeneous media and complicated domains organised by Lise-Marie Imbert-Gérard, Andrea Moiola and Euan Spence.

Asymptotic models for the wave propagation in presence of periodic structures organised by Sonia Fliss and Berangere Delourme.

Frames and PDEs organised by Peter Balazs and Helmut Harbrecht.

Modelling and numerical simulation of flow-acoustic interaction organised by Manfred Kaltenbacher and Claus-Dieter Munz.

Modern fast Boundary Element formulations for wave propagation problems organised by Martin Schanz and Stephanie Chaillat-Loseille.

Nonlinear acoustics: analytical and numerical aspects organised by Barbara Kaltenbacher and Mechthild Thalhammer.

Resonant-state expansion of waves in the near- and far-field organised by Stefan Rotter and Thomas Weiss.

Sweeping preconditioners and related iterative solvers for the Helmholtz equation organised by Martin Gander and Thorsten Hohage.

Tent-Pitching Space-Time Methods for Nonlinear Waves organised by Robert Haber and Joachim Schöberl.

Wave Phenomena: Analysis and Numerics organised by Wolfgang Reichel and Marlis Hochbruck.

Wave propagation and imaging in complex media organised by Chrysoula Tsogka and Arnold Kim.

The conference is supported and sponsored by



Practical Information

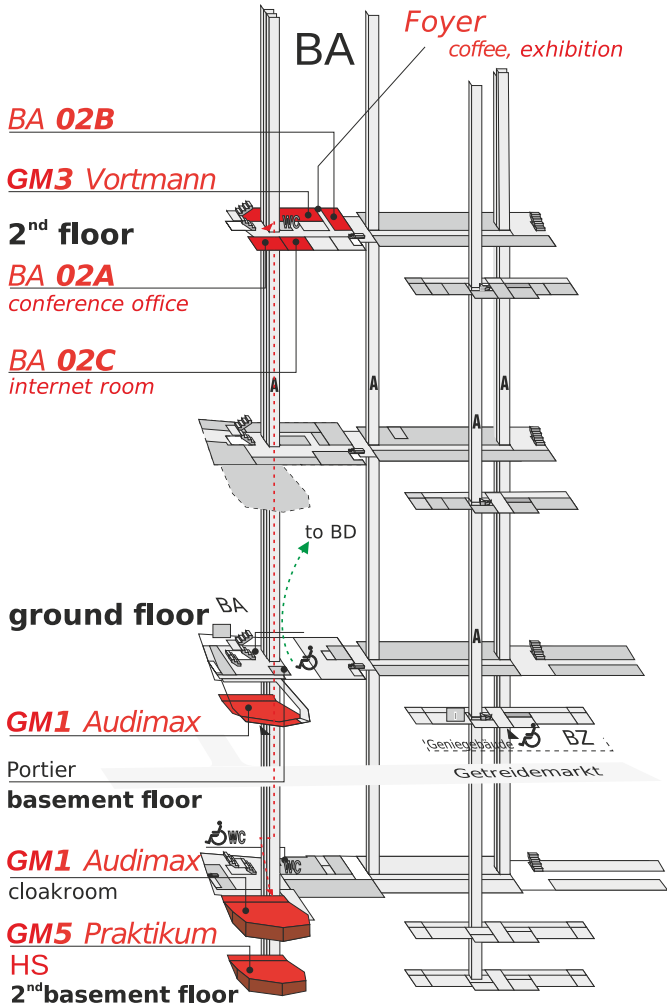
Conference Venue: TU Wien

The Conference will be held at main campus of Faculty of Mechanical and Industrial Engineering, TU Wien (Getreidemarkt 9, 1060 Vienna). The TU Wien (Vienna University of Technology) is located in the heart of Europe, in a cosmopolitan city of great cultural diversity. For more than 200 years, the TU Wien has been a place of research, teaching, and learning in the service of progress. TU Wien is among the most successful technical universities in Europe and is Austria's largest scientific-technical research and educational institution.

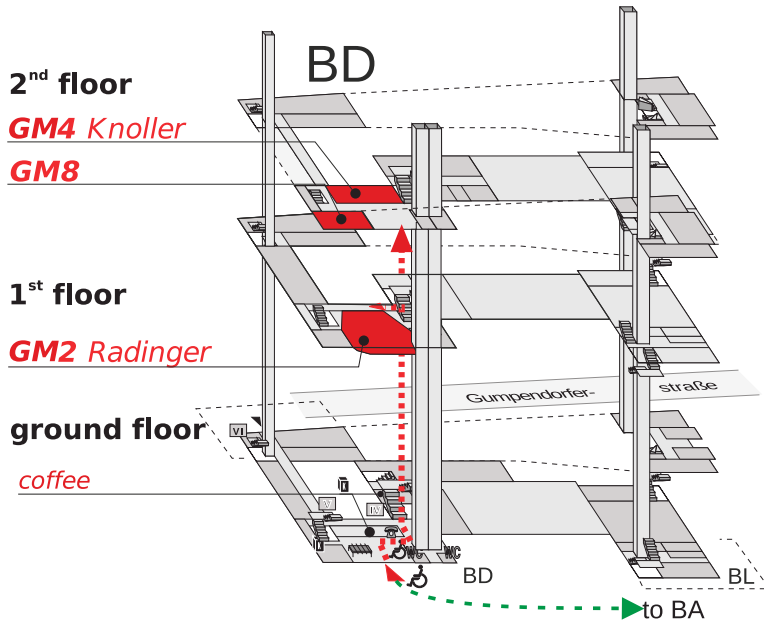
All sessions, coffee breaks, and exhibitions will take place on campus in Getreidemarkt 9, 1060 Vienna in the following two locations:

- Building **BA**, with rooms
 - Seminar Room **BA 02A**, 2nd floor: Conference office
 - Seminar Room **BA 02B**, 2nd floor
 - Seminar Room **BA 02C**, 2nd floor: Internet room
 - Foyer on 2nd floor: Coffee, Exhibition
 - **GM1** Audimax, 1st basement floor (U1)
 - **GM3** Vortmann Lecture Hall, 2nd floor
 - **GM5** Praktikums Lecture Hall, 2nd basement floor (U2)

- Building **BD**, with rooms
 - Seminar Room **GM8**, 2nd floor
 - Lecture hall **GM2** Radinger, 1st floor
 - Lecture hall **GM4** Knoller, 2nd floor
 - Ground floor: Coffee



Rooms in building BA



Rooms in building BD

Information for Presenters

All lecture rooms are equipped with projectors (VGA and HDMI connectors). A laptop computer and laser pointer will be provided by the conference organisation. Lecture rooms will be accessible 30 minutes prior to the start of the sessions. Please copy your presentation (PDF or PowerPoint) to the provided computer well before the session starts, and test if everything is working as expected. Our lecture room staff will be there to assist you.

Conference Office

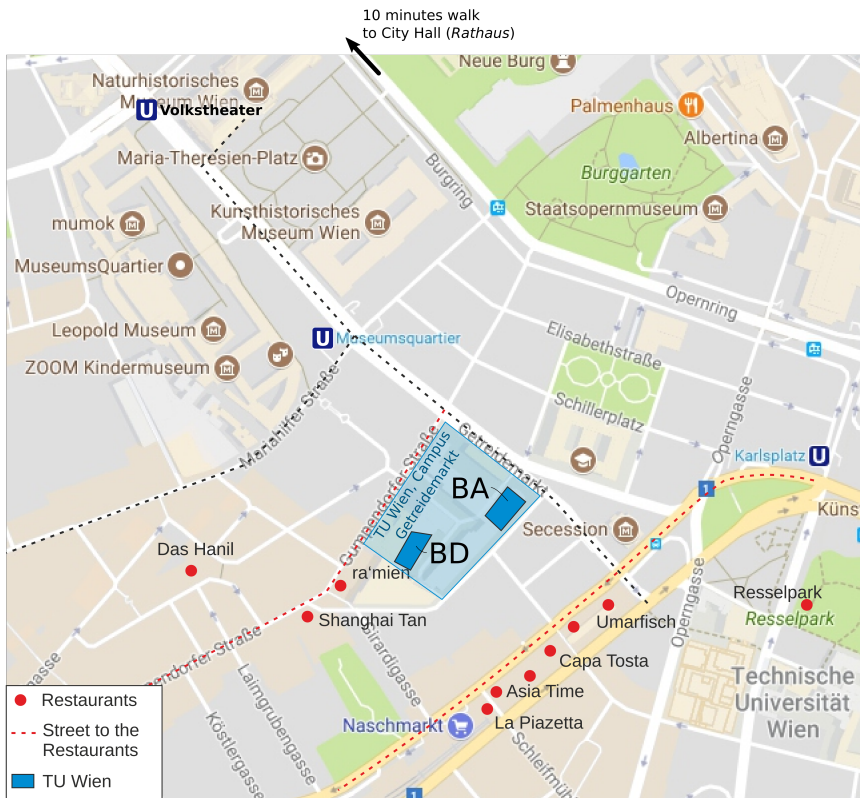
The conference office at Seminar Room BA 02A, 2nd floor of the BA building is available on:

- Sunday, 25. August; 16:00–20:00
- Monday, 26. August; 07:30–18:00
- Tuesday, 27. August; 08:00–17:00
- Wednesday, 28. August; 08:00–12:30
- Thursday, 29. August, 08:00–17:00
- Friday, 30. August, 08:00–13:00

Coffee & Lunch

During the coffee breaks, there will be drinks, coffee and snacks provided on the second floor of building BA, and at the assembly hall of building BD.

For lunch, there are several restaurants in walking distance. The famous *Naschmarkt*, located between the streets *Rechte Wienzeile* and *Linke Wienzeile*, is a market with over 100 different market stalls and offers food from traditional Austrian to Japanese buffet. Furthermore Austria's biggest shopping street, the *Mariahilfer Straße* offers a large variety of restaurants and shops. Both places are just five minutes away.



Surroundings of the conference venue

WiFi at the Venue

WiFi is available at the whole university. Conference participants with an *eduroam* account can use it on the campus. All participants without access to *eduroam* can

use their personalized account to access the network *tunetguest*. Participants have received the required login credentials (username and password) in the conference bag.

Cloakroom

Since we expect that many participants will have their luggage with them on the last conference day, a cloakroom will be available 07:45–09:30 and 08:00–13:00 on Friday, 30. August 2019 in building BA, basement floor (opposite of **GM1** Audimax). On all other conference days you have the possibility to store luggage at the conference office (building BA, 2nd floor, room **BA 02A**).

No Smoking Policy

There is a strict no-smoking-rule in all buildings of the conference venue. However, outside of the buildings smoking is allowed. Please use the provided ash trays.

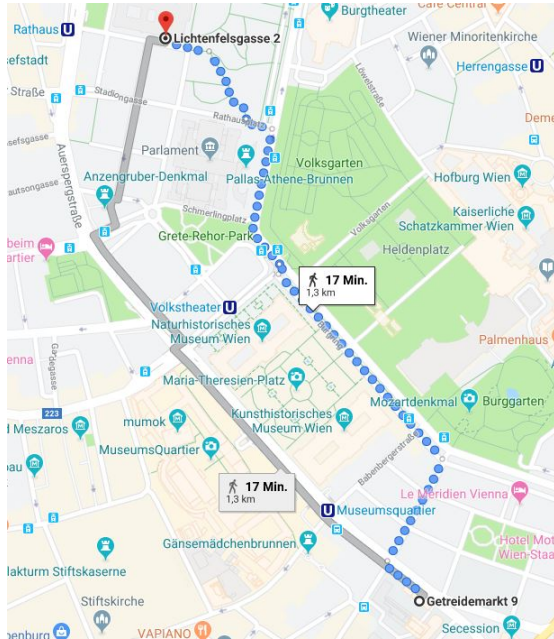
Social Events

Welcome Reception

Sunday, 25 August 2019, 17.00-20.00: The welcome reception, will be held on Sunday at TUtheSky on the 11th floor of the BA building, the main conference building, located at *Getreidemarkt 9, 1060 Vienna*. At the welcome reception drinks and finger food will be served, you will meet old and new friends, and you will have the possibility to get your conference bag. The BA building is an “energy-plus” office tower; it is the first office tower in the world capable to feed more energy into the power grid than is required to operate it.

Mayor’s Reception

Tuesday, 27 August 2019, 19.30, City Hall: On Tuesday evening, the Mayor’s Reception will be held at the Vienna City Hall (Rathaus), located in the center of Vienna and has to be entered through the side entrance at *Lichtenfelsgasse 2*. The City Hall is one of the most beautiful buildings in Vienna and serves as the seat of both the mayor and the city council of the city of Vienna. It was designed by Friedrich von Schmidt and built between 1872 and 1883. The distinctive Neo-Gothic style of the City Hall with its magnificent and fabulous halls provides a perfect setting for the conference reception. Please do not forget to bring along the invitation you have received with your conference bag.



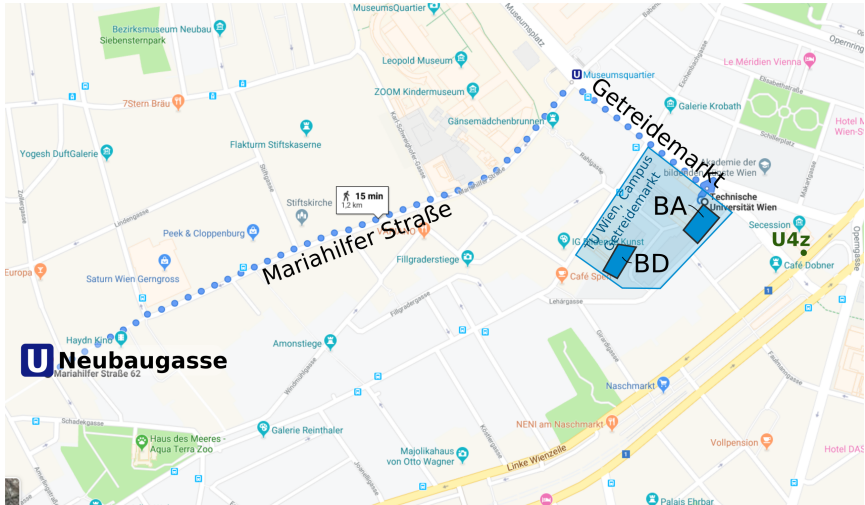
Walk from conference venue to Mayor's Reception

Conference Banquet

Thursday, 29 August 2019, 19.00, Brandauer's Schlossbräu: The banquet will take place at the Brandauer's Schlossbräu in a former aristocratic dancing hall, located at *Am Platz 5, 1130 Wien*, close to the famous castle Schönbrunn. In the previous restaurant, Der Weisse Engel, which was located at the same place, Johann Strauss, Johann Strauss Sohn, Franz Schubert and many more were among the guests.

The venue is reachable by subway line U4 (stop *Hietzing*). However, due to construction works line U4 is closed between Karlsplatz and Längenfeldgasse. The U4z replacement bus line operates between these stations (see information flyer in your conference bag).

Especially for larger groups, an alternative route by subway is: Walk up from the conference venue along *Mariahilfer Straße* to U3 stop *Neubaugasse*. Take subway line U3 (direction *Ottakring*) to *Westbahnhof* where you change to U6 (direction *Siebenhirten/Alterlaa*). At *Längenfeldgasse* change to U4 (direction *Hütteldorf*) and exit at stop *Hietzing* from where you can walk to the venue. There is a handy map on your banquet ticket.



Walk from conference venue via *Getreidemarkt* and *Mariahilfer Strasse* to subway stop *Neubaugasse* (line U3)



Walk from subway stop *Hietzing* (line U4) to Conference Banquet

Scientific Program

Overview

Monday

08:30–09:00 Opening Speech and General Information in **GM1 Audimax, Building BA**

09:00–10:00 Plenary Lecture

Assyr Abdulle (EPFL, Switzerland) *Numerical methods for wave propagation in heterogeneous media* in GM1 Audimax, Building BA

10:00–10:30 Coffee Break in buildings BA and BD

10:30–12:30 Parallel Sessions

Seismic and Hydroacoustic Problems in GM2 Radinger, Building BD

BEM and BIE in GM1 Audimax, Building BA

Transparent Boundary Conditions in Sem BA 02 B, Building BA

Optimization in GM8, Building BD

Resonant-state expansion of waves in the near- and far-field in GM5 Praktikum, Building BA

Asymptotic models for the wave propagation in presence of periodic structures in GM4 Knoller, Building BD

Modelling and numerical simulation of flow-acoustic interaction in GM3 Vortmann, Building BA

14:00–15:00 Plenary Lecture

Lexing Ying (Stanford University, United States of America) *Building neural networks for wave-based inverse problems* in GM1 Audimax, Building BA

15:00–15:30 Coffee Break in buildings BA and BD

15:30–17:00 Parallel Sessions

Modelling and numerical simulation of flow-acoustic interaction in GM3 Vortmann, Building BA

Nonlinear acoustics: analytical and numerical aspects in GM4 Knoller, Building BD

Resonant-state expansion of waves in the near- and far-field in GM5 Praktikum, Building BA

Time Stepping in GM2 Radinger, Building BD

BEM and BIE in GM1 Audimax, Building BA

Numerical Methods in GM8, Building BD

Transparent Boundary Conditions in Sem BA 02 B, Building BA

17:15–18:45 Parallel Sessions

Modelling and numerical simulation of flow-acoustic interaction in GM3 Vortmann, Building BA

Time Stepping in GM2 Radinger, Building BD

Numerical Methods in GM8, Building BD

Multiscale Problems in Sem BA 02 B, Building BA

Resonant-state expansion of waves in the near- and far-field in GM5 Praktikum, Building BA

Nonlinear acoustics: analytical and numerical aspects in GM4 Knoller, Building BD

Modern fast Boundary Element formulations for wave propagation problems in GM1 Audimax, Building BA

Tuesday

08:30–09:30 Plenary Lecture

Euan Spence (University of Bath, United Kingdom) *For most frequencies, strong trapping has a weak effect in frequency-domain scattering* in GM1 Audimax, Building BA

09:30–10:00 Coffee Break in buildings BA and BD

10:00–12:00 Parallel Sessions

Scattering in GM8, Building BD

Asymptotic models for the wave propagation in presence of periodic structures in GM4 Knoller, Building BD

Analysis and numerical methods for wave problems in heterogeneous media and complicated domains in GM2 Radinger, Building BD

Modelling and numerical simulation of flow-acoustic interaction in GM3 Vortmann, Building BA

Modern fast Boundary Element formulations for wave propagation problems in GM1 Audimax, Building BA

Sweeping preconditioners and related iterative solvers for the Helmholtz equation in GM5 Praktikum, Building BA

13:30–14:30 Plenary Lecture

Beth Wingate (University of Exeter, United Kingdom) *Nonlinear resonance and finite time-scale separation in highly oscillatory PDEs: examples in geo-*

physical fluid dynamics and numerical analysis in GM1 Audimax, Building BA

14:30–15:00 Coffee Break in buildings BA and BD

15:00–16:30 Parallel Sessions

Sweeping preconditioners and related iterative solvers for the Helmholtz equation in GM5 Praktikum, Building BA

Analysis and numerical methods for wave problems in heterogeneous media and complicated domains in GM2 Radinger, Building BD

Metamaterials in GM3 Vortmann, Building BA

Method of Images and Green's Functions in GM4 Knoller, Building BD

Numerical Methods in GM8, Building BD

BEM and BIE in GM1 Audimax, Building BA

16:45–18:15 Parallel Sessions

Modern fast Boundary Element formulations for wave propagation problems in GM1 Audimax, Building BA

Optics in GM3 Vortmann, Building BA

Numerical Methods in GM8, Building BD

Waveguides in GM4 Knoller, Building BD

Analysis and numerical methods for wave problems in heterogeneous media and complicated domains in GM2 Radinger, Building BD

Sweeping preconditioners and related iterative solvers for the Helmholtz equation in GM5 Praktikum, Building BA

Wednesday

08:30–09:30 Plenary Lecture

Marlis Hochbruck (Karlsruhe Institute of Technology, Germany) *Unified error analysis for certain full discretizations of wave-type problems* in GM1 Audimax, Building BA

09:30–10:00 Coffee Break in buildings BA and BD

10:00–12:00 Parallel Sessions

Periodic Structures in Sem BA 02 B, Building BA

Waveguides in GM4 Knoller, Building BD

Analysis and numerical methods for wave problems in heterogeneous media and complicated domains in GM2 Radinger, Building BD

Wave Phenomena: Analysis and Numerics in GM3 Vortmann, Building BA

Wave propagation and imaging in complex media in GM5 Praktikum, Building BA

Modern fast Boundary Element formulations for wave propagation problems in GM1 Audimax, Building BA

Tent-Pitching Space-Time Methods for Nonlinear Waves in GM8, Building BD

Thursday

08:30–09:30 Plenary Lecture

Andrii Khrabustovskiy (1: Graz University of Technology, Austria; 2: University of Trier, Germany) *Crushed ice problem revisited* in GM1 Audimax, Building BA

09:30–10:00 Coffee Break in buildings BA and BD

10:00–12:00 Parallel Sessions

Numerical Methods in GM8, Building BD

Inverse Problems in GM2 Radinger, Building BD

Analysis and Asymptotics in GM4 Knoller, Building BD

Frames and PDEs in Sem BA 02 B, Building BA

Wave Phenomena: Analysis and Numerics in GM3 Vortmann, Building BA

Wave propagation and imaging in complex media in GM5 Praktikum, Building BA

Modern fast Boundary Element formulations for wave propagation problems in GM1 Audimax, Building BA

13:30–14:30 Plenary Lecture

Josselin Garnier (Ecole Polytechnique, France) *Wave propagation in randomly perturbed waveguides* in GM1 Audimax, Building BA

14:30–15:00 Coffee Break in buildings BA and BD

15:00–16:30 Parallel Sessions

Modern fast Boundary Element formulations for wave propagation problems in GM1 Audimax, Building BA

Wave Phenomena: Analysis and Numerics in GM3 Vortmann, Building BA

Frames and PDEs in Sem BA 02 B, Building BA

High Frequency and Oscillatory Problems in GM5 Praktikum, Building BA

Numerical Methods in GM8, Building BD

Vibration in GM4 Knoller, Building BD

Inverse Problems in GM2 Radinger, Building BD

16:45–18:15 Parallel Sessions

Wave Phenomena: Analysis and Numerics in GM3 Vortmann, Building BA

High Frequency and Oscillatory Problems in GM5 Praktikum, Building BA

Elastodynamics in GM4 Knoller, Building BD

Inverse Problems in GM2 Radinger, Building BD

Domain Decomposition in GM8, Building BD

Modern fast Boundary Element formulations for wave propagation problems in GM1 Audimax, Building BA

Friday**08:30–10:30** Parallel Sessions

Analysis and Asymptotics in GM4 Knoller, Building BD

Domain Decomposition in GM8, Building BD

Wave Phenomena: Analysis and Numerics in GM3 Vortmann, Building BA

Wave propagation and imaging in complex media in GM5 Praktikum, Building BA

Modern fast Boundary Element formulations for wave propagation problems in GM1 Audimax, Building BA

10:30–11:00 Coffee Break in buildings BA and BD**11:00–12:00** Plenary Lecture

Anne-Sophie Bonnet-Ben Dhia (CNRS, France) *Combining integral representations on infinite boundaries and complex scaling for time-harmonic scattering problems* in GM1 Audimax, Building BA

12:00–12:30 Closing in **GM1 Audimax, Building BA**

Monday

08:30–09:00 Opening Speech and General Information

GM1 Audimax

09:00–10:00 Plenary Lecture

GM1 Audimax, Building BA

Chaired by Jens Markus Melenk

Assyr Abdulle *Numerical methods for wave propagation in heterogeneous media*

10:00–10:30 Coffee Break

Building BA and building BD

Seismic and Hydroacoustic Problems

GM2 Radinger, Building BD

Chaired by Piotr Borejko

10:30 *Comparison of Full-waveform and Travel-time Inversions in Helioseismology*

Majid Pourabdian, Laurent Gizon, Thorsten Hohage, Damien Fournier, Chris S. Hanson

11:00 *Imaging the Solar Interior with Seismic Holography*

Damien Fournier, Dan Yang, Laurent Gizon

11:30 *Low-rank representation of omnidirectional subsurface extended image volumes*

Mengmeng Yang, **Marie Graff**, Rajiv Kumar, Felix J. Herrmann

12:00 *Excitation and Propagation of Whispering Gallery Waves in a Vicinity of Curvilinear Isobath in Shallow Water*

Boris Katsnelson, Pavel Petrov

BEM and BIE

GM1 Audimax, Building BA

Chaired by Jens Markus Melenk

10:30 *Convergence analysis of boundary element methods for electromagnetic resonance problems for dielectric and plasmonic scatterers*

Gerhard Unger

11:00 *Model of electromagnetic scattering by breaking sea waves based upon the method of fundamental solutions*

Arnaud Coatanhay

11:30 *A Continuation Approach to Boundary Integral Equation for Steady-state Wave Scattering by a Crack with Contact Acoustic Nonlinearity*

Taizo Maruyama, Terumi Touhei

- 12:00** *P-SV wave scattering from an array of cylinders; tail-end asymptotics for the quasi-periodic Green's function*
Georgia M. Lynott, William J. Parnell, I. David Abrahams, Raphael C. Assier

Transparent Boundary Conditions

Sem BA 02 B, Building BA

Chaired by Eliane Becache

- 10:30** *Error analysis for transparent boundary conditions in fractal trees*
Patrick Joly, Maryna Kachanovska
- 11:00** *Computation of plasmon resonances localized at corners using frequency-dependent complex scaling*
 Anne-Sophie Bonnet-Ben Dhia, Christophe Hazard, **Florian Monteghetti**
- 11:30** *Complex Scaled Infinite Elements for Electromagnetic Problems in Open Domains*
 Bernhard Auinger, Karl Hollaus, **Michael Leumüller**, Lothar Nannen, Markus Wess
- 12:00** *Complex Scaled Infinite Elements for Wave Equations in Heterogeneous Open Systems*
 Lothar Nannen, Karoline Tichy, **Markus Wess**

Optimization

GM8, Building BD

Chaired by Martin Berggren

- 10:30** *Analysis of topological derivative as a means for qualitative identification*
Marc Bonnet, Fioralba Cakoni
- 11:00** *Topology optimisation for cloaking of arbitrary objects*
Hiroshi Isakari, Ryo Yamamoto, Kenta Nakamoto, Toru Takahashi, Toshiro Matsumoto
- 11:30** *Topological optimization of periodic materials to enhance anisotropic dispersive effects*
 Cédric Bellis, **Rémi Cornaggia**, Bruno Lombard
- 12:00** *Efficiently optimizing inclusion rotation angle for maximal power flow*
Boaz Blankrot, Clemens Heitzinger

Resonant-state expansion of waves in the near- and far-field

GM5 Praktikum, Building BA

Chaired by Thomas Weiss

- 10:30** *Microwave experiments on resonances and zeros of the scattering matrix: From spectral gaps and width shifts to random anti-lasing*
Ulrich Kuhl
- 11:00** *Modal correlation and modal selectivity in open disordered media*
Mathieu Davy, Azriel Z. Genack

11:30 *Spectral resonance expansion by Riesz projections***Lin Zschiedrich**, Felix Binkowski, Sven Burger

Asymptotic models for the wave propagation in presence of periodic structures

GM4 Knoller, Building BD

Chaired by Bérangère Delourme

10:30 *Effective equations of arbitrary order for wave propagation in periodic media*Assyr Abdulle, **Timothée Pouchon****11:00** *Electromagnetic shielding by thin periodic structures and the Faraday cage effect*Bérangère Delourme, **David Peter Hewett****11:30** *Homogenization of the time-harmonic Maxwell equations for a large class of periodic and perfectly conducting microstructures***Maik Urban**, Ben Schweizer, Klaas Hendrik Poelstra**12:00** *A homogenisation theory for a general class of high-contrast problems; asymptotics with error estimates***Ilia Kamotski**

Modelling and numerical simulation of flow-acoustic interaction

GM3 Vortmann, Building BA

Chaired by Manfred Kaltenbacher

10:30 *Stable acoustic operators for sound propagation using an adjoint based method***Étienne Spieser**, Christophe Bailly**11:00** *Low Mach number aeroacoustics in ducts using incompressible-flow wall pressure***Emmanuel Perrey-Debain**, Nicolas Papaxanthos**11:30** *Wave interaction with an infinite cascade of non-overlapping blades***Georg Maierhofer**, Nigel Peake**14:00–15:00** Plenary Lecture

GM1 Audimax, Building BA

Chaired by Martin J. Gander

Lexing Ying *Building neural networks for wave-based inverse problems***15:00–15:30** Coffee Break

Building BA and building BD

Modelling and numerical simulation of flow-acoustic interaction

GM3 Vortmann, Building BA

Chaired by Stefan Schoder

15:30 *Jet-Wing Interaction Noise Prediction with Forced Eddy Simulation*

Andrej Neifeld, Roland Ewert

16:00 *Turbulence modelling for flow-acoustic interaction of side mirror and gap noise*

Alexander Schell

16:30 *Mechanisms for wave generation in a turbulent air-water flow*

Francesco Zonta, Miguel Onorato, Alfredo Soldati

Nonlinear acoustics: analytical and numerical aspects

GM4 Knoller, Building BD

Chaired by Barbara Kaltenbacher

15:30 *A priori analysis for the finite element approximation of Westervelt's quasi-linear acoustic wave equation*

Vanja Nikolic, Barbara Wohlmuth

16:00 *Fundamental models in nonlinear acoustics*

Mechthild Thalhammer

16:30 *Optimal decay rates of the Moore-Gibson-Thompson equation*

Marta Pellicer, Belkacem Said-Houari, J. Sola-Morales

Resonant-state expansion of waves in the near- and far-field

GM5 Praktikum, Building BA

Chaired by Stefan Rotter

15:30 *Resonant-state expansion applied to photonic-crystal structures*

Sam Neale, **Egor Muljarov**

16:00 *Resonant mode approximation near Wood-Rayleigh anomalies*

Nikolay A. Gippius, Sergey G. Tikhodeev

16:30 *First-order perturbation theory for material changes in the surrounding of open optical resonators*

Steffen Both, Thomas Weiss

Time Stepping

GM2 Radinger, Building BD

Chaired by Marcus Grote

15:30 *Implicit-explicit scheme for the elastodynamic wave equation in plates*

Sonia Fliss, Alexandre Imperiale, Sébastien Imperiale, **Hajer Methenni**

16:00 *Semi-implicit time discretisation of incompressible elastodynamic equations*

Federica Caforio, **Sébastien Imperiale**

16:30 *High-order locally implicit time schemes*

Hélène Barucq, Marc Duruflé, **Mamadou N'Diaye**

BEM and BIE

GM1 Audimax, Building BA

Chaired by Holger Waubke

15:30 *A group theoretical approach for the numerical treatment of symmetries in multipole methods*

Igor Chollet, Xavier Claeys, Francis Collino, Laura Grigori

16:00 *Multi-Trace FEM-BEM formulation for acoustic scattering by composite objects*

Marcella Bonazzoli, Xavier Claeys

Numerical Methods

GM8, Building BD

Chaired by Joachim Schöberl

15:30 *A matrix-free Discontinuous Galerkin method for the time dependent Maxwell equations in open domains*

Bernard Kapidani, Joachim Schöberl

16:00 *Perturbed edge finite element method for the simulation of electromagnetic waves in magnetised plasmas*

Damien Chicaud, Patrick Ciarlet, Axel Modave

16:30 *An Inf-Sup Stable Space-Time Variational Formulation for the Scalar Second-Order Wave Equation*

Marco Zank, Olaf Steinbach

Transparent Boundary Conditions

Sem BA 02 B, Building BA

Chaired by Dan Givoli

15:30 *Stable Perfectly Matched Layers for a Class of Anisotropic Dispersive Models*

Eliane Becache, Maryna Kachanovska

16:00 *High Order Farfield Expansion ABC coupled with IGA and Finite Differences Applied to Acoustic Multiple Scattering*

Vianey Villamizar, Jacob Badger, Tahsin Khajah, Sebastian Acosta

16:30 *A high order impedance boundary condition with unique solutions for the time harmonic Maxwell's equations*

Pierre Payen, Olivier Lafitte, Bruno Stupfel

Modelling and numerical simulation of flow-acoustic interaction

GM3 Vortmann, Building BA

Chaired by Manfred Kaltenbacher

17:15 *Aeroacoustic formulation based on compressible flow data applying Helmholtz's decomposition*

Stefan Schoder, Klaus Roppert, Manfred Kaltenbacher

- 17:45** *Towards an efficient detection of hydrodynamic-acoustic feedback mechanisms in an industrial context*
Daniel Kempf, Claus-Dieter Munz
- 18:15** *A Stochastic Approach to Compute Cavity Noise using SNGR*
Michael Weitz, Stefan Schoder, Manfred Kaltenbacher

Time Stepping

- GM2 Radinger, Building BD Chaired by Sébastien Imperiale
- 17:15** *Efficient Uncertainty Quantification for Wave Propagation in Complex Geometry*
 Marcus J. Grote, **Simon Michel**
- 17:45** *Numerical methods for efficiently solving fractionally damped wave equations*
Katherine Baker, Lehel Banjai

Numerical Methods

- GM8, Building BD Chaired by Assyr Abdulle
- 17:15** *On Trefftz virtual element spaces*
 Alexey Chernov, **Lorenzo Mascotto**, Ilaria Perugia, Alexander Pichler
- 17:45** *A Trefftz discontinuous Galerkin method for acoustic scattering by small circular obstacles*
 Monique Dauge, Ilaria Perugia, **Alexander Pichler**
- 18:15** *A DPG Maxwell Approach for Studying Nonlinear Thermal Effects in Active Gain Fiber Amplifiers*
Stefan Henneking, Leszek Demkowicz, Jacob Grosek

Multiscale Problems

- Sem BA 02 B, Building BA Chaired by Josselin Garnier
- 17:15** *Heterogeneous Multiscale Method for Maxwell's Equations*
Bernhard Maier, Marlis Hochbruck
- 17:45** *Fast time-explicit micro-heterogeneous wave propagation*
Roland Maier, Daniel Peterseim
- 18:15** *Discrete Wave Equation Upscaling in 1-D and 2-D*
Cyrill Bösch, Dirk-Jan Van Manen, Andreas Fichtner

Resonant-state expansion of waves in the near- and far-field

GM5 Praktikum, Building BA

Chaired by Egor Muljarov

17:15 *Resonant States Expansions of Scattering Operators in the Harmonic and Time Domains*

Rémi Colom, Brian Stout, Ross Mcphedran, **Nicolas Bonod**

17:45 *Modal expansion of the T-matrix for resonant light scatterers*

Anton I. Ovcharenko, Jean-Paul Hugonin, **Christophe Sauvan**

18:15 *Expanding the Scattering Matrix through Quasi Normal Modes: a Numerical Case Study*

Maximilian Geismann, Faruk Salihbegovic, Matthias Kühmayer, Florian Libisch, Stefan Rotter

Nonlinear acoustics: analytical and numerical aspects

GM4 Knoller, Building BD

Chaired by Mechthild Thalhammer

17:15 *The Jordan-Moore-Gibson-Thompson equation of nonlinear acoustics: Well-posedness and singular limit for vanishing relaxation time*

Barbara Kaltenbacher, Vanja Nikolic

17:45 *Exact dispersion relation for strongly nonlinear elastic waves*

Romik Khajehtourian, **Mahmoud Hussein**

Modern fast Boundary Element formulations for wave propagation problems

GM1 Audimax, Building BA

Chaired by Timo Betcke

17:15 *Analytic preconditioners for 3D high-frequency elastic scattering problems*
Stéphanie Chaillat, **Marion Darbas**, Frédérique Le Louër

17:45 *Spectral coarse space for robust additive Schwarz preconditioning of hypersingular integral operators*

Xavier Claeys, Pierre Marchand, Frédéric Nataf

18:15 *Modelling the fluid-structure coupling caused by a far-field underwater explosion using a convolution quadrature based fast boundary element method*

Damien Mavaleix-Marchessoux, Stéphanie Chaillat, Bruno Leblé, Marc Bonnet

Tuesday

08:30–09:30 Plenary Lecture

GM1 Audimax, Building BA

Chaired by Ilaria Perugia

Euan Spence *For most frequencies, strong trapping has a weak effect in frequency-domain scattering*

09:30–10:00 Coffee Break

Building BA and building BD

Scattering

GM8, Building BD

Chaired by Paul Martin

10:00 *Near-Field Imaging of an Unbounded Elastic Rough Surface with a Direct Imaging Method*

Xiaoli Liu, Bo Zhang, Haiwen Zhang

10:30 *A Frequency Domain Method for Scattering Problems with Moving Boundaries*

David Gasperini, Xavier Antoine, Christophe Geuzaine, Hans Peter Beise, Udo Schroeder

11:00 *Scattering for NLS with a sum of two repulsive potentials*

David Lafontaine

Asymptotic models for the wave propagation in presence of periodic structures

GM4 Knoller, Building BD

Chaired by Sonia Fliss

10:00 *Numerical modeling for scattering of transient acoustic waves by resonant interfaces*

Marie Touboul, Cédric Bellis, Bruno Lombard

10:30 *Asymptotic analysis of the visco-acoustic equations for absorbing walls of arrays of Helmholtz resonators*

Kersten Schmidt, Adrien Semin

11:00 *Enriched homogenized model in presence of boundaries*

Clément Beneteau, Xavier Claeys, Sonia Fliss

11:30 *Effective description of waves in discrete and heterogeneous media*

Ben Schweizer

Analysis and numerical methods for wave problems in heterogeneous media and complicated domains

GM2 Radinger, Building BD

Chaired by Lise-Marie Imbert-Gerard

- 10:00** *Boundary element methods for scattering by fractal screens*
Simon N. Chandler-Wilde, David P. Hewett, **Andrea Moiola**
- 10:30** *Acoustic scattering by impedance screens with fractal boundary*
Joshua Bannister, **David P. Hewett**
- 11:00** *Electromagnetic scattering problems on perfectly-conducting complex domains: from Rayleigh-Sommerfeld integrals toward fractal screens*
James M. Christian, Holly A. J. Middleton-Spencer
- 11:30** *High-Order Galerkin Method for Helmholtz and Laplace Problems on Multiple Open Arcs*
José Andrés Pinto Denegri, Carlos Felipe Jerez-Hanckes
- 12:00** *Integral equation solution for two-dimensional simulations in nanoplasmonics; single layer vs multi-layer configurations.*
Harun Kurkcu
- 13:00** *Eigenoscillations and computation of surface waves in a water-basin with a conical bottom*
Ning Yan Zhu, Mikhail A. Lyalinov

Modelling and numerical simulation of flow-acoustic interaction

GM3 Vortmann, Building BA

Chaired by Manfred Kaltenbacher

- 10:00** *On the well-posedness of Galbrun's equation*
Linus Hägg, Martin Berggren
- 10:30** *Numerical analysis of the augmented Galbrun equation using discontinuous Galerkin finite elements*
Marcus Maeder, Andrew Peplow, Steffen Marburg
- 11:00** *Efficient Modeling Strategies for Thermoviscous Acoustics*
Florian Toth, Hamideh Hassanpour Guilvaiee, Manfred Kaltenbacher
- 11:30** *A computationally inexpensive visco-thermal boundary layer model for acoustic simulation and optimization*
Martin Berggren, Anders Bernland, André Massing, Daniel Noreland, Ed-die Wadbro

Modern fast Boundary Element formulations for wave propagation problems

GM1 Audimax, Building BA

Chaired by Naoshi Nishimura

- 10:00** *Efficient FEM solution of exterior wave propagation problems with weakly enforced integral non reflecting boundary conditions*
Silvia Falletta
- 10:30** *Generalization of Adaptive Cross Approximation for a Convolution Quadrature based Boundary Element Method*
 Anita M. Haider, **Martin Schanz**
- 11:00** *A superconvergence phenomenon in Runge-Kutta convolution quadrature for the wave equation*
 Jens Markus Melenk, **Alexander Rieder**
- 11:30** *On the development of a hybrid model based on the Convolution Quadrature Boundary Element Method*
Jacob Robert Rowbottom, David Chappell

Sweeping preconditioners and related iterative solvers for the Helmholtz equation

GM5 Praktikum, Building BA

Chaired by Thorsten Hohage

- 10:00** *On a Class of Iterative Solvers for Time Harmonic Wave Propagation: Factorizations, Sweeping Preconditioners, Source Transfer, Single Layer Potentials, Polarized Traces, and Optimal and Optimized Schwarz Methods*
Martin J. Gander
- 10:30** *L-Sweeps: A scalable parallel preconditioner for the high-frequency Helmholtz equation*
Matthias Taus, Leonard Zepeda-Núñez, Russell J. Hewett, Laurent Demanet
- 11:00** *Sweeping Preconditioner*
Lexing Ying
- 11:30** *Towards sweeping preconditioners for computational helioseismology*
Janosch Preuß, Christoph Lehrenfeld, Thorsten Hohage

13:30–14:30 Plenary Lecture

GM1 Audimax, Building BA

Chaired by Dan Givoli

Beth Wingate *Nonlinear resonance and finite time-scale separation in highly oscillatory PDEs: examples in geophysical fluid dynamics and numerical analysis*

14:30–15:00 Coffee Break

Building BA and building BD

Sweeping preconditioners and related iterative solvers for the Helmholtz equation

GM5 Praktikum, Building BA

Chaired by Martin J. Gander

15:00 *A time-domain approach for solving the Helmholtz equation*

Christiaan C. Stolk

15:30 *Scalable Parallel Methods for the Helmholtz Equation via Exact Controllability*

Jet Hoe Tang, Marcus Grote, Frédéric Nataf, Pierre-Henri Tournier

16:00 *Solving Helmholtz Equation via the Wave Equation*

Daniel Appelö, **Fortino Garcia**, Olof Runborg

Analysis and numerical methods for wave problems in heterogeneous media and complicated domains

GM2 Radinger, Building BD

Chaired by Andrea Moiola

15:00 *Uncertainty quantification for Helmholtz transmission problems with geometric uncertainties*

Laura Scarabosio

15:30 *Uncertainty Quantification for Helmholtz Scattering by Random Surfaces: Shape Calculus and Sparse Tensor Approximation*

Paul Escapil-Inchauspé, Carlos Jerez-Hanckes

16:00 *Nearby preconditioning for multiple realisations of the Helmholtz equation, with application to uncertainty quantification*

Owen R. Pembroey, Ivan G. Graham, Euan A. Spence

Metamaterials

GM3 Vortmann, Building BA

Chaired by Andrii Khrabustovskiy

15:00 *Essential spectrum generated by a negative material described by the Lorentz model*

Christophe Hazard, Sandrine Paolantoni

15:30 *Numerical study of the spectrum of cavities containing a negative-index material*

Sandrine Paolantoni, Christophe Hazard

16:00 *Constant-intensity waves in non-Hermitian media*

Andre Brandstötter, Konstantinos G. Makris, Etienne Rivet, Romain Fleury, Stefan Rotter

Method of Images and Green's Functions

GM4 Knoller, Building BD

Chaired by Ben Schweizer

15:00 *Use (and Misuse) of the Method of Images*

Paul Martin

15:30 *A step towards the embedding formula for the 'varying' Robin half-plane diffraction*

Marianthi Moschou, Raphael Assier

16:00 *Acoustic excitation of a layered scatterer by N internal point sources*

Andreas Kalogeropoulos, **Nikolaos Tsitsas**

Numerical Methods

GM8, Building BD

Chaired by Wolfgang Kreuzer

15:00 *A numerical algorithm to reduce the ill conditioning in meshless methods for the Helmholtz equation*

Pedro R. S. Antunes

15:30 *New Mass-Lumped Tetrahedral Elements for 3D Wave Propagation Modeling*

S. Geevers, W.A. Mulder, J.J.W. Van Der Vegt

16:00 *Study of a stable hybridization method to couple FVTD, GD scheme with FDTD/FEM scheme*

Xavier Ferrieres, Sebastien Pernet, Nicolas Deymier

BEM and BIE

GM1 Audimax, Building BA

Chaired by Xavier Claeys

15:00 *Boundary integral equations and block Jacobi preconditioner*

Bertrand Thierry

15:30 *A sinc-Fourier approach to an inverse problem in scattering*

S.-Sum Chow, Frank Stenger

16:00 *A high order method of boundary operators for the 3D time-dependent wave equation*

Sergey Petropavlovsky, Semyon Tsynkov, **Eli Turkel**

Modern fast Boundary Element formulations for wave propagation problems

GM1 Audimax, Building BA

Chaired by Marion Darbas

16:45 *Finite Element Discontinuous Galerkin and Fast Multipole BEM coupling for performing accurate scale resolved CAA simulations involving large geometries*

Stanislav Proskurov, Roland Ewert, Markus Lummer, Michael Möbner, Jan Delfs

17:15 *Synthetic Turbulence imposed as Boundary Condition for Fast Multipole BEM*

Nils Reiche, Markus Lummer, Roland Ewert, Jan Werner Delfs

17:45 *A BEM-FEM Model for Vibrations in Soils Caused by Railway Traffic in Tunnels*

Holger Waubke, Wolfgang Kreuzer, Tomasz Hrycak, Sebastian Schmutzhard

Optics

GM3 Vortmann, Building BA

Chaired by Stefan Rotter

16:45 *Designing symmetry-protected valley-Hall networks in phononic systems*
Mehul Makwana, Richard Craster, Sebastien Guenneau, Kun Tang, Patrick Sebbah, Gregory Chaplain

17:15 *Hybrid approach for modelling wave motion in a layered phononic crystal with multiple cracks and piezoelectric transducers*

Mikhail V. Golub, Alisa N. Shpak, Sergey I. Fomenko, Olga V. Doroshenko, Chuanzeng Zhang

17:45 *Optimal Wave Fields for Micromanipulation in Complex Scattering Environments*

Matthias Kühmayer, Michael Horodyski, Andre Brandstötter, Kevin Pichler, Yan V. Fyodorov, Ulrich Kuhl, Stefan Rotter

Numerical Methods

GM8, Building BD

Chaired by Eli Turkel

16:45 *A residual-based artificial viscosity finite difference method for scalar conservation laws*

Vidar Stiernström, Lukas Lundgren, Murtazo Nazarov, Ken Mattsson

17:15 *Globally Divergence-Free Discontinuous Galerkin Methods for Ideal Magnetohydrodynamic Equations*

Pei Fu, Fengyan Li, Yan Xu

17:45 *Compact fourth order scheme for the elastic wave equation in the frequency domain using a first order formulation*

Dan Gordon, Rachel Gordon, Eli Turkel

Waveguides

GM4 Knoller, Building BD

Chaired by Kersten Schmidt

16:45 *Transparent boundary conditions for periodic waveguides: analysis and extensions*

Sonia Fliss, Patrick Joly, Vincent Lescarret

17:15 *Wave Equation in a Periodic Waveguide with a Local Perturbation*

Marina Fischer

17:45 *Discrete nonlinear Schrödinger equations for periodic optical systems: pattern formation in $\chi^{(3)}$ coupled waveguide arrays*

James M. Christian, Richard Fox

Analysis and numerical methods for wave problems in heterogeneous media and complicated domains

GM2 Radinger, Building BD

Chaired by Euan Spence

16:45 *Generalized Plane Waves & Maxwell's equations*

Lise-Marie Imbert-Gerard, Jean-Francois Fritsch

17:15 *Frequency-domain wave propagation in hyperbolic metamaterials*

Patrick Ciarlet, **Maryna Kachanovska**

17:45 *Hamiltonian structure of the cold-plasma model and its discretization*

Omar Maj, Eric Sonnendrücker, Olivier Lafitte, Philip J. Morrison

Sweeping preconditioners and related iterative solvers for the Helmholtz equation

GM5 Praktikum, Building BA

Chaired by Thorsten Hohage

16:45 *An efficient domain decomposition method with cross-point treatment for Helmholtz problems*

Axel Modave, Xavier Antoine, Anthony Royer, Christophe Geuzaine

17:15 *A domain decomposition method for the Helmholtz equation using a DtN map*

Achim Schädle

Wednesday

08:30–09:30 Plenary Lecture

GM1 Audimax, Building BA

Chaired by Marcus Grote

Marlis Hochbruck *Unified error analysis for certain full discretizations of wave-type problems*

09:30–10:00 Coffee Break

Building BA and building BD

Periodic Structures

Sem BA 02 B, Building BA

Chaired by Anne-Sophie Bonnet-Ben Dhia

10:00 *Guided modes in a hexagonal periodic graph like domain : the zigzag and the armchair cases*

Bérangère Delourme, Sonia Fliss

10:30 *Reconstruction of a Local Perturbation in Inhomogeneous Periodic Layers*

Alexander Kohn

11:00 *Modelling of acoustic waves in fluid-saturated periodic scaffolds: Bloch wave decomposition and homogenization approaches*

Eduard Rohan, Robert Cimrman

11:30 *A high order numerical method for scattering from locally perturbed periodic surfaces*

Ruming Zhang

Waveguides

GM4 Knoller, Building BD

Chaired by Lothar Nannen

10:00 *An algorithm for the localization of exceptional points and the computation of Puiseux series with applications to acoustic waveguides*

Benoit Nennig, Emmanuel Perrey-Debain

10:30 *Recovering underlying graph for networks of 1D waveguides by reflectometry and transferometry*

Geoffrey Beck, Maxime Bonnaud, Jaume Benoit

11:00 *Exact zero transmission during the Fano resonance phenomenon in non symmetric waveguides*

Lucas Chesnel, Sergei A. Nazarov

11:30 *Bound States in the Continuum for a Class of Lattice Models*

Ya Yan Lu

Analysis and numerical methods for wave problems in heterogeneous media and complicated domains

GM2 Radinger, Building BD

Chaired by David Peter Hewett

10:00 *Finite element discretizations of high-frequency wave propagation problems in heterogeneous media*

Théophile Chaumont-Frelet, Serge Nicaise

10:30 *Two wave localisation effects and their impact on numerical simulation*

Céline Torres, Stefan Sauter

11:00 *Domain decomposition methods for heterogeneous Helmholtz problems*

Shihua Gong, Ivan G. Graham, Euan A. Spence

Wave Phenomena: Analysis and Numerics

GM3 Vortmann, Building BA

Chaired by Wolfgang Reichel

10:00 *The Limiting Absorption Principle for periodic Schrödinger operators*

Rainer Mandel

10:30 *Multiple solutions to a nonlinear curl-curl problem in \mathbb{R}^3*

Jarosław Mederski, Jacopo Schino, Andrzej Szulkin

11:00 *Bifurcation from Gap Eigenvalues for Nonlinear Schrödinger Equations*

Peter Rupp

11:30 *Coupled Mode Equations and Gap Solitons for Wavepackets in Nonlinear Periodic Media*

Tomas Dohnal, Lisa Wahlers

Wave propagation and imaging in complex media

GM5 Praktikum, Building BA

Chaired by Chrysoula Tsogka

10:00 *Imaging sparse reflectivities from noisy data*

Alexei Novikov

10:30 *Imaging in three-dimensional terminating waveguides with partial-aperture data*

Symeon Papadimitropoulos, Chrysoula Tsogka, Dimitrios Mitsoudis

11:00 *Adaptive Eigenspace Regularization for Inverse Scattering Problems*

Daniel H. Baffet, **Marcus J. Grote**, Jet H. Tang

11:30 *Obstacle Identification Using Learning*

Adar Kahana, Eli Turkel, Dan Givoli, Shai Dekel

Modern fast Boundary Element formulations for wave propagation problems

GM1 Audimax, Building BA

Chaired by Silvia Falletta

10:00 *Stability of the boundary integral equation methods for the two dimensional wave equation in time domain revisited*

Mio Fukuhara, Ryota Misawa, Kazuki Niino, **Naoshi Nishimura**

10:30 *Time domain CQBEM for wave scattering in complex media*

Akira Furukawa, **Sohichi Hirose**

11:00 *Space-Time Boundary Elements for the Acoustic Wave Equation*

Dominik Pözl, Martin Schanz

11:30 *The Fast Hybrid Method: Efficient ($O(1)$ sampling) and High-order, Dispersionless Long-time Transient Wave Scattering*

Thomas G. Anderson, Oscar P. Bruno, Mark Lyon

Tent-Pitching Space-Time Methods for Nonlinear Waves

GM8, Building BD

Chaired by Joachim Schöberl

10:00 *Distributed Parallel-Adaptive Causal Spacetime Discontinuous Galerkin Method with Application to Earthquake Simulation*

Robert Haber, Amit Madhukar, Xiao Ma, Ahmed Elbanna, Reza Abedi

10:30 *Applications of Adaptive Spacetime Meshing in the Asynchronous Space-time Discontinuous Galerkin Method*

Reza Abedi, Robert B Haber

11:00 *Tent pitching and a Trefftz-DG method for the acoustic wave equation*

Ilaria Perugia, Joachim Schöberl, **Paul Stocker**, Christoph Wintersteiger

11:30 *An explicit Runge-Kutta type time-stepping for Mapped Tent Pitching schemes*

Jay Gopalakrishnan, Joachim Schöberl, **Christoph Wintersteiger**

Thursday

08:30–09:30 Plenary Lecture

GM1 Audimax, Building BA

Chaired by Patrick Joly

Andrii Khrabustovskiy *Crushed ice problem revisited*

09:30–10:00 Coffee Break

Building BA and building BD

Numerical Methods

GM8, Building BD

Chaired by Achim Schädle

10:00 *High-order finite difference methods for the time-dependent Schrödinger equation on deforming domains*

Ylva Rydén, Jonatan Werpers, Ken Mattsson, Erik Sjöqvist

10:30 *Gypsilab, an open source efficient software for wave scattering simulation*

François Alouges, Matthieu Aussal, Marc Bakry

11:00 *Analysis of the hp-version of a first order system least squares method for the Helmholtz equation*

Maximilian Bernkopf, Jens Markus Melenk

Inverse Problems

GM2 Radinger, Building BD

Chaired by Eric Lunéville

10:00 *Calderón cavities inverse problem as a shape-from-moments problem*

Alexandre Munnier, **Karim Ramdani**

10:30 *On well-posedness of scattering problems in a Kirchhoff-Love infinite plate*

Laurent Bourgeois, Christophe Hazard

11:00 *The Linear Sampling Method applied to Kirchhoff-Love infinite plates*

Arnaud Recoquillay, Laurent Bourgeois

Analysis and Asymptotics

GM4 Knoller, Building BD

Chaired by Monique Dauge

10:00 *Asymptotic model for elastodynamic scattering by a small surface-breaking defect*

Marc Bonnet, Marc Deschamps, Eric Ducasse, Aditya Krishna

10:30 *Equivalent point-source modeling of small obstacles for electromagnetic waves*

Justine Labat, Victor Péron, Sébastien Tordeux

11:00 *Asymptotic expansions of Whispering Gallery Modes in graded index optical micro-cavities*

Stéphane Balac, Monique Dauge, **Zoïs Moitier**

- 11:30** *Dynamics and stability of a cold magnetic plasma*
Ibtissem Zaafrani, Simon Labrunie

Frames and PDEs

Sem BA 02 B, Building BA

Chaired by Peter Balazs

- 10:00** *Frames for the solution of operator equations in Hilbert spaces with fixed dual pairing*
Peter Balazs, Helmut Harbrecht
- 10:30** *U-cross Gram matrices and their invertibility*
 Peter Balazs, Mitra Shamsabadi, **Ali Arefijamaal**
- 11:00** *The invertibility of U-fusion cross Gram matrices of operators*
Mitra Shamsabadi, Ali Akbar Arefijamaal Arefijamaal, Peter Balazs
- 11:30** *Using B-spline frames to represent solutions of acoustics scattering problems*
Wolfgang Kreuzer

Wave Phenomena: Analysis and Numerics

GM3 Vortmann, Building BA

Chaired by Marlis Hochbruck

- 10:00** *Breather Solutions for a Quasilinear 1+1dim Wave Equation*
 Jiří Horák, **Simon Kohler**, Wolfgang Reichel
- 10:30** *Breathers on metric necklace graphs*
Daniela Maier
- 11:00** *Time-periodic solutions of a cubic wave equation*
Dominic Scheider
- 11:30** *Singularity formation in nonlinear wave equations*
 Irfan Glogic, **Birgit Schörkhuber**

Wave propagation and imaging in complex media

GM5 Praktikum, Building BA

Chaired by Chrysoula Tsogka

- 10:00** *Mixed-Dimensional Coupling for Time-Dependent Wave Problems*
Dan Givoli, Hanan Amar, Daniel Rabinovich
- 10:30** *Wave equation in a weakly randomly perturbed periodic medium*
Laure Giovangigli, Sonia Fliss
- 11:00** *Invisible floating objects*
Mahran Rihani, Lucas Chesnel
- 11:30** *Time Domain Full Waveform Inversion involving Discontinuous Galerkin approximation*
 Andreas Atle, H el ene Barucq, Henri Calandra, Julien Diaz, **Pierre Jacquet**

Modern fast Boundary Element formulations for wave propagation problems

GM1 Audimax, Building BA

Chaired by Xavier Claeys

10:00 *Bempp-cl: Fast GPU and CPU assembly of integral operators with OpenCL*
Timo Betcke, Matthew Scroggs

10:30 *A fast direct solver for multilayered quasi-periodic scattering*
Yabin Zhang, Adrianna Gillman

11:00 *High order impedance boundary condition for the three scattering problem in electromagnetism with the adaptive cross approximation*
Soumaya Oueslati, Christan Daveau, Brice Naisseline

11:30 *Convolution quadrature and BEM for scattering from generalized impedance boundary conditions*
 Lehel Banjai, Christian Lubich, **Jörg Nick**

13:30–14:30 Plenary Lecture

GM1 Audimax, Building BA

Chaired by Eliane Becache

Josselin Garnier *Wave propagation in randomly perturbed waveguides*

14:30–15:00 Coffee Break

Building BA and building BD

Modern fast Boundary Element formulations for wave propagation problems

GM1 Audimax, Building BA

Chaired by Eric Darrigrand

15:00 *Numerical resolution of boundary integral equations on some domains with singularities.*
Martin Averseng, Francois Alouges

15:30 *Shape Holomorphy of the Boundary Integral Operators in Acoustic Wave Scattering*
Fernando Henriquez, Christoph Schwab

16:00 *An implementation of the Galerkin method for the EFIE using the Hdiv inner product*
Kazuki Niino, Naoshi Nishimura

Wave Phenomena: Analysis and Numerics

GM3 Vortmann, Building BA

Chaired by Wolfgang Reichel

15:00 *Time integration and regularity theory of Maxwell equations in heterogeneous media*
Konstantin Zerulla

- 15:30** *Numerical analysis of nonlinear wave equations with dynamic boundary conditions*
Marlis Hochbruck, **Jan Leibold**
- 16:00** *Time-integration of semilinear wave equations with highly oscillatory solutions*
Benjamin Dörich, Marlis Hochbruck

Frames and PDEs

Sem BA 02 B, Building BA

Chaired by Helmut Harbrecht

- 15:00** *Multilevel frames for solving high-dimensional partial differential equations*
Helmut Harbrecht, Peter Zaspel
- 15:30** *Adaptive solution of PDEs using hybrid shearlet-wavelet frames*
Philipp Grohs, Gitta Kutyniok, Jackie Ma, Philipp Petersen, **Mones Raslan**
- 16:00** *Quarkonial frames with compression properties - theory and numerical applications*
Stephan Dahlke, Ulrich Friedrich, Philipp Keding, **Thorsten Raasch**, Alexander Sieber

High Frequency and Oscillatory Problems

GM5 Praktikum, Building BA

Chaired by Olof Runborg

- 15:00** *Galerkin boundary element methods for high-frequency sound-hard scattering problems*
Fatih Ecevit, Akash Anand, Yassine Boubendir, Souaad Lazergui
- 15:30** *Least squares collocation for a high-frequency scattering problem*
Andrew Gibbs, David Hewett, **Daan Huybrechs**, Emile Parolin
- 16:00** *PathFinder: a toolbox for oscillatory quadrature*
Andrew Gibbs, Daan Huybrechs

Numerical Methods

GM8, Building BD

Chaired by Ilaria Perugia

- 15:00** *Robust adaptive hp discontinuous Galerkin finite element methods for the Helmholtz equation*
Scott Congreve, **Joscha Gedicke**, Ilaria Perugia
- 15:30** *A discontinuous Galerkin Trefftz type method for solving the Maxwell equations*
Hakon Fure, **Sebastien Pernet**, Sebastien Tordeux

- 16:00** *High order discretization of seismic waves-problems based upon DG-SE methods*
Hélène Barucq, Henri Calandra, **Aurélien Citrain**, Julien Diaz, Christian Gout

Vibration

- GM4 Knoller, Building BD Chaired by Florian Toth
- 15:00** *Combining Dynamical Energy Analysis with Advanced Transfer Path Analysis*
Gregor Tanner, Timo Hartmann, Satoshi Morita, Martin Richter
- 15:30** *Sound radiation from complex vibrating mechanical structures using Wigner transformation technique*
Neekar Majeed Mohammed, Gregor Tanner, Stephen C Creagh
- 16:00** *3d Modeling and Simulation of a Harpsichord*
Lukas Larisch, Gabriel Wittum

Inverse Problems

- GM2 Radinger, Building BD Chaired by Lucas Chesnel
- 15:00** *Crack monitoring using transmission eigenvalues with artificial backgrounds*
Lorenzo Audibert, Housseem Haddar, Lucas Chesnel, **Kevish Napal**
- 15:30** *Near-Field Inverse Dipole Problems in Spherical Media*
Nikolaos Tsitsas
- 16:00** *Imaging small dielectric inclusions with polarization data*
Patrick Bardsley, **Maxence Cassier**, Fernando Guevara Vasquez

Wave Phenomena: Analysis and Numerics

- GM3 Vortmann, Building BA Chaired by Marlis Hochbruck
- 16:45** *Space-time discontinuous Galerkin method for the wave equation in polygonal domains*
Pratyuksh Bansal, Andrea Moiola, Ilaria Perugia, Christoph Schwab
- 17:15** *A space-time DPG method for acoustic waves in heterogeneous media*
Christian Wieners, Johannes Ernesti
- 17:45** *Uniform-in-time optimal convergent HDG method for transient elastic waves with strong symmetric stress formulation*
Shukai Du, Francisco-Javier Sayas

High Frequency and Oscillatory Problems

GM5 Praktikum, Building BA

Chaired by Euan Spence

- 16:45** *Ray density transport through a mesh using a phase-space integral operator with a direction preserving discretisation*
David James Chappell, Martin Richter, Gregor Tanner
- 17:15** *Convergence Properties of Transfer Operators for Billiards with a Mixed Phase-Space*
Martin Richter, David J. Chappell, Gregor Tanner
- 17:45** *Error estimates for Gaussian beams at a fold caustic*
Olof Runborg, Olivier Lafitte

Elastodynamics

GM4 Knoller, Building BD

Chaired by Sébastien Imperiale

- 16:45** *Linear isotropic elastodynamics by means of potentials: The case of transmission conditions for piecewise homogeneous media.*
Jorge Albella, Sébastien Imperiale, Patrick Joly, Jerónimo Rodríguez
- 17:15** *Numerical aspects of Energetic Boundary Element Method for 2D soft scattering in linear elastodynamics*
Giulia Di Credico, Alessandra Aimi, Mauro Diligenti, Chiara Guardasoni
- 17:45** *Spectral analysis of a nonhomogeneous rotating Timoshenko beam: Riesz basis property*
Jean-Luc Akian

Inverse Problems

GM2 Radinger, Building BD

Chaired by Marc Bonnet

- 16:45** *One-Way Operators for Time Dependent Wave Splitting and Echo Removal*
Daniel Henri Baffet, Marcus Grote
- 17:15** *How to solve inverse scattering problems without knowing the source term*
Marie Graff, Marcus J. Grote, Frédéric Nataf, Franck Assous
- 17:45** *Shape reconstruction of deposits inside a steam generator using eddy current measurements*
Hugo Girardon, Houssein Haddar, Lorenzo Audibert

Domain Decomposition

GM8, Building BD

Chaired by Joachim Schöberl

- 16:45** *High order transmission conditions for a Domain Decomposition Method applied to an efficient and accurate solution of EM scattering problems*
 Bruno Stupfel, **Matthieu Lecouvez**

- 17:15** *An integral equation on infinite boundaries when a global Green's function is not available*
Anne-Sophie Bonnet-Ben Dhia, Sonia Fliss, **Yohanes Tjandrawidjaja**
- 17:45** *Non-overlapping domain decomposition algorithm for time-harmonic elastic wave problems*
Marion Darbas, Christophe Geuzaine, **Vanessa Mattesi**

Modern fast Boundary Element formulations for wave propagation problems

GM1 Audimax, Building BA

Chaired by Martin Schanz

- 16:45** *Interior Penalty Discontinuous Galerkin BEM for the Helmholtz equation: Theoretical and numerical analysis*
Messai Nadir-Alexandre, Pernet Sébastien
- 17:15** *A stable integral equation for a mixed acoustic transmission problem*
Sarah Eberle, **Francesco Florian**, Ralf Hiptmair, Stefan Sauter
- 17:45** *FastMMLib: a generic library for Fast Multipole Methods*
Eric Darrigrand, Yvon Lafranche

Friday

Analysis and Asymptotics

GM4 Knoller, Building BD

Chaired by Christophe Hazard

08:30 *Homogenization of the time-dependent heat equation on plane mesh structures*

Adrien Semin, Kersten Schmidt, Josip Tambaca, Matko Ljulj

09:00 *Uniqueness of self-similar solutions obeying the problems of arbitrary discontinuity disintegration for the generalized Hopf equation*

Anna Chugaynova

09:30 *Water wave scattering by a submerged metamaterial*

Christos Marangos, Richard Porter

10:00 *Effective models for non-perfectly conducting thin coaxial cables*

Geoffrey Beck, Sébastien Imperiale, Patrick Joly

Domain Decomposition

GM8, Building BD

Chaired by Christian Wieners

08:30 *A Preconditioner for the Electric Field Integral Equation on Screens*

Ralf Hiptmair, **Carolina Urzúa-Torres**

09:00 *Non overlapping domain decomposition methods with non local transmission conditions for electromagnetic wave propagation*

Xavier Claeys, Francis Collino, Patrick Joly, **Emile Parolin**

09:30 *New transmission conditions for corners and cross-points*

Bruno Després, **Anouk Nicolopoulos**, Bertrand Thierry

Wave Phenomena: Analysis and Numerics

GM3 Vortmann, Building BA

Chaired by Wolfgang Reichel

08:30 *Solving inverse electromagnetic scattering problems via domain derivatives*

Felix Hagemann, Tilo Arens, Timo Betcke, Frank Hettlich

09:00 *Reconstructing thin tubular scattering objects in electromagnetic scattering*

Roland Griesmaier, **Marvin Knöller**

09:30 *On the analysis of perfectly matched layers for electromagnetic waves propagation in anisotropic media*

Éliane Bécache, Sonia Fliss, Maryna Kachanovska, **Maria Kazakova**

Wave propagation and imaging in complex media

GM5 Praktikum, Building BA

Chaired by Chrysoula Tsogka

08:30 *Reflection matrix approach for ultrasonic imaging in heterogeneous media*

Laura A. Cobus, William Lambert, Mathias Fink, Alexandre Aubry

- 09:00** *Introducing the Random Anti-laser: Coherent Perfect Absorption in Disordered Media*
Stefan Rotter, Kevin Pichler, Matthias Kühmayer, Julian Böhm, Andre Brandstötter, Philipp Ambichl, Ulrich Kuhl
- 09:30** *Maximum-likelihood estimation of target parameters in a time-evolving random medium*
 Clément Roussel, **Arnaud Coatanhay**, Alexandre Baussard
- 10:00** *Stochastic Models in Coordinate-Delay Synthetic Aperture Radar Imaging*
Mikhail Gilman, Semyon Tsynkov

Modern fast Boundary Element formulations for wave propagation problems

GM1 Audimax, Building BA Chaired by Martin Schanz

- 08:30** *Fast Calderón preconditioning of the PCMHWT formulation for scattering by multiple dielectric particles*
Antigoni Kleanthous, Timo Betcke, David Hewett, Carlos Jerez-Hanckes, Paul Escapil-Inchauspé, Anthony Baran
- 09:00** *Fast Calderón Preconditioning for Helmholtz Boundary Integral Equations*
Carlos Jerez-Hanckes, Ignacia Fierro
- 09:30** *FEM-BEM coupling for vibroacoustics using the open-source Gypsilab software*
Marc Bakry, François Alouges, Matthieu Aussal
- 10:00** *Parallelization techniques for the collocation boundary element method*
Caglar Guerbuez, Christopher Jelich, Steffen Marburg

10:30–11:00 Coffee Break

Building BA and building BD

11:00–12:00 Plenary Lecture

GM1 Audimax, Building BA Chaired by Manfred Kaltenbacher

Anne-Sophie Bonnet-Ben Dhia *Combining integral representations on infinite boundaries and complex scaling for time-harmonic scattering problems*

12:00–12:30 Closing

GM1 Audimax

PART II

Abstracts

Numerical methods for wave propagation in heterogeneous media

Assyr Abdulle¹

¹ANMC, Institute of Mathematics, École Polytechnique Fédérale de Lausanne, Station 8, CH-1015 Lausanne, Switzerland

Abstract

In this work we discuss effective models and numerical methods for wave propagation in heterogeneous media. For problems without scale separation we show that discrete coarse approximation spaces based on local orthogonal decomposition can be used to capture the wave dynamics. For locally-periodic problems, we discuss analytical and numerical models that are able to capture the dispersive effects that develops when the wave propagates over long time.

Keywords: second order hyperbolic problems, heterogeneous media, localized orthogonal decomposition, homogenization, dispersion

1 Wave in heterogeneous media

In this paper we discuss recent developments of numerical methods for the wave equation in heterogeneous media given by the following problem: find $u_\varepsilon : [0, T] \rightarrow \mathbb{R}$ such that

$$\partial_{tt}u_\varepsilon - \nabla \cdot (a^\varepsilon \nabla u_\varepsilon) = F \quad \text{in } \Omega \times (0, T), \quad (1)$$

with suitable initial and boundary conditions. The tensor a^ε , which describes the medium, is assumed to have *multiscale coefficients*, i.e., a^ε varies on a scale of order $\mathcal{O}(\varepsilon)$, where $0 < \varepsilon \ll 1$. At first we do not assign a particular value to ε , but we only assume that it is a very small parameter.

To illustrate our arguments we will assume that $\|a^\varepsilon\|_{W^{1,\infty}(\Omega)} = \mathcal{O}(\varepsilon^{-1})$. Let us also assume that $\Omega \subset \mathbb{R}^d$ is a bounded Lipschitz domain and that the matrix-valued function a^ε belongs to the space $\mathcal{M}(\alpha, \beta, \Omega)$ of symmetric matrix valued functions, uniformly elliptic and bounded by α and β , respectively,

2 Classical approximation

For a classical numerical approximation of the problem (1) we pick a $P1$ finite element (FE) space V_h with mesh size h (chosen for simplicity to be a quasi-uniform family of triangulation of the domain Ω in simplicial elements). The following standard approximation result can then

be obtained following Baker [8]:

$$\begin{aligned} \|u_\varepsilon - u_h\|_{L^\infty(L^2)} &\leq C(\|u_\varepsilon - \Pi_h(u_\varepsilon)\|_{L^\infty(L^2)} \\ &\quad + \|\partial_t u_\varepsilon - \partial_t \Pi_h(u_\varepsilon)\|_{L^1(L^2)}), \end{aligned}$$

where $\Pi_h : H_0^1(\Omega) \rightarrow V_h$ is the Ritz-projection onto V_h , i.e., the $(a_\varepsilon \nabla \cdot, \nabla \cdot)$ -orthogonal projection. The projection error can be further estimated (assuming $\partial_t u_\varepsilon \in L^1(H^1)$) by exploiting its quasi best-approximation property in $H^1(\Omega)$, an Aubin-Nitsche duality argument for the elliptic projection and the H^1 -stability of Π_h to obtain

$$\begin{aligned} \|u_\varepsilon - u_h\|_{L^\infty(L^2)} &\leq Ch \|a^\varepsilon\|_{W^{1,\infty}(\Omega)} (\|u_\varepsilon\|_{L^\infty(H^1)} \\ &\quad + \|\partial_t u_\varepsilon\|_{L^1(H^1)}) \leq C \frac{h}{\varepsilon^2}, \end{aligned}$$

where $C = C(T)$ is independent of ε . One power of ε originates from $\|a^\varepsilon\|_{W^{1,\infty}(\Omega)} = \mathcal{O}(\varepsilon^{-1})$, the other from the energy estimate for $\|\partial_t u_\varepsilon\|_{L^1(I)}$ that also scales as $\mathcal{O}(\varepsilon^{-1})$ (following classical arguments). The above estimate raises two observations. First, it scales poorly with respect to the parameter ε and requires a prohibitive mesh resolution if ε is small. Second, the estimate is not optimal in h . This is due to the fact that applying an Aubin-Nitsche duality argument to use an optimal first order convergence rate in the H^1 norm would require to bound $\|\partial_t u_\varepsilon\|_{L^1(H^2)}$ that however scales as $C\varepsilon^{-2}$. This issue also prevents the use of higher spatial approximation when using classical FE or finite difference (FD) methods for the approximation of (1).

In this contribution we consider two distinct classes of media that require different numerical strategies.

3 No scale separation and local orthogonal decomposition

For the first class of media, we assume no scale separation in the highly heterogeneous tensor a^ε , but only assume $\|a^\varepsilon\|_{W^{1,\infty}(\Omega)} = \mathcal{O}(\varepsilon^{-1})$. To construct a suitable method, we first need to design an appropriate multiscale space. For that we follow the idea of localized orthogonal decomposition (LOD) [11].

Consider a coarse quasi-uniform mesh and an associated FE space $V_H = \text{span}\{\Phi_z\}$, spanned by piecewise basis functions Φ_z . Here H can be much coarser than ε . We then consider the L^2 projection $I_H : H_0^1(\Omega) \rightarrow V_H$ and define $W_h = \text{Ker}(I_H|_{V_h})$, where V_h is a FE space spanned by piecewise basis functions with a quasi-uniform mesh with meshsize h that resolves the finest scale, i.e. $h < \varepsilon$.

Next we consider the corrector $Q : V_H \rightarrow W_h$ given by the elliptic projection

$$(a_\varepsilon \nabla Q(v_H), \nabla w_h) = -(a_\varepsilon \nabla v_H, \nabla w_h)$$

$\forall w_h \in W_h$ and we obtain a multiscale space $V_H^{ms} = \{\Phi_z + Q(\Phi_z), \Phi_z \text{ nodal macro basis fct}\}$. Building this space is very costly as it involves multiple solves of elliptic partial differential equations in Ω with resolved mesh $h < \varepsilon$. The crucial finding in [11] is that the elliptic projection can be localized on a patch around each coarse element, while maintaining good approximation properties of the multiscale space (the size of the neighbouring coarse elements involved in the patch usually scales as $|\log H|$). We denote this localized space by $V_{H,loc}^{ms}$ and assume that the local elliptic solution to build the multiscale FE space are sufficiently well resolved (see [2] for a precise statement).

Using $V_{H,loc}^{ms}$ for a FE solution of the wave equation (1) we can show for its corresponding solution u_H^{ms} the following error estimate

$$\begin{aligned} \|u_\varepsilon - u_H^{ms}\|_{L^\infty(L^2)} &\leq CH (\|u_\varepsilon\|_{L^\infty(H^1)} \\ &\quad + \|\partial_t u_\varepsilon\|_{L^1(H^1)}). \end{aligned}$$

However, as mentioned earlier, $\|\partial_t u_\varepsilon\|_{L^1(H^1)}$ scales as $\mathcal{O}(\varepsilon^{-1})$. Using a perturbation argument based on the notion of G -convergence from homogenization, we show in [2] that $\|\partial_t u_\varepsilon\|_{L^1(H^1)}$ can be bounded independently of ε , establishing a convergence rate that scales with a coarse meshsize H for a multiscale FE discretization of the wave equation in a medium with a continuum of (heterogeneous) scales. Fully discrete estimates with time-discretization for Newmark schemes (e.g. Crank-Nicolson method) can also be found in [2].

4 Locally periodic media: effective equations and numerical homogenization

For the second class of media, we assume scale separation in the tensor a^ε (e.g., periodic, locally periodic media). Multiscale methods based

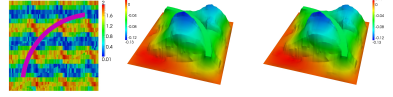


Figure 1: Heterogeneous medium (left), solution of the wave equation in the heterogeneous medium by a resolved FEM (middle) and a the multiscale solution u_H (right), see [2].

on homogenization theory can then be used, relying on the discretization of a homogenized version of (1)

$$\partial_t u_0 - \nabla \cdot (a^0 \nabla u_0) = F \quad \text{in } \Omega \times (0, T). \quad (2)$$

These multiscale methods, rely on a macroscopic finite element space V_H and a microscopic finite element space V_h that is used to solve the original highly oscillatory elliptic problem associated to (1) to recover on the fly the effective tensor a^0 at suitable quadrature points. This computation is done on patches that scales with ε , resulting in a computational cost independent of ε [1].

However as time evolves dispersive effects accumulate in the oscillatory wave u_ε given by (1) that are not captured by the homogenized wave u_0 [12]. Higher order models must then be computed. The first interesting time-scale where significant dispersion occur to make the homogenized model (2) invalid is $[0, T\varepsilon^{-2}]$. It is shown in [3] that a family of effective models (summation convention is used) of the form

$$\partial_{tt} \tilde{u} - a_{ij}^0 \partial_{ij}^2 \tilde{u} + \varepsilon^2 (a_{ijkl}^2 \partial_{ijkl}^4 \tilde{u} - b_{ij}^2 \partial_{ij}^2 \partial_{tt} \tilde{u}) = F,$$

can be defined upon appropriate choice of the tensors a^2 and b^2 . Solutions of these models are ε close to the solution u_ε in a norm equivalent to the $L^\infty(0, T\varepsilon^{-2}; L^2(\Omega))$ norm. The above family of models is appropriate when a^ε is a periodic tensor. Convergence of a multiscale method related to such models is proved in [4], effective models with locally periodic a^ε are derived in [5] and effective models on arbitrary timescales are presented in [6]. Related works can also be found in [7, 9, 10].

References

- [1] A. ABDULLE AND M. J. GROTE, *Finite element heterogeneous multiscale method*

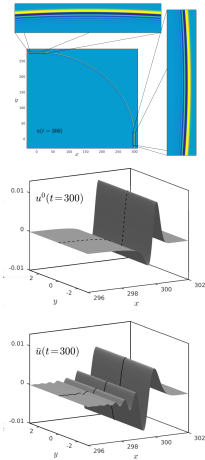


Figure 2: Wave propagating in layered medium (top figure), wave in the corresponding homogenized medium (middle figure), an effective solution given by the higher order model (bottom figure), see [3].

for the wave equation, *Multiscale Model. Simul.*, 9 (2011), 766–792.

- [2] A. Abdulle and P. Henning, *Localized orthogonal decomposition method for the wave equation with a continuum of scales*, *Math. Comp.* 86 (2017), no. 304, 549–587.
- [3] A. ABDULLE AND T. POUCHON, *Effective models for the multidimensional wave equation in heterogeneous media over long time and numerical homogenization*, *Math. Models Methods Appl. Sci.*, 26 (2016), 2651–2684.
- [4] —, *A priori error analysis of the finite element heterogeneous multiscale method for the wave equation over long time*, *SIAM J. Numer. Anal.*, 54 (2016), 1507–1534.
- [5] —, *Effective models for long time wave propagation in locally periodic media*, *SIAM J. Numer. Anal.*, 56 (2018), 2701–2730.
- [6] —, *Effective models and numerical homogenization for wave propagation in het-*

erogeneous media on arbitrary timescales. arXiv preprint arXiv:1905.09062, 2019.

- [7] G. ALLAIRE, A. LAMACZ, AND J. RAUCH, *Crime pays; homogenized wave equations for long times*. arXiv preprint arXiv:1803.09455, 2018.
- [8] G. A. Baker, *Error estimates for finite element methods for second order hyperbolic equations*, *SIAM J. Numer. Anal.*, 13 (1976), no 4, 564–576.
- [9] A. BENOIT AND A. GLORIA, *Long-time homogenization and asymptotic ballistic transport of classical waves*, arXiv preprint arXiv:1701.08600, (2017).
- [10] T. DOHNAL, A. LAMACZ, AND B. SCHWEIZER, *Dispersive homogenized models and coefficient formulas for waves in general periodic media*, *Asymptot. Anal.*, 93 (2015), 21–49.
- [11] A. Målqvist and D. Peterseim, *Localization of elliptic multiscale problems*, *Math. Comp.* 83 (2014), no. 304, 2583–2603.
- [12] F. Santosa and W. Symes, *A dispersive effective medium for wave propagation in periodic composites*, *SIAM J. Appl. Math.*, 51 (1991), no. 4, 984-1005.

Building Neural Networks for Wave-based Inverse Problems

Lexing Ying^{1,*}

¹Department of Mathematics, Stanford University, Stanford, CA, USA

*Email: lexing@stanford.edu

Abstract

This talk summarizes our recent work on developing neural networks for wave-based inverse problems.

Keywords: neural networks, inverse problems, Fourier-integral operators, butterfly algorithm

1 Introduction

In the past several years, deep learning has advanced the state-of-art of many topics in artificial intelligence, including vision, speech, etc. The main player of this success story is the architecture of deep neural networks, which is highly flexible in terms of representing high-dimensional functions and probability distributions and allows for automatic feature extraction. When combined with efficient optimization algorithms such as stochastic gradient descent and modern hardware (GPU, TPU, etc) and software (Tensorflow, Pytorch, etc) developments, they outperform traditional machine learning methods in many fields.

Wave-based imaging has been an important tool for scientific discovery in physical sciences. Unfortunately, many problems of wave-based imaging are mathematically challenging, due to the nonlinearity of the problem and the need to learn appropriate prior information from the data.

In this abstract, we present some recent work of applying deep learning to address some of these challenges. There are two main challenges in applying deep learning to inverse problems. First, in most applications of inverse problems, one is often faced with limited amount of data, when compared to the traditional machine learning tasks such as image and speech recognition. Second, since many inverse problems are often formulated as regression problems, i.e., learning a function rather than just a yes/no answer, they require much better accuracy. In order to overcome these main difficulties, our approach leverages the mathematical and physical structures of the inverse problems, by introducing compact neural network structures for the key mathematical operators, such as the pseudo-

differential operators and the Fourier-integral operators. At the same time, the weights of the neural networks along with the prior are trained end-to-end from the data.

2 Novel structural modules

Pseudo-differential operators (PDOs) and Fourier integral operators (FIOs) are key building blocks of mathematical treatments of the inverse problems.

PDOs of form

$$(Af)(x) \equiv \int K(x, y)f(y)dy,$$

are typically used to model the normal operator associated with the linearized forward operator. When viewed as a matrix, its off-diagonal blocks are often numerical low-rank. Based on this key property, we have recently proposed two types of neural networks for representing PDOs. The first type is motivated by the additive multiscale decomposition of PDOs (see Figure 1 top). When applied to an arbitrary vector, each scale of the decomposition can be encoded as a three-layer linear neural network (see Figure 1 bottom). By putting together the

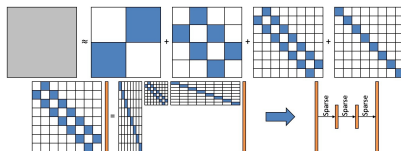


Figure 1: Pseudo-differential operators: additive multiscale decomposition in hierarchical matrix form.

three-layer linear neural networks at different scales and including nonlinear operators such as ReLU, we propose the multiscale neural networks in [1] (see Figure 2 top). By further exploiting the nested structures of the low-rank factorizations across different scales, one arrives at a more compact version proposed in [2] (see

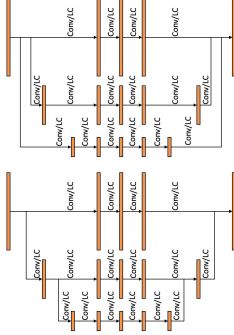


Figure 2: Multiscale neural network.

Figure 2 bottom). The second type is motivated by the multiplicative decomposition based on the non-standard wavelet from proposed by Beylkin, Coifman, and Rokhlin (see Figure 3 for a schematic decomposition and the matvec at a single scale). By putting together the linear neu-

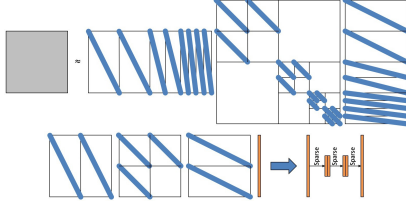


Figure 3: Pseudo-differential operators: multiplicative multiscale decomposition in non-standard wavelet form.

ral networks at each scale and including nonlinear operations such as ReLU, we arrive at the BCR-Net proposed in [3] (see Figure 4).

FIOs of form

$$(Af)(x) \equiv \int a(x, \xi) e^{2\pi i \Phi(x, \xi)} f(\xi) d\xi$$

are typically used to model the linearized forward and adjoint operators. If one partitions its matrix form into blocks that are square-root size of the dimension, a key property is that each block of the FIO is numerical low-rank. By applying low-rank approximations to each block,

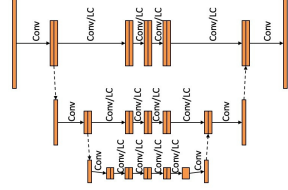


Figure 4: BCR-Net.

we arrive at the butterfly factorization (see Figure 5 top). When applied to an arbitrary vector, the whole computation can be encoded in a three-layer linear neural network (see Figure 5 bottom). By inserting the nonlinear operations,

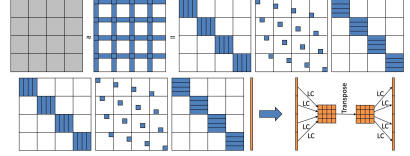


Figure 5: Fourier-integral operators: butterfly factorization in hierarchical.

we propose the Switch-Net module in [4] (shown in Figure 6) for applying the FIOs.

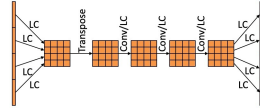


Figure 6: Switch-Net.

3 Applications

We have applied the neural network modules developed above to a few wave-based inverse problems. The first problem is inverse media scattering from the far field pattern (see Figure 8). This problem is modeled by the Helmholtz equation

$$Lu = \left(-\Delta - \frac{\omega^2}{c_0(x)^2} - \eta(x) \right) u = 0.$$

where ω is the frequency, $c_0(x)$ is the background velocity, and $\eta(x)$ is the unknown media. Given

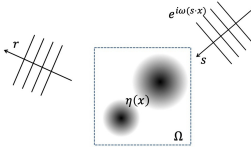


Figure 7: Inverse media scattering from far field pattern.

an incoming wave direction s and an outgoing wave direction r , the far field pattern $d(r, s)$ encodes the scaled and modulated scattering wave in the r direction. In the linearized regime, i.e., $\eta(x) \ll 1$, the following approximation holds

$$d(r, s) \approx (A\eta)(r, s) \equiv \sum_{x \in X} e^{i\omega(s-r)\cdot x} \eta(x),$$

where the linearized forward operator A , as an FIO from Ω to $\mathbb{S}^1 \times \mathbb{S}^1$, can be represented with a Switch-Net. Under the same assumption, the inverse operator is $(A^*A + \epsilon I)^{-1}A^*d$, where the part $(A^*A + \epsilon I)^{-1}$ can be shown to be a PDO. Based on these considerations, we propose in [4] the following neural network architecture for the full (nonlinear) inverse problem

$$d(r, s) \Rightarrow \text{SwitchNet} \Rightarrow \text{BCR-Net} \Rightarrow \eta(x).$$

The second case is a toy example of seismic imaging with surface observations in the frequency domain. To simplify the treatment, the

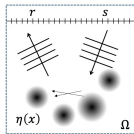


Figure 8: Seismic imaging with surface observations.

problem is modeled by the Helmholtz equation

$$Lu_s = \left(-\Delta - \frac{\omega^2}{c_0(x)^2} - \eta(x) \right) u_s = \delta_s(x),$$

where $\eta(x)$ is the unknown media and s is the source at surface. By imposing receivers r at the surface as well, the seismic data $d(r, s)$ can be approximated in the linearized regime as

$$d(r, s) \approx (A\eta)(r, s) \equiv \sum_{x \in X} G_0(r, x)G_0(x, s)\eta(x),$$

where G_0 is the Green's function of the background media $c_0(x)$. It can be shown that A is an FIO for sufficiently smooth background velocity $c_0(x)$ and hence can be represented with a Switch-Net. Following the same reasoning, the linearized normal operator $(A^*A + \epsilon I)^{-1}$ is a PDO and the same neural network architecture

$$d(r, s) \Rightarrow \text{SwitchNet} \Rightarrow \text{BCR-Net} \Rightarrow \eta(x)$$

can be used for this inverse problem as well [4].

References

- [1] Yuwei Fan, Lin Lin, Lexing Ying, and Leonardo Zepeda-Nunez. A multiscale neural network based on hierarchical matrices. arXiv:1807.01883.
- [2] Yuwei Fan, Jordi Feliu-Faba, Lin Lin, Lexing Ying, and Leonardo Zepeda-Nunez. A multiscale neural network based on hierarchical nested bases. Res. Math. Sci. 6, 2019.
- [3] Yuwei Fan, Cindy Orozco Bohorquez, and Lexing Ying. BCR-Net: a neural network based on the nonstandard wavelet form. Journal of Computational Physics, 384, 2019.
- [4] Yuehaw Khoo and Lexing Ying. Switch-Net: a neural network model for forward and inverse scattering problems. arXiv:1810.09675

For most frequencies, strong trapping has a weak effect in frequency-domain scattering

D. Lafontaine¹, E.A. Spence^{2,*}, J. Wunsch³

¹Department of Mathematical Sciences, University of Bath, Bath, BA2 7AY, UK

²Department of Mathematical Sciences, University of Bath, Bath, BA2 7AY, UK

³Department of Mathematics, Northwestern University, 2033 Sheridan Road, Evanston IL 60208-2730, US

*Email: E.A.Spence@bath.ac.uk

Abstract

It is well known that when the geometry and/or coefficients allow stable trapped rays, the solution operator of the Helmholtz equation (a.k.a. the resolvent of the Laplacian) grows *exponentially* through a sequence of real frequencies tending to infinity.

In this talk (based on the paper [21]) we show that, even in the presence of the strongest-possible trapping, if a set of frequencies of arbitrarily small measure is excluded, the Helmholtz solution operator grows at most *polynomially* as the frequency tends to infinity.

One significance application of this result is in the convergence analysis of several numerical methods for solving the Helmholtz equation at high frequency that are based on a polynomial-growth assumption on the solution operator (e.g. *hp*-finite elements, *hp*-boundary elements, certain multiscale methods). The result of this talk shows that this assumption holds, even in the presence of the strongest-possible trapping, for most frequencies.

Keywords: Helmholtz, high-frequency, a priori bound, resolvent, trapping, resonance.

1 Introduction

1.1 Motivation: bounds on the solution operator under trapping

Trapping and nontrapping are central concepts in scattering theory. This talk is concerned with the behaviour of the solution operator in frequency-domain scattering problems (a.k.a. the resolvent) in the presence of strong trapping. Our results (taken from the paper [21]) hold for a wide variety of boundary-value problems where the differential operator is the Helmholtz operator $\Delta + k^2$ outside some compact set; indeed, we work in the framework of *black-box scattering* introduced by Sjöstrand–Zworski in [36] and recapped briefly in [21, §2]. For simplicity, in this intro-

duction we focus on the exterior Dirichlet problem (EDP) for the Helmholtz equation; i.e. the problem of, given a bounded, open set $\mathcal{O} \subset \mathbb{R}^n$, $n \geq 2$, such that the open complement $\mathcal{O}_+ := \mathbb{R}^n \setminus \mathcal{O}$ is connected and $\partial\mathcal{O}_+$ is Lipschitz, $f \in L^2(\mathcal{O}_+)$ with compact support, and frequency $k > 0$, find $u \in H_{\text{loc}}^1(\mathcal{O}_+)$ such that

$$\Delta u + k^2 u = -f \quad \text{in } \mathcal{O}_+, \quad \gamma u = 0 \quad \text{on } \partial\mathcal{O}_+, \quad (1)$$

(where γ denotes the trace operator on $\partial\mathcal{O}_+$) and

$$\frac{\partial u}{\partial r}(x) - ik u(x) = o\left(\frac{1}{r^{(d-1)/2}}\right), \quad (2)$$

as $r \rightarrow \infty$, uniformly in $\widehat{x} := x/r$ (with this last condition the *Sommerfeld radiation condition*). One can show that the solution of the EDP is unique for all k , and then Fredholm theory implies that the solutions exist for all k and, given $R > 0$ such that $\text{supp} f \subset B_R := \{x : |x| < R\}$ and $k_0 > 0$,

$$\begin{aligned} \|\nabla u\|_{L^2(\mathcal{O}_+ \cap B_R)} + k \|u\|_{L^2(\mathcal{O}_+ \cap B_R)} \\ \leq \Upsilon(k, \mathcal{O}, R, k_0) \|f\|_{L^2(\mathcal{O}_+)} \end{aligned} \quad (3)$$

for all $k \geq k_0$, where $\Upsilon(k, \mathcal{O}, R, k_0)$ is some (a priori unknown) function of k, \mathcal{O}, R , and k_0 .

It is convenient to write bounds such as (3) in terms of the outgoing cut-off resolvent $\chi R(k) \chi$ $L^2(\mathcal{O}_+) \rightarrow H^1(\mathcal{O}_+)$ for $k \in \mathbb{R} \setminus \{0\}$, where $\chi \in C_{\text{comp}}^\infty(\overline{\mathcal{O}_+})$ and $R(k) := -(\Delta + k^2)^{-1}$, with Dirichlet boundary conditions on $\partial\mathcal{O}_+$, is defined by analytic continuation from $R(k) : L^2(\mathcal{O}_+) \rightarrow L^2(\mathcal{O}_+)$ for $\Im k > 0$ (this definition implies that the radiation condition (2) is satisfied for $k \in \mathbb{R} \setminus \{0\}$). The bound (3) then becomes

$$\begin{aligned} \|\chi R(k) \chi\|_{L^2(\mathcal{O}_+) \rightarrow L^2(\mathcal{O}_+)} &\leq \frac{\Upsilon(k, \mathcal{O}, \chi, k_0)}{k}, \\ \|\chi R(k) \chi\|_{L^2(\mathcal{O}_+) \rightarrow H^1(\mathcal{O}_+)} &\leq \frac{\Upsilon(k, \mathcal{O}, \chi, k_0)}{\min(k_0, 1)}, \end{aligned} \quad (4)$$

for all $k \geq k_0$. Having obtained an $L^2 \rightarrow L^2$ bound on $R_\chi(k)$, an $L^2 \rightarrow H^1$ bound can be obtained from Green's identity (i.e. multiplying the PDE in (1) by \bar{u} and integrating by parts; see, e.g., [37, Lemma 2.2]) and so we focus on $L^2 \rightarrow L^2$ bounds from now on.

When \mathcal{O}_+ has C^∞ boundary and is *nontrapping*, i.e. all billiard trajectories starting in an exterior neighbourhood of \mathcal{O} escape from that neighbourhood after some uniform time, one can show that Υ in (4) is independent of k , i.e. given $k_0 > 0$,

$$\|\chi R(k)\chi\|_{L^2(\mathcal{O}_+) \rightarrow L^2(\mathcal{O}_+)} \lesssim \frac{1}{k} \quad \text{for all } k \geq k_0, \quad (5)$$

where the notation $a \lesssim b$ means that there exists a $C > 0$, independent of k (but dependent on k_0 , \mathcal{O}_+ , and χ), such that $a \leq Cb$. This classic nontrapping resolvent estimate was first obtained by the combination of the results on propagation of singularities for the wave equation on manifolds with boundary by Melrose and Sjöstrand [29, 30] with either the parametrix method of Vainberg [40] (see [33]) or the methods of Lax and Phillips [22] (see [28]).

On the other hand, when \mathcal{O}_+ is *trapping*, a loss is unavoidable in the cut-off resolvent; indeed, at least in the case of semiclassical scattering by a potential, if trapping exists then one has a semiclassical lower bound by [4, Théorème 2], which in our notation corresponds to

$$\|\chi R(k)\chi\|_{L^2 \rightarrow L^2} \gtrsim \frac{\log(2+k)}{k}, \quad (6)$$

and one expects the strength of the loss to depend on the strength of the trapping. In the standard example of *hyperbolic trapping*, which is when \mathcal{O} equals the union of two disjoint convex obstacles with strictly positive curvature (see Figure 1(a), the lower bound (6) is achieved, since

$$\|\chi R(k)\chi\|_{L^2(\mathcal{O}_+) \rightarrow L^2(\mathcal{O}_+)} \lesssim \frac{\log(2+k)}{k}$$

for all $k \geq k_0$ by [9, Proposition 4.4]. In the standard example of *parabolic trapping*, which is when \mathcal{O} equals the union of two disjoint, aligned squares, in 2-d, or cubes, in 3-d, (see Figure 1(b)), the cut-off resolvent suffers a polynomial loss over the nontrapping estimate, with the bound

$$\|\chi R(k)\chi\|_{L^2(\mathcal{O}_+) \rightarrow L^2(\mathcal{O}_+)} \lesssim k \quad \text{for all } k \geq k_0$$

proved in [14, Theorem 1.9]; variable-power polynomial losses have also been exhibited in [16, Theorem 2] in cases of degenerate-hyperbolic trapping in the setting of scattering by metrics.

For general \mathcal{O}_+ with C^∞ boundary, the cut-off resolvent can grow at most exponentially in k by the bound of Burq [7, Theorem 2]

$$\|\chi R(k)\chi\|_{L^2(\mathcal{O}_+) \rightarrow L^2(\mathcal{O}_+)} \lesssim e^{\alpha k} \quad \text{for all } k \geq k_0$$

for some $\alpha = \alpha(\mathcal{O}, k_0) > 0$. In the presence of the strongest possible trapping – so called *elliptic trapping* – this exponential growth of the cut-off resolvent is achieved. Indeed, if \mathcal{O} has an ellipse-shaped cavity (see Figure 1(c)) then there exists a sequence of frequencies $0 < k_1 < k_2 < \dots$, with $k_j \rightarrow \infty$, and $\alpha > 0$ such that

$$\|\chi R(k_j)\chi\|_{L^2(\mathcal{O}_+) \rightarrow L^2(\mathcal{O}_+)} \gtrsim e^{\alpha k_j} \quad j = 1, 2, \dots, \quad (7)$$

see, e.g., [3, §2.5]. More generally, if there exists an elliptic trapped ray (i.e. an elliptic closed broken geodesic), and $\partial\mathcal{O}_+$ is analytic in neighbourhoods of the vertices of the broken geodesic, then the resolvent can grow at least as fast as $\exp(\alpha k_j^q)$, through a sequence k_j as above and for some range of $q \in (0, 1)$, by the quasimode construction of Cardoso and Popov [12] (note that Popov proved *superalgebraic* growth for certain elliptic trapped rays when $\partial\Omega_-$ is smooth in [32]).

The question this talk answers is *how does the cut-off resolvent behave under elliptic trapping when k is not equal to one of the “bad” frequencies k_j ?*

Our answer to this question uses this fact that the growth of the cut-off resolvent through the real sequence k_j under trapping is due to the presence of (complex) resonances lying in the lower-half complex k -plane, close to the real axis. The “bad” real frequencies k_j then correspond to the real parts of these (complex) resonances. The strength of the trapping and how close the resonances are to the real axis are intimately related. Indeed, in elliptic trapping, the resonances are super-algebraically close to the real axis, causing at least superalgebraic growth of the cut-off resolvent, whereas in hyperbolic trapping the resonances stay a fixed distance away from the real axis, hence the weak logarithmic loss over the nontrapping resolvent estimate; see the recent overview discussion in [41, §2.4] and the references therein.

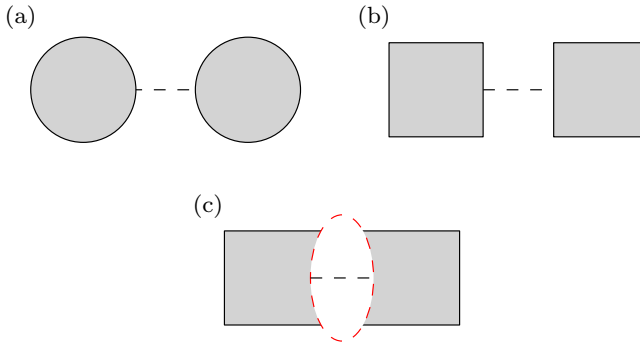


Figure 1: Examples of (a) hyperbolic trapping, (b) parabolic trapping, and (c) elliptic trapping, with a trapped ray for each indicated by a black dashed line.

1.2 Statement of main results (in the setting of impenetrable-Dirichlet-obstacle scattering)

In the setting of scattering by an impenetrable Dirichlet obstacle our main result is the following. This result is valid (and hence stated) for all Lipschitz obstacles, but is of primary interest when the obstacle contains an elliptic trapped ray.

Theorem 1 (Polynomial resolvent estimate for most frequencies [21, Theorem 1.1])

Let \mathcal{O} be an open set $\mathcal{O} \subset \mathbb{R}^n$, $n \geq 2$, such that the open complement $\mathcal{O}_+ := \mathbb{R}^n \setminus \overline{\mathcal{O}}$ is connected and $\partial\mathcal{O}_+$ is Lipschitz. Let $R(k)$ be defined as in §1.1. Then, given $k_0 > 0$, $\delta > 0$, and $\varepsilon > 0$, there exists $C = C(k_0, \delta, \varepsilon, n) > 0$ and a set $J \subset [k_0, \infty)$ with $|J| \leq \delta$ such that

$$\|\chi R(k)\chi\|_{L^2(\mathcal{O}_+) \rightarrow L^2(\mathcal{O}_+)} \leq Ck^{5n/2+\varepsilon}$$

for all $k \in [k_0, \infty) \setminus J$. (8)

In other words, even in the presence of elliptic trapping, outside an arbitrary-small set of frequencies, the resolvent is always polynomially bounded, with an exponent depending only on the dimension. We make the following remarks.

- The analogue of Theorem 1 in the black-box-scattering framework is given as [21, Theorem 3.4]; this result is that a resolvent estimate identical to (8) in its k -dependence

is valid in a wide range of settings, including scattering by an impenetrable Neumann obstacle, by a penetrable obstacle, by a potential, by elliptic and compactly-supported perturbations of Laplacian, and on finite volume surfaces (see [18, §4.1]).

- The proof of Theorem 1 uses the results of Tang and Zworski [39] about (i) the behaviour of resolvent away from resonances [38, Lemma 1], [39, Proposition 4.3] (see also [18, Theorem 7.5]) and (ii) the semiclassical maximum principle [38, Lemma 2], [39, Lemma 4.2] (see also [18, Lemma 7.7]). In fact [39, Proposition 4.6] notes that the cut-off resolvent is bounded polynomially in regions of the complex plane that include intervals of the real axis away from resonances; the difference here is that we seek to control the measure of these intervals.
- Under assumptions about the distribution of resonances, one can lower the exponent in (8) and also obtain a bound on the measure of the set $\{k : \|\chi R(k)\chi\|_{L^2 \rightarrow L^2} > \lambda^*\} \cap [\lambda, \lambda + 1)$; see [21, Theorem 3.6]. Scattering by a strictly convex, penetrable obstacle is one scenario where relatively-strong information is known about the distribution of resonances, and [21, Corollary 3.9] applies the general result of [21, Theorem 3.6] in this case.

- We do not know the sharp value of the exponent in the bound (8). Under an almost-equidistribution of resonances hypothesis, we obtain a lower bound of $\|\chi R(k)\chi\|_{L^2 \rightarrow L^2} \gtrsim k^{n-2}$: see [21, Lemma 3.10].
- Similar results to Theorem 1 about relatively “good” behaviour of the Helmholtz solution operator under elliptic trapping as long as k is outside some finite interval were proved for scattering by a penetrable ball in [10, Theorem 6.5] for 2-d and [11, Theorem 2.5] for 3-d. These results use the explicit expression for the solution in terms of an expansion in Fourier series (2-d) or spherical harmonics (3-d), with coefficients given by Hankel and Bessel functions, to bound the scattered field outside the obstacle in terms of the incident field, with a loss of derivatives (corresponding to a loss of powers of k). At least when the contrast in wave speeds inside and outside the obstacle is sufficiently large, [10, Lemma 6.2] and [11, Lemma 3.6] show that the scattered field everywhere outside the obstacle is polynomially bounded in k for k outside a set of small, finite measure.
- As noted in §1.1, when the obstacle \mathcal{O} contains an ellipse-shaped cavity, the resolvent grows exponentially through a sequence k_j (7); in this situation Theorem 1 implicitly contains information about the widths of the peaks in the norm of the resolvent at k_j . We are not aware of any results in the literature about the widths of these peaks in the setting of obstacle scattering, but precise information about the widths and heights of peaks in the transmission coefficient for model resonance problems in one space dimension can be found in [35], [1].
- Complementary results (in a different direction to Theorem 1) about “good” behaviour of the resolvent in trapping scenarios can be found in [13, Theorem 1.1], [8, Theorem 4], and [17, Theorems 1.1, 1.2]. Indeed, [13, Theorem 1.1] proves that, even in the presence of trapping, the nontrapping resolvent estimate (5) holds when the support of χ is sufficiently far away from the obstacle ([8, Theorem 4]

proves this result up to factors of $\log k$). The results [17, Theorems 1.1, 1.2] prove the analogue of this result in the setting of scattering by a potential and/or by a metric when the cut-off functions are replaced by semiclassical pseudodifferential operators restricting attention to areas of phase space isolated from the trapped set.

1.3 Applications to numerical analysis of Helmholtz scattering problems

The most exciting applications of the bound (8) are for numerical methods whose analyses require the resolvent to be *polynomially bounded in k , with the method depending only mildly on the degree of this polynomial*. Three such methods are

1. The hp -finite-element method (hp -FEM), where, under the assumption that the resolvent is polynomially bounded in k , the results of [19,26,27] establish that the finite element method when $h \sim k^{-1}$ and $p \sim \log k$ does not suffer from the pollution effect; i.e. under this choice of h and p , for which the total number of degrees of freedom $\sim k^n$, the method is quasi-optimal with constant independent of k . Similar results were then obtained for DG methods in [25,34], and for least-squares methods in [2,15].
2. The hp -boundary-element method (hp -BE) where, under a polynomial-boundedness assumption on the solution operator, the results of [23,24] establish that the boundary element method when $h \sim k^{-1}$ and $p \sim \log k$ does not suffer from the pollution effect.
3. The multiscale finite-element method of [20], [6], [5] [31], which, under the assumption that the resolvent is polynomially bounded in k , computes solutions that are uniformly accurate in k but with a total number of degrees of freedom $\sim k^n$, provided that a certain oversampling parameter grows logarithmically with k .

References

- [1] G. S. Abeynanda and S. P. Shipman. Dynamic resonance in the high- Q and near-

- monochromatic regime. In *2016 IEEE International Conference on Mathematical Methods in Electromagnetic Theory (MMET)*, pages 102–107. IEEE, 2016.
- [2] M. Bernkopf and J. M. Melenk. Analysis of the *hp*-version of a first order system least squares method for the Helmholtz equation. *arXiv preprint arXiv:1808.07825*, 2018.
- [3] T. Betcke, S. N. Chandler-Wilde, I. G. Graham, S. Langdon, and M. Lindner. Condition number estimates for combined potential boundary integral operators in acoustics and their boundary element discretisation. *Numer. Methods Partial Differential Eq.*, 27(1):31–69, 2011.
- [4] J.-F. Bony, N. Burq, and T. Ramond. Minoration de la résolvaite dans le cas captif. *Comptes Rendus Mathématique*, 348(23-24):1279–1282, 2010.
- [5] D. L. Brown and D. Gallistl. Multiscale sub-grid correction method for time-harmonic high-frequency elastodynamics with wavenumber explicit bounds. *arXiv preprint arXiv:1608.04243*, 2016.
- [6] D. L. Brown, D. Gallistl, and D. Peterseim. Multiscale Petrov-Galerkin method for high-frequency heterogeneous Helmholtz equations. In *Meshfree Methods for Partial Differential Equations VIII*, pages 85–115. Springer, 2017.
- [7] N. Burq. Décroissance des ondes absence de de l'énergie locale de l'équation pour le problème extérieur et absence de résonance au voisinage du réel. *Acta Math.*, 180:1–29, 1998.
- [8] N. Burq. Lower bounds for shape resonances widths of long range Schrödinger operators. *American Journal of Mathematics*, 124(4):677–735, 2002.
- [9] N. Burq. Smoothing effect for Schrödinger boundary value problems. *Duke Math. J.*, 123:403–427, 2004.
- [10] Y. Capdeboscq. On the scattered field generated by a ball inhomogeneity of constant index. *Asymptot. Anal.*, 77(3-4):197–246, 2012.
- [11] Y. Capdeboscq, G. Leadbetter, and A. Parker. On the scattered field generated by a ball inhomogeneity of constant index in dimension three. In *Multi-scale and high-contrast PDE: from modelling, to mathematical analysis, to inversion*, volume 577 of *Contemp. Math.*, pages 61–80. Amer. Math. Soc., Providence, RI, 2012.
- [12] F. Cardoso and G. Popov. Quasimodes with exponentially small errors associated with elliptic periodic rays. *Asymptotic Analysis*, 30(3, 4):217–247, 2002.
- [13] F. Cardoso and G. Vodev. Uniform estimates of the resolvent of the Laplace-Beltrami operator on infinite volume Riemannian manifolds. II. *Annales Henri Poincaré*, 3(4):673–691, 2002.
- [14] S. N. Chandler-Wilde, E. A. Spence, A. Gibbs, and V. P. Smyshlyaev. High-frequency bounds for the Helmholtz equation under parabolic trapping and applications in numerical analysis. *arXiv preprint arXiv:1708.08415*, 2017.
- [15] H. Chen and W. Qiu. A first order system least squares method for the Helmholtz equation. *Journal of Computational and Applied Mathematics*, 309:145–162, 2017.
- [16] H. Christianson and J. Wunsch. Local smoothing for the Schrödinger equation with a prescribed loss. *American Journal of Mathematics*, 135(6):1601–1632, 2013.
- [17] K. Datchev and A. Vasy. Propagation through trapped sets and semiclassical resolvent estimates. In *Microlocal Methods in Mathematical Physics and Global Analysis*, pages 7–10. Springer, 2013.
- [18] S. Dyatlov and M. Zworski. *Mathematical theory of scattering resonances*. American Mathematical Society, to appear, 2019. http://math.mit.edu/~dyatlov/res/res_final.pdf.
- [19] S. Esterhazy and J. M. Melenk. On stability of discretizations of the Helmholtz equation. In I. G. Graham, T. Y. Hou, O. Lakkis, and R. Scheichl, editors, *Numerical Analysis of Multiscale Problems*, pages 285–324. Springer, 2012.

- [20] D. Gallistl and D. Peterseim. Stable multiscale Petrov–Galerkin finite element method for high frequency acoustic scattering. *Comput. Method. Appl. M.*, 295:1–17, 2015.
- [21] D. Lafontaine, E. A. Spence, and J. Wunsch. For most frequencies, strong trapping has a weak effect in frequency-domain scattering. *arXiv preprint 1903.12172*, 2019.
- [22] P. D. Lax and R. S. Phillips. *Scattering Theory*. Academic Press, Boston, 2nd edition, 1989.
- [23] M. Löhndorf and J. M. Melenk. Wavenumber-Explicit *hp*-BEM for High Frequency Scattering. *SIAM Journal on Numerical Analysis*, 49(6):2340–2363, 2011.
- [24] J. M. Melenk. Mapping properties of combined field Helmholtz boundary integral operators. *SIAM Journal on Mathematical Analysis*, 44(4):2599–2636, 2012.
- [25] J. M. Melenk, A. Parsania, and S. Sauter. General DG-methods for highly indefinite Helmholtz problems. *Journal of Scientific Computing*, 57(3):536–581, 2013.
- [26] J. M. Melenk and S. Sauter. Convergence analysis for finite element discretizations of the Helmholtz equation with Dirichlet-to-Neumann boundary conditions. *Math. Comp.*, 79(272):1871–1914, 2010.
- [27] J. M. Melenk and S. Sauter. Wavenumber explicit convergence analysis for Galerkin discretizations of the Helmholtz equation. *SIAM J. Numer. Anal.*, 49:1210–1243, 2011.
- [28] R. B. Melrose. Singularities and energy decay in acoustical scattering. *Duke Math. J.*, 46(1):43–59, 1979.
- [29] R. B. Melrose and J. Sjöstrand. Singularities of boundary value problems. I. *Comm. Pure Appl. Math.*, 31(5):593–617, 1978.
- [30] R. B. Melrose and J. Sjöstrand. Singularities of boundary value problems. II. *Comm. Pure Appl. Math.*, 35(2):129–168, 1982.
- [31] D. Peterseim. Eliminating the pollution effect in Helmholtz problems by local sub-scale correction. *Mathematics of Computation*, 86(305):1005–1036, 2017.
- [32] G. S. Popov. Quasimodes for the Laplace operator and glancing hypersurfaces. In *Microlocal Analysis and Nonlinear Waves*, pages 167–178. Springer, 1991.
- [33] J. Ralston. Note on the decay of acoustic waves. *Duke Math. J.*, 46(4):799–804, 1979.
- [34] S. Sauter and J. Zech. A posteriori error estimation of *hp*-dG finite element methods for highly indefinite Helmholtz problems. *SIAM J. Num. Anal.*, 53(5):2414–2440, 2015.
- [35] S. P. Shipman and A. T. Welters. Resonant electromagnetic scattering in anisotropic layered media. *Journal of Mathematical Physics*, 54(10):103511, 2013.
- [36] J. Sjöstrand and M. Zworski. Complex scaling and the distribution of scattering poles. *J. Amer. Math. Soc.*, 4(4):729–769, 1991.
- [37] E. A. Spence. Wavenumber-explicit bounds in time-harmonic acoustic scattering. *SIAM Journal on Mathematical Analysis*, 46(4):2987–3024, 2014.
- [38] S.-H. Tang and M. Zworski. From quasimodes to resonances. *Math. Res. Lett.*, 5:261–272, 1998.
- [39] S.-H. Tang and M. Zworski. Resonance expansions of scattered waves. *Comm. Pure Appl. Math.*, 53(10):1305–1334, 2000.
- [40] B. R. Vainberg. On the short wave asymptotic behaviour of solutions of stationary problems and the asymptotic behaviour as $t \rightarrow \infty$ of solutions of non-stationary problems. *Russian Mathematical Surveys*, 30(2):1–58, 1975.
- [41] M. Zworski. Mathematical study of scattering resonances. *B. Math. Sci.*, 7(1):1–85, 2017.

**Nonlinear resonance and finite time-scale separation in highly oscillatory PDEs:
examples in geophysical fluid dynamics and numerical analysis**

Beth Wingate^{1,*}

¹Department of Mathematics, University of Exeter, Exeter, UK

*Email: b.wingate@exeter.ac.uk

Abstract

In highly oscillatory fluid dynamics, such as fluids that govern Earth's atmosphere and ocean, the role of the waves on developing and sustaining a mean flow is an open question with far-reaching consequences that include how we understand climate variability and how we perform numerical computations. In this talk we will discuss the role of nonlinear and linear resonance from time-scale separated PDEs on the formation and persistence of low-frequency phenomenon. We will rely on the use of the semi-group operator as a mapping that helps reveal the mathematical structure of the PDE. We will give examples from ODEs and an example from the Arctic Ocean. Finally, we will sketch a new proof of convergence for the parareal method when there is time-scale separation.

Keywords: resonance, numerical analysis, oscillations

1 Introduction

One of the most interesting challenges in dynamics is to understand the role of waves on the creation of low frequency (long-lived) mean flows. This type of phenomenon has long been of interest in fluid dynamics because it governs our understanding of the large-scale, low-frequency flow that we observe in atmospheres and oceans, plasmas, and other branches of physics. Having a deeper understanding of this type of phenomenon is also important in creating new numerical approximations to these PDEs required to use challenging new computer architectures and has long been of interested in mathematics. In this talk I will focus on highly oscillatory PDEs that exhibit time scale separation of the form,

$$\frac{d\mathbf{u}}{dt} + \frac{1}{\varepsilon}L\mathbf{u} + \mathcal{N}(\mathbf{u}) = 0, \quad (1)$$

$$\mathbf{u}(t)|_{t=0} = \mathbf{u}^0. \quad (2)$$

where the linear operator L has pure imaginary eigenvalues, the nonlinear term $\mathcal{N}(\mathbf{u}, \mathbf{u})$ is of

polynomial type, the operator D encodes a form of dissipation, and ε is a small non-dimensional parameter. For notational simplicity, we let $\mathbf{u}(t)$ denote the spatial (vector-valued) function

$$\mathbf{u}(t, \cdot) = (u_1(t, \cdot), u_2(t, \cdot), \dots).$$

The operator $\varepsilon^{-1}L$ results in time oscillations on an order $\mathcal{O}(\varepsilon)$ time scale. As $\varepsilon \rightarrow 0$, the oscillations become more rapid, leading to time-scale separation. It is these fast oscillations that generally require small time steps if standard explicit numerical integrators are used in numerical approximations.

When $\varepsilon \rightarrow 0$, (1), we encounter the case of a fast-singular limit (infinite time-scale separation). As such we expect small scale oscillations will remain a part of the solution even when the nonlinearity even in the limit as $\varepsilon \rightarrow 0$ [1–3]. To take a closer look at the oscillatory structure embedded in the PDE we apply an exponential mapping to (1) to arrive at,

$$\mathbf{u}(t) = e^{-\frac{1}{\varepsilon}Lt} \mathbf{v}(t) \quad (3)$$

$$\frac{d\mathbf{v}}{dt}(t) + e^{\frac{1}{\varepsilon}Lt} \mathcal{N}(e^{-\frac{1}{\varepsilon}Lt} \mathbf{v}(t)) = 0, \quad (4)$$

$$\mathbf{v}(t)|_{t=0} = \mathbf{u}^0. \quad (5)$$

Comparing (1) with (3-4) shows that the mapping (3) removes the stiff linear term from the evolutionary equation. However, though the stiff linear term is gone, taking another derivative of (4), which we call the Modulation equation, shows that there will still be oscillations present.

Inspired by the mathematical structure of fast singular limits, we take a next step and introduce a fast-wave-average approximation into (3)-(5),

$$\mathbf{u}(t) \approx e^{-\frac{1}{\varepsilon}Lt} \bar{\mathbf{v}}(t) \quad (6)$$

$$\frac{d\bar{\mathbf{v}}}{dt}(t) + \frac{1}{\eta} \int_0^\eta e^{\frac{1}{\varepsilon}Ls} \mathcal{N}(e^{-\frac{1}{\varepsilon}Ls} \bar{\mathbf{v}}(t)) ds = 0 \quad (7)$$

$$\bar{\mathbf{v}}(t)|_{t=0} = \mathbf{u}^0. \quad (8)$$

Notice that the integral in (7) is over a parameter s , which only appears in the nonlinear combination of the exponential operators, not in the solution itself.

Much is understood about (6-8) when $\epsilon \rightarrow 0$, but in some real-world applications the dynamics is not in the asymptotic limit, for example Earth's rotation rate does not go to infinity. And even in applications where ϵ is small enough to be considered within the asymptotic limit, it may not remain so as the solution evolves. This is because small nondimensional parameters are constructed using characteristic velocity, length, and time scales that change as solutions evolve. As a consequence we must take into account the finiteness of ϵ when studying the fluid dynamics that develops from equations of the form (1). A additional benefit would be to try and use what we learn from studies of finite ϵ when we consider time-descretizations.

In this talk I will discuss the relationships between the three equation sets above. I will give examples, including a real-world example of layer formation in the Arctic Ocean, and discuss a numerical approximation of (6-7) ([4] [5]) used to prove convergence of the parareal method ([6]). For quadratic nonlinearity this will involve ordered sequences of near-resonant sets.

References

- [1] N. BOGOLIUBOV AND Y. MITROPOLSKY, *Asymptotic Methods in the Theory of Nonlinear Oscillations*, Gordon and Breach, New York, 1961.
- [2] S. KLAINERMAN AND A. J. MAJDA, *Singular limits of quasilinear hyperbolic systems with large parameters and the incompressible limit of compressible fluids*, Communications in Pure and Applied Mathematics, 34 (1981), pp. 481–524.
- [3] S. SCHOCHET, *Fast singular limits of hyperbolic pdes*, Journal of Differential Equations, 114 (1994), pp. 476–512.
- [4] T. S. HAUT AND B. A. WINGATE, *An asymptotic parallel-in-time method for highly oscillatory pdes*, SIAM Journal on Scientific Computing, 36 (2014), pp. A693–A713.
- [5] A. G. PEDDLE AND T. S. HAUT AND B. A. WINGATE, *parareal Convergence for Oscillatory PDEs with Finite Time-Scale Separation*, In Press SIAM Journal on Scientific Computing (2019).
- [6] J. LIONS, Y. MADAY, AND G. TURINICI, *A "parareal" in time discretization of pde's*, Comptes Rendus de l'Academie des Sciences Series I Mathematics, 332 (2001), pp. 661–668.

Unified error analysis for certain full discretizations of wave-type problems

Marlis Hochbruck^{1,*}, Jonas Köhler¹¹Institute for Applied and Numerical Mathematics, Karlsruhe Institute of Technology, Germany

*Email: marlis.hochbruck@kit.edu

Abstract

We consider the full discretization of a class of linear wave-type problems in first order formulation, such as Maxwell's equations, the acoustic wave equation or the advection equation. In order to achieve this full discretization we use a method of lines approach, where we first discretize in space via the discontinuous Galerkin (dG) method. Subsequently, we use one of four schemes for time integration:

- the Crank–Nicolson scheme,
- the leapfrog scheme,
- a locally implicit scheme,
- the Peaceman–Rachford scheme.

In this paper we investigate the resulting fully discrete schemes. We show their stability (subject to an appropriate CFL condition where necessary) and error bounds that are optimal in space and time and robust under mesh refinement. These bounds are derived within a unified error analysis based on the fact that all schemes can be interpreted as perturbations of the Crank–Nicolson scheme.

1 Introduction

Let $\Omega \subset \mathbb{R}^d$ be a bounded domain and T be a finite time. We consider linear wave-type problems of the form

$$\begin{aligned} Mu' &= \mathcal{L}u + f, & (0, T) \times \Omega, \\ u(0) &= u^0, & \Omega. \end{aligned} \quad (1)$$

Here, \mathcal{L} is a first-order differential operator (also called Friedrichs' operator) given by

$$\mathcal{L}u = \sum_{i=1}^d L_i \partial_i u + L_0,$$

with $L_0 \in \mathbb{R}^{d \times d}$ such that $L_0 + L_0^T$ is negative semidefinite and symmetric $L_1, \dots, L_d \in \mathbb{R}^{d \times d}$. Further, $f \in L^2(\Omega)^d$ is a source term and $M \in L^\infty(\Omega)^{d \times d}$ is a symmetric positive definite material tensor.

Wellposedness of (1) in suitable function spaces can be shown under assumptions on the data [1, 6]. More general operators, where the coefficients are matrix-valued functions that possess certain regularity and positivity assumptions can be considered as well. However, for the sake of presentation, we restrict ourselves to the constant coefficient case and refer the reader to [1, 6] for more general problems.

2 Spatial discretization

Discretizing the wave-type problem (1) in space using a dG method with central fluxes [2] yields the semidiscrete problem

$$\begin{aligned} \mathbf{u}' &= \mathcal{L}\mathbf{u} + \mathbf{f}, & (0, T), \\ \mathbf{u}(0) &= \mathbf{u}^0, \end{aligned} \quad (2)$$

where \mathcal{L} is the discrete version of $M^{-1}\mathcal{L}$, $\mathbf{f} = \pi_h M^{-1}f$, and $\mathbf{u}^0 = \pi_h u^0$. Here, π_h denotes the L^2 -orthogonal projection onto the approximation space of the dG method.

3 Time integration

To obtain a fully discrete scheme, we consider the four different time integration schemes mentioned above. All four schemes are of classical order two and we will show that this order is retained in the stiff case.

Given a time stepsize τ we approximate the solution at times $t_n = n\tau$, i.e., $\mathbf{u}^n \approx \mathbf{u}(t_n)$. In what follows we abbreviate $\mathbf{f}^n = \mathbf{f}(t_n)$.

Crank–Nicolson scheme. Applying the Crank–Nicolson scheme to (2) yields the recursion

$$\mathbf{u}^{n+1} - \mathbf{u}^n = \frac{\tau}{2} \mathcal{L}(\mathbf{u}^{n+1} + \mathbf{u}^n) + \tau \bar{\mathbf{f}}^{n+1/2},$$

with $\bar{\mathbf{f}}^{n+1/2} = \frac{1}{2}(\mathbf{f}^{n+1} + \mathbf{f}^n)$. It is well known, that the Crank–Nicolson scheme is unconditionally stable.

Leapfrog or Verlet scheme. To apply the leapfrog scheme we need that (1), (2) exhibit a two field structure of the form

$$\mathbf{u} = \begin{pmatrix} \mathbf{p} \\ \mathbf{q} \end{pmatrix}, \quad \mathbf{f} = \begin{pmatrix} \mathbf{f}_p \\ \mathbf{0} \end{pmatrix}, \quad \mathcal{L} = \begin{pmatrix} 0 & \mathcal{L}_q \\ \mathcal{L}_p & 0 \end{pmatrix}. \quad (3)$$

Then, the leapfrog scheme applied to (2) is given by

$$\begin{aligned} \mathbf{q}^{n+1/2} - \mathbf{q}^n &= \frac{\tau}{2} \mathcal{L}_p \mathbf{p}^n, \\ \mathbf{p}^{n+1} - \mathbf{p}^n &= \tau \mathcal{L}_q \mathbf{q}^{n+1/2} + \tau \bar{\mathbf{f}}_p^{n+1/2}, \\ \mathbf{q}^{n+1} - \mathbf{q}^{n+1/2} &= \frac{\tau}{2} \mathcal{L}_p \mathbf{p}^{n+1}, \end{aligned}$$

with $\bar{\mathbf{f}}_p^{n+1/2} = \frac{1}{2}(\mathbf{f}_p^{n+1} + \mathbf{f}_p^n)$. The leapfrog scheme is stable under the CFL condition

$$\tau \leq C\theta h_{\min}, \quad \theta \in (0, 1),$$

where h_{\min} is the smallest mesh width of the spatial grid [9].

Locally implicit scheme. Next, we consider a locally implicit scheme [5, 10] that combines the implicit Crank–Nicolson and the explicit leapfrog scheme. Hence, we again assume the two-field structure (3). The locally implicit scheme reads

$$\begin{aligned} \mathbf{q}^{n+1/2} - \mathbf{q}^n &= \frac{\tau}{2} \mathcal{L}_p \mathbf{p}^n, \\ \mathbf{p}^{n+1} - \mathbf{p}^n &= \frac{\tau}{2} \mathcal{L}_q^i (\mathbf{q}^{n+1} + \mathbf{q}^n) \\ &\quad + \tau \mathcal{L}_q^e \mathbf{q}^{n+1/2} + \tau \bar{\mathbf{f}}_p^{n+1/2}, \\ \mathbf{q}^{n+1} - \mathbf{q}^{n+1/2} &= \frac{\tau}{2} \mathcal{L}_p \mathbf{p}^{n+1}, \end{aligned}$$

where $\mathcal{L}_q = \mathcal{L}_q^e + \mathcal{L}_q^i$ is split into an explicit and an implicit part in a suitable way, cf. [5, 9] for details. In particular, for $\mathcal{L}_q^e = 0$, we obtain the Crank–Nicolson scheme and for $\mathcal{L}_q^i = 0$, we obtain the leapfrog scheme. One can show that the scheme is stable under the CFL condition

$$\tau \leq C\theta h_{\min}^e, \quad \theta \in (0, 1),$$

where h_{\min}^e is the smallest mesh width of the explicitly treated part of the spatial grid [5, 9].

Peaceman–Rachford scheme. This is a splitting scheme, which is why we split $\mathcal{L} = \mathcal{A} + \mathcal{B}$. This splitting can, e.g., be a directional splitting leading to an ADI scheme [7, 8, 11]. The Peaceman–Rachford scheme is then given by

$$\begin{aligned} (I - \frac{\tau}{2} \mathcal{A})(I - \frac{\tau}{2} \mathcal{B})u^{n+1} \\ = (I + \frac{\tau}{2} \mathcal{A})(I + \frac{\tau}{2} \mathcal{B})u^n + \tau \bar{\mathbf{f}}_q^{n+1/2}. \end{aligned}$$

As for the Crank–Nicolson scheme, one can show that the Peaceman–Rachford scheme is unconditionally stable [3, 4].

Unified representation

Our analysis is based on the observation that we can represent all four schemes as perturbations of the Crank–Nicolson scheme. Namely, by introducing the operators

$$\mathcal{R}_{\pm} = \mathcal{I} \pm \frac{\tau}{2} \mathcal{L} + \frac{\tau^2}{4} \mathcal{D},$$

we can write all four schemes as

$$\mathcal{R}_- \mathbf{u}^{n+1} = \mathcal{R}_+ \mathbf{u}^n + \tau \bar{\mathbf{f}}_q^{n+1/2} \quad (4)$$

with different choices of \mathcal{D} for each scheme:

Crank–Nicolson: $\mathcal{D} = 0$.

Leapfrog: $\mathcal{D} = \begin{pmatrix} \mathcal{L}_q \mathcal{L}_p & 0 \\ 0 & 0 \end{pmatrix}$.

Locally implicit: $\mathcal{D} = \begin{pmatrix} \mathcal{L}_q^e \mathcal{L}_p & 0 \\ 0 & 0 \end{pmatrix}$.

Peaceman–Rachford: $\mathcal{D} = \mathcal{A}\mathcal{B}$.

4 Error analysis

To derive error bounds we consider the full discretization error

$$\begin{aligned} e^n = e_{\pi}^n + \mathbf{e}^n, \quad e_{\pi}^n = u(t_n) - \pi_h u(t_n), \\ \mathbf{e}^n = \pi_h u(t_n) - \mathbf{u}^n. \end{aligned}$$

Using standard interpolation bounds, it is easy to see that the projection error satisfies $\|e_{\pi}^n\| \leq C h^{k+1}$ with k being the polynomial degree used in the dG method. Here, $\|\cdot\|$ denotes a norm which is equivalent to the L^2 -norm. To bound the discretization error \mathbf{e}^n , we insert the projected exact solution $\pi_h u(t_n)$ into the numerical scheme (4). This yields the error recursion

$$\mathcal{R}_- \mathbf{e}^{n+1} = \mathcal{R}_+ \mathbf{e}^n + \tau d_{\pi}^n + \delta^n, \quad (5)$$

where the exact shape of the defects d_{π}^n and δ^n depends on the considered scheme. However, for all schemes, the projection defect satisfies $\|d_{\pi}^n\| \leq C h^k$ and it therefore only remains to bound the discretization defect δ^n .

For the Crank–Nicolson scheme, this defect corresponds to the quadrature error of the trapezoidal rule and can therefore be bounded by $\|\delta^n\| \leq C \tau^3$ if the exact solution is sufficiently smooth. Solving the error recursion (5) and using the stability of the Crank–Nicolson scheme then yields

$$\|\mathbf{e}^{n+1}\| \leq C(h^k + \tau^2). \quad (6)$$

The analysis of the leapfrog, locally implicit and Peaceman–Rachford scheme is more involved as additional perturbation terms arise stemming from the nonzero \mathcal{D} . However, we show that the above analysis can be adapted to deal with those additional terms, yielding equivalent error bounds to (6).

References

- [1] Burazin, K., Erceg, M., 2016. Non-stationary abstract Friedrichs systems. *Mediterr. J. Math.* **13**:6, 3777–3796.
- [2] Di Pietro, D. A., Ern, A., 2012. Mathematical aspects of discontinuous Galerkin methods. *Mathematics & Applications* **69**, Springer.
- [3] Faragó, I., Horváth, R., Schilders, W. H., 2005. Investigation of numerical time-integrations of Maxwell’s equations using the staggered grid spatial discretization. *Int. J. of Numer. Model. Electron. Netw. Dev. Fields* **18**:2, 149–169.
- [4] Hochbruck, M., Jahnke, T., Schnaubelt, R., 2015. Convergence of an ADI splitting for Maxwell’s equations. *Numer. Math.* **129**, 535–561.
- [5] Hochbruck, M., Sturm, A., 2016. Error analysis of a second-order locally implicit method for linear Maxwell’s equations. *SIAM J. Numer. Anal.* **54**:5, 3167–3191.
- [6] Köhler, J., 2019. The Peaceman–Rachford ADI-dG method for linear wave-type problems. PhD Thesis.
- [7] Namiki, T., 1999. A new FDTD algorithm based on alternating-direction implicit method. *IEEE Trans. Microwave Theory Tech.* **47**, 2003–2007.
- [8] Peaceman, D. W., Rachford, Jr., H. H., 1955. The numerical solution of parabolic and elliptic differential equations. *J. Soc. Indust. Appl. Math.* **3**, 28–41.
- [9] Sturm, A., 2017. Locally Implicit Time Integration for Linear Maxwell’s Equations. PhD Thesis.
- [10] Verwer, J. G., 2011. Component splitting for semi-discrete Maxwell equations. *BIT* **51**, 427–445.
- [11] Zhen, F., Chen, Z., Zhang, J., 2000. Toward the development of a three-dimensional unconditionally stable finite-difference time-domain method. *IEEE Trans. Microwave Theory Tech.* **48**, 1550–1558.

Crushed ice problem revisited

Andrii Khrabustovskyi^{1,*}, Olaf Post²¹Institute of Applied Mathematics, Graz University of Technology, Austria²Department IV - Mathematics, University of Trier, Germany

*Email: khrabustovskyi@math.tugraz.at

Abstract

We revisit one of the classical problems in homogenization theory – homogenization in a domain with a lot of tiny holes (also known as *crushed ice problem*). This problem concerns the Dirichlet Laplacian $\Delta_{\Omega_\varepsilon}$ on a perforated domain $\Omega_\varepsilon := \Omega \setminus (\cup_i D_{i\varepsilon})$, where $\Omega \subset \mathbb{R}^n$ and $\{D_{i\varepsilon}\}_i$ is a family of tiny identical holes distributed periodically with period ε . We denote by μ_ε the capacity of a single hole. It was known for a long time that $-\Delta_{\Omega_\varepsilon}$ converges to the operator $-\Delta_\Omega + q$ in strong resolvent sense provided the limit $q = \lim_{\varepsilon \rightarrow 0} \mu_\varepsilon \varepsilon^{-n}$ exists and is finite. In this talk we will discuss our recent improvements of this result. Namely, we show the norm resolvent convergence of the above operators and derive estimates in terms of operator norms. As an application, we establish the uniform convergence of the corresponding semigroups and convergence of spectra.

Keywords: domains with holes, Dirichlet Laplacian, homogenization, norm resolvent convergence, operator estimates

1 Introduction

Let $\Omega \subset \mathbb{R}^n$ be an open domain ($n \geq 2$) and $\{D_{i\varepsilon}\}_i$ be a family of small holes. The holes are identical (up to a rigid motion) and are distributed in Ω along the ε -periodic cubic lattice; more details will be given in Section 2. We set (see Figure 1)

$$\Omega_\varepsilon := \Omega \setminus \left(\bigcup_i D_{i\varepsilon} \right).$$

In Ω_ε we consider the problem

$$-\Delta_{\Omega_\varepsilon} u_\varepsilon + u_\varepsilon = f \upharpoonright_{\Omega_\varepsilon},$$

where $\Delta_{\Omega_\varepsilon}$ is the Dirichlet Laplacian in Ω_ε , $f \in L_2(\Omega)$ is a given function, $f \upharpoonright_{\Omega_\varepsilon}$ is the restriction of f to Ω_ε . The goal is to describe the behavior of the solution u_ε to this problem as $\varepsilon \rightarrow 0$.

In what follows we denote by μ_ε the capacity of $D_{i\varepsilon}$ (we recall its definition in Section 2).

One has the following celebrated result.

Theorem 1 *Let the limit*

$$q := \lim_{\varepsilon \rightarrow 0} \mu_\varepsilon \varepsilon^{-n}$$

exist and finite. Then for any $f \in L_2(\Omega)$

$$\|u_\varepsilon - u\|_{L_2(\Omega_\varepsilon)} \rightarrow 0 \text{ as } \varepsilon \rightarrow 0,$$

where u is the solution to the problem

$$-\Delta_\Omega u + qu + u = f.$$

This result was proven independently (and with quite different methods) by V.A. Marchenk and E.Ya. Khruslov [6, 7], J. Rauch and M. Taylor [11]¹, D. Cioranescu and F. Murat [3]. For more details we refer to monographs [1, 8, 12].

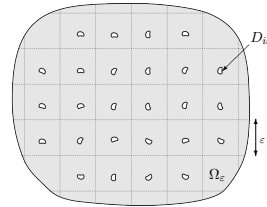


Figure 1: The domain Ω_ε .

On the language of operator theory Theorem 1 says that $-\Delta_{\Omega_\varepsilon}$ converges to $-\Delta_\Omega + q$ in a strong resolvent topology. Strictly speaking, we are not able to treat the classical resolvent convergence (since the underlying operators act in different Hilbert spaces), but we have its natural analogue for varying domains with $\Omega_\varepsilon \subset \Omega$: for any $f \in L_2(\Omega)$ one has

$$\lim_{\varepsilon \rightarrow 0} \|\mathcal{R}_\varepsilon J_\varepsilon f - J_\varepsilon \mathcal{R} f\|_{L_2(\Omega_\varepsilon)} = 0,$$

¹Strictly speaking for $q > 0$ J. Rauch and M. Taylor considered randomly distributed holes under assumptions resembling the case $q > 0$ in a deterministic case. The pioneer result in this direction was obtained by M. Kac in [4], who studied the case of uniformly distributed holes.

where $J_\varepsilon f := f|_{\Omega_\varepsilon}$ and

$$\mathcal{R}_\varepsilon := (-\Delta_{\Omega_\varepsilon} + \mathbf{I})^{-1}, \quad \mathcal{R} := (-\Delta_\Omega + (q+1)\mathbf{I})^{-1}.$$

In the talk we discuss the results of our recent paper [5], where we extend the above theorem by the proving *norm resolvent convergence with the estimate for its rate*. As a consequence of our main results, we establish uniform convergence of the corresponding semi-groups and convergence of spectra.

Let us stress that we do not assume that the domain Ω is bounded (except Theorem 6).

2 Main results

Let $n \geq 2$ and let $\Omega \subset \mathbb{R}^n$ be a domain with C^2 -boundary $\partial\Omega$ (also some mild additional assumptions on $\partial\Omega$ are required if Ω is unbounded).

We set $\square := (-1/2, 1/2)^n$.

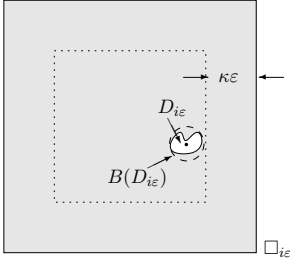


Figure 2: A scaled cells $\square_{i\varepsilon}$ and possible position of the obstacle $D_{i\varepsilon}$ (white). The smallest ball $B(D_{i\varepsilon})$ (dashed circle) containing the obstacle $D_{i\varepsilon}$ has security distance $\kappa\varepsilon$ from the boundary of $\square_{i\varepsilon}$, i.e., it should stay inside the dotted cube of side length $(1-2\kappa)\varepsilon$.

Now we describe a family of holes in Ω . Let D_ε be a Lipschitz domain in \mathbb{R}^n depending on a small parameter $\varepsilon > 0$. We denote by d_ε the radius of the smallest ball containing D_ε . It is assumed that

$$\begin{aligned} (d_\varepsilon)^{n-2} &\leq C\varepsilon^n & \text{as } n \geq 3, \\ |\ln d_\varepsilon|^{-1} &\leq C\varepsilon^2 & \text{as } n = 2 \end{aligned} \quad (1)$$

(hence, in particular, $d_\varepsilon = o(\varepsilon)$). For $i \in \mathbb{Z}^n$, let $D_{i\varepsilon}$ be a set enjoying the following properties (see Figure 2):

$$\begin{aligned} D_{i\varepsilon} &\text{ coincides with } D_\varepsilon \text{ up to a rigid motion,} \\ B(D_{i\varepsilon}) &\subset \square_{i\varepsilon} := \varepsilon(\square + i), \\ \text{dist}(B(D_{i\varepsilon}), \partial\square_{i\varepsilon}) &\geq \kappa\varepsilon \text{ for some } \kappa > 0, \end{aligned} \quad (2)$$

where $B(D_{i\varepsilon})$ is the smallest ball containing $D_{i\varepsilon}$ (the radius of this ball is d_ε).

Finally, we set (see Figure 1)

$$\Omega_\varepsilon := \Omega \setminus \left(\bigcup_{i \in \mathcal{I}_\varepsilon} \overline{D_{i\varepsilon}} \right),$$

where $\mathcal{I}_\varepsilon := \{i \in \mathbb{Z}^n : \square_{i\varepsilon} \subset \Omega\}$, i.e. the set of those indices for which the rescaled unit cell $\square_{i\varepsilon}$ is entirely in Ω .

By \mathcal{A}_ε we denote the Dirichlet Laplacian on Ω_ε , i.e. the operator acting in the Hilbert space $\mathcal{H}_\varepsilon := \mathbf{L}_2(\Omega_\varepsilon)$ associated with the closed densely defined positive sesquilinear form

$$\mathfrak{a}_\varepsilon[u, v] := \int_{\Omega_\varepsilon} \nabla u \cdot \nabla \bar{v} \, dx, \quad \text{dom}(\mathfrak{a}_\varepsilon) := \mathbf{H}_0^1(\Omega_\varepsilon).$$

Our goal is to describe the behaviour of the resolvent $(\mathcal{A}_\varepsilon + \mathbf{I})^{-1}$ as $\varepsilon \rightarrow 0$ under the assumption that the limit

$$q := \lim_{\varepsilon \rightarrow 0} \mu_\varepsilon \varepsilon^{-n}$$

exists and is finite; here μ_ε denotes the capacity of D_ε .

Recall that the capacity $\text{cap}(D)$ of the set $D \subset \mathbb{R}^n$ for $n \geq 3$ is defined via

$$\text{cap}(D) = \inf \int_{\mathbb{R}^n} |\nabla u(x)|^2 \, dx, \quad (3)$$

where the infimum is taken over $u \in C_0^\infty(\mathbb{R}^n)$ being equal to 1 on a neighbourhood of D . For $n = 2$ the right-hand-side of (3) is zero for an arbitrary domain D , hence we need a modified definition. It is as follows:

$$\text{cap}(D) = \inf \int_{B_1} |\nabla u(x)|^2 \, dx,$$

where B_1 is the unit ball concentric with $B(D)$ – the smallest ball containing D (here we assume that the set D is small enough so that $D \subset B(D) \subset B_1$), the infimum is taken over $u \in C_0^\infty(B_1)$ equal to 1 on a neighbourhood of D .

Finally, we introduce the limiting operator $\mathcal{A} = -\Delta_\Omega + q$. It acts in $\mathcal{H} := \mathbf{L}_2(\Omega)$ and is associated with the sesquilinear form

$$\begin{aligned} \mathfrak{a}[u, v] &:= \int_{\Omega} (\nabla u \cdot \nabla \bar{v} + qu\bar{v}) \, dx, \\ \text{dom}(\mathfrak{a}) &:= \mathbf{H}_0^1(\Omega). \end{aligned}$$

Now, we are in position to formulate the main result.

Theorem 2 *One has*

$$\|(\mathcal{A}_\varepsilon + \mathbf{I})^{-1} J_\varepsilon - J_\varepsilon (\mathcal{A} + \mathbf{I})^{-1}\|_{\mathcal{L}(\mathcal{H}, \mathcal{H}_\varepsilon)} \leq 4\delta_\varepsilon,$$

where δ_ε is defined by

$$\delta_\varepsilon = |\mu_\varepsilon \varepsilon^{-n} - q| + C_{\Omega, \kappa, \beta} \begin{cases} \varepsilon |\ln \varepsilon|, & n = 2, \\ \varepsilon, & n = 3 \\ \varepsilon^{1-\beta}, \beta > 0, & n = 4, \\ \max\{\varepsilon; d_\varepsilon \varepsilon^{-1}\}, & n \geq 5, \end{cases} \quad (4)$$

and the constant $C_{\Omega, \kappa, \beta}$ depends on the domain Ω , the relative distance κ of the obstacles from the period cell boundary (see (2)), and, in the case $n = 4$, on β .

Of course, the operator J_ε is not the only natural way to compare the resolvents of \mathcal{A}_ε and \mathcal{A} . Alternatively one can use $J'_\varepsilon: \mathcal{H}_\varepsilon \rightarrow \mathcal{H}$, which is the operator of extension by zero:

$$(J'_\varepsilon u)(x) = \begin{cases} u(x), & x \in \Omega_\varepsilon, \\ 0, & x \in \bigcup_{i \in \mathcal{I}_\varepsilon} D_{i\varepsilon}. \end{cases}$$

Theorem 3 *One has*

$$\|J'_\varepsilon (\mathcal{A}_\varepsilon + \mathbf{I})^{-1} - (\mathcal{A} + \mathbf{I})^{-1} J'_\varepsilon\|_{\mathcal{L}(\mathcal{H}_\varepsilon, \mathcal{H})} \leq 6\delta_\varepsilon,$$

where δ_ε is defined in (4). Moreover,

$$\begin{aligned} \|J'_\varepsilon (\mathcal{A}_\varepsilon + \mathbf{I})^{-1} J_\varepsilon - (\mathcal{A} + \mathbf{I})^{-1}\|_{\mathcal{L}(\mathcal{H}, \mathcal{H})} &\leq 9\delta_\varepsilon, \\ \|(\mathcal{A}_\varepsilon + \mathbf{I})^{-1} - J_\varepsilon (\mathcal{A} + \mathbf{I})^{-1} J'_\varepsilon\|_{\mathcal{L}(\mathcal{H}_\varepsilon, \mathcal{H}_\varepsilon)} &\leq 13\delta_\varepsilon. \end{aligned}$$

Remark 4 *Recently, using another methods, K. Cherednichenko, P. Dondl and F. Rösler [2] proved that*

$$\lim_{\varepsilon \rightarrow 0} \|J'_\varepsilon (\mathcal{A}_\varepsilon + \mathbf{I})^{-1} - (\mathcal{A} + \mathbf{I})^{-1} J'_\varepsilon\|_{\mathcal{L}(\mathcal{H}_\varepsilon, \mathcal{H})} = 0$$

(without the estimates for the rate of this convergence). The authors assumed that $D_{i\varepsilon}$ are balls distributed ε -periodically in Ω . For bounded Ω their proof resembles the variational approach developed in [3], for unbounded Ω they also utilize a rapid decay of the Green's function of $\mathcal{A} + \mathbf{I}$.

One important applications of the norm resolvent convergence is the uniform convergence of semi-groups generated by \mathcal{A}_ε and \mathcal{A} . Namely, we can approximate $\exp(-\mathcal{A}_\varepsilon t)$ in terms of simpler operators $\exp(-\mathcal{A}t)$, J_ε and J'_ε :

Theorem 5 *One has for each $t > 0$:*

$$\|\exp(-\mathcal{A}_\varepsilon t) - J_\varepsilon \exp(-\mathcal{A}t) J'_\varepsilon\|_{\mathcal{L}(\mathcal{H}_\varepsilon, \mathcal{H}_\varepsilon)} \leq c_t \delta_\varepsilon,$$

where δ_ε is defined in (4), and the constant c_t depends only on t .

Another important application is the convergence of spectra. In this note to simplify the presentation we formulate the result only for bounded domains Ω . In this case the operators \mathcal{A} and \mathcal{A} have discrete spectra; we denote by $\{\lambda_{k,\varepsilon}\}_{k \in \mathbb{N}}$ and $\{\lambda_k\}_{k \in \mathbb{N}}$ the sequences of the eigenvalues of \mathcal{A}_ε and \mathcal{A} , respectively, arranged in the ascending order and repeated according to their multiplicities.

Theorem 6 *For each $k \in \mathbb{N}$ one has*

$$\lim_{\varepsilon \rightarrow 0} \lambda_{k,\varepsilon} = \lambda_k, \quad (5)$$

moreover

$$|\lambda_{k,\varepsilon} - \lambda_k| \leq 4C_\varepsilon (\lambda_{k,\varepsilon} + 1)(\lambda_k + 1)\delta_\varepsilon, \quad (6)$$

where δ_ε is defined in (4), $|C_\varepsilon| \leq C$, $\lim_{\varepsilon \rightarrow 0} C_\varepsilon = 1$.

Our proofs are based on the abstract scheme for studying the convergence of operators in varying Hilbert spaces which was developed by O. Po in [9] and in more detail in the monograph [10]. The main ideas will be presented on the talk.

Acknowledgements

A.K. is supported by the Austrian Science Fund (FWF) under Project No. M 2310-N32.

References

- [1] A. Braides, *Γ -convergence for beginners*, Oxford University Press, Oxford, 2002, Oxford Lecture Series in Mathematics and its Applications, 22.
- [2] K. Cherednichenko, P. Dondl, F. Rösler, Norm-resolvent convergence in perforated domains, *Asymptot. Anal.* 110 (2018), 163–184.
- [3] D. Cioranescu and F. Murat, *Un terme étrange venu d'ailleurs*, Nonlinear partial differential equations and their applications. Collège de France Seminar, Vol. II (Paris, 1979/1980), Res. Notes in Math., vol. 60, Pitman, Boston, Mass.-London, 1982, pp. 98–138, 389–390.

- [4] M. Kac, *Probabilistic methods in some problems of scattering theory*, Rocky Mountain J. Math. **4** (1974), pp. 511–537.
- [5] A. Khrabustovskiy, O. Post, Operator estimates for the crushed ice problem, *Asymptot. Anal.* **110** (2018), pp. 137–161.
- [6] V. A. Marchenko and E. Y. Khruslov, *Boundary-value problems with fine-grained boundary*, Mat. Sb. (N.S.) **65 (107)** (1964), pp. 458–472.
- [7] V. A. Marchenko and E. Y. Khruslov, *Boundary value problems in domains with a fine-grained boundary* [in Russian], Izdat. “Naukova Dumka”, Kiev, 1974.
- [8] V. A. Marchenko and E. Y. Khruslov, *Homogenization of partial differential equations*, Birkhäuser Boston, Inc., Boston, MA, 2006.
- [9] O. Post, *Spectral convergence of quasi-one-dimensional spaces*, Ann. Henri Poincaré **7** (2006), 933–973.
- [10] O. Post, *Spectral analysis on graph-like spaces*, Lecture Notes in Mathematics, vol. 2039, Springer, Heidelberg, 2012.
- [11] J. Rauch and M. Taylor, *Potential and scattering theory on wildly perturbed domains*, J. Funct. Anal. **18** (1975), pp. 27–59.
- [12] B. Simon, *Functional integration and quantum physics*, Pure and Applied Mathematics, vol. 86, Academic Press Inc. [Harcourt Brace Jovanovich Publishers], New York, 1979.

Wave propagation in randomly perturbed waveguides

Josselin Garnier^{1,*}¹Centre de Mathématiques Appliquées, Ecole Polytechnique, Palaiseau, France

*Email: josselin.garnier@polytechnique.edu

Abstract

We consider wave propagation in randomly perturbed waveguides. The random perturbations may affect the index of refraction within the core of the waveguide or the core boundary. A separation of scales technique can be applied when the amplitude of the random perturbation is small, its correlation length is of the same order as the wavelength, and the propagation distance is large so that the net effect of the perturbations is of order one. The overall result is that the wavefield can be expanded on the complete basis of modes of the unperturbed waveguide and the complex mode amplitudes follow an effective Markovian dynamics that depends on the statistics of the random perturbations of the waveguide. In particular the analysis shows that wave intensity fluctuations can become very strong.

Keywords: waveguides, random media**1 Introduction**

We consider a two-dimensional waveguide with range axis denoted by $z \in \mathbb{R}$ and transverse coordinate denoted by $x \in \mathbb{R}$. This may model a dielectric slab waveguide for instance. A point-like source at a fixed position $(x, z) = (x_s, 0)$ transmits a time-harmonic signal. The wavefield $p(x, z)$ satisfies the Helmholtz equation:

$$[\Delta + k^2 n^2(x, z)]p(x, z) = \delta(z)\delta(x - x_s), \quad (1)$$

where $(x, z) \in \mathbb{R}^2$, $\Delta = \partial_x^2 + \partial_z^2$, k is the homogeneous wavenumber, and $n(x, z)$ is the index of refraction at position (x, z) .

When the waveguide is ideal (unperturbed), the index of refraction is range-independent:

$$n^{(0)}(x) = \begin{cases} n & \text{if } x \in (-d/2, d/2), \\ 1 & \text{otherwise,} \end{cases} \quad (2)$$

where $n > 1$ is the relative index of the core and $d > 0$ is its diameter.

We are interested in randomly perturbed waveguides. In this talk we address two types of random perturbations.

Type I perturbation: the index of refraction within the core region $x \in (-d/2, d/2)$ is randomly perturbed [5]:

$$n^{(\varepsilon)}(x, z) = \begin{cases} n + \varepsilon\nu(x, z) & \text{if } x \in (-d/2, d/2) \\ & \text{and } z \in (0, L^{(\varepsilon)}), \\ 1 & \text{otherwise.} \end{cases} \quad (3)$$

The fluctuations are modeled by the zero-mean, bounded, stationary in z random process $\nu(x, z)$ with smooth covariance function that satisfies strong mixing conditions in z . The typical amplitude of the fluctuations of index of refraction is assumed to be much smaller than 1 and it is modeled by the small and positive dimensionless parameter ε .

Type II perturbation: the boundaries of the core are randomly perturbed [6]:

$$n^{(\varepsilon)}(x, z) = \begin{cases} n & \text{if } x \in (\mathcal{D}_-^{(\varepsilon)}(z), \mathcal{D}_+^{(\varepsilon)}(z)) \\ & \text{and } z \in (0, L^{(\varepsilon)}), \\ 1 & \text{otherwise,} \end{cases} \quad (4)$$

where

$$\mathcal{D}_\pm^{(\varepsilon)}(z) = \pm d/2 \pm \varepsilon d\nu_\pm(z). \quad (5)$$

The fluctuations are modeled by the zero-mean, bounded, independent and identically distributed stationary random processes ν_+ and ν_- with smooth covariance function and mixing properties.

We study the wavefield at $z > 0$, satisfying

$$p \in \mathcal{C}^0((0, +\infty), H^2(\mathbb{R})) \cap \mathcal{C}^2((0, +\infty), L^2(\mathbb{R})),$$

and to set radiation conditions, we have assumed that the random fluctuations are supported in the range interval $(0, L^{(\varepsilon)})$. The net scattering effect of these fluctuations becomes of order one at range distances of order ε^{-2} , so we consider the interesting case $L^{(\varepsilon)} = L/\varepsilon^2$.

2 Effective Markovian dynamics

The overall result in the limit $\varepsilon \rightarrow 0$ is that the scalar wavefield $p(x, z)$ can be expanded on the complete basis of the unperturbed waveguide

(that contains guided modes, radiating modes and evanescent modes) and the complex mode amplitudes follow an effective Markovian dynamics. The infinitesimal generator of the effective Markov process depends on the unperturbed waveguide geometry and the two-point statistics of the random process ν (type I) or (ν_+, ν_-) (type II). The inspection of its form reveals different mode coupling mechanisms induced by scattering:

- 1) the coupling between guided modes gives rise to power exchange between the guided modes;
- 2) the coupling between guided and radiating modes gives rise to power leakage from the guided modes to the radiating ones (effective dissipation) and it adds frequency-dependent phases on the guided mode amplitudes (effective dispersion);
- 3) the coupling between guided and evanescent modes also adds frequency-dependent phases on the guided mode amplitudes (effective dispersion).

The effective Markovian description of the guided mode powers makes it possible to analyze their first- and second-order moments, which in turn gives a statistical description of the intensity distribution of the wavefield. In dramatic contrast with the situation in open random medium, the relative fluctuations of the intensity exponentially grow with the propagation distance in a randomly perturbed waveguide. The exponential growth rate can be identified as the difference of the first eigenvalues of two self-adjoint operators. When the effective dissipation is negligible, the exponential growth rate is zero and we recover the well-known equipartition result [4]: the energy becomes equipartitioned amongst the guided modes. When there is effective mode-dependent dissipation, the exponential growth rate is positive which may give rise to strong intensity fluctuations in such randomly perturbed waveguides.

3 Applications

We can discuss a few applications:

- 1) We address a directional coupler in integrated optics [1]. We consider a randomly perturbed system made of two parallel, single-mode waveguides. The goal is to quantify the transfer of power between the two waveguides in terms of their separation distance. The results show that, no matter how small the fluctuations of the interfaces are, they have significant effect at suf-

ficiently large distance of propagation, which manifests in two ways: The first effect consists of power leakage from the guided modes to the radiation ones. The second effect consists of blurring of the periodic transfer of power between the waveguides and the eventual equipartition of power.

- 2) We address a geoacoustic inverse problem in underwater acoustics [2]. The goal is to estimate the regional acoustic and geoacoustic shallow-water environment from data collected by a vertical hydrophone array and transmitted by distant time-harmonic point sources. We first show how to express the cross moments of the sound pressure in terms of the parameters to be estimated. We then show how the estimation problem can be formulated as a nonlinear inverse problem using this formulation, which can be solved by minimization of a misfit function or by a Bayesian approach. We apply this method to experimental data collected by the ALMA system (Acoustic Laboratory for Marine Applications) [3].

References

- [1] L. Borcea and J. Garnier, Wave propagation in randomly perturbed weakly coupled waveguides, arXiv:1812.01131.
- [2] L. Dumaz, J. Garnier, and G. Lepoutlier, Acoustic and geoacoustic inverse problems in randomly perturbed shallow-water environments, arXiv:1812.10141, to appear in *J. Acoust. Soc. Am.*
- [3] D. Fattaccioli, ALMA: A new experimental acoustic system to explore coastal and shallow waters, UACE 2015 Proceedings, Chania, Greece.
- [4] J.-P. Fouque, J. Garnier, G. Papanicolaou, and K. Sølna, *Wave Propagation and Time Reversal in Randomly Layered Media*, Springer, New York, 2007.
- [5] W. Kohler and G. Papanicolaou, *Wave Propagation in Randomly Inhomogeneous Ocean*, Lecture Notes in Physics, J. B. Keller and J. S. Papadakis, eds., Wave Propagation and Underwater Acoustics, Springer-Verlag, Berlin, 70, 1977.
- [6] D. Marcuse, *Theory of Dielectric Optical Waveguides*, Academic Press, New York, 1974.

Combining integral representations on infinite boundaries and complex scaling for time-harmonic scattering problems

Anne-Sophie Bonnet-Ben Dhia^{1,*}

¹POEMS (CNRS-INRIA-ENSTA Paristech), Palaiseau, France

*Email: anne-sophie.bonnet-bendhia@ensta-paristech.fr

Abstract

Nowadays integral methods or Perfectly Matched Layers allow to solve a large class of time-harmonic scattering problems in unbounded domains. But difficulties remain when the Green function is not available (or too expensive to compute) and when PML are not working (because of the presence of inverse modes). For several configurations of practical interest, a solution can be found by using integral representations on infinite boundaries, combined with complex scaling. The object of this presentation is to discuss some progress in this direction [1,5].

Keywords: scattering problems, integral representation, complex scaling, Fredholm theory

1 Motivations

Integral representations are commonly used in numerical methods when solving scattering problems in unbounded domains. In general, the integral is written on a bounded curve (in 2D) or surface (in 3D), typically the boundary of the scatterer or a boundary surrounding the scatterer. But for various reasons, one may have to consider integral representations on infinite boundaries. This arises for instance in stratified media, when one wants to avoid the heavy computation of the Green function of the stratified medium, by using integral representations written on the interfaces between two adjacent layers. But a difficulty comes from the slow decay of the scattered field at infinity, when truncating the boundary for numerical purposes [2].

Another motivation of the present work concerns scattering of elastic waves in anisotropic media. Such problems occur for instance in the context of ultrasonic non destructive testing of composite plates. The difficulty is that on one hand, the computation of the Green tensor is very expensive, and on the other hand, cartesian PML may fail [3]. In [4], we have developed a method which takes advantage of the fact that plane wave representations of the scattered field can be easily derived in half-spaces, based on a

partial Fourier transform. Imposing the compatibility of different representations written in overlapping half-spaces, one ends up with a system of integral equations, written on the infinite boundaries of four half-spaces surrounding the defect. This so-called Half-Space Matching method has been satisfactorily understood and analyzed in the dissipative case. But again, due to the slow decay of the scattered field at infinity, its validity in the non-dissipative case was still not clear, and the present work aims at clarifying this question.

For simplicity, the main ideas are presented below on the model case of a 2D Helmholtz equation: u denotes the outgoing solution of

$$\begin{aligned} \Delta u + k^2 u &= 0 && \text{in } \mathbb{R}^2 \setminus D \\ \frac{\partial u}{\partial \nu} &= -\frac{\partial u_{inc}}{\partial \nu} && \text{on } \partial D \end{aligned} \quad (1)$$

where $k \in \mathbb{R}$ is the wavenumber, D is a bounded obstacle and u_{inc} some incident wave.

2 Complex-scaled representations of Helmholtz solutions in half-planes

Suppose $D \subset \{|x_1| < a\} \cap \{|x_2| < a\}$ and let us focus on the half-space $\{x_1 > a\}$, where the solution u of (1) has the following representation:

$$u(x_1, x_2) = \int_{\mathbb{R}} K((x_1, x_2), (a, y_2)) u(a, y_2) dy_2$$

with a kernel related to the fundamental solution of the Helmholtz equation as follows:

$$\begin{aligned} K((x_1, x_2), (y_1, y_2)) &= \\ \frac{i}{2} \frac{\partial}{\partial y_1} (H_0^{(1)}(k \sqrt{(x_1 - y_1)^2 + (x_2 - y_2)^2})). \end{aligned}$$

Then, in the spirit of PML, thanks to the analyticity of $y_2 \mapsto K((x_1, x_2), (a, y_2)) u(a, y_2)$, we can deform the path of integration. More precisely we set for $b > 0$:

$$\mathcal{J}_\theta(y_2) = \begin{cases} y_2 & \text{for } |y_2| < b \\ \mp b + (y_2 \pm b) e^{i\theta} & \text{for } \pm y_2 > b \end{cases}$$

Then, since $u(a, y_2) \sim A^\pm \frac{e^{ik|y_2|}}{\sqrt{|y_2|}}$ when $|y_2| \rightarrow +\infty$, we can check that $\varphi_\theta(y_2) = u(a, \mathcal{J}_\theta(y_2))$ is

well-defined for $y_2 \in \mathbb{R}$ and exponentially decaying when $|y_2| \rightarrow +\infty$. The same result holds for the analytic extension of the Green function as soon as $(x_1 - a)^2 + (x_2 - \mathcal{J}_\theta(y_2))^2 \neq 0$. Summing up, we get the new representation of u :

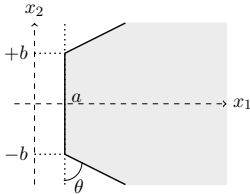
$$u(x_1, x_2) = \int_{\mathbb{R}} K_\theta(x_1, x_2, y_2) \varphi_\theta(y_2) dy_2 \quad (2)$$

whose kernel is now defined by

$$K_\theta(x_1, x_2, y_2) = K((x_1, x_2), (a, \mathcal{J}_\theta(y_2))) \mathcal{J}'_\theta(y_2)$$

Representation (2) holds in the domain

$$\{x_1 > a \text{ and } |x_2| < b + (x_1 - a) \cot \theta\}$$



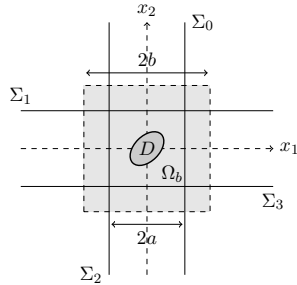
The advantage of the new formula is that now, the function to integrate is exponentially decaying, so that in practice, a truncation of the trace φ_θ will produce an exponentially small error. The price to pay is that the formula does not hold in the whole half-plane but only in the grey region.

3 Application to the complex-scaled Half-Space Matching method

Let us show now how these complex-scaled representations can be used to generalize the Half-Space Matching method of [4] to the non-dissipative problem (1). We first introduce 4 infinite straight lines Σ^j , $j = 0, 1, 2, 3$ as represented on the figure. Then the new idea is to consider as unknowns the complex-scaled traces of u on these lines, φ_θ^j , $j = 0, 1, 2, 3$. Then the equations linking the φ_θ^j are obtained as follows. Consider for instance the complex-scaled trace φ_θ^1 on the part of Σ_1 which is located at the right of Σ_0 . We can compute it by taking the analytic extension of (2) at the point $(\mathcal{J}_\theta(x_1), a)$. This gives a first equation linking φ_θ^0 and φ_θ^1 for $x_1 > a$:

$$\varphi_\theta^1(x_1) = \int_{\mathbb{R}} K_\theta(\mathcal{J}_\theta(x_1), a, y_2) \varphi_\theta^0(y_2) dy_2$$

Proceeding in the same way for all traces, we get 8 equations coupling all the φ_θ^j , which can be coupled to an equation for u in Ω_b where $\Omega_b = [-b, b]^2 \setminus D$ with $b > a$.



Thanks to the complex scaling, we can prove, with the same arguments as in the dissipative case [4], that the complete formulation is of Fredholm type in a standard functional framework where $\varphi_\theta^j \in L^2(\Sigma_j)$ and $u \in H^1(\Omega_b)$.

The next step consists in the conception of a similar method for anisotropic cases where cartesian PML do not work: in addition to previous ideas, a splitting of the traces has to be introduced, in order to handle differently the so-called direct and inverse waves.

References

- [1] A.-S. Bonnet-Ben Dhia, S. N. Chandler-Wilde, S. Fliss, C. Hazard, K.-M. Perfekt and Y. Tjandrawidjaja, The Halfspace Matching Method for Real Wavenumber, in preparation.
- [2] O. P. Bruno and C. Pérez-Arancibia, Windowed Green Function method for the Helmholtz equation in presence of multiply layered media, *PRSA*, **473** (2017).
- [3] E. Bécache, S. Fauqueux and P. Joly, Stability of perfectly matched layers, group velocities and anisotropic waves, *JCP*, **188** (2003), pp. 399–433.
- [4] A.-S. Bonnet-BenDhia, S. Fliss and A. Tonnoir, The Halfspace Matching Method: a New Method to Solve Scattering Problems in Infinite Media, *JCAM*, **338** (2018), pp. 44–68.
- [5] W. Lu, Y. Y. Lu, and J. Qian, Perfectly-Matched-Layer boundary integral equation method for wave scattering in a layered medium, *SIAM J. Appl. Math.*, **78** (2018), pp. 246–265.

Boundary element methods for scattering by fractal screens

Simon N. Chandler-Wilde¹, David P. Hewett², Andrea Moiola^{3,*}¹Department of Mathematics and Statistics, University of Reading, Reading, UK²Department of Mathematics, University College London, London, UK³Dipartimento di Matematica, Università degli Studi di Pavia, Pavia, Italy

*Email: andrea.moiola@unipv.it

Abstract

The scattering of time-harmonic acoustic waves by sound-soft (Dirichlet) screens, or cracks, its modeling via boundary integral equations (BIE) and discretisation with the boundary element method (BEM) are classical topics when the screens are sufficiently smooth. We extend the theory to include screens that are fractal or have fractal boundaries, such as the Sierpinski triangle, the Cantor dust and the Koch snowflake. Building on previous work on Sobolev spaces [1, 3] and BIE [2] we present well-posed BVPs for open and compact flat screens. We give conditions under which these problems can be approximated by similar ones on smoother “pre-fractal” sets, and results on the convergence of the associated BEM. Details, extensions, proofs and numerical experiments can be found in [4].

Keywords: Helmholtz equation, boundary element method, scattering, screen, sound-soft, fractal, non-Lipschitz set, Mosco convergence

1 Notation and Sobolev spaces

We consider a flat screen Γ that is a bounded subset of the plane $\Gamma_\infty := \mathbb{R}^2 \times \{0\} \subset \mathbb{R}^3$. (The case of 2-dimensional wave propagation $\Gamma \subset \mathbb{R} \times \{0\} \subset \mathbb{R}^2$ can easily be treated in the same way.)

We use fractional (Bessel) Sobolev spaces. For $s \in \mathbb{R}$, $\Omega \subset \mathbb{R}^2$ open and $F \subset \mathbb{R}^2$ closed, let

$$\begin{aligned} H^s(\mathbb{R}^2) &:= \{u \in \mathcal{S}'(\mathbb{R}^2) : \|u\|_{H^s(\mathbb{R}^2)} < \infty\} \\ \|u\|_{H^s(\mathbb{R}^2)}^2 &:= \int_{\mathbb{R}^2} (1 + |\xi|^2)^s |\hat{u}(\xi)|^2 d\xi, \\ H^s(\Omega) &:= \{u|_\Omega : u \in H^s(\mathbb{R}^2)\}, \\ \tilde{H}^s(\Omega) &:= \overline{C_0^\infty(\Omega)}^{H^s(\mathbb{R}^2)}, \\ H_P^s &:= \{u \in H^s(\mathbb{R}^2) : \text{supp } u \subset F\}. \end{aligned}$$

In general $\tilde{H}^s(\Omega) \subset H_\Omega^s$; they coincide if Ω is sufficiently regular but examples with $\tilde{H}^s(\Omega) \neq H_\Omega^s$ can be constructed [3, Thm. 3.19]. We denote γ^\pm the traces $\gamma^\pm : W^1(\mathbb{R}_\pm^3) \rightarrow H^{1/2}(\Gamma_\infty)$, where \mathbb{R}_\pm^3 are the upper and lower half-spaces.

2 Boundary value problems (BVP)

The classical sound-soft screen scattering BVP consists of looking for u satisfying the Helmholtz equation (1), the Sommerfeld condition (2) and the Dirichlet boundary condition (3):

$$\Delta u + k^2 u = 0 \quad \text{in } D := \mathbb{R}^3 \setminus \bar{\Gamma}, \quad (1)$$

$$\partial_r u(\mathbf{x}) - ik u(\mathbf{x}) = o(r^{-1}) \quad r := |\mathbf{x}| \rightarrow \infty, \quad (2)$$

$$u = -u^i \quad \text{on } \Gamma, \quad (3)$$

where $k > 0$ is the wavenumber and u^i is a given incident wave. To formulate a well-posed BVP, one needs to be more precise about the sense in which the boundary condition (3) holds.

We first describe the case when Γ is a relatively open subset of Γ_∞ .

Definition 1 (BVP $\mathcal{D}^{op}(\Gamma)$) *Let $\Gamma \subset \Gamma_\infty$ be bounded and open and $g \in H^{1/2}(\Gamma)$. Find $u \in C^2(D) \cap W^{1,loc}(D)$ satisfying (1)–(2) and*

$$(\gamma^\pm u)|_\Gamma = g.$$

Theorem 2 (Thm. 6.2 [2]) *If $\tilde{H}^{-1/2}(\Gamma) = H_\Gamma^{-1/2}$, then $\mathcal{D}^{op}(\Gamma)$ admits a unique solution u .*

Moreover, u satisfies the representation formula $u(\mathbf{x}) = -S_\Gamma \phi(\mathbf{x})$, $\mathbf{x} \in D$, where S_Γ is the single-layer potential and $\phi = [\partial_n u] := \partial_n^+ u - \partial_n^- u \in \tilde{H}^{-1/2}(\Gamma)$ is the unique solution of the BIE $S_\Gamma \phi = -g$, with $S_\Gamma : \tilde{H}^{-1/2}(\Gamma) \rightarrow H^{1/2}(\Gamma)$ the single-layer operator.

The main assumption for the well-posedness of the BVP is $\tilde{H}^{-1/2}(\Gamma) = H_\Gamma^{-1/2}$, equivalent to the density of $C_0^\infty(\Gamma)$ in $H_\Gamma^{-1/2}$. This is guaranteed if, e.g., (i) Γ is C^0 up to countably many points $P \subset \partial\Gamma$ such that P has only finitely many limit points [3, Thm. 3.24], or (ii) Γ is “thick” in the sense of Triebel [1]. All Lipschitz Γ , but also classical and exotic snowflakes with fractal boundaries, satisfy these conditions [1].

If the screen Γ is a compact set, we substitute the restriction operator $|_\Gamma$ in the boundary conditions with the orthogonal projection $P_\Gamma : H^{1/2}(\mathbb{R}^2) \rightarrow (\tilde{H}^{1/2}(\Gamma^c))^\perp$, where $\Gamma^c = \mathbb{R}^2 \setminus \Gamma$.

Definition 3 (BVP $D^{co}(\Gamma)$) Let $\Gamma \subset \Gamma_\infty$ be compact and $g \in (\tilde{H}^{-1/2}(\Gamma^c))^\perp$. Find $u \in C^2(D) \cap W^{1,loc}(D)$ satisfying (1)–(2) and

$$P_\Gamma \gamma^\pm u = g.$$

This choice of P_Γ ensures that if $\Omega \subset \Gamma_\infty$ is bounded, open, and $\tilde{H}^{-1/2}(\Omega) = H_\Omega^{-1/2}$, then the problems $D^{op}(\Omega)$ and $D^{co}(\bar{\Omega})$ are equivalent.

Theorem 4 (Thm. 6.4 [2]) Problem $D^{co}(\Gamma)$ admits a unique solution u .

Moreover, u satisfies the representation formula $u(\mathbf{x}) = -S_\Gamma \phi(\mathbf{x})$, $\mathbf{x} \in D$, with $\phi = [\partial_n u]$ the solution of the BIE $S_\Gamma \phi = -g$ for the single-layer operator $S_\Gamma : H_\Gamma^{-1/2} \rightarrow (\tilde{H}^{-1/2}(\Gamma^c))^\perp$.

3 Prefractal to fractal convergence

To study the scattering by a fractal screen Γ , we approximate it with simpler prefractal shapes $(\Gamma_j)_{j \in \mathbb{N}}$. The BVP $D^x(\Gamma)$ ($x \in \{op, co\}$) is correctly approximated by a sequence of BVPs $D^x(\Gamma_j)$ if the corresponding sequence of subspaces (either $\tilde{H}^{-1/2}(\Gamma_j)$ or $H_\Gamma^{-1/2}$) of $H^{-1/2}(\mathbb{R}^2)$ converges in the sense of Mosco [4]. In [4] we show:

Theorem 5 The solution ϕ_j of the BIE on Γ_j converges in $H^{-1/2}(\mathbb{R}^2)$ to the solution ϕ of the BIE on Γ and $S\phi_j \rightarrow S\phi$ in $W^{1,loc}(\mathbb{R}^2)$ if, e.g.,

- Γ and Γ_j are bounded, open with $\Gamma_j \subset \Gamma_{j+1}$ and $\Gamma = \bigcup_{j \in \mathbb{N}} \Gamma_j$, or
- Γ_j are compact, $\Gamma_j \supset \Gamma_{j+1}$ and $\Gamma = \bigcap_{j \in \mathbb{N}} \Gamma_j$.

We also show convergence for a class of non-nested prefractals such as those in Figure 1.



Figure 1: Non-nested prefractals Γ_j for the square snowflake Γ , for which $\phi_j \rightarrow \phi$ in $H^{-1/2}$.

4 BEM discretisation

We approximate the solution of scattering problems posed on a non-Lipschitz screen Γ (fractal or with fractal boundary) using a piecewise-constant boundary element methods (BEM) on prefractal screens Γ_j . In [4] we give general criteria on the mesh to guarantee convergence of the Galerkin BEM: the key is the Mosco convergence of the discrete spaces on Γ_j to the desired Sobolev space, either $\tilde{H}^{-1/2}(\Gamma)$ or $H_\Gamma^{-1/2}$.

E.g., if Γ_j are the classical prefractal approximations of the Koch snowflake, or the square snowflake prefractals of Figure 1, then any sequence of meshes \mathcal{T}_j on Γ_j with meshsize $h_j \searrow 0$ provides a provably convergent BEM scheme.

If Γ is a Cantor dust (the Cartesian product of two identical Cantor sets) then its scattered field is non-zero (for almost every incident plane waves) if and only if the Hausdorff dimension of Γ is larger than 1, [2]. We verify this numerically in Figure 2. For details and more extensive numerical tests, see [4].

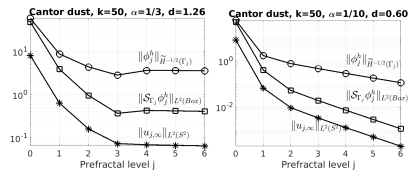


Figure 2: On-screen (o), near-field (□) and far-field (*) norms of the field scattered by Cantor dust prefractals $\Gamma_0, \dots, \Gamma_6$ computed with BEM. When the prefractal level is refined, for Hausdorff dimension $d = \frac{\log 4}{\log 3} > 1$ (left) the norms provably converge to a positive value, while for $d = \frac{\log 4}{\log 10} < 1$ (right) they converge to 0.

References

- [1] A. Caetano, D. P. Hewett and A. Moiola, Density results for Sobolev, Besov and Triebel-Lizorkin spaces on rough sets, arXiv:1904.05420, 2019.
- [2] S. N. Chandler-Wilde and D. P. Hewett, Well-posed PDE and integral equation formulations for scattering by fractal screens, *SIAM J. Math. Anal.*, **50** (2018), pp. 677–717.
- [3] S. N. Chandler-Wilde, D. P. Hewett and A. Moiola, Sobolev spaces on non-Lipschitz subsets of \mathbb{R}^n with application to boundary integral equations on fractal screens, *Integr. Equat. Operat. Th.*, **87** (2017), pp. 179–224.
- [4] S. N. Chandler-Wilde, D. P. Hewett and A. Moiola, Boundary element methods for acoustic scattering by fractal screens, *in preparation*.

Acoustic scattering by impedance screens with fractal boundary

Joshua Bannister¹, David P. Hewett^{1,*}¹Department of Mathematics, University College London, London, UK

*Email: d.hewett@ucl.ac.uk

Abstract

We present a well-posedness analysis of boundary value problem and boundary integral equation formulations for acoustic scattering by planar screens/cracks on which impedance boundary conditions are imposed. In contrast to previous works, our analysis is valid for screens with arbitrarily rough (possibly fractal) boundary.

Keywords: Boundary integral equations, Sobolev spaces, screen problems, Mosco convergence

The scattering of time-harmonic acoustic waves by thin “screens” or “cracks” is important in many applications, including noise barrier design and defect detection in non-destructive testing. To model the case where the screen acts as an absorber of wave energy one formulates the scattering problem as an impedance boundary value problem (BVP), which itself can be reformulated as a boundary integral equation (BIE) on the screen. Previous studies [1,2] establish well-posedness of such formulations when the boundary of the screen is smooth (in an unspecified sense). In this study we clarify the smoothness assumptions required for the analysis of [1,2] to be valid, and show how the addition of extra conditions in the BVP, along with a simple modification of the functional setting for the BIE, produce formulations which are well-posed for completely arbitrary bounded open planar screens, as was done previously for Dirichlet and Neumann screen problems in [3].

In order to focus attention on the regularity of the screen boundary, we simplify the problem as much as possible by restricting attention to a planar screen Γ , assumed to be a bounded open subset of the hyperplane $\mathbb{R}^{n-1} \times \{0\} \subset \mathbb{R}^n$, $n = 2, 3$. For $s \in \mathbb{R}$ let $H^s(\mathbb{R}^{n-1})$ be the standard Bessel potential Sobolev space on \mathbb{R}^{n-1} , normed by $\|u\|_{H^s(\mathbb{R}^{n-1})}^2 = \int_{\mathbb{R}^{n-1}} (1 + |\xi|^2)^s |\hat{u}(\xi)|^2 d\xi$, and for open $\Gamma \subset \mathbb{R}^{n-1}$ and closed $F \subset \mathbb{R}^{n-1}$ let

$$\tilde{H}^s(\Gamma) := \overline{C_0^\infty(\Gamma)}^{H^s(\mathbb{R}^{n-1})},$$

$$H_F^s := \{u \in H^s(\mathbb{R}^{n-1}) : \text{supp } u \subset F\},$$

and

$$H^\pm(\Gamma) = \{u|_\Gamma : u \in H^s(\mathbb{R}^{n-1})\},$$

$|_\Gamma$ denoting (distributional) restriction to Γ .

Given $k > 0$ and an incident field u^i (e.g. a plane wave $u^i = e^{ikd \cdot x}$), the standard BVP for the scattered field is [2]: find $u \in C^2(\mathbb{R}^n \setminus \bar{\Gamma}) \cap W^{1,\text{loc}}(\mathbb{R}^n \setminus \bar{\Gamma})$, outgoing at infinity, s.t.

$$(\Delta + k^2)u = 0, \quad \text{in } \mathbb{R}^n \setminus \bar{\Gamma}, \quad (1)$$

$$\partial_n^\pm u|_\Gamma \pm \lambda^\pm \gamma^\pm u|_\Gamma = g^\pm, \quad (2)$$

where γ^\pm and ∂_n^\pm are the Dirichlet and Neumann traces from the half spaces $\{\pm x_n > 0\}$ to the hyperplane \mathbb{R}^{n-1} , λ^\pm are impedance parameters (constants with $\Im \lambda^\pm \geq 0$ and $\lambda^+ + \lambda^- \neq 0$) and $g^\pm = -(\partial_n^\pm u^i|_\Gamma \pm \lambda^\pm \gamma^\pm u^i|_\Gamma) \in H^{-1/2}(\Gamma)$.

Theorem 1 *Let $g^+ - g^- \in \tilde{H}^{-1/2}(\Gamma)|_\Gamma$. The BVP (1)-(2) is well-posed if $\tilde{H}^{\pm 1/2}(\Gamma) = H_\mp^{\pm 1/2}$ and $H_{\partial\Omega}^{\pm 1/2} = \{0\}$. In particular, these conditions hold when Γ is “ C^0 except at a countable set of points with finitely many limit points” [4].*

The proof of Theorem 1 follows the approach in [2]. We first prove BVP uniqueness by a standard Rellich/unique continuation argument, then that the BVP solution (if it exists) is given by

$$u = \mathcal{D}\phi - \mathcal{S}\psi,$$

where \mathcal{D} and \mathcal{S} are the usual double- and single-layer potentials and $\phi := [u] \in H_\Gamma^{1/2} = \tilde{H}^{1/2}(\Gamma)$ and $\psi := [\partial_n u] \in H_\Gamma^{-1/2} = \tilde{H}^{-1/2}(\Gamma)$ are the Dirichlet and Neumann jumps, which must satisfy the BIE

$$A \begin{pmatrix} \phi \\ \psi \end{pmatrix} = \begin{pmatrix} \lambda^- g^+ + \lambda^+ g^- \\ g^+ - g^- \end{pmatrix},$$

where

$$A = \begin{pmatrix} \lambda^+ \lambda^- |_\Gamma + (\lambda^+ + \lambda^-)T & -\frac{1}{2}(\lambda^+ - \lambda^-)|_\Gamma \\ \frac{1}{2}(\lambda^+ - \lambda^-)|_\Gamma & |_\Gamma - (\lambda^+ + \lambda^-) \end{pmatrix};$$

with $S : \tilde{H}^{-1/2}(\Gamma) \rightarrow H^{1/2}(\Gamma)$ and $T : \tilde{H}^{1/2}(\Gamma) \rightarrow H^{-1/2}(\Gamma)$ denoting the usual single layer and hypersingular operators. (Note: the double layer contributions in [2] vanish when Γ is planar.)

Viewing A as an operator

$$A : \tilde{H}^{1/2}(\Gamma) \times \tilde{H}^{-1/2}(\Gamma) \rightarrow H^{-1/2}(\Gamma) \times \tilde{H}^{-1/2}(\Gamma)|_{\Gamma},$$

the assumptions of Theorem 1 guarantee that $|\Gamma : \tilde{H}^{-1/2}(\Gamma) \rightarrow H^{-1/2}(\Gamma)$ is injective, implying that A is Fredholm of index zero, so that well-posedness follows from BVP uniqueness.

But for general open Γ the above analysis can fail. In particular, the spaces $\tilde{H}^{\pm 1/2}(\Gamma)$ and $H_{\Gamma}^{\pm 1/2}$ may differ, the space $H_{\partial\Gamma}^{-1/2}$ may be non-trivial (which holds if the Hausdorff dimension of $\partial\Gamma$ exceeds $n - 2$), and $|\Gamma : \tilde{H}^{-1/2}(\Gamma) \rightarrow H^{-1/2}(\Gamma)$ may have a nontrivial kernel [4].

Our proposed remedy is to demand a little extra smoothness, namely that $g^+ - g^- \in H^0(\Gamma) \cong L^2(\Gamma)$, and supplement (1)-(2) with two additional conditions, namely

$$[u] \in \tilde{H}^{1/2}(\Gamma), \quad (3)$$

$$[\partial_n u] \in \tilde{H}^0(\Gamma) \cong L^2(\Gamma). \quad (4)$$

It is easily checked that, when the assumptions of Theorem 1 hold, the extra assumptions (3)-(4) are superfluous, i.e. they hold automatically.

Theorem 2 *Let $g^+ - g^- \in H^0(\Gamma) \cong L^2(\Gamma)$. The BVP (1)-(4) is well-posed for any bounded open screen Γ .*

Our proof follows that of Theorem 1, except now we view A as an operator

$$A : \tilde{H}^{1/2}(\Gamma) \times \tilde{H}^0(\Gamma) \rightarrow H^{-1/2}(\Gamma) \times H^0(\Gamma).$$

(Note that both $\tilde{H}^0(\Gamma)$ and $H^0(\Gamma)$ are isometrically isomorphic to $L^2(\Gamma)$ but we maintain the $\tilde{H}^0(\Gamma)$ and $H^0(\Gamma)$ notation to distinguish distributions on \mathbb{R}^{n-1} from those on Γ .) This new functional setting for A is attractive because now the codomain is the dual of the domain, so we have a symmetric variational framework. Furthermore, A is then not only Fredholm of index zero, but in fact one can decompose A as

$$A = A_{\text{coercive}} + A_{\text{compact}},$$

where, for a suitable choice of dual pairing on the product space,

$$A_{\text{coercive}} = \begin{pmatrix} (\lambda^+ + \lambda^-)T & 0 \\ 0 & |\Gamma \end{pmatrix}$$

is coercive (strongly elliptic) [5] and

$$A_{\text{compact}} = \begin{pmatrix} \lambda^+ \lambda^- |_{\Gamma} & -\frac{1}{2}(\lambda^+ - \lambda^-)|_{\Gamma} \\ \frac{1}{2}(\lambda^+ - \lambda^-)|_{\Gamma} & -(\lambda^+ + \lambda^-)S \end{pmatrix}$$

is compact.

This improved regularity result for A is a useful tool for the numerical analysis of boundary element approximations to impedance scattering problems. In particular, for a class of screens Γ with fractal boundary (including the von Koch snowflake) one can apply the theory of Mosco convergence for variational problems (detailed in [6]) and certain density results for function spaces on rough domains (derived in [7]) to prove that boundary element discretizations of scattering problems on smoother ‘‘prefractal’’ screens approximating Γ converge to the solution of (1)-(4) on the limiting fractal screen Γ .

References

- [1] R. Kress and K.-M. Lee, Integral equation methods for scattering from an impedance crack, *J. Comput. Appl. Math.*, 161 (2003), pp. 161–177.
- [2] F. Ben Hassen, Y. Boukari, and H. Haddar, Application of the linear sampling method to identify cracks with impedance boundary conditions, *Inverse Probl. Sci. En.*, 21 (2013), pp. 210–234.
- [3] S. N. Chandler-Wilde and D. P. Hewett, Well-posed PDE and integral equation formulations for scattering by fractal screens, *SIAM J. Math. Anal.*, 50 (2018), pp. 677–717.
- [4] S. N. Chandler-Wilde, D. P. Hewett, and A. Moiola, Sobolev spaces on non-Lipschitz subsets of \mathbb{R}^n with application to boundary integral equations on fractal screens, *Integr. Equat. Operat. Th.*, 87 (2017), pp. 179–224.
- [5] S. N. Chandler-Wilde and D. P. Hewett, Wavenumber-explicit continuity and coercivity estimates in acoustic scattering by planar screens, *Integr. Equat. Oper. Th.*, 82 (2015), pp. 423–449.
- [6] S. N. Chandler-Wilde, D. P. Hewett, and A. Moiola, Boundary element methods for acoustic scattering by fractal screens, *in preparation*.
- [7] A. Caetano, D. P. Hewett, and A. Moiola, Density results for Sobolev, Besov and Triebel-Lizorkin spaces on rough sets, arxiv.org/abs/1904.05420.

**Electromagnetic scattering problems on perfectly-conducting complex domains:
from Rayleigh-Sommerfeld integrals toward fractal screens**

J. M. Christian^{1,*}, H. A. J. Middleton-Spencer¹

¹Joule Physics Laboratory, University of Salford, Greater Manchester M5 4WT, UK

*Email: j.christian@salford.ac.uk

Abstract

The diffraction of light by an aperture in an otherwise perfectly conducting plane screen of infinite extent is a phenomenon of fundamental interest in electromagnetics. Here, we consider classes of problems where the aperture domain is *complex* (possessing self-similar structure across a range of spatial scales) and modelled on finite iterations of the fractal shapes devised by Cantor and Sierpinski.

Rayleigh-Sommerfeld (RS) integrals are deployed to predict electric fields in the space behind the screen. This approach captures more fully the details of wave scattering, eliminating many of the approximations inherent with simpler analyses in Fraunhofer and Fresnel regimes. The solutions are essentially exact for Cantor-set apertures, at least within Kirchoff's treatment of the boundary conditions. Diffraction patterns from Cantor dust and Sierpinski triangle apertures are computed by transforming integrations over the domain into circulations around the constituent subdomain boundaries.

Keywords: Fractal screens, Cantor set, Cantor dust, Sierpinski triangle

1 Introduction

We consider an infinite screen Γ_∞ that is a perfect conductor of zero thickness and which occupies an entire axis (in 2D) or an entire plane (in 3D). If Γ denotes a bounded aperture in Γ_∞ , then the *Dirichlet* and *Neumann* RS integrals for the electric field E behind the screen are

$$E^D(\mathbf{x}) = -2 \int_{\Gamma} d\Gamma' E(\mathbf{x}') \frac{\partial}{\partial n'} G_0(\mathbf{x}|\mathbf{x}'), \quad (1a)$$

$$E^N(\mathbf{x}) = 2 \int_{\Gamma} d\Gamma' G_0(\mathbf{x}|\mathbf{x}') \frac{\partial}{\partial n'} E(\mathbf{x}'), \quad (1b)$$

respectively, where G_0 is the free space Green's function of the corresponding Helmholtz equation [1]. These formulations of the diffraction problem inherently respect the Sommerfeld radiation condition [2]. Since either $E(\mathbf{x}')$ or its (outward) normal derivative $(\partial/\partial n')E(\mathbf{x}')$ are

anticipated to vanish on the screen, one needs to specify their values on Γ . Following Kirchoff's prescription, we set these quantities to match those of the incident plane wave; Eqs. (1a) and (1b) are then internally self-consistent [1].

2 Cantor set

Consider removing a closed interval of width $2a$ from the centre of an infinite screen Γ_∞ that is defined along a straight line. This initiator stage, labelled by index $n = 0$, creates a gap of empty space $[-a, a]$ which represents a bounded aperture Γ (see Fig. 1). At the first pre-fractal level ($n = 1$), the open middle third of that gap is filled-in to produce two closed sub-intervals of empty space, $[-a, -a/3]$ and $[a/3, a]$. The iterative process of filling-in the open middle thirds may continue indefinitely, with the limit $n \rightarrow \infty$ defining a Cantor set whose capacity dimension is $\log 2/\log 3 \approx 0.63$ [3]. We then take the complex domain Γ as the union of 2^n closed aperture sub-intervals, each of width $2a/3^n$.

When the electric vector of the incident wave is linearly polarized and perpendicular to the propagation plane, Eqs. (1a) and (1b) prescribe

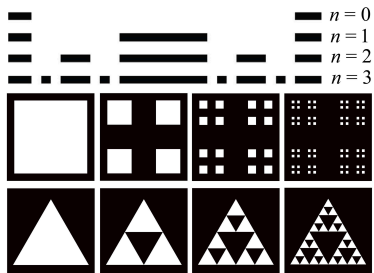


Figure 1: Examples of complex domains—the initiator and first three pre-fractal levels of the Cantor set (top), Cantor dust (middle), and Sierpinski triangle (bottom). White: bounded aperture Γ . Black: unbounded screen $\Gamma_\infty \setminus \Gamma$.

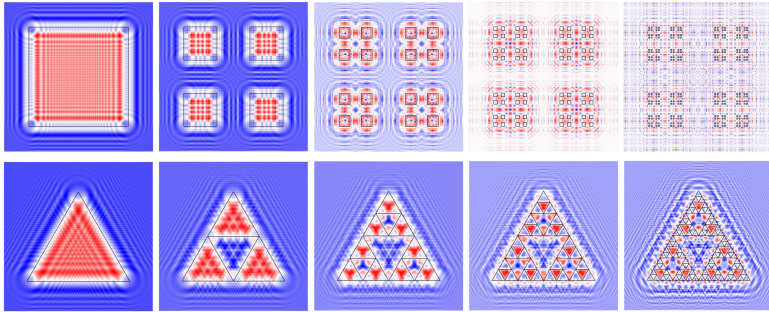


Figure 2: Numerical calculations of the Dirichlet RS integral [that is, $\Re(E^D)$] for the initiator and first four pre-fractal levels of the (top) Cantor dust and (bottom) Sierpinski triangle. Black lines correspond to the geometrical projections of the aperture domain boundaries onto the observation plane.

the vector $\mathbf{E} = (0, 0, E^{D,N})$. In this case, $E^{D,N}$ and its partial derivatives must be zero on the unlit surface of the screen. One may then calculate the magnetic field components from $\mathbf{B} = -(i/c\kappa)\nabla \times \mathbf{E}$, prove that $\nabla \cdot \mathbf{E} = 0$ and $\nabla \cdot \mathbf{B} = 0$ (as required by Maxwell's equations), and work out the energy flow from the Poynting vector. It is also possible to reconstruct the electromagnetic field in front of the screen by restoring the incident and reflected waves, and to devise a moderate form of Babinet's principle by considering a complementary problem [2].

3 Cantor dust & Sierpinski triangle

We now consider apertures based on the Cantor dust and Sierpinski triangle (see Fig. 1) [3]. In the limit, these shapes have capacity dimensions of $\log 4/\log 3 \approx 1.26$ and $\log 3/\log 2 \approx 1.58$, respectively. In these cases, the relationship between the scalar fields of Eqs. (1a) and (1b) and the full vector solution for the electromagnetic wave is not so obvious. Polarization effects are thus neglected here, but we expect $E^{D,N}$ to capture the dominant contribution in \mathbf{E} .

Evaluating the RS integrals for a given 2D domain is nontrivial, but progress can be facilitated by applying the divergence theorem and transforming integrations over area Γ into circulations around the boundaries $\partial\Gamma$ of all the constituent subdomains. Such a technique renders the calculations more manageable (see Fig. 2) but they can still remain computationally expensive as the pre-fractal level increases.

4 Concluding remarks

The RS diffraction formulae are best suited to high-frequency regimes and have many advantages over their far field (Fraunhofer) and paraxial (Fresnel) counterparts. One must be particularly mindful of limitations [1, 2], however, within the complex-domains arena. All three apertures have a Lebesgue measure of zero, interpreted physically as *vanishing area* for $n \rightarrow \infty$. Equations (1a) and (1b) will inevitably return a wave with zero amplitude as Γ shrinks to a set of points (though the validity of Kirchhoff's approximation will have been compromised well before then). Formulating the scattering problem more rigorously, it has recently been proved that classes of zero-measure screens *can* sometimes support a transmitted wave [4].

References

- [1] G. Barton, *Elements of Green's Functions and Propagation*, Clarendon Press, Oxford, 2005.
- [2] J. D. Jackson, *Classical Electrodynamics*, 3rd edition, John Wiley, New York, 1999.
- [3] K. Falconer, *Fractal Geometry*, 2nd edition, John Wiley, Chichester, 2003.
- [4] S. N. Chandler-Wilde and D. P. Hewett, Well-posed PDE and integral equation formulations for scattering by fractal screens, *SIAM J. Math. Anal.* **50** (2018), pp. 677–717.

High-Order Galerkin Method for Helmholtz and Laplace Problems on Multiple Open Arcs

Carlos Jerez-Hanckes^{1,*}, José Pinto^{2,*}

¹Faculty of Engineering and Sciences, Universidad Adolfo Ibáñez, Santiago, Chile

²School of Engineering, Pontificia Universidad Católica de Chile, Santiago, Chile

*Email: jspinto@uc.cl

Abstract

In this work we present a spectral numerical solver for Laplace and Helmholtz problems with Dirichlet boundary conditions on a finite set of open arcs in \mathbb{R}^2 . An indirect boundary integral method is employed, giving rise to a first kind formulation whose variational form is discretized using weighted Chebyshev polynomials. Convergence rates under the existence of smooth maps to describe the arcs are proved. In order to reduce computation times, a simple matrix compression technique based on sparse kernel approximations is developed. Numerical results provided validate our claims.

Keywords: Boundary integral equations, spectral methods, crack problems

1 Introduction

The scattering of waves by open arcs is a well-studied problem with applications ranging from structural cracks modeling to acoustic engineering and medical images. The problem is characterized by: (i) unbounded domain with a non-Lipschitz boundary, (ii) solutions which exhibit singular behaviors in the end points of each arc, (iii) large number of degrees of freedom for high frequency, and (iv) bad accuracy when the number of arcs and frequency increase. The problem is re-formulate as a system of boundary integral equations using standard boundary operators theory. This last formulation can be analysed with the techniques presented by [2]. In particular we are able to show that the boundary integral formulation is well posed for an arbitrary number of arcs.

For the approximation of the solutions we do a Galerkin discretization of the problem. In order to obtain a fast convergence method we employ an spectral method with weighed polynomials, whose weight mimics the singular behavior of the solutions at the end points. We are able to characterize the rate of converge for this basis functions under regularity assumptions of

the geometry and the arcs, but without previous knowledge of the singularity of the solution.

Finally in order to be able to solve geometries with hundred or more arcs, we present a compression algorithm, which give an sparse approximation of the matrix corresponding to the Galerkin discretization, and thus we can accelerate the solution of the linear system when iterative methods are employed.

2 Boundary Integral Formulation

Consider $\Gamma \subset \mathbb{R}^2$ a finite collection of M open arcs, and denote $\Omega = \mathbb{R}^2 \setminus \bar{\Gamma}$. For $\kappa \geq 0$, $\mathbf{g} = (g_1, \dots, g_M) \in H^{1/2}(\Gamma_1) \times \dots \times H^{1/2}(\Gamma_M)$ we consider the problem. Seek $u \in H_{loc}^1(\Omega)$ such that

$$\begin{aligned} -\Delta u - \kappa^2 u &= 0 && \text{in } \Omega, \\ \gamma_i^\pm u &= g_i && i = 1, \dots, M, \\ &&& \text{condition at infinity}(\kappa). \end{aligned}$$

Where the conditions of infinity for $k = 0$ are $\nabla u \in (L^2(\Omega))^2$ and

$$\frac{u(\mathbf{x})}{\sqrt{1 + \|\mathbf{x}\|_2^2} \log(2 + \|\mathbf{x}\|_2^2)} \in L^2(\Omega)$$

whereas for $k > 0$ we use the standard Sommerfeld condition. The solution u can be written as

$$u(\mathbf{x}) = \sum_{i=1}^M (S_{\Gamma_i}[\kappa]\lambda_i)(\mathbf{x}), \quad \forall \mathbf{x} \in \Omega,$$

where

$$(S_{\Gamma_i}[\kappa]\lambda_i)(\mathbf{x}) := \int_{\Gamma_i} G_\kappa(\mathbf{x}, \mathbf{y})\lambda_i(\mathbf{y})d\Gamma_i(\mathbf{y})$$

denotes the single layer potential generated by the arc Γ_i with fundamental solution G_κ .

Hence the boundary integral problem is to find $\lambda_1, \dots, \lambda_M$ such that

$$\sum_{i=1}^M \gamma_j(S_{\Gamma_i}[\kappa]\lambda_i)(\mathbf{x}) = g_j(\mathbf{x}).$$

where γ_j is the Dirichlet trace on the arc Γ_j . The following result is a simple extension of the work done in [2].

Theorem 1 *The boundary integral problem is well-posed.*

3 Galerkin Discretization

We detail the discrete spaces used to form the approximation of the solution of equation (2).

Let $\mathbb{T}_N(\widehat{\Gamma}) = \text{span}\{T_n\}_{n=0}^N$, where T_n denote the n -degree first kind Chebyshev, polynomials orthogonal under the weight $w^{-1}(t) = (1-t^2)^{-1/2}$ over $(-1, 1)$. Now, let us construct elements $p_n^i = T_n \circ \mathbf{r}_i^{-1}$, where \mathbf{r}_i is the parametrization of Γ_i , spanning the space $\mathbb{T}_N(\Gamma_i)$. We define the normalized space:

$$\overline{\mathbb{T}}_N(\Gamma_i) = \left\{ \bar{p}_n^i = \frac{p_n^i}{\|\mathbf{r}_i \circ \mathbf{r}_i^{-1}\|_2}, p_n^i \in \mathbb{T}_N(\Gamma_i) \right\}$$

Since the solutions $\boldsymbol{\lambda}$ exhibit singular behavior at the end points of each arc, we consider the weighted polynomial space:

$$\mathbb{Q}_N(\Gamma_i) := \{q_n^i := w_i^{-1} \bar{p}_n^i : \bar{p}_n^i \in \overline{\mathbb{T}}_N(\Gamma_i)\},$$

wherein $w_i := w \circ \mathbf{r}_i^{-1}$. The corresponding basis for $\mathbb{Q}_N(\Gamma_i)$ will be denoted $\{q_n^i\}_{n=0}^N$.

Theorem 2 (Theorem 4.23 [1]) *Let $\kappa > 0$, $m \in \mathbb{N}$ with $m > 2$, $\Gamma \in C^m$, $\mathbf{g} \in C^m(\Gamma)$, $\boldsymbol{\lambda}$ be the only solution of the boundary integral problem, and $\boldsymbol{\lambda}_N \in \mathbb{Q}_N(\Gamma_1) \times \dots \times \mathbb{Q}_N(\Gamma_M)$ the solution of the Galerkin discretization. Then, there exists $N_0 \in \mathbb{N}$ such that for every $N > N_0 \in \mathbb{N}$ there is a unique $\boldsymbol{\lambda}_N$ that converge as*

$$\|\boldsymbol{\lambda} - \boldsymbol{\lambda}_N\|_{\overline{\mathbb{H}}^{-\frac{1}{2}}(\Gamma)} \leq C(\Gamma, \kappa) N^{-m+1};$$

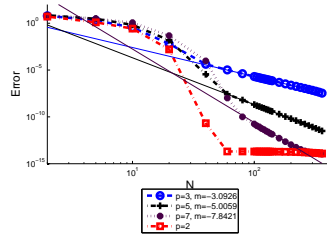
Moreover, if Γ , and \mathbf{g} are analytic, there exists $\rho > 1$ such that

$$\|\boldsymbol{\lambda} - \boldsymbol{\lambda}_N\|_{\overline{\mathbb{H}}^{-\frac{1}{2}}(\Gamma)} \leq C(\Gamma, \kappa) \rho^{-N+2} \sqrt{N}.$$

with $C(\Gamma, \kappa)$ being a positive constant.

The case $\kappa = 0$ works similar, but the vector densities $\boldsymbol{\lambda}$ and $\boldsymbol{\lambda}_N$ have to be chosen such that $\langle \boldsymbol{\lambda}, \mathbf{1} \rangle = \langle \boldsymbol{\lambda}_N, \mathbf{1} \rangle = 0$ over each arc. The result of the theorem is illustrated on Figure 1.

Figure 1: Convergence for Γ given by $\mathbf{r}(t) = (t, |t|^p)$, m is the measured rate of convergence.



4 Matrix Compression

Let's denote $\mathbf{L}[\kappa]$ the matrix associated with the Galerkin discretization, the entries are given by

$$(\mathbf{L}_{ji}[\kappa])_{lm} = \left\langle \gamma_j \widehat{\mathcal{S}}_{\Gamma_i}[\kappa] w^{-1} T_m, w^{-1} T_l \right\rangle_{(-1,1)},$$

where $\widehat{\mathcal{S}}_{\Gamma_i}[\kappa]$ is the weakly integral operator with kernel $G_k(r_j(t), r_i(s))$. Hence the matrix terms correspond to the Chebyshev coefficients of the kernel. By the Approximation theory this coefficients decay super-algebraically with respect to the indices m and l [1], when the kernel is smooth, which is the case for $i \neq j$. Hence since the terms decay fast, we can approximate the blocks of the cross interactions matrices by sparse matrices.

References

- [1] C. JEREZ-HANCKES AND J. PINTO, *High-order Galerkin method for Helmholtz and Laplace problems on multiple open arcs*, Tech. Rep. 2018-49, Seminar for Applied Mathematics, ETH Zürich, Switzerland, 2018.
- [2] E. P. STEPHAN AND W. L. WENDLAND, *An augmented Galerkin procedure for the boundary integral method applied to two-dimensional screen and crack problems*, *Applicable Analysis*, 18 (1984), pp. 183–219.

Integral equation solution for two-dimensional simulations in nanoplasmonics; single layer vs multi-layer configurations.

Harun Kurkcu^{1,*}

¹Department of Mathematics and NS, Gulf University of Science and Technology, Kuwait

*Email: kurkcu.h@gust.edu.kw

Abstract

Nanoplasmonics forms a major part of the field of nanophotonics, which explores how electromagnetic fields can be confined over dimensions on the order of or smaller than the wavelength. Here, we present an integral-equation formulation of the mathematical model that delivers accurate solutions in small computational times for surface plasmons coupled by periodic corrugations of flat surfaces of single layer and multi layered configurations along with experimental comparisons.

Keywords: nanoplasmonics, integral-equations, periodic structures

1 Introduction

Nanoplasmonics forms a major part of the field of nanophotonics, which explores how electromagnetic fields can be confined over dimensions on the order of or smaller than the wavelength. Initiated in 1902 by R.W. Wood [1] with the discovery of grating anomalies, this phenomenon has attracted significant attention over the last hundred years [2, 3]. Mie in 1908 gave a mathematical description of light scattering from spherical particles of sizes comparable to the wavelength [2], describing an effect that would come to be known as localized surface plasmons in the context of nanoplasmonics. It is based on interaction processes between electromagnetic radiation and conduction electrons at metallic interfaces or in small metallic nanostructures, leading to an enhanced optical near-field at sub-wavelength dimension. In 1899, Sommerfeld had described surface waves (waves propagating at the surface of metals) mathematically, and in 1902 Wood observed anomalous drops in the intensity of light reflected by a metallic grating [2]. But theory and observation would not be linked until 1941, by Fano [4]. Further experimental validation came in 1968, when Kretschmann and Raether used prism coupling to excite surface waves with visible light [5]. Other forms of coupling to surface plasmons have been thoroughly

investigated since then. All of the phenomena mentioned above are based entirely on classical electromagnetics, and thus can be mathematically described by Maxwell's equations. In this paper, an integral-equations formulation is given for an infinitely periodic metal surface whose period d is on the nanometer scale. The metal is assumed to extend infinitely below this surface, while a dielectric material extends infinitely above the surface. In this paper, we also, offer to extend this achievement to a more challenging case; multilayer configurations. The new configuration will be composed of a thin layer of noble metal (gold, silver, etc.) with depth larger than skin depth of the material, buried into different epoxies on top (glass/polymer substrate) and the bottom (liquid/water/blood). Some details of the numerical implementation and the results of a few numerical simulations and experimental comparisons are also given.

2 Formulation and Algorithm

In this section, a system of integral equations for the total exterior field u ($u = E_z$ in Transverse Electric -TE- and $u = H_z$ in Transverse Magnetic -TM- polarizations) and its normal derivative $\frac{\partial u}{\partial n}$ on the surface $\partial\Gamma$ are given. The metal surface $\partial\Gamma$ is infinitely thick and periodic and satisfies $f(x + d, y) = f(x, y)$. These fields $[u, \frac{\partial u}{\partial n}]$ satisfy [5];

$$u^i(r) = \int_P G_i(r, r') \frac{\partial u^i(r')}{\partial n(r')} - \frac{\partial G_i}{\partial n(r')}(r, r') u^i(r'),$$

$$u^e(r) = \int_P u^e(r') \frac{\partial G_e}{\partial n(r')}(r, r') - G_e(r, r') \frac{\partial u^e(r')}{\partial n(r')}$$

for $x \in \Gamma$, and for $x \in \Gamma^e$, respectively where n is the unit normal to $\partial\Gamma$ directed into the exterior of Γ and P is a single period of the surface $\partial\Gamma$. Here, $G(r, r')$ is the quasi-periodic Green's function [6] given by

$$G_Q(r, r') = \frac{i}{4} \sum_{n=-\infty}^{\infty} e^{i\alpha nd} H_0^{(1)}(kr_n)$$

where $\alpha = k \sin(\theta)$ and θ is incidence angle.

As $x \rightarrow \partial\Gamma$ and using the boundary conditions, the surface integral equations become

$$\begin{aligned} u^{\text{inc}}(r) &= \psi(r) + \int_P \frac{\partial(G_i - G_e)}{\partial n(r')}(r, r')\psi(r')dr' \\ &\quad - \int_P (\nu G_i - G_e)(r, r') \frac{\partial\psi(r')}{\partial n(r')}dr', \\ \frac{\partial u^{\text{inc}}(r)}{\partial n(r)} &= \frac{\nu + 1}{2} \frac{\partial\psi(r)}{\partial n(r)} + \int_P \frac{\partial^2(G_i - G_e)}{\partial n(r)\partial n(r')}(r, r')\psi(r')dr' \\ &\quad - \int_P \frac{\partial(\nu G_i - G_e)}{\partial n(r)}(r, r') \frac{\partial\psi(r')}{\partial n(r')}dr', \end{aligned}$$

for $r \in \partial D$ with the unknowns $\psi(r) = u_e(r) + u^{\text{inc}}(r)$ and $\partial\psi(r)/\partial n(r)$. Here $u^{\text{inc}}(r)$ denotes the incoming incident wave and $\nu = 1$ for TE polarization and $\nu = k_i/k_e$ for TM polarization.

The multi-layer formulation on the other hand follows similarly;

$$\left(A_1 + [A_{21}|A_{22}] \right) \begin{bmatrix} u_1(x) \\ \frac{\partial u_1(x)}{\partial n(x)} \\ u_2(x) \\ \frac{\partial u_2(x)}{\partial n(x)} \end{bmatrix} = \begin{bmatrix} u^{\text{inc}}(x) \\ 0 \\ \frac{\partial u^{\text{inc}}(x)}{\partial n(x)} \\ 0 \end{bmatrix}$$

where

$$\begin{aligned} A_1 &= \begin{pmatrix} 1 & 0 & 0 & 0 \\ 0 & 0 & -1 & 0 \\ 0 & \frac{1+\nu_1}{2} & 0 & 0 \\ 0 & 0 & 0 & -\frac{1+\nu_2}{2} \end{pmatrix} \\ A_{21} &= \begin{pmatrix} D_m^1 - D_e^1 & S_e^1 - \nu_1 S_m^1 \\ -D_m^1 & \nu_1 S_m^1 \\ -(N_e^1 - N_m^1) & D_e^{*1} - \nu_1 D_m^{*1} \\ -N_m^1 & \nu_1 D_m^{*1} \end{pmatrix} \\ A_{22} &= \begin{pmatrix} D_m^2 & -S_m^2 \\ D_i^2 - D_m^2 & S_m^2 - \nu_2 S_i^2 \\ N_m^2 & -D_m^{*2} \\ -(N_m^2 - N_i^2) & D_m^{*2} - \nu_2 D_i^{*2} \end{pmatrix} \end{aligned}$$

and the operators are

$$\begin{aligned} S_a^i(\mu) &= \int_{\Gamma_i} G_a(x, y)\mu(y)dy \\ D_a^i(\mu) &= \int_{\Gamma_i} \frac{\partial G_a(x, y)}{\partial n(y)}\mu(y)dy \\ D_a^{*i}(\mu) &= \int_{\Gamma_i} \frac{\partial G_a(x, y)}{\partial n(x)}\mu(y)dy \\ N_a^i(\mu) &= \int_{\Gamma_i} \frac{\partial^2 G_a(x, y)}{\partial n(x)\partial n(y)}\mu(y)dy \end{aligned}$$

and $G_a(x, y)$ is the quasi periodic Green's function. Here $u^{\text{inc}}(r)$ denotes the incoming incident wave and $\nu = 1$ for TE polarization and $\nu = k_i/k_e$ for TM polarization.

Our numerical algorithm depends on seeking the unknowns on the surface of the grating, and the matrix elements are evaluated through the derivation of a careful decomposition that allows for explicit evaluation of the singular and non-singular parts of the kernels [7].

References

- [1] R. W. Wood, *On a remarkable case of uneven distribution of light in a diffraction grating spectrum*, Philos. Mag. 4, 396-402 (1902).
- [2] G. Mie, *Contributions to the optics of turbid media, particularly of colloidal metal solutions*, 25, vol. 3, no. Annalen der Physik, pp. 377-445, 1908.
- [3] M. I. Stockman, *Nanoplasmonics: The physics behind the applications*, Physics Today, vol. 64.
- [4] Fano U., *The theory of anomalous diffraction gratings and of quasi-stationary waves on metallic surfaces (Sommerfeld's waves)*, Journal of the Optical Society of America 31, 213-222 1941.
- [5] Colton D. and Rainer K., *Inverse Acoustic and Electromagnetic Scattering Theory*, Springer-Verlag, 1992.
- [6] Kurkcü H. and Reitech F., *Stable and efficient evaluation of periodized Green's functions for the Helmholtz equation at high frequencies*, in Journal of Comp. Physics, 228, 2009 pp. 75-95.
- [7] Kurkcü H., *An efficient algorithm for the solution of high-frequency scattering by infinite rough surfaces*, PhD Thesis 2008.
- [8] Reitech F., Johnson T., Oh S., and Meyer G., *A fast and high-order accurate boundary perturbation method for nanoplasmonic simulations: basic concepts, analytic continuation and applications*, in Journal of the Optical Society of America A, Vol. 30, Issue 11, 2013 pp. 2175-2187.

Eigenoscillations and computation of surface waves in a water-basin with a conical bottom

Ning Yan Zhu^{1,*}, Mikhail A. Lyalinov²

¹Institute of Radio Frequency Technology, University of Stuttgart, Stuttgart, Germany

²Department of Mathematical Physics, St. Petersburg University, St. Petersburg, Russia

*Email: ningyan.zhu@ihf.uni-stuttgart.de

Abstract

This paper is centred on the numerical study of eigenoscillations and the corresponding surface waves in a water-basin with a conical bottom, whose closed-form exact solution is given in [1] by means of the Mellin transform and functional difference-equations. As revealed by an asymptotic analysis, the Mellin transform is slowly decreasing and highly oscillatory at the water surface, rendering a combination of a Filon-Cleenshaw-Curtis rule and uniform stationary phase method necessary for the computation of the velocity-potential; for a close neighbourhood of the tip, the path of integration has been shifted. Numerical examples are included to demonstrate the behaviour of surface waves in such a canonical domain.

Keywords: Surface waves, eigenoscillations, water-basin with a conical bottom, asymptotical-numerical computation

1 Statement of the problem and its exact solution

In a spherical co-ordinate system with the z -axis pointed vertically downwards, the conical bottom is located at $\vartheta = \vartheta_1 < \pi/2$ and the water surface at $\vartheta = \pi/2$. The velocity-potential $u(r, \vartheta, \varphi)$ solves the Laplace equation in water ($0 \leq r < \infty, \vartheta_1 \leq \vartheta \leq \pi/2, -\pi < \varphi \leq \pi$):

$$\operatorname{div} \operatorname{grad} u(r, \vartheta, \varphi) = 0,$$

is subject to the boundary condition at the water surface

$$\left[\frac{1}{r} \frac{\partial}{\partial \vartheta} u(r, \vartheta, \varphi) - K u(r, \vartheta, \varphi) \right]_{\vartheta=\pi/2} = 0$$

($K > 0$ plays the role of the spectral parameter and corresponds to the continuous spectrum) and at the bottom of the basin

$$\left. \frac{1}{r} \frac{\partial}{\partial \vartheta} u(r, \vartheta, \varphi) \right|_{\vartheta=\vartheta_1} = 0.$$

We are seeking for classical solutions of the homogeneous problem that satisfy a Meixner's type condition at the vertex and vanish slowly at infinity.

On use of the Mellin transform

$$u(r, \vartheta, \varphi) = \frac{1}{2\pi i} \int_{-i\infty}^{+i\infty} u_\nu(\omega) r^{\nu-1/2} d\nu, \quad (1)$$

the problem of solving the Laplace equation for the velocity-potential $u(r, \vartheta, \varphi)$ has been converted into one for resolving a functional difference equation for $u_\nu(\omega)$. As detailed in [1], the Mellin transform, save for a constant, reads

$$u_\nu(\omega) = e^{-in\varphi} K^\nu \left[P_{\nu-1/2}^{-|n|}(\cos \vartheta) - \frac{d_{\vartheta_1} P_{\nu-1/2}^{-|n|}(\cos \vartheta_1)}{d_{\vartheta_1} P_{\nu-1/2}^{-|n|}(-\cos \vartheta_1)} P_{\nu-1/2}^{-|n|}(-\cos \vartheta) \right] \times \frac{\Gamma(-\nu + |n| + 1/2) \gamma_n(\nu)}{1 + \frac{d_{\vartheta_1} P_{\nu-1/2}^{-|n|}(\cos \vartheta_1)}{d_{\vartheta_1} P_{\nu-1/2}^{-|n|}(-\cos \vartheta_1)}}. \quad (2)$$

In addition to the associated Legendre function $P_{\nu-1/2}^{-|n|}(\cdot)$ and the Euler Gamma function $\Gamma(\cdot)$, a new special function $\gamma_n(\cdot)$ has been constructed, cf [1].

2 Computational aspects and examples

As a preparation for the computation of the Mellin transform (1), let us consider the behaviour of $u_\nu(\omega)$ as $\nu \rightarrow \pm i\infty$. On use of the respective properties of the employed special functions, we have

$$u_\nu(\omega) r^{\nu-1/2} \sim \frac{e^{\mp i\nu(\vartheta-\pi) + \nu - \nu \ln \nu + \nu \ln(Kr)}}{\sqrt{r\nu \sin \vartheta}} \gamma_n^\pm$$

with $\gamma_n^\pm = \lim_{\nu \rightarrow \pm i\infty} \gamma_n(\nu)$.

Hence it is evident that, on the water surface with $\vartheta = \pi/2$, the integrand of the Mellin transform is a highly oscillatory function whose envelope decreases with $\nu^{-1/2}$ as $\nu \rightarrow \pm i\infty$.

To compute efficiently the highly oscillatory integral over an infinite interval (1), it is advantageous to divide the imaginary axis in the ν -plane into a finite, central part and two semi-infinite parts:

$$u(r, \vartheta, \varphi) = \frac{1}{2\pi i} \left(\int_{-i\infty}^{-i\mu_0} + \int_{-i\mu_0}^{+i\mu_0} + \int_{+i\mu_0}^{+i\infty} \right) u_\nu(\omega) r^{\nu-1/2} d\nu, \quad (3)$$

with $\mu_0 \gg 1$.

The integration over the central finite part is executed by means of a Filon-Clenshaw-Curtis rule as suggested in [2]. The remaining two semi-infinite integrals are evaluated by means of the uniform stationary-phase method, cf [3]. To this end, let us write

$$\begin{aligned} I_+ &= \int_{i\mu_0}^{+i\infty} \frac{u_\nu(\omega) r^{\nu-1/2}}{2\pi i} d\nu \\ &= \int_1^\infty f(m) e^{i\mu_0 q(m)} dm \end{aligned}$$

with $q(m) = m(1 + \ln \frac{Kr}{\mu_0 m})$. Therefore,

$$\begin{aligned} I_+ &\approx \left\{ \mathbf{F}^* \left[\frac{\sqrt{\mu_0 |q(1) - q(m_s)|}}{e^{-i\pi/4 + i\mu_0(q(1) - q(m_s))}} \right] \right. \\ &\quad \left. + \frac{2\sqrt{\pi} \sqrt{\mu_0 |q(1) - q(m_s)|}}{\mu_0} \right\} \\ &\quad \times f(m_s) e^{iKr - i\pi/4} \frac{\sqrt{2\pi Kr}}{\mu_0} \\ &\quad + \frac{f(1) e^{i\left[\mu_0 \left(1 + \ln \frac{Kr}{\mu_0}\right) + \frac{\pi}{2}\right]}}{\mu_0 \ln(Kr/\mu_0)}. \end{aligned} \quad (4)$$

Here, $m_s = Kr/\mu_0$ is the stationary point of $q(m)$, $\mathbf{F}(\cdot)$ stands for the Fresnel integral (see [3]) and $\sqrt{\mu_0 |q(1) - q(m_s)|}$ represents the detour-parameter.

The Mellin transform (1) is not directly suitable for numerical computation of the velocity-potential in a neighbourhood of the tip with $Kr < 1$. As an alternative, the path of integration has been shifted to $1 + iR$, say:

$$\begin{aligned} u(r, \vartheta, \varphi) &= - \sum \text{Res}_{\nu_j} \left[u_\nu(\omega) r^{\nu-1/2} \right] \\ &\quad + \int_{-i\infty}^{+i\infty} \frac{u_{\nu+1}(\omega) r^{\nu+1/2}}{2\pi i} d\nu, \end{aligned} \quad (5)$$

with ν_j ($0 < \text{Re } \nu_j < 1$) being the poles of $u_\nu(\omega)$ eventually captured during the deformation of the integration path.

On inspection of (2), there is merely one such pole located at $\nu = 1/2$ for $n = 0$. Hence,

$$-\text{Res}_{\nu=1/2} \left[u_\nu(\omega) r^{\nu-1/2} \right] = \frac{\sqrt{K} \gamma_0(\frac{1}{2})}{\cos \vartheta_1}. \quad (6)$$

It can be shown that the integrand at the right-hand side of (5) remains highly oscillatory, but its envelope decreases with $\nu^{-3/2}$ at the water surface. Therefore, the integral in (5) is evaluated in a similar fashion as the Mellin transform (1).

As an example Figure 1 displays the velocity-potential with $n = 0$ on the water surface away from the tip.

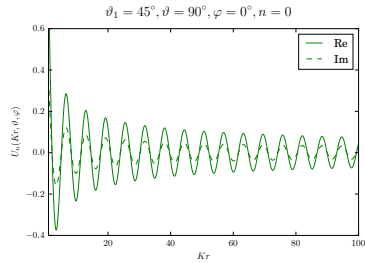


Figure 1: Velocity-potential at the water surface away from the tip (solid line: real part; broken line: imaginal part).

References

[1] M. A. Lyalinov, Eigenmodes in the water-wave problems for infinite pools with cone-shaped bottom, *Journal of Fluid Mechanics* **800** (2016), pp. 645–665.
 [2] V. Dominguez, I. G. Graham and V. P. Smyshlyaev, Stability and error estimates for Filon-Clenshaw-Curtis rules for highly oscillatory integrals, *IMA Journal of Numerical Analysis* **31** (2011), pp. 1253–1280.
 [3] V. M. Babich, M. A. Lyalinov and V. E. Grikurov, *Diffraction Theory: The Sommerfeld-Malyuzhinets Technique*, Alpha Science, Oxford, 2008.

Uncertainty quantification for Helmholtz transmission problems with geometric uncertainties

Laura Scarabosio¹

¹Department of Mathematics, Technical University of Munich, Munich, Germany

Abstract

We address how to compute statistics of quantities of interest depending on the solution to a Helmholtz transmission problem with random interface. A mapping to a reference configuration allows for an efficient computational treatment and a rigorous numerical analysis building on the well-established results for PDEs on deterministic domains with uncertain coefficients. For quantities of interest depending smoothly on the stochastic parameters, a dimension-adaptive Smolyak algorithm proves to be much more efficient than Monte Carlo rules, without suffering from the so-called curse of dimensionality. Multilevel Monte Carlo is instead a viable alternative for non-smooth quantities of interest.

Keywords: random geometry, high-dimensional approximation, Helmholtz equation.

1 Model problem

To define the random interface, we introduce a probability space $(\Omega, \mathcal{A}, \mathbb{P})$, where Ω is the set of elementary events, \mathcal{A} a sigma-algebra on Ω and \mathbb{P} a probability measure. For every $\omega \in \Omega$, we formally define $\Gamma(\omega)$ to be the boundary of the scatterer, $D_{in}(\omega)$ the domain occupied by the latter and $D_{out}(\omega)$ the outer, unbounded domain. The transmission problem reads:

$$\begin{cases} -\nabla \cdot (\alpha(\Gamma(\omega); x) \nabla u) - \kappa^2(\Gamma(\omega); x) u = 0, \\ \llbracket u \rrbracket_{\Gamma(\omega)} = 0, \quad \llbracket \alpha(\Gamma(\omega); x) \nabla u \cdot \mathbf{n} \rrbracket_{\Gamma(\omega)} = 0, \\ \text{+ Sommerfeld radiation condition on } u - u_i, \end{cases}$$

where $u = u(\omega)$ is the total field, the first equation is posed on $D_{in}(\omega) \cup D_{out}(\omega) \subset \mathbb{R}^2$, the second line denotes continuity of the tangential and conormal traces across the interface (with \mathbf{n} the unit normal pointing to the outer domain) and, in the third equation, u_i is an incoming plane wave. The coefficients α and κ are real-valued, piecewise constant in each subdomain and uniformly positive. Our goal is to compute efficiently the mean of quantities of interest depending on the solution u to the model problem. These could be, for instance, the solution u itself, the far-field pattern or point values of u .

2 Interface parametrization

For a star-shaped scatterer, we model the stochastic interface as

$$r(\mathbf{y}; \varphi) = r_0 + \sum_{j=1}^J c_j y_{2j-1} \cos(j\varphi) + s_j y_{2j} \sin(j\varphi),$$

for $\varphi \in [0, 2\pi)$, $J \in \mathbb{N}$ and $c_j, s_j \in \mathbb{R}$ for every $j = 1, \dots, J$. The quantity $r_0 \in \mathbb{R}$ describes a nominal circular interface, while the terms in the summation model the random shape variations. The parameter $\mathbf{y} = (y_1, \dots, y_{2J})$ is the image of a random variable $\mathbf{Y}(\omega) := (Y_1(\omega), \dots, Y_{2J}(\omega))$, $\omega \in \Omega$, whose entries are independent, identically distributed $\sim \mathcal{U}([-1, 1])$. Consequently, \mathbf{y} takes values in the high-dimensional parameter space $[-1, 1]^{2J}$. In the model problem we can now substitute the dependence on $\omega \in \Omega$ by a dependence on $\mathbf{y} \in [-1, 1]^{2J}$, and computing the average of a quantity of interest means performing an integration over the high-dimensional space $[-1, 1]^{2J}$ with respect to the image measure $\mu_{\mathbf{y}} = (\frac{1}{2})^{2J}$. To ensure positivity of the radius and convergence of the sum for J arbitrarily large, we assume the following [2].

Assumption 1 *The coefficient sequences $(c_j)_{j \geq 1}$ and $(s_j)_{j \geq 1}$ have a monotonically decreasing majorant in $\ell^p(\mathbb{N})$ for $0 < p < \frac{1}{2}$. Moreover, they fulfill $\sum_{j \geq 1} (|c_j| + |s_j|) \leq \frac{r_0}{2}$.*

3 Mapping to a reference configuration

We follow the mapping approach described in [5] to work on a reference configuration with fixed, parameter-independent interface. First, we truncate the outer domain with a circle of radius $R \in \mathbb{R}_+$ that contains every realization of the scatterer in its interior, and denote by D_R the truncated domain; the Sommerfeld radiation condition for the unbounded domain is replaced by a Neumann boundary condition involving the DtN map [2]. Then, we construct a \mathbf{y} -dependent, orientation preserving diffeomorphism $\Phi(\mathbf{y}) : D_R \rightarrow D_R$, $\mathbf{y} \in [-1, 1]^{2J}$ from a reference configuration with interface r_0 to the

configuration with interface $r(\mathbf{y}; \cdot)$. We ask that Φ maps ∂D_R to itself and the circle with nominal radius r_0 to $r(\mathbf{y}; \cdot)$. In particular, from now on, we consider

$$\Phi(\mathbf{y}; \hat{x}) = \hat{x} + \chi(\hat{x})(r(\mathbf{y}; \arg(\hat{x})) - r_0) \frac{\hat{x}}{\|\hat{x}\|},$$

for every $\hat{x} \in D_R$, with $\chi : D_R \rightarrow \mathbb{R}_{0,+}$ a smooth mollifier acting on the radial direction [2].

4 Computing statistics of smooth quantities of interest

To compute the mean of some quantity of interest, different quadrature rules can be used, depending on the smoothness of the quantity with respect to $\mathbf{y} \in [-1, 1]^{2J}$. In this section we focus on the smooth case, and address the non-smooth case in the next section. We have the following result, proved in [2].

Theorem 1 *Let Assumption 1 hold. Moreover, assume that $(|c_j|)_{j \geq 1}$ and $(|s_j|)_{j \geq 1}$ have a monotonically decreasing majorant, and that the wavelengths inside and outside the scatterer are large compared to the scatterer size, in the sense that κ fulfills Assumption 4.4 in [2]. Then $\hat{u}(\mathbf{y}; \hat{x}) := u(\mathbf{y}; \Phi(\mathbf{y}; \hat{x}))$, as mapping from $[-1, 1]^{2J}$ to $H^1(D_R)$, admits a holomorphic extension to any open set $\mathcal{O}_\rho := \bigotimes_{l \geq 1} \mathcal{O}_{\rho_l}$, with $\mathcal{O}_{\rho_l} := \{z \in \mathbb{C} : \text{dist}(z, [-1, 1]) \leq \rho_l - 1\}$ and*

$$\sum_{l \geq 1} (\rho_l - 1)l(|c_l| + |s_l|) \leq \varepsilon,$$

for $\varepsilon > 0$ sufficiently small.

As a consequence of this result, high-order quadrature rules on $[-1, 1]^{2J}$ allow to attain convergence rates for the computation of $\mathbb{E}_{\mu_{\mathbf{y}}}[\hat{u}]$ which are much higher than those of Monte Carlo and do not degenerate for J large. In particular, application of the dimension-adaptive Smolyak algorithm described in [4] using, for instance, \mathfrak{R} -Leja nodes, shows a convergence rate of N^{-s} , where N is the number of function evaluations for \hat{u} (i.e. the number of PDE solves) and $s = \frac{1}{p} - 2$, p being as in Assumption 1. The same convergence rate is attained for the average of the far field pattern [2].

5 Computing statistics of non-smooth quantities of interest

For quantities of interest that do not depend smoothly on $\mathbf{y} \in [-1, 1]^{2J}$, in general we cannot

expect high-order convergence rates from high-order quadrature rules, but it is still possible to devise a multilevel Monte Carlo (MLMC) strategy to obtain considerable computational savings compared to plain Monte Carlo. We show this for the point evaluation of the solution u at a fixed point x_0 that can be crossed by the interface for some realizations [3]. We consider a hierarchy of meshes on the reference configuration, obtained by uniform refinement, and denote by $E^L[u(\mathbf{y}; x_0)]$ the MLMC estimator of $\mathbb{E}_{\mu_{\mathbf{y}}}[u(\mathbf{y}; x_0)]$ using L levels [1].

Theorem 2 *Let Assumption 1 hold, and assume that the values of the wavenumber κ inside and outside the scatterer fulfill Assumption 4.4 in [2]. On each mesh in the hierarchy, we consider a linear finite element discretization (that resolves the interface r_0) and an algebraic multi-grid solver for the linear system. Then, for any tolerance $TOL > 0$, there exist $L \in \mathbb{N}$, a sequence of number of samples per level $(M_l)_{l=1}^L$ and a constant $C > 0$ such that*

$$\|E^L[u(\mathbf{y}; x_0)] - \mathbb{E}_{\mu_{\mathbf{y}}}[u(\mathbf{y}; x_0)]\|_{L^2([-1, 1]^{2J}, \mathbb{R})} \leq TC$$

and the work to compute the estimator is bounded as $\mathcal{W}(E^L[u(\mathbf{y}; x_0)]) \leq CTOL^{-2}$.

For the proof of this result, we refer to [3].

References

- [1] Giles, M. B. (2015). *Multilevel monte carlo methods*. Acta Numerica, 24, 259-328.
- [2] Hiptmair, R., Scarabosio, L., Schillings, C., & Schwab, C. (2018). *Large deformation shape uncertainty quantification in acoustic scattering*. Advances in Computational Mathematics, 44(5), 1475-1518.
- [3] Scarabosio, L. (2019). *Multilevel Monte Carlo on a high-dimensional parameter space for transmission problems with geometric uncertainties*. International Journal for Uncertainty Quantification (accepted).
- [4] Schillings, C., & Schwab, C. (2013). *Sparse, adaptive Smolyak quadratures for Bayesian inverse problems*. Inverse Problems, 29(6), 065011.
- [5] Xiu, D., & Tartakovsky, D. M. (2006). *Numerical methods for differential equations in random domains*. SIAM Journal on Scientific Computing, 28(3), 1167-1185.

Uncertainty Quantification for Helmholtz Scattering by Random Surfaces: Shape Calculus and Sparse Tensor Approximation

Paul Escapil-Inchauspé^{1,*}, Carlos Jerez-Hanckes²

¹School of Engineering, Pontificia Universidad Católica de Chile, Santiago, Chile

²Faculty of Engineering and Sciences, Universidad Adolfo Ibáñez, Santiago, Chile

*Email: pescapil@uc.cl

Abstract

We consider the numerical solution of acoustic wave scattering by obstacles with uncertain geometries. In particular, we analyze fields diffracted by small stochastic perturbations of a nominal shape. Using the shape derivative, we derive deterministic boundary integral equations for the statistical moments of the fields. These are approximated by sparse tensor Galerkin discretization –via the combination technique. We show numerically predicted convergence rates with poly-logarithmic growth in the number of degrees of freedom and accuracy in approximation of the moments, and discuss implementation details.

Keywords: Helmholtz scattering, UQ

1 Introduction

Acoustic wave scattering modeling and simulation is key in numerous areas such as in aeronautics, biology or astrophysics, to name a few. As the complexity of applications increases, quantifying the effects of random perturbations originated by actual manufacturing or operation conditions becomes ever more relevant for efficient and robust design.

The present work seeks to provide an accurate and fast method for computing the mean field and higher statistical moments due to small random perturbations of a nominal deterministic shape. Model problems here considered involve solving Helmholtz equations in unbounded domains. Thanks to the small perturbation assumption and following the technique proposed in [3, 6], we employ suitable shape Taylor expansions through shape derivatives (SD) to approximate the statistical moments by quantities defined on the nominal shape, leading to an equation with stochastic right-hand side. We then combine the theory of boundary integral equations (BIEs) and boundary element method (BEM) with the sparse tensor approximation theory [1, 2, 5].

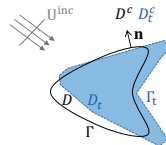


Figure 1: Problem geometry.

2 Random Domains

Throughout, we consider an open bounded Lipschitz –nominal– domain $D \subset \mathbb{R}^d$, $d = 2, 3$, of class $C^{1,1}$ with $\Gamma := \partial D$. Let $(\Omega, \mathcal{A}, \mathbb{P})$ be a suitable probability space. For an index $k \in \mathbb{N}$ and for $U : \Omega \rightarrow X$ a random field in the Bochner space $L^k(\Omega, \mathbb{P}; X)$ [3, Section 4.1] we define the statistical moments:

$$\mathcal{M}^k[U(\mathbf{x}, \omega)] := \int_{\Omega} U(\mathbf{x}_1, \omega) \cdots U(\mathbf{x}_k, \omega) d\mathbb{P}(\omega),$$

with the case $k = 1$ being the expectation. Accordingly, for suitably defined random vector fields \mathbf{v} we introduce families of random surfaces via mappings $\Omega \ni \omega \mapsto \Gamma_t(\omega) = \{\mathbf{x} + t\mathbf{v}(\omega), \mathbf{x} \in \Gamma\}$ (see Figure 2).

Definition 1 (Shape Derivative) *Consider a random shape dependent scalar field $U_t(\omega)$ defined in a domain $D_t(\omega)$ for each $t \in [0, \varepsilon]$. We say that $U_t(\omega)$ admits a SD U' in D along $\mathbf{v}(\omega)$, if the following limit exists*

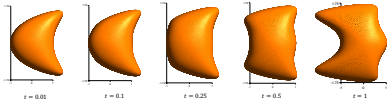
$$U'(\omega) := \lim_{t \rightarrow 0} \frac{U_t(\omega) - U}{t}. \quad (1)$$

If U_t admits a SD, for small t , the quantities of interest can be approximated accurately for $k \geq 2$ on proper domains by

$$\begin{aligned} \mathbb{E}[U_t(\omega)] &= U + \mathcal{O}(t^2), \\ \mathcal{M}^k[U_t(\omega) - U] &= t^k \mathcal{M}^k[U'(\omega)] + \mathcal{O}(t^{k+1}). \end{aligned}$$

3 Boundary Reduction and Sparse Tensor Approximation

For an incident wave, we introduce the sound-soft, -hard, impedance and transmission prob-


 Figure 2: Γ_t function to t (3249 vertices)

lems. Besides, k -fold tensors are denoted with parenthesized subscripts for $k \in \mathbb{N}$. The technique presented consists in using the boundary value problems satisfied by the SD, as detailed in [4, Table 5.6], and performing a boundary reduction, leading to well-posed BIEs:

Generic Formulation for the BIEs For $k \geq 2$, X, Y Hilbert spaces, $g \in Y$, and $\mathcal{M}^k[g] \in Y^{(k)}$, we seek $\xi \in X, \Sigma \in X^{(k)}$ such that

$$\begin{cases} Z\xi &= g & \text{on } \Gamma, \\ Z^{(k)}\Sigma &= \mathcal{M}^k[g] & \text{on } \Gamma^{(k)}. \end{cases} \quad (2)$$

Then, solving via the Galerkin method and nested spaces $\{V_L\}_{L \in \mathbb{N}_0}$, leads to an $\mathcal{O}(h^{\min(p+1, s)})$ asymptotic error bound for $\xi \in X^s$ a smoothness space and p the polynomial degree. Classical results for sparse tensor elements guarantee the existence of $L_0(k) \in \mathbb{N}$ such that the solution converges quasi-optimally as follows [5].

Lemma 2 *The following error bound holds for $L \geq L_0(k) \in \mathbb{N}$ and $\Sigma \in (X^s)^{(k)}$:*

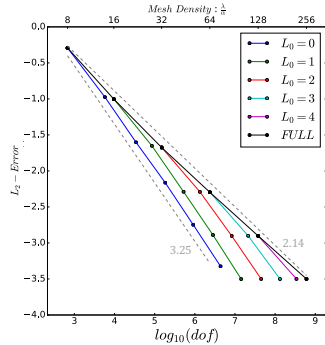
$$\|\Sigma - \hat{\Sigma}_L\|_{X^{(k)}} \leq Ch^{\min(p+1, s)} |\log h|^{(k-1)/2}.$$

4 Numerical Results

We perturb a kite-shaped object (see Figure 2) for different t values and test the accuracy of the first-order shape approximation. Then, we verify the expected convergence rates for the sparse tensor approximation (see Figure 3 for the sound-soft problem on \mathbb{S}^2).

5 Conclusion

In this work, we tackled the UQ for random shape Helmholtz scattering. Under small perturbation assumptions, we applied the SD-UQ framework and allowed for an accurate approximation of the statistical moments with a poly-logarithmic complexity. Numerical results evidenced the applicability of the technique and showed good scalability and robustness when coupled with fast resolution methods and efficient preconditioners.


 Figure 3: Convergence results of the solution in full (black) versus sparse tensor spaces for $k = 2$, $\Gamma = \mathbb{S}^2$ and $\kappa = 1$ function to L_0 .

References

- [1] H. Harbrecht, M. Peters and M. Siebenmorgen, Combination technique based k -th moment analysis of elliptic problems with random diffusion, *Journal of computational physics* **252** (2013), pp. 128–141.
- [2] M. Griebel, M. Schneider and C. Zenger, A combination technique for the solution of sparse grid problems, *Citeseer* (1990).
- [3] C. Jerez-Hanckes and C. Schwab, Electromagnetic wave scattering by random surfaces: uncertainty quantification via sparse tensor boundary elements, *IMA Journal of Numerical Analysis* **3** (2016), pp. 1175–1210.
- [4] R. Hiptmair and J. Li, Shape Derivatives in Differential Forms II: Shape Derivatives for Scattering Problems, *Foundations of computational mathematics* (2017).
- [5] T. von Petersdorff and C. Schwab, Sparse finite element methods for operator equations with stochastic data, *Applications of Mathematics* **51** (2006), pp. 145–180.
- [6] H. Harbrecht, R. Schneider and C. Schwab, Sparse second moment analysis for elliptic problems in stochastic domains, *Numerische Mathematik* **3** (2008), pp. 385–414.

Nearby preconditioning for multiple realisations of the Helmholtz equation, with application to uncertainty quantification

Ivan G. Graham¹, Owen R. Pemberty^{1,*}, Euan A. Spence¹

¹Department of Mathematical Sciences, University of Bath, Bath, UK

*Email: o.r.pemberty@bath.ac.uk

Abstract

We present a technique for speeding up the solution of multiple linear systems arising from multiple realisations of the heterogeneous Helmholtz equation; the main idea is to calculate a preconditioner for one realisation exactly and then use it for many ‘nearby’ realisations. We prove, and give numerical evidence, of how the effectiveness of the technique depends on the wavenumber, and apply the technique to a problem in uncertainty quantification, demonstrating significant speedup.

Keywords: Helmholtz equation, random, heterogeneous, preconditioning, uncertainty quantification, GMRES

Motivation

The motivation for this work comes from uncertainty quantification (UQ) where one seeks to compute properties of the solution of the stochastic Helmholtz equation

$$\nabla \cdot (A \nabla u) + k^2 n u = -f, \quad (1)$$

where A and n are random fields, and therefore u is also a random field (i.e., A , n , and u are both random and spatially heterogeneous). If one uses a sampling-based approach, one will have to solve many (potentially thousands) of linear systems which arise from discretising many realisations of (1). If one is using a preconditioned linear solver (such as GMRES) then one must, it seems, construct a different preconditioner for each realisation of (1). This may incur a significant computational cost. Therefore we propose re-using preconditioners for problems that are ‘nearby’ in some sense.

Model Problem and aim

To focus on the convergence of GMRES applied to ‘nearby preconditioned’ linear systems, consider the two deterministic Helmholtz equations

$$\nabla \cdot (A^{(j)} \nabla u^{(j)}) + k^2 n^{(j)} u^{(j)} = -f, \quad j = 1, 2, \quad (2)$$

where A is matrix-valued, n is real-valued, and A equals the identity and n equals one outside some compact set. We combine (2) with either the Sommerfeld radiation condition or an impedance boundary condition. Let $\mathbf{A}^{(j)}$, $j = 1, 2$ denote the matrices arising from fixed-order finite-element discretisations of (2).

The aim of this work is to study the behaviour of GMRES applied to $(\mathbf{A}^{(1)})^{-1} \mathbf{A}^{(2)}$, and to give sufficient conditions on $\|A^{(1)} - A^{(2)}\|_{L^\infty}$ and $\|n^{(1)} - n^{(2)}\|_{L^\infty}$ such that GMRES converges in a number of iterations that is independent of the wavenumber k .

Main Results

We work with h -finite elements with polynomial degree p . We prove results for GMRES in the weighted norm $\|\cdot\|_{\mathbf{D}_k}$, where the matrix $\mathbf{D}_k := \mathbf{S} + k^2 \mathbf{M}$, where \mathbf{S} and \mathbf{M} are the finite-element stiffness and mass matrices respectively. Whilst we state the results below only for left preconditioning, analogous results also hold for right preconditioning. Related results also hold when working in the standard norm $\|\cdot\|_2$, and we discuss these below.

Theorem 1 *Assume $A^{(1)}$, $n^{(1)}$ and the domain are nontrapping (see, e.g., [4, p.2871 and Definition 7.6]), and h depends on k and p such that the finite-element error is bounded uniformly in k . Given $k_0 > 0$, there exist C_1 and C_2 independent of h and k (but dependent on $A^{(1)}$, $n^{(1)}$, p , k_0 , and the domain) such that for all $k \geq k_0$*

$$\begin{aligned} \|\mathbf{I} - (\mathbf{A}^{(1)})^{-1} \mathbf{A}^{(2)}\|_{\mathbf{D}_k} &\leq \\ C_1 k \|A^{(1)} - A^{(2)}\|_{L^\infty} + C_2 k \|n^{(1)} - n^{(2)}\|_{L^\infty}. \end{aligned} \quad (3)$$

From (3), we can conclude the following result on the convergence of GMRES for the ‘nearby preconditioned’ system $(\mathbf{A}^{(1)})^{-1} \mathbf{A}^{(2)}$ using the analogue of the Elman estimate for GMRES in the weighted norm $\|\cdot\|_{\mathbf{D}_k}$, see [3, Theorem 5.1].

Corollary 2 Under the assumptions of Theorem 1, if

$$C_1 k \|A^{(1)} - A^{(2)}\|_{L^\infty} + C_2 k \|n^{(1)} - n^{(2)}\|_{L^\infty} \leq \frac{1}{2}, \tag{4}$$

then weighted GMRES in $\|\cdot\|_{\mathbf{D}_k}$ applied to

$$(\mathbf{A}^{(1)})^{-1} \mathbf{A}^{(2)} \mathbf{u} = \mathbf{f}$$

converges in a k -independent number of iterations for all $k \geq k_0$.

We also obtain similar results to Theorem 1 and Corollary 2 for standard GMRES (i.e., working in $\|\cdot\|_2$). The only substantial difference is that the term $C_1 k \|A^{(1)} - A^{(2)}\|_{L^\infty}$ on the right-hand side of (3) and left-hand side of (4) is replaced by

$$\tilde{C}_1 \frac{1}{h} \|A^{(1)} - A^{(2)}\|_{L^\infty}, \tag{5}$$

for some constant \tilde{C}_1 . The new condition (5) is typically more restrictive, as practical values of h are $< 1/k$. However, as discussed below, numerical experiments show that (5) is not necessary for nearby preconditioning to perform well.

Observe that (4) is more restrictive on $\|A^{(1)} - A^{(2)}\|_{L^\infty}$ and $\|n^{(1)} - n^{(2)}\|_{L^\infty}$ for larger k . Therefore the set of problems for which $\mathbf{A}^{(1)}$ is a good preconditioner decreases as k grows. However, as discussed below, when this technique is applied to a UQ model problem we obtain speedup for a range of physically relevant k .

Numerical Confirmation

Numerical results show that the condition (4) is sufficient in standard GMRES, despite the fact it is only proved for weighted GMRES. I.e., if $\|A^{(1)} - A^{(2)}\|_{L^\infty}$ and $\|n^{(1)} - n^{(2)}\|_{L^\infty}$ decrease like $1/k$ as $k \rightarrow \infty$, the the number of GMRES iterations is bounded independently of k .

We note that [3] observed similar behaviour with domain-decomposition preconditioners for the Helmholtz equation; results on GMRES convergence were proved for weighted GMRES, but the numerically observed behaviour for weighted and standard GMRES was essentially the same.

Application to UQ

To test the effectiveness of the nearby preconditioning technique applied to UQ, we consider the model problem of computing samples of

$$\begin{aligned} \Delta u + k^2 n u &= -f & (6) \\ \partial_\nu u - iku &= g, \end{aligned}$$

with n given by the artificial Karhunen–Loève expansion

$$n(\omega, \mathbf{x}) = n_0(\mathbf{x}) + \sum_{j=1}^J y_j(\omega) \psi_j(\mathbf{x})$$

for some $J \in \mathbb{N}$, spatially varying n_0 and ψ_j (chosen so that n is positive almost surely), and independent $\text{Unif}(-1/2, 1/2)$ random variables y_j . We generate many realisations of n by generating many vectors $\mathbf{y} = (y_j)_{j=1}^J$ using a Monte-Carlo or a Quasi-Monte-Carlo (see, e.g., [2]) method. We then solve the realisations of (6) given by each realisation of n .

To use nearby preconditioning in this setting, we calculate a preconditioner for a realisation of (6), and then reuse this preconditioner on nearby realisations (where $n^{(1)}$ and $n^{(2)}$ are ‘nearby’ if (4) with $A^{(1)} = A^{(2)}$ holds). We recalculate the preconditioner (corresponding to another realisation of (6)) when the number of GMRES iterations needed to solve $(\mathbf{A}^{(1)})^{-1} \mathbf{A}^{(2)}$ grows too large. With this strategy, we obtain speedup for a range of physically relevant k .

References

[1] M. J. Gander, I. G. Graham and E. A. Spence, Applying GMRES to the Helmholtz equation with shifted Laplacian preconditioning: what is the largest shift for which wavenumber-independent convergence is guaranteed?, *Numerische Mathematik* **131** (3) (2015), pp. 567-614.

[2] F. Y. Kuo and D. Nuyens, Application of Quasi-Monte Carlo Methods to Elliptic PDEs with Random Diffusion Coefficients: A Survey of Analysis and Implementation, *Foundations of Computational Mathematics* **16** (2016), pp. 1631-1696.

[3] I. G. Graham, E. A. Spence and E. Vainikko, Domain decomposition preconditioning for high-frequency Helmholtz problems with absorption, *Mathematics of Computation* **86** (307) (2017), pp. 2089-2127.

[4] I. G. Graham, Owen R. Pembrey and E. A. Spence, The Helmholtz equation in heterogeneous media: A priori bounds, well-posedness, and resonances, *Journal of Differential Equations* **266** (6) (2019), pp. 2869-2923.

Generalized Plane Waves & Maxwell's equations

Lise-Marie Imbert-Gérard^{1,*}, Jean-François Fritsch²¹Department of Mathematics, University of Maryland, College Park, USA²ENSTA-ParisTech, Palaiseau, France

*Email: lmig@math.umd.edu

Abstract

Modeling for wave propagation in magnetically confined plasma motivates the development of numerical methods for smooth variable coefficient time-harmonic Maxwell's equations. The simplest of these models, the cold plasma model, reads

$$\nabla \times \nabla \times \mathbf{E} - \kappa^2 \epsilon \mathbf{E} = 0 \quad (1)$$

where the 3×3 tensor epsilon is both homogeneous and anisotropic. Generalized Plane Waves (GPWs) were introduced in the 2D variable refractive index Helmholtz framework. These functions are constructed to satisfy approximately the PDE, and a set of linearly independent GPWs can easily be constructed for discretization purposes. They were designed as exponential of polynomials, using Taylor expansions. The first extension of the GPW construction to the 3D vector-valued Maxwell's equation is introduced, including a discussion on possible ansatz for the amplitude and phase functions, and emphasizing the challenges related to the construction algorithm.

Keywords: Generalized Plane Waves, Time-harmonic Maxwell, variable coefficients.

1 Introduction

GPWs have been introduced in the framework of Trefftz methods: Trefftz methods are Galerkin methods that rely on basis functions chosen as local solutions to the homogeneous partial differential equation (PDE), but for variable coefficient PDEs such solutions are generally not available; GPWs are basis functions tailored for a given partial differential operator \mathcal{L} to solve locally approximately the homogeneous PDE $\mathcal{L}\varphi \approx 0$.

They were first initially proposed, in two dimensions, for scalar Helmholtz operator:

$$\mathcal{L}_H := -\Delta - \kappa^2 \eta(\mathbf{x})$$

with a scalar coefficient η , see [1, 2], were then coupled to a Trefftz formulation in [4], and were

also used to study mode conversion for the following operator:

$$\mathcal{L}_{MC} := \left(\partial_x^2 + (d + \bar{d}) \partial_x \partial_y + |d|^2 \partial_y^2 \right. \\ \left. + (d - \bar{d}) x \partial_y - \left(1 + \frac{1}{\mu} + x(x+y) \right) \right),$$

with parameters $(d, \mu) \in \mathbb{C}^2$.

A GPW φ associated to a partial differential operator \mathcal{L} was designed as an approximated solution in the following sense: it is constructed locally, at a point \mathbf{x}_0 to ensure that the Taylor expansion of $\mathcal{L}\varphi$ at \mathbf{x}_0 cancels up to a given order q .

2 GPW ansatz, vector-valued operators & normalization

For scalar valued operators, the original GPW ansatz studied in [2] corresponds to adding high order terms to the phase function of a classical plane wave $\mathbf{x} \mapsto \exp i\kappa \mathbf{d} \cdot (\mathbf{x} - \mathbf{x}_0)$ for a given direction \mathbf{d} with $|\mathbf{d}| = 1$:

$$\varphi(\mathbf{x}) = \exp(i\kappa \mathbf{d} \cdot (\mathbf{x} - \mathbf{x}_0) + H.O.T.)$$

where the higher order terms *H.O.T.* were constructed to ensure that $\mathcal{L}\varphi(\mathbf{x}) = O(\|\mathbf{x} - \mathbf{x}_0\|^q)$.

A vector valued classical plane wave, $\mathbf{x} \mapsto \mathbf{p} \exp i\kappa \mathbf{d} \cdot (\mathbf{x} - \mathbf{x}_0)$, has a direction \mathbf{d} with $|\mathbf{d}| = 1$ as in the scalar valued case, but also has a polarization \mathbf{p} . Hence for vector valued operators, there is a priori several possibilities to define a GPW starting from a classical plane wave, since higher order corrections could be added either to the phase function or to the amplitude function: each component of a GPW could be designed as follows:

$$\phi_\alpha(\mathbf{x}) = (\mathbf{p}_\alpha + H.O.T.) \exp(i\kappa \mathbf{d} \cdot (\mathbf{x} - \mathbf{x}_0) + H.O.T.).$$

However, as described in [3], it is natural to preserve the fact that each component of a GPW, as those of a classical plane wave, have the same unique phase function: we therefore propose to study the construction of vector-valued GPWs constructed with the ansatz

$$\phi_\alpha(\mathbf{x}) = (\mathbf{p}_\alpha + H.O.T.) \exp i\kappa \mathbf{d} \cdot (\mathbf{x} - \mathbf{x}_0). \quad (2)$$

The normalization of a GPW, corresponding to choosing the lowest order terms of its phase and amplitude functions, is performed naturally following the compatibility conditions between the phase and amplitude of a classical plane wave in the constant coefficient case. The challenge, in order to construct GPWs to satisfy the Taylor approximation $\mathcal{L}\phi(\mathbf{x}) = O(\|\mathbf{x} - \mathbf{x}_0\|^q)$, then lies in the construction of a solution to the system coupling the higher order terms of the components (2) of the amplitude of ϕ .

3 Maxwell's equations

In the particular case of Maxwell's equations (1), the normalization condition reads:

$$\mathbf{d} \times \mathbf{d} \times \mathbf{p}(\mathbf{x}_0) - \kappa^2 \epsilon(\mathbf{x}_0) \mathbf{p}(\mathbf{x}_0) = 0.$$

It corresponds, see [3], to the WKB approximation in the high frequency regime. The construction of a GPW $\phi(\mathbf{x}) = \mathbf{A}(\mathbf{x}) \exp i\kappa \mathbf{d} \cdot (\mathbf{x} - \mathbf{x}_0)$, as in the scalar case, relies on a careful study of the quantity:

$$\begin{aligned} \mathcal{L}\phi(\mathbf{x}) &= \kappa^2 \left[-\mathbf{d} \times \mathbf{d} \times \mathbf{A} - \epsilon \mathbf{A} \right] e^{i\kappa \mathbf{d} \cdot (\mathbf{x} - \mathbf{x}_0)} \\ &\quad + i\kappa \left[\mathbf{d} \times \nabla \times \mathbf{A} \right] e^{i\kappa \mathbf{d} \cdot (\mathbf{x} - \mathbf{x}_0)} \\ &\quad + \left[\nabla \times \nabla \times \mathbf{A} \right] e^{i\kappa \mathbf{d} \cdot (\mathbf{x} - \mathbf{x}_0)}. \end{aligned}$$

Thanks to the choice of a unique phase function, it is sufficient to construct the amplitude function \mathbf{A} to cancel the Taylor expansion, up to order q , of the following quantity:

$$\begin{aligned} \mathbf{Q}(\mathbf{x}) &:= -\kappa^2 \mathbf{d} \times \mathbf{d} \times \mathbf{A} - \epsilon \mathbf{A} \\ &\quad + i\kappa \mathbf{d} \times \nabla \times \mathbf{A} + \nabla \times \nabla \times \mathbf{A}. \end{aligned}$$

The the amplitude components $\mathbf{A}_\alpha(\mathbf{x})$ are constructed as polynomials, denoted

$$\sum_{0 \leq i+j+k \leq \text{deg}_\alpha} \lambda_{i,j,k}^\alpha (x - x_K)^i (y - y_K)^j (z - z_K)^k,$$

thanks to a careful examination of the system obtained from canceling the Taylor expansion terms of \mathbf{Q} :

$$\forall (i, j, k) \in \mathbb{N}^3, i + j + k < q, \partial_x^i \partial_y^j \partial_z^k \mathbf{Q}(\mathbf{x}) = 0$$

Despite the coupling of the three components of \mathbf{A} in \mathbf{Q} , we will present an algorithm to construct a solution to this system, and as in the scalar case this will be achieved via the construction of an analytic formula.

References

[1] L.-M. Imbert-Gerard, & B. Després, A generalized plane-wave numerical method for smooth nonconstant coefficients, *IMA Journal of Numerical Analysis*, (2014) **34** (3): 1072–1103, doi:10.1093/imanum/drt030.

[2] L.-M. Imbert-Gérard, Interpolation properties of generalized plane waves, *Numerische Mathematik* (2015) doi:10.1007/s00211-015-0704-y.

[3] L.-M. Imbert-Gérard, Generalized Plane Waves, variable amplitude and vector valued equations, *The 12th International Conference on Mathematical and Numerical Aspects of Wave Propagation Book of abstracts* (2017).

[4] L.-M. Imbert-Gerard, & P. Monk, Numerical simulation of wave propagation in inhomogeneous media using Generalized Plane Waves, *M2AN* (2017) doi:10.1051/m2an/2016067.

Frequency-domain wave propagation in hyperbolic metamaterials

Patrick Ciarlet¹, Maryna Kachanovska^{2,*}

¹POEMS (UMR CNRS-ENSTA-INRIA), ENSTA ParisTech, Palaiseau, France

²POEMS (UMR CNRS-ENSTA-INRIA), INRIA, Palaiseau, France

*Email: maryna.kachanovska@inria.fr

Abstract

In this work we address the question of theoretical justification of problems arising in the wave propagation in hyperbolic metamaterials [1]. Such phenomena are described by anisotropic, dispersive Maxwell equations, which, in the frequency domain, correspond to a problem that is hyperbolic for a range of frequencies. For a particular case of such materials (highly magnetized plasmas), we prove the well-posedness of the corresponding model in the free space, providing a suitable radiation condition, as well as study its regularity and demonstrate the limiting amplitude and limiting absorption principles.

Keywords: hyperbolic metamaterials, radiation condition, Maxwell equations, limiting amplitude principle, limiting absorption principle

1 Introduction

We consider the wave propagation in hyperbolic metamaterials, for the simplest case of the 2D strongly magnetized plasma. In the time domain, it is modelled by the Maxwell's equations

$$\partial_t E_x - \partial_y H_z = 0, \quad (1)$$

$$\partial_t E_y + \partial_x H_z + \omega_p j_y = 0, \quad \partial_t j_y = \omega_p E_y,$$

$$\partial_t H_z + \partial_x E_y - \partial_y E_x = f(x, t), \quad (x, t) \in \mathbb{R}^2 \times \mathbb{R}_+,$$

with given initial conditions. The energy

$$E(t) = \frac{1}{2} (\|E_x\|^2 + \|E_y\|^2 + \|H_z\|^2 + \|j_y\|^2)$$

is preserved in the absence of sources ($f = 0$).

With $\hat{u} = \mathcal{F}u = \frac{1}{\sqrt{2\pi}} \int_0^\infty e^{i\omega t} u(t) dt$, and assuming zero initial conditions, we can rewrite the above problem in the frequency domain as follows:

$$\begin{aligned} \omega^2 \hat{H}_z + \partial_y^2 \hat{H}_z + \varepsilon_\perp(\omega)^{-1} \partial_x^2 \hat{H}_z &= i\omega \hat{f}, \\ \varepsilon_\perp(\omega) &= \left(1 - \frac{\omega_p^2}{\omega^2}\right), \quad x \in \mathbb{R}^2. \end{aligned} \quad (2)$$

Thus, for $0 < \omega < \omega_p$ the above problem is hyperbolic (Klein-Gordon equation), and for $\omega >$

ω_p it is elliptic. Here we address the hyperbolic regime. A similar problem, but in a different setting, was studied in [2].

2 Well-posedness in the hyperbolic case

We start with the case with absorption ($\omega \notin \mathbb{R}$), and next consider the case $\omega \in \mathbb{R}$.

Theorem 1 (Case with absorption) *Let $\omega \in \mathbb{C} \setminus \mathbb{R}$. For any $\hat{f} \in L^2(\mathbb{R}^2)$, the problem (2) has a unique solution $\hat{H}_z \in H^1(\mathbb{R}^2)$. Moreover, $\|\hat{H}_z\|_{H^1} \leq C(\omega) \|\hat{f}\|_{L^2}$.*

The solution to (2), when $\Im\omega \neq 0$, is given by convolution of \hat{f} with the corresponding fundamental solution G_ω . Taking $\omega = \omega_0 + i\varepsilon$, $0 < \omega_0 < \omega_p$, $\varepsilon \rightarrow 0+$, it is possible to show the existence of a solution to (2) with $\omega = \omega_0$. The uniqueness is assured with the help of a radiation condition. We suggest to use a radiation condition which resembles the Fourier radiation condition in the rough surface scattering [4]. Let

$$\mathcal{F}_x u(k_x, y) = \frac{1}{\sqrt{2\pi}} \int_{-\infty}^{\infty} e^{ik_x x} u(x, y) dx.$$

Let us fix $0 < \omega < \omega_p$; importantly, $\varepsilon_\perp(\omega) < 0$.

Definition 2 (Radiation Condition) *A function \hat{H}_z satisfies the radiation condition (RC) if*

- $\hat{H}_z(\cdot, y) \in L^2(\mathbb{R})$ for all $y \in \mathbb{R}$ (a.e.)
- $\mathcal{F}_x \hat{H}_z$ satisfies for all $k_x \in \mathbb{R}$ (a.e.),

$$\lim_{|y| \rightarrow +\infty} \left(\partial_{|y|} - i\sqrt{-\frac{k_x^2}{\varepsilon_\perp(\omega)} + \omega^2} \right) \mathcal{F}_x \hat{H}_z = 0.$$

To formulate the well-posedness result, we will need the anisotropic weighted Sobolev spaces:

$$\|u\|_{\perp, s}^2 = \int_{\mathbb{R}^2} (1 + |y|^2)^s |u(x, y)|^2 dx dy, \quad s \in \mathbb{R},$$

$$L_{\perp, s}^2 = \{u \in L_{loc}^2(\mathbb{R}^2) : \|u\|_{\perp, s} < \infty\},$$

$$H_{\perp, s}^1 = \{u \in L_{loc}^2(\mathbb{R}^2) : \|u\|_{\perp, s}^2 + \|\nabla u\|_{\perp, s}^2 < \infty\}$$

We assume throughout that $s > \frac{1}{2}$. The principal result of this section reads.

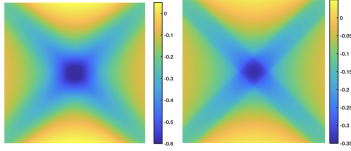


Figure 1: $\text{Im } \hat{H}_z$, for $\hat{f} = \mathbf{1}\{x \in \Omega\} \in \bigcap_{\varepsilon > 0} H^{\frac{1}{2}-\varepsilon}$.

Left: $\Omega = [-1, 1]^2$. Here $\hat{H}_z \in H_{loc}^{\frac{5}{2}-\varepsilon}$, $\varepsilon > 0$.
 Right: $\Omega = R_{\frac{\pi}{4}}[-1, 1]^2$ (R_ϕ is a rotation by ϕ).
 In this case $\hat{H}_z \in H_{loc}^{\frac{3}{2}-\varepsilon}$, $\varepsilon > 0$, $\hat{H}_z \notin H_{loc}^{\frac{3}{2}}$.

Theorem 3 (Case without absorption) *Let $0 < \omega < \omega_p$. For all $\hat{f} \in L_s^2(\mathbb{R}^2)$, the problem (2) equipped with the radiation condition (RC) admits a unique solution $\hat{H}_z \in H_{1,-s}^1(\mathbb{R}^2)$. Also, there exists $C > 0$, s.t. for all $\hat{f} \in L_s^2(\mathbb{R}^2)$,*

$$\|\hat{H}_z\|_{H_{1,-s}^1} \leq C \|\hat{f}\|_{L_{1,s}^2}.$$

Let us define the resolvent for (2): $N_\omega \hat{f} = \hat{H}_z$, $N_\omega \in \mathcal{B}(L_{1,s}^2, H_{1,-s}^1)$. It is analytic in $\omega \in \mathbb{C} \setminus \mathbb{R}$, and is continued to $(0, \omega_p)$ according to Thm 3.

Theorem 4 (Limit. absorp., $\omega \in (0, \omega_p)$) *For all $\hat{f} \in L_{1,s}^2$,*

$$\lim_{\varepsilon \rightarrow 0^+} N_{\omega+i\varepsilon} \hat{f} = N_\omega \hat{f} \text{ in } H_{1,-s}^1.$$

3 Regularity in the hyperbolic case

In the elliptic regime ($\omega > \omega_p$), $\hat{H}_z \in H_{loc}^2(\mathbb{R}^2)$, while in the hyperbolic it holds only that $\hat{H}_z \in H_{loc}^1(\mathbb{R}^2)$. Denoting by $L_{comp}^2 = \{u \in L^2 : u \text{ is compactly supported}\}$, we obtain

Theorem 5 *Let $0 < \omega < \omega_p$. Then*

$$N_\omega \in \mathcal{B}(L_{comp}^2, H_{1,-s}^{1+\sigma}) \iff \sigma \leq 0.$$

This result can be refined: it appears that reduced regularity is induced by the lines of discontinuity of \hat{f} , which are aligned with characteristics of (2), see Figure 1. Solutions are computed with the help of the PMLs of [5].

4 Limiting amplitude principle

Adapting the classical proof of the limiting amplitude principle by Eidus [3], we obtain

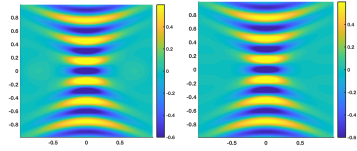


Figure 2: Left: limiting amplitude solution $\lim_{t \rightarrow \infty} \text{Re}(H_z e^{-i\omega t})$, where H_z solves (1) with $f = e^{i\omega t} g(x)$.

Right: limit. absorpt. sol. $\lim_{\varepsilon \rightarrow 0^+} \text{Re } \hat{H}_z(\omega_0 + i\varepsilon)$ where \hat{H}_z solves (2) with $\hat{f} = \hat{g}$

Theorem 6 (Limit. amplit., $\omega \in (0, \omega_p)$) *Given $f(x, t) = e^{i\omega t} g(x)$, $g(x) \in L_s^2$, let H_z solve (1) and \hat{H}_z solve (2) with \hat{f} replaced by \hat{g} , equipped with the radiation condition (RC). Then*

$$\lim_{t \rightarrow +\infty} \|H_z(t) - \hat{H}_z e^{i\omega t}\|_{L_{1,s}^2} = 0.$$

This result is shown in Figure 2 ($0 < \omega_0 < \omega_p$).

5 Future work

A continuation of this work consists in the development of accurate numerical methods for (2) and studying frequency-domain hyperbolic problems in more general geometric configurations (bounded domains, higher dimensions).

References

- [1] A. Poddubny, I. Iorsh, P. Belov, Yu. Kivshar, Hyperbolic metamaterials. *Nature Photon.* 7, 948–957 (2013)
- [2] E. Bonnetier, H.-M. Nguyen, Superlensing using hyperbolic metamaterials: the scalar case. *JEP (Mathématiques)*, Vol. 4 (2017), p. 973-1003.
- [3] D. M. Eidus, The principle of limiting amplitude. *Uspehi Mat. Nauk* 24 (1969), no. 3(147), 91–156.
- [4] T. Arens, T. Hohage, On radiation conditions for rough surface scattering problems. *IMA J. Appl. Math.* (2005) 70, 839–847.
- [5] E. Bécache, M. Kachanovska, Stable perfectly matched layers for a class of anisotropic dispersive models. Part I: necessary and sufficient conditions of stability. *ESAIM: M2AN*, vol. 51, 6, pp. 2399 – 2434, 2017.

Hamiltonian structure of the cold-plasma model and its discretization

Omar Maj^{1,*}, Eric Sonnendrücker¹, Olivier Lafitte², Philip J. Morrison³

¹Max Planck Institute for Plasma Physics, D-85748 Garching, Germany.

²Université Paris 13, Sorbonne Paris Cité, LAGA (UMR 7539) 93430 - Villetaneuse, France.

³Department of Physics and Institute for Fusion Studies, University of Texas, Austin, USA.

*Email: Omar.Maj@ipp.mpg.de

Abstract

In this work we consider Maxwell's equations coupled to an evolution equation for the electric current density. The coupled system is known as the cold-plasma model and describes high-frequency waves in magnetically confined plasmas, with application in nuclear fusion research. We show formally that the system has a natural Hamiltonian structure, which can be exploited in order to design a structure-preserving numerical scheme.

Keywords: Electromagnetic waves; Hamiltonian systems; Finite element exterior calculus.

1 Introduction

In certain conditions, the propagation of electromagnetic waves in a magnetized plasma can be described by the *cold-plasma model*, which comprises Maxwell's equations coupled to an evolution equation for the current density induced in the plasma by the wave electric field (cf. Brambilla [1] for a physics derivation and the validity conditions of the cold-plasma model). The system of equations reads

$$\begin{cases} \partial_t E = \text{curl } B - \omega_p Y, \\ \partial_t B = -\text{curl } E, \\ \partial_t Y = \omega_p E - Y \times \omega_c, \end{cases} \quad (1)$$

with the constraint

$$\text{div } B = 0, \quad (2)$$

where E, B are the electromagnetic fields of the wave, Y is proportional to the induced current density, and the dimensionless coefficients $\omega_p = \omega_p(x) \in \mathbb{R}_+$ and $\omega_c = \omega_c(x) \in \mathbb{R}^3$ depend on the spatial position $x = (x_1, x_2, x_3)$ in a domain Ω . Time and spatial coordinates are normalized to a given frequency ω_0 and to the corresponding wave number ω_0/c , respectively, with c being the speed of light in free space.

For simplicity, let the domain Ω be either the full space \mathbb{R}^3 or the torus $(\mathbb{R}/2\pi\mathbb{Z})^3$, hence

$\partial\Omega = \emptyset$, and let Cauchy data

$$E(0) = E_0, \quad B(0) = B_0, \quad Y(0) = Y_0, \quad (3)$$

be given at $t = 0$, with $\text{div } B_0 = 0$.

Formally, the L^2 -norm of $u = (E, B, Y)$ is constant for a solution of system (1), that is, the total energy

$$H(u) = \frac{1}{2} (\|E\|_{L^2}^2 + \|B\|_{L^2}^2 + \|Y\|_{L^2}^2), \quad (4)$$

is preserved.

Motivated by many applications in plasma physics, several codes have been developed for the cold-plasma model. Most of these codes implement the standard Yee scheme [2] enhanced with an *ad hoc* update rule for the current density. The Yee scheme is an energy preserving variational scheme for Maxwell's equations [3], but the choice of the update rule for the current density may destroy such desirable properties; for instance, special care needs to be taken in order to ensure energy conservation [4].

In this work we show that system (1) defines an infinite-dimensional Hamiltonian system [5] and constraint (2) corresponds to a family of Casimir invariants. We use this fact to obtain a structure-preserving numerical scheme.

2 Hamiltonian structure

A Poisson structure on a Banach space U is a Lie-algebra structure on $C^\infty(U) = C^\infty(U, \mathbb{R})$ satisfying the Leibniz rule, that is, a bi-linear anti-symmetric map $\{\cdot, \cdot\} : C^\infty(U) \times C^\infty(U) \rightarrow C^\infty(U)$, called Poisson brackets, satisfying the Leibniz and Jacobi identities,

$$\begin{aligned} \{F, GH\} &= \{F, G\}H + \{F, H\}G, \\ \{F, \{G, H\}\} &+ \{G, \{H, F\}\} + \{H, \{F, G\}\} = 0, \end{aligned}$$

for all $F, G, H \in C^\infty(U)$.

An evolution equation for $u \in C^1(\mathbb{R}, U)$ of the form $du/dt = f(u)$, where $f : U \rightarrow U$, is Hamiltonian if there exist a Poisson structure

$\{ \cdot, \cdot \}$ and a functional $H \in C^\infty(U)$, referred to as the Hamiltonian, such that

$$\frac{d}{dt}F(u(t)) = \{F, H\}(u(t)), \quad (5)$$

for all functional $F \in C^\infty(U)$.

With $u = (E, B, Y)$, we define formally

$$\{F, G\} = \{F, G\}_0 + \{F, G\}_p - \{F, G\}_c, \quad (6)$$

where

$$\begin{aligned} \{F, G\}_0 &= \int_{\Omega} \left[\operatorname{curl} \frac{\delta F}{\delta E} \cdot \frac{\delta G}{\delta B} - \operatorname{curl} \frac{\delta G}{\delta E} \cdot \frac{\delta F}{\delta B} \right] dx, \\ \{F, G\}_p &= \int_{\Omega} \omega_p \left[\frac{\delta F}{\delta Y} \cdot \frac{\delta G}{\delta E} - \frac{\delta G}{\delta Y} \cdot \frac{\delta F}{\delta E} \right] dx, \\ \{F, G\}_c &= \int_{\Omega} \omega_c \cdot \left[\frac{\delta F}{\delta Y} \times \frac{\delta G}{\delta Y} \right] dx, \end{aligned}$$

with all functional derivatives computed with respect to the L^2 -pairing. Brackets (6) define an anti-symmetric bi-linear form which satisfies both the Leibniz and Jacobi identities formally. Upon using (4) as Hamiltonian, equation (5) amounts to a weak formulation of (1).

The divergence constraint (2) is recovered from Casimir invariants, that are all functionals $C \in C^\infty(U)$ such that

$$\{C, F\} = 0, \quad \text{for all } F \in \mathcal{A}.$$

For every scalar function $\varphi = \varphi(x)$,

$$C_\varphi(u) = \int_{\Omega} \varphi \operatorname{div} B dx \quad (7)$$

is a Casimir invariant of brackets (6). If the initial condition satisfies (2), the existence of this family of invariants implies (2) for $t \geq 0$.

3 Finite element exterior calculus

Let us assume $\omega_p \in L^\infty(\Omega)$, $\omega_c \in (L^\infty(\Omega))^3$. The variable $u = (E, B, Y) \in U$ is approximated by $u_h \in U_h = V_1 \times V_2 \times V_1$, with conforming spaces V_j such that the diagram

$$\begin{array}{ccccccc} H^1(\Omega) & \rightarrow & H(\operatorname{curl}, \Omega) & \rightarrow & H(\operatorname{div}, \Omega) & \rightarrow & L^2(\Omega) \\ \downarrow \pi_0 & & \downarrow \pi_1 & & \downarrow \pi_2 & & \downarrow \pi_3 \\ V_0 & \rightarrow & V_1 & \rightarrow & V_2 & \rightarrow & V_3 \end{array}$$

is commutative and each row is an exact sequence. Here the arrows represent the operators grad, curl, and div respectively in the upper row and their discrete counterparts in the lower

row. Possible choices of the discrete spaces V_j are available [6, 7].

We denote by $\mathbf{u} \in \mathbb{R}^N$ the vector of degrees of freedom of the discrete field $u_h \in U_h$. The restriction of a functional F to U_h amounts to a function $\mathbf{F} = \mathbf{F}(\mathbf{u}) = F(u_h)$ on \mathbb{R}^N . The discretization of (5) then reads

$$\frac{d}{dt}\mathbf{F}(\mathbf{u}(t)) = \{\mathbf{F}, \mathbf{H}\}_h(\mathbf{u}(t)), \quad (8)$$

for all $\mathbf{F} \in C^\infty(\mathbb{R}^N)$, where the discrete brackets $\{\mathbf{F}, \mathbf{G}\}_h = \nabla_{\mathbf{u}} \mathbf{F} \cdot \mathbf{P} \nabla_{\mathbf{u}} \mathbf{G}$, with \mathbf{P} a constant anti-symmetric matrix (the Poisson tensor), define a Poisson structure on \mathbb{R}^N and admit a family of Casimir invariants corresponding to (7). The Hamiltonian structure is preserved, and the discrete energy $\mathbf{H}(\mathbf{u}(t))$ of a solution is constant.

Equation (8) has to be integrated in time. Since \mathbf{H} is quadratic, the problem reduces to a linear evolution equation and it is sufficient to evaluate the matrix exponential. On the other hand the Hamiltonian structure opens the way to integrators based on splitting either the Poisson brackets (preserving energy) or the Hamiltonian (preserving the Poisson structure). In Hamiltonian splitting, it is critical to find an exact solution of each step. To this end, we introduce a time-dependent change of variables which yields time-dependent Poisson brackets, and show how such a structure can be useful.

References

- [1] M. Brambilla, *Kinetic Theory of Plasma Waves*, Oxford Un. Press, Oxford, 1998.
- [2] A. Taflove and S. Hagness, *Computational Electrodynamics*, Artech House, 2005.
- [3] A. Stern et al., in *Geometry, Mechanics, and Dynamics: The Legacy of Jerry Marsden*, Springer, New York 2015, pp. 437–425.
- [4] F. da Silva et al., *Journal of Computational Physics* **295** (2015), pp. 24–45.
- [5] P. Morrison, *Rev. Mod. Phys.* **70** (1998), pp. 467–521.
- [6] D. Arnold, R. Falk and R. Winther, *Acta numerica* **15** (2006), pp. 1–155.
- [7] A. Ratnani and E. Sonnendrücker, *J. Sci. Comput.* **51** (2012), pp. 87–106.

Finite element discretizations of high-frequency wave propagation problems in heterogeneous media

T. Chaumont-Frelet^{1,*}, S. Nicaise²

¹Univ. Côte d'Azur, Inria, CNRS, LJAD, France

²Univ. Valenciennes, LAMAV, France

*Email: theophile.chaumont@inria.fr

Abstract

We analyze the convergence of finite element discretizations of time-harmonic wave propagation problems. We propose a general methodology to derive stability conditions and error estimates that are explicit with respect to the frequency. The method is developed under general assumptions and is illustrated on particular cases including the propagation of acoustic and elastic waves in heterogeneous media. We provide numerical experiments that illustrate our analysis and indicate that our results are sharp.

Keywords: Helmholtz problems; High order methods; Finite element methods; Pollution effect

Time-harmonic wave propagation problems arise in a variety of applications, which motivate the design of efficient and robust simulation tools. When the domain of propagation is heterogeneous, finite element methods (FEMs) are routinely employed to discretize the problem.

While FEMs are very efficient to accurately take into account complex geometries, they suffer from the so-called “pollution effect” in the high-frequency regime where the domain of propagation is large compared to the characteristic wavelength [2]. This “pollution effect” manifests itself by a loss of stability of FEMs when the frequency is high. Specifically, there is a gap between the error of the finite element solution, and the one of the best possible representation of the continuous solution in the discrete space.

The pollution effect has been thoroughly studied in the literature for the propagation of acoustic waves in homogeneous media [2–4]. The key conclusions of these works is that the pollution effect can be eliminated if the mesh size h is sufficiently small. More precisely, in the case of a non-trapping problem at angular frequency ω , the authors show that the pollution effect vanishes under the condition that

$$\omega^{p+1}h^p \leq C, \quad (1)$$

where p is the degree of the polynomial basis functions and C is a generic constant that is independent of h and ω . We can restate stability condition (1) as

$$N_\lambda \geq C\omega^{1/p} \quad (2)$$

where $N_\lambda = (\omega h)^{-1}$ is the number of elements per wavelength. A key observation is that high order FEMs are less sensitive to the pollution effect, as stability condition (2) is less restrictive when p is large.

Stability condition (1) is established using an approach known as the “Schatz argument” [5]. The crucial step of the proof is a duality technique in which a solution to the wave propagation problem with an $L^2(\Omega)$ right-hand side is introduced. The stability of the FEM is then linked to the ability of the discrete space to approximate the aforementioned solution. As this dual right-hand only belongs to $L^2(\Omega)$, the corresponding solution possesses low regularity, and it is not clear why high-order methods are performant. As a result, the key idea introduced in [3] is to perform a “regularity splitting” where the dual solution is decomposed into two components. The first component belongs to $H^2(\Omega)$ only, but its norm does not grow as the frequency increases. The other component is highly oscillatory and analytic. It is the dominant part in the high-frequency regime, and since it is smooth, it is efficiently captured by high-order FEMs, which explains there enhanced stability.

The regularity splitting introduced in [2, 3] focuses on the acoustic Helmholtz equation in homogeneous media. As the proposed splitting heavily relies on the Green’s function of the wave operator, it is not clear how it can be extended to more complex wave propagation systems, including heterogeneous media.

In this work, we propose a new strategy to derive stability condition (1) in more general settings [1]. Specifically, we consider a problem

of the form

$$-\omega^2 \mathcal{L}_0 u - i\omega \mathcal{L}_1 u + \mathcal{L}_2 u = f \text{ in } \Omega,$$

with additional boundary conditions that we discretize with a FEM of order p . We assume that the operators \mathcal{L}_j satisfy

$$\begin{aligned} \|\mathcal{L}_0 v\|_{\ell,\Omega} &\leq C\|v\|_{\ell,\Omega}, \\ \|\mathcal{L}_1 v\|_{\ell,\Omega} &\leq C\|v\|_{\ell+1,\Omega}, \\ \|\mathcal{L}_2^{-1} v\|_{\ell+2,\Omega} &\leq C\|v\|_{\ell,\Omega}, \end{aligned} \quad (3)$$

for all $v \in C^\infty(\bar{\Omega})$ and $0 \leq \ell \leq p-1$. This hypothesis is rather general, as it is satisfied if the boundary of Ω and the heterogeneous coefficients appearing in the operators \mathcal{L}_j are sufficiently smooth. In addition, we can weaken this hypothesis by assuming piecewise smoothness only.

Instead of relying on the Green's function, our analysis exploits the expansion

$$u = \sum_{j=0}^{p-1} \omega^j u_j + r_p, \quad (4)$$

where the $u_j \in H^{j+2}(\Omega)$ are iteratively defined and independent of ω , and $r_p \in H^{p+1}(\Omega)$ is a remainder, whose norm is controlled explicitly in ω . Then, we employ splitting (4) within the Schatz argument technique to establish (2).

We derive the method in generality under assumption (3) on the domain of propagation and the differential operators appearing in the boundary value problem. We illustrate our analysis on acoustic, convected and elastic Helmholtz equations in heterogeneous media.

In Figure 1, we have simulated the propagation of a superposition of elastic plane waves with a FEM of degree p for different frequencies ω and mesh sizes h . In each case, we compute both the finite element error, and the best approximation error. For a given frequency ω , we denote by $h^*(\omega)$ the largest value of h such that

$$|u - u_h|_{1,\Omega} \leq 2|u - \pi_h u|_{1,\Omega}$$

for all $h \leq h^*(\omega)$, where u_h and $\pi_h u$ are the finite element solution and the best approximation of u . The curves presented on Figure 1 show that $h^*(\omega) \simeq \omega^{-1-1/p}$, which is in agreement with stability condition (1).

The main conclusion of our work is that, as in the case of acoustic wave propagation in homogeneous media, high order FEMs are less sensitive to the pollution effect, and should be preferred in the high-frequency regime.

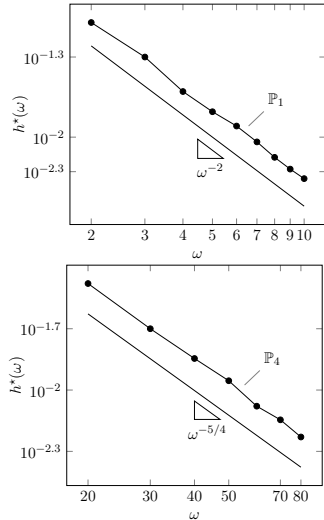


Figure 1: Asymptotic ranges $h^*(\omega)$ for \mathbb{P}_1 (top) and \mathbb{P}_4 (bottom) elements

References

- [1] T. Chaumont-Frelet and S. Nicaise, Wavenumber explicit convergence analysis for finite element discretization wave propagation problems, accepted for publication in *IMA J. Numer. Anal.* (2019) preprint: [hal-01685388](https://hal.archives-ouvertes.fr/hal-01685388).
- [2] F. Ihlenburg and I. Babuška, Finite element solution of the Helmholtz equation with high wave number. Part II: The h - p version of the FEM, in *SIAM J. Numer. Anal.* **34**, pp 315–358.
- [3] J.M. Melenk and S.A. Sauter, Convergence analysis for finite element discretizations of the Helmholtz equation with Dirichlet-to-Neumann boundary conditions, in *Math. Comp.* **79** (2010), pp. 1871–1914.
- [4] J.M. Melenk and S.A. Sauter, Wavenumber explicit convergence analysis for Galerkin discretizations of the Helmholtz equation, in *SIAM J. Numer. Anal.* **49** (2011) pp. 1210–1243.
- [5] A.H. Schatz, An observation concerning Ritz-Galerkin methods with indefinite bilinear forms, in *Math. Comp.*, **28**, (1974) pp. 959–962.

Two wave localisation effects and their impact on numerical simulation

Céline Torres^{1,*}, Stefan Sauter¹¹University of Zurich

*Email: celine.torres@math.uzh.ch

Abstract

We study the wave propagation in \mathbb{R}^d modelled in the frequency domain by the Helmholtz equation in heterogeneous media. In particular, we are interested in media with highly oscillating contrast and derive stability estimates which are explicit in the wave number and wave speed of the media. We consider two different mechanisms of wave localisations: (a) Wave localisation appearing at a single discontinuity in the geometry or the material (“whispering gallery” modes), (b) wave localisation caused by highly varying wave speed. The latter can be studied in an isolated way in 1D, since whispering gallery modes are absent in this regime.

Keywords: stability, resonance, localisation, heterogeneous Helmholtz

1 Setting

We consider the Helmholtz Equation of the form

$$-\Delta u - \left(\frac{\omega}{c}\right)^2 u = f \text{ in } \Omega \quad (1a)$$

for a bounded Lipschitz domain Ω , right hand side $f \in L^2(\Omega)$ and a wave number ω in \mathbb{R} , corresponding to the “pure” Helmholtz problem (for wave scattering in lossy media ω is complex valued and its stability is analysed, e.g., in [3]). We impose impedance boundary conditions

$$\frac{\partial u}{\partial n} - i\frac{\omega}{c}u = g \text{ on } \partial\Omega. \quad (1b)$$

Existence and uniqueness for a bounded wave speed c s.t. $\frac{1}{c} \in L^\infty(\Omega)$ is proved by the Fredholm alternative (see [2] for details). We are interested in the stability of the solution of (1) with variable and possibly non-smooth or oscillatory coefficients.

Conjecture 1 *For any bounded Lipschitz domain $\Omega \subset \mathbb{R}^d$, $c \in L^\infty(\Omega)$, with $0 < c_{\min} \leq c \leq c_{\max} < \infty$, $\omega \geq \omega_0 > 0$ the stability constant C_{stab} in*

$$\left(\int_{\Omega} |\nabla u|^2 + \left(\frac{\omega}{c}\right)^2 |u|^2 \right)^{\frac{1}{2}} \leq C_{\text{stab}} \left(\|f\|_{L^2(\Omega)}^2 + \|g\|_{H^{1/2}(\partial\Omega)}^2 \right)^{\frac{1}{2}}. \quad (2)$$

satisfies

$$C_{\text{stab}} \leq C_1 \exp(C_2 \omega), \quad (3)$$

with $C_1, C_2 > 0$ depending only on c_{\min} , c_{\max} and Ω .

2 Localisation effect in 1D

For the following we assume that the wave speed c is piecewise constant (possibly highly varying). Such situations are also considered in [1]. Our investigation of localisations in 1D is based on a new recursive representation of the Green’s function of the problem. We derive a very simple scalar sequence (Q_j) , represented as iterated Möbius transformations, which has as inputs the wave speed c as a piecewise constant function and the wave number ω and which fully encodes the localisation effect. The sequence can be used to design media which exhibits localisation phenomena (see Fig. 1) at prescribed locations. It turns out that, in order to observe localisation, the number of jumps n needs to be chosen such that $n \sim \omega$, i.e. is “in resonance” with the wave number ω .

We show that Conjecture 1 holds in 1D and for piecewise constant wave speed c . Moreover, we use the sequence (Q_j) to construct explicitly localisation waves as in Fig. 1, we show that the estimate in (3) is sharp.

We note that the effect of localisation is very unstable w.r.t. perturbations of the wave speed, the location of discontinuities, or the wave number and is therefore “rare” in the set of piecewise constant and bounded wave speeds. Our sequence (Q_j) can also be used to find regions in the set of given data (wave speed, position and number of discontinuities,...) where the solution is “well-behaved”, i.e. solutions whose stability constant is independent of ω .

We note that in our analysis, we allow discontinuous wave speeds which are non-periodic, non-monotonic and not a small perturbation of the constant case.

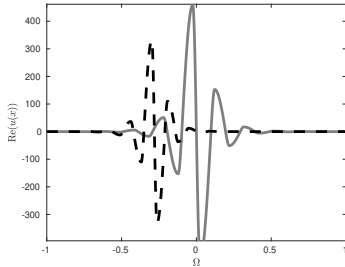


Figure 1: Two examples of a solution u with localisation effect in 1D.

3 Localisation effects in 3D

In contrast to the 1-dimensional case, in 3D we may observe a localisation effect of type (a). A rigorous analysis of these localisation effects can be found in [4, 5], for smooth or discontinuous coefficients with one interface. We present new stability results for discontinuous (in particular highly varying non-periodic) heterogeneous media in 3D. We will see that, besides whispering gallery modes, the solution can also show localisation effects caused by many jumps.

References

- [1] T. Chaumont-Frelet. *Finite element approximation of Helmholtz problems with application to seismic wave propagation*. PhD thesis, INSA de Rouen, Dec. 2015.
- [2] I.G. Graham and S. Sauter. Stability and error analysis for the Helmholtz equation with variable coefficients. *ArXiv e-prints*, Mar. 2018. arXiv:1803.00966
- [3] J.M. Melenk, S. Sauter and C. Torres. Wavenumber-Explicit Analysis for Galerkin Discretizations of Lossy Helmholtz Problems. *ArXiv e-prints*, 2019
- [4] G. Popov and G. Vodev. Resonances near the real axis for transparent obstacles. *Comm. Math. Phys.*, 207(2):411–438, 1999.
- [5] J.V. Ralston. Trapped rays in spherically symmetric media and poles of the scattering matrix. *Comm. Pure Appl. Math.*, 24:571–582, 1971.

- [6] S. Sauter and C. Torres. Stability estimate for the Helmholtz equation with rapidly jumping coefficients. *Zeitschrift für angewandte Mathematik und Physik*, Oct. 2018.
- [7] S. Sauter and C. Torres. Stability estimate for the Helmholtz equation with rapidly jumping coefficients Part 2: the 3-dimensional case. *in prep.*

Domain decomposition methods for heterogeneous Helmholtz problems

Shihua Gong^{1,*}, Ivan G. Graham¹, Euan A. Spence¹¹Department of Mathematical Sciences, University of Bath, Bath BA2 7AY, UK

*Email: sg2328@bath.ac.uk

Abstract

We consider one-level additive Schwarz preconditioners for a family of Helmholtz problems of increasing difficulty (characterised by increasing wavenumber). These are discretized using nodal conforming finite elements of any (fixed) order on fine meshes with mesh diameter chosen to maintain accuracy as the wavenumber increases. The action of the preconditioner requires the solution of independent subproblems (with impedance boundary conditions) on overlapping subdomains. These are linked together using prolongation/restriction operators defined using a partition of unity. In this talk we will study (both theoretically and experimentally) the effect of heterogeneity in the coefficients on the properties of the preconditioner.

1 Previous results

These (and related) preconditioners were studied experimentally in the papers [5–7]. In numerical experiments we observe robust (wavenumber k -independent) GMRES convergence as k increases, with subdomain diameter decreasing moderately as k increases. This provides a highly-parallel, k -robust one-level domain-decomposition method for this class of problems. The cost of the method is dominated by the cost of solving the subdomain problems, but the size of the required direct solves can be reduced by further recursive subdivision (and inner-outer iteration), or by adding an additional coarse space. Supporting theory for this preconditioner in the case of homogeneous Helmholtz problems is given in [7]. A distinctive feature of the theory is that it applies to problems posed on general Lipschitz polyhedral domains such as those which arise from exterior sound-soft scattering problems in truncated domains. The subdomain problems can all be solved in parallel at each iteration and the domain may contain cavities. The theory in the homogeneous case is obtained by considering “nearby” absorptive problems with the level of absorption appropriately chosen so that (a) the preconditioner works well

for the absorptive problem and (b) the absorptive problem is not too far away from the pure Helmholtz problem. [2, 7]. The performance of related preconditioners for Maxwell problems is discussed in [1].

2 This talk

In this talk we will present new theoretical results and numerical experiments for the method when it is applied to heterogeneous Helmholtz problems of the form

$$-\nabla \cdot (A\nabla u) - \omega^2 nu = f$$

subject to mixed impedance/Dirichlet boundary conditions, with variable A and n , where ω is the angular frequency. (The wavenumber $k = \omega$ when $A = I$ and $n = 1$.) We will focus in particular on the role of the ‘non-trapping’ criterion from [3], [4] in the theory and performance of preconditioners.

Keywords: Helmholtz equation, high frequency domain decomposition, absorbing boundary condition, heterogeneity

References

- [1] M. Bonazzoli, V. Dolean, I. G. Graham, E. A. Spence, and P.-H. Tournier, Domain decomposition preconditioning for the high-frequency time-harmonic Maxwell equations with absorption, [arXiv:1711.03789](https://arxiv.org/abs/1711.03789) (2017), to appear in *Mathematics of Computation*.
- [2] M.J. Gander, I.G. Graham, E.A. Spence, Applying GMRES to the Helmholtz equation with shifted Laplacian preconditioning: What is the largest shift for which wavenumber-independent convergence is guaranteed? *Numerische Mathematik* **131** (2015), pp 38-60.
- [3] I.G. Graham, O.R. Pembrey and E.A. Spence, The Helmholtz equation in heterogeneous media: a priori bounds, well-posedness, and resonances, *J. Differ. Equations*, **266** (2019), 2869-2923 .

- [4] I.G. Graham and S.A. Sauter, Stability and error analysis for the Helmholtz equation with variable coefficients. preprint, 2018. [arxiv:1803.00966](https://arxiv.org/abs/1803.00966)
- [5] I. G. Graham, E. A. Spence, and E. Vainikko, *Domain decomposition preconditioning for high-frequency Helmholtz problems with absorption*, Math. Comp., 86 (2017), pp. 2089–2127.
- [6] I. G. Graham, E. A. Spence, and E. Vainikko, *Recent results on domain decomposition preconditioning for the high-frequency Helmholtz equation using absorption*, in Modern solvers for Helmholtz problems, D. Lahaye, J. Tang, and K. Vuik, eds., Birkhauser series in Geosystems Mathematics, 2016.
- [7] I.G. Graham, E.A. Spence and J. Zou, Domain Decomposition with local impedance conditions for the Helmholtz equation, preprint, 2018 <https://arxiv.org/abs/1806.03731>.

Effective equations of arbitrary order for wave propagation in periodic media

Assyr Abdulle¹, **Timothée Pouchon**^{1,*}

¹ANMC, Institute of Mathematics, École Polytechnique Fédérale de Lausanne, Station 8, CH-1015 Lausanne, Switzerland

*Email: timothee.pouchon@epfl.ch

Abstract

While the standard homogenized wave equation describes the effective behavior of the wave at short times, it fails to capture the macroscopic dispersion that appears at long times. To describe the dispersion, the effective model must include additional operators of higher order. In this work, we present a practical way to construct effective equations of arbitrary order in periodic media, with a focus on their numerical approximation. In particular, we exhibit an important structure hidden in the definition of the high order effective tensors which allows a significant reduction of the computational cost for their approximation.

Keywords: homogenization, long time behavior, dispersion

1 Introduction

Let $a(y)$ be a $[0, 1]^d$ -periodic tensor, $\Omega \subset \mathbb{R}^d$ be a hypercube and for $\varepsilon > 0$ let $u^\varepsilon : [0, T] \times \Omega \rightarrow \mathbb{R}$ be the solution of the wave equation

$$\partial_t^2 u^\varepsilon(t, x) - \nabla_x \cdot \left(a\left(\frac{x}{\varepsilon}\right) \nabla_x u^\varepsilon(t, x) \right) = f(t, x), \quad (1)$$

for $(t, x) \in (0, T] \times \Omega$, where we impose Ω -periodic boundary conditions, the initial conditions and the source f are assumed to have $\mathcal{O}(1)$ frequencies and $\mathcal{O}(1)$ support, and Ω is arbitrarily large. To accurately approximate u^ε , standard numerical methods require a grid resolution of order $\mathcal{O}(\varepsilon)$ in the whole domain, which leads to a prohibitive computational cost as $\varepsilon \rightarrow 0$. In the regime $\varepsilon \ll 1$, homogenization theory provides a way to approximate u^ε at a cost that is independent of ε : the result states that $\lim_{\varepsilon \rightarrow 0} u^\varepsilon = u^0$ in $L^\infty(0, T; L^2(\Omega))$, where u^0 solves the *homogenized equation*

$$\partial_t^2 u^0(t, x) - a_{ij}^0 \partial_{ij}^2 u^0(t, x) = f(t, x), \quad (2)$$

equipped with the same initial and boundary conditions as (1). The homogenized tensor a^0 is constant and can be computed by means of (first

order) correctors, solutions of (first order) *cell problems*, i.e., periodic elliptic PDEs in $[0, 1]^d$ involving $a(y)$. In practice, we observe that for long times $t = \mathcal{O}(\varepsilon^{-\alpha})$ $\alpha \geq 2$, dispersion effects that appear in the L^2 behavior of $u^\varepsilon(t, \cdot)$ are not captured by $u^0(t, \cdot)$. *High order effective equations* are effective models that describe the dispersion (with an accuracy that should increase with the order). Several definitions of high order effective equations were recently proposed [1–3]. Although the form of the equations are not the same, they all involve the same high order effective quantities.

2 Family of effective equations of arbitrary order

We present the high order models introduced in [1]. For $q \in \text{Sym}^n(\mathbb{R}^d)$, a symmetric tensor of order n , we denote the operator $q \nabla_x^n = \sum q_{i_1 \dots i_n} \partial_{i_1 \dots i_n}^n$. For a timescale $\mathcal{O}(\varepsilon^{-\alpha})$, the effective equations have the form

$$\partial_t^2 \tilde{u} - a^0 \nabla_x^2 \tilde{u} - \sum_{r=1}^{\lfloor \alpha/2 \rfloor} (-1)^r \varepsilon^{2r} L^{2r} \tilde{u} = Qf, \quad (3)$$

where the operators L^{2r} and Q are defined as

$$L^{2r} = a^{2r} \nabla_x^{2r+2} - b^{2r} \nabla_x^{2r} \partial_t^2, \\ Q = 1 + \sum_{r=1}^{\lfloor \alpha/2 \rfloor} (-1)^r \varepsilon^{2r} b^{2r} \nabla_x^{2r},$$

and $a^{2r} \in \text{Sym}^{2r+2}(\mathbb{R}^d)$, $b^{2r} \in \text{Sym}^{2r}(\mathbb{R}^d)$. Note that if a^{2r} , b^{2r} are non-negative, (3) is well-posed

To derive the values of the effective tensors a^{2r} , b^{2r} , we use asymptotic expansion. We look for an adaptation $\mathcal{B}^\varepsilon \tilde{u}$ that approximates u^ε . An error estimate tells us that for \tilde{u} to be close to u^ε up to $\mathcal{O}(\varepsilon^{-\alpha})$ timescales, $\mathcal{B}^\varepsilon \tilde{u} - u^\varepsilon$ must satisfy the wave equation with a right hand side of order $\mathcal{O}(\varepsilon^{\alpha+1})$ in the $L^\infty(0, \varepsilon^{-\alpha} T; L^2(\Omega))$ -norm. We then combine (i) the ansatz

$$\mathcal{B}^\varepsilon \tilde{u}(t, x) = \tilde{u}(t, x) + \sum_{k=1}^{\alpha+2} \chi^k(t, x, y) \nabla_x^k \tilde{u}(t, x),$$

where the k -th order corrector $\chi^k = \{\chi_{i_1 \dots i_k}^k\}$ has value in $\text{Sym}^k(\mathbb{R}^d)$, and (ii) inductive Boussinesq tricks (use (3) to replace time derivatives with space derivatives) and obtain the *cell problems*, which have the cascade form:

$$\begin{aligned} \mathcal{A}\chi_{i_1}^1 &= \mathcal{F}_{i_1}^1(a), \\ \mathcal{A}\chi_{i_1 i_2}^2 &= \mathcal{F}_{i_1 i_2}^2(a, \chi^1, a^0), \\ \mathcal{A}\chi_{i_1 \dots i_{2r+1}}^{2r+1} &= \mathcal{F}_{i_1 \dots i_{2r+1}}^{2r+1}(a, \chi^1, \dots, \chi^{2r}), \\ \mathcal{A}\chi_{i_1 \dots i_{2r+2}}^{2r+2} &= \mathcal{F}_{i_1 \dots i_{2r+2}}^{2r+2}(a, \chi^1, \dots, \chi^{2r+1}, a^{2r} - a^0 \otimes b^{2r}), \end{aligned} \quad (4)$$

where $\mathcal{A} = -\nabla_y \cdot (a \nabla_y \cdot)$ and $\mathcal{F}_{i_1 \dots i_k}^k$ are specified in [1]. While the odd order cell problems are well-posed unconditionally, the solvability of the even order cell problems provides constraints on the tensors a^{2r}, b^{2r} :

$$a^{2r} - a^0 \otimes b^{2r} =_S \bar{q}^r(\chi^1, \dots, \chi^{2r+1}), \quad (5)$$

where $\bar{q}^r(\chi^1, \dots, \chi^{2r+1})$ is a constant tensor of order $2r+2$ computed by means of the correctors χ^1 to χ^{2r+1} and $=_S$ means that the equality holds up to symmetry.

Theorem 1 *Assume sufficient regularity of the data and let $\{a^{2r}, b^{2r}\}_{r=1}^{\lfloor \alpha/2 \rfloor}$ be symmetric, non-negative tensors satisfying (5). Then it holds*

$$\|u^\varepsilon - \bar{u}\|_{L^\infty(0, \varepsilon^{-\alpha} T; W)} \leq C\varepsilon,$$

where the constant C is independent of ε and Ω and the norm $\|\cdot\|_W$ is equivalent to the $L^2(\Omega)$ -norm up to the Poincaré constant.

Theorem 1 ensures that any set $\{a^{2r}, b^{2r}\}_{r=1}^{\lfloor \alpha/2 \rfloor}$ satisfying the requirements gives an effective equation. Hence, this result implicitly defines a family of effective equations over timescales $\mathcal{O}(\varepsilon^{-\alpha})$.

3 Substantial cost reduction to compute the high order effective tensors

In [1], we provide an explicit procedure to compute the effective tensors $\{a^{2r}, b^{2r}\}$ in practice. As \bar{q}^r may happen to be negative, the main challenge is to build non-negative a^{2r} that satisfy (5). The preeminent computational cost of the procedure is the calculation of \bar{q}^r . The natural—but naive—formula for \bar{q}^r requires to solve the cell problems for χ^1 to χ^{2r+1} . However, exploiting a hidden structure of the cell problems, we prove the following result:

Theorem 2 *The tensor \bar{q}^r involved in (5) can in fact be computed from $\chi^1, \dots, \chi^{r+1}$.*

Thanks to this result, the computational cost to compute the effective tensors $\{a^{2r}, b^{2r}\}_{r=1}^{\lfloor \alpha/2 \rfloor}$ is significantly reduced. Specifically, it allows to avoid solving

$$N(\alpha, d) = \binom{2\lfloor \alpha/2 \rfloor + 1 + d}{d} - \binom{\lfloor \alpha/2 \rfloor + 1 + d}{d}$$

cell problems (e.g., $N(6, 2) = 21$, $N(6, 3) = 85$).

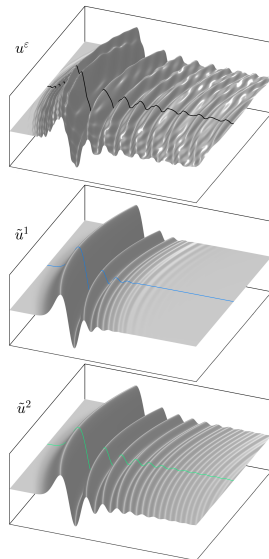


Figure 1: Comparison between u^ε (top) and high order effective solutions for $\alpha=2$ (\bar{u}^1 , middle) and $\alpha=4$ (\bar{u}^2 , bottom). See [1] for details.

References

- [1] A. ABDULLE AND T. POUCHON, *Effective models and numerical homogenization for wave propagation in heterogeneous media on arbitrary timescales*. arXiv preprint arXiv:1905.09062, 2019.
- [2] GRÉGOIRE ALLAIRE, AGNES LAMACZ, AND JEFFREY RAUCH, *Crème pays; homogenized wave equations for long times*. arXiv preprint arXiv:1803.09455, 2018.
- [3] ANTOINE BENOIT AND ANTOINE GLORIA, *Long-time homogenization and asymptotic ballistic transport of classical waves*, arXiv preprint arXiv:1701.08600, 2017.

Electromagnetic shielding by thin periodic structures and the Faraday cage effect

Bérangère Delourme^{1,*}, David P. Hewett^{2,*}

¹Laboratoire Analyse Géométrie et Applications (LAGA), Université Paris 13, Villetaneuse, France

²Department of Mathematics, University College London, London, UK

*Email: d.hewett@ucl.ac.uk

Abstract

The ability of wire meshes to block electromagnetic waves (the “Faraday cage” effect) is well known to physicists and engineers. We consider the scattering of electromagnetic waves (governed by the time-harmonic Maxwell equations) by a thin periodic layer of perfectly conducting obstacles. The size of the obstacles and the distance between neighbouring obstacles are both small compared to the wavelength. We derive homogenized interface conditions for three model configurations, namely (i) discrete obstacles, (ii) parallel wires, (iii) a wire mesh, and observe that the leading order behaviour depends strongly on the topology of the periodic layer, with shielding of incident waves of all polarizations occurring only in the case of a wire mesh.

Keywords: Homogenized interface conditions, Maxwell equations, Faraday cage

Our aim is to derive homogenized interface conditions for electromagnetic scattering by a thin periodic layer of perfectly-conducting obstacles

$$\mathcal{L}^\delta = \text{int} \left(\bigcup_{(i,j) \in \mathbb{Z}^2} \delta \left\{ \bar{\Omega} + i\mathbf{e}_1 + j\mathbf{e}_2 \right\} \right),$$

where $\delta > 0$ is small and $\bar{\Omega} \subset [0, 1]^2 \times \mathbb{R} \subset \mathbb{R}^3$ is the canonical obstacle in the period cell. In particular we consider three model cases:

- (i) $\hat{\Omega} = (\frac{3}{8}, \frac{5}{8})^2 \times (-\frac{1}{8}, \frac{1}{8})$, i.e. a cube;
- (ii) $\hat{\Omega} = [0, 1] \times (\frac{3}{8}, \frac{5}{8}) \times (-\frac{1}{8}, \frac{1}{8})$, i.e. a wire (of square section) parallel to the direction \mathbf{e}_1 .
- (iii) $\hat{\Omega} = \{[0, 1] \times (\frac{3}{8}, \frac{5}{8}) \times (-\frac{1}{8}, \frac{1}{8})\} \cup \{(\frac{3}{8}, \frac{5}{8}) \times [0, 1] \times (-\frac{1}{8}, \frac{1}{8})\}$, i.e. a cross-shaped domain with branches parallel to \mathbf{e}_1 and \mathbf{e}_2 .

We seek a solution \mathbf{u}^δ of the Maxwell equations

$$\mathbf{curl} \mathbf{curl} \mathbf{u}^\delta - \omega^2 \varepsilon \mathbf{u}^\delta = \mathbf{f} \quad \text{in } \Omega^\delta := \mathbb{R}^3 \setminus \overline{\mathcal{L}^\delta},$$

subject to the PEC boundary condition

$$\mathbf{u}^\delta \times \mathbf{n} = \mathbf{0} \quad \text{on } \Gamma^\delta := \partial\Omega^\delta.$$

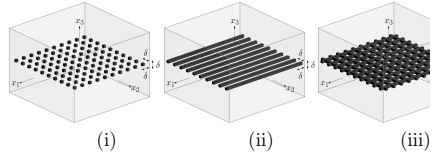


Figure 1: The domain Ω^δ in cases (i)–(iii).

It is well-known that, under appropriate assumptions on \mathbf{f} , ω and ε and the far-field behaviour, this problem is well-posed. Our aim is to identify the limit \mathbf{u}^0 of \mathbf{u}^δ as δ tends to 0. This limit solution is defined in the union of two distinct domains $\Omega^\pm = \{\mathbf{x} \in \mathbb{R}^3 : \pm x_3 > 0\}$, whose common interface is $\Gamma = \{\mathbf{x} \in \mathbb{R}^3 : x_3 = 0\}$.

Theorem 1 *The limit solution \mathbf{u}^0 satisfies*

$$\mathbf{curl} \mathbf{curl} \mathbf{u}^0 - \omega^2 \varepsilon \mathbf{u}^0 = \mathbf{f} \quad \text{in } \Omega^+ \cup \Omega^-,$$

and the following interface conditions on Γ (when $[\cdot]_\Gamma$ denotes the jump across Γ):

Case (i): $[\mathbf{u}_0 \times \mathbf{e}_3]_\Gamma = \mathbf{0}$ and $[\mathbf{curl} \mathbf{u}_0 \times \mathbf{e}_3]_\Gamma = 0$, so the interface is transparent to leading order.

Case (ii): $\mathbf{u}_0 \cdot \mathbf{e}_1 = 0$ on Γ , $[\mathbf{u}_0 \cdot \mathbf{e}_2]_\Gamma = 0$, and $[(\mathbf{curl} \mathbf{u}_0 \times \mathbf{e}_3) \cdot \mathbf{e}_2]_\Gamma = 0$, so the interface reflects waves polarized parallel to the wires.

Case (iii): $\mathbf{u}_0 \times \mathbf{e}_3 = \mathbf{0}$ on Γ , so the interface reflects waves of all polarizations.

To prove Theorem 1 we approximate \mathbf{u}^δ using matched asymptotic expansions, as in [1–7] when closely related problems are studied. It is convenient to work with the first-order formulation

$$\begin{aligned} -i\omega \mathbf{h}^\delta + \mathbf{curl} \mathbf{u}^\delta &= \mathbf{0} && \text{in } \Omega^\delta, \\ -i\omega \mathbf{u}^\delta - \mathbf{curl} \mathbf{h}^\delta &= -\frac{1}{i\omega} \mathbf{f} && \text{in } \Omega^\delta, \\ \mathbf{u}^\delta \times \mathbf{n} &= \mathbf{0} \text{ and } \mathbf{h}^\delta \cdot \mathbf{n} = 0 && \text{on } \Gamma^\delta. \end{aligned}$$

Far from the periodic layer \mathcal{L}^δ we expand

$$\begin{aligned} \mathbf{h}^\delta &= \mathbf{h}_0(\mathbf{x}) + \delta \mathbf{h}_1(\mathbf{x}) + \dots, \\ \mathbf{u}^\delta &= \mathbf{u}_0(\mathbf{x}) + \delta \mathbf{u}_1(\mathbf{x}) + \dots, \end{aligned}$$

and, in the vicinity of \mathcal{L}^δ ,

$$\mathbf{h}^\delta = \mathbf{H}_0(x_1, x_2, \frac{\mathbf{x}}{\delta}) + \delta \mathbf{H}_1(x_1, x_2, \frac{\mathbf{x}}{\delta}) + \dots,$$

$$\mathbf{u}^\delta = \mathbf{U}_0(x_1, x_2, \frac{\mathbf{x}}{\delta}) + \delta \mathbf{U}_1(x_1, x_2, \frac{\mathbf{x}}{\delta}) + \dots,$$

where, for $i \in \{0, 1\}$, $\mathbf{H}_i(x_1, x_2, y_1, y_2, y_3)$ and $\mathbf{U}_i(x_1, x_2, y_1, y_2, y_3)$ are 1-periodic in both y_1 and y_2 . The near and far field expansions satisfy matching conditions, the $O(1)$ one being

$$\lim_{x_3 \rightarrow 0^\pm} \mathbf{h}_0 = \lim_{y_3 \rightarrow \pm\infty} \mathbf{H}_0, \quad \lim_{x_3 \rightarrow 0^\pm} \mathbf{u}_0 = \lim_{y_3 \rightarrow \pm\infty} \mathbf{U}_0. \tag{1}$$

The near fields \mathbf{U}_0 and \mathbf{H}_0 satisfy

$$\begin{aligned} \mathbf{curl} \mathbf{U}_0 &= \mathbf{curl} \mathbf{H}_0 = \mathbf{0} && \text{in } \mathcal{B}_\infty, \\ \operatorname{div} \mathbf{U}_0 &= \operatorname{div} \mathbf{H}_0 = 0 && \text{in } \mathcal{B}_\infty, \\ \mathbf{U}_0 \times \mathbf{n} &= \mathbf{0} \text{ and } \mathbf{H}_0 \cdot \mathbf{n} = 0 && \text{on } \partial \mathcal{B}_\infty, \end{aligned}$$

where $\mathcal{B}_\infty = \mathbb{R}^3 \setminus \bigcup_{(i,j) \in \mathbb{Z}^2} \{\overline{\Omega} + i\mathbf{e}_1 + j\mathbf{e}_2\}$. A key step in our analysis is to prove that \mathbf{U}_0 and \mathbf{H}_0 are uniquely defined respectively as elements of the normal and tangential cohomology spaces K_N and K_T [8, 9], which are subspaces of $H_{loc}(\mathbf{curl}; \mathcal{B}_\infty) \cap H_{loc}(\operatorname{div}; \mathcal{B}_\infty)$ with a periodicity condition in y_1 and y_2 and appropriate decay conditions at $y_3 = \pm\infty$. In the following theorem let $\mathbf{U}^{i,\pm} := \lim_{y_3 \rightarrow \pm\infty} \mathbf{U} \cdot \mathbf{e}_i$.

Theorem 2 *For each of the three cases (i)-(iii), K_N and K_T are spanned by gradients of certain scalar potentials satisfying the Laplace equation with appropriate boundary/decay conditions.*

Case (i): K_N and K_T have dimension 4 and 3 respectively. If $\mathbf{U} \in K_N$ and $\mathbf{H} \in K_T$ then $\mathbf{U}^{i,+} = \mathbf{U}^{i,-}$ and $\mathbf{H}^{i,+} = \mathbf{H}^{i,-}$ for $i \in \{1, 2\}$.

Case (ii): K_N and K_T have dimension 3 and 4 respectively. If $\mathbf{U} \in K_N$ and $\mathbf{H} \in K_T$ then $\mathbf{U}^{1,\pm} = 0$, $\mathbf{U}^{2,+} = \mathbf{U}^{2,-}$, and $\mathbf{H}^{1,+} = \mathbf{H}^{1,-}$.

Case (iii): K_N and K_T have dimension 2 and 5 respectively. If $\mathbf{U} \in K_N$ then $\mathbf{U}^{1,\pm} = \mathbf{U}^{2,\pm} = 0$.

Theorem 1 then follows by combining Theorem 2 with the matching conditions (1). For details see [9]. We note that a study of case (iii), using a different approach to that outlined above, appeared recently in [4], where the first order correction terms were also considered.

The convergence of \mathbf{u}^δ to \mathbf{u}_0 in the limit $\delta \rightarrow 0$ can be made rigorous by justifying the asymptotic expansions considered above. This can be done a posteriori by constructing an approximation of \mathbf{u}^δ on Ω^δ (based on truncated

expansions) and using a δ -explicit stability estimate, cf. [10]. This is the subject of ongoing work by the authors of the talk.

References

- [1] Chapman S.J., Hewett D.P., Trefethen L.N., Mathematics of the Faraday cage, *SIAM Review*, 57 (2015), pp. 398–417.
- [2] Hewett D.P., Hewett I.J., Homogenized boundary conditions and resonance effects in Faraday cages, *Proc. R. Soc. A*, 472 (2016), 20160062.
- [3] Holloway C.L., Kuester E.F., Dienstfrey, A., A homogenization technique for obtaining generalized sheet transition conditions for an arbitrarily shaped coated wire grating, *Radio Sci.*, 49 (2014), pp. 813–850.
- [4] Holloway, C.L., Kuester, E.F., Generalized sheet transition conditions for a metascreen - a fishnet metasurface, *IEEE T. Antenn. Propag.*, 66 (2018), pp. 2414–2427.
- [5] Marigo J.J., Maurel A., Two-scale homogenization to determine effective parameters of thin metallic-structured films, *Proc. R. Soc. A*, 472 (2016), 20160068.
- [6] Delourme B., Haddar H., Joly P., On the well-posedness, stability and accuracy of an asymptotic model for thin periodic interfaces in electromagnetic scattering problems, *Math. Meth. Appl. Sci.*, 23 (2013), pp. 2433–2464.
- [7] Delourme B., High-order asymptotics for the electromagnetic scattering by thin periodic layers, *Math. Method Appl. Sci.*, 38 (2015), pp. 811–833.
- [8] Amrouche C., Bernardi C., Dauge M., Girault V., Vector potentials in three-dimensional non-smooth domains, *Math. Meth. Appl. Sci.*, 21 (1998), pp. 823–864.
- [9] Delourme B., Hewett D. P., Electromagnetic shielding by thin periodic structures and the Faraday cage effect, *arXiv:1806.10433*, 2018
- [10] Maz'ya V., Nazarov S., Plamenevskij B., *Asymptotic Theory of Elliptic Boundary Value Problems in Singularly Perturbed Domains*, Birkhäuser, 2012.

Homogenization of the time-harmonic Maxwell equations for a large class of periodic and perfectly conducting microstructures

Klaas Hendrik Poelstra¹, Ben Schweizer¹, Maik Urban^{1,*}

¹Department of Mathematics, TU Dortmund University, Dortmund, Germany

*Email: maik.urban@tu-dortmund.de

Abstract

Inspired by experimental observations, homogenization of the time-harmonic Maxwell equations has been an active field of research in recent years. We contribute by studying periodic meta-materials consisting of perfectly conducting microstructures and void space. Contrary to the most known results, we do not focus on a microstructure with a particular topology but consider a large class of microstructures. We show that topological characteristics of the microstructure determine the structure of the effective equations as well as transmission properties of the effective medium. The definition of the effective magnetic field requires a new notion of average, the so called geometric average. As we consider a large class of microstructures we present a new definition of the geometric average, which extends the known definitions.

Keywords: Maxwell's equations, homogenization, meta-material, periodic structures

1 Description of the problem

We consider a periodic meta-material placed in a bounded domain $\Omega \subset \mathbb{R}^3$. In this context, a meta-material is a periodic assembly of perfect conductors, and we are interested in the behaviour of the electromagnetic fields when the period of the meta-material tends to zero. Denoting the period of the meta-material by $\eta > 0$, we assume that the perfect conductors fill the set $\Sigma_\eta \subset \Omega$. We study distributional solutions $(E^\eta, H^\eta) \in L^2(\Omega; \mathbb{R}^3) \times L^2(\Omega; \mathbb{R}^3)$ to the time-harmonic Maxwell equations

$$\operatorname{curl} E^\eta = i\omega\mu_0 H^\eta \quad \text{in } \Omega, \quad (1)$$

$$\operatorname{curl} H^\eta = -i\omega\varepsilon_0 E^\eta \quad \text{in } \Omega \setminus \overline{\Sigma}_\eta, \quad (2)$$

$$E^\eta = H^\eta = 0 \quad \text{in } \Sigma_\eta, \quad (3)$$

in the limit $\eta \rightarrow 0$. In this system, $\omega > 0$ is a fixed frequency, $\varepsilon_0 > 0$, and $\mu_0 > 0$ are material parameters.

This problem has already been investigated in [3] but with stronger assumptions on the perfectly conducting microstructure.

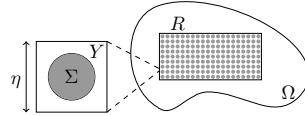


Figure 1: The meta-material is located in a sub-domain $R \Subset \Omega$ and is obtained by periodization of microstructures $\Sigma \subset Y$.

2 Geometry and assumptions

We remain in the framework of standard periodic homogenization; that is, the set Σ_η is assumed to be locally periodic. A reference microstructure $\Sigma \subset Y$ is considered, where Y denotes the unit cube $[0, 1]^3 \subset \mathbb{R}^3$. Identifying opposite faces, we can think of Y as the flat three-dimensional torus. The topology of Σ plays an important role in the effective equations; we make the following assumptions:

- (i) Σ is a proper subdomain of the three dimensional torus Y that has a Lipschitz boundary;
- (ii) $\Sigma^* := Y \setminus \overline{\Sigma}$ is connected as a subset of the three-dimensional torus Y .

We assume that the meta-material is located in a second domain $R \Subset \Omega$. In its complement, $\Omega \setminus R$, the relative permittivity as well as the relative permeability are equal to unity. The perfect conductor Σ_η is given by

$$\Sigma_\eta := \bigcup_{k \in \mathcal{K}} \eta(k + \Sigma),$$

where $\mathcal{K} := \{k \in \mathbb{Z}^3 : \eta(k + Y) \subset R\}$. In Figure 1 we sketched the setting.

We use the tool of two-scale convergence. In order to apply this, we have to assume that we are given a sequence $(E^\eta, H^\eta)_\eta$ of distributional solutions to the time-harmonic Maxwell equations (1)-(3) that satisfies the energy-bound

$$\sup_{\eta > 0} \int_{\Omega} |E^\eta|^2 + |H^\eta|^2 < \infty.$$

3 The notion of a geometric average

Denote by $E_0, H_0 \in L^2(\Omega \times Y; \mathbb{R}^3)$ the two-scale limits of $(E^\eta)_\eta$ and $(H^\eta)_\eta$, respectively. It is classical that the effective fields \hat{E} and \hat{H} are defined as suitable averages of E_0 and H_0 . For physical reasons, the averaging procedure has to be chosen in such a way that the tangential components of (\hat{E}, \hat{H}) are continuous across the boundary of the meta-material. Setting $\hat{E} := \int_Y E_0$ yields the right effective electric field. The volume average of H_0 , however, possesses tangential discontinuities [1]. To overcome this difficulty, Bouchitté et al. introduced a new averaging procedure for periodic magnetic fields; the key idea is to handle them as one-forms. We use this idea and extend the definition of the geometric average given in [1] to the microstructures $\Sigma \subset Y$ that we consider.

Define the function space

$$V(\Sigma^*) := \left\{ \phi \in L^2(Y; \mathbb{R}^3) : \begin{array}{l} \text{curl } \phi = 0 \text{ in } Y \\ \text{and } \phi = 0 \text{ in } \Sigma \end{array} \right\}$$

and the space of attainable averages of fields from $V(\Sigma^*)$,

$$A^V(\Sigma^*) := \left\{ \int_Y \phi : \phi \in V(\Sigma^*) \right\} \subset \mathbb{R}^3.$$

We write \wedge for the cross-product in \mathbb{R}^3 .

Definition 1 For every $u \in L^2(\Sigma^*; \mathbb{R}^3)$ that satisfies $\text{curl } u = 0$ in Σ^* there is at least one vector $b \in \mathbb{R}^3$ such that the identity

$$\int_{\Sigma^*} u \wedge \phi = b \wedge \int_{\Sigma^*} \phi, \quad (4)$$

holds for all $\phi \in V(\Sigma^*)$. The vector of minimal Euclidean norm among all vectors $b \in \mathbb{R}^3$ satisfying (4) is called the geometric average of u , and is denoted by $\mathfrak{f}_{\Sigma^*} u$.

In [2] we prove that the geometric average is well-defined. As H_0 satisfies $\text{curl } H_0(x, \cdot) = 0$ in Σ^* for almost all $x \in \Omega$, we may define \hat{H} by $\hat{H}(x) := \mathfrak{f}_{\Sigma^*} H_0(x, \cdot)$. Some components of this effective magnetic field \hat{H} satisfy the continuity condition across the boundary of the meta-material. More precisely, for almost all $x \in \Omega$,

$$\pi_{A^V}(\text{curl } \hat{H}(x, \cdot)) \in L^2(\Omega; \mathbb{R}^3),$$

where $\pi_{A^V}: \mathbb{R}^3 \rightarrow \mathbb{R}^3$ is the orthogonal projection onto the space $A^V(\Sigma^*)$. In particular, if $A^V(\Sigma^*) = \mathbb{R}^3$, then all tangential components of the effective field \hat{H} are continuous.

4 Effective equations

The space of all $\phi \in V(\Sigma^*)$ with $\text{div } \phi = 0$ in Σ^* is denoted by $V^E(\Sigma^*)$. By $X^H(\Sigma^*)$ we denote the space of all vector fields $u \in L^2(Y; \mathbb{R}^3)$ that satisfy $\text{curl } u = 0$ in Σ^* , $\text{div } u = 0$ in Y , and $u = 0$ in Σ . Denoting by $X_0^H(\Sigma^*)$ the set of vector fields $u \in X^H(\Sigma^*)$ with $\mathfrak{f}_{\Sigma^*} u = 0$, we have the decomposition $X^H(\Sigma^*) = X_0^H(\Sigma^*) \oplus X_\perp^H(\Sigma^*)$, which is orthogonal with respect to the L^2 -scalar product. Similar to $A^V(\Sigma^*)$ we define the set of attainable geometric averages,

$$A^X(\Sigma^*) := \left\{ \int_Y \phi : \phi \in X_\perp^H(\Sigma^*) \right\}.$$

The effective permittivity ε^{eff} is the linear map $A^V(\Sigma^*) \rightarrow A^V(\Sigma^*)$ that satisfies

$$\varepsilon^{\text{eff}} \left(\int_Y \phi \right) \cdot \left(\int_Y \phi' \right) = \int_Y \phi \cdot \phi'$$

for all $\phi, \phi' \in V^E(\Sigma^*)$. We further set $\hat{\varepsilon}(x) := \varepsilon^{\text{eff}}$ for $x \in R$ and $\hat{\varepsilon}(x) := \text{id}$ for $x \in \Omega \setminus R$. The effective permeability μ^{eff} is the linear map $A^X(\Sigma^*) \rightarrow \mathbb{R}^3$, $\mathfrak{f}_{\Sigma^*} u \mapsto \int_{\Sigma^*} u$. We define $\hat{\mu}(x) := \mu^{\text{eff}}$ for $x \in R$ and $\hat{\mu}(x) := \text{id}$ for $x \in \Omega \setminus R$.

Theorem 2 Let (\hat{E}, \hat{H}) be the effective fields defined above, and let $\hat{\varepsilon}$ and $\hat{\mu}$ be as above. Then there holds

$$\begin{aligned} \text{curl } \hat{E} &= i\omega\mu_0\hat{\mu}\hat{H} && \text{in } \Omega, \\ \pi_{A^V}(\text{curl } \hat{H}) &= -i\omega\varepsilon_0\pi_{A^V}(\hat{\varepsilon}\hat{E}) && \text{in } \Omega, \\ \text{curl } \hat{H} &= -i\omega\varepsilon_0\hat{E} && \text{in } \Omega \setminus R, \\ \hat{E}(x) &\in A^V(\Sigma^*) && \text{for } x \in R, \\ \hat{H}(x) &\in A^X(\Sigma^*) && \text{for } x \in R. \end{aligned}$$

References

- [1] G. Bouchitté, C. Bourel, and D. Felbacq, Homogenization Near Resonances and Artificial Magnetism in Three Dimensional Dielectric Metamaterials, *Arch. Ration. Mech. Anal.*, **225(3)** (2017), pp. 1233-1277
- [2] K. H. Poelstra, B. Schweizer, and M. Urban, The geometric average of curl-free fields in periodic geometries, *in preparation*
- [3] B. Schweizer and M. Urban, Effective Maxwell's equations in general periodic microstructures, *Appl. Anal.*, **97(13)** (2017), pp. 2210-2230

A homogenisation theory for a general class of high-contrast problems; asymptotics with error estimates

Ilia Kamotski^{1,*}, Shane Cooper², Valery Smyshlyaev¹

¹Department of Mathematics, UCL, UK

²Department of Mathematics, Durham University, UK

*Email: i.kamotski@ucl.ac.uk

Abstract

In this talk, we present a framework to study the asymptotic behaviour of (a large class of) periodic *non-uniformly elliptic* systems with respect to a (small period) parameter. We determine, under very few readily verifiable assumptions, the leading-order approximation of the solution and derive error estimates, uniform in right-hand-side. Asymptotics for the spectrum with error estimates directly follow.

Keywords: Homogenisation, High contrast, Error estimates

1 Motivating examples and Problem formulation

We are motivated by the asymptotic behaviour of the solution $u \in H^1(\mathbb{R}^d)$ to the problem

$$\operatorname{div} A_\varepsilon \nabla u - u = f \in L^2(\mathbb{R}^d), \tag{1}$$

as $\varepsilon \rightarrow 0$. Here $A_\varepsilon(\cdot) = a_1(\frac{\cdot}{\varepsilon}) + \varepsilon^2 a_2(\frac{\cdot}{\varepsilon})$, a_1, a_2 are non-negative measurable periodic matrix-functions such that the sum is uniformly elliptic and bounded:

$$c|\xi|^2 \leq (a_1(y) + a_2(y))\xi \cdot \xi \leq c^{-1}|\xi|^2, \quad \forall \xi, y \in \mathbb{R}^d,$$

for some $c > 0$, cf [1, 2]. If $a_2 = 0$ then (1) reduces to the problem of *classical* homogenisation with uniformly elliptic matrix. If a_2 is an identity matrix and $a_1 = \chi a_2$, where χ is a characteristic function of connected periodic set, then (1) corresponds to the generalised “double porosity model”, see [3]. Other problems we are interested in include (but are by no means limited to) : Schrödinger’s equation with a strong periodic magnetic field b :

$$(\nabla - i\varepsilon^{-1}b(\frac{\cdot}{\varepsilon}))^*(\nabla - i\varepsilon^{-1}b(\frac{\cdot}{\varepsilon}))u - u = f,$$

and differential-difference equations, e.g. in the one-dimensional setting:

$$\begin{aligned} \varepsilon^{-2}b(\frac{x}{\varepsilon})(u(x + \varepsilon) - 2u(x) + u(x - \varepsilon)) \\ + (a(\frac{x}{\varepsilon})u(x))' - u(x) = f(x), \end{aligned}$$

with 1-periodic positive functions a and b .

Upon rescaling $x/\varepsilon \rightarrow y$ and an application of the Floquet transform $y \rightarrow (y, \theta)$, all these problems fall into the following general class of problems: For fixed $\varepsilon > 0$ and each θ in given compact set $\Theta \subset \mathbb{R}^d$,

$$\begin{cases} \text{Find } u_\theta \in H \text{ such that} \\ \varepsilon^{-2}a_\theta(u_\theta, \phi) + (u_\theta, \phi)_\theta = \langle f, \phi \rangle, \quad \forall \phi \in H. \end{cases} \tag{2}$$

Here, H is a (complex) Hilbert space with a family of equivalent scalar products $(\cdot, \cdot)_\theta$, $f \in H^*$ and a_θ is a non-negative, continuous sesquilinear form on H . Our aim is to find the leading-order approximation to u_θ (with respect to ε) and to derive error estimates uniform in $\theta \in \Theta$. We assume that $(\cdot, \cdot)_\theta$ and a_θ are merely Lipschitz continuous with respect to θ , that is there exist $c > 0$ such that

$$|(u, v)_{\theta_1} - (u, v)_{\theta_2}| \leq c|\theta_1 - \theta_2||u|_{\theta_1}|v|_{\theta_1},$$

$$|a_{\theta_1}(u, v) - a_{\theta_2}(u, v)| \leq c|\theta_1 - \theta_2||u|_{\theta_1}|v|_{\theta_1},$$

for all $u, v \in H, \forall \theta_1, \theta_2 \in \Theta$. Denote $a_\theta[u] = a_\theta(u, u)$, $V_\theta = \{u \in H \mid a_\theta[u] = 0\}$ and $W_\theta = \{w \in H \mid (w, v)_\theta = 0, \forall v \in V_\theta\}$. Let

$$\nu_\theta = \inf\{a_\theta[w]||w|_\theta^{-2} : w \in W_\theta, w \neq 0\}.$$

Our main assumption is the following *Spectral gap condition*: ν_θ is positive, for all $\theta \in \Theta$. Let us stress that this condition is easily verifiable in applications, see [2] for the extensive list of physically relevant examples of divergence type *systems* that satisfy this condition. Other interesting examples include homogenisation problems on periodic quantum graphs and their generalisations. Some problems in *thin* domains also fall into the above framework.

2 Main results

First we assume that the family of spaces V_θ is Lipschitz continuous: there is $c > 0$ such that

$$\inf_{v_2 \in V_{\theta_2}} \|v_1 - v_2\|_{\theta_2} \leq c|\theta_1 - \theta_2||v_1|_{\theta_1}, \tag{3}$$

$\forall v_1 \in V_{\theta_1}, \forall \theta_1, \theta_2 \in \Theta$. This is the case e.g. in the *inverse* double porosity model, where the stiff phase is formed by periodic isolated inclusions.

Theorem 1 *If V_θ is Lipschitz continuous then $\inf_{\theta \in \Theta} \nu_\theta = \nu > 0$, and*

$$\varepsilon^{-2} a_\theta [u_\theta - v_\theta] + \|u_{\varepsilon, \theta} - v_\theta\|_\theta^2 \leq \varepsilon^2 \nu^{-1} \|f\|_{*\theta}^2,$$

where $v_\theta \in V_\theta$ solves

$$(v_\theta, \bar{v})_\theta = \langle f, \bar{v} \rangle, \quad \forall \bar{v} \in V_\theta.$$

In applications, condition (3) is often violated at some point $\theta_0 \in \Theta$ (without loss of generality we assume that $\theta_0 = 0$), and the family of spaces V_θ has a removable singularity at this point. By this we mean that there exists a closed subspace V_\star of H such that

$$V_\theta^\star = \begin{cases} V_\theta, & \theta \neq 0, \\ V_\star, & \theta = 0 \end{cases} \text{ is Lipschitz continuous.} \tag{4}$$

For a wide class of applications one has $V_\theta = V$ for $\theta \neq 0$ and (4) trivially holds for $V_\star = V$. Set Z to be orthogonal complement of V_\star in V_0 (with respect to $(\cdot, \cdot)_0$).

We further assume that there exist sesquilinear bounded forms $a'_0 : H \times H \rightarrow \mathbb{C}^d, a''_0 : H \times H \rightarrow \mathbb{C}^{d \times d}$ and a constant $c \geq 0$ such that

$$|a_\theta(u, v) - a_0(u, v) - a'_0(u, v) \cdot \theta - a''_0(u, v) \theta \cdot \theta| \leq c|\theta|^3 \|u\|_0 \|v\|_0, \quad \forall u, v \in H, \forall \theta \in \Theta \tag{5}$$

((5) holds with $c = 0$ for second order differential systems). Our final assumption is

$$\exists \nu_\star > 0 : \nu_\theta \geq \nu_\star |\theta|^2, \quad \forall \theta \in \Theta, \tag{6}$$

which condition is a well-known to hold in the classical homogenisation.

We introduce the generalisation of the *homogenised matrix*: the positive sesquilinear (quadratic in θ) form $a_\theta^{\text{hom}} : Z \times Z \rightarrow \mathbb{C}$ given by

$$a_\theta^{\text{hom}}(z, \bar{z}) := a''_0(z, \bar{z}) \theta \cdot \theta - a_0(\theta \cdot Nz, \theta \cdot N\bar{z}), \quad z, \bar{z} \in Z,$$

where the *corrector* $Nz \in W_0^d$ is the solution to

$$a_0(\theta \cdot Nz, \bar{w}_0) = -a'_0(z, \bar{w}_0) \cdot \theta, \quad \forall \bar{w}_0 \in W_0, \quad \forall \theta \in \Theta.$$

Theorem 2 *Assume (4)-(6). Consider the solutions $v_\theta^\star \in V_\theta^\star$ to*

$$(v_\theta^\star, \bar{v})_\theta = \langle f, \bar{v} \rangle, \quad \forall \bar{v} \in V_\theta^\star,$$

and $z_\theta \in Z$ to

$$\varepsilon^{-2} a_\theta^{\text{hom}}(z_\theta, \bar{z}) + (z_\theta, \bar{z})_0 = \langle f, \bar{z} \rangle, \quad \forall \bar{z} \in Z. \tag{7}$$

Set

$$u_\theta^{\text{approx}} = v_\theta^\star + z_\theta + \theta \cdot Nz_\theta.$$

Then, there exists constant $c > 0$ independent of ε, θ and f such that

$$\varepsilon^{-2} a_\theta [u_\theta - u_\theta^{\text{approx}}] + \|u_\theta - u_\theta^{\text{approx}}\|_\theta^2 \leq \varepsilon^2 c \|f\|_{*\theta}^2,$$

and

$$\|u_\theta - (v_\theta^\star + z_\theta)\|_\theta^2 \leq \varepsilon^2 c \|f\|_{z_\theta}^2,$$

$\forall \theta \in \Theta, \forall \varepsilon > 0$.

We note that Z is finite dimensional under an additional easily verifiable condition and (7) is then a linear algebraic system. This theorem recovers some of the results from [4] in the context of classical homogenisation and of the results from [5] for the “double porosity” model.

Theorem 2 implies uniform in θ estimates of the spectrum of the operator generated by the form $\varepsilon^{-2} a_\theta(u, v) + (u, v)_\theta$, which in turn allows us to establish the gaps in the spectrum of the original operator with error estimates.

References

- [1] V.P. Smyshlyaev, Propagation and localization of elastic waves in highly anisotropic periodic composites via two-scale homogenization, *Mechanics of Materials* **41** (2009), pp. 434–447.
- [2] I. Kamotski, V.P. Smyshlyaev, Two-scale homogenization for a general class of high contrast PDE systems with periodic coefficients, *Applicable Analysis* **98(1-2)** (2019), pp.64–90.
- [3] V.V. Zhikov, On an extension and an application of the two-scale convergence method. *Sbornik Math* **191** (2000), pp. 973–1014.
- [4] M.Sh. Birman, T.A. Suslina, Homogenization with corrector for periodic differential operators. Approximation of solutions in the Sobolev class $H^1(\mathbb{R}^d)$, *St. Petersburg Math. J.* **18(6)** (2007), pp. 857–955.
- [5] K.D. Cherednichenko, S. Cooper, Resolvent Estimates for High-Contrast Elliptic Problems with Periodic Coefficients. *Archive for Rational Mechanics and Analysis* **219(3)** (2016), pp. 1061–1086.

Numerical modeling for scattering of transient acoustic waves by resonant interfaces

Marie Touboul^{1,*}, Cédric Bellis¹, Bruno Lombard¹

¹Aix Marseille Univ, CNRS, Centrale Marseille, LMA UMR 7031, Marseille, France

*Email: touboul@lma.cnrs-mrs.fr

Abstract

With an adequate scaling on the physical parameters, a thin micro-structured medium can be such that resonances are possible in the inclusions. The homogenization of such media yields jump conditions that apply across an interphase and involve frequency-dependant coefficients in the harmonic regime. Auxiliary variables are used to take into account these resonances and perform time-domain simulations.

Keywords: homogenization, resonant interfaces, time-domain wave propagation, immersed interface method

1 Physical modeling

The physical problem concerns the propagation of acoustic waves through scatterers disposed periodically in a 2D media with a spacing h . The spatial coordinates are denoted by $\mathbf{x} = (x_1, x_2)$. The mass density ρ and the compressibility χ are piecewise constants:

$$(\rho, \chi)(\mathbf{x}) = \begin{cases} (\rho_m, \chi_m) & \text{in the matrix} \\ (\rho_i, \chi_i) & \text{in the inclusions.} \end{cases} \quad (1)$$

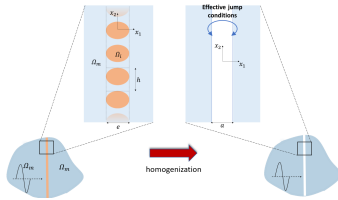


Figure 1: Homogenization process on a single array of resonant inclusions.

Resonances are possible with a low contrast in the compressibility $\chi_i/\chi_m = \mathcal{O}(1)$ and a high contrast in the mass density $\rho_m/\rho_i = (kh)^2$, where $k = \frac{2\pi}{\lambda}$ is the wavenumber in the matrix and λ is the wavelength supposed to be much larger than h .

Under these assumptions, the microstructured problem can be replaced by an equivalent homogenized problem [1]. It consists in solving the volumic equations around an interphase of thickness a , and jump conditions on the pressure p and the normal velocity v_1 across this interphase. These jump conditions take into account the microstructure characteristics and read in the frequency domain :

$$\begin{cases} \llbracket \hat{p} \rrbracket_a &= B_1 \langle \partial_{x_1} \hat{p} \rangle_a + B_2 \langle \partial_{x_2} \hat{p} \rangle_a, \\ \llbracket \hat{v}_1 \rrbracket_a &= C_{11} \langle \partial_{x_1} \hat{v}_1 \rangle_a + C_{12} \langle \partial_{x_2} \hat{v}_1 \rangle_a \\ &+ C_{22} \langle \partial_{x_2} \hat{v}_2 \rangle_a + hD(k) \langle \nabla \cdot \hat{\mathbf{v}} \rangle_a, \end{cases} \quad (2)$$

where we have defined

$$\llbracket f \rrbracket_a(x_2) = f\left(\frac{a}{2}, x_2\right) - f\left(-\frac{a}{2}, x_2\right), \quad (3)$$

$$\langle f \rangle_a(x_2) = \frac{1}{2} \left(f\left(\frac{a}{2}, x_2\right) + f\left(-\frac{a}{2}, x_2\right) \right) \quad (4)$$

being the jump of f across the homogenized interphase and the mean value of f respectively. $D(k)$ encapsulates the resonant behaviour of the inclusions and can be written as:

$$D(k) = \alpha_0 - \sum_{n \geq 1} \alpha_n^2 \frac{k^2}{k^2 - k_n^2}, \quad (5)$$

where the set of $\{k_n\}$ denote resonant frequencies, with $\{k_n^2\}$ eigenvalues of the problem $\Delta P + \kappa^2 P = 0$ solved in an inclusion.

Stability of such system is linked to energy considerations and is guaranteed for a specific interphase thickness that will be detailed in a future work.

2 Auxiliary variables

Because of $D(k)$, formulating the system in the time domain involves a convolution product. This is very costly numerically and it reduces the computational gains obtained from homogenization. To avoid this, auxiliary fields [3] \hat{J}_r are introduced:

$$\hat{J}_r = \alpha_r^2 \frac{k^2}{k^2 - k_r^2} \nabla \cdot \hat{\mathbf{v}} \quad \text{for } r = 1, \dots, N_R. \quad (6)$$

We introduce N_R the number of resonances chosen in (5), $c_m = 1/\sqrt{\rho_m \chi_m}$, $\tilde{C}_{11} = C_{11} + h\alpha_0$, $\tilde{C}_{22} = C_{22} + h\alpha_0$, and the N_R auxiliary fields $G_r = \partial_t J_r$. We combine (2) and (6) and get formally in the time domain and on the interfaces:

$$\left\{ \begin{array}{l} \partial_t G_r + (c_m k_r)^2 J_r = (\alpha_r c_m)^2 \Delta(\nabla \cdot v), \\ \partial_t J_r = G_r, \\ \llbracket p \rrbracket_a = B_1 \langle \partial_{x_1} p \rangle_a + B_2 \langle \partial_{x_2} p \rangle_a, \\ \llbracket v_1 \rrbracket_a = \tilde{C}_{11} \langle \partial_{x_1} v_1 \rangle_a + C_{12} \langle \partial_{x_2} v_1 \rangle_a \\ \quad + \tilde{C}_{22} \langle \partial_{x_2} v_2 \rangle_a - h \sum_{r=1}^{N_R} \langle J_r \rangle_a. \end{array} \right. \quad (7)$$

The system (7) is a first-order boundary-value problem. This formulation is at price of handling $2N_R$ auxiliary variables J_r and G_r . But contrary to v and p they are introduced only along the interfaces.

3 Time-domain simulations

An explicit finite-difference scheme is used to solve numerically the homogenized problem. The scheme has to be adapted because the solution is not defined in the interphase. This modification will take into account the jump conditions. A point M is called an irregular point if the stencil at M requires nodes that are in the interphase where the solution is not defined. For these points, some modified values will be used in the interphase, and direct numerical values will be used otherwise. These modified values are constructed as a smooth extension of the solution on the interface using the jump conditions. Their construction is detailed in [2] for the non-resonant case and is adapted here in the resonant case.

For a plane wave and a resonant plane interphase (tilted or not), a semi-analytical solution of the homogenized problem can be computed. Comparisons of both solutions along x_1 are shown in Figure 2. A comparison with a semi-analytical solution is also possible for a plane wave on a circular interphase and gives the same type of results.

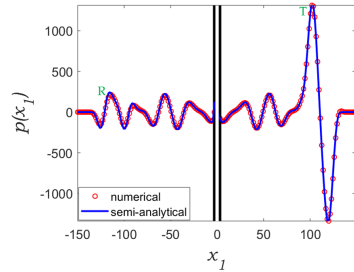


Figure 2: Semi-analytical pressure p^r (blue line) and numerical pressure p (red symbols).

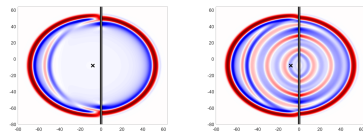


Figure 3: $p(x_1, x_2, t = 0.02375)$ without (left panel) and with resonances (right panel) for a short pulse emitted at the black cross location.

This numerical method then allows to investigate other types of sources (Figure 3 displays the numerical solution for a source point in the non-resonant and resonant cases) or interphases for which analytical solutions are not known.

References

- [1] K. Pham, A. Maurel, and J.-J. Marigo, Two scale homogenization of a row of locally resonant inclusions - the case of shear waves, *Journal of the Mechanics and Physics of Solids*, **106** (2017), pp. 80–941
- [2] B. Lombard, A. Maurel, and J.-J. Marigo, Numerical modeling of the acoustic wave propagation across an homogenized rigid microstructure in the time domain, *Journal of Computational Physics*, **335** (2017), pp. 558–577
- [3] C. Bellis and B. Lombard, Simulating transient wave phenomena in acoustic metamaterials using auxiliary fields, *Wave motion*, **86** (2019), pp. 175–194

Asymptotic analysis of the visco-acoustic equations for absorbing walls of arrays of Helmholtz resonators

Kersten Schmidt^{1,*}, Adrien Semin¹

¹Department of Mathematics, Technische Universität Darmstadt, Germany

*Email: kscheidt@mathematik.tu-darmstadt.de

Abstract

We will consider the visco-acoustic equations in a three-dimensional domain that contains a wall constituted of arrays of Helmholtz resonators. These arrays of resonators are used to suppress reflections from walls. Due to the smallness of the periodicity and of the perforations a direct numerical simulation is only possible for very large costs. We introduce a *surface homogenization with three scales* that combines a multiscale approach for the homogenization of the array of Helmholtz resonators with a matched asymptotic method around their aperture to prove that the solution of the visco-acoustic problem admits a limit as the characteristic sizes of the periodicity and of the perforation tend to 0. We justify that the limit model takes the array of Helmholtz resonators into account through *equivalent impedance boundary conditions*, which integrated into numerical methods leads to much lower computational costs.

1 Introduction

We consider a three-dimensional domain Ω that is for simplicity a simply connected smooth bounded domain in $\mathbb{R}^2 \times \mathbb{R}_+$, and we consider Γ as a connected, smooth subset of $\partial\Omega \cap \{x_3 = 0\}$ and of measure non-zero. We extend the domain Ω to a domain containing an array of Helmholtz resonators as follow: we assume this array to be periodic, *i.e.* there exists two fixed vectors \mathbf{a}_1 and \mathbf{a}_2 such that the centered parallelogram \mathcal{A} spanned by these two vectors has an area of 1, and there exists $\delta > 0$ such that the set Γ^δ describing the aperture centers is given by

$$\Gamma^\delta := \Gamma \cap (\delta \mathbf{a}_1 \mathbb{Z} + \delta \mathbf{a}_2 \mathbb{Z}).$$

We assume then that the array of resonators is described as follow: given a resonator position $\mathbf{x}_\Gamma^\delta \in \Gamma^\delta$, the resonator $\Omega_H^\delta(\mathbf{x}_\Gamma^\delta)$ is decomposed into a chamber part

$$\Omega_C^\delta(\mathbf{x}_\Gamma^\delta) := \mathbf{x}_\Gamma^\delta + \delta \mathcal{A}_C \times (-L, -\delta^2 h_0)$$

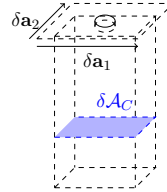


Figure 1: Example of one resonator (square-shaped constant cross-sections) that connects through one hole.

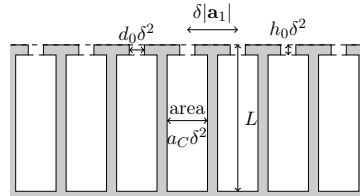


Figure 2: Representation of the array of resonators (cut along one periodicity direction).

and a neck part

$$\Omega_N^\delta(\mathbf{x}_\Gamma^\delta) := \mathbf{x}_\Gamma^\delta + \delta^2 \mathcal{D}_2(0.5d_0) \times (-\delta^2 h_0, 0),$$

where $\mathcal{A}_C \subset \mathcal{A}$ is a simply connected fixed domain of area $a_C < 1$, \mathcal{D}_2 designates the centered two-dimensional disc, and the lengths $L, d_0, h_0 > 0$ are independent of δ (see Fig. 1).

We finally extend the domain Ω^δ into the open domain Ω^δ containing the periodic array of resonators, *i.e.* whose closure is defined by

$$\overline{\Omega^\delta} = \overline{\Omega} \cup \bigcup_{\mathbf{x}_\Gamma^\delta \in \Gamma^\delta} \overline{\Omega_H^\delta(\mathbf{x}_\Gamma^\delta)}.$$

On the domain Ω^δ we introduce the acoustic equations in the framework of Landau and Lifschitz [1] as a perturbation of the Navier-Stokes equations around a stagnant uniform fluid with mean density ρ_0 . We consider the-harmonic ve-

locity \mathbf{v}^δ and acoustic pressure p^δ (the time regime is $\exp(-i\omega t)$, $\omega > 0$), which are described by the coupled system

$$\begin{aligned} -i\omega\mathbf{v}^\delta + \frac{1}{\rho_0}\nabla p^\delta - \nu(\delta)\Delta\mathbf{v}^\delta &= \mathbf{f}, & \text{in } \Omega^\delta, \\ -i\omega p^\delta + \rho_0 c^2 \operatorname{div} \mathbf{v}^\delta &= 0, & \text{in } \Omega^\delta, \\ \mathbf{v}^\delta &= \mathbf{0}, & \text{on } \partial\Omega^\delta, \end{aligned} \quad (1)$$

with the speed of sound c , the kinematic viscosity $\nu(\delta) = \nu_0\delta^4$ and a source term \mathbf{f} independent of δ and compactly supported in Ω away from its boundary with a positive distance.

2 Main result

We embed domain geometry Ω^δ and the associated Navier-Stokes problem (1) in a family of problems that are δ -dependent, and we are interested by the limit problem posed on Ω as $\delta \rightarrow 0$. Coupling a three-scale expansion technique developed in [2] for an interface problem and a periodic homogenization technique [3, 4] for the array of Helmholtz resonators, we show that the non-trivial limit (\mathbf{v}_0, p_0) is solution of an inviscid Helmholtz problem posed on Ω , stated by the following theorem.

Theorem 1 (Limit problem) *The solution $(\mathbf{v}^\delta, p^\delta)$ of the linearized Navier-Stokes problem in Ω^δ converges weakly in $H(\operatorname{div}, \Omega) \times H^1(\Omega)$ to (\mathbf{v}_0, p_0) solution of the following problem*

$$\begin{aligned} -i\omega\mathbf{v}_0 + \frac{1}{\rho_0}p_0 &= \mathbf{f}, & \text{in } \Omega, \\ -i\omega p_0 + \rho_0 c^2 \operatorname{div} \mathbf{v}_0 &= 0, & \text{in } \Omega, \\ \mathbf{v}_0 \cdot \mathbf{n} &= 0, & \text{on } \partial\Omega \setminus \Gamma, \end{aligned}$$

and

$$\left(\frac{i c \rho_0}{a c} \cos \frac{\omega L}{c} + \frac{2i \omega \rho_0}{k_R} \sin \frac{\omega L}{c}\right) \mathbf{v}_0 \cdot \mathbf{n} + p_0 \sin \frac{\omega L}{c} = 0$$

on Γ , where \mathbf{n} designates the outer unit normal vector of Ω , and k_R is a complex constant with $\operatorname{Im}(k_R) > 0$, the so-called effective Rayleigh conductivity [2], obtained by solving an instationary Stokes problem in an infinite domain $\widehat{\Omega}_N$ that is the union of two infinite half-spaces glued by one cylindrical domain of diameter d_0 and height h_0 , see Fig. 3. More precisely, we seek for $(\mathbf{V}, P) \in H^1(\widehat{\Omega}_N)^2 \times H_{\text{loc}}^1(\widehat{\Omega}_N)$ with $\nabla P \in L^2(\widehat{\Omega}_N)^2$ solution of the problem

$$\begin{aligned} -i\omega\mathbf{V} + \frac{1}{\rho_0}\nabla P - \nu_0\Delta\mathbf{V} &= \mathbf{0}, & \text{in } \widehat{\Omega}_N, \\ \operatorname{div} \mathbf{V} &= 0, & \text{in } \widehat{\Omega}_N, \\ \mathbf{V} &= \mathbf{0}, & \text{on } \partial\widehat{\Omega}_N, \\ \lim_{S \rightarrow \infty} P|_{\widehat{\Gamma}_\pm(S)} &= \pm \frac{1}{2}, \end{aligned}$$

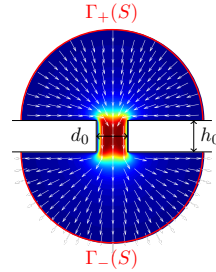


Figure 3: Domain $\widehat{\Omega}_N$ and representation of the imaginary part of \mathbf{V} .

and k_R is given by

$$k_R := \lim_{S \rightarrow \infty} \frac{i\omega\rho_0}{2} \left(\int_{\widehat{\Gamma}_+(S)} \mathbf{V} \cdot \mathbf{n} - \int_{\widehat{\Gamma}_-(S)} \mathbf{V} \cdot \mathbf{n} \right).$$

Keywords: Helmholtz resonators, visco-acoustic impedance boundary conditions

References

- [1] L. D. Landau and E. M. Lifshitz, *Course of theoretical physics Vol. 6*, 1st edition, Pergamon Press, New York, 1959.
- [2] K. Schmidt, A. Semin, A. Thöns-Zueva and F. Bake, On impedance conditions for circular multiperforated acoustic liners, *J. Math. Ind.* **8:15** (2018).
- [3] X. Claeys and B. Delourme, High order asymptotics for wave propagation across thin periodic interfaces, *Asymptot. Anal.*, **83:1-2** (2013), 35–82.
- [4] B. Delourme, K. Schmidt and A. Semin, On the homogenization of thin perforated walls of finite length, *Asymptot. Anal.*, **97:3-4** (2016), 211–264.

Enriched homogenized model in presence of boundaries

Clément BENETEAU^{1,*}, Xavier CLAEYS², Sonia FLISS¹¹POEMS (CNRS-INRIA-ENSTA-Paristech), Palaiseau, FRANCE²Sorbonne Université, CNRS, Inria, Laboratoire Jacques-Louis Lions, équipe Alpines, Paris, FRANCE

*Email: clement.beneteau@ensta-paristech.fr

Abstract

We study the wave equation set in periodic half-space when the period is small compared to the wave length. The classical homogenization theory enables to derive an effective model which provides an approximation of the solution. However it is well known that these models are not accurate near the boundaries. In this work, we propose an enriched asymptotic expansion which enables to derive high order effective models.

Keywords: homogenization, asymptotic model

1 Introduction

In this work, we consider the time-harmonic wave equation in a periodic half-space :

$$-\nabla \cdot \left[a \left(\frac{\mathbf{x}}{\varepsilon} \right) \nabla u_\varepsilon \right] - \omega^2 \rho \left(\frac{\mathbf{x}}{\varepsilon} \right) u_\varepsilon = f \text{ in } \Omega \quad (1)$$

$$u_\varepsilon = g \text{ on } \partial\Omega$$

where $\mathbf{x} = (x_1, x_2) \in \Omega = \mathbb{R}^+ \times \mathbb{R}$, $\text{Im}(\omega^2) > 0$ (so that the problem is well-posed in $H^1(\Omega)$), $f \in L^2(\Omega)$, $g \in H^{1/2}(\partial\Omega)$, a and ρ are 1-periodic functions in the two directions which are uniformly bounded from above and below by strictly positive constants, and ε is the period of the medium. We are interested in the situation where the period is small compared to the wave length. In order to simplify the physical model and to reduce the computational cost, we want to propose an asymptotic model. The homogenization theory justifies that the periodic medium can be replaced by an effective homogeneous medium [1]. It is well-known that the homogenized model gives a good approximation of the macroscopic behavior of the solution but it poorly takes into account interfaces or boundaries. In this work, we propose an effective model which is enriched near the boundary. Note that this can be directly applied to the time-dependent wave equation.

2 Asymptotic expansion : ansatz and equations

The method consists in postulating the ansatz

$$u_\varepsilon(\mathbf{x}) = u_0(\mathbf{x}) + \varepsilon u_1 \left(\mathbf{x}; \frac{\mathbf{x}}{\varepsilon} \right) + \varepsilon^2 u_2 \left(\mathbf{x}; \frac{\mathbf{x}}{\varepsilon} \right) + \dots$$

$$+ \varepsilon U_1 \left(x_2; \frac{\mathbf{x}}{\varepsilon} \right) + \varepsilon^2 U_2 \left(x_2; \frac{\mathbf{x}}{\varepsilon} \right) + \dots \quad (2)$$

The first line of (2) is the two-scale asymptotic expansion of the classical homogenization theory which is relevant far from the boundary: the u_n 's are such that $\mathbf{y} = (y_1, y_2) \mapsto u_n(\mathbf{x}; \mathbf{y})$ is 1-periodic. For all $\mathbf{x} \in \Omega$, the study of $u_n(\mathbf{x}; \cdot)$ can be restricted to the periodicity cell $Y = (0, 1)^2$. The second line of (2) contains the so called near field terms which take account the boundary without polluting the two-scale expansion far from the boundary : the U_n 's are such that $y_2 \mapsto U_n(x_2; y_1, y_2)$ is 1-periodic and $y_1 \mapsto U_n(x_2; y_1, y_2)$ is exponentially decreasing as $y_1 \rightarrow +\infty$. For all x_2 , the study of $U_n(x_2; \cdot)$ can be restricted to a semi-infinite strip $\mathcal{S} = \mathbb{R} \times (0, 1)$. Formally, we inject this ansatz in the equation (1) and we show by induction that for all n , u_n is a sum of a so called oscillating part $u_n^{osc}(\mathbf{x}; \mathbf{y})$ which can be expressed thanks to the previous terms and the solutions of cell problems, and a so called macroscopic part $\hat{u}_n(\mathbf{x})$. Moreover, the necessary condition of existence of u_{n+2} leads to the volume equation satisfied by \hat{u}_n (as in classical homogenization) and the necessary condition of existence of U_n leads to its boundary condition. Finally, we recover for the first term the classical effective problem:

$$\begin{cases} -\nabla \cdot [A^* \nabla u_0] - \omega^2 \rho^* u_0 = f & \text{in } \Omega \\ u_0 = g & \text{on } \partial\Omega \end{cases} \quad (3)$$

where $A^* = (a_{ij}^*)$ is the homogenized tensor calculated from the periodic solutions w_i with vanishing mean value of the cell problems

$$-\nabla \cdot [a(\mathbf{y}) \nabla w_i] = -\partial_{y_i} a(\mathbf{y}) \text{ in } Y, \quad (4)$$

and $\rho^* = \int_Y \rho(\mathbf{y}) d\mathbf{y}$. For the second term, we have $u_1(\mathbf{x}; \mathbf{y}) = w_i(\mathbf{y}) \partial_{x_i} u_0(\mathbf{x}) + \hat{u}_1(\mathbf{x})$ where its macroscopic part \hat{u}_1 is solution of

$$\begin{cases} -\nabla \cdot [A^* \nabla \hat{u}_1] - \omega^2 \rho^* \hat{u}_1 = 0 & \text{in } \Omega \\ \hat{u}_1 = d_1^{(i)} \partial_{x_i} u_0 & \text{on } \partial\Omega \end{cases}$$

The coefficients $d_1^{(i)}$ are derived from the solution of problems set in the semi-infinite peri-

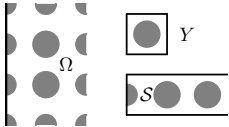


Figure 1: The domains Ω , Y and S

odic strip S (which can be solved by using for instance periodic DtN operators). Those coefficients take into account the way the boundary cuts the periodic medium.

Besides, for the third term, we have

$$u_2(\mathbf{x}; \mathbf{y}) = \partial_{x_i x_j}^2 u_0(\mathbf{x}) \theta_{ij}(\mathbf{y}) + \partial_{x_i} \hat{u}_1(\mathbf{x}) w_i(\mathbf{y}) + \omega^2 u_0(\mathbf{x}) \gamma(\mathbf{y}) + \hat{u}_2(\mathbf{x})$$

where θ_{ij} and γ are periodic solutions with vanishing mean value of cell problems similar to (4), and the macroscopic part \hat{u}_2 is solution of

$$\begin{cases} -\nabla \cdot [A^* \nabla \hat{u}_2] - \omega^2 \rho^* \hat{u}_2 = b_{ijkl}^* \partial_{ijkl}^4 u_0 + \omega^2 c_{ij}^* \partial_{ij}^2 u_0 + \omega^4 d^* u_0 & \text{in } \Omega \\ \hat{u}_2 = d_1^{(i)} \partial_i \hat{u}_1 + d_2^{(ij)} \partial_{ij}^2 u_0 + d_2^{(0)} u_0 & \text{on } \partial\Omega \end{cases}$$

Similarly to $d_1^{(i)}$, the coefficients $d_2^{(ij)}$ and $d_2^{(0)}$ are obtained thanks to the solution of strip problems. Let us remark that this third term is important for the homogenization of the time-dependent wave equation and more precisely to capture the long-time dispersion of the solution (see for instance [2]). So far, the long-time homogenization was studied without boundaries and in this work, we treat the presence of boundaries and propose appropriate boundary conditions.

This construction can be done at any order. Finally, under regularity assumptions on f and g , error estimates justify the expansion :

$$\forall n, \quad \left\| u_\varepsilon - \sum_{k=0}^n \varepsilon^k (u_k + U_k) \right\|_{L^2(\Omega)} = \mathcal{O}(\varepsilon^{n+1}),$$

$$\left\| u_\varepsilon - \sum_{k=0}^n \varepsilon^k (u_k + U_k) \right\|_{H^1(\Omega)} = \mathcal{O}(\varepsilon^n).$$

In classical homogenization, the near field terms are not considered and homogeneous boundary conditions are imposed for each macroscopic term. In that case, the error estimate in the H^1 norm is locked at any order at $\mathcal{O}(\sqrt{\varepsilon})$.

3 Approximate models

From the asymptotic expansion, it is possible to derive effective models which provide an approximation of the solution u_ε at a fixed order. Indeed, it is easy to see that $u_0 + \varepsilon \hat{u}_1$ satisfies up to an error $\mathcal{O}(\varepsilon^2)$:

$$\begin{cases} -\nabla \cdot [A^* \nabla v_\varepsilon] - \omega^2 \rho^* v_\varepsilon = f & \text{in } \Omega \\ v_\varepsilon - \varepsilon d_1^{(i)} \partial_{x_i} v_\varepsilon = g & \text{on } \partial\Omega \end{cases} \quad (5)$$

This problem can be ill-posed (unstable for the corresponding time-dependent problem) if $d_1^{(i)} < 0$. As the sign of this coefficient is not known a priori, we want to modify it without deteriorating the consistency order of the approximation. A first method consists in shifting artificially the boundary as in [3]. A simpler strategy consists in choosing another solution of the cell problem (4). More precisely, if w_i^M is the solution of (4) with the mean value equal to $M \in \mathbb{R}$, and if the asymptotic is performed with this cell solution, the coefficient $d_1^{(i)}$ is simply replaced by $d_1^{(i)} + M$. Thus for M large enough, the corresponding problem (5) is well-posed.

Then, $u_0 + \varepsilon \hat{u}_1 + \varepsilon^2 \hat{u}_2$ satisfies up to an error $\mathcal{O}(\varepsilon^3)$ an equation in which appears a fourth order operator. It is well known in the long time homogenization, even without boundaries, that this problem has to be modified in order to be well-posed. Because fourth order PDEs are not easy to discretize, we propose another approximate model. It consists (for sufficiently regular datas) in considering u_0 as a source term for the problem satisfied approximately by $\varepsilon \hat{u}_1 + \varepsilon^2 \hat{u}_2$. We end up with the volume equation set in Ω

$$\begin{aligned} -\nabla \cdot [A^* \nabla w_\varepsilon] - \omega^2 \rho^* w_\varepsilon &= \varepsilon^2 b_{ijkl}^* \partial_{ijkl}^4 u_0 \\ &+ \varepsilon^2 \omega^2 c_{ij}^* \partial_{ij}^2 u_0 + \varepsilon^2 \omega^4 d^* u_0 \end{aligned}$$

with the boundary condition

$$w_\varepsilon - \varepsilon d_1^{(i)} \partial_i w_\varepsilon = \varepsilon d_1^{(i)} \partial_i u_0 + \varepsilon^2 d_2^{(ij)} \partial_{ij}^2 u_0 + \varepsilon^2 d_2^{(0)} u_0$$

To make this problem well-posed, we adopt the same strategy than before. Numerical results will be shown for the time-harmonic and the time-dependent wave equations.

Acknowledgement.

This work is supported by DGA and Labex LMH

References

- [1] A.Bensoussan, J-L.Lions, G.Papanicolau, *Asymptotic Analysis for Periodic Structures*, 1st edition, North Holland, 1978
- [2] A.Lamacz, *Dispersive effective models for waves in heterogeneous media*, M3AS, 21(9), 1871–1899, 2011
- [3] B.Delourme, *Asymptotic models for thin periodic layers in electromagnetism*, PhD thesis, UPMC, 2010

Effective description of waves in discrete and heterogeneous media

Ben Schweizer^{1,*}, Agnes Lamacz², Florian Theil³, Tomas Dohnal⁴¹Fakultät für Mathematik, TU Dortmund, Germany²U Duisburg-Essen³U Warwick⁴U Halle-Wittenberg

*Email: ben.schweizer@tu-dortmund

Abstract

Our analysis is motivated by the wave equation on \mathbb{R}^d with periodic coefficients,

$$\partial_t^2 u^\varepsilon = \nabla \cdot (a(\frac{x}{\varepsilon}) \nabla u^\varepsilon(x)).$$

Homogenization theory predicts that solutions can be described, in the limit of small periodicity $\varepsilon > 0$, by an effective wave equation

$$\partial_t^2 u(x, t) = AD^2 u(x, t),$$

where the effective coefficient A can be constructed with the help of cell-problems. Nevertheless, when we consider large time intervals of order $1/\varepsilon^2$, the effective equation from above leads to predictions that are off by the order 1. In the two papers [2,3], the authors showed that a good effective equation (with constant coefficients) has the form

$$\partial_t^2 w^\varepsilon = AD^2 w^\varepsilon + \varepsilon^2 ED^2 \partial_t^2 w^\varepsilon - \varepsilon^2 FD^4 w^\varepsilon. \quad (1)$$

The authors supplied a rigorous proof that, for appropriate coefficient tensors A, E , and F , the solution w^ε to the above equation approximates u^ε on time intervals $[0, T/\varepsilon^2]$. The result is based on a Bloch-wave representation of solutions and uses the “replacement trick” in order to transform the “bad Bousinesq equation” into a well posed partial differential equation.

Starting from this result, we considered the following two research questions.

Long time behavior of lattice dynamics

In this project with F. Theil we are interested in discrete wave equations on a lattice, $\gamma \in \varepsilon\mathbb{Z}^d$,

$$\partial_t^2 u^\varepsilon(\gamma, t) = \frac{1}{\varepsilon^2} \sum_{j \in \mathbb{Z}^d} a_j u^\varepsilon(\gamma + \varepsilon j, t)$$

with correlation numbers a_j . The lattice points are undistinguishable; nevertheless, by its discrete character, the system has an ε -periodicity.

We may therefore expect that a weakly dispersive equation similar to (1) appears in the limit. This fact was derived rigorously in [1].

Description with profile dynamics

The work [1] actually contains an additional result, which was further developed in [4]. We describe the solution of the weakly dispersive equation (1) with profile functions.

In order to introduce the idea, let us first describe the 1-dimensional situation: The long time behavior of the dispersive equation

$$\partial_t^2 u = c^2 \partial_x^2 u + \varepsilon^2 p \partial_x^4 u$$

can be described by the linearized KdV-equation

$$\partial_\tau V(z, \tau) = -\frac{p}{2c} \partial_z^2 V(z, \tau).$$

This fact can easily be shown with the ansatz $u(x, t) = V(x - ct, \varepsilon^2 t)$. What is interesting already in the 1-dimensional situation is the selection of initial values: In terms of the Fourier transforms, we must choose, for the right-going pulse V and its initial data V_0 :

$$\hat{V}_0^\varepsilon(\xi) := \begin{cases} \hat{u}_0^\varepsilon(\xi) & \text{for } \xi > 0 \\ 0 & \text{else.} \end{cases}$$

The result can be obtained also in higher space dimension. We consider a solution of a (dispersive) wave equation, in Fourier space given by $\hat{u}(k, \tau/\varepsilon^2) = \hat{u}_0(k) e^{-i(c|k|/\varepsilon^2 + b(|k|))\tau}$. The result of [4] is that this solution can be reconstructed in physical space with profile functions. The reconstruction is done in three steps. With an operator \mathcal{R} , we extract from the Fourier transform of initial data the Fourier transform of profile equation initial data:

$$\mathcal{R}\hat{u}_0(\xi, q) := \left(\frac{|\xi|}{2\pi i} \right)^{\frac{d-1}{2}} \hat{u}_0(|\xi|q \mathbf{1}_{\{\xi>0\}}).$$

In this equation, a vector $q \in S^{d-1}$ is used to select a direction of interest. The profile evolution is given in Fourier space for initial data \hat{V}_0 with a multiplication,

$$(J_b \hat{V}_0)(\xi, q, \tau) := e^{-ib(\xi)\tau} \hat{V}_0(\xi, q).$$

We note that the choice $b(\xi) = b_3 \xi^3$ leads to the linearized KdV-equation mentioned above.

Finally, from the profiles $V = V(z, q, \tau)$, we can reconstruct a function in physical space with a shell-like distribution of the profiles,

$$(SV)(x, t) := \frac{1}{(ct)^{(d-1)/2}} V\left(|x| - ct, \frac{x}{|x|}, \varepsilon^2 t\right) \mathbf{1}_{\{|x| < 2ct\}}.$$

The main result of [4] provides an approximation result for the reconstruction operator

$$\mathcal{Q}_b = \mathcal{S} \circ \mathcal{F}_1^{-1} \circ J_b \circ \mathcal{R}.$$

We obtain, for initial data \hat{u}_0 with some smoothness properties, the convergence

$$(\hat{\mathcal{Q}}_b \hat{u}_0)(k, \tau/\varepsilon^2) e^{ic|k|\tau/\varepsilon^2} - e^{-ib(|k|)\tau} \hat{u}_0(k) \rightarrow 0.$$

The proof uses the method of stationary phase and is performed in dimensions $d \in \{1, 2, 3\}$.

Keywords: Heterogeneous media, discrete media, dispersion, profile equation

References

- [1] B. Schweizer and F. Theil, Lattice dynamics on large time scales and dispersive effective equations, *SIAM J. Appl. Math.*. Vol. 78(6), (2018), pp. 3060-3086.
- [2] T. Dohnal, A. Lamacz, and B. Schweizer, Dispersive homogenized models and coefficient formulas for waves in general periodic media, *Asymptot. Anal.* Vol. 93(1-2), (2015), pp. 21-49.
- [3] T. Dohnal, A. Lamacz, and B. Schweizer, Bloch-wave homogenization on large time scales and dispersive effective wave equations, *Multiscale Model. Simul.* Vol. 12(2), (2014), pp. 488-513.
- [4] A. Lamacz, and B. Schweizer, Representation of solutions to wave equations with profile functions, *Preprint TU Dortmund* (2019).

Frames for the solution of operator equations in Hilbert spaces with fixed dual pairing

Peter Balazs¹, Helmut Harbrecht²¹Acoustics Research Institute Austrian Academy of Sciences, Vienna, AUSTRIA²Department of Mathematics and Computer Science, University of Basel, Basel, SWITZERLAND**Abstract**

For the solution of operator equations, Stevenson introduced a definition of frames, where a Hilbert space and its dual are *not* identified. We are going to revisit the concept of Stevenson frames and introduce it for Banach spaces, show that in this setting the investigation of ℓ^2 -Banach frames make sense and apply them to the discretization of operator equations.

Details and proofs can be found in [3].

Keywords: Banach frames, Stevenson frames, matrix representation, discretization of operators.

1 Introduction

The standard definition of frames in a Hilbert space \mathcal{H} by Duffin and Schaefer [10] is the following:

$$\|f\|_{\mathcal{H}} \approx \|\langle f, \psi_k \rangle_{\mathcal{H}}\|_{\ell^2} \text{ for all } f \in \mathcal{H}. \quad (1)$$

Here, $x \approx y$ means that there are constants $0 < A \leq B < \infty$ such that $A \cdot x \leq y \leq B \cdot x$.

This concept led to a lot of theoretical work, see e.g. [6, 7], but has been used also extensively in signal processing [5], quantum mechanics [11], acoustics [4] and various other fields.

Frames can be used also to represent operators. For the numerical solution of operator equations, the (Petrov-) Galerkin scheme [15] is used, where operators are represented by

$$\langle O\psi_k, \phi_l \rangle_{k,l \in K},$$

called the *stiffness* or *system matrix*. The collection $\Psi = (\psi_k)_{k \in K}$ consists of the ansatz functions, the collection $\Phi = (\phi_k)_{k \in K}$ are the test functions.

In finite and boundary element approaches, bases were used [9], but also frames have been applied, e.g. in [13, 16]. Recently, such operator representations got also a more theoretical treatment [1, 2].

Partial differential operators are typically operators of the form $O : \mathcal{H} \rightarrow \mathcal{H}'$, while boundary integral operators might also be smoothing operators which map in accordance with

$O : \mathcal{H}' \rightarrow \mathcal{H}$. One possible solution is to work with Gelfand triples i.e. $\mathcal{H} \subset \mathcal{H}_0 \subset \mathcal{H}'$. This is explicitly done for the concept of Gelfand frames [8].

Another possibility is the following, introduced by Stevenson in [16]: A collection $\Psi = (\psi_k)_{k \in K} \subset \mathcal{H}$ is called a (Stevenson) frame for \mathcal{H} , if

$$\|f\|_{\mathcal{H}'} \approx \|\langle f, \psi_k \rangle_{\mathcal{H}', \mathcal{H}}\|_{\ell^2} \text{ for all } f \in \mathcal{H}'. \quad (2)$$

Clearly, the definitions (1) and (2) are equivalent by the Riesz isomorphism, i.e. considering $\mathcal{H} \cong \mathcal{H}'$. If another isomorphism is utilized, for example, considering the triple $\mathcal{H} \subset \mathcal{H}_0 \subset \mathcal{H}'$, using the Riesz isomorphism on the pivot space $\mathcal{H}_0 \cong \mathcal{H}'_0$, \mathcal{H} and \mathcal{H}' cannot be considered to be equal.

On a more theoretical level, let us consider Banach frames [12]. For a Banach space X , a sequence space X_d , a sequence $\Psi \subset X'$ is a X_d -frame if

$$\|f\|_X \approx \|\langle f, \psi_k \rangle_{X, X'}\|_{X_d} \text{ for all } f \in X.$$

It is called a Banach frame if a reconstruction operator exists, i.e. there exists $R : X_d \rightarrow X$ with $R(\langle f, \psi_k \rangle_{X, X'}) = f$ for all $f \in X$.

In this presentation, we look at ℓ^2 -Banach Stevenson frames and apply them for the matrix discretization of operator equations.

2 Stevenson Banach Frames

Definition 1 Let (X, X') be a dual pair of reflexive Banach spaces. Let $\Psi = (\psi_k)_{k \in K} \subset X$. It is called a *Stevenson Banach frame* for X , if there exist bounds $0 < A_{\Psi} \leq B_{\Psi} < \infty$ such that

$$A_{\Psi} \|f\|_{X'}^2 \leq \|\langle f, \psi_k \rangle_{X', X}\|_{\ell^2}^2 \leq B_{\Psi} \|f\|_{X'}^2$$

for all $f \in X'$.

Consider the frame operator $S_{\Psi} f = \sum \langle f, \psi_k \rangle_{X', X} \psi_k$, which is a mapping $S_{\Psi} : X' \rightarrow X$. In this setting one can show [3]:

Theorem 2 *The sequence $\tilde{\Psi} = (\tilde{\psi}_k)_{k \in K} := (S_{\Psi}^{-1}\psi_k)_{k \in K} \subset X'$ is a Stevenson Banach frame for X' with bounds $\frac{1}{B_{\Psi}}$ and $\frac{1}{A_{\Psi}}$. For $f \in X$ and $g \in X'$, we have the reconstructions*

$$f = \sum_{k \in K} \langle f, \tilde{\psi}_k \rangle_{X, X'} \psi_k$$

and

$$g = \sum_{k \in K} \langle g, \psi_k \rangle_{X', X} \tilde{\psi}_k.$$

Set $\langle\langle u, v \rangle\rangle := \langle u, S_{\Psi}v \rangle_{X', X}$. This is, trivially, a symmetric and positive bilinear form and, therefore, an inner product on X' making $(X', \langle\langle \cdot, \cdot \rangle\rangle)$ a Hilbert space with equivalent norm.

But note that for things like condition numbers, constants in convergence rates, etc. the concrete norms are important. So in this case distinguishing ℓ^2 -Banach frames from Hilbert frames is necessary and useful.

3 Matrix Representation

If we have an operator $O : X \rightarrow X'$ and look at the equation $Ou = b$, we use

$$Ou = b \iff \sum_k \langle u, \tilde{\psi}_k \rangle_{X, X'} O\psi_k = b,$$

which implies

$$\sum_k \langle u, \tilde{\psi}_k \rangle_{X, X'} \langle O\psi_k, \psi_l \rangle_{X', X} = \langle b, \psi_l \rangle_{X', X}$$

for all $l \in K$. Setting $\mathbf{M} = \langle O\psi_n, \psi_m \rangle_{X', X}$, $\vec{u}_k = \langle u, \tilde{\psi}_k \rangle$ and $\vec{b}_k = \langle b, \psi_k \rangle$, we thus have

$$Ou = b \iff \mathbf{M}\vec{u} = \vec{b}.$$

Solving the system of linear equations $\mathbf{M}\vec{u} = \vec{b}$ gives a solution to $Ou = b$ by $u = \sum_k \vec{u}_k \psi_k$. Note that this avoids the numerically expensive calculation of a dual frame [14].

References

[1] P. Balazs. Matrix-representation of operators using frames. *Sampling Theory in Signal and Image Processing (STSIPI)*, 7(1):39–54, 2008.

[2] P. Balazs and K. Gröchenig. A guide to localized frames and applications to Galerkin-like representations of operators. In I. Pesenson, H. Mhaskar, A. Mayeli, Q. T. L. Gia, and D.-X. Zhou, editors, *Frames and Other Bases in Abstract and Function Spaces*, Applied and Numerical Harmonic Analysis series (ANHA). Birkhauser/Springer, 2017.

[3] P. Balazs and H. Harbrecht. Frames for the solution of operator equations in Hilbert spaces with fixed dual pairing. *Numerical Functional Analysis and Optimization*, 40(1):65–84, 2019. preprint.

[4] P. Balazs, N. Holighaus, T. Necciarì, and D. Stoeva. Frame theory for signal processing in psychoacoustics. In R. Balan, J. J. Benedetto, W. Czaja, and K. Okoudjou, editors, *Excursions in Harmonic Analysis Vol. 5*, pages 225–268. Springer, 2017.

[5] H. Bölcskei, F. Hlawatsch, and H. G. Feichtinger. Frame-theoretic analysis of oversampled filter banks. *IEEE Trans. Signal Processing*, 46(12):3256–3268, 1998.

[6] P. Casazza. The art of frame theory. *Taiwanese J. Math.*, 4(2):129–202, 2000.

[7] O. Christensen. *An Introduction to Frames and Riesz Bases*. Birkhäuser, 2016.

[8] S. Dahlke, M. Fornasier, and T. Raasch. Adaptive Frame Methods for Elliptic Operator Equations. *Adv. Comput. Math.*, 27(1):27–63, 2007.

[9] W. Dahmen and R. Schneider. Composite wavelet basis for operator equations. *Math. Comp.*, 68:1533–1567, 1999.

[10] R. J. Duffin and A. C. Schaeffer. A class of non-harmonic Fourier series. *Trans. Amer. Math. Soc.*, 72:341–366, 1952.

[11] J.-P. Gazeau. *Coherent states in quantum physics*. Wiley, Weinheim, 2009.

[12] K. Gröchenig. Describing functions: atomic decompositions versus frames. *Monatsh. Math.*, 112(3):1–41, 1991.

[13] H. Harbrecht, R. Schneider, and C. Schwab. Multilevel frames for sparse tensor product spaces. *Numer. Math.*, 110(2):199–220, 2008.

[14] A. J. Janssen and P. Sondergaard. Iterative algorithms to approximate canonical Gabor windows: Computational aspects. *J. Fourier Anal. Appl.*, 13(2):211–241, April 2007.

[15] S. Sauter and C. Schwab. *Boundary Element Methods*. Springer Series in Computational Mathematics. Springer Berlin Heidelberg, 2010.

[16] R. Stevenson. Adaptive solution of operator equations using wavelet frames. *SIAM J. Numer. Anal.*, 41(3):1074–1100, 2003.

[17] D. T. Stoeva. X_d -frames in Banach spaces and their duals. *Int. J. Pure Appl. Math.*, 52(1):1–14, 2009.

U-cross Gram matrices and their invertibility

Peter Balazs¹, Mitra Shamsabadi², Ali Akbar Arefijamaal^{3,*}

¹Acoustics Research Institute Austrian Academy of Sciences, Vienna, AUSTRIA.

²Department of Mathematics and Computer Sciences, Hakim Sabzevari University, Sabzevar, IRAN.

³Department of Mathematics and Computer Sciences, Hakim Sabzevari University, Sabzevar, IRAN.

*Email: arefijamaal@hsu.ac.ir

Abstract

The Gram matrix is defined for Bessel sequences by combining synthesis with subsequent analysis operators. If different sequences are used and an operator U is inserted we reach so called U -cross Gram matrices. Many authors investigated how to find a matrix representation of operators on a Hilbert space \mathcal{H} with Bessel sequences, frames and Riesz bases. In this talk, we show that under mild conditions the pseudo-inverse of a U -cross Gram matrix can always be represented as a U -cross Gram matrix with dual frames of the given ones. Details and proofs can be found in [4].

Keywords: Frames, dual frames, U -cross Gram matrices, pseudo-inverses.

1 Introduction

From practical experience it soon has become apparent that the concept of an orthonormal basis is not always useful. Sometimes it is more important for a decomposing set to have other special properties rather than guaranteeing unique coefficients. For example it is impossible to have good time-frequency localization for Gabor ONBs or a wavelet ONB with a mother wavelet which has exponentially decay and is infinitely often differentiable with bounded derivatives [9]. Furthermore suitable ONBs are often difficult to construct in a numerical efficient way. This led to the concept of frames, which was introduced by Duffin and Schaefer [8].

Some operator equations, e.g. in acoustics [10] and vibration simulation [5] cannot be treated analytically, but have to be solved numerically. Depending on the problem this can be done using a boundary element method [11] or finite element method [7] approach. Thereby operator equations $Of = b$, are transferred to matrix levels to be able to be treated numerically [11]. A standard approach for that, the Galerkin

method, is using orthonormal basis (ONB) $\{e_i\}_{i \in I}$ and investigate the matrix

$$M_{k,l} := \langle Oe_l, e_k \rangle$$

solving $Mc = d$ for $d = \{d_l\}_{l \in I} = \{\langle b, e_l \rangle\}_{l \in I}$. More recently frames are used for such a discretization (3, 6).

A sequence $\Phi = \{\phi_i\}_{i \in I}$ in a separable Hilbert space \mathcal{H} is a *frame* if there exist constants $A_\Phi, B_\Phi > 0$ such that for all $f \in \mathcal{H}$

$$A_\Phi \|f\|^2 \leq \sum_{i \in I} |\langle f, \phi_i \rangle|^2 \leq B_\Phi \|f\|^2. \quad (1)$$

The numbers A_Φ and B_Φ are called the *frame bounds*. We call a complete Bessel sequence an *upper semi-frame* (1, 2). If $\{\phi_i\}_{i \in I}$ is assumed to satisfy the right hand of (1), then it is called a *Bessel sequence* with Bessel bound B_Φ . For a Bessel sequence $\Phi = \{\phi_i\}_{i \in I}$, the *synthesis operator* $T_\Phi : \ell^2 \rightarrow \mathcal{H}$ is defined by

$$T_\Phi \{c_i\}_{i \in I} = \sum_{i \in I} c_i \phi_i.$$

Its adjoint operator $T_\Phi^* : \mathcal{H} \rightarrow \ell^2$; the so called *analysis operator* is given by

$$T_\Phi^* f = \{\langle f, \phi_i \rangle\}_{i \in I}.$$

The operator $S_\Phi : \mathcal{H} \rightarrow \mathcal{H}$, which is defined by $S_\Phi f = T_\Phi T_\Phi^* f = \sum_{i \in I} \langle f, \phi_i \rangle \phi_i$, for all $f \in \mathcal{H}$, is called the *frame operator*. For a frame Φ the operator T_Φ is onto, T_Φ^* is one-to-one, and S_Φ is positive, self-adjoint and invertible [9]. A *dual* for a Bessel sequence $\Phi = \{\phi_i\}_{i \in I} \subseteq \mathcal{H}$ is a Bessel sequence $\Psi = \{\psi_i\}_{i \in I}$ in \mathcal{H} such that

$$f = \sum_{i \in I} \langle f, \psi_i \rangle \phi_i, \quad (f \in \mathcal{H}).$$

For a frame Φ it is obvious to see that the Bessel sequence $\{S_\Phi^{-1} \phi_i\}_{i \in I}$ is a dual and is itself a frame again. This dual, denoted by $\tilde{\Phi} = \{\tilde{\phi}_i\}_{i \in I}$ is called the *canonical dual*. A *Riesz basis* for \mathcal{H}

¹This work was supported by FWF project Y 551-N13.

is a family of the form $\{Ue_i\}_{i \in I}$, where $\{e_i\}_{i \in I}$ is an orthonormal basis for \mathcal{H} and $U : \mathcal{H} \rightarrow \mathcal{H}$ is a bounded bijective operator. Every Riesz basis is a frame and has a biorthogonal sequence which is also its unique dual. In this talk, we present U -cross Gram matrices and their properties.

2 Main Results

Definition 1 Let $\Psi = \{\psi_i\}_{i \in I}$ and $\Phi = \{\phi_i\}_{i \in I}$ be Bessel sequences in Hilbert spaces \mathcal{H}_1 and \mathcal{H}_2 , respectively. For $U \in \mathbf{B}(\mathcal{H}_1, \mathcal{H}_2)$, the matrix $\mathbf{G}_{U, \Phi, \Psi}$ given by

$$(\mathbf{G}_{U, \Phi, \Psi})_{i,j} = \langle U\psi_j, \phi_i \rangle, \quad (i, j \in I), \quad (2)$$

is called the U -cross Gram matrix. If $\mathcal{H}_1 = \mathcal{H}_2$ and $U = I_{\mathcal{H}_1}$ it is called the cross Gram matrix and denoted by $\mathbf{G}_{\Phi, \Psi}$. We use \mathbf{G}_Φ for $\mathbf{G}_{\Phi, \Phi}$; the so called Gram matrix [9].

Obviously, $\mathbf{G}_{U, \Phi, \Psi} = T_\Phi^* U T_\Psi$ and $\|\mathbf{G}_{U, \Phi, \Psi}\| \leq \sqrt{B_\Phi B_\Psi} \|U\|$. It is a compact operator when U is compact. In the next theorem, we study sufficient conditions for the invertibility of the U -cross Gram matrix associated to Riesz sequences.

Theorem 2 Let $U \in \mathbf{B}(\mathcal{H}_1, \mathcal{H}_2)$, $\Phi = \{\phi_i\}_{i \in I}$ and $\Psi = \{\psi_i\}_{i \in I}$ be two Bessel sequences in \mathcal{H}_2 and \mathcal{H}_1 , respectively, such that $\mathbf{G}_{U, \Phi, \Psi}$ is invertible. Then Φ and Ψ are Riesz sequences in \mathcal{H}_2 and \mathcal{H}_1 , respectively. If Φ and Ψ are assumed to be upper semi-frames, Φ and Ψ are Riesz bases and U is invertible. In this case,

$$(\mathbf{G}_{U, \Phi, \Psi})^{-1} = \mathbf{G}_{U^{-1}, \tilde{\Psi}, \tilde{\Phi}},$$

For a closed range operator $U \in \mathbf{B}(\mathcal{H}_1, \mathcal{H}_2)$, the pseudo-inverse of U is the unique operator $U^\dagger \in \mathbf{B}(\mathcal{H}_1, \mathcal{H}_2)$ satisfying that

$$\mathbf{N}(U^\dagger) = \mathbf{R}(U)^\perp, \quad \mathbf{R}(U^\dagger) = \mathbf{N}(U)^\perp,$$

and $UU^\dagger U = U$.

If U has closed range, then U^* has closed range and $(U^*)^\dagger = (U^\dagger)^*$, see e.g. Lemma 2.5.2 of [9]. Similar to the case for multipliers [12] we can show that there exist duals that allow the representation of the pseudo-inverse as a matrix of the same class.

Theorem 3 Let Ψ and Φ be frames in Hilbert space \mathcal{H} , $U \in \mathbf{B}(\mathcal{H})$ be an invertible operator and $\mathbf{G}_{U, \Phi, \Psi}$ have closed range. Then the following assertions hold:

(1) There exists a unique dual $\Phi^{(U, \Psi)}$ of Φ such that

$$(\mathbf{G}_{U, \Phi, \Psi})^\dagger = \mathbf{G}_{U^{-1}, \tilde{\Psi}, \Phi^{(U, \Psi)}}.$$

(2) There exists a unique dual $\Psi^{(\overline{U, \Phi})}$ of Ψ such that

$$(\mathbf{G}_{U, \Phi, \Psi})^\dagger = \mathbf{G}_{U^{-1}, \Psi^{(\overline{U, \Phi})}, \tilde{\Phi}}.$$

References

1. J.-P. Antoine and P. Balazs. Frames and semi-frames. *J. Phys. A*, 44:205201, 2004.
2. J.-P. Antoine and P. Balazs. Frames, semi-frames, and Hilbert scales. *Numer. Funct. Anal. Optim.*, 33(7-9):736-769, 2012.
3. P. Balazs. Basic definition and properties of Bessel multipliers. *J. Math. Anal. Appl.*, 325(1):571-585, 2007.
4. P. Balazs, M. Shamsabadi, A. Arefijamaal and A. Rahimi. U -cross Gram matrices and their invertibility. *J. Math. Anal. Appl.*, accepted, 2019.
5. P. Balazs, W. Kreuzer and H. Waubke. A stochastic 2D-model for calculating vibrations in liquids and soils. *J. Comput. Acoust.*, 15(3)(2007), pp.271-283.
6. P. Balazs and H. Harbrecht. Frames for the solution of operator equations in Hilbert spaces with fixed dual pairing. *Numer. Funct. Anal. Optim.*, accepted, 2018.
7. S. Brenner and L. Scott. The mathematical theory of finite element methods. 2nd ed., Springer New York, 2002.
8. R. J. Duffin and A. C. Schaeffer. A class of non-harmonic Fourier series. *Trans. Amer. Math. Soc.*, 72 (1952), pp.341-366.
9. O. Christensen. Frames and Bases: An Introductory Course. Birkhäuser, Boston, 2008.
10. W. Kreuzer, P. Majdak and Z. Chen. Fast multipole boundary element method to calculate head-related transfer functions for a wide frequency range. *J. Acoust. Soc. Am.*, 126(3) (2009), pp.1280-1290.
11. S. Sauter and C. Schwab. Boundary Element Methods. Springer Berlin Heidelberg, 2010.
12. D. T. Stoeva and P. Balazs. Invertibility of multipliers. *Appl. Comput. Harmon. Anal.*, 33(2) (2012), pp.292-299.

The invertibility of U -fusion cross Gram matrices of operatorsMitra Shamsabadi^{1,*}, Ali Akbar Arefijamaal², Peter Balazs³¹Department of Mathematics and Computer Sciences, Hakim Sabzevari University, Sabzevar, IRAN.²Department of Mathematics and Computer Sciences, Hakim Sabzevari University, Sabzevar, IRAN.³Acoustics Research Institute Austrian Academy of Sciences, Vienna, AUSTRIA.

*Email: mi.shamsabadi@hsu.ac.ir

Abstract

For applications like the numerical solution of physical equations a discretization scheme for operators is necessary. Recently frames have been used for such an operator representation. In this paper, we do this with fusion frames. We interpret the operator representation using fusion frames as a generalization of fusion Gram matrices. Also we study the (pseudo-)invertibility of the U -cross Gram matrices, characterize fusion orthonormal bases and fusion Riesz bases by those properties and give formulas for the (pseudo-)inverses. For more details see [2, 10].

Keywords: Fusion frames, Dual, U - fusion cross Gram matrices, pseudo-inverses.

1 Introduction

For a numerical treatment of operator equations, used for example for solving integral equations in acoustics [7], the involved operators have to be discretized to be handled numerically. Applying (Petrov-)Galerkin approach [5]. For an operator O , the matrix M defined by $M_{k,l} = \langle O\psi_l, \phi_k \rangle$ is called the matrix corresponding to the operator O , or the system matrix. The standard way for the discretization of operators is using bases, but recently the general theory for frames has been developed. Frames were also used in numerics (6), in particular in an adaptive approach (1). As the concept of domain decomposition is a particularly relevant topic in this field, the investigation of operators with fusion frame is very important (9).

Let $\{W_i\}_{i \in I}$ be a family of closed subspaces of \mathcal{H} and $\{\omega_i\}_{i \in I}$ be a family of weights, i.e. $\omega_i > 0, i \in I$. The sequence $\{(W_i, \omega_i)\}_{i \in I}$ is called a *fusion frame* for \mathcal{H} if there exist constants $0 < A_W \leq B_W < \infty$ such that

$$A_W \|f\|^2 \leq \sum_{i \in I} \omega_i^2 \|\pi_{W_i} f\|^2 \leq B_W \|f\|^2, \quad (f \in \mathcal{H}).$$

³This work was supported by FWF project Y 551-N13.

The constants A_W and B_W are called *fusion frame bounds*. If we have the upper bound, we call $\{(W_i, \omega_i)\}_{i \in I}$ a *Bessel fusion sequence*. A fusion frame $\{(W_i, \omega_i)\}_{i \in I}$ is said to be an *fusion orthonormal basis* if $\mathcal{H} = \bigoplus_{i \in I} W_i$ and a *fusion Riesz basis* for \mathcal{H} if there exist constants $0 < C \leq D < \infty$ such that for each finite subset $J \subseteq I$

$$C \sum_{j \in J} \|f_j\|^2 \leq \left\| \sum_{j \in J} \omega_j f_j \right\|^2 \leq D \sum_{j \in J} \|f_j\|^2, \quad (f_j \in \mathcal{H}) \quad (1)$$

for a given fusion Riesz basis $W = \{(W_i, \omega_i)\}_{i \in I}$ denote by W' the 1-uniform family of subspaces $\{(W_i, 1)\}_{i \in I}$. Furthermore, the *synthesis operator*

$T_W : (\sum_{i \in I} \bigoplus W_i) \ell^2 \rightarrow \mathcal{H}$ for a Bessel fusion sequence $\{(W_i, \omega_i)\}_{i \in I}$ is defined by

$$T_W(\{f_i\}_{i \in I}) = \sum_{i \in I} \omega_i f_i, \quad \text{for } (f_i)_{i \in I} \in \left(\sum_{i \in I} \bigoplus W_i \right) \ell^2$$

The adjoint operator $T_W^* : \mathcal{H} \rightarrow (\sum_{i \in I} \bigoplus W_i) \ell^2$ which is called the *analysis operator* is given by

$$T_W^* f = \{\omega_i \pi_{W_i} f\}_{i \in I}, \quad (f \in \mathcal{H}).$$

Both are bounded by $\sqrt{B_W}$. If $\{(W_i, \omega_i)\}_{i \in I}$ is a fusion frame, the *fusion frame operator* $S_W : \mathcal{H} \rightarrow \mathcal{H}$, which is defined by $S_W f = T_W T_W^* f = \sum_{i \in I} \omega_i^2 \pi_{W_i} f$, is bounded (with bound B_W), invertible and positive (3, 8).

Every Bessel fusion sequence $\{(W_i, \omega_i)\}_{i \in I}$ is called a *Gävruta-dual* of $\{(W_i, \omega_i)\}_{i \in I}$, if

$$f = \sum_{i \in I} \omega_i v_i \pi_{V_i} S_W^{-1} \pi_{W_i} f, \quad (f \in \mathcal{H}).$$

The sequence of subspaces $\widetilde{W} := \{(S_W^{-1} W_i, \omega_i)\}_i$ is also a fusion frame for \mathcal{H} and a dual of $\{(W_i, \omega_i)\}_i$ called the *canonical dual* of W

2 Main Results

Definition 1 Let $W = \{(W_i, \omega_i)\}_{i \in I}$ be a Bessel fusion sequence for \mathcal{H} and $V = \{(V_i, v_i)\}_{i \in I}$ a

fusion frame for \mathcal{H} . For $U \in B(\mathcal{H})$, the matrix operator $\mathcal{G}_{U,W,V} : (\sum_{i \in I} \oplus W_i)_{\ell^2} \rightarrow (\sum_{i \in I} \oplus W_i)_{\ell^2}$ given by

$$\mathcal{G}_{U,W,V} = \phi_{WV} T_V^* U T_W = \{\pi_{W_i} S_V^{-1} T_V^* U T_W\}_{i \in I},$$

is called the U -fusion cross Gram matrix. If $U = I_{\mathcal{H}}$, it is called fusion cross Gram matrix and denoted by $\mathcal{G}_{W,V}$. We use \mathcal{G}_W for $\mathcal{G}_{W,W}$; the so called fusion Gram matrix.

Theorem 2 Let $W = \{(W_i, \omega_i)\}_{i \in I}$ be a fusion frame in \mathcal{H} and U an invertible operator in $B(\mathcal{H})$. Then the following assertions hold.

(1) If W is a fusion orthonormal basis, then the inverse of $\mathcal{G}_{U,W,W}$ is also a Gram matrix and $\mathcal{G}_{U,W,W}^{-1} = \mathcal{G}_{U^{-1},W,W}$.

(2) If $\mathcal{G}_{U,W,W}$ is invertible, then W is a fusion Riesz basis and

$$\mathcal{G}_{U,W,W}^{-1} = \mathcal{G}_{S_W^{-1} U^{-1} S_W^{-1}, W, W}.$$

(3) If $\mathcal{G}_{U, \widetilde{W}, W}$ is invertible, then W is a fusion Riesz basis and $\mathcal{G}_{U, \widetilde{W}, W}^{-1} = \mathcal{G}_{U^{-1}, \widetilde{W}, W}$.

(4) If $\mathcal{G}_{U, W, \widetilde{W}}$ is invertible, then W is a fusion Riesz basis and

$$\mathcal{G}_{U, W, \widetilde{W}}^{-1} = \mathcal{G}_{(O U S_{W'}^{-1})^{-1}, W, W},$$

$$\text{where } O = T_W \phi_{W \widetilde{W}} T_{\widetilde{W}}^*.$$

(5) If $\mathcal{G}_{U, \widetilde{W}, \widetilde{W}}$ is invertible, then W is a fusion Riesz basis and

$$\mathcal{G}_{U, \widetilde{W}, \widetilde{W}}^{-1} = \mathcal{G}_{S_{\widetilde{W}}^{-1} U^{-1} S_{\widetilde{W}}^{-1}, W, W}.$$

For a closed range operator $U \in \mathbf{B}(\mathcal{H}_1, \mathcal{H}_2)$, the pseudo-inverse of U is the unique operator $U^\dagger \in \mathbf{B}(\mathcal{H}_1, \mathcal{H}_2)$ satisfying that

$$\mathbf{N}(U^\dagger) = \mathbf{R}(U)^\perp, \quad \mathbf{R}(U^\dagger) = \mathbf{N}(U)^\perp,$$

and $U U^\dagger U = U$ (4).

Theorem 3 Let $W = \{(W_i, \omega_i)\}_{i \in I}$ be a fusion frame in \mathcal{H} and U a closed range operator in $B(\mathcal{H})$, also let $\mathcal{G}_{U, \widetilde{W}, W}$ have closed range. Then

$$\mathcal{G}_{U, \widetilde{W}, W}^\dagger = \mathcal{G}_{U^\dagger, \widetilde{W}, W}$$

if and only if $S_W^{-1} \pi_{W_i} = \pi_{\widetilde{W}_i}$ on $\mathbf{R}(U^*) \cup \mathbf{R}(U)$.

Definition 4 Let $W = \{(W_i, w_i)\}_{i \in I}$ be a fusion frame with bounds A_W and B_W , respectively. The alternate fusion frame operator $L_W : \mathcal{H} \rightarrow \mathcal{H}$ is defined by

$$L_W = T_W \phi_{W W} T_W^*.$$

It follows that L_W is bounded, positive, self-adjoint and invertible operator.

Theorem 5 Let $W = \{(W_i, \omega_i)\}_{i \in I}$ be a fusion frame in \mathcal{H} and $U \in B(\mathcal{H})$ be onto. If $\mathcal{G}_{U,W,W}$ is a closed range operator, then

$$(\mathcal{G}_{U,W,W})^\dagger = \mathcal{G}_{L_W U^\dagger L_W^{-1}, W, W}$$

if and only if

$$\pi_{W_i} S_W^{-1} \pi_{W_i} = \pi_{W_i} L_W^{-1}, \quad (i \in I)$$

on $\mathbf{R}(U^*) \cup \mathbf{R}(U)$.

References

1. P. Balazs. Matrix-representation of operators using frames. *Sampl. Theory Signal Image Process.*, 7(1):39–54, 2008.
2. P. Balazs, M. Shamsabadi, A. A. Arefijamaal, and A. Rahimi. U -cross Gram matrices and their invertibility. *J. Math. Anal. Appl.*, preprint .
3. P. G. Casazza and G. Kutyniok. Frames of subspaces. *Cont. Math.*, 2004.
4. O. Christensen. *Frames and Bases. An Introductory Course*. Applied and Numerical Harmonic Analysis. Basel Birkhäuser, 2008.
5. L. Gaul, M. Kögler, and M. Wagner. *Boundary Element Methods for Engineers and Scientists*. Springer, 2003.
6. H. Harbrecht, R. Schneider, and C. Schwab. Multilevel frames for sparse tensor product spaces. *Numer. Math.*, 110(2):199–220, 2008.
7. W. Kreuzer, P. Majdak, and Z. Chen. Fast multipole boundary element method to calculate head-related transfer functions for a wide frequency range. *J. Acoust. Soc. Am.*, 126(3):1280–1290, 2009.
8. P. Găvruta. On the duality of fusion frames. *J. Math. Anal. Appl.*, 333(2):871–879, 2007.
9. P. Oswald. Stable space splittings and fusion frames. In *Wavelets XIII (V. Goyal, M. Papadakis, D. Van de Ville, eds.)*, *Proceedings of SPIE San Diego*, volume 7446, 08 2009.
10. M. Shamsabadi, P. Balazs, A. A. Arefijamaal. The invertibility of U -fusion cross Gram matrices. arXiv:1711.00091.

Using B-spline frames to represent solutions of acoustics scattering problems

Wolfgang Kreuzer^{1,*}¹Acoustics Research Institute, Austrian Academy of Sciences, Vienna

*Email: wolfgang.kreuzer@oeaw.ac.at

Abstract

Frames have been used in signal processing for some time now, however in other fields of mathematics and engineering they haven't found much attention yet. In the talk we want to investigate approximations of solutions of wave scattering problems by Gabor frames, where B-splines are used as generating windows. We will discuss different ways to determine the unknown expansion coefficients and numerical examples are presented showing the efficiency of the different representation in terms of number of coefficients used versus approximation error.

Keywords: Frames, Helmholtz equation, approximation

1 Introduction

For simulating acoustic scattering problems finite element (FEM) or boundary element (BEM) methods have a long tradition. The application of these methods range from calculating the efficiency of noise barriers to determining filter functions for 3D audio. Both FEM and BEM depend on a discretization of the scatterer's geometry or in case of the BEM its surface, respectively. For the BEM, it is, as a general rule, recommended to use at least six elements per wavelength (cf. [1]).

One way to deal with this frequency dependence of the mesh is to use ansatz functions for the unknown solution $u(\mathbf{x}) = \sum_{i \in I} u_i \phi_i(\mathbf{x})$ that already contain oscillating components (cf. [2]). Alternatively, we want to investigate the approximation properties of *Gabor* frames, i.e. a family of functions that is generated by translating and modulating a given window function.

Compared to a basis, representations using frames are in general not unique, on the other hand, frames are more flexible and still can provide efficient and stable representations.

In this manuscript we will only look at one-dimensional functions, the extension to higher dimensions is straightforward using tensor products of one-dimensional frames.

2 Frames

In a Hilbert space \mathcal{H} a countable family of functions $\{\phi_i\}_{i \in \mathcal{I}}$ is called *frame* if there exist constants $A, B > 0$ such that

$$A\|f\|^2 \leq \sum_{i \in \mathcal{I}} |\langle f, \phi_i \rangle|^2 \leq B\|f\|^2, \forall f \in \mathcal{H}, \quad (1)$$

where $\mathcal{I} \subset \mathbb{N}$ is some countable index set and $\langle f, g \rangle$ denotes the scalar product in \mathcal{H} . The values A and B are called lower and upper frame-bound, respectively. If the frame bounds are close to each other Eq. (1) ensures a stable reconstruction of every element of the Hilbert space by the frame. It is known that for every frame there exists at least one *dual* frame $\tilde{\phi}$ such that

$$f = \sum_{i \in \mathcal{I}} \langle f, \tilde{\phi}_i \rangle \phi_i = \sum_{i \in \mathcal{I}} \langle f, \phi_i \rangle \tilde{\phi}_i.$$

In the Hilbert space of square integrable functions $L^2(\mathbb{R})$ Gabor systems $G(g, a, b)$ are collections of functions that are constructed by translating and modulating a given window function $g(x)$:

$$\phi_{m,n}(x) = g(x - na)e^{2\pi imbx}. \quad (2)$$

It can be show (cf. [3]) that under certain conditions on the window and on the parameters a and b a Gabor system is a frame, additionally it is known that some of the dual frames also can be constructed by translation and modulation of a window function, the so called *dual* window.

3 B-splines

In numerical and applied mathematics and especially in computer graphics cardinal B-splines are often used for curve-fitting, representing surfaces, or approximating functions in general. The B-splines of different order can be constructed by

$$N_1(x) = \begin{cases} 1, & x \in [0, 1], \\ 0, & \text{otherwise,} \end{cases}$$

$$N_{\ell+1}(x) = (N_\ell * N_1)(x) = \int_0^1 N_\ell(x-t)dt,$$

where $*$ denotes the convolution operator.

The B-Splines N_ℓ are $\ell - 2$ times continuously differentiable, have compact support, are linear independent, and the shifted versions of a fixed order form a partition of unity. Especially the partition of unity and the compact support make B-splines interesting generating windows for Gabor frames (cf. [3] where several theorems with respect to B-splines, Gabor frames and their duals can be found).

4 Implementation

When using (Gabor) frames in connection with BEM or FEM two points have to be addressed. 1) The restriction of the frames to a finite interval and 2) the calculation of the expansion coefficients. Since a frame may have many possible duals there are several ways for representing the target function. If the coefficients are calculated using a known dual frame, a numerical algorithm for the inner space vector product needs to be implemented. Alternatively there is also the possibility to determine the unknown coefficients by setting up a least squares problem

$$\operatorname{argmin}_c \|f(x) - \sum_{i=1}^N c_i g_i(x)\|^2 \quad (3)$$

that can be solved for example by a greedy algorithm like the orthogonal matching pursuit (OMP). Note, that solving Eq. 3 using the pseudoinverse is equivalent to the canonical dual window approach.

In general, Gabor frames are constructed for the whole real line, whereas for BEM and FEM the frames need to be restricted to one element. Assuming periodicity of the solution may lead to possible discontinuities at the element boundaries, thus it is advisable to extend the target functions over the element to cover the support of the dual frames needed for determining the frame coefficients or by using the least squares approach.

5 Numerical Experiments

As an example we use the sound field on a sound hard cylinder caused by a plane wave, which can be reduced to a problem in 2D:

$$f(\mathbf{x}) = \frac{2}{\pi k r} \sum_{n=0}^{\infty} \epsilon_n (-i)^{(n-1)} \frac{\cos(n\varphi)}{H'_n(kr)},$$

where $\mathbf{x} = r e^{i\varphi}$, $\epsilon_0 = 1$, $\epsilon_n = 2$, $n > 0$ and H'_n is the derivative of the Hankel function of order

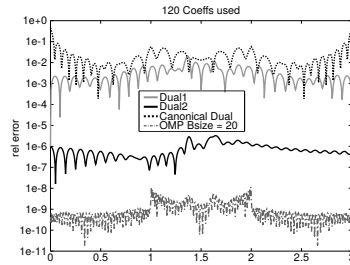


Figure 1: Relative approximation error using Gabor frames based on the B-spline $N_2(x)$. The coefficients are calculated using three dual frames and the OMP algorithm (cf. [4]).

n . $r = 1$, $k = 5$ and the above sum is truncated appropriately to achieve sufficient accuracy. φ is discretized in the interval $[0, 2\pi]$ with 601 equidistant nodes and scaled to the interval $[0, 3]$ to avoid having to rescale the B-spline window $N_2(\mathbf{x})$. The frame parameters are set to $a = 1$ and $b = \frac{1}{3}$. In Fig. 1 the relative approximation error when using the 120 biggest (in absolute value) coefficients calculated with either three types of dual frames or a modified OMP algorithm are depicted (for more details refer to [4]). In general, using Eq. (3) in combination with a modified OMP yields the best ratio between approximation error and number of coefficients used.

References

- [1] S. Marburg, Six boundary elements per wavelength. Is that enough?, *J. Comput. Acoust.* **10** (2002), pp. 25–51.
- [2] S. N. Chandler-Wilde, I. G. Graham, S. Langdon and E. A. Spence, Numerical-asymptotic boundary integral methods in high-frequency acoustic scattering, *Acta Numerica* **21** (2012), pp. 89–305.
- [3] O. Christensen, *An introduction to frames and Riesz bases*, 2nd expanded edition, Birkhäuser, Basel, 2016.
- [4] W. Kreuzer, Using B-spline frames to represent solutions of acoustics scattering problems, *J. Comput. and Appl. Math.*, **351** (2019), pp. 331-343.

Multilevel frames for solving high-dimensional partial differential equations

Helmut Harbrecht^{1,*}, Peter Zaspel¹¹Department of Mathematics and Computer Science, University of Basel, Basel, Switzerland

*Email: helmut.harbrecht@unibas.ch

Abstract

We consider the numerical solution of elliptic problems on the tensor product of two physical domains as e.g. present in the approximation of the solution's covariance of elliptic partial differential equations with random input. In order to approximate such problems in sparse tensor product spaces, we use multilevel frames. They are usually based on a geometrically constructed multilevel hierarchy, but can also be constructed by means of the algebraic multigrid method. Thus, we are able to apply sparse approximation techniques also to problems given on complex geometries and for discretizations arising from unstructured grids, which was not feasible before. Numerical results show that our algebraic construction exhibits the same convergence behaviour as the geometric construction, while being applicable even in black-box type PDE solvers.

Keywords: sparse tensor product approximation, multilevel frames, algebraic multigrid

1 Introduction

The solution of elliptic problems on tensor products of a polygonally bounded domain $\Omega \subset \mathbb{R}^d$ with e.g. $d = 2, 3$ given by

$$\begin{aligned} (\Delta \otimes \Delta)u &= f && \text{on } \Omega \times \Omega, \\ u &= 0 && \text{on } \partial(\Omega \times \Omega), \end{aligned} \quad (1)$$

is an important high-dimensional problem. As an example, this problem arises from the estimation of the output covariance of an elliptic partial differential equation with random input data that is given on a domain Ω . The problem becomes high-dimensional since the dimensionality of the elliptic problem on Ω is doubled. In case of real-world problems in $d = 3$, we end up solving a six-dimensional problem, which might become prohibitively expensive.

2 Sparse tensor product spaces

There have been developments to overcome this strong limitation. These developments are based

on the introduction of a *geometrically constructed multilevel frame* to solve the elliptic problem on Ω . Standard Galerkin discretizations of this problem approximate the solution with respect to a *basis* of a finite-dimensional trial and test space V_J , which is connected to a triangulation \mathcal{T}_J of the domain Ω . A multilevel frame discretization uses more functions to construct the trial and test space. In fact, it uses all basis functions of a (nested) hierarchy of subspaces

$$V_0 \subset V_1 \subset \dots \subset V_J \subset H_0^1(\Omega), \quad (2)$$

which are associated to a (nested) *geometric* hierarchy of triangulations $\mathcal{T}_0, \mathcal{T}_1, \dots, \mathcal{T}_J$ with an increasing number of nodes $|\mathcal{T}_0| < |\mathcal{T}_1| < \dots < |\mathcal{T}_J|$. This set with many redundant basis functions is no longer a basis for V_J , but a *frame*, compare [1, 2].

The multilevel frame gives rise to a sparse approximation with respect to the energy space $H_0^1(\Omega) \otimes H_0^1(\Omega)$ of the tensor product type boundary value problem (1). It has been shown that the approximation in the *sparse* trial and test space

$$\widehat{V_J \otimes V_J} = \sum_{0 \leq j+j' \leq J} V_j \otimes V_{j'}$$

instead of the *full* trial and test space

$$V_J \otimes V_J = \sum_{0 \leq j, j' \leq J} V_j \otimes V_{j'}$$

allows to solve the tensor product problem at a computational complexity that stays essentially (i.e. up to a poly-logarithmic factor) proportional to the number of degrees of freedom to discretize a function on the single domain Ω with respect to the trial space

3 Algebraic multilevel frames

The currently available geometric construction of the multilevel hierarchy imposes limitations on the discretization for real-world problems. First, the coarsest triangulation \mathcal{T}_0 in the geometrical hierarchy of triangulations has to fully represent the boundary of the geometry Ω . This

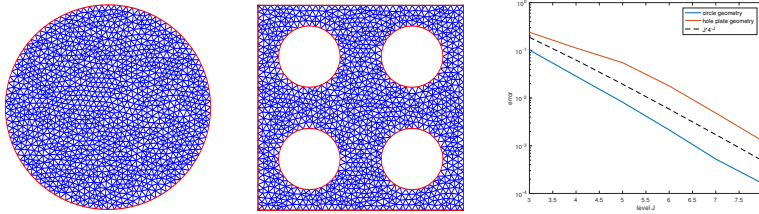


Figure 1: Meshes on a circle (left) and a square with four holes (middle). The convergence with respect to the level is plotted on the right.

either limits the types of geometry to consider or the computational efficiency (in case even the coarsest mesh has to be fine at the boundary). Second, the use of a fully unstructured mesh \mathcal{T}_J becomes barely possible, since we are missing a coarsening strategy for such a mesh.

To overcome the obstruction of geometrically constructing multilevel sequences (2), their algebraic construction has been proposed in [4]. It starts with the discretization of the problem

$$-\Delta u = f \text{ on } \Omega, \quad u = 0 \text{ on } \partial\Omega$$

on the finest (potentially unstructured) mesh \mathcal{T}_J . The coarser spaces are then obtained by using algebraic coarsening known from the classical *Ruge-Stüben algebraic multigrid* (AMG) [5]. Thus, the classical multilevel discretizations for elliptic partial differential equations are replaced by a purely matrix-based construction.

4 Iterative solution

The discretization of the tensor product type boundary value problem (1) with respect to the multilevel frame discretization leads to a system of linear equations, which has a huge kernel. Nonetheless, all nonzero eigenvalues stay constant independently of the mesh size. Therefore, the numerical solution is order-optimal by using an appropriate iterative solver.

As shown in [3], the multilevel frame discretization is equivalent to the *sparse grid combination technique*. This fact enables a second way of solving (1) with respect to the multilevel frame. Instead of solving one, large system of linear equations, one can also solve a couple of small systems of linear equations and *combine* their approximate solutions appropriately to get the sparse multilevel frame representation.

5 Numerical illustration

In our numerical studies, we consider the solution of (1) with right-hand side $f \equiv 1$ on a disc and on a square domain with holes. The unstructured triangulation on level $J = 5$ is found in Figure 1. In the right plot of this figure, we compare the approximate solution in the sparse tensor product space against the exact solution, which can simply be computed by tensorizing the numerical solution $u \in H_0^1(\Omega)$ of the Poisson equation $-\Delta u = 1$ on Ω for the level J . Convergence results for the choices $J = 3, \dots, 8$ are given, showing the expected convergence rate $\mathcal{O}(J4^{-J})$, which is indicated by the dashed line.

References

- [1] J. Bramble, J. Pasciak, and J. Xu. Parallel multilevel preconditioners. *Mathematics of Computation* **55**:1–22 (1990).
- [2] H. Harbrecht, R. Schneider, and C. Schwab. Multilevel frames for sparse tensor product spaces. *Numerische Mathematik* **110**(2):199–220 (2008).
- [3] H. Harbrecht, M. Peters, and M. Siebenmorgen. Combination technique based k -th moment analysis of elliptic problems with random diffusion. *Journal of Computational Physics* **252**:128–141 (2013).
- [4] H. Harbrecht and P. Zaspel. On the algebraic construction of sparse multilevel approximations of elliptic tensor product problems. *Journal of Scientific Computing* **78**(2):1272–1290 (2019).
- [5] J. Ruge and K. Stüben. Algebraic multigrid (AMG). In: S. McCormick (ed.), *Multigrid Methods*, SIAM, Philadelphia (1986).

Adaptive solution of PDEs using hybrid shearlet-wavelet frames

Philipp Grohs¹, Gitta Kutyniok², Jackie Ma³, Philipp Petersen⁴, Mones Raslan^{2,*}¹Faculty of Mathematics and Research Platform Data Science, University of Vienna, Vienna, Austria²Institut für Mathematik, Technische Universität Berlin, Berlin, Germany³Fraunhofer-Institut, Heinrich-Hertz-Institut, Berlin, Germany⁴Mathematical Institute, University of Oxford, Oxford, United Kingdom

*Email: raslan@math.tu-berlin.de

Abstract

We present a hybrid shearlet-wavelet frame for Sobolev spaces defined on bounded domains. This representation system yields best N -term approximation rates that are superior when compared to pure wavelet frames for solutions of elliptic partial differential equations (PDEs) with right-hand sides (RHSs) that contain curvilinear singularities. It constitutes the starting point for the development of an efficient, adaptive shearlet-based solver for the solution of such problems.

Keywords: shearlets, wavelets, frames, approximation rates, PDEs, adaptivity

1 Motivation

In [1], the authors developed a numerical, adaptive wavelet-based solver for the solution of elliptic PDEs with optimal convergence rates to solutions with high Besov-regularity. However, for solutions which cannot be adequately described in terms of Besov regularity, the convergence rates are suboptimal in general. As a special case, consider the Poisson equation $-\Delta u = f$ on a bounded domain $\Omega \subset \mathbb{R}^2$ with homogeneous boundary conditions such that $f \in L^2(\Omega)$ is a *cartoon-like function* (see [2]), i.e. a function which is in C^2 apart from a C^2 -curvilinear singularity. It has been shown in [3] that the higher-order derivatives of u are cartoon-like (see Figure 1).

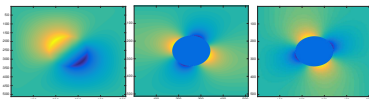


Figure 1: **Left:** u ; **Middle:** $\frac{\partial^2}{\partial x_1^2} u$; **Right:** $\frac{\partial^2}{\partial x_2^2} u$.

2 Frame discretization of PDEs

In an abstract setting, consider a Hilbert space H and an operator equation $Lu = f$, where

$L : H \rightarrow H^* \cong H$ is a linear, bounded, symmetric, elliptic operator, $f \in H^*$ is the RHS and $u \in H$ is the uniquely determined solution. Then, given a frame $\Phi = (\varphi_i)_{i \in \mathbb{N}}$ for H , it is possible to reformulate the operator equation $Lu = f$ as a discrete system of linear equations $\mathbf{L}\mathbf{u} = \mathbf{f}$, with $\mathbf{L} = T_\Phi^* L T_\Phi$, $\mathbf{f} = T_\Phi^* f$, where T_Φ^*, T_Φ are the analysis and synthesis operators of Φ , respectively and $u = \sum_{i \in \mathbb{N}} \mathbf{u}_i \varphi_i$. In [5], an asymptotically optimal, adaptive algorithm **SOLVE** has been developed which under certain assumptions converges with the same rate to \mathbf{u} as the error of best N -term approximation rate of u with respect to Φ , denoted by $\sigma_{N,\Phi,H}(u)$. Hence, a sufficient prerequisite towards the efficient solution of PDEs with cartoon-like RHS is the construction of a frame for the solution space $H^1(\Omega)$, which exhibits efficient best N -term approximation rates for functions whose higher-order derivatives are cartoon-like. We will describe such a system in the next section.

3 Shearlet-wavelet frames for Sobolev Spaces

A *shearlet* frame for $L^2(\mathbb{R}^2)$ is an anisotropic multiscale system based on the *parabolic scaling* and *shearing* (see [2] for further information and Figure 2 for the induced frequency tiling) of a few generator functions. It yields provably optimal best N -term approximation rates for cartoon-like functions with respect to the L^2 -norm not achievable by wavelet systems.

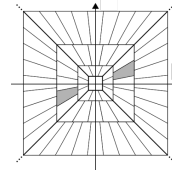


Figure 2: Anisotropic shearlet frequency tiling.

The intuitive reason behind this observation is depicted in Figure 3: Shearlets are able to capture a curvilinear singularity better than wavelets due to their anisotropy.

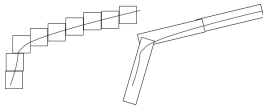


Figure 3: Capturing of a curvilinear singularity by **left**: isotropic wavelets, and **right**: anisotropic shearlets.

To employ shearlets for the efficient solution of PDEs, it is desirable to construct a shearlet frame for the space $H^1(\Omega)$ yielding efficient approximation rates for functions with cartoon-like derivatives and whose elements are boundary-adapted in order to incorporate boundary conditions given by the PDE. However, there is no known construction of boundary-adapted shearlet elements. A remedy to overcome this drawback is the construction of a hybrid system: It consists of compactly supported shearlet elements to provide efficient approximation rates, and boundary adapted wavelets (see Figure 4). To be more precise, the following holds:

Theorem 1 ([2, 4]) *There exists a frame Φ for $H^1(\Omega)$ with dual frame Φ_d consisting of shearlets fully supported in Ω as well as boundary-adapted wavelets close to the boundary of Ω such that $\sigma_{N, \Phi_d, H^1(\Omega)}(u) \in \mathcal{O}(N^{-1})$ for $N \rightarrow \infty$ and for all $u \in H^1(\Omega)$ with cartoon-like higher-order derivatives. In particular, the approximation rate provided by pure wavelet systems cannot be better than $\mathcal{O}(N^{-1/2-\epsilon})$ for $N \rightarrow \infty$ and all $\epsilon > 0$.*

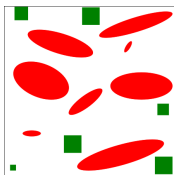


Figure 4: **Red**: Compactly supported shearlets, **Green**: Boundary adapted wavelets

4 Numerical examples

Having constructed a hybrid shearlet-wavelet frame for $H^1(\Omega)$ for $\Omega \subset \mathbb{R}^2$, we conclude this note with a numerical experiment implementing a simulated version of SOLVE based on thresholding for the solution of the Poisson equation with cartoon-like RHS. We see in Figure 5, in particular the right part, that after just a few iterations we already obtain a reconstruction of u which is close to the ground truth. This is due to the ability of shearlets to capture the singular behavior of the derivatives of u .

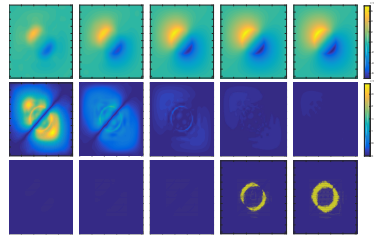


Figure 5: **Top**: Reconstructed solutions; **Middle**: Errors of the reconstructions; **Bottom**: Active shearlet elements.

References

- [1] A. Cohen, W. Dahmen and R. DeVore, Adaptive wavelet methods for elliptic operator equations: convergence rates, *Math. Comp.*, **70** (2001), pp. 27–75.
- [2] P. Grohs, G. Kutyniok, J. Ma, P. Petersen and M. Raslan, Anisotropic Multiscale Systems on Bounded Domains, *arXiv:1510.04538v4* (2018).
- [3] Y. Li and L. Nirenberg, Estimates for elliptic systems from composite material, *Comm. Pure Appl. Math.*, **56** (2003), pp. 892–925.
- [4] P. Petersen and M. Raslan, Approximation properties of hybrid shearlet-wavelet frames for Sobolev spaces, *Adv. Comp. Math.* (2019), in press.
- [5] R. Stevenson, Adaptive solution of operator equations using wavelet frames, *SIAM J. Numer. Anal.*, **44** (2004), pp. 1074–1100.

Quarkonial frames with compression properties — theory and numerical applications

Stephan Dahlke¹, Ulrich Friedrich¹, Philipp Keding¹, Thorsten Raasch², Alexander Sieber¹

¹Philipps University of Marburg, Germany

²University of Siegen, Germany

Abstract

We discuss the design and numerical applications of compressive quarkonial frames. Such so-called quarklet systems are wavelet versions of hp -finite element systems. Smooth functions with local singularities can be approximated from quarkonial systems at exponential rates. Moreover, rescaled quarklet systems are frames in Lebesgue and negative-order Sobolev spaces, enabling their application in numerical solvers for differential and singular integral equations, and in anisotropic tensor product approximation.

Keywords: quarkonial frames, partition-of-unity methods, operator compression, adaptivity

1 Atomic decompositions

The stable decomposition of function spaces by atoms and molecules [12] is a well-studied field of research with manifold applications, e.g., in the convergence analysis of basis-oriented adaptive numerical schemes for local and nonlocal operator equations, cf. [6,9] for recent overviews.

Atomic decompositions are given by a dictionary which allows for equivalences between smoothness norms and weighted sequence norms of expansion coefficients. Prominent examples are wavelet systems and multilevel h -finite element systems on a domain $\Omega \subset \mathbb{R}^n$, both of which are designed via dilation and spatial translation of a finite set of basis functions. Such dictionaries are stable in a range of Besov, Sobolev and Triebel-Lizorkin spaces over Ω .

The approximation order of both wavelet and h -finite element dictionaries is polynomial, in the sense that under generic assumptions on the approximand, the best N -term approximation errors from wavelet or h -finite element dictionaries scale like N^{-s} for some $s > 0$, N being the number of active basis functions. In the last decades, intensive research on the convergence properties of adaptive h -FEM and wavelet methods for well-posed local and nonlocal operator equations has revealed that these very rates s can also be realized in practice, most often at

a linear computational complexity [6,9].

2 Quarkonial frames

In order to achieve superalgebraic or even exponential approximation rates for piecewise smooth approximands, the underlying dictionary has to be enlarged appropriately. This idea has some history in numerical analysis and involves hp -finite element systems [2,7], the partition of unity method [1] and related multiscale schemes [8], and meshless methods. It is well-known that, e.g., hp -adaptive finite element methods can in principle achieve discretization errors that scale like $e^{-\alpha N^\beta}$ in N , with $\alpha, \beta > 0$. Despite significant progress in the last years, however, a full convergence analysis of hp -adaptive finite element schemes is not yet available.

In [10], quarkonial decompositions of function spaces (“quarks” \leftrightarrow “finer than atoms”) have been proposed to characterize spaces of smooth functions over general domains. Quarkonial systems are constructed from a partition of unity $\{\phi_{j,k}\}_k$ of locally supported bump functions, centered at points $x_{j,k}$ in a cloud of meshsize $h_j \approx 2^{-j}$. j is the scale, while k navigates through the point cloud at level j . A quarkonial system

$$\Phi := \{\phi_{p,j,k}\}_{p,j,k} \quad (1)$$

is achieved by adding a third degree of freedom p standing for the degree of the polynomial part of $\phi_{p,j,k}$. If $\Omega = \mathbb{R}^n$, and if the point clouds stem from dilation of a single lattice, the quarkonial system can be produced via modulation $\phi_p(x) = g_p(x)\phi(x)$ of a single bump function ϕ with an enrichment function g_p , and by subsequent dilation and translation, e.g., $\phi_{p,j,k}(x) = \phi_p(2^j x - k)$ in a shift-invariant setting. Such quarkonial systems combine features of local refinement and spectral approximation.

Under generic conditions, it was shown in [11] that properly scaled quarkonial systems of this type are frames in Besov-Sobolev spaces of positive order, and the numerical stability could be significantly improved by an alternative approach [5], relaxing the decay assumptions on

the p -dependent scaling. The stability properties and the similarity to hp -finite element and partition-of-unity dictionaries render quark systems appealing for numerical applications.

3 Compressive quarkonial frames

While such non-compressive quarkonial systems can already be used in an adaptive numerical scheme, just as an hp -finite element dictionary, it is not immediately possible to work with such systems in scenarios where the frame property in Lebesgue and nonnegative-order Sobolev spaces is essential, e.g., in anisotropic tensor product approximation, in space-time variational methods for evolution problems, or in the numerical treatment of singular integral equations.

By borrowing a leaf from the construction principles of wavelet systems, it could be shown in [4] how to augment a compactly supported, biorthogonal spline wavelet basis on the real line by polynomially enriched oscillatory functions, so-called quarklets. The resulting compactly supported quarklet systems can be considered as an hp versions of a wavelet system, and it has the frame property in L_2 and certain negative-order Sobolev spaces. In [3], the quarklet construction from [4] could be adapted to the case of bounded intervals, as well as to a class of polyhedral domains in \mathbb{R}^n , by means of anisotropic tensor product techniques.

What is more, the cancellation properties of the individual quarklets enable operator compression techniques, just as in the case of wavelet frames [3]. In the adaptive numerical discretization of elliptic boundary value problems, the attainable convergence rates of adaptive quarklet schemes are yet polynomial, but significantly higher than those of adaptive wavelet schemes that work with the embedded wavelet Riesz basis alone. The anisotropic structure of the overall quarklet frame can also be used to show that the attainable convergence rates do not depend on the spatial dimension.

Current research focuses on the question how to ensure exponential convergence rates of the numerical quarklet solver. In the talk, we will report on the latest developments.

References

[1] I. Babuška and J.M. Melenk, The partition of unity finite element method: Basic

theory and applications, *Comput. Methods Appl. Mech. Eng.* 139 (1996), 289–314

- [2] I. Babuška and M. Suri, The p - and h - p versions of the finite element method. An overview, *Comput. Methods Appl. Mech. Eng.* 80 (1990), 5–26
- [3] S. Dahlke, U. Friedrich, P. Keding, T. Raasch and A. Sieber, Adaptive quarkonial domain decomposition methods for elliptic partial differential equations, Preprint, 2018, submitted
- [4] S. Dahlke, P. Keding and T. Raasch, Quarkonial frames with compression properties, *Calcolo* 54 (2017), 823–855
- [5] S. Dahlke, P. Oswald and T. Raasch, A note on quarkonial systems and multilevel partition of unity methods, *Math. Nachr.* 286 (2013), 600–613
- [6] R.H. Nochetto, K. Siebert and A. Veiser, Theory of adaptive finite element methods: An introduction, in: *Multiscale, Nonlinear and Adaptive Approximation*, 409–542, Springer, Berlin, 2009
- [7] C. Schwab, *p - and hp -Finite Element Methods. Theory and Applications in Solid and Fluid Mechanics*, Clarendon Press, Oxford, 1998
- [8] M. Schweitzer, *A Parallel Multilevel Partition of Unity Method for Elliptic Partial Differential Equations*, Lecture Notes in Computational Science and Engineering, vol. 29, Springer, Berlin, 2003
- [9] R. Stevenson, Adaptive wavelet methods for solving operator equations: an overview, in: *Multiscale, Nonlinear and Adaptive Approximation*, 543–597, Springer, Berlin, 2009
- [10] H. Triebel, *Fractals and spectra related to Fourier analysis and function spaces*, Birkhäuser, Basel, 1997
- [11] H. Triebel, Wavelet frames for distributions: local and pointwise regularity, *Stud. Math.* 154 (2003), 59–88
- [12] H. Triebel, *Function spaces and wavelets on domains*, EMS Tracts in Mathematics, vol. 7, Zürich, 2008

Stable acoustic operators for sound propagation using an adjoint based method

Étienne Spieser^{1,*}, Christophe Bailly²¹Safran Aircraft Engines, Rond Point René Ravaud - Réau, 77550 Moissy Cramayel, France²Laboratoire de Mécanique des Fluides et d'Acoustique, UMR CNRS 5509, Ecole Centrale de Lyon, Université de Lyon, 69134 Ecully Cedex, France

*Email: etienne.spieser@ec-lyon.fr

Abstract

Adjoint method is a clever technique to tackle acoustic propagation effects of broadband sources in the presence of a flow and diffracting surfaces. The theory is first presented and validated numerically in considering the acoustic propagation of a source in a sheared and stratified flow. Physical instability waves may occur for such sheared flows, but corrupt the computed acoustic field and render it unusable. Some *ad hoc* stable wave equation are given here by taking benefit of the energy conservation property of self-adjoint operators. In this study acoustic predictions computed with these new stable propagation operators and with some others from literature are compared. Unexpectedly Pierce's wave equation [3] for potential acoustics is found to be the best compromise. The question on how to generalise acoustic potential theory for non-potential mean-flows is also addressed. In addition Euler Wave Equation (EWE), a new wave equation almost equivalent to LEE is presented in this work.

Keywords: adjoint method, wave equation**1 Adjoint method in propagation problems**

The methodology introduced by Tam and Auriault [4] to assess mean-flow refraction effects for jet noise is synthesised and generalised here. Consider a pressure field p and a source term s , a linear acoustic propagation problem may be described by an operator \mathcal{L}_0 so that the physical problem of interest - the direct problem - may be written as:

$$\begin{cases} \mathcal{L}_0(p) = s & \text{in } \Omega \\ \mathcal{B}_0(p) = 0 & \text{on } \partial\Omega \end{cases} \equiv (\mathcal{D})$$

Green-Lagrange's identity relates the direct and adjoint fields with help of a given scalar product. That is the cornerstone of the methodology: given a scalar product \langle, \rangle , there exist a

unique operator \mathcal{L}_0^\dagger and specific boundary conditions \mathcal{B}_0^\dagger such that for any field p^\dagger :

$$\langle p^\dagger, \mathcal{L}_0(p) \rangle = \langle \mathcal{L}_0^\dagger(p^\dagger), p \rangle$$

p^\dagger is referred to as the adjoint field. Introducing the adjoint source s^\dagger , such that $s^\dagger = \mathcal{L}_0^\dagger(p^\dagger)$, the adjoint problem associated with (\mathcal{D}) reads:

$$\begin{cases} \mathcal{L}_0^\dagger(p^\dagger) = s^\dagger & \text{in } \Omega \\ \mathcal{B}_0^\dagger(p^\dagger) = 0 & \text{on } \partial\Omega \end{cases} \equiv (\mathcal{A})$$

The adjoint Green function $G_{\mathbf{x}_m}^\dagger$ for a point source in \mathbf{x}_m is now considered. Green-Lagrange identity can be used to solve locally the direct propagation problem,

$$p(\mathbf{x}_m) = \langle G_{\mathbf{x}_m, t_m}^\dagger, s \rangle$$

2 Application to propagation over a parallel mean-flow

Acoustic propagation over parallel mean-flows is governed by Lilley's wave equation [2]:

$$\begin{aligned} \mathcal{L}_0(p) = & D_{\mathbf{u}_0}(D_{\mathbf{u}_0}^2(p) - \nabla \cdot (a_0^2 \nabla p)) \\ & + 2a_0^2 \nabla u_{0,z} \cdot \nabla \left(\frac{\partial p}{\partial z} \right) \end{aligned}$$

The mean-flow is aligned with \mathbf{z} , that is $\mathbf{u}_0 = u_{0,z}\mathbf{z}$, and the material derivative is denoted by $D_{\mathbf{u}_0} = \{\partial/\partial t + \mathbf{u}_0 \cdot \nabla\}$. From Green-Lagrange's identity, using integration by parts, the adjoint linear operator \mathcal{L}_0^\dagger to Lilley's equation can be obtained for the classic scalar product,

$$\begin{aligned} \mathcal{L}_0^\dagger(p^\dagger) = & -D_{\mathbf{u}_0}(D_{\mathbf{u}_0}^2(p^\dagger) - \nabla \cdot (a_0^2 \nabla p^\dagger)) \\ & + 4a_0^2 \nabla u_{0,z} \cdot \nabla \left(\frac{\partial p^\dagger}{\partial z} \right) \\ & + 3a_0^2 \Delta u_{0,z} \frac{\partial p^\dagger}{\partial z} \\ & + 3 \frac{\partial p^\dagger}{\partial z} \nabla a_0^2 \cdot \nabla u_{0,z} \end{aligned}$$

The boundary conditions for the direct problem \mathcal{B}_0 correspond to free-field radiating conditions while the boundary conditions to the adjoint problem \mathcal{B}_0^\dagger are anti-radiating conditions. The adjoint source can be seen as a sink.

3 Numerical illustration

Lilley's equation \mathcal{L}_0 and its adjoint operator \mathcal{L}_0^\dagger have been implemented in a finite difference direct frequency solver. Radiating boundary conditions are achieved with PML. The acoustic propagation of a source in a mean sheared flow is computed [1], but the frequency is chosen so not to trigger instability waves. The direct pressure field p is shown in figure 1.

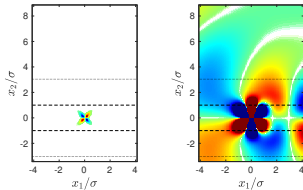


Figure 1: Source and fluctuating pressure p . Dotted and dashed lines represent the maximal shear position and the approximative width σ of the Gaussian mean flow considered.

Adjoint Green functions $G_{\mathbf{x}_m}^\dagger$ are computed for a sample of \mathbf{x}_m along the line $\mathbf{x}_2/\sigma = 7.25$ as illustrated in figure 2.

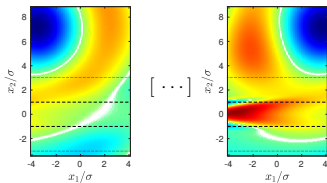


Figure 2: Sample of 17 adjoint Green functions.

$p(\mathbf{x}_m)$ is rebuilt at these locations. A comparison between the direct problem and the reconstructed field is finally plotted in figure 3.

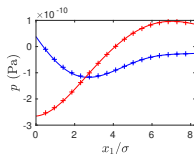


Figure 3: Validation along $\mathbf{x}_2/\sigma = 7.25$. Reference (-) adjoint method (+). $Re(p)$, $Im(p)$.

4 Stable operators

For the adjoint approach as for the direct method there is a need of stable accurate wave equations which do not describe the physical acoustic-vorticity coupling. Starting from the LEE for a parallel mean-flow, the Euler Wave Equation (EWE) can be obtained for the fluctuating velocity \mathbf{u} :

$$\mathcal{E}_0(\mathbf{u}) = D_{\mathbf{u}_0}^2(\mathbf{u}) + [(\nabla\mathbf{u}_0) + (\nabla\mathbf{u}_0)^T] \cdot D_{\mathbf{u}_0}(\mathbf{u}) + (\nabla\mathbf{u}_0)^T \cdot (\nabla\mathbf{u}_0) \cdot \mathbf{u} - a_0^2 \nabla(\nabla \cdot \mathbf{u})$$

This new wave equation, equivalent to Lilley's one may present some interest in analytical mode developments. Assuming a potential description of the fluctuations, $\rho_0 \mathbf{u} = \nabla\Phi$, the following wave equation can be derived:

$$\rho_0 \mathcal{E}_0 \left(\frac{\nabla\Phi}{\rho_0} \right) = \nabla \left[D_{\mathbf{u}_0}^2(\Phi) - \nabla \cdot (a_0^2 \nabla\Phi) \right] + (\nabla \times \mathbf{u}_0) \times \left[\nabla(D_{\mathbf{u}_0}(\Phi)) - [(\nabla\mathbf{u}_0) + (\nabla\mathbf{u}_0)^T] \right]$$

From the latter, it appears that Pierce's wave equation [3],

$$\mathcal{P}_0(\Phi) = D_{\mathbf{u}_0}^2(\Phi) - \nabla \cdot (a_0^2 \nabla\Phi)$$

is not only exact in the high-frequency limit, but also stands for propagation in the presence of a potential mean flow.

References

- [1] M. D. Dahl. Fourth CAA workshop on benchmark problems. Technical report, NASA/CP-2004-212954, 2004.
- [2] G. M. Lilley, H. E. Plumlee, W. C. Strahle, S. Y. Ruo, and P. E. Doak. The generation and radiation of supersonic jet noise. volume IV. theory of turbulence generated jet noise, noise radiation from upstream sources, and combustion noise. Technical report, Lockheed-Georgia Co. Marietta, 1972.
- [3] A. D. Pierce. Wave equation for sound in fluids with unsteady inhomogeneous flow. *The Journal of the Acoustical Society of America*, 87(6):2292-2299, 1990.
- [4] C. K. Tam and L. Auriault. Mean flow refraction effects on sound radiated from localized source in a jet. *Journal of Fluid Mechanics*, 1998.

Low Mach number aeroacoustics in ducts using incompressible-flow wall pressure.

Emmanuel Perrey-Debain^{1,*}, Nicolas Papaxanthos¹¹Sorbonne universités, Université de Technologie de Compiègne, Laboratoire Roberval CNRS FRE 2012, CS 60319, 60203 Compiègne cedex, France.

*Email: emmanuel.perrey-debain@utc.fr

Abstract

This work deals with numerical prediction of noise produced by interaction of a low Mach number flow with fixed obstacles inserted in a duct. The computation of the flow-generated noise is accomplished following a hybrid approach. In a first step, a Large Eddy Simulation for incompressible flows is performed in order to obtain wall pressure fluctuations. An integral formulation for the pressure correction term taking into account compressibility effects is presented. Comparisons with experimental data show good agreement and confirm the interest for the proposed formulation.

Keywords: Low Mach number internal flow noise, Lighthill's analogy, integral equation.

1 Introduction

The prediction of flow noise in ducts is essential for noise control in industrial ducts, such as HVAC or pipelines. The presence of obstacles with a low Mach number flow will result in unsteady aerodynamic fluctuations which generate sound waves propagating along the duct. These can be constrictions (orifices, diaphragms) or other obstacles (flap, splitter...). The numerical approach presented in this work permits to predict the radiated acoustic power in an efficient manner as it only requires the discretization of the surface of the fluid domain which includes the duct wall and the obstacle.

2 Integral form of Lighthill's equation

In the frequency domain, Lighthill's analogy can take the form of an inhomogeneous wave equation for the pressure which relates the noise generated by a turbulent flow to the noise emitted by quadrupoles of strength T_{ij} per unit volume in a medium at rest:

$$(\Delta + k^2)p = q \quad \text{with} \quad q = -\frac{\partial^2 T_{ij}}{\partial x_i \partial x_j}. \quad (1)$$

The unknown pressure p comprises both the hydrodynamic pressure fluctuations in the turbu-

lent flow and the sought-after propagating pressure waves which are dominant outside the source region. In an isentropic low Mach number flow, Lighthill's stress tensor becomes $T_{ij} \approx \rho_0 u_i u_j - \tau_{ij}$ which an incompressible-flow simulation approximates adequately and, within these assumptions, the incompressible flow pressure p_0 is known to obey the Poisson's equation $\Delta p_0 = q$.

We are interested in solving (1) in a bounded domain Ω with rigid walls terminated by openings Γ which act as semi-infinite waveguides. In these regions, it is assumed that the source term q is negligible so the acoustic pressure p can be described as outgoing waves and $\partial_n p = T(p)$ where n is the outward unit normal and T stands for the Dirichlet-to-Neumann map. Solution of (1) must satisfy the integral equation

$$S_\Omega[p](\mathbf{x}) = \int_\Omega q G d\Omega_y \quad (2)$$

where $S_\Omega[p]$ is the scattering operator for the open domain Ω

$$S_\Omega[p](\mathbf{x}) = C(\mathbf{x})p(\mathbf{x}) - \int_{\partial\Omega} p \partial_n G d\Gamma_y + \int_\Gamma G T(p) d\Gamma_y. \quad (3)$$

where G refers to the free-field Green's function, and $\partial\Omega$ delimits the volume of interest Ω . The literature mentions several difficulties linked to the volume integral calculation, such as numerical errors of sources estimation and memory requirement (see [1] and references therein). In order to ease the computation of the volume integral, the integral equation can be modified in order to include the incompressible-flow pressure, this gives the alternative form for the pressure correction

$$S_\Omega[p_c](\mathbf{x}) \approx \int_{\partial\Omega} p_0 \partial_n (G - G_0) d\Gamma_y + \int_\Gamma [G_0 \partial_n p_0 - G T(p_0)] d\Gamma_y$$

where $p_c = p - p_0$. The volume integral

$$\Pi = \int_\Omega q (G - G_0) d\Omega_y$$

can be seen as the compressible part of the incident field from quadrupoles and is intentionally omitted in the right-hand side. It is found in [2] that Π negligible for the case of a non-compact wing in an unbounded domain as a result of the proximity of the main sources to the trailing edge. The fact that the reflected part of the incident wavefield accounts for most of the radiated power is discussed in detail in Refs. [3, 4]

3 Results for a flap inserted in a straight duct

Figure 1 shows the computational domain for the flow simulation. The flap is made with a 8 mm thickness rectangular plate of duct section dimensions ($20 \times 10 \text{ cm}^2$) inclined 30 degrees about the duct axis. Meshes are both built with approximately 9 millions hexahedral cells with refinement boxes around the obstacle, especially near edges where cells size reach 0.5 mm.

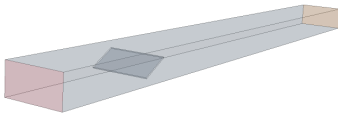


Figure 1: Computational domain

The flow simulation is carried out on 160 CPUs with the finite volume commercial software STAR-CCM+. A RANS calculation is first performed and gives the initial conditions to the LES. The averaged velocity over the inlet cross-section is 4.6 m/s. Simulations are carried out during a physical time of 0.3125 s with a time step $\delta t = 10^{-5}$ s. Figure 2 illustrate the Lighthill's stress tensor on the midplane at 200 and 2000 Hz. It permits to identify the location of the main noise sources. Here, only the longitudinal component T_{33} of Lighthill's stress tensor is shown as it dominates over the other terms. Figure 3 shows the calculated as well as the measured total sound power radiated upstream and downstream. Results match fairly well with experimental data (obtained from our aeracoustics bench), except near cut-off, and this confirms the interest for the proposed formulation.

References

- [1] N. Papaxanthos, E. Perrey-Debain, S. Benouna, B. Ouédraogo, S. Moreau and J.-

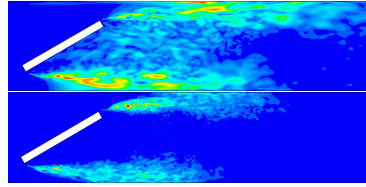


Figure 2: Component T_{33} of Lighthill's stress tensor at $f = 200$ Hz and $f = 2000$ Hz.

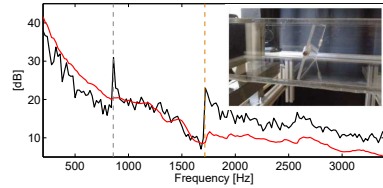


Figure 3: Total sound power radiating upstream and downstream, black: computed, red: measured. The gray and orange vertical lines indicate the cut-off frequencies of the rectangular duct.

M. Ville, Pressure-based integral formulations of Lighthill-Curle's analogy for internal aeroacoustics at low Mach numbers, *Journal of Sound and Vibration*, **393** (2017) pp. 176–186.

- [2] P. Martínez-Lera, C. Schram, H. Bériot and R. Hallez, An approach to aerodynamic sound prediction based on incompressible-flow pressure, *Journal of Sound and Vibration*, **333**, (2014) pp. 132–143.
- [3] N. Curle, The influence of solid boundaries upon aerodynamic sound, *Proc. R. Soc. Lond. A* **231** (1955) pp. 505–514.
- [4] D.G. Crighton, Basic principles of aerodynamic sound generation, *Prog. Aerospace Sciences* **16**(1) (1975) 31–96.

Wave interaction with an infinite cascade of non-overlapping blades

Georg Maierhofer^{1,*}, Nigel Peake¹¹Department of Applied Mathematics and Theoretical Physics, University of Cambridge, UK

*Email: g.maierhofer@maths.cam.ac.uk

Abstract

We consider the acoustic scattering problem on an infinite cascade of finite-length blades. This problem has its origins as a model for the components in turbofan engines and is of correspondingly wide interest. Analytical studies of the problem, however, have only been successful thus far in the case of overlapping blades. We present the first analytical solution in the case of non-overlapping blades, which is found to be valid for an arbitrary choice of blade spacing. This solution exploits the Wiener-Hopf technique and is based on the use of a novel additive splitting in a system of coupled scalar Wiener-Hopf equations. The solution allows us to understand the far-field behaviour of scattered acoustic waves, as well as the lift exerted on the blades by vortex waves that are incident on the structure.

Keywords: acoustics, Wiener-Hopf method, analytical methods, scattering

1 Introduction

We consider an infinite cascade of blades of zero thickness and camber as sketched in figure 1, which provides a model for sound propagation through the fan components of turbofan engines. One of the earliest formulations of this problem was given by [1], and analytical solutions were first studied in [2], then later using asymptotic kernel factorisations and incident harmonic gusts in [3], and the setting was extended to include spanwise waves in a three-dimensional setting in [4]. All of these studies apply the Wiener-Hopf method in a coupled scalar formulation and specifically rely on overlapping blades.

Similar to previous work, our method builds on the idea of reformulating a periodic three-part boundary value problem (BVP) as a system of coupled two-part BVPs on a strip – an approach related to Schwarzschild’s method. This facilitates the use of classical Wiener-Hopf techniques for scalar equations. A careful analysis of the Wiener-Hopf system shows that it is possible to apply an additive splitting that is valid for arbitrary blade spacing, and this allows the

analytical reduction to an infinite algebraic system. We demonstrate that this method of solution applies to multiple types of incident fields and that we can use the finite section method to evaluate solutions numerically. This allows for the study of physical observables, including the scattered radiation from an incident acoustic wave and the blade lift generated by incident vortical gusts.

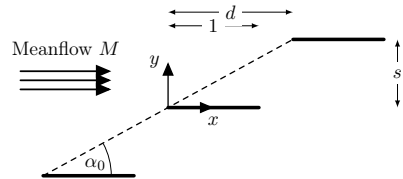
2 Model problem

Figure 1: A cascade of blades with mean flow.

Non-dimensionalising all physical variables allows us to consider blades of length 1, with blade overlap d (non-overlapping cascades have $d \geq 1$). Irrotational perturbations to the mean flow are then given in terms of a velocity potential ϕ , which satisfies

$$\beta^2 \frac{\partial^2 \phi}{\partial x^2} + \frac{\partial^2 \phi}{\partial y^2} - 2iM^2 \Omega \frac{\partial \phi}{\partial x} + M^2 \Omega^2 \phi = 0, \quad (1)$$

on $(x, y) \in \mathbb{R}^2 \setminus \{(nd + t, ns) \mid t \in [0, 1], n \in \mathbb{Z}\}$. Here $\beta^2 = 1 - M^2$, M is the Mach number of the flow, and Ω is the reduced frequency. For an incident harmonic wave (e.g. gust, or acoustic waves) the upwash on the n^{th} blade of the cascade is

$$V_g \exp(i\Omega t - iK_1 x + i\sigma),$$

where σ describes its change of phase between adjacent blades. K_1 is the first component of the incident wave vector and V_g is a constant describing the incident amplitude. Additionally ϕ must satisfy a Neumann boundary condition on the blades, together with continuity of pressure

p away from the blades and a radiation condition (we assume that the incident wave is damped by a small $\text{Im } \Omega < 0$ and the radiation condition is $\phi(\cdot, y) \in L^1(\mathbb{R}) \cap L^2(\mathbb{R})$ for each y), which altogether result in a periodic three-part BVP.

3 Method of solution

It is possible to distribute these boundary conditions onto $\phi_1 + \phi_2 + \phi_3 = \phi$, such that each $\phi_j, j = 1, 2, 3$, satisfies (1) and a two-part boundary condition on the strip $0 \leq y \leq s$. Fourier transforming those allows us to arrive at the following system of scalar Wiener-Hopf equations relating the pressure jumps $[p_j]$ and ϕ_j :

$$\begin{aligned} \frac{[P_1^+](\alpha)}{\kappa(\alpha)} &= \frac{\partial \Phi_1^-(\alpha, 0)}{\partial y} - \frac{iV_g}{\alpha - K_1}, \\ \frac{\partial \Phi_2^+(\alpha, 0)}{\partial y} &= \frac{1}{\kappa(\alpha)} \left([\tilde{P}_2^-](\alpha) - [\tilde{P}_1^+](\alpha) - [\tilde{P}_3^+](\alpha) \right), \\ \frac{\partial \Phi_3^-(\alpha, 0)}{\partial y} &= \frac{1}{\kappa(\alpha)} \left([P_3^+](\alpha) - [P_2^-](\alpha) \right). \end{aligned}$$

Here the capitals $[P_j]^\pm$ and Φ_j^\pm denote half-line Fourier transforms and κ is determined by the geometry of the cascade. Via an additive Cauchy-type splitting and careful analysis it is possible to reduce the problem to an infinite algebraic system. Approximate solutions to this system and hence to the original scattering problem can be found using the finite section method.

4 Numerical results

We can use these approximate solutions to understand the effect of mean-flow and cascade geometry on the scattered potential. Figure 2 shows the total lift exerted by an incident gust on each blade in the cascade for a range of mean-flow speeds – in this example $d < 1$. The solution is found to be in very good agreement with previous work by [3]. In figure 3 we see the effect of changing the blade spacing (far into the non-overlapping regime) on the transmission amplitude of the first cut-on radiation mode. Each jump in the figure corresponds to the point where a new mode begins to propagate (i.e. becomes cut-on). Thus larger gaps make the cascade more permeable and allow for a greater number of propagating modes.

5 Concluding remarks

Our solution also generalises naturally to the three-dimensional setting, and the corresponding analysis and further numerical results will be presented at the conference.

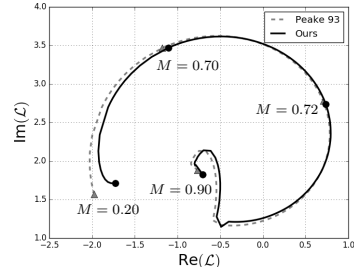


Figure 2: Total lift \mathcal{L} for $M \in [0.2, 0.9]$.

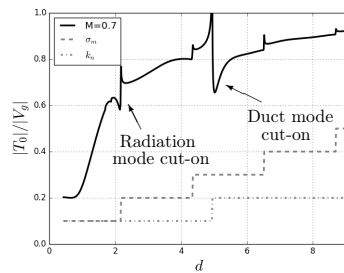


Figure 3: Transmission amplitude for s/d fixed. The jumps correspond to new modes becoming cut-on. The dashed lines represent the number of cut-on radiation and duct modes.

References

- [1] S. Kaji and T. Okazaki, Propagation of sound waves through a blade row: II. Analysis based on the acceleration potential method, *Journal of Sound and Vibration* **11(3)** (1970), 355–375.
- [2] W. Koch, On the transmission of sound waves through a blade row, *Journal of Sound and Vibration* **18(1)** (1971), pp. 111–128.
- [3] N. Peake, The scattering of vorticity waves by an infinite cascade of flat plates in subsonic flow, *Wave Motion* **18(3)** (1993), pp. 255–271.
- [4] S. A. L. Glegg, The response of a swept blade row to a three-dimensional gust, *Journal of Sound and Vibration* **227(1)** (1999), pp. 29–64.

Jet-Wing Interaction Noise Prediction with Forced Eddy Simulation

Andrej Neifeld^{1,*}, Roland Ewert¹

¹German Aerospace Center (DLR), Institute of Aerodynamics and Flow Technology, Technical Acoustics Branch, Braunschweig, Germany

*Email: Andrej.Neifeld@dlr.de
Roland.Ewert@dlr.de

Abstract

The present work concerns the numerical prediction of jet-wing interaction noise for the geometry specified in the European project JERON-IMO, which consists of a **Ultra High Bypass Ratio (UHBR)** nozzle mounted in close proximity to a swept wing with deployed flap ($\alpha_F = 14^\circ$). The geometrical setup provides a realistic scenario for a modern aircraft at 1:10 model scale but slightly reduced complexity neglecting details such as pylon, struts, and slat.

Results are obtained using a newly extended block structured mesh that resolves the high-lift wing with the UHBR nozzle and applying the latest version of the Forced Eddy Simulation approach based on a combined active/dissipative subgrid scale model. In agreement with experiment, the jet flow interacts with the trailing edge and generates additional installation noise, which predominates the low frequency part of the acoustic spectrum.

Keywords: Computational Aeroacoustics, LES, DNC, FRPM, FES, Jet Noise, Jet-Airframe Interaction

1 Methodology

A Direct Noise Computation (DNC) is carried out with DLR's 4th order structured multi-block code PIANO solving the compressible Navier-Stokes equations with Non-Linear Disturbance Equations (NLDE). With the triple decomposition of the flow variables

$$\mathbf{U} = \mathbf{U}^0 + \mathbf{U}' + \mathbf{U}'', \quad (1)$$

into \mathbf{U}^0 for the mean part, \mathbf{U}' for the resolved fluctuations, and \mathbf{U}'' for the non-resolved subgrid scale fluctuations, the Navier-Stokes equations in the applied disturbance form read

$$\frac{\partial \mathbf{U}'}{\partial t} + \mathcal{N}(\mathbf{U}^0 + \mathbf{U}') = \mathbf{S}, \quad (2)$$

where \mathcal{N} represents the Navier-Stokes operator and the right-hand side source term contains the

subgrid scale contributions, $\mathbf{S} = (0, \mathbf{f}_{sgs}, \theta_{sgs})^T$, e.g. refer to the discussion in [1]. The background mean-flow part is provided by a precursor RANS simulation of the envisaged flow problem. The sum of the resolved fluctuating part and the mean-flow part provides the resolved turbulent scales over the NLDE zone (that might represent a sub-zone of RANS) and as such altogether realizes a zonal RANS/LES method [3].

In the Forced Eddy Simulation (FES) approach [2, 4], a combined dissipative/active subgrid scale model replaces the standard purely dissipative LES subgrid scale model. The active part provides a model for the turbulence production by the non-resolved scales, which represents an important physical aspect of the subgrid scales, especially on relatively coarse meshes. Chances are that a subgrid scale model with extended physics might help to lower general LES resolution requirements. Furthermore, the transition to fully developed turbulence is enforced thus avoiding grey areas. The active part of the model is provided by a stochastic forcing method based on the Fast Random Particle-Mesh Method (FRPM). The applied vector force model reads

$$\mathbf{f}_{sgs} = -\nabla \times [\bar{\rho} \nu_r (\boldsymbol{\omega}' - \boldsymbol{\omega}^f)] / \bar{\rho}, \quad (3)$$

Eq. (3) consists of a combined dissipation and production term, where $\bar{\rho} = \rho^0 + \rho'$ is the resolved density, ν_r is the residual eddy viscosity, $\boldsymbol{\omega}'$ are the resolved vorticity fluctuations and $\boldsymbol{\omega}^f$ represents the stochastic forcing [2, 4].

2 Results

The resulting turbulent flow distribution of this computation is illustrated in Fig. 1 with the aid of Q-criterion. It is defined as

$$Q = \frac{1}{2} \|\bar{\boldsymbol{\Omega}}\|^2 - \|\bar{\mathbf{S}}\|^2 \quad (4)$$

which describes the imbalance between the vorticity and strain rate magnitude.

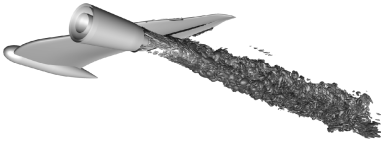


Figure 1: Q-criterion of JERONIMO configuration computed with Forced Eddy Simulation

Fig. 2 shows the corresponding fluctuating part of the pressure field. The plot includes both, acoustical waves as well as non-acoustical hydrodynamic fluctuations. Despite the hydrodynamic pressure fluctuations are not directly contributing to the far-field noise radiation, it is crucial to reproduce correctly these structures beneath the wing. The driving mechanism for the circular wave radiation as observable in Fig. 2 is the passing-by of coherent hydrodynamic structures over the flap trailing edge and thus the generation of a dipole source with orthogonal orientation to the flap cord.

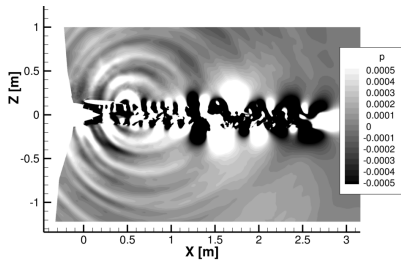


Figure 2: Distribution of non-dimensional pressure fluctuations $p' = (p_{tot} - p^0) / (\rho_{\infty} c_{\infty}^2)$ in the x - z -plane on jet axis

Fig. 3 demonstrates a quantitative evaluation of FES computation with the comparison of power spectral density to the measurement of the same setup. Two different microphone locations are considered for this comparison, i.e. one above and one below the wing at a polar angle of $\theta = 90^\circ$ with the origin at the bypass nozzle exit on jet axis. A second measurement of isolated nozzle is also included in this plot for evaluation of noise increase from the installation with the wing. The numerical prediction slightly over-

estimates the peak value and frequency with approx. $1.2kHz$ while the measurement yields the maximum around $0.9kHz$. In terms of maximum frequency resolution with approx. $3kHz$, the range of installation noise is well captured. The noise contribution above this frequency can be rather attributed to jet mixing noise, which is partly shielded to the upper side and reflected to the bottom side⁸.

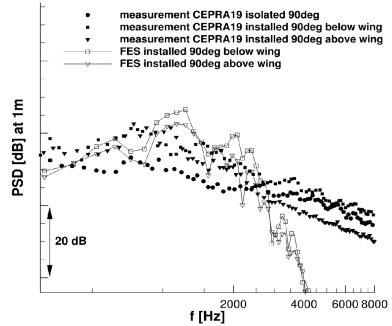


Figure 3: Comparison of power spectral density between measurement and FES computation at 1m distance and a polar angle $\theta = 90^\circ$ with (triangle symbol) above and (square symbol) below the wing geometry; (circle symbol) represents the isolated nozzle as reference without installation noise contribution

References

- [1] M. Terracol, E. Manoha, B. Lemoine, Investigation of the Unsteady Flow and Noise Generation in a Slat Cove, *AIAA Journal* **54**(2) (2016), pp. 1–21.
- [2] R. Ewert, J. Dierke, A. Neifeld, Simulation of Cold Jet Installation Noise using a Stochastic Backscatter Model, *AIAA Paper* 2017-3017.
- [3] E. Labourasse and P. Sagaut, Advance in RANS-LES coupling, a review and an insight on the NLDE approach, *Archives of Computational Methods in Engineering* **11**(3) (2004), pp. 199–256.
- [4] Neifeld, A., Ewert, R.: Towards Forced Eddy Simulation of Airframe Induced Noise Radiation from Coherent Hydrodynamic Structures of Jet Flow, *AVIATION Conference*, AIAA 2018-3463.

⁸This work has received funding from the Clean Sky 2 Joint Undertaking under the European Union's Horizon 2020 program under JERONIMO grant agreement No. 314692 and ASPIRE grant agreement No. 681856.

Turbulence modelling for flow-acoustic interaction of side mirror and gap noise

Alexander Schell^{1,*}¹Aerodynamics & Aeroacoustics, Daimler AG, Sindelfingen, Germany

*Email: alexander.schell@daimler.com

Abstract

This work deals with the numerical calculation of aeroacoustic excitations to estimate the wind noise entrainment into a passenger car. Based on in-/compressible detached and large eddy simulations with the commercial CFD code *Star-CCM+* [1], direct and hybrid computational aeroacoustic methods are investigated and validated. Beside classical side mirror noise, with its broadband noise character, more challenging applications like gape noise and aeroacoustic feedback phenomena are focused.

Keywords: computational aeroacoustics, direct noise calculation, aeroacoustic feedback

1 Introduction

Wind noise is becoming increasingly important for automotive development due to significant reductions in road and engine noise. For many vehicles, wind noise is the dominant contributor to interior noise at higher vehicle speeds. Beside the typical broadband noise character of wind noise, tonal noise phenomena like resonant gap noise and aeroacoustic feedback are more critical. These narrow band noise components can be a lot more disturbing independent of the overall interior noise quality of the vehicle. Increases in computational resources have made it feasible to implement different direct and hybrid computational aeroacoustic (CAA) strategies using a variety of numerical approaches, beside the original integral methods.

2 Methods

A direct noise calculation (DNC) uses the compressible Navier-Stokes equations to solve the hydrodynamic and acoustic field at once. Therefore, effects of both physical fields are considered on each other. Unfortunately, the benefit of a direct approach and its natural behavior is faced with several challenges. In order to avoid the difficulties associated with a direct noise calculation (e.g. disparity of scales, accurate numerical methods, disturbances and acoustic reflections at boundary conditions and mesh transi-

tions, hydrodynamic masking of acoustic near field content), it is useful to instead describe the contributions to hydrodynamic and acoustic surface pressures separately by using an acoustic analogy. Due to this separation no backward coupling of the acoustics to the flow field is considered, which might be for instance necessary to capture resonant buffeting phenomena, but is negligible for broadband side mirror noise.

The hybrid computational aeroacoustic approach used in the following studies is based on incompressible large and detached eddy simulations, meaning the solved unsteady pressure fluctuations contain no acoustic information. Starting from the APE-2 equation set [2], assuming an incompressible flow and neglecting the minor source term of mean vorticity - acoustic interaction, one can derive a scalar wave equation for the acoustic pressure without mean convection and refraction effects [3]:

$$\frac{1}{c^2} \frac{\partial^2 p^a}{\partial t^2} - \nabla^2 p^a = -\frac{1}{c^2} \frac{\partial^2 p^{ink}}{\partial t^2} \quad (1)$$

Independent of the used CAA method the correct flow field has to be determined first. As acoustics is of transient nature, the challenge is about correct and appropriate turbulence modelling and one has to find the best suitable CFD method for each application.

3 Side mirror noise (broadband)

For classical side mirror noise it can be assumed that the hydrodynamic flow field is independent of any resulting acoustics and a separate calculation of both is applicable. This also allows a differentiated analysis of both physical excitations and their contribution to the interior noise level [4, 5], which is not straightforward in wind tunnel measurements.

By using a detached eddy simulation (DES) the advantages of a large eddy simulation (LES) and an unsteady Reynolds Averaged Navier-Stokes simulation (URANS) are combined. Within the LES region, which requires a highly resolved mesh, the turbulent flow structures and acoustic

source mechanisms can be captured accurately. The unsteady RANS part in coarse regions and the inner boundary layer reduces the computational effort and enables the usage for larger industrial applications.

4 Gap noise

This works fine as long as the aeroacoustic relevant flow mechanisms are dominated by fully turbulent separated flow topologies, hence, resolved by DES and not modelled. Whenever upstream turbulence information for the aeroacoustic source mechanism is necessary, both, DES and LES, struggle due to missing unsteady inflow turbulence information. Or it would be computationally too expensive by resolving the entire boundary layer in case of a LES.

To overcome this, the turbulent boundary fluctuations, which drive the noise mechanism in case of a rear door gap, are amplified by anisotropic linear forcing [6]. The gap noise simulation, independent of the used CAA method, is based on a two-step approach: a steady RANS simulation based on an elliptic-blending Reynolds stress model of the entire setup with a subsequent LES of a small region around the gap. Here, anisotropic linear forcing close to the inlet of the LES region introduces necessary turbulent boundary layer fluctuations [7]. Comparison of different CAA methods show that a direct noise computation is able to consistently reproduce the experimental results, while simulations based on the acoustic wave equation cannot predict the varying excitation strength of the gap's Helmholtz frequency. This indicates that flow-acoustic interaction above the gap's opening leads to acoustic dissipation which is not considered in the current formulation of the wave equation.

5 Side mirror noise (narrow band)

Whistling sounds usually occur by flow over sharp edges and resonant gaps, but can also be caused by the feedback of sound waves with laminar boundary layers or separation bubbles and the resulting frequency-selective growth of boundary layer instabilities. Such aeroacoustic feedback can e.g. occur at the side mirror of a vehicle [8] and one compellingly needs the coupling of acoustic and flow field. A compressible LES is in principle suitable but one has to take care of any numerical artifacts which can disturb the

entire acoustic field. The provided compressible simulations are using non-reflecting boundary conditions in combination with a sponge zone approach to reduce hydrodynamic fluctuations a priori to the non-reflective acoustic boundary conditions.

References

- [1] STAR-CCM+ Release 13, Siemens PLM Software Inc., 2018.
- [2] Ewert, R., Schroeder, W., "Acoustic perturbation equations based on flow decomposition via source filtering", *Journal of Computational Physics* 188, pp. 365-398, 2003.
- [3] Schell, A., "Entwicklung einer Berechnungsmethode zur Vorhersage der Schallausbreitung im Nahfeld eines umströmten Kraftfahrzeugs", Ph.d. thesis, Universität Stuttgart 2014, ISBN: 978-3-8439-1907-4.
- [4] Schell, A., Cotoni, V., "Prediction of Interior Noise in a Sedan Due to Exterior Flow", *SAE Int. J. Passeng. Cars - Mech. Syst.* 8(3):2015, doi:10.4271/2015-01-2331.
- [5] Schell, A., Cotoni, V., "Flow Induced Interior Noise Prediction of a Passenger Car", *SAE Int. J. Passeng. Cars - Mech. Syst.* 9(3):2016, doi:10.4271/2016-01-1809.
- [6] De Laage de Meux, B., Audebert, B., Manceau, R., and Perrin, R., "Anisotropic linear forcing for synthetic turbulence generation in large eddy simulation and hybrid RANS/LES modeling", *Physics of Fluids*, Vol. 27, No. 3, 2015, p. 035115.
- [7] Erbig, L., Hu, N., Lardeau, S., "Experimental and Numerical Study of Passive Gap Noise", 24th AIAA/CEAS Aeroacoustics Conference, 2018, AIAA 2018-3595.
- [8] Frank, H., Munz, C.-D., "Direct aeroacoustic simulation of acoustic feedback phenomena on a side-view mirror", *Journal of Sound and Vibration*, Vol. 371, pp. 132-149, 2016.

Mechanisms for wave generation in a turbulent air-water flow

Francesco Zonta^{1,*}, Miguel Onorato², Alfredo Soldati¹¹Institute of Fluid Mechanics and Heat Transfer, TU Wien, Vienna, Austria²Department of Physics, University of Torino, Torino, Italy

*Email: francesco.zonta@tuwien.ac.at

Abstract

Using the Direct Numerical Simulation (DNS) of the Navier Stokes equations, we analyze the dynamics of the interface between air and water when they are driven by opposite pressure gradients (countercurrent configuration). At each time step, the physical domain is transformed into a rectangular domain (using a nonorthogonal transformation) where Continuity and Navier-Stokes equations are solved using a pseudospectral method. The problem is described by the Reynolds number (Re_τ), the Weber number (We), and the Froude number (Fr). Keeping Re_τ constant and varying We and Fr , we show that, in the initial stages of the wave generation process, the amplitude of the interface elevation grows in time as $t^{2/5}$. At steady state, our data are in good agreement with the prediction of the Wave Turbulence Theory.

Keywords: Wave generation, Turbulence, DNS**1 Introduction**

Interfacial waves at the air/water interface interact with turbulence modifying mass, momentum and energy transfer rates between the phases. These processes are crucial in many industrial applications, including condensers/evaporators and heat exchangers, where air and water usually flow countercurrent to promote interfacial transfer [1]. In such instances, predicting the evolution of the interface deformation according to flow conditions is essential since interface transfer mechanisms depend on magnitude and structure of interface deformation. However, mechanisms controlling interfacial waves generation and growth in air/water flow systems are not yet clear and still require investigation. Experimental measurements of turbulence/interface interactions occurring at the tiny scale of the near-interface region are extremely challenging, and progresses in this direction have been observed only recently [2]. Obtaining a description of the flow field above and below the interface is still an open issue using exper-

imental techniques. Direct Numerical Simulation (DNS) can help providing at any given time the entire velocity/pressure fields as well as the interface deformation, ensuring a level of detail sufficient to characterize the phenomena occurring in the proximity of the interface (where experimental measurements are difficult). For this reason, we decided to perform DNS to analyze the process of wave generation and growth in a countercurrent air/water turbulent flow. We let the air/water interface evolve starting from flat interface conditions, and we focus in particular on the transient behavior of the interface dynamics, deriving a simplified model capable of predicting the initial growth of the surface elevation.

2 Governing equation and numerical modelling

We consider a turbulent air-water flow. The reference geometry consists of two different domains (one for air and one for water) separated by a deformable interface. The origin of the coordinate system is located at the center of each domain, and the x -, y - and z -axes point in the streamwise, spanwise and interface normal direction. Air and water, which are considered incompressible and Newtonian, are driven by an imposed pressure gradient and flow in opposite directions. We consider a Cartesian coordinate system where air is placed above water. The dimensionless continuity and Navier-Stokes equations are:

$$\nabla \cdot \mathbf{u} = 0, \quad (1)$$

$$\frac{\partial \mathbf{u}}{\partial t} + \mathbf{u} \cdot \nabla \mathbf{u} = -\nabla p + \frac{1}{Re_\tau} \nabla^2 \mathbf{u}, \quad (2)$$

where \mathbf{u} is the velocity vector and p is pressure. Variables are made dimensionless using the half depth of each subdomain h , the thermophysical properties of each phase (the density ρ and the kinematic viscosity ν) and the corresponding shear velocity $u_\tau = \sqrt{\tau_{int}/\rho}$ (τ_{int} being the shear stress at the interface). Free-slip boundary conditions for the velocity field and zero-

gradient conditions for the pressure field are employed at the outer boundaries for both gas and liquid side. Periodic boundary conditions are employed in the streamwise and spanwise directions. At the interface, air and water are coupled by the continuity of the velocity and of the normal/shear components of the stress tensor (dynamic boundary conditions). The dimensionless numbers that describe the problem are the Weber, $We = \rho_L h u_{\tau L}^2 / \gamma$, Froude, $Fr = \rho_L u_{\tau L}^2 / (gh(\rho_L - \rho_G))$ and Reynolds $Re_{\tau} = u_{\tau G} 2h / \nu_G$ (but also $Re_{\tau} = u_{\tau L} 2h / \nu_L$) numbers: Note that the subscripts G and L are for gas (air) and liquid (water) and γ is the surface tension (u_{τ} being evaluated at the beginning of the simulation). The kinematic boundary condition for the interface is prescribed using an advection equation for the vertical elevation of the interface (boundary-fitted approach): At each time step, the distorted physical domain is transformed onto a Cartesian domain where governing equations are solved using a pseudospectral technique which employs Fourier series in the homogeneous directions (x and y) and Chebichev polynomials in the interface-normal direction (z). Time marching is realized by a two-stage fractional step splitting method [3]. We run three different simulations, each characterized by a specific set of dimensionless numbers and corresponding to a specific choice of the domain height h ($h = 0.045$ m for S1, $h = 0.05$ m for S2 and $h = 0.06$ m for S3).

3 Results

The dynamics of the deformable interface separating air and water currents is governed by the interaction between external forcing (pressure/velocity fluctuations and large scale coherent structures) and restoring forces (surface tension and gravity). The interface dynamics is strongly time-dependent and can support the propagation of waves with different amplitudes and wavelengths. To characterize the time-behavior of the interface deformation, we computed the root mean square (rms) of the interface amplitude in time, $\eta_{rms}(t) = \langle \eta(t)^2 \rangle^{1/2}$, where brackets $\langle \cdot \rangle$ implies averaging in space. Results are shown in Fig. 1. We first focus on the initial stage up to $t \simeq 6$ s; in this stage, the trend of the growth of $\eta_{rms}(t)$ seems to be independent of the physical parameters of the simulations. A simple phenomenological model of the wave gen-

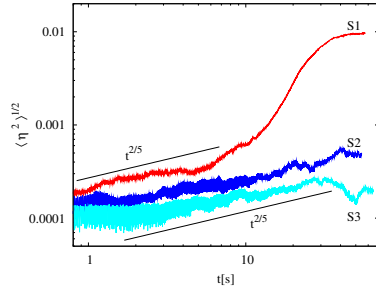


Figure 1: Time behavior of the root mean square (rms) of the interface amplitude, $\eta_{rms} = \langle \eta(t)^2 \rangle^{1/2}$, for simulation with $\sqrt{Fr}/We = 2.03$ (simulation S1, red line), $\sqrt{Fr}/We = 1.9$ (simulation S2, blue line) and $\sqrt{Fr}/We = 1.4$ (simulation S3, cyan line). The theoretical scaling law predicted by the simplified physical model proposed in the present study (thin line) is also shown.

eration during this initial stage gives $\eta \propto t^{2/5}$, a behavior that seems in good agreement with the numerical results and indicates that the process is dominated by capillarity.

4 References

References

- [1] Bartrand, T. A., Farouk, B., & Haas, C. N., “Counter-current gas/liquid flow and mixing: Implications for water disinfection,” *Int. J. Multiphase Flow*, **35**, 171 (2009).
- [2] Berhanu, M. & Falcon, E., “Space-Time-Resolved Capillary Wave Turbulence,” *Phys. Rev. E*, **87**, 033003 (2013).
- [3] Fulgosi, M., Lakehal, D., Banerjee, S. & De Angelis, V., “Direct numerical simulation of turbulence in a sheared air-water flow with a deformable interface,” *J. Fluid Mech.*, **482**, 319 (2003).

Aeroacoustic formulation based on compressible flow data applying Helmholtz's decomposition

Stefan Schoder^{1,*}, Klaus Roppert¹, Manfred Kaltenbacher¹

¹Institute of Mechanics and Mechatronics, TU Wien, Vienna, Austria

*Email: stefan.schoder@tuwien.ac.at

Abstract

Aeroacoustic analogies, in combination with a hybrid approach, represent a computationally efficient way to predict sound radiation. The classical hybrid approach, of first performing an incompressible flow computation, evaluate the acoustic sources and finally compute the acoustic field does not consider any feedback of the acoustic field on the flow. Therefore, we propose the following adapted approach: (1) Perform a compressible flow simulation on a restricted domain, which incorporates two-way coupling of flow and acoustics; (2) Filter the flow data by Helmholtz's decomposition, such that we obtain a pure non-radiating field, which the acoustic sources are computed with; (3) Perform the acoustic propagation computation. In this work, we present the theoretical fundamentals of this adapted hybrid approach and in particular Helmholtz's decomposition of the flow data using the finite element method.

Keywords: Aeroacoustic, CFD, Helmholtz decomposition, FEM

Introduction

A general aeroacoustic analogy, in combination with a hybrid approach, assumes a causal forward coupling of the forcing (obtained by an independent flow simulation) on fluctuating quantities, e.g. the fluctuating pressure p' . The nature of flow and acoustic fluctuations allows to speak of the acoustic pressure p^a at large distances from the turbulent region. Thereby, the differential equation of an acoustic analogy composes a hyperbolic left hand side (e.g. wave operator \square) and a generic right hand side $\mathbf{RHS}(\star)$

$$\square p' = \mathbf{RHS}(p, \mathbf{u}, \rho, \dots). \quad (1)$$

Lighthill's inhomogeneous wave equation perfectly fits into this class of equations [1]. It is obvious that $\mathbf{RHS}(\star)$ of Lighthill's inhomogeneous wave equation contains not only source terms, but also interaction terms between the sound and flow field, which includes effects, such

as convection and refraction of the sound by the flow. Regarding physics, the whole set of compressible flow dynamics equations, including acoustics, has to be solved in order to calculate the right hand side. This flow simulation must already resolve the acoustics as implicit part of the right hand side $\mathbf{RHS}(\star)$, which is a challenge for any numerical scheme. The computational noisy errors itself may strongly disturb the physical radiating wave components [2]. Phillips and Lilley [3, 4] moved interaction effects, at least to some extent, to the wave operator \square and predicted certain aspects of jet-noise quite accurately. These effects are neglected by Lighthill's wave operator and are often not present in Lighthill's source term due to the restricted numerical resolution of interactions during a preceding flow simulation [5].

In year 2003, Goldstein [6] proposed a method to split flow variables (p, \mathbf{u}, \dots) into a base flow $\tilde{\star}$ and a remaining component \star'

$$\star = \tilde{\star} + \star'. \quad (2)$$

Although Goldstein's idea has a different perspective, a separation into a base flow and a remaining component shows distinctive features of sound in the source terms. In this contribution, we develop a formal construct to derive and analyze aeroacoustic analogies. We introduce a non-radiating base flow as a flow state around the flow equations are linearized. A non-radiating flow solution is defined as a flow that has not emitted the sound (e.g. an incompressible flow) but has the potential to do so, either due to the physical model or the computational algorithm. The remaining component is the perturbation of the base flow and is usually small for subsonic flows. Using a non-radiating base flow, the remaining component describes all radiating component, including the sound field.

Applying the decomposition to the right hand side of the wave equation yields

$$\square p' = \mathbf{RHS}(\tilde{p}, \tilde{\mathbf{u}}, \tilde{\rho}, p', \mathbf{u}', \rho', \dots). \quad (3)$$

Now interaction terms can be moved to the differential operator to take, e.g., convection and refraction effects or even nonlinear interactions into account. Exactly this approach has been applied in the theories of Phillips and Lilley, and furthermore in the derivation of perturbation equations [7–9].

Following this modeling approach, the main interaction terms between the flow and the acoustic field are modeled by an appropriate wave operator $\tilde{\square}$, e.g. convection and refraction effects, and the right hand side is modeled by the base flow

$$\tilde{\square}p' = \mathbf{RHS}(\tilde{p}, \tilde{\mathbf{u}}, \tilde{\rho}, \dots). \quad (4)$$

Following the hybrid approach, we perform a compressible flow simulation, which incorporates two-way coupling of flow and acoustics and extends aeroacoustic analogies to physical phenomena, where feedback matters. Based on this compressible flow results, we use Helmholtz's decomposition to obtain the non-radiating base flow (incompressible part of the flow result) that is used as base flow in the wave equation.

Helmholtz's decomposition

In this contribution, we discuss Helmholtz's decomposition of the compressible flow field in the vector potential formulation and the finite element method implementation in CFS++ [11]. Using Helmholtz's theorem, the curl-curl equation for the vector potential \mathbf{A}^{ic} is obtained

$$\nabla \times \nabla \times \mathbf{A}^{\text{ic}} = \nabla \times \mathbf{u}, \quad (5)$$

forced by the vorticity $\nabla \times \mathbf{u}$. We derive the weak formulation of (5) and prescribe boundary conditions that are based on fluid dynamics [10]. The weak formulation is discretized with edge elements. Having the vector potential, the incompressible part of the velocity field is computed by

$$\tilde{\mathbf{u}} := \mathbf{u}^{\text{ic}} = \nabla \times \mathbf{A}^{\text{ic}}. \quad (6)$$

This incompressible part of the velocity field can be used as the non-radiating base flow. Finally, we apply Helmholtz's decomposition to a Mach 0.8 flow over a rectangular cavity [12].

References

[1] M. J. Lighthill, On sound generated aerodynamically I. General theory, *Proceedings of the Royal Society of London*, **211**:564–587, 1951.

- [2] D. G. Crighton, Computational aeroacoustics for low Mach number flows, In *Computational aeroacoustics*, pages 50–68. Springer, 1993.
- [3] O. M. Phillips, On the generation of sound by supersonic turbulent shear layers, *Journal of Fluid Mechanics*, **9**(1):1–28, 1960.
- [4] G. M. Lilley, *On the noise from jets*, AGARD-CP-131, 1974.
- [5] M. E. Goldstein, *Aeroacoustics*, McGraw-Hill International Book Co., New York, 1976.
- [6] M. E. Goldstein, A generalized acoustic analogy, *Journal of Fluid Mechanics*, **488**:315–333, 2003.
- [7] R. Ewert and W. Schröder, Acoustic perturbation equations based on flow decomposition via source filtering, *Journal of Computational Physics*, **188**(2):365–398, 2003.
- [8] J. Seo and Y. J. Moon, Perturbed compressible equations for aeroacoustic noise prediction at low mach numbers, *AIAA journal*, **43**(8):1716–1724, 2005.
- [9] C.-D. Munz, M. Dumbser, and S. Roller, Linearized acoustic perturbation equations for low Mach number flow with variable density and temperature, *Journal of Computational Physics*, **224**(1):352–364, 2007.
- [10] S. J. Schoder, *Aeroacoustic analogies based on compressible flow data*, PhD thesis, TU Wien, 2019.
- [11] M. Kaltenbacher, *Numerical Simulation of Mechatronic Sensors and Actuators: Finite Elements for Computational Multiphysics*, Springer Berlin Heidelberg, 2015.
- [12] T. Colonius, Modeling artificial boundary conditions for compressible flow, *Annu. Rev. Fluid Mech.*, **36**:315–345, 2004.

**Towards an efficient detection of hydrodynamic-acoustic
feedback mechanisms in an industrial context**

Daniel Kempf^{1,*}, Claus-Dieter Munz¹

¹Institute of Aerodynamics and Gas Dynamics, University of Stuttgart, Stuttgart, Germany

*Email: kempf@iag.uni-stuttgart.de

Abstract

Direct noise computation (DNC) offers some advantages compared to hybrid approaches in simulating aeroacoustic feedback mechanisms. In DNC, hydrodynamics and acoustics are solved in a coupled manner which allows to depict intricate interactions between both fields. However, this approach intrinsically requires the resolution of the occurring disparate length and time-scales which is computationally expensive. The aim of this work is to draw the attention to an efficient method for the detection of aeroacoustic feedback. It can be effectively predicted by a global stability analysis. Here, an impulse response analysis on a time averaged flow field is carried out. The underlying baseflow is maintained constant through volume forcing terms. To overcome the drawback of long time-averaging of LES-data a computationally less expensive numerical method like a RANS-solver can be employed to generate the time-averaged baseflow, which is then used by our high order framework FLEXI to simulate the response of small perturbations. Results of a side-view mirror will demonstrate the advantages of the latter approach.

Keywords: Aeroacoustic feedback loop, Global instability, Side-view mirror

1 Introduction

Tonal noise due to aeroacoustic feedback is well understood, e.g. trailing edge noise of the NACA 0012 airfoil [1]. Lounsberry et al. [2] suggested that the tonal noise seen at smooth surfaces, such as a side-view mirror, is based on the same mechanism. The mechanism is associated to laminar boundary layer separation and the associated coherent vortex shedding. Within the developing shear layer, instabilities are amplified and eventually roll up to coherent vortices. The interaction of those structures with the trailing edge leads to acoustic radiation. The upstream travelling acoustic wave interacts with the shear layer through receptivity and excites instabilities

at a certain frequency. This mechanism can trigger a self-sustaining oscillatory state at a certain frequency, which is the source of tonal noise.

To depict the interaction between hydrodynamics and acoustics DNC is necessary. Frank [3] successfully demonstrated the occurrence of aeroacoustic feedback on a side-view mirror by applying DNC. Furthermore, he applied a global stability analysis to detect acoustic feedback proposed by Jones et. al [1]. Here, an initial time averaged flow field obtained from compressible high-fidelity large eddy simulation (LES) is disturbed by a small perturbation, while the underlying baseflow is maintained through volume forcing terms. To overcome this drawback of computational expensive time averaging, we propose a more efficient method by using a less expensive numerical method, based on the Reynolds averaged Navier-Stokes equations (RANS), to generate the time-averaged baseflow. We apply this method to a submodel of a side-view mirror and will demonstrate the applicability of this approach.

2 Numerical method

The mechanism of acoustic feedback is based on an complex interaction between the hydrodynamics and the acoustics, which requires a direct numerical simulation of the compressible Navier-Stokes equations (NSE). In this work we apply the high-order discontinuous Galerkin spectral element method (DGSEM) implemented in our framework FLEXI as described in Hindele et. al [4] and extended by a perturbation formulation. The perturbation formulation is implemented according to Jones et. al [1] and Frank [3]:

$$U'_t = R(U_0 + U') - R(U_0). \quad (1)$$

With $U_t = R(U)$ being the nonlinear Navier-Stokes operator, U' the fluctuating values and U_0 the baseflow. The second part of the right-hand side can be interpreted as a forcing back onto the baseflow. This method allows us to

analyze the impulse response of a small perturbation to any provided baseflow, which is like a global stability analysis. To obtain the baseflow we use a steady state, incompressible RANS-solver implemented in OpenFOAM. The RANS-equations are closed by the Langtry-Menter 4-equation transitional SST model. Conducting a perturbation analysis of a disturbed baseflow obtained from a RANS solver, followed by a dynamic mode decomposition (DMD) of the obtained time series reveals the frequencies which are considered for feedback.

3 Perturbation analysis

In the following, the results of the perturbation analysis applied to a two-dimensional side-view mirror at freestream velocity of $U_\infty = 27.78 \text{ m/s}$ are presented. Figure 1 shows the Ritz values of the associated time series analyzed by means of a DMD. In the diagram you can see the real part plotted over the imaginary part of the complex eigenvalues ω , which are associated to the growth rate and the angular frequency of the mode. The size of the plotted modes is encoded with the Euclidean norm of the respective mode which can be seen as a measure of energy of the modes. The least damped energetic modes which is seen as the acoustic feedback mode is found to be at 2555 Hz . Compared to the dominant tonal frequency found in DNC at $f = 2550 \text{ Hz}$, the results of the DMD are in good agreement with the dominant frequency found in the perturbation analysis.

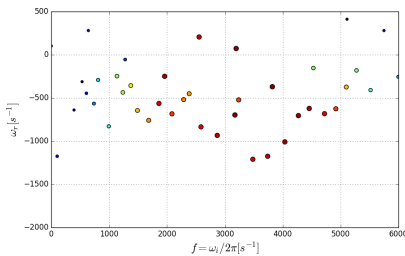


Figure 1: Spectrum of Ritz values delivered by the DMD algorithm.

Those promising results for the baseline velocity shows great potential of the new proposed method. A variation of the freestream velocities shows that the newly proposed method can re-

produce the Reynolds dependency of the tonal frequency, compared to DNC by Frank [3], well.

4 Conclusions

The present work deals with an efficient method to capture aeroacoustic feedback induced by the flow around a side-view mirror. A global perturbation ansatz based on a mean flow is proposed. The potential of such a stability analysis has been demonstrated in the literature, with the downside of computationally expensive time averaging of transient LES or DNS to obtain the baseflow. Using a RANS solver to compute the baseflow as well as a geometric submodel the computational effort reduces significantly. Conducting a perturbation analysis of a submodel based on the RANS baseflow, followed by a dynamic mode decomposition reveals the selection of discrete frequencies by the mechanism. Good agreement of the least damped modes with the tonal frequency found by DNC as well as the literature was found. This leads to the conclusion that RANS simulations are suitable as a baseflow for a high order disturbance analysis in order to detect acoustic feedback.

5 Acknowledgements

We thank the AUDI AG for their financial support. This work used HPC resources on the CRAY XC40 hazelhen at the High Performance Computing Center Stuttgart (HLRS).

References

- [1] L. E. Jones and R. D. Sandberg. Numerical analysis of tonal airfoil self-noise and acoustic feedback-loops. *Journal of Sound and Vibration*, 330(25):6137–6152, 2011.
- [2] T. H. Lounsberry, M. E. Gleason, and M. M. Puskarz. Laminar flow whistle on a vehicle side mirror. Technical report, SAE Technical Paper, 2007.
- [3] H. Frank. High order large eddy simulation for the analysis of tonal noise generation via aeroacoustic feedback effects at a side mirror. *Dr. Hut, München*, 2017.
- [4] F. Hindenlang, G. J. Gassner, C. Altmann, A. Beck, M. Staudenmaier, and C.-D. Munz. Explicit discontinuous galerkin methods for unsteady problems. *Computers & Fluids*, 61:86–93, 2012.

A Stochastic Approach to Compute Cavity Noise using SNGR

Michael Weitz^{1,*}, Stefan Schoder¹, Manfred Kaltenbacher¹

¹Institute of Mechanics and Mechatronics, TU Wien, Vienna, Austria

*Email: michael.weitz@tuwien.ac.at

Abstract

Stochastic methods represent a highly efficient way to recreate turbulent velocity fluctuations based on Reynolds-averaged Navier-Stokes (RANS) simulations. In this work, we present how to compute source terms from the generated stochastic velocity field and how to apply it to the aeroacoustic simulation of a deep cavity with a lip to compute broadband noise and aeroacoustic modes.

Keywords: Computational Aeroacoustics, Fluid Dynamics, Stochastic Methods

1 Introduction

Stochastic methods constitute a low-cost computational fluid dynamics (CFD) approach to reconstruct the turbulent velocity fluctuations using results from RANS simulations. This approach was introduced by Béchara *et al.* in 1994 and is known as stochastic noise generation and radiation (SNGR) [1].

As proposed by Billson *et al.* [2], a stochastic turbulent velocity field can be generated as a finite sum of N unsteady random Fourier modes

$$\mathbf{u}_t(\mathbf{x}, t) = 2 \sum_{n=1}^N \tilde{u}_n \cos(\mathbf{k}_n \cdot (\mathbf{x} - t\mathbf{u}_c)) + \psi_n + \omega_n t) \boldsymbol{\sigma}_n. \quad (1)$$

where \mathbf{x} is the spatial position, and \mathbf{k}_n , \tilde{u}_n , ψ_n , and $\boldsymbol{\sigma}_n$ are the wave vector, the amplitude, the phase, and the direction of the n^{th} mode, respectively. The wave vector \mathbf{k}_n is randomly chosen on a sphere of radius $k_n = \|\mathbf{k}_n\|$ to ensure isotropy of the generated turbulent velocity field and is thus defined by the coordinates $(k_n, \varphi_n, \theta_n)$ as depicted in Fig. 2. Additionally, incompressibility of the turbulent flow field implies $\partial u_{ti}/\partial x_i = 0$, and hence

$$\mathbf{k}_n \cdot \boldsymbol{\sigma}_n = 0 \quad \text{for } n = 1, \dots, N. \quad (2)$$

Therefore, the unit vector $\boldsymbol{\sigma}_n$ lying in the $(k'_1-k'_2)$ -plane is perpendicular to the wave vector \mathbf{k}_n and solely defined by its polar angle α_n (see Fig. 2). The probability density functions that

determine the randomly drawn angles φ_n , α_n , ψ_n , and θ_n are listed in Tab. 1.

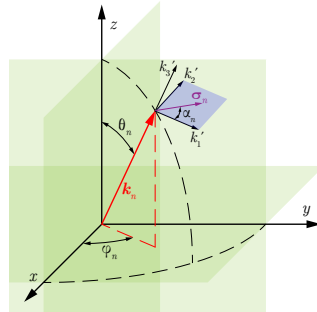


Figure 1: Geometry of the wave vector corresponding to the n^{th} Fourier mode.

Table 1: Probability distributions of random variables used to generate stochastic turbulent velocity field [3].

Probability density	Interval
$p(\varphi_n) = 1/(2\pi)$	$0 \leq \varphi_n \leq 2\pi$
$p(\alpha_n) = 1/(2\pi)$	$0 \leq \alpha_n \leq 2\pi$
$p(\psi_n) = 1/(2\pi)$	$0 \leq \psi_n \leq 2\pi$
$p(\theta_n) = (1/2) \sin \theta_n$	$0 \leq \theta_n \leq \pi$

Homogeneous isotropic turbulence may be characterized by an energy spectrum $E(k)$ with $k = \|\mathbf{k}\|$, which allows to compute the amplitude \tilde{u}_n of the n^{th} mode as

$$\tilde{u}_n = \sqrt{E(k_n)\Delta k_n}. \quad (3)$$

The spectrum $E(k)$ used to simulate the complete spectral range is a von Kármán-Pao spectrum [4,5]

$$E(k) = \alpha \frac{u'^2}{k_e} \frac{(k/k_e)^4}{[1 + (k/k_e)^2]^{17/6}} \exp \left[-2 \left(\frac{k}{k_\eta} \right)^2 \right] \quad (4)$$

where $k_\eta = (\varepsilon/\nu^3)^{1/4}$ is the Kolmogorov wave number, and $u' = \sqrt{2K/3}$ is the root mean square value of the velocity fluctuations, where ε is the rate of dissipation of turbulence energy, ν is the kinematic viscosity, and K is the turbulent kinetic energy. Moreover, k_c is the wave number of the most energetic eddies and α is a numerical constant.

In Eq. (1), \mathbf{u}_c is the local convection velocity and ω_n is the angular frequency of the n^{th} mode. As opposed to the convection velocity \mathbf{u}_c , which is a function of the known local mean flow, the angular frequency ω_n is a random variable drawn from a distribution associated to a Gaussian probability density function

$$p_n(\omega) = \frac{1}{\bar{\omega}_n \sqrt{2\pi}} \exp\left(-\frac{(\omega - \bar{\omega}_n)^2}{2\bar{\omega}_n^2}\right), \quad (5)$$

where the mean angular frequency of the n^{th} mode $\bar{\omega}_n$ is connected to the wave number k_n by $\bar{\omega}_n = u'k_n$.

2 Application to a cavity

The presented stochastic approach is applied to a generic cavity that was presented in [6]. In this contribution, we generate a velocity field $\mathbf{u} = \mathbf{U} + \mathbf{u}_t$, where \mathbf{U} is the solution of the RANS simulation and \mathbf{u}_t are the turbulent velocity fluctuations resulting from the SNGR approach described above. This velocity field can be employed to compute the Lighthill source term $\partial^2 L_{ij}/(\partial x_i \partial x_j)$. For low Mach numbers, Lighthill's tensor may be approximated by $L_{ij} = \rho_0 u_i u_j$, where ρ_0 is the mean density [7].

With this procedure, it is possible to compute both acoustic modes and the broadband noise associated to a turbulent flow over the orifice of the cavity.

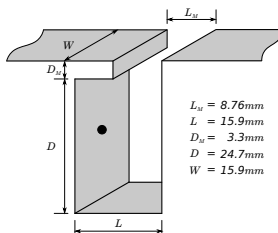


Figure 2: Geometry of the investigated cavity [8].

References

- [1] Walid Béchara, Christophe Bailly, Philippe Lafon, and Sebastien M. Candel. Stochastic approach to noise modeling for free turbulent flows. *AIAA Journal*, 32(3):455–463, 1994.
- [2] Christophe Bailly and Daniel Juvé. A stochastic approach to compute subsonic noise using linearized euler's equations. In *5th AIAA/CEAS Aeroacoustics Conference and Exhibit*, page 1872, 1999.
- [3] Anthony Lafitte, Thomas Le Garrec, Christophe Bailly, and Estelle Laurendeau. Turbulence generation from a sweeping-based stochastic model. *AIAA Journal*, 52(2):281–292, 2014.
- [4] Theodore Von Karman. Progress in the statistical theory of turbulence. *Proceedings of the National Academy of Sciences of the United States of America*, 34(11):530, 1948.
- [5] Yih-Ho Pao. Structure of turbulent velocity and scalar fields at large wavenumbers. *The Physics of Fluids*, 8(6):1063–1075, 1965.
- [6] Bence Farkas and György Paál. Numerical study on the flow over a simplified vehicle door gap – an old benchmark problem is revisited. *Periodica Polytechnica Civil Engineering*, 59(3):337–346, 2015.
- [7] S. C. Crow. Aerodynamic sound emission as a singular perturbation problem. *Studies in applied mathematics*, 49(1):21–46, 1970.
- [8] Ivan Lazarov. Strömungsakustische simulation einer tiefen kavität mit lippe. Master's thesis, TU Wien, Vienna, Austria, 2018.

On the well-posedness of Galbrun's equation

Linus Hägg^{1,*}, Martin Berggren¹¹Department of Computing Science, Umeå University, SE-901 87 Umeå, Sweden

*Email: linush@cs.umu.se

Abstract

We investigate well-posedness of Galbrun's equation, which is a reformulation of linearized Euler's equations that model propagation of sound in moving fluids.

Keywords: Galbrun's equation, linearized Euler's equations, Friedrichs' systems, flow-acoustic interaction

1 Introduction

Linearized Euler's equations, which are obtained by linearizing Euler's equations around some given flow, constitute the standard model for loss-less sound propagation in moving fluids. We consider flows where the entropy is everywhere constant; that is, either the flow is homentropic or the fluid is elastic. In such cases, Euler's equations describe the evolution of the fluid velocity u , pressure p and density ρ given the volume force density φ acting on the fluid and suitable initial and boundary conditions. Introducing the linearization ansatz $\phi(x, t) = \phi_0(x, t) + \delta\phi(x, t)$ —where ϕ denotes a generic flow field, ϕ_0 is given, $\delta\phi$ denotes the so-called Eulerian perturbation and where u_0, p_0, ρ_0 and φ_0 fulfill Euler's equations—into Euler's equations and retaining terms that are at most linear in the perturbations, yields linearized Euler's equations [2]

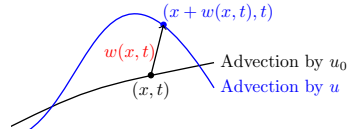
$$D_0\delta u + \frac{\nabla\delta p}{\rho_0} + (\delta u \cdot \nabla)u_0 - \frac{\nabla p_0}{\rho_0^2}\delta\rho = \delta\varphi, \quad (1a)$$

$$D_0\delta\rho + \nabla \cdot (\rho_0\delta u) + (\nabla \cdot u_0)\delta\rho = 0, \quad (1b)$$

$$\delta p - c_0^2\delta\rho = 0, \quad (1c)$$

where $D_0 = \partial_t + u_0 \cdot \nabla$ denotes the material derivative with respect to the background flow, and where c_0 denotes the isentropic speed of sound.

Less known is the reduction of linearized Euler's equations (1) to a vector wave equation in the Lagrangian displacement w , which has been attributed to H. Galbrun [3]. As depicted in Figure 1, the Lagrangian displacement describes the displacement of individual fluid particles induced by the perturbations.

Figure 1: The Lagrangian displacement w .

For homentropic flows (or elastic fluids), Galbrun's equation reads [2]

$$\rho_0 D_0^2 w - \nabla(\rho_0 c_0^2 \nabla \cdot w) + (\nabla p_0) \nabla \cdot w - (\nabla w)^T \nabla p_0 = \rho_0 (\delta\varphi + (w \cdot \nabla) \varphi_0), \quad (2)$$

where $(\nabla w)_{ij} = \partial_j w_i$. The derivation of Galbrun's equation (2) relies critically on the so-called no resonance assumption, which will be discussed in the sequel.

A series of papers that consider increasingly complicated steady background flows has established well-posedness of a spatially regularized formulation in two spatial dimensions of the time harmonic counterpart to Galbrun's equation (2) (culminating paper [4]). For general time dependence in two spatial dimensions, the regularized formulation is also known to be well-posed for homogenous background flows [1]. To the best of our knowledge, no other results regarding well-posedness of Galbrun's equation (2) have been reported in the literature.

2 Our approach to Galbrun's equation

Instead of introducing the Lagrangian displacement w in the spirit of Figure 1, we propose to define w abstractly as the solution to the transport equation¹

$$\underbrace{(\partial_t + \mathcal{L}_{u_0})w}_{D_0 w - (w \cdot \nabla)u_0} = \delta u, \quad (3)$$

where $\mathcal{L}_{u_0} w = (u_0 \cdot \nabla)w - (w \cdot \nabla)u_0$ denotes the Lie derivative of w along u_0 . We show that definition (3) and equation (1b) implies that

$$\rho_0 D_0 \left(\frac{\delta\rho + \nabla \cdot (\rho_0 w)}{\rho_0} \right) = 0. \quad (4)$$

¹To make w well-defined, adequate initial and boundary conditions need to be supplied.

One formulation of the no resonance assumption is that the only solution to equation (4) is the trivial solution; that is,

$$\delta\rho = -\nabla \cdot (\rho_0 w). \quad (5)$$

We remark that relation (5) provides the only solution to equation (4) when posed on a bounded domain, if and only if relation (5) holds initially and at the part of the boundary where the background flow enters the domain. In particular, when the background flow is everywhere tangential to the boundary, we note that the initial condition of w may be chosen so that relation (5) holds initially and thereby for all subsequent times.

Definition (3) and expressions (5) and (1c) substituted into equation (1a) yields Galbrun's equation

$$\begin{aligned} \rho_0 D_0(D_0 w - (w \cdot \nabla)u_0) - \nabla(c_0^2 \nabla \cdot (\rho_0 w)) \\ + \rho_0 ((D_0 w - (w \cdot \nabla)u_0) \cdot \nabla) u_0 \\ + \frac{\nabla p_0}{\rho_0} \nabla \cdot (\rho_0 w) = \rho_0 \delta\varphi. \end{aligned} \quad (6)$$

The equivalence of formulations (2) and (6) can be established by a direct, albeit lengthy, calculation.

Our approach to Galbrun's equation indicates that if $(\delta u, \delta\rho)$ is a solution to linearized Euler's equations (1), then w defined by relation (3) is a solution to Galbrun's equation (6) provided that relation (5) holds. Moreover, we have shown that if the background flow is everywhere tangential to the boundary of the domain, then the initial condition needed to make w in definition (3) well-defined can be chosen so that relation (5) holds.

In order to proceed, we establish mild well-posedness of an initial boundary value problem of linearized Euler's equations (1) in the particular case that the background flow is everywhere tangential to the boundary of the domain and where the boundary condition is given by

$$Y \delta p - \rho_0 c_0 n \cdot \delta u = \rho_0 c_0 g. \quad (7)$$

In boundary condition (7), Y is a non-negative Lipschitz continuous dimensionless admittance function that allows interpolation between the boundary conditions $-n \cdot \delta u = g$ and $\delta p - \rho_0 c_0 n \cdot \delta u = \rho_0 c_0 g$ that holds at a vibrating impenetrable wall and can be used as an artificial in/out boundary condition, respectively.

Our proof of well-posedness is carried out within a recently developed framework for Friedrichs' systems [5, 6] and relies on results obtained by Rauch [7].

Within the same framework for Friedrichs' systems, we establish mild well-posedness of the initial boundary value problem for transport equation (3); that is, we show that the Lagrangian displacement is well-defined.

Finally, we demonstrate that if the background flow is sufficiently regular, then sufficiently regular solutions to the initial boundary value problem of Galbrun's equation (6) satisfy the estimate

$$\begin{aligned} \frac{d}{dt} \left\| \left(\tau_0^{-1} w, (\partial_t + \mathcal{L}_{u_0}) w, c_0 \rho_0^{-1} \nabla \cdot (\rho_0 w) \right) \right\|_{\rho_0}^2 \leq \\ \gamma \left\| \left(\tau_0^{-1} w, (\partial_t + \mathcal{L}_{u_0}) w, c_0 \rho_0^{-1} \nabla \cdot (\rho_0 w) \right) \right\|_{\rho_0}^2 + \\ \tau_0 \|\delta\varphi\|_{\rho_0}^2 + \alpha \|g\|_{\rho_0 c_0, \partial\Omega}^2, \end{aligned} \quad (8)$$

where $\tau_0 > 0$ has been introduced to homogenize dimensions, $\gamma, \alpha > 0$ depends on the background flow and on the admittance function Y , and where we have introduced weighted L^2 -norms $\|\xi\|_q^2 = \int q |\xi|^2$ on the domain and on the boundary. From estimate (8) follows a so-called energy estimate for Galbrun's equation (6). Due to the presence of zeroth order terms of indefinite signs, our energy estimate incorporates solutions that grow exponentially with time.

References

- [1] K. Berriri. PhD thesis, ENSTA ParisTech, 2006.
- [2] G. Gabard. PhD thesis, Université de Technologie de Compiègne, 2003.
- [3] H. Galbrun. *Propagation d'une onde sonore dans l'atmosphère et théorie des zones de silence*. Gauthier-Villars, Paris, 1931.
- [4] AS. Bonnet-Ben Dhia et al. *Commun. Comput. Phys.*, 11(2):555–572, 2012.
- [5] K. Burazin and M. Erceg. *Mediterr. J. Math.*, 13(6):3777–3796, 2016.
- [6] A. Ern et al. *Commun. Part. Diff. Eq.*, 32(2):317–341, 2007.
- [7] J. Rauch. *T. Am. Math. Soc.*, 291(1):167–187, 1985.

Numerical analysis of the Galbrun equation using discontinuous Galerkin finite elements

Marcus Maeder^{1,*}, Andrew Peplow², Steffen Marburg¹

¹Chair of Vibroacoustics of Vehicles and Machines, TU-Munich, Munich, Germany

²College of Natural and Health Sciences, Zayed University, Abu Dhabi, UAE

*Email: Marcus.Maeder@tum.de

Abstract

In the engineering field of aeroacoustics, a number of reformulations of the Navier-Stokes equations known as Linearized Euler Equations (LEE), the Linearized Navier-Stokes Equations (LNSE), the Acoustic Perturbation Equations (APE) or Galbrun's equation can be used to analyze acoustic wave propagation in moving media. Galbrun used a mixed Lagrangian-Eulerian frame to describe perturbations of the field quantities only in terms of the Lagrangian particle displacement. Despite the reduced number of degrees of freedom, Galbrun's equation suffers from numerical difficulties, for example the onset of pollution errors due to spurious-like modes, when utilizing standard finite element approaches. Preliminary studies have shown that by using DG-FEM, numerical difficulties such as spurious modes can be omitted.

In this paper, the authors numerically investigate the Galbrun equation using a discontinuous Galerkin finite element method (DG-FEM) to solve aeroacoustic problems in shear flow.

Keywords: Galbrun, discontinuous Galerkin, finite element method

1 Introduction

Besides well studied theories for aeroacoustic problems, Galbrun's equation is not widely applied. Known drawbacks and solutions to solve Galbrun's equation can be found in the literature, cf. [1, 3, 6, 7].

We apply a discontinuous Galerkin finite element method in order to gain solution stability and further to separate acoustically relevant from non-relevant eigenvalues in the frame of a numerical modal analysis.

2 Theory

We consider a fluid filled domain $\Omega_F \subset \mathbb{R}^2$ which is bounded by Γ_F . Further, a Cartesian coordinate system is assumed while a vector component description together with Einstein's sum-

mation convention is applied. Following the considerations of Treysède et al. [7] and assuming that the reference pressure field is uniform, the displacement based formulation of Galbrun's equation can be stated such that

$$\rho_0 \frac{d^2 w_k}{dt^2} - (c_0^2 \rho_0 w_{l,l})_{,k} = 0, \quad \text{in } \Omega_F, \quad (1)$$

$$w_j n_j = 0, \quad \text{on } \Gamma_F. \quad (2)$$

with the material time derivative

$$\frac{dw_k}{dt} = \frac{\partial w_k}{\partial t} + v_{0l} w_{k,l} \quad (3)$$

where the abbreviation $w_{k,l}$ can be understood as the spatial derivative of w_k with respect to the l -direction. We consider a harmonic time dependency in the form of $w_k(x_k, t) = w_k(x_k) e^{-i\omega t}$ with the angular frequency $\omega = 2\pi f$ and the imaginary unit i .

3 Numerical Method

We apply the well known principles of the finite element method where the weak form of equation (1) is set up and discretized using discontinuous finite elements. For a complete description we refer to the literature, cf. [2, 4, 5].

4 Simulations

As a test case, we use an annulus with an inner radius $r_1 = 0.75$ m and an outer radius $r_2 = 1$ m to study the proposed method for a shear flow problem. Figure 1 displays the geometry of the annulus together with the flow direction.

$$v_{0k} = \begin{bmatrix} v_{01} \\ v_{02} \end{bmatrix} = \begin{bmatrix} 0 \\ -Ma c_0 \frac{1}{r_2 - r_1} (2r - (r_1 + r_2)) \end{bmatrix} \quad (4)$$

Equation (4) describes the flow velocity dependency on the radial coordinate r . The boundaries of the domain can be seen as acoustically hard. After discretizing the domain with DG finite elements we are interested in the solutions of the associated eigenvalue problem. In a first step we

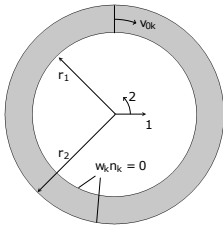


Figure 1: Geometry of annulus

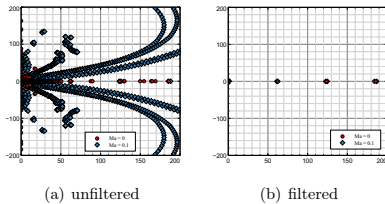


Figure 2: Solution of eigenvalue problem

consider the unfiltered Galbrun equation. The results are shown in Figure 2.

It can be seen that for $Ma = 0$ the eigenvalues are distributed close to the real axis in the complex plane, cf. Figure 2(a). As the flow velocity increases to $Ma = 0.1$ the main portion of the eigenvalues show an increasing imaginary part. Only some of the eigenvalues remain close to the real axis. For the remaining, the system is set up so that the real value of the eigenvalue solution is associated with the oscillating frequency. In a second step as an example we introduce a Lagrange multiplier enforcing the rotational components of the solution field to be zero. This way, it is possible so study the which eigenvalues have strong rotational components and which don't. Figure 2(b) shows the solutions of the filtered Galbrun equation. It can be seen that only these eigenvalues remain which have a vanishing rotational component. Further, it is possible to analyze the relative change in the frequency in order to understand the influence of the rotational components to the eigenvalue.

5 Conclusion

We analyzed an annulus with shear flow and acoustically hard walls and applying a discon-

tinuous Galerkin finite element method. By introducing Lagrange multipliers that enforce, e.g. the rotational components of the solution field to be zero, one can analyze the nature of the eigenvalues associated to the shear flow problem.

In future work the augmented version of Galbrun proposed by Bonnet-Ben Dhia [1] will be implemented and further analyzed.

References

- [1] A.-S. Bonnet-Ben Dhia, È.-M. Duclairoir, G. Legendre, J.-F. Mercier, Time-harmonic acoustic propagation in the presence of a shear flow, *Journal of Computational and Applied Mathematics*, 204, 2007 pp. 428–439.
- [2] B. Cockburn, G. E. Karniadakis, C.-W. Shu, *Discontinuous Galerkin Methods*, Springer Berlin Heidelberg, 2000.
- [3] F. Dietzsch, L. Hervella-Nieto, S. Marburg, R. Rodríguez, H. Weisbecker, Physical and spurious modes in mixed finite element formulation for the Galbrun equation, *Acta Acustica united with Acustica*, 100, 2014 pp. 493–512.
- [4] J. S. Hesthaven and T. Warburton, *Nodal discontinuous galerkin methods*, Springer New York, 2008.
- [5] M. Maeder, A. Peplow, M. Meindl and S. Marburg, Solving Galbrun's equation with a discontinuous Galerkin finite element method, *submitted for publication*
- [6] S. Retka and S. Marburg, An in finite element for the solution of Galbrun equation, *ZAMM - Journal of Applied Mathematics and Mechanics*, 93, 2012 pp. 154–162.
- [7] F. Treysède, G. Gabard, M. Ben Tahar, A mixed finite element method for acoustic wave propagation in moving fluids based on an Eulerian-Lagrangian description, *The Journal of Acoustical Society of America*, 113, 2003 pp. 705–716.

Efficient Modeling Strategies for Thermoviscous Acoustics

Florian Toth^{1,*}, Hamideh Hassanpour Guilvaiee¹, Manfred Kaltenbacher¹¹Institute of Mechanics and Mechatronics, TU Wien, Vienna, Austria

*Email: florian.toth@tuwien.ac.at

Abstract

Several formulations exist to model viscous and thermal boundary layers in fluids close to solid boundaries, ranging from the linearised Navier-Stokes equations to standard pressure acoustics with impedance-type boundary conditions. We critically assess the existing methods and propose a hybrid approach coupling the linearised Navier-Stokes and Helmholtz equations via non-conforming grids. The formulation is validated via simple example problems and subsequently applied to more complex modeling tasks.

Keywords: acoustics, linearised Navier-Stokes, viscous and thermal losses, non-conforming grid

1 Introduction

Viscous and thermal effects are often neglected when modeling acoustic phenomena. However, these dissipative effects become important in applications like hearing aids or microelectromechanical systems (MEMS). In general, viscous and thermal effect must be considered whenever the viscous and thermal boundary layer thickness become non-negligible in comparison to a) the acoustic wave length, or b) the model dimension.

2 Modelling

We assume small, harmonic perturbations of the state variables particle velocity \mathbf{v} , pressure p , density ρ , specific entropy s and temperature T of the form $f(t) = f_0 + \Re\{\hat{f}e^{j\omega t}\}$, where f_0 denotes the value of the state variable at equilibrium and $\hat{f} \in \mathbb{C}$ the perturbation. Furthermore, we assume that the relation between the thermodynamic quantities obey the ideal gas law, and that the viscous stress tensor is described by an isotropic Newtonian fluid, i.e.

$$\hat{\boldsymbol{\tau}} = \mu(\nabla\hat{\mathbf{v}} + (\nabla\hat{\mathbf{v}})^T) - \left(\frac{2}{3}\mu - \eta\right)\mathbf{I}\nabla\cdot\hat{\mathbf{v}}, \quad (1)$$

where the parameters μ and η denote the shear and bulk viscosity, respectively, and \mathbf{I} is the unit tensor. The linearized conservation equations

for momentum, mass and energy are then

$$j\omega\rho_0\hat{\mathbf{v}} + \nabla\hat{p} - \nabla\cdot\hat{\boldsymbol{\tau}} = 0, \quad (2)$$

$$j\omega\frac{\rho_0}{\rho_0}\hat{p} - j\omega\frac{\rho_0}{T_0}\hat{T} + \rho_0\nabla\cdot\hat{\mathbf{v}} = 0, \quad (3)$$

$$j\omega\rho_0c_p\hat{T} - \nabla\cdot\kappa\nabla\hat{T} - j\omega\hat{p} = 0, \quad (4)$$

where c_p denotes the heat capacity at constant pressure and κ denotes the thermal conductivity. Prescribing suitable boundary conditions, above equations can be solved for the unknown pressure, temperature and velocity components by the finite element method.

Above formulation may be modified in several ways: The velocity field may be split into a rotational and solenoidal part, leading to two scalar Helmholtz equations for acoustic and entropic temperatures, and a vectorial Helmholtz equation for the rotational velocity [2, 3]. By taking the time derivative of (2) and the divergence of (3) one may eliminate the pressure and thus obtain a coupled equation system for the temperature and velocity components [4]. Retaining the pressure in a mixed formulation may avoid numerical problems associated with near incompressibility, but requires appropriate stable discretisations [5].

3 Numeric Efficiency

As the thermoviscous formulation requires the solution of coupled equations with 5 unknowns and thin viscous and thermal boundary layers need to be resolved, the computational effort is much larger than for standard acoustics with a scalar unknown and the requirement to resolve the acoustic wave length. As thermoviscous effects are only active close to the boundaries, one can couple thermoviscous and purely acoustic descriptions. This can be elegantly done using non-conforming grids [6], removing the necessity of a transition mesh between fine and coarse discretisation.

Another recent approach uses classical pressure acoustics (neglecting viscosity and thermal conductivity) in the fluid domain but introduces thermal and viscous effects as boundary condi-

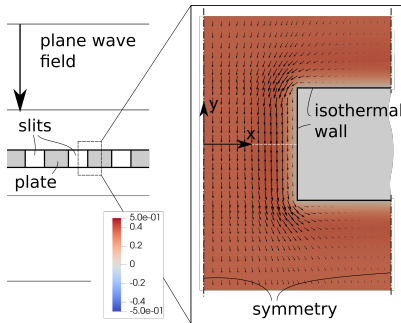


Figure 1: 2D model of a plane wave traveling through an isothermal plate with narrow slits (left), and computed velocity (vectors) and temperature (in color) fields in the slit (right).

tions derived by integrating the known boundary layer profiles [1, 7]. The aim of this work is to critically assess and compare the numerical performance as well as the range of applicability of the different available methods.

4 Application

The above formulation has been implemented in the finite element software CFS++ [8], which is used to solve representative example problem, e.g. the propagation of a plane wave through a rigid plate with thin slits (see Fig. 1). The slits are much smaller than the acoustic wave length, however they are in the order of magnitude of the viscous and thermal boundary layer. Thus, the arising damping effects must be accurately modeled. Figure 2 shows the computed velocity and temperature profile in the middle of the slit.

References

- [1] Berggren M, Bernland A, Noreland D. Acoustic boundary layers as boundary conditions. *Journal of Computational Physics* oct 2018; **371**:633–650.
- [2] Cotterill PA, Nigro D, Abrahams ID, Garcia-Neefjes E, Parnell WJ. Thermo-viscous damping of acoustic waves in narrow channels: A comparison of effects in air and water. *The Journal of the Acoustical Society of America* dec 2018; **144**(6):3421–3436.

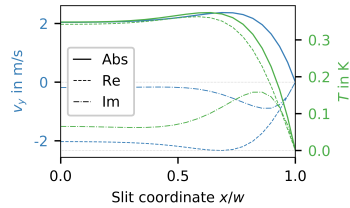


Figure 2: Velocity and temperature profile in the center of the slit. The real and imaginary parts show two instantaneous profiles of the evanescent wave originating from the boundary at $x/w = 1$.

- [3] Beltman WM. Viscothermal wave propagation including acousto-elastic interaction, part i: Theory. *Journal of Sound and Vibration* oct 1999; **227**(3):555–586.
- [4] Joly N, Bruneau M, Bossart R. Coupled Equations for Particle Velocity and Temperature Variation as the Fundamental Formulation of Linear Acoustics in Thermo-Viscous Fluid at Rest. *Acta Acustica united with Acustica* 2006; **92**:202–209.
- [5] Kampinga WR, Wijnant YH, de Boer A. Performance of several viscothermal acoustic finite elements. *Acta Acustica united with Acustica* jan 2010; **96**(1):115–124.
- [6] Flemisch B, Kaltenbacher M, Wohlmuth BI. Elasto-acoustic and acoustic-acoustic coupling on nonmatching grids. *Int. J. Numer. Meth. Engng* 2006; **67**(13):1791–1810.
- [7] Bach JS, Bruus H. Theory of pressure acoustics with viscous boundary layers and streaming in curved elastic cavities. *The Journal of the Acoustical Society of America* aug 2018; **144**(2):766–784.
- [8] Coupled Field Simulation in C++. <http://cfs-doc.mdmt.tuwien.ac.at>.

A computationally inexpensive visco–thermal boundary layer model for acoustic simulation and optimization

**Martin Berggren^{1,*}, Anders Bernland¹, André Massing², Daniel Noreland¹,
Eddie Wadbro¹**

¹Department of Computing Science, Umeå University, Umeå, Sweden

²Department of Mathematics and Mathematical Statistics, Umeå University, Umeå, Sweden

*Email: martin.berggren@cs.umu.se

Abstract

To model the effects of acoustic boundary layers close to solid surfaces, we have derived a generalized admittance boundary condition to the Helmholtz equation for the acoustic pressure. The admittance operator acts on the acoustic pressure and its surface Laplacian in order to account for thermal and viscous effects, respectively. For a model problem with significant visco–thermal effects, this model yields virtually identical results to a hybrid Helmholtz/linearized Navier–Stokes model; however, our model needs about two orders of magnitude less memory and computational time. We have recently incorporated the model in a shape optimization framework to design a device for which visco–thermal losses are important to model.

Keywords: acoustics, visco–thermal boundary layers, Helmholtz equation, shape optimization

1 Background

For devices such as hearing aids, microphones, micro loudspeakers, and compression drivers for loudspeaker horns, the presence of visco–thermal boundary layers in the vicinity of solid walls significantly affects the overall performance. These effects thus have to be accounted for in the modeling and optimization of such devices. Although the linearized Navier–Stokes equations provide accurate modeling, the computational cost of solving these equations is generally very high. The high cost stems from the need to resolve the extremely thin boundary layers, which are in the order of 20–400 μm in the audio range.

2 The acoustic boundary-layer model

Under isentropic assumptions, sound propagation in air can in frequency domain be modeled by the first-order system

$$\frac{i\omega}{c^2}p + \nabla \cdot \rho_0 \mathbf{U} = 0, \quad (1a)$$

$$i\omega \rho_0 \mathbf{U} + \nabla p = 0, \quad (1b)$$

where p and \mathbf{U} are the acoustic pressure and velocity, and ρ_0 and c the static density and the speed of sound of air. Eliminating \mathbf{U} , the system reduces to the Helmholtz equation in the pressure,

$$-\Delta p - k_0^2 p = 0, \quad (2)$$

where $k_0 = \omega/c$. Equations (1) or (2) accurately model acoustic wave propagation except close to solid walls, where boundary layers form. Boundary-layer theory yields, in the case of a smooth wall, an explicit formula for the acoustic velocity and density as a function of wall distance. From their boundary values, the acoustic velocity and density will exponentially attain isentropic values governed by equation (1) with decay constants $\delta_V = \sqrt{2\nu/\omega}$ and $\delta_T = \sqrt{2\kappa/(\omega\rho_0 c_p)}$, the viscous and thermal boundary-layer thicknesses. Here, ν and κ are the thermal conductivity and the kinematic viscosity, and c_p the specific heat at constant pressure.

Plugging these formulas into the equation of mass conservation and integrating in the wall-normal direction, we have shown that the *isentropic* mass conservation law (1a) holds to first order in δ_V and δ_T , provided that the solid-wall boundary condition on $\mathbf{n} \cdot \mathbf{u}$ (or $\partial p/\partial n$ for the Helmholtz equation (2)) is modified [1]. We have recently learned that this modification has previously been derived, using a different approach, by Pierce [2, Eq. 10–4.12]. Somewhat surprisingly, it seems, to the best of our knowledge, that Pierce’s condition has not been translated into a boundary condition for numerical computations.

In the case of a closed acoustic cavity with vibrating walls, the boundary-value problem for the Helmholtz equation using the resulting boundary condition becomes

$$-k_0^2 p - \Delta p = 0 \quad (\Omega), \quad (3a)$$

$$\delta_T k_0^2 \frac{1}{2}(i-1)(\gamma-1)p - \delta_V \frac{1}{2}(i-1)\Delta_T p + \partial p/\partial n = g \quad (\Gamma_w), \quad (3b)$$

where γ is the heat capacity ratio and g is proportional to the imposed vibration amplitude. Boundary condition (3b) constitutes a perturbation of the wall boundary condition $\partial p/\partial n = g$, where $g = 0$ for a motionless wall. The *viscous* part of boundary condition (3b) has previously appeared in a report by Schmidt and Thöns-Zueva [3], derived by different means. The current model requires that boundary layer thickness is much smaller than the radius of curvature of the wall and that possible opposite-facing walls are well outside the boundary layer.

In a recent article [1], we assessed the model by computing the radiated power out of a generic compression driver. Figure 1 shows the power spectrum for three different models: a lossless Helmholtz model (dashed), a model where the linearized Navier–Stokes equations were used in narrow regions (circles), and our boundary-loss model (solid).

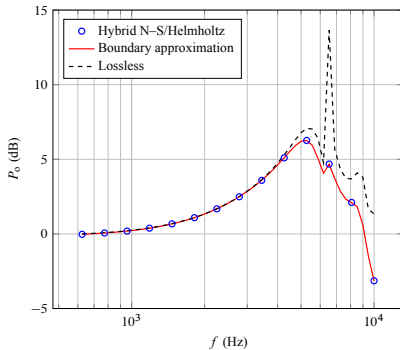


Figure 1: Compression-driver power output for different models

Our model gives virtually identical results to the more accurate one, but in our model, the memory requirement was reduced from 102 Gbytes down to 1 Gbytes and the computational times from 2100 s down to 12 s per frequency.

Since the new model does not need meshes that resolve boundary layers and due to its computational efficiency, we here apply it for the first time in the context of shape optimization of devices for which boundary-layer effects need to be considered. Figures 2 and 3 shows initial results of an optimization in 3D of the so-called phase plug of a compression driver. We use gradient-based shape optimization, adjoint

equations to compute gradients, and a geometry represented with a level-set function. Boundary condition (3b) is imposed using the CutFEM method [4]. The figure shows one half of 32 circumferentially symmetric sections. The membrane is located to the left, and the outlet into the throat of the horn is to the right.

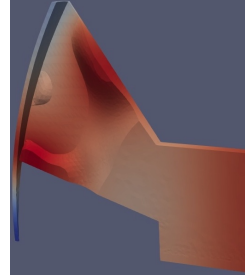


Figure 2: A shape-optimized phase plug

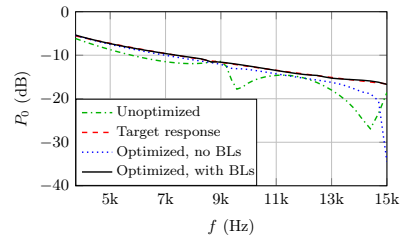


Figure 3: Frequency response. Target and results when optimized with and without accounting for boundary-layer effects

References

- [1] M. Berggren, A. Berland, D. Noreland, Acoustic boundary layers as boundary conditions, *J. Comput. Phys.* 371 (2018), pp. 633–650.
- [2] A. D. Pierce, *Acoustics, An Introduction to its Physical Principles and Applications*, ASA, 1994.
- [3] K. Schmidt, A. Thöns-Zueva, Impedance boundary conditions for acoustic time harmonic wave propagation in viscous gases. Preprint 6-2014, Technische Universität Berlin, 2014.
- [4] E. Burman, S. Claus, P. Hansbo, M.G. Larson, A. Massing, CutFEM: discretizing geometry and partial differential equations, *Int. J. Numer. Meth. Engrg.* 104 (2015), pp. 472–501.

Analytic preconditioners for 3D high-frequency elastic scattering problems

Stéphanie Chaillat¹, Marion Darbas^{2,*}, Frédérique Le Louër³¹Laboratoire POEMS, ENSTA-UMA, Université Paris-Saclay, Palaiseau, France²LAMFA UMR CNRS 7352, Université de Picardie Jules Verne, Amiens, France³LMAC EA 2222, Université de Technologie de Compiègne, Compiègne, France

*Email: marion.darbas@u-picardie.fr

Abstract

The work is concerned with the numerical solution of 3D high-frequency elastic scattering problems by a bounded obstacle, namely the exterior Navier problem with a Dirichlet or a Neumann boundary condition. We propose the combination of analytic preconditioners [2] and the Fast Multipole Method (FMM).

Keywords: Elastodynamics, boundary integral equations, FMM, analytic preconditioners

1 Introduction

The numerical solution of high-frequency scattering problems of time-harmonic elastic waves by a three-dimensional obstacle is a challenging task. The fast multipole method is an efficient technique to accelerate the solution of large scale 3D scattering problems with boundary integral equations. However, the fast multipole accelerated boundary element method (FM-BEM) is intrinsically based on an iterative solver. It has been shown that the number of iterations can significantly hinder the overall efficiency of the FM-BEM. The derivation of robust preconditioners for FM-BEM is inevitable to increase the size of the problems that can be considered. The main constraint in the context of the FM-BEM is that the complete system is not assembled to reduce computational times and memory requirements. Analytic preconditioners offer a very interesting strategy by improving the spectral properties of the boundary integral equations ahead from the discretization. We propose to combine an approximate adjoint Dirichlet to Neumann (DtN) map as an analytic preconditioner with a FM-BEM solver to treat Dirichlet exterior scattering problems in 3D elasticity. We compare usual and preconditioned Combined Field Integral Equations (CFIEs).

2 The Navier exterior problem

We consider a bounded domain Ω^- in \mathbb{R}^3 , with a closed smooth boundary $\Gamma := \partial\Omega^-$. Let Ω^+ de-

note the exterior domain $\mathbb{R}^3 \setminus \overline{\Omega^-}$ and \mathbf{n} the outer unit normal vector to the boundary Γ . The scattering problem is formulated as follows : Given an incident displacement wave \mathbf{u}^{inc} , find the solution \mathbf{u} of the Navier exterior problem:

$$\begin{aligned} \mu \Delta \mathbf{u} + (\lambda + \mu) \nabla \operatorname{div} \mathbf{u} + \rho \omega^2 \mathbf{u} &= 0, \text{ in } \Omega^+, \\ \mathbf{u} &= -\mathbf{u}^{inc}, \text{ on } \Gamma, \\ \Delta \mathbf{u}_p + \kappa_p^2 \mathbf{u}_p &= 0, \operatorname{curl} \operatorname{curl} \mathbf{u}_s - \kappa_s^2 \mathbf{u}_s = 0, \end{aligned} \quad (1)$$

where $\omega > 0$ is the frequency, and the Lamé parameters μ , λ and the density ρ are positive constants. The field \mathbf{u} is decomposed into a longitudinal field \mathbf{u}_p with vanishing curl and a transverse divergence-free field \mathbf{u}_s solutions to with respective wavenumbers $\kappa_p^2 = \rho \omega^2 (\lambda + 2\mu)^{-1}$ and $\kappa_s^2 = \rho \omega^2 \mu^{-1}$.

3 Usual and preconditioned CFIEs

Integral equation method is based on the potential theory. The field \mathbf{u} is uniquely determined by the knowledge of the Cauchy data $(\mathbf{u}_\Gamma, \mathbf{t}_\Gamma)$. The Neumann trace $\mathbf{t}_\Gamma := \mathbf{T}\mathbf{u}$ is given by the traction operator

$$\mathbf{T} = 2\mu \frac{\partial}{\partial \mathbf{n}} + \lambda \mathbf{n} \operatorname{div} + \mu \mathbf{n} \times \operatorname{curl}.$$

For any real-valued constant α , we introduce the modified Neumann trace $\mathbf{t}_\alpha \in \mathbf{H}^{-\frac{1}{2}}(\Gamma)$ defined by

$$\mathbf{t}_\alpha = \mathbf{t}_\Gamma - \alpha \mathcal{M} \mathbf{u}_\Gamma$$

where \mathcal{M} is the tangential G unter derivative. The standard CFIE consists in finding the physical unknown $\varphi = -(\mathbf{t}_\Gamma + \mathbf{t}_\Gamma^{inc})$ solution to

$$\left(\frac{1}{2} + D' + i\eta S\right)\varphi = -(\mathbf{t}^{inc} + i\eta \mathbf{u}_\Gamma^{inc}), \quad \text{on } \Gamma, \quad (2)$$

with $\mathbf{t}_\Gamma^{inc} = \mathbf{T}\mathbf{u}^{inc}$, η a non-zero real constant and the single- and double-layer boundary integral operators

$$\begin{aligned} S\varphi(\mathbf{x}) &= \int_\Gamma \Phi(\mathbf{x}, \mathbf{y}) \varphi(\mathbf{y}) \, ds(\mathbf{y}), \\ D\psi(\mathbf{x}) &= \int_\Gamma [\mathbf{T}_\mathbf{y} \Phi(\mathbf{x}, \mathbf{y})]^\top \psi(\mathbf{y}) \, ds(\mathbf{y}). \end{aligned}$$

It is well known that the standard CFIE is not suited for an iterative solution. To expect an eigenvalue clustering and hence a fast convergence of GMRES, the approach we consider is to derive preconditioned CFIEs: Find $\varphi = -(\mathbf{t}_\Gamma + \mathbf{t}_\Gamma^{inc})$ solution to

$$\left(\frac{I}{2} + D' - \Lambda' S\right)\varphi = -(\mathbf{t}_\Gamma^{inc} - \Lambda' \mathbf{u}_\Gamma^{inc}), \quad \text{on } \Gamma, \quad (3)$$

where Λ' is an approximation of the exact adjoint DtN map

$$\Lambda^{\text{ex}} : \mathbf{u}_\Gamma \in \mathbf{H}^{\frac{1}{2}}(\Gamma) \mapsto \Lambda^{\text{ex}} \mathbf{u}_\Gamma := \mathbf{t}_\Gamma \in \mathbf{H}^{-\frac{1}{2}}(\Gamma),$$

4 Approximation of the adjoint DtN map and new boundary integral equations

The spectral properties of (3) depend on the choice of the approximate adjoint DtN map Λ' . We want to compare several approximations of different orders. In [2], new approximations of the DtN map have been obtained in the spirit of OSRC methods. The idea is to consider only the principal part of the exact adjoint operator $\Lambda_\alpha^{\text{ex}}$ and the decomposition

$$\Lambda^{\text{ex}} = \Lambda_\alpha^{\text{ex}} + \alpha \mathcal{M}$$

where $\Lambda_\alpha^{\text{ex}}$ is the exact exterior Modified Dirichlet-to-Neumann (MDtN) map defined by

$$\Lambda_\alpha^{\text{ex}} : \mathbf{u}_\Gamma \in \mathbf{H}^{\frac{1}{2}}(\Gamma) \mapsto \Lambda_\alpha^{\text{ex}} \mathbf{u}_\Gamma := \mathbf{t}_\alpha \in \mathbf{H}^{-\frac{1}{2}}(\Gamma).$$

We compare low- and high-order adjoint DtN approximations, and the corresponding LO and HO preconditioned CFIEs [1]. The high-order adjoint DtN approximations are expressed in terms of surface differential operators, square-root operators and their inverse. Complex Padé rational approximants provide local and uniform representations of the square-root operators.

5 Numerical results

The numerical efficiency of the different proposed preconditioned CFIEs is illustrated for several more or less complex geometries. An analytical study for the spherical case underlines an "ideal" eigenvalue clustering around the point (1, 0) for the preconditioned CFIEs. This is not the case for the standard CFIE which has small eigenvalues close to zero. The number of GMRES iterations is drastically reduced when the preconditioned CFIEs are considered, independently of the frequency.

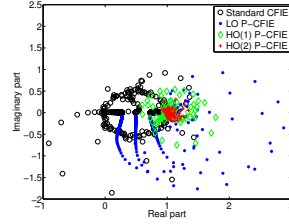


Figure 1: Distribution of the eigenvalues of the standard and different P-CFIEs ($\eta = 1$, $\kappa_s = 16\pi$ and $n_{\lambda_s} = 10$).

#DOFs	ω	# iter CFIE	# iter HO(1) P-CFIE	# iter P-
1 926	4	18	7	5
7 686	8.25	27	6	4
30 726	16.5	51	6	3
122 886	33	180	6	3
490 629	66.5	> 500	6	3

Table 1: Diffraction of P-waves by the unit sphere. Number of GMRES iterations for a fixed density of 10 points per wavelength.

6 Perspectives

Ongoing work concerns the derivation of such preconditioners for Neumann (or cavity) elastic exterior problems. Contrary to the acoustic and electromagnetic cases, the definition of the Neumann-to-Dirichlet preconditioner as the inverse of the DtN preconditioner is not sufficient to construct well-conditioned BIEs for Neumann scattering problems. A more extensive analysis of the DtN and Neumann-to-Dirichlet maps has to be realized in the transition region corresponding to the grazing modes.

References

- [1] S. Chaillat, M. Darbas and F. Le Louër, Fast iterative boundary element methods for high-frequency scattering problems in 3D elastodynamics *JCP*, **41** (2017), pp. 429–446.
- [2] M. Darbas and F. Le Louër, Analytic preconditioners for the iterative solution of elasticity scattering problems *M2AS*, **38** (2015), pp. 1705–1733.

Spectral coarse space for robust additive Schwarz preconditioning of hypersingular integral operators

X.Claeys¹, P.Marchand¹, F.Nataf¹

¹Sorbonne Université, Université Paris-Diderot SPC, CNRS,Inria, Laboratoire Jacques-Louis Lions, équipe Alpines, F-75005 Paris

Abstract

Considering hypersingular integral operators discretised by Lagrange finite elements, we present a preconditionner based on a two level additive Schwarz domain decomposition strategy. This preconditionner relies on a coarse space defined through the solution, in parallel, of generalised eigenvalue problems in each subdomain. The construction of the coarse space is fully automatic and guarantees scalability of iterative solvers. We provide theoretical bounds for the condition number of the preconditionned problem as well as numerical results supporting the theory.

Keywords: domain decomposition, boundary integral operator, preconditioning

1 Model problem

Let $\Omega \subset \mathbb{R}^d, d = 2, 3$ refer to a polyhedral domain with $\Gamma := \partial\Omega$, denote $V_h \subset H^{1/2}(\Gamma)$ the space of \mathbb{P}_k -Lagrange functions constructed over a triangulation \mathcal{T} of Γ , and V_h^* its dual. Given $\ell \in V_h^*$, we study the problem of finding $u \in V_h$ solving $A(u) = \ell$ with $A : V_h \rightarrow V_h^*$ defined by

$$\begin{aligned} A(u), v := & \int_{\Gamma \times \Gamma} \mathcal{G}(\mathbf{x} - \mathbf{y}) [\text{curl}_{\Gamma} u(\mathbf{x}) \cdot \text{curl}_{\Gamma} v(\mathbf{y}) \\ & + \gamma^2 u(\mathbf{x}) v(\mathbf{y}) \mathbf{n}(\mathbf{x}) \cdot \mathbf{n}(\mathbf{y})] d\sigma(\mathbf{x}, \mathbf{y}). \end{aligned}$$

where \mathcal{G} refer to the Green kernel of the operator $\gamma^2 - \Delta$. Numerous past contributions have already proposed domain decomposition based preconditionners for such a model problem, e.g. Additive Schwarz Method (ASM), the most efficient of which encompassing coarse space corrections, see e.g. [3]. However, most of the coarse spaces proposed so far depend a priori on the discretisation procedure and are ad-hoc problem dependent constructions.

Following the so-called GenEO strategy previously developed for preconditioning Laplace-like equations discretised by \mathbb{P}_1 -Lagrange finite elements [2], we propose a new coarse space construction.

2 Domain decomposition

Consider a decomposition $\Gamma = \cup_{j=1}^J \bar{\Gamma}_j$ into overlapping subdomains, each Γ_j being a union of cells of the triangulation \mathcal{T} , and set

$$\begin{aligned} n_{\chi} &= \text{chromatic number} \\ n_{\mu} &= \sup_{\mathbf{x} \in \Gamma} \sum_{j=1}^J 1_{\Gamma_j}(\mathbf{x}) \end{aligned} \quad (1)$$

The chromatic number is defined as the minimum number of colours required to guarantee that any two adjacent subdomains have different colours. We suppose that the subdomain covering $\{\Gamma_j\}_{j=1}^J$ has been generated so that n_{χ}, n_{μ} remain bounded uniformly with respect to J . This is a reasonable assumption met by standard automatic mesh partitionners.

Define $\check{V}_h^j := \{v \in V_h, \text{supp}(v) \subset \Gamma_j\}$ and $\check{V}_h := \check{V}_h^1 \times \dots \times \check{V}_h^J$. We have $V_h = \check{V}_h^1 + \dots + \check{V}_h^J$ so that the operator $R : \check{V}_h \rightarrow V_h$ defined by $R(u_1, \dots, u_J) = u_1 + \dots + u_J$ is surjective. Define also $B : \check{V}_h \rightarrow \check{V}_h^*$ by

$$B(\mathbf{u}), \mathbf{v} := \sum_{j=1}^J \langle A(u_j), v_j \rangle$$

for $\mathbf{u} = (u_j), \mathbf{v} = (v_j)$ in \check{V}_h . With the one-level ASM preconditionner defined by $RB^{-1}R^*$, the conditioning of the system is admittedly stable with respect to meshwidth, but deteriorates as $J =$ "number of subdomains" grows.

3 Spectral coarse space

This is our motivation for introducing a coarse space correction. Denote $V_h^j := \{v|_{\Gamma_j}, v \in V_h\}$ and $\mathbb{V}_h = V_h^1 \times \dots \times V_h^J$. Let $\psi_j \in V_h^j$ satisfy $\psi_1 + \dots + \psi_J = 1$, and define $D : \mathbb{V}_h \rightarrow \mathbb{V}_h$ by

$$D((u_j)_{j=1}^J) := (\Pi_h(\psi_j u_j))_{j=1}^J$$

where Π_h is the Lagrange interpolator on V_h . Let $h_{\mathcal{T}}(\mathbf{x}) := |\tau|^{1/(d-1)}$ for $\mathbf{x} \in \tau$ and τ any cell of the triangulation \mathcal{T} , and define the operator $B' : \mathbb{V}_h \rightarrow \mathbb{V}_h^*$ by

$$B'(\mathbf{u}), \mathbf{v} := \sum_{j=1}^J \int_{\Gamma_j} h_{\mathcal{T}} \nabla_{\Gamma} u_j \cdot \nabla_{\Gamma} v_j d\sigma.$$

Given a parameter $\Lambda > 0$ to be fixed heuristically, our coarse space $V_h^0 \subset V_h$ is defined by

$$V_h^0 := \text{span}\{ \text{RD}(\mathbf{v}) \in V_h \mid \exists \lambda > \Lambda \\ \text{such that } D^* \text{BD}\mathbf{v} = \lambda B' \mathbf{v} \}$$

Since both B and B' are subdomain-wise block diagonal, this eigenvalue problem can be solved in parallel. Next set $\mathbb{W}_h := V_h^0 \times \mathbb{V}_h$ and define $B_w : \mathbb{W}_h \rightarrow \mathbb{W}_h^*$ and $R_w : \mathbb{W}_h \rightarrow V_h$ by

$$\langle B_w(\mathbf{u}), \mathbf{v} \rangle := \sum_{j=0}^J \langle A(u_j), v_j \rangle \\ R_w(\mathbf{u}) := u_0 + \dots + u_J$$

Our two level preconditionner is then given by $R_w B_w^{-1} R_w^*$.

4 Condition number estimates

We provide a complete analysis of this preconditionner. First consider the Sobolev-Slobodecki norm

$$\|u\|_{1/2,\Gamma}^2 := \int_{\Gamma \times \Gamma} \frac{|u(\mathbf{x}) - u(\mathbf{y})|^2}{|\mathbf{x} - \mathbf{y}|^d} d\sigma(\mathbf{x}, \mathbf{y})$$

for all $u \in H^{1/2}(\Gamma)$, and define the condition number of A with respect to this norm

$$\kappa_A := \sup W(A) / \inf W(A)$$

$$W(A) := \left\{ \frac{\langle A(u), \bar{u} \rangle}{\|u\|_{1/2,\Gamma}^2}, u \in H^{1/2}(\Gamma) \setminus \{0\} \right\}$$

Finally we also need to define

$$c_{B'} := \sup_{v \in V_h \setminus \{0\}} \frac{\int_{\Gamma} |\nabla_{\Gamma} v|^2 h_{\mathcal{T}} d\sigma}{\langle A(v), \bar{v} \rangle}. \quad (2)$$

Left apart Γ and A , the constant $c_{B'}$ only depends on the shape regularity of the triangulation \mathcal{T} and the polynomial degree k , but not on the meshwidth $h = \sup_{\Gamma} h_{\mathcal{T}}$, see [1, Prop.5].

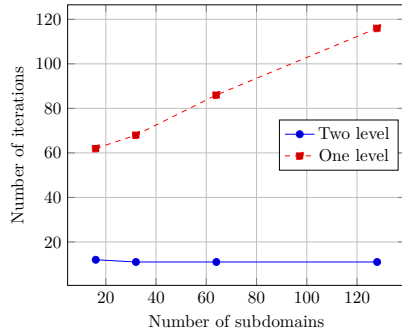
Defining $\text{cond}(R_w B_w^{-1} R_w^* A) := \sup \mathfrak{S} / \inf \mathfrak{S}$, where \mathfrak{S} refers to the spectrum of $R_w B_w^{-1} R_w^* A$, we can establish the following bound

$$\text{cond}(R_w B_w^{-1} R_w^* A) \leq \\ \max(2, 5n_{\chi} \kappa_A) (c_{B'} n_{\mu} \Lambda (1 + 5n_{\chi} \kappa_A) + 2) \quad (3)$$

The upper bound above only depends on the discretisation through n_{χ} , n_{μ} and $c_{B'}$. Our previous remarks thus show that this bound depends neither on the mesh width h nor on the number of subdomains J .

5 Numerical validation

The figure below presents strong scaling results obtained for the case where $\Omega := (-2, +2)^2 \setminus [-1, +1]^2 \subset \mathbb{R}^2$ with $\gamma = 0.1$. For both one and two level preconditionners, this picture provides the number of iterations of a conjugate gradient solver versus the number of subdomains J for a fixed problem size $\text{dim}(V_h)$. It confirms the strong scalability of our two-level preconditionner. During the talk, we shall provide further numerical proofs of the efficiency of this preconditionning strategy.



6 Acknowledgement

This work was supported by French National Research Agency (ANR) through the project NonlocalDD, grant ANR-15-CE23-0017-01.

References

- [1] M.Aurada, M.Feischl, T.Führer, M.Karkulik and D.Praetorius, Energy norm based error estimators for adaptive BEM for hypersingular integral equations, *Appl. Numer. Math.* **95** (2015), 15–35.
- [2] N.Spillane, V.Dolean, P.Hauret, F.Nataf, C.Pechstein, R.Scheichl, Abstract robust coarse spaces for systems of PDEs via generalized eigenproblems in the overlaps. *Numer. Math.* 126 (2014), no. 4, 741–770.
- [3] N.Heuer, E.P.Stephan, An additive Schwarz method for the h-p version of the boundary element method for hypersingular integral equations in R3. *IMA J. Numer. Anal.* 21 (2001), no. 1, 265–283.

Modelling the fluid-structure coupling caused by a far-field underwater explosion using a convolution quadrature based fast boundary element method

Damien Mavaleix-Marchessoux^{1,2,*}, Stéphanie Chaillat¹, Bruno Leblé², Marc Bonnet¹

¹POEMS (CNRS, INRIA, ENSTA), ENSTA, Palaiseau, France

²Naval Group Research, Nantes, France

*Email: mavaleix@ensta.fr

Abstract. This contribution concerns the modelling of the impact of a far-field underwater explosion shock wave on a structure, in deep water. An iterative fluid-structure coupling is developed to solve the problem. Two complementary methods are used: the Finite Element Method (FEM), that offers a wide range of tools to appreciate the structure response; and the Boundary Element Method (BEM), more suitable to deal with large fluid domains. The issues addressed are the conception of a temporal fast BEM procedure and the implementation of the FEM-BEM coupling.

A frequency-based BEM, accelerated by the Fast Multipole Method (FMM) and extended to the time domain by the Convolution Quadrature Method (CQM), permits an accurate resolution of the Helmholtz equation, despite the high frequencies considered when dealing with underwater explosions (UNDEX).

Keywords: Boundary Element Method, Fast Multipole Method, Convolution Quadrature Method, underwater explosion

Assessing the impact of underwater explosions on submerged structures (submarines) is an important naval engineering problem. An underwater explosion mainly induces two distinct phenomena: a “shock wave” (fast acoustic perturbation) followed by an oscillating bubble of gas (slow incompressible flow) [4]. Our overall goal is to create an efficient numerical method that accounts for the effects of both phenomena on submerged structures.

This contribution focuses on the interaction for the shock wave phenomenon. Computational challenges arise: (a) the relevant structures are large, and (b) the interaction is fast (lasting a few milliseconds) and hence involves high frequencies. Strong simplifying assumptions are often proposed, such as the *Doubly Asymptotic Approximations* (DAA) [5]. The goal of this work is to develop accurate numerical methods allowing to deal with complex geometries.

Formulation of the problem, radiated and reflected pressures Consider a structure Ω_s of surface Γ submerged in an infinite fluid domain Ω_f (see Figure 1). The fluid and the structure are both at initial rest. At $t = 0$, a known spherical wave emerges from an explosion (re-

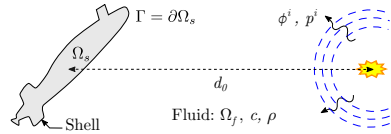


Figure 1: Shell submerged in an acoustic medium, submitted to a far-field UNDEX.

mote point source). At a distance r far from the explosion, the incident pressure p^{inc} is given by an empirical law [4]:

$$p^{\text{inc}}(r, t) = p_m(r) \exp\left(-\frac{t-r/c}{\tau(r)}\right) H(t-r/c),$$

where $p_m(r)$ and $\tau(r)$ depend on parameters of the explosive material (typically $p_m \approx 1$ Mpa and $\tau \approx 1$ ms), and H is the Heaviside step function. The velocity potential ϕ is such that

$$\vec{v} = \vec{\nabla}\phi, \quad p = -\rho \frac{\partial \phi}{\partial t}, \quad \Delta \phi - \frac{1}{c^2} \frac{\partial^2 \phi}{\partial t^2} = 0.$$

A set of structure equations, not specified here, governs the dynamical response of the structure. The fluid and structure equations are coupled by requiring the continuity of the normal velocity and the normal stress on Γ . For the fluid-structure interaction (FSI) problem, the potential ϕ is decomposed upon three parts [6]:

$$\phi^{\text{tot}} = \phi^{\text{inc}} + \phi^{\text{ref}} + \phi^{\text{rad}}.$$

The incident field ϕ^{inc} defines the acoustic field in the absence of the structure. The reflected field ϕ^{ref} is the perturbation that would be observed in the fluid if the structure were motionless. The radiated field ϕ^{rad} corresponds to the modification of the fluid state due to the motion of the structure, which radiates an acoustic wave into the fluid. On Γ , the boundary conditions verified by $\phi^{\text{ref}}, \phi^{\text{rad}}$ stem from the required continuity of the normal velocity:

$$\vec{\nabla}(\phi^{\text{ref}}) \cdot \vec{n} = -\vec{\nabla}(\phi^{\text{inc}}) \cdot \vec{n}, \quad \vec{\nabla}(\phi^{\text{rad}}) \cdot \vec{n} = \vec{v}_s \cdot \vec{n},$$

where $\vec{v}_s(\vec{x})$ is the structure velocity at $\vec{x} \in \Gamma$, and \vec{n} is the outward normal to Γ . The potentials $\phi^{\text{ref}}, \phi^{\text{rad}}$ are to be computed using the boundary element method.

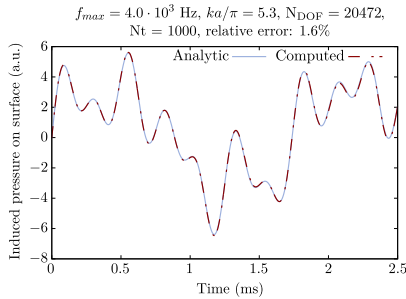


Figure 2: Pressure induced on a breathing sphere surface, submerged in water.

Convolution quadrature based fast boundary element method The BEM [1, 9] allows to solve 3D linear problems by discretising only a 2D surface (such as Γ), making it very suitable for unbounded propagation domains. The BEM used in this work is accelerated using the FMM [2, 7]. Combining the CQM [8] and the \mathcal{Z} -transform, a time-marching solution algorithm can be set up using a set of suitably chosen Laplace-domain BEM solutions. The latter are computed using the FMM code COFFEE [2, 3].

This acoustic CQM-BEM formulation has been validated on two simple problems: (a) the acoustic pressure radiated by a breathing sphere in water, and (b) the scattering of the wave emerging from an underwater explosion by a rigid infinite cylinder. Figure 2 shows results obtained for a breathing sphere whose prescribed normal velocity is of the form $\sum_i C_i \sin(2\pi f_i t)$, with the largest excitation frequency $f_{max} = 4.0$ kHz being of an order typically observed in underwater explosion analysis.

Iterative fluid-structure coupling The problem is solved through an iterative fluid-structure coupling which alternates solutions for the entire time interval in the fluid and structure domains (Figure 3), making it easier to couple our CQM-FMM treatment with a commercial FEM code for the structure part:

- The reflected pressure is computed from the incident field using the BEM;
- At iteration $k = 0$, the total field is expressed as $p_{[0]}^{tot} = p^{ref} + p^{inc} + 0$. A FEM based procedure is used to compute the structure motion due to this pressure field;
- The structure motion implies a radiated

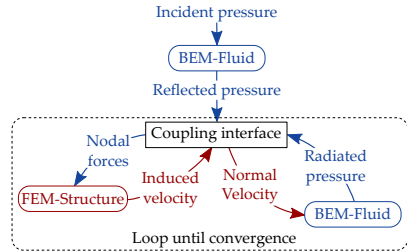


Figure 3: Fluid-structure coupling procedure.

pressure $p_{[k+1]}^{rad}$ computed with the BEM;

- The total field $p_{[k+1]}^{tot} = p^{ref} + p^{inc} + p_{[k+1]}^{rad}$ is updated, and it goes back to step 2 until convergence (stagnation criterion).

Modified forms of the above basic scheme involving relaxation are also studied. The communication will include preliminary numerical results.

Closing remarks. This contribution focuses on computing the effect on a structure of the “shock wave” created by an underwater explosion. The treatment of the FSI associated with the follow-up oscillating bubble phenomenon is currently being developed. Merging the two phenomena into a single two-scale model will then permit to address the challenges of the naval engineering problem motivating this study.

References

- [1] M. Bonnet. *Boundary integral equation methods in solids and fluids*. John Wiley & sons, 1999.
- [2] S. Chaillat, M. Bonnet, and J.-F. Semblat. A multi-level fast multipole BEM for 3-D elastodynamics in the frequency domain. *Comput. Methods Appl. Mech. Engrg.*, 197(49):4233–4249, 2008.
- [3] S. Chaillat, uma.ensta-paristech.fr/soft/COFFEE/
- [4] R. H. Cole. *Underwater explosions*. Princeton University Press, 1948.
- [5] T. L. Geers and C. A. Felippa. Doubly asymptotic approximations for vibration analysis of submerged structures, *J. Acoust. Soc. Am.* 73:1152–1159, 1983.
- [6] M. C. Junger and D. Feit. *Sound, structures, and their interaction*. The MIT Press, 2nd edition, 1986.
- [7] N. Nishimura. Fast multipole accelerated boundary integral equation methods. *Appl. Mech. Rev.*, 55: 299–324, 2002.
- [8] F. J. Sayas. *Retarded Potentials and Time Domain Boundary Integral Equations. A Road Map*. Springer International Publishing, 2016.
- [9] S. Sauter and C. Schwab. *Boundary element methods*. Springer, 2010.

Efficient FEM solution of exterior wave propagation problems with weakly enforced integral non reflecting boundary conditions

Silvia Falletta^{1,*}

¹Department of Mathematical Sciences, Politecnico di Torino, Torino, Italy

*Email: silvia.falletta@polito.it

Abstract

We consider waves scattered by rigid bodies and propagating in 2D unbounded domains. We propose a numerical method that approximates the solution using computations only in an interior finite domain, bounded by an artificial boundary \mathcal{B} . Transmission conditions between the interior domain, discretized by a FEM, and the exterior one, which is reduced to the boundary \mathcal{B} via a BEM, are imposed weakly using a mortar approach. The main advantage of this approach is that non matching grids can be used at the interface \mathcal{B} of the interior and exterior domains. This allows to exploit the higher accuracy of the BEM with respect to the FEM, which justifies the choice of the discretization in space of the BEM coarser than the one inherited by the spatial discretization of the finite computational domain.

Keywords: boundary element method, finite element method, non reflecting boundary conditions, non matching grids.

1 Introduction

Let $\mathcal{O}^e = \mathbb{R}^2 \setminus \overline{\mathcal{O}}$ be the complement of a bounded rigid obstacle $\mathcal{O} \subset \mathbb{R}^2$, having a smooth boundary Γ . We consider the following exterior wave propagation problem:

$$\begin{cases} u_{tt}(\mathbf{x}, t) - \Delta u(\mathbf{x}, t) = f(\mathbf{x}, t) & \text{in } \mathcal{O}^e \times [0, T] \\ u(\mathbf{x}, t) = 0 & \text{on } \Gamma \times [0, T] \\ u(\mathbf{x}, 0) = u_0 & \text{in } \mathcal{O}^e \\ u_t(\mathbf{x}, 0) = v_0 & \text{in } \mathcal{O}^e. \end{cases}$$

To solve it by means of a finite element method, we truncate the infinite external domain by an artificial boundary \mathcal{B} , defined by a smooth curve. This boundary divides \mathcal{O}^e into two open subdomains: a finite computational domain Ω^i , which is bounded internally by Γ and externally by \mathcal{B} , and an unbounded domain $\Omega^e = \mathbb{R}^2 \setminus \overline{\Omega^i \cup \mathcal{O}}$. We assume that the data are locally supported and that the artificial boundary \mathcal{B} is chosen in such a way that their supports are included in

Ω^i . Then, the above problem can be split into two problems: a problem set on the interior domain

$$\begin{cases} u_{tt}^i(\mathbf{x}, t) - \Delta u^i(\mathbf{x}, t) = f(\mathbf{x}, t), & \text{in } \Omega^i \times [0, T] \\ u^i(\mathbf{x}, t) = 0, & \text{on } \Gamma \times [0, T] \\ u^i(\mathbf{x}, 0) = u_0 & \text{in } \Omega^i \\ u_t^i(\mathbf{x}, 0) = v_0 & \text{in } \Omega^i. \end{cases}$$

and a problem set on the exterior one

$$\begin{cases} u_{tt}^e(\mathbf{x}, t) - \Delta u^e(\mathbf{x}, t) = 0, & \text{in } \Omega^e \times [0, T] \\ u^e(\mathbf{x}, 0) = 0 & \text{in } \Omega^e \\ u_t^e(\mathbf{x}, 0) = 0 & \text{in } \Omega^e. \end{cases}$$

Denoting by $\lambda^i = \partial_{\mathbf{n}_i} u^i$ and $\lambda^e = \partial_{\mathbf{n}_e} u^e$, \mathbf{n}_i and \mathbf{n}_e being the unit normal vectors on \mathcal{B} pointing outward of Ω^i and Ω^e , respectively, the two problems are coupled by the conditions $u^i = u^e$ and $\lambda^i + \lambda^e = 0$ on \mathcal{B} . It is known that the solution u^e in Ω^e can be represented by

$$u^e(\mathbf{x}, t) = \mathcal{V}\lambda^e(\mathbf{x}, t) - \mathcal{K}u^e(\mathbf{x}, t), \quad (1)$$

where

$$\mathcal{V}\lambda^e(\mathbf{x}, t) = \int_0^t \int_{\mathcal{B}} G(\mathbf{x} - \mathbf{y}, t - \tau) \lambda^e(\mathbf{y}, \tau) d\mathcal{B}_{\mathbf{y}} d\tau$$

$$\mathcal{K}u^e(\mathbf{x}, t) = \int_0^t \int_{\mathcal{B}} \partial_{\mathbf{n}_i} G(\mathbf{x} - \mathbf{y}, t - \tau) u^e(\mathbf{y}, \tau) d\mathcal{B}_{\mathbf{y}} d\tau$$

are the single and double layer integral operators; $G(\mathbf{x}, t) = H(t - \|\mathbf{x}\|) / (2\pi\sqrt{t^2 - \|\mathbf{x}\|^2})$ is the fundamental solution of the wave equation (being $H(\cdot)$ the Heaviside function). We introduce the spaces

$$V^i = H_{0,\Gamma}^1(\Omega^i) = \{u \in H^1(\Omega^i) : u = 0 \text{ on } \Gamma\},$$

$$V^e = H^{1/2}(\mathcal{B}), \quad \Lambda = H^{-1/2}(\mathcal{B}),$$

and, for any $w \in H^1(\Omega^i)$, we denote by $\gamma_{\mathcal{B}} w$ its trace on \mathcal{B} , which belongs to $H^{1/2}(\mathcal{B})$. Then, introducing the bilinear form

$$a : H^1(\Omega^i) \times H^1(\Omega^i) \rightarrow \mathbb{R}$$

$$a(v, w) = \int_{\Omega^i} \nabla v(\mathbf{x}) \cdot \nabla w(\mathbf{x}) dx,$$

and denoting by $(v, w)_{\Omega^i} = \int_{\Omega^i} v(\mathbf{x})w(\mathbf{x})dx$ the $L^2(\Omega^i)$ scalar product, we write the weak formulation of the coupled problem as follows: for any $t > 0$, given $f(t) \in L^2(\Omega^i)$, find $u^i(t) \in V^i$, $\lambda^i(t) \in \Lambda$, $u^e(t) \in V^e$, $\lambda^e(t) \in \Lambda$ such that for all $v^i \in V^i$, $v^e \in V^e$, $\mu^i \in \Lambda$ and $\mu^e \in \Lambda$

$$\begin{cases} \frac{d^2}{dt^2} (u^i, v^i)_{\Omega^i} + a(u^i, v^i) - \langle \lambda^i, \gamma_B v^i \rangle = (f, v^i)_{\Omega^i} \\ \langle \mu^e, \mathbf{N}\lambda^e \rangle - \frac{1}{2} \langle \mu^e, u^e \rangle - \langle \mu^e, \mathcal{K}u^e \rangle = 0 \\ \langle \lambda^i + \lambda^e, v^e \rangle = 0 \\ \langle \mu^i, \gamma_B u^i - u^e \rangle = 0. \end{cases}$$

where $\langle \cdot, \cdot \rangle$ denotes the duality pairing between $H^{-1/2}(\mathcal{B})$ and $H^{1/2}(\mathcal{B})$. Note that the transmission conditions on \mathcal{B} , obtained as the trace of (1) on \mathcal{B} (see [1]), are enforced in a weak form.

For the numerical approximation of the proposed method, we present a full discretization by finite elements in space and a Crank-Nicolson time stepping scheme in the interior of the computational domain. For the discretization of the NRBC, we construct a numerical scheme which is based on a second order Lubich discrete convolution quadrature formula for the discretization of the time integral, coupled with a classical Galerkin method in space. We remark that the spatial discretization of the NRBC is decoupled from that of the FEM.

Example We consider the scattering of a wave by a circular obstacle of radius 2. The wave propagates radially, starting from an initial configuration $u_0(x, y) = e^{-5((x-5)^2+y^2)}$, with null initial velocity and without external source. The artificial boundary \mathcal{B} is the circle of radius $R = 8$. We compare the solution u^S , obtained by using the standard (strong) FEM-BEM coupling, with the solution u^W obtained by using the new proposed weak coupling method. The former has been obtained by a decomposition of Ω^i into $n_T = 41554$ triangles, which induces a non uniform decomposition of \mathcal{B} into $M^i = 408$ segments. The solution u^W has been obtained by using the same triangular decomposition of Ω^i , and using $M^e = 128$ subintervals of equal length for the decomposition of the artificial boundary \mathcal{B} . The time interval $[0, 20]$ has been decomposed into $N = 256$ time steps. In Figure 1, left plot, we show the comparison of the reference

solution u^{BEM} (obtained by solving the associated BEM) with the solutions u^S and u^W at the point $P \approx (8, 0)$, and the associated absolute errors. In the right plot, we show the behavior of u^S and u^W on \mathcal{B} for $t \in [0, 20]$. In Figure 2 we show the snapshots of the solution u^W at some time instants. We will show that the

Figure 1: Behavior of the solution at $P \approx (8, 0)$ and associated absolute error (left plot). Plot of the solutions u^S and u^W at the artificial boundary in the time interval $[0, 20]$ (right plot).

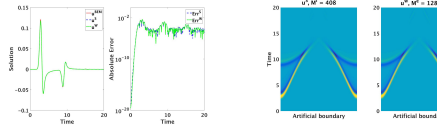
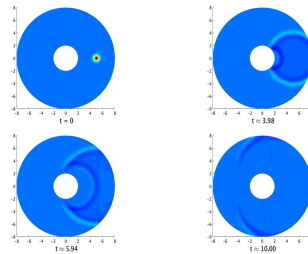


Figure 2: Snapshots of the solution u^W at different times.



new approach allows to reduce significantly the computational cost of the NRBC, preserving the accuracy. One further advantage is that the use of different spatial discretizations for the FEM and the BEM is allowed. For example, the use of wavelet type discretization for the BEM will allow sparse representation of the matrices associated to the integral operators, thus reducing further the computational cost (see [2]).

References

- [1] S. Falletta, G. Monegato, An exact non reflecting boundary condition for 2D time-dependent wave equation problems. *Wave Motion* 51 (2014), no. 1, pp. 168–192.
- [2] S. Bertoluzza, S. Falletta, L. Scuderi, Wavelets and convolution quadrature for the efficient solution of a 2D space-time BIE for the wave equation. *Submitted*.

Generalization of Adaptive Cross Approximation for a Convolution Quadrature based Boundary Element Method

Anita M. Haider¹, Martin Schanz^{2,*}

¹Institute of Applied Mechanics, Graz University of Technology, Graz, Austria

²Institute of Applied Mechanics, Graz University of Technology, Graz, Austria

*Email: m.schanz@tugraz.at

Abstract

The acoustic wave equation is solved in time domain with a boundary element formulation. The time discretisation is performed with the convolution quadrature method and for the spatial approximation standard elements and a collocation schema is applied. In the interest of increasing the efficiency of the boundary element method a low-rank approximation such as the adaptive cross approximation is carried out. We discuss about a generalization of the adaptive cross approximation to approximate a three-dimensional array of data, i.e. usual boundary element matrices at several complex frequencies. First results are presented for some simple problems.

Keywords: BEM, generalised ACA, CQM

1 Problem setting

We consider the time domain boundary element method for the homogeneous wave equation with vanishing initial conditions and given Dirichlet and/or Neumann boundary conditions. The convolution quadrature method (CQM) is used for the temporal discretization and collocation for the spatial discretization. Essentially, the CQM requires to establish boundary element matrices of the corresponding elliptic problem in Laplace domain at several complex frequencies (usually as much as time steps). Consequently, we get an array of system matrices. This array of system matrices can be interpreted as a three-dimensional array of data which we want to approximate by a data-sparse representation.

2 Generalization of the adaptive cross approximation

The idea of a generalization of adaptive cross approximation has been proposed in [1] and is sketched in Algorithm 1. As discussed above, we generate a three-dimensional array of data $C_{ij,k}$. The first two indices corresponds to the spatial discretization. One is related to the collocation

Algorithm 1 idea generalized ACA

For $\ell = 1, 2, 3 \dots$

1. compute face \mathcal{H}^ℓ via low-rank approximation $h_{ij}^\ell = C_{ij,k_\ell}$
2. define pivot position $(i_\ell, j_\ell) := \arg \max_{i,j} |h_{ij}^\ell|$
3. compute fiber \mathcal{F}^ℓ $f_k^\ell = C_{i_\ell, j_\ell, k}$

Stop if $\|\widetilde{\mathcal{H}}^\ell\|_F \|\widetilde{\mathcal{F}}^\ell\|_F \leq \varepsilon \|\mathcal{S}^\ell\|_F$

point and the other to the basis function. The third index of the 3D array corresponds to the complex frequencies from the CQM. The algorithm starts by assembling the system matrix at an arbitrary chosen but fixed frequency. Let the corresponding index be k_ℓ . This system matrix, which we call face \mathcal{H} , is compressed by the standard adaptive cross approximation. Therefore, we have to decompose the system matrix into a hierarchical scheme first. This hierarchical structure is based on the usual geometrical considerations and used for all further assembled faces. After the low-rank approximated face is determined, we have to define the position of the pivot element. In principle, the maximum entry of the matrix determines the pivot position, where h_{ij}^ℓ denotes the entries of the current face. Regarding to this position we compute the fiber \mathcal{F} , an array with all frequencies where the indices related to the spatial discretization are fixed, i.e. one matrix entry at all frequencies for a distinct collocation point and shape function is assembled, f_k^ℓ . In this way the first cross with an approximated face and a fiber is generated. An schematic sketch of the fiber and face can be found in Fig.1. For the next cross, the face or the fiber has to be updated. At further iterations the residual of the face and of the fiber has to be determined and based on this residual the position of the pivot element is computed.

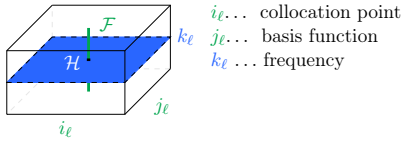


Figure 1: Sketched idea of generalized ACA

The algorithm terminates successfully if a suitable stopping criterion with a given accuracy ε is satisfied. The current approximation is defined as $\mathcal{S}^\ell = \sum_{d=1}^{\ell} \tilde{\mathcal{H}}^d \otimes \tilde{\mathcal{F}}^d$.

The crucial task to determine the pivot position is how to find the maximum entry in a low-rank approximated face in an appropriate time for admissible blocks, i.e. ACA approximated blocks. Certainly, it is no option to compute the matrix entry of face \mathcal{H} by multiplying the low-rank matrices. Instead, we define the index i or j by the maximum of the absolute row sum of the low rank matrices, respectively. To get the idea, let assume the block \mathcal{A} is approximated by the truncated singular value decomposition $\mathcal{A} \approx \mathcal{A}_r = \mathbf{U}\Sigma\mathbf{V}^H$, where the low-rank matrices \mathbf{U} and \mathbf{V} consists of orthonormal columns. In this caes, we define the index i of the pivot position by

$$\begin{aligned} \arg \max_{i,j} |a_{ij}| &= \arg \max_{i,j} \sum_{k=1}^r |u_{ik}\sigma_k| \underbrace{|v_{jk}|}_{\leq 1} \\ &\leq \arg \max_i \sum_{k=1}^r |u_{ik}\sigma_k| \end{aligned}$$

and, analogously, for index j . This concept is based on the fact that the columns of \mathbf{U} and \mathbf{V} are orthonormal. To adopt this to an ACA approximated block, a QR-decomposition of the low-rank matrix \mathbf{U} and \mathbf{V} is performed

$$\begin{aligned} \mathcal{A} \approx \mathcal{A}_r &= \mathbf{U}\mathbf{V}^H = Q_U(R_U R_V^H)Q_V^H \\ &= Q_U \check{\mathbf{U}}\check{\Sigma}\check{\mathbf{V}}^H Q_V^H = \check{\mathbf{U}}\check{\Sigma}\check{\mathbf{V}}^H \end{aligned}$$

and, secondly, we use the SVD for the smaller inner matrix $R_U R_V^H$. Finally, we end up with low-rank matrices $\check{\mathbf{U}}$ and $\check{\mathbf{V}}$ where their columns are orthonormal. This allows to use the above described selection of the pivot position. Additionally, this process makes an implicit recompression of the block by the SVD of the inner matrix product.

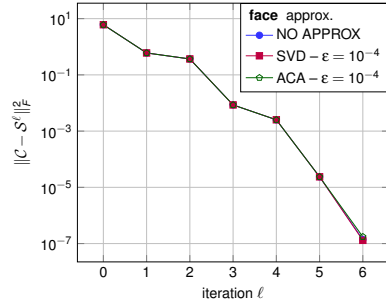


Figure 2: Approximation error in the Frobenius norm versus frequency

3 First result

How the introduced algorithm performs is shown by a numerical experiment. In this example, the three-dimensional array of data \mathcal{C} is computed by assembling the single layer operator at 11 different frequencies given by the CQM. The squared error of the approximation in the Frobenius norm is plotted in Fig. 2 against the iteration counter of the algorithm. Note, the iteration number corresponds to the number of necessary complex frequencies. The accuracy of the generalized ACA is chosen as $\varepsilon = 10^{-4}$. We perform the numerical experiment first without any low-rank approximation of the face, then with an approximation by a singular value decomposition and, last, by adaptive cross approximation. The accuracy of the low-rank approximated face is set as well to $\varepsilon = 10^{-4}$ for both approximation methods. For all three alternatives, the stopping criterion is satisfied after five iterations. At the fifth iteration, the ACA approximated face exhibits a slightly different approximation error. This indicates that the low-rank approximation error of the faces has already an effect. Nevertheless, it may be concluded that it is sufficient to evaluate the single layer operator only at a few instead of all frequencies and still a sufficiently quality of the data is maintained, resulting in a reduction of the computation time and the memory consumption.

References

- [1] M. Bebendorf, A. Kühnemund, and S. Rjasanow, *Appl. Numer. Math.* **74**, (2013), pp. 1–16 .

A superconvergence phenomenon in Runge-Kutta convolution quadrature for the wave equation

Jens Markus Melenk¹, Alexander Rieder^{1,*}

¹Institute for Analysis and Scientific Computing, TU Wien, Vienna, Austria

*Email: alexander.rieder@tuwien.ac.at

Abstract

For Runge-Kutta convolution quadrature (CQ), the convergence rate is usually analyzed by s -explicit bounds of the convolution symbol in the Laplace domain. When looking at scattering problems, this does not tell the whole story, as dividing by s has larger impact on the observed rate. We provide an explanation and a proof for such phenomena.

Keywords: Convolution Quadrature, Wave equation, Boundary Element Methods

1 Introduction

When discretizing by Runge-Kutta convolution quadrature, the expected convergence rate is usually determined by bounds of the form

$$|K(s)| \leq C |s|^\mu, \quad (1)$$

where $K(s)$ is the Laplace transform of the convolution kernel, $\mu \in \mathbb{R}$ and s is taken in a complex sector in the right half-plane. The convergence rate is then given as $\min(q+1-\mu, p)$, where q and p are the stage order and classical order of the underlying Runge-Kutta method respectively.

When considering boundary element methods, such estimates may fail to be sharp. Namely, for the Dirichlet-to-Neumann map, the estimates read

$$\|\text{DtN}\|_{H^{1/2} \rightarrow H^{-1/2}} \leq C |s|^{\mu-1}.$$

When looking at DtN and s^{-1} DtN, one would therefore expect rates q and $q+1$ respectively. But the numerical results show a different picture, see Figure 1. Even though the estimates seem sharp for the DtN operator, the integrated version shows an increased rate of $q+2$ instead.

We give an explanation for this phenomenon based on a decomposition of the Dirichlet-to-Neumann map. Similar techniques can also be used to derive sharp bounds for the Neumann problem of the wave equation, which are not covered by direct bounds of the Neumann-to-Dirichlet map of the form (1).

2 Runge-Kutta convolution quadrature

Runge-Kutta CQ was introduced by Lubich and Ostermann in [1] to approximate convolution integrals of the form

$$K(\partial_t)g := \int_0^t k(\cdot - \tau)g(\tau) d\tau,$$

where the symbol $K(\cdot)$ is the Laplace transform of the convolution kernel k .

The approximation is computed by

$$K(\partial_t^k)g := \sum_{n=0}^{\infty} W_n g(\cdot - t_n + kc),$$

where the weights W_j can be computed by sampling K at appropriate points, c are the Runge-Kutta nodes and $k > 0$ is the step size.

State of the art for analyzing CQ approximations is the following result:

Proposition 1 ([2]) *Let g be sufficiently smooth. Assume that K satisfies*

$$\begin{aligned} |K(s)| &\lesssim |s|^{\mu_1} \quad \text{for } \text{Re}(s) \geq \sigma_0 > 0, \\ |K(s)| &\lesssim |s|^{\mu_2} \quad \text{for } \text{Arg}(s) \in (-\pi/2 + \delta, \pi/2 - \delta). \end{aligned}$$

Then the error of the CQ-approximation can be bounded by:

$$\left| K(\partial_t)g - K(\partial_t^k)g \right| \leq C(g)k^{\min(q+1-\mu_2, p)}.$$

3 The Dirichlet Problem

Let $\Omega^- \subseteq \mathbb{R}^2$ be a smooth bounded domain or a polygon with boundary Γ . We start by considering the sound-soft scattering problem. Given a function $g : \mathbb{R} \rightarrow H^{1/2}(\Gamma)$ with $g(-t) = 0$, $t > 0$ we solve

$$\ddot{u}(t) = \Delta u(t) \quad \text{in } \mathbb{R}^2 \setminus \Omega^-, t > 0, \quad (2a)$$

$$u(t)|_{\Gamma} = g(t) \quad \text{for } t > 0, \quad (2b)$$

$$u(t) = 0 \quad \text{for } t \leq 0. \quad (2c)$$

We are interested in discretizing the time domain Dirichlet-to-Neumann map $g \mapsto \partial_n u$. Using the frequency-domain operator $\text{DtN}(s)$, and

convolution quadrature, we approximate $\lambda = \partial_n u = \text{DtN}(\partial_t)g$ by two schemes,

$$\lambda^k := \text{DtN}(\partial_t^k)g \quad \text{and} \quad \tilde{\lambda}^k := J(\partial_t^k) \text{DtN}(\partial_t^k)g.$$

where $J(s) := s^{-1}$ and $J(\partial_t^k)$ is the (discrete) integration operator.

Theorem 1 *Let g be sufficiently smooth, then*

$$\begin{aligned} \left\| \lambda(t_n) - \lambda^k(t_n) \right\|_{H^{-1/2}} &\lesssim C(g)k^q, \\ \left\| \lambda(t_n) - \tilde{\lambda}^k(t_n) \right\|_{H^{-1/2}} &\lesssim C(g)k^{\min(q+2,p)}. \end{aligned}$$

$C(g)$ depends on the time t_n and on the data g .

This result is surprising in the light of Proposition 1, as the convolution symbol only differs by one power of s .

3.1 The underlying mechanism

We work in the frequency domain. For the (modified) Helmholtz equation, the scaled Dirichlet-To-Neumann map can be decomposed into

$$\begin{aligned} s^{-1} \text{DtN}(s) &= s^{-1}(\text{DtN}(s) + s\text{I}) - \text{I} \\ &=: s^{-1} \text{DtI}(s) + \text{I}. \end{aligned}$$

Since the identity operator does not depend on s , it is reproduced exactly by CQ. The DTI map has improved bounds in the frequency domain:

Theorem 2 *For $s \in \mathbb{C}_+$ with $\text{Arg}(s) \in (-\pi/2 + \delta, \pi/2 - \delta)$ and all $g \in H^1(\Gamma)$:*

$$\|\text{DtI}(s)g\|_{H^{-1/2}(\Gamma)} \leq C \|g\|_{H^1(\Gamma)} \quad (3)$$

with constant $C > 0$ independent of s .

For the case of the half-plane and the unit sphere, a similar estimate to (3) was proved in [3] and conjectured for general convex scatterers.

Our proof of (3) relies on three observations:

1. In 1d, the DtN map is given by $g \mapsto -sg$.
2. The bad s dependence of DtN is mainly caused by boundary layers.
3. Boundary layers are essentially a 1d phenomenon, so observation 1 applies.

For the Neumann problem, similar observations can be made for the Neumann-to-Dirichlet map:

$$\text{NtD}(s) = (\text{NtD}(s) + s^{-1}\text{I}) - s^{-1}\text{I}.$$

The $s^{-1}\text{I}$ part corresponds to a discrete integral which is realized with order p by the RK-method. The Neumann-to-Impedance map also has more favorable bounds than the NtD map. We note the additional complication, that the Neumann-to-Impedance map only maps to $H^{1/2}$ if the Neumann data is also at least $H^{1/2}$. This discrepancy needs to be taken care of by an additional decomposition step of the data into a smooth part and remainder.

4 Numerical example

We compare the approximations λ^k and $\tilde{\lambda}^k$ for a model problem on an L-shaped domain. To discretize, we use a 5-stage RadauIa method and prescribe the exact solution as a travelling wave. Figure 1 shows the predicted rates, as the RK-method has stage order $q = 5$.

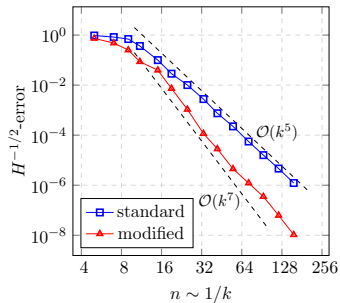


Figure 1: Convergence using 5-stage Radau Ia

References

- [1] Ch. Lubich and A. Ostermann, *Runge-Kutta methods for parabolic equations and convolution quadrature*, Math. Comp. **60** (1993), no. 201, 105–131.
- [2] L. Banjai, C. Lubich, and J. M. Melenk, *Runge-Kutta convolution quadrature for operators arising in wave propagation*, Numer. Math. **119** (2011), no. 1, 1–20.
- [3] L. Banjai, *Time-domain Dirichlet-to-Neumann map and its discretization*, IMA J. Numer. Anal. **34** (2014), no. 3, 1136–1155.

On the development of a hybrid model based on the Convolution Quadrature Boundary Element Method.

Jacob Rowbottom^{1,*}, David Chappell¹

¹Department of Physics and Mathematics, Nottingham Trent University, Nottingham, United Kingdom

*Email: jacob.rowbottom2017@my.ntu.ac.uk

Abstract

An overview of the Convolution Quadrature Boundary Element Method (CQBEM) for solving the wave equation will be presented. We discuss the computational issues arising when wave problems containing broadband frequency content are of interest. A hybrid model is proposed to address these issues, where the lower frequency content will be modelled via the CQBEM which provides an explicit connection to the frequency content of the wave modelled via the Z-transform, making it the ideal candidate for a hybrid scheme. The higher frequency content will be modelled using a statistical, or energetic, approach such as ray tracing.

Keywords: Convolution Quadrature, Boundary Element Method, Wave equation, Ray tracing, Hybrid method.

1 Introduction

Numerical wave equation solvers share the limitation that high frequency content in the time domain signal requires a discretised model containing many degrees of freedom. The computational cost depends on the choice of method and the number of spatial dimensions to be modelled [1]. A hybrid model is proposed to address these issues at high frequencies, where the lower frequency content will be modelled via the CQBEM and the higher frequency content will be modelled using a statistical approach. The CQ approach was developed by Lubich [2,3] and provides a simple way to obtain a stable time stepping scheme using the Laplace transform of the kernel function. Since then, the CQ method has made significant progress in time-dependent wave simulation methods including high-order Runge Kutta implementations for a variety of wave equations [4, 5]. It possesses favourable stability properties due to an implicit regularization in time. For the discretisation of boundary integral equations, its main advantage is that it avoids having to evaluate the convolution ker-

nel in the time domain and instead solving a simplified system of frequency domain boundary integral equations in the spatial region [6]. We employ a direct BEM for the spatial discretisation. Other examples of work on the CQBEM for solving a range of problems can be found in [7] as well as for a Neumann BVP, such as the one considered here, in [8]. For high frequencies in the CQBEM we require a larger number of boundary elements to model the rapidly oscillating waves. The hybrid method will be more computationally efficient as we can solve in terms of phase-space density, which is frequency independent [9]. At higher frequencies, wave problems in industry also exhibit a greater sensitivity to small uncertainties in the models, meaning a hybrid method with less sensitivity to these uncertainties is of more interest to engineers or manufacturers.

2 Solving the wave equation via CQBEM

Let $\Omega \subset \mathbb{R}^2$ be a domain with boundary $\Gamma = \partial\Omega$. We define the following Neumann boundary value problem for the homogeneous wave equation as follows

$$\partial_t^2 u = c^2 \Delta u \quad \text{in } \Omega \times (0, T), \quad (1a)$$

with initial conditions

$$u(\cdot, 0) = \partial_t u(\cdot, 0) = 0, \quad \text{in } \Omega \quad (1b)$$

and boundary conditions

$$\frac{\partial u}{\partial \hat{\mathbf{n}}_{\mathbf{y}}} = h \quad \text{on } \Gamma \times (0, T) \quad (1c)$$

for some $T > 0$, where $\hat{\mathbf{n}}$ is the unit outward normal to the boundary at $\mathbf{y} \in \Gamma$. The solution can be calculated by reformulating the above boundary value problem into an integral equation via a direct formulation. The direct method involves applying Green's identities to derive a boundary integral representation of the wave equation in space and time, which takes the form of a

convolution integral in time. The main advantage of using a direct method is that our solution is expressed in terms of physical quantities. The CQBEM is then applied to rewrite the space-time boundary integral equation as a system of Helmholtz boundary integral problems for N complex wave numbers $k_l = \frac{i\gamma(z_l)}{c\Delta t}$, where $z_l = \lambda e^{-2\pi il/N}$, $l = 0, 1, \dots, N-1$, and $\lambda \in (0, 1)$ is a constant. The function $\gamma(z) = \frac{1}{2}(z^2 - 4z + 3)$ is the quotient of the generating polynomials of the second order backward difference formula applied to discretise in time [4]. The system of Helmholtz equations is then given by

$$-\frac{1}{2}\tilde{u}_l(\mathbf{x}) + \left(\int_{\Gamma} \frac{\partial G_k}{\partial \mathbf{n}} (\|\mathbf{x} - \mathbf{y}\|, k_l) \tilde{u}_l(\mathbf{y}) d\Gamma_{\mathbf{y}} \right) = \tilde{g}_l(\mathbf{x}), \tag{2}$$

for $l = 0, 1, \dots, N-1$. Here $G_k(r, s)$ is the free space Green's function for the Helmholtz equation and $\tilde{g}_l(\mathbf{x})$ is calculated using the z-transform

$$\tilde{g}_l(\mathbf{x}) = \sum_{n=0}^{N-1} \lambda^n g_n(\mathbf{x}) e^{-2\pi i ln/N}, \tag{3}$$

where

$$g_n(\mathbf{x}) = \int_0^{t_n} \int_{\Gamma} k(\|\mathbf{x} - \mathbf{y}\|, t - \tau) h(\mathbf{y}, \tau) d\Gamma_{\mathbf{y}} d\tau.$$

Here $k(r, s)$ is the fundamental solution of the wave equation in \mathbb{R}^2 . The solution to (1a) can then be approximated via a trapezoidal method for the inverse z-transform

$$u_l = \frac{\lambda^{-l}}{N} \sum_{j=0}^{N-1} \tilde{u}_j e^{2\pi ilj/N}. \tag{4}$$

3 Transformation to phase-space densities and outlook

We aim to develop a hybrid method that is capable of efficiently modelling waves with broadband frequency content. At high frequencies, the Helmholtz solution \tilde{u} may be well approximated in terms of the phase ϕ and amplitude A along a ray, which can be provided via a high frequency energy method such as ray tracing [9]. We therefore require a direct link between the Helmholtz equation and a phase-space density function obtained from the ray tracing method. In particular, one can express the phase-space density ρ on Γ in the form

$$\rho(s, p) = \sum_{m=1}^M A_m^2(s) \delta \left(p - \frac{d\phi_m}{ds} \right), \tag{5}$$

where s is the arc-length boundary parameter, p is the tangential slowness and the sum corresponds to a superposition of plane waves.

References

- [1] F. Fahy, Statistical energy analysis: a critical overview, *Phil. Trans. R. Soc. Lond. A* **346** (1994), pp. 431–447.
- [2] C. Lubich, Convolution quadrature and discretized operational calculus I, *Numer. Math.* **52** (1988), pp. 129–145.
- [3] C. Lubich, On the multistep time discretization of linear initial-boundary value problems and their boundary integral equations, *Numer. Math.* **67** (1994), pp. 365–389.
- [4] L. Banjai and S. Sauter, Rapid solution of the wave equation on unbounded domains, *SIAM J. Num. Anal.* **47** (2008), pp. 229–247.
- [5] L. Banjai, M. Lopez-Fernandez and A. Schadle, Fast and oblivious algorithms for dissipative and 2D wave equations, *SIAM J. Num. Anal.* **55** (2017), pp. 621–639.
- [6] A. Reider, Convolution quadrature and boundary element methods in wave propagation: a time domain point of view, *PhD thesis, Vienna University of Technology* (2017).
- [7] W. Hackbusch, W. Kress and S.Sauter, Sparse convolution quadrature for the time domain boundary integral formulations of the wave equation, *IMA J. Numer. Anal.* **29** (2008), pp. 158–179.
- [8] D.J. Chappell, Convolution quadrature Galerkin boundary element method for the wave equation with reduced quadrature weight computation, *IMA J. Numer. Anal.* **31**(2) (2011), pp. 640–666.
- [9] O. Runborg, Mathematical models and numerical methods for high frequency waves, *Commun. Comput. Phys.* **2**(5) (2007), pp. 827–878.

Finite Element Discontinuous Galerkin and Fast Multipole BEM coupling for performing accurate scale resolved CAA simulations involving large geometries

S. Proskurov^{1,*}, R. Ewert¹, M. Lummer¹, M. Mößner¹, J. Delfs¹

¹German Aerospace Centre (DLR), Braunschweig, Germany

*Email: stanislav.proskurov@dlr.de

Abstract

The primary focus of our research is on the weak and strong coupling of two advanced Computational Aero-Acoustic (CAA) methods for performing efficient fan tone shielding simulations of aerial vehicles with unconventional engine intake installations. In this work the Fast Multipole Boundary Element Method (FM-BEM) which can solve the surface integral based on the Kirchhoff-Helmholtz wave equation for large geometries [1, 2] (e.g. a full scale aircraft) is combined with a volume resolving Discontinuous Galerkin (DG) method which is very well suited for the region around a jet inlet where strong mean flow gradients are present. [3] Weak coupling results are presented for a generic test problem. The extension to a strongly coupled method utilising the Möhring-Howe acoustic analogy is discussed.

Keywords: Discontinuous Galerkin, Fast Multipole Boundary Element Method, acoustic shielding, acoustic scattering

1 Introduction

A high order DG method which solves the system of Acoustic Perturbation Equations (APE) [4] has been converted into the frequency domain to cope with the frequency domain formulation of FM-BEM. Solving a sound propagation problem for a full-scale aircraft with volume resolving CAA methods requires substantial high-performance resources as for today. To some extent, computational effort can be reduced by placing an integration surface in the linear region and applying the Ffowcs Williams and Hawkins (FW-H) method for determining the far-field pressure. However, such trick can only produce a meaningful acoustic solution for isolated components where acoustic scattering by other bodies is of minor importance. In contrast, DG / FM-BEM coupling does not only account for acoustic scattering and shielding but the FM-BEM can also enforce global boundary conditions on the DG sub-domain as “feedback”.

As a result, such hybrid approach has a much reduced turnaround time in comparison to solving the wave propagation in the entire domain yet it should be capable of producing a solution of similar quality.

2 Boundary Element Method

BEM simulations are performed using the DLR FMCAS code (Fast Multipole Code for Acoustic Shielding). This section introduces the reader to the fundamental physical concept of the method. Starting from the Helmholtz equation for pressure,

$$(\nabla^2 + \kappa^2)p(x) = -f \quad x \in \Omega_+ \quad (1)$$

where Ω_+ is the exterior CAA domain, f is the forcing term, $\kappa c = \omega$ where c is the speed of sound and $p(x)$ is the acoustic pressure at the far-field point x , we follow the derivation in [1] for obtaining the boundary integral equation:

$$\begin{aligned} \xi(x)p(x) &= \int_{\partial\Omega} p(y) \frac{\partial \mathcal{G}(x, y)}{\partial n_y} d\Omega_y \\ &\quad - i\omega\rho_0 \int_{\partial\Omega} \mathcal{G}(x, y) v_f(y) d\Omega_y + p_{inc}(x) \quad (2) \end{aligned}$$

where $\xi(x)$ is a free term coefficient $\{0, 1/2 \text{ or } 1\}$, \mathcal{G} is the free field Green's function, v_f is related to the fluid particle velocity expressed via the normal derivative of pressure at y : $v_f = \frac{1}{i\omega\rho_0} \frac{\partial p(y)}{\partial n_y}$ and $p_{inc} = \int_{\Omega} -Q(z)\mathcal{G}(x, y) d\Omega_z$ is the incident pressure term which accounts for the source strength $Q(z)$ inside the domain, Ω_- .

In a classic BEM approach the surface pressure $p(y)$ is computed from an incident source. However, if part of the surface already has a solution of $p(y)$ and $\frac{\partial p(y)}{\partial n_y}$ (e.g. interpolated from DG) then it can be treated as a permeable source surface. Hence, by solving a scattering problem $p(x)$ can be obtained following the standard procedure.

The FM-BEM represents a *fast summation method* for the quadrature of the integrals of the boundary integral equation reducing the number of operations for each integral evaluation from $\mathcal{O}(N^2)$ to $\mathcal{O}(N \log N)$, where N denotes the number of surface elements.

3 Surface sources from DG

For acoustic sources definition on the coupling surface we rely on the DISCO++ (Discontinuous Galerkin) code developed by the DLR. The initial step consists of the wave propagation in a highly non-uniform flow. The DG pressure solution at the radiation surface becomes part of a broader BEM surface representing the entire geometry. Eventually, based on the partly given surface solution, the entire BEM problem can be solved for the remaining unknowns.

The coupling concept may be demonstrated by considering a simple monopole scattering problem. Figure 1 shows the triangulated BEM geometry which consists of two parts: a solid rectangular shield and a protruded permeable source surface. Both parts feature an opening but together form a common watertight surface.

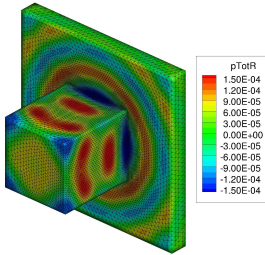


Figure 1: Triangulated BEM geometry: Total $p_{\{Re\}}$ solution computed by the FMCAS code.

For concept validation the above solution is compared to a classic incident-scattering problem of a distributed monopole source placed in front of the same rectangular shield. For consistency, the spherical FMCAS source is located at the origin of the DG monopole with its radius matching the half width of the original source. Figure 2 shows the noise footprint comparison on a plane which is placed 6 shield widths below the source region. For comparison, the amplitude of the monopole source has been rescaled to unity and a good agreement between noise shielding contours is reported.

If a source surface is located in the vicinity of a solid body, in some cases, its scattering may have the influence on the DG solution. Therefore, two-way coupling is necessary to appropriately satisfy the boundary conditions.

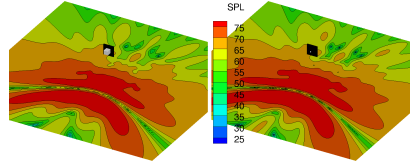


Figure 2: Noise footprint: the SPL contour obtained with the DG source surface (a) and with the reference monopole source (b).

4 Two-way coupling

The feedback information arriving to the DISCO+ boundary ghost points must contain a full velocity matrix in addition to pressure. Since this missing information cannot be recovered directly from the FMCAS solution, the idea is to reformulate the BEM equations in terms of the acoustic potential, B' . [5] Then one can apply the Möhring-Howe acoustic analogy which by definition, also, accounts for the mean flow.

$$B' = \frac{p'}{\rho_0} + \mathbf{v}_0 \cdot \hat{\mathbf{v}}' \quad \nabla B' = -i\omega \hat{\mathbf{v}}' \quad (3)$$

The gradient of the acoustic potential is evaluated as part of the FMCAS solution for the required boundary coordinates. As soon as the DG solution converges the data is passed back to FMCAS. The iterative process repeats until the residual is sufficiently small.*

References

- [1] Lummer M.: Aircraft noise generation and assessment. Installation: numerical investigation. *CEAS Aeronautical Journal* (2019)
- [2] Lummer M., Richter C., Pröber C., Delfs J.: Validation of a model for open rotor noise predictions and calculation of shielding effects using a fast bem. *19th AIAA/CEAS Aeroacoustics Conference, 27-29 May, 2013, Berlin, Germany*
- [3] Mößner M., Delfs J., Kissner C., Enghardt L.: Computational chain for virtual fly-over simulations applied to fan noise. *24th AIAA/CEAS Aeroacoustics Conference, 25-29 June, 2018, Atlanta, GA, USA*
- [4] Ewert R., Schröder W.: Acoustic perturbation equations based on flow decomposition via source filtering. *Journal of Computational Physics* **188**, pp. 365-398 (2003)
- [5] Heitmann D., Ewert R., Delfs J.: A novel extrapolation approach in aeroacoustics: development & validation. *22d AIAA/CEAS Aeroacoustics Conference, 30 May - 1 June, 2016, Lyon, France*

*The work has been partly funded by Airbus Defence & Space. We further acknowledge valuable discussions with Simone Mancini and Alexander Kolb from AD&S.

Synthetic Turbulence imposed as Boundary Condition for Fast Multipole BEM

Nils Reiche^{1,*}, Markus Lummer¹, Roland Ewert¹, Jan Werner Delfs¹¹Institute of Aerodynamics and Flow Technology, Technical Acoustics, German Aerospace Center (DLR), Braunschweig, Germany

*Email: Nils.Reiche@dlr.de

Abstract

A non-empirical approach for airframe noise simulation is realised by coupling synthetically modelled turbulence and a fast multipole boundary element method. The approach is applied to and validated against a benchmark case for trailing edge noise.

1 Introduction

Broadband noise from interaction of turbulent flows with surfaces plays an important role for many technical applications, such as aircrafts. For their acoustic assessment and for low noise aircraft design research and industry invest in the development of numerical, non-empirical simulation approaches that accurately capture all important flow effects. However, the challenge for this simulation approach is to resolve the very small turbulent structures and the aircraft parts of all sizes. This requirement results in a numerical setup with a huge number of degrees of freedom. An idea to minimize this number is achieved by the presented strategy that combines modelled, synthetic turbulence, i.e. sound sources, in the region of interest and a fast multipole boundary element method for sound propagation [1]. Both algorithms as well as their coupling interface are designed to be fast, accurate and efficient and scale with $\mathcal{O}(N \log N)$.

2 Numerical Approach

Sound wave propagation through a homogeneous medium at rest can be described by the Helmholtz equation for the pressure \hat{p} in frequency domain

$$(\nabla^2 + k) \hat{p}_x = -\hat{f}, \quad x \in \Omega \quad (1)$$

where k is the wave number and $-\hat{f}$ defines an arbitrary source. Using the free-field Green's function G_0 for eq. (1) and integration over the domain Ω leads to the Kirchoff-Integral

$$\hat{p}_x - \int_{\partial\Omega} \left[\hat{p}_y \frac{\partial G_0}{\partial n_y} - G_0 \frac{\partial \hat{p}_y}{\partial n_y} \right] d\Omega_y = \hat{p}_V, \quad (2)$$

where the subscripts indicate observer (x) and surface location (y). $\hat{p}_V = \int_{\partial\Omega_y} -\hat{f} G_0 d\Omega$ accounts for some volume contribution, which is not present in the later problem statement and thus neglected.

Note, the solution of eq. (2) can be contaminated if k is an eigenvalue of the inner problem of surface $\partial\Omega$. However, a unique solution can be enforced by the proposal of Burton-Miller (BM) which entails the application of the linear operator $\mathcal{B}_x = 1 + \alpha \frac{\partial}{\partial n_x}$ to eq. (2). The coupling constant α for a sphere might be $\alpha = \frac{i}{k}$.

Eq. (2) allows coupling with surface sources using a von Neumann boundary condition

$$\frac{\partial \hat{p}_y}{\partial n_y} = Y_y \hat{p}_y + V_y(\hat{v}_n) \quad (3)$$

with wall admittance Y_y and some surface excitation $V_y(\hat{v}_n)$ that according to the splitting theorem [4, 5] is a function of the wall normal velocity \hat{v}_n . Application of the boundary condition (3) and the BM operator to eq. (2) leads to

$$\frac{1}{2} \mathcal{B}_x \hat{p}_x - \int_{\partial\Omega} \left[\hat{p}_y \frac{\partial}{\partial n_y} - Y_y \right] \mathcal{B}_x G_0 d\Omega_y = \int_{\partial\Omega} V_y(\hat{v}_n) \mathcal{B}_x G_0 d\Omega_y \quad (4)$$

Turbulence interaction with the surface can be established by coupling acoustic and incompressible velocity $\hat{v}_{n,a} = \hat{v}_{n,i}$. Latter is induced by turbulence vortices Ω' and can be obtained by solving a Poisson equation for the stream function Ψ'

$$\hat{v}_{n,i} = \mathcal{F} \{ \mathbf{n} \cdot (\nabla \times \Psi') \}, \quad \nabla^2 \Psi' = -\Omega'. \quad (5)$$

Here, \mathbf{n} is the wall normal vector and \mathcal{F} indicates the Fourier transform. The turbulence vorticity Ω' is synthesised using the fast random particle mesh (FRPM) method which provides

spatio-temporal resolved turbulence that fulfills turbulence statistics from a RANS solution.

Discretisation of the surface integrals of (4) into surface elements yields a boundary element formulation which can be written as an equation system $\mathbf{B}\hat{p} = -\hat{q}$. This system is solved using an iterative solver such as GMRES. Since the size of the matrix \mathbf{B} depends quadratically on the number of elements the method becomes inefficient for very large problems. But, implementation of a Fast Multipole Method (FMM) splits the matrix \mathbf{B} into near- and far-field signatures and reduces the number of matrix vector multiplication for the iterative solver. A more detailed description of the fast multipole code for acoustic scattering (FMCAS) is given in [2].

3 Application

The interaction of a turbulent flow with a surface is studied for a turbulent boundary layer trailing edge noise problem. A large validation data base is given by the BANC-benchmark for a flow around a NACA0012 airfoil [3]. The benchmark case#1 describes an incompressible flow of flow Mach number $Ma = 0.1664$ at an angle of attack of $\alpha = 0^\circ$, see top of Figure 1.

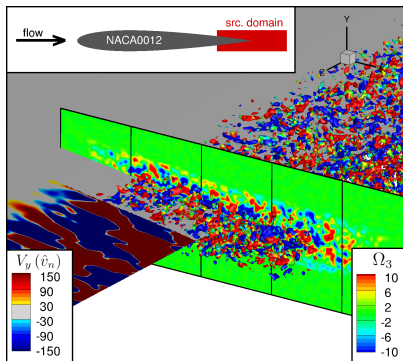


Figure 1: Simulation setup (top); Ω_3 iso-surface / Slice across source domain displaying Ω_3 / Surface excitation V_y (bottom).

The steady flow state is computed by the DLR TAU code that solves the RANS equations using a $k-\omega$ Menter SST turbulence model. The obtained 3-dimensional mean flow data and turbulence statistics are interpolated to acoustic

source region, displayed in Figure 1, and used for the reconstruction of turbulence. The airfoil is extruded to a wing and discretised for an acoustic resolution of $f_{max} = 5kHz$. Figure 1 shows the surface excitation V_y for a single frequency of $f \approx 800Hz$. An acoustic simulation is performed for each single frequency of the entire Fourier transformed excitation signal. This acoustic signal is propagated to the far-field and evaluated at an observer point 2.5 chord lengths underneath the trailing edge of the airfoil.

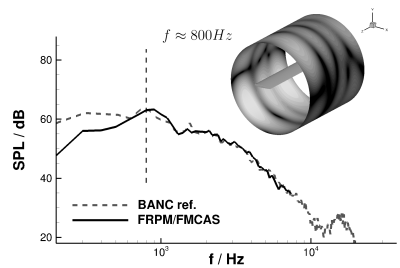


Figure 2: Far-field cylinder with sound pressure level contours (top); Acoustic spectrum at observer point underneath trailing edge (bottom).

Figure 2 shows the obtained spectrum for sound pressure level and compares it to a validated reference simulation of the benchmark case performed by the DLR code PIANO [3]. The FRPM/ FMCAS spectrum matches the reference spectrum very well for the location of the maximum and high frequency trend. This results indicate promising capabilities for full-scale simulations of large, complex problems.

References

- [1] N. Reiche et al. *23rd AIAA/CEAS Aeroacoustics Conference* (2017-3515)
- [2] M. Lummer et al. *19th AIAA/CEAS Aeroacoustics Conference* (2013-2096)
- [3] M. Herr et al. *21st AIAA/CEAS Aeroacoustics Conference* (2015-2847)
- [4] M.S. Howe *Journal of Sound and Vibration* **225** (1999), pp. 211–238.
- [5] M. E. Goldstein, *Aeroacoustics*, 1st edition, McGraw-Hill International Book Company, New-York, 1976.

A BEM-FEM Model for Vibrations in Soils Caused by Railway Traffic in Tunnels

Holger Waubke^{1,*}, Wolfgang Kreuzer¹, Tomasz Hrycak¹, Sebastian Schmutzhard¹

¹Acoustics Research Institute, Austrian Academy of Sciences, Vienna, Austria

*Email: holger.waubke@oeaw.ac.at

Abstract

Railway traffic in tunnels produces vibrations in the soil. Assuming that the tunnel is straight and has a constant cross-section the model is defined in the wave-number domain w.r.t. the longitudinal direction x . In the current model the soil is modeled as a horizontally layered linear elastic anisotropic medium. By a Fourier transformation in space and time the waves in the medium are derived in the wave-number domain about the horizontal axes x and y . Assuming a Dirac load the Green's function is derived in this domain and the element integrals are solved in the transformed domain. The numerical results have to be transformed from the wave-number domain to the original domain for the horizontal axis y . A collocation approach with linear shape functions is used for the BEM part in 2.5D.

Keywords: 2.5D approach, anisotropic medium, FEM-BEM coupling

1 Introduction

Railway traffic in tunnels produces vibration in the soil that can annoy inhabitants in houses directly or by secondary airborne noise. Some mitigation measures e.g. ballast mats and floating slabs can be used to reduce the vibrations at the source or an elastic foundation of the houses can be used to reduce the vibrations in the house. These measures are costly and therefore a prediction of the needed measures is needed during the planning phase of the tunnel. Prediction models used today show differences of up to 10 dB with respect to the measurements and are therefore not helpful [1].

A stratification of an isotropic soil is taken into account by Clouteau [2] using a Floquet transformation in the longitudinal direction.

2 Highspeed trains

New lines are often build for high-speed trains. The moving source can be simply introduced into the model in the frequency wave-number

domain:

$$\omega = \Omega - k_x \cdot v. \quad (1)$$

The angular frequency in the moving system is Ω , ω is the angular frequency for a fixed observer, k_x the wave-number in the longitudinal direction x and v the velocity of the moving load.

3 Waves in the medium

The solution for the waves in an anisotropic medium are derived in the frequency wave-number domain applying the Fourier transformation with respect to all coordinates in space and in time [5]. The differential relationships become simple matrix equation depending on the wave-numbers k_x , k_y , k_z and the angular frequency ω .

Assuming no load in a single layer six generalized eigenvalues $k_{z,i}$ and corresponding eigenvectors describing the displacements and stresses can be derived. An inverse Fourier transformation of the equations for the displacements and stresses with respect to z leads to equations consisting of complex exponential functions.

The equations for the media of the multiple layered soil are coupled at the interfaces. Three equations for the displacements and three equations for the stresses at the interface can be derived. At the top only three equations for the stresses can be derived. Adding an isotropic half-space below the layers setting the three upward traveling waves to zero assures causality and reduces the number of unknowns to the number of equations.

If the material axes are rotated with respect to the global coordinates the stiffness tensor can be derived by 4 rotations using the cosines between the normal vectors.

4 Green's function

So far it was assumed that loads are only allowed at the interfaces. Therefore, an additional interface is needed in the depth of the Dirac loading needed for the Green's function. The

possibility to add a load in the interior of the layer is discussed in [4].

5 Boundary Element Method

The difficulty that occurs is the need to integrate the boundary elements with singularities in the original y, z domain, but the Greens function is only known in the k_y, z domain. The solution of the BEM is to transform the element integral into the wave-number domain and solve the element integrals analytically [3]. A constant shape function leads to a sinc function and a linear shape function gives a derivative of the sinc function. Only the inverse transformation to the y domain has to be done numerically. This function is oscillating and thus the Filon method is used to demodulate the kernel.

6 Finite elements

Volume elements in 2.5D will be used for the simulation of the concrete shell of the tunnel and the superstructure. The element will be reduced in 2.5D to a flat shell element. Linear shape functions will be applied for the 3 node triangle and 4 node quadrilateral elements to be consistent with the shape functions in the BEM part. The rail is simulated using a beam in 2.5D, there the element is reduced to a point element.

7 Coupling FEM with BEM

The matrices of the FEM and BEM are of medium size in 2.5D. Therefore, direct coupling for FEM and BEM will be used. A direct solver seems to be appropriate.

8 Results

First results for the BEM part without FEM are presented in Fig. 1. The unit load is assumed to act directly at the base of the tunnel. The vibrations at the surface are clearly visible. The parameters are presented in [4].

9 Conclusions

A new model is presented that includes stratification and anisotropy of the soil. The effect of a fast moving load can also be added to the model in a simple manner using a simulation in 2.5D. The degrees of freedom of the task are reduced using the 2.5D approach and a BEM formulation of the stratified medium. Overall the memory size needed for the task is small and

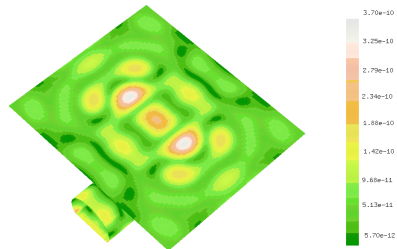


Figure 1: Vibrations in the soil caused by a unit load at the base of the tunnel.

the time for computing the solution can be reduced by parallel computing, because the computation can be split up to several tasks. Only the results have to be collected at the end.

References

- [1] L. Andersen and C. Jones, Coupled boundary and finite element analysis of vibration from railway tunnels a comparison of two- and three-dimensional models, *Journal of Sound and Vibration* **293** (2006), pp. 611–625.
- [2] D. Clouteau, M. Arnst, T. M. Al-Hussaini and G. Degrande, Freefield vibrations due to dynamic loading on a tunnel embedded in a stratified medium, *Journal of Sound and Vibration* **283** (2005), pp. 173–199.
- [3] G. Rieckh, W. Kreuzer, H. Waubke, P. Balazs, A 2.5D-Fourier-BEM-model for vibrations in a tunnel running through layered anisotropic soil, *Engineering Analysis with Boundary Elements* **36** (2012), pp. 960–967.
- [4] H. Waubke, Transform methods for horizontally layered isotropic and anisotropic media with obstacles, *30. Deutsche Jahrestagung für Akustik DAGA, Strasbourg, France, 22-25 March 2004*, pp. 331–332.
- [5] J. P. Wolf, *Dynamic Soil-Structure Interaction*, Prentice-Hall, Eaglewood Cliffs N.J., 1985.

Stability of the boundary integral equation methods for the two dimensional wave equation in time domain revisited

Mio Fukuhara¹, Ryota Misawa², Kazuki Niino¹, Naoshi Nishimura^{1,*}

¹Graduate School of Informatics, Kyoto University, Kyoto, Japan

²Graduate School of Engineering, Kyoto University, Kyoto, Japan

*Email: nchml@i.kyoto-u.ac.jp

Abstract

This study considers the stability of the traditional time domain collocation BIEMs for the wave equation in 2D. We show that the question of stability of time domain BIEMs is reduced to a nonlinear eigenvalue problem related to frequency domain integral equations. We propose to solve this eigenvalue problem numerically with the Sakurai-Sugiura method (SSM). The proposed approach is validated numerically with standard BIEs for exterior and transmission problems.

Keywords: stability, time domain, BIEM, eigenvalue problems

Introduction

Boundary integral equation methods (BIEMs) for the wave equation in time domain have a long standing stability problem. Among various efforts to stabilise BIEMs for wave equations, the three dimensional space-time variational approach by Ha Duong and his colleagues [1] appears to be the first successful attempt. Unfortunately, however, implementing a space-time variational BIEM is not very easy, which is why engineers still prefer fully collocated approaches. Recent developments of CQM by Lulich [2] made it possible to stabilise collocation BIEMs, but there still remain demands for simpler traditional methods. In the traditional collocation BIEM, however, there exist few effective methods of checking stability except for solving large eigenvalue problems for the space-time discretised system matrices. Even this "last resort" is not very practical in 2D problems because of the slow decay of the fundamental solution with respect to time.

In this presentation we propose to resolve this difficulty by carrying out the required stability analysis in frequency domain. Namely, we convert the stability analysis for BIEMs in the wave equation in 2D to a non-linear eigenvalue problem similar to those for the Helmholtz

equation and solve it with SSM using techniques proposed in Misawa et al. [3]. This approach has an additional benefit of making the relation between eigenvalues of the integral operators in frequency domain and the stability of the time domain BIEM clearer. We use the proposed technique to investigate stability of various time domain integral equations for exterior and transmission problems.

Stability

We consider the following integral equation

$$f(t) = \int_0^t K(t-s)v(s) ds \quad (1)$$

where K and f are given functions and v is an unknown function. Equation (1) is typically obtained as one discretises the time domain BIEs for the wave equation in the spatial direction using N collocation points, in which case K is an $N \times N$ matrix and v and f are N -vectors, respectively. Discretising the unknown function $v(s)$ in (1) using time interpolation functions $\phi_m(s)$ as $v(s) \approx \sum_m \phi_m(s)v_m$ ($v_m \in \mathbb{R}^N$), we obtain the following algebraic equation:

$$f(l\Delta t) = \sum_{m=1}^l \int_0^{l\Delta t} K(l\Delta t - s)\phi_m(s) ds v_m \quad l = 1, 2, \dots \quad (2)$$

where $\phi_m(s) = \phi_{\Delta t}(s - m\Delta t)$ and $\phi_{\Delta t}(t)$ is a basis function which satisfies $\phi_{\Delta t}(k\Delta t) = \delta_{k0}$ (where δ_{ij} is the Kronecker delta), respectively. One shows that the stability of this equation is related to the following eigenvalue problem: find $\Omega \in \mathbb{C}$ with which the following equation

$$0 = \sum_{m=-\infty}^{\infty} \frac{1}{\Delta t} \hat{K}(\Omega_m) \hat{\phi}_{\Delta t}(\Omega_m) v \quad (3)$$

has a non-trivial solution $v \in \mathbb{C}^N$, where $\Omega_m = \Omega - \frac{2m\pi}{\Delta t}$ and $\hat{\cdot}$ stands for the Fourier transform

with respect to time. One finds that (2) is stable (unstable) if $\text{Im } \Omega \leq 0$ ($\text{Im } \Omega > 0$) holds for all the eigenvalues (an eigenvalue) of (3). The stability issue of the time domain BIEM is thus reduced to a non-linear eigenvalue problem in frequency domain given by (3). One may use methods based on contour integrals such as the Sakurai-Sugiura Method (SSM) in the solution of non-linear eigenvalue problem in (3).

In the special case where the boundary of the domain is a unit circle Γ , one may consider a semi-discretisation in which only the time direction is discretised. Actually, we can simplify the non-linear eigenvalue problem in (3) using the Fourier series with respect to the angular variable. In the exterior Dirichlet problem in 2D, for example, one has the following BIE:

$$\int_0^t \int_{\Gamma} G(x-y, t-s) q(y, s) dS_y ds = u^{\text{inc}}(x, t) \quad x \in \Gamma, \quad t > 0 \quad (4)$$

where $G(x, t) = 1/(2\pi\sqrt{t^2 - |x|^2}_+)$, $u^{\text{inc}}(x, t)$ is a given function (incident wave) and q is the unknown function. One shows that the eigenvalues of (3) for this special case are the zeros of

$$\sum_m H_n^{(1)}(\Omega_m) J_n(\Omega_m) \hat{\phi}_{\Delta t}(\Omega_m), \quad (5)$$

for an $n \in \mathbb{Z}$, where J_n and $H_n^{(1)}$ are Bessel and Hankel functions.

Numerical experiments

We now carry out numerical experiments to see if the stability analysis given in the previous section can predict the behaviour of the time domain BIEM correctly. We consider (4) with the incident wave given by

$$u^{\text{inc}} = \begin{cases} 0 & (t - x_1 - t_0 \leq 0) \\ \frac{(t - x_1 - t_0)^2}{2} & (t - x_1 - t_0 > 0) \end{cases} \quad (6)$$

where $t_0 = 1 + 2\Delta t$. We use piecewise constant boundary elements, piecewise linear time elements and the collocation method to discretise the BIE in (4). The boundary is discretised into 100 elements, the time increment is set as $\Delta t = \frac{2\pi}{100}$ and the number of time steps is 1000. Also, the eigenvalues of (3) are calculated with (5) and SSM, neglecting the effect of spatial discretisation. The equation obtained by taking the time derivative of (4) is also considered.

Figs.1 (a) and (b) show the plot of q for every 10 time steps obtained with time domain BIEs. We see that (4) leads to instability, while its time derivative gives stable results. Figs.2(a)

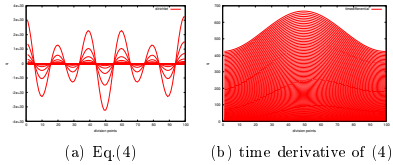


Figure 1: q obtained with various integral equations vs point number.

and (b) show the eigenvalues (green symbols) of (3) for the corresponding time domain BIEs in Figs.1 (a)–(b). Also shown in red are the eigenvalues of the frequency domain BIEs given by $\hat{K}(\Omega)v = 0$. These figures show that the

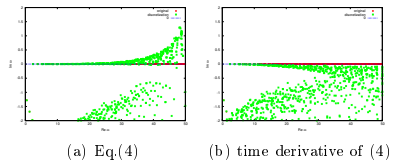


Figure 2: Eigenvalues of (3) for time domain integral equations

stability of BIEs considered and the behaviour of the eigenvalues of (3) are consistent.

References

- [1] A. Bamberger and T. Ha Duong, Formulation variationnelle espace-temps pour le calcul par potentiel retardé de la diffraction d'un onde acoustique (I), *Math Meth Appl Sci* **8** (1986), pp.405–435.
- [2] C. Lubich, On the multistep time discretization of linear initial-boundary value problems and their boundary integral equations, *Num Math* **67** (1994) pp.365–389.
- [3] R. Misawa, K. Niino and N. Nishimura, Boundary integral equations for calculating complex eigenvalues of transmission problems, *SIAM J Appl Math* **77** (2017), pp.770–788.

Time domain CQBEM for wave scattering in complex media

Akira Furukawa¹, Sohichi Hirose^{2,*}¹Department of Civil and Environmental Engineering, Tokyo Institute of Technology, Tokyo, Japan²Department of Civil and Environmental Engineering, Tokyo Institute of Technology, Tokyo, Japan

*Email: shirose@cv.titech.ac.jp

Abstract

A time domain boundary element method (BEM) based on the CQM (convolution quadrature method) is applied to analyze wave scattering in fluid-saturated porous solid and its formulation is verified via numerical analysis for wave propagation of an incident wave in the complex media.

Keywords: wave scattering, Biot media, boundary element method, CQM

1 Introduction

In general, ground has complex materials consisting of soil, water and air, and it is very important to investigate wave propagation behavior in the ground from the view point of earthquake engineering, ground exploration and so on.

In this paper, a time domain BEM based on the CQM is applied to analyze wave scattering in complex media like ground. The CQM is used to evaluate numerically convolution integrals with use of a kernel function in Laplace domain. One advantage of the CQBEM is to produce very stable solutions even if small time increment is chosen, compared with the conventional one. Another advantage is to make possible the formulation of time domain boundary integral equations whenever the fundamental solution in Laplace domain is available. These advantages expand the application of a time domain CQBEM to the analysis of very complicated problems, such as wave propagation and scattering with attenuation, even if a fundamental solution is not available explicitly in time domain.

In the following, Biot's theory for fluid-saturated porous solid is briefly introduced as an example of complex media and the formulation and numerical example of a time domain BEM based on the CQM are presented.

2 Biot's theory

For general anisotropic fluid-saturated porous solid under infinitesimal deformation, the con-

stitutive equations for the Biot's model are given by

$$\sigma_{ij} = C_{ijkl}u_{k,l} - \alpha_{ij}p \quad (1)$$

$$p = -M(\alpha_{kl}u_{k,l} + w_{k,k}) \quad (2)$$

where σ_{ij} is the total stress in solid, p is the pressure in fluid, and u_i and w_i are displacements of solid skeleton and flow of the fluid relative to the solid, respectively. C_{ijkl} , α_{ij} and M are elastic moduli of solid skeleton, Biot's effective-stress coefficients, and Biot's elastic modulus, respectively.

The equations of motion with no body force are expressed as

$$\sigma_{ij,j} = \rho\ddot{u}_i + \rho_f\ddot{w}_i \quad (3)$$

$$p_{,i} = -\rho_f\ddot{u}_i - m_{ij}\ddot{w}_j - \eta r_{ij}\dot{w}_j \quad (4)$$

where ρ and ρ_f are densities of porous solid and pore fluid, respectively. m_{ij} , η and r_{ij} are mass matrix determined by geometry of pores, fluid viscosity, and the flow resistivity matrix, respectively.

Assuming zero initial values at time $t = 0$, the Laplace transform is applied to eqs.(1)–(4), and the variables w and σ_{ij} are eliminated to have the following governing equations with the parameter s in Laplace domain for $\bar{q}_K = \{\bar{u}_k, \bar{p}\}^T$ ($K = 1, \dots, 4$ and $k = 1, 2, 3$).

$$\bar{L}_{IK}\bar{q}_K = 0 \quad (5)$$

where

$$\bar{L}_{IK} = \begin{bmatrix} C_{ijkl}\partial_j\partial_l - \tilde{\rho}_{ik}s^2 & -\tilde{\alpha}_{ij}\partial_j \\ \{\tilde{\alpha}_{kl}\partial_l\}^T & -\frac{1}{s^2}Y_{jl}^{-1}\partial_j\partial_l + \frac{1}{M} \end{bmatrix} \quad (6)$$

where $\tilde{\rho}_{ik} = \rho\delta_{ik} - \rho_f^2Y_{ik}^{-1}$, $\tilde{\alpha}_{ij} = \alpha_{ij} - \rho_fY_{ij}^{-1}$, $Y_{ik} = m_{ik} + \eta r_{ik}/s$.

The fundamental solution $\bar{U}_{QK}(\mathbf{x}, \mathbf{y}, s)$ in La domain, indicating the general displacement in Q direction at \mathbf{x} due to the general body force in K direction at \mathbf{y} in Biot's media, is governed by

$$\bar{L}_{IQ}\bar{U}_{QK} = -\delta(\mathbf{x} - \mathbf{y})\delta_{IK}. \quad (7)$$

Following a similar procedure derived for the fundamental solution for elastodynamics in general anisotropic solids [1], the fundamental solution \bar{U}_{QK} is obtained in the integral form, and is evaluated numerically.

3 Formulation of CQBEM

We consider the wave propagation problem shown in Fig. 1. The incident wave q_I^n is generated

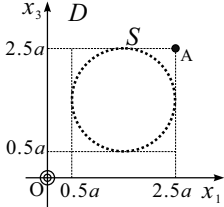


Figure 1: Model for wave scattering analysis.

due to a body force at the origin O, and scattered by a scatterer with the surface S. Applying the reciprocal theorem to \bar{q}_K in eq.(5) and \bar{U}_{QK} in eq.(7) in Laplace domain and transferring formally from Laplace domain to time domain, then the general wave displacement in the outer domain D is expressed by

$$q_I^n(\mathbf{x}, t) + \int_S U_{IK}(\mathbf{x}, \mathbf{y}, t) * s_K(\mathbf{y}, t) dS_y - \int_S W_{IK}(\mathbf{x}, \mathbf{y}, t) * q_K(\mathbf{y}, t) dS_y = c(\mathbf{x})q_I(\mathbf{x}, t) \quad (8)$$

where $c(\mathbf{x})$ is the free term defined by $c(\mathbf{x}) = 1(\mathbf{x} \in D), 1/2(\mathbf{x} \in S)$, and $0(\mathbf{x} \notin \bar{D})$ and $*$ is the time convolution integral. s_K and W_{IK} are general traction and double layer kernels, corresponding to q_K and U_{IK} , respectively.

The time convolution integral in eq.(8) is evaluated by using CQM [2], i.e.,

$$K(t) * g(t)|_{t=N\Delta t} \approx \sum_{k=0}^n w_{n-k}(\Delta t)g(k\Delta t) \quad (9)$$

where Δt is the time increment and $w_m(\Delta t)$ is the weight function given by

$$w_m(\Delta t) = \frac{R^{-m}}{L} \sum_{l=0}^{L-1} \bar{K}\left(\frac{\gamma(z_l)}{\Delta t}\right) e^{-2\pi i m l / L} \quad (10)$$

where $\bar{K}(s)$ is the Laplace transferred function of the kernel function $K(t)$, and other parameters of γ, z_l, R and L are referred to [2].

The boundary integral equation of eq.(8) for $\mathbf{x} \in S$ is solved by discretizing the boundary S with constant element for unknown boundary values of s_K or q_K , applying the CQM for the time convolution, introducing the boundary conditions, and taking the time marching scheme.

4 Numerical example

We consider the wave propagation problem in Fig. 1, where the interior domain enclosed by the boundary S is occupied by the same material of sand stone as the outer one [3]. The boundary integral equation (8) for the exterior problem can be solved with combination of the boundary integral equation for the interior problem. In this case, no scattered wave is generated and the obtained solution is exactly the same as the incident wave.

Fig.2 shows the time variations of the solid displacements u_1 and u_3 and the fluid pressure p at the point A in Fig. 1. Numerical solutions for total wave obtained by time domain CQBEM are the same as analytical solutions of the incident wave.

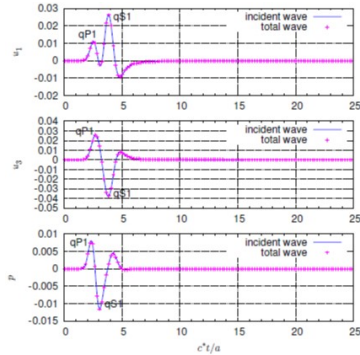


Figure 2: Time variations of u_1, u_3 and p at the point A in Fig. 1.

References

- [1] C.-Y. Wang and J. D. Achenbach, Geophys. J. Int. **118** (1994), pp.384–392.
- [2] C. Lubich, Numeri. Math. **52** (1988), pp.129–145.
- [3] J. M. Carcione, J. Acoust. Soc. Am., **99** (1996), pp.2655–2666.

Space-Time Boundary Elements for the Acoustic Wave Equation

Dominik Pözl^{1,*}, Martin Schanz¹¹Institute of Applied Mechanics, Graz University of Technology, Graz, Austria

*Email: poelz@tugraz.at

Abstract

Many acoustic scattering problems are modelled by the 3d wave equation. The use of boundary integral equations enables an elegant handling of problems posed on the unbounded exterior of the scatterer. In this work, we discuss space-time discretizations of these time domain integral equations. The philosophy of space-time methods is to treat time like an additional spatial coordinate. Consequently, the operator equation is discretized in the 3+1-dimensional space-time cylinder. In the context of boundary integrals, only a discretization of the lateral space-time boundary is required. We employ standard finite element spaces based on simplex meshes of this boundary.

In the space-time setting, the numerical computation of the underlying integral operators is challenging. We present a tailored quadrature technique for point-wise evaluations of integral operators of the 3d wave equation. The method is verified via numerical experiments.

Keywords: time domain, boundary integral equation, retarded potential, space-time mesh

1 Wave equation and integral form

Let $\Omega^- \subset \mathbb{R}^3$ be a bounded open domain with polyhedral Lipschitz boundary $\Gamma = \partial\Omega^-$ and exterior $\Omega^+ = \mathbb{R}^3 \setminus \overline{\Omega^-}$. For a fixed wave velocity $c > 0$ we employ the scaled time $t = c\tau$, where τ denotes the physical time. We define the space-time cylinders $Q^* = (0, T) \times \Omega^*$ for $*$ $\in \{-, +\}$ with lateral boundary $\Sigma = (0, T) \times \Gamma$ where $T > 0$ is the simulation end time. We are concerned with the solution u of the wave equation

$$(\partial_t^2 - \Delta_x)u = 0 \quad \text{in } Q^+ \quad (1)$$

$$u = 0 \wedge \partial_t u = 0 \quad \text{on } \{0\} \times \Omega^+ \quad (2)$$

$$u = g \quad \text{on } \Sigma \quad (3)$$

for some given Dirichlet datum g . Note that Δ_x denotes the Laplace operator differentiating with respect to spatial coordinates only. In this work, we shall use a boundary integral representation of the solution of (1)-(3), which is convenient since Q^+ is unbounded. For a sufficiently

smooth surface density $w : \Sigma \rightarrow \mathbb{R}$ the Huygens (also known as *retarded*) single layer potential SL has the integral representation [1]

$$\text{SL } w(t, x) = \int_{\Gamma} \frac{w(t - \|x - y\|, y)}{4\pi\|x - y\|} dS(y) \quad (4)$$

with the extension $w(t, \cdot) = 0$ for $t \leq 0$. It holds

$$(\partial_t^2 - \Delta_x)\text{SL } w = 0 \quad \text{in } Q^+ \cup Q^-$$

for any admissible w , in particular, the ansatz $u = \text{SL } w$ satisfies (1) and (2) for any surface density w . To find w such that (3) is satisfied, the trace is applied, yielding the equation

$$V w = g \quad \text{on } \Sigma, \quad (5)$$

where the integral representation of V is exactly (4) since SL is continuous across the boundary.

2 Space-time boundary elements

We devise a discretization method for (5) based on a decomposition of the lateral boundary Σ into space-time boundary elements. Since Σ is a 3d hypersurface embedded in \mathbb{R}^4 we employ a mesh Σ_N composed of $N \in \mathbb{N}$ tetrahedral boundary elements. Each tetrahedron $\sigma \in \Sigma_N$ is the image of the reference element $\hat{\sigma} \subset \mathbb{R}^3$ under a smooth bijection $\chi_\sigma : \hat{\sigma} \rightarrow \sigma$. We use standard trial spaces, e.g. for $p \in \mathbb{N}_0$

$$S_N^p = \{v : \Sigma \rightarrow \mathbb{R} : v|_\sigma \circ \chi_\sigma \in \mathbb{P}^p(\hat{\sigma}), \sigma \in \Sigma_N\}.$$

These are *space-time* boundary element spaces, since there is no distinction between space and time variables. In [2], we derived the representation of Huygens layer potentials that genuinely matches the space-time setting

$$\text{SL } w(t, x) = \sum_{\sigma \in \Sigma_N} k_\sigma^w(t, x)$$

with

$$k_\sigma^w(t, x) = \int_{\chi_\sigma^{-1}(\Xi \cap \sigma)} \frac{w \circ \chi_\sigma(\xi) v_\sigma(\xi)}{4\pi\|x - y(\xi)\|} dS(\xi) \quad (6)$$

where $v_\sigma : \hat{\sigma} \rightarrow \mathbb{R}$ is some smooth function and the 3d hypersurface Ξ is the backward light cone

$$\Xi = \{(\zeta, y) \in \mathbb{R} \times \mathbb{R}^3 : t - \zeta = \|x - y\|\}.$$

A robust and accurate quadrature technique for evaluating (6) is proposed in [2], which exploits that $\chi_\sigma^{-1}(\Xi \cap \sigma)$ is a subset of a quadric if χ_σ is affine. This quadric is parametrized by well-known maps $\psi : \text{dom } \psi \rightarrow \text{ran } \psi$ with $\text{dom } \psi \subset \mathbb{R}^2$ and $\text{ran } \psi \cap \hat{\sigma} = \chi_\sigma^{-1}(\Xi \cap \sigma)$. By transforming (6) to the parameter domain $\text{dom } \psi$ the singularity of the kernel function is lifted, enabling the application of standard quadrature rules.

An example space-time collocation scheme that approximates solutions of (5) is to find

$$w_N \in S_N^1 \cap C(\Sigma) : \forall w_N(t, x) = g(t, x) \quad (7)$$

for any vertex (t, x) of the mesh Σ_N .

3 Numerical examples

To test the method, we apply it to a simple problem setting, for which an exact solution of (5) is known. We consider the unit ball $\Omega^- = \{x \in \mathbb{R}^3 : \|x\| < 1\}$ and Dirichlet data of the form

$$g(t, x) = \varphi(t), \quad (t, x) \in \Sigma$$

where $\varphi : \mathbb{R} \rightarrow \mathbb{R}$ is sufficiently smooth and $\varphi(t) = 0$ for $t \leq 0$. In this case the solution w of (5) is known [3]. In particular, we use $\varphi(t) = t^4 \exp(-2t)$ for $t > 0$ in our tests.

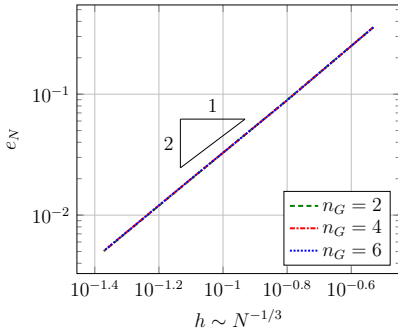


Figure 1: Convergence test: quadrature scheme

The tetrahedral mesh Σ_N is an approximation of the smooth space-time boundary, which is the extrusion of the unit sphere in time up to end time T . To measure the approximation error, we compute the arithmetic mean

$$e_N = \frac{1}{6} \sum_{i=1}^6 |\tilde{w}(T, x_i) - g(T, x_i)|,$$

where x_i are six vertices of the mesh Σ_N located at time $T = 6$. The tilde in above formula indicates that the integral operator is approximated by Gaussian quadrature of order $n_G \in \mathbb{N}$ [2]. The result displayed in Fig. 1 shows the expected second-order convergence rate in the mesh size h for a sequence of uniform meshes. Further tests that illustrate the capacity of the quadrature scheme can be found in [2].

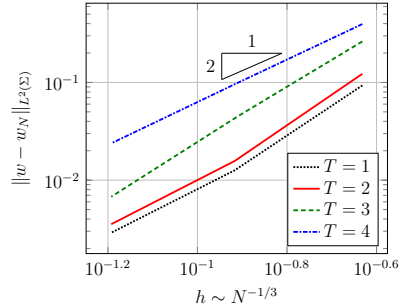


Figure 2: Convergence test: collocation method

As a second test, consider the collocation method (7). The error of the approximation $\|w - w_N\|_{L^2(\Sigma)}$ is computed for a sequence of uniform meshes. A convergence study is exhibited in Fig. 2 for various values of T . While the approach yields quadratic convergence in the examined scenarios, there are cases where it may fail, see [2]. Instabilities of collocation methods, independent of the space-time setting, are already well-known. The stability of space-time schemes is subject of further investigations.

References

- [1] F.-J. Sayas, *Retarded Potentials and Time Domain Boundary Integral Equations: A Road Map*, Springer, 2016.
- [2] D. Pözl and M. Schanz, Space-Time Discretized Retarded Potential Boundary Integral Operators: Quadrature for Collocation Methods, *submitted* (2019).
- [3] S. Sauter and A. Veit, Retarded Boundary Integral Equations on the Sphere: Exact and Numerical Solution, *IMA Journal of Numerical Analysis* **34.2** (2014), pp. 675–699.

The Fast Hybrid Method: Efficient ($\mathcal{O}(1)$ sampling) and High-order, Dispersionless Long-time Transient Wave Scattering

Thomas G. Anderson^{1,*}, Oscar P. Bruno¹, Mark Lyon²

¹Applied & Computational Mathematics, Caltech, Pasadena, USA

²Mathematics & Statistics, University of New Hampshire, Durham, USA

*Email: tanderson@caltech.edu

Abstract

We propose a frequency/time hybrid integral-equation method for transient wave scattering. The method uses Fourier-time transformation, resulting in required solution of a fixed set (with size independent of the desired solution time) of frequency-domain integral equations to evaluate transient solutions for arbitrarily long times. Two main concepts are introduced, namely 1) A smoothly-windowed time-partitioning methodology that enables accurate band-limited representations for arbitrary long time signals, and 2) A novel Fourier transform approach which delivers dispersionless spectrally-accurate solutions. The proposed algorithm is computationally parallelizable and exhibits high-order convergence for scattering from complex geometries while, crucially, enabling time-parallel solution with an $\mathcal{O}(1)$ -cost of sampling at large times T .

Keywords: transient wave propagation, integral equations, Fourier transform methods

1 Introduction

The simulation of transient (i.e. non-zero incident field bandwidth) wave propagation and scattering phenomena is an important problem in science and engineering. Hybrid methods for the problem

$$\frac{\partial^2 u}{\partial t^2}(\mathbf{r}, t) - c^2 \Delta u(\mathbf{r}, t) = 0, \quad \mathbf{r} \in \Omega, \quad (1a)$$

$$u(\mathbf{r}, 0) = \frac{\partial u}{\partial t}(\mathbf{r}, 0) = 0, \quad (1b)$$

$$u(\mathbf{r}, t) = b(\mathbf{r}, t) \quad (\mathbf{r}, t) \in \Gamma \times [0, T^{inc}], \quad (1c)$$

are characterized by use of solutions to well-studied frequency-domain problems to construct transient scattering solutions. A prominent example in this class is the Convolution Quadrature method [2] which proceeds by application of a discrete Z-transform to time-stepped approximations to equation (1a), solution of integral equations for resulting modified Helmholtz problems, and approximate numerical inversion

via a certain complex contour integral. A number of difficulties—including dispersion and inversion errors, as well as a growing number of required integral equations solutions for long-time simulation arise in this approach which we seek to avoid in the proposed methodology.

2 Temporal Partitioning

The proposed Fast Hybrid Method is based on Fourier time transformation of incident fields; we propose to partition and window in time the incident field $b(\mathbf{r}, t)$ using a smooth window function $w_k(t) = w(t - s_k)$ which vanishes for H time units away from certain well-spaced time-window centers $s_k \in [0, T^{inc}]$. The window functions satisfy a partition of unity (POU) property $\sum_k w_k(t) = 1$ so that $b_k(\mathbf{r}, t) = w_k(t)b(\mathbf{r}, t)$ satisfies $\sum_k b_k(\mathbf{r}, t) = b(\mathbf{r}, t)$. Due to the POU property the desired scattering solutions u_k corresponding to boundary condition $b_k(\mathbf{r}, t)$ also satisfy $\sum_k u_k(\mathbf{r}, t) = u(\mathbf{r}, t)$. The intent of this decomposition is to re-center the temporal variable t in the transform and limit the oscillatory character of the frequency-domain solutions due to the oscillatory kernel $e^{i\omega t}$ in the transform—hence the “slow” superscripts in our notation. Concretely, for incident fields of the form

$$b_k(\mathbf{r}, t) = \frac{1}{2\pi} \int_{-\infty}^{\infty} B_k^t(\omega) e^{i(\kappa(\omega)\mathbf{p}\cdot\mathbf{r} - \omega t)} d\omega \quad (2)$$

in a given single direction \mathbf{p} , the temporally-partitioned boundary condition function $b_k(t)$ (the inverse Fourier transform of $B_k^t(\omega)$) has the Fourier transform,

$$B_k^{slow}(\omega) = \int_{-H}^H b_k(t + s_k) e^{i\omega t} dt, \quad (3)$$

and it follows that $B_k^t(\omega) = e^{i\omega s_k} B_k^{slow}(\omega)$, so that B_k^{slow} is a slowly-varying function of ω .

The resulting boundary densities $\psi_k^{slow}(\mathbf{r}, \omega)$ and near-field solutions $U_k^{slow}(\mathbf{r}, \omega)$ can be obtained for *all time partitions* k on a *fixed* (time independent) set $\{\psi_{\mathbf{p}}^t\}$ of boundary integral densities for each ω in a frequency sample set \mathcal{F}

(with maximum frequency W , the bandlimit of b_k), using the representation formula

$$\begin{aligned} U_k^{slow}(\mathbf{r}, \omega) &= \int_{\Gamma} \psi_k^{slow}(\mathbf{r}', \omega) G_{\omega}(\mathbf{r}, \mathbf{r}') d\sigma(\mathbf{r}') \\ &= B_k^{slow}(\omega) \int_{\Gamma} \psi_{\mathbf{p}}^t(\mathbf{r}', \omega) G_{\omega}(\mathbf{r}, \mathbf{r}') d\sigma(\mathbf{r}'). \end{aligned} \quad (4)$$

3 FFT-accelerated Transform Inversion

The proposed method produces transient approximations $u_k^W \approx u_k$ from U_k^{slow} using inverse Fourier transforms of W -bandlimited frequency domain solutions:

$$u_k^W(\mathbf{r}, t) = \int_{-W}^W U_k^{slow}(\mathbf{r}, \omega) e^{-i\omega(t-s_k)} d\omega \quad (5)$$

A certain special treatment of this transform required for 2D scattering due to a singularity at $\omega = 0$ is used (but not described here). The proposed treatment for the 3D case begins with the M -term truncated Fourier series expansion $U_k^{slow} \approx \sum_{m=-M/2}^{M/2} c_m e^{i2\pi m\omega/W}$.

Exact integration on an arbitrary (no CFL restriction is present in the fast hybrid method) equi-spaced temporal sampling grid $\{t_n = n\Delta t\}$ leads to the scaled-convolution sum:

$$\begin{aligned} u_k^W(\mathbf{r}, t_n) &\approx \sum_m c_m \int_{-W}^W e^{-i\frac{\pi}{W}(\beta n - m)\omega} d\omega \\ &= \sum_m c_m b_{\beta n - m}, \quad \beta = \frac{W\Delta t}{\pi}, \end{aligned} \quad (6)$$

with the convolution kernel $b_q = 2W \operatorname{sinc}(q)$. This expression displays the $\mathcal{O}(1)$ sampling cost of the fast hybrid method, but rapid evaluation for a range of temporal samples t_n , ($N_1 \leq n \leq N_2$) is facilitated using FFT-accelerated Fractional Fourier Transform methods [3].

4 Numerical Examples

Analysis guarantees that errors decrease super-algebraically as the two approximation parameters $W, M \rightarrow \infty$, and excellent convergence properties are observed to confirm the theory. The fast hybrid method has been successfully demonstrated in a variety of wave scattering contexts. Figure 1 displays snapshots from the long-time simulation of a certain 2D “whispering gallery” geometry, while Figure 2 shows scattering off a 3D glider geometry, the boundary of which is discretized with a high-order multipatch strategy based on a CAD description.

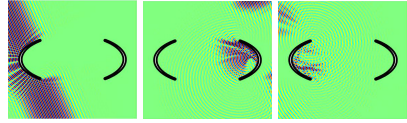


Figure 1: “Whispering Gallery” scattering; 30 multiple scattering events were computed.

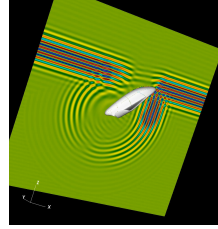


Figure 2: 3D Glider scattering

5 Conclusion

The proposed method [1] is effective for dispersive media and complex physical structures, straightforwardly permits temporal and spatial parallelization, and enables time leaping, that is, solution sampling at time T at $\mathcal{O}(1)$ -bounded sampling cost, without requirement of evaluation of the solution at intermediate times. The fast hybrid method, which generalizes to any linear partial differential equation in the time domain for which frequency-domain solutions can be obtained, yields an attractive time-domain wave solver.

References

- [1] T. G. Anderson, O. P. Bruno, and M. Lyon. High-order, dispersionless “fast-hybrid” wave equation solver. Part I: $\mathcal{O}(1)$ sampling cost via incident-field windowing and recentering, 2018. arXiv:1807.02718.
- [2] Christian Lubich. On the multistep time discretization of linear initial-boundary value problems and their boundary integral equations. *Numerische Mathematik*, 67(3):365–389, 04 1994.
- [3] Victor Nascov and Petre Cătălin Logofătu. Fast computation algorithm for the rayleigh-sommerfeld diffraction formula using a type of scaled convolution. *Appl. Opt.*, 48(22):4310–4319, 08 2009.

Bempp-cl: Fast GPU and CPU assembly of integral operators with OpenCL

Timo Betcke^{1,*}, Matthew Scroggs¹¹Department of Mathematics, University College London, London, UK

*Email: t.betcke@ucl.ac.uk

Abstract

We present Bempp-cl, a successor of the Bempp library for the Galerkin discretisation of boundary integral operators.

Bempp-cl is built on OpenCL and allows explicit use of AVX/AVX-512 vectorisation on CPUs and supports AMD, Intel, and Nvidia GPUs. On an Nvidia Volta GPU it can on-the-fly assemble and apply to a vector an electric field boundary operator with 20,000 elements in less than one second.

Keywords: integral equations, GPU acceleration, Galerkin assembly, OpenCL

1 Introduction

The Bempp boundary element library is a UCL lead project that has been developed since 2011. It consists of a fast C++ core and a user friendly Python interface. It supports the Galerkin discretisation of Laplace, Helmholtz and Maxwell boundary integral operators, either as dense matrices or via ACA based H-Matrix compression.

However, over the last 10 years a revolution has taken place in advanced computing architectures. Massively multicore Xeon CPUs with up to 48 cores are expected to be released in 2019. Each of these cores supports AVX-512 registers that allow the parallel execution of eight double precision or sixteen single precision instructions. At the same time GPU architectures have become mainstream with the fastest Nvidia Volta V100 GPUs having over 5000 compute cores with a peak performance of almost 16 TFlops per second in single precision.

While Bempp performs well on classical multicore architectures with a few parallel cores, performance issues arise in massive multicore environments. Moreover, it is not able to take advantage of modern vectorized instructions or GPU computing environments.

These considerations have lead to the decision to completely reimplement the library with modern compute architectures in mind. The new library should support advanced vector instruction sets on CPUs and vendor-independent

GPU computing. Moreover, the new library should consist only of Python code that would not require any pre-compilation of C or C++ modules. The outcome of these efforts is the Bempp-cl library, which is expected to be released in April 2019. So far it supports the dense Galerkin assembly of Laplace, Helmholtz and Maxwell operators. The performance profiles are significantly improved compared to Bempp, making it possible to assemble dense matrices in the dimension of tens of thousands within seconds on a modern CPU or GPU node. This is especially useful for highly oscillatory problems, which are challenging for standard H-Matrix compression algorithms. Indeed, we will demonstrate high-frequency examples, where the dense assembly in Bempp-cl is significantly more performant than the H-Matrix assembly in previous Bempp versions.

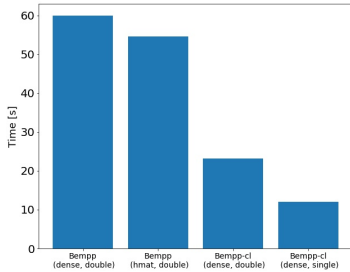
2 An overview of Bempp-cl

Bempp-cl is a pure Python library with essentially the same interface as the previous Bempp library. The big difference is what goes on under the hood. Consider the function to assemble an electric field boundary operator in Bempp-cl.

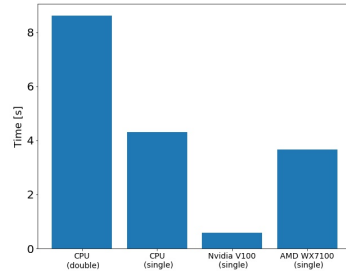
```
op = maxwell.electric_field(
    domain, range_,
    dual_to_range,
    wavenumber,
    precision='single',
    assembler='dense',
    device_interface=cl_device)
```

The new parameters *precision*, *assembler*, and *device_interface* are crucial. Based on this information (or the corresponding default parameters) Bempp-cl proceeds as follows:

1. Select the suitable assembler interface (see below for available assemblers)
2. Based on the chosen compute device select either a GPU compute kernel, or in the case of a CPU device, one of several CPU kernels depending on the hardware support for vectorisation.



(a) Performance of Bempp-cl in dense mode on a 10 Core Xeon CPU compared to Bempp in dense and H-Matrix mode on the same CPU.



(b) Performance of the dense evaluator assembly mode of Bempp-cl on a 10 Core Xeon CPU vs Nvidia and AMD GPUs.

- Configure the chosen precision level (single or double precision) and just-in-time compile the code for the compute device. This is handled by the PyOpenCL library developed by Andreas Klöckner, which provides a convenient Python interface to the underlying OpenCL drivers.
- Run the compiled compute kernel.

Currently, two assembler types are available, a dense assembler which returns a dense matrix discretisation of the operator, and a dense evaluator. The latter one does not pre-assemble the matrix. Rather, during a matrix-vector product it generates the required matrix elements on the fly and then discards them again. This allows us to handle also larger problems with tens of thousands of unknowns on a memory restricted device such as a GPU.

3 Performance tests

In the following we present benchmarks for the assembly of an electric field boundary operator on the unit sphere with wavenumber $k = 15$. The sphere is discretised with 19572 elements (around 8 elements per wavelength), giving 29358 edge degrees of freedom. In Figure 1a we present results for Bempp-cl in dense assembler mode compared to dense assembly and H-Matrix assembly in the current Bempp release version. The tests were performed on an Intel Xeon W-2155 CPU with 10 cores. AVX-512 was used for the Bempp-cl compute kernels.

The H-Matrix timings are not much better than the dense results in this case due to the high-frequency discretisation with 8 elements per wave length. Bempp-cl is three times faster than Bempp in double precision and almost six times faster in single precision (Bempp only supports double precision). The results are even more impressive on GPUs. Figure 1b shows timings for the dense evaluator of Bempp-cl, which performs a matrix-vector product by assembling the matrix on the fly and not storing the elements, reducing memory access significantly. On an Nvidia Volta GPU this on-the-fly assembly/matvec only takes 0.6s, making this highly efficient even compared to standard H-Matrices for the demonstrated element sizes. Only for very large element sizes beyond 100,000 does this evaluation become noticeably slow on a single V100 GPU due to its quadratic complexity.

4 Outlook

Bempp-cl is already highly usable and will be released in summer 2019. We are currently implementing optimised Calderón and transmission operators. The corresponding results will be reported at a later stage. Multi GPU and distributed computing support is also in the work, as well as an OpenCL based FMM implementation for Bempp-cl.

A fast direct solver for multilayered quasi-periodic scattering

Yabin Zhang^{1,*}, Adrianna Gillman¹¹Department of Computational and Applied Mathematics, Rice University, Houston, USA

*Email: yabin.zhang@rice.edu

Abstract

This paper presents a fast direct solver for solving two dimensional wave scattering problems from quasi-periodic multilayered structures. It is based upon an existing boundary integral formulation that is robust at the Wood's anomalies and recent developments on hierarchical matrix representations and inversions. The proposed scheme scales linearly with respect to the total number of unknowns on the interfaces. It is efficient in handling multiple incident angles and requires minimal extra calculations if a certain layer or interface in the structure is modified, as what may often happen in an optimal design setting.

Keywords: fast direct solver, Helmholtz equation, multilayered media, matrix compression

1 Introduction

Wave scattering from multilayered quasi-periodic geometries arises in the design of optical and electromagnetic devices. Some specific examples include solar cells (thin-film photovoltaic cells [1]), dielectric gratings for high-powered laser [7] and wideband [5] applications. Most of such applications require solving a scattering problem with a large number of incident angles. For example, a Bragg diagram created from the solution of 200 boundary value problems is desirable in many engineering applications. Additionally, in the case of optimal design, a scattering problem is often nested inside an optimization loop and solved with slightly different geometry or material properties for each iteration. Thus, having access to a robust and efficient numerical method that can well handle multiple incident angles and changes in geometry and/or material properties will significantly reduce the cost of developing such devices.

Consider a L layered geometry $\Omega = \bigcup_{i=1}^L \Omega_i$ where Ω_i denotes a layer with material property ω_i and Γ_i denotes the interface between Ω_i and Ω_{i+1} . There are $L - 1$ interfaces. The geometry is infinite both horizontally and vertically but d -periodic in the horizontal direction. A

plane wave u^{inc} with angle $\theta^{\text{inc}} \in (-\pi, 0)$ is incident to the top layer. The incident wave and the resulting scattered field are quasi-periodic; i.e. $u^{\text{inc}}(x+d, y) = \alpha u^{\text{inc}}(x, y)$, where the Bloch phase α depends on the incident angle θ^{inc} via $\alpha = e^{id\omega_1 \cos \theta^{\text{inc}}}$. Let u_i denote the scattered field in layer Ω_i . The scattered field satisfies the boundary value problem

$$\begin{aligned} (\Delta + \omega_i^2)u_i(\mathbf{x}) &= 0 & \mathbf{x} \in \Omega_i, 1 \leq i \leq L \\ u_1 - u_2 &= -u^{\text{inc}}(\mathbf{x}) & \mathbf{x} \in \Gamma_1 \\ \frac{\partial u_1}{\partial \nu} - \frac{\partial u_2}{\partial \nu} &= -\frac{\partial u^{\text{inc}}}{\partial \nu} & \mathbf{x} \in \Gamma_1 \\ u_i - u_{i+1} &= 0 & \mathbf{x} \in \Gamma_i, 1 < i < L - 1 \\ \frac{\partial u_i}{\partial \nu} - \frac{\partial u_{i+1}}{\partial \nu} &= 0 & \mathbf{x} \in \Gamma_i, 1 < i < L - 1 \end{aligned} \quad (1)$$

plus radiation conditions in the top and bottom layer. The first equation in (1) is the Helmholtz equation. The remainder equations enforce continuity of the solution and the flux through the interfaces. Figure 1(a) illustrates a model problem in a five layered geometry.

2 The formulation and solution scheme

Since the wave speed in any layer is constant, it is possible to recast the boundary value problem as a boundary integral equation. This means that instead of discretizing all of \mathbb{R}^2 , only the interfaces need to be discretized. The proposed direct solver is constructed for the boundary integral formulation presented in [2]. This integral formulation is robust even at Wood's anomalies by utilizing the free space Green's function and introducing additional unknowns to enforce periodicity.

Upon discretization, this formulation results in a block linear system where the largest block (in general) is a tridiagonal matrix corresponding to discretized boundary integral operators. The diagonal blocks correspond to the discretized operator on $\Gamma_i^{(0)}$ (single period) evaluated on itself plus contributions from the left and right neighboring periods, Γ_i^{-1} and Γ_i^{+1} , respectively. The off-diagonal blocks correspond to the evaluation of the discretized integral operators from the top and bottom neighbor interfaces Γ_{i-1} and

Γ_{i+1} . Figure 1(b) illustrates the notation for the five layered geometry.

Since the tri-diagonal matrix is the largest in the block linear system, the proposed solver is based on creating a fast direct solver for this matrix. Specifically, the tri-diagonal matrix is written as a block diagonal matrix \mathbf{D} plus a block tridiagonal matrix \mathbf{B} . The diagonal blocks of \mathbf{D} correspond to discretized integral operators evaluated on the same interface. This matrix can be approximated and inverted for a cost that scales linearly with the number of discretization points on each interface via a fast direct solver such as [4]. The matrix \mathbf{B} has all the non-self interaction matrices which can be approximated via low rank factorizations to high accuracy. All of these approximations can be done independently of the incident angle θ^{inc} and Bloch phase α . The full tridiagonal matrix $\mathbf{D} + \mathbf{B}$ can then be inverted rapidly via a Woodbury formula as in [3] and [6].

This approach allows lots of the expensive calculations to be performed independently of the incident angle and the Bloch phase as pre-computation, and thus multiple incident angles can be processed rapidly. Furthermore, in the case where one (or several) particular interface or layer property changes, a new self inversion and a low rank approximation capturing neighbor interactions for this particular interface can be reconstructed and replaces the previous one without touching the rest of the precomputed operators.

3 Numerical results

The numerical results will show the following:

- The solver can handle complex interface geometries (e.g. sharp corners) and low to intermediate frequency problems (the largest tested value for ω_i is about 50) to very high accuracy (with matrix compression tolerance set to be 1×10^{-12} , the observed relative error is about 1×10^{-10}).
- The cost scales linearly with respect to the total number of unknowns on the interfaces. The precomputation is expensive, but once done, solving for one incident angle is cheap. (e.g. for the model geometry in Figure 1 with 8.4×10^4 total points on the interfaces, the Bloch phase independent precomputation takes 536 seconds,

the Bloch phase dependent precomputation takes 75 seconds, and one incident angle solve takes 8 seconds.)

- The proposed solver is efficient in handling multiple incident angle problems.
- Once the direct solver is constructed, the cost of changing an interface or wave number ω_i depends only on the interfaces affected by the change. The rest of the direct solver can be reused.

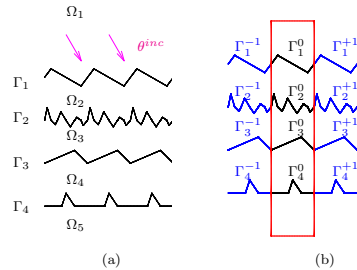


Figure 1: (a) A five-layer model geometry ($L = 5$) with plane wave of angle θ^{inc} incident to the top layer. Three periods are drawn for each interface. (b) Same geometry with the center period in red box. Γ_i^0 , Γ_i^{-1} , and Γ_i^{+1} denote the self, left neighbor, and right neighbor period of the i th interface Γ_i , respectively.

References

- [1] H. Atwater and A. Polman, Plasmonics for improved photovoltaic devices, *Nature Materials* **9** (2010), pp. 205-213.
- [2] M. Cho and A. Barnett, Robust fast direct integral equation solver for quasi-periodic scattering problems with a large number of layers, *Optics Express* **23** (2015), pp. 1775-1799.
- [3] A. Gillman and A. Barnett, A fast direct solver for quasi-periodic scattering problems, *Journal of Computational Physics* **248** 92013, pp. 309-322.
- [4] A. Gillman, P. Yound, and P. Martinsson, A direct solver with $O(N)$ complexity for integral equations on one-dimensional domains, *Frontiers of Mathematics in China* **7** (2012), pp. 217-247.
- [5] G.A. Kalinchenko and A. M. Lerer, Wideband all-dielectric diffraction grating on chirped mirror, *Journal of Lightwave Technology* **28** (2010), pp. 2743-2749.
- [6] G. Marple, A. Barnett, A. Gillman, and S. Veerapaneni, A fast algorithm for simulating multiphase flows through periodic geometries of arbitrary shape, *SIAM Journal of Scientific Computing* **38** (2016), pp. B740-B772.
- [7] M. D. Perry, R.D. Boyd, J. A. Britten, D. Decker, B. W. Shore, C. Shannon, and E. Shults, High-efficiency multilayer dielectric diffraction gratings. *Opt. Lett.* **20** (1995), pp/ 940-942

High order impedance boundary condition for the three scattering problem in electromagnetism with the adaptive cross approximation

Soumaya Oueslati^{1,*}, Christian Daveau¹, Brice Naisseline¹

¹Department of Mathematics, University of Cergy-Pontoise, Paris, France

*Email: soumaya.oueslati1@u-cergy.fr

Abstract

In this paper, we propose a new variational formulation for the electromagnetic scattering problem which derives from an integral method with the use of high order impedance boundary condition (HOIBC) to improve the accuracy Leontovitch impedance boundary condition (SIBC). The performances of the HOIBC are evaluated by calculating the radar cross section (RCS).

Keywords: HOIBC, boundary element method, scattering problem.

1 Introduction

We consider the scattering problem of electromagnetic waves (\mathbf{E} , \mathbf{H}) by perfectly conducting obstacles coated with a thin layer of dielectric. The coating is modeled by the SIBC on its outer surface Γ . More accurate models can be obtained with high order impedance boundary condition [2]. In this model the tangential values of the electric and magnetic fields on the surface of an object are related with the incident angle at each point of the surface.

This paper deals with the implementation of HOIBC in 3D MoM codes using Rao-Wilton-Glisson (RWG) basis functions. To improve efficiency, the MPI method is used to accelerate fast boundary elements formulation based on Hierarchical compression of matrices by adaptive cross approximation (ACA).

2 Approximation of the HOIBC

The impedance boundary condition (IBC) is approximated with a ratio of polynomials of second order. Equivalently, it can be written as a second order IBC with Hodge operator [1]. It is worth noting that three-dimensional HOIBC approximation as

$$(I+b_1L_D-b_2L_R)\mathbf{E}_{tg}=(a_0I+a_1L_D-a_2L_R)\mathbf{n}\times\mathbf{H} \quad (1)$$

where \mathbf{n} is the outer unit normal vector, Γ is the boundary of the illuminated object and \mathbf{E}_{tg} and \mathbf{H} designates, respectively, the tangential electric and magnetic fields. The Leontovitch

impedance boundary condition is the case with $a_1 = a_2 = b_1 = b_2 = 0$. We find method to calculate these coefficients (a_0, a_j, b_j) for HOIBC in [2]. We define the operators L_D and L_R for all vector function \mathbf{A} sufficiently smooth, such that $\mathbf{A} \cdot \mathbf{n} = 0$

$$L_D\mathbf{A} = \nabla_{tg}(\text{div}_{tg}\mathbf{A}), \quad L_R\mathbf{A} = \text{rot}_{tg}(\text{rot}_{tg}\mathbf{A}).$$

3 Variational problem with HOIBC

In this section, we give a new variational formulation with unknowns $\mathbf{J} = \mathbf{n}\times\mathbf{H}$ and $\mathbf{M} = \mathbf{E}\times\mathbf{n}$.

Find $U = (\mathbf{J}, \mathbf{M}) \in V = [H^{-1/2}(\text{div}, \Gamma)]^2$ such that:

$$A(U, \Psi) = \langle I\mathbf{E}^{inc}, \Psi_J \rangle + \langle I\mathbf{H}^{inc}, \Psi_M \rangle,$$

for all $\Psi = (\Psi_J, \Psi_M) \in V$, where the bilinear form $A(U, \Psi)$ is defined as:

$$\begin{aligned} A(U, \Psi) = & \langle Z_0(B - S)\mathbf{J}, \Psi_J \rangle + \frac{a_0}{2} \langle \mathbf{J}, \Psi_J \rangle \\ & + \frac{b_1}{2a_0} \langle L_D(\mathbf{n} \times \mathbf{M}), \mathbf{n} \times \Psi_M \rangle - \langle Q\mathbf{J}, \Psi_M \rangle \\ & + \frac{1}{Z_0} \langle (B - S)\mathbf{M}, \Psi_M \rangle + \frac{b_2}{2} \langle L_R\mathbf{n} \times \mathbf{M}, \Psi_J \rangle \\ & + \frac{a_1}{2} \langle L_D\mathbf{J}, \Psi_J \rangle + \frac{1}{2a_0} \langle \mathbf{n} \times \mathbf{M}, \mathbf{n} \times \Psi_M \rangle \\ & - \frac{a_1}{2a_0} \langle L_D\mathbf{J}, \mathbf{n} \times \Psi_M \rangle + \frac{a_2}{2a_0} \langle L_R\mathbf{J}, \mathbf{n} \times \Psi_M \rangle \\ & + \langle Q\mathbf{M}, \Psi_J \rangle - \frac{b_2}{2a_0} \langle L_R(\mathbf{n} \times \mathbf{M}), \mathbf{n} \times \Psi_M \rangle \\ & - \frac{b_1}{2} \langle L_D(\mathbf{n} \times \mathbf{M}), \Psi_J \rangle - \frac{a_2}{2} \langle L_R\mathbf{J}, \Psi_J \rangle, \end{aligned}$$

where k is the wave number. The operators $(B - S)$ and Q are defined in [3].

The operators arising in the discretization of HOIBC are not easily computed with basis functions. The surface RWG is discontinuous when crossing the edge that borders the two elements on which they are defined. We propose a new approximation of the high order impedance boundary condition which is Hodge operator. To overcome the difficulty of the discretization of $\text{div}(\mathbf{n} \times \mathbf{w})$ and $\text{rot}(\mathbf{w}) \forall \mathbf{w} \in H(\text{div})$, we use the theory of distributions.

4 Hierarchical compression by ACA approximation

The discretization of the integral operators described in section 3 leads to dense matrices. The overall simulation time and the memory footprint of the method are very high. To solve this problem, we use a matrix approximation method called the ACA method introduced in [4] and MPI parallelization of our computation code. Our work, which was written with MPI functions is mainly intended to reduce the user's parallel programming cost and the overall simulation time.

5 Numerical validation

To illustrate our approach, we compute the RCS of a unit sphere coated with a thin dielectric layer. The comparison of the calculation time is given by the following table:

Unknowns	Direct solve	ACA solve
229740	32	4

The effect of coating thickness on the complexity of the impedance terms is illustrated in the next few Figures. Figure 1 illustrates that thin layers the SIBC is an excellent approximation. The increasing complexity of the impedance terms as the coating becomes thicker is illustrated in Figures 2 and 3. In the case of $d = 0.3 \lambda_0$ clearly show the increased accuracy of the HOIBC solution relative to the SIBC solution. As illustrated in Figure 3, when $d = \lambda_0$ the HOIBC is found to be unsatisfactory. In the case derivatives of higher than second order must be included in the boundary condition in order to obtain an accurate model of the bistatic RCS. The second example, Figure 4, is chosen to include increasing a wave number. In this cas, the HOIBC is quite satisfactory.

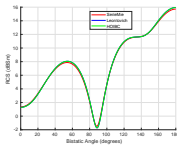


Figure 1: Bistatic RCS of the sphere coating thickness of $d = 0.1 \lambda_0$ with $\epsilon = 4$.

Acknowledgment This work was funded by Labex MME-DII.

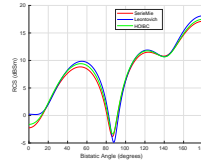


Figure 2: Bistatic RCS of the sphere coating thickness of $d = 0.3 \lambda_0$ with $\epsilon = 4$.

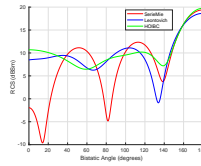


Figure 3: Bistatic RCS of the sphere coating thickness of $d = \lambda_0$ with $\epsilon = 4$.

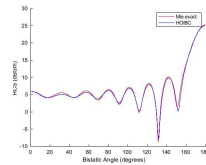


Figure 4: Bistatic RCS of the sphere coating thickness of $d = 0.01 \lambda_0$ with $\epsilon = 2$.

References

- [1] A. Aubakirov, P. Soudais and C. Daveau, High Order Impedance Boundary Condition for MoM Scattering, *IEEE on Antennas and propagation, July 7-13 2013, Orlando Florida, USA*
- [2] Y. Rahmat-Samii and D. J. Hoppe, *Impedance boundary conditions in electromagnetics, Taylor & Francis, 1995.*
- [3] S. Oueslati, *A new variational formulation for scattering problem with high order impedance boundary condition, UCP,2019*
- [4] M. Bebendorf, Approximation of boundary element matrices, *Numerische Mathematik, 86 (2000), pp. 565–589.*

Convolution quadrature and BEM for scattering from generalized impedance boundary conditions

Lehel Banjai¹, Christian Lubich², Jörg Nick^{2,*}

¹The Maxwell Institute for Mathematics in the Sciences; School of Mathematical & Computer Sciences, Heriot-Watt University, Edinburgh, UK

²Mathematisches Institut, Universität Tübingen, Germany

*Email: nick@na.uni-tuebingen.de

Abstract

We consider the acoustic wave equation on an exterior domain with linear generalized impedance boundary conditions. A boundary integral formulation is developed and then discretized in time with the convolution quadrature (CQ) method. We prove stability and convergence of the semi-discretized systems.

A boundary element (BEM) spatial-semi-discretization is then applied and analyzed. Similarly as before, we prove a stability result and use it to obtain a convergence result. Finally, a full discretization that couples both discretizations is employed and analyzed. The combination of the results obtained before gives a stability result that leads to the convergence result of the fully discretized scheme.

Keywords: Acoustic wave equation, Convolution quadrature, Generalized impedance boundary conditions

1 Introduction

The simulation of scattered waves in unbounded exterior domains is a challenge both in theory and in practice. This work considers the acoustic wave equation, with two generalized boundary conditions. We denote with u^{inc} an incidental incoming wave from an exterior domain $\Omega \subset \mathbb{R}^3$, with boundary Γ . The first boundary condition considered is then a kinetic-type boundary condition, i.e.

$$\partial_n u = \epsilon(\partial_t^2(u + u^{\text{inc}}) - \Delta_\Gamma(u + u^{\text{inc}})) - \partial_n u^{\text{inc}}, \quad (1)$$

which is a model for a material with a thin coating, which .

The second boundary condition analyzed, a model for highly absorbing materials, is a fractional-type boundary condition, namely

$$\partial_n u = \partial_t^{1/2}(u + u^{\text{inc}}) - \partial_n u^{\text{inc}}. \quad (2)$$

2 Calderon operator system

We start with Kirchhoff's integral representation theorem

$$u = S(\partial_t)\varphi + D(\partial_t)\partial_\Gamma^{-1}\psi,$$

and take the limit towards the boundary. The jump conditions of the potential operators then yield an operator system that is solved by boundary densities φ and ψ , corresponding to a solution of the wave equation u .

Plugging in the boundary conditions then gives an operator system that is solved by densities, corresponding to a solution u , that fulfills these same boundary conditions. In the case of (2) this gives the system

$$\begin{pmatrix} B_{\text{imp}}(\partial_t) + \begin{pmatrix} 0 & 0 \\ 0 & \epsilon(\partial_t - \Delta_\Gamma \partial_\Gamma^{-1}) \end{pmatrix} \end{pmatrix} \begin{pmatrix} \varphi \\ \psi \end{pmatrix} = \begin{pmatrix} 0 \\ g^{\text{inc}} \end{pmatrix},$$

where the Operator $B_{\text{imp}}(s)$ is the translated Calderon operator for the Helmholtz equation, which was already analyzed in [1]. The g^{inc} is purely depending on the incidental wave u^{inc} . The kinetic boundary condition yields a similar system.

3 Time discretization with the Convolution Quadrature method

Both boundary conditions lead to such a transformed Calderon operator. By using the Convolution Quadrature method based on A-stable backward difference formulae, we discretize these systems in time.

The key to the convergence analysis is to analyze the corresponding Helmholtz operators in the frequency domain. We choose fitting Hilbert spaces that keep the coercivity property of the Calderon operator, shown in [1], which plays a key role in the analysis.

Using an operator valued Herglotz theorem, formulated in [1], then gives an energy estimate

and results from [2] give an optimal order error estimate of the semi-discretization in time.

4 Space Discretization with the Boundary Element method

Discretization of the boundary sobolev spaces by boundary element spaces of piecewise constant and linear functions allows us to formulate differential-algebraic systems.

By relying heavily on the properties of the corresponding elliptic operators, in particular the coercivity property, a stability result is shown for these systems. The regularity of the defects here is handled in a way, that a factor ϵ^{-1} of the right-hand side of the error estimate is avoided.

The defects are then estimated using standard arguments of finite element theory and the bound of the Calderon operator in the frequency domain.

5 Full discretization

Combining both estimates gives an error bound on the fully discrete system. For both boundary conditions we at least achieve the error bound

$$\begin{aligned} & \sum_{j=0}^n \left\| \varphi_{\Delta x}^j - \varphi(j\Delta t, \cdot) \right\|_{H^{-1/2}(\Gamma)}^2 \\ & + \sum_{j=0}^n \left\| \psi_{\Delta x}^j - \psi(j\Delta t, \cdot) \right\|_{H^{1/2}(\Gamma)}^2 \\ & \leq C_T (\tau^p + h)^2, \end{aligned}$$

where C_T at most grows polynomially in T and p is the order of the corresponding A-stable backward difference formulae.

References

- [1] Banjai, Lehel and Lubich, Christian and Sayas, Francisco-Javier, Stable numerical coupling of exterior and interior problems for the wave equation *Numerische Mathematik*, **129**, (2015), pp. 611–646
- [2] Lubich, Christian, On the multistep time discretization of linear initial-boundary value problems and their boundary integral equations *Numerische Mathematik*, **67**, pp. 365–389

Numerical resolution of boundary integral equations on some domains with singularities.

Martin Averseng^{1,*}, François Alouges¹

¹Centre de Mathématiques Appliquées, École polytechnique

*Email: martin.averseng@polytechnique.edu

Abstract

The standard Galerkin method for wave scattering problems in 2D by open arcs has a slow convergence in terms of the mesh-size, due to the singular nature of the exact solution. Moreover, the usual preconditioning techniques prove inefficient, due to the singularity of the domain itself and the lack of efficient pseudo-differential theories on this kind of geometries. Here, we solve both problems by introducing a new Galerkin setting in weighted L^2 spaces, and two new preconditioners for the exterior Dirichlet and Neumann problems. The preconditioners take the form of square roots of local operators. We demonstrate the efficiency of this method on several numerical examples. We also introduce an adapted pseudo-differential calculus on open curves to analyze the proposed preconditioners. An extension to the case of scattering by a flat disk in 3 dimensions is also presented.

Keywords: integral equations, boundary element method, preconditioning

1 Introduction

The problem of preconditioning the linear systems coming from the discretization of first kind integral equations has received considerable attention since two decades. Among the possible strategies are the so-called pseudo-differential preconditioners [1–3, 5, 6, 15]. Roughly speaking, if the original problem is written in the abstract form

$$\mathcal{L}u = f, \quad (1)$$

where \mathcal{L} is a linear operator, the strategy consists in left multiplying equation (1) by an operator \mathcal{K} and solve

$$\mathcal{K}\mathcal{L}u = \mathcal{K}f. \quad (2)$$

Now, if $\mathcal{K}\mathcal{L}$ is a compact perturbation of the identity, the condition number of the discretized underlying linear system becomes independent of the mesh size, enabling the efficient use of iterative methods such as GMRES [13]. This is

in particular the case when \mathcal{K} is a parametrix of \mathcal{L} , which is usually proven using tools from pseudo-differential calculus [14].

Several strategies, depending on the problem to solve (e.g. Helmholtz or Maxwell equations) have been studied in the literature to propose such operators \mathcal{K} , that often turn out to be very effective in practice, when numerical applications are considered. Among those, we would like to emphasize the viewpoint first proposed in [1, 2], where, for Helmholtz equation, the authors consider integral formulations of the problem that involve the Dirichlet-Neumann map Λ which leads to well-conditioned systems after discretization. Combined with the approximation of Λ proposed first in [3] under the form of the square root operator

$$\Lambda \sim \sqrt{-\Delta_\Gamma - k^2}, \quad (3)$$

where Δ_Γ stands for the Laplacian operator on the surface Γ , the method (called GCSIE) yields a very impressive reduction of the number of iterations.

However, all the preceding results and theories are limited to smooth surfaces Γ and very little is known when the integral equation is posed on non-smooth domains, such as domains with corners (in 2D), wedges or conical points (in 3D). One of the reasons might be the fact that pseudo-differential calculus is difficult to generalize on such manifolds and the existing theories such as the ones presented in e.g. [9, 11, 12] do not seem to be adequate for the analysis of such problems.

Nevertheless, attempts to precondition the integral equations that come from the discretization of single-layer or double-layer potentials for Laplace equation on singular domains has started a few years ago [4, 6–8, 10] in dimension 2 or 3, but for very particular domains such as a straight and then curved segments in 2D and a unit disc in 3D. In most of these works, weighted versions of the single layer and hypersingular op-

erators are introduced,

$$S_{k,\omega} = S_{k,\omega}^{-1}, \quad N_{k,\omega} = N_{k,\omega},$$

where $\omega(x) \propto \sqrt{d(x, \partial\Omega)}$. Those weighted operators enjoy better mapping properties than the standard operators, and the analysis is obtained “by hand” without any explicit use of pseudo-differential calculus.

Here, we describe an analytical framework and a Galerkin method in weighted L^2 spaces suited to the inversion of these weighted operators. We introduce two scale of interpolating Hilbert spaces, T^s and U^s , based on Chebyshev polynomials of first and second kind. Namely,

$$T^s = \{u \in L^2_\omega \mid \sum_{n \geq 0} (1 + n^2)^s |\hat{u}_n|^2\}$$

where \hat{u}_n are the first kind Fourier-Chebyshev coefficients of u . U^s is defined analogously, using this time the second kind Fourier-Chebyshev coefficients. The operators $S_{k,\omega}$ and $N_{k,\omega}$ are shown to map continuously T^s to T^{s+1} and U^s to U^{s-1} for all $s \in \mathbb{R}$. Using the properties of T^s and U^s , we prove optimal rates of convergence for the piecewise linear Galerkin discretization of the corresponding first-kind integral equations. Furthermore, using a novel kind of pseudo-differential calculus on open arcs, we are able to derive asymptotic expansions of the symbols of $S_{k,\omega}$ and $N_{k,\omega}$. This allows us to build efficient preconditioners P_1 and P_2 for the linear systems arising from the previous Galerkin method, respectively for the Dirichlet and the Neumann problem. Those preconditioners are defined at the continuous level as

$$P_1 = \sqrt{(\omega \partial_\tau)^2 - k^2 \omega^2}$$

$$P_2 = \sqrt{(\partial_\tau \omega)^2 - k^2 \omega^2}^{-1}$$

and discretized using Padé approximants. Lastly, we show how a large part of this analysis can be put forward in 3 dimensions with minimal modifications to treat the case of a flat disk.

References

[1] F. Alouges, S. Borel and D. Levadoux. A Stable well conditioned integral equation for electromagnetism scattering. *J. Comput. Appl. Math.* 204(2):440–451, 2007.
 [2] F. Alouges, S. Borel and D. Levadoux. A new well-conditioned integral formulation for Maxwell equations in three-dimensions. *IEEE Trans. on Antennas and Propagation* 53(9), 2005.

[3] X. Antoine and M. Darbas. Generalized combined field integral equations for the iterative solution of the three-dimensional helmholtz equation. *ESAIM: Mathematical Modelling and Numerical Analysis*, 41(1):147–167, 2007.
 [4] O. P. Bruno and S. K. Lintner. Second-kind integral solvers for TE and TM problems of diffraction by open arcs. *Radio Science*, 47(6), 2012.
 [5] S. H. Christiansen and J.-C. Nédélec. A preconditioner for the electric field integral equation based on calderon formulas. *SIAM Journal on Numerical Analysis*, 40(3):1100–1135, 2002.
 [6] R. Hiptmair, C. Jerez-Hanckes, and C. A. Urzúa Torres. Mesh-independent operator preconditioning for boundary elements on open curves. *SIAM Journal on Numerical Analysis*, 52(5):2295–2314, 2014.
 [7] R. Hiptmair, C. Jerez-Hanckes, and C. A. Urzúa Torres. Closed-form exact inverses of the weakly singular and hypersingular operators on disks. *arXiv preprint arXiv:1703.08556*, 2017.
 [8] C. Jerez-Hanckes and J.-C. Nédélec. Explicit variational forms for the inverses of integral logarithmic operators over an interval. *SIAM Journal on Mathematical Analysis*, 44(4):2666–2694, 2012.
 [9] R. Melrose. Transformation of boundary problems. *Acta Mathematica*. 147:149–236, 1981.
 [10] P. Ramaciotti and J.-C. Nédélec. About some boundary integral operators on the unit disk related to the laplace equation. *SIAM Journal on Numerical Analysis*, 55(4):1892–1914, 2017.
 [11] S. Rempel and B. Schulze. Parametrices and boundary symbolic calculus for elliptic boundary problems without the transmission property. *Math. Nachr.* 105:45–149, 1982.
 [12] S. Rempel and B. Schulze. Asymptotics for elliptic mixed boundary problems. Pseudo-differential and Mellin operators in spaces with conormal singularity. *Mathematical Research* 50, 1989.
 [13] Y. Saad and M. H. Schultz. GMRES: A generalized minimal residual algorithm for solving nonsymmetric linear systems. *SIAM J. Sci. Stat. Comput.*, 7:856–869, 1986.
 [14] O. Steinbach and W. L. Wendland. The construction of some efficient preconditioners in the boundary element method. *Advances in Computational Mathematics*, 9(1-2):191–216, 1998.
 [15] O. Steinbach and W.L. Wendland. The construction of some efficient preconditioners in the boundary element method. *Adv. Comput. Math.*, 9(1-2):191–216, 1998.

Shape Holomorphy of the Boundary Integral Operators in Acoustic Wave Scattering

Fernando Henríquez^{1,*}, Christoph Schwab¹¹Seminar for Applied Mathematics, ETH Zürich, CH-8092 Zürich, Switzerland.

*Email: fernando.henriquez@sam.math.ethz.ch

Abstract

In this work, we consider the boundary integral operators (BIOs for short) for the Helmholtz equation in domains of class \mathcal{C}^2 and in two dimensions. We prove that these operators, as elements of the Banach spaces of bounded linear operators, depend holomorphically on the shape of the boundary on which they are posed. Furthermore, we explore the implications of these findings in forward and inverse shape uncertainty quantification (UQ).

Keywords: Shape Holomorphy, Boundary Integral Operators, Uncertainty Quantification.

1 Introduction

We establish the holomorphic dependence of the BIOs, as well as the solution of any well-posed boundary integral equations (BIEs), in the shape of the boundary on which these are posed, assuming that the boundary is of class \mathcal{C}^2 in two dimensions. This property, referred to as *shape holomorphy*, is key to mathematically justify the use of several cutting-edge computational tools in forward and inverse UQ [1]. In particular, this result implies sparse approximation of the solution of any family of parametric and well-posed BIEs. As a particular application in UQ, we consider the Bayesian approach to inverse problems in acoustic wave scattering for the approximation of the unknown shape of the scatterer by incorporating noisy measurements, a technique known as *Bayesian shape inversion* [2, 3].

2 Shape Holomorphy of the BIOs

Set $I := [0, 1]$. Let $\{\Gamma_r\}_{r \in \mathfrak{T}}$ be a family of \mathcal{C}^2 -smooth, Jordan curves given by

$$\Gamma_r := \{\mathbf{x} \in \mathbb{R}^2 : \mathbf{x} = r(t), t \in I\},$$

where $r \in \mathfrak{T}$ is a regular boundary representation of the Jordan curve Γ_r and $\mathfrak{T} \subset \mathcal{C}_{\text{per}}^2(I, \mathbb{R}^2)$. Let τ_r denote the pullback between Γ_r and the reference domain I . For $r \in \mathfrak{T}$, $\tau_r : H^\sigma(\Gamma_r) \rightarrow H_{\text{per}}^\sigma(I)$ is an isomorphism, for all $|\sigma| \leq 1$, being $H_{\text{per}}^\sigma(I)$ the periodic Sobolev spaces in I . For

$r \in \mathfrak{T}$, we recall the Calderón projector

$$\mathcal{C}_r^{(\omega)} := \begin{pmatrix} \frac{1}{2} \text{Id} - \mathcal{K}_r^{(\omega)} & \mathcal{V}_r^{(\omega)} \\ \mathcal{W}_r^{(\omega)} & \frac{1}{2} \text{Id} + \mathcal{K}_r^{(\omega)'} \end{pmatrix},$$

where $\mathcal{V}_r^{(\omega)}$, $\mathcal{K}_r^{(\omega)}$, $\mathcal{K}_r^{(\omega)'}$ and $\mathcal{W}_r^{(\omega)}$ are the *single layer*, *double layer*, *adjoint double layer* and *hypersingular* BIOs for the Helmholtz operator with angular frequency ω and defined on the Jordan curve Γ_r (here Id stands for the identity operator). Using the pullback operator, we define $\hat{\mathcal{C}}_r := \tau_r \circ \mathcal{C}_r \circ \tau_r^{-1}$ (the application of τ_r is understood component-wise). Provided $\delta > 0$, we define

$$\mathfrak{T}_\delta := \left\{ r \in \mathcal{C}_{\text{per}}^2(I, \mathbb{C}^2) : \begin{array}{l} \exists \tilde{r} \in \mathfrak{T} \text{ s.t.} \\ \|\tilde{r} - r\|_{\mathcal{C}_{\text{per}}^2(I)} < \delta \end{array} \right\}.$$

We proceed to state the main result, namely shape holomorphy of the BIOs.

Theorem 1 *There exists $\delta > 0$ such that the Calderón projector $\hat{\mathcal{C}}_r$ admits an extension to the set \mathfrak{T}_δ , denoted by $\tilde{\mathcal{C}}_{r, \mathbb{C}}$, such that*

$$r \in \mathfrak{T}_\delta \mapsto \tilde{\mathcal{C}}_{r, \mathbb{C}}^{(\omega)} \in \mathcal{L} \left(\begin{array}{cc} H_{\text{per}}^{\frac{1}{2}}(I) & H_{\text{per}}^{\frac{1}{2}}(I) \\ \times & \times \\ H_{\text{per}}^{-\frac{1}{2}}(I) & H_{\text{per}}^{-\frac{1}{2}}(I) \end{array} \right),$$

is holomorphic and uniformly bounded.

3 Shape Holomorphy of the Combined Integral Operator

For $r \in \mathfrak{T}$, we consider the *combined integral operator* on Γ_r

$$\mathbf{A}_r^{(\omega, \eta)} := \frac{1}{2} \text{Id} + \mathcal{K}_r^{(\omega)} - \eta \mathcal{V}_r^{(\omega)},$$

where $\eta \in \mathbb{R} \setminus \{0\}$ is the coupling parameter. It is well-known that $\mathbf{A}_r^{(\omega, \eta)} : L^2(\Gamma_r) \rightarrow L^2(\Gamma_r)$ is an isomorphism for boundaries of class \mathcal{C}^2 and for all angular frequencies $\omega \in \mathbb{R}_+$. By means of the pullback operator, for $r \in \mathfrak{T}$, we now define

$$\hat{\mathbf{A}}_r^{(\omega, \eta)} := \tau_r \circ \mathbf{A}_r^{(\omega, \eta)} \circ \tau_r^{-1} \in \mathcal{L}_{\text{iso}}(L^2(I), L^2(I)),$$

Theorem 2 *There exists $\delta > 0$ such that the operator $\hat{\mathbf{A}}_r^{(\omega, \eta)}$ admits an extension to \mathfrak{T}_δ , denoted by $\tilde{\hat{\mathbf{A}}}_{r, \mathbb{C}}^{(\omega, \eta)}$, such that the map $r \in \mathfrak{T}_\delta \rightarrow \tilde{\hat{\mathbf{A}}}_{r, \mathbb{C}}^{(\omega, \eta)}$ is holomorphic and uniformly bounded.*

By means of BIODs, the sound-soft scattering problem by an incoming plane wave $\exp(i\omega \mathbf{d} \cdot \mathbf{r})$ (\mathbf{d} is unitary direction of propagation) may be reduced to the following BIE: find $\hat{\varphi}_r \in L^2(\Gamma)$ such that $\hat{\mathbf{A}}_r^{(\omega, \eta)} \hat{\varphi}_r := \hat{f}_r$, where $\hat{f}_r^{(\omega)} = -\exp(i\omega \mathbf{d} \cdot \mathbf{r}) \in L^2(\Gamma)$, for all $r \in \mathfrak{T}$. The aforementioned BIE is well-posed for all $\omega \in \mathbb{R}_+$ and all $r \in \mathfrak{T}$. We define the so-called *domain-to-solution map* $r \in \mathfrak{T} \rightarrow \hat{\varphi}_r := \left(\hat{\mathbf{A}}_r^{(\omega, \eta)}\right)^{-1} \hat{f}_r^{(\omega)}$. As a consequence of Theorem 2, the fact that linear isomorphisms are open in the space of bounded linear operators and that the inversion operation of linear isomorphisms is holomorphic, one may establish the following result.

Theorem 3 *There exists $\delta > 0$ such that the domain-to-solution map $\hat{\varphi}_r \in L^2(\Gamma)$ admits an extension to \mathfrak{T}_δ , denoted by $\hat{\varphi}_{r, \mathbb{C}}$, such that $r \in \mathfrak{T}_\delta \rightarrow \hat{\varphi}_{r, \mathbb{C}} := \left(\hat{\mathbf{A}}_{r, \mathbb{C}}^{(\omega, \eta)}\right)^{-1} \hat{f}_{r, \mathbb{C}}^{(\omega)}$, is holomorphic and uniformly bounded, where $\hat{f}_{r, \mathbb{C}}^{(\omega)} := -\exp(i\omega \mathbf{d} \cdot \mathbf{r})$, for $r \in \mathfrak{T}_\delta$.*

4 Bayesian Shape Inversion

Our goal is to compute the expected value of the boundary by taking into account noisy measurements. We consider the following set of affine, parametric boundary representations $\mathfrak{T} = \{r_{\mathbf{y}} : \mathbf{y} \in \mathbb{U}\}$, where $r(\mathbf{y}) := r_0 + \sum_{j=1}^s y_j r_j$, $\mathbf{y} := \{y_j\}_{j \in \mathbb{N}} \in \mathbb{U} := [-1, 1]^s$ and $s \in \mathbb{N}$ is the dimension truncation. Here $r_j \in \mathcal{C}_{\text{per}}^2(\Gamma, \mathbb{R}^2)$ and $\{\|r_j\|_{\mathcal{C}_{\text{per}}^2(\Gamma, \mathbb{R}^2)}\}_{j \in \mathbb{N}} \in \ell^p(\mathbb{N})$, for some $p \in (0, 1)$. Provided $\text{ND} \in \mathbb{N}$ unitary directions $\{\mathbf{d}_i\}_{i=1}^{\text{ND}}$, we define the uncertainty-to-observation $\mathcal{G} : \mathbf{y} \rightarrow \mathbb{C}^{\text{ND}^2}$, where the output vector contains the far-field measured in the unitary directions \mathbf{d}_i , $i = 1, \dots, \text{ND}$, and produced by the domain-to-solution map, namely $\hat{\varphi}_{\mathbf{y}} := \hat{\varphi}_{r_{\mathbf{y}}}$ when the scattered object is illuminated by an incoming plane wave with direction \mathbf{d}_j , $j = 1, \dots, \text{ND}$.

The measured data Υ is modeled as the observation produced by a fixed boundary \mathbf{y}^* plus an additive Gaussian noise ϱ , namely $\Upsilon = \mathcal{G}(\mathbf{y}^*) + \varrho$, where $\varrho \sim \mathcal{N}(0, \Sigma)$ and $\Sigma \in \mathbb{R}_{\text{sym}}^{\text{ND}^2 \times \text{ND}^2}$ is the covariance matrix. We measure the misfit between the available noisy data and the output of the uncertainty-to-observation map using the following *least square potential*: $\Phi_\Sigma^\Upsilon(\mathbf{y}) = \frac{1}{2}(\Upsilon - \mathcal{G}(\mathbf{y}))^\top \Sigma^{-1}(\Upsilon - \mathcal{G}(\mathbf{y}))$.

According to Bayes' Theorem [2], the expected value of $r(\mathbf{y})$ with respect to the conditional distribution of \mathbf{y} provided noisy mea-

surements Υ is given by

$$\mathbb{E}^{\mathbf{y}|\Upsilon}[r] = \frac{1}{Z_\Sigma} \int_{\mathbb{U}} r(\mathbf{y}) \exp(-\Phi_\Sigma^\Upsilon(\mathbf{y})) \mu_0(d\mathbf{y}),$$

where

$$Z_\Sigma := \int_{\mathbb{U}} \exp(-\Phi_\Sigma^\Upsilon(\mathbf{y})) \mu_0(d\mathbf{y})$$

and $\mu_0(d\mathbf{y}) := \prod_{j=1}^s dy_j$.

5 Numerical Results

In Figure 1 we obtain the expected value of the boundary by incorporating noisy measurements and using the Bayesian framework. The high-dimensional integrals arising in this approach are computed using higher order Quasi-Monte Carlo integration rules, as in [3]. This technique is immune to the *curse of dimensionality*, namely convergence rates do not depend on the dimension of the parameter space \mathbb{U} . Shape holomorphy of the BIODs is the key mathematical concept to justify this property.

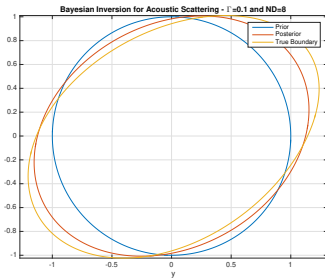


Figure 1: Prior and posterior expectations of the boundary for $\text{ND} = 8$, $s = 48$, $\omega = 1$ and $\Sigma = 1$.

6 Acknowledgments

This work was partially funded by ETH Zürich through Grant ETH4417-1.

References

- [1] A. Chkifa, A. Cohen, and Ch. Schwab. Breaking the curse of dimensionality in sparse polynomial approximation of parametric PDEs. *Journal de Mathématiques Pures et Appliquées*, 103(2):400–428, 2015.
- [2] Ch. Schwab and A. M. Stuart. Sparse deterministic approximation of Bayesian inverse problems *Inverse Problems*, 28(4), 2012.
- [3] R. N. Gantner and M. D. Peters. Higher-Order Quasi-Monte Carlo for Bayesian shape inversion. *SIAM/ASA J. Uncertainty Quantification*. 6(2):707–736, 2018.

**Discretisation of the EFIE using the H_{div} inner product
without the Buffa-Christiansen basis function**

Kazuki Niino^{1,*}, Naoshi Nishimura²

¹Graduate School of Informatics, Kyoto University, Kyoto, Japan

²Graduate School of Informatics, Kyoto University, Kyoto, Japan

*Email: niino@i.kyoto-u.ac.jp

Abstract

A discretisation method for the electric field integral equation (EFIE) using the H_{div} inner product is discussed. The EFIE is known to suffer from the low-frequency breakdown, which makes the EFIE have bad accuracy for problems with small frequencies. In a proceeding study, we found that using the H_{div} inner product for the Galerkin method with the Buffa-Christiansen (BC) basis function resolves the low-frequency breakdown. In this paper, we propose a new implementation of the discretisation method using the H_{div} inner product without the use of the Buffa-Christiansen (BC) basis function. In this implementation, the EFIE can be discretised with only the Raviart-Thomas function and the piecewise constant function.

Keywords: EFIE, Low-frequency breakdown

1 Introduction

The EFIE [1], which is one of formulations of integral equations for solving electromagnetic wave scattering problems, is known to have several problems from the numerical point of view, such as the low-frequency breakdown. Many formulations of EFIEs avoiding the low-frequency breakdown have been studied [2, 3]. We also found that using the H_{div} inner product instead of the standard L^2 inner product in the Galerkin method solves the low-frequency breakdown [4]. This method, however, requires the implementation of the BC basis functions, which are defined on the barycentric elements having six times more triangular elements than an original mesh used for discretising the EFIE. In this paper, we propose a new implementation of the discretisation method using the H_{div} inner product without the use of the Buffa-Christiansen (BC) basis function.

2 Formulation

The domain of a scatterer is denoted by Ω^i and its surface Γ is sufficiently smooth. We consider

the following electric field integral equation

$$i\omega\mu Q\mathbf{j} = \mathbf{E}^{\text{inc}} \times \mathbf{n}, \quad (1)$$

defined on Γ , where ω is the frequency, μ is the permeability, \mathbf{j} is the unknown electric current on Γ ,

$$Q\mathbf{j} = \mathbf{n} \times \int_{\Gamma} \left\{ G(\mathbf{x} - \mathbf{y}) + \frac{1}{k^2} \nabla \nabla G(\mathbf{x} - \mathbf{y}) \right\} \mathbf{j}(\mathbf{y}) dS_{\mathbf{y}},$$

and G is Green's function of the Helmholtz equation: $G(\mathbf{x} - \mathbf{y}) = \frac{e^{ik|\mathbf{x} - \mathbf{y}|}}{4\pi|\mathbf{x} - \mathbf{y}|}$.

3 Discretisation of the EFIE with the H_{div} inner product

In this section, we briefly introduce the discretisation method using the H_{div} inner product for the EFIE in (1) and describe an implementation of this method without the BC basis function. Readers can refer to [4] for more details.

A standard Galerkin method for the EFIE utilises the L^2 inner product to discretise the EFIE in (1) as follows:

$$(\mathbf{n} \times \mathbf{t}_i, i\omega\mu Q\mathbf{j})_{L^2_{\Gamma}(\Gamma)} = (\mathbf{n} \times \mathbf{t}_i, \mathbf{E}^{\text{inc}} \times \mathbf{n})_{L^2_{\Gamma}(\Gamma)}, \quad (2)$$

where $(\cdot, \cdot)_{L^2_{\Gamma}(\Gamma)}$ denotes the L^2 inner product of tangent-vector functions on Γ and \mathbf{t}_i is the Raviart-Thomas function of first order. This equation is known to suffer from the so called low-frequency breakdown, in which the discretised EFIE shows bad accuracy for small frequencies. Also, solving this equation with iteration methods such as the GMRES requires much computational time since the coefficient matrix is ill-conditioned.

Instead of the L^2 inner product, one can use the H_{div} inner product

$$(\mathbf{u}, \mathbf{v})_{H_{\text{div}}(\Gamma)} := (\mathbf{u}, \mathbf{v})_{L^2_{\Gamma}(\Gamma)} + c(\nabla_S \cdot \mathbf{u}, \nabla_S \cdot \mathbf{v})_L$$

for applying the Galerkin method to the EFIE:

$$(\mathbf{s}_i, i\omega\mu Q\mathbf{j})_{H_{\text{div}}(\Gamma)} = (\mathbf{s}_i, \mathbf{E}^{\text{inc}} \times \mathbf{n})_{H_{\text{div}}(\Gamma)},$$

where \mathbf{s}_i is the Buffa-Christiansen (BC) basis function. The LHS of this equation is calculated as

$$(\mathbf{s}_i, i\omega\mu Q\mathbf{j})_{H_{\text{div}}(\Gamma)} = (\mathbf{s}_i, i\omega\mu Q\mathbf{j})_{L^2_\Gamma(\Gamma)} - i\omega\mu c(\nabla_S \cdot \mathbf{s}_i, \mathbf{n} \cdot \Psi\mathbf{j})_{L^2(\Gamma)} \quad (3)$$

where ∇_S denotes the surface gradient on Γ and $\Psi\mathbf{j} = \int_\Gamma \nabla G \times \mathbf{j} dS_y$. It is known that this formulation can solve the low-frequency breakdown by setting the parameter $c = 1/k^2$ [4]. Also one can easily find a preconditioner for this equation. The LHS in (3), which corresponds to the coefficient matrix of the discretised EFIE, can be calculated as

$$(\mathbf{s}_i, i\omega\mu Q\mathbf{j})_{H_{\text{div}}(\Gamma)} = (\mathbf{s}_i, i\omega\mu \tilde{Q}\mathbf{j})_{L^2_\Gamma(\Gamma)}$$

where $\tilde{Q} = Q + \nabla_S \mathbf{n} \cdot \Psi$. One can prove that the operator \tilde{Q} multiplied with $i\omega\varepsilon\mathcal{S} = i\omega\varepsilon\mathbf{n} \times \int_\Gamma G(x-y) \cdot dS_y$ is well-conditioned in a sense that the equation $i\omega\varepsilon\mathcal{S} \cdot \tilde{Q} = \mathcal{R} + \mathcal{K}$ is satisfied, where \mathcal{R} is an operator on Γ whose eigenvalues are $1/4$ and $-1/4$ and \mathcal{K} is a compact operator [4]. Hence the matrix $T_{L^2}^{\prime-1} \tilde{S}_{L^2}^{BC} T_{L^2}^{\prime-1} A_{H_{\text{div}}}^{BC}$ is expected to be well-conditioned where

$$\begin{aligned} (A_{H_{\text{div}}}^{BC})_{ij} &= (\mathbf{s}_i, i\omega\mu Q\mathbf{t}_j)_{H_{\text{div}}(\Gamma)}, \\ (\tilde{S}_{L^2}^{BC})_{ij} &= (\mathbf{n} \times \mathbf{s}_i, i\omega\varepsilon \tilde{S}\mathbf{s}_j)_{L^2(\Gamma)}, \\ (T_{L^2}^{\prime})_{ij} &= (\mathbf{n} \times \mathbf{s}_i, \mathbf{t}_j)_{L^2(\Gamma)}, \\ (T_{L^2}^{\prime\prime})_{ij} &= (\mathbf{s}_i, \mathbf{s}_j)_{L^2(\Gamma)}. \end{aligned}$$

Now we propose an implementation of the discretisation method with the H_{div} inner product without the BC basis function. The first term of the RHS in (3) with the preconditioner \tilde{S} can be discretised with only the Raviart-Thomas function as $T_{L^2}^{-1} \tilde{S}_{L^2}^{RT} T_{L^2}^{-1} A_{H_{\text{div}}}^{RT}$ where

$$\begin{aligned} (A_{H_{\text{div}}}^{RT})_{ij} &= (\mathbf{n} \times \mathbf{t}_i, i\omega\mu Q\mathbf{t}_j)_{H_{\text{div}}(\Gamma)}, \\ (\tilde{S}_{L^2}^{RT})_{ij} &= (\mathbf{t}_i, i\omega\varepsilon \tilde{S}(\mathbf{n} \times \mathbf{t}_j))_{L^2(\Gamma)}, \\ (T_{L^2})_{ij} &= (\mathbf{t}_i, \mathbf{t}_j)_{L^2(\Gamma)}. \end{aligned}$$

Although the second term cannot be discretised in the same way, one can move the surface derivative ∇_S in the operator $\nabla_S \mathbf{n} \cdot \Psi$ to \tilde{S} . This operation leads us to the discretisation of the second

term as $T_{L^2}^{-1} D T_c^{-1} M$ where

$$\begin{aligned} (D)_{ij} &= \left(\mathbf{t}_i, \mathbf{n} \times \int_\Gamma \nabla G q_j dS \right)_{L^2_\Gamma(\Gamma)}, \\ (M)_{ij} &= \left(q_i, \mathbf{n} \cdot \int_\Gamma \nabla G \times \mathbf{t}_j dS \right)_{L^2_\Gamma(\Gamma)}, \\ (T_c)_{ij} &= (q_i, q_j)_{L^2(\Gamma)}, \end{aligned}$$

and q_i is the piecewise constant function.

4 Numerical example

We consider a spherical scatterer with the radius 0.25 illuminated by a plane wave. We compare the proposed discretisation method and the conventional method in (2). The linear equation is solved by the GMRES with the error tolerance 10^{-5} and the maximum iteration number 1500. Figure 1 shows the iteration number of the GMRES for the three kinds of preconditioning. The

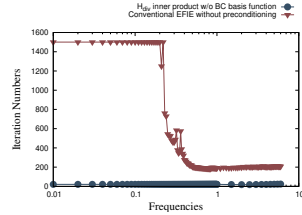


Figure 1: The iteration number of the GMRES.

iteration number of the proposed method is less than that of the standard EFIE even in small frequencies.

5 Conclusions

We proposed an implementation of the discretisation method using the H_{div} inner product without the BC basis function.

References

- [1] W. C. Chew. *Waves and fields in inhomogeneous media*. IEEE press New York, 1995.
- [2] Zhi Guo Qian and Weng Cho Chew. *Microwave and Optical Technology Letters*, 50(10):2658–2662, 2008.
- [3] F.P. Andriulli, K. Cools, I. Bogaert, and E. Michielssen. *IEEE Transactions on Antennas and Propagation*, 61(4):2077–2087, 2013.
- [4] Kazuki Niino, Sho Akagi, and Naoshi Nishimura. *Antennas and Propagation, IEEE Transactions on*, 65(6):3102–3113, 2017.

Interior Penalty Discontinuous Galerkin BEM for the Helmholtz equation: Theoretical and numerical analysis

Messai Nadir-Alexandre^{1,*}, Pernet Sébastien²

¹ONERA/DTIS, Université fédérale de Toulouse F-31000, Toulouse France

²ONERA/DTIS, Université fédérale de Toulouse F-31000, Toulouse France

*Email: nadir-alexandre.messai@onera.fr

Abstract

In this study we propose the construction and the first *a priori* error analysis of an interior penalty Galerkin numerical scheme applied to the integral equation related to the Helmholtz problem. Our main results are an error bound in a broken norm suited to the problem and in a more classic L^2 norm. Various formulation choices and penalty functions are theoretically and numerically discussed. We confirm the advantage of using a symmetric formulation in the context of a DG in integral equations. We will present an extensive numerical study of the scheme, particularly the h and p convergence. The very important case of nonconforming mesh and varying polynomial order are treated, and indicates the method's ability to handle hp refinement strategies.

Keywords: discontinuous Galerkin method, integral equation, acoustics

1 Introduction

In this study we explore a discontinuous approach for solving the family of integral equations arising in the field of acoustics. The use of this nonconforming methodology could indeed bring significant advantages in the processes of local refining procedure and mesh generation of complex objects. As far as we know very little was investigated about discontinuous approximation of integral problems. Our work is an extension of [1] to oscillating kernels.

Here we deal with the following problem model:

$$\mathcal{W}u = f \text{ in } H^{\frac{1}{2}}(\Gamma) \quad (1)$$

which arises in the integral formulation of a sound-hard scattering problem. We note Γ a polyhedral closed surface, u the unknown of the problem and \mathcal{W} the double layer potential operator defined for all $x \in \Gamma$:

$$\mathcal{W}u(x) = -\frac{\partial}{\partial \mathbf{n}(x)} \int_{\Gamma} u(y) \frac{\partial g(x, y)}{\partial \mathbf{n}(y)} d\Gamma(y) \quad (2)$$

with g being the Helmholtz kernel. We also need the simple layer potential operator defined by $\mathcal{V}u = g \star u$, with \star being the convolution product.

2 Discontinuous Galerkin scheme

A discontinuous numerical scheme is obtained from (1) by a classic procedure: we split the weak formulation on each element K of the mesh \mathcal{T}_h and use integration per parts formula in order to exhibit the trace of the trial function on the skeleton of the mesh γ_h . At the end, we seek a numerical solution u_h such that:

$$\forall v \in X_{hp}, \quad A_h^\theta(u_h, v) = \langle f, v \rangle_{\Gamma} \quad (3)$$

with A_h^θ being a bilinear form such that:

$$\begin{aligned} A_h^\theta(u, v) = & \langle \mathcal{V} \mathbf{curl}_h u, \mathbf{curl}_h v \rangle_{\Gamma} \\ & - k^2 \langle \mathcal{V}(u_h \mathbf{n}), v \mathbf{n} \rangle_{\Gamma} \\ & + \langle T u_h, v \rangle_{\gamma_h} + P^\sigma(u_h, v) + \theta \langle T v, u_h \rangle_{\gamma_h} \end{aligned} \quad (4)$$

with $\langle T u, v \rangle_{\gamma_h} = \langle \mathbf{t}_e \cdot \mathcal{V} \mathbf{curl}_h u, v \rangle_{\gamma_h}$. The parameter θ can be tuned in order to get symmetric ($\theta = 1$) or anti symmetric ($\theta = -1$) flux. A penalty term denoted P^σ must be added to stabilise the formulation. We classically choose $P^\sigma(u, v) = \sigma_h \langle [u], [v] \rangle_{\gamma_h}$, with $[u]$ being the jump and $\sigma_h : \gamma_h \rightarrow \mathbb{R}^+$ the penalty function which is essential in order to stabilise the discrete problem. In this work we choose $\sigma_h = \sigma_o \frac{h^{n_h}}{p^{n_p}}$, with $n_h > 0$, $n_p > 0$ and $\sigma_o > 0$ being parameters to determine.

The approximation space X_{hp} is a piece-wise polynomial space of order p_K on each element $K \in \mathcal{T}_h$. We equip this latter with the following broken norm:

$$\begin{aligned} \|u\|_{dg}^2 = & \|\mathbf{curl}_h u\|_{H^{-\frac{1}{2}}(\Gamma)}^2 + \|u\|_{L^2(\Gamma)}^2 \\ & + \|\sigma_h^{\frac{1}{2}} u\|_{L^2(\gamma_h)}^2. \end{aligned} \quad (5)$$

We obtain the following *a priori* error bound.

Theorem 1 Let $u \in H^r(\Gamma)$ be the solution of problem (1), with $r \geq 1$. Let σ_h be the penalty function from definition above with $n_h > 3$ and $n_p > 4$.

Let u_h denote the DG approximation defined in problem (3). There exists $h_o > 0$ and $p_o > 1$ such that for all $0 < h < h_o$ and $p > p_o$ with $X_{hp} \subset X_{h_o p_o}$, the following error estimate holds:

$$\|u - u_h\|_{dg} \leq \max_{K \in \mathcal{T}_h} \left\{ \frac{h_K^{\frac{n_h-3}{2} + \mu_K}}{p_K} \right\} \|u\|_{H^r(\Gamma)} + \max_{K \in \mathcal{T}_h} \left\{ \frac{h_K^{\min(0, \frac{n_h-4}{2})}}{p_K} \right\} \inf_{v \in X_{hp} \cap C^o(\Gamma)} \|v - u\|_{dg},$$

with $\mu_K = \min(p_K + 1, r)$.

One can see that the theoretical rate of convergence explicitly depends on the penalty parameters. More precisely depending on the selected values three ranges of convergence appear (in the case of h convergence):

- $r + \frac{n_h-5}{2} \leq 0$: the error isn't controlled by the theorem. Nothing can be said about the convergence of the numerical scheme.
- $\frac{1}{2} \leq r + \frac{n_h-4}{2} \leq r$: convergence rate of $\mathcal{O}(h^{r + \frac{n_h-5}{2}})$ which is slower than the BEM rate of convergence.
- $n_h \geq 4$: convergence rate of $\mathcal{O}(h^{r-\frac{1}{2}})$, as fast as the conforming BEM method.

3 Numerical results

In the presentation we will present numerical experiments which illustrate the convergence rates predicted by the theorem. We show below two illustrative examples.

3.1 Nonconforming experiment

We show some numerical results in a hp nonconforming situation. We consider a cube illuminated by plane wave. We consider the mesh in figure 3.1, with the upper part being a P^4 approximation and the lower part a P^2 approximation. The corresponding solution is can be seen figure 3.1. It tends to show the nonconforming interface doesn't pollute (at least visually) the numerical solution.

Those preliminary tests give hope in the actual possibility of using this kind of methods for solving real problems.

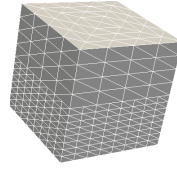


Figure 1: Mesh used

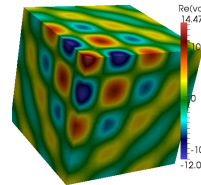


Figure 2: Real part of the numerical solution

3.2 Comparison of the formulations

On figure 3.2 we compare the three formulations (symmetric, anti symmetric and natural). We run an example with the same setting. As for other DG, we note the symmetric formulation reestablish a lot better the continuity of the numerical solution.

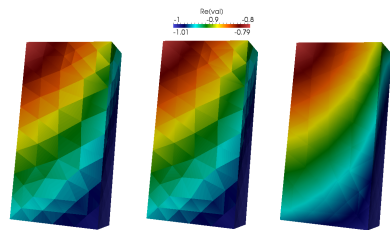


Figure 3: real part of the solutions for all the formulations. From left to right: anti-symmetric ($\theta = -1$), natural ($\theta = 0$) and symmetric formulation ($\theta = 1$)

4 References

References

- [1] Norbert Heuer and Salim Meddahi. Discontinuous Galerkin hp -BEM with quasi-uniform meshes. *arXiv:1206.6351 [math]*, June 2012.

A stable integral equation for a mixed acoustic transmission problem

Sarah Eberle¹, Francesco Florian^{2,*}, Ralf Hiptmair³, Stefan Sauter²

¹Institut für Mathematik, Goethe-Universität Frankfurt am Main, Frankfurt am Main, Germany

²Institut für Mathematik, Universität Zürich, Zürich, Switzerland

³Seminar für Angewandte Mathematik, ETH Zürich, Zürich, Switzerland

*Email: francesco.florian@uzh.ch

Abstract

In physics and engineering there are many important applications where it is essential to obtain information on material properties inside (large) solid objects. For this purpose, typically, time-depending waves are sent into the solid and the scattered waves are recorded and used to solve the governing mathematical equations for the quantity of interest.

In this paper we consider the acoustic wave equation as our model problem and derive a stable formulation as retarded potential integral equations for general boundary and transmission conditions.

An efficient solution of the resulting problem is addressed by means of the boundary element method and convolution quadrature.

Keywords: Boundary Element Methods, wave equation, impedance boundary condition, convolution quadrature

1 Introduction

We consider the *wave equation*

$$\begin{cases} \rho_1^2 \partial_t^2 u_1 + a_1^2 \Delta u_1 = 0 & \text{in } \Omega_1 \times [0, T] \\ \rho_2^2 \partial_t^2 u_2 + a_2^2 \Delta u_2 = 0 & \text{in } \Omega_2 \times [0, T] \\ [u]_{\Gamma_{1,2}} = [a^2 \frac{\partial u}{\partial n}]_{\Gamma_{1,2}} = 0 & \text{on } \Gamma_J \times [0, T] \\ u = g_D & \text{on } \Gamma_D \times [0, T] \\ a \frac{\partial u}{\partial n_I} - T * \dot{u} = d_I & \text{on } \Gamma_I \times [0, T] \\ a \frac{\partial u}{\partial n_N} = d_N & \text{on } \Gamma_N \times [0, T] \\ u(0, x) = \dot{u}(0, x) = 0 & \text{in } \Omega \end{cases} \quad (1)$$

in a domain $\Omega \subseteq \mathbb{R}^3$ split into $\Omega = \bar{\Omega}_1 \cup \bar{\Omega}_2$ for some positive parameters $a_i = a|_{\Omega_i}$, $\rho_i = \rho|_{\Omega_i}$ for $i \in \{1, 2\}$; Ω_1 and Ω_2 are open sets, $\bar{\Gamma}_D \cup \bar{\Gamma}_N \cup \bar{\Gamma}_I = \partial\Omega$, $\Gamma_J := \partial\Omega_1 \cap \partial\Omega_2$ and T is a dissipative operator acting on the boundary Γ_I . Typical examples include operators giving rise to impedance type and DtN type boundary conditions.

In order to transform the problem to a boundary integral equation, we introduce $\Gamma_j := \partial\Omega_j$, $j \in \{1, 2\}$, $\Gamma := \Gamma_1 \cup \Gamma_2$, and γ_D, γ_N the trace and

co-normal trace operators. This allows to introduce the single and double layer potentials, defined for functions φ and $\psi : \Gamma_j \rightarrow \mathbb{C}$ by

$$(\mathcal{S}_j * \varphi)(x, t) := \int_{\Gamma_j} \varphi(y, t - \frac{\rho_j \|x-y\|}{a_j}) \frac{1}{4\pi a_j^2 \|x-y\|} ds_y$$

$$(\mathcal{D}_j * \psi)(x, t) := \int_{\Gamma_j} \left(\gamma_{N, \Gamma_j, y} \frac{\psi(z, t - \frac{\rho_j \|x-y\|}{a_j})}{4\pi a_j^2 \|x-y\|} \right) \Big|_{z=y} ds_y,$$

$\forall (x, t) \in (\mathbb{R}^3 \setminus \Gamma_j) \times [0, T]$, where ds_y denotes the surface measure on Γ_j .

We will extend the approach developed in [2] to the more general interface and boundary conditions considered in eq. (1): we use Green's representation formula and insert boundary conditions and jump relations from eq. (1), to obtain a system of *retarded potential integral equations* of convolution type:

$$\mathcal{B} * \eta = \mathbf{d}, \quad (2)$$

where η is a function (consisting of the unknown Cauchy data) in an appropriate Sobolev space of the boundary $\partial\Omega_1 \cup \partial\Omega_2$; \mathbf{d} collects the right hand side of the jump relations (i.e. 0) and boundary conditions (i.e. g_D, d_N, d_I) in eq. (1); \mathcal{B} is built from the boundary operators

$$\begin{aligned} \mathcal{V}_j * \varphi_j &= \gamma_D \Gamma_j (\mathcal{S}_j * \varphi_j) \\ \mathcal{K}_j * \psi_j &= \gamma_D \Gamma_j (\mathcal{D}_j * \psi_j) \\ \mathcal{K}'_j * \varphi_j &= \gamma_N \Gamma_j (\mathcal{S}_j * \varphi_j) \\ \mathcal{W}_j * \psi_j &= -\gamma_N \Gamma_j (\mathcal{D}_j * \psi_j) \end{aligned}$$

for $j \in \{1, 2\}$, their restrictions to certain subsets of the surface Γ_j , the Dirac distribution δ and the operator T ; we refer to [3] for the details.

This system can be equivalently restated by applying a Laplace transform with respect to time to all equations; in [3] a proof is given that the derived formulation in the Laplace domain is continuous, coercive, and hence well posed;

by standard techniques, this carries over to the well posedness of eq. (2).

2 Integro-differential equations in the Laplace domain

We start from a generic convolution integral $h(t) = f * g(t) = \int_0^t f(t-\tau)g(\tau)d\tau$. We replace f by the inverse Laplace transform of its Laplace transform:

$$h(t) = \int_0^t \frac{1}{2\pi i} \int_{c+i\mathbb{R}} e^{s(t-\tau)} \hat{f}(s) ds g(\tau) d\tau = \frac{1}{2\pi i} \int_{c+i\mathbb{R}} \hat{f}(s) \int_0^t e^{s(t-\tau)} g(\tau) d\tau ds. \tag{3}$$

The inner integral $U(s, t) := \int_0^t e^{s(t-\tau)} g(\tau) d\tau$ is the solution of the initial value problem

$$y'(t) = sy(t) + g(t) \quad y(0) = 0. \tag{4}$$

We rewrite our problem (2) using this method; applying the inverse Laplace transform to the Laplace transformed equation, we end up with a system of *integro-differential equations*:

$$\begin{cases} \frac{1}{2\pi i} \int_{\gamma} \mathbf{BZ} = \mathbf{d} \\ \partial_t \mathbf{Z}(s, t) = s\mathbf{Z}(s, t) + \boldsymbol{\eta}(t), \mathbf{Z}(s, 0) = 0; \end{cases} \tag{5}$$

now g, \hat{f}, h in eq. (3) are substituted by the unknown $\boldsymbol{\eta}$, the Laplace transform of \mathcal{B} (denoted by \mathbf{B}), and the boundary conditions and jump relations \mathbf{g} ; the auxiliary function U is now replaced by \mathbf{Z} ; we emphasize that here $\boldsymbol{\eta}, \mathbf{g}, \mathbf{U}$ are vector-valued¹.

3 Convolution quadrature (CQ)

In this section we propose a method for discretizing eq. (5). We start again with a general setting, and follow [1]: eq. (4) can be approximated by a discretization, e.g. by an implicit A -stable Runge-Kutta scheme on equidistant points² $t_j := j\Delta t$; we consider $h_n := h(t_n)$ at these discrete points, so that a z -transform yields:

$$\sum_{n=0}^{\infty} h_{n+1} z^t = \mathbf{b}^T \mathbf{A}^{-1} \hat{f} \left(\frac{\Delta(z)}{\Delta t} \right) \sum_{n=0}^{\infty} \mathbf{g}_n z^n, \tag{6}$$

where $\Delta(z) = \left(\mathbf{A} - \frac{z}{1-z} \mathbb{1} \mathbf{b}^T \right)^{-1}$, \mathbf{g}_k is the vector containing the values of g at $t_n + c_j \Delta t$ and $\mathbf{A}, \mathbf{b}, \mathbf{c}$ define the Runge-Kutta method.

¹We refer to [3] for the details

²This can be generalized to consider intervals of variable length, see e.g. [4]

Suppose now that \hat{f} is analytic, thus

$$\hat{f} \left(\frac{\Delta(z)}{\Delta t} \right) = \sum_{n=0}^{\infty} W_n^{\Delta t}(\hat{f}) z^n, \tag{7}$$

where

$$W_n^{\Delta t}(\hat{f}) = \frac{1}{2\pi i} \int_{\gamma} \hat{f} \left(\frac{\Delta(z)}{\Delta t} \right) z^{-n-1} dz \approx \frac{R^{-n}}{L} \sum_{l=0}^{L-1} \hat{f} \left(\frac{\Delta(R\zeta^{-l})}{\Delta t} \right) \zeta^{nl}, \quad \zeta = e^{\frac{2\pi i}{L}}$$

for $\gamma = Re^{i\theta}$, $0 \leq \theta \leq 2\pi$, and the last sum can be computed via a fast Fourier transform. We insert this and eq. (7) into eq. (6), to obtain a discrete convolution:

$$h_{n+1} = \mathbf{b}^T \mathbf{A}^{-1} \sum_{j=0}^n W_{n-j}^{\Delta t}(\hat{f}) g_j. \tag{8}$$

Next we apply CQ to our original problem in the form of eq. (5). It can be treated as eqs. (6) and (7), resulting in a discretization of the form (8). The resulting system is then block-triangular and has to be solved for $\boldsymbol{\eta}$.

References

- [1] L. Banjai, M. Messner, and M. Schanz. "Runge-Kutta convolution quadrature for the Boundary Element Method". In: *Comput. Methods Appl. Mech. Engrg.* (2012), pp. 90-101.
- [2] X. Claeys, R. Hiptmair, C. Jerez-Hanckes, and S. Pintarelli. "Novel Multi-Trace Boundary Integral Equations for Transmission Boundary Value Problems". *Unified Transform for Boundary Value Problems: Applications and Advances*. SIAM, 2014, pp. 227-258.
- [3] S. Eberle, F. Florian, R. Hiptmair, and S. Sauter. "Stable Boundary Integral Formulation of an Acoustic Wave Transmission Problem with Mixed Boundary Conditions". (In preparation)
- [4] M. Lopez-Fernandez and S. Sauter. "Generalized convolution quadrature with variable time stepping". In: *IMA Journal of Numerical Analysis* 33.4 (2013), pp. 1156-1175.

FastMMLib: a generic library for Fast Multipole Methods

Eric DARRIGRAND^{1,*}, Yvon LAFRANCHE¹¹IRMAR, University Rennes 1, Rennes, France

*Email: eric.darrigrand-lacarrieu@univ-rennes1.fr

Abstract

FastMMLib is a library which provides a generic framework for Fast Multipole Methods (FMM) usable in various applications and physical contexts. The library deals with all the FMM aspects (clustering, kernel expansion, pre-calculation, matrix-vector product) but the user keeps the entire control of the application background (physics, solved equations, discretisation). The library is written in C++. Dedicated classes ensure the interaction with the user, and offer the tools to inform precisely the user application (finite element / point-wise approach; Helmholtz equation / Coulomb potential).

Keywords: FMM, C++ library, Helmholtz kernel, Coulomb potential

1 Introduction

The Fast Multipole Method (FMM) has been widely used and studied in the context of integral equations for the resolution of wave propagation phenomena in exterior domains (e.g. [2, 4]). However, the method is still rather unaccessible for academic studies due to its complicated implementation. One can find some existing codes or libraries (e.g. [3]). To complete this offer, FastMMLib has been developed with the idea to provide a generic framework for the use of Fast Multipole Methods in various applications and physical contexts. The most popular uses of the FMM are matrix-vector products where the matrix is obtained either from the discretisation of an integral equation involving the Helmholtz Green kernel or from interactions governed by the Coulomb potential. As an example, solving boundary integral equations on a domain Γ by finite elements, one has to consider matrices like

$$[M]_{ij} = \iint_{\Gamma \times \Gamma} G(x, y) \varphi_j(y) \varphi_i(x) d\gamma(y) d\gamma(x), \quad (1)$$

where $G(x, y) = e^{ik\|x-y\|} / (4\pi\|x-y\|)$, and φ_i are the finite element basis functions. In the context of the Coulomb point-wise interactions,

the matrix would reduce to $[M]_{ij} = G(x_i, y_j)$ with G the Coulomb potential.

The library is written in C++ and deals with all the FMM aspects (geometry clustering, pre-calculation, kernel expansions, FMM product, ...) but the user keeps the entire control of the discretisation of his model (finite element or point-wise discretisation, quadrature rules, calculation of the singular integrals, ...). This is made possible due to specific C++ classes which organise the interfaces between the user problem and the library. In the next section, we present the generic expansion for the kernel and show its use for the Helmholtz equation. The third section is devoted to a brief presentation of the generic class which defines the geometric context of the user.

2 The generic formulation

A fundamental ingredient of the library is the choice of a generic expansion of the interaction function G :

$$G(x, y) \approx \sum_{p=1}^S c_p g_{x,B}^{(p)} \sum_{\tilde{p}=1}^{\tilde{S}} \mathcal{T}_{B,\tilde{B}}^{(p,\tilde{p})} f_{y,\tilde{B}}^{(p,\tilde{p})}, \quad (2)$$

where S and \tilde{S} are generally truncation or discretisation parameters; c_p is a coefficient which depends only on p ; $\mathcal{T}_{B,\tilde{B}}^{(p,\tilde{p})}$ is named the *translation operator*, with B and \tilde{B} two FMM clusters containing resp. x and y (generally cubic boxes); $f_{y,\tilde{B}}^{(p,\tilde{p})}$ is named a *far moment* and is independent of the point x ; $g_{x,B}^{(p)}$ is named a *local moment* and is independent of the point y .

As an example, the Helmholtz Green kernel can be approximated by such an expansion using Gegenbauer series and the Funk-Hecke formula

$$G(x, y) \approx \sum_{p=1}^S c_p g_{x,B}^{(p)} \mathcal{T}_{B,\tilde{B}}^{(p)} f_{y,\tilde{B}}^{(p)}, \quad (3)$$

with S a discretisation parameter related to the integration on the unit sphere (from the Funk-

Hecke formula); $c_p = \frac{ik}{(4\pi)^2} w_p$, with w_p a quadrature weight; $f_{y,\tilde{B}}^{(p)} = e^{-ik\langle s_p, y - C_{\tilde{B}} \rangle}$ where $C_{\tilde{B}}$ is the center of the box \tilde{B} , and s_p a quadrature point; $g_{x,B}^{(p)} = e^{ik\langle s_p, x - C_B \rangle}$ where C_B is the center of the box B ; $\mathcal{T}_{B,\tilde{B}}^{(p)}$ the translation operator, from \tilde{B} to B derived from a truncation of the Gegenbauer series

$$\mathcal{T}_{B,\tilde{B}}^{(p)} = \sum_{\ell=1}^L (-i)^\ell (2\ell + 1) h_\ell^{(1)}(k|C_B - C_{\tilde{B}}|) P_\ell(\cos(s_p, C_B - C_{\tilde{B}})),$$

with $h_\ell^{(1)}$ the spherical Hankel function of the first kind of degree ℓ , P_ℓ the Legendre polynomial of degree ℓ , L and S estimated thanks to empirical formulae.

From the expansion of the interaction function G , e.g. (3), we deduce the expansion of the matrix $[M]$. For the matrix defined in (1),

$$[M]_{ij} \approx \sum_{p=1}^S c_p \sum_{\substack{B/B \cap \text{supp} \varphi_i \neq \emptyset \\ \tilde{B}/\tilde{B} \cap \text{supp} \varphi_j \neq \emptyset}} g_{i,B}^{(p)} \mathcal{T}_{B,\tilde{B}}^{(p)} f_{j,\tilde{B}}^{(p)}, \quad (4)$$

with

$$f_{j,\tilde{B}}^{(p)} = \int_{\tilde{B} \cap \text{supp} \varphi_j} f_{y,\tilde{B}}^{(p)} \varphi_j(y) d\gamma(y), \quad (5)$$

and $g_{i,B}^{(p)}$ defined similarly from $g_{x,B}^{(p)}$.

3 Interface with the user

The interface with the user consists of the description of the geometrical context and the discretisation strategy (e.g. a finite element method or a point-wise approach), and the identification of the physics through the interaction function (e.g. the Helmholtz Green kernel, the Coulomb potential). One of the main ingredients of this interface is the C++ class, named **Particle**, which defines the geometrical objects inducing the structure of the matrix $[M]$ of the matrix-vector product to be evaluated. The problem specific configuration is described by the user through a class of particles which derives from the **Particle** abstract class. The particles are typically finite element degrees of freedom or geometrical points in a domain. They follow a rigorous identification through a C++ class which

contains different mandatory geometrical data (localisation, close influence area, ...). The particle is also the object that should evaluate itself if it is contained in a FMM cluster, and explain how the related moments are calculated. For example, the far moment $f_{j,\tilde{B}}^{(p)}$, given in (5) is computed thanks to a member function of the class **Particle** that should corresponds to the operator which returns the quantity $f_{j,\tilde{B}}^{(p)}$ from a given function $f^{(p)} : y \mapsto f_{y,\tilde{B}}^{(p)}$. This function $f^{(p)}$ is defined in a class dedicated to the kernel.

4 State of the art and futur of FastMM-Lib

First validation results and asymptotic behaviours will be presented for the single-level FMM in the case of Helmholtz kernel. The multilevel version of the FMM is in progress. The generic aspect and the squeueleton of FastMMLib are designed in such a way that the library is also able to cope with other developments of the method like the regularized FMM introduced in [1] or kernel-independent versions of the FMM [5].

References

- [1] Philippe Chartier, Eric Darrigrand and Erwan Faou, A regular fast multipole method for geometric numerical integrations of Hamiltonian systems, *BIT*, **50** (2010), pp. 23–40.
- [2] Ronald Coifman, Vladimir Rokhlin and Stephen Wandzura, The Fast Multipole Method for the Wave Equation: A Pedestrian Prescription, *IEEE Ant. and Propag. Mag.*, **35** (1993), pp. 7–12.
- [3] Leslie Greengard and Zydrunas Gimbutas, <https://cims.nyu.edu/cmcl/fmm3dlib/fmm3dlib.html>, Courant Institute of New-York University (2012).
- [4] Jiming M. Song and Weng Cho Chew, Multilevel Fast Multipole Algorithm for Solving Combined Field Integral Equations of Electromagnetic Scattering, *Microwave Opt. Tech. Letter* **10**(1) (1995), pp. 14–19.
- [5] Lexing Ying, George Biros and Denis Zorin, A kernel-independent adaptive fast multipole algorithm in two and three dimensions, *J. Comput. Phys.* **196** (2004), pp. 591–626.

Fast Calderón preconditioning of the PCMHWT formulation for scattering by multiple dielectric particles

Antigoni Kleanthous^{1,*}, Timo Betcke¹, David P. Hewett¹, Carlos Jerez-Hanckes², Paul Escapil-Inchauspé³, Anthony J. Baran^{4, 5}

¹University College London, London, UK.

²Universidad Adolfo Ibañez, Santiago, Chile.

³Pontificia Universidad Católica de Chile, Santiago, Chile.

⁴Met Office, Exeter, UK.

⁵University of Hertfordshire, Hatfield, UK.

*Email: antigoni.kleanthous.12@ucl.ac.uk

Abstract

The discrete PMCHWT formulation for the single and multi-particle transmission problem suffers from ill-conditioning. Calderón preconditioning is a well-known technique to remedy this, reducing the number of iterations required by the linear solver, albeit at the expense of an increased number of matvecs per iteration. For single-particle problems, we find that the Calderón method is often outperformed by a simple mass-matrix preconditioner. For multi-particle problems a block-diagonal Calderón preconditioner provides a significant reduction in computational cost. We explore the capabilities of a bi-parametric Calderón preconditioner, which uses high quadrature orders and small \mathcal{H} -matrix tolerances for the assembly of the operator, but low quadrature orders and larger \mathcal{H} -matrix tolerances for the preconditioner. Finally, we investigate the effect of using only near-field interactions in the preconditioner. The performance of the different approaches is compared using the Bemp software package.

Keywords: Boundary element method, electromagnetic scattering, multiple bodies, Bemp

1 Introduction

We consider 3D electromagnetic scattering by M disjoint isotropic homogeneous dielectric scatterers in a homogeneous exterior medium. The electric and magnetic fields in the interior domains ($\mathbf{E}_m^i, \mathbf{H}_m^i$), and the exterior domain ($\mathbf{E}^e, \mathbf{H}^e$) are assumed to satisfy the time-harmonic Maxwell equations, which, written in second-order form for the electric fields $\mathbf{E}_m^i, \mathbf{E}^e$, are

$$\nabla \times (\nabla \times \mathbf{E}) - k^2 \mathbf{E} = 0,$$

where $k = k_m = \omega \sqrt{\mu_m \epsilon_m}$ and $k = k_e = \omega \sqrt{\mu_e \epsilon_e}$ are the wavenumbers for the respective domains.

The exterior field is assumed to satisfy the Silver-Müller radiation condition.

2 Boundary Integral Operators

We define electric and magnetic potentials

$$\begin{aligned} \mathcal{E}\mathbf{v}(\mathbf{x}) &:= ik \int_{\Gamma} \mathbf{v}(\mathbf{y}) G(\mathbf{x}, \mathbf{y}) d\Gamma(\mathbf{y}) \\ &\quad - \frac{1}{ik} \nabla_{\mathbf{x}} \int_{\Gamma} \nabla_{\mathbf{y}} \cdot \mathbf{v}(\mathbf{y}) G(\mathbf{x}, \mathbf{y}) d\Gamma(\mathbf{y}), \\ \mathcal{H}\mathbf{v}(\mathbf{x}) &:= \nabla_{\mathbf{x}} \times \int_{\Gamma} \mathbf{v}(\mathbf{y}) G(\mathbf{x}, \mathbf{y}) d\Gamma(\mathbf{y}), \end{aligned}$$

with $G(x, y) = \frac{\exp(ik|\mathbf{x} - \mathbf{y}|)}{4\pi|\mathbf{x} - \mathbf{y}|}$, and interior (−) and exterior (+) Dirichlet and Neumann traces

$$\begin{aligned} \gamma_D^{\pm} \mathbf{u}^{\pm}(\mathbf{x}) &= \mathbf{u}^{\pm}(\mathbf{x}) \times \mathbf{n}(\mathbf{x}), \quad \mathbf{x} \in \Gamma, \\ \gamma_N^{\pm} \mathbf{u}^{\pm}(\mathbf{x}) &= \frac{1}{ik} \gamma_D^{\pm} (\nabla \times \mathbf{u}^{\pm}(\mathbf{x})), \quad \mathbf{x} \in \Gamma. \end{aligned}$$

We define the electric and magnetic boundary integral operators (with $\{\gamma_{\cdot}\} := (\gamma_{\cdot}^+ + \gamma_{\cdot}^-)/2$)

$\mathcal{S} := \{\gamma_D\} \mathcal{E} - \{\gamma_N\} \mathcal{H}$, $\mathcal{C} := \{\gamma_D\} \mathcal{H} - \{\gamma_N\}$

and the block operators and vectors

$$\begin{aligned} \mathcal{A}_m^i &= \begin{bmatrix} C_m^i & \frac{\mu_m}{k_m} S_m^i \\ -\frac{k_m}{\mu_m} S_m^i & C_m^i \end{bmatrix}, \quad \mathbf{u}_m^i = \begin{bmatrix} \gamma_{D,m}^- \mathbf{E}_r^i \\ \frac{k_m}{\mu_m} \gamma_{N,m}^- \mathbf{I} \end{bmatrix} \\ \mathcal{A}_m^e &= \begin{bmatrix} C_m^e & \frac{\mu_e}{k_e} S_m^e \\ -\frac{k_e}{\mu_e} S_m^e & C_m^e \end{bmatrix}, \quad \mathbf{u}_m^e = \begin{bmatrix} \gamma_{D,m}^+ \mathbf{E}^s \\ \frac{k_e}{\mu_e} \gamma_{N,m}^+ \mathbf{E} \end{bmatrix} \\ \mathcal{A}_{m\ell} &= \begin{bmatrix} C_{m\ell}^e & \frac{\mu_e}{k_e} S_{m\ell}^e \\ -\frac{k_e}{\mu_e} S_{m\ell}^e & C_{m\ell}^e \end{bmatrix}, \quad \mathbf{u}_m^{inc} = \begin{bmatrix} \gamma_{D,m}^+ \mathbf{E}^{ii} \\ \frac{k_e}{\mu_e} \gamma_{N,m}^+ \mathbf{E} \end{bmatrix} \end{aligned}$$

where e.g. $S_{m\ell}^e$ is \mathcal{S} acting on scatterer ℓ , evaluated on scatterer m , with wavenumber $k = k_e$.

3 The PMCHWT formulation

The multi-particle PMCHWT formulation is

$$\mathbf{A}\mathbf{u}^s = \left(\frac{1}{2} \mathcal{I} - \mathcal{A}^i \right) \mathbf{u}^{inc}, \quad (1)$$

where

$$\mathcal{A} = \begin{bmatrix} \mathcal{A}_1^e + \mathcal{A}_1^i & \mathcal{A}_{12} & \cdots & \mathcal{A}_{1M} \\ & \mathcal{A}_{21} & \ddots & \vdots \\ & \vdots & \ddots & \mathcal{A}_{(M-1)M} \\ \mathcal{A}_{M1} & \cdots & \mathcal{A}_{M(M-1)} & \mathcal{A}_M^e + \mathcal{A}_M^i \end{bmatrix},$$

$$\mathcal{A}^i = \begin{bmatrix} \mathcal{A}_1^i & 0 & \cdots & 0 \\ & \ddots & \ddots & \vdots \\ & & & 0 \\ 0 & \cdots & 0 & \mathcal{A}_M^i \end{bmatrix}, \quad \mathbf{u}^s = \begin{bmatrix} \mathbf{u}_1^s \\ \mathbf{u}_2^s \\ \vdots \\ \mathbf{u}_M^s \end{bmatrix},$$

$$\mathcal{I} = \begin{bmatrix} \mathcal{I}_1 & 0 & \cdots & 0 \\ & \ddots & \ddots & \vdots \\ & & & 0 \\ 0 & \cdots & 0 & \mathcal{I}_M \end{bmatrix}, \quad \mathbf{u}^{inc} = \begin{bmatrix} \mathbf{u}_1^{inc} \\ \mathbf{u}_2^{inc} \\ \vdots \\ \mathbf{u}_M^{inc} \end{bmatrix}.$$

4 Calderón Preconditioning

Galerkin discretisation of (1) produces an ill-conditioned linear system, leading to slow convergence of iterative solvers. This occurs because \mathcal{C}_m^i and \mathcal{C}_m^e are compact, with eigenvalues accumulating at zero, while \mathcal{S}_m^i and \mathcal{S}_m^e are the sum of a compact operator, with eigenvalues accumulating at zero, and a hypersingular operator, with eigenvalues accumulating at infinity. As was shown in [1], one can remedy this at the continuous level by applying \mathcal{A} to (1), obtaining the preconditioned system

$$\mathcal{A}^2 \mathbf{u}^s = \mathcal{A} \left(\frac{1}{2} \mathcal{I} - \mathcal{A}^i \right) \mathbf{u}^{inc}, \quad (2)$$

which has better spectral properties than (1) due to the Calderón identities

$$\mathcal{S}^2 = -\frac{1}{4} \mathcal{I} + \mathcal{C}^2, \quad \mathcal{C}\mathcal{S} + \mathcal{S}\mathcal{C} = 0.$$

In a recent study of Calderón preconditioners for single- and multi-particle dielectric scattering [2], we found that the standard Calderón preconditioner (2) is actually no more efficient than a simple mass-matrix preconditioner in terms of the total matvecs required to reach GMRES convergence. But for the multi-particle case we found that a significant saving in computational cost can be obtained by performing block-diagonal Calderón preconditioning in which (1)

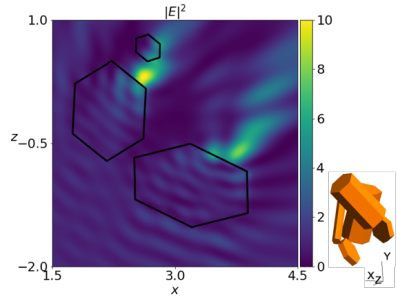


Figure 1: Squared magnitude of the electric field created by a plane incident wave travelling across an aggregate of ice crystals.

is multiplied by only the block-diagonal part \mathcal{D} of \mathcal{A} . Numerical experiments were performed for scatterers representing complex ice crystals, an example of which is shown in Fig. 1.

In [3], a bi-parametric Calderón preconditioner was introduced for the EFIE problem. We apply this bi-parametric approach to the PMCHWT multi-particle problem, with the operator \mathcal{A} discretised by RWG basis functions and assembled with a high order quadrature and small \mathcal{H} -matrix tolerance, and the preconditioner \mathcal{D} discretised by BC functions and assembled with a minimum number of quadrature points and a larger \mathcal{H} -matrix tolerance. In addition, we explore the possibility of including only the near-field interactions in the preconditioner, which results in a sparse matrix.

References

- [1] Cools, K., Andriulli, F. P. and Michielssen, A., A Calderón multiplicative preconditioner for the PMCHWT integral equation. *IEEE T. Antenn. Propag.* 59 (2011), pp. 4579–4587.
- [2] Kleanthous, A. et al., Calderón preconditioning of PMCHWT boundary integral equations for scattering by multiple absorbing dielectric particles. *J. Quant. Spectrosc. Ra.* 224 (2019), pp. 383–395.
- [3] Escapil-Inchauspé, P. and Jerez-Hanckes, C., Fast Calderón preconditioning for the electric field integral equation. *IEEE T. Antenn. Propag.* (2019).

Fast Calderón Preconditioning for Helmholtz Boundary Integral Equations

Carlos Jerez-Hanckes^{1,*}, Ignacia Fierro²¹Faculty of Engineering and Sciences, Universidad Adolfo Ibañez, Santiago, Chile²School of Engineering, Pontificia Universidad Católica de Chile, Santiago, Chile

*Email: carlos.jerez@uai.cl

Abstract

The computational performance of Calderón multiplicative preconditioners worsens as mesh size decreases due to the barycentric refinement used to construct dual basis functions. Based on coarser quadrature rules over dual cells and \mathcal{H} -matrix compression, we propose a family of fast preconditioners that significantly reduce assembly and computation times when compared to standard versions of Calderón preconditioning for the Helmholtz three-dimensional BIOs.

Keywords: Calderón Preconditioning, Hierarchical Matrices, Fast solvers

1 Introduction

Many applications require the modeling of time-harmonic wave scattering in unbounded domains by solving boundary integral equations (BIEs). Due to the non-local character of the resulting boundary integral operators (BIOs), arising linear systems are dense. Moreover, if first kind integral equations are employed, their condition numbers will worsen as discretization accuracy is improved. Consequently, the performance of iterative solvers is foiled and preconditioning techniques become mandatory.

One preconditioning strategy involves so-called *Calderón identities*, which for Helmholtz BIEs read:

$$\mathbf{V}_\kappa \mathbf{W}_\kappa = \frac{1}{4} \mathbf{1}_{H^{\frac{1}{2}}(\Gamma)} - \mathbf{K}_\kappa^2, \quad (1)$$

$$\mathbf{W}_\kappa \mathbf{V}_\kappa = \frac{1}{4} \mathbf{1}_{H^{-\frac{1}{2}}(\Gamma)} - \mathbf{K}_\kappa'^2, \quad (2)$$

wherein the weakly singular BIO (\mathbf{V}_κ) can serve as a preconditioner for the hyper-singular one (\mathbf{W}_κ) and viceversa.

Numerically, Calderón Multiplicative Preconditioners (CMP) are built as follows [1, 2]. Let $\mathbf{A} : X \rightarrow Y$ and $\mathbf{B} : Y \rightarrow X$ denote \mathbf{V}_κ and \mathbf{W}_κ and vice-versa, (cf. (1) and (2) wherein X and Y are alternatively $H^{\pm 1/2}(\Gamma)$). Set discrete spaces $X_h \subset X$ and $Y_h \subset Y$ over meshes of characteristic length h , such that $\dim(X_h) =$

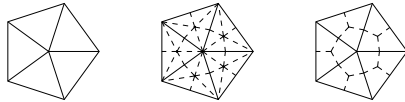


Figure 1: Primal, barycentric and dual meshes for piecewise-constant basis functions.

$\dim(Y_h)$, to find discretizations for \mathbf{A} and \mathbf{B} (\mathbf{A}_h and \mathbf{B}_h , respectively). Assume that X and Y are dual to each other and use a stable L^2 -pairing, $\mathbf{G}_h^{X_h, Y_h} = (\phi_h, \varphi_h)_{L^2}$ for $\phi_h \in X_h$ and $\varphi_h \in Y_h$. With these elements, the preconditioned matrix takes the general form:

$$(\mathbf{G}_h^{X_h, Y_h})^{-1} \mathbf{B}_h (\mathbf{G}_h^{X_h, Y_h})^{-T} \mathbf{A}_h. \quad (3)$$

In practice, dual basis are based on barycentric refinements of the primal mesh [3]. This entails a six-fold increase in computational complexity, rendering the method often impractical in realistic scenarios and recent efforts have been devoted to tackle this issue [4, 5].

In this note, we devise an effective yet much cheaper CMP preconditioner built by heavily compressing far-field interaction as in [5], along with coarse quadrature rules to integrate directly over dual basis functions.

2 Modified Calderón Preconditioning

Let \mathcal{T}_h refer to either primal (Γ_h), dual ($\hat{\Gamma}_h$) or barycentrically refined primal ($\bar{\Gamma}_h$) mesh (see Figure 1). For $p = 0, 1$, we write $P_p \equiv P_p(\Gamma_h)$ for the space of piecewise constant or linear functions over Γ_h , respectively. Similarly for barycentric (\bar{P}_p) and dual (\hat{P}_p) basis functions. We seek to solve

$$\mathbf{W}_{\kappa, h} \mathbf{u} = \mathbf{b}, \quad (4)$$

$$\mathbf{V}_{\kappa, h} \mathbf{v} = \boldsymbol{\eta}. \quad (5)$$

The standard CMP matrix reads:

$$(\mathbf{G}_h^{X_h, Y_h})^{-1} \boldsymbol{\Sigma} \mathbf{B}_h^{\bar{Y}_h, \bar{Y}_h} \boldsymbol{\Sigma}^T (\mathbf{G}_h^{X_h, Y_h})^{-T} \mathbf{A}_h^{X_h, X_h},$$

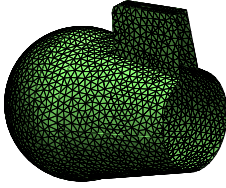


Figure 2: Interior view of the submarine mesh.

None	\mathcal{H} -mCMP1E-8	\mathcal{H} -CMP1E-8
9,745	1,751	1,734

 Table 1: GMRES iteration counts. Compression tolerance of \mathcal{H} -matrices: $\epsilon = 1E - 8$

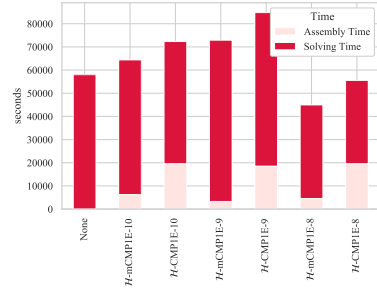
where Σ is an averaging matrix. We build preconditioners directly on approximations of the dual mesh employing low accuracy integration routines.

Consider (1) and the associated matrix $\mathbf{V}_{\kappa,h}^{\widehat{P}_0, \widehat{P}_0}$. As shown in Figure 1, the supports of \widehat{P}_0 -basis functions are obtained as the sum of barycentric piecewise-constant basis functions, \overline{P}_0 , that occupy the dual basis function support. Ideally, integration should be performed over the whole support, but we can also consider a quadrilateral mesh in which dual supports are divided into coarser partitions than the barycentric one. Computationally, self-interaction matrix entries $\mathbf{V}_{\kappa,h}^{\widehat{P}_0, \widehat{P}_0}$ are obtained as prescribed in standard CMP. For cross-interaction terms, quadrilateral elements are first built by merging couples of barycentric triangles into quadrilaterals. A hierarchical version of the mCMP can also be obtained by performing a \mathcal{H} -matrix compression of the mCMP (\mathcal{H} -mCMP).

3 Numerical Results

We show a submarine-like mesh containing 44,338 nodes. The boundary condition used was $\gamma_{Nu} = \hat{n}_z e^{i\kappa z}$ and $\kappa = 30$. Table 1 compares the number of iterations that takes to solve the induced system, by using hierarchical versions of mCMP and standard CMP. Results show that the mCMP performs as good as the CMP.

Assembly and solving times for each preconditioner (Figure 3) confirm the standard \mathcal{H} -CMP poor's performance when compared against \mathcal{H} -mCMP assembly time. In some cases, to-


 Figure 3: Assembly and solving time for \mathcal{H} -mCMP and \mathcal{H} -CMP. Tolerances used to build the compressions are indicated by the names of the preconditioners.

tal execution time of the mCMP does not exceed that of the unpreconditioned system. Also, solving times in the case of hierarchical preconditioners are prohibitively long, as the preconditioner is applied in each GMRES iteration. However, more efficient methods should be employed in order to reduce this bottleneck.

References

- [1] R. Hiptmair, Operator preconditioning, *Computers and mathematics with Applications*, **52** (2006), 699–706.
- [2] F. P. Andriulli, K. Cools, H. Bagci, F. Olyslager, A. Buffa, S. Christiansen, E. Michielssen, A multiplicative Calderón preconditioner for the electric field integral equation, *IEEE TAP*, **56** (2008), 2398–2412.
- [3] A. Buffa, S. Christiansen, A dual finite element complex on the barycentric refinement, *Math. Comp.* **76** (2007), 1743–1769.
- [4] S. B. Adrian, F. P. Andriulli, T. F. Eibert, On a refinement-free Calderón multiplicative preconditioner for the electric field integral equation, *arXiv preprint arXiv:1803.08333*.
- [5] P. Escapil-Inchauspé, C. Jerez-Hanckes, Fast Calderón preconditioning for the electric field integral equation, *IEEE Trans. Antennas and Propagation*, **67** (2019), 2555–2564.

FEM-BEM coupling for vibroacoustics using the open-source GYPSILAB software

Marc Bakry^{1,*}, François Alouges¹, Matthieu Aussal¹¹Centre de Mathématiques Appliquées, Ecole polytechnique, Palaiseau, France

*Email: marc.bakry@gmail.com

Abstract

We show the capabilities of the open-source software GYPSILAB developed at the Ecole polytechnique. Available under the GPL3.0 license, GYPSILAB is a prototyping library entirely written in the MATLAB language. It enables the natural writing of variational formulations as the code reflects the mathematical formulation, and features natively an entire algebra for \mathcal{H} -matrices. In this work, we study a strong coupling FEM and BEM in vibroacoustics using GYPSILAB.

Keywords: open-source, FEM-BEM coupling, hierarchical matrices, vibroacoustics

1 Introduction

GYPSILAB [1, 3] is a high-level coding interface (whose purpose may be compared to other APIs like FreeFEM++, XLIFE++, Phoenix, Drake, this is not exhaustive). It aims at providing the user a portable and fast prototyping tool, taking advantage of the powerful MATLAB API, for the assembling of variational formulations arising from the classical Finite Element Method or Boundary Element Method. Until recently, it only focused on pure FEM or pure BEM problems. In this work, we will show how one can easily compute the strong coupling between an acoustic wave propagating in an exterior medium and an elastic wave in a solid in the frequency domain. The elastic part will be computed using a classical FEM formulation. The acoustic scattering part will be computed using the well-known Brakhage-Werner BEM formulation [4, 5] by taking advantage of the full \mathcal{H} -matrix algebra [6].

2 Coupling equations, implementation

We study the interaction between an acoustic wave with angular frequency ω propagating in an *exterior* medium and a vibrating solid Ω with surface Γ and *outbound* normal \vec{n} . The solid has a density ρ_s and Lamé coefficients (λ, μ) . The unknown is the displacement vector field \mathbf{u} . The propagation equation may be found in [7]. On

the other side, the acoustic medium has a density ρ_0 . The total pressure field is the sum of the incident field p^i (given) and the scattered field p^s . The propagation of the acoustic wave is computed using the Brakhage & Werner boundary integral equation [5] which we shorten such that

$$p^s(x) = BW\alpha(x), \quad (1)$$

$$\frac{\partial p^s}{\partial n}(x) = \frac{\partial BW}{\partial n}\alpha(x), \quad (2)$$

where α is some scalar non-physical unknown. We have the coupling conditions extrapolated from [2, 7]

$$\rho_0\omega^2(\mathbf{u} \cdot \vec{n}) = \frac{\partial p^{\text{tot}}}{\partial n}, \quad (3)$$

and reciprocity of the constraint

$$\sigma(\mathbf{u}) \cdot \vec{n} + p^{\text{tot}}\vec{n} = 0, \quad (4)$$

where $\sigma(\mathbf{u})$ is the stress-tensor in Ω . We obtain the following variational formulations

$$\int_{\Omega} (\sigma(\mathbf{u}) : \bar{\mathbf{v}} - \rho_s\omega^2(\mathbf{u} \cdot \bar{\mathbf{v}})) d\Omega + \int_{\Gamma} (BW\alpha)(\vec{n} \cdot \bar{\mathbf{v}}) d\gamma = - \int_{\Gamma} p^i(\vec{n} \cdot \bar{\mathbf{v}}) d\gamma, \quad (5)$$

$$\rho_0\omega^2 \int_{\Gamma} \bar{w}(\vec{n} \cdot \mathbf{u}) d\gamma - \int_{\Gamma} \bar{w} \left(\frac{\partial BW}{\partial n} \alpha \right) d\gamma = \int_{\Gamma} \bar{w} \frac{\partial p^i}{\partial n} d\gamma, \quad (6)$$

where \mathbf{v} is the "FEM" test function and w is the "BEM" test function.

Implementation The key point with GYPSILAB is that the implementation will mirror the way variational formulations are written. The system defined by (5) and (6) is a 2×2 block-system which can be rewritten as

$$\begin{pmatrix} A & B \\ C & D \end{pmatrix} \cdot \begin{pmatrix} \mathbf{u} \\ \alpha \end{pmatrix} = \begin{pmatrix} e \\ f \end{pmatrix}, \quad (7)$$

where all terms A, B, C, D, e, f are computed using a combination of the same generic interface function `integral(...)` whose behaviour and return-type is determined by the number and kind of arguments which are given as input. The block system is then solved using a Schur complement to avoid mixing the different types of matrices. The unknown α is computed by solving iteratively

$$(D - C \cdot A^{-1} \cdot B) \alpha = f - C \cdot A^{-1} \cdot e. \quad (8)$$

The left-hand-side may be preconditioned by using the LU-decomposition of the \mathcal{H} -matrix D . The post-processing (for example near- and far-field computations based on the representation formula (1)) is performed in the same fashion using the `integral()` interface.

3 Numerical results

The coupling has been validated in 2D and 3D. For example, it was used to compute numerically the transmission and reflexion coefficients of a dispersive solid screen as it can be seen on Fig. 1. The computation was performed

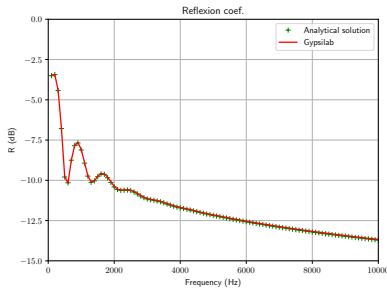


Figure 1: Reflexion coefficient for a dispersive thick screen.

by solving a 2D (or 3D) problem for a slab by forbidding lateral displacement and shear-wave propagation, and using a beamed incident field smaller than the surface. Note that the source code for the 2D and 3D examples are available at [1].

Another example is the scattering by a 3D steel cylinder where the source is a spherical wave placed at the middle. The main dimension is along the \vec{e}_x axis. GYPSILAB was used to

compute the radiation diagrams which are represented on Fig. 2 for a frequency $f = 1000$ Hz.

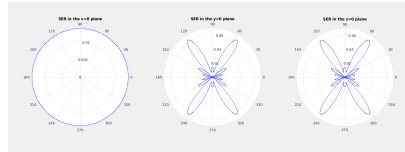


Figure 2: Radiation diagram for a cylinder at 1000 Hz

4 Conclusion

Using the GYPSILAB library, we quickly design a readable and synthetic code for the resolution of vibroacoustics problems. We are able to couple efficiently a FEM formulation for the elastic part and a complex BEM formulation for the acoustic part as GYPSILAB is able to mix finite elements spaces defined on surfacic or volumic meshes. Moreover, the \mathcal{H} -matrix algebra can be used to accelerate the BEM by simply adding a tolerance parameter to the `integral()` routine.

References

- [1] <https://github.com/matthieuauussal/gypsilab/>
- [2] J.-C. Nédélec, *Acoustic and Electromagnetic Equations, Integral Representations for Harmonic Problems*, Springer, 2001
- [3] F. Alouges and M. Aussal, *FEM and BEM simulations with the GYPSILAB framework*, SMAI Journal of Computational Mechanics 4, 2018, pp. 297–318
- [4] D. Colton and R. Kress, *Integral Equation Methods in Scattering Theory*, SIAM, 2013
- [5] R. Kress, *Minimizing the condition number of boundary integral operators in acoustic and electromagnetic scattering*, A. JI Mech. appl. Math. **38** (2), 1985
- [6] S. Börm, L. Grasedyck and W. Hackbusch, *Hierarchical Matrices*, tech. report, 2015
- [7] E. A. Skelton and J. H. James, *Theoretical Acoustics of Underwater Structures*, Imperial College Press, 1997

Parallelization techniques for the collocation boundary element method

Caglar Guerbuez^{1,*}, Christopher Jelich¹, Steffen Marburg¹¹Chair of Vibroacoustics of Vehicles and Machines, Technical University of Munich, Munich, Germany

*Email: caglar.guerbuez@tum.de

Abstract

We introduce a parallel implementation strategy for the collocation boundary element method (BEM) applied to the interior boundary value problem of the three-dimensional Helmholtz equation. This contribution presents an implementation strategy in order to accelerate the matrix assembly process. For this purpose, we take advantage of the fact that each matrix element is evaluated independently. Thus, we transform the nested loop of the matrix assembly procedure into a large iteration space. Then, the associated work can be efficiently distributed among the threads. Moreover, we present an acceleration technique for the iterative solving scheme, especially for the matrix-vector product, by using parallelized routines from PETSc or the Math Kernel Library provided by Intel®. The performance of the presented strategies is demonstrated for a numerical benchmark problem and for an industrial application, a fluid model of a sedan cabin compartment.

Keywords: boundary element method, Helmholtz equation, high performance computing, parallel programming

1 Introduction

Sound radiation and scattering problems play an important role in many engineering applications. In this contribution, we will investigate the sound radiation in a sedan cabin compartment in order to reduce noise in the interior of a vehicle. For this application, we consider the time-harmonic wave equation, i.e. the Helmholtz equation, for the sound pressure p in a domain Ω

$$\Delta p(\mathbf{x}) + k^2 p(\mathbf{x}) = 0 \quad \mathbf{x} \in \Omega \subset \mathbb{R}^3 \quad (1)$$

where $k = \omega/c$ denotes the wavenumber. The angular frequency and the speed of sound are described by ω and c respectively. Moreover, admittance boundary conditions are applied on the boundary Γ , which are equivalent to Robin boundary conditions

$$v_f(\mathbf{x}) - v_s(\mathbf{x}) = Y(\mathbf{x})p(\mathbf{x}) \quad \mathbf{x} \in \Gamma \subset \mathbb{R}^2 \quad (2)$$

with Y representing the boundary admittance. The sound radiation can now be formulated in a boundary integral equation, i.e. the Kirchhoff-Helmholtz integral equation, which can be discretized by the collocation boundary element method. Even if fast boundary element methods, such as the fast multipole method or hierarchical matrices exist, the presented parallelization method is firstly applied to the classical BEM. The presented method can then be easily adapted to the matrix assembly of the dense blocks in the accelerated methods. In general, the BEM is highly advantageous since it only requires the discretization of the boundary. However, the resulting system matrices are dense and generally neither Hermitian nor positive definite. Subsequently, the matrix assembly and the iterative solving procedure are both associated with high computational efforts.

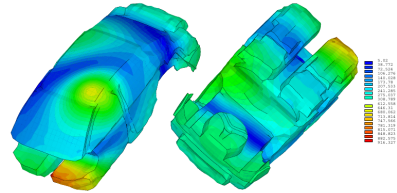


Figure 1: Sedan Cabin Compartment, interior acoustic problem [2].

In order to accelerate the matrix assembly, we transform the nested loop, which underlies the assembly process, into a loop with a large iteration space. This provides the opportunity to share the work among the threads and to parallelize the matrix assembly process. The parallelization is implemented by using OpenMP [7]. Moreover, we present a basic mechanism to accelerate the iterative solving procedure by applying parallelized routines from PETSc [9] and the Intel® Math Kernel Library (MKL) [8]. Finally, some aspects associated with code optimization are covered.

2 Parallelization strategies

In the matrix assembly in the collocation boundary element method, the elements in the system matrix are evaluated independently from each other. Hence, the matrix assembly can be parallelized by transforming the nested loop into a large iteration space. Then, more work can be distributed among the threads, which makes the parallelization more efficient. This parallelization strategy is implemented by using OpenMP [7]. More specifically, we applied the collapse clause in OpenMP in order to parallelize all loop levels instead of just the outer loop. The basic idea of the parallelized matrix assembly is depicted in the pseudo-code below.

Algorithm 1 Parallel matrix assembly

```

1: #pragma omp for collapse(2)
2: for all collocation points do
3:   for all elements do
4:     perform integration on element level
5:     assemble the system matrix

```

In addition to the parallelized matrix assembly, the authors demonstrate an elementary parallelization technique in order to accelerate the iterative solving procedure. For this purpose, the linear system of equations is solved by using parallelized routines from Intel® MKL [8] and PETSc [9].

3 Numerical results

The performance of the implemented parallelization techniques are analyzed for two numerical examples. At first, a typical numerical benchmark case in the field of computational acoustics, the three-dimensional duct problem, is investigated. Then, the presented method is applied to an industrial problem, a sedan cabin compartment [2].

4 Conclusions and outlook

In this contribution, we presented a parallelization method in order to accelerate the matrix assembly process in the collocation boundary element method. Even if modern boundary element methods omit the full assembly of the dense system matrix, the presented method can still be applied on accelerated methods, in order to perform the matrix assembly of dense blocks, which are still present in the fast BEM. Moreover, the iterative solving scheme is accelerated by using parallelized libraries. Finally, the performance of the presented method is analyzed for two examples: the three-

dimensional duct problem and the sedan cabin compartment. Besides further parallelization of the BEM, the BEM code will be optimized toward an efficient distribution of data.

References

- [1] M. Hornikx, M. Kaltenbacher and S. Marburg: A Platform for Benchmark Cases in Computational Acoustics. *Acta Acustica united with Acustica* 101 (2012), 811-820.
- [2] S. Marburg, Boundary element method for time-harmonic acoustic problems. In: M. Kaltenbacher, editor, *Computational Acoustics*, CISM International Centre for Mechanical Sciences, Courses and Lectures, Vol. 579, Springer, Berlin, Heidelberg, (2017), 69-158.
- [3] S. Marburg, B. Nolte, A unified approach to finite and boundary element discretization in linear acoustics. In: S. Marburg, B. Nolte, editor, *Computational Acoustics of Noise Propagation in Fluids. Finite and Boundary Element Methods.*, Springer, Berlin (200/), 1-34
- [4] G. Hager and G. Wellein, *Introduction to high performance computing for scientists and engineers*. CRC Press (2010)
- [5] B. Chapman, G. Jost, R. Van Der Pas, *Using OpenMP: portable shared memory parallel programming.*, Vol. 10, MIT press (2008)
- [6] V. Eijkhout, R. van de Geijn, E. Chow *Introduction to High Performance Scientific Computing.*, lulu.com, (2011)
- [7] <https://www.openmp.org/>.
- [8] <https://software.intel.com/en-us/mkl>.
- [9] <https://www.mcs.anl.gov/petsc/>.

A priori analysis for the finite element approximation of Westervelt's quasilinear acoustic wave equation

Vanja Nikolić^{1,*}, Barbara Wohlmuth²

¹Department of Mathematics, Technical University of Munich, Munich, Germany

²Department of Mathematics, Technical University of Munich, Munich, Germany

*Email: vanja.nikolic@ma.tum.de

Abstract

We analyze the spatial discretization of Westervelt's quasilinear strongly damped wave equation by piecewise linear finite elements. The main challenges lie in handling the underlying nonlinearities which involve temporal derivatives of the acoustic pressure and ensuring the non-degeneracy of the model. The talk is based on [2].

Keywords: finite element method, a priori analysis, nonlinear acoustics

1 Introduction

We study a spatial discretization of Westervelt's wave equation for the acoustic pressure u :

$$(1 - 2ku)u_{tt} - c^2\Delta u - b\Delta u_t = 2ku_t^2. \quad (1)$$

This equation represents a classical model for nonlinear ultrasound propagation through thermoviscous fluids [3]. In (1), the constant c denotes the speed of sound, b is the sound diffusivity, $k = \beta_a/(\rho c^2)$, where ρ is the mass density and β_a the coefficient of nonlinearity of the medium. We consider equation (1) with homogeneous Dirichlet conditions and non-zero initial data $(u, u_t)|_{t=0} = (u_0, u_1)$.

The motivation to study (1) comes from many applications of nonlinear ultrasound in medicine and industry. For instance, high-intensity ultrasound waves are often used in treatments of kidney stones to break them into smaller pieces.

An interesting feature of Westervelt's quasilinear equation is that the non-degeneracy is *not* a priori given. In our proofs, we have to ensure that the factor $1 - 2ku$ next to the second time derivative remains positive.

In the continuous analysis of the Westervelt equation, non-degeneracy is typically ensured by a higher-regularity result for the solution and the use of an embedding, e.g., $H^2(\Omega) \hookrightarrow L^\infty(\Omega)$, combined with an assumption of sufficiently small data; cf. [1, Theorem 3.1]. We cannot directly transfer this strategy to the semi-discrete setting

since we use piecewise linear basis functions. Instead, we rely on inverse estimates for finite element functions and the stability and approximation properties of the interpolation operator.

It is also worth noting that the strong damping (i.e., $b > 0$) is needed for the continuous problem to be well-posed in 2D and 3D; the same holds for the semi-discrete equation.

2 Linearized Westervelt's equation

Let $S_h \subset H_0^1(\Omega)$ denote a finite element space that consists of piecewise polynomials of degree 1 on a quasi-uniform simplicial tessellation \mathcal{T} of $\bar{\Omega} \subset \mathbb{R}^d$, where $d \in \{2, 3\}$.

Our theoretical approach employs the Banach fixed-point theorem in combination with a priori analysis of a non-degenerate linear wave model with variable coefficients:

$$\alpha(x, t)u_{tt} - c^2\Delta u - b\Delta u_t + \beta(x, t)u_t = f(x, t), \quad (2)$$

where $0 < \alpha_0 \leq \alpha \leq \alpha_1$ a.e. in $\Omega \times (0, T)$, coupled with the initial conditions and homogeneous Dirichlet data. The error analysis of the discretization of (2) in S_h has to take into account approximation errors of the coefficients α and β to make later use of a fixed-point approach possible.

3 A priori analysis of Westervelt's equation

The analysis of the nonlinear problem is then performed by defining an iterative map on which we can apply the Banach fixed-point theorem while relying on the error analysis for the linearized equation (2). In this way, we obtain optimal convergence rates in L^2 -based spatial norms for sufficiently small data and mesh size, and a suitable choice of initial approximations.

Theorem 1 [A priori error estimate, [2]] *Let $c^2, b, k > 0$, and let $T > 0$. Assume that the initial-boundary value problem for (1) has*

a unique solution which satisfies

$$\begin{aligned} u &\in L^\infty(0, T; L^\infty(\Omega) \cap \dot{H}^s(\Omega)), \\ u_t &\in L^2(0, T; L^\infty(\Omega)) \cap L^\infty(0, T; \dot{H}^s(\Omega)), \\ u_{tt} &\in L^2(0, T; L^\infty(\Omega) \cap \dot{H}^s(\Omega)), \end{aligned}$$

where $\max\{1, d/2\} < s \leq 2$. Then for sufficiently small

$$\begin{aligned} m &= \|u\|_{L^\infty L^\infty}, \\ M &= \max \{ \|u\|_{L^\infty H^s}, \|u_t\|_{L^\infty H^s}, \|u_t\|_{L^2 L^\infty}, \\ &\quad \|u_{tt}\|_{L^2 H^s}, \|u_{tt}\|_{L^2 L^\infty} \}, \end{aligned}$$

and h , there exists a unique u_h in a neighbourhood of u which satisfies the equation

$$\begin{aligned} ((1 - 2ku_h)u_{h,tt}, \phi)_{L^2} + c^2(\nabla u_h, \nabla \phi)_{L^2} \\ + b(\nabla u_{h,t}, \nabla \phi)_{L^2} = 2k(u_{h,t}^2, \phi)_{L^2}, \end{aligned}$$

for all $\phi \in S_h$ a.e. in time, and $(u_h(0), u_{h,t}(0)) = (R_h u_0, R_h u_1)$. Furthermore, there exists a positive constant C that depends on m , M , and T , but not on h , such that

$$\begin{aligned} \|u - u_h\|_{L^\infty L^2} + \|u_t - u_{h,t}\|_{L^\infty L^2} \\ + h\|\nabla(u - u_h)\|_{L^\infty L^2} + h\|\nabla u_t - u_{h,t}\|_{L^\infty L^2} \\ \leq Ch^s. \end{aligned}$$

In the talk, we will illustrate our theoretical findings by numerical experiments in a setting of a 1D channel as well as for a focused-ultrasound problem.

References

[1] B. Kaltenbacher and I. Lasiecka, *Global existence and exponential decay rates for the Westervelt equation*, Discrete and Continuous Dynamical Systems Series S, 2(3), 503–523, 2009.

[2] V. Nikolić and B. Wohlmuth, *A priori error estimates for the finite element approximation of Westervelt’s quasi-linear acoustic wave equation*, submitted, arXiv:1901.08510, 2019.

[3] Peter J. Westervelt, *Parametric acoustic array*, The Journal of the Acoustical Society of America, 35(4), 535–537, 1963.

Fundamental models in nonlinear acoustics

Barbara Kaltenbacher¹, Mechthild Thalhammer^{2,*}¹Institut für Mathematik, Universität Klagenfurt, Klagenfurt, Austria²Institut für Mathematik, Universität Innsbruck, Innsbruck, Austria

*Email: mechthild.thalhammer@uibk.ac.at

Abstract

Recent advances on the numerical simulation of fundamental models from nonlinear acoustics will be presented. A hierarchy of nonlinear damped wave equations arising in the description of sound propagation in thermoviscous fluids will be introduced. Former investigations imply that two classical models, the Kuznetsov and Westervelt equations, are retained as limiting systems for vanishing thermal conductivity and consistent initial data. Numerical comparisons confirm and complement this theoretical result.

Keywords: Nonlinear acoustics; Nonlinear damped wave equations; Limiting systems; Numerical simulation

1 Introduction

Wave equations naturally arise in the field of nonlinear acoustics; in view of various medical and industrial applications, the investigation of nonlinear damped wave equations is of particular importance in high-intensity ultrasonics, see for instance [1] and references given therein.

Pursuing former work [2], our main objective is to provide numerical simulations for a hierarchy of nonlinear damped wave equations modelling sound propagation in thermoviscous fluids; our study confirms and complements a rigorous theoretical result which implies that two classical models, the Kuznetsov and Westervelt equations, are retained as limiting systems for vanishing thermal conductivity and consistent initial data.

2 Kuznetsov and Westervelt equations

The Kuznetsov equation [3] is a widely-used model for the propagation of sound in thermoviscous fluids that neglects thermal effects. In accordance with [2], we employ a formulation as abstract evolution equation for the space-time-dependent acoustic velocity potential

$$\psi : \Omega \times [0, T] \subset \mathbb{R}^d \times \mathbb{R} \longrightarrow \mathbb{R}, \quad (1a)$$

$$d \in \{1, 2, 3\},$$

defined on a certain space-time domain; setting $\sigma = 1$ as well as

$$\begin{aligned} \beta_1^{(0)} &= \nu \Lambda, \\ \beta_3 &= c_0^2, \\ \beta_5(\sigma) &= \frac{1}{c_0^2} (2(1-\sigma) + \frac{B}{A}), \\ \beta_6(\sigma) &= \sigma, \\ \sigma &\in \{0, 1\}, \end{aligned} \quad (1b)$$

with kinematic viscosity ν , quantity $\Lambda = \frac{\mu_B}{\mu} + \frac{4}{3}$ given by the ratio of the bulk and shear viscosities μ_B and μ , speed of sound c_0 , and parameter of nonlinearity $\frac{B}{A}$, the Kuznetsov equation reads as follows

$$\begin{aligned} \partial_t \psi(t) - \beta_1^{(0)} \Delta \partial_t \psi(t) - \beta_3 \Delta \psi(t) \\ + \partial_t \left(\frac{1}{2} \beta_5(\sigma) (\partial_t \psi(t))^2 \right. \\ \left. + \beta_6(\sigma) |\nabla \psi(t)|^2 \right) = 0, \end{aligned} \quad (1c)$$

$$t \in (0, T),$$

$$\psi(0) = \psi_0,$$

$$\partial_t \psi(0) = \psi_1.$$

The special choice $\sigma = 0$ leads to the Westervelt equation [4], which in addition disregards local nonlinear effects.

3 Nonlinear damped wave equation

An extended model is obtained from the fundamental conservation laws for mass, momentum, and energy as well as an equation of state, see [2] for details on the derivation. In accordance with (1), we denote by $a > 0$ the thermal conductivity and set

$$\begin{aligned} \beta_1^{(a)} &= a \left(1 + \frac{B}{A} \right) + \nu \Lambda, \\ \beta_2^{(a)}(\sigma_0) &= a \left(\nu \Lambda + a \frac{B}{A} \right. \\ &\quad \left. + \sigma_0 \frac{B}{A} (\nu \Lambda - a) \right), \\ \beta_3 &= c_0^2, \\ \beta_4^{(a)}(\sigma_0) &= a \left(1 + \sigma_0 \frac{B}{A} \right) c_0^2, \\ \beta_5(\sigma) &= \frac{1}{c_0^2} \left(2(1-\sigma) + \frac{B}{A} \right), \\ \beta_6(\sigma) &= \sigma, \\ \sigma, \sigma_0 &\in \{0, 1\}; \end{aligned} \quad (2a)$$

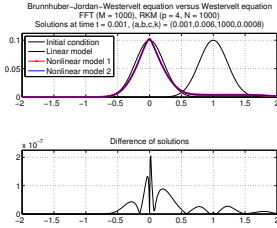


Figure 1: Comparison of solution profiles for consistent initial data.

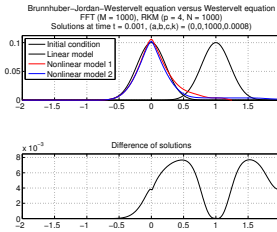


Figure 2: Comparison of solution profiles for inconsistent initial data.

evidently, $\beta_1^{(a)} \rightarrow \beta_1^{(0)}$ and $\beta_2^{(a)}(\sigma_0) \rightarrow 0$ as well as $\beta_4^{(a)}(\sigma_0) \rightarrow 0$ if $a \rightarrow 0_+$. The heuristic observation that the nonlinear damped wave equation

$$\begin{aligned} & \partial_{tt}\psi^{(a)}(t) - \beta_1^{(a)} \Delta \partial_{tt}\psi^{(a)}(t) \\ & + \beta_2^{(a)}(\sigma_0) \Delta^2 \partial_t \psi^{(a)}(t) \\ & - \beta_3 \Delta \partial_t \psi^{(a)}(t) \\ & + \beta_4^{(a)}(\sigma_0) \Delta^2 \psi^{(a)}(t) \\ & + \partial_{tt} \left(\frac{1}{2} \beta_5(\sigma) (\partial_t \psi^{(a)}(t))^2 \right. \\ & \left. + \beta_6(\sigma) |\nabla \psi^{(a)}(t)|^2 \right) = 0, \end{aligned} \quad (2b)$$

$$\begin{aligned} & t \in (0, T), \\ & \psi^{(a)}(0) = \psi_0, \\ & \partial_t \psi^{(a)}(0) = \psi_1, \\ & \partial_{tt} \psi^{(a)}(0) = \psi_2, \end{aligned}$$

includes as special cases the Kuznetsov and Westervelt equations is made rigorous in [2].

4 Numerical simulations

The general model (2) defines a hierarchy of nonlinear damped wave equations, see refer-

ences given in [2]. The Brunnhuber–Jordan–Kuznetsov equation is cast into the general formulation with $\sigma = 1$ and $\sigma_0 = 1$. The Blackstock–Crighton–Kuznetsov equation arises in situations, where the quantity $(\nu\Lambda - a) \frac{B}{A}$ is negligible, for instance in the description of monatomic gases; it is embedded for $\sigma = 1$ and $\sigma_0 = 0$. In both cases, the Kuznetsov equation results as limiting system for vanishing thermal conductivity $a \rightarrow 0_+$ and initial data satisfying a certain consistency condition. Westervelt-type equations do not take into account local nonlinear effects; this is reflected by the absence of the term $c_0^2 |\nabla \psi|^2 - (\partial_t \psi)^2$ and corresponds to the value $\sigma = 0$.

A natural approach for the space and time discretisation of these partial differential equations is to combine standard methods such as finite element approximations with Runge–Kutta methods; as alternative, we favour operator splitting methods, as this provides the possibility to use tailored solvers.

In Figures 1 and 2, we display preliminary results obtained for the Brunnhuber–Jordan–Westervelt equation (nonlinear model 1) versus the Westervelt equation (nonlinear model 2) and a linearised wave equation (linear model); restricting ourselves to a single space dimension, the simple geometry of the spatial domain permits the use of fast Fourier techniques. As expected, for smaller values such as $a = 10^{-3}$ and consistent initial data the solutions to the nonlinear models coincide (Figure 1), whereas inconsistent initial data lead to different solution profiles, even in the special case $a = 0$ (Figure 2).

References

- [1] O. V. ABRAMOV, *High-Intensity Ultrasonics*. Gordon and Breach Science Publishers, Amsterdam, 1998.
- [2] B. KALTENBACHER, M. THALHAMMER, *Fundamental models in nonlinear acoustics: Part I. Analytical comparison*. M3AS 28/12 (2018) 2403–2455.
- [3] V. KUZNETSOV, *Equations of nonlinear acoustics*. Soviet Physics-Acoustics 16 (1971) 467–470.
- [4] P. J. WESTERVELT, *Parametric acoustic array*. The Journal of the Acoustic Society of America 35 (1963) 535–537.

Optimal decay rates of the Moore-Gibson-Thompson equation.

M. Pellicer^{1,*}, B. Said-Houari², J. Solà-Morales³¹Dpt. d'Informàtica, Matemàtica Aplicada i Estadística, U. de Girona, Girona, (Catalonia, Spain)²Dpt. of Mathematics, University of Sharjah, Sharjah (United Arab Emirates)³Dpt. de Matemàtiques, Universitat Politècnica de Catalunya, Barcelona, (Catalonia, Spain)

*Email: martap@imae.udg.edu

Abstract

The Moore–Gibson–Thompson equation is a well-known model in Acoustics and, under the name of standard linear viscoelastic model, it also appears in Viscoelasticity. We present the results of two recent works where we study the asymptotic stability of this problem under a certain dissipative condition in a bounded domain and in \mathbb{R}^N , giving optimal decay rates in both situations. In both cases, an accurate and precise description of the spectrum of the related operators will be very important.

Keywords: Moore-Gibson-Thompson model, standard linear viscoelastic model, optimal decay rate, optimal scalar product, energy method, eigenvalues expansion method.

1 Motivation of the problem

Our aim is to study the asymptotic stability of the so-called Moore–Gibson–Thompson equation, a well-known model in Acoustics which is given by the following third order in time linear dissipative wave equation:

$$\tau u_{ttt} + u_{tt} - a^2 \Delta u - a^2 \beta \Delta u_t = 0, \quad (1)$$

where u represents the acoustic velocity potential. This equation arises in Acoustics as the linearization of the important Jordan–Moore–Gibson–Thompson equation (see [2], [3] or [4] and the references therein for more details). The JMGT equation, together with its linearization (1), has applications in medical and industrial use of high intensity ultrasound such as lithotripsy, thermotherapy or ultrasound cleaning. Actually, the JMGT equation pretends to be an alternative (and more realistic) model for viscous thermally relaxing fluids, instead of other classical acoustic models such as the Kuznetsov equation (see previous references). It appears when we want to overcome the paradox of infinite speed propagation in thermal waves that is usually used. This is achieved by considering

the Cattaneo law $\tau q_t + q = -\kappa \nabla \theta$ instead of the usual Fourier one for the heat conduction. Here, q and θ are representing the heat flux and temperature difference, respectively, and τ is the relaxation time of the heat flux (usually small with respect to the other parameters of the model).

Surprisingly, the same equation is a well-known model in Mechanics, but then under the name of *standard linear viscoelastic* model. In this case, u stands for the linear deformations of a viscoelastic solid (that is, a solid exhibiting both a viscous fluid and an elastic solid response) with an approach that is considered to be more realistic than the usual Kelvin-Voigt one (that is actually recovered if we take $\tau = 0$). The main idea in modelling this type of deformations is that (1) can be obtained by considering the following constitutive relation between σ (the stress) and e (the strain):

$$\sigma + \tau \sigma' = E(e + \beta e')$$

with E being the Young modulus of the elastic structure and the constants τ and β being small and satisfying $0 < \tau < \beta$. As references for this problem under the viscoelastic approach see, for instance, [1] or [4] and the references therein.

In spite of being a linear equation, (1) exhibits very different behaviours depending on the physical parameters of the equation. As we are going to see, the relation between the relaxation parameter τ and β is indeed very important when determining the stability of problem (1). From previous references ([2] and references therein) we know that, in a bounded domain, $0 < \tau < \beta$ is a dissipative condition that makes the problem exponentially stable. When $0 < \tau = \beta$ the energy of the problem is conserved and when $\tau > \beta > 0$ the solutions turn out to have a chaotic behaviour. In the next sections we summarize the results of the two recent works [5] (bounded domain case) and [4] (problem in \mathbb{R}^N), both dealing with optimal de-

decay rates of the solutions of the MGT problem under the dissipative condition.

2 Optimal decay rate of the MGT equation in a bounded domain in \mathbb{R}^N

In [5] we study the asymptotic behaviour of the following general version of the MGT equation (1) in a bounded domain under the previous dissipative condition $0 < \tau < \beta$

$$\tau u_{ttt} + u_{tt} + Lu + \beta Lu_t = 0,$$

with L being a self-adjoint and strictly positive operator in a Hilbert space with compact resolvent. Observe that, in particular, when $L = -a^2\Delta$ we have the MGT given in (1).

By completing the description of the spectrum given in [3] (with the accurate description of the cases in which we have eigenvalues with algebraic multiplicity higher than one), we give a new equivalent and explicit scalar product under which the operator will be proved to be normal, which is the best we can expect in this case. Hence, the operator admits a complete set of orthonormal eigenfunctions. This will be true except from some exceptional values of the parameters (corresponding to cases with eigenvalues with algebraic multiplicity higher than one), in which case we will prove that the operator cannot be made normal (see Theorem 1.1 of [5]). We will use this result to obtain optimal exponential decay rates in the asymptotic behaviour of the solutions, and will adapt it to achieve the same kind of results when the operator is not normal (see Theorem 1.2 of [5]). These results slightly improve previous ones related to the asymptotic decay rate of this problem.

3 Optimal decay of the MGT equation in \mathbb{R}^N

In [4] we study the MGT equation (1) in \mathbb{R}^N also when $0 < \tau < \beta$. First, we give the appropriate functional setting to prove that this Cauchy problem is well-posed. Then, we are interested in the asymptotic stability of this problem in \mathbb{R}^N . We first apply the energy method in the Fourier space and find the appropriate some Lyapunov functionals to show that a norm related to the solution decays with a rate $(1+t)^{-N/4}$ (see Theorem 3.6 in [4]). Similar results are given for the decay rate of this norm involving derivatives of the solution. As the previous result does not give the asymptotic decay rate of the solution

itself, we use the eigenvalues expansion method to give it. That is, we show an explicit representation of the solution in the Fourier domain using the the accurate and explicit description of the operator given in [5]. The optimal decay rate we obtain with this method for the solution (and also of its derivatives), is $(1+t)^{1-N/4}$ for $N = 1, 2$ and $(1+t)^{1/2-N/4}$ when $N \geq 3$ (see Theorems 5.1, 5.3 and 5.5 in [4]).

Acknowledgments

J.Solà-Morales has been supported by the grant s MTM2014-52402-C3-1-P and MTM2017-84214-C2-1-P (Spain). M. Pellicer has been supported by the grants MTM2014-52402-C3-3-P, MTM2017-84214-C2-2-P (Spain) and by MPC UdG 2016/047 (U. of Girona, Catalonia). These authors are part of the Catalan research group 2017 SGR 1392.

References

- [1] G.C. Gorain, Stabilization for the vibrations modeled by the standard linear model of viscoelasticity. *Proc. Indian Acad. Sci. Math. Sci.* **120** (4) (2010), pp.495–506.
- [2] B. Kaltenbacher, I. Lasiecka, and R. Marchand, Wellposedness and exponential decay rates for the Moore-Gibson-Thompson equation arising in high intensity ultrasound. *Control and Cybernetics* **40** (2011), pp.971–988.
- [3] R. Marchand, T. McDevitt, and R. Triggiani. An abstract semigroup approach to the third-order Moore–Gibson–Thompson partial differential equation arising in high-intensity ultrasound: structural decomposition, spectral analysis, exponential stability. *Math. Methods. Appl. Sci.* **35** (15) (2012), pp. 1896–1929.
- [4] M. Pellicer and B.Said-Houari, Wellposedness and decay rates for the Cauchy problem of the Moore-Gibson-Thompson equation arising in high intensity ultrasound. *Appl Math. Optim* (2017), DOI 10.1007/s00245-017-9471-8.
- [5] M. Pellicer and J. Solà-Morales, Optimal scalar products in the Moore-Gibson-Thompson equation. *Evol. Eqs. and Control Theory* **8** (1) (2019), pp. 203-220.

**The Jordan-Moore-Gibson-Thompson equation of nonlinear acoustics:
Well-posedness and singular limit for vanishing relaxation time**

Barbara Kaltenbacher^{1,*}, Vanja Nikolić²

¹Department of Mathematics, Alpen-Adria-Universität Klagenfurt, Klagenfurt, Austria

²Department of Mathematics, Technical University of Munich, Garching, Germany

*Email: barbara.kaltenbacher@aau.at

Abstract

The Jordan-Moore-Gibson-Thompson equation is a third order in time wave equation describing the nonlinear propagation of sound that avoids the infinite signal speed paradox of classical second order in time strongly damped models of nonlinear acoustics, such as the Westervelt and the Kuznetsov equation. We show well-posedness in an acoustic velocity potential formulation with and without gradient nonlinearity. Moreover, we consider the limit as the parameter of the third order time derivative that plays the role of a relaxation time tends to zero, which again leads to the classical Kuznetsov and Westervelt models. The proofs rely on appropriate energy estimates for the linearized equations as well as fixed-point arguments for well-posedness of the nonlinear equations. These results extend to the practically relevant setting of Neumann boundary conditions for modelling excitation, as well as absorbing boundary conditions.

Keywords: nonlinear acoustics, Jordan-Moore-Gibson-Thompson equation, Kuznetsov's equation, Westervelt equation, singular limit

Introduction

Nonlinear propagation of sound arises in numerous applications. We here especially mention high-intensity ultrasound used in medical imaging and therapy, but also for industrial purposes, such as ultrasound cleaning or welding. One of the most established models of nonlinear acoustics is Kuznetsov's equation (Kuznetsov 1971; Lesser and Seebass 1968); by ignoring local nonlinear effects modeled by the quadratic velocity term, we arrive at the Westervelt equation, (Westervelt 1963). In terms of the acoustic velocity potential ψ , these equations can be rewritten as

$$\psi_{tt} - c^2 \Delta \psi - \delta \Delta \psi_t = \mathcal{N}^K(\psi) \quad (1)$$

and

$$\psi_{tt} - c^2 \Delta \psi - \delta \Delta \psi_t = \mathcal{N}^W(\psi), \quad (2)$$

respectively, where c is the speed of sound, δ is the diffusivity of sound, and the nonlinear terms are defined by

$$\mathcal{N}^K(\psi) = \left(\frac{1}{c^2} \frac{B}{2A} (\psi_t)^2 + |\nabla \psi|^2 \right)_t,$$

$$\mathcal{N}^W(\psi) = \left(\frac{\beta_a}{c^2} (\psi_t)^2 \right)_t,$$

with the parameter of nonlinearity $B/(2A)$ and the coefficient $\beta_a = 1 + B/(2A)$.

As has been observed, e.g., in [1] (see also the references therein), the use of classical Fourier's law leads to an infinite signal speed paradox, which appears to be unnatural in wave propagation. Therefore in [1], several other constitutive relations for the heat flux within the derivation of nonlinear acoustic wave equations are considered. Among these is the Maxwell-Cattaneo law, whose combination with the balance equations for mass and momentum, as well as the equation of state, leads to the third order in time PDE model:

$$\tau \psi_{ttt} + \psi_{tt} - c^2 \Delta \psi - b \Delta \psi_t = \mathcal{N}^K(\psi), \quad (3)$$

where τ is a positive constant accounting for relaxation (the relaxation time), and $b = \delta + \tau c^2$. If one neglects local nonlinear effects modeled by the quadratic velocity term $|\nabla \psi|^2$, one replaces \mathcal{N}^K by \mathcal{N}^W in (3) analogously to the reduction of the Kuznetsov to the Westervelt equation; cf. [2].

Our results rely on energy estimates for the linearized equation

$$\tau \psi_{ttt} + \alpha \psi_{tt} - c^2 \Delta \psi - b \Delta \psi_t = f, \quad (4)$$

also called the (Stokes-)Moore-Gibson-Thompson equation, see also Kaltenbacher, Lasiecka, and Marchand 2012; Marchand, McDevitt, and Triggiani 2012; Dell'Oro and Pata 2017; Pellicer and Solá-Morales 2019.

This paper reports on recent contributions to the analysis of the JMGT equation in two

ways. Firstly, its well-posedness with a quadratic gradient nonlinearity arising when taking into account local nonlinear effects (cf. the additional $(|\nabla\psi|^2)_t$ term in $\mathcal{N}^K(\psi)$ as compared to $\mathcal{N}^W(\psi)$). Since maximal parabolic regularity and Implicit Function Theorem arguments do not apply here, the arguments are based on energy estimates for a fixed-point reformulation (4) with $\alpha = \alpha(\psi) = (1 - k\psi_t)$, $f = f(\psi) = 2\nabla\psi \cdot \nabla\psi_t$ of (3) where we use the abbreviation $k = \frac{2}{c^2} \frac{B}{2A}$. We rely on the formulation in terms of the acoustic velocity potential ψ which more easily than the acoustic pressure formulation from [2] allows to include the quadratic velocity term $(|\nabla\psi|^2)_t$ on the right hand side of (3).

Secondly, we consider the limit $\tau \rightarrow 0$ and state that solutions of (3) converge to a solution of (1) as $\tau \rightarrow 0$. Also for this purpose, the previously derived energy estimates are crucial.

Theorem 1 [3] *Let $c^2, b, T > 0$, and $k \in \mathbb{R}$. Then there exist $\bar{\tau}, \rho > 0, \rho_0 > 0$ such that for all $(\psi_0, \psi_1, \psi_2) \in X_0^W = H_0^1(\Omega) \cap H^2(\Omega) \times H_0^1(\Omega) \cap H^2(\Omega) \times H_0^1(\Omega)$ satisfying*

$$\|\psi_0\|_{H^2(\Omega)}^2 + \|\psi_1\|_{H^2(\Omega)}^2 + \tau\|\psi_2\|_{H^1(\Omega)}^2 \leq \rho_0^2,$$

and all $\tau \in (0, \bar{\tau})$, there exists a solution $\psi \in X^W$ of

$$\begin{cases} \tau\psi_{ttt} + \psi_{tt} - c^2\Delta\psi - b\Delta\psi_t = \mathcal{N}^W(\psi) & \text{in } \Omega \times (0, T), \\ \psi = 0 & \text{on } \partial\Omega \times (0, T), \\ (\psi, \psi_t, \psi_{tt}) = (\psi_0, \psi_1, \psi_2) & \text{in } \Omega \times \{0\}, \end{cases} \quad (5)$$

and satisfies the energy estimate

$$\tau^2\|\psi_{ttt}\|_{L^2L^2}^2 + \tau\|\psi_{tt}\|_{L^\infty H^1}^2 + \|\psi_{tt}\|_{L^2H^1}^2 + \|\psi\|_{W^{1,\infty}H^2}^2 \leq \rho^2.$$

Theorem 2 [3] *Let $c^2, b, T > 0, k \in \mathbb{R}$. Then there exist $\bar{\tau}, \rho > 0, \rho_0 > 0$ such that for all $(\psi_0, \psi_1, \psi_2) \in X_0^K = H_0^1(\Omega) \cap H^3(\Omega) \times H_0^1(\Omega) \cap H^2(\Omega) \times H_0^1(\Omega)$ satisfying*

$$\|\psi_0\|_{H^3(\Omega)}^2 + \|\psi_1\|_{H^2(\Omega)}^2 + \tau\|\psi_2\|_{H^1(\Omega)}^2 \leq \rho_0^2,$$

and all $\tau \in (0, \bar{\tau})$, there exists a unique solution $\psi \in X^K$ of (5) with $\mathcal{N}^W(\psi)$ replaced by $\mathcal{N}^K(\psi)$ and satisfies the energy estimate

$$\begin{aligned} \tau\|\psi_{tt} + \frac{c^2}{b}\psi_t\|_{L^\infty H^1}^2 + \|\psi_{tt} + \frac{c^2}{b}\psi_t\|_{L^2H^1}^2 \\ + \|\psi_t + \frac{c^2}{b}\psi\|_{L^\infty H^2}^2 + \|\psi\|_{L^\infty H^3}^2 \leq \rho^2. \end{aligned}$$

The function space setting for the limiting case is determined by the respective τ -independent part of the energies defined in Theorems 1 and 2, respectively, i.e.,

$$\begin{aligned} \bar{X}^W &:= H^2(0, T; H_0^1(\Omega)) \cap W^{1,\infty}(0, T; H^2(\Omega)), \\ \bar{X}^K &:= \bar{X}^W \cap L^\infty(0, T; H^3(\Omega)). \end{aligned}$$

Theorem 3 [3] *Let $c^2, b, T > 0$, and $k \in \mathbb{R}$. Then there exist $\bar{\tau}, \rho_0 > 0$ such that for all $(\psi_0, \psi_1, \psi_2) \in X_0^W$, the family $(\psi^\tau)_{\tau \in (0, \bar{\tau})}$ of solutions to (5) converges weakly* in \bar{X}^W to a solution $\bar{\psi} \in \bar{X}^W$ of (2) with homogeneous Dirichlet boundary conditions and initial conditions $\bar{\psi}(0) = \psi_0, \bar{\psi}_t(0) = \psi_1$.*

The statement remains valid with the Westervelt nonlinearity \mathcal{N}^W , the equation (2) and the spaces X_0^W, \bar{X}^W replaced by the Kuznetsov nonlinearity \mathcal{N}^K , the equation (1), and the space X_0^K, \bar{X}^K , respectively.

In [4], the above results have been extended to the practically relevant setting of Neumann and absorbing boundary conditions

$$\frac{\partial\psi}{\partial n} = g \text{ on } \Gamma, \quad \frac{\partial\psi}{\partial n} = -\beta\psi_t \quad \text{on } \partial\Omega \setminus \Gamma,$$

References

- [1] P. M. Jordan, Second-sound phenomena in inviscid, thermally relaxing gases, *Discrete & Continuous Dynamical Systems-Series B* **19** (2014).
- [2] B. Kaltenbacher, I. Lasiecka, and M. K. Pospieszalska, Well-posedness and exponential decay of the energy in the nonlinear Jordan–Moore–Gibson–Thompson equation arising in high intensity ultrasound, *Mathematical Models and Methods in Applied Sciences*, **22** (2012), p. 1250035.
- [3] B. Kaltenbacher, V. Nikolić, On the Jordan–Moore–Gibson–Thompson equation: well-posedness with quadratic gradient nonlinearity and singular limit for vanishing relaxation time, arXiv:1901.02795 [math.AP], and submitted.
- [4] B. Kaltenbacher, V. Nikolić, Vanishing relaxation time limit of the Jordan–Moore–Gibson–Thompson wave equation with Neumann and absorbing boundary conditions, arXiv:1902.10606 [math.AP], and submitted.

Exact dispersion relation for strongly nonlinear elastic waves

Romik Khajehtourian¹, Mahmoud I. Hussein^{2,*}¹Department of Mechanical and Process Engineering, ETH Zürich, Zürich, 8092, Switzerland²Ann and H.J. Smead Department of Aerospace Engineering Sciences, University of Colorado Boulder, Boulder, Colorado

*Email: mih@colorado.edu

Wave motion lies at the heart of many disciplines in the physical sciences and engineering. For example, problems and applications involving light, sound, heat, or fluid flow are all likely to involve wave dynamics at some level. In this extended abstract, we present our recent work on large-strain elastic waves in solids, focusing on both homogeneous and periodic media.

Specifically, we examine the propagation of large-amplitude elastic waves in an elastic one-dimensional medium that is undeformed at its initial state. In this context, our focus is on the effects of inherent nonlinearities on the dispersion relation. Considering a slender rod, where the thickness is small compared to the wavelength, we present an exact formulation for the treatment of nonlinearity in the strain-displacement gradient relation. As examples, we consider Green-Lagrange strain (for which the conjugate stress is second Piola-Kirchhoff stress) and Hencky strain (for which the conjugate stress is Kirchhoff stress). The ideas presented, however, apply generally to other types of geometric nonlinearities, and also to material nonlinearities regardless of type or order. The only limitation is that the nonlinearity has to be expressed analytically and integrable. Furthermore, a thick rod may be considered by simply accounting for lateral inertia in the model.

The derivation starts with an implementation of Hamilton's principle and terminates with an expression for the finite-strain dispersion relation in closed form [1]. The derivation is then verified by direct time-domain simulations, examining both instantaneous dispersion (by direct observation; see Figure 4 in Ref. [1]) and short-term, pre-breaking dispersion (by Fourier transformations; see Figure 1). As can be seen in Figure 1, the theory (solid lines) matches corresponding results shown as a contour of the energy spectrum. This contour is obtained by running a series of separate simulations where each involves a different excitation

wavenumber, and finally plotting the superposition of the space-time Fourier transform of the field variable in these simulations; what emerges is a profile of the fundamental harmonic spanning the various simulations. Moreover, we reveal that an otherwise linearly nondispersive elastic solid may exhibit dispersion solely due to the presence of a nonlinearity. The same approach is also applied to flexural waves in an Euler-Bernoulli beam, demonstrating qualitatively different nonlinear dispersive effects compared to longitudinal waves [1]. Finally, we present a method for extending this analysis to a continuous periodic thin rod, i.e., a one-dimensional phononic crystal (see Figure 2) [2]. The method, which is based on a standard transfer matrix augmented with a nonlinear enrichment at the constitutive material level, yields an approximate band structure that accounts for the finite wave amplitude. The effects of the nonlinearity on the Bragg band gap are also highlighted, among other intriguing outcomes. In Ref. [1], it was shown that this technique gives accurate results for up to an amplitude-to-unit cell length ratio of one-eighth. The same technique is also applicable to one-dimensional locally resonant elastic metamaterials [3].

The present theory is not limited by the strength of the nonlinearity, unlike perturbation-based analysis which is commonly used in the literature for weakly nonlinear waves. A validated dispersion relation for a strongly nonlinear problem provides new understanding of the physics of nonlinear waves in general. This result is relevant to the study of waves in both natural and engineered problems, and in principle is applicable to a range of topics including dislocation and crack dynamics, geophysical and seismic waves, material nondestructive evaluation, biomedical imaging, elastic metamaterial engineering, nanoscale thermal transport, among others.

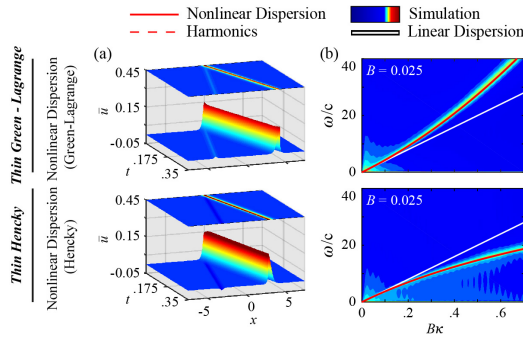


Figure 1: Finite-strain dispersion curves for a thin homogeneous rod. Top panel show case with Green Lagrange strain [1], and bottom panel show case with Hencky strain. The contours shown are obtain by direction space-time simulation (left) and corresponding Fourier transform (right).

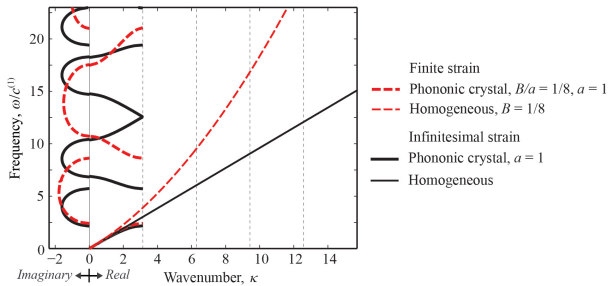


Figure 2: Finite-strain dispersion curves for a phononic-crystal thin rod under finite strain. For comparison, the dispersion curves under infinitesimal strain are included. Also, corresponding dispersion curves for a statically equivalent one-dimensional homogeneous elastic medium are overlaid. [2]

References

- [1] M. H. Abedinnasab and M. I. Hussein, Wave dispersion under finite deformation, *Wave Motion* **50** (2013), pp. 374–388.
- [2] M. I. Hussein and R. Khajehtourian, Nonlinear Bloch waves and balance between hardening and softening dispersion, *Proc. R. Soc. A* **474** (2018), 20180173.
- [3] R. Khajehtourian and M. I. Hussein, Dispersion characteristics of a nonlinear elastic metamaterial, *AIP Advances* **4** (2014), 124308.

Microwave experiments on resonances and zeros of the scattering matrix: From spectral gaps and width shifts to random anti-lasing

Ulrich Kuhl^{1,*}

¹Institut de Physique de Nice, Université Côte d'Azur, CNRS, Nice, France

*Email: ulrich.kuhl@unice.fr

Abstract

I will present versatile microwave set-ups addressing such different questions as the fractal Weyl law, the spectral Gap, width shifts, and zeros of the scattering matrix. The starting point is a detailed description of the experiments including the extraction of complex resonances from the measured reflections. Thereafter, results on the fractal Weyl law and the spectral gap are presented for strongly open systems with thin and thick classical repellers. The results are in agreement with predictions from resonance theory. Next the width shifts, i.e. change of resonance widths under local or global perturbations, are investigated. The experimental distributions agree with predictions from random matrix theory. Last but not least, I will concentrate on zeros of the scattering matrix, related to coherent perfect absorbers. Is it experimentally realizable in a q1D-setting with adjustable local absorption and corresponds to a random anti-laser.

Keywords: Resonances, Random Matrix Theory, Random Media, Wave front shaping, Coherent Perfect Absorber

In microwave experiments the complex scattering S is measured using vector network network analyzers [1]. In the experiments reflection S_{aa} and transmission S_{ab} are measured and can be described approximately by $S_{ab}(E) = \delta_{ab} - i \sum_n \frac{a_n}{\nu - \nu_n + \frac{i}{2}\Gamma_{\nu,n}}$, where a_n is the complex amplitude, ν_n the eigenfrequency and $\Gamma_{\nu,n}$ the width in frequency units. The complex eigenfrequencies ν_n can be related to the complex eigenenergies of a quantum-mechanical Hamiltonian. From the theoretical side, random matrix theory often in combination with the effective Hamiltonian approach is used to obtain prediction of the statistical behaviour of systems with corresponding classically chaotic systems. Apart from this theory from the mathematical side also interest on resonances of the Laplacian on an open space, see for example [2]. In this case the well founded Weyl law and width distributions need to be revisited. I will present

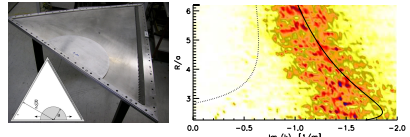


Figure 1: Left: Photograph of the microwave three-disk experiment with a sketch included. Right: Shade plots of the distribution of imaginary parts of k_n using a color code from white to dark blue for the three-disk experiment as a function of the R/a parameter. The classical escape rate is the solid black line and the pressure $P(1/2)$ corresponds to the dotted line. For details see [4].

microwave experiments on the three disk system agreeing with the prediction from mathematics. In Fig. 1 the experimental setup is shown on the left hand side and the experimental results for the spectral gap are shown on the right. For details on the microwave experiments and results on the fractal Weyl law refer to [3] and the spectral gap to [4].

The change of resonance widths in an open system under a perturbation of its interior has been introduced by Fyodorov and Savin [5] as a sensitive indicator of the nonorthogonality of resonance states. I present an experimental study on the universal statistics of this quantity in weakly open two-dimensional microwave cavities. Global as well as local perturbations are treated. In Fig. 2 the system used for local perturbations is shown (upper left) with the corresponding resonance position in normalized energies E_n . The resonance width of width Γ_n is indicated by the vertical lines. On the lower part the experimental width shift distributions for two types of perturbations (global and local) are presented. The theory prediction obtained by random matrix theoretical (RMT) studies are in good agreement with the experimental results. For further details see [6].

We will now turn from resonances to zeros

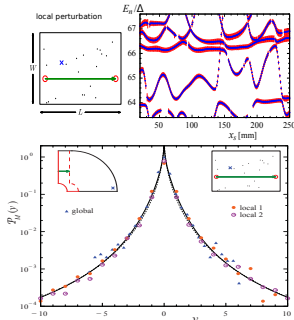


Figure 2: The experimental setup (upper, left) together with the parametric dependence (right) of energies and widths (red vertical lines). The eigenvalue dynamics are generated by moving a scatterer along the green arrow. The lower part shows the experimental normalized width velocities distribution $P(y)$ for systems with local and global perturbations. The solid (dashed) curve stand for the prediction for the global (local) perturbations. For further details see [6].

of the scattering matrix, more precisely to zeros of an eigenvalue of the scattering matrix. This is related to the coherent perfect absorber and time reversed lasing [7]. The experimental set-up is based on a quasi-one dimensional waveguide supporting four propagating modes. An arbitrary mode combination can be excited using four dipole antennas which are driven by a vector network analyzer via four IQ-modulators. The full complex scattering matrix can be detected using the set-up shown in the left part of Fig. 3. The scattering system presented here consists of randomly placed teflon scatterers and an additional local absorber (a dipole antenna connected to a 50Ω) is placed in the central part of the scattering region. The coupling of the antenna can be adjusted by changing its length. Within the frequency interval defined by the four mode propagating range for each realization we found a minimal eigenvalue of the scattering matrix with very low power reflection. An example is presented on the right hand side of Fig. 3 showing that the relative reflected power is less than 0.3%. As the local absorber is a dipole antenna we can also measure the reflection R_{abs} of this absorber and a minima is present at the same frequency as well showing

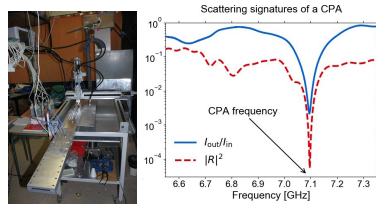


Figure 3: Left: Experimental set-up situated in the Waves in Complex Systems group at the University of Côte d'Azur in Nice, for the realization of a coherent perfect absorber corresponding to a random anti-laser. Right: Scattering signatures of a CPA state showing less than 0.3% reflection from the injected microwave power.

the connection to the random anti-laser. For further details refer to [8].

References

- [1] U. Kuhl et al., Direct processes in chaotic microwave cavities in the presence of absorption, *PRL* **94**, p. 144101 (2005)
- [2] M. Zworski, Resonances in physics and geometry, *Not. AMS* **43**, p. 319 (1999)
- [3] A. Potzauweit et al., Weyl asymptotics: From closed to open systems, *PRE* **86**, p. 066205 (2012)
- [4] S. Barkhofen et al., Experimental observation of the spectral gap in microwave n -disk systems, *PRL* **110**, p. 164102 (2013)
- [5] Y. V. Fyodorov and D. V. Savin, Statistics of resonance width shifts as a signature of eigenfunction nonorthogonality, *PRL* **108**, p. 184101 (2012)
- [6] J.-B. Gros et al., Experimental width shift distribution: A test of nonorthogonality for local and global perturbations, *PRL* **113**, p. 224101 (2014)
- [7] Y. D. Chong et al., Coherent perfect absorbers: Time-reversed lasers, *PRL* **105**, p. 053901 (2010)
- [8] K. Pichler et al., Random anti-lasing through coherent perfect absorption in a disordered medium, *Nature* **567**, p. 351 (2019)

Modal correlation and modal selectivity in open disordered media

Matthieu Davy^{1,*}, Azriel Z. Genack²

¹Univ Rennes, CNRS, Institut d'Electronique et de Télécommunications de Rennes - UMR 6164, F-35000 Rennes, France

²Department of Physics, Queens College and Graduate Center of the City University of New York, Flushing, New York 11367, USA

*Email: matthieu.davy@univ-rennes1.fr

Abstract

Open systems that are coupled to its surroundings through channels are described by non Hermitian Hamiltonians with complex eigenvalues. The bi-orthogonality of eigenfunctions leads to many exciting physical phenomena such as the existence of exceptional points or an excess noise in random lasers. Here, using microwave measurements, we explore the degree of correlation of eigenfunctions in chaotic and random systems. We demonstrate that the non-Hermiticity leads to the enhancement of modal strengths in transmission. Transmission is then reduced with negative correlations between overlapping modes so that the net transmission is bounded by unity. We then explore the selective excitation of quasi-normal modes by controlling the incoming wavefront. We show that the energy of a mode can be enhanced within a sample by a factor equal to the number of channels but the correlation between eigenfunctions limits modal selectivity.

Keywords: non-Hermitian, correlation of eigenfunctions, modal selectivity

1 Introduction

Quasi-normal modes, referred as modes in the following, are solutions of the wave equation with outgoing boundary conditions. In open systems, the eigenvalues and eigenfunctions of the wave equation are complex as a result of losses through channels. This stands in contrast to closed system for which they are real. The complex eigenvalues $\tilde{\omega}_n = \omega_n - i\Gamma_n/2$ are the poles of the scattering matrix $S(\omega)$ and can be extracted from spectral measurement of elements of $S(\omega)$. Here ω_n correspond to the central frequency and Γ_n to the linewidths. The statistics of modes are crucial to analyze transport through random systems. Thouless showed that the average of the dimensionless conductance g is determined by the degree of level or

modal overlap, which is the ratio of the average level width and spacing, so that $\delta = g$ [1]. The modal overlap parameter, known as the Thouless number, reflects the degree of spatial localization of waves within the sample. Thus the degree of modal overlap and spatial localization can be inferred from a measurement of steady-state conductance or transmission. The eigenfunctions of open systems, which are hence non-Hermitian, are nonorthogonal [2]. They form a bi-orthogonal set with a degree of correlation between eigenfunctions which increases with modal overlap [3, 4]. Measuring the degree of non-Hermiticity is however challenging since this requires probing the field inside the medium.

2 Experimental results

We measure the transmission matrix (TM) of a two-dimensional microwave multichannel system (see Fig. 1a). The TM is the part of scattering matrix associated with transmission coefficients between incoming and outgoing channels on the left and right side of the sample, respectively. We first show in Fig. 1b that spectra of the TM can be decomposed into a superposition of modal transmission matrices of unit rank. We then demonstrate that this modal analysis makes it possible to probe the degree of correlation of the eigenfunctions within the sample. The coupling coefficients between modes and channels are the projection of eigenfunctions at the interfaces of the sample and give the correlation between eigenfunctions. This is demonstrated for samples with high quality factor and moderate modal overlap which are chaotic cavities with weakly coupled antennas to the sample and random media with strong disorder.

We observe that the degree of correlation of eigenfunctions increases with the coupling of channels to the sample and with modal overlap. Experimental results of the correlation as a function of the spacing in the complex plane

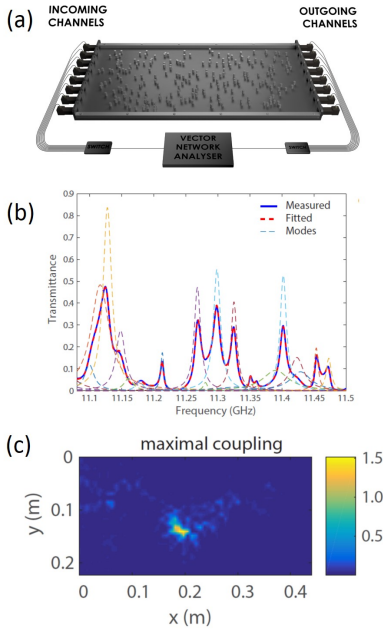


Figure 1: (a) Experimental setup. (b) Spectrum of the transmittance through a weakly localized sample (red curve), reconstruction using a modal analysis (blue dashed line) and contributions of modes to the transmittance (dashed lines). (c) Illustration of a spatial intensity profile inside the sample obtained for maximal enhancement of a mode.

between two resonances are in very good agreement with the theoretical eigenvector statistics given in Ref. [4, 5]. We then show that the non-Hermiticity is accompanied by an enhancement of modal strength in transmission T_n . The modal strength is related to the Petermann factor which characterizes an excess spontaneous emission for laser cavities [4–6]. The distribution of T_n is found to be bimodal for localized waves and extend over a very broad range for diffusive waves. Since transmission is bounded by unity, transmission is then suppressed relative to the incoherent sum of modal contributions by the coherent sum of overlapping modes

due to the negative correlation of modal speckle patterns.

Finally, we demonstrate that the energy density of a mode can be enhanced by a factor equal to the number of channels by shaping the incoming wavefront [6]. This provides a new approach to control waves in complex media in addition to the control of transmission and delay time [7]. Modal selectivity however is limited in open systems by the correlation between eigenfunctions leading to the correlation of output speckle patterns of neighboring modes. In accord with results of an effective Hamiltonian model, the degree of modal selectivity decreases with increasing modal spectral overlap and non-Hermiticity.

References

- [1] D. J. Thouless, *Phys. Rev. Lett.* **39** (1977), pp. 1167.
- [2] E. S. C. Ching, et al., *Rev. Mod. Phys.* **70** (1998), pp. 1545; F. Alpegiani, et al., *Phys. Rev. X* **7** (2017), pp. 021035; I. Rotter, *J. Phys. A* **42** (2009), pp. 153001
- [3] J. T. Chalker and B. Mehlig, *Phys. Rev. Lett.* **81** (1998), pp. 3367; Y. V. Fyodorov, *Commun. Math. Phys.* **363** (2018), pp. 579;
- [4] B. Mehlig and M. Santer, *Phys. Rev. E* **63** (2001), pp. 020105.
- [5] R. A. Janik, et al., *Phys. Rev. E* **60** (1999), pp. 2699.
- [6] M. Davy and A. Z. Genack, *Nat. Comm.* **9** (2018), pp. 4714.
- [7] S. Rotter and S. Gigan, *Rev. Mod. Phys.* **89** (2017), pp. 015005.

Spectral resonance expansion by Riesz projections

Lin Zschiedrich^{1,*}, Felix Binkowski², Sven Burger^{1,2}¹JCMwave GmbH, Berlin, Germany²Zuse Institute Berlin, Germany

*Email: lin.zschiedrich@jcmwave.com

Abstract

We review a spectral expansion approach for light-matter interaction problems as arising in nano-optical applications. The expansion is based on Riesz projections, which are given as contour integrals in the complex frequency plane to precisely quantify the coupling of an emitter to the eigenmodes and to the background continuum of modes of a nanoresonator. The approach is in particular also applicable in the case of general material dispersion.

Keywords: Riesz projection, resonance expansion, QNMs

Riesz projection expansion

In the past decades, the concept of a modal eigenfield expansion has been successfully generalized to open dissipative optical devices to study light-matter interaction [1–4]. In a nutshell, non-normalizable resonant states, also called quasinormal modes (QNMs), are used instead of eigenmodes. An orthogonality relation for QNMs together with an unconjugated scalar product has been formulated [5] and generalized for common dispersive media [6] allowing for a projection of a light scattering problem onto a finite set of discrete resonances. However, for weakly coupled systems, the discrete set of QNMs must be supplemented by the continuous spectrum of the operator capturing the nonresonant background scattering [7].

In this contribution, we discuss Riesz projections as an alternative approach for a resonance expansion of the electromagnetic field [8]. We show that with Riesz projections the nonresonant background interaction can be incorporated in a closed form. Riesz projections are a well-known concept in spectral theory [9] and they do not rely on orthogonality relations and the explicit knowledge of eigenfunctions and are therefore applicable for material dispersion beyond the Drude model.

To decompose the electric field solution $\mathbf{E}(\mathbf{r}, \omega_0)$ of time-harmonic Maxwell's equations into its

resonant and nonresonant parts, we consider the $z = \omega^2$ plane and write $\mathbf{E}(\mathbf{r}, z) = \mathbf{E}(\mathbf{r}, \omega = \sqrt{z})$. Cauchy's residue theorem gives

$$\mathbf{E}(\mathbf{r}, \omega_0) = \frac{1}{2\pi i} \oint_{C_0} \frac{\mathbf{E}(\mathbf{r}, z)}{z - \omega_0^2} dz, \quad (1)$$

where C_0 is a closed curve around ω_0^2 so that $\mathbf{E}(\mathbf{r}, z)$ is holomorphic inside of C_0 , as shown in Fig. 1(a). Then, deforming the path of integration so that an outer curve C_{nr} includes ω_0^2 , the resonance poles $\omega_1^2, \dots, \omega_M^2$ and no further poles yields

$$\begin{aligned} \oint_{C_0} \frac{\mathbf{E}(\mathbf{r}, z)}{z - \omega_0^2} dz &= - \oint_{C_1} \frac{\mathbf{E}(\mathbf{r}, z)}{z - \omega_0^2} dz - \dots - \oint_{C_M} \frac{\mathbf{E}(\mathbf{r}, z)}{z - \omega_0^2} dz \\ &\quad + \oint_{C_{nr}} \frac{\mathbf{E}(\mathbf{r}, z)}{z - \omega_0^2} dz, \end{aligned}$$

see Figs. 1(b) and (c). Thereby, we obtain the expansion

$$\mathbf{E}(\mathbf{r}, \omega_0) = \sum_{m=1}^M \mathbf{E}_m(\mathbf{r}, \omega_0) + \mathbf{E}_{nr}(\mathbf{r}, \omega_0), \quad (2)$$

where the fields

$$\mathbf{E}_m(\mathbf{r}, \omega_0) = -\frac{1}{2\pi i} \oint_{C_m} \frac{\mathbf{E}(\mathbf{r}, z)}{z - \omega_0^2} dz \quad (3)$$

are related to the resonance poles $\omega_1^2, \dots, \omega_M^2$. The field

$$\mathbf{E}_{nr}(\mathbf{r}, \omega_0) = \frac{1}{2\pi i} \oint_{C_{nr}} \frac{\mathbf{E}(\mathbf{r}, z)}{z - \omega_0^2} dz \quad (4)$$

quantifies the nonresonant components and contributions from possible resonance poles outside of the integration curve C_{nr} . It has to be ensured that C_{nr} does not cross the branch cut in the $z = \omega^2$ plane starting from $z = 0$. The fields in Eq. (3) are essentially Riesz projections applied to the governing time-harmonic Maxwell's equations, see results from spectral theory [9].

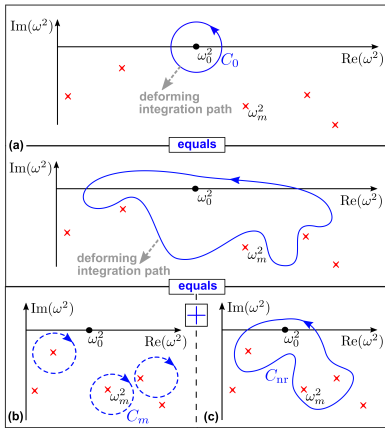


Figure 1: Contour integration in the complex ω^2 plane for computing the Riesz projection expansion. The red crosses represent resonance poles ω_m^2 , the blue curves are the integration curves. (a) Top: Integration path C_0 around ω_0^2 . Bottom: Deforming the integration path without enclosing resonance poles does not modify the integral. (b) Integration curves C_m in negative direction for computing Riesz projections. (c) Outer integration path C_{nr} for quantifying the interaction with nonresonant components. (figure from [8])

The numerical implementation of the Riesz projection is straightforward and essentially requires solving time-harmonic scattering problems for complex frequencies. We demonstrate the method by computing modal decay rates of a dipole emitter embedded in a diamond nanodisk antenna showing a weak coupling to the QNMs and a significant background coupling [8].

Acknowledgments

We acknowledge the collaboration with G. Kewes, N. Nikolay and O. Benson of Humboldt Universität zu Berlin. This project has received funding from the DFG Cluster of Excellence MATH+ (project AA4-6). This project has received funding from the European Union's Horizon 2020 research and innovation programme under the Marie Skłodowska-Curie grant agreement No 675745 (MSCA-ITN-EID NOLOSS).

References

- [1] E. A. Muljarov, W. Langbein, and R. Zimmermann. Brillouin-Wigner perturbation

theory in open electromagnetic systems. *EPL*, 92:50010, 2010.

- [2] C. Sauvan, J.-P. Hugonin, I. S. Maksymov, and P. Lalanne. Theory of the Spontaneous Optical Emission of Nanosize Photonic and Plasmon Resonators. *Phys. Rev. Lett.*, 110:237401, 2013.
- [3] P. T. Kristensen and S. Hughes. Modes and Mode Volumes of Leaky Optical Cavities and Plasmonic Nanoresonators. *ACS Photonics*, 1:2, 2014.
- [4] E. A. Muljarov and W. Langbein. Resonant-state expansion of dispersive open optical systems: Creating gold from sand. *Phys. Rev. B*, 93:075417, 2016.
- [5] P. T. Leung, S. Y. Liu, and K. Young. Completeness and orthogonality of quasinormal modes in leaky optical cavities. *Phys. Rev. A*, 49:3057, 1994.
- [6] W. Yan, R. Faggiani, and P. Lalanne. Rigorous modal analysis of plasmonic nanoresonators. *Phys. Rev. B*, 97:205422, 2018.
- [7] B. Vial, FF. Zolla, A. Nicolet, and M. Comandré. Quasimodal expansion of electromagnetic fields in open two-dimensional structures. *Phys. Rev. A*, 89:023829, 2014.
- [8] L. Zschiedrich, F. Binkowski, N. Nikolay, O. Benson, G. Kewes, and S. Burger. Riesz-projection-based theory of light-matter interaction in dispersive nanoresonators. *Phys. Rev. A*, 98:043806, 2018.
- [9] P.D. Hislop and I.M. Sigal. *Introduction to spectral theory. With applications to Schrödinger operators*. Springer, New York, 1996.

Resonant-state expansion applied to photonic-crystal structures

Sam Neale¹, Egor A. Muljarov^{1,*}¹School of Physics and Astronomy, Cardiff University, Cardiff CF24 3AA, United Kingdom

*Email: egor.muljarov@astro.cf.ac.uk

The resonant state expansion (RSE) is a novel rigorous method for calculating resonant states (RSs) of a photonic system [1]. These are the eigenolutions of Maxwell's wave equation (MWE) with outgoing boundary conditions. Using a complete set of RSs of a simpler system as a basis, the RSE makes a mapping of MWE onto a linear eigenvalues problem, determining the full set of the RSs of a complex system.

In addition to higher numerical efficiency [2,3] compared to other computational methods, the RSE provides an intuitive physical picture of resonant phenomena, capable of explaining features observed in optical spectra. So far the RSE has been applied to finite open optical systems of different geometry and dimensionality, as well as to homogeneous and inhomogeneous planar waveguides [3]. Very recently, the RSE was generalized to magnetic, chiral and bi-anisotropic optical systems [4], enabling its further application to metamaterials. The RSE has been also used in first perturbation order for photonic crystal (PC) structures to describe the refractive index sensing [5], and a rigorous analytic normalization of the RSs in PC structures has been presented [5,6].

Here, we develop a PC-RSE, a new rigorous approach for accurate calculation of RSs in planar PC structures using a homogeneous slab as basis system. The key advantage of treating periodic modulations of a homogeneous slab as perturbations is that all diagonal elements of the perturbation matrix are vanishing due to periodicity, which guarantees a low level of numerical errors in the RSE even for small basis sizes. Using for illustration a dielectric slab periodically modulated in one direction, we demonstrate the accuracy and efficiency of the PC-RSE in finding the RSs of photonic crystal structures.

The periodicity of PC structures mixes all possible Bragg harmonics. Therefore, the basis RSs have to be taken with different in-plane wave numbers. As a result, the Green's function of MWE has branch cuts in the complex

frequency plane, which have to be taken into account in the PC-RSE along with the RSs. This presents the major complication of the PC-RSE which we have dealt with by splitting the cuts into series of discrete, artificial cut states added for completeness to the basis of RSs [3].

We further study bound states in the continuum (BIC) of a dielectric photonic-crystal slab. We show in particular how different types of RSs of a homogeneous slab contribute to BIC and compare these contributions with other resonances of the photonic-crystal system, such as waveguide, quasi-guided [7] and Fabry-Pérot modes.

References

- [1] E. A. Muljarov, W. Langbein, and R. Zimmermann, *Europhys. Lett.* **92**, 50010 (2010).
- [2] M. B. Doost, W. Langbein, and E. A. Muljarov, *Phys. Rev. A* **90**, 013834 (2014).
- [3] S. V. Lobanov, G. Zorinants, W. Langbein, and E. A. Muljarov, *Phys. Rev. A* **95**, 053848 (2017).
- [4] E. A. Muljarov and T. Weiss, *Opt. Lett.* **43**, 1978 (2018).
- [5] T. Weiss, M. Mesch, M. Schäferling, H. Giessen, W. Langbein, and E. A. Muljarov, *Phys. Rev. Lett.* **116**, 237401 (2016).
- [6] T. Weiss, M. Schäferling, H. Giessen, N. A. Gippius, S. G. Tikhodeev, W. Langbein, and E. A. Muljarov, *Phys. Rev. B* **96**, 045129 (2017).
- [7] S. G. Tikhodeev, A. L. Yablonskii, E. A. Muljarov, N. A. Gippius, and T. Ishihara, *Phys. Rev. B* **66**, 045102 (2002).

Resonant mode approximation near Wood-Rayleigh anomalies

Nikolay A. Gippius^{1,*}, Sergey G. Tikhodeev²¹Skolkovo Institute of Science and Technology, Moscow, Russia² Prokhorov General Physics Institute, RAS and Faculty of Physics, Lomonosov Moscow State University, Moscow, Russia

*Email: n.gippius@skoltech.ru

Abstract

The optical properties of Fano resonances near diffraction threshold are addressed. The resonant mode approximation for the optical scattering matrix in respect to the propagation constant of the opening diffraction channel provides good description of the optical scattering matrix near the diffraction threshold anomalies.

Keywords: resonances, Wood-Rayleigh anomalies

1 Introduction

Layered periodic structures or photonic crystal slabs (PCS) [1] attract a great interest in modern nanooptics. A very convenient formalism for the numerical investigation of periodic structures is the Fourier modal method in the form of the optical scattering matrix (S -matrix) approach [2–4]. It is based on a decomposition of the solutions of the Maxwell's equations into a set of the Bloch waves. S -matrix connects the hypervectors of complex amplitudes of Bloch harmonics corresponding to the incoming and outgoing waves, $|I\rangle$ and $|O\rangle$,

$$S|I\rangle = |O\rangle. \quad (1)$$

The S -matrix method has been greatly improved in recent years with several techniques, such as factorization rules [5] and adaptive spacial resolution [6] (see, e.g., [7]). Due to this progress it is now possible to consider periodic structures with a complicated unit cell consisted of arbitrary materials including metals and/or anisotropic crystals. However, the needed computational time can still be very long. Therefore, physically clear approximations giving a qualitative, and, if possible, quantitative prediction of the system's properties are crucially important.

2 Resonant mode approximation

In this paper we analyze a generalization of the resonant mode approximation (RMA) [8,9], which

allows one to describe correctly the optical properties of PCS with the Fano-type resonances [10] near the Wood-Rayleigh diffraction threshold anomalies [11]. The approximation is free of fitting parameters: all needed quantities are calculated from the eigenproblem for the linearized inverse S -matrix [12].

Far from the diffraction thresholds, if N different poles are located near the frequency range of interest, S -matrix can be represented [8,9] as a sum of slowly varying background and resonant parts S_b and S_r ,

$$S = S_b + S_r = S_b + \sum_{r=1}^N \frac{A_r}{\omega - \Omega_r}. \quad (2)$$

Here matrices A_r depend on the corresponding input and output resonant vectors, $|I_r\rangle$ and $|O_r\rangle$,

$$A_r = |O_r\rangle\langle I_r|. \quad (3)$$

The details of this resonant mode approximation can be found in [9,13].

On the other side, as shown in [14], S -matrix in the vicinity of the threshold can be represented as $S = S_0 + B\kappa$, where the parameter $\kappa = \frac{\sqrt{\varepsilon}}{c} \sqrt{\omega^2 - \Omega_t^2}$ is a z -component of the wavevector of the new diffracted wave. This parameter is real above the threshold ($\omega > \Omega_t$) where the diffracted wave is propagating, and pure imaginary below the threshold.

Following [12] we consider the simplest case of two poles κ_1 and κ_2 in the vicinity of the diffraction opening. Instead of Eq. (2) we can now write the Breit-Wigner type expression for the S -matrix as a function of κ as

$$S = S_b + S_r = S_b + \sum_{r=1,2} |O_r\rangle \frac{1}{\kappa - \kappa_r} \langle I_r|. \quad (4)$$

Figures 1-2 show the trajectories of the poles $\kappa_{1,2}$ spanned with the change of k_x , i. e., the in-plane wavevector. Figure 3 and 4 show the dependencies of the reflection coefficient on complex κ for $k_x = 0.13\mu m^{-1}$ (diffraction chan-

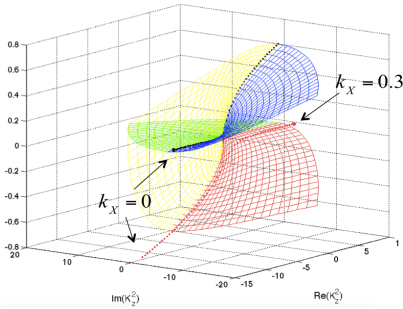


Figure 1: Trajectories of the poles in energy plane.

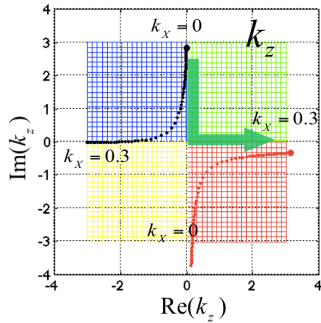


Figure 2: Trajectories of the poles in k_z plane.

nel for the quided mode is closed) and, respectively at the opening of the diffraction at $k_x = 0.17\mu\text{m}^{-1}$.

References

[1] K. Sakoda, *Optical Properties of Photonic Crystals*, Berlin: Springer-Verlag, 2001.
 [2] L. Li, *J. Opt. Soc. Am.* **A13**, 1024 (1996).
 [3] D.M. Whittaker, I.S. Culshaw, *Phys. Rev. B* **60**, 2610 (1999).
 [4] S.G. Tikhodeev et al., *Phys. Rev. B* **66**, 045102 (2002).
 [5] L. Li, *J. Opt. Soc. Am.* **A14**, 2758 (1997).
 [6] G. Granet, *J. Opt. Soc. Am.* **A16**, 2510 (1999).

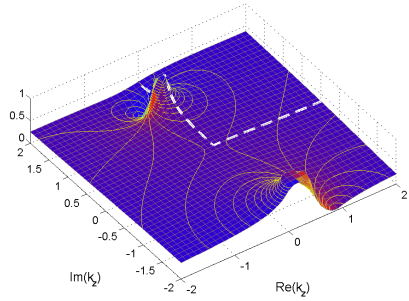


Figure 3: Reflectance vs k_z at $k_x = 0.13\mu\text{m}^{-1}$. White dashed line shows the κ_x corresponding the real energy.

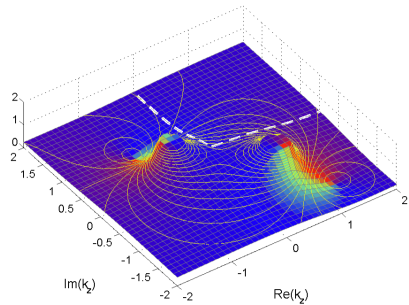


Figure 4: Reflectance vs k_z at $k_x = 0.17\mu\text{m}^{-1}$.

[7] T. Weiss et al., *Opt. Express* **17**, 8051 (2009).
 [8] N.A. Gippius et al., *Phys. Rev. B.* **72**, 045138 (2005).
 [9] N.A. Gippius et al., *Opt. Exp.*, **18**, 7569 (2010).
 [10] U. Fano, *J. Opt. Soc. Am.* **31**, 213 (1941).
 [11] Lord Rayleigh, *Philos. Mag.* **14**, 60 (1907).
 [12] A.B. Akimov, N.A. Gippius, S.G. Tikhodeev, *JETP Letters*, **93** 427 (2011)
 [13] T. Weiss et al., *J. Opt. Soc. Am. A*, **28**, 238 (2011).
 [14] B. M. Bolotovskii, A. N. Lebedev, *Sov. Phys. JETP* **26**, 784 (1968).

First-order perturbation theory for material changes in the surrounding of open optical resonators

Steffen Both^{1,*}, Thomas Weiss¹

¹4th Physics Institute and Research Center SCoPE, University of Stuttgart, Stuttgart, Germany

*Email: s.both@pi4.uni-stuttgart.de

Abstract

We present a first-order perturbation theory to predict resonance shifts and linewidth changes under small variations of the surrounding materials in almost any kind of open optical resonator. Our method allows to drastically reduce computational efforts and has potential applications in developing advanced sensor designs.

Keywords: computational methods, resonant sensing, plasmonics

1 Introduction

In recent years, nanophotonics has evolved into a powerful platform for various kinds of optical sensing applications. The typical operation principle is the following: Changes in the local environment of an open optical resonator lead to shifts of its resonance frequencies, and these shifts are then detected optically [1]. Examples for open resonators are plasmonic nanoantennas, dielectric nanoparticles, as well as photonic crystals. In order to design and optimize such systems with regard to their sensing capabilities, theoretical modeling becomes important. Usually this relies on full numerical simulations, which, however, have the disadvantage that they can be very time consuming, since, in order to calculate the response of the sensor to variations of the analyte substances, the simulations have to be repeated several times.

2 Perturbative approach

A way to drastically reduces the computational effort consists in perturbative theories. Such theories are based on the eigenmodes of the system, also known as resonant states or quasi-normal modes [1, 2]. The idea is the following: Once the eigenmodes of the unperturbed system are known, e.g., from a single simulations, the influence of perturbations to the system can be calculated analytically without relying on repetitive simulations. Such theories have been proven to be very efficient for describing all kinds of changes within or in close proxim-

ity to open optical resonators. However, a general rigorous way to incorporate perturbations of the surrounding medium into the theory is missing so far. The main difficulty arises from the fact that nanophotonic systems exhibit resonant states that radiate to the far field, so that their field distributions grow with distance to the resonator. Hence, conventional perturbative formulations for bound states, e.g., known from quantum mechanics, cannot be applied. Based on existing works [1–4], we recently have developed a way to also account for changes within the surrounding of the resonator [5]. Our main result is a simple integral expression over the fields of the unperturbed mode, that, in first-order approximation, directly provides the resonance shift and linewidth change as a function of the perturbation.

3 Results

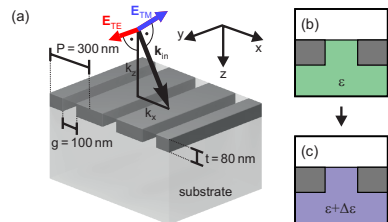


Figure 1: Exemplary test system: one-dimensional photonic crystal slab. (a) The structure consists of a periodic grating (dark gray), embedded into a substrate with permittivity ϵ , and air on top. (b,c) As a perturbation, we change ϵ to $\epsilon + \Delta\epsilon$.

To verify our theory, we apply it to different example systems. One of them is a one-dimensional photonic crystal slab, as depicted figure 1(a). The structure was initially introduced in Ref. [6] and was further discussed in Ref. [3]. All parameters are chosen as in the

forementioned references. The geometry consists of a periodic grating (dark gray, period $P = 300$ nm) of a material with refractive index 2.5, embedded into a substrate with permittivity ϵ , and air on top. As indicated in figure 1(b,c), we introduce a perturbation by changing ϵ to $\epsilon + \Delta\epsilon$. In figure 2(a,b), we display the normalized electric field distribution of exemplary resonant states in the unperturbed system. The example uses exactly the same modes as discussed in Ref. [3], which are a TE resonance at $k_x = \pi/(2P) = 5.236 \mu\text{m}^{-1}$ (a), and a TM resonance at $k_x = 0.2 \mu\text{m}^{-1}$ (b). Panels (c) and (d) depict the corresponding resonance energy (black) and linewidth (blue) as a function of ϵ . The solid lines represent the result of the first-order perturbation theory, while the squares have been derived from exact numerical calculations based on the Fourier modal method. It can be seen that for both modes, perturbation theory and exact results exhibit a good agreement, as long as the change in ϵ is not too big. Note that for the TE mode, the linear perturbation theory works over a much larger range of ϵ than for the TM mode. The reason is that the TM resonance depicted here is coincidentally very close to a Rayleigh anomaly [3] that strongly affects the far-field coupling, which in turn significantly depends on the substrate index that is changed here as the perturbation parameter.

4 Conclusion

We have generalized the single-mode approximation of the resonant state expansion to perturbations in the exterior of open optical resonators. We have tested our theory on different example systems, and found that, as long as the perturbations are not too big, our method exhibits a good agreement with exact calculations, while having the advantage of a reduced computational effort. Hence, we believe that our theory provides an efficient tool for the design and modeling of nanophotonic sensors.

References

- [1] T. Weiss, et al., From Dark to Bright: First-Order Perturbation Theory with Analytical Mode Normalization for Plasmonic Nanoantenna Arrays Applied to Refractive Index Sensing, *Phys. Rev. Lett.* **116** (2016), 237401.

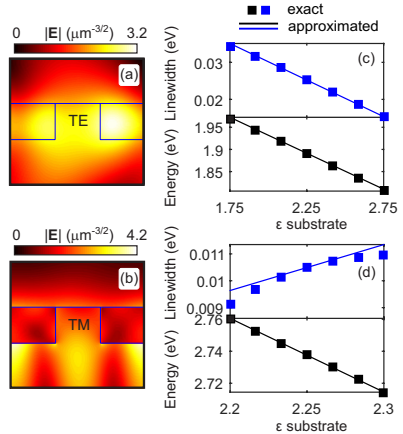


Figure 2: (a,b) Exemplary modes of the unperturbed system. (c,d) Corresponding resonance energy (black) and linewidth (blue) as a function of ϵ . Solid lines represent the results of the perturbation theory, while the squares are derived by numerically exact calculations.

- [2] J. Yang, H. Giessen, and P. Lalanne, Simple Analytical Expression for the Peak-Frequency Shifts of Plasmonic Resonances for Sensing, *Nano Lett.* **15** (2015), pp. 3439–3444.
- [3] T. Weiss, et al., Analytical normalization of resonant states in photonic crystal slabs and periodic arrays of nanoantennas at oblique incidence, *Phys. Rev. B* **96** (2017), 045129.
- [4] E. A. Muljarov, and T. Weiss, Resonant-state expansion for open optical systems: generalization to magnetic, chiral, and bianisotropic materials, *Opt. Lett.* **43** (2018), pp. 1978–1981.
- [5] S. Both and T. Weiss, First-order perturbation theory for material changes in the surrounding of open optical resonators, preprint: arXiv:1902.08120.
- [6] A. B. Akimov, N. A. Gippius, and S. G. Tikhodeev, Optical fano resonances in photonic crystal slabs near diffraction threshold anomalies, *JETP Lett.* **93** (2011), 427.

Resonant States Expansions of Scattering Operators in the Harmonic and Time Domains

Remi Colom¹, Brian Stout¹, Ross McPhedran², Nicolas Bonod^{1,*}

¹CNRS, Aix Marseille Univ, Centrale Marseille, Institut Fresnel, Marseille, France

²Institute for Photonics and Optical Science (IPOS), University of Sydney NSW 2006 Australia

*Email: nicolas.bonod@fresnel.fr

Abstract

In this work, we consider the S and T -matrices of dispersionless spherical scatterers and expand their elements with respect to their resonant states. This resonant state expansion features two terms: a non-resonant term and a resonant term composed of a phase term multiplied by a sum of lorentzian functions. The modal expansion of the T -matrix allows for a modal calculation of the scattering Mie coefficients which in turn provide the optical cross-sections. In a second step, we address the problem of the eigenfield divergence in the far field region. We show that this divergence vanishes when calculating the modal expression of the eigenfields in the time domain when invoking causality principle.

Keywords: Resonant states; Multipolar Formalism; Resonant Light Scattering; Open Systems

1 Introduction

The resonant interaction between light and plasmonic or Mie scatterers is of particular interest to enhance light-matter interactions through resonant light scattering, internal or near field enhancements. Such particles behave like open cavities for light and a lot of attention has been paid to describe their optical response in terms of their resonant states, also called quasi-normal modes [1-4].

In the multipolar description of light scattering, the electromagnetic properties of the scatterers can be predicted thanks to S and T -matrix operators. The matrix elements are of particular importance to calculate the scattering Mie coefficients with which are calculated the electromagnetic response of the scatterer, in particular their scattering and extinction cross-sections. They are also of high interest since the polarizabilities of the scatterer are proportional to these coefficients.

Here, we aim at expanding the coefficients of

these scattering operators in terms of the resonant states of the scatterer. We first derive the resonant states expansion in the harmonic domain of the three main S , T and Ω matrix operators. The second objective is to show that the well-identified divergence of the eigenfields observed in the harmonic domain far from the scatterer is removed in the time domain thanks to causality. The analytic expression of the scattered field in the time domain is derived when considering a causal incident field [5].

2 Resonant States Expansion in the Harmonic domain

In the multipolar framework theory, the incoming $\mathbf{E}_{\text{in}}(k\mathbf{r})$, outgoing $\mathbf{E}_{\text{out}}(k\mathbf{r})$, incident $\mathbf{E}_{\text{inc}}(k\mathbf{r})$ and scattered $\mathbf{E}_{\text{sca}}(k\mathbf{r})$ fields are expanded on the appropriate set of vector partial waves (VPW). The S -matrix operator links the outgoing field to the incoming field, $\mathbf{E}_{\text{out}}(\omega) = S(\omega)\mathbf{E}_{\text{in}}(\omega)$, while the T -matrix operator links the scattered field to the incident field, $\mathbf{E}_{\text{sca}}(\omega) = T(\omega)\mathbf{E}_{\text{inc}}(\omega)$. The poles of the scatterer satisfy the condition $S_n^{(i)-1}(p_{\alpha,n}^{(i)}) = 0$, where $i = e$ or h denotes the electric and magnetic modes, and n the multipolar order. We started this study in 2013 by describing the S matrix operator under the form:

$$S_n^{(i)}(\omega) = A_n^{(i)} e^{iB_n^{(i)}\omega} \left(1 + \sum_{\alpha} \frac{r_{n,\alpha}^{(i)}}{\omega - p_{n,\alpha}^{(i)}} \right)$$

where $r_{n,\alpha}^{(i)}$ are the residues at the pole $p_{n,\alpha}^{(i)}$, $A_n^{(i)}$ and $B_n^{(i)}$ being constant [1]. This expression unveils the existence of two kinds of contributions. The first term, $A_n^{(i)} e^{iB_n^{(i)}\omega}$, is a non-resonant contribution while the second term, composed of a sum of lorentzian functions, is a resonant contribution. We recently derived the analytic expression of the $A_n^{(i)}$ and $B_n^{(i)}$ constants and managed to derive the fully analytic modal expansion of the 3 matrix operators [5]:

$$S_n^{(i)}(\omega) \simeq e^{-2ikR} \left(S_{nr,n}^{(i)} + \sum_{\alpha=-M}^M \frac{r_{n,\alpha}^{(i)}}{\omega - p_{n,\alpha}^{(i)}} \right), \quad (1)$$

$$T_n^{(i)}(\omega) \simeq \frac{S_{nr,n}^{(i)} e^{-2ikR} - 1}{2} + \frac{e^{-2ikR}}{2} \sum_{\alpha=-M}^{+M} \frac{r_{n,\alpha}^{(i)}}{\omega - p_{n,\alpha}^{(i)}}, \quad (2)$$

where $S_{nr,n}^{(i)} = 1 + \sum_{\alpha=-M}^{+M} \frac{r_{n,\alpha}^{(i)}}{p_{n,\alpha}^{(i)}}$, R being the radius of the spherical scatterer. The convergence of the modal expansion can be studied with respect to the number of poles, M , taken into account in the expansion. It turns out that the convergence cannot be achieved if the non-resonant contribution is not taken into account. This kind of expansion was recently derived for the Ω -matrix coefficients linking the internal field to the incident field:

$$\Omega_n^{(i)}(\omega) \simeq \frac{1}{2} \sum_{\alpha=-M}^{+M} \frac{r_{\Xi,n,\alpha}^{(i)}}{\omega - p_{n,\alpha}^{(i)}}, \quad (3)$$

where $r_{\Xi,n,\alpha}^{(i)}$ is the residue of $\Omega_n^{(i)}(\omega)$ at pole $p_{n,\alpha}^{(i)}$. This modal expansion does not feature any non-resonant term. Lastly, we benefited from the modal expansions of external and internal to analyze the link between the Fano anomalies and anapoles observed in the scattering spectrum of dielectric Mie resonators with internal field enhancements inside the particle [6].

3 Resonant States Expansion in the Time domain

The problem of divergence experienced by the eigenfields has been studied by several authors and some of them suggested that causality could solve the problem [7]. However, despite significant advances, the problem of divergence of eigenfields still remains. Divergence-free expansion of the time-dependent scattered field may be derived from the pole expansions of the scattering operators by means of an inverse Fourier transform. One has however to consider a causal excitation field, $g(t)$ with a cut-off in the time domain, and to use the causality principle. In that case, we can obtain the analytic expression of the scattered field in the time domain and the far field with respect to the poles $p_{n,\alpha}^{(i)}$ of the

scatterer:

$$\mathbf{E}_{\text{scat},n,m}^{(\epsilon),\text{FF}}(\mathbf{r}, t) = \frac{\mathbf{D}_{n,m}(\theta, \phi)}{2k_0 r} g(t) * \left(S_{nr,n}^{(\epsilon)} \delta(t - \tau) - \delta\left(t - t_s - \frac{r}{c}\right) - iH(t - \tau) \sum_{\alpha=-M}^M r_{n,\alpha}^{(\epsilon)} e^{-i\omega_{p,n,\alpha}^{(\epsilon)}(t-\tau)} \right) \quad (4)$$

with $\mathbf{D}_{n,m}(\theta, \phi)$ being defined in ref.[5], $\tau = t_s + \frac{r}{c} - \frac{2R}{c}$ with t_s an additional time delay. A very similar expression can be obtained for $\mathbf{E}_{\text{scat},n,m}^{(h),\text{FF}}(\mathbf{r}, t)$ [5]. This expression shows that the scattered field of an optical cavity results from the convolution between the excitation field $g(t)$ and the response of the scatterer that is composed of two terms. The first term depends on the non-resonant contribution $S_{nr,n}^{(\epsilon)}$ and the second term includes the far-field expression of the eigenfield. The Heaviside distribution in front of this QNM field term comes from causality. This term is very important since it solves the divergence problem, the outgoing field being different from zero only when $t - t_s - \frac{r}{c} + \frac{2R}{c} \geq 0$ so that $e^{\omega_{p,n,\alpha}^{(\epsilon)}(t-t_s-\frac{r}{c}+\frac{2R}{c})} < 1$.

4 References

- [1] V. Grigoriev, A. Tahri, S. Varault, B. Rolly, B. Stout, J. Wenger, N. Bonod, Optimization of resonant effects in nanostructures via Weierstrass factorization, *Phys. Rev. A* **88** (2013), 011803(R).
- [2] C. Sauvan, J. P. Hugonin, I. Maksymov, P. Lalanne, Theory of the spontaneous optical emission of nanosize photonic and plasmon resonators, *Phys. Rev. Lett.* **110** (2013), 237401.
- [3] E. Muljarov, W. Langbein, Exact mode volume and Purcell factor of open optical systems, *Phys. Rev. B* **94** (2016), 235438.
- [4] P. Lalanne, W. Yan, K. Vynck, C. Sauvan, J. P. Hugonin, Light interaction with photonic and plasmonic resonances, *Laser & Photonics Reviews* **12** (2018), 1700113.
- [5] R. Colom, R. McPhedran, B. Stout, N. Bo Modal expansion of the scattered field: Causality, nondivergence, and nonresonant contribution, *Physical Review B* **98** (8), 085418 (2018).
- [6] R. Colom, R. McPhedran, B. Stout, N. Bo Modal Analysis of Anapoles, Internal Fields and Fano Resonances in Dielectric Particles, *J. Opt. Soc. Am. B* **36** (8), 2052-2061 (2019).
- [7] H. M. Nussenzveig, *Causality and dispersion relations*, Academic Press New York, 1972

Modal expansion of the T-matrix for resonant light scatterers

Anton I. Ovcharenko¹, Jean-Paul Hugonin¹, Christophe Sauvan^{1,*}

¹Laboratoire Charles Fabry, Institut d'Optique Graduate School, CNRS, Université Paris-Saclay, Palaiseau, France

*Email: christophe.sauvan@institutoptique.fr

Abstract

We propose a modal formalism to calculate semi-analytically the T -matrix of a single resonant scatterer from the sole knowledge of its eigenmodes. We use the reconstructed T -matrix to calculate the response of an ensemble of scatterers with the multipole method. This formalism allows calculating semi-analytically light scattering by various assemblies of resonant scatterers from the sole knowledge of a few eigenmodes of a single object.

Keywords: Quasinormal modes, T-matrix

1 Introduction

The development of micro- and nanotechnologies has recently opened a wide range of possibilities for controlling light at the wavelength scale or below. A fine control of the light (emission, transport and detection) in small volumes is at the heart of various applications, such as high-performance sensors, light focusing below the diffraction limit, nanolasers, solid-state single-photon sources, or photovoltaic devices. Most of these applications rely on the use of localized optical resonances supported by photonic or plasmonic micro and nanoresonators. Moreover, applications often require the use of an ensemble of resonators. For design and optimization purposes, it is crucial to calculate accurately the optical response of an ensemble of resonant light scatterers as fast as possible.

Multiple light scattering from an ensemble of scatterers, be it ordered or disordered, in a homogeneous environment or inside a layered medium, can be calculated from the T -matrix of each scatterer with the multipole method [1–4]. The T -matrix links the scattered field to the incident field, both expanded in the vector spherical waves basis. Once the T -matrix of each scatterer has been calculated, the calculation of light scattering by any arrangement of these scatterers can be easily calculated with the multipole method. The critical step is thus the calculation of the T -matrix. For spherical scatterers (sim-

ple spheres or core-shell spheres), the calculation can be done analytically with Mie theory. For scatterers with a more complex geometry, one has to rely on numerical calculations, see for instance [5].

Light scattering by a single resonant scatterer can be calculated semi-analytically from a modal expansion of the scattered field with quasinormal modes (QNM, also known as resonant states) [6–8]. Very recently, a few works have shown that such a modal expansion can be applied to reconstruct the T -matrix of a single scatterer or the scattering matrix of a periodic array [9–11]. However, the proposed formalisms do not rely on the sole knowledge of the object eigenmodes: either the fit of a non-resonant background [9, 10] or the calculation of the residues are needed [11].

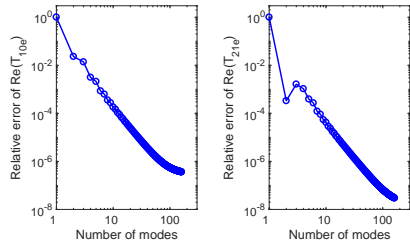


Figure 1: Relative error on the T -matrix calculated with a QNM expansion for a silver sphere of radius $R = 25$ nm. Left: relative error on the electric term with $n = 1$ and $m = 0$. Right: relative error on the electric term with $n = 2$ and $m = 1$. The reference calculation for the error evaluation is performed with Mie theory.

We propose a modal formalism that allows calculating semi-analytically the T -matrix of a single scatterer from the sole knowledge of its eigenmodes. Figure 1 displays the relative error on two different coefficients of the T -matrix for a silver nanosphere. The wavelength is chosen

close to the resonance.

Then, from the sole knowledge of the eigenmodes of a single scatterer, we calculate the optical response of an ensemble of scatterers by using a multipole method [2, 3]. We apply our formalism to dimers and periodic arrays of plasmonic nanoparticles. For instance, Fig. 2 shows the extinction cross-section of a dimer made of two gold nanorods illuminated by a plane wave with an incident angle shown by the red arrow. The solid blue curve corresponds to the calculation made from the T -matrix of a single nanorod reconstructed with a single QNM. It is compared to the results of a rigorous calculation (red circles). The calculation of a single QNM provides the extinction cross-section of the dimer with a good accuracy. Once the QNM of a single nanorod has been calculated, it can be used to calculate light scattering by any assembly of nanorods illuminated by any incident field.

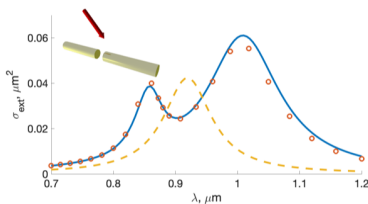


Figure 2: Extinction cross-section of a dimer made of two gold nanorods. The dimer is illuminated by a plane wave with an incident angle shown by the red arrow. We compare rigorous calculations (red circles) with the results obtained from the multipole method with the T -matrix of a single nanorod reconstructed with a single QNM (solid blue curve).

References

- [1] M.I. Mishchenko, G. Videen, V.A. Babenko, N.G. Khlebtsov and T. Wriedt, T -matrix theory of electromagnetic scattering by particles and its applications: a comprehensive reference database, *J. Quant. Spectrosc. Radiat. Transf.* **88** (2004), pp. 357–406.
- [2] B. Stout, C. Andraud, D. Prot, J. Lafait, J.C. Auger and S. Stout, Complete field description in three-dimensional multiple

scattering problems: a transfer-matrix approach, *J. Opt. A: Pure Appl. Opt.* **4** (2002), pp. S182–S187.

- [3] B. Stout, A. Devilez, B. Rolly and N. Bonod, Multipole methods for nanoantennas design: applications to Yagi-Uda configurations, *J. Opt. Soc. Am. B* **28** (2011), pp. 1213–1223.
- [4] A. Egel and U. Lemmer, Dipole emission in stratified media with multiple spherical scatterers: enhanced outcoupling from OLEDs, *J. Quant. Spectrosc. Radiat. Transf.* **148** (2014), pp. 165–176.
- [5] G. Demésey, J.C. Auger and B. Stout, Scattering matrix of arbitrarily shaped objects: combining finite elements and vector partial waves, *J. Opt. Soc. Am. A* **35** (2018), pp. 1401–1409.
- [6] Q. Bai, M. Perrin, C. Sauvan, J.P. Hugonin and P. Lalanne, Efficient and intuitive method for the analysis of light scattering by a resonant nanostructure, *Opt. Express* **21** (2013), pp. 27371–27382.
- [7] P. Lalanne, W. Yan, K. Vynck, C. Sauvan and J.P. Hugonin, Light interaction with photonic and plasmonic resonances, *Laser and Photonics Reviews* **12** (2018), pp. 1700113.
- [8] W. Yan, R. Faggiani and P. Lalanne, Rigorous modal analysis of plasmonic nanoresonators, *Phys. Rev. B* **97** (2018), pp. 205402.
- [9] F. Alleggiani, N. Parappurath, E. Verhagen and L. Kuipers, Quasinormal-Mode Expansion of the Scattering Matrix, *Phys. Rev. X* **7** (2017), pp. 021035.
- [10] T. Weiss and E. A. Muljarov, How to calculate the pole expansion of the optical scattering matrix from the resonant states, *Phys. Rev. B* **98** (2018), pp. 085433.
- [11] R. Colom, R. McPhedran, B. Stout and N. Bonod, Modal expansion of the scattered field: causality, divergence and nonresonant contribution, *Phys. Rev. B* **98** (2018), pp. 085418.

Expanding the Scattering Matrix through Quasi Normal Modes: a Numerical Case Study

Maximilian Geismann^{1,*}, Faruk Salihbegović¹, Matthias Kühmayer¹, Florian Libisch¹,
Stefan Rotter¹

¹Institute for Theoretical Physics, Vienna University of Technology (TU Wien), Vienna, Austria

*Email: e1125349@student.tuwien.ac.at

Abstract

Calculating the scattering-matrix (S -matrix) of a complex system typically requires an immense computational effort. Here we present a semi-analytical expansion of the S -matrix based solely on the far-field of Quasi-Normal Modes (QNMs) and on their complex eigen-energies. We showcase this approach by reconstructing the S -matrix of a disordered medium and demonstrate its superiority as compared to standard approaches, which have to repeat their numerical routines for every real scattering energy in a given energy-interval. For our QNM-expansion, on the other hand, similar routines are run only for a much smaller number of energies, which are in this case, however, complex. The resulting expansion thus requires only a comparatively short computation time and allows one to interpret the calculated scattering quantities through resonances in the system.

Keywords: Complex Scattering Systems, Quasi Normal Mode Expansion

1 Introduction

Scattering problems in quantum mechanics or classical electrodynamics typically require explicit solutions of the corresponding wave equations, i.e., the Schrödinger equation and the Maxwell equations, respectively. Imposing outgoing wave boundary conditions outside the system under study leads to special solutions called Quasi Normal Modes (QNMs) or resonant states. Their complex eigen-energies correspond to poles of the S -matrix located in the lower half of the complex plane. Along the real axis each pole forms a resonance-peak of width proportional to the modulus of its imaginary part such that a QNM-expansion is at the same time a pole expansion. Also, QNMs decay exponentially in time (they leak out of the system) but diverge in space for points far away from the scattering region due to their negative imaginary part. Normalisation is thus not trivial but possible [1, 2].

Furthermore, QNMs can form complete sets rendering them a suitable basis for perturbative techniques [3].

QNM-expansions of the S -matrix for specific cases have been proposed before: in [4] – on which our approach is based – the authors present a normalisation-independent derivation for real-valued far-fields starting from a coupled mode formalism, while the authors of [5] employ a normalisation-scheme for QNMs in order to expand the resonant part of the S -matrix.

In this contribution we will discuss limitations of the approach of [4] and new strategies for how to evaluate the non-resonant contribution to the S -matrix. Specifically, we will work with the example presented in Figure 1, consisting of a wave-guide with randomly distributed scattering elements placed inside of it. Comparing the QNM-expansion for this system with a conventional recursive Green’s function algorithm, we find a speed-up by a factor larger than 20 [6]. Furthermore, our approach provides considerable insight into the actual scattering physics that can be used for optimisation of such structures for any desired purpose [7].

2 Simulation and Results

The S -matrix expansion we use is given by [6]:

$$S(\omega) = C + iB(\omega - \bar{\Omega})^{-1}Q^{-1}B^\dagger \quad (1)$$

where C is the direct coupling matrix or the non-resonant background-term and the matrix B consists of the far-field column-vectors (evaluated at the boundaries) of the QNMs. The entries of $\bar{\Omega}$ and Q are given by

$$\bar{\Omega}_{ij} = \delta_{ij}\omega_i \quad (2)$$

$$Q_{ij} = i \frac{\vec{b}_i^\dagger \vec{b}_j}{\omega_j - \omega_i^*} \quad (3)$$

with δ_{ij} being the Kronecker-delta and ω_i and \vec{b}_i being the energy and far-field of the i -th QNM.

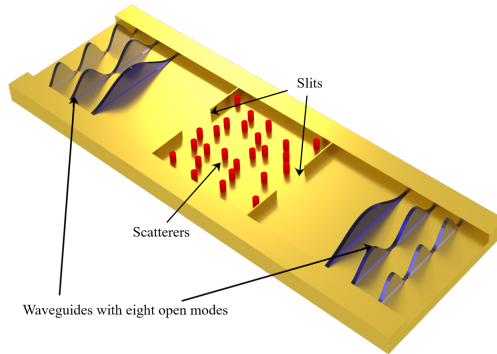


Figure 1: Geometry and potential of the two dimensional system under study: the square scattering region of length $L=4.35$ consists of 25 randomly placed scatterers (red rods) featuring a radius $r = 0.025L$ and a constant potential $V = 98.86E_0$ inside with $E_0 = \frac{1}{2}(\frac{\pi}{L})^2$. The scattering region is connected to two semi-infinite wave-guide leads with 8 open modes via a slit of width $L/3$ on each side (only six modes are shown in the asymptotic region).

In the example problem of Figure 1, we first evaluate a reference S -matrix using the modular recursive Green's function method [8, 9]. Next, we calculate the QNMs as eigen-states of a discretised Hamiltonian with perfectly matched layers attached at the boundaries via an iterative Krylov subspace routine. Both approaches show excellent agreement with each other, e.g., on the level of the transmission through the structure. Calculating the QNMs and evaluating the expansion took about 30 minutes, while computation of the reference S -matrix took about 11 hours on the same cluster.

References

- [1] A. J. F. Siegert, On the Derivation of the Dispersion Formula for Nuclear Reactions, *Physical Review* **56** (1939), pp. 750–752.
- [2] P. Lalanne, W. Yan, K. Vynck, C. Sauvan, and J.-P. Hugonin, Light Interaction With Photonic and Plasmonic Resonances, *Laser & Photonics Reviews* **12** (2017), p. 1700113.
- [3] A. Tanimu and E. A. Muljarov, Resonant-state expansion applied to one-dimensional quantum system, *Physical Review A* **98** (2018), p. 022127.
- [4] F. Alpeggiani, N. Parappurath, E. Verhagen, and L. Kuipers, Quasinormal-Mode Expansion of the Scattering Matrix, *Physical Review X* **7** (2017), pp. 2160–3308.
- [5] T. Weiss and E. A. Muljarov, How to Calculate the Pole Expansion of the Optical Scattering Matrix From the Resonant States, *Physical Review B* **98** (2018), p. 085433.
- [6] F. Salihbegović, M. Geismann, M. Kühmayer, F. Libisch, and S. Rotter, (manuscript in preparation).
- [7] V. Grigoriev, A. Tahri, S. Varault, B. Rolly, B. Stout, J. Wenger, and N. Bonod, Optimization of Resonant Effects in Nanostructures via Weierstrass Factorization, *Physical Review A* **88**, p. 011803.
- [8] S. Rotter, J.-Z. Tang, L. Wirtz, T. Ludger, and J. Burgdörfer, Modular Recursive Green's Function Method for Ballistic Quantum Transport, *Physical Review B* **62** (2000), pp. 1950–1960.
- [9] F. Libisch, S. Rotter, and J. Burgdörfer, Coherent Transport Through Graphene Nanoribbons in the Presence of Edge Disorder, *New Journal of Physics* **14** (2012), p. 123006.

**On a Class of Iterative Solvers for Time Harmonic Wave Propagation:
Factorizations, Sweeping Preconditioners, Source Transfer, Single Layer Potentials,
Polarized Traces, and Optimal and Optimized Schwarz Methods**

Martin J. Gander^{1,*}

¹Department of Mathematics, University of Geneva, Geneva, Switzerland

*Email: martin.gander@unige.ch

Abstract

There have been many recent developments for iterative solvers for time harmonic wave propagation. The methods mentioned in the title seem all to be quite different, and their invention followed quite different path¹. They are however very closely related, and I will show the precise relations, both at the continuous and the discrete level.

Keywords: Domain Decomposition, Time Harmonic Wave Propagation.

Introduction

Time harmonic wave propagation problems are difficult to solve by iterative methods, for a review, see [1]. Sweeping type preconditioners have received a lot of attention over the past few years, following the publication by Engquist and Ying [2, 3]. In the original version of the sweeping preconditioner, the problem is solved grid layer by grid layer, first sweeping in one direction over the computational domain, and then sweeping back.

Sweeping Type Preconditioners

An intense development of iterative methods based on sweeping motion followed. In the source transfer domain decomposition method by Chen and Xiang [4, 5], a Green's function representation is used to describe how a source on one side of the domain is transferred over the domain and the sources contained in it to the other side, and then back, in order to obtain an iterative solver. In the method of Stolk [6], which is based on single layer potentials, the domain is decomposed into a so called one way decomposition, leading to a decomposition into strips, and a subdomain iteration is introduced which uses a single layer potential representation at the interfaces to transmit information from one subdomain to the next, first from left to right, and then back. Then there is also the method of polarized traces

by Zepeda-Núñez and Demanet [7], and all these methods have sparked a wealth of followup publications.

Underlying Mathematical Techniques

All these methods use Perfectly Matched Layers (PML) or (high-order) Absorbing Boundary Conditions (ABCs) as an essential ingredient in transmission conditions on what can be interpreted as subdomain interfaces. They are very much related to earlier developments: on the one hand to the so called Analytic Incomplete LU (AILU) preconditioners by Gander and Nataf [8, 9] going back to the Filtering Frequency Decomposition by Wagner and Wittum [10, 11]. On the other hand, and even more importantly, they are related to the development of optimal and optimized Schwarz methods [12–17], see [18, 19] for an introduction.

The common formulation of optimal and optimized Schwarz methods allows us to explain in detail how and why these methods work. All these methods are based on one-dimensional decompositions of the problem in space into a sequence of subproblems, and they have in their optimal form the property to lead to nilpotent iterations, like an exact block LU factorization. They thus represent at the discrete level approximate block LU decomposition preconditioners. The continuous analog of the exact block LU factorization at the PDE level is what is called an optimal Schwarz method, where optimal here does not refer to scalability, but to the fact that better transmission conditions are not possible. The optimal transmission conditions involve Dirlet to Neumann operators, and in situations where those can be well approximated by PML, the methods can work extremely well. While we focus in the presentation on the specific case of the Helmholtz equation, our formulations are completely general and hold for other partial differential equations as well. This talk is based on joint work with Hui Zhang that just appeared

in a comprehensive article in SIAM Review [20].

References

- [1] Ernst, O., Gander, M.J.: Why it is difficult to solve Helmholtz problems with classical iterative methods. In: I. Graham, T. Hou, O. Lakkis, R. Scheichl (eds.) *Numerical Analysis of Multiscale Problems*, 325–363. Springer-Verlag, Berlin (2012)
- [2] Engquist, B., Ying, L.: Sweeping preconditioner for the Helmholtz equation: Hierarchical matrix representation. *Comm. Pure Appl. Math.* **LXIV**, 0697–0735 (2011)
- [3] Engquist, B., Ying, L.: Sweeping preconditioner for the Helmholtz equation: Moving perfectly matched layers. *Multiscale Model. Sim.* **9**, 686–710 (2011)
- [4] Chen, Z., Xiang, X.: A source transfer domain decomposition method for Helmholtz equations in unbounded domain. *SIAM J. Numer. Anal.* **51**, 2331–2356 (2013)
- [5] Chen, Z., Xiang, X.: A source transfer domain decomposition method for Helmholtz equations in unbounded domain Part II: Extensions. *Numer. Math. Theor. Meth. Appl.* **6**, 538–555 (2013)
- [6] Stolk, C.C.: A rapidly converging domain decomposition method for the Helmholtz equation. *J. Comput. Phys.* **241**, 240–252 (2013)
- [7] Zepeda-Núñez, L., Demanet, L.: The method of polarized traces for the 2D Helmholtz equation. *J. Comput. Phys.* **308**, 347–388 (2016)
- [8] Gander, M.J., Nataf, F.: AILU: a preconditioner based on the analytic factorization of the elliptic operator, *Numer. Linear Algebra Appl.*, **7**, 505–526 (2000)
- [9] Gander, M.J., Nataf, F.: An incomplete LU preconditioner for problems in acoustics. *J. Comput. Acoust.* **13**, 455–476 (2005)
- [10] Wittum, G.: An ILU-based smoothing correction scheme. In *Parallel algorithms for partial differential equations, Proc. 6th GAMM-Semin., Kiel/Ger., Notes Numer. Fluid Mech.*, **31**, 228–240 (1991)
- [11] Wagner C.: Tangential frequency filtering decompositions for symmetric matrices. *Numer. Math.*, **78**(1), 119–142 (1997)
- [12] Gander, M.J., Magoules, F., Nataf, F.: Optimized Schwarz methods without overlap for the Helmholtz equation. *SIAM J. Sci. Comput.* **24**, 38–60 (2002)
- [13] Gander, M.J., Halpern, L, and Magoules, F.: An optimized Schwarz method with two-sided Robin transmission conditions for the Helmholtz equation, *Int. J. Numer. Meth. Fluids*, **55**, 163–175 (2007)
- [14] Gander, M.J. and Zhang, H.: Domain decomposition methods for the Helmholtz equation: a numerical investigation, in *Domain Decomposition Methods in Science and Engineering XX*, R. Bank, M. Holst, O. Widlund, and J. Xu, eds., Berlin, Springer-Verlag, 215–222 (2013)
- [15] Gander, M.J. and Zhang, H.: Optimized Schwarz methods with overlap for the Helmholtz equation, *SIAM J. Sci. Comput.*, **38** A3195–A3219 (2016)
- [16] Kim, S. and Zhang, H.: Optimized Schwarz method with complete radiation transmission conditions for the Helmholtz equation in waveguides, *SIAM J. Numer. Anal.*, **53**, 1537–1558 (2015)
- [17] Kim, S. and Zhang, H.: Optimized double sweep Schwarz method by complete radiation boundary conditions, *Computers Math. Applic.*, **72**, 1573–1589 (2016)
- [18] Gander, M.J.: Optimized Schwarz methods. *SIAM Journal on Numerical Analysis* **44**(2), 699–731 (2006)
- [19] Gander, M.J.: Schwarz methods over the course of time, *Electron. T. Numer. Ana.*, **31**, 228–255 (2008)
- [20] Gander, M.J., Zhang, H.: A class of iterative solvers for the Helmholtz equation: Factorizations, sweeping preconditioners, source transfer, single layer potentials, polarized traces, and optimized Schwarz methods. *SIAM Review* **61**(1), 3–76 (2019)

L-Sweeps: A scalable parallel preconditioner for the high-frequency Helmholtz equation

Matthias Taus^{1,*}, Leonardo Zepeda-Núñez², Russell J. Hewett³, Laurent Demanet⁴

¹Institute for Analysis and Scientific Computing, TU Wien, Austria

²Lawrence Berkley National Laboratory, USA

³Department of Mathematics, Virginia Tech, USA

⁴Department of Mathematics, MIT, USA

*Email: matthias.taus@gmail.com

Abstract

We introduce a new preconditioning technique for the high-frequency Helmholtz equation based on a checkerboard domain decomposition. The novelty of the new technique is that it can be applied in parallel and is independent of the discretization. In particular, the preconditioner can be applied in $O(N/p)$ complexity where N is the number of degrees of freedom and $p = O(N^{1/d})$ is the number of processors. We consider several numerical examples involving constant and non-constant wave speeds. In all examples, using a preconditioned GMRES method, the preconditioner results in a logarithmic growth of the number of iterations with respect to the frequency ω .

Keywords: High-frequency Helmholtz equation, Preconditioning, Parallel computing

1 Introduction

In many science and engineering applications, solving time-harmonic high-frequency wave propagation problems quickly and accurately is of paramount importance. For example, in geophysics, particularly in oil exploration, such problems can be the forward problem in an iterative process for solving the inverse problem of subsurface inversion. It is important to solve these wave propagation problems accurately in order to efficiently obtain meaningful solutions of the inverse problems: low order forward modeling can hinder convergence. Additionally, due to the volume of data and the iterative nature of most optimization algorithms, the forward problem must be solved many times. Therefore, a fast solver is necessary to make solving the inverse problem feasible. For time-harmonic high-frequency wave propagation, obtaining both speed and accuracy is historically challenging.

Recently, there have been many advances in the development of fast solvers for such prob-

lems, including methods which have linear complexity with respect to the number of degrees of freedom. While most methods scale optimally only in the context of low-order discretizations and smooth wave speed distributions, the method of polarized traces [1] has been shown to retain optimal scaling for high-order discretizations, such as hybridizable discontinuous Galerki methods and for highly heterogeneous (and even discontinuous) wave speeds [4]. The resulting fast and accurate solver is consequently highly attractive for geophysical applications. To date, this method relies on a layered domain decomposition together with a preconditioner applied in a sweeping fashion, which has limited straightforward parallelization.

In this work, we introduce a new technique which reveals more parallel structure than previous versions while preserving all of other advantages of the method of polarized traces. We achieve this by introducing the preconditioner based on a checkerboard domain decomposition (DD) resulting in a preconditioner that can be applied in optimal parallel complexity. All considered numerical examples result in a logarithmic growth of the number of iterations in a preconditioned GMRES solver showing the almost optimal complexity to invert the linear system. To the best of our knowledge, this is the first preconditioner for the high-frequency Helmholtz equation that reveals this almost optimal parallel complexity.

As a model problem we use the high-frequency Helmholtz equation with varying wave speed on a square (or cube) Ω with transparent boundary conditions. We discretize the problem using finite difference methods and perfectly matched layers. However, all techniques presented in this work can be directly extended to other discretizations or transparent boundary conditions.

2 Method

The method is based on a checkerboard DD of the domain Ω . Corresponding to each subdomain we define a local problem by gluing transparent boundary conditions to its boundaries. The global wave field is then reconstructed in two stages. The first stage simply consists of the method of polarized traces applied to each row and column of the checkerboard DD, see Figure 1.

The second stage constructs the wave field in the remaining subdomains. A sweep over the domain on a layer-by-layer basis is applied where the layers are defined as the diagonals of the checkerboard DD. Then each subdomain in one layer can be processed independently by solving a quarter-space problem based on L-shaped incoming traces from the previous layer. We show that on the algebraic level, the solution of these quarter-space problem can be computed using similar techniques as in [1].

Using this procedure, we sweep over the diagonally defined layered domain decomposition. The sweep from the bottom left corner to the top right corner is illustrated in Figure 1.

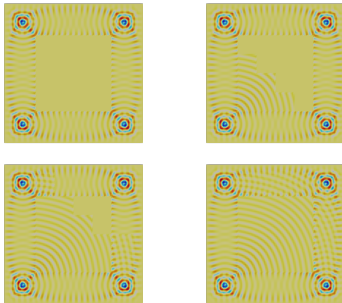


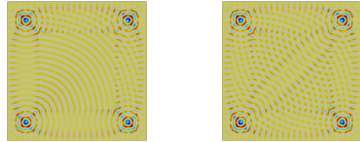
Figure 1: The reconstructed wave fields after stage 1 (top left), and at snapshots during stage 2. The snapshots were taken during (top right, bottom left) and at the end of (bottom right) the first diagonal sweep over the domain.

To get a good approximation of the global wave field, we sweep over each diagonal in both directions, see Figure 2. Combined with a windowing technique to avoid ill-defined restrictions of delta distributions appearing in the residuals of the reconstructed wave field, this technique is

used as a preconditioner for the iterative solution of the global linear system.

We consider several numerical examples to show that the resulting iteration count is logarithmic with respect to the frequency ω and that for appropriately defined domain decompositions, the new preconditioner can be applied in $O(N/p)$ complexity where $p = O(N^{1/d})$.

Sweep 1: bottom left to top right: Sweep 2: top right to bottom left



Sweep 3: bottom right to top left: Sweep 4: top left to bottom right

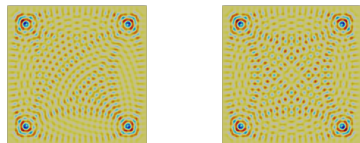


Figure 2: Summary of stage 2.

3 Outlook

Our solution strategy can be applied for $d = 2, 3$ as long as $p = O(N^{1/d})$. In 3D, this can be further improved by parallelizing the quasi-one-dimensional problems in each subdomain using multi-frontal methods. This allows one to use $p = O(N^{\frac{d-1}{d}})$ processors resulting in the $O(N^{1/d})$ complexity for $d = 2, 3$. In the presence of several right hand sides this can be even further improved using pipelining [2]. The end result is that in average in a parallel environment the preconditioner can be applied in $O(1)$ time per right hand side as long as there are at least $O(N^{1/d})$ right hand sides and $p = O(N^{\frac{d-1}{d}})$ processors. All of these extensions are the topic of current research.

References

- [1] L. Zepeda-Núñez and L. Demanet, The method of polarized traces for the 2D Helmholtz equation, *Journal of Computational Physics* **308** (2016), pp. 347–388.
- [2] L. Zepeda-Núñez, A. Scheuer, R. J. Hewett and L. Demanet, The method of polarized traces for the 3D Helmholtz equation, *arXiv e-prints* arXiv:1801.08655
- [3] M. Taus, L. Zepeda-Núñez, R. J. Hewett and L. Demanet, L-Sweeps: A scalable parallel preconditioner for the Helmholtz equation, In preparation.
- [4] M. Taus, L. Demanet, L. Zepeda-Núñez, A short note on a fast and high-order hybridizable discontinuous Galerkin solver for the 2D high-frequency Helmholtz equation, SEG Technical Program Expanded Abstracts 2016, pp. 3835–3840

Sweeping Preconditioner

Lexing Ying^{1,*}¹Department of Mathematics, Stanford University, Stanford, CA, USA

*Email: lexing@stanford.edu

Abstract

This talk reviews the main ideas behind the sweeping preconditioner for solving high-frequency time-harmonic wave equations and its extensions.

Keywords: sweeping preconditioner, Helmholtz equation, Maxwell equation, elasticity equation

1 Introduction

Let us start by considering the Helmholtz equation

$$\Delta u(x) + \frac{\omega^2}{c^2(x)} u(x) = f(x),$$

on the unit box $D = (0, 1)^d$ with $d = 2, 3$ with Sommerfeld boundary condition at infinity, where ω is the angular frequency, $c(x)$ is the velocity field, and $f(x)$ is the external force. It is convenient to assume that $c(x)$ is of order $O(1)$ and $\lambda = \frac{2\pi}{\omega}$ is the typical wavelength.

A popular treatment of the Sommerfeld boundary condition is the perfectly matched layer developed by Berenger [1]. By introducing appropriate complex damping at the domain boundary, the PML solution for $d = 2$ satisfies

$$\left(\partial_1 \left(\frac{s_1}{s_2} \partial_1 \right) + \partial_2 \left(\frac{s_2}{s_1} \partial_2 \right) + \frac{\omega^2}{s_1 s_2 c^2} \right) u = f,$$

where s_1 and s_2 are functions of x_1 and x_2 , respectively.

In a typical setting, the Helmholtz equation is discretized with at least a constant number of points per wavelength. Therefore, the number of samples n in each dimension is proportional to ω , the total number of samples N for a uniform Cartesian discretization is $n^d = O(\omega^d)$. For simplicity, assume that the 5-point stencil finite difference method is used for the discretization of the second order differential operator and the unknowns are order slice-by-slice by going through the x_1 coordinate first, we end up with a matrix equation

$$\mathbf{A} \mathbf{u} = \mathbf{f}.$$

By denoting the unknowns and forcing terms in the i -th slice by \mathbf{u}_i and \mathbf{f}_i , the system takes the

form

$$\begin{pmatrix} \mathbf{A}_{1,1} & \mathbf{A}_{1,2} & & & \\ \mathbf{A}_{2,1} & \mathbf{A}_{2,2} & \ddots & & \\ & \ddots & \ddots & \mathbf{A}_{n-1,n} & \\ & & & \mathbf{A}_{n,n-1} & \mathbf{A}_{n,n} \end{pmatrix} \begin{pmatrix} \mathbf{u}_1 \\ \mathbf{u}_2 \\ \vdots \\ \mathbf{u}_{n-1} \\ \mathbf{u}_n \end{pmatrix} = \begin{pmatrix} \mathbf{f}_1 \\ \mathbf{f}_2 \\ \vdots \\ \mathbf{f}_{n-1} \\ \mathbf{f}_n \end{pmatrix}$$

2 Sweeping preconditioner

The starting point of the sweeping preconditioner [3] is the LDL^T factorization of \mathbf{A} :

$$\mathbf{A} = \mathbf{L}_1 \cdots \mathbf{L}_{n-1} \begin{pmatrix} \mathbf{S}_1 & & & \\ & \mathbf{S}_2 & & \\ & & \ddots & \\ & & & \mathbf{S}_n \end{pmatrix} \mathbf{L}_{n-1}^T \cdots \mathbf{L}_1^T,$$

where \mathbf{S}_i are the Schur complements. Inverting this factorization gives an explicit representation of the solution

$$\mathbf{u} = (\mathbf{L}_1^T)^{-1} \cdots (\mathbf{L}_{n-1}^T)^{-1} \begin{pmatrix} \mathbf{S}_1^{-1} & & & \\ & \mathbf{S}_2^{-1} & & \\ & & \ddots & \\ & & & \mathbf{S}_n^{-1} \end{pmatrix} \mathbf{L}_{n-1}^{-1} \cdots$$

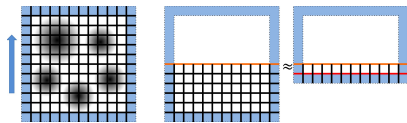


Figure 1: Left: the domain discretization and the sweeping direction. Middle: the half-space problem for each Schur complement \mathbf{S}_m . Right: the truncated domain.

The key challenge is how to apply \mathbf{S}_m^{-1} to an arbitrary vector efficiently and accurately. The main observation is that the matrix \mathbf{S}_m^{-1} is the restriction to the m -th slice of the discrete half-space Green's function with zero boundary condition at the $(m+1)$ -th slice. The key idea is that,

since only the restriction at the m -th slice is of interest, one can approximate by truncating the domain and moving the PML the beginning all the way close to the m -th slice.

This is the *moving PML* idea of the sweeping preconditioner.

The main computational advantage is that, for each matrix-vector multiplication of \mathbf{S}_m^{-1} , we have traded a d -dimensional half-space problem with and a quasi $(d-1)$ -dimensional sub-problem. When $d = 2$, the quasi 1D sub-problem can be solved efficiently by banded LU factorization. The costs for constructing and applying the factorization are both $O(n)$. When $d = 3$, the quasi 2D sub-problem can be solved efficiently using the nested dissection algorithm by George [5] (or the more general multifrontal method). The costs for constructing and applying the factorization are $O(n^3)$ and $O(n^2)$, respectively.

The resulting algorithm serves as a reasonably accurate approximate inverse of the operator \mathbf{A} . When combined with general iterative solvers (e.g. GMRES or TFQMR) as a preconditioner, the iterative solver typically converge in a small number of iterations, as witnessed by a wide variety of numerical examples. In 2D, the overall costs for constructing the preconditioner and solving the Helmholtz problem iteratively are $O(N)$ and $O(Nm_{\text{it}})$, respectively, where m_{it} is the number of iterations. In 3D, the costs are $O(N^{4/3})$ and $O(N \log Nm_{\text{it}})$, respectively.

We would like to point out that the idea of using LU or LDE^T factorization for solving the Helmholtz equation has appeared earlier in the work of Gander and Nataf [4]. The main novel ingredients of the sweeping preconditioner are (1) truncating the domain with the moving PML to reduce the dimensionality, and (2) incorporating the nested dissection for the rapid solution of the quasi 2D sub-programs.

3 Extensions

When the sweeping preconditioner was first proposed, the quasi 2D sub-problems are solved [2] with the hierarchical matrix algebra developed by Hackbusch et al. However, theoretical and numerical studies seem to suggest that the nested dissection approach is more efficient and robust.

Over the past several years, the sweeping preconditioner has been extended in several directions. First, it has been applied to the time-harmonic Maxwell's equations, in the settings of the Yee's scheme and the curl-conforming edge element. We have also implemented it to time-harmonic elasticity equation in the setting of

spectral elements with local Gauss-Lobatto grids

For 3D large-scale (i.e. high-frequency) problems, the main computational task of the sweeping preconditioner is the construction and application of the nested dissection solver for each slice. We have designed a parallel multifrontal solver to speed up these calculations and have applied the parallel solver to 3D large-scale seismic simulations.

For 3D problems, another approach for speeding up the quasi 2D sub-problems relies on the simple observation that these sub-problems are approximately Helmholtz equations themselves. Therefore, it is natural to applying the sweeping preconditioner to solve them. This line of idea results the recursive sweeping preconditioners.

As we have seen, the starting point of the sweeping preconditioner is the (multiplicative) LDL^T factorization of the operator \mathbf{A}^{-1} . Alternatively, one can also write down an additive $\mathbf{L} + \mathbf{D} + \mathbf{U}$ decomposition for \mathbf{A}^{-1} . It turns out that one can also use the same moving PML sweeping idea to accelerate the matrix-vector multiplications of \mathbf{L} and \mathbf{U} . This results an additive version of the sweeping preconditioner.

Finally, the sweeping preconditioner has also been applied to solve the (integral) Lippman-Schwinger equation of the time-harmonic acoustic scattering. The key idea here is to design a problem-specific transformation that turns the Lippman-Schwinger approximately to a sparse linear system. This sparse linear system can be viewed as a Helmholtz-type equation and the sweeping preconditioner can be applied to speed up its solution.

References

- [1] J. Berenger, *Journal of Computational Physics* **114** (1994)
- [2] B. Engquist and L. Ying, *Communications in Pure and Applied Mathematics* **6** (2011)
- [3] B. Engquist and L. Ying, *Multiscale Modeling and Simulation* **9** (2011)
- [4] M. Gander and F. Nataf, *Journal of Computational Acoustics* **13** (2005)
- [5] J. George, *SIAM Journal on Numerical Analysis* **10** (1973)

Towards sweeping preconditioners for computational helioseismology

Janosch Preuß^{1,*}, Christoph Lehrenfeld², Thorsten Hohage^{1,2}¹Max Planck Institute for Solar System Research, Göttingen, Germany²Institute for Numerical and Applied Mathematics, University of Göttingen, Germany

*Email: janosch.preuss@stud.uni-goettingen.de

Abstract

The propagation of acoustic waves in the Sun can be described by a Helmholtz-type equation. We aim to construct efficient preconditioners for the iterative solution of the arising linear systems based on a sweeping approach. The resonating nature of the Sun poses a major challenge for the application of sweeping preconditioners. In this talk we discuss why this is the case based on an investigation of the Dirichlet-to-Neumann operator. Furthermore, we sketch our approach to overcome these problems employing symmetry and spherical harmonic transforms.

Keywords: helioseismology, sweeping preconditioners, Dirichlet-to-Neumann operator, resonances

1 Introduction

The propagation of acoustic waves in the Sun is approximately described by the Helmholtz equation

$$-\frac{\sigma^2}{\rho c^2} u - \nabla \cdot \left(\frac{1}{\rho} \nabla u \right) = f, \quad (1)$$

where u is the divergence of the wave displacement. The density ρ and sound speed c are determined by a given solar model and $\sigma^2 = \omega^2 + 2i\gamma\omega$ with damping $\gamma = \gamma(\omega)$ chosen to fit the solar data.

In [1] wave propagation in the Sun has been treated under the assumption of axial symmetry. We further refer to [2] in which Atmospheric Radiation Boundary Conditions were developed that model the behavior of outward propagating waves. In the fully three-dimensional case or for a more accurate vector-valued version of (1) a direct solution of the arising linear systems may become unfeasible. Hence, we aim to construct efficient preconditioners for the iterative solution of these problems.

Our aim is to develop sweeping preconditioners as introduced in [3]. In [4] this preconditioner has been described as a special op-

timized Schwarz method which uses as transmission condition between subdomain interfaces an approximation of the Dirichlet-to-Neumann (DtN) operator by a moving Perfectly Matched Layer (PML). Applying this preconditioner in combination with GMRES to an axisymmetric version of the problem yields iteration numbers:

$\omega/2\pi$	9.0	6.0	4.5	4.0	3.5	3.0
#iterations	5	5	10	22	68	> 100

Contrary to expectation, the preconditioner is very efficient for high frequencies but its performance deteriorates dramatically for low frequencies. Next, we want to explain this behavior and the arising challenges.

2 Challenges for applying sweeping preconditioners

The Sun is a resonator: Inward propagating waves are refracted by an increase in sound speed towards the core while outward propagating wave with frequency lower than a certain cutoff ($\omega/2\pi$ 5.3 mHz) are reflected by the sharp decrease in density towards the surface. While sweeping preconditioners have shown impressive results for many problems their usefulness in the presence of resonances, as for the Sun, appears to be an open question. Indeed, our tests indicate that the sweeping preconditioner performs poorly in this setting. To understand why this happens it is instructive to consider the one-dimensional case:

Assuming spherical symmetry, i.e. $c = c(r)$, $\rho = \rho(r)$ with r denoting the radial distance from the Sun's core, the solution decomposes into spherical harmonics

$$u(r, \theta, \phi) = \sum_{\ell=0}^L \sum_{m=-\ell}^{\ell} u^{\ell,m}(r) Y_{\ell}^m(\theta, \phi). \quad (2)$$

Plugging this ansatz into (1) yields the ODE

$$-\frac{\partial}{\partial r} \left(\frac{r^2}{\rho} \frac{\partial u^{\ell,m}}{\partial r} \right) + \left(\frac{\ell(\ell+1)}{\rho} - \frac{\sigma^2 r^2}{\rho c^2} \right) u^{\ell,m} = r^2 f^{\ell,m}. \quad (3)$$

The success of the sweeping preconditioner is determined by how well the DtN operator can be approximated by the moving PML [5]. Figure 1 shows this approximation close to the Sun's surface obtained with a moving PML that contains about ten degrees of freedom. The exact DtN numbers have outliers that occur close to the nodes of a nearby resonance eigenfunction. Apparently, the PML fails completely to capture the behavior of the DtN numbers.

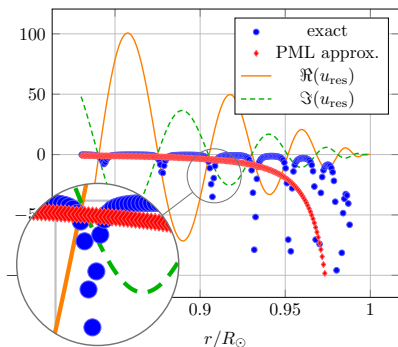


Figure 1: Moving PML approximation of the imaginary part of the DtN numbers for equation (3) with $\omega = 3.0$ mHz, $\ell = 0$. Also shown is an eigenfunction u_{res} corresponding to a nearby resonance. Distance on the abscissa given in terms of the solar radius R_{\odot} .

3 Towards more accurate transmission conditions

Spherical symmetry of the reference model suggests to decompose the Sun into spherical shells which can serve as layers for the sweeping method. This requires an approximation of the DtN operator on spheres. For boundary data $g(\theta, \phi) = \sum_{\ell=0}^L \sum_{m=-\ell}^{\ell} g^{\ell,m} Y_{\ell}^m(\theta, \phi)$ given in terms of spherical harmonics the solution of the corresponding exterior problem can easily be written down in the form (2). From this expression the normal derivative $\partial u / \partial r$ can be obtained by differentiating the radial coefficients $\partial u^{\ell,m} / \partial r$. Hence, for the purely spherically symmetric case the DtN operator can be determined by solving the ODEs (3), which are actually independent of m . Combining this observation with spherical harmonic transforms allows to apply the DtN operator to arbitrary boundary data.

We realized this idea for a two-dimensional model problem on the unit disk employing a

general framework for the sweeping methods (see Algorithm 2 of [4]). To demonstrate the shortcomings of the moving PML we use a similar strategy as in [5]: The disk is partitioned into ten circular layers in between which the wavenumber is discontinuous. On the first layer the wavenumber is $16(1 - \alpha/2)$, on the second $16(1 + \alpha/2)$, on the third $16(1 - \alpha/2)$ and so on continuing this sequence. Increasing the contrast α leads to a dramatic growth of the iteration numbers:

α	moving PML	our approach
0.0	7	17
0.5	63	18
1.0	137	19

However, our approach appears to be nearly robust. Encouraged by this result we aim to extend this technique for our applications in helioseismology.

References

- [1] L. Gizon, H. Barucq, M. Duruflé, C. S. Hanson, M. Leguèbe, A. C. Birch, et al., Computational helioseismology in the frequency domain: acoustic waves in axisymmetric solar models with flows, *Astronomy and Astrophysics* **600** (2017), A35.
- [2] H. Barucq, J. Chabassier, M. Duruflé, L. Gizon and M. Leguèbe, Atmospheric Radiation Boundary Conditions for the Helmholtz Equation, *ESAIM: Mathematical Modelling and Numerical Analysis* **52** (2018), pp. 945–964.
- [3] B. Engquist and L. Ying, Sweeping preconditioner for the Helmholtz equation: moving perfectly matched layers, *Multiscale Model. Simul.*, **9** (2011), pp. 686–710.
- [4] M. J. Gander and H. Zhang, A Class of Iterative Solvers for the Helmholtz Equation: Factorizations, Sweeping Preconditioners, Source Transfer, Single Layer Potentials, Polarized Traces, and Optimized Schwarz Methods, *SIAM Review*, **61** (2019), pp. 3–76.
- [5] M. J. Gander and H. Zhang, Restrictions on the Use of Sweeping Type Preconditioners for Helmholtz Problems, in *Domain Decomposition Methods in Science and Engineering XXIV, LNCSE*, Springer-Verlag (2018), pp. 321–332.

A time-domain approach for solving the Helmholtz equation

Christiaan C. Stolk^{1,*}

¹Korteweg-de Vries Institute for Mathematics, University of Amsterdam, Amsterdam, The Netherlands

*Email: C.C.Stolk@uva.nl

Abstract

In this work we present a novel finite-difference time domain (FDTD) method specifically designed to simulate time-harmonic waves with minimal dispersion errors. The method uses recently developed spatial discretizations of the Helmholtz equation and a time discretization adapted to the narrow band wave field, so that relatively coarse meshes can be used. The scheme is suitable for comparison of the FDTD approach with other approaches for solving finite-difference discretizations of the Helmholtz equation, such as those based on sparse direct solvers, domain decomposition, multigrid or complex-shifted Laplacians. A study of overall performance is forthcoming.

Keywords: Helmholtz equation, finite differences, solvers

1 Introduction

In application fields, FDTD is regularly used to simulate solutions to Helmholtz equations. At the same time, in the literature on Helmholtz solvers usually little is said about this methodology (e.g. in papers on domain decomposition, multigrid methods or complex shifted-Laplacian methods). This raises the question whether numerical mathematicians should give more attention to this approach.

We start with some a priori observations about time domain simulation and its computational cost. (i) If both the frequency and the number of unknowns in each direction is increased, also the number of time steps must be increased. If d is the dimension, assuming a constant number of time-steps per period, and a constant number of spatial discretization points per wavelength in each direction, then a first estimate is that computational cost increases with $N^{1+1/d}$. (ii) The CFL condition implies a minimum number of time steps per period, which may be quite large in absolute numbers. Large differences in velocities worsen the situation in this respect. (iii) Time discretization errors, if not handled prop-

erly, may also mean that many time steps per period are required. (iv) FDTD algorithms are often well suited for modern hardware (in terms of vectorization and memory locality).

While (i) to (iii) *appear* to be disadvantages of the time domain, this is mostly not the case. Issue (i) is not unique to time domain methods. For complex-shifted Laplacians, the number of iterations also scales at least linear with problem size (we are not aware of any hard bounds in fact). In 3-D the solve cost of sparse direct solvers scales similarly. Issue (ii) can be addressed by using relatively coarse spatial grids. Recent discretizations of the Helmholtz equation allow for this [3] and this is part of our approach. However, large differences in velocities do pose challenges, because appropriate adaptive meshes are not easily combined with our methodology. To mitigate (iii), an adapted time discretization will be presented below. Observation (iv) is of course a main reason that time domain methods are of interest.

We will assume, as is commonly done, that some damping is present in the Helmholtz equations to be solved, for example from absorbing layers included for modeling an unbounded domain. Previous works documenting large scale Helmholtz solvers include [1, 2, 4].

2 A novel FDTD scheme

With standard low order discretizations, the use of coarse grids leads to large numerical dispersion. We next outline a scheme that involves relatively small stencils, but nevertheless obtains small dispersion errors when simulating time harmonic waves of a specific angular frequency ω . This scheme incorporates recently developed discretizations of the Helmholtz operator in a time-domain scheme. We start with the homogeneous wave equation without damping. The inclusion of inhomogeneous terms and damping will be briefly discussed afterwards. Once a discrete wave equation is available, it can be solved with a time harmonic right hand side. For typical systems that include some form of

damping, the solution becomes approximately time-periodic after some time, and a solution to the Helmholtz equation can then be extracted (“limiting-amplitude principle”).

The continuous equation to be discretized is

$$\left(\frac{1}{c(x)^2} \frac{\partial^2}{\partial t^2} - \Delta \right) u(t, x) = f(t, x)$$

Here $u(t, x)$ is the wave field to be simulated.

The first step is the spatial discretization. Let H denote a discrete Helmholtz equation of [3], section 5.1. This operator is a good approximations of $-\Delta - k^2$, in the sense that the propagating wave solutions to the Helmholtz equation have closely similar wave numbers (small numerical dispersion). Thus the continuous time, discrete space wave equation is

$$\left(\frac{1}{c(x)^2} \frac{\partial^2}{\partial t^2} + H + k^2 \right) u(t, x) = f(t, x). \quad (1)$$

Here $u(t, x)$ denotes a function of $t \in \mathbb{R}$ and x in a regular grid with grid spacing h .

For the time discretization, the equality

$$\left(\frac{\partial^2}{\partial t^2} + \omega^2 \right) e^{\pm i\omega t} = 0.$$

should remain true when $\frac{\partial^2}{\partial t^2}$ is replaced by the discrete second order time derivative. (This follows by inserting a solution $U(x)e^{\pm i\omega t}$ into (1) where U is a solution to the discrete homogeneous Helmholtz equation $HU = 0$, and multiplying by $c(x)^2$.) Discretizing by replacing

$$\frac{\partial^2 u}{\partial t^2} \rightarrow \frac{\alpha u^{(n+1)} - 2\beta u^{(n)} + \gamma u^{(n-1)}}{\Delta t^2}.$$

the equation becomes

$$\alpha e^{i\omega\Delta t} - 2\beta + (\Delta t)^2 \omega^2 + \gamma e^{-i\omega\Delta t} = 0.$$

To obtain zero imaginary part, one sets $\gamma = \alpha$. Then one parameter is free due to overall scaling so that one can set $\beta = \alpha$. Solving for α then results in

$$\alpha = \frac{(\Delta t \omega)^2}{2 - 2 \cos(\omega \Delta t)}.$$

The resulting discrete scheme for the homogeneous equation is then

$$\frac{\alpha(u^{(n+1)} - 2u^{(n)} + u^{(n-1)})}{\Delta t^2} + (H + k^2)u^{(n)} = 0.$$

from which an explicit expression for $u^{(n+1)}$ in terms of $u^{(n)}$ and $u^{(n-1)}$ can be easily extracted.

For the inhomogeneous equation an overall scaling of the right hand side can be established and the operators Q of [3], section 5.2 can be applied. Damping can be included by adding a contribution $\beta \frac{u^{(n+1)} - u^{(n-1)}}{\Delta t}$ were $\beta = \beta(x)$ is a local damping constant (not the same β as above).

3 Discussion

In wave field processing it is common to go back and forth between time and frequency domains, or between position and k-space. Examples are for example the processing of seismic data or in some simulation approaches (e.g. k-Wave). We present a new instance of such mixed domain computing. It will be of interest to compare the computational cost of the FDTD approach for solving the Helmholtz equation with that of other Helmholtz solvers. Numerical results are forthcoming.

References

- [1] H. Calandra, S. Gratton, X. Pinel and X. Vasseur, An improved two-grid preconditioner for the solution of three-dimensional Helmholtz problems in heterogeneous media, *Numer. Linear Algebra Appl.*, **20** (2013), pp. 663–688.
- [2] J. Poulson, B. Engquist, S. Li, and L. Ying. A parallel sweeping preconditioner for heterogeneous 3D Helmholtz equations. *SIAM J. Sci. Comput.*, 35(3):C194–C212, 2013.
- [3] C.C. Stolk, A dispersion minimizing scheme for the 3-D Helmholtz equation based on ray theory, *J. Comput. Phys.* **314** (2016), pp. 618–646.
- [4] C.C. Stolk, An improved sweeping domain decomposition preconditioner for the Helmholtz equation *Adv. Comput. Math.* **43** (2017), pp. 45–76.

Scalable Parallel Methods for the Helmholtz Equation via Exact Controllability

M. J. Grote¹, F. Nataf², J. H. Tang^{1,*}, P.-H. Tournier²¹Dept. of Mathematics and Computer Science, University of Basel, Basel, Switzerland²Laboratoire J.L. Lions and ALPINES INRIA, Université Pierre et Marie Curie, Paris, France

*Email: jet.tang@unibas.ch

Abstract

Large-scale Helmholtz problems are notoriously difficult to solve with standard iterative methods, in fact increasingly so, the higher the frequency $\omega > 0$. Controllability methods (CM) offer an alternative approach [1–4] for the numerical solution of the Helmholtz equation. Instead of solving the problem directly in the frequency domain, we first transform it back to the time domain where we seek the time-periodic solution $y(\cdot, t)$ of the corresponding time-dependent wave equation with known period $T = (2\pi)/\omega$. By minimizing a cost functional, which penalizes the mismatch after one period, CM iteratively steer y towards the desired periodic state.

Here, we consider two different approaches based either on the first or second-order formulation of the wave equation [1, 5]. Both are extended to general boundary-value problems governed by the Helmholtz equation and lead to robust and inherently parallel algorithms. Numerical results illustrate the accuracy and strong scalability of CM with up to a billion unknowns on massively parallel architectures [4].

Keywords: time-harmonic waves, controllability method, parallel computing

1 Second-order wave equation

Let $\Omega \subset \mathbb{R}^d$ be a connected, bounded Lipschitz domain with boundary $\partial\Omega = \Gamma_D \cup \Gamma_N \cup \Gamma_S$ and u denote the solution of the Helmholtz equation,

$$\begin{aligned} -\Delta u(x) - k(x)^2 u(x) &= f(x) \quad x \in \Omega, \\ \frac{\partial u(x)}{\partial n} &= g(x) \quad x \in \Gamma_N, \\ u(x) &= 0 \quad x \in \Gamma_D, \\ \frac{\partial u(x)}{\partial n} - ik(x)u(x) &= g(x) \quad x \in \Gamma_S, \end{aligned} \quad (1)$$

where Γ_D and Γ_N are physical boundaries, Γ_S is an artificial boundary, $k = \omega/c$ is the wave number, and $c(x)$ is the speed of propagation.

Instead of solving (1) directly in the frequency domain, we consider the T -periodic time-harmonic solution

$$y(x, t) = \operatorname{Re}\{u(x) e^{-i\omega t}\}.$$

It satisfies the second-order wave equation

$$\frac{1}{c^2} \frac{\partial^2 y}{\partial t^2} - \Delta y = \operatorname{Re}\{f e^{-i\omega t}\} \quad \text{in } \Omega \times (0, T), \quad (2)$$

with corresponding time-harmonic initial and boundary conditions

$$y(\cdot, 0) = y_0, \quad y_t(\cdot, 0) = y_1 \quad \text{in } \Omega. \quad (3)$$

Once the (unknown) initial conditions y_0 and y_1 have been determined, the solution u of (1) is immediately given by

$$u = y_0 + (i/\omega)y_1. \quad (4)$$

2 Controllability methods

To determine (y_0, y_1) , Glowinski et al. [1] proposed to reformulate the problem as a least-squares optimization problem over $H^1 \times L^2$ for the quadratic energy functional

$$J(y_0, y_1) = \frac{1}{2} \|\nabla y(T) - \nabla y_0\|^2 + \frac{1}{2} \left\| \frac{1}{c} (y_t(T) - y_1) \right\|^2$$

where y satisfies (2)–(3). The minimizer (y_0, y_1) of J is determined by the conjugate gradient (CG) method. To ensure that all CG-iterates remain in $H^1 \times L^2$, each iteration requires the solution of a coercive elliptic problem independent of ω .

Instead of using the wave equation (3) in second-order form, we can also reformulate it in first-order (or mixed) form [5] as

$$\begin{aligned} \frac{1}{c^2} \frac{\partial v}{\partial t} - \operatorname{div} \mathbf{p} &= \operatorname{Re}\{f e^{-i\omega t}\} \quad \text{in } \Omega \times (0, T), \\ \frac{\partial \mathbf{p}}{\partial t} &= \nabla v \quad \text{in } \Omega \times (0, T), \end{aligned} \quad (5)$$

with corresponding initial and boundary conditions. Since the initial values $(\mathbf{p}_0, v_0) \in (L^2)^{d+1}$, the solution of an elliptic problem at each CG iteration is no longer necessary. To discretize (5), we consider a recent hybrid discontinuous Galerkin (HDG) method. First, it leads to a block-diagonal mass-matrix and, therefore, becomes trivially parallel when combined with explicit time integration of (5). Second, it also

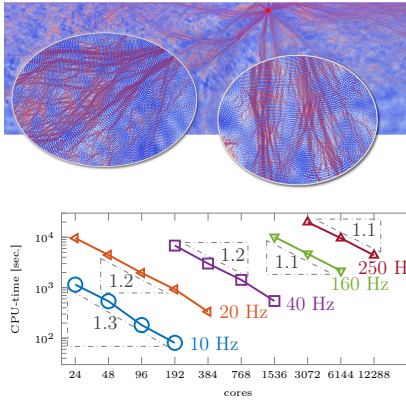


Figure 1: 2D-Marmousi: (top) wave field u , (bottom) CPU-time w.r.t. numbers of cores

yields superconvergence in space after a local post-processing step.

When applied to general boundary-value problems governed by the Helmholtz equation (1), the original CMCG method with J generally yields a time-periodic solution of (2)-(3) (or (5)), which contains u , but also a constant shift, a linearly growing part determined by a constant η , and higher frequency harmonics. In [3, 4], we showed that the shift and higher eigenmodes can be removed by a simple *filtering procedure*:

$$u = \hat{y} + \frac{i\eta}{\omega}, \quad \hat{y} = \frac{1}{T} \int_0^T (y(\cdot, t) + \frac{i}{\omega} y_t(\cdot, t)) e^{i\omega t} dt.$$

Then, η is determined by the following *compatibility condition* directly derived from (1):

$$\frac{i\eta}{\omega} = -\frac{1}{\|k\|^2} \left(\int_{\Omega} f dx + \int_{\Gamma_N} g ds + \int_{\Omega} k^2 \hat{y} dx \right).$$

3 HPC parallel results

We apply the CMCG method with \mathcal{P}^2 -FE to the Marmousi model ($\omega = 2\pi\nu$, $\nu = 10 - 250$) and with \mathcal{P}^1 -FE to the 3d-cavity problem ($k = \omega = 2\pi\nu$, $\nu = 2 - 6$), both with mass-lumping. For the time integration of (2), (5), we use the explicit leap-frog method. The implementation is written in FreeFem++ and the elliptic problem is solved in parallel by using the hpddm

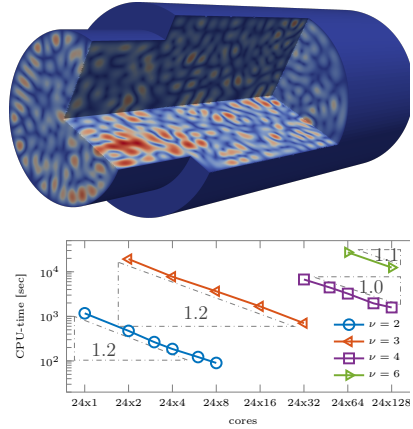


Figure 2: 3D-cavity: (top) wave field u , (bottom) CPU-time w.r.t. numbers of cores

library. As shown in Figures 1 and 2, the parallel implementation of the CMCG method scales perfectly for a fixed FE mesh as the number of cores increases.

References

- [1] M.-O. Bristeau, R. Glowinski and J. Périaux, “Controllability Methods for the Calculation of Time-Periodic Solutions. Application to Scattering”, J. Comp. Phys., 1998.
- [2] E. Heikkola, S. Mönkölä, A. Pennanen and T. Rossi, “Controllability method for the Helmholtz equation with higher-order discretizations”, J. Comp. Phys., 2007.
- [3] M. J. Grote, J. H. Tang, “On controllability methods for the Helmholtz equation”, J. Comp. Appl. Math., 2019.
- [4] M. J. Grote, F. Nataf, J. H. Tang, P.-H. Tournier, “Parallel controllability methods for the Helmholtz equation”, arXiv:1903.12522, 2019.
- [5] S. Kähkönen, R. Glowinski, T. Rossi and R. A. E. Mäkinen “Solution of time-periodic wave equation using mixed finite elements and controllability techniques”, J. Theor. Comput. Acoust., 2011.

Solving Helmholtz Equation via the Wave Equation

Daniel Appelö¹, Fortino Garcia^{1,*}, Olof Runborg²¹Department of Applied Mathematics, University of Colorado, Boulder, CO USA²Department of Mathematics, KTH, Stockholm, Sweden

*Email: fortino.garcia@colorado.edu

Abstract

We introduce a novel idea inspired by recent work on exact controllability (EC) methods, [4]. As in EC methods our method make use of time domain methods for wave equations to design frequency domain Helmholtz solvers but unlike EC methods we don't require adjoint solves. Numerical examples with various discretization techniques are presented.

Keywords: Helmholtz, Wave Equation.

1 Introduction

Designing efficient iterative solvers for the Helmholtz equation

$$c(x)^2 \Delta u + \omega^2 u = f(x), \quad (1)$$

is notoriously difficult when $\omega \gg 1$ and has been the subject of much research. The main difficulties in solving the Helmholtz equation are the resolution requirements and the highly indefinite character of the discretized problem.

Assuming that (1) has been scaled so that the mean of $c(x)$ is about 1 then the typical wavelength is $\lambda = 2\pi/\omega$ and the typical wavenumber is $\omega/2\pi$. In order to numerically propagate solutions to the time dependent wave equation corresponding to (1) with small errors it is crucial to control the dispersion by using high order methods. The basic estimate by Kreiss and Olinger [1] shows that in order to propagate a wave over J wavelengths with a p th order finite difference method and with an error no greater than ϵ one must choose the number of points per wavelength $\text{PPW}(J, p)$ as $\text{PPW}(J, p) \geq C(p, \epsilon) J^{\frac{1}{p}}$, where $C(p, \epsilon)$ depends on the tolerance but decreases with increasing order of accuracy p . Consequently, for a problem in d -dimensions and with fixed physical size the number of wavelengths in the domain will scale as ω^d and to maintain a fixed tolerance the total number of degrees of freedom needed, $N_p(\omega) = \mathcal{O}(\omega^{d(1+\frac{1}{p})})$, is very large for high frequencies.

The dependence on p and ω in $N_p(\omega)$ immediately reveals two fundamental criteria for

designing high frequency Helmholtz solvers: 1.) The solvers must be **parallel, memory lean** and they must **scale well**. In 3D the number of degrees of freedom representing the solution cannot be stored on a single computer, and even on a parallel computer it is important to preserve the sparsity of the discrete version of (1). 2.) The underlying discretizations must be **high order accurate**. At high frequencies and in 3D the extra penalty due to pollution / dispersion errors becomes prohibitive.

2 A New Idea for Designing Scalable Parallel Helmholtz Solvers

Note that for suitable initial conditions $w(0, x)$ and $w_t(0, x)$, the unique $T = 2\pi/\omega$ -periodic solution to $w_{tt} = c(x)^2 \Delta w - f(x)e^{i\omega t}$ is also the unique solution to the Helmholtz equation. We can thus find $u(x)$ by finding initial conditions that gives a T -periodic solution to (2). Without loss of generality, we may take $w_t(0, x) = 0$ and $w(t, x) = u(x) \cos(\omega t)$, since for a T -periodic solution there is a time when $w_t(0, x) = 0$. Thus

$$\begin{cases} w_{tt} &= c(x)^2 \Delta w - f(x) \cos(\omega t), \\ w(0, x) &= v(x), \quad w_t(0, x) = 0, \end{cases} \quad (2)$$

where $0 \leq t \leq T$. In other words, to find $u(x)$, rather than solving (1) directly, we will find the initial data $v(x)$ that produces the unique T -periodic solution to (2).

We now propose a fixed point iteration that can be used to construct highly scalable parallel solvers for Helmholtz type equations. The proposed iteration is defined as follows

$$\boxed{v^{(n+1)} = \Pi v^{(n)}, \quad v^{(0)} \equiv 0,} \quad (3)$$

where

$$\Pi v = \frac{2}{T} \int_0^T \left(\cos(\omega t) - \frac{1}{4} \right) w(t, x) dt, \quad T = \frac{2\pi}{\omega}$$

with $w(t, x)$ solving the wave equation (2) with initial data $v(x) \equiv v^{(n)}$. It is not hard to show that the above iteration can be expressed as a

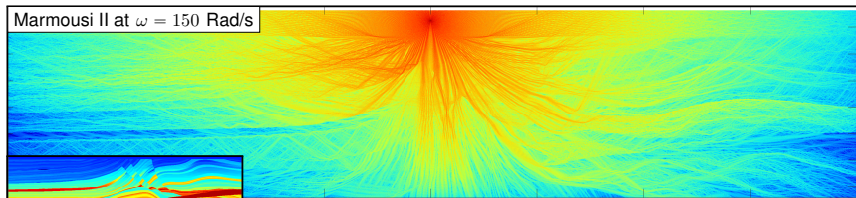


Figure 1: Plotted is the magnitude of the solution to Helmholtz equation due to a point source at 150Rad/s. The color scale is logarithmic. The inlay displays the velocity (compressional) structure with regions ranging from 1km/s to ~ 4.6 km/s.

Frequency	5π	10π	15π	20π	25π	30π	35π	40π
Iterations using ILU + GMRES	44	47	21	28	29	35	37	43
Iterations using QMR	55	104	152	200	251	301	357	396
Fill-in L vs. A	3.95%	4.04%	4.28%	4.04%	4.09%	4.06%	4.07%	4.12%

Figure 2: The behavior of classic ILU preconditioning under constant fill in ratio.

system of equations where the system matrix is symmetric positive definite (unlike systems that stem from the direct discretization of Helmholtz eq.). Note that this method shares the feature of finding time-periodic solutions with so called exact controllability methods that were considered in the late 1990's by Bristeau [3] for Dirichlet and impedance conditions and, more recently, general boundary value problems in Grote et al. [4]. The latter was an inspiration for the work presented here but we stress that our method is distinct from [4], e.g. we do not need to compute gradients at each step.

3 A Numerical Examples

Consider the interior 1D problem with constant wave speed of one and with homogenous Dirichlet boundary conditions on the domain with a very narrow forcing placed near the middle of the domain. The discretization is an energy based DG method, [2] with 4 elements and a basis of Legendre polynomials of degree 32 together with a Taylor series method of order 32 in time. We increase the resolution with ω so that the problem is resolved and solve it using Matlab's built-in QMR solver as a baseline. We compare the QMR results with results using Matlab's ILU preconditioner with the `crout` and `milu = 'off'` options together with GMRES. The results, displayed in Figure 2 are intriguing: the number of iterations appears to be less sensitive to wavenumber than the un-

preconditioned case. As a more realistic problem we compute the solution of the Marmousi 2 test problem on the full grid (13601×2801 grid-points or $38 \cdot 10^6$ degrees of freedom). The wave equation is discretized using 6th order accurate summation-by-parts operators, and we impose homogenous Dirichlet boundary conditions at the surface and non-reflecting super-grid on the other boundaries. We force the solution at a point near the surface at $\omega = 150$ Rad/s. The amplitude of the solution is plotted in logarithmic scale in Figure 1.

References

- [1] H.-O. Kreiss and J. Oliger, Comparison of accurate methods for the integration of hyperbolic equations, *Tellus*, 1972.
- [2] D. Appelö and T. Hagstrom, A new discontinuous Galerkin formulation for wave equations in second order form, *SIAM J. Num. Anal.*, 53(6):2705-2726, 2015.
- [3] M. O. Bristeau, R. Glowinski, and J. Péri-aux, Controllability methods for the computation of time-periodic solutions; application to scattering, *J. Comp. Phys.*, 147(2):265-292, 1998.
- [4] M. J. Grote and J. H. Tang, On controllability methods for the Helmholtz equation. Preprint 2018-06, Universität Basel, 2018.

**An efficient domain decomposition method with cross-point treatment
for Helmholtz problems**

A. Modave^{1,*}, X. Antoine², A. Royer³, C. Geuzaine³

¹POEMS (CNRS-ENSTA-Imria), Palaiseau, France

²Université de Lorraine, CNRS, Inria, IECL, France

³Université de Liège, Belgium

*Email: axel.modave@ensta-paristech.fr

Abstract

The parallel finite-element solution of large-scale time-harmonic scattering problems is addressed with a non-overlapping domain decomposition method (DDM). It is well known that the efficiency of this method strongly depends on the transmission condition enforced on the interfaces between the subdomains. Local conditions based on high-order absorbing boundary conditions (HABCs) are well suited for configurations without cross points (*where more than two subdomains meet*). In this work, we extend this approach to efficiently deal with cross points. Two-dimensional finite-element results are presented.

Keywords: Helmholtz solvers, finite elements, domain decomposition, fast comput. technique

1 Introduction

Optimized Schwarz DDMs are currently a very promising approach for the parallel solution of high-frequency time-harmonic problems. With these methods, subproblems of smaller sizes are solved in parallel using direct solvers, and are combined in an iterative procedure [1, 2, 4].

The convergence rate of the DDM procedure depends on the transmission condition enforced on the interfaces between the subdomains. Local conditions based on HABCs represent a good compromise between basic impedance conditions (*which lead to suboptimal convergence*) and the exact Dirichlet-to-Neumann (DtN) map related to the complementary of the subdomain (*which is expensive to compute*). They are well suited for configurations without cross points [1], but a direct application of this approach with cross points does not provide satisfactory results.

Noting that cross points actually are corners for the subdomains, we propose a novel strategy which consists in incorporating a corner treatment developed for HABCs [3] into the DDM procedure for configurations with cross points and right angles.

2 DDM method

We consider a 2D Helmholtz problem defined on a rectangular computational domain Ω :

$$\begin{cases} \Delta u + k^2 u = s, & \text{in } \Omega, \\ \partial_{n_f} u - iku = 0, & \text{on each } \Gamma_f, \end{cases}$$

where k is the wavenumber, s is a source term, Γ_f is an edge of the domain, and ∂_{n_f} is the exterior normal derivative, with $f = 1 \dots 4$.

The domain Ω is partitioned into a structured grid of non-overlapping rectangular subdomains Ω_I , with $I = 1 \dots N^{\text{dom}}$. Each edge $\Gamma_{I,f}$ can be either a *boundary edge* (if $\subset \partial\Omega$) or an *interface edge* (if $\not\subset \partial\Omega$). In the standard DDM procedure, the solution u_I of each subdomain Ω_I is obtained by solving the subproblem

$$\begin{cases} \Delta u_I + k^2 u_I = s, & \text{in } \Omega_I, \\ \partial_{n_{I,f}} u_I - iku_I = 0, & \text{on each } \Gamma_{I,f} \subset \partial\Omega, \\ \partial_{n_{I,f}} u_I + \mathcal{B}u_I = g_{I,f}, & \text{on each } \Gamma_{I,f} \not\subset \partial\Omega, \end{cases}$$

where \mathcal{B} is an impedance operator and $g_{I,f}$ is a transmission variable. For any interface edge, the transmission variable is computed using

$$g_{I,f} = \partial_{n_{I,j}} u_j + \mathcal{B}u_j = -g_{J,g} + 2\mathcal{B}u_j, \quad (1)$$

where $g_{J,g}$ and u_j belong to the neighboring subdomain Ω_J with the shared edge $\Gamma_{I,f} = \Gamma_{J,g}$. Each iteration of the DDM procedure then consists in solving concurrently the subproblems and updating the transmission variables using equation (1). See [1] for further details.

With our approach, the transmission operator \mathcal{B} is an approximation of an exact half-space DtN operator, where a rational approximation of the square root is used in the symbol. The application of \mathcal{B} on u_I is written as

$$\mathcal{B}u_I = -i\kappa\alpha \left[u_I + \frac{2}{M} \sum_{i=1}^N c_i (u_I + \varphi_{I,f,i}) \right],$$

where $\alpha = e^{i\phi/2}$, $c_i = \tan^2(i\pi/M)$, $M = 2N + 1$, N and ϕ are parameters, and $\{\varphi_{I,f,i}\}_{i=1 \dots N}$ are 1D auxiliary fields living on the edge $\Gamma_{I,f}$.

$$\left\{ \begin{array}{ll} \partial_{n_{I,f'}} \varphi_{I,f,i} - ik\varphi_{I,f,i} = 0, & \text{on each } P_{I,ff'} \subset \partial\Omega, \\ \partial_{n_{I,f'}} \varphi_{I,f,i} + \mathcal{C}(\varphi_{I,f,i}, \varphi_{I,f',1}, \dots, \varphi_{I,f',N}) = g_{I,f,i}, & \text{on each } P_{I,ff'} \not\subset \partial\Omega. \end{array} \right. \quad (2)$$

For each interface edge $\Gamma_{I,f}$, each auxiliary field $\varphi_{I,f,i}$ is governed by a 1D Helmholtz equation (first equation in system (2), where ∂_{τ_i} is the tangent derivative). Because of the second-order partial derivative, a boundary condition is required at each extremity of the edge [3], which are corners of the subdomain. In the DDM procedure, that condition becomes a transmission condition if the adjacent edge is an interface.

The corner shared by $\Gamma_{I,f}$ and any adjacent edge $\Gamma_{I,f'}$ is denoted $P_{I,ff'} = \Gamma_{I,f} \cap \Gamma_{I,f'}$. Depending on the type of $\Gamma_{I,f'}$, the auxiliary field $\varphi_{I,f,i}$ verifies one of the two last equations of system (2). In the last one, \mathcal{C} is a linear function taking $\varphi_{I,f,i}$ and all the auxiliary fields living on $\Gamma_{I,f'}$ (the expression is easily obtained from [3]). The transmission variable $g_{I,f,i}$ verifies

$$g_{I,f,i} = -g_{J,f,i} + 2\mathcal{C}(\varphi_{J,f,i}, \varphi_{J,g',1}, \dots, \varphi_{J,g',N}),$$

where $\Gamma_{I,f}$ and $\Gamma_{J,f}$ have the same position in Ω_I and Ω_J , and $\Gamma_{I,g'} = \Gamma_{J,g'}$ is the shared edge.

3 Preliminary finite element results

To analyse the efficiency of the method, we consider the scattering of a plane wave by the unit disk in a squared domain partitioned into 6 subdomains (figure 1). A Neumann BC is used on the boundary of the disk, and the basic ABC is prescribed on the exterior border. Simulations are performed with P1 elements and a Galerkin method adapted from [1] using GetDDM [4]. The GMRES is used on the top of the procedure.

The convergence is faster when the HABC transmission condition is used with the cross-pointing treatment (figure 2). If the number of auxiliary fields N is large enough, the number of iteration does not vary when increasing the

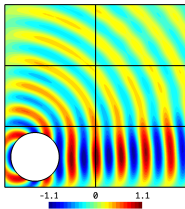


Figure 1: Configuration and reference solution.

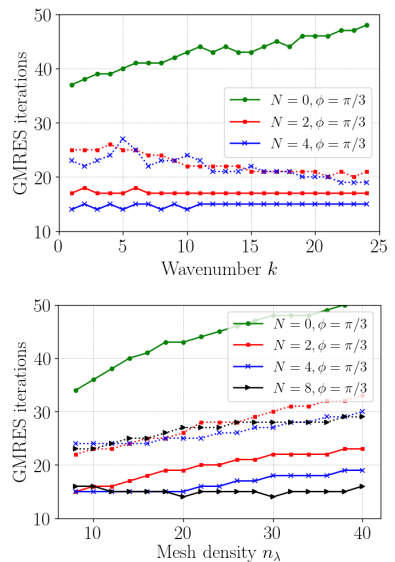


Figure 2: Number of iterations to reach relative residual 10^{-6} vs wavenumber k (with $n_\lambda = 15$) and mesh density n_λ (with $k = 2\pi$), without (dot. lines) or with (cont. lines) c.-p. treatment.

frequency or the mesh density. The procedure always converges towards the correct solution, even without the treatment (results not shown).

Our approach can be used with other exterior boundary conditions. In future works, we will consider other physical waves and combination with preconditioning techniques.

References

- [1] Y. Boubendir, X. Antoine, C. Geuzaine. *J. Comput. Phys.* 231 (2), 262–280, 2012
- [2] M. Gander, F. Magoules, F. Nataf. *SIAM J. Sci. Comput.* 24 (1), 38–60, 2002
- [3] A. Modave, C. Geuzaine, X. Antoine. *Corner treatments for high-order absorbing boundary conditions in high-frequency acoustic scattering problems*, preprint hal-01925160
- [4] B. Thierry, A. Vion, S. Tournier, M. El Bouajaji, D. Colignon, N. Marsic, X. Antoine, C. Geuzaine. *Comput. Phys. Commun.* 203, 309–330, 2016

A domain decomposition method for the Helmholtz equation using a DtN map

Achim Schädle^{1,*}

¹Mathematisches Institut, Heinrich-Heine-Universität, Düsseldorf, Germany

*Email: achim.schaedle@hhu.de

Abstract

In this talk I will try to analyze what can be expected from a Schwarz iteration using some sort of Dirichlet to Neumann (DtN) operator to exchange information among sub-domains applied to the Helmholtz equation on an unbounded domain with circular scatterers. For the analysis ideas from multiple scattering are combined with the non-overlapping Schwarz algorithm.

Keywords: domain decomposition, Helmholtz equation, DtN operator

Introduction

Our model problem is the Helmholtz equation in \mathbb{R}^2 with several circular non-intersecting holes given by

$$\begin{aligned} \Delta v_{to}(x) + \omega^2 v_{to}(x) &= f \text{ for } x \in \tilde{\Omega} \\ \partial_\nu v_{to}(x) &= 0 \text{ for } x \in \Gamma \quad (1) \\ &+ \text{boundary condition for } |x| \rightarrow \infty \end{aligned}$$

where $\tilde{\Omega} := \mathbb{R}^2 \setminus \{\cup_{j=1}^M B_{r_j}(x_j)\}$ with $B_{r_j}(x_j)$, $j=1, \dots, M$ pairwise disjoint discs of radius r_j and midpoint x_j . By $\Gamma := \partial\tilde{\Omega}$ we denote the boundary of the discs.

The motivation behind this problem are photonic crystals. There the size of the computational domain is several wavelengths and the typical structure size is below the wavelength.

Domain Decomposition

Restricting (1) to a bounded computational domain Ω , an artificial boundary Γ_{ext} and an exterior domain Ω_{ext} are introduced.

The solution u_{to} , the total field, of equation (1) for an incoming wave u_{in} is given by

$$\begin{aligned} \Delta u_{to} + \omega^2 u_{to} &= f \text{ in } \Omega, \\ \partial_\nu u_{to} &= 0 \text{ on } \Gamma, \\ \partial_\nu u_{to} &= \partial_\nu u_{sc} + \partial_\nu u_{in} \text{ on } \Gamma_{ext}. \end{aligned} \quad (2)$$

The scattered field u_{sc} on the boundary is calculated using the DtN map from

$$\partial_\nu u_{sc} = \text{DtN}(u_{sc}) \text{ on } \Gamma_{ext}, \quad (3)$$

where the coupling of (2) and (3) is given by $u_{sc} = u_{to} - u_{in}$. By definition of the DtN map u_{to} coincides with v_{to} restricted to Ω . In total we get

$$\begin{aligned} \Delta u_{to} + \omega^2 u_{to} &= f \text{ in } \Omega \\ \partial_\nu u_{to} &= 0 \text{ on } \Gamma, \\ \partial_\nu u_{to} &= \text{DtN}(u_{to} - u_{in}) + \partial_\nu u_{in} \text{ on } \Gamma_{ext}. \end{aligned} \quad (4)$$

The DtN operator for the scattered field on the exterior boundary Γ_{ext} of Ω is defined as the operator that:

1. Solves Equation (1) on the exterior domain Ω_{ext} with given Dirichlet data on Γ_{ext} and Sommerfeld radiation condition.
2. Evaluates and returns the Neumann data of the solution on Γ_{ext} .

For the definition of the DtN operator we do not require, that there are no ‘‘holes’’ in Ω_{ext} .

A wave from outside Ω is given by u_{in} and $\partial_\nu u_{in}$ on Γ_{ext} . Equation (4) is the key to our understanding of the domain decomposition algorithm.

Let Ω_m , $m = 1, \dots, M$, form a decomposition of Ω into M non-overlapping sub-domains with interfaces $\Sigma_{k,l} = \Sigma_{l,k} := \partial\Omega_l \cap \partial\Omega_k$. Set $\Sigma_{k,ext} := \partial\Omega_k \cap \Gamma_{ext}$ and $\Sigma_{k,int} := \partial\Omega_k \cap \Gamma_{int}$. The out-going normal to Ω_k is $\nu(k)$.

Starting with $v^{-1+\frac{j}{M}}$ a full iteration of the multiplicative Schwarz method is performed thro M fractional steps, where $v^{\frac{j}{M}}$ is the solution of the following problem

$$\begin{aligned} \Delta v^{\frac{j}{M}} + \omega^2 v^{\frac{j}{M}} &= f \text{ in } \Omega_j, \\ \partial_\nu v^{\frac{j}{M}} &= \begin{cases} \text{DtN}(v^{\frac{j}{M}} - v^{\frac{k}{M}}) + \partial_{\nu(j)} v^{\frac{k}{M}} & \text{on } \Sigma_{j,k} \text{ for } j < k, \\ \text{DtN}(v^{\frac{j}{M}} - v^{-1+\frac{k}{M}}) + \partial_{\nu(j)} v^{-1+\frac{k}{M}} & \text{on } \Sigma_{j,k} \text{ for } j > k, \end{cases} \\ \partial_{\nu(j)} v^{\frac{j}{M}} &= 0 \text{ on } \Sigma_{j,int}, \\ \partial_\nu v^{\frac{j}{M}} &= \text{DtN}(v^{\frac{j}{M}} - v_{in}) + \partial_\nu v_{in} \text{ on } \Sigma_{j,ext}. \end{aligned} \quad (5)$$

For the additive Schwarz method a similar iteration can be written down. In the above iterative method the DtN operator differs from sub-domain to sub-domain, taking into account the “holes” and sources in the respective exterior domain. It seems hopeless to ever be able to evaluate the DtN operator.

This leads to the notion of a pseudo Dirichlet to Neumann operator, which does not take into account “holes” and sources f in the exterior domain.

Definition 1 (pDtN Operator) *The pseudo DtN operator for the scattered field on the exterior boundary Γ_{ext} of Ω is defined as the operator that given Dirichlet data g :*

1. Solves the exterior Helmholtz equation

$$\begin{aligned} \Delta w(x) + \omega^2 w(x) &= 0 \text{ for } x \in \mathbb{R}^2 \setminus \Omega \\ w &= g \text{ on } \Gamma_{ext} \\ \lim_{|x| \rightarrow \infty} (\partial_\nu u - iku) &= 0. \end{aligned}$$

2. Evaluates and returns the Neumann data of the solution on Γ_{ext} .

In case Ω is a disk and ω is constant in the exterior the pDtN operator can be written down explicitly. For Ω a convex polygon and assuming ω to be constant along rays in the exterior the pDtN operator can be approximated using the PML method or a non-reflecting boundary condition such as the pole condition.

Multiple Scattering

Consider the simple situation of only two circular scatterers, i.e. $\Omega := \mathbb{R}^2 \setminus \{B_{R_1}(p) \cup B_{R_2}(q)\}$. A separation in angular and radial variables with respect to disc $\ell = 1, 2$ gives the following representation of u_ℓ , cf. [1].

$$u_\ell(r_\ell, \phi_\ell) = \sum_{n=-\infty}^{\infty} \exp(in\phi_\ell) (b_n^{(\ell)} H_n(r_\ell k)) \quad (6)$$

where $H_n(z) := H_n^{(1)}(z)$ are the cylindrical Hankel functions. Denoting by Γ_1 the boundary of ball 1 and by Γ_2 the boundary of ball 2 we have the following system of equations

$$\begin{aligned} \partial_\nu u_1|_{\Gamma_1} &= -\partial_\nu u_{in}|_{\Gamma_1} - \partial_\nu u_2|_{\Gamma_1}, \\ \partial_\nu u_2|_{\Gamma_2} &= -\partial_\nu u_{in}|_{\Gamma_2} - \partial_\nu u_1|_{\Gamma_2}, \end{aligned}$$

equivalently

$$\begin{bmatrix} Id & \partial_\nu|_{\Gamma_1} A_2 \\ \partial_\nu|_{\Gamma_2} A_1 & Id \end{bmatrix} \begin{bmatrix} \partial_\nu|_{\Gamma_1} u \\ \partial_\nu|_{\Gamma_2} u \end{bmatrix} = \begin{bmatrix} \partial_\nu|_{\Gamma_1} u_{in} \\ \partial_\nu|_{\Gamma_2} u_{in} \end{bmatrix}$$

where A_1 is the linear mapping that maps the Neumann data on Γ_1 to the solution defined in $\mathbb{R}^2 \setminus B_{R_1}(p)$. $\partial_\nu|_{\Gamma_2}$ denotes the restriction to Γ_2 and evaluating the normal derivative there, similar A_2 is defined. Differentiating (6) one obtains

$$\partial_\nu|_{\Gamma_\ell} u_\ell(R_\ell, \phi_\ell) = \sum_{n=-\infty}^{\infty} e^{in\phi_\ell} b_n^{(\ell)} k H'_n(kR_\ell).$$

Only $2N$ discrete points on each boundary are taken into account corresponding to $2N$ Fourier modes of the angular variable. The Fourier coefficients $b_n^{(\ell)}$ of $\partial_\nu u_\ell$ allow to evaluate $\partial_\nu u_1$ on Γ_2 resp. $\partial_\nu u_2$ on Γ_1 .

A lengthy calculation yields a formula for a discretization of the operators $\partial_\nu|_{\Gamma_j} A_i$.

This ansatz can be easily extended to N circular scatterers. And it is the basis to study a Schwarz like iteration on a purely algebraic level. In contrast to a standard domain decomposition ansatz the information in this case is not only passed between neighbouring domains through a common interface.

In this talk a convergence result for the algorithm sketched above and numerical experiments will be presented.

References

- [1] P. A. Martin, Multiple scattering: an invitation, *Third International Conference on Mathematical and Numerical Aspects of Wave Propagation* (Philadelphia), SIAM, 1995, pp. 3–16.
- [2] A. Schädle and L. Zschiedrich, Additive Schwarz Method for Scattering Problems Using the PML Method at Interfaces, in *LNCSE*, **55**, (2007), pp 205–212.

Distributed Parallel-Adaptive Causal Spacetime Discontinuous Galerkin Method with Application to Earthquake Simulation

Robert B. Haber^{1,*}, Amit Madhukar¹, Xiao Ma², Ahmed Elbanna², Reza Abedi³

¹Department of Mechanical Science & Engineering, University of Illinois, Urbana, USA

²Department of Civil & Environmental Engineering, University of Illinois, Urbana, USA

³Department of Mechanical, Aerospace & Biomedical Eng., University of Tennessee, Knoxville, USA

*Email: rbh3@illinois.edu

Abstract

Serial versions of the causal Spacetime Discontinuous Galerkin (cSDG) method compete with other methods running on multi-host platforms for challenging wave problems with wide ranges of length and time scales. This performance reflects the method's asynchronous structure and fine-grained adaptive meshing. However, an effective parallel-adaptive cSDG scheme using traditional domain decomposition has proven elusive. Rebalancing decompositions introduces severe synchronous barriers and is unable to keep pace with dynamic cSDG adaptive meshing.

We use lazy mesh refinement to localize adaptive meshing and, in place of domain decomposition, and a probabilistic scheme for distributing data and tasks continuously maintains load balance. We obtain a fully asynchronous, barrier-free software architecture that delivers excellent performance and scaling efficiency on multi-host platforms. Earthquake simulations exemplify the distributed cSDG implementation's multiscale simulation capabilities.

Keywords: parallel, adaptive, spacetime, discontinuous Galerkin, earthquake

1 Introduction

The cSDG method depends on specialized spacetime finite element mesh generation. Figure 1 (left) shows a spacetime solution domain with one spatial dimension. Arrows on cell A indicate characteristic trajectories for waves travel-

ling left and right. We impose a *causality constraint* on interior cell faces: they must be space-like (closer to horizontal than the characteristic trajectories). This ensures that the solution in cell A depends only on solutions in cells B and C. If the overall solution is cell-wise discontinuous and the predecessor-cell solutions are available, the solution in cell A is fully determined and can be solved locally. Level-1 cells on the initial-time boundary can be solved in parallel using only initial data and boundary data. Any level-2 cell can be solved as soon as its level-1 predecessors have been solved, etc.

At any stage of the solution process, there is a *front mesh* (shown in red in Fig. 1) below which all cells have been solved. Each step in the cSDG solution process involves advancing a vertex to form a new cell, computing a local solution on the new cell, and updating the front mesh to its new configuration. We repeat this process until the spacetime mesh fills the spacetime analysis domain.

Adaptive refinement of the front mesh induces spacetime mesh refinement. If the solution on a larger cell constructed to the dashed outline near cell D in Fig. 1 has excessive error, we discard the larger cell, bisect its inflow (red) faces to refine locally the front mesh, and restart the cSDG meshing/solution process. This generates cell D which, due to the causality constraint, is refined in both space and time.

In practice, we use the Tent Pitcher algorithm [1] to fill the region between the old and new fronts with a small *patch* of simplex cells. Inter-cell boundaries within the patch are not necessarily causal, so the entire patch has to be solved simultaneously. Fig. 1 (right) shows an adaptively refined cSDG mesh at an intermediate stage of a $2d \times$ time simulation of crack-tip wave scattering in which high-resolution cSDG adaptive meshing captures moving wavefronts and quasi-singular crack-tip fields.

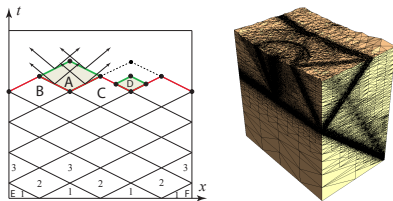


Figure 1: left: cSDG solution scheme in $1d \times$ time; right: adapted causal mesh in $2d \times$ time.

2 Parallel-Adaptive Implementation

Figure 2 diagrams a previous parallel-adaptive cSDG software architecture for a single multi-core, shared-memory host with two hardware threads per core. The front mesh and the *Pitchable Vertex Queues* (PVQs determine the patch-building order) are the only global, shared data. On each core i , one hardware thread handles meshing while the other solves patches. Threads run asynchronously and communicate exclusively via queues. All meshing and solve operations are embarrassingly parallel, with the exception of operations that access the global data to build and store front-mesh fragments called *footprints*.

In our new architecture, a templated *distributed vector* container class distributes front-mesh and PVQ data across meshing threads on multiple hosts. The distributed vector class handles internally non-blocking MPI access commands, recycling of storage freed by delete operations, and a probabilistic load-balancing distribution scheme. Solve threads only access private local data and are unchanged in the distributed architecture.

3 Simulation of Super-Shear Earthquake

Earthquake simulations present extreme computational challenges due to the wide range of scales — regional fault systems extend over thousands of kilometers while rupture process zones measure in hundreds of microns. State-of-the-art earthquake simulations are unable to bridge this range of scales, so it is common practice to use much larger process zone sizes in numerical models. For example, the Southern California Earthquake Center (SCEC) TPV205-2D benchmark problem uses a critical slip-weakening

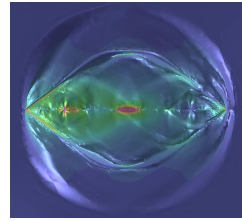


Figure 3: Super-shear rupture for reduced d_c in SCEC TPV205-2D benchmark problem.

We combined adaptive cSDG models for elastodynamics, dynamic contact, and dynamic fracture [2] with a slip-weakening friction model to obtain a powerful new earthquake simulation tool. When we modeled SCEC TPV205-2D as specified, our cSDG solutions were in good agreement with previous results where rupture-tip speeds remained below the shear-wave speed. Figure 3 shows the cSDG solution when we reduced D_c by a factor of 10. The left and right Mach cones confirm the presence of super-shear rupture speeds that approach the dilatational wave speed.

4 Conclusions

The SCEC TPV205-2D results underline the importance of resolving all relevant length and time scales in science and engineering simulation. The results shown here, obtained with a serial cSDG code, demonstrate the power of adaptive cSDG methods. Parallel-adaptive cSDG codes running on HPC platforms promise break-through performance capable of solving problems with realistic material-parameter values on regional-scale fault systems. New results will demonstrate the the distributed cSDG scheme's performance and scalability.

References

- [1] R. Abedi, S.-H. Cheng, J. Erickson, Y. Fan, M. Garland, D. Guoy, R. Haber, J. Sullivan, S. Thite and Y. Zhou. Spacetime meshing with adaptive refinement and coarsening, in *20th Ann. Symp. Comp. Geometry, New York, USA, June 8–11, 2004*, pp. 300–309.
- [2] R. Abedi, R.B. Haber and P.L. Clark, Effect of random defects on dynamic fracture in quasi-brittle materials, *Int J Fract* **208** (2017), pp. 241–268.

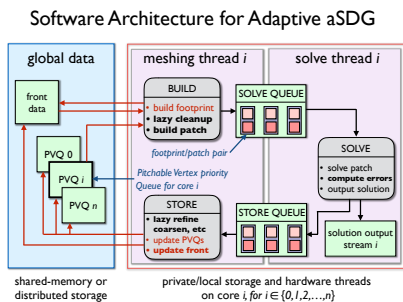


Figure 2: Parallel software architecture

Applications of Adaptive Spacetime Meshing in the Asynchronous Spacetime Discontinuous Galerkin Method

Reza Abedi^{1,*}, Robert B Haber²

¹Department of Mechanical, Aerospace & Biomedical Eng., University of Tennessee, Knoxville, USA

²Department of Mechanical Science & Engineering, University of Illinois, Urbana, USA

*Email: rabedi@utk.edu

Abstract

Asynchronous Spacetime Discontinuous Galerkin (aSDG) methods use robust adaptive meshing to construct unstructured grids on spacetime analysis domains with no global time-step constraints. While traditional adaptive remeshing is performed only once per N time steps, aSDG solvers perform many thousands of adaptive operations per layer of spacetime elements to capture fast-moving wavefronts and track rapidly-evolving interfaces. We present applications in dynamic fracture and electromagnetics to demonstrate these capabilities.

Keywords: adaptive meshing, spacetime, discontinuous Galerkin, front capturing, interface tracking, dynamic fracture, electromagnetics

1 Introduction

The *Tent Pitcher* algorithm [1] is the point of departure for aSDG adaptive meshing. Tent Pitcher advances a space-like *front mesh* with non-uniform time coordinates by incrementing the time coordinate of one vertex at a time. The increment of time advancement is limited by a *causality constraint* that ensures that the front remains space-like. Tessellations of the spacetime volume between fronts define *patches* of spacetime elements on which local aSDG solutions are computed. If the solution is successful, the old front is discarded and the process repeats on updated fronts until the spacetime analysis domain is covered.

Adaptive refinement is triggered whenever a patch solution fails adaptive error criteria. In that case, the adaptive meshing procedure discards the failed patch and the updated front, locally refines the old front mesh, and resumes the Tent Pitcher procedure. The result is new patches that are simultaneously refined in space and time. In addition to front refinement, adaptive vertex-deletion, edge-flip, and vertex-moving operations are available.

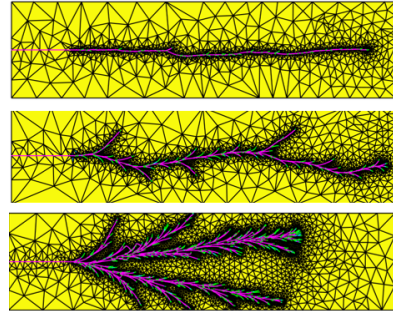


Figure 1: Dynamic tensile fracture under increasing load amplitudes.

2 Dynamic fracture: tracking interfaces

Simulation of dynamic fracture poses significant challenges: capturing fast-moving crack-tip field; and wavefronts as well as fracture nucleation, extension, and coalescence — all while ensuring that the physics model alone determines the crack patterns. We combined aSDG adaptive meshing capabilities with a stochastic fracture nucleation model to meet these challenges.

Figure 1 shows crack patterns due to dynamic fracture in identical pre-cracked strips subject to increasing mode-I load amplitudes. For the lowest loading (top), crack extension in near; a straight line is sufficient to absorb the applied energy. As the loading increases (middle, bottom), so do crack-path undulation, micro-crack formation, and crack branching. The emergence of these mechanisms are also observed experimentally; they serve as means to dissipate excess input power.

Figure 2 compares predicted fracture patterns for homogeneous and inhomogeneous fracture strength. Crack nucleation is pervasive for homogeneous fracture strength, as in Fig. 2(a). A more realistic sparse nucleation pattern emerges for inhomogeneous fracture strength in Figs. 2(b) and 2(c) where only the weakest flaws trigger

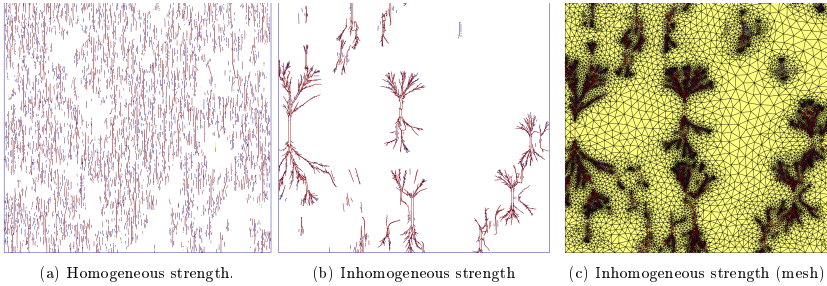
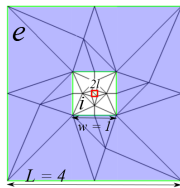


Figure 2: Effects of inhomogeneous fracture strength on fragmentation patterns

failure.

3 Electromagnetics: capturing wavefronts

The two-dimensional *Transverse Magnetic* electromagnetic problem depicted at the right involves an inner square region filled with a low-electric-permittivity material (white) and an outer region containing a second material (purple) with 10 times higher electric permittivity. A short-duration excitation within the red square at the center of the domain generates a sharp wavefront that propagates to the bi-material interface where it is reflected and transmitted into the outer region.



We compare non-adaptive and adaptive aSDG simulations to demonstrate the flexibility and efficiency of asynchronous spacetime meshing. The non-adaptive front is, at all times, an unstructured mesh of 83071 triangles. The initial front mesh for the adaptive simulation with just 46 triangles is shown in the figure. We depend on adaptive spacetime meshing to generate sufficient refinement to capture the initial pulse as well as evolving patterns of sharp wavefronts over the course of the simulation, as depicted by the sequence in Fig. 3. The adaptive run generates 2.77 million patches over the course of the simulation with a minimum element diameter of 9.77×10^{-4} . This compares favorably with the non-adaptive run's minimum element diameter, 0.0134, as well as 5.6 times more patches, 7.5 times higher computation time, and about double the energy error of the adaptive simulation.

4 Conclusions

Adaptive aSDG methods support front capturing and interface tracking in some of the most challenging dynamic simulations. We will present additional examples that showcase emerging parallel adaptive and 3d×time aSDG technologies.

References

[1] R. Abedi, S.-H. Cheng, J. Erickson, Y. Fan, M. Garland, D. Guoy, R. Haber, J. Sullivan, S. Thite and Y. Zhou. Spacetime meshing with adaptive refinement and coarsening, in *20th Ann Symp Comp Geometry, New York, USA, June 8–11, 2004*, pp. 300–309.

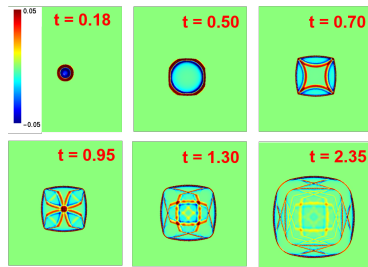


Figure 3: Time sequence; H_3 mapped to color.

Tent pitching and a Trefftz-DG method for the acoustic wave equation

Ilaria Perugia¹, Joachim Schöberl², Paul Stocker^{1,*}, Christoph Wintersteiger²¹Faculty of Mathematics, University of Vienna, Vienna, Austria²Institute for Analysis and Scientific Computing, Vienna University of Technology, Vienna, Austria

*Email: paul.stocker@univie.ac.at

Abstract

We present a space-time Trefftz discontinuous Galerkin method for the first-order transient acoustic wave equation. The method uses discontinuous test and trial functions that enforce properties of the wave equation. Optimal convergence, in terms of mesh size, was proven by A. Moiola, I. Perugia, (Numer. Math. 138, 2 (2018), 389-435), for arbitrary space dimensions. The method was implemented in NG-Solve, using a tent pitching algorithm to advance in time.

Keywords: Space-time finite elements, discontinuous Galerkin, Trefftz functions, tent pitching

1 Introduction

Standard finite element methods approximate the solution of a given partial differential equation (PDE) by piecewise polynomial functions. Instead of following the classic approach, where one uses finite element methods to discretize space and then use time stepping schemes to advance in time, we take a different approach, using finite element approximation simultaneously in space and time. This requires to mesh the full space-time domain and increases the dimension of the approximation space by the dimension of time. On the upside, *hp*-refinement is made possible in space-time, and we are able to use unstructured meshes.

The method we present combines a space-time discontinuous Galerkin (DG) method with the following two tools: tent pitched meshes and Trefftz functions. Tent pitching techniques give a possible way of generating a space-time mesh, which complies with the causality properties of the hyperbolic PDE, allowing to solve the PDE locally, circumventing the CFL-condition, which usually limits the global time-step size by the size of the smallest spatial element. Trefftz methods allow to enforce properties of the PDE in the test and trial spaces, resulting in smaller approximation spaces, but preserving approxi-

mation properties.

2 The Trefftz-DG method for the acoustic wave equation

We consider the acoustic wave equation in first order formulation, given by the initial boundary value problem (IBVP)

$$\begin{cases} \nabla \cdot \boldsymbol{\sigma} + c^{-2} \frac{\partial v}{\partial t} = 0 & \text{in } Q \\ \nabla v + \frac{\partial \boldsymbol{\sigma}}{\partial t} = \mathbf{0} & \text{in } Q \\ v(\cdot, 0) = v_0, \boldsymbol{\sigma}(\cdot, 0) = \boldsymbol{\sigma}_0 & \text{on } \Omega \\ v = g_D & \text{on } \Gamma_D \times [0, T] \end{cases}$$

on the space-time domain $Q = \Omega \times (0, T)$, with Ω a Lipschitz bounded domain in \mathbb{R}^n . We assume that the wavespeed $c > 0$ is piecewise constant on Ω .

2.1 The space-time mesh

The mesh $\mathcal{T}_h(Q)$ of the space-time domain Q is assumed to consist of non-overlapping Lipschitz polytopes. Either vertical faces or faces below the characteristic speed are allowed, an example and special notation for the faces is shown in Figure 1. If only faces below the characteristic speed are present, we call the mesh a tent pitched mesh, which can be obtained algorithmically as shown in [2].

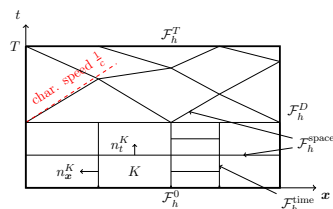


Figure 1: A Cartesian product mesh on the bottom and a tent pitched mesh on the top.

2.2 The Trefftz spaces

The main property of Trefftz functions is that they are in the kernel of the considered differential operator. For an element $K \subset \mathbb{R}^{n+1}$ in the mesh $\mathcal{T}_h(Q)$, we define the local polynomial Trefftz space as

$$\mathbb{T}^p(K) := \left\{ (w, \boldsymbol{\tau}) \in \mathbb{P}^p(K)^{n+1} : \nabla \cdot \boldsymbol{\tau} + c^{-2} \frac{\partial w}{\partial t} = 0, \nabla w + \frac{\partial \boldsymbol{\tau}}{\partial t} = \mathbf{0} \right\},$$

where we denote by \mathbb{P}^p the space of polynomials of degree $\leq p$. The global Trefftz-DG space on the whole mesh is then given by $\mathbb{T}^p(\mathcal{T}_h) := \prod_{K \in \mathcal{T}_h} \mathbb{T}^p(K)$. A possible way to construct a basis for the space is given in [1].

2.3 The method

The method is derived, as in [1], from the local weak formulation of IBVP by integrating by parts. Then the volume integrals over K vanish, since the test functions $(w, \boldsymbol{\tau}) \in \mathbb{T}^p(K)$ are Trefftz, and we get

$$\int_{\partial K} [\hat{v}_{hp} (\boldsymbol{\tau} \cdot \mathbf{n}_K^x + c^{-2} w n_K^t) + \hat{\boldsymbol{\sigma}}_{hp} \cdot (w \mathbf{n}_K^x + \boldsymbol{\tau} n_K^t)] = 0.$$

The solution $(v, \boldsymbol{\tau})$ in the boundary integral is replaced by the numerical fluxes $(\hat{v}_{hp}, \hat{\boldsymbol{\sigma}}_{hp}) \in \mathbb{T}^p(K)$. Suitably defining numerical fluxes for each face type and summing over all elements in the mesh results in the following method:

Find $(v_{hp}, \boldsymbol{\sigma}_{hp}) \in \mathbb{T}_p(\mathcal{T}_h)$ s.t.

$$\mathcal{A}(v_{hp}, \boldsymbol{\sigma}_{hp}; w, \boldsymbol{\tau}) = \ell(w, \boldsymbol{\tau}), \quad \forall (w, \boldsymbol{\tau}) \in \mathbb{T}_p(\mathcal{T}_h)$$

with

$$\begin{aligned} \mathcal{A}(v_{hp}, \boldsymbol{\sigma}_{hp}; w, \boldsymbol{\tau}) := & \int_{\mathcal{F}_h^{\text{space}}} \hat{v}_{hp} (c^{-2} [w]_t + [\boldsymbol{\tau}]_N) + \boldsymbol{\sigma}_{hp}^- \cdot ([\boldsymbol{\tau}]_t + [w]_N) \\ & + \int_{\mathcal{F}_h^T} c^{-2} v_{hp} w + \boldsymbol{\sigma}_{hp} \cdot \boldsymbol{\tau} + \int_{\mathcal{F}_h^D} (\boldsymbol{\sigma} \cdot \mathbf{n}_\Omega + \alpha v_{hp}) w \\ & + \int_{\mathcal{F}_h^{\text{time}}} [(\langle \hat{v}_{hp} \rangle + \beta [\boldsymbol{\sigma}_{hp}]_N) [\boldsymbol{\tau}]_N \\ & \quad + (\langle \hat{\boldsymbol{\sigma}}_{hp} \rangle + \alpha [v_{hp}]_N) \cdot [w]_N] \\ \ell(w, \boldsymbol{\tau}) := & \int_{\mathcal{F}_h^0} c^{-2} v_0 w + \boldsymbol{\sigma} \cdot \boldsymbol{\tau} \\ & + \int_{\mathcal{F}_h^D} g(\alpha w - \boldsymbol{\tau} \cdot \mathbf{n}_\Omega), \end{aligned}$$

where $\alpha, \beta \in L^\infty(\mathcal{F}_h^{\text{time}} \cup \mathcal{F}_h^D)$ are parameters penalizing the jump term. By w^+ and w^- we

denote the trace of the function w on space-like faces from the adjacent element at higher and lower times, respectively. We have used some standard DG notation for

$$\begin{aligned} \text{averages: } \langle \boldsymbol{\tau} \rangle &:= \frac{1}{2} (\boldsymbol{\tau}|_{K_1} + \boldsymbol{\tau}|_{K_2}) \\ \text{jumps: } \llbracket \boldsymbol{\tau} \rrbracket_N &:= \boldsymbol{\tau}|_{K_1} \cdot \mathbf{n}_{K_1}^x + \boldsymbol{\tau}|_{K_2} \cdot \mathbf{n}_{K_2}^x \\ \llbracket \boldsymbol{\tau} \rrbracket_t &:= \boldsymbol{\tau}|_{K_1} n_{K_1}^t + \boldsymbol{\tau}|_{K_2} n_{K_2}^t, \end{aligned}$$

between two elements $K_1, K_2 \in \mathcal{T}_h(Q)$.

On a product mesh the method can be solved sequentially on each time-slab, on each of which the method is implicit. On a tent pitched mesh it is semi-explicit, meaning that the solution on each tent only depends on the tents below, allowing to solve the tents sequentially, possibly in parallel.

3 Numerical results

For this example we use tent pitching in 2 + 1 dimensions until $T = 1$ solving tents sequentially. On the unit square initial and Dirichlet boundary conditions are chosen, such that the standing wave is the solution. The results of this are shown in Figure 2. We see a conver-

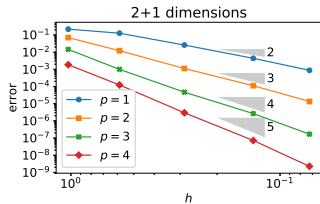


Figure 2: Tent pitching in (2+1)D, convergence comparison to the maximum mesh size.

gence rate of $O(h^{p+1})$, as the one we would expect from non-Trefftz polynomials of degree p in space and time.

References

- [1] A. Moiola, and I. Perugia, A space–time Trefftz discontinuous Galerkin method for the acoustic wave equation in first-order formulation. *Numer. Math.* 138, 2 (2018), 389–435
- [2] J. Gopalakrishnan, J. Schöberl, and C. Wintersteiger, Mapped tent pitching schemes for hyperbolic systems, *SIAM J. Sci. Comput.*, 39(6), (2016), B1043–B1063

An explicit Mapped Tent Pitching scheme for hyperbolic systems

Jay Gopalakrishnan¹, Joachim Schöberl², Christoph Wintersteiger^{2,*}

¹F. Maseeh Department of Mathematics and Statistics, Portland State University, Portland, USA

²Institute for Analysis and Scientific Computing, TU Wien, Wien, Austria

*Email: christoph.wintersteiger@tuwien.ac.at

Abstract

The presented Mapped Tent Pitching (MTP) method is based on a tent pitching algorithm, which partitions the spacetime domain into tent-shaped regions that respect causality. Instead of discretizing these tents in spacetime, we introduce a transformation, which maps each tent to a domain with tensor product structure of the spatial domain with a time interval. Using a discontinuous Galerkin method space, we observed a convergence order reduction when using standard explicit Runge-Kutta methods in time. Therefore we present a Runge-Kutta type time-stepping which overcomes this issue and can be applied to non-linear hyperbolic systems.

Keywords: tent pitching, local time stepping, non-linear hyperbolic systems

1 Introduction

In this work we consider hyperbolic systems, which fit into the following generic description. The integer $L > 0$ denotes the number of equations and $N > 0$ the spatial dimension. Further we denote the spatial domain with $\Omega_0 \subset \mathbb{R}^N$ and the cylindrical spacetime domain with $\Omega = \Omega_0 \times (0, t_{\max})$. With sufficiently smooth functions $g : \Omega \times \mathbb{R}^L \rightarrow \mathbb{R}^L$ and $f : \Omega \times \mathbb{R}^L \rightarrow \mathbb{R}^L \times \mathbb{R}^N$, the problem is to find a function $u : \Omega \rightarrow \mathbb{R}^L$ such that

$$\partial_t g(x, t, u) + \operatorname{div}_x f(x, t, u) = 0 \quad (1)$$

is satisfied. We use the notation $\partial_t = \partial/\partial t$ for the temporal derivative and div_x for the row-wise divergence operator.

Based on an unstructured mesh \mathcal{T} of the spatial domain Ω_0 a tent pitching algorithm is used to generate a discretization of Ω . Details of the tent pitching algorithm can be found in [1], which is based on the ideas presented in [2]. The main idea is that the time coordinates of the vertices are consecutively incremented such that the causality condition of the hyperbolic system is respected. Thus the algorithm consecutively

creates advancing fronts and the spacetime region between the old and the new front is denoted as tent. These tent pitched meshes are mostly used in combination with spacetime discontinuous Galerkin (SDG) methods as in [3]. In contrast to these methods we construct a fully explicit method by mapping the tents to a tensor product domain, such that space and time of the local problems can be discretized separately.

2 Mapped Tent Pitching scheme

The tents can be easily characterized in the following way. For each vertex V we denote the vertex patch by ω_V . The functions φ_b and φ_t describe the bottom and top advancing fronts restricted to ω_V . This allows us to define a tent

$$K := \{(x, t) : x \in \omega_V, \varphi_b(x) \leq t \leq \varphi_t(x)\}. \quad (2)$$

To separate space and time for the local problem on K , we introduce a transformation $\Phi : \hat{K} \rightarrow K$, with $\hat{K} := \omega_V \times (0, 1)$. This transformation is defined by $\Phi(x, \hat{t}) := (x, \varphi(x, \hat{t}))$, where

$$\varphi(x, \hat{t}) := (1 - \hat{t})\varphi_b(x) + \hat{t}\varphi_t(x). \quad (3)$$

Further we rewrite (1) using the spacetime divergence, which allows us to apply the Piola transform. This then leads to the equivalent system on \hat{K}

$$\begin{aligned} \partial_{\hat{t}} (g(x, \hat{t}, \hat{u}) - f(x, \hat{t}, \hat{u}) \nabla \varphi(\hat{t})) \\ + \operatorname{div}_x (\delta(x) f(x, \hat{t}, \hat{u})) = 0, \end{aligned} \quad (4)$$

with $\hat{u} = u \circ \Phi$ and the height of the tent $\delta = \varphi_t - \varphi_b$.

Equation (4) is then discretized a using discontinuous Galerkin (DG) method with polynomials of order p . Given that $n \in \mathbb{N}$ is the dimension of the discrete space \mathcal{V}_h restricted to the vertex patch ω_V , we are left to solve the system of ordinary differential equations for $U : [0, 1] \rightarrow \mathbb{R}^n$ such that

$$(M(\hat{t})(U(\hat{t})))' - A(U(\hat{t})) = 0. \quad (5)$$

The arising operators $M(\hat{t})(\cdot)$ and $A(\cdot)$ might be non-linear, depending on the structure of the considered problem (1).

h	RK3		RK3type	
	e	eoC	e	eoC
2.50e-02	1.96·10 ⁻⁴	1.99	1.96·10 ⁻⁴	1.99
1.25e-02	3.55·10 ⁻⁵	2.46	3.56·10 ⁻⁵	2.46
6.25e-03	4.72·10 ⁻⁶	2.91	4.75·10 ⁻⁶	2.91
3.13e-03	6.26·10 ⁻⁷	2.92	6.15·10 ⁻⁷	2.95
1.56e-03	1.18·10 ⁻⁷	2.41	7.87·10 ⁻⁸	2.96
7.81e-04	4.47·10 ⁻⁸	1.40	9.91·10 ⁻⁹	2.99
3.91e-04	2.27·10 ⁻⁸	0.98	1.25·10 ⁻⁹	2.99
1.95e-04	1.09·10 ⁻⁸	1.06	1.57·10 ⁻¹⁰	3.00
9.77e-05	5.84·10 ⁻⁹	0.89	1.98·10 ⁻¹¹	2.99

Table 1: $L^2(\Omega_0)$ -error and convergence rates of the one-dimensional Burgers using a DG finite element space with polynomial order $p = 2$.

3 Runge-Kutta type time-stepping

Defining the variable $Y(\hat{t}) := M(\hat{t})(U(\hat{t}))$, equation (5) reads

$$Y(\hat{t})' - A(M(\hat{t})^{-1}(U(\hat{t}))) = 0. \quad (6)$$

Applying a standard Runge-Kutta method to (6) leads to a reduction of the spatial convergence order and we obtain a method which converges only linearly in h , where h denotes the mesh size $\text{diam}(\mathcal{T})$.

This can be illustrated for the one-dimensional Burgers equation

$$\partial_t u(x, t) + \partial_x u(x, t)^2 = 0, \quad \forall (x, t) \in \Omega, \quad (7)$$

with initial values

$$u(x, 0) = \exp\left(-50\left(x - \frac{1}{2}\right)^2\right), \quad \forall x \in \Omega_0.$$

solved on $\Omega_0 = [0, 1]$. The final time $t_{\max} = 0.1$ is chosen such that the exact solution is still smooth. The boundaries are defined as inflow boundary at $x = 0$ and outflow boundary at $x = 1$. The results shown in Table 1 were calculated using the third order Heun method and second order polynomials in space. The second column contains the spatial L^2 -errors $e := \|u - u_h\|_{L^2(\Omega_0)}$ at $t = t_{\max}$ and the ‘‘experimental order of convergence’’ (eoC). We see the expected third order convergence for the first few refinement levels before the rate drops to first order.

The explicit time dependency of $M(\hat{t})$ arises from the definition (3) of φ . Since φ is affine in \hat{t} , we get $M(\hat{t}) = M_0 - \hat{t}M_1$ with the time independent operators $M_0(\cdot)$ and $M_1(\cdot)$. Recalling

the definition of $Y(\hat{t})$ and integrating (5) from 0 to \hat{t} gives

$$\begin{aligned} Y(\hat{t}) &= M_0(U(\hat{t})) - \hat{t}M_1(U(\hat{t})) \\ &= M_0(U(0)) + \int_0^{\hat{t}} A(U(s))ds. \end{aligned} \quad (8)$$

For the additional variable $Z(\hat{t}) := M_0(U(\hat{t}))$ equation (8) reads

$$Z(\hat{t}) = Z(0) + \hat{t}\tilde{M}_1(Z(\hat{t})) + \int_0^{\hat{t}} \tilde{A}(Z(s))ds, \quad (9)$$

with $\tilde{M}_1 := M_1 \circ M_0^{-1}$ and $\tilde{A} = A \circ M_0^{-1}$. This allows us to define the following new time-stepping method.

Definition 1 For a given explicit Runge-Kutta method with s -stages and the Butcher tableau (A, b) , the explicit Runge-Kutta type method is defined by

$$Z_i = Z_0 + \hat{t} \sum_{j < i} d_{ij} \tilde{M}_1(Z_j) + a_{ij} \tilde{A}(Z_j), \quad (10a)$$

for $1 \leq i \leq s$ and

$$Y_1 = Y_0 + \hat{t} \sum_{i=1}^s b_i \tilde{A}(Z_i), \quad (10b)$$

with $Y_0 = Y(0)$ and $Z_0 = Z(0)$. The additional coefficients of this method are given by a lower triangular matrix $\mathcal{D} \in \mathbb{R}^{s \times s}$ with the entries $(\mathcal{D})_{ij} := d_{ij}$.

Applying the Runge-Kutta type time-stepping of order 3 to the previously discussed example we now obtain optimal convergence order. The third column of Table 1 contains the L^2 -errors and the experimental convergence order.

References

- [1] J. Gopalakrishnan, J. Schöberl, and C. Wintersteiger, Mapped tent pitching schemes for hyperbolic systems, *SIAM J. Sci. Comput.* **39** (2017), B1043-B1063.
- [2] J. Erickson, D. Guoy, J. M. Sullivan, and A. Üngör, Building spacetime meshes over arbitrary spatial domains, *Engineering with Computers*, **20** (2005), pp. 342–353.
- [3] S. T. Miller and R. B. Haber, A spacetime discontinuous Galerkin method for hyperbolic heat conduction, *Computer Methods in Applied Mechanics and Engineering* **198** (2008), pp. 194–209.

The Limiting Absorption Principle for periodic Schrödinger operators

Rainer Mandel^{1,*}

¹Institute for Analysis, Karlsruhe Institute of Technology, Karlsruhe, Germany

*Email: Rainer.Mandel@kit.edu

Abstract

We present a new Limiting Absorption Principle for periodic Schrödinger operators $-\Delta + V(x)$ as well as its applications to nonlinear Helmholtz equations. It is demonstrated how this result depends on the shape of the associated Fermi surfaces (also called isoenergetic surfaces).

Keywords: Limiting Absorption principles, Periodic Schrödinger operators, Nonlinear Helmholtz Equations

1 Introduction

Standing wave ansatzes for wave equations in periodic Kerr-type media lead to the study of nonlinear Helmholtz equations of the form

$$-\Delta u + V(x)u - \lambda u = \Gamma(x)|u|^{p-2}u \quad \text{in } \mathbb{R}^n. \quad (1)$$

Here, u describes the profile of the wave that oscillates in time with frequency $\lambda \in \mathbb{R}$. For $\lambda \notin \sigma(-\Delta + V(x))$ variational techniques and other tools may be employed to prove the existence of nontrivial localized solutions of this equation. Typically, these solutions are smooth, exponentially decaying and have at most finitely many zeros. Positive solutions are called ground states. Our intention is to show that in the complementary case $\lambda \in \sigma(-\Delta + V(x))$ localized solutions still exist even though most of the well-established techniques for Nonlinear Schrödinger equations break down due to the weak decay rates and oscillatory behaviour of solutions at infinity. Ground states and other finite energy solutions do in general not exist in this case so that different analytical tools have to be developed. We provide here such a tool and discuss its applications.

One possibility to tackle (1) is to use a dual formulation based on a Limiting Absorption Principle. This principle, explained in more detail below, allows to find solutions $u \in L^p(\mathbb{R}^n)$ of (1) by solving

$$u = \mathcal{R}_\lambda(\Gamma|u|^{p-2}u) + \varphi \quad (2)$$

where $-\Delta\varphi + V(x)\varphi - \lambda\varphi = 0$ and \mathcal{R}_λ is a kind of right inverse of the Schrödinger operator $-\Delta + V(x) - \lambda$. Following [1, 2, 4] the dual

equation (2) may be solved via fixed point or variational techniques once the mapping properties of $\mathcal{R}_\lambda : L^{p'}(\mathbb{R}^n) \rightarrow L^p(\mathbb{R}^n)$ are established. In [3] this was for the first time achieved for a class Schrödinger operators with nonconstant periodic potential V .

2 The Limiting Absorption Principle

The Limiting Absorption Principle consists in proving the well-definedness of the operator

$$\mathcal{R}_\lambda := \lim_{\varepsilon \rightarrow 0^+} \operatorname{Re}((-\Delta + V(x) - \lambda - i\varepsilon)^{-1}).$$

For applications to nonlinear problems such as (2) the boundedness of \mathcal{R}_λ between Lebesgue spaces is required. In the special case of the trivial potential $V \equiv 0$ Fourier analysis can be used to prove the corresponding estimates and thereby establish a Limiting Absorption Principle, see Theorem 6 in [2]. This technique does not apply in the general periodic setting which we are interested in, but Floquet-Bloch theory may act as a substitute. Using the tools from this theory and defining the notion of a ‘‘Fermi surface’’ in an appropriate and physically reasonable manner, we find the following sufficient conditions for a good Limiting Absorption principle for the operator $-\Delta + V(x)$:

- (A1) $V \in L^\infty(\mathbb{R}^n)$ is \mathbb{Z}^n -periodic.
- (A2) The Fermi surface of $-\Delta + V(x)$ at the energy λ is smooth, regular, with positive Gaussian curvature.
- (A3) The Floquet-Bloch eigenfunctions associated with $-\Delta + V(x)$ are pointwise equibounded.

In Fig. 1 resp. Fig. 2 we depict numerically computed Fermi surfaces for two different potentials and various values of λ . We can analytically verify (A2) in two dimensions for separated potentials $V(x) = V_1(x_1) + V_2(x_2)$ that are close to constants and low frequencies λ in the first band of the spectrum $\sigma(-\Delta + V(x))$. The assumption (A3) is less problematic.

Theorem 1 Assume (A1), (A2), (A3) as well as $\frac{2(n+1)}{n-1} < p < \frac{2n}{n-2}$. Then $\mathcal{R}_\lambda : L^{p'}(\mathbb{R}^n) \rightarrow L^p(\mathbb{R}^n)$ is well-defined and bounded.

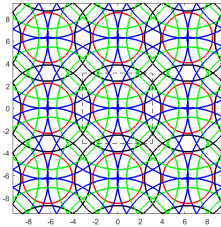


Figure 1: $V(x_1, x_2) = 0.2 \sin(2\pi x_1)^2 \cos(2\pi x_2)$

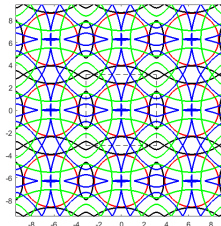


Figure 2: $V(x_1, x_2) = 10 \sin(2\pi x_1)^2 \cos(2\pi x_2)$

3 Applications

As indicated above, Theorem 1 may be used to find $L^p(\mathbb{R}^n)$ -solutions of (2) and hence of (1). Following [2], one may use the Contraction Mapping Theorem to get small nontrivial solutions of (1) that are parametrized by small Herglotz waves φ as above.

Theorem 2 [4] Assume (A1), (A2), (A3) and $p > \frac{2(n+1)}{n-1}$, $\Gamma \in L^\infty(\mathbb{R}^n)$. Then (2) admits a continuum of small mutually different solutions in $L^p(\mathbb{R}^n)$.

For exponents bigger than $\frac{2n}{n-2}$ a truncation is used in the proof. In [1] Evequoz and Weth demonstrated in the special case $V \equiv 0$ how large solutions may be constructed using dual variational methods and the Symmetric Mountain

Pass Theorem. We could partly adapt their approach to the periodic setting.

Theorem 3 [3] Assume (A1), (A2), (A3) and $\frac{2(n+1)}{n-1} < p < \frac{2n}{n-2}$ and let $\Gamma \in L^\infty(\mathbb{R}^n)$ be positive and evanescent at infinity. Then (2) admits an unbounded sequence of solutions.

References

- [1] G. Evequoz, T. Weth, Dual variational methods and nonvanishing for the nonlinear Helmholtz equation in *Adv. Math.* 280 (2015), pp. 690–728.
- [2] S. Gutiérrez, Non trivial L^q solutions to the Ginzburg-Landau equation in *Math. Ann.* 328 (2004), pp.1–25.
- [3] R. Mandel, The Limiting Absorption Principle for Periodic Differential Operators and Applications to Nonlinear Helmholtz Equations in *Comm. Math. Phys.* (2019), doi= 10.1007/s00220-019-03363-1.
- [4] R. Mandel, Uncountably many solutions for nonlinear Helmholtz and curl-curl equations with general nonlinearities, arXiv:1811.08168 (2018).

Multiple solutions to a nonlinear curl-curl problem in \mathbb{R}^3 Jarosław Mederski^{1,*}, Jacopo Schino¹, Andrzej Szulkin²¹Institute of Mathematics, Polish Academy of Sciences, Warsaw, Poland²Department of Mathematics, Stockholm University, Stockholm, Sweden

*Email: jmederski@impan.pl

Abstract

We look for ground states and bound states $E : \mathbb{R}^3 \rightarrow \mathbb{R}^3$ to the curl-curl problem

$$\nabla \times (\nabla \times E) = f(x, E), \quad x \in \mathbb{R}^3, \quad (1)$$

which originates from nonlinear Maxwell equations. The energy functional associated with this problem is strongly indefinite due to the infinite dimensional kernel of $\nabla \times (\nabla \times \cdot)$. The growth of the nonlinearity f is controlled by an N -function $\Phi : \mathbb{R} \rightarrow [0, \infty)$ such that $\lim_{s \rightarrow 0} \Phi(s)/s^6 = \lim_{s \rightarrow +\infty} \Phi(s)/s^6 = 0$. We prove the existence of a ground state, i.e. a least energy nontrivial solution, and the existence of infinitely many geometrically distinct bound states. Multiplicity results for our problem have not been studied so far in \mathbb{R}^3 and in order to do this we construct a suitable critical point theory. It is applicable to a wide class of strongly indefinite problems, including this one and Schrödinger equations. The talk is based on a joint work with Jacopo Schino and Andrzej Szulkin [3].

Keywords: Time-harmonic Maxwell equations, ground state, variational methods, strongly indefinite functional, curl-curl problem

1 Main result

We look for weak solutions to the semilinear curl-curl problem (1) originating from the Maxwell equations, where $\bar{E}(x, t) = E(x) \cos(\omega t)$ is a time-harmonic electric field in a nonlinear medium and $f(x, E)$ models a nonlinear polarization in the medium. $\bar{E}(x, t)$ solves the so-called electromagnetic wave equation. Another motivation has been provided by Benci and Fortunato [2] who introduced a model for a unified field theory for classical electrodynamics based on a semilinear perturbation of the Maxwell equations in the spirit of the Born-Infeld theory [1]. In the magnetostatic case in which the electric field vanishes and the magnetic field is independent of time, this leads to an equation of the form (1)

with E replaced by A , the gauge potential related to the magnetic field.

The problem (1) has a variational structure and the energy functional is given by

$$\mathcal{E}(E) = \frac{1}{2} \int_{\mathbb{R}^3} |\nabla \times E|^2 dx - \int_{\mathbb{R}^3} F(x, E) dx$$

where $f = \partial_E F$, and is unbounded from above and from below and its critical points may have infinite Morse index. For instance, this is the case, if $f(x, E) = \Gamma(x) \min\{|E|^{p-2}, |E|^{q-2}\} E$ with $2 < p < 6 < q$, where $\Gamma \in L^\infty(\mathbb{R}^3)$ is \mathbb{Z}^3 -periodic, positive and bounded away from 0. Here \mathcal{E} is of class C^1 on the Banach space $\mathcal{D}(\text{curl}, \Phi)$, see [3] for details.

Our principal aim is to prove the following result under suitable growth conditions controlled by Φ .

Theorem 1 (a) Equation (1) has a ground state solution, i.e. there is a critical point $E \in \mathcal{N}$ of \mathcal{E} such that $\mathcal{E}(E) = \inf_{\mathcal{N}} \mathcal{E} > 0$, where

$$\mathcal{N} = \{E \in \mathcal{D}(\text{curl}, \Phi) : E \neq 0, \mathcal{E}'(E)[E] = 0, \text{ and } \mathcal{E}'(E)[\nabla \varphi] = 0 \text{ for any } \varphi \in \mathcal{C}_0^\infty(\mathbb{R}^3)\}$$

(b) If in addition F is even in u , there is an infinite sequence $(E_n) \subset \mathcal{N}$ of geometrically distinct solutions of (1), i.e. solutions such that $(\mathbb{Z}^3 * E_n) \cap (\mathbb{Z}^3 * E_m) = \emptyset$ for $n \neq m$, where $\mathbb{Z}^3 * E_n := \{E_n(\cdot + y) : y \in \mathbb{Z}^3\}$.

References

- [1] M. Born, L. Infeld: *Foundations of the new field theory*, Proc. Roy. Soc. Lond. A **144** (1934), 425–451.
- [2] V. Benci, D. Fortunato: *Towards a unified field theory for classical electrodynamics*, Arch. Rat. Mech. Anal. **173** (2004), 379–414.
- [3] J. Mederski, J. Schino, A. Szulkin: *Multiple solutions to a nonlinear curl-curl problem in \mathbb{R}^3* , submitted arXiv:1901.05776

Bifurcation from Gap Eigenvalues for Nonlinear Schrödinger Equations

Peter Rupp^{1,*}

¹Institut für Analysis, KIT, Karlsruhe, Germany

*Email: peter.rupp@kit.edu

Abstract

A global bifurcation for the (stationary) nonlinear Schrödinger equation originating from the trivial solutions at a gap eigenvalue of the corresponding linearized operator is proved. These problems originate inserting a standing wave Ansatz in the time dependent Schrödinger equation. Aside from the existence of such standing waves for certain frequencies, we also obtain some information about the topological structure of the connected component of the set of solutions containing the bifurcation point.

Keywords: nonlinear Schrödinger equation, bifurcation

1 Introduction

We consider the equation

$$-\Delta u + V(x)u - \lambda u - g(x, u) = 0, \quad (1)$$

where the functions $V : \mathbb{R}^N \rightarrow \mathbb{R}$ and $g : \mathbb{R}^N \times \mathbb{R} \rightarrow \mathbb{R}$ fulfill the following assumptions: Let $V \in L^\infty(\mathbb{R}^N)$ be a potential such that the spectrum $\sigma(T)$ of the corresponding linear selfadjoint Schrödinger operator

$$T : L^2(\mathbb{R}^N) \supset D(T) \rightarrow L^2(\mathbb{R}^N), \\ Tu := -\Delta u + V(x)u$$

admits

$$\sigma(T) \cap (-a, a) = \{\lambda_0, \lambda_1, \dots, \lambda_m\} \subset \sigma_p(T)$$

for some $a > 0$, where σ_p denotes the set of eigenvalues of finite multiplicity. Such a spectral pattern can occur considering periodic potential with a relatively compact perturbation or interface potentials consisting of a junction of two periodic potentials at an interface. However, the approach presented here does not rely on any structural properties aside from the spectral pattern.

For the function g we assume all linear (in u) parts of the equation already to be absorbed in V such that T is the linearization of the left hand side in $u = 0$. Hence, some minimal

growth condition in 0 is imposed. Moreover we need some subcritical growth for large u as well as some bounds for its derivative. Let $s > 0$ be fixed, then it is assumed:

(G1) $g \in C(\mathbb{R}^N \times \mathbb{R}, \mathbb{R})$ and $g(x, \cdot) \in C^2(\mathbb{R})$ for almost every $x \in \mathbb{R}^N$.

(G2) There is $\varepsilon_0, C > 0$ and $\alpha < \frac{\varepsilon_0 \cdot s}{2}$ such that:

$$|g(x, v)| \leq C \langle x \rangle^\alpha |v|^{1+\varepsilon_0} \\ ((x, v) \in \mathbb{R}^N \times (-1, 1)).$$

(G3) For $N \geq 4$ there is $C > 0, p_0 \in (2, \frac{2N}{(N-4)_+})$ and $\beta < \frac{p_0 s}{2}$ such that:

$$|g(x, v)| \leq C \langle x \rangle^\beta |v|^{p_0} \\ ((x, v) \in \mathbb{R}^N \times \mathbb{R}).$$

(G4) For $N \geq 4$ there is $C > 0,$

$$q_0 \in (2, \min\{\frac{N}{(N-4)_+} - 1, \frac{4}{(N-4)_+}\})$$

and $\vartheta < \frac{q_0 s}{2}$ such that:

$$|\partial_v g(x, v)| \leq C \langle x \rangle^\vartheta |v|^{q_0}, ((x, v) \in \mathbb{R}^N \times \mathbb{R})$$

(G5) There is $\gamma > 2$ such that

$$0 \leq \gamma \cdot G(x, v) \leq g(x, v) \cdot v, \\ ((x, v) \in \mathbb{R}^N \times \mathbb{R}), \text{ where } G(x, \cdot) \text{ is a primitive of } g(x, \cdot).$$

2 Results

The following theorem can be found in [2] Let

$$L^{2,s}(\mathbb{R}^N) = \{u \in L^2(\mathbb{R}^N) : \langle x \rangle^s u \in L^2(\mathbb{R}^N)\}$$

and

$$H^{2,s}(\mathbb{R}^N) = \{u \in H^2(\mathbb{R}^N) : \langle x \rangle^s u \in H^2(\mathbb{R}^N)\}$$

be the weighted Lebesgue and Sobolev space. Moreover let $\mathcal{S}(s)$ be the set of nontrivial $H^{2,s}$ -solutions to (1), i.e a pair

$$(\lambda, u) \in ((-a, a), H^{2,s}(\mathbb{R}^N)) \setminus ((-a, a) \times \{0\}).$$

The result reads as follows:

Theorem 1 Let $s_0 > 0$ small enough and $\lambda_0 \in (-a, a)$ be a gap eigenvalue of odd multiplicity of T in $L^2(\mathbb{R}^N)$. Let $C_{\lambda_0}(s)$ be the connected component of $\overline{\mathcal{S}(s)}$ containing $(\lambda_0, 0)$. Then at least one of the following statements holds true:

1. $\exists s^* \in (0, s_0)$: $C_{\lambda_0}(s)$ is unbounded for all $s \in [s^*, s_0)$.
2. $\exists \lambda_1 \in (-a, a) \setminus \{\lambda_0\}$ and $s^* \in (0, s_0)$ such that $(\lambda_1, 0) \in C_{\lambda_0}(s)$ for all $s \in (0, s^*)$.
3. $\exists s^* \in (0, s_0)$, such that for any $s \in (0, s^*)$ either for all $\lambda \in (-b_s, \lambda_0]$ or for all $\lambda \in [\lambda_0, b_s)$ there exists $u_\lambda \in H^{2,s}(\mathbb{R}^N)$ such that $(\lambda, u_\lambda) \in C_{\lambda_0}(s)$ for some $b_s \rightarrow a$ as $s \rightarrow 0$.

3 Outline of the proof

The result is based on the global bifurcation result of Rabinowitz in [1]. Formally, the problem is reformulated into a fix point problem

$$\begin{aligned} -\Delta u + V(x)u - \lambda u - g(x, u) &= 0 \\ (-\Delta + V(x) + W - \lambda)^{-1}(g(x, u) + Wu) &= u, \end{aligned} \tag{2}$$

where $W : L^2(\mathbb{R}^N) \rightarrow L^2(\mathbb{R}^N)$ is a compact operator to be chosen later. In order to make it rigorous, we have to overcome two obstacles: Firstly, the Rabinowitz result requires a compact operator, which will be guaranteed by using weighted Sobolev spaces introduced above. This way the compactness of the map

$$H^{2,s}(\mathbb{R}^N) \rightarrow L^{2,s}(\mathbb{R}^N), u \mapsto g(x, u)$$

under the assumptions **(G1)-(G4)** is shown.

In order to provide the invertibility of the linear operator we introduce the perturbation W , defined by $W := M \cdot Pu$, where P denotes the projection on the common eigenspace of $\{\lambda_0, \dots, \lambda_m\}$ and M is large enough. In this way, W shifts the eigenvalues outside the gap while preserving the essential part of the spectrum of T . This property is preserved using weighted spaces provided that $M > 0$ is large enough in relation to the weight. This property furthermore relies on the eigenfunctions to gap eigenvalues being exponentially decaying. Moreover, we obtain a bound on the resolvent $(-\Delta + V(x) + W - \lambda)^{-1}$ uniformly in $s \in [0, s_0]$ for some $s_0 > 0$ and $\lambda \in [-b, b] \subset (-a, a)$.

Finally, assumption **(G5)** provides the differentiability of the left hand side of (2). The

application of Rabinowitz' theorem yields the global bifurcation result firstly for fixed $s > 0$ and in an s -independent formulation stated in Theorem 1

References

- [1] Paul H. Rabinowitz, Some global results for nonlinear eigenvalue problems, *Journal of functional analysis* **7** (1971), pp. 487–513.
- [2] Peter Rupp, Globale Bifurkation von Lückeneigenwerten bei nichtlinearen Schrödingergleichungen, *KITopen-Katalog* KITopen-ID: 1000086743 (2018)

Coupled Mode Equations and Gap Solitons for Wavepackets in Nonlinear Periodic Media

Tomas Dohnal^{1,*}, Lisa Wahlers²

¹Department of Mathematics, Martin Luther University Halle-Wittenberg, Germany

²Dortmund, Germany

*Email: tomas.dohnal@mathematik.uni-halle.de

Abstract

Wavepackets in the periodic Gross-Pitaevskii equation in arbitrary dimension are studied. For asymptotically small wavepackets with N carrier Bloch waves a system of first order coupled mode equations (CMEs) is justified as the effective system. The CMEs are then shown to possess standing solitary wave solutions bifurcating from spectral edges into a spectral gap.

Keywords: wavepacket, periodic medium, coupled mode equations, solitary waves

1 Introduction

We consider small amplitude wavepackets in the Gross-Pitaevskii equation in \mathbb{R}^d

$$i\partial_t u + \Delta u - (V + \varepsilon W)u - \sigma|u|^2 u = 0, \quad (1)$$

$x \in \mathbb{R}^d, t \in \mathbb{R}$ where $V, \sigma \in C(\mathbb{R}^d, \mathbb{R})$ are $2\pi\mathbb{Z}^d$ -periodic, $\varepsilon > 0$ is a small parameter, and

$$W(x) = \sum_{m=-m_*}^{m_*} a_m e^{i l^{(m)} \cdot x}$$

is a real periodic function with $l^{(m)} \in \mathbb{R}^d \forall m$.

In contrast with the traditional asymptotic ansatz with one carrier wave leading to the nonlinear Schrödinger equation [1,3] effective equation we study wavepackets with N carrier waves (and N envelopes). In general these carrier waves have different group velocities. The approximate ansatz is

$$u^{\text{app}}(x, t) := \varepsilon^{1/2} \sum_{j=1}^N A_j(\varepsilon x, \varepsilon t) p_j(x) e^{i(k^{(j)} \cdot x - \omega_0 t)}$$

where $p_j(x) e^{i(k^{(j)} \cdot x - \omega_0 t)}$, $j = 1, \dots, N$ are the carrier Bloch waves. A formal asymptotic calculation shows that the envelopes (A_1, \dots, A_N) have to satisfy the coupled mode equations (CMEs)

$$i(\partial_t A_j + v_y^{(j)} \cdot \nabla A_j) + \sum_{r=1}^N \kappa_{jr} A_r + N_j(\vec{A}) = 0, \quad (2)$$

$j = 1, \dots, N$, where for $j, r \in \{1, \dots, N\}$

$$N_j(\vec{A}) := \sum_{\substack{(\alpha, \beta, \gamma) \in \{1, \dots, N\}^3 \\ k^{(\alpha)} - k^{(\beta)} + k^{(\gamma)} \in k^{(j)} + \mathbb{Z}^d}} \gamma_j^{(\alpha, \beta, \gamma)} A_\alpha \bar{A}_\beta A_\gamma,$$

$$\gamma_j^{(\alpha, \beta, \gamma)} := - \int_{\mathbb{T}} \sigma(x) p_\alpha(x) \bar{p}_\beta(x) p_\gamma(x) \times \\ \times \bar{p}_j(x) e^{i(k^{(\alpha)} - k^{(\beta)} + k^{(\gamma)} - k^{(j)}) \cdot x} dx,$$

$$\kappa_{jr} := - \sum_{\substack{m \in \{-m_*, \dots, m_*\} \\ k^{(r)} + l^{(m)} \in k^{(j)} + \mathbb{Z}^d}} a_m \int_{\mathbb{T}} e^{i(k^{(r)} + l^{(m)} - k^{(j)}) \cdot x} \times \\ \times p_r(x) \bar{p}_j(x) dx,$$

and where $\mathbb{T} := \mathbb{R}^d / (2\pi\mathbb{Z}^d)$ is a d -dimensional torus.

2 Justification of the CMEs

It is essential to justify the above formal asymptotics, i.e. to prove that the ansatz u^{app} , with suitable solutions \vec{A} of (2), produces an approximation of a solution u of (1) on time intervals $[0, O(\varepsilon^{-1})]$.

System (2) with $\kappa = 0$ (due to the choice $W \equiv 0$) was considered and justified in [2]. The authors work in a scaled H^s -space. Because of the loss of powers of ε when evaluating the $L^2(\mathbb{R}^d)$ norm of a function $f(\varepsilon \cdot)$, they are forced to consider higher order terms in the asymptotics and to impose a certain closed mode system condition. We work in an L^1 space in the Bloch variables avoiding the need for higher order terms as well as the closed mode condition.

Our justification result is [4]:

Theorem 1 *Under non-resonance and smoothness assumptions on the band structure of $-\Delta + V$, assumptions on the smoothness of V and σ and the assumption of Lipschitz continuity with respect to k for the Bloch functions let \vec{A} be a solution of (2) with $\vec{A}_j \in C([0, T_0], L^1_{s_A}(\mathbb{R}^d) \cap L^2(\mathbb{R}^d))$, $\partial_T \vec{A}_j \in C([0, T_0], L^1(\mathbb{R}^d))$ for some $T_0 > 0$, all $j = 1, \dots, N$ and some $s_A > 2[\frac{d}{2}] + d + 2$. Then there are constants $c > 0$ and $\varepsilon_0 > 0$, such that if $u(\cdot, 0) = u^{\text{app}}(\cdot, 0)$, then*

for all $\varepsilon \in (0, \varepsilon_0)$ the solution u of (1) satisfies $u(x, t) \rightarrow 0$ as $|x| \rightarrow \infty$ and

$$\|u(\cdot, t) - u^{app}(\cdot, t)\|_{C_0^0} \leq c\varepsilon^{3/2} \quad (3)$$

for all $t \in [0, \varepsilon^{-1}T_0]$.

The proof is carried out in the Bloch variables in $L^1(\mathbb{B}, l_{s/d}^2)$ with $s > d/2$. The supremum norm in physical variables is controlled by the $L^1(\mathbb{B}, l_{s/d}^2)$ norm in Bloch variables. The proof is based on an improvement of the asymptotic ansatz, an estimate of the residual and a Gronwall inequality argument.

3 Existence of Solitary Waves for CMEs

A natural question in nonlinear dispersive problem is the existence of localized solitary waves. The shape of these solutions balances the dispersive and the nonlinear effects of the equation. Solitary waves of the CMEs (2) produce approximate solitary waves of (1) via Theorem 1. Localized solitary waves are most easily found in spectral gaps. These are called gap solitons. In the case $d = 1$ (and $N = 2$) the CMEs are known to possess a family of explicit gap solitons parametrized by velocity (for a special case of γ). For $d \geq 2$ spectral gaps in CMEs can exist only for even N . In the moving frame ansatz $\vec{A} = \vec{B}(X - vT)e^{-i\Omega T}$ in all studied examples the problem for \vec{B} lacks a spectral gap when $v \neq 0$. We study standing gap solitons ($v = 0$) with the asymptotic ansatz

$$\widehat{\vec{B}}_{app}(k) = \varepsilon^{1-d} \widehat{C} \left(\frac{k - k_0}{\varepsilon} \right) \vec{\eta}^{(j_0)}(k_0),$$

where $\vec{\eta}^{(j_0)}(k_0)$ is an eigenvector corresponding to the dispersion relation of the CMEs. The scalar function C has to satisfy the effective nonlinear Schrödinger equation

$$\omega_1 C + \nabla^T (G_0 \nabla C) + \Gamma |C|^2 C = 0, \quad (4)$$

where $\omega_1, \gamma \in \mathbb{R}$ and $2G_0 \in \mathbb{R}^{d \times d}$ is the Hessian of the dispersion relation at k_0 . We prove [5]:

Theorem 2 Choose $\omega_0 \in \{\alpha, \beta\}$, where (α, β) is a spectral gap for (2) and let the edge ω_0 be simple. Let $\omega_1 \in \mathbb{R}$ be such that $sign(\omega_1) = 1$ if $\omega_0 = \alpha$ and $sign(\omega_1) = -1$ if $\omega_0 = \beta$. If C is a PT -symmetric solution of (4) with $\widehat{C} \in L^1_4(\mathbb{R}^d)$ and the kernel of the Jacobian of (4) is three dimensional, then there are constants $c_1, \varepsilon_0 > 0$

such that for each $\varepsilon \in (0, \varepsilon_0)$ there is a solution $e^{-i\Omega t} \vec{B}(X)$ of CMEs with $\Omega = \omega_0 + \varepsilon^2 \omega_1$ which satisfies $\vec{B} \in L^2_2(\mathbb{R}^d)$ and

$$\|\widehat{\vec{B}} - \widehat{\vec{B}}_{app}\|_{L^1(\mathbb{R}^d)} \leq c_1 \varepsilon^{9/5}.$$

We have found coefficients $\kappa \in \mathbb{R}^{4 \times 4}$ such that the spectral conditions of Theorem 2 are satisfied. The proof of Theorem 2 is based on a decomposition of the solution \vec{B} and a nested Banach fixed point argument.

Figure 1 (from [5]) shows the first component of the approximation \vec{B}_{app} for a radially symmetric solution of (4) and the corresponding numerical solution B_1 .

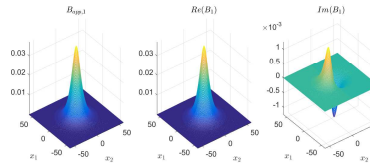


Figure 1: Asymptotic approximation $B_{app,1}$ and the numerical solution B_1 (real and imag. part) at $\varepsilon = 0.05$.

References

- [1] K. Busch, G. Schneider, L. Tkeshelashvili, and H. Uecker. Justification of the nonlinear Schrödinger equation in spatially periodic media. *Z. Angew. Math. Phys.*, **57**:905–939, 2006.
- [2] J. Giannoulis, A. Mielke, and Ch. Sparber. Interaction of modulated pulses in the nonlinear Schrödinger equation with periodic potential. *J. Diff. Equ.*, **245**(4):939–963, 2008.
- [3] T. Dohnal and D. Rudolf. NLS Approximation for Wavepackets in Periodic Cubically Nonlinear Wave Problems in \mathbb{R}^d , accepted to *Applicable Analysis*, 2018.
- [4] T. Dohnal and L. Wahlers. Coupled Mode Equations and Gap Solitons in Higher Dimensions. submitted, arXiv:1810.04944.
- [5] T. Dohnal and L. Wahlers, Bifurcation of Gap Solitons in Coupled Mode Equations in d Dimensions, submitted, 2019. arXiv:1903.02631.

Breather Solutions for a Quasilinear 1+1dim Wave Equation

Jiří Horák¹, Simon Kohler^{2,*}, Wolfgang Reichel²

¹Faculty of Mechanical Engineering, THI, Ingolstadt, Germany

²Department of Mathematics, KIT, Karlsruhe, Germany

*Email: simon.kohler@kit.edu

Abstract

For the 1+1-dimensional quasilinear wave equation

$$g(x)\partial_t^2 u - \partial_x^2 u + \Gamma(x)\partial_t((\partial_t u)^3) = 0, \quad (1)$$

with $(x, t) \in \mathbb{R}^2$, we prove the existence of a breather solution, i.e., a solution which is localized in space and periodic in time.

Here $g \in L^\infty(\mathbb{R})$ is a periodic potential such that 0 lies in a spectral gap of the operators $L_k = -\frac{d^2}{dx^2} - k^2\omega^2 g(x)$ on $L^2(\mathbb{R})$ for all $k \in 2\mathbb{Z} - 1$. A typical example for g is a periodic step potential. The main feature of the problem is the choice of $\Gamma(x)$ as a multiple of a delta-distribution located at 0. Using a Fourier ansatz in time we obtain the breather solution as a minimizer of a functional on a suitable sequence space of Fourier coefficients. The analytical results are complemented by numerical simulations.

Keywords: calculus of variations, quasilinear wave equation, breather

1 Physical Motivation

One way to deduce the quasilinear equation (1) is the following: We consider a nonlinear Maxwell model without charges and currents

$$\begin{aligned} \nabla \cdot \mathbf{D} &= 0, & \nabla \times \mathbf{E} &= -\partial_t \mathbf{B}, \\ \nabla \cdot \mathbf{B} &= 0, & \nabla \times \mathbf{H} &= \partial_t \mathbf{D}, \end{aligned}$$

and with Kerr-type nonlinear material laws

$$\mathbf{B} = \mu_0 \mathbf{H}, \quad \mathbf{D} = \epsilon_0(1 + \chi_1(\mathbf{x}) + \chi_3(\mathbf{x})|\mathbf{E}|^2)\mathbf{E}$$

to obtain the vector-valued equation

$$\nabla \times \nabla \times \mathbf{E} + \partial_t^2 \left(g(\mathbf{x})\mathbf{E} + \Gamma(\mathbf{x})|\mathbf{E}|^2 \mathbf{E} \right) = 0.$$

Assuming that g and Γ only depend on x_1 , $\mathbf{E} = (0, v(x_1, t), 0)$ and writing x instead of x_1 we get

$$g(x)\partial_t^2 v - \partial_x^2 v + \Gamma(x)\partial_t^2 (v^3) = 0.$$

Finally we write $v = \partial_t u$ and integrate once in t to obtain (1), which has a variational structure.

2 Main Result

Our problem consists in finding requirements on the potential g such that a spatially localized and time-periodic solution u exists for (1).

After the explicit breather family for the sine-Gordon equation was found, also non-existence result for breathers for perturbed sine-Gordon equations were discovered: the sine nonlinearity is the *only* nonlinearity in the class of nonlinearities f with $f(0) = 0, f'(0) \neq 0$ close to sine such that a breather exist, cf. [3] and [1]. Only few other results on the existence of breathers are known, e.g., cf. [2] for small breathers via bifurcation methods and [5] for large breathers via variational calculus. These works considered semi-linear equations. By using a multiple scale approximation ansatz the authors in [6] find strong evidence, that coherent spatially localized solutions of a quasilinear 1+1 dimensional Maxwell model exist. Similar multiple scale ansatzes are used in [7] to verify coherent multiscale structures arising from wave packet type initial conditions in numerical simulations.

Our result for (1) reads as follows.

Theorem 1 For $a, b > 0, a \neq b$ and $\Theta \in (0, 1)$ let

$$g(x) := \begin{cases} a, & |x| < \pi\Theta \\ b, & \pi\Theta < |x| < \pi \end{cases}$$

and extend g as a 2π -periodic function to \mathbb{R} . Assume in addition

$$\sqrt{\frac{b}{a}} \frac{1 - \Theta}{\Theta} \in 2\mathbb{Z} + 1.$$

For every ω such that $2\sqrt{a}\Theta\omega - \frac{1}{2} \in \mathbb{N}_0$ there exists a nontrivial, real-valued, spatially localized and time-periodic weak solution u of (1) with period $T = \frac{2\pi}{\omega}$. Furthermore there are constants $C, \rho > 0$ such that $|u(x, t)| \leq Ce^{-\rho|x|}$.

3 Outline of the Ideas

Solutions are obtained by finding critical points of an energy functional whose Euler-Lagrange

equation is (1). We write \mathbb{T}_T for the 1-dim torus of period T .

Definition 2 A function $u \in H^1(\mathbb{R} \times \mathbb{T}_T)$ with $\partial_t u(0, \cdot) \in L^3(0, T)$ is called a weak solution of (1), if for every $\varphi \in C_c^\infty(\mathbb{R} \times \mathbb{T}_T)$

$$\int_{\mathbb{R} \times \mathbb{T}_T} -g(x) \partial_t u \partial_t \varphi + \partial_x u \partial_x \varphi \, d(x, t) - \gamma \int_{\mathbb{T}_T} (\partial_t u(0, t))^3 \partial_t \varphi(0, t) \, dt = 0.$$

If we assume that u is even in x , we can formally rewrite (1) as a wave equation on the half-axis with nonlinear Neumann boundary conditions:

$$\begin{cases} g(x)u_{tt} - u_{xx} = 0, & \text{for } x \in (0, \infty) \\ 2u_x(0_+, t) = \gamma (u_t(0, t))^3, & t \in \mathbb{R} \end{cases}$$

We choose the following ansatz

$$u(x, t) = \sum_{k \in \mathbb{Z}_{\text{odd}}} \frac{\widehat{z}_k}{k} \Phi_k(|x|) \frac{1}{\sqrt{T}} e^{ik\omega t} \quad (2)$$

with unknowns $\widehat{z}_k \in \mathbb{C}$, where Φ_k is the exponentially decaying Bloch-mode of $L_k = -\frac{d^2}{dx^2} - k^2 \omega^2 g(x)$. Here a function $\Phi_k: \mathbb{R} \rightarrow \mathbb{R}$ is called a Bloch mode, if it solves $L_k \Phi_k = 0$ and $\Phi_k(\cdot + 2\pi) = \rho_k \Phi_k(\cdot)$ for some $\rho_k \in \mathbb{C}$, cf. [4]. The formal energy functional

$$\begin{aligned} I(u) = & \int_{\mathbb{R} \times \mathbb{T}_T} -g(x) |\partial_t u|^2 + |\partial_x u|^2 \\ & - \frac{1}{2} \Gamma(x) |\partial_t u|^4 \, d(x, t) \end{aligned}$$

then (up to constants) becomes

$$J(\widehat{z}) = \frac{1}{4} (\widehat{z} * \widehat{z} * \widehat{z} * \widehat{z})_0 + \frac{1}{\gamma \omega^4} \sum_k \frac{\Phi'_k(0)}{k^2} |\widehat{z}_k|^2$$

for sequences $\widehat{z} = (\widehat{z}_k)_k$, where $*$ denotes convolution. Theorem 1 follows by minimizing J on a suitable Banachspace of sequences. We then show that the reconstruction of u by (2) yields a solution of (1) in the sense of Definition 2.

4 Numerical Results

We implemented numerical steepest decent methods to construct approximate minimizers of J in suitable l -dimensional subspaces. We also prove analytically, that minimizers in such l -dimensional subspaces converge towards a global minimizer of J as $l \rightarrow \infty$.

5 Further Analytical Results

By exploiting the Euler-Lagrange equation for J we prove additional regularity for solutions u , in particular we obtain $u \in H^{1+\nu}(\mathbb{T}_T, L^2(\mathbb{R})) \cap H^\nu(\mathbb{T}_T, H^1(\mathbb{R}))$ for any $\nu \in (0, \frac{1}{4})$.

Furthermore we prove the existence of countably many solutions of (1) on different energy levels.

Moreover we have formulated abstract conditions on the Bloch modes Φ_k , such that the minimization procedure of J , the reconstruction procedure of u and the additional smoothness of u can be performed.

References

- [1] B. Birnir, H. P. McKean, A. Weinstein, *The rigidity of sine-gordon breathers*. Communications on Pure and Applied Mathematics, 47(8), 1043-1051,(1994).
- [2] C. Blank, M. Chirilus-Brukner, V. Lescarret, G. Schneider, *Breather solutions in periodic media*. Communications in mathematical physics, 302(3), 815-841, (2011).
- [3] J. Denzler, *Nonpersistence of breather families for the perturbed sine Gordon equation*. Communications in Mathematical physics, 158(2), 397-430,(1993).
- [4] M. S. P. Eastham, *The spectral theory of periodic differential equations*. Scottish Academic Press, distributed by Chatto & Windus, London, (1973).
- [5] A. Hirsch, W. Reichel, *Real-valued, time-periodic localized weak solutions for a semilinear wave equation with periodic potentials*, arXiv:1709.08443v2, 2017
- [6] D. E. Pelinovsky, G. Simpson, M. I. Weinstein: *Polychromatic solitary waves in a periodic and nonlinear Maxwell system*. SIAM Journal on Applied Dynamical Systems 11.1: 478-506, (2012).
- [7] G. Simpson, M. I. Weinstein: *Coherent structures and carrier shocks in the nonlinear periodic Maxwell equations*. Multiscale Model. Simul., 9(3):955-990, 2011. URL <https://doi.org/10.1137/100810046>.

Breathers on metric necklace graphs

Daniela Maier^{1,*}¹ Department of Mathematics and Physics, University of Stuttgart, Stuttgart, Germany
new address (from 04-15-2019 onwards):

Department of Mathematics, Karlsruhe Institute of Technology, Karlsruhe, Germany

*Email: daniela.maier@mathematik.uni-stuttgart.de

Abstract

We provide a rigorous proof for the existence of breather solutions for nonlinear Klein-Gordon equations on periodic metric necklace graphs with Kirchhoff boundary conditions. The proof relies on a spatial dynamics approach combined with center manifold reduction. It requires a careful control of the Floquet Bloch spectrum of the underlying linearized differential operators.

Keywords: nonlinear Klein Gordon equation, breathers, spatial dynamics, center manifold reduction

1 Introduction**1.1 Quantum graphs**

Applications of periodic graphs arise in many fields of science, for instance as models for complex physical structures such as photonic crystals, nano-tubes or graphene.

What is meant by posing differential equations on metric graphs?



Figure 1: Geometry of the metric necklace graph. We assign length π to each edge.

The differential operator acts on functions defined on the edges together with appropriate boundary conditions. For instance, the Laplacian becomes self-adjoint by imposing *Kirchhoff boundary conditions* (continuity and conservation of the flows).

1.2 The problem

We are interested in real-valued, time-periodic and spatially structures in nonlinear Klein Gordon equations on periodic necklace graphs. From a mathematical point of view,

the existence of these so called *breather solutions* for PDEs is very rare. In the spatially homogeneous situation, a nonlinear wave equation known to admit small-amplitude breather solutions of pulse form is the Sine-Gordon equation. These solutions do not persist under analytic perturbations. However, the situation is different if one introduces spatial inhomogeneities and breather solutions are back.

Our approach is motivated by the existence result of small-amplitude breathers of Blank, Chirilus-Brukner, Lescarret, and Schneider [1].

2 Existence of breather solutions

Theorem 1 *Let k be an odd integer. For sufficiently small $\varepsilon > 0$, the cubic Klein-Gordon equation*

$$\partial_t^2 u(x, t) = \partial_x^2 u(x, t) - \left(\frac{k^2}{4} + \varepsilon \right) u(x, t) + u(x, t)^3$$

with Kirchhoff boundary conditions at the vertices possesses breather solutions of amplitude $\mathcal{O}(\sqrt{\varepsilon})$ and frequency $\omega = k/2$. These solutions are symmetric in the upper and lower semicircle.

Precisely, there exist functions $u : \mathbb{R} \times \mathbb{R} \rightarrow \mathbb{R}$ satisfying

- $u(x, t) = u(x, t + \frac{4\pi}{k})$, for all $t, x \in \mathbb{R}$,
- $\lim_{|x| \rightarrow \infty} u(x, t) e^{\beta|x|} = 0$, for all $t \in \mathbb{R}$ and a constant $\beta > 0$.

By construction we get polychromatic, long-wave breathers.

3 Method of proof

Using a Fourier series expansion with respect to time

$$u(t, x) = \sum_{m \in \mathbb{N}_{\text{odd}}} u_m(x) \cos(m\omega t),$$

the original problem transforms into countably many coupled second order ordinary differential equations

$$-m^2\omega^2 u_m = \partial_x^2 u_m - (\alpha + \varepsilon^2)u_m + (u * u * u)_m, \quad (1)$$

for the Fourier coefficients with $m \in \mathbb{N}_{\text{odd}}$ and new dynamic variable x (*spatial dynamics formulation*). The cubic nonlinearity transforms into a discrete convolution term. Since we are interested in spatially localized solutions, i.e.,

$$\lim_{|x| \rightarrow \infty} u(t, x) = 0, \quad t \in \mathbb{R},$$

we construct a *homoclinic orbit to zero* in the phase space of the infinite dimensional system above. The key idea is to perform a center manifold reduction in order to reduce (1) to a finite dimensional system. However, because of the Kirchhoff boundary conditions, the system is non-autonomous and the first derivatives of the solutions have jumps and the flow on the center manifold is no longer continuous. Therefore, we apply a *discrete version of the center manifold theorem* to the family of time- P -maps. To do so, we require a careful control of the Floquet Bloch spectrum of the underlying linearized differential operators.

Floquet-characterization of the spectrum:

Let $M(\lambda)$ denote the monodromy matrix of system (1), which is the canonical fundamental matrix evaluated after one period. Then,

$$\lambda \in \sigma_{\text{ac}}(-\partial_x^2|_{\Gamma}) \Leftrightarrow |\text{tr}(M(\lambda))| \leq 2.$$

Discrete center manifold reduction: There exists an invariant manifold with same dimension as the center subspace and dynamics of small solutions are determined on this center manifold.

Key relation and choice of breather frequency:

- 1. $|\text{tr}M(m^2\omega^2 - \alpha)| \leq 2 \Leftrightarrow$ Eigenvalues of $M(m^2\omega^2 - \alpha)$ on unit circle,
- 2. $\#\{\text{Eigenvalues of } M(m^2\omega^2 - \alpha) \text{ on unit circle}\} =$ dimension of center manifold.

We choose constants $\omega = k/2$, $\alpha = \omega^2$ with $k \in \mathbb{N}_{\text{odd}}$ such that $|\text{tr}M(\omega^2 - \alpha)| = 2$ and $|\text{tr}M(m^2\omega^2 - \alpha)| > 2$ for all odd integers $m \geq 3$, cf. Figure 2.

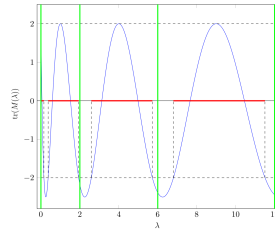


Figure 2: Band-gap structure of the spectrum and odd multiples of ω (vertical lines)

Analysis of the reduced system: The lowest order approximation of the dynamics on the center manifold is given by the ODE for u_1 with $u_m = 0$ for all $m \geq 3$:

$$\partial_x^2 u_1(x) = \varepsilon u_1(x) - u_1^3(x).$$

The existence of a homoclinic to zero of this ODE was proved in [2]. The persistence of homoclinics under higher order perturbations is obtained by symmetry and reversibility arguments, cf. Figure 3.

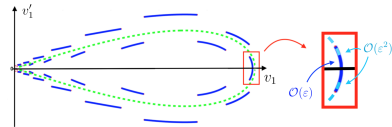


Figure 3: Transversal intersection

Remark: This work is part of my PhD-Thesis supervised by Guido Schneider and will be published soon.

References

- [1] Blank, Chirilus-Brukner, Lescarret and Schneider, *Breather solutions in periodic media*, Comm. Math. Phys., 2011
- [2] Pelinovsky and Schneider, *Bifurcations of standing localized waves on periodic graphs*, Ann. Henri Poincaré, 2017

Time-periodic solutions of a cubic wave equation

Dominic Scheider^{1,*}

¹Institute for Analysis, Karlsruhe Institute of Technology, Karlsruhe, Germany

*Email: dominic.scheider@kit.edu

Abstract

We construct time-periodic “polychromatic” solutions of a cubic wave equation set on the full three-dimensional space. Our solutions are localized and radially symmetric in the space variable. This is achieved by reduction to an infinite system of stationary Helmholtz-type wave equations, which can be solved using bifurcation theory. The key element is a detailed analysis of the oscillatory behavior of the components in the far field, which will give rise to infinitely many distinct families of time-dependent solutions of the original wave equation bifurcating from any time-independent solution.

Keywords: Nonlinear wave equation, Nonlinear Helmholtz system, Bifurcation.

1 Introduction

There have been recent advances in constructing time-periodic, spatially localized and real-valued solutions $U = U(t, x)$ of wave equations

$$V(x)\partial_t^2 U - \partial_x^2 U + q(x)U = \Gamma(x)U^3 \text{ on } \mathbb{R} \times \mathbb{R}$$

with periodic $V(x) \geq 0$, $q(x) = c \cdot V(x) \geq 0$, $\Gamma(x)$. The first construction of such kind in [1] has been done for a very specific choice of the periodic coefficient functions; it relies on spatial dynamics and center manifold reduction. The approach in [2] incorporates more general potentials and nonlinearities and is based on variational techniques. Both articles use a polychromatic ansatz of the form

$$U(t, x) = \sum_k u_k(x)e^{ik\omega t} \quad (t, x \in \mathbb{R}),$$

which reduces the time-dependent equation to an infinite set of stationary problems with periodic coefficients. Floquet-Bloch theory then provides the required spectral properties of the associated differential operators, in particular the occurrence of spectral gaps. It is required that 0 lies in such spectral gaps, and moreover that the distance between 0 and the spectra has a positive lower bound. This is realized by assuming a certain “roughness” of the potentials.

We present an entirely different approach, which yields time-periodic, spatially localized, real-valued solutions of the cubic wave equation

$$\partial_t^2 U - \Delta U - U = U^3 \text{ on } \mathbb{R} \times \mathbb{R}^3 \quad (1)$$

in three space dimensions, but assuming radial symmetry. Our solutions also have the form

$$U(t, x) = \sum_{k \in \mathbb{Z}} u_k(x)e^{ikt} \quad (t \in \mathbb{R}, x \in \mathbb{R}^3) \quad (2)$$

where the coefficients u_k , $k \in \mathbb{Z}$, are chosen as radially symmetric solutions of an infinite system of nonlinear Helmholtz equations similar to [4]. Concerning mathematical methods, the fundamental difference is that this construction does not require conditions ensuring the existence of spectral gaps of sufficient size; on the contrary, Helmholtz methods allow to work inside the essential spectrum.

2 The main result

Let us consider some radially symmetric solution of the stationary equation

$$-\Delta w_0 - w_0 = w_0^3 \quad \text{on } \mathbb{R}^3. \quad (3)$$

For the existence, see [3]; it is shown there in particular that $w \in C_{\text{loc}}^2(\mathbb{R}^3) \cap X$ where we let

$$X := \{u \in C_{\text{rad}}(\mathbb{R}^3, \mathbb{R}) \mid \|(1 + |\cdot|)u\|_{\infty} < \infty\}.$$

Then, the following Theorem holds:

Theorem 1 *There exist an open interval $I \subseteq \mathbb{R}$ containing 0 and a continuum $(U^{(\alpha)})_{\alpha \in I}$ in $C(\mathbb{R}, X)$ of twice differentiable, classical solutions of the wave equation (1) of the form*

$$U^{(\alpha)}(t, x) = \sum_{k \in \mathbb{Z}} u_k^{(\alpha)}(x)e^{ikt}$$

with $U^{(0)}(t, x) = w_0(x)$ and $U^{(\alpha)}$ nonstationary for $\alpha \neq 0$.

Theorem 1 is proved via bifurcation from a simple eigenvalue. We will put special emphasis on the verification of simplicity, which will be

achieved by fixing suitable parameters governing the asymptotic behavior of the components $u_k^{(\alpha)}(x)$ as $|x| \rightarrow \infty$. It will be demonstrated that such a freedom of choice is a particular feature of the nonlinear Helmholtz equations governing $u_k^{(\alpha)}$. In particular, the bifurcation parameter we introduce only affects the asymptotic behavior and hence does not appear in the wave equation (1).

We add some remarks.

- (a) For every $\nu \in \mathbb{N}$, the proof yields solutions with $\frac{d}{d\alpha} \Big|_{\alpha=0} U^{(\alpha)}(t, x) = \tilde{u}(x) \cos(\nu t)$.
- (b) Generalizations: Pass from (1) to

$$\partial_t^2 U - \Delta U - \xi U = \Gamma(x)U^3 \quad (1')$$

where $\xi \in \mathbb{R} \setminus \{0\}$ and $\Gamma(x)$ is radially symmetric, C^1 and bounded with $\Gamma \neq 0$ almost everywhere.

- (c) Still open: Extension to non-constant periodic potentials $q(x)$. This requires, most of all, extensions of the linear theory.

3 Methods

We give a sketch of the main steps and tools.

- ▷ Step 1: Infinite Helmholtz system.
Insert (2) into (1) (with $u_{-k} = u_k$):

$$-\Delta u_k - (k^2 + 1)u_k = t_k(\mathbf{u}) \quad (4a)$$

where $t_k(\mathbf{u}) = \sum_{l+m+n=k} u_l u_m u_n$.

- ▷ Step 2: Limiting Absorption Principle.
LAPs provide resolvent-type operators for Helmholtz equations. By [4], we pass to

$$u_k = \mathcal{R}_{k^2+1}^{\tau_k}[t_k(\mathbf{u})] \quad (4b)$$

for suitable $\tau_k \in [0, \pi)$ and with a convolution operator $\mathcal{R}_{k^2+1}^{\tau_k} : X \rightarrow X$. Then (4b) implies (4a) with, as $|x| \rightarrow \infty$,

$$u_k(x) \sim \frac{\sin(|x|\sqrt{k^2+1} + \tau_k)}{4\pi|x|} + O(|x|^{-2}). \quad (4c)$$

The bifurcation parameter λ is included by replacing τ_ν with $\tau_\nu - \lambda$.

- ▷ Step 3: Solving the system (4b) by means of the Crandall-Rabinowitz Theorem.

Most importantly, this requires that the linearization of (4b) close to $(u_k)_{k \in \mathbb{Z}} \approx (\dots, 0, w_0, 0, \dots)$ has a simple kernel. Motivated by (4b), every element $(q_k)_{k \in \mathbb{Z}}$ of that kernel satisfies

$$q_k = 3\mathcal{R}_{k^2+1}^{\tau_k}[w_0^2 q_k]. \quad (4d)$$

As in (4a), (4c) this yields a differential equation with an asymptotic condition.

Following [4], there is a unique $\tau_k \in [0, \pi)$ such that (4d) has a radial nonzero solution. We choose this value only for $k = \nu$, cf. Remark (a).

- ▷ Step 4: Regularity estimates complete the proof.

Acknowledgements

The author gratefully acknowledges financial support by the Deutsche Forschungsgemeinschaft (DFG) through CRC 1173 “Wave phenomena: analysis and numerics”.

References

- [1] C. Blank, M. Chirilus-Brukner, V. Lescarret and G. Schneider, Breather Solutions in Periodic Media, *Communications in Mathematical Physics* **3** (2011), pp. 815–841.
- [2] A. Hirsch and W. Reichel, Real-valued, time-periodic localized weak solutions for a semilinear wave equation with periodic potentials, *Nonlinearity* (2019), to appear.
- [3] R. Mandel, E. Montefusco and B. Pellacci, Oscillating solutions for nonlinear Helmholtz equations, *Zeitschrift für angewandte Mathematik und Physik* **6** (2017), article 121.
- [4] R. Mandel and D. Scheider, Bifurcations of nontrivial solutions of a cubic Helmholtz system, *preprint*. URL: http://www.waves.kit.edu/downloads/CRC1173_Preprint_2018-32.pdf

Singularity formation in nonlinear wave equations

Irfan Glogić¹, Birgit Schörkhuber^{2,*}¹Department of Mathematics, University of Vienna, Austria²Department of Mathematics, Karlsruhe Institute of Technology, Germany

*Email: birgit.schoerhuber@kit.edu

Abstract

In this talk, we review recent results on singularity formation for the focusing semilinear wave equation. In particular, we discuss the existence of non-trivial self-similar blowup solutions and their role in the time evolution of generic initial data.

Introduction

We consider the focusing wave equation

$$(\partial_t^2 - \Delta)u = |u|^{p-1}u, \quad p > 1 \quad (1)$$

for $u : (t, x) \in I \times \mathbb{R}^d \rightarrow \mathbb{R}$, $I \subset \mathbb{R}$, $0 \in I$ and $d \geq 3$. In the past years this model has been studied extensively as a natural toy model for more involved problems. Despite the simple form of Eq. (1), its solutions exhibit rather complex dynamics, depending of course on the space dimension and the strength of the nonlinearity. It is well-known that Eq. (1) has solutions that blow up in finite time for all $p > 1$ and $d \geq 1$. In view of the scale invariance $u_\lambda(t, x) = \lambda^{\frac{2}{p-1}}u(\lambda t, \lambda x)$ one can look for self-similar blowup solutions

$$u(t, x) = (T - t)^{-\frac{2}{p-1}}f\left(\frac{x}{T-t}\right), \quad T > 0.$$

A trivial example is given by the ODE blowup profile $f_0 = c_p$, where $c_p > 0$ is a constant depending on p . Apart from this, infinitely many smooth, non-trivial radial profiles $\{f_n\}_{n \in \mathbb{N}}$ are known to exist at least for $d = 3$ and each odd $p \geq 7$, see [2]. The trivial ground state f_0 and the excited profile f_1 seem to play a special role in the generic time evolution. In fact, numerical experiments performed in [1] suggest the following picture: For small initial data, solutions disperse as $t \rightarrow \infty$. For large generic data, solutions blowup in finite time $T < \infty$ in a self-similar manner and approach f_0 locally around the blowup point as $t \rightarrow T^-$. For data fine-tuned to the threshold between blowup and dispersion, f_1 is approached for some intermediate period before one of the two scenarios occurs eventually.

Analysis of self-similar blowup solutions

We are far from understanding this picture from a rigorous point of view. However, in the recent years, the nonlinear asymptotic stability of the ODE blowup has been established in various works covering basically all $p > 1$ and all (odd) space dimensions, see e.g. [3] and the references therein. Little is known about the stability properties of non-trivial self-similar profiles. One difficulty is that so far such solutions were not known in closed form. In [4] we gave the first example of an *explicit* non-trivial self-similar profile f^* for the cubic wave equation in $d \geq 5$ and analyzed its stability properties. In $d = 5$, we proved that the corresponding blowup solution is codimension one stable in a local sense (i.e., in a backward lightcone). In this talk, we review these results and discuss the role of f^* as a threshold for blowup. We address generalizations to higher space dimensions and report on new findings for other nonlinearities.

Keywords: Nonlinear wave equations, finite-time blowup, self-similar, stability

References

- [1] P. Bizoń, T. Chmaj, Z. Tabor, *On blowup for semilinear wave equations with a focusing nonlinearity*, *Nonlinearity* **17** (2004), 2187–2201.
- [2] P. Bizoń, D. Maison, A. Wasserman, *Self-similar solutions of semilinear wave equations with a focusing nonlinearity*, *Nonlinearity* **20** (2007), 2061–2074.
- [3] R. Donninger, B. Schörkhuber, *Stable blowup for wave equations in odd space dimensions*, *Annales de l'Institut Henri Poincaré. Analyse Non Linéaire* **34** (2017), 1181–1213.
- [4] I. Glogić, B. Schörkhuber, *Co-dimension one stable blowup for the supercritical cubic wave equation*, Preprint arXiv:1810.07681.

Time integration and regularity theory of Maxwell equations in heterogeneous media

Konstantin Zerulla^{1,*}¹Karlsruhe Institute of Technology, Karlsruhe, Germany

*Email: konstantin.zerulla@kit.edu

Abstract

We consider linear isotropic Maxwell equations on a cuboid consisting of two different media. To account for sharp material interfaces, the material parameters are allowed to have discontinuities at an interface. We first focus on the smoothness of the associated solutions and give a result stating piecewise regularity of second order up to the boundary.

The second part deals with ADI schemes for the time integration of linear Maxwell equations on cuboids. These are attractive since they have only linear complexity and are still unconditionally stable. Based on our regularity results for the continuous system, we establish a rigorous error bound in the abstract time-discrete setting, requiring only regularity of the initial data.

Keywords: Regularity theory, heterogeneous media, Maxwell equations, time integration

1 Introduction

Maxwell equations belong to the most important PDEs in physics and describe the propagation of electromagnetic waves in matter. We treat the homogeneous, linear, and isotropic case

$$\partial_t \mathbf{E} = \frac{1}{\varepsilon} \operatorname{curl} \mathbf{H} \quad Q \times [0, \infty), \quad (1a)$$

$$\partial_t \mathbf{H} = -\frac{1}{\mu} \operatorname{curl} \mathbf{E} \quad Q \times [0, \infty), \quad (1b)$$

$$\operatorname{div}(\varepsilon \mathbf{E}) = \operatorname{div}(\mu \mathbf{H}) = 0 \quad Q \times [0, \infty), \quad (1c)$$

$$\varepsilon \mathbf{E} \times \nu = 0, \quad \mu \mathbf{H} \cdot \nu = 0 \quad \partial Q \times [0, \infty), \quad (1d)$$

$$\mathbf{E}(0) = \mathbf{E}_0, \quad \mathbf{H}(0) = \mathbf{H}_0 \quad Q, \quad (1e)$$

on a cuboid $Q \subset \mathbb{R}^3$ with perfectly conducting boundary. The fields $\mathbf{E} = \mathbf{E}(x, t)$, $\mathbf{H} = \mathbf{H}(x, t) \in \mathbb{R}^3$ are the electric and magnetic field. The functions $\varepsilon, \mu : Q \rightarrow (0, \infty)$ further describe the electric permittivity, and the magnetic permeability, respectively. Finally, $\nu \in \mathbb{R}^3$ is the outer unit normal vector at the boundary ∂Q .

If the functions ε and μ are sufficiently regular and strictly positive, system (1a)-(1e) has a unique classical solution (\mathbf{E}, \mathbf{H}) belonging to $C([0, \infty), H^2(Q)^6) \cap C^1([0, \infty), L^2(Q)^6)$, for appropriate initial data $(\mathbf{E}_0, \mathbf{H}_0)$, see e.g. [4].

We however want to treat here heterogeneous media to cover a broader range of applications. In our model, the cuboid Q is divided into two smaller cuboids Q_1 and Q_2 and their common interface is denoted by \mathcal{F}_{int} . On both subcuboids the functions ε and μ are supposed to be constant, expressing piecewise homogeneous media. At the interface however, both coefficients are allowed to have discontinuities.

In this setting arise two issues. First, the regularity of solutions to the system (1a)-(1e) is treated. Second, we aim at a rigorous error result for the Peaceman-Rachford ADI scheme integrating the Maxwell system in time. So far, an error analysis seems to be missing in the case of piecewise regular coefficients.

2 Regularity analysis

We write $w = (\mathbf{E}, \mathbf{H})$ and interpret system (1a)-(1e) as an evolution equation

$$\partial_t w = Mw, \quad t \geq 0, \quad (2)$$

$$w(0) = w_0,$$

employing the Maxwell operator

$$M \begin{pmatrix} \mathbf{E} \\ \mathbf{H} \end{pmatrix} = \begin{pmatrix} \frac{1}{\varepsilon} \operatorname{curl} \mathbf{H} \\ -\frac{1}{\mu} \operatorname{curl} \mathbf{E} \end{pmatrix}$$

on its domain

$$\mathcal{D}(M)$$

$$:= \{(\mathbf{E}, \mathbf{H}) \in L^2(Q)^6 \mid \operatorname{curl} \mathbf{E}, \operatorname{curl} \mathbf{H} \in L^2(Q)^3, \\ \operatorname{div}(\varepsilon \mathbf{E}) = \operatorname{div}(\mu \mathbf{H}) = 0, \\ \mathbf{E}, \mathbf{H} \text{ satisfy (1d)}\}.$$

For the wellposedness of system (2) and the regularity of its solutions, we obtain the following result. Note that a function is called piecewise regular here if its restrictions to both cuboids Q_1 and Q_2 are regular.

Theorem 1 *The domain $\mathcal{D}(M^2)$ embeds continuously into $PH^2(Q)^6$, the space of piecewise H^2 -regular functions. Moreover, the Cauchy problem (2) has a unique classical solution w belonging to $C^1([0, \infty), L^2(Q)^6) \cap C([0, \infty), PH^2(Q)^6)$ for all initial data $w_0 \in \mathcal{D}(M^2)$.*

The first step of the proof is concerned with piecewise first order regularity for solutions of (2), arguing in parts similar to [1]. Then, a detailed regularity analysis for transmission problems involving interpolation theory follows. Similar techniques are applied in [3] and [4] for the case of ε and μ regular on Q . Note however that the regularity of solutions to (2) on general Lipschitz domains can be far below H^2 , see [2].

3 ADI schemes

The main idea of alternating direction implicit (ADI) schemes is to split the Maxwell system (1a)-(1e) into two smaller problems that are solved separately. In both subproblems, the space derivatives decouple and one solves essentially one-dimensional elliptic problems implicitly, leading to linear complexity of the scheme, see [5] and [6].

In the current framework, the Maxwell operator M is splitted into two operators

$$M = \begin{pmatrix} 0 & \frac{1}{\varepsilon}C_1 \\ \frac{1}{\mu}C_2 & 0 \end{pmatrix} + \begin{pmatrix} 0 & -\frac{1}{\varepsilon}C_2 \\ -\frac{1}{\mu}C_1 & 0 \end{pmatrix} =: A + B$$

employing

$$C_1 := \begin{pmatrix} 0 & 0 & \partial_2 \\ \partial_3 & 0 & 0 \\ 0 & \partial_1 & 0 \end{pmatrix} \text{ and } C_2 := \begin{pmatrix} 0 & \partial_3 & 0 \\ 0 & 0 & \partial_1 \\ \partial_2 & 0 & 0 \end{pmatrix}.$$

The Peaceman-Rachford ADI scheme for (1a)-(1e) then approximates the exact solution at time $t_n = n\tau$ by

$$w^n = (I - \frac{\tau}{2}B)^{-1}(I + \frac{\tau}{2}A)(I - \frac{\tau}{2}A)^{-1} \cdot (I + \frac{\tau}{2}B)w^{n-1}, \quad (3)$$

where $w^0 = w_0$ and $\tau > 0$ is the chosen time step size, see [6].

While it is known that (3) is second order accurate when the material parameters ε and μ are sufficiently regular, see [4], a rigorous error bound for piecewise regular coefficients seems not to be known. In fact, experiments in [4] indicate that (3) suffers from a loss of convergence order in case of discontinuous ε and μ .

By means of Theorem 1, we can show the following rigorous error result in the time-discrete setting. We stress that it only requires regularity of the initial data. Note moreover that $\|\cdot\|_{\mathcal{D}(M^3)}$ denotes the graph norm of M^3 with respect to $\|\cdot\|_{L^2(Q)}$ and that $\mathcal{D}(M^3)$ contains $PH^3(Q)^6$ with appropriate boundary, transmission and divergence conditions.

Theorem 2 *Let $T > 0$. There are uniform constants $C, \tau_0 > 0$ such that the error estimate*

$$\|w^n - w(n\tau)\|_{L^2(Q)} \leq CT\tau^{3/2}\|w(0)\|_{\mathcal{D}(M^3)}$$

is true for the iterates w^n of (3) for all initial data $w^0 = w(0) \in \mathcal{D}(M^3)$, $\tau \in (0, \tau_0)$ and $n \in \mathbb{N}$ with $n\tau \leq T$. The constants C and τ_0 depend only on ε, μ and Q .

Our error analysis in parts transfers arguments from [4] for the case of regular ε and μ .

4 Extensions

We are currently investigating a generalization to include charges, currents and conductivity.

Acknowledgment

The author gratefully acknowledges financial support by the Deutsche Forschungsgemeinschaft (DFG) through CRC 1173.

References

- [1] A.-S. Bonnet-BenDhia, C. Hazard, and S. Lohrengel: A singular field method for the solution of Maxwell's equations in polyhedral domains. *SIAM J. Appl. Math.* **59** (6) (1999), 2028–2044.
- [2] M. Costabel, M. Dauge, and S. Nicaise: Singularities of Maxwell interface problems. *M2AN Math. Model. Numer. Anal.* **33** (3) (1999), 627–649.
- [3] J. Eilinghoff, and R. Schnaubelt: Error estimates in L^2 of an ADI splitting scheme for the inhomogeneous Maxwell equations. *Preprint 2017/32 of CRC 1173*. See www.waves.kit.edu/downloads/CRC1173_Preprint_2017-32.pdf
- [4] M. Hochbruck, T. Jahnke, and R. Schnaubelt: Convergence of an ADI splitting for Maxwell's equations. *Numer. Math.* **129** (2015), 535–561.
- [5] J. Lee, and B. Fornberg: A split step approach for the 3-D Maxwell's equations. *J. Comput. Appl. Math.* **158** (2003), 485–505.
- [6] F. Zhen, Z. Chen, and J. Zhang: Toward the development of a three-dimensional unconditionally stable finite-difference time-domain method. *IEEE Trans. Microwave Theory Tech.* **48** (9) (2000), 1550–1558.

Numerical analysis of nonlinear wave equations with dynamic boundary conditions

Marlis Hochbruck¹, Jan Leibold^{1,*}

¹Institute for Applied and Numerical Mathematics, Karlsruhe Institute of Technology, Karlsruhe, Germany

*Email: jan.leibold@kit.edu

Abstract

In this paper we present and analyze a full discretization of semilinear acoustic wave equations with dynamic boundary conditions. Dynamic boundary conditions do not neglect the momentum of the wave on the boundary and are typically posed on domains with (piecewise) smooth, curved boundaries. Hence, numerical schemes have to approximate the domain which leads to non-conforming approximations. This makes the error analysis much more involved. We present a framework that can be used to analyze non-conforming space- and time discretizations of such problems. Using this we derive an a-priori error estimate for a discretization with an efficient implicit-explicit scheme in time and finite elements in space. To our knowledge this is the first full discretization error result for nonlinear wave equations with dynamic boundary conditions.

Keywords: dynamic boundary conditions, error analysis, wave-type equation, finite element method, time integration

Introduction

In this paper we consider the following semilinear wave equation with kinetic boundary conditions

$$\begin{aligned} u_{tt} + \alpha_{\Omega} u_t - c_{\Omega} \Delta u &= |u|^2, & \text{in } \Omega, \\ \mu u_{tt} + c_{\Gamma} \partial_n u - c_{\Gamma} \Delta_{\Gamma} u &= |u|^3, & \text{on } \Gamma, \\ u(0, \cdot) = u_0, \quad u_t(0, \cdot) &= v_0, & \text{in } \bar{\Omega} \end{aligned} \quad (1)$$

as a guiding example. Here, Ω is a domain with C^k boundary Γ , $k \geq 2$ and Δ_{Γ} denotes the Laplace-Beltrami operator. The wellposedness of generalizations of this equation is analyzed in [4].

We will use equation (1) to demonstrate the difficulties that occur in the construction and error analysis of numerical methods for such problems and how to deal with them.

Non-conformal space discretization

The weak formulation of (1) is given by

$$m(u'', v) + b(u', v) + a(u, v) = m(f(u), v) \quad (2)$$

for all $v \in V$ in the Hilbert space

$$V = \{v \in H^1(\Omega) \mid \gamma(v) \in H^1(\Gamma)\} \\ \xrightarrow{\text{dense}} H = L^2(\Omega) \times L^2(\Gamma),$$

where γ denotes the trace operator.

The bilinear forms a, b , and m contain integrals over Ω as well as over Γ due to the dynamic boundary condition. We have, e.g.,

$$m(u, v) = \int_{\Omega} u(x)v(x) \, dx + \mu \int_{\Gamma} u(x)v(x) \, ds.$$

To discretize (1) in space, we use the bulk-surface finite element method presented in [1]. For problems with dynamics boundary conditions, such discretizations have been considered in [2] for the linear and in [3] for the semilinear case.

Let V_h be the isoparametric finite element space of degree $p \leq k$ with mesh width h and let $\Omega_h \approx \Omega$ be the discretized domain. Then, the finite element discretization is then given by

$$\begin{aligned} m_h(u_h'', v_h) + b_h(u_h', v_h) + a_h(u_h, v_h) \\ = m_h(f_h(u_h), v_h) \end{aligned}$$

for all $v_h \in V_h$. The discrete bilinear forms are obtained from the continuous ones by adjusting the domains in the integrals, e.g.,

$$\begin{aligned} m_h(u_h, v_h) &= \int_{\Omega_h} u_h(x)v_h(x) \, dx \\ &+ \mu \int_{\Gamma_h} u_h(x)v_h(x) \, ds. \end{aligned}$$

In general, this leads to non-conformal discretizations since due to the smooth boundary we have $V_h \not\subseteq V$ and thus $m \neq m_h$, $a \neq a_h$, and $b \neq b_h$.

Time integration

For the time integration we rewrite the spatially discretized equation as evolution equation in V_h :

$$u_h'' + B_h u' + A_h u = f_h(u_h).$$

We propose the following implicit-explicit (IMEX) time integration scheme:

$$\begin{aligned} v_h^{n+1/2} &= v_h^n - \frac{\tau}{2} A_h v_h^n - \frac{\tau^2}{4} A_h v_h^{n+1/2} \\ &\quad - \frac{\tau}{2} B_h v_h^{n+1/2} + \frac{\tau}{2} f_h(u_h^n) \\ u_h^{n+1} &= u_h^n + \tau v_h^{n+1/2} \\ v_h^{n+1} &= v_h^n - \frac{\tau}{2} A_h v_h^n - \frac{\tau^2}{4} A_h v_h^{n+1/2} \\ &\quad - \frac{\tau}{2} B_h v_h^{n+1/2} + \frac{\tau}{2} f_h(u_h^{n+1}) \end{aligned} \tag{3}$$

This scheme can be rewritten in such a way, that only one application of A_h and B_h , one evaluation of the nonlinearity, and the solution of one linear system of equations is necessary in each timestep.

Full discretization error bound

The full discretization error analysis is quite involved, since the error of the IMEX scheme has to be combined with error bounds of the non-conforming space discretization provided by the unified error analysis [2, 3].

To relate the discrete and the continuous solution we use a lift operator $\mathcal{L}_h: V_h \rightarrow V$ as in [1] and make the following rather general assumptions:

- The bilinear form m is an inner product on H .
- There exists a constant $c_G > 0$ s.t. $a + c_G m$ is an inner product on V .
- The bilinear form $b: V \times H \rightarrow \mathbb{R}$ is bounded and quasi-monotone.
- The function $f: V \rightarrow H$ is locally Lipschitz-continuous.

For the corresponding discrete quantities we require the same properties, with constants independent of h .

In the framework of the unified error analysis we proved the following result:

Theorem 1 *Let u be a sufficient smooth solution of (2) on $[0, T]$ and let u_h^n, v_h^n be the fully discrete approximations given by (3). Then there exists $\tau^* > 0$ s.t. for all $\tau < \tau^*$ and $t_n < T$ the lifted fully discrete solution satisfies*

$$\begin{aligned} \|\mathcal{L}_h u_h^n - u(t_n)\|_V + \|\mathcal{L}_h v_h^n - u'(t_n)\|_H \\ \leq C(\tau^2 + E_h). \end{aligned}$$

The constants C and τ^* are independent of h . E_h contains interpolation errors of the solution as well as geometric errors and discretization errors of the initial values, the bilinear forms and the nonlinearity.

Theorem 1 can be applied to all equations and space discretizations fitting in the general setting, for instance to (1).

Corollary 2 *Let u be a sufficiently smooth solution of (1) and let u_h^n, v_h^n be the fully discrete approximation obtained with isoparametric elements of order $p \leq k$. Then there exists $\tau^* > 0$ s.t. for all $\tau < \tau^*$ and $t_n < T$ the lifted fully discrete solution satisfies the error bound*

$$\begin{aligned} \|\mathcal{L}_h u_h^n - u(t_n)\|_V + \|\mathcal{L}_h v_h^n - u'(t_n)\|_H \\ \leq C(\tau^2 + h^p). \end{aligned}$$

The constants C and τ^* are independent of h .

Acknowledgement

We gratefully acknowledge financial support by the Deutsche Forschungsgemeinschaft (DFG) through CRC 1173.

References

- [1] C. M. Elliott, T. Ranner, Finite element analysis for a coupled bulk-surface partial differential equation, *IMA Journal of Numerical Analysis* **33** (2013), pp. 377–402.
- [2] D. Hipp, M. Hochbruck, C. Stohrer, Unified error analysis for nonconforming space discretizations of wave-type equations, *IMA Journal of Numerical Analysis* (2018), dry036.
- [3] J. Leibold, Semilineare Wellengleichungen mit dynamischen Randbedingungen, *Master's Thesis*, Karlsruhe Institute of Technology (2017).
- [4] E. Vitillaro, Strong solutions for the wave equation with a kinetic boundary condition, *Contemp. Math.* **594** (2013), pp. 295–307.

Time-integration of semilinear wave equations with highly oscillatory solutions

Benjamin Dörich^{1,*}, Marlis Hochbruck¹

¹Institute for Applied and Numerical Mathematics, Karlsruhe Institute of Technology, Germany

*Email: benjamin.doerich@kit.edu

Abstract

In this talk we consider the time-integration of abstract semilinear wave equations. We are interested in problems, where the solution lacks spatial regularity and thus standard numerical integrators require the use of very small time step sizes. By exploiting the connection of trigonometric integrators and splitting methods we construct and analyze numerical schemes which circumvent these issues.

Keywords: highly oscillatory, wave equation, splitting methods, non-standard error analysis, summation by parts, filter functions.

Trigonometric integrators

We consider the abstract semilinear wave equation

$$\begin{aligned} q''(t) &= -\Lambda^2 q(t) + G(q(t)), \\ q(0) &= q_0, \quad q'(0) = q'_0 \end{aligned} \tag{1}$$

with a positive, self-adjoint operator Λ . We assume $G : L^2(\Omega) \rightarrow L^2(\Omega)$ to be bounded and that the solution q satisfies the finite energy condition

$$\|\Lambda q(t)\|_{L^2}^2 + \|q'(t)\|_{L^2}^2 \leq K, \quad t \in [0, T],$$

but no bounds on q'' . This means that we cannot use higher order Taylor expansions of the solution. In such situations, numerical experiments show resonances in the error at certain time step sizes which are related to the largest eigenvalues of Λ (dotted line, Figure 1). For these step sizes, the order deteriorates.

In the ODE case, where Λ^2 is a matrix, integration by trigonometric integrators yields convergence of second order with a constant independent of the norm of Λ [2–4]. In first-order formulation trigonometric integrators for (1) are given by

$$\begin{aligned} \begin{pmatrix} q_{n+1} \\ q'_{n+1} \end{pmatrix} &= \begin{pmatrix} \cos(\tau\Lambda) & \Lambda^{-1} \sin(\tau\Lambda) \\ -\Lambda \sin(\tau\Lambda) & \cos(\tau\Lambda) \end{pmatrix} \begin{pmatrix} q_n \\ q'_n \end{pmatrix} \\ &+ \frac{\tau}{2} \begin{pmatrix} \tau\psi(\tau\Lambda)G_n \\ \psi_0(\tau\Lambda)G_n + \psi_1(\tau\Lambda)G_{n+1} \end{pmatrix} \end{aligned} \tag{2}$$

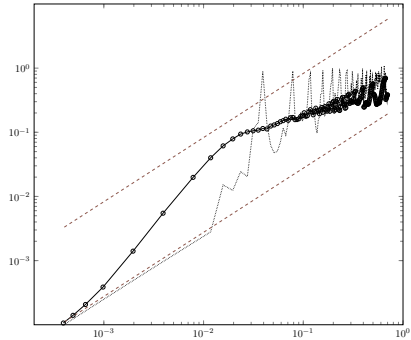


Figure 1: dotted line: Lie splitting without filter, solid line: Lie splitting with filter

with suitable filter functions $\psi, \psi_0, \psi_1, \phi$, and $G_n = G(\phi(\tau\Lambda)q_n)$.

The key ingredient is the appropriate choice of filters depending on τ and Λ . For a symmetric scheme, such functions χ should be even and satisfy

$$\chi(0) = 1, \quad \chi(k\pi) = 0, \quad k = 1, 2, 3, \dots$$

Roughly speaking these filters smooth the interaction of the nonlinearity and the stiff part Λ in such a way that resonances in the error cancel out (solid line, Figure 1).

Averaged equations and splitting methods

It is well known that trigonometric integrators can also be written as splitting methods applied to an averaged equation, where the nonlinearity G is replaced by

$$\tilde{G}(q) = \widehat{\Psi}G(\widehat{\Phi}q).$$

Indeed, if we define

$$A = \begin{pmatrix} 0 & I \\ -\Lambda^2 & 0 \end{pmatrix}, \quad u = \begin{pmatrix} q \\ q' \end{pmatrix}, \quad \tilde{b}(u) = \begin{pmatrix} 0 \\ \tilde{G}(q) \end{pmatrix}$$

and the flow

$$\varphi_b^\tau(u) = u + \tau\tilde{b}(u),$$

we can rewrite (2) as the Strang splitting

$$u_{n+1} = \varphi_b^{\tau/2} \left(e^{\tau A} \varphi_b^{\tau/2}(u_n) \right).$$

Recently, in [1], this observation was used to prove error bounds in a different way. The idea is to first bound the error induced by replacing G by \tilde{G} in (1). The second step consists of the error analysis of a Strang splitting applied to the averaged equation by techniques developed for splitting methods.

Generalizations

We investigate the construction of splitting methods or variants of exponential integrators under different assumptions on the regularity of the solution or on the nonlinearity G than in [1–4].

The Lie splitting

$$u_{n+1} = e^{\tau A} \varphi_b^{\tau}(u_n)$$

based on a modified function \tilde{b} is analyzed in two different scenarios.

(a) We still assume the finite energy condition, but allow the perturbation G to map from L^2 to H^{-1} .

Proposition 1 *Let u be the solution of the first order formulation of (1) in $L^2 \times H^{-1}$. If $\hat{\Phi} = I$ and $\hat{\Psi}$ is suitably chosen, then*

$$\|u(t_n) - u_n\|_{L^2 \times H^{-1}} \leq C\tau,$$

where C is independent of τ .

(b) Assume G to be linear and bounded from L^2 to L^2 . Then we can weaken the finite energy assumption and obtain the following result.

Proposition 2 *Let u be the solution of the first order formulation of (1) in $L^2 \times H^{-1}$. If $\hat{\Psi} = I$ and $\hat{\Phi}$ is suitably chosen, then*

$$\|u(t_n) - u_n\|_{L^2 \times H^{-1}} \leq C\tau,$$

where C depends on $\|u(t)\|_{L^2 \times H^{-1}}$, but is independent of τ and $\|u(t)\|_{H^1 \times L^2}$.

Note that not only the position of the filters, but also the error analysis needs to be carefully adapted to the problem at hand.

Acknowledgement

We gratefully acknowledge financial support by the Deutsche Forschungsgemeinschaft (DFG) through CRC 1173.

References

- [1] S. Buchholz, L. Gauckler, V. Grimm, M. Hochbruck, and T. Jahnke. Closing the gap between trigonometric integrators and splitting methods for highly oscillatory differential equations. *IMA J. Numer. Anal.*, 38(1):57–74, 2018.
- [2] B. García-Archilla, J. M. Sanz-Serna, and R. D. Skeel. Long-time-step methods for oscillatory differential equations. *SIAM J. Sci. Comput.*, 20(3):930–963, 1999.
- [3] V. Grimm and M. Hochbruck. Error analysis of exponential integrators for oscillatory second-order differential equations. *J. Phys. A*, 39(19):5495–5507, 2006.
- [4] M. Hochbruck and C. Lubich. A Gautschi-type method for oscillatory second-order differential equations. *Numer. Math.*, 83(3):403–426, 1999.

Space-time discontinuous Galerkin method for the wave equation in polygonal domains

Pratyuksh Bansal^{1,*}, Andrea Moiola², Ilaria Perugia³, Christoph Schwab¹

¹Seminar for Applied Mathematics, ETH Zurich, Switzerland

²University of Pavia, Italy

³University of Vienna, Austria

*Email: pratyuksh.bansal@sam.math.ethz.ch

Abstract

Corners in a polygon may lead to singularities in the solution of the wave equation. These singularities can be resolved using meshes with appropriate local refinement near the corners. We propose a novel non-Trefftz space-time discontinuous Galerkin method, which yields *optimal* asymptotic rates of convergence with these locally refined meshes in polygons. It is *unconditionally stable*, thus, no restriction needs to be imposed on the size of the space-time cells. We prove a priori error estimates for the proposed method.

Use of hierarchies of locally, corner-refined meshes in the spatial, polygonal domain (e.g. by bisection-tree refinement) and corresponding adapted multi-level time-stepping allows to apply the combination formula to approximate the wave propagation in polygons in time-domain at work vs. accuracy scaling as one elliptic solve on the finest spatial grid.

Numerical results confirm the theory.

Keywords: polygon, corner singularities, space-time DG, local refinement, sparse-grids.

1 Introduction

Let $Q = \Omega \times I$ be a space-time domain, where $\Omega \subset \mathbb{R}^2$ is an open, bounded, Lipschitz polygon with outward unit normal \mathbf{n}_Ω^x and $I = (0, T)$ is a time interval, for $T \in \mathbb{R}^+$. Let $\Gamma = \Gamma_D \cup \Gamma_N$ be the boundary of Ω , where Γ_D and Γ_N are mutually disjoint and correspond to Dirichlet and Neumann boundary conditions, respectively. We consider the following initial boundary value problem (IBVP) for the linear, first-order acoustic wave equation:

$$\begin{aligned} \nabla v + \frac{\partial \boldsymbol{\sigma}}{\partial t} &= \mathbf{0} && \text{in } Q, \\ \nabla \cdot \boldsymbol{\sigma} + c^{-2} \frac{\partial v}{\partial t} &= f && \text{in } Q, \\ v(\cdot, 0) = v_0, \boldsymbol{\sigma}(\cdot, 0) &= \boldsymbol{\sigma}_0 && \text{on } \Omega, \\ v &= g_D && \text{on } \Gamma_D \times \bar{I}, \\ \boldsymbol{\sigma} \cdot \mathbf{n}_\Omega^x &= g_N && \text{on } \Gamma_N \times \bar{I}. \end{aligned} \tag{1}$$

Here c is the wave speed and $f, v_0, \boldsymbol{\sigma}_0, g_D, g_N$ are the given data.

Results on the regularity of solutions of the second-order acoustic wave equation in spatial, polygonal domains have been established in the recent years, see [1] and references therein. These results imply that the solution of IBVP (1),

$$(v, \boldsymbol{\sigma}) \in C^{s-1}(\bar{I}; H_\delta^{k+1,2}(\Omega)) \times C^s(\bar{I}; H_\delta^{k,2}(\Omega)^2),$$

for $s, k \in \mathbb{N}$, under suitable regularity assumptions for the data in our setting. It is well-known that for functions in weighted Sobolev spaces $H_\delta^{k,2}(\Omega)$ one can recover optimal convergence rates for finite element methods with local mesh refinement in the vicinity of corners, refer [1].

2 Numerical scheme

Let $\mathcal{T}_{h_x}^{(x)}$ be a shape-regular mesh on Ω with N_x elements and $\mathcal{T}_{h_t}^{(t)}$ be a partitioning of I into N_t sub-intervals $I_n := (t_{n-1}, t_n)$, $n = 1, 2, \dots, N_t$. Define the space-time mesh \mathcal{T}_h on the domain Q as a Cartesian tensor product of the spatial mesh $\mathcal{T}_{h_x}^{(x)}$ and the time partitioning $\mathcal{T}_{h_t}^{(t)}$,

$$\mathcal{T}_h := \{K_x \times I_n : K_x \in \mathcal{T}_{h_x}^{(x)}, I_n \in \mathcal{T}_{h_t}^{(t)}\}. \tag{2}$$

Define a finite element space of discontinuous piecewise polynomials on the mesh \mathcal{T}_h as

$$\mathbf{V}_p(\mathcal{T}_h) := \prod_{K \in \mathcal{T}_h} \mathbb{P}_K^v(K) \times (\mathbb{P}_K^z(K))^2, \tag{3}$$

where $\mathbb{P}_K^{(\cdot)}(K) := \mathbb{P}_{x,K}^{(\cdot)}(K_x) \otimes \mathbb{P}_{t,K}^{(\cdot)}(I_n)$ is the polynomial space on a space-time element $K \in \mathcal{T}_h$ and $P_{x,K}^{(\cdot)}, P_{t,K}^{(\cdot)} \in \mathbb{N}_0$ are polynomial degrees.

We propose a non-Trefftz space-time discontinuous Galerkin (xt-DG) method based on the formulation developed in [2]. We keep the same definitions for numerical fluxes, but choose the approximation space $\mathbf{V}_p(\mathcal{T}_h)$ (3). This implies that the volume integrals in the variational formulation from [2] do not vanish. The fully discrete formulation reads: find $(v_h, \boldsymbol{\sigma}_h) \in \mathbf{V}_p(\mathcal{T}_h)$

such that $\mathcal{A}_{\text{DG}}(v_h, \sigma_h; w, \tau) = \ell(w, \tau), \forall (w, \tau) \in \mathbf{V}_p(\mathcal{T}_h)$.

For ease of notation, assume $p_x = p_{x,K}^v = p_{x,K}^\sigma + 1$ and $p_t = p_{t,K}^v = p_{t,K}^\sigma, \forall K \in \mathcal{T}_h$. Let h_x and h_t denote maximum meshwidth measures in space and time, respectively. Then the xt-DG solution (v_h, σ_h) satisfies the *a priori* error bounds in Thm. 1.

Theorem 1 *Let (v, σ) be the solution of IBVP (1) and (v_h, σ_h) be the xt-DG solution. Under certain regularity assumptions, the following estimate holds:*

$$\begin{aligned} & \|c^{-1}(v - v_h)\|_{L^2(\Omega \times \{T\})} + \|\sigma - \sigma_h\|_{L^2(\Omega \times \{T\})}^2 \\ & \leq C_1 h_x^q + C_2 h_t^{p_t+1}, \end{aligned} \tag{4}$$

where $q = p_x$ for locally, corner-refined spatial meshes and $q = 1 - \delta, \delta > 0$, for quasi-uniform spatial meshes. Here C_1 and C_2 are constants independent of mesh size.

3 Sparse Grids

We devise a sparse approximation of the finite element space $\mathbf{V}_p(\mathcal{T}_h)$ based on the *combination formula* from *sparse grids* [3]. Consider a nested hierarchy of locally, corner-refined meshes on Ω and a dyadic hierarchy of uniform partitions of I . Build a sequence \mathfrak{T} of space-time meshes, such that for a *fine* spatial mesh, a *coarse* time partitioning is used, and vice-versa. Next, compute the xt-DG solution for each mesh in \mathfrak{T} . In the end, we take an appropriate linear combination of these mutually independent solutions to obtain the *sparse-xt-DG* solution.

4 Results

Choose $\Omega = (-1, 1)^2 \setminus \{(0, 1) \times (-1, 0)\}$ and $T = 1.125$. For $r = \|\mathbf{x}\|_2$ and $\theta = \arctan(x_2/x_1)$, we consider the solution $v = \partial_t u, \sigma = -\nabla_x u, u = r^{\frac{2}{3}} \sin(\frac{2}{3}\theta) \sin(\pi t)$. We generate graded spatial meshes using local bisection tree refinement on uniform meshes, refer [1], and choose a uniform partitioning in time.

From the convergence behaviour in Figure 1, we verify that the xt-DG method converges with *sub-optimal* rates for uniform meshes and *optimal* rates for graded meshes.

A comparative study of accuracy vs. work scaling for the full-xt-DG solution, i.e. without any sparse approximation, against that of the sparse-xt-DG solution is shown in Figure 2. Here $O(M_L^{-1})$ corresponds to the scaling for a

single elliptic solve on the finest spatial mesh and we observe that sparse-xt-DG solution approaches it asymptotically.

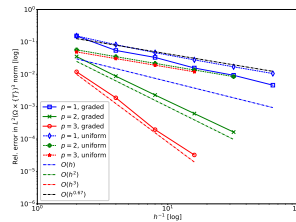


Figure 1: Relative error vs. $h^{-1}, h = h_x = h_t$ is the meshwidth, for $p = p_x = p_t$. For uniform meshes - $O(h^{0.67})$ convergence; for graded meshes - $O(h^p)$ convergence.

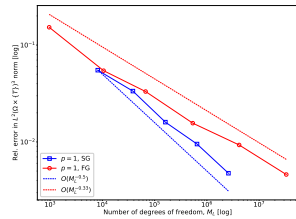


Figure 2: FG: full-xt-DG solution, SG: sparse-xt-DG solution, $p = p_x = p_t = 1$. Relative error vs. the number of degrees of freedom M_L .

5 Acknowledgements

The research presented above is partially supported by ModCompShock project 642768.

References

- [1] F. Müller and C. Schwab, Finite elements with mesh refinement for wave equations in polygons, *Journal of Computational and Applied Mathematics*, 283 (2015), 163–181.
- [2] A. Moiola and I. Perugia, A space-time Trefftz discontinuous Galerkin method for the acoustic wave equation in first-order formulation, *Numerische Mathematik*, 138 (2018), pp. 389–435.
- [3] H.-J. Bungartz and M. Griebel, Sparse grids, *Acta Numerica*, 13 (2004), pp. 147–269.

A space-time DPG method for acoustic waves in heterogeneous media

Christian Wieners^{1,*}, Johannes Ernesti²

¹KIT, Institute of Applied and Numerical Mathematics, Karlsruhe, Germany

²KIT, Institute of Applied and Numerical Mathematics, Karlsruhe, Germany

*Email: christian.wieners@kit.edu

Abstract

We apply the discontinuous Petrov-Galerkin method (DPG) to linear acoustic waves in space and time using the framework of first-order Friedrichs systems. We show that the ideal DPG method is well-posed on a suitable subset of the space-time cylinder. We use the graph norm of the space-time differential operator, and traces are implicitly defined as distributions. Then, the practical DPG method is analyzed by constructing a Fortin operator numerically, and non-conforming traces are considered by comparison with an equivalent conforming scheme. For our numerical experiments we introduce a simplified DPG method with discontinuous ansatz functions on the faces of the space-time skeleton. Examples include results for a benchmark configuration in seismic imaging with a point source and a small region with measurement points. We show that the computation on a truncated space-time cylinder allows for a substantial reduction of DoFs.

Keywords: space-time finite elements, DPG

The linear wave equation

On a Lipschitz domain Ω_0 , we consider the evolution equation

$$Lu := M\partial_t u + Au = f \text{ in } (0, T) \times \Omega_0 \subset \mathbb{R} \times \mathbb{R}^d$$

subject to initial conditions $u(0) = u_0$ in Ω_0 , where $f \in L_2((0, T) \times \Omega_0; \mathbb{R}^m)$ is a source function, and with

- a) a symmetric positive definite operator M represented by $M \in L_\infty(\Omega_0; \mathbb{R}_{\text{sym}}^{m \times m})$;
- b) a hyperbolic operator A with domain $\mathcal{D}(A) \subset L_2(\Omega_0; \mathbb{R}^m)$ such that

$$(Av, z)_{0, \Omega_0} = -(v, Az)_{0, \Omega_0}, \quad v, z \in \mathcal{D}(A)$$

and such that $M + A$ is surjective, i.e.,

$$(M + A)(\mathcal{D}(A)) = L_2(\Omega_0; \mathbb{R}^m).$$

In this setting, the operator $M^{-1}A$ generates a semigroup in $L_2(\Omega_0; \mathbb{R}^m)$, and for sufficiently regular f the solution is given by

$$u(t) = \int_0^t \exp((t-s)M^{-1}A)M^{-1}f(s) \, ds.$$

Our basic example is the acoustic wave equation for velocity and pressure with $(v, p) \in \mathcal{D}(A) = H(\text{div}, \Omega_0) \times H_0^1(\Omega_0)$, $M(v, p) = (\rho v, \kappa^{-1}p)$, and $A(v, p) = -(\nabla p, \nabla \cdot v)$ where $\rho, \kappa \in L_\infty(\Omega_0)$ model the spatially varying mass density and the bulk modulus of the material.

A main property of the linear wave equation is the finite speed of propagation $c_{\max} > 0$, which allows – in case of local support of the source function f – to restrict the computation to the cone

$$\begin{aligned} \mathcal{C}_+(\text{supp } f) &= \{(t, x) \in (0, T) \times \Omega_0 : \\ &|x - x_0| \leq c_{\max}(t - t_0), t_0, x_0 \in \text{supp } f\}, \end{aligned}$$

i.e., for the solution of $Lu = f$ holds $\text{supp } u \in \mathcal{C}_+(\text{supp } f)$. E.g., in the acoustic case we have $c(x) = \sqrt{\kappa(x)/\rho(x)}$.

Correspondingly, if the solution is evaluated only in a domain of interest $\omega \subset [0, T] \times \Omega_0$, the solution in ω only depends on the backward cone $\mathcal{C}_-(\bar{\omega})$.

The space-time discretization

Let $\Omega \supset \mathcal{C}_+(\text{supp } f) \cup \mathcal{C}_-(\bar{\omega})$, and let $\Omega_h = \bigcup K \subset \Omega$ be a decomposition into open convex subsets K with skeleton $\partial\Omega_h$. Integration by parts defines the operator D_{Ω_h} by

$$\langle D_{\Omega_h} v, z \rangle = (Lv, z)_{0, \Omega_h} - (v, L^*z)_{0, \Omega_h}$$

with $L^* = -L$, and formally we obtain for the solution u and its distributional trace $\hat{u} = D_{\Omega_h} u$

$$(u, L^*z)_{0, \Omega_h} + \langle \hat{u}, z \rangle = (f, z)_{0, \Omega_h}$$

for all test functions $z \in H(L^*, \Omega_h)$.

The DPG method is defined by selecting and ansatz space Y_h and test space Z_h such that the

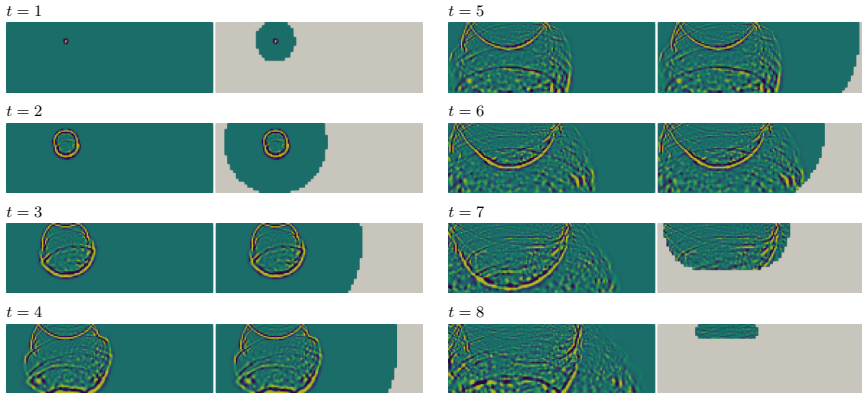


Figure 1: Acoustic parallel space-time DPG simulation for the Marmousi benchmark configuration in Fig. 2: pressure distribution computed with a time stepping method with DG discretization in Ω_0 and with a space-time DPG method on a truncated domain $\Omega \subset (0, T) \times \Omega_0$.

discrete solution $(u_h, \hat{u}_h) \in Y$ is uniquely defined by

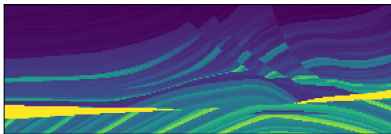
$$(u_h, L^* z_h)_{0, \Omega_h} + \langle \hat{u}_h, z_h \rangle = (f, z_h)_{0, \Omega_h}, \quad z_h \in Z_h.$$

Suitable spaces are constructed and the convergence is analyzed in [1–3].

Numerical results

Many applications rely on accurate numerical simulations of waves through complex material structures. A typical example is the problem of full waveform inversion (FWI), where the material distribution is reconstructed from measurements of the wave field close to the surface. Here, in a field survey a wave is excited at some point $S_0 \in \Omega_0$, and the scattered wave field is measured by receiver devices located in ω .

Figure 2: Density distribution for the Marmousi



To demonstrate the flexibility and the accuracy of the space-time DPG method for heterogeneous media, we consider a numerical example corresponding to the forward problem within FWI. We use the acoustic wave equation for the

Marmousi benchmark, a synthetic model problem for geophysical structures, cf. Fig. 2. The results are illustrated in Fig. 1.

References

- [1] J. Ernesti. *Space-Time Methods for Acoustic Waves and Applications to Full Waveform Inversion*. PhD thesis, Dept. of Mathematics, Karlsruhe Institute of Technology, 2017.
- [2] J. Ernesti and C. Wieners. A space-time DPG method for acoustic waves. In U. Langer and O. Steinbach, editors, *Space-Time Methods. Applications to Partial Differential Equations*, volume 21 of *Radon Series on Computational and Applied Mathematics*. Walter de Gruyter, 99–127, 2019.
- [3] J. Ernesti and C. Wieners. Space-time discontinuous Petrov-Galerkin methods for linear wave equations in heterogeneous media. to appear in *Comput. Meth. Appl. Math.*
- [4] C. Wieners and B. Wohlmuth. Robust operator estimates and the application to substructuring methods for first-order systems. *ESAIM Math. Model. Numer. Anal.*, 48(5): 1473–1494, 2014.

Uniform-in-time optimal convergent HDG method for transient elastic waves with strong symmetric stress formulation

Shukai Du^{1,*}, Francisco-Javier Sayas¹

¹Department of Mathematical Sciences, University of Delaware

*Email: shukaidu@udel.edu

Abstract

We present a semi-discrete Hybridizable Discontinuous Galerkin (HDG) method for transient elastic waves and prove it is optimal convergent uniformly-in-time. The method uses polynomial spaces of degree k and $k+1$ for the approximations of stress and displacement respectively, and the symmetry of the stress tensor is enforced strongly. The core in the design and the analysis of the method is a newly devised tailored projection for the Lehrenfeld-Schöberl type HDG (HDG+ for simplicity) methods. The projection enables us to recycle existing projection-based error analysis of HDG methods and render the analysis of our method simple and concise. We show some numerical experiments at the end to support our analysis.

Keywords: elastic waves; discontinuous Galerkin method; hybridization

1 Introduction

The first HDG for elasticity [6] uses piecewise $\mathcal{P}_k^{\text{sym}}(K)$, $\mathcal{P}_k^3(K)$ and $\mathcal{P}_k^3(F)$ as approximation spaces for the stress $\boldsymbol{\sigma}_h$, the displacement \mathbf{u}_h and the numerical trace $\widehat{\mathbf{u}}_h$. It was proved in [2] that the method is suboptimal. One simple and efficient way to recover optimal convergence is to use a variant of HDG which we call HDG+ in this paper. HDG+ method uses a special type of numerical flux first proposed by Lehrenfeld and Schöberl for elliptic diffusion [4], then applied to steady-state elasticity in [5] and time-harmonic elasticity in [3]. In this paper, we consider the design and the analysis of HDG+ for transient elastic waves. To be more specific, the elastic waves equations we consider are

$$\mathcal{A}\boldsymbol{\sigma}(t) - \boldsymbol{\varepsilon}(\mathbf{u}(t)) = 0 \quad \text{in } \Omega \times [0, \infty), \quad (1a)$$

$$\rho\ddot{\mathbf{u}}(t) - \text{div } \boldsymbol{\sigma}(t) = \mathbf{f}(t) \quad \text{in } \Omega \times [0, \infty), \quad (1b)$$

$$\boldsymbol{\gamma}\mathbf{u}(t) = \mathbf{g}(t) \quad \text{on } \partial\Omega \times [0, \infty), \quad (1c)$$

$$\mathbf{u}(0) = \mathbf{u}_0 \quad \text{in } \Omega, \quad (1d)$$

$$\dot{\mathbf{u}}(0) = \mathbf{v}_0 \quad \text{in } \Omega, \quad (1e)$$

where \mathcal{A} is the compliance tensor and ρ is the mass density. For the input of the PDE system, we have $(\mathbf{f}, \mathbf{g}) : [0, \infty) \rightarrow L^2(\Omega; \mathbb{R}^3) \times H^{1/2}(\partial\Omega; \mathbb{R}^3)$ as the forcing term and the Dirichlet data, and $(\mathbf{u}_0, \mathbf{v}_0) \in [L^2(\Omega)]^2$ as the initial displacement and velocity.

2 A semi-discrete HDG+ method

We next propose a semidiscrete HDG+ method for (1): Find (for all $t \in [0, \infty)$)

$$\begin{aligned} \boldsymbol{\sigma}_h(t)|_K &\in \mathcal{P}_k^{\text{sym}}, & \mathbf{u}_h(t)|_K &\in \mathcal{P}_{k+1}^3, \\ \widehat{\mathbf{u}}_h(t)|_F &\in \mathcal{P}_k^3, \end{aligned}$$

satisfying (we will hide the dependence on t)

$$\begin{aligned} (\mathcal{A}\boldsymbol{\sigma}_h, \boldsymbol{\theta})_{\mathcal{T}_h} + (\mathbf{u}_h, \text{div } \boldsymbol{\theta})_{\mathcal{T}_h} - \langle \widehat{\mathbf{u}}_h, \boldsymbol{\theta}\mathbf{n} \rangle_{\partial\mathcal{T}_h} \\ = 0, \end{aligned} \quad (2a)$$

$$\begin{aligned} (\rho\ddot{\mathbf{u}}_h, \mathbf{w})_{\mathcal{T}_h} + (\boldsymbol{\sigma}_h, \boldsymbol{\varepsilon}(\mathbf{w}))_{\mathcal{T}_h} - \langle \widehat{\boldsymbol{\sigma}}_h\mathbf{n}, \mathbf{w} \rangle_{\partial\mathcal{T}_h} \\ = (\mathbf{f}, \mathbf{w})_{\mathcal{T}_h}, \end{aligned} \quad (2b)$$

$$\langle \widehat{\boldsymbol{\sigma}}_h\mathbf{n}, \boldsymbol{\mu} \rangle_{\partial\mathcal{T}_h \setminus \Gamma} = 0, \quad (2c)$$

$$\langle \widehat{\mathbf{u}}_h, \boldsymbol{\mu} \rangle_{\Gamma} = \langle \mathbf{g}, \boldsymbol{\mu} \rangle_{\Gamma}, \quad (2d)$$

where the numerical flux is defined as

$$\widehat{\boldsymbol{\sigma}}_h\mathbf{n} := \boldsymbol{\sigma}_h\mathbf{n} - \boldsymbol{\tau}\mathbf{P}_M(\mathbf{u}_h - \widehat{\mathbf{u}}_h). \quad (3)$$

In the above, the stabilization function $\boldsymbol{\tau}|_K = \mathcal{O}(h_K^{-1})$ and \mathbf{P}_M is the L_2 projection onto $\mathcal{R}_k(\partial K)$, which we denote as the piecewise $\mathcal{P}_k^3(F)$ space on the boundary ∂K .

For the initial conditions, we use ideas from [1], where a HDG method for acoustic waves is proposed and analyzed, and the HDG projection is used to define the initial conditions for the HDG scheme. Following similar ideas, we next complete the scheme (2) by using a HDG+ projection (which will be defined and explained in section 3) to define the initial conditions:

$$(\times, \widehat{\mathbf{u}}_h(0))|_K := \Pi^{\text{HDG+}}|_K(\mathcal{A}^{-1}\boldsymbol{\varepsilon}(\mathbf{v}_0), \mathbf{v}_0; \boldsymbol{\tau}),$$

and $\mathbf{u}_h(0)$ is simply defined as the solution of the HDG+ discretization of the steady-state linear elasticity system with input $-\text{div}(\mathcal{A}^{-1}\boldsymbol{\varepsilon}(\mathbf{u}_0))$ and $\mathbf{g}(0)$ as the forcing term and Dirichlet boundary condition.

3 HDG+ projection

We present the HDG+ projection in this section. A novelty of the projection is the fact that it has an associated boundary remainder term, which does not affect the error bounds or the simplicity of the proofs. The boundary remainder allows us to more flexibly design the HDG projection, since the standard HDG projection now only corresponds to the very limited case where the boundary remainder vanishes, and an important observation is that the optimal convergence of a HDG scheme only requires a small enough boundary remainder instead of a vanishing one. We will see this in section 4, where we use the projection defined here for the error analysis of the scheme we proposed in section 2.

The HDG+ projection is (for $k \geq 1$):

$$\begin{aligned} \Pi^{\text{HDG}+} : H_{\text{sym}}^1 \times [H^1]^3 &\rightarrow \mathcal{P}_k^{\text{sym}}(K) \times \mathcal{P}_{k+1}^3(K), \\ (\boldsymbol{\sigma}, \mathbf{u}) &\mapsto (\boldsymbol{\sigma}_K, \mathbf{u}_K), \\ \text{R} : H_{\text{sym}}^1 \times [H^1]^3 &\rightarrow \mathcal{R}_k(\partial K), \\ (\boldsymbol{\sigma}, \mathbf{u}) &\mapsto \boldsymbol{\delta}_K, \end{aligned}$$

satisfying

$$\begin{aligned} (\mathbf{u}_K - \mathbf{u}, \mathbf{v})_K &= 0, \\ -(\text{div}(\boldsymbol{\sigma}_K - \boldsymbol{\sigma}), \mathbf{w})_K \\ + \langle \boldsymbol{\tau} \mathbf{P}_M(\mathbf{u}_K - \mathbf{u}), \boldsymbol{\mu} \rangle_{\partial K} &= \langle \boldsymbol{\delta}_K, \mathbf{w} \rangle_{\partial K}, \\ -\langle (\boldsymbol{\sigma}_K - \boldsymbol{\sigma}) \mathbf{n} - \boldsymbol{\tau}(\mathbf{u}_K - \mathbf{u}), \boldsymbol{\mu} \rangle_{\partial K} &= \langle \boldsymbol{\delta}_K, \boldsymbol{\mu} \rangle_{\partial K}, \end{aligned}$$

for all $\mathbf{v} \in \mathcal{P}_{k-1}^3(K)$, $\mathbf{w} \in \mathcal{P}_{k+1}^3(K)$ and $\boldsymbol{\mu} \in \mathcal{R}_k(\partial K)$. The convergence properties are

$$\begin{aligned} \|\boldsymbol{\sigma}_K - \boldsymbol{\sigma}\|_K + h_K^{-1} \|\mathbf{u}_K - \mathbf{u}\|_K + h_K^{1/2} \|\boldsymbol{\delta}_K\|_{\partial K} \\ \leq C h_K^m (|\boldsymbol{\sigma}|_{m,K} + |\mathbf{u}|_{m+1,K}), \end{aligned}$$

with $m = 1, 2, \dots, k+1$.

4 Projection-based error analysis

We define $\boldsymbol{\varepsilon}_h^* = \Pi * - *_h$ and $\mathbf{e}_* = \Pi * - *$, where $*$ = $\boldsymbol{\sigma}$ or \mathbf{u} . We aim to control the terms $\boldsymbol{\varepsilon}_h^*$ by the local projection error \mathbf{e}_* and boundary remainder $\boldsymbol{\delta}$ (which we have a control by the convergence properties of the HDG+ projection). For a fixed constant $C > 0$, the following estimate holds:

$$\begin{aligned} \|\boldsymbol{\varepsilon}_h^*(T)\|_{\mathcal{A}} + \|\mathbf{P}_M(\boldsymbol{\varepsilon}_h^*(T) - \boldsymbol{\varepsilon}_h^*(T))\|_{\boldsymbol{\tau}} + \|\boldsymbol{\varepsilon}_h^*(T)\|_{\rho} \\ \leq C \left(\|\mathbf{e}_{\boldsymbol{\sigma}}(0)\|_{\mathcal{A}} + \|\dot{\mathbf{e}}_{\boldsymbol{\sigma}}\|_{\mathcal{A},1}^{[0,T]} \right. \\ \left. + \|\dot{\mathbf{e}}_{\mathbf{u}}\|_{\rho,1}^{[0,T]} + \|\boldsymbol{\delta}\|_{\boldsymbol{\tau}^{-1},\infty}^{[0,T]} + \|\dot{\boldsymbol{\delta}}\|_{\boldsymbol{\tau}^{-1},1}^{[0,T]} \right), \end{aligned}$$

If $k \geq 1$, the meshes are shape-regular, and the elliptic regularity holds, then

$$\begin{aligned} \|\boldsymbol{\varepsilon}_h^*(T)\|_{\Omega} \leq \\ C(1+T)^2 \left(h \|\mathbf{e}_{\boldsymbol{\sigma}}(0)\|_{\Omega} + h \|\boldsymbol{\delta}(0)\|_{\boldsymbol{\tau}^{-1}} + \|\mathbf{e}_{\mathbf{u}}(0)\|_{\Omega} \right. \\ \left. + h \|\dot{\mathbf{e}}_{\boldsymbol{\sigma}}\|_{\Omega,\infty}^{[0,T]} + h \|\dot{\boldsymbol{\delta}}\|_{\boldsymbol{\tau}^{-1},\infty}^{[0,T]} + \|\ddot{\mathbf{e}}_{\mathbf{u}}\|_{\Omega,\infty}^{[0,T]} \right. \\ \left. + h \|\ddot{\mathbf{e}}_{\boldsymbol{\sigma}}\|_{\Omega,\infty}^{[0,T]} + h \|\ddot{\boldsymbol{\delta}}\|_{\boldsymbol{\tau}^{-1},\infty}^{[0,T]} + \|\ddot{\mathbf{e}}_{\mathbf{u}}\|_{\Omega,\infty}^{[0,T]} \right), \end{aligned}$$

where the constant C is independent of the mesh size h and the time T .

5 Numerical experiments

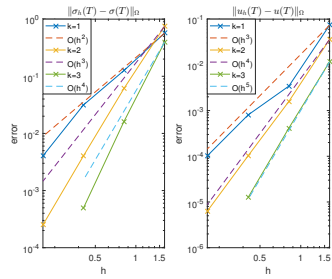


Figure 1: History of convergence for $\boldsymbol{\sigma}(T)$ and $\mathbf{u}(T)$ with sequence of uniform refinements in space and over-refinements in time.

References

- [1] B. Cockburn, Z. Fu, A. Hungria, L. Ji, M. A. Sánchez and F.-J. Sayas, Störmer-Numorov HDG methods for acoustic waves, *J. Sci. Comput.* **75(2)** (2018), pp. 597–624.
- [2] G. Fu, B. Cockburn and H. K. Stolarski, Analysis of an HDG method for linear elasticity, *Internat. J. Numer. Methods Engrg.* **102(3-4)** (2015), pp. 551–575.
- [3] A. Hungria, D. Prada and F.-J. Sayas, HDG methods for elastodynamics, *Comput. Math. Appl.* **74(11)** (2017), pp. 2671–2690.
- [4] C. Lehrenfeld, Hybrid discontinuous Galerkin methods for solving incompressible flow problems, *Rheinisch-Westfälischen Technischen Hochschule Aachen* (2010).
- [5] W. Qiu, J. Shen and K. Shi, An HDG method for linear elasticity with strong symmetric stresses, *Math. Comp.* **87(309)** (2018), pp. 69–93.
- [6] S.-C. Soon, B. Cockburn and H. K. Stolarski, A hybridizable discontinuous Galerkin method for linear elasticity, *Internat. J. Numer. Methods Engrg.* **80(8)** (2009), pp. 1058–1092.

Solving inverse electromagnetic scattering problems via domain derivatives

Felix Hagemann^{1,*}, Tilo Arens¹, Timo Betcke², Frank Hettlich¹

¹Department of Mathematics, KIT, Karlsruhe, Germany

²Department of Mathematics, University College London, United Kingdom

*Email: felix.hagemann@kit.edu

Abstract

We employ domain derivatives to solve inverse electromagnetic scattering problems for obstacles which are either penetrable or impenetrable with perfect conducting or impedance boundary conditions. A new proof of the characterization of the domain derivative for an impedance boundary condition using variational methods is shown. We consider the inverse scattering problem of reconstructing the scatterer from far field measurements for a single incident field and solve it by a regularized iterative Newton scheme. Both the direct scattering problem and the problem characterizing the domain derivative are formulated as boundary integral equations and numerically solved using the boundary element library Bempp. Numerical examples of shape reconstructions are presented.

Keywords: inverse scattering problem, maxwell, domain derivative

1 Impedance boundary value problem

We consider time harmonic Maxwell's equations

$$\operatorname{curl} E - ikH = 0, \quad \operatorname{curl} H + ikE = 0 \quad (1)$$

with constant wavenumber $k = \omega\sqrt{\varepsilon\mu}$ in a linear isotropic homogeneous medium with electric permittivity ε , magnetic permeability μ and frequency ω . Given an incident field (E^i, H^i) , a solution of (1) in \mathbb{R}^3 , a bounded scatterer $D \subset \mathbb{R}^3$ gives rise to a scattered field (E^s, H^s) in $\mathbb{R}^3 \setminus \overline{D}$, a solution of (1) which satisfies the Silver Müller radiation condition. The impedance boundary condition reads as

$$\nu \times H = \lambda(\nu \times (E \times \nu)) \quad \text{on } \partial D,$$

for some positive impedance $\lambda : \partial D \rightarrow \mathbb{R}$ and the outwards directed unit normal ν . Due to the boundary condition, the appropriate Hilbert space for the weak formulation is

$$H_{\text{imp}} := \{E \in H(\operatorname{curl}, \Omega) : \nu \times E \in L^2_t(\partial D)\},$$

with $\Omega = B_R(0) \setminus \overline{D}$ and $R > 0$ large enough. The corresponding inner product is

$$\langle E, V \rangle_{H_{\text{imp}}} = \langle E, V \rangle_{H(\operatorname{curl}, \Omega)} + (\nu \times E, \nu \times V)_{L^2_t(\partial D)}$$

The weak formulation reads as: Find $E \in H_{\text{imp}}$ with

$$\begin{aligned} & \langle \operatorname{curl} E, \operatorname{curl} V \rangle_{L^2(\Omega)} - k^2 \langle E, V \rangle_{L^2(\Omega)} \\ & \quad - ik \langle \lambda \nu \times E, \nu \times V \rangle_{L^2(\partial D)} \\ & \quad + ik \langle \Lambda(E \times \nu), V \rangle_{L^2(\partial B_R(0))} \\ & = \langle ik \Lambda(\nu \times E^i) - \nu \times \operatorname{curl} E^i, V \rangle_{L^2(B_R(0))} \end{aligned}$$

for all $V \in H_{\text{imp}}$. The impedance boundary value problem is uniquely solvable in H_{imp} and depends continuously on the right hand side [1]. The variational approach of finding the derivative of the solution E with respect to the boundary ∂D starts by considering variations of the boundary ∂D , generated by small, compactly in $B_R(0)$ supported vector fields $h \in C^1(\mathbb{R}^3, \mathbb{R}^3)$. Then, one considers solutions E_h of the boundary value problem with respect to the perturbed scatterer

$$D_h := \{y = \varphi(x) = x + h(x) : x \in D\}.$$

By investigations of the behaviour of E_h as $h \rightarrow 0$ in $C^1(\mathbb{R}^3, \mathbb{R}^3)$, we prove the following theorems.

Theorem 1 *The solution E depends continuously on D . To be more precise: Let $\widehat{E}_h := J^T_\varphi(E_h \circ \varphi)$. Then*

$$\|E - \widehat{E}_h\|_{H_{\text{imp}}} \rightarrow 0, \quad \|h\|_{C^1} \rightarrow 0.$$

Theorem 2 *The solution E is differentiable with respect to the boundary: There exists a unique $W \in H_{\text{imp}}$, depending linear and continuously on h , such that*

$$\lim_{\|h\|_{C^1} \rightarrow 0} \frac{1}{\|h\|_{C^1}} \|\widehat{E}_h - E - W\|_{H_{\text{imp}}} = 0.$$

The function W is called *material derivative* of E and can be used to characterize the known [2, 5] *domain derivative* $E' \in H_{\text{imp}}$.

Theorem 3 We have

$$E' = W - J_h^\top E - J_E h \in H_{\text{imp}},$$

where (E', H') are weak solutions of (1) with boundary condition

$$\begin{aligned} \nu \times H' - \lambda(\nu \times (E' \times \nu)) &= \text{Grad}(h_\nu H_\nu) \times \nu + \lambda \text{Grad}(E_\nu h_\nu) \\ &+ h_\nu \left(\frac{\partial \lambda}{\partial \nu} + ik - 2\lambda(\mathcal{R} + \kappa) \right) (\nu \times (E \times \nu)) \\ &+ ik\lambda h_\nu (H \times \nu) \end{aligned} \quad (2)$$

2 Solving inverse problems

We define the boundary to far field operator \mathbf{F} by

$$\mathbf{F}(\partial D) = E^\infty,$$

where E^∞ is the far field of the solution E with respect to the scatterer D . We want to solve the following inverse problem. Fixing an incoming plane wave

$$\begin{pmatrix} E^i \\ H^i \end{pmatrix} (x) = \begin{pmatrix} p \\ (d \times p) \end{pmatrix} e^{ikd \cdot x}$$

with direction $d \in \mathbb{S}^2$ and polarization $p \in \mathbb{C}^3$, satisfying $p \cdot d = 0$, solve the equation

$$\mathbf{F}(\partial D) = E^\infty.$$

Theorems 2 and 3 show differentiability of \mathbf{F} . We employ a regularized iterative Newton scheme as follows. First, we chose an initial guess ∂D^0 . In every iteration $i \in \mathbb{N}$, we check the residual $r = \|\mathbf{F}(\partial D^i) - E^\infty\|$. We solve for the variation h in the linearized equation $\mathbf{F}(\partial D_h^i) = E^\infty$ and update our current boundary ∂D^i by h . Regularization comes in play by applying Tikhonov regularization, i.e. solving

$$\begin{aligned} (\mathbf{F}'[\partial D^i]^* \mathbf{F}'[\partial D^i] + \alpha \mathbf{I}) h &= \mathbf{F}'[\partial D^i]^* (E^\infty - \mathbf{F}(\partial D^i)) \end{aligned}$$

for some $\alpha > 0$. This algorithm has been successfully carried out for the three-dimensional acoustic scattering [4]. We have applied this technique to electromagnetic wave scattering from obstacles which are either penetrable or impenetrable with perfect conductiong or impedance boundary condition. We have formulated both the direct scattering problem and the characterization of the domain derivative as integral equations. In order to solve these numerically,

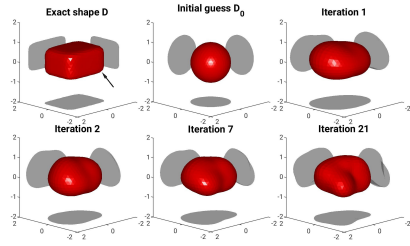


Figure 1: Reconstruction of a rounded cuboid using 64 shape functions and noisy data. The black arrow indicates the direction of the incoming plane wave.

we have used the boundary element method library BEMPP [6]. The implementation of the right hand side of (2) requires stable discretizations of surface differential operators, the rotation $\nu \times \cdot$ and the mean curvature κ . In figure 1, an actual reconstruction for a penetrable object is shown. For further details and more reconstructions, we refer to our paper [3].

References

- [1] F. Cakoni, D. Colton and P. Monk, The electromagnetic inverse-scattering problem for partly coated Lipschitz domains, *Proc. of the R. Soc. of Edin.*, 134A, 661–682, 2004.
- [2] H. Haddar and R. Kress, On the Frechet derivative for obstacle scattering with an impedance boundary condition, *SIAM J. on Appl. Math.*, **65**, 194–208, 2004.
- [3] F. Hagemann, T. Arens, T. Betcke and F. Hettlich, Solving inverse electromagnetic scattering problems via domain derivatives, *CRC 1173-Preprint (submitted, provisionally accepted)*, KIT, 2018.
- [4] H. Harbrecht and T. Hohage, Fast methods for three-dimensional inverse obstacle scattering problems, *Int. Eq. and Appl.*, 72:509–535, 2012.
- [5] R. Hiptmair and J. Li, Shape derivatives for scattering problems, *Inv. Prob.*, 34:105001 (25pp), 2018.
- [6] W. Śmigaj, T. Betcke et al, Solving boundary integral problems with BEM++, *ACM Trans. on math. soft.*, **42**, 6:1–6:40, 2015

Reconstructing thin tubular scattering objects in electromagnetic scattering

Roland Griesmaier¹, Marvin Knöller^{1,*}¹Department of Mathematics, KIT, Karlsruhe, Germany

*Email: marvin.knoeller@kit.edu

Abstract

We derive an efficient regularized Newton algorithm for reconstructing thin tubular scattering objects in electromagnetic scattering. The algorithm is based on an asymptotic perturbation formula for the Maxwell transmission problem in three dimensional free space. Due to this formula, in contrast to classical Newton schemes, no partial differential equation has to be numerically solved during the whole reconstruction process. We will first discuss the asymptotic perturbation formula, building on the abstract framework in [2], and study its basic components for the case of a thin tubular scatterer. Then we set up the regularized Newton method, discuss its implementation and present numerical results, which illustrate the performance of the reconstruction algorithm.

Keywords: inverse scattering, thin tubular scatterers, Newton method, Maxwell equations

1 The Maxwell transmission problem

Let $k = \omega \sqrt{\varepsilon_0 \mu_0}$ be the wave number with frequency ω , electric permittivity ε_0 , and magnetic permeability μ_0 . Denote by E^i and H^i the incident electric and magnetic field respectively, which solve the time-harmonic Maxwell equations, i.e.

$$\begin{aligned} \operatorname{curl} E^i - i\omega \mu_0 H^i &= 0 \quad \text{in } \mathbb{R}^3, \\ \operatorname{curl} H^i + i\omega \varepsilon_0 E^i &= 0 \quad \text{in } \mathbb{R}^3. \end{aligned}$$

For a C^2 -curve K with length $L > 0$ we consider thin tubular scattering objects of the form

$$D_\rho = \{x \in \mathbb{R}^3 \mid \operatorname{dist}(x, K) < \rho\}.$$

The incident wave is scattered by such an object, for which we assume homogenous electric permittivity $\varepsilon_1 > 0$ and magnetic permeability $\mu_1 > 0$. The total fields $E_\rho^s = E^i + E_\rho^s$ and $H_\rho^s = H^i + H_\rho^s$ satisfy the Maxwell system

$$\begin{aligned} \operatorname{curl} E_\rho - i\omega \mu_\rho H_\rho &= 0 \quad \text{in } \mathbb{R}^3, \\ \operatorname{curl} H_\rho + i\omega \varepsilon_\rho E_\rho &= 0 \quad \text{in } \mathbb{R}^3, \end{aligned}$$

where

$$\gamma_\rho(x) = \begin{cases} \gamma_1, & \text{if } x \in D_\rho \\ \gamma_0, & \text{if } x \in \mathbb{R}^3 \setminus \overline{D}_\rho \end{cases}$$

for $\gamma \in \{\mu, \varepsilon\}$. The tangential components of E and H are assumed to be continuous on the interface of D_ρ . Additionally, E_ρ^s and H_ρ^s have to satisfy the Silver-Müller radiation condition. The scattered field permits a representation of the form

$$E_\rho^s(x) = \frac{e^{ik|x|}}{4\pi|x|} \left(E_\rho^\infty(\hat{x}) + O\left(\frac{1}{|x|}\right) \right),$$

where $E_\rho^\infty : S^2 \rightarrow \mathbb{C}^3$ is called far field. Our approach to scattering by thin tubular objects is supported by the following theorem.

Theorem 1 *The far field of E_ρ^s satisfies*

$$\begin{aligned} E_\rho^\infty(\hat{x}) &= \\ \rho^2 \pi &\left(\int_K \alpha_1 (\operatorname{curl}_x \mathbb{G}(\hat{x}, y))^\infty \mathbb{M}^\mu(y) \operatorname{curl}_y E^i(y) \right. \\ &\quad \left. - \alpha_2 (\mathbb{G}(\hat{x}, y))^\infty \mathbb{M}^\varepsilon(y) E^i(y) \, ds(y) \right) + o(\rho^2) \end{aligned}$$

with $\alpha_1 = \mu_1/\mu_0 - 1$ and $\alpha_2 = k^2(1 - \varepsilon_1/\varepsilon_0)$ as $\rho \rightarrow 0$. Here, \mathbb{G} denotes the dyadic Green's function and the matrix-valued functions \mathbb{M}^ε and \mathbb{M}^μ denote the electric and magnetic polarization tensors.

We discretize the curve K as a linear spline

$$K \approx \tilde{K} = \bigcup_{j=1}^n [x^j, x^{j+1}],$$

where $[x^j, x^{j+1}]$ denotes the line segment from x^j to x^{j+1} . Using results from [1], we conclude that for $\gamma \in \{\mu, \varepsilon\}$, the polarization tensors can be diagonalized,

$$\mathbb{M}^\gamma(y) = V(y) M^\gamma V^\top(y),$$

where $V(y)$ contains the Frenet-Serret frame at $y \in \tilde{K}$ as its columns and

$$M^\gamma = \operatorname{diag}(1, 2\gamma_0/(\gamma_1 + \gamma_0), 2\gamma_0/(\gamma_1 + \gamma_0)).$$

Convergence of this discretization of the formula from theorem 1 for fixed ρ with respect to the number of subsegments of \tilde{K} is depicted in figure 1. The reference solution has been numerically approximated by means of the boundary element method library BEM++ (see [5] and <https://bempp.com/>).

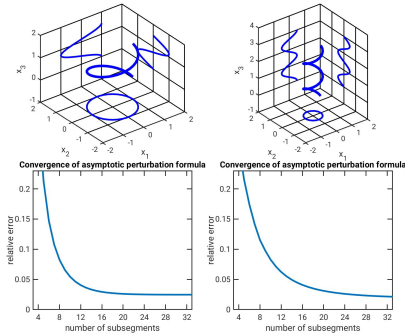


Figure 1: **Top row:** Two different curves together with their projections onto the 3 coordinate planes. **Bottom row:** Relative error between the result of the discretized perturbation formula and the far field computed by means of BEM++ with respect to the number of subsegments of the linear spline \tilde{K} for fixed ρ .

2 A regularized Newton method

Next we consider the operator $\mathcal{T} : K \mapsto g_\rho^\infty$, which maps the curve K to the leading order term g_ρ^∞ of the perturbation formula in theorem 1. The inverse problem consists in solving $\mathcal{T}(K) = E_\rho^\infty$ for the unknown curve K . The idea is to minimize the nonlinear functional

$$F(x^1, \dots, x^{n+1}) = \left\| E_\rho^\infty - \sum_{j=1}^n \mathcal{T}([x^j, x^{j+1}]) \right\|_{L^2}^2 + \lambda_1^2 \psi_1(x^1, \dots, x^{n+1}) + \lambda_2^2 \psi_2(x^1, \dots, x^{n+1})$$

with regularization parameters $\lambda_1, \lambda_2 > 0$ and penalty terms ψ_1 and ψ_2 , which prevent the subsegments of the reconstructed linear spline from getting entangled and from having strongly varying lengths. A combination of the Gauß-Newton method and the golden search line method is now used to minimize F . A visualization of the reconstruction process is shown in figure 2.

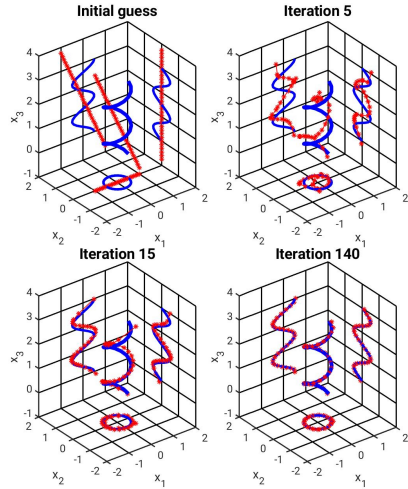


Figure 2: Reconstruction of a helix using 30 subsegments in the discretization of K .

References

- [1] E. Beretta et al. Thin cylindrical conductivity inclusions in a three-dimensional domain: a polarization tensor and unique determination from boundary data *Inverse Problems*, 25(6):065004, 22, 2009
- [2] Y. Capdeboscq and M. Vogelius. A general representation formula for boundary voltage perturbations caused by internal conductivity inhomogeneities of low volume fraction. *M2AN Math. Model. Numer. Anal.*, 37(1):159-173, 2003
- [3] R. Griesmaier. A general perturbation formula for electromagnetic fields in presence of low volume scatterers *ESAIM Math. Model. Numer. Anal.*, 45(6):1193-1218, 2011
- [4] R. Griesmaier and N. Hyvönen. A regularized Newton method for locating thin tubular conductivity inhomogeneities *Inverse Problems*, 27(11): 115008, 22, 2011
- [5] F. Hagemann et al. Solving inverse electromagnetic scattering problems via domain derivatives *CRC 1173-Preprint (submitted, provisionally accepted)*, KIT, 2018.

On the analysis of perfectly matched layers for electromagnetic waves propagation in anisotropic media

Éliane Bécache¹, Sonia Fliss¹, Maryna Kachanovska¹, Maria Kazakova^{1,*}

¹Poems (CNRS/Inria/ENSTA ParisTech), Palaiseau, France

*Email: maria.kazakova@ensta-paristech.fr

Abstract

The work deals with the analysis of Cartesian Perfectly Matched Layers (PMLs) in the context of electromagnetic wave propagation in a 3D infinite anisotropic homogeneous medium with a diagonal dielectric tensor. Contrary to the 2D case some anisotropies lead to the existence of backward waves giving rise to instabilities of the PMLs in the time-domain and a lack of convergence in the frequency domain.

Keywords: Anisotropic Maxwell's equation, Perfectly Matched Layers, Backward waves

1 Introduction

We are interested in simulating wave propagation in three-dimensional infinite anisotropic media which can be described with Maxwell's equations. Since the medium is infinite, one needs to introduce an equivalent formulation posed in a bounded domain which is suitable for numerical purposes. The widely-used PML method (see [1]) consists in surrounding the computational domain by a layer which absorbs outgoing waves. PML techniques are very popular because they are efficient and easy to implement for a large class of problems. They can be used in the time and frequency domains. It is well known that classical Cartesian PMLs fail in the presence of backward waves in the PML direction: one can observe instabilities in time-domain (see e.g. [2]), and a lack of convergence towards the physical solution in the frequency domain (see [4]).

Although backward waves do not exist for diagonal anisotropy for the 3D scalar wave equation as well as for 2D Maxwell's equations, surprisingly they do exist for 3D Maxwell's equations for a class of diagonal anisotropic dielectric tensors. This is counter-intuitive and a more detailed analysis follows. In the sequel, we consider the time-domain problem, but this can be transposed to the frequency regime.

2 Problem statement

We consider electromagnetic wave propagation in a diagonal anisotropic medium described by Maxwell's equations

$$\underline{\underline{\epsilon}} \partial_{tt} \mathbf{E}(t, \mathbf{x}) + \nabla \times \nabla \times \mathbf{E}(t, \mathbf{x}) = 0, \quad \mathbf{x} \in \mathbb{R}^3 \quad (1)$$

with compactly supported initial conditions, and $\underline{\underline{\epsilon}} = \text{diag}\{\epsilon_x, \epsilon_y, \epsilon_z\}$, with $\epsilon_j > 0$, $j = x, y, z$.

In order to allow for numerical simulation of (1) in unbounded space, we surround the computational domain by a PML. Inside this layer one modifies (1) by an appropriate complex scaling. The layer is truncated and vanishing Dirichlet/Neumann boundary conditions are imposed. To analyse the stability of the PMLs we perform the plane-wave analysis of the original system (1). This consists in considering particular solutions of (1) of the form

$$\mathbf{E}(t, \mathbf{x}) = \hat{\mathbf{E}} e^{i(\omega t - \mathbf{k}\mathbf{x})},$$

where $\hat{\mathbf{E}}$ is the amplitude vector, $\mathbf{k} = (k_x, k_y, k_z)$ is the wave vector. This yields the *dispersion relation*

$$\omega^2 F(\omega, k_x, k_y, k_z) = 0. \quad (2)$$

Here F is a biquadratic equation in ω , with four roots denoted as $\omega_j^\pm(\mathbf{k})$, $j = 1, 2$, which define four almost everywhere different *modes*.

For a given mode, we can define the *phase velocity* \mathbf{v}_p and the *group velocity* \mathbf{v}_g :

$$\mathbf{v}_p(\mathbf{k}) = \frac{\omega_j^\pm(\mathbf{k})}{|\mathbf{k}|} \frac{\mathbf{k}}{|\mathbf{k}|}, \quad \mathbf{v}_g(\mathbf{k}) = \nabla_{\mathbf{k}} \omega_j^\pm(\mathbf{k}),$$

In the following, we will analyse the stability of PMLs for (1) relying on these quantities.

3 Condition on the tensor $\underline{\underline{\epsilon}}$

The necessary condition of the stability of PML methods in time domain for anisotropic media was established in [2]. For systems with constant coefficients this criterion is based on the analysis of (2). The classical PML method is unstable in a given direction \mathbf{e}_j if

$$\exists \mathbf{k} \in \mathbb{R}^3 : (\mathbf{v}_p(\mathbf{k}) \cdot \mathbf{e}_j)(\mathbf{v}_g(\mathbf{k}) \cdot \mathbf{e}_j) < 0. \quad (3)$$

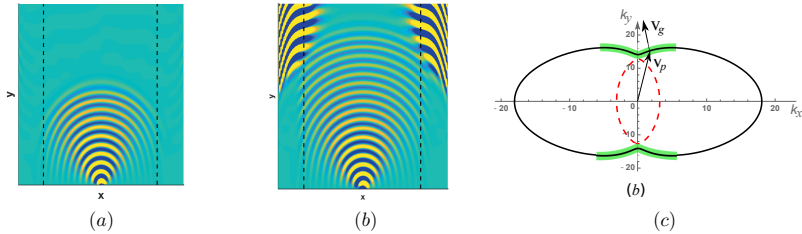


Figure 1: Snapshots of the electric field component $E_x(t, x, y, 0)$ at (a) $t = 2.5$, (b) $t = 4$. (c) Solution of dispersion relation (2) for $\varepsilon_y < \varepsilon_x < \varepsilon_z$ with $k_z = \text{const.}$

By definition this corresponds to the presence of *backward propagating* modes in the direction \mathbf{e}_j . For example, if the PML is applied in x -direction, the necessary stability condition is written as

$$\frac{k_x}{\omega_j^\pm(\mathbf{k})} \frac{\partial \omega_j^\pm(\mathbf{k})}{\partial k_x} \geq 0 \quad \forall \mathbf{k} \in \mathbb{R}^3.$$

As demonstrated in [2], this condition has a simple geometrical interpretation, expressing the fact that along the dispersive surfaces, the phase and the group velocity are oriented in the same direction with respect to the \mathbf{e}_x direction (see figure 1,(c)).

The following result establishes the necessary condition of stability of the PML applied for (1) in x -direction:

Theorem 1

(i) if $\min(\varepsilon_y, \varepsilon_z) < \varepsilon_x < \max(\varepsilon_y, \varepsilon_z) \exists \mathbf{k}_0, \varepsilon > 0$ such that $\forall \mathbf{k} : \|\mathbf{k} - \mathbf{k}_0\| < \varepsilon$ there are backward propagating modes in the \mathbf{e}_x direction (see Figure 1(c)).

(ii) otherwise there are no backward propagating waves in the \mathbf{e}_x direction.

The criterion (3) being a necessary stability condition, the classical PML method is unstable in the time-domain if (i) is satisfied. Since the analysis is not specific to the \mathbf{e}_x direction, we conclude that if $\varepsilon_x \neq \varepsilon_y \neq \varepsilon_z$ backward waves will exist in one of the axis direction, but if two of the coefficients are equal no backward waves exist. Numerical simulations confirm the instabilities of PML in the x -direction for a medium satisfying (i) (see Figure 1 (a,b)). On the other hand, no instabilities appear in the two other directions. The justification of this constitutes part of future research.

It is known that the extension of classical PML methods can be proposed for some models with backward propagating modes (see [3] for dispersive metamaterials and plasmas) via a new change of variables for the PML construction. However in the present case a similar techniques seem to be inappropriate, and an alternative solution should be proposed. A new strategy is currently under investigation first in the frequency domain, and then in time-domain.

Acknowledgement. The forth author was supported by a public grant as part of the "Investissement d'avenir" project, reference ANR-11-LABX-0056-LMH, LabEx LMH.

References

- [1] J.-P. Bérenger, A perfectly matched layer for the absorption of electromagnetic waves. *J. of Comp. Phys.*, **114**(2) (1994) pp. 185–200.
- [2] É. Bécache, S. Fauqueux, P. Joly, Stability of perfectly matched layers, group velocities and anisotropic waves *J. of Comp. Phys.*, **188**(2) (2003) pp. 399–433.
- [3] É. Bécache, P. Joly, M. Kachanovska, V. Vinoles, Perfectly matched layers in negative index metamaterials and plasmas *ESAIM: Proceedings and Surveys*, **50** (2015) pp. 113–132.
- [4] A.-S. Bonnet-Ben Dhia, C. Chambeyron, G. Legendre, On the use of perfectly matched layers in the presence of long or backward propagating guided elastic waves", *Wave Motion*, **51** (2014) pp. 266–283.

Imaging sparse reflectivities from noisy data

Miguel Moscoso¹, Alexei Novikov^{2,*}, Chrysoula Tsoyka³, George Papanicolaou⁴¹Department of Mathematics, Universidad Carlos III de Madrid, Leganes, Madrid 28911, Spain²Mathematics Department, Penn State University, University Park, PA 16802, USA³Applied Math Unit, University of California, Merced, Merced, USA⁴Department of Mathematics, Stanford University, Stanford, CA 94305, USA

*Email: novikov@psu.edu

Abstract

We consider the problem of imaging sparse scenes from a few noisy data using an ℓ_1 -minimization approach. This problem can be cast as a linear system of the form $\mathcal{A}\boldsymbol{\rho} = \mathbf{b}$, where \mathcal{A} is a sensing matrix. We assume that the dimension of the unknown sparse vector $\boldsymbol{\rho}$ is much larger than the dimension of the data vector \mathbf{b} . Our main contribution is a new method for exact support recovery in the presence of additive noise. We propose to solve the augmented linear system $\mathcal{A}\boldsymbol{\rho} + \mathcal{C}\boldsymbol{\eta} = \mathbf{b}$, where the matrix \mathcal{C} is a noise collector.

Keywords: array imaging, sparse recovery, l_1 -minimization

1 Formulation of the problem

Consider point sources located inside the image window IW. The goal of array imaging is to determine their positions and amplitudes using measurements obtained on an array of receivers. The array of size a has N receivers separated by a distance h located at positions $\vec{\mathbf{x}}_r$, $r = 1, \dots, N$ (see Figure 1). They can measure single or multifrequency signals with frequencies ω_l , $l = 1, \dots, S$. The M point sources, whose positions $\vec{\mathbf{z}}_j$ and (complex-valued) amplitudes $\alpha_j \in \mathbb{C}$, $j = 1, \dots, M$, we seek to determine, are at a distance L from the array. In order to form the images we discretize the IW using a uniform grid of points $\vec{\mathbf{y}}_k$, $k = 1, \dots, K$, and we introduce the *true source vector*

$$\boldsymbol{\rho} = [\rho_1, \dots, \rho_K]^\top \in \mathbb{C}^K,$$

such that

$$\rho_k = \begin{cases} \alpha_j, & \text{if } \|\vec{\mathbf{z}}_j - \vec{\mathbf{y}}_k\|_\infty < \text{grid-size}, \\ & \text{for some } j = 1, \dots, M, \\ 0, & \text{otherwise.} \end{cases}$$

To write the data received on the array in a compact form, we define the Green's function

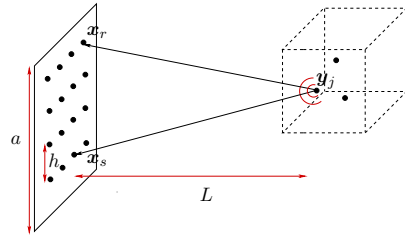


Figure 1: General setup of array imaging.

vector

$$\mathbf{g}(\vec{\mathbf{y}}; \omega) = [G(\vec{\mathbf{x}}_1, \vec{\mathbf{y}}; \omega), \dots, G(\vec{\mathbf{x}}_N, \vec{\mathbf{y}}; \omega)]^\top \quad (1)$$

at location $\vec{\mathbf{y}}$ in the IW, where $G(\vec{\mathbf{x}}, \vec{\mathbf{y}}; \omega)$ denotes the free-space Green's function of the homogeneous medium. The signal received at $\vec{\mathbf{x}}_r$ at frequency ω_l is given by

$$b(\vec{\mathbf{x}}_r, \omega_l) = \sum_{j=1}^M \alpha_j G(\vec{\mathbf{x}}_r, \vec{\mathbf{z}}_j; \omega_l). \quad (2)$$

If we normalize the columns of \mathcal{A} to have length one and stack the data in a column vector

$$\mathbf{b} = \frac{1}{\sqrt{NS}} [b(\vec{\mathbf{x}}_1, \omega_1), \dots, b(\vec{\mathbf{x}}_N, \omega_S)]^\top, \quad (3)$$

then the source vector $\boldsymbol{\rho}$ solves the system of equations $\mathcal{A}\boldsymbol{\rho} = \mathbf{b}$, with the $(N \cdot S) \times K$ matrix

$$\mathcal{A} = \frac{1}{\sqrt{NS}} \begin{pmatrix} \mathbf{g}(\vec{\mathbf{y}}_1; \omega_1) & \dots & \mathbf{g}(\vec{\mathbf{y}}_K; \omega_1) \\ \vdots & & \vdots \\ \mathbf{g}(\vec{\mathbf{y}}_1; \omega_S) & \dots & \mathbf{g}(\vec{\mathbf{y}}_K; \omega_S) \end{pmatrix}.$$

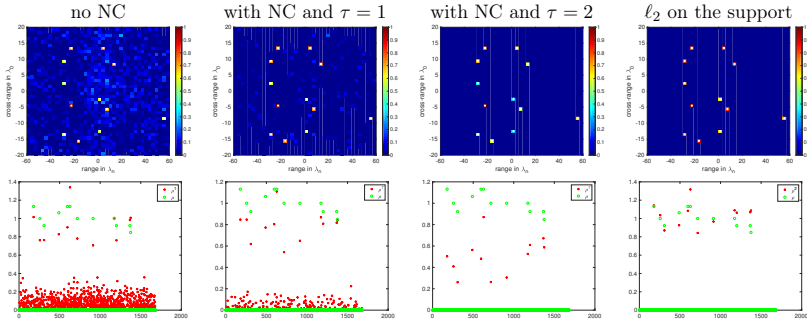


Figure 2: High level of noise; SNR = 1. From left to right: ℓ_1 -norm minimization without the noise collector; ℓ_1 -norm minimization with a noise collector with $\Sigma = 10^4$ columns, and the weight $\tau = 1$; ℓ_1 -norm minimization with a noise collector, and the correct $\tau = 2$; ℓ_2 -norm solution restricted to the support. In the top row we show the images, and in the bottom row the solution vector with red stars and the true solution vector with green circles.

2 Main Results

When data is perturbed by small noise, the following qualitative description of the image could be observed. Firstly, the points where the sources are located become blobs containing several nearby pixels. Secondly, a few pixels away from the sources are also visible. The latter is usually referred as grass. In order to quantify the observed results we introduce the vicinities.

Let $\rho \in \mathbb{C}^K$ be an M -sparse solution of $\mathcal{A}\rho = \mathbf{b}$, with support $T = \{i : \rho_i \neq 0\}$. For any $j \in T$ define the corresponding vicinity of \mathbf{a}_j as

$$S_j = \left\{ k : |\langle \mathbf{a}_k, \mathbf{a}_j \rangle| \geq \frac{1}{3M} \right\}. \quad (4)$$

For any vector $\boldsymbol{\eta} \in \mathbb{C}^K$ its coherent misfit to ρ is

$$\mathbf{Co}(\rho, \boldsymbol{\eta}) = \sum_{j \in T} \left| \rho_j - \sum_{k \in S_j} \langle \mathbf{a}_j, \mathbf{a}_k \rangle \eta_k \right|, \quad (5)$$

whereas its incoherent remainder with respect to ρ is

$$\mathbf{In}(\rho, \boldsymbol{\eta}) = \sum_{k \notin \Upsilon} |\eta_k|, \quad \Upsilon = \cup_{j \in T} S_j. \quad (6)$$

Proposition 1. Suppose the vicinities S_j do not overlap, and let

$$\gamma = \sup_{\mathbf{c}} (\|\boldsymbol{\xi}\|_{\ell_1} / \|\mathbf{c}\|_{\ell_2}), \quad (7)$$

where $\boldsymbol{\xi}$ is the minimal ℓ_1 -norm solution of $\mathcal{A}\boldsymbol{\xi} = \mathbf{c}$. Let

$$\rho_\delta = \arg \min \|\rho_e\|_{\ell_1}, \text{ subject to } \mathcal{A}\rho_e = \mathbf{b}_\delta, \quad (8)$$

with noise $\|\mathbf{b} - \mathbf{b}_\delta\|_{\ell_2} \leq \delta$. Then, $\mathbf{Co}(\rho, \rho_\delta) \leq 3\gamma\delta$, and $\mathbf{In}(\rho, \rho_\delta) \leq 5\gamma\delta$. If $\delta = 0$, and Υ does not contain collinear vectors, then $\rho_\delta = \rho$.

Proposition 1 implies that a key to control the noise is the constant γ defined in (7). In general, we have $\gamma = O(\sqrt{N})$. This means that the quality of the image deteriorates as the number of measurements $N \rightarrow \infty$. We can remedy that by augmenting the imaging matrix \mathcal{A} with a “noise collector” matrix \mathcal{C} , and solving the system

$$\begin{aligned} (\rho_\tau, \boldsymbol{\eta}_\tau) &= \arg \min_{\rho, \boldsymbol{\eta}} (\tau \|\rho\|_{\ell_1} + \|\boldsymbol{\eta}\|_{\ell_1}), \quad (9) \\ &\text{subject to } \mathcal{A}\rho + \mathcal{C}\boldsymbol{\eta} = \mathbf{b}_\delta, \end{aligned}$$

with $\tau = 1$, see the second column on Figure 2. The $\Sigma = N^\beta$ columns of \mathcal{C} are chosen at random from the unit sphere. We further can remove all the grass from the image by correctly choosing the weight τ , see the third column on Figure 2. The last column of Figure 2 shows the ℓ_2 projection of the measurement \mathbf{b}_δ on the recovered support of ρ .

Imaging in three-dimensional terminating waveguides with partial-aperture data

Symeon Papadimitropoulos^{1,*}, Chrysoula Tzogka², Dimitrios A. Mitsoudis³

¹Faculty of Aerospace Engineering, Technion - Israel Institute of Technology, Haifa, Israel

²Applied Math Unit, University of California, Merced, Merced, USA & IACM/FORTH, Greece

³Department of Naval Architecture, University of West Attica & IACM/FORTH, Greece

*Email: symeon@campus.technion.ac.il

Abstract

We study the problem of imaging extended reflectors in a three-dimensional terminating waveguide using an active planar array. Our imaging method relies on the back propagation of an appropriate projection of the usual array response matrix and allows us to obtain good reconstructions of the reflector with partial-aperture arrays that cover a small fraction of the waveguide's cross-section.

Keywords: array imaging, waveguide, partial aperture, prolates

1 Formulation of the problem

We consider a three-dimensional (3D) Cartesian coordinate system $\vec{x} = (z, \mathbf{z}') \in \mathbb{R}^3$, where z is the range coordinate, the cross-range coordinates \mathbf{z}' lie on the xy -plane, and x is taken to be positive downwards. We denote by Ω a 3D cylindrical waveguide, as shown in Figure 1, that consists of two parts: a semi-infinite cylindrical waveguide Ω_{L-} of constant (bounded, Lipschitz) cross-section \mathcal{C} for range $z < L$, filled with a homogeneous medium, and a bounded domain $\Omega_{L+} \subset \mathbb{R}^3$ where the cross-section may vary with range and/or the medium may be inhomogeneous. For simplicity, we restrict ourselves to the acoustic case with a sound-soft boundary but our approach applies to other boundary conditions as well. An active planar array \mathcal{A} of N transducers is placed parallel to the waveguide's cross-section at range $z = z_a < L$; the array may span the entire cross-section or just a part of it. In this setup we want to create images in order to locate an extended reflector contained somewhere in Ω_{L+} ; the term extended refers to a reflector with typical size comparable to a reference wavelength.

Our data set for imaging is contained in a matrix $\widehat{\Pi}(\omega) \in \mathbb{C}^{N \times N}$ whose (r, s) entry is the Fourier coefficient at frequency ω of the time traces of the echoes recorded at the r -th receiver when the s -th source emits a signal. This is the

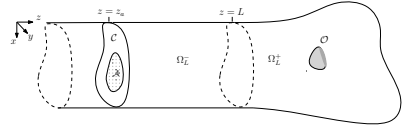


Figure 1: Imaging setup in a 3D terminating waveguide.

so-called *array response matrix*.

We denote by $\widehat{G}(\vec{x}, \vec{x}_s; \omega)$ the Green's function for the Helmholtz operator evaluated at $\vec{x} \in \Omega$, due to a point source located at $\vec{x}_s \in \Omega$, for a single frequency ω , *i.e.* $\widehat{G}(\vec{x}, \vec{x}_s; \omega)$ solves

$$-\Delta \widehat{G}(\vec{x}, \vec{x}_s; \omega) - k^2 \eta(\vec{x}) \widehat{G}(\vec{x}, \vec{x}_s; \omega) = \delta(\vec{x} - \vec{x}_s),$$

supplemented with Dirichlet boundary conditions. Moreover, let $\{\mu_n, \Phi_n\}_{n=1}^{\infty}$ be the eigenvalues (in ascending order) and corresponding orthonormal eigenfunctions of the Dirichlet transverse Laplacian $-\Delta$ in \mathcal{C} . It is well-known that $\mu_n \in \mathbb{R}$ and are positive, while $\{\Phi_n\}_{n=1}^{\infty}$ forms an orthonormal basis of $L^2(\mathcal{C})$. Let also M be the number of propagating modes in Ω_{L-} , *i.e.* M is an index that satisfies $\mu_M < k^2 < \mu_{M+1}$, where k is the constant wavenumber in Ω_{L-} .

Finally, let $\beta_n = \begin{cases} \sqrt{k^2 - \mu_n}, & 1 \leq n \leq M, \\ i\sqrt{\mu_n - k^2}, & n \geq M + 1. \end{cases}$

2 Imaging

To create an image, we define a search domain $\mathcal{S} \subset \Omega$ and we compute the values of an appropriate imaging functional, which has the property that its values, when computed and graphically displayed, exhibit peaks that indicate the location of the scatterer.

The full-aperture array case. In [2] we have proposed an imaging approach, inspired by phase conjugation, for the case of a two-dimensional (2D) terminating waveguide. The extension in our current 3D setting, leads to the imaging

functional

$$\mathcal{I}^a(\tilde{\mathbf{y}}^s) = \sum_{i=1}^M \sum_{j=1}^M \beta_i \beta_j \overline{\hat{\mathbb{Q}}_{ij}} \hat{G}_i(z_a, \tilde{\mathbf{y}}^s) \hat{G}_j(z_a, \tilde{\mathbf{y}}^s),$$

where $\tilde{\mathbf{y}}^s \in \mathcal{S}$ and $\hat{G}_i(z_a, \cdot)$ are the Fourier coefficients of the Green's function with respect to the orthonormal basis $\{\Phi_n\}_{n=1}^\infty$ of $L^2(\mathcal{C})$, *i.e.*, $\hat{G}_i(z_a, \cdot) = \int_{\mathcal{C}} \hat{G}((z_a, \mathbf{z}'), \cdot) \Phi_i(\mathbf{z}') dz'$.

The matrix $\hat{\mathbb{Q}}$ in the case of the full-aperture array ($\mathcal{A} = \mathcal{C}$) is defined as the projection of $\hat{\Pi}_{rs} := \hat{\Pi}(\tilde{\mathbf{x}}_r, \tilde{\mathbf{x}}_s; \omega)$ on $\Phi_i(x, y)$. Therefore it is an $M \times M$ matrix with entries

$$\hat{\mathbb{Q}}_{ij} = \int_{\mathcal{A}} \int_{\mathcal{A}} \hat{\Pi}_{rs}(\omega) \Phi_i(\mathbf{z}'_s) \Phi_j(\mathbf{z}'_r) dz'_s dz'_r. \quad (1)$$

Following similar arguments as in [2] we may show that the functional \mathcal{I}^a for a point scatterer behaves like the square of the imaginary part of the Green's function.

The partial-aperture array case. For $\mathcal{A} \subset \mathcal{C}$ the eigenfunctions Φ_i are no longer orthonormal along \mathcal{A} . As a result the efficiency of \mathcal{I}^a deteriorates as $|\mathcal{A}|$ decreases. In [1], in the case of a 2D waveguide, we have introduced a method, that is based on a projection of the array response matrix on proper orthogonal functions, which remarkably improves the performance of \mathcal{I}^a for small array apertures. A key role to our approach, and to the extension to the 3D case, plays the real, symmetric (Gram) matrix A_{arr} :

$$(A_{\text{arr}})_{ij} = \int_{\mathcal{A}} \Phi_i(\mathbf{z}') \Phi_j(\mathbf{z}') dz', \quad i, j = 1, \dots, M.$$

Let $\{\nu_n, \mathbf{w}^{(n)}\}$ be the eigenvalues (in descending order) and corresponding orthonormal eigenvectors of A_{arr} . It is easy to show that $\nu_n \in [0, 1]$. Then, we define the functions

$$S_j(\mathbf{z}') = \sum_{i=1}^M w_i^{(j)} \Phi_i(\mathbf{z}'), \quad j = 1, \dots, M.$$

The S_j 's are doubly orthogonal in the sense that they are orthonormal along \mathcal{C} and orthogonal along \mathcal{A} and exhibit a prolate-like behavior. In fact, in the 2D case they are clearly identified as prolate or prolate-like wavefunctions; for details see [1] and the references therein. Next, we project $\hat{\Pi}$ on S_j , *i.e.*

$$\hat{\mathbb{S}}_{ij} = \frac{1}{\nu_i \nu_j} \int_{\mathcal{A}} \int_{\mathcal{A}} \hat{\Pi}_{rs}(\omega) S_i(\mathbf{z}'_s) S_j(\mathbf{z}'_r) dz'_s dz'_r,$$

where it is to be understood that $\hat{\mathbb{S}}_{ij} = 0$ whenever ν_i or $\nu_j = 0$ (or, in practice, whenever they are below a certain threshold). Finally, we define the projected array response matrix $\hat{\mathbb{Q}}$ as

$$\hat{\mathbb{Q}} = W \hat{\mathbb{S}} W^T, \quad (2)$$

where $W = (\mathbf{w}^{(1)}, \mathbf{w}^{(2)}, \dots, \mathbf{w}^{(M)})$. In the case of a point scatterer, it can be shown that in this way, as long as the eigenvalues ν_n remain above a certain threshold, we recover the exact same matrix as in (1) and, subsequently, the same image as in the full-aperture case.

3 Numerical results

We consider a 3D terminating homogeneous waveguide with constant rectangular cross-section $\mathcal{C} = ([0, 10] \times [0, 20])\lambda_0$, where λ_0 is a reference wavelength that corresponds to $k_0 = \pi/10$. We use a single frequency with $k = 0.9875k_0$. A 2D square perfect reflector with sidelength $2\lambda_0$ is placed parallel to the waveguide's cross-section centered at $\tilde{\mathbf{x}}^* = (19, 5, 10)\lambda_0$. In Figure 2 we present some imaging results using \mathcal{I}^a with arrays of various shapes that cover roughly the same area which is about 30% of the waveguide's (full-aperture) cross-section.

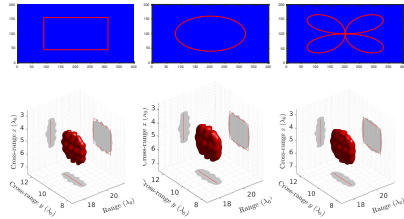


Figure 2: Imaging using \mathcal{I}^a with arrays of various shapes covering covering about 30% of the waveguide's full aperture (with area $\simeq 0.3|\mathcal{C}|$).

References

- [1] C. Tsogka, D. A. Mitsoudis, and S. Papadimitropoulos. Partial-aperture array imaging in acoustic waveguides. *Inverse Problems*, **32**(12), 2016.
- [2] C. Tsogka, D. A. Mitsoudis, and S. Papadimitropoulos. Imaging extended reflectors in a terminating waveguide. *SIAM Journal on Imaging Sciences*, **11**(2), 2018 pp. 1680–1716.

Adaptive Eigenspace Regularization for Inverse Scattering Problems

Daniel H. Baffet¹, Marcus J. Grote^{1,*}, Jet H. Tang¹¹Dept. of Mathematics and Computer Science, University of Basel, Basel, Switzerland

*Email: marcus.grote@unibas.ch

Abstract

A nonlinear optimization method is proposed for inverse scattering problems in the frequency domain. The time-harmonic inverse medium problem is formulated as a PDE-constrained optimization problem and solved by an inexact truncated Newton-type method combined with frequency stepping. Instead of a grid-based discrete representation combined with standard Tikhonov regularization, the unknown medium is projected to a small finite-dimensional subspace, which is iteratively adapted using dynamic thresholding. Rigorous error estimates of the adaptive eigenspace approximation are proved for an arbitrary piecewise constant medium.

Keywords: Helmholtz equation, inverse scattering, total variation, regularization

1 Inverse scattering problem

Let y be the solution of the Helmholtz equation,

$$-\nabla \cdot (u \nabla y) - \omega^2 y = f \quad \text{in } \Omega, \quad (1)$$

$$\frac{\partial y}{\partial n} - i \frac{\omega}{c} y = g \quad \text{on } \Gamma, \quad (2)$$

in a bounded connected polygonal domain $\Omega \subset \mathbb{R}^d$, with boundary Γ . Here $\omega > 0$ denotes the wave frequency, $u(x) = c^2(x)$ denotes the (unknown) squared wave speed inside Ω , n is the unit outward normal to Γ , and $f \in L^2(\Omega)$ and $g \in L^2(\Gamma)$ are known sources.

To determine u , the inverse problem is formulated as a PDE-constrained optimization problem with the standard L^2 -least-squares misfit functional

$$J[u] = \frac{1}{2} \sum_{\ell=1}^{N_s} \|y_\ell - y_\ell^{\text{obs}}\|_{L^2(\Gamma)}^2 \quad (3)$$

where for each $\ell = 1, \dots, N_s$, $y_\ell = y_\ell[u]$ is the solution to (1)-(2) with $f = f_\ell$ and $g = g_\ell$, and $y_\ell^{\text{obs}} \in L^2(\Gamma)$ is the observed data on the boundary. To minimize $J[u]$, we use a standard (inexact, truncated CG) Newton-like iteration.

Since the inverse problem is in general severely ill-posed, a Tikhonov (TV) regularization

term is typically added to the cost functional. Here, we instead seek u in a finite-dimensional subspace spanned by the first few eigenfunctions of a linear elliptic operator, which itself depends on the medium.

2 Adaptive eigenspace (AE) basis

During the optimization, we compute at each iteration an approximation u^* of the solution u as a truncated expansion

$$u^*(x) = \sum_{k=1}^K \beta_k \varphi^k(x) \quad (4)$$

where $\{\varphi^k\}_{k \geq 1}$ are the eigenfunctions of the linear elliptic operator [1-3]

$$Lv = L_\varepsilon[u]v = -\nabla \cdot (\mu_\varepsilon[u] \nabla v), \quad (5)$$

with

$$\mu_\varepsilon[u] = \frac{1}{\sqrt{|\nabla u|^2 + \varepsilon^2}}, \quad \varepsilon > 0. \quad (6)$$

More precisely, for each k , the eigenpair (φ^k, λ_k) satisfies

$$\begin{aligned} L_\varepsilon[u] \varphi^k &= \lambda_k \varphi^k & \text{in } \Omega, \\ \varphi^k &= 0 & \text{on } \Gamma, \end{aligned} \quad (7)$$

the sequence $\{\lambda_k\}$ is nondecreasing with each eigenvalue repeated according to its multiplicity, and $\{\varphi^k\}$ is orthonormal w.r.t. the $L^2(\Omega)$ inner product.

Note that for a piecewise constant function u , (6) is not well-defined. Instead, we thus use a more regular approximation u_δ of u , e.g., a projection of u into an H^1 -conforming finite element (FE) space. Although our analysis assumes that u_δ satisfy certain conditions, it does not require u_δ to be obtained by any specific method. Hence, we distinguish the parameter δ from the FE mesh parameter h .

3 Analysis of the AE approximation

We assume that u is piecewise constant,

$$u = \sum_{k=1}^K u^k \chi^k, \quad u^k \in \mathbb{R}, u^k \neq 0, \quad (8)$$

where for each k , χ^k is the characteristic function of a set A^k compactly contained in Ω . For $\delta > 0$ and $k = 1, \dots, K$, let U_δ^k be the δ -neighborhood of the boundary of A^k , $U_\delta = \bigcup_{k=1}^K U_\delta^k$ and $D_\delta = \Omega \setminus \overline{U_\delta}$ their complement.

Next, we introduce the more regular approximation u_δ of u . To include FE approximations in our analysis, we consider the eigenvalue problem (7) in a closed subspace $\mathcal{V}_\delta \subset H_0^1(\Omega)$. For each $k = 1, \dots, K$, let $\{\chi_\delta^k\}_{\delta>0}$ be such that $\chi_\delta^k \in \mathcal{V}_\delta$, and $\lim_{\delta \rightarrow 0} \chi_\delta^k = \chi^k$ in $L^2(\Omega)$, and set

$$u_\delta = \sum_{k=1}^K u^k \chi_\delta^k. \quad (9)$$

Theorem 1 *Let the sets A^1, \dots, A^K be open, connected, satisfy the strong Lipschitz condition, and with mutually disjoint boundaries. Suppose for each k , the function $\chi_\delta^k \in \mathcal{V}_\delta$ satisfies $\nabla \chi_\delta^k \in L^\infty(\Omega)$, $\nabla \chi_\delta^k = 0$ a.e. in $\Omega \setminus \overline{U_\delta^k}$, and there exist $p \in [1, \infty]$ and $C_1 > 0$, such that for every sufficiently small δ , there holds*

$$\delta^{1-1/p} \|\nabla \chi_\delta^k\|_{L^p(\Omega)} \leq C_1 \quad (10)$$

(with the usual convention $1/\infty := 0$). Then there exists a constant $C > 0$, such that for every $\varepsilon > 0$, $k = 1, \dots, K$ and $\delta > 0$ sufficiently small there holds

$$\|\nabla \varphi^k\|_{L^2(D_\delta)}^2 \leq \frac{C\varepsilon}{\min_j |u^j|}. \quad (11)$$

Here (φ^k, λ_k) are the eigenvalues and eigenfunctions of $L_\varepsilon[u_\delta]$ in \mathcal{V}_δ .

Essentially, estimate (11) implies that the first K eigenfunctions φ^k of (7) are ‘‘almost’’ constant in each connected component of D_δ . Thus, for sufficiently small δ and ε , u in (8) can be well approximated in the K dimensional subspace spanned by $\varphi^1, \dots, \varphi^K$.

4 Numerical results

Here we consider a profile u which consists of characteristic functions of two sets in $\Omega = (0, 1)^2$. Figure 1 shows u_δ , discretized with P^1 -FE, and the first two eigenfunctions $\varphi^1, \varphi^2 \in \mathcal{V}_\delta$ of L_ε .

Figure 2 shows results for an inverse medium problem, given scattered wave data on Γ recorded from eight separate Gaussian sources located in Ω . Here, the AE Inversion Algorithm employs frequency stepping; it starts at a low frequency and iteratively computes minimizers for



Figure 1: (left) true profile u_δ ; (middle-right) the eigenfunctions φ^1, φ^2 of L_ε in (7), $\varepsilon = 10^{-8}$.

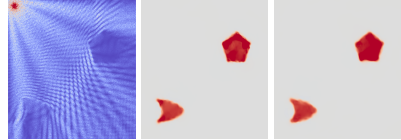


Figure 2: (left) observation y_δ^{obs} ; reconstruction without (middle) or with 20% noise (right).

data obtained at increasingly higher frequencies, where each minimizer $u^{(\ell)}$ obtained for a frequency ω_ℓ is used as an initial guess for the minimization for $\omega_{\ell+1}$. At each frequency ω_ℓ , we use the BFGS method to seek a minimizer of (3) in the span of a finite dimensional basis B^ℓ constructed iteratively as follows: At each iteration, B^ℓ is obtained by combining the basis $B^{\ell-1}$ from the previous frequency $\omega_{\ell-1}$ with the first few eigenfunctions of (5), with u replaced by $u^{(\ell-1)}$, truncated via SVD. To ensure that B^ℓ remains L^2 orthogonal, we apply the modified Gram-Schmidt algorithm. Thus, we ensure that the misfit essentially decreases monotonically even when we update the basis.

References

- [1] M. de Buhan and M. Kray-Graff, A new approach to solve the inverse scattering problem for waves: combining the TRAC and the adaptive inversion methods, *Inverse Problems* (2017), pp. 085009.
- [2] M. J. Grote, M. Kray-Graff and U. Nahum, Adaptive eigenspace method for inverse scattering problems in the frequency domain, *Inverse Problems* (2017), pp. 025006.
- [3] M. J. Grote and U. Nahum, Adaptive eigenspace for multi-parameter inverse scattering problems, *Comput. Math. Appl.* (2019), pp. 3264–3280.

Obstacle Identification Using Learning

Adar Kahana^{1,*}, Eli Turkel¹, Shai Dekel¹, Dan Givoli²¹Department of Mathematics, Tel-Aviv University, Tel-Aviv, Israel²Department of Aerospace engineering, Technion, Haifa, Israel

*Email: Adarkahana@mail.tau.ac.il

Abstract

The field of machine learning is growing very fast, with applications to many other fields. We propose applying advanced methods of learning to the classical numerical solution for the wave equation, allowing the solution of ill-posed problems with high accuracy for obstacle identification.

Keywords: learning, inverse problem, source, scatterer, sensors, neural network, convolution

1 Introduction

We investigate the solution of the acoustic wave equation in a homogeneous medium with reflecting or absorbing boundaries. We synthetically create a small eruption that generates a wave propagation and insert a small number of sensors in the medium. Information is stored, in time, only at these sensors. We formulate our main questions as inverse problems [1] -

- Source refocusing [6] - Given the medium properties (boundary condition, scatterers, wave velocity, sensors, etc.) we are interested in finding the location of the source that started transmitting the acoustic waves.
- Obstacle identification [4, 5] - Given the medium properties and the source location, but excluding the scatterers, we are interested in the properties of the scatterers (location, size, shape, penetrability, etc.).

Both problems are ill-posed so that a solution does not necessarily exist and even when it does it might not be unique. In addition, the solution is highly sensitive to perturbations in the input data. Hence, when we have only noisy partial knowledge - since we only record in a small amount of sensors - we cannot retrieve the solution in the entire domain. To aid us with the lack of information we use learning.

In this work we discuss the problem of obstacle identification. The main goal is to locate an

arbitrary obstacle together with its shape. We simulate a physical experiment with synthetic data using the propagation of waves. Data is stored at a small number of sensors for every time step of the forward calculation of the wave equation. We wish to use this stored data to find the properties of the scatterers using learning techniques. In previous works [4–6] we found that solving the wave equation backward in time using this sensor information significantly adds to the robustness of the method especially with regard to noise.

The proposed method involves using classical numerical methods for solving the problems previously discussed, both forward and backward in time, within a learning framework. We construct physically informed models so the process of learning will be part of the physical solution (rather than a pre/post process).

2 Learner architecture

Given the measurements recorded in the sensors we propose several methods of inferring the properties of the scatterer. First, we address the problem as a segmentation problem - modeling the scatterer as a binary segment (each voxel is either inside or outside the segment). We apply several learning techniques such that the output will be a probability tensor including the obstacle (each voxel has a probability to be inside the segment).

To enhance the robustness of our model to noise and achieve faster convergence of the learner we introduce a method that mimics the classical regularization procedure for PDEs and adapt it to the training process of the learner. Instead of a common loss function we take in account a weighted loss penalized with an equivalent to a regularization term.

Another proposed method is exploiting the time-reversibility of the wave equation. Instead of using the recorded values in the sensors directly, we use the Time Reversal (TR) [2,3] procedure and a feature extraction algorithm specially constructed for the backward step of the

TR. The interesting results we achieved using this method show that using the TR procedure adds additional independent information to the learner, giving us better inferences (even though the backward step was in fact simulated using the same data from the sensors).

3 Noise

To determine how reliable our inferences are, we introduce artificial noise to the data. There are two types of noise to take into account -

- Noisy data (the more common type of noise) - Every electrical component generates internal noise. Also, the wave equation does not take in account all the physical processes in the wave propagation. An underwater environment may include noise from unknown sources. Therefore, after simulating the recording in the sensors we synthetically add artificial normally distributed noise to the measurements.
- Noisy labels - When training the models we use a learning set including recordings with known scatterers. Some of the measurements may have false labels.

We propose several methods to overcome the negative effect of these types of noises on our model and present the models accuracy given the amount of noise.

4 Numerical results

Using a convolutional neural network with a very simple architecture, we trained the model on only 25,000 measurements (10% of them used for testing) of arbitrarily shaped polygons (not necessarily convex). After only 5 computer hours of training (using nVidia's GTX1050 GPU) we achieved an average of 60% intersection over union score, i.e

$$IOU = \frac{\#(y_{truth} \cap y_{pred})}{\#(y_{truth} \cup y_{pred})}$$

Training with more samples produced more accurate results. As an example, we display a non convex polygon in Figure 1.

5 Conclusion

We considered the use of learning techniques for ill-posed problems in partial differential equations. By using learning techniques that incorporate the numerical solution of the wave equation we were able to well approximate the shape

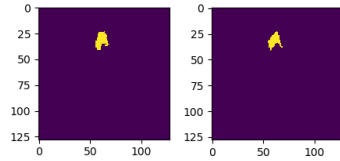


Figure 1: Non-convex polygon. Left: Prediction, Right: Ground truth

and position of the scatterer based on time data at only a few sensors.

References

- [1] V. Isakov, *Inverse Problems for Partial Differential Equations* 2nd edition, Applied Mathematical Sciences **127**, (Springer 2006).
- [2] C. Bardos and M. Fink, Mathematical foundations of the time reversal mirror, *Asymptotic Anal.* **29** (2002), pp. 157–182.
- [3] P. Blomgren, G. Papanicolaou and H. Zhao, Super-resolution in time-reversal acoustics, *J. Acoust. Soc. Am.* **111** (2002), pp. 230–248.
- [4] D. Givoli and E. Turkel, Time reversal with partial information for wave refocusing and scatterer identification, *Comput. Methods Appl. Mech. Eng.* **213** (2012), pp. 223–242.
- [5] I. Levi, E. Turkel and D. Givoli, Time reversal for elastic wave refocusing and scatterer location recovery, *J. Comput. Acoust.* **23(1450013)** (2015), pp. 1–29.
- [6] A. Kahana, E. Turkel and D. Givoli, Convective Wave Equation and Time Reversal Process for Source Refocusing, *J. Comput. Acoust.* **26(1850016)** No.02 (2018).

Mixed-Dimensional Coupling for Time-Dependent Wave Problems

Dan Givoli^{1,*}, Hanan Amar¹, Daniel Rabinovich¹¹Dept. of Aerospace Engineering, Technion, Haifa, Israel

*Email: givolid@technion.ac.il

Abstract

The coupling of two-dimensional (2D) and one-dimensional (1D) models to form a single hybrid 2D-1D model is considered, for the time-dependent linear scalar wave equation and for the equations of elastodynamics. The 1D model is used to represent a 2D computational domain where the solution behaves approximately in a 1D way. This hybrid model, if designed properly, is a more efficient way to solve the full 2D model for the entire problem. The paper focuses on the way the 2D-1D coupling is done, and on the coupling error generated, and in doing so compares three methods of coupling: the Panasenko method, the Nitsche method and the Dirichlet-to-Neumann (DtN) mapping method.

Keywords: coupling, mixed-dimensional, 2D-1D, 1D-2D, Nitsche, Panasenko, DtN

1 Introduction

A reoccurring theme in computational mechanics in recent years is the need to reduce the size of large discrete models. One type of such a reduction is spatial dimensional reduction, which one may perform in cases where the solution in some region of a high-dimensional (HighD, say 3D) computational domain behaves in a low-dimensional (LowD, say 1D) way. There are several scenarios where this could be the case. Most significant is the scenario where the solution in a certain region behaves in a way that is weakly (or hardly) dependent on a certain coordinate, relative to the other coordinates. Another possible scenario is when we are interested in the solution within a geometrically slender region. In this case we might be interested in the lateral average of the solution within this region rather than in its lateral distribution. Alternatively we might already know the nature of the lateral distribution of the solution within this region and wish to know the axial distribution. In these cases, the lateral dimension is the dimension we would eliminate, resulting in a LowD model.

Typically, the LowD model is employed as an approximation to the HighD model in a par-

tial region of the spatial domain. The HighD region is the region of interest where the LowD approximation does not hold or does not provide the details required for the analysis. The LowD region is the ‘outer region’ where the LowD approximation is believed to be valid (e.g., based on asymptotic analysis). The LowD solution is possibly of less interest in its details to the analyzer, yet it affects the solution in the HighD region significantly. Denoting the LowD region by Ω_1 and the complementary HighD region by Ω_2 , it is beneficial to represent the problem by a LowD model in Ω_1 and by a HighD model in Ω_2 . Then, one has to couple the two models via the interface between them. The hybrid HighD-LowD model, if designed properly, is much more efficient than the standard HighD model taken for the entire problem. An important issue related to such hybrid models is the way in which the mixed-dimensional coupling is done on the interface, and the coupling error generated. If the mixed-dimensional coupling performs poorly, this may deteriorate the accuracy of the whole computation.

In recent years, along with the increase in the size and complexity of computational models, the scenario of mixed-dimensional (LowD-HighD) coupling has drawn a lot of attention. Fields of application where this scenario is of special interest include, among others, the following:

- *Blood-flow analysis.* Typically the HighD model corresponds to a specific blood vessel of interest in the human body and the LowD model corresponds to the rest of the blood system. An example can be found in [1].
- *Hydrological and geophysical flow models.* Here the LowD region represents a collection of channel-like entities (rivers, flood streams, etc.) and the HighD region is that of a large water body (a river delta, a lake, etc.).
- *Elastic structures.* A number of LowD-

HighD configurations exist in this application field. In one of them the LowD model consists of the slender parts of the structure that have rod- or beam- or plate- or shell-like behavior, and which typically constitute most of the structure volume, while the HighD parts are the regions that have to be modeled as 3D elastic bodies. Examples include the frame structure of a car or an aircraft. The beam-like parts of the structure exhibit 1D behavior, but some small regions (the joints and parts of the base) behave in a fully 3D manner. Panasenko *et al.* have developed an asymptotic-variational approach for such structural problems, under static conditions. See, e.g., [2].

Our focus in this work is the latter application, although the coupling methods developed are general and may be useful for other applications as well. We apply the proposed coupling methods to wave problems governed by the scalar wave equation and by the equations of elastodynamics.

2 The hybrid model

After splitting the given problem into a 2D part and a 1D part, thus creating a hybrid 2D-1D model, we need to consider the interface conditions imposed at the continuous level (i.e., before any discretization takes place). There are two interface conditions: on the wave function u (the pressure in acoustics, the displacement vector in elastodynamics) and on its “flux” (the normal derivative $\partial u/\partial n$ in acoustics, the traction in elastodynamics). We impose pointwise continuity on u (which also implies that u is uniform along the interface), and continuity in the average sense on the “flux.” *We prove that the hybrid model involving these two interface conditions is well-posed.*

3 The coupling methods

We shall consider three coupling methods. The methods themselves are not new, but to the best of our knowledge they have not been adopted to the scenario of mixed-dimensional coupling, except in the previous work of the first author (but then only in the steady-state regime).

- *The Panasenko coupling method.* Here the u -continuity condition is imposed strongly

and the flux-continuity condition is imposed weakly. See [2] and [3]. The advantage of this method is that it is very simple to implement and produces accurate solutions if one places the 2D-1D interface in an appropriate location.

- *The Nitsche coupling method.* Here both the u -continuity condition and the flux-continuity condition are imposed weakly; see [4]. The Nitsche method results in a symmetric finite element formulation which is stabilized via a special stabilization term. We show that the Nitsche method is more forgiving than the Panasenko method in situations where the interface is placed deep in the 2D regime.
- *The Dirichlet-to-Neumann (DtN) coupling method.* Here information is passed at each time-step between the 2D model and the 1D model by using the numerically-obtained DtN mapping of the 1D model on the interface. This method outperforms the other two methods, although its implementation is more involved.

By experimenting with various numerical examples, we shall investigate the performance of the three methods, estimate the errors that each of them generates, and compare between them in accuracy and efficiency.

References

- [1] C. D’Angelo and A. Quarteroni, On the Coupling of 1D and 3D Diffusion-Reaction Equations, Application to Tissue Perfusion Problems, *Math. Models & Meth. Appl. Sci.* **18** (2008), pp. 1481–1504.
- [2] G. P. Panasenko, The Partial Homogenization: Continuous and Semi-discretized Versions, *Math. Models & Meth. Appl. Sci.* **8** (2007), pp. 1183–1209.
- [3] H. Amar and D. Givoli, Mixed-Dimensional Modeling of Time-Dependent Wave Problems Using the Panasenko Construction, *J. Theor. Comput. Acoust.* **26** (2018), pp. 1850034-1–11.
- [4] H. Amar and D. Givoli, Mixed-Dimensional Coupling for Time-Dependent Wave Problems Using the Nitsche Method, *Comp. Meth. Appl. Mech. & Engng.*, to appear.

Wave equation in a weakly randomly perturbed periodic medium

Laure Giovangigli^{1,*}, Sonia Fliss²

¹POEMS (CNRS-INRIA-ENSTA Paristech), Palaiseau, France

²POEMS (CNRS-INRIA-ENSTA Paristech), Palaiseau, France

*Email: laure.giovangigli@ensta.paristech.fr

Abstract

In this work we consider the solution of the time harmonic wave equation in a periodic medium and we want to study the effects of rare random perturbations of the medium. More precisely, we study a one-dimensional periodic setting, in which each period have a probability η to have its coefficients modified, independently of the other periods. The perturbation is weak in the sense that it happens rarely but when it happens the correction is of the order of the initial coefficient. Our goal is to derive an asymptotic approximation of the solution u_η with respect to η .

Keywords: random media, periodic media, defects, wave equation

1 Introduction

In this work, which is at its very first stage, we consider the solution of the time harmonic wave equation in a periodic medium and we want to study the effects of rare random perturbations of the medium. More precisely, we study a one-dimensional periodic medium, in which each period have a probability η to have its coefficients modified, independently of the other periods. Our goal is to derive an asymptotic approximation of the solution u_η with respect to η .

Our motivations are twofold. The idea of this problem originates from a paper [2] by C. Le Bris and A. Anantharaman who worked on this particular problem but in the context of homogenization to model composite materials with defects. [3] and [4] extend the framework to other random perturbations but are still considering the homogenized problem. We want here to investigate the general regime where homogenization techniques can not necessarily be applied.

Our second motivation concerns the numerical approximation of the solutions of the wave equations in weakly perturbed periodic media in order to propose transparent boundary conditions. We wish to build an easily computable and good approximation of the random solution u_η by using our expertise on periodic media [1].

We present the model in Section 1 before proving the convergence of u_η to the solution of the periodic problem in Section 2 and developing first-order approximations of $\mathbb{E}(u_\eta)$ and u_η in the last section.

2 Problem settings

Let $(\Omega, \mathcal{F}, \mathbb{P})$ be a probability space. Let $(B_j^i)_{j \in \mathbb{N}}$ be independent Bernouilli random variables with parameter $\eta \in [0, 1]$. We consider a random medium occupying N periods of length $L > 0$, characterised by the following coefficients for $(x, \omega) \in [0, NL] \times \Omega$

$$\kappa_\eta(x, \omega) = \kappa_{\text{per}}(x) + b_\eta(x, \omega)\tilde{\kappa}_{\text{per}}(x),$$

$$\rho_\eta(x, \omega) = \rho_{\text{per}}(x) + b_\eta(x, \omega)\tilde{\rho}_{\text{per}}(x),$$

where $\kappa_{\text{per}}, \tilde{\kappa}_{\text{per}}, \rho_{\text{per}}, \tilde{\rho}_{\text{per}}$ are L -periodic functions and $b_\eta(x, \omega) = \sum_{j=0}^{N-1} \mathbb{1}_J(x)B_j^i(\omega), J = [jL, (j+1)L]$.

We are interested in the solution u_η of the wave equation in this medium in the frequency domain. More precisely, u_η is the solution in $L^2(\Omega, H^2((0, NL)))$ of the equation

$$\begin{cases} -\frac{\partial}{\partial x} \kappa_\eta \frac{\partial}{\partial x} u_\eta - \rho_\eta k^2 u_\eta = 0 & \text{in } (0, NL), \\ u_\eta(0) = 1, \quad u_\eta(NL) = 0. \end{cases} \quad (1)$$

where we suppose to simplify that $\Im(k^2) > 0$. We assume furthermore that there exist strictly non negative constants $\kappa_+, \kappa_-, \rho_+, \rho_-$ such that almost everywhere

$$0 < \kappa_- \leq \kappa_{\text{per}} \leq \kappa_+, \quad 0 < \kappa_- \leq \kappa_{\text{per}} + \tilde{\kappa}_{\text{per}} \leq \kappa_+,$$

$$0 < \rho_- \leq \rho_{\text{per}} \leq \rho_+, \quad 0 < \rho_- \leq \rho_{\text{per}} + \tilde{\rho}_{\text{per}} \leq \rho_+.$$

We equip $L^2(\Omega, V)$ for $V = L^2((0, NL)), H^1((0, NL))$ or $H^2((0, NL))$ with the norm

$$\forall u \in L^2(\Omega, V), \quad \|u\|_{L^2(\Omega, V)} = \sqrt{\mathbb{E}(\|u\|_V^2)}.$$

3 Convergence of u_η

We introduce u_{per} the solution of the wave equation in the unperturbed domain. u_{per} is the unique solution in $H^2((0, NL))$ of

$$\begin{cases} -\frac{\partial}{\partial x} \kappa_{\text{per}} \frac{\partial}{\partial x} u_{\text{per}} - k^2 \rho_{\text{per}} u_{\text{per}} = 0 & \text{in } (0, NL), \\ u_{\text{per}}(0) = 1, \quad u_{\text{per}}(NL) = 0. \end{cases}$$

We prove that u_η converges to u_{per} as $\eta \rightarrow 0$ in $L^2(\Omega, H^1((0, NL)))$ at a rate of $\sqrt{\eta}$.

Theorem 1

$$\|u_\eta - u_{\text{per}}\|_{L^2(\Omega, H^1((0, NL)))} \leq C\sqrt{\eta}\|u_{\text{per}}\|_{H^1((0, NL))},$$

$$\text{where } C = \frac{\max(\kappa_+, \rho_+ |k|^2)}{\Im(k) |k| \min\left(\frac{\kappa_-}{|k|^2}, \rho_-\right)}.$$

4 First-order corrections

In order to refine this approximation, we introduce u_{j_1, \dots, j_p} , the solution in a medium where exactly only the periods J_1, \dots, J_p are perturbed.

Let $p \geq 1$. Let $j_1 < \dots < j_p$ in $\llbracket 0, N-1 \rrbracket$. u_{j_1, \dots, j_p} is the unique solution in $H^2((0, NL))$

$$\left\{ \begin{array}{l} -\frac{\partial}{\partial x} \left(\kappa_{\text{per}} + \sum_{m=1}^p \mathbb{1}_{J_m} \tilde{\kappa}_{\text{per}} \right) \frac{\partial}{\partial x} u_{j_1, \dots, j_p} \\ -k^2 \left(\rho_{\text{per}} + \sum_{m=1}^p \mathbb{1}_{J_m} \tilde{\rho}_{\text{per}} \right) u_{j_1, \dots, j_p} = 0 \\ \text{in } (0, NL), \\ u_{j_1, \dots, j_p}(0) = 1, \quad u_{j_1, \dots, j_p}(NL) = 0. \end{array} \right.$$

For all $\omega \in \Omega$, we denote by \mathcal{P}_ω the set of integers $j \in \llbracket 0, N-1 \rrbracket$ such that $B_j^\omega(\omega) = 1$. u_η can then be written for all $(x, \omega) \in (0, NL) \times \Omega$

$$u_\eta(x, \omega) = \mathbb{1}_{\mathcal{P}_\omega = \emptyset}(\omega) u_{\text{per}}(x) + \sum_{p=1}^N \sum_{j_1 < \dots < j_p} \mathbb{1}_{\mathcal{P}_\omega = \{j_1, \dots, j_p\}}(\omega) u_{j_1, \dots, j_p}(x). \tag{2}$$

The expectation of u_η has therefore the following expression

$$\mathbb{E}(u_\eta) = (1 - \eta)^N u_{\text{per}} + \eta^p (1 - \eta)^{N-p} \sum_{p=1}^N \sum_{j_1 < \dots < j_p} u_{j_1, \dots, j_p}, \tag{3}$$

which yields directly to the following result.

Theorem 2

$$\|\mathbb{E}(u_\eta) - u_{\text{per}} - \eta \sum_{j=0}^{N-1} v_j\|_{H^1((0, NL))} = \mathcal{O}(\eta^2),$$

where $v_j, j \in \llbracket 0, N-1 \rrbracket$ denotes $u_j - u_{\text{per}}$.

The first-order correction for $\mathbb{E}(u_\eta)$ is the sum of the difference between the solutions in a medium with exactly one defect and u_{per} , for all the different possible defects. Higher order approximation can also be derived from (3). The advantage of such expansion is that each term is solution of a deterministic problem set on a locally perturbed periodic medium. Using (1), these problems can be solved considering only cell problems with $(\kappa_{\text{per}}, \rho_{\text{per}})$ or $(\kappa_{\text{per}} + \tilde{\kappa}_{\text{per}}, \rho_{\text{per}} + \tilde{\rho}_{\text{per}})$. Computationally, the resolution is then really cheap.

Unfortunately, adding this corrector to u_η does not change the rate of convergence of $\sqrt{\eta}$ found in Theorem 1 in $L^2(\Omega, H^1((0, NL)))$, even if the approximation seems to be slightly better. Figure 1 illustrates the different rates of convergence that we exhibited so far.

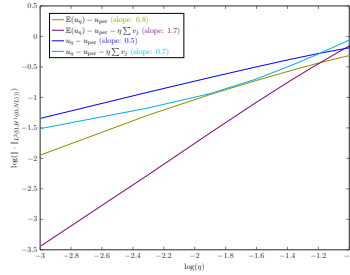


Figure 1: Rate of convergence of $\mathbb{E}(u_\eta)$ and u_η and their first-order corrections

However, similarly as (3), one can obtain from (2) asymptotic expansions for the expectation of any smooth function of u_η . This can be seen as an approximation in law in the first order in η of u_η . Higher order approximations can also be derived.

Theorem 3 For any $\varphi \in C^\infty((0, NL))$

$$\|\mathbb{E}(\varphi(u_\eta)) - \varphi(u_{\text{per}}) - \eta \sum_{j=0}^{N-1} \varphi(v_j)\|_{H^1((0, NL))} = \mathcal{O}(\eta^2) \tag{4}$$

We are currently working on improving the approximation that we built for u_η . One of the question reads: Is it possible to provide a good and deterministic approximation of u_η in a stronger sense than (4)? We are also investigating other types of weakly randomly perturbed periodic media such as stationary weakly correlated environments.

References

- [1] P. Joly, J.R. Li and S. Fliss, Exact boundary conditions for periodic waveguides containing a local perturbation, *Communications in Computational Physics*, **1** (6), 945-973, 2006.
- [2] A. Anantharaman and C. Le Bris, Elements of mathematical foundations for a numerical approach for weakly random homogenization problems, *Communications in Computational Physics*, Global Science Press, **11** (4) (2012), pp. 1103-1143.
- [3] A. Anantharaman and C. Le Bris, A numerical approach related to defect-type theories for some weakly random problems in homogenization, *Multiscale Modeling and Simulation*, SIAM, **9** (2) (2011), pp. 513-544.
- [4] J-C. Mourrat, First-order expansion of homogenized coefficients under Bernoulli perturbations, *J. Math. Pures Appl.*, **103** (2015), pp. 68-101.

Invisible floating objects

Lucas Chesnel¹, Mahran Rihani^{2,*}

¹ INRIA/CMAP, Ecole Polytechnique, Université Paris-Saclay, Palaiseau, France

² POEMS, ENSTA-ParisTech, Palaiseau, France

*Email: mahran.rihani@ensta-paristech.fr

Abstract

We consider a time-harmonic water waves problem in a 2D waveguide. The geometry is symmetric with respect to an axis orthogonal to the direction of propagation of waves. Moreover, the waveguide contains two floating obstacles separated by a distance L . We study the behaviours of R (the reflection coefficient) and T (the transmission coefficient) as L tends to $+\infty$. From this analysis, we exhibit situations of non reflectivity ($R = 0, |T| = 1$) or perfect invisibility ($R = 0, T = 1$).

Keywords: water waves, waveguides, invisibility, asymptotic analysis

Introduction

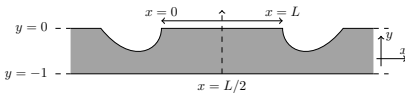


Figure 1: The waveguide Ω_L .

We consider the propagation of water waves in a 2D waveguide Ω_L which coincides with $\mathbb{R} \times (-1; 0)$ outside of a bounded domain. We assume that Ω_L is symmetric with respect to the vertical line $x = L/2$ and contains two floating objects separated by a distance L (see Figure 1). This leads us to study the problem

$$\begin{cases} \Delta u = 0 & \text{in } \Omega_L \\ \partial_n u = \lambda u & \text{on } \Gamma_0 := \mathbb{R} \times \{0\} \\ \partial_n u = 0 & \text{on } \partial\Omega_L \setminus \Gamma_0 \end{cases} \quad (1)$$

where $\lambda > 0$ is proportional to the square of the frequency and ∂_n stands for the outward normal derivative. Define $\beta > 0$ such that $\beta \tan(\beta) = \lambda$. Only two waves $w^\pm(x, y) = e^{\pm i\beta x} \cosh(\beta(y + 1))$ can propagate in Ω_L . And (1) admits the scattering solution

$$u = \begin{cases} w^+ + R w^- + \dots & \text{for } x < 0 \\ T w^+ + \dots & \text{for } x > 0, \end{cases}$$

where $R, T \in \mathbb{C}$ and where the dots are terms which are exponentially decaying at $\pm\infty$. Due

to conservation of energy, the reflection and transmission coefficients satisfy $|R|^2 + |T|^2 = 1$. Thus, perfect invisibility implies non reflectivity but the converse is not true in general. Working as in [1], we compute an explicit asymptotic expansion of R and T as $L \rightarrow +\infty$. This allows us to exhibit non reflecting geometries. Then playing with an additional parameter, we explain how to get not only $|T| = 1$ but also $T = 1$ (perfect invisibility).

Half waveguide problems

In this section, we use the symmetry of the problem to decompose it into two half waveguide problems. Set $\omega_L := \{(x, y) \in \Omega_L, x < L/2\}$ and $\Sigma := \{0\} \times (-1; 0)$ (see Figure 2).

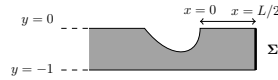


Figure 2: The half waveguide ω_L .

Consider the two problems

$$\begin{cases} \Delta u_D = 0 & \text{in } \omega_L \\ \partial_n u_D = \lambda u_D & \text{in } \Gamma_0 \\ \partial_n u_D = 0 & \text{in } \partial\omega_L \setminus \Gamma_0 \\ u_D = 0 & \text{in } \Sigma \end{cases} \quad \begin{cases} \Delta u_N = 0 & \text{in } \omega_L \\ \partial_n u_N = \lambda u_N & \text{in } \Gamma_0 \\ \partial_n u_N = 0 & \text{in } \partial\omega_L \setminus \Gamma_0 \\ \partial_n u_N = 0 & \text{in } \Sigma. \end{cases}$$

They admit solutions such that $u_D = w^+ + R_D w^- + \dots$ and $u_N = w^+ + R_N w^- + \dots$. Here $R_D, R_N \in \mathbb{C}$ and the dots are terms which are exponentially decaying at $-\infty$. Due to conservation of energy, we have $|R_D| = |R_N| = 1$. We can show that

$$R = \frac{R_N + R_D}{2}; \quad T = \frac{R_N - R_D}{2} e^{-i\beta L}. \quad (2)$$

Therefore, to obtain an asymptotic expansion of R, T as $L \rightarrow +\infty$, it is enough to work on R_D, R_N .

When $L \rightarrow +\infty$, the limit geometry of ω_L is the domain ω_∞ with just one floating object pictured in Figure 3. We denote by

$$s = \begin{pmatrix} r & t \\ t & \tilde{r} \end{pmatrix} \in \mathbb{C}^{2 \times 2}$$

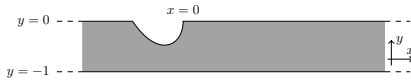


Figure 3: The limit geometry ω_∞ .

the unitary scattering matrix of the propagation problem set in ω_∞ . When $rt \neq 0$, as $L \rightarrow +\infty$, we can prove the expansions $R_D = R_D^{asy} + \dots$ and $R_N = R_N^{asy} + \dots$ with

$$R_D^{asy} = r - \frac{t^2}{e^{-i\beta L} + \tilde{r}}; \quad R_N^{asy} = r - \frac{t^2}{-e^{-i\beta L} + \tilde{r}}.$$

One can check that $|R_D^{asy}| = |R_N^{asy}| = 1$. Introduce $\theta_D, \theta_N, \theta_D^{asy}, \theta_N^{asy} \in \mathbb{R}/(2\pi\mathbb{Z})$ the phases of $R_D, R_N, R_D^{asy}, R_N^{asy}$. Finally, define

$$e := \theta_D - \theta_N - \pi; \quad e^{asy} := \theta_D^{asy} - \theta_N^{asy} - \pi.$$

Non reflectivity

From (2), we see that we have $R(L) = 0$ if and only if $e(L) = 0$. To prove that this occurs for certain L , first we show that there is L^* such that $e^{asy}(L^*) = 0$ and $\partial_L e^{asy}(L^*) \neq 0$. Then using the exponential convergence of $e(L)$ to $e^{asy}(L)$ when $L \rightarrow +\infty$, as well as the continuous dependence of $e(L)$ with respect to L , we can obtain the desired result.

Theorem 1 Assume that $rt \neq 0$. Then there is a sequence (L_n) of values of L such that $R(L_n) = 0$. And we have $L_{n+1} - L_n \underset{n \rightarrow +\infty}{\sim} \pi/\beta$.

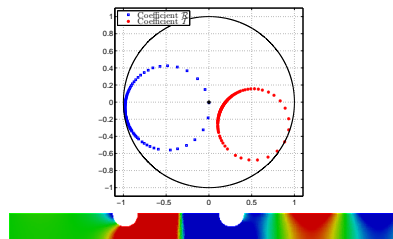


Figure 4: $R(L), T(L)$ for $L \in (0.5; 7)$ (top). Real part of the scattered field $u_s = u - w^+$ for $L = 3.15$ (bottom). In this case, $R(L) \approx 0$ and u_s is exponentially decaying in the left branch.

We illustrate this theorem in Figure 4. The floating objects are half disks of radius 0.5. We approximate numerically (FEM) the scattering coefficients $R(L), T(L)$ for $L \in (0.5; 7)$. And we

observe that the curve $L \mapsto R(L)$ indeed passes through zero. An example of non reflecting geometry is given in Figure 4.

Perfect transmission

Now we study the problem of imposing $T = 1$. Using (2) and the expansions of R_D, R_N , we get

$$T = T^{asy} + \dots \quad \text{with} \quad T^{asy} = \frac{t^2 e^{-2i\beta L}}{e^{-2i\beta L} - \tilde{r}^2}.$$

Then a direct calculus shows that the curve $L \mapsto T^{asy}(L)$ passes through 1 if and only if $t \in \mathbb{R}$. This occurs for example when the floating object is a demi ellipse of semi minor axe 0.3 and semi major axe l for $l = l^* \approx 3.6$ (see Figure 5). With this notation, with the inverse function theorem, we can prove the following result.

Theorem 2 Assume that $r(l^*)t(l^*) \neq 0$. Then there is a sequence (l_n, L_n) converging to $(l^*, +\infty)$ such that $T(l_n, L_n) = 1$. And we have $L_{n+1} - L_n \underset{n \rightarrow +\infty}{\sim} \pi/\beta$.

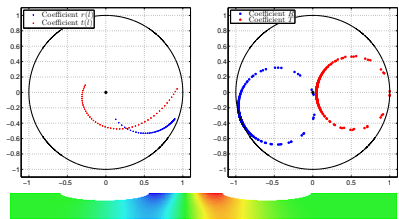


Figure 5: Coefficients $r(l), t(l)$ for $l \in (0.5; 3.9)$ (top left). Coefficients $R(l^*, L), T(l^*, L)$ for $L \in (0.5; 10)$ (top right). Real part of the scattered field $u_s = u - w^+$ for $L = 2.9$ and $l = 3.6$. In this case, $T(l, L) \approx 0$ and u_s is almost exponentially decaying in the two branches.

References

[1] L. Chesnel, S.A. Nazarov, V. Pagneux, Invisibility and perfect reflectivity in waveguides with finite length branches, *SIAM J. Appl. Math.*, vol. 78, 4:2176-2199, 2018.

Time Domain Full Waveform Inversion involving Discontinuous Galerkin approximation

Andreas Atle¹, H el ene Barucq², Henri Calandra³, Julien Diaz¹, Pierre Jacquet^{1,*}¹TOTAL E&P Research & Technology, USA, LLC²Inria Team Project Magique-3D, DIP, UPPA, E2S, CNRS, Pau, FRANCE³TOTAL SA, CSTJF, Pau, FRANCE

*Email: pierre.jacquet@inria.fr

Abstract

Geophysical exploration can be formulated as a minimization problem under constraints to get quantitative information of the subsurface with numerical simulations. In this work, we focus on the Full Waveform Inversion governed by the time-domain acoustic wave equation. Our objective is to revisit the inversion algorithm to assess the influence of the numerical discretization on the capability of FWI in retrieving the characteristics of the propagation medium. In particular, we propose to analyze different methods for time integration while the space variations are approximated with a Discontinuous Galerkin scheme.

Keywords: Full Waveform Inversion, Acoustic, Time domain, Discontinuous Galerkin

1 Introduction

Geophysical exploration is increasingly using numerical experiments to get information of the subsurface, either kinematic or dynamic. The underlying physical phenomenon is a wave equation like

$$\frac{1}{\mu} \frac{\partial^2 u}{\partial t^2} - \operatorname{div} \left(\frac{1}{\rho} \nabla u \right) = s(x, t),$$

where μ denotes the bulk modulus and ρ the density of the propagation medium. We omit here the boundary and initial conditions. The wavefield u is the solution of the forward problem generated by the sourcefield s . By traveling inside the subsurface, u is transformed into different waves including reflected waves recorded by receivers. The objective of the Full Waveform Inversion (FWI) is to use this set of data to reconstruct the propagation medium. It consists in solving an inverse problem which aims at retrieving μ and ρ from the seismic traces provided by the receivers. The inversion algorithm heavily involves the solution of the forward problem and its adjoint. In 2D, the FWI

is mainly based upon harmonic wave equations because its computational cost is really below the one in time domain. In 3D, the competition is in favor of time-domain simulations regarding both the computational burden and the treatment of the data which are intrinsically temporal. The objective of this talk is to analyze how the discretization of the forward and adjoint problems impacts on the efficiency of the Time Domain FWI (TDFWI).

2 Full Waveform Inversion Algorithm

Let P be the map relating the physical parameters $\alpha = (\mu, \rho)$ to the recorded seismic traces coming from u . Let d_{obs} be the set of real data obtained from acquisition. Then, the result of FWI is the set of parameters α_{opt} which makes the misfit between $P(\alpha, u)$ and d_{obs} minimal. We introduce the least-square misfit function defined by

$$J(\alpha, u) = \frac{1}{2} \|P(\alpha, u) - d_{obs}\|^2,$$

where $\|\cdot\|$ stands for the L^2 -norm in time and space. The minimization of J can be conducted by applying a gradient descent algorithm which is based upon an iterative process related to the update of α as follows:

$$\alpha_{i+1} = \alpha_i - \delta \nabla_{\alpha} J(\alpha_i)$$

The parameter δ corresponds to the step length of the descent and i is the number of iterate. This method requires then to compute the Fr chet derivatives of the forward solution which can be very expensive. Fortunately, there is a way to avoid the computation of the Fr chet derivatives by introducing an auxiliary unknown λ solution to

$$\frac{1}{\mu} \frac{\partial^2 \lambda}{\partial t^2} - \operatorname{div} \left(\frac{1}{\rho} \nabla \lambda \right) = s^*(x, t).$$

The unknown λ defines the adjoint state. The adjoint problem depends on the source term s^* which is defined by [1] $s^* = P^*(P(\alpha, u) - d_{obs})$.

We can for instance consider the gradient obtained by taken the derivative of the cost function by μ parameters.

$$\nabla_{\mu} J = - \int_0^{T_{max}} \int_{\Omega} \lambda \frac{1}{\mu^2} \frac{\partial^2 u}{\partial t^2} d\Omega dt.$$

Here, T_{max} denotes the final time of acquisition.

The FWI algorithm can then be pictured as in Fig. 1.

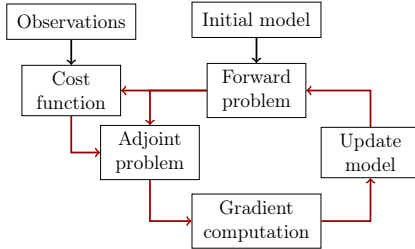


Figure 1: FWI algorithm

3 Numerical implementation

Mechanical waves are very sensitive to the topography of the subsurface. In order to keep as much information as possible from the seismic traces, it is important to use accurate discretization for the simulations. For that purpose, we use DG elements which in addition allow h and p adaptivity and are also suitable for massively parallel computations [2]. In Fig. 2, we have displayed the result obtained for the Marmousi model. We have used 3^{rd} order finite elements and the time discretization has been done with a Runge Kutta 2 time scheme.

We can see in Fig. 2 the cost function gradient by the μ model (with noiseless sources). This result validates the first loop of the FWI algorithm. It remains to finalize the optimization and make tests with different models.

Regarding the FWI algorithm, we have seen that the gradient of the cost function is carried out by solving an auxiliary problem defining the adjoint state. At this point, we have two options: the first one consists in using the same numerical scheme to discretize both the adjoint problem and the forward one; the second option consists in deriving the adjoint of the numerical scheme used for the forward problem. The

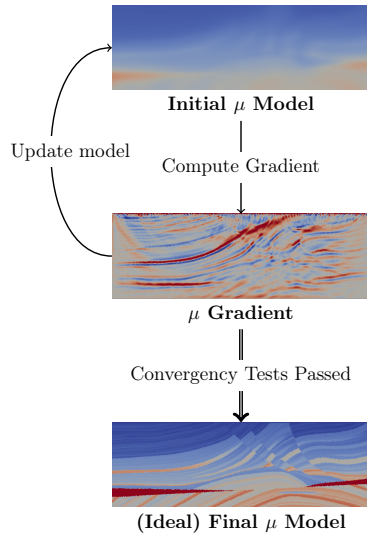


Figure 2: Algorithm illustration on Marmousi

second method passes exactly the adjoint test and guarantees the invertibility of the Hessian of J . However, it requires to implement and to optimize two different numerical schemes.

This question has been addressed in [4] for finite difference methods and the conclusion is that the best option could be the first one. We compare, here, the impact of the two strategies in a RK-DG schemes context. We also analyze the effect of the basis functions (Lagrange or Bézier polynomials) and of the time schemes (RK2, RK4, AB3) on the efficiency of the FWI algorithm.

References

- [1] R-E Plessix, *Geophysical Journal International* 167(2):495–503, 2006.
- [2] Bernardo Cockburn. *ZAMM-Journal of Applied Mathematics and Mechanics*, 83(11):731–754, 2003.
- [3] Ziv Sirkes and Eli Tziperman, *Monthly Weather Review*, 125(12):3373–3378, 1997.
- [4] Alain Sei and William W. Symes, *Mathematical and Computer Modelling*, 1995

Reflection matrix approach for ultrasonic imaging in heterogeneous media

L. A. Cobus^{1,*}, William Lambert¹, Mathias Fink¹, Alexandre Aubry¹

¹Institut Langevin, ESPCI Paris, CNRS, PSL University, 1 rue Jussieu, 75005 Paris, France

*Email: laura.cobus@espci.fr

Abstract

We present a reflection matrix approach for wave imaging through heterogeneous media. The idea is that a wide range of information can be obtained via the mathematical projection of the reflection matrix between various geometrical bases. This approach enables compensation for common imaging problems such as aberration, multiple scattering and multiple reflections. Here, the concepts are introduced and demonstrated in the context of ultrasound imaging.

Keywords: matrix approach, acoustics, imaging, scattering, wave propagation

1 Introduction

Classical wave imaging is limited in depth and resolution by variations in the refractive index of the medium under investigation. When such variations cause the equivalence of time-of-flight and target to be lost, then conventional imaging techniques fail. Slow variations cause distortion of the propagating wavefront, aberrating the resulting image, while smaller variations cause multiple scattering, adding noise to the image. Most conventional imaging modalities in reflection, such as ultrasonic echography or optical coherence tomography, are based on a temporal and confocal discrimination of singly-scattered waves. However, effects such as distortion result in a temporal and spatial ‘spreading’ of the point spread function. This loss of information inherent in the confocal approach is especially significant in heterogeneous media.

To overcome the fundamental limits of aberration and multiple scattering, there has been a growing interest in *matrix approaches* for imaging. These consist of the acquisition of an entire matrix of responses between different inputs and outputs, whether in transmission or reflection. While most of the work in this area has to date been performed in the transmission geometry, the reflection matrix [1] (the more relevant for non-invasive medical imaging) also has diverse potential for transport and control. However, only a few studies have attempted to apply this

approach to imaging [2–4]. Here, we present a reflection matrix approach for wave imaging that can cope with issues such as aberration and multiple scattering. The method is based on the projection of the reflection matrix between various geometrical bases, which enables information not available with confocal approaches to be extracted and exploited.

2 Imaging with the reflection matrix

In general, the reflection matrix \mathbf{R} can be described as mapping the responses between points of a geometrical basis to points located in another (or the same) basis. For ultrasound imaging performed with a transducer array, three bases are relevant: the *transducer*, *far-field* and *focused* bases [Fig. 2(a)]. In principle, \mathbf{R} can be acquired experimentally in any of these bases via beamforming: for example, by emitting and receiving with individual elements of the array (whose locations are defined by vector \mathbf{u}), \mathbf{R} is acquired in the transducer basis, now expressed as $\mathbf{R}_{\mathbf{u}\mathbf{u}}$. Emitting/receiving plane waves of different angles θ gives $\mathbf{R}_{\theta\theta}$ (the far-field). Using focused beams would give $\mathbf{R}_{\mathbf{r}\mathbf{r}}$ in the focused basis (focal points located at $\mathbf{r} \equiv \mathbf{x} + \hat{z}z$, where \mathbf{x} is lateral position and z is depth); however, such acquisition sequences are prohibitively time-consuming, as scanning of the focused beam in reception is required for each emission. Happily $\mathbf{R}_{\mathbf{r}\mathbf{r}}$ can be calculated from \mathbf{R} in any other basis.

Sound propagation between points of any two bases can be described by a matrix of appropriate Green’s functions. For example, propagation between the far-field and the focused bases is modeled by $\mathbf{G}_{\theta\mathbf{r}}(\omega)$, whose elements are

$$\mathbf{G}_{\theta\mathbf{r}}(\mathbf{r}_{\text{in}}, \theta_{\text{in}}, \omega) = e^{[ik(z_{\text{in}} \cos \theta_{\text{in}} + x_{\text{in}} \sin \theta_{\text{in}})]}, \quad (1)$$

where $\omega = 2\pi f$ is the angular frequency of the waves and $k = \omega/c$ is the wave number. Thus, $\mathbf{R}_{\theta\theta}$ can be projected into the focused basis via:

$$\mathbf{R}_{\mathbf{r}\mathbf{r}} = \sum_{\delta\omega} \mathbf{G}_{\theta\mathbf{r}}^*(\omega) \times \mathbf{R}_{\theta\theta}(\omega) \times \mathbf{G}_{\theta\mathbf{r}}^\dagger(\omega) \quad (2)$$

where $*$ is the complex conjugate, \dagger the conjugate transpose, \times represents a matrix product

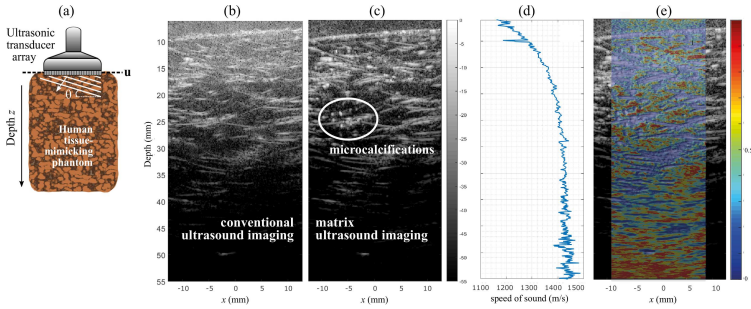


Figure 1: (a) The ultrasonic transducer array is placed in contact with a breast phantom. The transducer basis corresponds to points \mathbf{s} in vect \mathbf{u} . The far-field basis corresponds to \mathbf{t} emission/reception of plane-waves with different angles θ . Images are calculated from the diagonal of $\mathbf{R}_{\mathbf{r}\mathbf{r}}$, (b) assuming a spatially-invariant speed of sound, and (c) using $c(z)$. (d) $c(z)$ for the breast phantom is shown. (e) A map of multiple scattering inside the phantom is shown superimposed on the image.

and $\delta\omega$ is the acoustic bandwidth.

$\mathbf{R}_{\mathbf{r}\mathbf{r}}$ can be thought of as containing responses between *virtual transducers* distributed throughout the medium [2]. The signal in the diagonal elements of $\mathbf{R}_{\mathbf{r}\mathbf{r}}$ is equivalent to that obtained using confocal methods; thus, images [Fig. 2(b,c)] are calculated via $I(x, z) \equiv \mathbf{R}(\mathbf{r}_{\text{in}} = \mathbf{r}_{\text{out}})$. However, the off-diagonal elements hold an abundance of additional information. In particular, they enable a direct measurement of focus quality everywhere inside the medium – an objective measure of image reliability. We can furthermore calculate spatial maps of medium parameters such as the amount of multiple scattering (an important bio-marker for tissue), and sound speed as a function of depth $c(z)$ [Fig. 2(e,d)]. Knowledge of $c(z)$ enables the calculation of a clean image even through layers of fat or muscle tissue. As shown in Fig. 2(c), this method can uncover hidden features such as microcalcifications (a bio-marker for cancer).

Finally, examining the reflection matrix in different bases gives different information; for example, $\mathbf{R}_{\theta\theta}$ is sensitive to multiple reflections between parallel surfaces, thus enabling suppression of this signal for better imaging.

3 Conclusion

The reflection matrix holds much more information than is available with conventional imaging techniques. By studying this matrix in various geometrical bases, we can measure the spatial

variation of sound speed and multiple scattering, and compensate for wavefront distortion and multiple reflections in heterogeneous media.

References

- [1] S. M. Popoff, A. Aubry, G. Lerosey, M. Fink, A. C. Boccara, and S. Gigan, Exploiting the Time-Reversal Operator for Adaptive Optics, Selective Focusing, and Scattering Pattern Analysis, *Physical Review Letters* **107** (2011), pp. 263901.
- [2] J.-L. Robert and M. Fink, Green's function estimation in speckle using the decomposition of the time reversal operator: Application to aberration correction in medical imaging, *Journal of the Acoustical Society of America* **123** (2008), pp. 866–77.
- [3] A. Badon, D. Li, G. Lerosey, A. C. Boccara, M. Fink, and A. Aubry, Smart optical coherence tomography for ultra-deep imaging through highly scattering media, *Science Advances* **2** (2016), pp. e1600370.
- [4] S. Kang, P. Kang, S. Jeong, Y. Kwon, T. D. Yang, J. H. Hong, M. Kim, K.-D. Song, J. H. Park, J. H. Lee, M. J. Kim, K. H. Kim, and W. Choi, High-resolution adaptive optical imaging within thick scattering media using closed-loop accumulation of single scattering, *Nature Communications* **8** (2017), pp. 2157.

**Introducing the Random Anti-laser:
Coherent Perfect Absorption in Disordered Media**

Stefan Rotter^{1,*}, Kevin Pichler¹, Matthias Kühmayer¹, Julian Böhm², Andre Brandstötter¹, Philipp Ambichl¹, Ulrich Kuhl²

¹Institute for Theoretical Physics, Vienna University of Technology (TU Wien), Austria

²Institut de Physique de Nice, Université Côte d'Azur, CNRS, Nice, France

*Email: stefan.rotter@tuwien.ac.at

Abstract

I will present the concept of random anti-lasing, i.e., the time-reverse of random lasing. In the same way as a random laser emits a spatially complex but coherent wave at its first lasing threshold, the random anti-laser absorbs such a complex incoming field perfectly. We recently implemented this concept in a microwave experiment, where an absorber is embedded in the middle of a disordered medium [1]. Measuring the 8×8 scattering matrix of this structure allows us to calculate and then generate an incoming wave field that gets absorbed by more than 99.7% inside the disorder. Our setup is scalable in the number of involved modes and can easily be transferred to other wave scattering systems.

Keywords: wave scattering, disordered media, wave front shaping

1 Introduction and Theory

A very promising concept that has emerged from the field of non-Hermitian wave engineering is that of coherent perfect absorption [2–4] – an effect corresponding to the time-reversal of coherent emission of radiation at the lasing threshold. Coherent perfect absorbers (CPAs) have already been realized in a number of experiments [3, 4], but have remained limited to setups involving simple slab geometries. Here we combine the concept of coherent perfect absorption with that of random lasing [5]. A random laser is a disordered gain medium that is pumped sufficiently strongly to emit coherent laser light. Time-reversing such a random laser mode results in a highly complex wave state that impinges on the disordered structure and gets perfectly absorbed there (without any back-reflection to the asymptotic region).

The crucial quantity behind the CPA concept is the scattering matrix S , which relates the injected fields to the outgoing ones, $\psi_{\text{out}} = S\psi_{\text{in}}$. In Hermitian systems, zeros of the S -

matrix are generally located in the upper half ($\text{Im}(\nu) > 0$) of the complex plane of frequency ν , whereas poles are located in the lower half ($\text{Im}(\nu) < 0$). Adding gain to the system moves the poles up towards the real ν -axis where the system turns into a random laser as soon as the first pole hits the real ν -axis. Conversely, adding loss to the medium will turn it into a random anti-laser (disordered CPA) at those frequencies and loss values where one of the S -matrix zeros crosses the real ν -axis. At these parameter configurations, a random anti-laser mode ψ_{CPA} is an eigenstate of the S -matrix with eigenvalue $\lambda_{\text{CPA}} = 0$, i.e. $S\psi_{\text{CPA}} = 0$, where ψ_{CPA} is the incoming radiation field and the empty 0-field is the outgoing one.

2 Experimental realization

Our experimental setup consists of an aluminum waveguide where a disordered medium is implemented by 60 randomly placed cylindrical Teflon scatterers, see Fig. 1a. Four transverse modes are open at the operation frequency, requiring four antennas on each side (left and right) to control all degrees of freedom of the injected microwave field. The absorption strength inside the waveguide can be tuned by simply varying the length of a monopole antenna placed in the center of the scattering region. This microwave setup allows us to measure the full scattering matrix of the disordered medium as well as to inject arbitrarily shaped wavefronts into the disorder. Our experimental procedure to realize a random anti-laser is now the following: we first measure the S -matrix of the system as a function of frequency (in a broad interval to ensure that many S -matrix zeros are contained in it) and of the absorption strength of the central absorbing antenna (as determined by the penetration depth into the waveguide). In a next step, we evaluate the eigenvalues of these S -matrices and identify those parameter configurations for which the absolute value of the small-

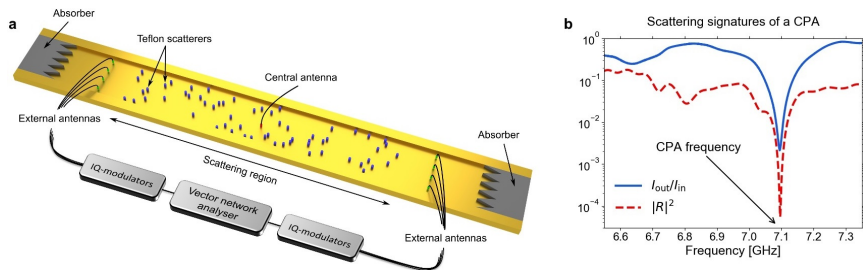


Figure 1: (a) Experimental setup of the random anti-laser: microwaves are injected through eight external antennas into an aluminum waveguide, which contains a set of randomly placed Teflon scatterers emulating a disordered medium (the top plate covering the entire waveguide is not shown). A monopole antenna in the center of the disordered region (central antenna) absorbs the microwave field with a degree that can be tuned by its penetration into the waveguide. (b) Scattering signatures of a CPA state: Ratio between outgoing (I_{out}) and incoming (I_{in}) intensity of a CPA state injected by the external antennas compared to the reflection signal R measured at the central antenna when injecting microwaves there.

est S -matrix eigenvalue dips almost to zero. In the last step, we inject the S -matrix eigenstate with the smallest eigenvalue (the CPA state) into the system and evaluate its properties, in particular its degree of absorption.

3 Results and Discussion

Following the protocol outlined in section 2, we find CPA states whose injected intensity gets absorbed by more than 99.78%, as illustrated by the blue curve in Fig. 1b that shows the ratio between the outgoing and the incoming microwave intensity (I_{out}/I_{in}) of a CPA state as a function of the signal frequency. Since we expect that a CPA state is primarily absorbed by the central antenna (and less by global absorption in the metallic waveguide), the time-reverse of this state should be a harmonic signal that enters through the central antenna without any back-reflection. Indeed, we find by injecting microwaves through the central antenna that its frequency-dependent reflection coefficient $|R|^2$ shows a pronounced minimum close to the frequency where we found the CPA state independently, see red dashed curve in Fig. 1b.

4 Conclusions

In summary, we present the first experimental realization of a random anti-laser, which provides proof of principle that coherent perfect ab-

sorption can also be realized in arbitrarily composed systems such as in disordered media. We expect our findings [1] to be relevant for practical applications such as perfect focusing of electromagnetic signals and sound fields in complex environments such as in an office space or in biological tissue. Our results also serve as a bridge between the two highly active communities of wavefront shaping and non-Hermitian physics.

References

- [1] K. Pichler et al., Random anti-lasing through coherent perfect absorption in a disordered medium, *Nature* **567**, 351 (2019).
- [2] Y.D. Chong et al., Coherent Perfect Absorbers: Time-Reversed Lasers, *Phys. Rev. Lett.* **105**, 053901 (2010).
- [3] W. Wan et al., Time-Reversed Lasing and Interferometric Control of Absorption, *Science* **331**, 889 (2011).
- [4] D.G. Baranov et al., Coherent perfect absorbers: linear control of light with light, *Nat. Rev. Mater.* **2**, 17064 (2017).
- [5] D.S. Wiersma, The physics and applications of random lasers, *Nat. Phys.* **4**, 359 (2008).

Maximum-likelihood estimation of target parameters in a time-evolving random medium

Clément J. Roussel^{1,*}, Arnaud Coatanhay¹, Alexandre Baussard¹

¹ENSTA Bretagne, Lab-STICC (UMR CNRS 6285), Brest, France

*Email: clement.roussel@ensta-bretagne.org

Abstract

We derive the stochastic differential equation (SDE) that models the scattering by a target embedded in a dynamic random medium for two target models: homodyned K scattering (HK) and generalized K scattering (GK). Using Euler-Maruyama’s scheme, we approximate the transition probabilities of the reflectivity. Using the Markov property, we can express the likelihood of a time-series. We show that it is possible to analytically maximize the likelihood with respect to a complex parameter Ψ_c . Using numerical experiments, the performances of the resulting maximum likelihood (ML) estimator for Ψ_c are assessed and illustrated.

Keywords: random media, stochastic differential equations, Markov processes, target

1 Introduction

For remote sensing applications, a target of interest should generally be placed in a complex natural or urbanized environment. A typical approach to model these multiple and heterogeneous environments is to consider them as gatherings of random scatterers. In static case, the quantification of the electromagnetic field reflected by these random scatterers and what is scattered by the target can raise some modeling difficulties. However, for fluctuating problems, the modeling issue becomes significantly harder and the identification of model parameters is far more challenging. This is due to the fact that, when electromagnetic waves are emitted toward a time-evolving random medium, the complex reflectivity of the medium, called clutter, is unpredictable.

Statistical models for the clutter Ψ_t have long been developed. More specifically, the random walk model (see [1]) represents $\Psi_t^{(cl)}$ as a sum of contributions from a population of discrete scatterers in the limit of infinitely many scatterers. $z_t = |\Psi_t|^2$ is known to be K -distributed for all t , but the dynamics of Ψ_t or z_t are unspecified and independence for $t, t + \Delta t$ is usually

assumed [2]. This is a limit for target detection schemes since this assumption breaks down for small Δt . We propose to use Field’s model (see [3] and [4]), which is an extension of the random walk model and represents the clutter as a product $\Psi_t^{(cl)} = x_t^{1/2} \gamma_t$ where x_t and $\gamma_t = \gamma_t^{(R)} + i \gamma_t^{(I)}$ solve the SDEs:

$$\begin{cases} dx_t = \mathcal{A}(1 - x_t)dt + (2\frac{\mathcal{A}}{\alpha}x_t)^{\frac{1}{2}} dW_t^{(x)} \\ d\gamma_t^{(R)} = -\frac{1}{2}\mathcal{B}\gamma_t^{(R)}dt + \frac{1}{\sqrt{2}}\mathcal{B}^{\frac{1}{2}}dW_t^{(R)} \\ d\gamma_t^{(I)} = -\frac{1}{2}\mathcal{B}\gamma_t^{(I)}dt + \frac{1}{\sqrt{2}}\mathcal{B}^{\frac{1}{2}}dW_t^{(I)}. \end{cases} \quad (1)$$

x_t is a \mathbb{R}^+ -valued slow process for the local power and γ_t is a \mathbb{C} -valued fast process for the scatterers phase coherence, and the W_t processes are brownian motions. The model is parameterized by three constants \mathcal{A} , \mathcal{B} and α , whose estimation has been addressed in [5].

2 Contributions

Two models of target are proposed in [3]. HK scattering assumes that the target reflectivity is a complex constant Ψ_c , while GK scattering assumes that the target reflectivity is $\Psi_c x_t$, *i.e.*:

$$\begin{aligned} \Psi_t &= x_t^{1/2} \gamma_t + \Psi_c \quad (\text{HK scattering}) \\ \Psi_t &= x_t^{1/2} \gamma_t + \Psi_c x_t \quad (\text{GK scattering}). \end{aligned}$$

If Ψ_t has real and imaginary parts R_t and I_t , we derive SDEs for the multidimensional stochastic process $Y_t = [x_t \ R_t \ I_t]^T$. We obtain:

$$\begin{aligned} \begin{bmatrix} dx_t \\ dR_t \\ dI_t \end{bmatrix} &= \beta_{\Psi_c}^{(iK)}(x_t, R_t, I_t) dt \\ &+ \Sigma_{\Psi_c}^{(iK)}(x_t, R_t, I_t) \begin{bmatrix} dW_t^{(x)} \\ dW_t^{(R)} \\ dW_t^{(I)} \end{bmatrix} \end{aligned} \quad (2)$$

where iK refers either to HK or GK, $\beta_{\Psi_c}^{(iK)}$ is a 3D vector and $\Sigma_{\Psi_c}^{(iK)}$ a 3×3 matrix. Applying Euler-Maruyama’s scheme [6] to (2), we get:

$$\begin{aligned} Y_{t+\Delta t} &\approx Y_t + \beta_{\Psi_c}^{(iK)}(Y_t) \Delta t \\ &+ \Sigma_{\Psi_c}^{(iK)}(Y_t) \Delta W_t, \end{aligned} \quad (3)$$

where the brownian increment ΔW_t is multivariate Gaussian distributed. Equation (3) is used to obtain Gaussian approximations for the transition probabilities $p_{\Psi_c}(Y_{t+\Delta t} = y | Y_t = x)$. This approximation is relevant for small Δt , which is the case for high sampling frequency observation systems, such as radars over the sea surface [7]. If a time series $\tilde{Y} = \{\tilde{Y}_0, \tilde{Y}_1, \dots, \tilde{Y}_n\}$ of Y_t is observed at times $t_0 < t_1 < \dots < t_n$, its likelihood is then by the Markov property:

$$\mathcal{L}_{\Psi_c} = p_{\Psi_c}(\tilde{Y}_0) \prod_{k=1}^n p_{\Psi_c}(Y_{t_k} = \tilde{Y}_k | Y_{t_{k-1}} = \tilde{Y}_{k-1}). \quad (4)$$

If Ψ_c is unknown, we state that a good estimator for it is the value $\tilde{\Psi}_c$ which maximizes the likelihood (4). Expression the optimality condition:

$$\frac{\partial \mathcal{L}_{\Psi_c}}{\partial \Psi_c}(\tilde{\Psi}_c) = 0, \quad (5)$$

we obtain analytical expressions for $\tilde{\Psi}_c$ in both HK and GK scattering as a function of the observed time series \tilde{Y} :

$$\begin{aligned} \tilde{\Psi}_c^{(HK)} &= F(\tilde{Y}) & (6) \\ \tilde{\Psi}_c^{(GK)} &= G(\tilde{Y}). & (7) \end{aligned}$$

Equations (6) and (7) express ML estimators for the target constant Ψ_c . They would lead naturally to target detection scheme in a random medium. Numerical simulations more specific to radar remote sensing of the sea surface are carried out to evaluate the ML estimators of Ψ_c in comparison with a naive ergodicity-based estimator. It is shown that the estimation bias is negligible and that the estimation variance is low for both HK and GK scattering. Dependence to the intensity $|\Psi_c|^2$ of the target and to the duration of \tilde{Y} are studied. It is shown that mostly in GK scattering (interaction between the target and random medium) does ML provide a significant advantage over the ergodicity-based estimator. The contribution reported above corresponds to an area of research on which we are working very actively and we continue to improve, [8].

References

[1] E. Jakeman and K. D. Ridley, *Modeling Fluctuations in Scattered Waves*, CRC Press: Series in Optics and Optoelectronics, Boca Raton, 2006.

- [2] K. Ward, R. Tough and S. Watts, *Sea Clutter: Scattering, the K distribution and Radar Performance*, 2nd edition, IET Radar, Sonar and Navigation, 2006.
- [3] T. R. Field, *Electromagnetic Scattering from Random Media*, Oxford University Press, Oxford, 2009.
- [4] C. J. Roussel, A. Coatanhay and A. Baussard, Forward and backward probabilistic inference of the sea clutter, to be published in *Waves in Random and Complex Media*, 2018.
DOI: 10.1080/17455030.2018.1453956
- [5] C. J. Roussel, A. Coatanhay and A. Baussard, Estimation of the parameters of stochastic differential equations for sea clutter, to be published in *IET Radar, Sonar and Navigation*, 2018.
DOI: 10.1049/iet-rsn.2018.5445
- [6] D. J. Higham, An Algorithmic Introduction to Numerical Simulation of Stochastic Differential Equations, in *Society for Industrial and Applied Mathematics*, Volume 43, Issue 3, pp. 525-546, 2001.
- [7] I. G. Cumming and F. H. Wong, *Digital Processing of Synthetic Aperture Radar Data*, Artech House, Norwood, 2005.
- [8] C. J. Roussel, A. Coatanhay and A. Baussard, Detection of a coherent scatterer in a random medium: an approach based on transition probabilities, submitted to *Waves in Random and Complex Media*, 2018.

Stochastic Models in Coordinate-Delay Synthetic Aperture Radar Imaging

Mikhail Gilman^{1,*}, Semyon Tsynkov¹¹Department of Mathematics, North Carolina State University, Raleigh, North Carolina, USA

*Email: mgilman@ncsu.edu

Abstract

We build stochastic models for synthetic aperture radar (SAR) imaging of targets that exhibit delayed scattering. Detection of scattering delay in SAR is hindered by the range-delay ambiguity, and the stochasticity of scattering adds uncertainty to the result. Using Monte-Carlo simulations, we obtain ensembles of coordinate-delay SAR images of instantaneous and delayed targets. Then, we explore the separation of likelihood-based metrics for those ensembles.

Keywords: SAR, range-delay ambiguity, Monte-Carlo simulation, Hellinger distance

1 Coordinate-delay SAR

By detecting and analyzing the scattering delay, we can learn important geometrical information about radar targets such as the presence of cavities, their internal structure, and characteristic size. Following [1], we will consider targets for which the relation between the incident u^i and scattered u^s fields is local in space and non-local in time. It is rendered by the spatio-temporal reflectivity function $\nu(t_z, \mathbf{z})$:

$$u^s(t, \mathbf{z}) = \int_0^\infty u^i(t - t_z, \mathbf{z}) \nu(t_z, \mathbf{z}) dt_z. \quad (1)$$

The coordinate-delay SAR (cdSAR) image is built from a series of scattering events with signals transmitted and received from the locations \mathbf{x}^n spaced over the synthetic aperture: $I(t_y, \mathbf{y}) = \sum_n \int \overline{P(t - t_{y,n})} u^s(t, \mathbf{x}^n) dt$. In this formula, $t_{y,n} = t_y + 2|\mathbf{x}^n - \mathbf{y}|/c$ is the sum of scattering and propagation delays, and \overline{P} is the complex conjugate of the frequency modulated transmitted pulse: $P(t) = e^{-i\omega_0 t} e^{-iBt^2/(2\tau)}$, $|t| \leq \tau$, where B and τ are pulse bandwidth and duration, respectively. In the linearized setting (1), the image is given by a convolution operator

$$I(t_y, \mathbf{y}) = \int_0^\infty dt_z \int d\mathbf{z} \nu(t_z, \mathbf{z}) W(t_y, \mathbf{y}; t_z, \mathbf{z}), \quad (2)$$

with the kernel defined as

$$\frac{W}{N\tau} = e^{-2i\xi\omega_0/B} \operatorname{sinc} \xi \int_{-1/2}^{1/2} e^{2i\eta s} e^{i\kappa\xi s^2} ds. \quad (3)$$

In (3), $\operatorname{sinc} x = \sin(x)/x$, $\xi_r = B(y_2 - z_2) \sin \theta/c$, $\xi_d = B(t_y - t_z)/2$, $\xi = \xi_r + \xi_d$, $\kappa = \varphi_T^2 \omega_0/B$, N is the number of pulses per the synthetic array, $\eta = \varphi_T \omega_0(y_1 - z_1) \sin \theta/c$, φ_T is the angular aperture size, θ is the incident angle, and the indices 1 and 2 denote the cross-range and range coordinates, respectively.

The range-delay ambiguity is due to a combination of range- and time-dependent terms in ξ , and is controlled by the value of κ . If $\kappa \rightarrow 0$, then the integral in (3) is just $\operatorname{sinc} \eta$. Hence, the dependence of W on ξ_r disappears and the two terms in ξ cannot be separated. In this case, we see that the cdSAR image (2) will be constant along the lines $y_2 \sin \theta + ct_y/2 = \text{const}$.

2 Stochastic scatterers and cdSAR

Speckle in SAR [2] is seen as rapid and strong variations of the observed reflectivity of an extended scatterer whereas the true quantities of interest vary gradually and smoothly. Due to a large parameter ω_0/B in the exponent in (3), the kernel in (2) oscillates rapidly and thus emphasizes the singularities of ν in the directions z_2 and t_z . Typically, the reflectivity is rough on the scale of the wavelength $\lambda_0 = 2\pi c/\omega_0$, while the size of the resolution cell in range is $\sim c/B \gg \lambda_0$. The following stochastic model proved effective in standard SAR [2]. It simulates a large number of point scatterers that are randomly positioned inside each resolution cell and represent the singularities of ν :

$$\nu_b(t_z, \mathbf{z}) = \delta(t_z) \mu_b(\mathbf{z}). \quad (4)$$

In (4), $\mu_b(\mathbf{z})$ is a two-dimensional circular Gaussian white random field:

$$\langle \mu_b(\mathbf{z}) \rangle = 0, \quad \langle \overline{\mu_b(\mathbf{z})} \mu_b(\mathbf{z}') \rangle = \sigma_b^2 \delta(\mathbf{z} - \mathbf{z}'). \quad (5)$$

In (5), σ_b^2 is a deterministic parameter that characterizes the average reflectivity of a homogeneous extended scatterer.

As an extension to (4)–(5), we introduce two new stochastic scatterer models: ν_l is a delayed point scatterer and ν_s is an inhomogeneous in-

stantaneous scatterer:

$$\nu_t(t_z, \mathbf{z}) = \mu_t(Bt_z/2)\delta(\mathbf{z} - \mathbf{z}_d), \quad (6)$$

$$\nu_s(t_z, \mathbf{z}) = \mu_s(B(z_2 - z_{d2}) \sin \theta/c) \cdot \delta(t_z)\delta(z_1 - z_{d1}), \quad (7)$$

where $\mathbf{z}_d = (z_{d1}, z_{d2}, 0)$ is the reference location of the inhomogeneity. In (6)–(7), $\mu_{s,t}(\xi)$ are inhomogeneous one-dimensional circular Gaussian white random processes described by

$$\langle \overline{\mu_{s,t}(\xi)\mu_{s,t}(\xi')} \rangle = \sigma_{s,t}^2 F(\xi)\delta(\xi - \xi'),$$

where σ_s^2 and σ_t^2 are the averaged reflectivities of the corresponding scatterers, $0 \leq F \leq 1$, and we choose $F(\xi) = 0$ for $\xi < 0$ to account for the causality in (1). The justification for introducing stochasticity for ν_t may be seen in the presence of multiple cavity eigenmodes and/or multipath reflection. The form of F will characterize the scatterer: we choose $F(\xi) = 1$ for $0 \leq \xi \leq \xi_{\max}$ and zero otherwise, where ξ_{\max} describes the maximum scattering delay.

The reflectivities ν_s and ν_t of (6)–(7) are built so that they produce similar cdSAR images when the range-delay ambiguity is not resolved, e.g., when $\kappa \rightarrow 0$ (Section 1). Hence, we will use (6)–(7) to explore our ability to distinguish between the instantaneous and delayed scatterers. The background (clutter) (4)–(5) is added to (6)–(7) to create the overall reflectivity

$$\nu = \nu_b + \nu_t \quad \text{or} \quad \nu = \nu_b + \nu_s. \quad (8)$$

3 Monte-Carlo simulations

The autocorrelation of a cdSAR image can be obtained by substituting models (8) with (4)–(7) into (2) and subsequent averaging. Then, for given intensities σ_b^2 , σ_s^2 , and σ_t^2 , we can use the Monte-Carlo method to manufacture ensembles of cdSAR images (i.e., arrays of pixel values \mathbf{Q}) due to one of the two models in (8) with the corresponding multivariate Gaussian statistics. Optionally, we can add to the result an uncorrelated circular Gaussian term to represent the noise. If, on the other hand, we have an array \mathbf{Q} randomly generated as above or obtained by observations, then we can use the same statistics to calculate the probability density function (pdf) of \mathbf{Q} due to either of these models. Denoting these likelihood functions by $p_s(\mathbf{Q}) \equiv p_s(\mathbf{Q}; \sigma_b^2, \sigma_s^2)$ and $p_t(\mathbf{Q}) \equiv p_t(\mathbf{Q}; \sigma_b^2, \sigma_t^2)$, we calculate

$$\check{p}_t(\mathbf{Q}) = \max_{\sigma_b^2, \sigma_t^2} p_t(\mathbf{Q}), \quad \check{p}_s(\mathbf{Q}) = \max_{\sigma_b^2, \sigma_s^2} p_s(\mathbf{Q}).$$

Other parameters, such as \mathbf{z}_d , can be added to the set of optimization variables.

Although the multivariate Gaussian models can yield any data with nonzero pdf, we expect that on average, $\check{p}_t(\mathbf{Q}) \geq \check{p}_s(\mathbf{Q})$ for the data produced from the first model in (8), and $\check{p}_t(\mathbf{Q}) \leq \check{p}_s(\mathbf{Q})$ for the second one. In order to characterize the separation between the two models numerically, we use the Hellinger distance $H[f, g]$ between two pdfs, $f(x)$ and $g(x)$, defined as $H[f, g] = \frac{1}{2} \int (\sqrt{f(x)} - \sqrt{g(x)})^2 dx$, see [3]. In the limiting cases, $H[f, g] = 1$ when f and g are completely disjoint, and $H[f, f] = 0$.

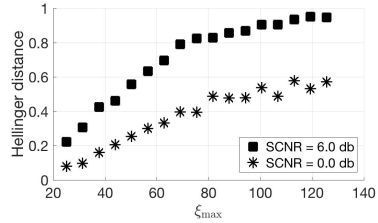


Figure 1: Plot of the Hellinger distance vs. ξ_{\max} .

We calculate the Hellinger distance between the pdfs of $\log(\check{p}_t(\mathbf{Q})/\check{p}_s(\mathbf{Q}))$ for the ensembles generated according to the two models in (8). Figure 1 plots this distance for two different values of signal to clutter and noise ratio (SCNR) and $\kappa = 1/4$. We can see that with high SCNR and large scattering delays ξ_{\max} , the models in (8) are safely distinguishable.

Acknowledgements

This material is based upon work supported by the US Air Force Office of Scientific Research under award number FA9550-17-1-0230.

References

- [1] Matthew Ferrara, Andrew Homan, and Margaret Cheney, Hyperspectral SAR, *IEEE Transactions on Geoscience and Remote Sensing*, **55**(3) (2017), pp. 1–14.
- [2] Chris Oliver and Shaun Quegan, *Understanding Synthetic Aperture Radar Images*, Artech House, Boston, 1998.
- [3] David Pollard, *A User's Guide to Measure Theoretic Probability*, Cambridge University Press, 2002.

Asymptotic model for elastodynamic scattering by a small surface-breaking defect

Marc Bonnet^{1,*}, Marc Deschamps², Eric Ducasse², Aditya Krishna²

¹POEMS (CNRS, INRIA, ENSTA), ENSTA, Palaiseau, France

²Univ. Bordeaux, I2M-APy, UMR 5295, Talence, France

*Email: mbonnet@ensta.fr

Abstract. We establish a leading-order asymptotic model for the scattering of elastodynamic fields by small surface-breaking defects in elastic solids. The asymptotic form of the representation formula of the scattered field is written in terms of the elastodynamic Green's tensor, which is in fact available in semi-analytical form for some geometrical configurations that are of practical interest in ultrasonic NDT configurations.

Keywords: elastodynamics, surface-breaking defect, asymptotic expansion

Asymptotic formulations for the scattering of waves by small obstacles embedded in the interior of the propagation domain has elicited significant attention (especially so for obstacles in the free space \mathbb{R}^d), see e.g. [1, 2]. This communication addresses a different case which has received comparatively little attention so far, namely that of *superficial* obstacles (such as indentations) lying at the (possibly curved) surface of a spatially bounded medium.

As a practical motivation, asymptotic models of the kind considered here will be useful for modelling non-destructive testing of embedded pipes, tubes and composite plates. In addition to permitting good interpretation of fields scattered by small superficial defects at moderate computational costs, even for 3D situations, this work paves the way towards versions of imaging methods such as the topological derivative [2, 3] specifically aimed at finding flaws lying at the inner or outer surface of tested structures.

Elastodynamic scattering by a small surface-breaking defect Let a reference elastic solid body occupy the open domain $\Omega \subset \mathbb{R}^3$ (with material characterized by the elasticity tensor \mathcal{C} and the mass density ρ). We consider a flawed solid $\Omega_{\varepsilon,z}$ featuring a small indentation of characteristic radius ε around a point \mathbf{z} of the surface $S := \partial\Omega$, consisting in matter removal occurring in a small volume $v_{\varepsilon,z} \subset \Omega$ adjacent to S (Fig. ??). The surface S is smooth and traction-free in a neighborhood of \mathbf{z} . A time-harmonic excitation (e.g. tractions on a surface portion separated from \mathbf{z}) is applied to either

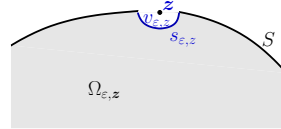


Figure 1: Two-scale asymptotics: notation.

solid Ω and $\Omega_{\varepsilon,z}$, giving rise to displacement fields \mathbf{u} and \mathbf{u}_ε , respectively.

The scattered displacement field $\mathbf{v}_\varepsilon := \mathbf{u}_\varepsilon - \mathbf{u}$ caused by the superficial flaw can be shown to satisfy the boundary integral equation (BIE)

$$\begin{aligned} \frac{1}{2} \mathbf{v}_\varepsilon(\mathbf{x}) + \int_{s_{\varepsilon,z}} \mathbf{t}[\mathbf{G}_\omega^k(\mathbf{y}, \mathbf{x})] \cdot \mathbf{v}_\varepsilon dS_y \\ = - \int_{s_{\varepsilon,z}} \mathbf{G}_\omega(\mathbf{y}, \mathbf{x}) \cdot \mathbf{t}[\mathbf{u}](\mathbf{y}) dS_y \quad \mathbf{x} \in s_{\varepsilon,z}, \end{aligned} \quad (1)$$

where $s_{\varepsilon,z} := \Omega \cap \partial v_{\varepsilon,z}$, $\mathbf{t}[\mathbf{w}] := \mathbf{n} \cdot \mathcal{C} : \nabla^s \mathbf{w}$ defines the traction operator, and \mathbf{G}_ω is the elastodynamic Green's tensor of Ω satisfying suitable homogeneous boundary conditions on S (in particular $\mathbf{t}[\mathbf{G}_\omega^k(\cdot, \mathbf{x})] = \mathbf{0}$ on S near \mathbf{z}).

Following the intuitive idea that the flawed solid resembles an indented half-space when observed near \mathbf{z} at the (small) length scale ε , we introduce the half-space $E := \{\tilde{\mathbf{x}} = (\tilde{x}_1, \tilde{x}_3), \tilde{x}_3 < 0\}$ (with $\tilde{\mathbf{x}}' := (\tilde{x}_1, \tilde{x}_2)$) and let points $\mathbf{x} \in \Omega$ in a neighborhood U of \mathbf{z} be parameterized as

$$\mathbf{x} = \Phi(\tilde{\mathbf{x}}) := \mathbf{z} + \tilde{\mathbf{x}}' + F(\tilde{\mathbf{x}}')\mathbf{e}_3 + \tilde{x}_3\mathbf{n}(\tilde{\mathbf{x}}')$$

where the C^2 function F is such that $\mathbf{x} = \mathbf{z} + \tilde{\mathbf{x}}' + F(\tilde{\mathbf{x}}')\mathbf{e}_3$ gives a local parametrization of S , and verifies $F(\mathbf{0}) = \partial_1 F(\mathbf{0}) = \partial_2 F(\mathbf{0}) = \partial_{12} F(\mathbf{0}) = 0$. Then, letting \mathcal{V} denote a fixed indentation made to E around its origin, a family of indentations $v_{\varepsilon,z}$ of vanishing size ε is defined through

$$\mathbf{x} = \Phi(\varepsilon\tilde{\mathbf{x}}), \quad \mathbf{x} \in v_{\varepsilon,z}, \quad \tilde{\mathbf{x}} \in \mathcal{V}$$

allowing to map $v_{\varepsilon,z}$ and $s_{\varepsilon,z}$ on fixed sets of parametric coordinates as ε varies.

The asymptotic behavior of \mathbf{v}_ε as $\varepsilon \rightarrow 0$ is now found by (a) setting $\mathbf{y} = \Phi(\varepsilon\tilde{\mathbf{y}})$ and $\mathbf{x} = \Phi(\varepsilon\tilde{\mathbf{x}})$ in (1), (b) seeking the leading-order limiting form of the resulting integral equation (whose support is now the fixed surface $S :=$

$\partial V \cap E$) and (c) interpreting that limiting equation in terms of a BVP. Step (b) relies on the following representation of \mathbf{G}_ω near \mathbf{z} :

Proposition 1 *Let $(\tilde{\mathbf{y}}, \tilde{\mathbf{x}}) \in E \times E \mapsto \mathbf{G}_0^E(\tilde{\mathbf{y}}, \tilde{\mathbf{x}})$ denote the elastostatic Green's tensor of E satisfying the traction-free condition on ∂E . Let $V := U \cap \Omega$. There exist tensor-valued kernel functions \mathbf{H} and \mathbf{H}_c such that for any $V \times V \ni (\mathbf{y}, \mathbf{x}) = \Phi(\tilde{\mathbf{y}}, \tilde{\mathbf{x}})$ the decomposition*

$$\mathbf{G}_\omega(\mathbf{y}, \mathbf{x}) = \mathbf{G}_0^E(\tilde{\mathbf{y}}, \tilde{\mathbf{x}}) + \mathbf{H}(\tilde{\mathbf{y}}, \tilde{\mathbf{x}}; \tilde{\mathbf{x}}) + \mathbf{H}_c(\mathbf{y}, \mathbf{x})$$

holds. Moreover: (i) $\mathbf{H}_c(\cdot, \mathbf{x}) \in H^1(V)$ with $\|\mathbf{H}_c(\cdot, \mathbf{x})\|_{H^1(V)} \leq C$ uniformly in $\mathbf{x} \in V$, (ii) $\mathbf{c} \mapsto \mathbf{H}(\mathbf{a}, \mathbf{b}; \mathbf{c})$ is C^1 for all $\mathbf{a} \neq \mathbf{b}$, (iii) $(\mathbf{a}, \mathbf{b}) \mapsto \mathbf{H}(\mathbf{a}, \mathbf{b}; \mathbf{c})$ is positively homogeneous with degree -1, and (iv) $\mathbf{H}(\mathbf{a}, \mathbf{b}; \mathbf{0}) = \mathbf{0}$ for all $\mathbf{a} \neq \mathbf{b}$.

Proof. The given decomposition is established by recasting a BVP governing \mathbf{G}_z in V using the rectified coordinates $\tilde{\mathbf{x}}$, in particular (i) finding the BVP in E defining \mathbf{H} and using its partial Fourier version to show homogeneity, and (ii) (by linear superposition) showing that \mathbf{H}_c solves a weak problem to which the Lax-Milgram lemma is applicable. \square

Using Prop. 1 with $\mathbf{y} = \Phi(\varepsilon\tilde{\mathbf{y}})$, $\mathbf{x} = \Phi(\varepsilon\tilde{\mathbf{x}})$, and observing that $(\tilde{\mathbf{y}}, \tilde{\mathbf{x}}) \mapsto \mathbf{G}_0^E(\tilde{\mathbf{y}}, \tilde{\mathbf{x}})$ is also positively homogeneous with degree -1, we find

$$\begin{aligned} \mathbf{G}_\omega(\mathbf{y}, \mathbf{x}) &= \varepsilon^{-1} \mathbf{G}_0^E(\tilde{\mathbf{y}}, \tilde{\mathbf{x}}) + o(1), \\ t[\mathbf{G}_\omega](\mathbf{y}, \mathbf{x}) &= \varepsilon^{-2} t[\mathbf{G}_0^E](\tilde{\mathbf{y}}, \tilde{\mathbf{x}}) + o(\varepsilon^{-1}) \end{aligned}$$

i.e. \mathbf{G}_ω is dominated as the length scale vanishes by \mathbf{G}_0^E . This, together with $dS_{\tilde{\mathbf{y}}} = (1 + o(1))\varepsilon^2 dS_{\tilde{\mathbf{y}}}$, allows to show that the limiting form of (1) is an *elastostatic* integral equation for a displacement field in $E_V := E \setminus \bar{V}$ (the half-space with a normalized indentation). More precisely, the asymptotic approximation of \mathbf{v}_ε on the flaw surface $s_{\varepsilon, z}$ is found as follows:

Theorem 1 *The following expansion holds, in $H^{1/2}(s_{\varepsilon, z})$ norm:*

$$\mathbf{v}_\varepsilon(\mathbf{x}) = \varepsilon \mathbf{V}(\tilde{\mathbf{x}}) + o(\varepsilon), \quad \mathbf{x} = \Phi(\varepsilon\tilde{\mathbf{x}}), \tilde{\mathbf{x}} \in S,$$

where \mathbf{V} solves the elastostatic BVP in E_V :

$$\begin{aligned} \mathcal{L}_0 \mathbf{V} &= \mathbf{0} \quad \text{in } E_V, \quad |\mathbf{V}| \rightarrow 0 \quad \text{for } |\tilde{\mathbf{x}}| \rightarrow \infty \\ t[\mathbf{V}] &= \mathbf{n} \cdot \mathbf{C} : \nabla^s \mathbf{u}(z) \quad \text{on } S, \\ t[\mathbf{V}] &= \mathbf{0} \quad \text{on } \partial E_V \setminus S \end{aligned}$$

Proof. The shown BVP results from interpreting the leading-order limiting BIE. The given expansion of \mathbf{v}_ε is justified using the BIE solved by the expansion error, showing that its r.h.s. decays fast enough in $H^{1/2}(s_{\varepsilon, z})$ norm w.r.t. ε and its governing integral operator is boundedly invertible (uniformly for small enough ε). \square

Then, the limiting form of the integral representation theorem applied to $\mathbf{v}_\varepsilon(\mathbf{x})$, $\mathbf{x} \neq \mathbf{z}$ becomes

$$\begin{aligned} \mathbf{v}_\varepsilon(\mathbf{x}) &= \varepsilon^3 |\mathcal{V}| \{ \nabla^s \mathbf{G}_\omega(\mathbf{z}, \mathbf{x}) : \mathcal{A} : \nabla^s \mathbf{u}(z) \\ &\quad - \rho \omega^2 \mathbf{G}_\omega(\mathbf{z}, \mathbf{x}) \cdot \mathbf{u}(z) \} + o(\varepsilon^3), \quad (2) \end{aligned}$$

where the *elastic moment tensor* (EMT) \mathcal{A} is given explicitly in terms of \mathbf{V} .

Discussion The asymptotic representation formula (2) relies on the elastodynamic Green's tensor \mathbf{G}_ω for the defect-free solid. While \mathbf{G}_ω has in general to be evaluated numerically, it is available in analytical form (in Fourier/Laplace variables associated with space/time) for some configurations (plates, tubes) that are of interest in NDT modelling, including in cases where material properties are anisotropic or layered [4].

The structure of formula (2) is the same as in the case of small internal defects. The surface-breaking nature of the defect is reflected in (i) the choice of Green's tensor and (ii) the value of the EMT \mathcal{A} being determined by \mathbf{V} . The latter does not depend on whether S is planar or curved at \mathbf{z} (while \mathbf{G}_ω depends on the curvature of S). In Prop. 1, $\mathbf{H} = \mathbf{0}$ if S is locally planar.

The foregoing analysis applies equally when time is treated in the Laplace domain rather than the frequency domain.

Numerical examples. We will present simulations of the scattering of an incident field by corrosion pits at the external surface of a cylindrical tube, considering various shapes for the flaw (half-ball, half-cube, triangular occlusion) for which the EMT is first computed using the FEM. These simulations exploit a previously-established semi-analytic formulation of the relevant Green's tensor [4].

References

- [1] Bendali A., Cocquet P.H., Tordeux S. Approximation by multipoles of the multiple acoustic scattering by small obstacles in three dimensions and application to the Foldy theory of isotropic scattering. *Arch. Ration. Mech. An.*, **219**:1017–1059 (2016).
- [2] Bonnet M. Inverse acoustic scattering using high-order topological derivatives of misfit functional. *Inverse Probl. Imag.*, **12**:921–953 (2018).
- [3] Dominguez N., Gibiat V., Esquerré Y. Time domain topological gradient and time reversal analogy: an inverse method for ultrasonic target detection. *Wave Motion*, **42**:31–52 (2005).
- [4] Mora P., Ducasse E., Deschamps M. Transient 3D elastodynamic field in an embedded multilayered anisotropic plate. *Ultrasonics*, **69**:106–115 (2016).

Equivalent point-source modeling of small obstacles for electromagnetic waves

Justine Labat^{1,*}, Victor Péron¹, Sébastien Tordeux¹¹EPC Magique 3D, UPPA-E2S, Inria Bordeaux Sud-Ouest, LMAP UMR CNRS 5142, Pau, France

*Email: justine.labat@inria.fr

Abstract

We develop reduced models to approximate the solution of scattering problem by electromagnetic obstacles that are small in comparison with the wavelength. Using the matched asymptotic expansions method, we investigate a meshless multi-scale approach where the scatterers are represented by equivalent point-sources. In the context of multiple scattering, we deduce from this a Foldy-Lax approximation whose accuracy and efficiency are illustrated with numerical simulations.

Keywords: Reduced models, Maxwell's equations, Multiple scattering

Introduction

The propagation of time-harmonic electromagnetic waves of angular frequency $\omega > 0$ in a homogeneous and isotropic dielectric infinite medium of electric permittivity $\varepsilon > 0$ and magnetic permeability $\mu > 0$ is described by an incident wave

$$\text{Re}(\mathbf{E}^{\text{inc}}(x) \exp(-i\omega t)), \quad x \in \mathbb{R}^3, \quad t > 0.$$

In the presence of a small and smooth auto-similar obstacle $\omega_\delta = \delta\omega \subset \mathbb{R}^3$ centered at the origin, whose characteristic length δ is very small compared to the wavelength $\lambda = \frac{2\pi}{\omega\sqrt{\mu\varepsilon}}$, the wave is scattered and gives birth to electromagnetic fields \mathbf{E}_δ and \mathbf{H}_δ satisfying the time-harmonic Maxwell equations

$$\begin{cases} \nabla \times \mathbf{E}_\delta - i\kappa \mathbf{H}_\delta = 0, \\ \nabla \times \mathbf{H}_\delta + i\kappa \mathbf{E}_\delta = 0, \end{cases}$$

where $\kappa = \frac{2\pi}{\lambda}$ denotes the wave-number. For a perfectly conducting obstacle, the domain of propagation Ω_δ is the exterior domain $\mathbb{R}^3 \setminus \overline{\omega_\delta}$ and the boundary condition reads as

$$\mathbf{n} \times \mathbf{E}_\delta = -\mathbf{n} \times \mathbf{E}^{\text{inc}} \quad \text{on } \partial\omega_\delta.$$

The existence of a unique solution is guaranteed by the hypothesis of outgoing wave at infinity given by the Silver-Müller radiation condition,

$$\lim_{|x| \rightarrow \infty} |x|(\mathbf{H}_\delta \times \hat{x} - \mathbf{E}_\delta) = 0 \quad \text{unif. in } \hat{x} = \frac{x}{|x|}.$$

Numerical techniques based on a discrete approximation of the geometry are limited and very expensive due to the smallness of the obstacle. To overcome these difficulties, we investigate two meshless approaches involving approximate solutions of the exterior Maxwell problem.

Equivalent point-source modeling

The first one is a volumical approach based on the method of matched asymptotic expansions [1]. This method consists in constructing distinct expansions of the solution in different regions of the domain of propagation with appropriate scales, and matching them in an intermediate region called the matching area. Far from the obstacle, the obstacle is modeled like a dipolar source around the origin. As a result,

$$\mathbf{E}_\delta \underset{\delta \rightarrow 0}{\sim} \mathcal{E}_{\text{elec}}[\mathbf{d}_\delta^{\text{E}}] + \mathcal{E}_{\text{mag}}[\mathbf{d}_\delta^{\text{H}}], \quad (1)$$

where $\mathcal{E}_{\text{elec}}[\mathbf{d}_\delta^{\text{E}}]$ (resp. $\mathcal{E}_{\text{mag}}[\mathbf{d}_\delta^{\text{H}}]$) is the electric field generated by an electric (resp. magnetic) dipole of moment $\mathbf{d}_\delta^{\text{E}} \in \mathbb{C}^3$ (resp. $\mathbf{d}_\delta^{\text{H}} \in \mathbb{C}^3$), given by

$$\begin{aligned} \mathcal{E}_{\text{elec}}[\mathbf{d}](x) = \frac{\exp(i\kappa r)}{r} \left[\left(\frac{2}{r^2} - \frac{2i\kappa}{r} \right) (\mathbf{d} \cdot \hat{x}) \hat{x} \right. \\ \left. + \left(-\frac{1}{r^2} + \frac{i\kappa}{r} + \kappa^2 \right) (\hat{x} \times \mathbf{d}) \times \hat{x} \right], \end{aligned}$$

$$\mathcal{E}_{\text{mag}}[\mathbf{d}](x) = \frac{\exp(i\kappa r)}{r} \left(\frac{1}{r} - i\kappa \right) (i\kappa \mathbf{d}) \times \hat{x},$$

where $r = |x|$. For the single-scattering case, the dipole moments will depend on the incident field, size and location of the scatterer. In particular, for a spherical obstacle, we have $\mathbf{d}_\delta^{\text{E}} = \delta^3 \mathbf{E}^{\text{inc}}(0)$ and $\mathbf{d}_\delta^{\text{H}} = -\frac{\delta^2}{2} \mathbf{H}^{\text{inc}}(0)$. For the multiple-scattering case, each obstacle $\omega_\delta^k = c_k + \delta\omega$ ($k = 1, \dots, N_{\text{obs}}$) is modeled as a dipolar source around its center c_k . Following (1), the electric field is approximated by

$$\sum_{k=1}^{N_{\text{obs}}} \mathcal{E}_{\text{elec}}[\mathbf{d}_{\delta,k}^{\text{E}}](x - c_k) + \mathcal{E}_{\text{mag}}[\mathbf{d}_{\delta,k}^{\text{H}}](x - c_k).$$

According to Foldy-Lax theory, the dipole moments depend not only on the incident fields, but also on all the other scattered fields,

$$\mathbf{d}_{\delta,k}^{\text{E}} = \delta^3 \alpha(\delta) \left\{ \mathbf{E}^{\text{inc}}(c_k) + \sum_{\ell=1, \ell \neq k}^{\text{N}_{\text{obs}}} \mathcal{E}_{\text{elec}}[\mathbf{d}_{\delta,\ell}^{\text{E}}](c_k - c_\ell) + \mathcal{E}_{\text{mag}}[\mathbf{d}_{\delta,\ell}^{\text{H}}](c_k - c_\ell) \right\},$$

with a similar expression for the magnetic moments $\mathbf{d}_{\delta,k}^{\text{H}}$. These expressions lead to a vectorial formulation involving 6N_{obs} unknowns. The coefficient $\alpha(\delta)$ differs with different levels of approximation. We define

$$\alpha(\delta) = \begin{cases} 1 & \text{: first Foldy model,} \\ 1 + \frac{3(\kappa\delta)^2}{10} & \text{: collected Foldy model,} \\ \frac{3i}{2(\kappa\delta)^3} \frac{j_1(\kappa\delta)}{h_1^{(1)}(\kappa\delta)} & \text{: modified Foldy model,} \end{cases}$$

where j_1 and $h_1^{(1)}$ denote the bessel function and the hankel function of the first kind, of order 1. The Born approximations are defined by neglecting the interactions between the obstacles.

Spectral method: the reference solution

The electric field has the integral representation

$$\mathbf{E}_\delta(x) = \sum_{k=1}^{\text{N}_{\text{obs}}} \nabla \times \int_{\partial\omega_k^\delta} \Phi(x, y) \mathbf{p}_k(y) ds_y, \quad x \in \Omega_\delta,$$

where $\Phi(x, y) = \frac{\exp(i\kappa|x-y|)}{4\pi|x-y|}$ denotes the Green function associated to the Helmholtz equation. The tangential densities \mathbf{p}_k solve the following boundary integral equations

$$\sum_{\ell=1}^{\text{N}_{\text{obs}}} \mathcal{M}_\Gamma^{k\ell} \mathbf{p}_\ell = -\mathbf{n} \times \mathbf{E}^{\text{inc}} \quad \text{on } \partial\omega_\delta^k, \quad (2)$$

where the magnetic potentials $\mathcal{M}_\Gamma^{k\ell} \boldsymbol{\lambda}$ are defined as an extension of

$$\mathbf{n}(x_\Gamma) \times \lim_{x \rightarrow x_\Gamma} \left(\nabla \times \int_{\partial\omega_\delta^\xi} \Phi(x, y) \boldsymbol{\lambda}(y) ds_y \right),$$

with $x_\Gamma \in \partial\omega_\delta^k$. The spectral method [2] consists in discretizing (2) into a local spectral basis associated with the vectorial Laplace-Beltrami operator with N_{mod} modes. For spherical obstacles, the basis is composed of the vector spherical harmonics $\nabla_{\mathbb{S}} Y_{n,m}$, $\text{curl}_{\mathbb{S}} Y_{n,m}$,

$$\mathbf{p}_\ell = \sum_{n=1}^{\text{N}_{\text{mod}}} \sum_{m=-n}^n p_{n,m}^{\ell,\perp} \nabla_{\mathbb{S}} Y_{n,m}^\ell + p_{n,m}^{\ell,\times} \text{curl}_{\mathbb{S}} Y_{n,m}^\ell,$$

where $Y_{n,m}^\ell(\hat{x}) = Y_{n,m}(\widehat{x - c_\ell})$. This formulation leads to the linear system developed in [3] with $2\text{N}_{\text{mod}}(\text{N}_{\text{mod}} + 2)\text{N}_{\text{obs}}$ degrees of freedom. The matrix becomes more ill-conditioned as the number of obstacles grows or the size of obstacles decreases. We make use of linear algebra tools, preconditionners and iterative solvers to perform simulations with thousands of spheres.

Numerical tests

The asymptotic models are validated with the spectral method, itself validated with finite element solutions provided by Montjoie code, in spherical geometries. Figure 1 shows the performance of the reduced models. The incident wave is an electromagnetic plane wave of wavelength $\lambda = 1.0$ and the medium contains five aligned spheres of radius δ varying between 10^{-6} and $10^{-2.75}$. The reference solution is the spectral solution truncated at the order $\text{N}_{\text{mod}} = 10$.

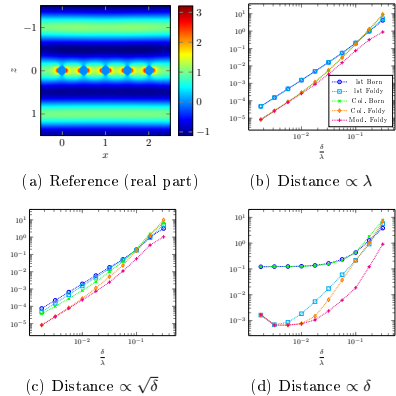


Figure 1: Relative L^2 -error depending on the obstacle size computed in the domain delimited by spheres of respective radius 15λ and 16λ .

References

- [1] J. Labat, V. Péron, S. Tordeux, *Asymptotic modeling of the electromagnetic scattering by small spheres perfectly conducting*, Research Report, 2018.
- [2] M. Ganesh, S. C. Hawkins, *A high-order algorithm for multiple electromagnetic scattering in three dimensions*, Numerical Algorithms, 2009.
- [3] Y. L. Xu, *Electromagnetic scattering by an aggregate of spheres*, Applied Optics, 1995.

Asymptotic expansions of Whispering Gallery Modes in graded index optical micro-cavities

Stéphane Balac¹, Monique Dauge¹, Zoïs Moitier^{1,*}

¹Univ Rennes, CNRS, IRMAR - UMR 6625, F-35000 Rennes, France

*Email: zois.moitier@univ-rennes1.fr

Abstract

We are interested in resonance frequencies of two dimensional dielectric cavities—a component of optical micro-resonators—and more specifically in resonances corresponding to whispering gallery modes (WGM). WGM are optical waves with high polar mode index, circling around the cavity and almost perfectly guided by total internal reflection. For a cavity of general shape with a varying optical index n (graded index optical cavity), using a phase amplitude ansatz, we have obtained asymptotic expansions of resonances as the polar mode index becomes large. We have also found sufficient conditions linking the curvature of the cavity boundary and the optical index for such expansions to hold.

Keywords: Helmholtz transmission problem; Resonances; WKB method.

1 Problem setting

Resonant modes in an optical micro-cavity are particular time-harmonic solutions to the source free Maxwell equations inside and outside the dielectric cavity. We consider a 2D setting, a situation that arises as a simplification of the 3D resonance problem, e.g. by using the effective index approach. It is well known that the 2D Maxwell setting is the combination of two sub-systems of equations referred to as transverse electric (TE) and transverse magnetic (TM). For brevity we report here only for the TM case.

We denote by Ω the bounded domain in \mathbb{R}^2 describing the dielectric cavity. The optical index n is 1 outside $\bar{\Omega}$ and coincides with a smooth function $n > 1$ in $\bar{\Omega}$. The resonance problem can be formulated as: Find $(k, u) \in \mathbb{C} \times H_{loc}^2(\mathbb{R}^2)$ with $u \neq 0$ such that

$$-\Delta u - k^2 n^2 u = 0 \quad \text{in } \mathbb{R}^2, \quad (1a)$$

$$u(r, \theta) = \sum_{m \in \mathbb{Z}} c_m H_m^{(1)}(kr) e^{im\theta} \quad r > R_0. \quad (1b)$$

Here $H_m^{(1)}$ refers to Hankel function of the first kind of order m . Equation (1b) expresses the ra-

diation condition at infinity in polar coordinates for R_0 large enough. For real k , it corresponds to the outgoing Sommerfeld's condition. It is known that the solutions (k, u) to problem (1) are such that k has a negative imaginary part.

For a circular cavity with constant index, asymptotic expansions of the resonances can be obtained using expansions of Bessel functions [1]. When n is not constant in $\bar{\Omega}$, this approach is not applicable.

2 Disk cavity with radially varying index

Let R be the radius of the disk and assume n is a smooth radial function $r \mapsto n(r)$. Then problem (1) can be reduced to a family of 1D radial problems depending on an integer $m \in \mathbb{Z}$ referred as the *polar mode index*:

$$-\frac{1}{m^2} \mathcal{L}w + Vw = \lambda w \quad (4)$$

where $V(r) = \left[\frac{n(R)R}{n(r)r} \right]^2 - 1$ is an effective potential, $k = \frac{m}{Rn(R)} \sqrt{1 + \lambda}$ and $\mathcal{L}w = \frac{n(R)^2 R^2}{n(r)^2 r} (rw)'$ is an elliptic operator. Since $V(R^-) = 0$ and $V(R^+) = n(R)^2 - 1 > 0$, we have a potential barrier at $r = R$. We note that $V'(R^-) = -2\tilde{\kappa}$ where

$$\tilde{\kappa} = \frac{1}{R} + \frac{n'(R)}{n(R)}. \quad (5)$$

We have identified three typical behaviors [2] for the solutions of (4), depending on the sign of $\tilde{\kappa}$, relying on the spectral theory of Schrödinger operators.

a) Half-triangular potential well. If $\tilde{\kappa} > 0$ then V is decreasing in a left neighborhood of R and has a local minimum at R . We have obtained an asymptotic expansion of the resonances in the form $k = m \mathcal{K}_a(m^{-\frac{1}{3}})$ for a function \mathcal{K}_a in $C^\infty([0, 1])$ with determined Taylor expansion at 0. Moreover, the (quasi)mode u localizes at the boundary.

b) Half-quadratic potential well. If $\tilde{\kappa} = 0$, under the additional condition $\frac{2}{R^2} - \frac{n''(R)}{n(R)} > 0$ the effective potential V has a local minimum

at R . Our expansion is now $k = m\mathcal{K}_b(m^{-\frac{1}{2}})$ for another function $\mathcal{K}_b \in C^\infty([0, 1])$. Again, the (quasi)mode u localizes at the boundary.

c) Internal quadratic potential well. If $\tilde{\kappa} < 0$, since $\lim_{r \searrow 0} V(r) = +\infty$, the effective potential V has at least a global minimum r_0 in $(0, R)$. Under the condition $\frac{2}{r_0} - \frac{n''(r_0)}{n(r_0)} > 0$ and that r_0 is the unique global minimum of V , our expansion has again the form $k = m\mathcal{K}_c(m^{-\frac{1}{2}})$ with a different function $\mathcal{K}_c \in C^\infty([0, 1])$, and now u localizes inside the cavity around $r = r_0$.

3 General cavity with variable index

In the general case, the phase function is not known and we have used a phase amplitude ansatz, the famous WKB method, to find asymptotic expressions of the resonances in tubular coordinates along the boundary of Ω [2]. This leads to an eikonal equation coupled with a Schrödinger equation. A small parameter h appears naturally, and has to be quantized so that the phase is well-defined, giving rise to a generalized notion of polar mode index. We have constructed quasi-resonances (k, u) in the sense of [3] in a similar, but more general, form than in case a) above, when the condition $\kappa + \frac{\partial_n \kappa}{n} > 0$ is fulfilled all along $\partial\Omega$ where κ is the curvature of $\partial\Omega$. The asymptotic expansions are computed using a computer algebra system.

The advantage of the asymptotic formulas we have obtained is twofold. They provide accurate approximations of resonances at high frequencies when the use of standard numerical approximation is difficult. For lower frequencies, combined with finite element (FE) computations, they provide information on the localization of the resonances in the FE matrix spectrum.

4 Numerical Experiments

For numerical illustration we consider an elliptic cavity with perimeter L and constant index n . Our 4-term asymptotic expansion of k reads

$$k_j^{[4]}(m) = \frac{2\pi m}{Ln} \left[1 + \frac{a_j}{2} \langle \kappa^{\frac{2}{3}} \rangle h_m^{\frac{2}{3}} - \frac{n \langle \kappa \rangle}{2\sqrt{n^2 - 1}} h_m \right. \\ \left. + \frac{a_j^2}{12} \left(\langle \kappa^{\frac{2}{3}} \rangle^2 - \frac{\langle \kappa^{\frac{4}{3}} \rangle}{10} - \frac{4}{45} \langle \kappa^{\frac{2}{3}} \kappa^{-\frac{8}{3}} \rangle \right) h_m^{\frac{4}{3}} \right. \\ \left. - \frac{a_j n_0}{12\sqrt{n^2 - 1}} \left(\langle \kappa^{\frac{2}{3}} \rangle \langle \kappa \rangle + \frac{\langle \kappa^{\frac{5}{3}} \rangle}{n^2 - 1} \right) h_m^{\frac{5}{3}} \right]$$

as $m \rightarrow +\infty$, where $h_m = \frac{L}{\pi m}$ and $\langle \cdot \rangle$ is the mean value along $\partial\Omega$. Here j is a natural integer (radial mode index) and a_j is the j -th zero of the reverse Airy function $x \mapsto \text{Ai}(-x)$.

On Figure 1, we have compared our N -terms asymptotic expansion to FE computation for an ellipse of semi-major axis 1 and eccentricity 0.5 with constant index $n = 5$. We have used a *Perfectly Matched Layer* with a structured quadrangular mesh of geometric degree 3 and a FE space of degree 7 with 64156 dofs. For $N = 0$, $k_0^{[0]}(m)$ is the principal term $\frac{2\pi m}{Ln}$, for $N = 1$, $k_0^{[1]}(m)$ is $k_0^{[0]}(m)$ plus one corrective term, etc. Note that, problem (1) has two solutions for each m .

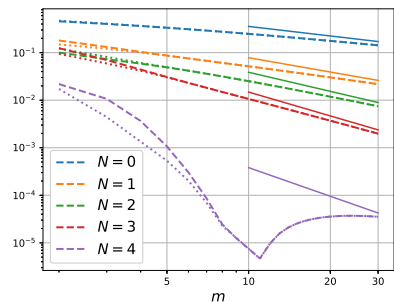


Figure 1: Relative difference between FE resonances and N -terms asymptotic expansions, for $j = 0$. The slopes of the solid lines are $-\frac{N+2}{3}$.

References

- [1] B.R. Johnson, *Theory of morphology dependent resonances: shape resonances and width formulas*, J. Opt. Soc. Am. A., 1993.
- [2] Z. Moitier, *Étude mathématique des résonances dans une micro-cavité optique*, PhD thesis in preparation, University of Rennes 1, 2019.
- [3] S.H. Tang, M. Zworski, *From quasimodes to resonances*, Math. Res. Lett., 1998.

This work has been performed within the framework of the CNRS INFINITI project SONATINE in collaboration with FOTON Laboratory. The authors also acknowledge support of the Centre Henri Lebesgue ANR-11-LABX-0020-01.

Dynamics and stability of a cold magnetic plasma

Ibtissem Zaafrani^{1,*}, Simon Labrunie¹¹Institut Élie Cartan, Université de Lorraine, Vandœuvre-lès-Nancy, France

*Email: ibtissem.zaafrani@univ-lorraine.fr

Abstract

We study the stabilization of Euler–Maxwell model in a cold plasma in the presence of a static external magnetic field. This model corresponds to the coupling between linearized Euler equation in two particle species and a Maxwell system. We show that the model is well-posed for two types of boundary conditions: perfectly conducting (metallic) and Silver–Müller (absorbing). We prove the strong stability of the system in a closed subspace of the energy space.

Keywords: electromagnetism, stabilization

1 Introduction

Let $\Omega \subset \mathbb{R}^3$ be a bounded open set, which represents the plasma volume in the tokamak with static external time-invariant magnetic field [3]. We consider the following linearised Euler–Maxwell model for $(t, \mathbf{x}) \in \mathbb{R}^+ \times \Omega$:

$$\frac{\partial \mathbf{J}_1}{\partial t} = \varepsilon_0 \omega_{p1}^2 \mathbf{E} + \Omega_{c1} \mathbf{J}_1 \wedge \mathbf{b} - \nu_1 \mathbf{J}_1; \quad (1)$$

$$\frac{\partial \mathbf{J}_2}{\partial t} = \varepsilon_0 \omega_{p2}^2 \mathbf{E} + \Omega_{c2} \mathbf{J}_2 \wedge \mathbf{b} - \nu_2 \mathbf{J}_2; \quad (2)$$

$$\frac{\partial \mathbf{E}}{\partial t} = c^2 \mathbf{rot} \mathbf{B} - \frac{1}{\varepsilon_0} \mathbf{J}_1 - \frac{1}{\varepsilon_0} \mathbf{J}_2; \quad (3)$$

$$\frac{\partial \mathbf{B}}{\partial t} = -\mathbf{rot} \mathbf{E}; \quad (4)$$

where the indices 1 and 2 denote the particle species: ion and electron. The variable coefficients depending on \mathbf{x} are: ν_s the collision frequency, ω_{ps} the plasma pulsation, Ω_{cs} the cyclotron pulsation of the species s , and \mathbf{b} the direction of the external magnetic field.

The boundary conditions on $\Gamma = \partial\Omega$ are as follows. On the conducting part $\Gamma_P \neq \emptyset$, it holds that

$$\mathbf{E} \wedge \mathbf{n} = 0 \quad \text{on } \Gamma_P, \quad (5)$$

while on the (possibly vanishing) absorbing part $\Gamma_A = \Gamma \setminus \Gamma_P$, one has the Silver–Müller boundary condition:

$$\mathbf{E} \wedge \mathbf{n} + c\mathbf{B}_T = \mathbf{g}(t, \mathbf{x}) \quad \text{on } \Gamma_A, \quad (6)$$

where \mathbf{g} is given. Moreover, \mathbf{J}_s , \mathbf{E} and \mathbf{B} are given at time $t = 0$.

2 Well-posedness of the system

To prove an existence and uniqueness result for the Euler–Maxwell model (1)–(4) with various boundary conditions, we re-write it as a system of evolution equations:

$$\begin{cases} \mathbf{u}'(t) = \mathbb{A}\mathbf{u}(t), \\ \mathbf{u}(0) = \mathbf{u}_0, \end{cases} \quad (7)$$

where \mathbb{A} is a linear operator given by the formula

$$\mathbb{A} = \begin{pmatrix} -\mathbb{M}_1 & 0 & \varepsilon_0 \omega_{p1}^2 & 0 \\ 0 & -\mathbb{M}_2 & \varepsilon_0 \omega_{p2}^2 & 0 \\ -\frac{1}{\varepsilon_0} & -\frac{1}{\varepsilon_0} & 0 & c^2 \mathbf{rot} \\ 0 & 0 & -\mathbf{rot} & 0 \end{pmatrix},$$

with $\mathbb{M}_s \in \mathcal{M}_{3,3}(\mathbb{R})$ such that

$$\Omega_{cs} \mathbf{b} \wedge \mathbf{v} + \nu_s \mathbf{v} = \mathbb{M}_s \mathbf{v}, \quad \forall \mathbf{v} \in \mathbb{R}^3,$$

$$\mathbf{u}(t) = \begin{pmatrix} \mathbf{J}_1(t) \\ \mathbf{J}_2(t) \\ \mathbf{E}(t) \\ \mathbf{B}(t) \end{pmatrix} \quad \text{and } \mathbf{u}'(t) \text{ its derivative.}$$

The well-posedness of problem (7) follows from semi-group theory, in particular the Hille–Yosida theorem, in the appropriate Hilbert space, namely $\mathbf{X} = \mathbf{L}^2(\Omega)^4$, endowed with the scalar product and norm $(\mathbf{u} | \mathbf{w})_{\mathbf{X}} := \left(\frac{1}{\varepsilon_0 \omega_{p1}^2} \mathbf{u}_1 | \mathbf{w}_1 \right) + \left(\frac{1}{\varepsilon_0 \omega_{p2}^2} \mathbf{u}_2 | \mathbf{w}_2 \right) + (\varepsilon_0 \mathbf{u}_3 | \mathbf{w}_3) + (c^2 \varepsilon_0 \mathbf{u}_4 | \mathbf{w}_4)$ and $\|\mathbf{u}\|_{\mathbf{X}} := (\mathbf{u} | \mathbf{u})_{\mathbf{X}}^{\frac{1}{2}}$. There are two cases, according to the boundary conditions.

2.1 Perfectly conducting boundary conditions

We assume that (5) holds on the whole boundary, i.e., $\Gamma_P = \Gamma$, $\Gamma_A = \emptyset$. The unbounded operator associated with the abstract problem (7) on \mathbf{X} , noted $(D(\mathbb{A}_1), \mathbb{A}_1)$, is defined as

$$D(\mathbb{A}_1) = \mathbf{L}^2(\Omega) \times \mathbf{L}^2(\Omega) \times \mathbf{H}_0(\mathbf{rot}; \Omega) \times \mathbf{H}(\mathbf{rot}; \Omega)$$

and $\mathbb{A}_1 \mathbf{u} = \mathbb{A} \mathbf{u}$ for all \mathbf{u} in $D(\mathbb{A}_1)$. The operator \mathbb{A}_1 is a maximal dissipative [5]; thus if $\mathbf{u}_0 \in D(\mathbb{A}_1)$ there exists a unique strong solution $\mathbf{u} \in C^1([0, +\infty]; \mathbf{X}) \cap C([0, +\infty]; D(\mathbb{A}_1))$.

2.2 Silver–Müller boundary conditions

In this case, we assume that $\Gamma_A \neq \emptyset$ and $\Gamma_P \neq \emptyset$.

First, we study the *homogeneous* case $\mathbf{g} = 0$. We define the operator \mathbb{A}_2 from \mathbf{X} into itself associated with the evolution problem (7) with conditions (5)–(6) as follows:

$$D(\mathbb{A}_2) = \mathbf{L}^2(\Omega) \times \mathbf{L}^2(\Omega) \times \mathcal{H},$$

where

$$\mathcal{H} = \{(\mathbf{w}_1, \mathbf{w}_2) \in \mathbf{H}_0^p(\mathbf{rot}; \Omega) \times \mathbf{H}(\mathbf{rot}; \Omega) : \mathbf{w}_1 \wedge \mathbf{n} + c\mathbf{w}_2 \top = 0 \text{ on } \Gamma_A\},$$

and $\mathbb{A}_2 \mathbf{u} = \mathbb{A} \mathbf{u}$ for all \mathbf{u} in $D(\mathbb{A}_2)$. Again [5], \mathbb{A}_2 is maximal dissipative, hence the existence and uniqueness of a strong solution to this problem. The non-homogeneous case $\mathbf{g} \neq 0$ can then be handled by a lifting of the boundary data under appropriate conditions on \mathbf{g} .

In a second step, one recovers in both cases [5] Maxwell’s divergence equations and the condition $\mathbf{B} \cdot \mathbf{n} = 0$ on Γ_P as usual.

3 Strong stability

The decay of the energy of the system

$$\mathcal{E}(t) = \frac{1}{2} \|(\mathbf{J}_1, \mathbf{J}_2, \mathbf{E}, \mathbf{B})^T\|_{\mathbf{X}}^2$$

is guaranteed under suitable conditions on ν_s , ω_{ps} and Ω_{cs} .

As the resolvents of our operators are not compact, in order to show strong stability we will use the following theorem due to Arendt–Batty and Lyubich–Vu [1, 4].

Theorem 1 (Arendt–Batty/Lyubich–Vu). *Let \mathbf{X} be a reflexive Banach space and let $(\mathbf{T}(t))_{t \geq 0}$ be a C^0 semi-group on \mathbf{X} of generated \mathbf{A} . Assume that $(\mathbf{T}(t))_{t \geq 0}$ is bounded and that no eigenvalues of \mathbf{A} lie on the imaginary axis. If $\sigma(\mathbf{A}) \cap i\mathbb{R}$ is countable, then $(\mathbf{T}(t))_{t \geq 0}$ is stable i.e for all $\mathbf{x} \in \mathbf{X}$, $\lim_{x \rightarrow \infty} \mathbf{T}(t)\mathbf{x} = 0$.*

With the aim of applications to tokamaks, we consider that the domain Ω is not simply connected, but its boundary Γ is connected. We introduce the cuts $(\Sigma_j)_{1 \leq j \leq J}$ as usual [2]. We begin with the perfectly conducting case. Setting $\mathbf{H}_0^\Sigma(\text{div}0; \Omega) := \{\mathbf{v} \in \mathbf{H}_0(\text{div}0; \Omega) : (\mathbf{v} \cdot \mathbf{n}, 1)_{\Sigma_j} = 0, 1 \leq j \leq J\}$, we define

$$\tilde{\mathbf{X}} := \mathbf{L}^2(\Omega) \times \mathbf{L}^2(\Omega) \times \mathbf{L}^2(\Omega) \times \mathbf{H}_0^\Sigma(\text{div}0; \Omega).$$

$\tilde{\mathbf{X}}$ is a closed subspace of \mathbf{X} endowed by the same scalar product $(\cdot | \cdot)_{\tilde{\mathbf{X}}}$.

After a spectral analysis of the operator \mathbb{A}_1 carried out on the imaginary axis, we introduce a unbounded operator on $\tilde{\mathbf{X}}$, noted $(D(\tilde{\mathbb{A}}_1), \tilde{\mathbb{A}}_1)$ defined by

$$D(\tilde{\mathbb{A}}_1) = D(\mathbb{A}_1) \cap \tilde{\mathbf{X}},$$

and $\tilde{\mathbb{A}}_1 \mathbf{u} = \mathbb{A}_1 \mathbf{u}$, for all \mathbf{u} in $D(\tilde{\mathbb{A}}_1)$.

As a consequence of Theorem 1, it holds that:

Theorem 2 *The operator $\tilde{\mathbb{A}}_1$ is strongly stable.*

The proof of strong stability with the Silver–Müller condition is similar and in progress.

References

- [1] W. ARENDT & C. J. K. BATTY. Tauberian theorems and stability of one-parameter semigroups. *Trans. Amer. Math. Soc.*, **305**(2):837–852, 1988.
- [2] F. ASSOUS, P. CIARLET & S. LABRUNIE. *Mathematical foundations of computational electromagnetism*. Applied Mathematical Sciences vol. **198**, Springer, 2018.
- [3] R.J. GOLDSTON & P.H. RUTHERFORD. *Introduction to plasma physics*. Institute of Physics Publishing, Bristol (1995).
- [4] Y. I. LYUBICH & Q. P. VU. Asymptotic stability of linear differential equations in Banach spaces. *Studia Math.*, **88**(1):37–42, 1988.
- [5] S. LABRUNIE & I. ZAAFRANI. Dynamique d’un plasma magnétique froid. 2017. <https://hal.archives-ouvertes.fr/hal-01572067v2/document>

Homogenization of the time-dependent heat equation on plane mesh structures

Adrien Semin^{1,*}, Matko Ljulj², Kersten Schmidt¹, Jossip Tambaca²

¹Department of Mathematics, Technische Universität Darmstadt, Germany

²University of Zagreb, Croatia

*Email: semin@mathematik.tu-darmstadt.de

Abstract

In this paper we use the homogenization theory and a definition of two-scale convergence to elliptic problems defined on domains consisting of curves located in a plane with certain periodic properties. Using this approach we prove that family of solutions of diffusion equations defined on graphs in a plane with repeating periodic unit cells converges to the solution of appropriate diffusion equation defined on the subset of plane, when unit cells size converge to zero. We additionally show how to perform formal analysis (which in this setting gives the correct limit model) and show several examples of various unit cells appearing in the domain.

1 Introduction

Let us consider a one-dimensional manifold $\Gamma_Y \subset (0, 1)^2$ that can be described as an oriented, connected and periodic graph structure whose edges admit a regular enough parametrization. Let Ω be a connected Lipschitz domain, and let Γ^δ be the plane mesh illustrated in Fig. 1 and defined by

$$\Gamma^\delta := \Omega \cap \left(\bigcup_{(n_1, n_2) \in \mathbb{Z}^2} \delta(\Gamma_Y + n_1 \mathbf{e}_1 + n_2 \mathbf{e}_2) \right)$$

Let $\Gamma_D \subset \partial\Omega$ be a part of the boundary of Ω that corresponds to a finite union of line segments of positive length. For any δ , let us introduce $\Gamma_D^\delta := \partial\Gamma_D \cap \partial\Gamma^\delta$ and

$$\mathcal{H}^\delta := \{v \in H^1(\Gamma^\delta) \text{ such that } v = 0 \text{ on } \Gamma_D^\delta\}$$

On this domain, we consider the heat equation, written in a weak formulation: given $T > 0$, $f^\delta \in L^2(0, T; L^2(\Gamma^\delta))$ and the initial temperature $u_{\text{init}}^\delta \in \mathcal{H}^\delta$, find $u^\delta \in L^2(0, T; \mathcal{H}^\delta)$ such that, for any $v \in \mathcal{H}^\delta$,

$$\begin{aligned} &\rho c_p \int_{\Gamma^\delta} \partial_t u^\delta(t, \mathbf{x}) v(\mathbf{x}) \, ds(\mathbf{x}) \\ &+ \int_{\Gamma^\delta} a(\mathbf{x}) \partial_\Gamma u^\delta(t, \mathbf{x}) \partial_\Gamma v(\mathbf{x}) \, ds(\mathbf{x}) \\ &= \int_{\Gamma^\delta} f^\delta(t, \mathbf{x}) v(\mathbf{x}) \, ds(\mathbf{x}), \quad (1) \end{aligned}$$

and

$$u^\delta(0, \cdot) = u_{\text{init}}^\delta;$$

here ρ is the mass density of the material, c_p is the specific heat capacity that are considered as constants, $a : \Omega \rightarrow \mathbb{R}$ the thermal conductivity that is a positive continuous function that is uniformly bounded from below, *i.e.*,

$$\min_{\mathbf{x} \in \Omega} a(\mathbf{x}) > 0,$$

and $\partial_\Gamma v$ designates the derivate of v along the graph Γ^δ or Γ_Y .

To stress the passage from the 1D mesh Γ^δ to the 2D domain Ω we call the two-scale convergence in this paper the *mesh two-scale convergence*.

Definition 1 (Mesh two-scale convergence)

We say that family of function $(v^\delta) \in L^2(0, T; L^2$ for $\delta \rightarrow 0$ is "mesh two-scale convergent" to $v^0 \in L^2(0, T; L^2(\Omega; L^2(\Gamma_Y)))$ if for each $\psi \in C^\infty(0, T; C^\infty(\Omega; C^\infty(\Gamma_Y)))$ we have

$$\begin{aligned} &\lim_{\delta \rightarrow 0} \int_0^T \int_{\Gamma^\delta} v^\delta(t, \mathbf{x}) \psi(t, \mathbf{x}, \frac{\mathbf{x}}{\delta}) \, ds(\mathbf{x}) \, dt \\ &= \int_0^T \int_{\Omega} \int_{\Gamma_Y} v^0(t, \mathbf{x}, \mathbf{y}) \psi(t, \mathbf{x}, \mathbf{y}) \, ds(\mathbf{y}) \, dx \, dt. \end{aligned}$$

In the following, we are interested by the two-scale limit u^0 of the solution u^δ of the heat equation (1). To do so, we develop a two-scale homogenization procedure, in a spirit of what

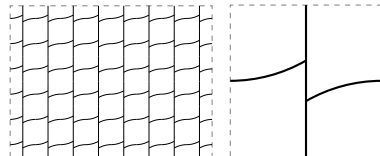


Figure 1: Example of an admissible one-dimensional periodic domain Γ^δ (left) and the associated unit pattern Γ_Y (right).

can be found in [1, 2], with the additional presence of the time-dependency. In particular, the two-scale limit u^0 is stated by the following theorem.

Theorem 2 (Two-scale convergence)

Let $f^\delta(t, \mathbf{x}) = f(t, \mathbf{x}, \frac{\mathbf{x}}{\delta})$ for all $\delta > 0$ with

$$f \in L^2(0, T; L^2(\Gamma_Y; C(\Omega))),$$

and $u_{init}^\delta(\mathbf{x}) = u_{init}(\mathbf{x})$ with

$$u_{init} \in C^1(\Omega), \quad u_{init} = 0 \text{ on } \Gamma_D,$$

and let for $\delta > 0$, $u^\delta \in L^2(0, T; \mathcal{H}^\delta)$ be such that $\partial_t u^\delta \in L^2(0, T; L^2(\Gamma^\delta))$ be the unique solution of (1). Then $(u^\delta)_{\delta > 0}$ mesh two-scale converges to the function u^0 which is the unique solution of the problem: find $u^0 \in L^2(0, T; \mathcal{H})$ such that $\partial_t u^0 \in L^2(0, T; L^2(\Omega))$, where

$$\mathcal{H} := \{v \in H^1(\Omega) : v = 0 \text{ on } \Gamma_D\},$$

such that

$$\begin{aligned} \rho c_p \int_{\Omega} \partial_t u^0(t, \mathbf{x}) v(\mathbf{x}) \, d\mathbf{x} \\ + \int_{\Omega} (\mathbf{A}_{hom}(\mathbf{x}) \nabla u^0(t, \mathbf{x})) \cdot \nabla v(\mathbf{x}) \, d\mathbf{x} \\ = \int_{\Omega} f_{hom}(t, \mathbf{x}) v(\mathbf{x}) \, d\mathbf{x}, \end{aligned} \quad (2)$$

and

$$u^0(t, \mathbf{x}) = u_{init}(\mathbf{x}), \quad \mathbf{x} \in \Omega,$$

where

$$f_{hom} = \frac{1}{|\Gamma_Y|} \int_{|\Gamma_Y|} f(\cdot, \cdot, \mathbf{y}) \, ds(\mathbf{y})$$

and where the 2-by-2 symmetric and positive definite homogenized thermal conductivity tensor $\mathbf{A}_{hom}(\mathbf{x})$ is given by

$$\begin{aligned} \mathbf{A}_{hom}(\mathbf{x}) := \frac{a(\mathbf{x})}{|\Gamma_Y|} \int_{|\Gamma_Y|} (\mathbf{t}(\mathbf{y}) + \partial_\Gamma \Phi(\mathbf{y})) \\ (\mathbf{t}(\mathbf{y}) + \partial_\Gamma \Phi(\mathbf{y}))^T \, ds(\mathbf{y}), \end{aligned}$$

where $\mathbf{t}(\mathbf{y})$ is the tangent vector defined on Γ_Y and $\Phi := (\phi_1, \phi_2) \in H^1(\Gamma_Y)^2$ is a periodic function defined componentwise on Γ_Y as any solution of the canonical problem

$$\begin{aligned} \int_{\Gamma_Y} \partial_\Gamma \phi_i(\mathbf{y}) \partial_\Gamma \psi(\mathbf{y}) \, ds(\mathbf{y}) \\ = - \int_{\Gamma_Y} \mathbf{t}(\mathbf{y}) \cdot \mathbf{e}_i \partial_\Gamma \psi(\mathbf{y}) \, ds(\mathbf{y}), \end{aligned}$$

for any smooth periodic function ψ .

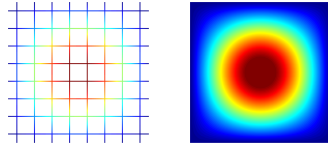


Figure 2: Left: plot of the solution $u^\delta(T)$ for $T = 2$ and $\delta = 1/8$. Right: Plot of the homogenized solution $u^0(T)$ for the same time and using the same color values.

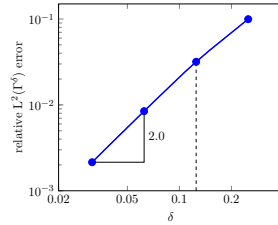


Figure 3: Relative $L^2(\Gamma^\delta)$ error as a function of δ for $T = 2$. The dashed line is at $\delta = 1/8$.

We shall also see that numeric computation of the solution of (1) tends to the solution of (2), qualitatively (see Fig. 2) and quantitatively. In particular, we will seek numerically that the relative L^2 -error on Γ^δ between u^δ and u^0 scales like at most like δ and reduces fast depending on the pattern of Γ_Y (see Fig.2).

Keywords: Heat equation, two-scale homogenization, numerical methods

References

- [1] G. Allaire, A. Damlamian and U. Hornung, Two-Scale Convergence On Periodic Surfaces And Applications. *Proceedings of the International Conference on Mathematical Modelling of Flow through Porous Media* (1996), pp. 15–25.
- [2] G. Bouchitté and I. Fragalà, Homogenization of elastic thin structures: a measure-fattening approach. *Journal of Convex Analysis* **9** (2002), pp. 339–362.
- [3] M. Ljulj, K. Schmidt, A. Semin and J. Tambaca, Homogenization of the time-dependent heat equation on planar one-dimensional periodic structures. *In preparation*.

Uniqueness of self-similar solutions obeying the problems of arbitrary discontinuity disintegration for the generalized Hopf equation

Anna Chugaynova^{1,*}

¹Steklov Mathematical Institute of Russian Academy of Sciences, Moscow, Russia

*Email: anna_ch@mi-ras.ru

Abstract

Solutions of a problem about an arbitrary discontinuity disintegration for the generalized Hopf equation are under investigation. The solution is constructed from a sequence of the non-overturning Riemann waves and discontinuities having the stable stationary and non-stationary structure. The influence of small-scale effects of dissipation and dispersion are analyzed. Small-scale processes determine a discontinuity structure and a set of discontinuities with stationary structures. Among discontinuities with stationary structures there are special ones on which (in addition to relations following from conservation laws) some additional relations should be satisfied which follow from the requirement for the discontinuity structure to exist. The existence of special discontinuities leads to non-unique way to construct self-similar solutions to the problem of arbitrary discontinuity disintegration.

Keywords: special discontinuities, nonlinear hyperbolic systems of equations, travelling wave solution

1 Introduction

Special discontinuities, for example, deflagration waves, are known for a long time. These discontinuities are described as undercompressive shock wave [1, 2] and non-classical one [3] are used. We shall use the term a special discontinuity introduced in [4].

The solutions of nonlinear hyperbolic systems of equations are studied. To the hyperbolic system we add terms describing small-scale processes of dispersion and dissipation. Solutions of this supplemented system are smoothed discontinuous solutions of the initial system. The solution in the form of travelling wave for the supplemented system is called a stationary discontinuity structure. Among all discontinuities with stationary structures we select special discontinuities, their structures are described by integral curves joining two saddle points. The

condition for such a curve to exist is called an additional condition on a discontinuity [4]. This condition following from the requirement for a stationary structure to exist provides the evolutionary character of a discontinuity [5].

If the initial system can have a special discontinuity as a solution, the problem of arbitrary discontinuity disintegration for this system can have non-unique solution [4, 6–9].

2 Special discontinuities for longitudinal waves propagating in visco-elastic rods with complicated nonlinearity

Special discontinuities in longitudinal waves propagating in visco-elastic rods were considered in [4, 6–8] (see also the references). Special discontinuities can occur if the function responsible for nonlinearity is specified in a special way. The discontinuity structure is described by the generalized KdV-Burgers equation

$$\frac{\partial v}{\partial t} + \frac{\partial \varphi(v)}{\partial x} = \mu \frac{\partial^2 v}{\partial x^2} - m \frac{\partial^3 v}{\partial x^3}, \quad (1)$$

$$m, \mu = \text{const}, \quad v = v(x, t)$$

The term involving the coefficient m in the right-hand side of Eq. (1) describes the dispersion effects (m is the dispersion parameter). The term involving the coefficient μ takes into account the viscous effects and dissipation (μ is the dissipation parameter). The nonlinearity is specified by the function $\varphi(v)$, which is not a quadratic one and will be defined below. One should analyze the traveling wave solutions representing shock structures in solutions of the equation

$$\frac{\partial v}{\partial t} + \frac{\partial \varphi(v)}{\partial x} = 0, \quad (2)$$

to which Eq.(1) is reduced when considering solutions characterized by variations of large scale L in x (both terms on the right-hand side of Eq. (1) become small as compared with the left-hand-side terms).

Equation (2) can be called a generalized Hopf equation, with the Hopf equation it coincides when $\varphi(v)$ is a quadratic function of v .

Equation (2) (as well as (1)) represents a conservation law, so the corresponding relation at the discontinuity can be written as

$$W = \frac{[\varphi(v)]}{[v]}. \quad (3)$$

Here, W is the discontinuity velocity and square brackets denote the difference in the functions values behind and ahead of the discontinuity.

The function $\varphi(v)$ is defined as

$$\varphi(v) = v^4 - v^2. \quad (4)$$

We consider self-similar solutions of arbitrary discontinuity disintegration which consist only of stable discontinuities with a stationary or non-stationary structure and simple waves. The conclusive criterion has been formulated of an admissible discontinuity problem of arbitrary discontinuity disintegration governed by the Hopf equation (2). Admissible discontinuities were treated as discontinuities with a stable structure, which can be stationary or periodic in time. Accordingly, discontinuities with stationary unstable structures were excluded from the set of discontinuities regarded previously as admissible and time-periodic structures were added to this set (their stability and periodicity were verified by direct numerical computation). As a result we showed that the solution of the problem of arbitrary discontinuity disintegration constructed in this work uniquely exists for all parameter values.

Acknowledgments The research was funded by a grant from the Russian Science Foundation (Project No. 19-71-30012).

References

- [1] D. Jacobs, B. McKinney, M. Shearer, Travelling wave solutions of the modified Korteweg-de Vries-Burgers equation, *Journ. Diff. Equations* **116**(1995), pp. 448–467.
- [2] G.A. El, M.A. Hoefer, M. Shearer, Dispersive and diffusive-dispersive shock waves for non-convex conservation laws, *SIAM Review* **59**(1)(2016), pp. 3–61.
- [3] B. Hayes, M. Shearer, Undercompressive shocks and Riemann problems for scalar conservation laws with non-convex fluxes, *Proc. Roy. Soc. Edinburgh* **129**(1999), 733–754.
- [4] A.G. Kulikovskii, The possible effect of oscillations in a discontinuity structure on the set of admissible discontinuities, *Soviet Phys. Dokl.* **29**(1984), pp. 283–285.
- [5] P.D. Lax, Hyperbolic systems of conservation laws, *Comm. Pure Appl. Math.* **10**(1957), pp. 537–566.
- [6] A.G. Kulikovskii, A.P. Chugainova, Classical and non-classical discontinuities in solutions of equations of non-linear elasticity theory, *Russ. Math. Surv.* **63**(2)(2008), pp. 283–350.
- [7] A.P. Chugainova, V.A. Shargatov, Stability of discontinuity structures described by a generalized KdV–Burgers equation, *Comput. Math. Math. Phys.* **56**(2)(2016), pp. 263–277.
- [8] A.P. Chugainova, A.T. Il'ichev, A.G. Kulikovskii, V.A. Shargatov, Problem of arbitrary discontinuity disintegration for the generalized Hopf equation: selection conditions for a unique solution, *J. Appl. Math.* **82**(2017), pp. 496–525.
- [9] A.P. Chugainova, Special discontinuities in nonlinearly elastic media, *Comput. Math. Math. Phys.* **57**(6)(2017), pp. 1013–1021.

Water wave scattering by a submerged metamaterial

Christos Marangos^{1,*}, Richard Porter²¹School of Mathematics, University of Bristol, UK

*Email: cm14737@my.bristol.ac.uk

Abstract

This work presents solutions to several water wave problems, in the presence of a fixed metamaterial on the bed. Typically, in these problems, metamaterial can be viewed as an infinite array of parallel thin plates, placed infinitely closed to each other. After the governing equation of the wave inside and outside the metamaterial is derived and solved, then the reflection and transmission coefficients, will be found using a variety of semi-analytical techniques. By adjusting the geometry of the array structure, the behaviour of the reflected and transmitted wave can be manipulated and get a plethora of phenomena.

Keywords: water waves, metamaterials, homogenisation

1 Introduction

Linear, time-harmonic water wave theory is used to derive the model in the fluid domain of finite depth, while in the presence of the metamaterial, homogenisation theory and the continuum hypothesis is used to derive the governing equation. So after the surface gravity wave strikes the metamaterial, which looks like a waveguide, there will be some transmission and some reflection. The unknown Fourier coefficients (that rise from the separation of variables and give information about the reflection and transmission), can be found by matching the wave across the boundaries of the metamaterial.

2 Geometry of the 3D problems

In the first problem, thin rectangular arrays, that are aligned with the x -axis and separated by some infinitesimal distance, are placed in the bottom of an inviscid fluid and they interact with an incident surface gravity water wave of wavenumber k , arriving from a point in $x < -b$ and travelling at an acute angle θ_0 with the positive x -axis. The origin is sitting on the surface of the water, directly above the midpoint of the plates, with the z direction pointing normally outwards the fluid.

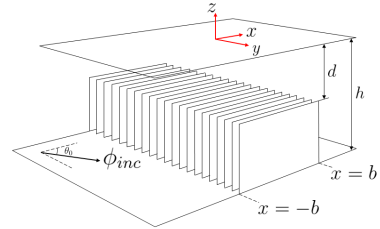


Figure 1: Geometry of the "x-aligned" problem

The second problem is exactly the same as the first one, but this time the plates are aligned with the y -axis. So, the plates will have infinite length.

3 The Continuum Hypothesis

Assuming time-harmonic motion of the wave, the governing equations outside the structure, are

$$\begin{aligned} \nabla^2 \phi(x, y, z) = 0, \quad \phi_z(x, y, -h) = 0, \\ \phi_z(x, y, 0) = K\phi(x, y, 0) \end{aligned} \quad (1)$$

where ϕ is the complex velocity potential, with time dependence removed and $K = \omega^2/g$ with ω be the angular velocity of the incident wave. But to derive the model in the metamaterial, we use homogenisation theory [1], [2]. So in the x -aligned problem, we have that in the single channel $x \in (-b, b)$, $y \in (0, l)$, with l be the spacing of the plates and λ be the incident wavelength ($l \ll \lambda$)

$$\nabla^2 \phi = 0, \quad \phi_y = 0 \text{ on } y = 0, l \quad (2)$$

Now by introducing the new microscopic variable $y = lY$ and expanding $\phi = \phi_0 + l\phi_1 + l^2\phi_2 + \dots$, then the orders of l^0 , l^1 will imply that ϕ_0 , ϕ_1 are functions of the macroscopic variables x, z only, while the orders of l^2 will imply $(\partial_{xx}^2 + \partial_{zz}^2)\phi_0 = 0$, after integrating in $Y \in (0, 1)$. Therefore, by the continuum hypothesis

$$(\partial_{xx}^2 + \partial_{zz}^2)\phi(x, y, z) = 0 \quad (3)$$

inside the metamaterial (using $\phi \sim \phi_0$). The accuracy of the continuum description compared to the exact results, is confirmed in [3].

4 Extensions

The main focus of the talk will be about the two previous problems, where the plates are aligned with the x -axis and y -axis, but we will show what happens when the plates are tilted at a random angle too. Also, we might compare it with the problems involving the replacement of thin plates with thick barriers (again infinitely close to each other). This kind of problems, are analysed in [4].

5 Numerical Results

Then we apply the matching conditions to get he Fourier coefficients numerically.

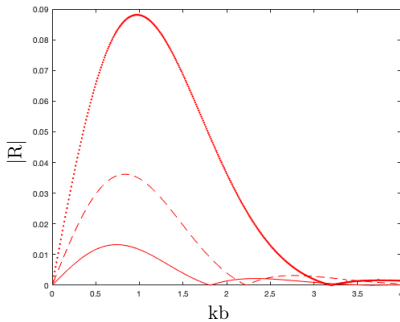


Figure 2: Reflection coefficient against kb (y -aligned problem), with $d/h = 0.9$, $b/h = 1$, for $\theta_0 = \pi/6, \pi/4, \pi/3$ (—, - - -, ...)

This kind of plots, will always go through the origin because of the penetration of the motion of the fluid. In long waves ($kb \ll 1$) the decay of the wave as we go down to the bottom, is very small, because of e^{kz} and so the wave can somehow travel above the obstacle unaffected (the energy of a long wave sits on the top surface). Also, as we increase θ_0 from 0 to $\pi/2$, the sliding ability of the wave (through the plates) is reduced, causing more reflection. Moreover, the period of $|R|$ is not constant in kb , even if we fix θ_0 . This happens due to the effect of multiple scattering interference and it has to do with how many wavelengths can fit in the distance travelled by the wave in the channel. The en-

ergy $|R|^2 + |T|^2$ was conserved in all the possible choice of parameters, with the trivial case of $\theta_0 = 0$ giving $R = 0$ and $T = 1$. Now, by solving the second problem, but now developing an integral equation and solving it efficiently using the Galerkin method, the analogous result is

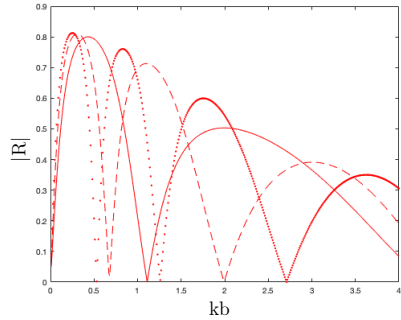


Figure 3: Reflection coefficient against kb (y -aligned problem), with $d/h = 0.1$, $b/h = 1$, for $\theta_0 = \pi/6, \pi/4, \pi/3$ (—, - - -, ...)

First, we can see that, compared to the previous result, the interaction increases as the height of the arrays becomes larger. Also, the special case of $\theta_0 = 0$, gives the same results as if there was a rigid step in the region of the metamaterial [5], which makes sense, since incompressibility implies no z variation in between the plates in the limit $kl \rightarrow 0$.

References

- [1] D. Cioranescu, P. Donato, An introduction to Homogenization, 1999.
- [2] C.C. Mei, B. Vernescu, Homogenization Methods for multiscale mechanics, 2010.
- [3] R. Porter, Plate arrays as a water wave metamaterial, 2018.
- [4] A. Maurel, J.-J. Marigo, P. Cobelli, P. Petitjeans and V. Pagneux, Revisiting the anisotropy of metamaterials for water waves, 2017.
- [5] R. Porter, Transparency of structures in water waves, 2014.

Effective models for non-perfectly conducting thin coaxial cables

Geoffrey Beck^{1,*}, Sébastien Imperiale², Patrick Joly¹

¹POEMS (CNRS-INRIA-ENSTA Paristech), Palaiseau, France

²Inria & LMS, Ecole polytechnique, CNRS, Université Paris-Saclay, France

*Email: geoffrey.beck.poems@gmail.com

Abstract

Continuing past work on the modelling of coaxial cables, we investigate the question of the modeling of non-perfectly conducting thin coaxial cables. Starting from 3D Maxwell's equations, we derive, by asymptotic analysis with respect to the (small) transverse dimension of the cable, a simplified effective 1D model. This model involves a fractional time derivatives that accounts for the so-called skin effects in highly conducting regions.

Keywords: Maxwell's equations, Coaxial cables, Asymptotic analysis

Statement of the problem

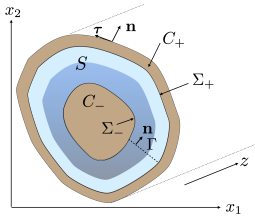


Figure 1: Section the coaxial cable. Σ_+ and Σ_- are the outer and inner boundary of S .

Denoting $\delta > 0$ a small parameter, we consider a family of (thin) domains $\Omega^\delta = \mathcal{G}_\delta(\Omega)$ where

$$\mathcal{G}_\delta : (x_1, x_2, z) \longrightarrow (\delta x_1, \delta x_2, z).$$

and Ω is the disjoint union of a conducting domain Ω_c and a dielectric one Ω_d ,

$$\Omega_c = C \times \mathbb{R}, \quad \Omega_d = S \times \mathbb{R},$$

where $C = C^+ \cup C^-$, C^+ corresponding to the outer metallic shield and C^- to the inner metallic wire and S is non-simply connected, see Figure 1. Accordingly, we have, with obvious notation

$$\Omega^\delta = \Omega_d^\delta \cup \Omega_c^\delta.$$

We are interested in the solution (E^δ, H^δ) of 3D Maxwell's equation in Ω^δ :

$$\begin{cases} \varepsilon^\delta \partial_t E^\delta + \sigma^\delta E^\delta - \text{curl } H^\delta = \mathbf{j}^\delta, \\ \mu^\delta \partial_t H^\delta + \text{curl } E^\delta = \mathbf{0}, \end{cases} \quad (1)$$

with zero initial data. In Ω_c^δ , $(\varepsilon^\delta, \mu^\delta)$ are constant equal to (ε_c, μ_c) and $\mathbf{j}^\delta = \mathbf{0}$. In Ω_d^δ , $(\varepsilon^\delta, \mu^\delta)$ do not depend on z and are obtained by a scaling in the transverse variable $\mathbf{x}_T = (x_1, x_2)$ of fixed distributions in the reference domain Ω_d , for instance

$$\varepsilon^\delta(\mathbf{x}_T, z) = \varepsilon(\mathbf{x}_T/\delta).$$

The source term \mathbf{j}^δ is defined similarly, moreover it is compactly supported, it has no longitudinal component and is divergence free. The conductivity is weak in the dielectric Ω_d^δ , but very high in Ω_c^δ . More precisely

$$\sigma^\delta(\mathbf{x}_T, z) = \begin{cases} \delta^{-4} \sigma_c & \text{in } \Omega_c^\delta, \\ \delta \sigma(\mathbf{x}_T/\delta), & \text{in } \Omega_d^\delta. \end{cases} \quad (2)$$

Note that the $O(\delta^{-4})$ magnitude of σ^δ in Ω_c^δ gives rise to a skin depth in $O(\delta^2)$, small with respect to δ .

Our approach consists in obtaining the formal behaviour of the solution for small δ . To do so, we propose two distinct asymptotic expansions of the solution Ω_d^δ and Ω_c^δ that we match using our transmission conditions. We present below our main results.

Electromagnetic field in the dielectric

We introduce the following notations.

- ∇ for the 2D transverse gradient in \mathbf{x}_T , identified to a 3D vector with third component 0,
- $S_\Gamma := S \setminus \Gamma$ where Γ is a cut that makes S_Γ simply connected (see Figure 1),
- $[\cdot]_\Gamma$ for the jump across Γ in the direction \mathbf{n} ,
- $\tilde{\nabla}$ is the 2D transverse gradient in S_Γ ,
- $\partial_{\tilde{\mathbf{n}}}$ is the normal derivative, and $\partial_\tau \psi = \tilde{\nabla} \psi \cdot \tau$ the tangential derivative.

We obtain that, for small δ and all $\mathbf{x}_T \in S^\delta$,

$$\begin{aligned} E^\delta(\mathbf{x}_T, z, t) &\sim V^\delta(z, t) \nabla \varphi_e(\mathbf{x}_T/\delta) \\ &\quad + \delta \left(\int_0^t V^\delta(z, s) ds \right) \nabla \varphi_r(\mathbf{x}_T/\delta), \\ &\quad + \delta \partial_z V^\delta(z, t) (\varphi_e - \varphi_m)(\mathbf{x}_T/\delta) \mathbf{e}_z, \end{aligned}$$

$$\begin{aligned} H^\delta(\mathbf{x}_T, z, t) &\sim I^\delta(z, t) \nabla \psi_m(\mathbf{x}_T/\delta), \\ &\quad + \delta \left(\int_0^t \frac{1}{2} I^\delta(z, s) ds \right) \nabla \psi_r(\mathbf{x}_T/\delta), \\ &\quad + \delta \partial_z I^\delta(z, t) (\psi_e - \psi_m)(\mathbf{x}_T/\delta) \mathbf{e}_z, \end{aligned}$$

where $\mathbf{e}_z = (0, 0, 1)^t$. Moreover:

i) The potential $\varphi_e \in H^1(S)$ satisfies,

$$\operatorname{div} \varepsilon \nabla \varphi_e = 0(S), \quad \varphi_e = 0(\Sigma_+), \quad \varphi_e = 1(\Sigma_-),$$

and the same for φ_m with μ^{-1} instead of ε .

ii) The potential $\psi_m \in H^1(S_\Gamma)$ satisfies

$$\operatorname{div} \mu \nabla \psi_m = 0(S_\Gamma), \quad \partial_n \psi_m = 0(\partial S),$$

and $[\psi_m]_\Gamma = 1$, $[\partial_n \psi_m]_\Gamma = 0$. The same holds for ψ_e with ε^{-1} instead of μ . Moreover

$$\int_S \mu \psi_e = \int_S \mu \psi_m = 0.$$

iii) The function $\varphi_r \in H_0^1(S)$ is the solution of

$$\operatorname{div} \varepsilon \nabla \varphi_r = -\operatorname{div} \sigma \nabla \varphi_e.$$

iv) The function $\psi_r \in H^1(S)$ satisfies

$$\operatorname{div} \mu \nabla \psi_r = 0(S), \quad \mu \partial_n \psi_r = -\sqrt{\frac{\mu_c}{\sigma_c}} \partial_\tau^2 \psi_m(\partial S).$$

v) The electric potential $V^\delta(z, t)$ and current $I^\delta(z, t)$ are 1D unknowns governed by generalized telegrapher's equations:

$$\begin{cases} C \partial_t V^\delta + \delta G V^\delta + \partial_z I^\delta = j, \\ L \partial_t I^\delta + \delta R \partial_t^{\frac{1}{2}} I^\delta + \partial_z V^\delta = 0, \end{cases} \quad (3)$$

where $j(z, t)$ is an effective source term,

$$j(z, t) = \int_S \mathbf{j}(\mathbf{x}_T, z, t) \cdot \nabla \varphi_e(\mathbf{x}_T), \quad (4)$$

and $\partial_t^{\frac{1}{2}}$ is the square root derivative in the sense of Caputo

$$\partial_t^{\frac{1}{2}} u(t) = \frac{1}{\sqrt{\pi}} \int_0^t \frac{\partial_\tau u(\tau)}{\sqrt{t-\tau}} d\tau.$$

As in [1], the capacity C , inductance L and conductance G are given by:

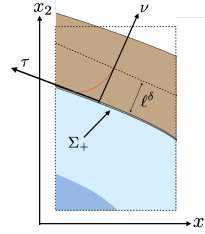
$$C = \int_S \varepsilon |\nabla \varphi_e|^2, \quad L = \int_S \mu |\tilde{\nabla} \psi_m|^2, \quad G = \int_S \sigma |\nabla \varphi_e|^2$$

Moreover, we obtain an explicit expression for the resistance R , which takes into account skin effects:

$$R = \int_{\partial S} \sqrt{\frac{\mu_c}{\sigma_c}} |\partial_\tau \psi_m|^2. \quad (5)$$

This generalizes formulas of the literature (see [2], chapter 13) already derived in very simple cases.

Electric field in the outer conductor



In the rescaled conducting domain C_+ the electromagnetic fields are described using tangential and normal coordinates (τ, ν) . The penetration depth ℓ^δ of the fields is in $O(\delta)$.

L^+ being the length of Σ_+ , one shows that there exists a 3D field

$$E^+ : [0, L^+] \times \mathbb{R}^+ \times \mathbb{R} \times \mathbb{R}^+ \rightarrow \mathbb{R}^3$$

such that in $C_+^\delta \times \mathbb{R}$ and for small δ ,

$$E^\delta(\mathbf{x}_T(\tau, \nu), z, t) \sim \delta^2 E^+(\tau/\delta, \nu/\delta^2, z, t),$$

(and a similar property holds for the magnetic field). The important fact is that the component E_z^+ is solution of the 1D heat equation

$$\mu_c \sigma_c \partial_t E_z^+ - \partial_\nu^2 E_z^+ = 0, \quad (6)$$

and thus satisfies, at the boundary $\nu = 0$:

$$\partial_\nu E_z^+ + \sqrt{\mu_c \sigma_c} \partial_t^{\frac{1}{2}} E_z^+ = 0.$$

The above equation is used when writing transmission conditions across $\Sigma_+^\delta \times \mathbb{R}$.

This explains the appearance of $\partial_t^{\frac{1}{2}}$ in the effective model (3).

References

- [1] G. Beck, S. Imperiale, P. Joly *Mathematical modelling of multi conductor cables*, Disc. & Cont. Dynamical Systems, (2014).
- [2] W. H. Hayt, J. A. Buck, *Engineering Electromagnetics*, 6th Edition, (2001).

Convergence analysis of boundary element methods for electromagnetic resonance problems for dielectric and plasmonic scatterers

Gerhard Unger^{1,*}

¹Institute of Applied Mathematics, Graz University of Technology, Graz, Austria

*Email: gunger@math.tugraz.at

Abstract

We present a convergence analysis of Galerkin boundary element methods for the approximation of electromagnetic resonances and modes of dielectric and plasmonic scatterers. The analysis is based on the analytic Fredholm theory and on the concept of regular approximations of operators.

Keywords: electromagnetic scattering, resonances, boundary element method

1 Boundary integral formulation

We consider resonance problems for dielectric and plasmonic scatterers occupying a bounded Lipschitz domain Ω_1 with boundary Γ . The embedding domain is denoted by $\Omega_2 := \mathbb{R}^3 \setminus \overline{\Omega_1}$. We assume that the permittivity ε and the permeability μ are homogeneous in Ω_1 and Ω_2 , respectively, and define $\varepsilon = \varepsilon_1 \chi(\Omega_1) + \varepsilon_2 \chi(\Omega_2)$ and $\mu = \mu_1 \chi(\Omega_1) + \mu_2 \chi(\Omega_2)$, where χ denotes the characteristic function. The permittivity and permeability may depend on the angular frequency ω , but the dependency is assumed to be holomorphic within the interested frequency range $\Lambda \subset \mathbb{C}$. The resonance problem reads as follows: find $\omega \in \Lambda$ and non-trivial $(\mathbf{E}, \mathbf{H}) \in (\mathbf{H}_{\text{loc}}(\text{curl}, \mathbb{R}^3))^2$ such that:

$$\begin{aligned} \nabla \times \mathbf{E} &= i\omega\mu\mathbf{H} && \text{in } \mathbb{R}^3 \setminus \Gamma, \\ \nabla \times \mathbf{H} &= -i\omega\varepsilon\mathbf{E} && \text{in } \mathbb{R}^3 \setminus \Gamma, \\ \gamma_t^{(1)}\mathbf{E} &= \gamma_t^{(2)}\mathbf{E} && \text{and } \gamma_t^{(1)}\mathbf{H} = \gamma_t^{(2)}\mathbf{H} && \text{on } \Gamma, \end{aligned} \tag{1}$$

where $\gamma_t^{(j)}\mathbf{F} := \mathbf{n} \times \mathbf{F}|_{\partial\Omega_j}$, $j = 1, 2$, and \mathbf{n} is the unit normal vector field on Γ pointing into Ω_2 . In addition we impose that (\mathbf{E}, \mathbf{H}) satisfies an outgoing radiation condition, see [5]. If $(\omega, \mathbf{E}, \mathbf{H})$ satisfies (1), then \mathbf{E} can be represented in terms of the tangential traces

$$\mathbf{j} := \mathbf{n} \times \mathbf{E}|_{\Gamma} \quad \text{and} \quad \mathbf{m} := i\omega(\mathbf{n} \times \mathbf{H})|_{\Gamma}$$

by the Stratton-Chu representation formula

$$\mathbf{E} = \begin{cases} -(\frac{\mu_1}{\varepsilon_1\omega^2})^{\frac{1}{2}} \Psi_{\text{SL}}^1(\omega)\mathbf{m} - \Psi_{\text{DL}}^1(\omega)\mathbf{j}, & \text{in } \Omega_1, \\ (\frac{\mu_2}{\varepsilon_2\omega^2})^{\frac{1}{2}} \Psi_{\text{SL}}^2(\omega)\mathbf{m} + \Psi_{\text{DL}}^2(\omega)\mathbf{j}, & \text{in } \Omega_2, \end{cases} \tag{2}$$

where Ψ_{SL}^j and Ψ_{DL}^j are the single and double layer potential of Maxwell's equations [1]. A similar formula holds for \mathbf{H} . Applying the tangential trace operators $\gamma_t^{(1)}$ and $\gamma_t^{(2)}$ to the Stratton-Chu formula (2) yields the interior and exterior Calderón identity [1]

$$(\frac{1}{2}I - A_1(\omega)) \begin{pmatrix} \mathbf{j} \\ \mathbf{m} \end{pmatrix} = 0 = (\frac{1}{2}I + A_2(\omega)) \begin{pmatrix} \mathbf{j} \\ \mathbf{m} \end{pmatrix} \tag{3}$$

with

$$A_j(\omega) := \begin{pmatrix} C^j(\omega) & \frac{\sqrt{\mu_j}}{\omega\sqrt{\varepsilon_j}} S^j(\omega) \\ \frac{\omega\sqrt{\varepsilon_j}}{\sqrt{\mu_j}} S^j(\omega) & C^j(\omega) \end{pmatrix},$$

where $C^j := \frac{1}{2}(\gamma_t^{(1)}\Psi_{\text{DL}}^j + \gamma_t^{(2)}\Psi_{\text{DL}}^j)$ and $S^j := \gamma_t^{(j)}\Psi_{\text{SL}}^j$. Combining the identities in (3) leads to the following boundary integral formulation of the resonance problem (1): find $\omega \in \Lambda$ and non-trivial $(\mathbf{j}, \mathbf{m}) \in \mathbf{X}^2$ such that

$$A(\omega)(\mathbf{j}, \mathbf{m})^T = 0, \tag{4}$$

where $\mathbf{X} := \mathbf{H}^{-1/2}(\text{div}_{\Gamma}, \Gamma)$ and $A := A_1 + A_2$. The boundary integral formulation of the resonance problem in (4) is a nonlinear eigenvalue problem, even in the non-dispersive case, since ω appears nonlinearly in the kernel of the boundary integral operators $S^j(\omega)$ and $C^j(\omega)$. However, on the discrete level the resulting eigenvalue problem can be reduced to an equivalent linear eigenvalue problem by the contour integral method.

For the analysis of the eigenvalue problem (4) it is crucial that $A(\omega)$ satisfies a generalized Gårding's inequality in \mathbf{X}^2 , i. e., there exist a compact operator $K(\omega)$ and an isomorphism $T(\omega)$ such that

$$\langle A(\omega)\mathbf{u}, T(\omega)\mathbf{u} \rangle + \langle K(\omega)\mathbf{u}, \mathbf{u} \rangle \geq c(\omega)\|\mathbf{u}\|_{\mathbf{X}^2}^2 \tag{5}$$

for all $\mathbf{u} \in \mathbf{X}^2$ [1, 5]. The operator $T(\omega)$ is a block diagonal operator with diagonal elements T and/or $I_{\mathbf{X}}$ depending on the frequency. The operator T is constructed as projection which

is related to a Helmholtz-type decomposition of \mathbf{X} [1]. The generalized Gårding's inequality (5) shows that $A(\omega)$ is a Fredholm operator of index zero. This together with the holomorphy of the integral operators implies that the eigenvalue problem (4) can be treated within the analytic Fredholm theory [2].

2 Boundary element approximation

We consider a conforming Galerkin boundary element approximation of the eigenvalue problem (4). Let $(\mathbf{X}_h^2)_h$ be a sequence of finite-dimensional subspaces of \mathbf{X}^2 such that

$$\inf_{\mathbf{u}_h \in \mathbf{X}_h^2} \|\mathbf{u}_h - \mathbf{u}\|_{\mathbf{X}^2} \rightarrow 0 \text{ as } h \rightarrow 0 \quad \forall \mathbf{u} \in \mathbf{X}^2. \quad (6)$$

We denote by $Q_h : \mathbf{X}^2 \rightarrow \mathbf{X}_h^2$ is the orthogonal projection.

The Galerkin approximation of the eigenvalue problem (4) reads as follows: find $\omega_h \in \Lambda$ and a non-trivial $\mathbf{u}_h \in \mathbf{X}_h^2$ such that

$$\langle A(\omega_h)\mathbf{u}_h, \mathbf{v}_h \rangle = 0 \quad \forall \mathbf{v}_h \in \mathbf{X}_h^2. \quad (7)$$

The Galerkin eigenvalue problem (7) results in a nonlinear matrix eigenvalue problem which can be solved by the contour integral method [5].

The application of abstract convergence results of [2,3] to the Galerkin approximation (7) requires a regular approximation of the operator $A(\omega)$ by the sequence $(Q_h A(\omega) Q_h)_h$, i. e., for any $(Q_h A(\omega) Q_h \mathbf{u}_h)_h$, $\|\mathbf{u}_h\|_{\mathbf{X}^2} \leq 1$, which has a convergent subsequence, it holds that $(\mathbf{u}_h)_h$ has already a convergent subsequence.

For the case of an operator which satisfies a generalized Gårding's inequality sufficient conditions for the regular approximation are specified in [4]. These imply that a regular approximation of $A(\omega)$ by $(Q_h A(\omega) Q_h)_h$ is guaranteed if the following condition is satisfied:

- (A) For $T(\omega)$ as given in (5) there exists a sequence $(T_h(\omega))_h$, $T_h(\omega) : \mathbf{X}_h^2 \rightarrow \mathbf{X}_h^2$ linear and continuous, such that

$$\sup_{\mathbf{u}_h \in \mathbf{X}^2 \setminus \{0\}} \frac{\|(T(\omega) - T_h(\omega))\mathbf{u}_h\|_{\mathbf{X}^2}}{\|\mathbf{u}_h\|_{\mathbf{X}^2}} \xrightarrow{h \rightarrow 0} 0.$$

If \mathbf{X}_h is the space generated by Raviart-Thomas elements defined on a sequence of regular triangulations of Γ , then (6) holds [1] and also condition (A) is satisfied for

$$T_h[i, j](\omega) := P_h T[i, j](\omega), \quad 1 \leq i, j \leq 2,$$

where $P_h : \mathbf{X} \rightarrow \mathbf{X}_h$ is the orthogonal projection [5].

In the following theorem the error estimates for the Galerkin approximations are presented.

Theorem 1 *Suppose that (6) and (A) holds. Let $\omega \in \Lambda$ be an eigenvalue of (4) and $D \subset \Lambda$ be compact such that ω is the only eigenvalue in D . Then there exists an $h_0 > 0$ and a constant $c > 0$ such that for all $0 < h \leq h_0$ we have:*

$$|\omega - \omega_h| \leq c\delta(G(\omega), \mathbf{X}_h^2)^{2/\ell}$$

for all eigenvalues $\omega_h \in D$ of (7), where

$$\delta(G(\omega), \mathbf{X}_h^2) := \sup_{\mathbf{u} \in G(\omega)} \inf_{\mathbf{u}_h \in \mathbf{X}_h^2} \frac{\|\mathbf{u} - \mathbf{u}_h\|_{\mathbf{X}^2}}{\|\mathbf{u}\|_{\mathbf{X}^2}}.$$

Here $G(\omega)$ denotes the generalized eigenspace corresponding to ω , and ℓ is the maximal length of a Jordan chain corresponding to ω . Further, if (ω_h, \mathbf{u}_h) is an eigenpair of (7) with $\omega_h \in D$ and $\|\mathbf{u}_h\|_{\mathbf{X}^2} = 1$, then it holds

$$\inf_{\mathbf{u} \in G(\omega)} \|\mathbf{u} - \mathbf{u}_h\|_{\mathbf{X}^2} \leq c(\delta(G(\omega), \mathbf{X}_h^2) + |\omega - \omega_h|).$$

Numerical examples in [5] confirm the theoretical results of Thm. 1.

References

- [1] A. Buffa, R. Hiptmair, T. von Petersdorff and C. Schwab, Boundary element methods for Maxwell transmission problems in Lipschitz domains, *Numer. Math.* **95(3)** (2003), pp. 459–485.
- [2] O. Karma, Approximation in eigenvalue problems for holomorphic Fredholm operator functions. I. *Numer. Funct. Anal. Optim.*, **17(3-4)**, (1996), pp. 365–387 .
- [3] O. Karma, Approximation in eigenvalue problems for holomorphic Fredholm operator functions. II. *Numer. Funct. Anal. Optim.*, **17(3-4)**, (1996), pp. 389– 408.
- [4] M. Halla, Regular Galerkin approximations of holomorphic T-Gårding operator eigenvalue problems, ASC Report 4, TU Wien, 2016.
- [5] G. Unger, Convergence analysis of a Galerkin boundary element method for electromagnetic eigenvalue problems, *Berichte aus dem Institut für Numerische Mathematik*, 17/2, TU Graz, 2017.

Model of electromagnetic scattering by breaking sea waves based upon the method of fundamental solutions

Arnaud Coatanhay^{1,*}, Yves-Marie Scolan²

¹ENSTA Bretagne, Lab-STICC (UMR CNRS 6285), Brest, France

²ENSTA Bretagne, IRDL (UMR CNRS 6027), Brest, France

*Email: arnaud.coatanhay@ensta-bretagne.fr

Abstract

Two issues arise from modeling of the electromagnetic scattering by breaking sea waves: first, the simulation of the breaking sea waves which is matter of fluid mechanics theory and, secondly, the computation of the electromagnetic scattered field which is matter of electromagnetic physics. The purpose of this study is modeling these two issues with the same approach: the method of fundamental solutions.

Keywords: electromagnetic scattering, breaking waves, method of fundamental solutions

1 Introduction

At a fundamental level, models in fluid dynamics are based on non-linear partial differential equations leading to very complex numerical estimations and time-consuming simulations for the sea waves. Fortunately, considering fluid as ideal, incompressible and irrotational, the fluid mechanics issue becomes much easier to treat. In fact, on these assumptions, the velocity potential ϕ can be described by a Laplace equation:

$$\Delta\phi = 0 \quad \text{in the fluid} \quad (1a)$$

$$\phi = e(\vec{M}, t) \quad \text{on the free surface,} \quad (1b)$$

where \vec{M} denotes the two-dimensional position of point M on the free surface and the function e follows from the solution of the time differential system composed of kinematic and dynamic free surface boundary conditions.

The method of fundamental solutions (MFS) is to express the velocity potential in the form of a series of elementary solutions:

$$\phi(\vec{x}, t) \approx \sum_{j=1}^N q_j(t) G(\vec{x}, \vec{X}_j(t)), \quad (2)$$

where $\vec{X}_j(t)$ are the location of source number j and q_j is its strength. We denote G the fundamental solution (one point source) for the Laplace equation.

The position of the sources is not arbitrary and must be tuned to be optimized, but, in any case, sources are located outside the fluid domain. In fact, the distance from the boundary is chosen so that mass and energy are well conserved. Several years ago, Y.-M. Scolan combined conformal transformations with MFS and developed a very efficient algorithm to simulate sea breaking waves. This algorithm is implemented in the code FSID (Free Surface Identification) and is fully described in [1]. Here we use that code to produce realistic overturning crest and its dynamics as illustrated in figure 1:

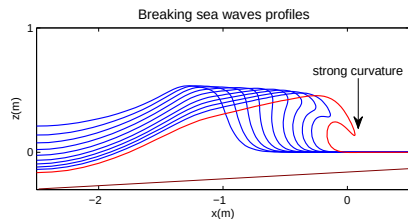


Figure 1: Breaking sea wave profile generated by the code FSID.

2 Electromagnetic field

A standard approach to compute the electromagnetic field scattered by these breaking wave profiles is to use the electric field integral equation (EFIE) and standard numerical methods, method of moments (MoM) for instance, to solve this equation. Unfortunately, breaking wave profiles involve the presence of strong local curvature area. For standard MoM, strong curvatures create numerical convergence problems [2]. To overcome these difficulties, different numerical strategies can be applied [4–6].

From a numerical viewpoint, these strategies enable to solve the convergence problem. How-

ever, the strategies does not clarify the physical interpretations of the complex interaction between time-evolving sea surface and the electromagnetic scattering. Strictly speaking, the scattering by sea surface is not a coupled phenomenon since the electromagnetic field has no influence on the fluid. However, we think that a common numerical model for the fluid mechanics and the electromagnetics may be helpful in understanding the interaction between sea surface and the scattered electromagnetic field. With this aim in mind, we suggest to applied the same numerical approach (MFS) previously used in fluid mechanics as for the electromagnetic issue.

From a formal point of view, the scattering problem of a monochromatic plane electromagnetic wave can be summarized as the following boundary value problem:

(Helmholtz equation)

$$\Delta u + k^2 u = 0 \quad \text{in } \Omega \quad (3a)$$

$$u = v \quad \text{on } \partial\Omega, \quad (3b)$$

where $\Omega \subset \mathcal{R}^2 = \mathcal{C}$ is a connected planar domain with analytic boundary $\partial\Omega$.

In the same way as for fluid modeling, the idea of the MFS is to approximate u by a linear combination of fundamental solutions of the form:

$$u(\vec{x}, t) \approx \frac{i}{4} \sum_{j=1}^N \alpha_j H_0^{(1)}(k|\vec{x} - \vec{X}_j|) \quad (4)$$

where \vec{X}_j is the position of the source number j . $H^{(1)} = J_0 + iY_0$ is an Hankel function of the first kind of zero order, J_0 is a Bessel function of the first kind of order zero and Y_0 is a Bessel function of the second kind of order zero.

The application of MFS for Helmholtz equation has been validated by already published studies [7,8] for various canonical configurations. In this study, we propose to apply this numerical method in the case of breaking wave profiles and to present the connection between fluid mechanics source points and the electromagnetic ones.

References

[1] Y.-M. Scolan, Some aspects of the flip-through phenomenon: A numerical study based on the desingularized technique, *Journal of Fluids and Structures* **26** (2010), pp. 918–953.

- [2] C. Davis, K. Warnick, Error analysis of 2-D MoM for MFIE/EFIE/CFIE based on the circular cylinder, *Antennas and Propagation* **53** (2005), pp. 321–331.
- [3] R. Khairi, A. Coatanhay, A. Khenchaf, Optimal High-Order Method of Moment combined with NURBS for the scattering by a 2D cylinder, *Advanced Electromagnetics* **2(1)** (2013), pp. 33–43.
- [4] W. Yang, Z. Zhao, Electromagnetic Modeling of Breaking Waves at Low Grazing Angles With Adaptive Higher Order Hierarchical Legendre Basis Functions, *IEEE Transactions on Geoscience and Remote Sensing*, **49(1)** (2011), pp. 346–352.
- [5] R. Khairi, A. Coatanhay, A. Khenchaf and Y.-M. Scolan, Numerical modeling of electromagnetic waves scattering from 2D coastal breaking sea wave, *The European Physical Journal Applied Physics* **64(2)** (2013), pp. 24505–24510.
- [6] A. Coatanhay and Y.-M. Scolan, Adaptive multiscale moment method applied to the electromagnetic scattering by coastal breaking sea waves, *Mathematical Methods in the Applied Sciences* **38(10)** (2015), pp. 2041–2052.
- [7] S. Yu. Reutskiy, The method of fundamental solution for Helmholtz eigenvalue problems in simply and multiply connected domains, *Engineering Analysis with Boundary Elements* **30** (2006), pp. 150–159.
- [8] A.H. Barnetta, T. Betcke, Stability and convergence of the method of fundamental solutions for Helmholtz problems on analytic domains, *Journal of Computational Physics* **227** (2008), pp. 7003–7026.

A Continuation Approach to Boundary Integral Equation for Steady-state Wave Scattering by a Crack with Contact Acoustic Nonlinearity

Taizo Maruyama^{1,*}, Terumi Touhei¹

¹Department of Civil Engineering, Tokyo University of Science, Japan

*Email: taizo_maruyama@rs.tus.ac.jp

Abstract

The present study deals with steady-state wave scattering by a crack with contact acoustic nonlinearity. The authors propose a continuation approach to the boundary integral equation for the wave scattering in order to investigate nonlinear resonance with higher- and sub-harmonic generation. To derive the system of nonlinear equations, a harmonic balance method is integrated into the boundary element method. A numerical continuation method is applied to track the solution of the system of nonlinear equations.

Keywords: Elastic wave, Contact acoustic nonlinearity, Continuation method, Boundary element method, Harmonic balance method

1 Introduction

Nonlinear ultrasonic testing (NLUT) based on contact acoustic nonlinearity (CAN) has been developed for inspection of closed cracks [1]. Accurate NLUT requires an understanding of the behavior of higher- and sub-harmonic waves, which are used for the defect evaluation. However, the theoretical explanation of the nonlinear scattering phenomena with CAN is not sufficient at present. In particular, there remains investigation of nonlinear resonance due to the interaction among incident frequency and amplitude, size of crack, and CAN.

In order to investigate the behavior of nonlinear resonance with higher- and sub-harmonic generation, the present study deals with steady-state wave scattering by a crack with contact boundary conditions. Under pre-opening displacement or static compressive stress, a crack in an unbounded elastic solid is subjected to a time-harmonic incident wave, and clapping motion and dynamic friction on the crack face are induced as a nonlinear phenomenon.

2 Wave scattering by a crack with CAN

An incident wave \mathbf{u}^{in} is scattering by a crack $S \subset \mathbb{R}^2$ having edges ∂S , as shown in Fig. 1(a).

The base material $D(= \mathbb{R}^2 \setminus \bar{S})$ is assumed to be a homogeneous, isotropic, and linear elastic solid. The unit normal vector \mathbf{n} is defined as pointing to the positive side of S .

From a microscopic viewpoint, the crack has rough surfaces as shown in Fig. 1(b). However, the wavelength of the waves dealt with herein is much larger than the roughness height and length, which enables us to analyze the crack from a macroscopic viewpoint. Therefore, average displacement \mathbf{u}^\pm and average stress $\boldsymbol{\sigma}^\pm$ are treated on S , where the superscript $+$ ($-$) indicates the field variables limited to S from the positive (negative) side of S . It is assumed that the traction $\mathbf{t}^\pm(= \mathbf{n} \cdot \boldsymbol{\sigma}^\pm)$ and the crack opening displacement (COD) $[\mathbf{u}]$ satisfy

$$\mathbf{t}^+ = \mathbf{t}^- (= \mathbf{t}) \quad \text{on } S, \quad (1)$$

$$[\mathbf{u}] (= \mathbf{u}^+ - \mathbf{u}^-) = \mathbf{0} \quad \text{on } \partial S. \quad (2)$$

In order to describe the clapping motion and dynamic friction on the crack, we consider separation and closed phases. It is assumed that S can be separated into S_s and S_c , where S_s and S_c denote portions of S in the separation and closed phases, respectively. At the separation phase, the traction-free condition is assumed:

$$\mathbf{t} = \mathbf{0} \quad \text{on } S_s. \quad (3)$$

For the closed phase, we consider the displacement continuity and Coulomb's friction law:

$$[\mathbf{u}] \cdot \mathbf{n} = 0, \quad (4a)$$

$$\mathbf{t} \cdot \mathbf{s} = -\mu_d (\dot{\mathbf{t}} \cdot \mathbf{n}) \text{sgn}([\dot{\mathbf{u}}] \cdot \mathbf{s}) \quad \text{on } S_c, \quad (4b)$$

where \mathbf{s} is the unit tangential vector, μ_d is the dynamic friction coefficient, and $(\dot{\quad})$ indicates the time differentiation.

When the incident wave \mathbf{u}^{in} reaches S under the static displacement field \mathbf{u}^{st} , the scattered wave \mathbf{u}^{sc} is generated by the interaction of \mathbf{u}^{st} and \mathbf{u}^{in} with S and radiates into infinity. Hence, the total displacement field \mathbf{u} is represented as $\mathbf{u} = \mathbf{u}^{\text{st}} + \mathbf{u}^{\text{in}} + \mathbf{u}^{\text{sc}}$, and \mathbf{u}^{sc} satisfies

$$\begin{aligned} & \mu \nabla^2 \mathbf{u}^{\text{sc}}(\mathbf{x}, t) + (\lambda + \mu) \nabla \nabla \cdot \mathbf{u}^{\text{sc}}(\mathbf{x}, t) \\ & = \rho \ddot{\mathbf{u}}^{\text{sc}}(\mathbf{x}, t) \quad \text{for } (\mathbf{x}, t) \in D \times [0, \infty), \end{aligned} \quad (5)$$

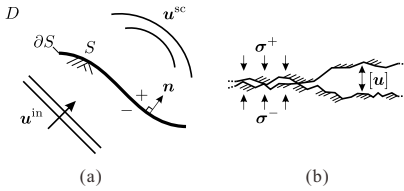


Figure 1: (a) Wave scattering by a crack in an unbounded elastic solid and (b) microscopic view of crack faces.

and the outgoing radiation condition, where ρ is the mass density, and λ and μ are the Lamé parameters.

3 Solution procedure

It is expected for the above stated problem that a time-harmonic incident wave leads to periodic responses after a sufficient elapsed time. Therefore, we introduce the nonlinear steady-state scattering due to time-harmonic \mathbf{u}^{in} with circular frequency ω^{in} as asymptotic behavior after a sufficient elapsed time. The solution procedure is briefly summarized.

The wave scattering by a crack is described in the time-domain BIE with unknown variables $[\mathbf{u}]$ and \mathbf{t} on S . Then, $[\mathbf{u}]$ and \mathbf{t} are approximated by means of the finite Fourier series. For example,

$$[\mathbf{u}](\mathbf{x}, t) \simeq \frac{\mathbf{a}^{(0)}(\mathbf{x})}{2} + \sum_{n=1}^{N_h} \left[\mathbf{a}^{(n/\kappa)}(\mathbf{x}) \cos\left(\frac{n\omega^{in}t}{\kappa}\right) + \mathbf{b}^{(n/\kappa)}(\mathbf{x}) \sin\left(\frac{n\omega^{in}t}{\kappa}\right) \right], \quad (6)$$

where the Fourier series are truncated by N_h , and κ is an integer used to represent possible sub-harmonic components. Substituting Eq.(6) into the time-domain BIE and taking limit of $t \rightarrow \infty$ to express the asymptotic behavior, we can obtain a system of nonlinear equations without time factors, whose unknown variables are $\mathbf{a}^{(n/\kappa)}$ and $\mathbf{b}^{(n/\kappa)}$. The system of nonlinear equations can be written as

$$\mathbf{f}(\phi, \alpha) = \mathbf{0} \quad (7)$$

$$\phi = \left\{ \mathbf{a}^{(0)}, \dots, \mathbf{a}^{(N_h/\kappa)}, \mathbf{b}^{(1/\kappa)}, \dots, \mathbf{b}^{(N_h/\kappa)} \right\}^T,$$

where α is a physical parameter such as ω^{in} . Solving Eq. (7) with some spatial discretization

is called a harmonic balance-boundary element method (HB-BEM) [2].

We want to track the solution ϕ of Eq. (7) when α is changed, and the numerical continuation method (NCM) [3] is therefore used for the purpose. In the NCM procedure, we may encounter the turning and branch points of the solution path, which are related with important phenomena such as jump and bifurcation in the nonlinear dynamical system. Thus, investigation of these points is an important role in the NCM procedure.

The HB-BEM provides steady-state solution without distinction of stability, though we have to distinguish the stability to understand the physical phenomenon. For the stability analysis, assuming that an infinitesimal perturbation ϵ arises around the obtained COD solution $[\tilde{\mathbf{u}}]$, we investigate whether or not the amplitude of ϵ grows with time. As a result of the formulation based on Hill’s method, the stability analysis comes to the nonlinear eigenvalue problem, which is solved by the Sakurai-Sugiura method [4] in this study.

4 Conclusions

We developed a numerical method for the steady state wave scattering by a crack with contact acoustic nonlinearity. The numerical solutions and their comparison to the transient solutions will be presented in the talk.

References

- [1] I. Yu. Solodov, D. Doring, and G. Busse, New opportunities for NDT using nonlinear interaction of elastic waves with defects, *Journal of Mechanical Engineering* **57** (2011), pp. 169–182.
- [2] T. Maruyama and T. Touhei, Steady-state anti-plane shear wave scattering by a crack with friction, *The Journal of the Acoustical Society of America* **143** (2018) pp. 3545–3556.
- [3] E. L. Allgower and K. Georg, Introduction to numerical continuation methods, Springer-Verlag (1990).
- [4] J. Asakura, T. Sakurai, H. Tadano, T. Ikegami, and K. Kimura, A numerical method for nonlinear eigenvalue problems using contour integrals, *JSIAM Letters* **1** (2009), pp. 52–55.

P-SV scattering from a periodic array of cylinders; tail-end asymptotics for efficient evaluation of the quasi-periodic Green's function

Georgia M. Lynott^{1,*}, William J. Parnell¹, I. David Abrahams², Raphaël C. Assier¹

¹School of Mathematics, University of Manchester, Manchester, UK

²Isaac Newton Institute, University of Cambridge, Cambridge, UK

*Email: georgia.lynott@manchester.ac.uk

Abstract

We study the scattering of time-harmonic P- and SV-waves from an infinite periodic array of cylindrical scatterers via the use of boundary element methods and the quasi-periodic elastodynamic Green's function. The slow convergence of the quasi-periodic Green's function is well known; we present a novel method of calculation that allows for rapid and accurate approximation of the functions, while remaining relatively easy to implement. This approach is based on an asymptotic expansion of the summand in the quasi-periodic Green's functions in order to derive tail-end correction terms, as was recently demonstrated for the acoustic case [1]. We extend this method to the elastodynamic case, which combined with BEM allows us to efficiently calculate the transmission and reflection coefficients associated with arrays of cylinders of different cross-sections and varying aspect ratios.

Keywords: Elastic scattering, periodic Green's function, BEM

1 Introduction

The reflection and transmission of elastic waves from an array of cylinders or voids is a canonical scattering problem with a wide range of potential applications. Previous work by [1] presented a novel method of calculation for the quasi-periodic Green's function in the acoustic case. Numerous alternative methods exist for periodic and quasi-periodic Greens functions in the acoustic case, as discussed in the review by [2], as well as more recent works [3], [4]. Methods for the elastodynamic case are less common in the literature. We demonstrate an extension of the method in [1] to the quasi-periodic elastic Green's functions that arise from the BEM scheme.

2 Problem formulation

We consider an infinite periodic array of cylinders of arbitrary shape along the x_1 axis, as shown in Fig. 1, surrounded by an isotropic, elastic medium with Lamé constants μ, λ and density ρ . We denote the m th cylinder by V^m , with surface ∂V^m . We seek time-harmonic so-

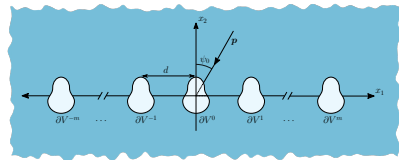


Figure 1: Time-harmonic wave, with incident angle ψ_0 and wavevector \mathbf{p} , scattering from a periodic array of cavities with spacing d .

lutions of the form $\mathbf{u}(\mathbf{x}e^{-i\omega t})$, where the displacement $\mathbf{u}(\mathbf{x})$ satisfies the elastodynamic wave equation

$$\mu \nabla^2 \mathbf{u}(\mathbf{x}) + (\mu + \lambda) \nabla(\nabla \cdot \mathbf{u}(\mathbf{x})) + \rho \omega^2 \mathbf{u}(\mathbf{x}) = 0$$

where $\mathbf{x} = (x_1, x_2)$. Let us consider an incident compressional wave of the form

$$\mathbf{u}^{\text{in}}(\mathbf{x}) = u_0 \mathbf{p} e^{ik_l \mathbf{p} \cdot \mathbf{x}},$$

with the wavevector

$$\mathbf{p} = -(\sin \psi_0, 0, \cos \psi_0),$$

and the compressional and shear wavenumbers, k_l , and k_s .

The total displacement field may be written as the sum of the scattered and incident fields, which allows us to introduce the BIE formulation for the displacement on the surface of a cylinder

$$\frac{1}{2} \delta_{ik} u_k(\mathbf{x}) = u_k^{\text{in}}(\mathbf{x}) + \int_{\partial V^m} U_{ik}(\mathbf{x}, \mathbf{y}) t_i(\mathbf{y}) dS(\mathbf{y}) - \int_{\partial V^m} T_{ik}(\mathbf{x}, \mathbf{y}) u_i(\mathbf{y}) dS(\mathbf{y}), \quad \mathbf{x} \in \partial V^m,$$

where f denotes the CPV integral, and U_{ik}, T_{ik} are the fundamental elastodynamic solutions, or Green's functions, for the displacement and traction. The displacement for the entire array is given simply by summing over the surfaces ∂V^m , owing to the superposition principle.

To reduce the surface of integration from an infinite array of cylinders to that of a single reference cylinder, we apply the quasi-periodic conditions

$$x_1^p = x_1^0 + pd, \quad x_2^p = x_2^0, \quad y_1^p = y_1^0 + qd, \quad y_2^p = y_2^0,$$

so that the incident field satisfies

$$\mathbf{u}^{\text{in}}(\mathbf{x}^p) = \mathbf{u}^{\text{in}}(\mathbf{x}^0)e^{-ik_1pd \sin \psi_0}.$$

This suggests the total displacement field also satisfies the Bloch-Floquet type condition

$$\mathbf{u}(\mathbf{x}^p) = \mathbf{u}(\mathbf{x}^0)e^{-ik_1pd \sin \psi_0}.$$

We can therefore rewrite the boundary integral equation in terms of the zeroth cell coordinates, integrating over the reference cylinder ∂V^0 to get

$$\frac{1}{2} \delta_{ik} u_k(\mathbf{x}^0) = u_k^{\text{in}}(\mathbf{x}^0) + \int_{\partial V^0} \tilde{U}_{ik}(\mathbf{x}^0, \mathbf{y}^0) t_i(\mathbf{y}^0) dS(\mathbf{y}^0) - \int_{\partial V^0} \tilde{T}_{ik}(\mathbf{x}^0, \mathbf{y}^0) u_i(\mathbf{y}^0) dS(\mathbf{y}^0), \quad \mathbf{x}^0 \in \partial V^0,$$

and defining the quasi-periodic forms of the fundamental solutions as

$$\begin{aligned} \tilde{U}_{ik}(\mathbf{x}^0, \mathbf{y}^0) &= \sum_{m=-\infty}^{\infty} e^{ik_l dm \sin \psi_0} U_{ik}(r_m), \\ \tilde{\Sigma}_{ik}^j(\mathbf{x}^0, \mathbf{y}^0) &= \sum_{m=-\infty}^{\infty} e^{ik_l dm \sin \psi_0} \Sigma_{ik}^j(r_m) \end{aligned}$$

where $r_m = \sqrt{(x_1^0 - y_1^0 + (m)d)^2 + (x_2^0 - y_2^0)^2}$.

3 Asymptotics of the quasi-periodic Green's function

In order to speed up computation of the quasi-periodic forms of the fundamental elastodynamic solutions, in each case we seek to truncate the sum at some integer M , and then approximate the remaining 'tail ends' of the sum, i.e. the sum for $|m| \geq M$, using an asymptotic expansion for the summand for each term $|m| \geq M$. We define the truncated sum as

$$S_M = \sum_{m=-(M-1)}^{M-1} e^{ik_l \sin \psi_0 dm} U_{ik}(r_m),$$

and seek correction terms $s_{\pm}(M)$ such that

$$\tilde{U}_{ik} \sim S_M + s_+(M) + s_-(M),$$

where σ_+ and σ_- denote the tail ends $m \geq M$ and $-m \leq -M$ respectively. By asymptotically expanding the terms of U_{ik} for large m , we find an expression for the tail ends in terms of a series of Lerch transcendent. We then exploit the integral representation of the Lerch transcendent, along with Watson's lemma, to replace the partial sums with an series of terms of increasing order $M^{-\frac{1}{2}}, M^{-\frac{3}{2}}, M^{-\frac{5}{2}}, \dots$, for truncation point M . The same method can be applied to the quasi-periodic fundamental traction.

While the resulting expressions for the correction terms are somewhat involved, they are still relatively straightforward to implement and allow for more accurate approximation of the Green's functions than the truncated sums alone

References

- [1] G. Lynott, V. Andrew, I.D. Abrahams *et al*, Acoustic scattering from a one-dimensional array; tail-end asymptotics for efficient evaluation of the quasi-periodic Green's function, *Journal of Wave Motion* DOI: 10.1016/j.wavemoti.2019.01.012
- [2] C. M. Linton, The Green's function for the two-dimensional Helmholtz equation in periodic domains, *Journal of Engineering Mathematics* **33**(4) (1998) pp. 377-401
- [3] O. P. Bruno and B. Delourme, Rapidly convergent two-dimensional quasi-periodic Green function throughout the spectrum – including Wood anomalies, *Journal of Computational Physics* **262** (2014) pp. 262-290
- [4] C. M. Linton, Lattice sums for the Helmholtz equation, *SIAM review* **54**(4) (2010) pp. 630-674

**A group theoretical approach for the numerical treatment
of symmetries in multipole methods**

Igor Chollet^{1,*}, Xavier Claeys², Francis Collino, Laura Grigori²

¹Sorbonne Université, Institut des Sciences du Calcul et des Données, ISCD, Université Paris-Diderot SPC, CNRS, Inria, Laboratoire Jacques-Louis Lions, équipe Alpines, F-75005, Paris, France

²Sorbonne Université, Université Paris-Diderot SPC, CNRS, Inria, Laboratoire Jacques-Louis Lions, équipe Alpines, F-75005 Paris

*Email: igor.chollet@inria.fr

Abstract

Multilevel acceleration methods for integral equations, such as the Fast Multipole Method (FMM), are commonly optimized by taking advantage of symmetry invariance properties of certain matrices involved in their hierarchical structure. Although such optimizations are well documented in the case where the invariance group under consideration is commutative, we present a unified approach that can also deal with the general non-commutative case. We apply this methodology to the particular case of HF-FMM in conjunction with Lebedev cubature grids.

Keywords: Symmetries, Helmholtz, High frequency, FMM, Cubature, Block diagonalization

Introduction

We consider the problem of computing sums of the form

$$f(\mathbf{x}) = \sum_{\mathbf{y} \in Y} G(\mathbf{x} - \mathbf{y})u(\mathbf{y}), \quad \mathbf{x} \in X$$

$$\text{where } G(\mathbf{z}) = \exp(i\kappa|\mathbf{z}|)/(4\pi|\mathbf{z}|)$$

where $X, Y \subset \mathbb{R}^3$ are large point clouds. Fast Multipole Methods (FMM) aims at computing such sums as fast as possible [4]. In the high frequency regime, the classical FMM for Helmholtz kernel heavily relies [3] on the formula:

$$G(\mathbf{r} + \mathbf{d}) = \int_{\mathbb{S}^2} \exp(i\kappa\mathbf{r} \cdot \boldsymbol{\lambda})T(\boldsymbol{\lambda}, \mathbf{d})d\sigma(\boldsymbol{\lambda}) \quad (1)$$

with \mathbb{S}^2 the unit sphere and $T(\boldsymbol{\lambda}, \mathbf{d})$ is a kernel involving Hankel and Legendre functions. There are many possible cubature strategies to evaluate the integral above, and their efficiency can be measured with respect to the ratio

$$\frac{\#\{\text{integrated spherical harmonics}\}}{\#\{\text{cubature nodes}\}} \quad (2)$$

where $\#\{\text{integrated spherical harmonics}\}$ refers to the number of spherical harmonics that are

exactly integrated on \mathbb{S}^2 by the cubature rule under consideration.

Interpolation over the unit sphere

The choice of the cubature order relies on the requested accuracy and on the size of the smallest box containing all vectors \mathbf{r} in (1). In a multilevel procedure, this size varies between levels, and so does the cubature grid. It is important to be able to realize interpolation between different cubature grids.

In practice, the FMM involves interpolation steps where nodal values distributed on one cubature grid $C_s = \{\boldsymbol{\lambda}_k\}_{k=1}^{N_s}$ are mapped to values on the grid $C_t = \{\boldsymbol{\mu}_j\}_{j=1}^{N_t}$ of the next level. These steps take the form of a matrix-vector product $\mathbf{q} \mapsto \mathbf{M}\mathbf{q}$ where

$$\mathbf{M}_{j,k} := \sum_{l=0}^L \frac{2l+1}{4\pi} P_l(\boldsymbol{\mu}_j \cdot \boldsymbol{\lambda}_k). \quad (3)$$

Here L is a heuristically chosen truncation order, taking account of the consistency order of both C_s and C_t , and P_l denotes the l^{th} Legendre polynomial. A priori, the matrix \mathbf{M} is rectangular $N_s \neq N_t$ and cannot be compressed through a truncated singular value decomposition.

These interpolation steps can become very costly when the size of boxes becomes large, and the global speed of the FMM depends on efficient matrix-vector products with (3). The aim of the present work is to reduce this cost.

Exploiting symmetries

We investigated block-diagonalisation of (3) by taking maximal advantage of the symmetries of the cubature grids $C_s, C_t \subset \mathbb{S}^2$. Let us point that \mathfrak{H} , the symmetry group of transformations leaving both C_s and C_t invariant, can be non-commutative in which case such a block diagonalisation becomes non-trivial. We use finite group representation theory [6] to tackle this.

This approach can be applied in the general situation where the matrix \mathbf{M} stems from the discretisation of a kernel $\Phi : \mathbb{R}^d \times \mathbb{R}^d \rightarrow \mathbb{C}$ satisfying the symmetry property:

$$\begin{aligned} \Phi(h \cdot \mathbf{x}, h \cdot \mathbf{y}) &= \Phi(\mathbf{x}, \mathbf{y}), \\ \forall \mathbf{x}, \mathbf{y} \in \mathbb{R}^3, \forall h \in \mathfrak{H}. \end{aligned} \quad (4)$$

In our case $\Phi(\mathbf{x}, \mathbf{y}) = \sum_{l=0}^L P_l(\mathbf{x} \cdot \mathbf{y})(2l+1)/(4\pi)$ clearly satisfies this property as soon as \mathfrak{H} is any rotation group.

This exact block-diagonalization, including the number of blocks and their sizes, only relies on the irreducible group representations of \mathfrak{H} [6].

Choice of cubature rules

The most common choices for cubature grids on \mathbb{S}^2 are based on tensorized 1D rules: for example Gauss-Legendre rules combined with 1D uniform rules (GL-U). In this situation \mathfrak{H} is a cyclic group of rotations along a fixed axis, and block-diagonalisation can be achieved efficiently using Fast Fourier Transform (FFT).

We dedicate particular attention to Lebedev cubature rules [5] that do not fall into the previously mentioned category of tensorized 1D rules. Lebedev cubature grids enjoy the same symmetry group \mathfrak{D} as the normalised octahedron, a non-commutative group of cardinal 48. Although Lebedev cubature does not lend itself to FFT, its efficiency in terms of (2) appears superior compared to tensorized rules (approximately $\frac{3}{2}$ times better than GL-U).

This last point has a particular interest in an important part of HF-FMM (namely the horizontal pass) where the cost of computation depends on the number of cubature nodes.

Other highly efficient group-invariant cubatures, based on the icosahedral group [1] exist. However, working on Lebedev cubatures allows to consider the symmetries appearing in the octree structure. This information can be used in practice to reduce the cost of precomputation.

The figure below provides a comparison of application timings for the interpolation between cubature grids over the sphere with regard to integration order of C_s . The order of C_t is twice the order of C_s . FFT based interpolation for GL-U is confronted to block-diagonalisations (BD) of \mathbf{M} for Lebedev rules. We shall discuss in further detail how those methods compare, commenting on the various low-level optimization.

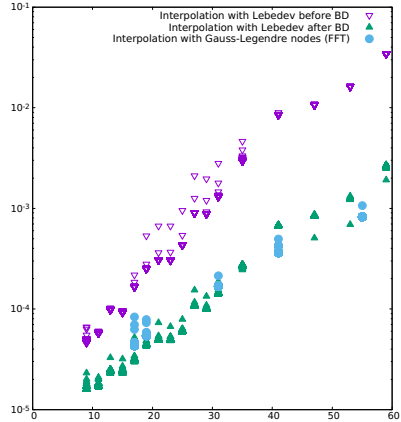


Figure 1: Application times (sec.) vs order of $C_s := (\#integrated\ spherical\ harmonics)^{1/2} - 1$.

Acknowledgment

This work was funded by the Institut des Sciences du Calcul et des Données (ISCD) of Sorbonne Université.

References

- [1] C. Ahrens, G. Beylkin, Rotationally invariant quadratures for the sphere, *Proc. R. Soc. Lond. Ser. A Math. Phys. Eng. Sci* **465** (2009), 3103–3125
- [2] A. Aimi, M. Diligenti, Restriction matrices for numerically exploiting symmetry, *Adv. Comput. Math.* **28** (2008), 201–235.
- [3] R. Coifman, V. Rokhlin, S. Wandzura, The fast multipole method for the wave equation: a pedestrian prescription, *IEEE Antennas and Propag. Mag.* **35** (1993), 7–12
- [4] L. Greengard, V. Rokhlin, A fast algorithm for particle simulations, *J. Comput. Phys.* **73** (1987), 325–348
- [5] V. I. Lebedev, Quadratures on the sphere *Z. Vycisl. Mat. i Mat. Fiz* **16** (1976), 293–306.
- [6] J-P. Serre, Linear representations of finite groups, *Graduate texts in Mathematics* **42** (1977).

Multi-Trace FEM-BEM formulation for acoustic scattering by composite objects

Marcella Bonazzoli^{1,*}, Xavier Claeys²

¹Inria Saclay Île-de-France, Centre de Mathématiques Appliquées, Palaiseau, France

²Laboratoire Jacques-Louis Lions, Sorbonne Université, Paris, France

*Email: marcella.bonazzoli@inria.fr

Abstract

This talk is about the scattering of an acoustic wave by an object composed of piecewise homogenous parts and an arbitrarily heterogeneous part. We propose and analyze a formulation that couples, adopting a Costabel-type approach, boundary integral equations for the homogenous subdomains with domain variational formulations for the heterogeneous subdomain.

Keywords: FEM-BEM coupling, boundary integral equations, Helmholtz, junction points

Acknowledgement This work was supported by NonlocalDD project, ANR-15-CE23-0017-01.

1 Introduction

We propose an extension of the global multi-trace formulation (MTF) introduced in [2, 3] for acoustic scattering by composite objects, allowing the wavenumber to vary arbitrarily in a part of the domain. This can be seen also as an extension of Costabel FEM-BEM coupling to a multi-domain configuration, with junction points allowed, i.e. points where three or more subdomains abut. Usually just the exterior unbounded subdomain is treated with the BEM; here we wish to exploit the BEM whenever it is applicable, that is for all the homogenous parts of the scattering object, since it yields a reduction in the number of unknowns compared to the FEM. This talk is based on the upcoming paper [1], where proofs will be included.

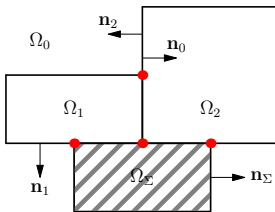


Figure 1: Geometric setting.

We consider a partition into Lipschitz subdomains $\mathbb{R}^d = \bigcup_{j=0}^n \bar{\Omega}_j \cup \bar{\Omega}_\Sigma$ (see Figure 1), where Ω_Σ and the Ω_j for $j \neq 0$ are bounded; in addition, $\Omega_\Sigma, \mathbb{R}^d \setminus \bar{\Omega}_\Sigma$, and each Ω_j are connected. This partition reflects the material properties of the propagation medium, which is homogeneous in each Ω_j , with wavenumbers $\kappa_j \in \mathbb{R}$, and heterogeneous in Ω_Σ , with wavenumber $\kappa_\Sigma \in L^\infty(\Omega_\Sigma)$. We set $\Gamma := \bigcup_{j=0}^n \partial\Omega_j, \Sigma := \partial\Omega_\Sigma$.

For each subdomain Ω_j (and similarly for Ω_Σ), denote by γ_D^j and γ_N^j the interior Dirichlet and Neumann trace operators, and by $\gamma_{D,c}^j$ and $\gamma_{N,c}^j$ the exterior ones. The orientation of both γ_N^j and $\gamma_{N,c}^j$ is fixed by the outward normal \mathbf{n}_j . Gathering traces, we define the interior and exterior Cauchy trace operators

$$\begin{aligned} \gamma^j &: \mathbb{H}_{\text{loc}}^1(\Delta, \bar{\Omega}_j) \rightarrow \mathbb{H}^{1/2}(\partial\Omega_j) \times \mathbb{H}^{-1/2}(\partial\Omega_j) \\ \gamma_c^j &: \mathbb{H}_{\text{loc}}^1(\Delta, \mathbb{R}^d \setminus \bar{\Omega}_j) \rightarrow \mathbb{H}^{1/2}(\partial\Omega_j) \times \mathbb{H}^{-1/2}(\partial\Omega_j) \\ \gamma^j(V) &:= \begin{pmatrix} \gamma_D^j(V) \\ \gamma_N^j(V) \end{pmatrix}, \quad \gamma_c^j(V) := \begin{pmatrix} \gamma_{D,c}^j(V) \\ \gamma_{N,c}^j(V) \end{pmatrix}. \end{aligned}$$

2 Multi-trace FEM-BEM formulation

First of all, consider the trace space

$$\begin{aligned} \widehat{\mathbb{H}}(\Gamma) &:= \mathbb{H}(\partial\Omega_1) \times \dots \times \mathbb{H}(\partial\Omega_n) \times \mathbb{H}^{-\frac{1}{2}}(\Sigma), \\ \text{where } \mathbb{H}(\partial\Omega_j) &:= \mathbb{H}^{+\frac{1}{2}}(\partial\Omega_j) \times \mathbb{H}^{-\frac{1}{2}}(\partial\Omega_j), \end{aligned}$$

equipped with the standard norm of the Cartesian product on the spaces $\mathbb{H}^{\pm 1/2}(\partial\Omega_j)$. We write $\langle \cdot, \cdot \rangle_j$ for the duality pairing between $\mathbb{H}^{+1/2}(\partial\Omega_j)$ and $\mathbb{H}^{-1/2}(\partial\Omega_j)$, and for $\mathbb{H}(\partial\Omega_j)$ we define the skew-symmetric pairing

$$\left[\begin{pmatrix} u_j \\ p_j \end{pmatrix}, \begin{pmatrix} v_j \\ q_j \end{pmatrix} \right]_j := \langle u_j, q_j \rangle_j - \langle v_j, p_j \rangle_j,$$

and similarly for $[\cdot, \cdot]_\Sigma$.

Let the function $\mathcal{G}_\kappa(\mathbf{x})$ be the κ -outgoing fundamental solution for the Helmholtz operator $-\Delta - \kappa^2, \kappa \in \mathbb{R}$. For each subdomain Ω_j , for

any $\mathbf{v}_j = (v, q) \in \mathbb{H}(\partial\Omega_j)$ and any $\mathbf{x} \in \mathbb{R}^d \setminus \partial\Omega_j$, define the potential operators

$$\begin{aligned} \text{SL}_\kappa^j(q)(\mathbf{x}) &:= \int_{\partial\Omega_j} q(\mathbf{y})\mathcal{G}_\kappa(\mathbf{x} - \mathbf{y})d\sigma(\mathbf{y}) \\ \text{DL}_\kappa^j(v)(\mathbf{x}) &:= \int_{\partial\Omega_j} v(\mathbf{y})\mathbf{n}_j(\mathbf{y}) \cdot (\nabla\mathcal{G}_\kappa)(\mathbf{x} - \mathbf{y})d\sigma(\mathbf{y}) \\ \mathbf{G}_\kappa^j(\mathbf{v}_j)(\mathbf{x}) &:= \text{DL}_\kappa^j(v)(\mathbf{x}) + \text{SL}_\kappa^j(q)(\mathbf{x}). \end{aligned}$$

Applying traces to potentials yields boundary integral operators: in our compact notation we will use

$$\mathbf{A}_\kappa^j := \{\gamma^j\} \circ \mathbf{G}_\kappa^j := \frac{1}{2}(\gamma^j + \gamma_\kappa^j) \circ \mathbf{G}_\kappa^j.$$

Finally, set $\theta_j(\mathbf{v}_j) := (-v, q)^\top$, and

$$a_\Sigma(U, V) := \int_{\Omega_\Sigma} (\nabla U \cdot \nabla V - \kappa_\Sigma^2(\mathbf{x})UV).$$

Given a source term $f \in L^2(\Omega_\Sigma)$ and an incident field $U_{\text{inc}} \in \mathbf{H}_{\text{loc}}^1(\mathbb{R}^d)$, the global multi-trace formulation with Costabel-type coupling is: find $U \in \mathbf{H}^1(\Omega_\Sigma)$, $\hat{\mathbf{u}} \in \hat{\mathbb{H}}(\Gamma)$, $\hat{\mathbf{u}} = (\hat{\mathbf{u}}_1, \dots, \hat{\mathbf{u}}_n, p_\Sigma)$ such that

$$\begin{aligned} &\sum_{j=1}^n [(A_{\kappa_j}^j + A_{\kappa_0}^j)(\hat{\mathbf{u}}_j), \theta_j(\hat{\mathbf{v}}_j)]_j \\ &+ \sum_{j=1}^n \sum_{q=1, q \neq j}^n [\gamma^q \mathbf{G}_{\kappa_0}^j(\hat{\mathbf{u}}_j), \theta_q(\hat{\mathbf{v}}_q)]_q \\ &+ \left[\mathbf{A}_{\kappa_0}^\Sigma \left(\begin{matrix} \gamma_D^\Sigma U \\ p_\Sigma \end{matrix} \right), \theta_\Sigma \left(\begin{matrix} \gamma_D^\Sigma V \\ q_\Sigma \end{matrix} \right) \right]_\Sigma \\ &+ \sum_{j=1}^n \left[\gamma^\Sigma \mathbf{G}_{\kappa_0}^j(\hat{\mathbf{u}}_j), \theta_\Sigma \left(\begin{matrix} \gamma_D^\Sigma V \\ q_\Sigma \end{matrix} \right) \right]_\Sigma \\ &+ \sum_{q=1}^n \left[\gamma^q \mathbf{G}_{\kappa_0}^\Sigma \left(\begin{matrix} \gamma_D^\Sigma U \\ p_\Sigma \end{matrix} \right), \theta_q(\hat{\mathbf{v}}_q) \right]_q \\ &+ \frac{1}{2} \left[\left(\begin{matrix} \gamma_D^\Sigma U \\ p_\Sigma \end{matrix} \right), \left(\begin{matrix} \gamma_D^\Sigma V \\ q_\Sigma \end{matrix} \right) \right]_\Sigma + a_\Sigma(U, V) \\ &= \sum_{j=1}^n [\gamma^j U_{\text{inc}}, \theta_j(\hat{\mathbf{v}}_j)]_j \\ &+ \left[\gamma^\Sigma U_{\text{inc}}, \theta_\Sigma \left(\begin{matrix} \gamma_D^\Sigma V \\ q_\Sigma \end{matrix} \right) \right]_\Sigma + \int_{\Omega_\Sigma} fV \end{aligned} \tag{1}$$

for all $V \in \mathbf{H}^1(\Omega_\Sigma)$, $\hat{\mathbf{v}} \in \hat{\mathbb{H}}(\Gamma)$, $\hat{\mathbf{v}} = (\hat{\mathbf{v}}_1, \dots, \hat{\mathbf{v}}_n, q_\Sigma)$. The first five lines could be written in a matrix form, with diagonal terms $A_{\kappa_j}^j + A_{\kappa_0}^j$, $\mathbf{A}_{\kappa_0}^\Sigma$, and off-diagonal terms $\gamma^q \mathbf{G}_{\kappa_0}^j$, $\gamma^\Sigma \mathbf{G}_{\kappa_0}^j$, $\gamma^q \mathbf{G}_{\kappa_0}^\Sigma$ that couple all subdomains with all other subdomains, hence the attribute *global*.

In the MTF the unknown traces are doubled on each interface that separates two (bounded) subdomains and the transmission conditions are imposed weakly by the equation itself.

Theorem 1 *If $U \in \mathbf{H}^1(\Omega_\Sigma)$, $\hat{\mathbf{u}} \in \hat{\mathbb{H}}(\Gamma)$, solve (1), then $\tilde{U} \in L_{\text{loc}}^2(\mathbb{R}^d)$ defined by*

$$\begin{aligned} \tilde{U}(\mathbf{x}) &:= U(\mathbf{x}) \quad \text{for } \mathbf{x} \in \Omega_\Sigma, \\ \tilde{U}(\mathbf{x}) &:= \mathbf{G}_{\kappa_j}^j(\hat{\mathbf{u}}_j)(\mathbf{x}) \quad \text{for } \mathbf{x} \in \Omega_j, j = 1, \dots, n, \\ \tilde{U}(\mathbf{x}) &:= \left(U_{\text{inc}} - \mathbf{G}_{\kappa_0}^\Sigma \left(\begin{matrix} \gamma_D^\Sigma U \\ p_\Sigma \end{matrix} \right) - \sum_{j=1}^n \mathbf{G}_{\kappa_0}^j(\hat{\mathbf{u}}_j) \right)(\mathbf{x}) \end{aligned}$$

for $\mathbf{x} \in \Omega_0$, solves the standard transmission problem (see e.g. [2, §1]) for multi-domain acoustic scattering.

Theorem 2 (Gårding inequality) *Let $\mathfrak{a}_{\text{MTF}}$ designate the bilinear form on the left-hand side of (1). There exist a compact bilinear form \mathbf{k} and a constant $\beta > 0$ such that*

$$\begin{aligned} \Re \left[\mathfrak{a}_{\text{MTF}} \left((V, \hat{\mathbf{v}}), (\bar{V}, \bar{\hat{\mathbf{v}}}) \right) + \mathbf{k} \left((V, \hat{\mathbf{v}}), (\bar{V}, \bar{\hat{\mathbf{v}}}) \right) \right] \\ \geq \beta (\|V\|_{\mathbf{H}^1(\Omega_\Sigma)}^2 + \|\hat{\mathbf{v}}\|_{\hat{\mathbb{H}}(\Gamma)}^2) \end{aligned}$$

for all $V \in \mathbf{H}^1(\Omega_\Sigma)$, $\hat{\mathbf{v}} \in \hat{\mathbb{H}}(\Gamma)$.

A consequence of Theorem 2 is that the operator induced by $\mathfrak{a}_{\text{MTF}}$ is of Fredholm type with index 0, hence injectivity is sufficient for bijectivity and for stability of (1).

Theorem 3 *Let $U \in \mathbf{H}^1(\Omega_\Sigma)$, $\hat{\mathbf{u}} \in \hat{\mathbb{H}}(\Gamma)$, solve (1) with $f = 0$, $U_{\text{inc}} = 0$. Then $U = 0$; moreover, $\hat{\mathbf{u}} = 0$ if and only if κ_0 is not an interior Dirichlet eigenvalue of $-\Delta$ on Ω_Σ .*

A combined field formulation immune to spurious resonances can be constructed.

References

- [1] M. Bonazzoli and X. Claeys, FEM-BEM coupling with Multi-Trace formulations for acoustic scattering, *in preparation*.
- [2] X. Claeys and R. Hiptmair, Multi-Trace Boundary Integral Formulation for Acoustic Scattering by Composite Structures, *Communications on Pure and Applied Mathematics*, 66(8):1163–1201, 2013.
- [3] X. Claeys and R. Hiptmair, Integral Equations for Acoustic Scattering by Partially Impenetrable Composite Objects, *IEOT*, 81 (2015), no. 2, pp. 151–189.

Boundary integral equations and block Jacobi preconditioner

Bertrand Thierry^{1,*}¹CNRS - Laboratoire Jacques Louis Lions, Sorbonne Université, Paris, France

*Email: bertrand.thierry@sorbonne-universite.fr

Abstract

Boundary integral equation (BIE) is a powerful method and a large number of BIEs with different properties have been proposed in the literature. In multiple scattering context, BIEs can be rewritten in a block matrix form and consequently, the block Jacobi preconditioner becomes an attractive choice. This presentation focuses on the action of this preconditioning technique on all BIEs and is mainly based on the following result: every preconditioned BIEs become either identical or equals, up to a change of basis. The main result of this contribution has been proven in [2] and even though it can be considered as “old”, it has never been presented at Waves conference.

Keywords: Boundary Integral Equation, Multiple scattering, Preconditioning, Helmholtz, Block Jacobi

1 Direct BIEs

In a homogeneous medium, when illuminated by an incident time-harmonic acoustic wave u^{inc} , the $M > 1$ obstacles $\Omega_p, p = 1, \dots, M$, generate a scattered wave u solution of the Helmholtz equation:

$$\begin{cases} \Delta u + k^2 u = 0 & \mathbb{R}^3 \setminus \overline{\cup_{p=1}^M \Omega_p} \\ u = -u^{inc} & \Gamma := \cup_{p=1}^M \Gamma_p \\ u \text{ is radiating.} \end{cases}$$

The quantity k is the positive wavenumber, the radiation condition stands for the Sommerfeld one and Γ_p is the boundary of Ω_p . The boundary condition is here of Dirichlet type but another condition can be imposed.

It is well known that this problem can be rewritten equivalently under the form of a system of boundary integral equations (BIEs) with the densities ρ and λ as unknown. If \mathcal{S} and \mathcal{D} respectively represent the volume single- and double-layer integral operators, then the scattered field is sought as

$$u(x) = \mathcal{S}\rho(x) + \mathcal{D}\lambda(x), \quad \forall x \notin \overline{\cup_{p=1}^M \Omega_p}.$$

Following [1], the BIEs can be classified as direct or indirect, depending on whether or not the unknown densities (λ, ρ) are equal to the Cauchy data. For Direct BIEs and Dirichlet boundary value problem, the quantity λ vanishes and the single-layer BIE, sometimes called *Electric Field Integral Equation* (EFIE), is obtained by applying the interior Dirichlet trace on Γ on the quantity u :

$$\begin{cases} u = \mathcal{S}\rho \\ \mathcal{S}\rho = -u^{inc}|_{\Gamma}, \quad S = \mathcal{S}|_{\Gamma}. \end{cases}$$

Applying the Neumann interior trace leads to the MFIE and a Fourier trace to the CFIE ($=\alpha$ EFIE + $(1 - \alpha)$ MFIE). For an abstract framework, a general interior trace γ^A is introduced and the associated (direct) BIE is then given by:

$$\begin{cases} u = \mathcal{S}\rho \\ \mathcal{S}^A \rho = -\gamma^A u^{inc}, \quad \gamma^A \mathcal{S} = S^A. \end{cases}$$

2 Multiple Scattering and Block Jacobi

In this context, BIE can be rewritten in a matrix form $(S_{p,q}^A)$ where the diagonal block $S_{p,p}^A$ corresponds to the boundary integral operator when considering only the obstacle Ω_p (*single scattering*) and where the off-diagonal block $S_{p,q}^A$ for $q \neq p$ represents the interaction between the two obstacles Ω_p and Ω_q . For example and for two obstacles, the BIE $S^A \rho = \gamma^A u^{inc}$ reads as:

$$\begin{pmatrix} S_{1,1}^A & S_{1,2}^A \\ S_{2,1}^A & S_{2,2}^A \end{pmatrix} \begin{pmatrix} \rho_1 \\ \rho_2 \end{pmatrix} = - \begin{pmatrix} \gamma^A u^{inc}|_{\Gamma_1} \\ \gamma^A u^{inc}|_{\Gamma_2} \end{pmatrix}.$$

The block Jacobi preconditioner \widehat{S}^A , composed by the M blocks located on the diagonal of this matrix, is here given by:

$$\widehat{S}^A = \begin{pmatrix} S_{1,1}^A & 0 \\ 0 & S_{2,2}^A \end{pmatrix}$$

When applying it to the above BIE, the matrix of the system has now the following form:

$$(\widehat{S}^A)^{-1} S^A = \begin{pmatrix} I_{1,1} & (S_{1,1}^A)^{-1} S_{1,2}^A \\ (S_{2,2}^A)^{-1} S_{2,1}^A & I_{2,2} \end{pmatrix} \quad (1)$$

This preconditioner is classical and known as the *block Jacobi preconditioner*. In this context, it can also be seen as *geometric* as it takes into account only the single scattering effects and be thus named *single scattering preconditioner*. It is also linked to the *Reflexion Method*, *Lax-Foldy model* or the *Boundary Decomposition Method*.

3 Main Result

As it has been proven in [2], the three direct boundary integral equations cited above become exactly the same after being preconditioned (by the block Jacobi). In other words, (1) is totally independent of the choice of γ^A . This result is also independent of the geometry, provided that the obstacles do not touch each other.

For other BIEs, such as the indirect boundary integral equations of Brakhage-Werner, the result can be extended. For this case, the linear systems become similar, that is, equal up to an invertible operator (the *passing operator*). For example, if S^{BW} is the operator of Brakhage-Werner and \widehat{S}^{BW} its block jacobi preconditioner, then there exists an invertible operator U such that

$$(\widehat{S}^A)^{-1}S^A = U \left[(\widehat{S}^{BW})^{-1}S^{BW} \right] U^{-1}.$$

These properties imply in particular that the convergence rate of a Krylov subspaces solver will be exactly the same for every preconditioned integral equations.

4 Numerical Illustration

This result will be illustrated using either μ -diff [3] or GypsiLab [4], two open-source Matlab toolboxes for solving two dimensionnal scattering problem using BIE. The first one is restricted to disks (using Fourier series) while the second one is based on BEM and is thus more flexible. As an example, for 30 obstacles of unit length and a wavenumber $k = 20$, the eigenvalues of the four preconditioned BIEs are shown on figure 4 and up to a numerical error, they match. On figure 4 is shown the histories of convergence of the GMRES for the four BIEs with and without preconditioner, these last four curves being superimposed (dashed line).

References

[1] A. Bendali and M. Fares, Computational Methods for Acoustics Problems, *chapter*

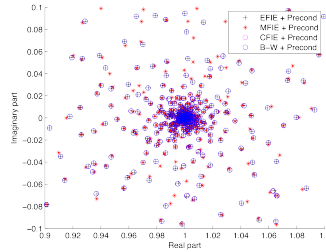


Figure 1: Eigenvalues (zoom) of the four preconditioned operators in the complex plane: they are equals up to a relative error of 2.7%

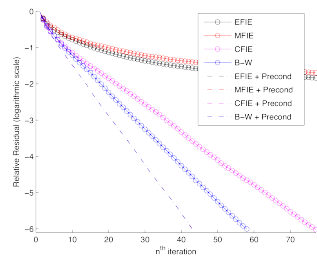


Figure 2: Histories of convergence of the GMRES (zoom): the four curves of the preconditioned BIEs are superimposed (dashed lines)

Boundary Integral Equations Methods in Acoustics, Saxe-Coburg Publications, 2007

[2] B. Thierry, A remark on the single scattering preconditioner applied to boundary integral equations. *Journal of Mathematical Analysis and Applications* **413** (2014), pp. 212–228.

[3] B. Thierry, X. Antoine, C. Chniti and H. Alzubaidi, μ -diff: An open-source Matlab toolbox for computing multiple scattering problems by disks. *Computer Physics Communications* **192** (2015) pp. 348–362.

[4] F. Alouges and M. Aussal, FEM and BEM simulations with the Gypsilab framework. *SMAI-Journal of computational mathematics*, **4** (2018), pp. 297–318.

A sinc-Fourier approach to an inverse problem in scattering

Sum Chow^{1,*}, Frank Stenger²¹Department of Mathematics, Brigham Young University, Provo, Utah, USA²SINC, LLC, Utah, USA

*Email: schow@math.byu.edu

Abstract

In this paper, we discuss a Sinc-Fourier transform solution method for determining the refractive index of an inhomogeneous medium acoustic scattering problem in a three dimensional region. We formulate the problem as a 3D Lippmann—Schwinger equation. The direct problem is solved iteratively by first applying a 2D Fourier transform that takes advantage of the simple form of the free space Green's function and then solving the transformed equation using the sinc convolution method for one dimensional problems, and finally by an inverse Fourier transform. By using a regularization method, we extend the sinc-Fourier approach to the inverse problem and examine the numerical performance of the method.

Keywords: sinc convolution, Lippmann-Schwinger, inverse medium problem

1 Introduction

In applications such as biomedical imaging, it is important to determine material properties of the underlying medium. In this paper we discuss a Sinc-Fourier transform solution method for determining the refractive index of an inhomogeneous medium acoustic scattering problem in a three dimensional region.

The scattering problem under consideration is modelled by a Helmholtz equation in a non-homogeneous medium inside a bounded domain $V = [-X, X] \times [-Y, Y] \times [-Z, Z]$:

$$\Delta f + \kappa^2(1 + \gamma(\mathbf{x})) f = 0$$

with given boundary data:

$$f = v, \quad \frac{\partial f}{\partial \nu} = w \quad \text{on } \partial V$$

The differential equation with boundary data may be reformatted as a 3D Lippmann—Schwinger integral equation. With $G(\mathbf{r}) = \frac{e^{i\kappa r}}{4\pi r}$, $r = |\mathbf{r}| = |(x, y, z)|$, denoting the Green's function for free

space constant coefficient Helmholtz problem, we have the Lippmann—Schwinger equation

$$f(\mathbf{r}) - \int_V \kappa^2(1 + \gamma(\mathbf{r}')) f G(|\mathbf{r} - \mathbf{r}'|) d\mathbf{r}' = f^{\text{in}}(\mathbf{r})$$

where

$$f^{\text{in}}(\mathbf{r}) = \int_{\partial V} w G(\mathbf{r} - \mathbf{r}') - v \frac{\partial G(\mathbf{r} - \mathbf{r}')}{\partial \nu'} dS(\mathbf{r}').$$

In practice, it is often more realistic to assume that the incident wave f^{in} is known in place of the function and derivative values on the boundary.

For the direct problem of finding f , the integral equation is a Fredholm equation of the second kind while for the inverse problem of finding γ , it is a Fredholm equation of the first kind. The solution the full 3D problem typically requires high computational resource. An efficient method using a sinc-Fourier approach was recently introduced by Stenger, Anderssen and Chow [1] to handle the direct problem. This is done using a combination of 2F Fourier transform and a 1D sinc convolution method that effectively reduces the solution process to a sequence of 1D problems. By using a regularization method, we extend the sinc-Fourier approach to the inverse problem.

With the refractive index γ assumed known, the direct problem of calculating the solution to the Helmholtz may be solved efficiently using a sinc-Fourier method.

First a 2D Fourier transform for the y, z variables is applied to the integral equation. The 2D Fourier transform of the corresponding free space Green's function has the simple and explicit form

$$\tilde{G}(x, \boldsymbol{\lambda}) = \frac{i}{2\beta} \exp(i\beta|x|)$$

where $\bar{\boldsymbol{\lambda}} = [\lambda_y, \lambda_z]^T$ are the Fourier variables corresponding to y and z , and

$$\beta = \sqrt{\kappa^2 - |\bar{\boldsymbol{\lambda}}|^2}.$$

Under the further assumption that the incident wave is a plane wave, and set

$$\begin{aligned} f &= f^{sc} + f^{in}, \\ f^{sc} &= f^{in} u, \end{aligned}$$

the transformed Lippmann-Schwinger equation takes the form

$$\tilde{u}(x, \bar{\lambda}) = \kappa^2 \int_{-X}^X \tilde{H}(x-t, \bar{\lambda}) \{ \tilde{\gamma} u(t, \bar{\lambda}) + \tilde{\gamma}(t, \bar{\lambda}) \} dt,$$

where

$$\tilde{H}(x, \bar{\lambda}) = \frac{i}{2\beta} \exp(-i\kappa x + i\beta|x|).$$

The equation is then solved iteratively. For each fixed Fourier variable pair, the transformed equation is a one dimensional equation involving integral of convolution type. With a known approximate solution u^n , the convolution integral involving γu^n is evaluated using the highly accurate sinc convolution method [2], which allows us to handle the singularity in the integral equation effectively, and a new function \tilde{u}^{n+1} is found from the integral equation. An inverse 2D Fourier transform is then applied to obtain a new approximation u^{n+1} .

For the inverse problem of determining the reflective index γ , we introduce a small regularization term to the Lippmann-Schwinger equation:

$$\begin{aligned} \alpha \tilde{\gamma}(x, \bar{\lambda}) &= -\tilde{u}(x, \bar{\lambda}) \\ + \kappa^2 \int_{-X}^X \tilde{H}(x-t, \lambda) \{ \tilde{\gamma} u(t, \bar{\lambda}) + \tilde{\gamma}(t, \bar{\lambda}) \} dt, \end{aligned}$$

where α is the regularization parameter. Iteration process based on the sinc-Fourier approach described above is then applied to determine the reflective index. We will report the numerical performance of different iterative schemes and discuss the convergence of the iterative method.

2 Numerical example

To illustrate the method we note that for any nice F , by setting

$$\gamma = -\frac{\Delta F + 2i\kappa F_x}{\kappa^2(1+F)}.$$

we have a solution to the Lippmann-Schwinger equation.

For

$$F(\bar{r}) = b \exp(-a|\bar{r} - \bar{r}_0|^2),$$

where a and b constants, with a is positive,

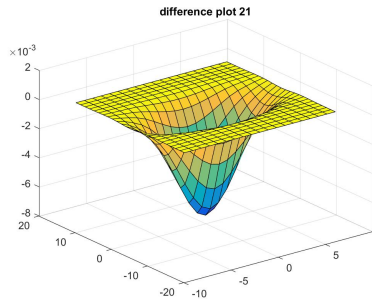
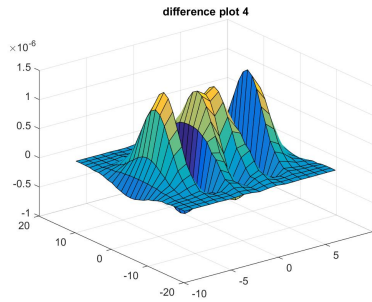
$$\gamma(\bar{r}) = \frac{4i a \kappa (x - x_0) + 6a - 4a^2 |\bar{r} - \bar{r}_0|^2}{\kappa^2(1+F(\bar{r}))} F(\bar{r})$$

Note γ has a ‘‘peak’’ at $\bar{r} = \bar{r}_0 = (x_0, y_0, z_0)$. With parameters

$$a = 0.03, b = 0.05, (x_0, y_0, z_0) = (0, 0, 0), \kappa = 2\pi$$

$$X = 20, Y = 15, Z = 8, N_x = 16, N_y = 12, N_z =$$

the error of real and imaginary parts of F are



3 References

References

- [1] F. Stenger, R.S Anderssen and S.-Sum Chow, A sinc-Fourier approach to an inverse problem in scattering, submitted.
- [2] F. Stenger, *Handbook of Sinc numerical methods*, CRC Press, Boca Raton, FL, 2011.

A high order method of boundary operators for the 3D time-dependent wave equation

S. V. Petropavlovsky¹, S. V. Tsynkov^{2,*}, E. Turkel³¹National Research University Higher School of Economics, Moscow 101000, Russia²Department of Mathematics, North Carolina State University, Raleigh, NC, USA³School of Mathematical Sciences, Tel Aviv University, Tel Aviv, Israel*Email: tsynkov@math.ncsu.edu**Abstract**

We propose an efficient high order accurate boundary algorithm for the numerical solution of unsteady exterior initial boundary problems for the three-dimensional wave equation. The algorithm relies on the method of difference potentials combined with the Huygens' principle.

Keywords: method of difference potentials, Huygens' principle, unsteady wave propagation

1 Introduction

Consider an exterior initial boundary value problem (IBVP) for the three-dimensional homogeneous wave (d'Alembert) equation:

$$\frac{1}{c^2} \frac{\partial^2 u}{\partial t^2} - \Delta u = 0, \quad \text{on } \mathbb{R}^3 \setminus \Omega \times [0, T], \quad (1a)$$

$$\mathcal{L}_\Gamma u = \phi, \quad \text{on } \partial\Omega \times [0, T], \quad (1b)$$

$$u|_{t=0} = \partial u / \partial t|_{t=0} = 0, \quad (1c)$$

where c is the speed of light. The boundary condition (1b) is inhomogeneous. For example, if u is the field scattered off the given shape Ω , then the operator \mathcal{L}_Γ defines the type of scattering on $\partial\Omega$ and the data ϕ represent the impinging field.

The numerical method we propose for solving the IBVP (1) combines the flexibility and ease of finite differences with the advantages of a boundary approach. It reduces the dimension of the problem by one and handles non-conforming boundaries $\partial\Omega$ on regular grids with no loss of accuracy. These features are enabled by the method of difference potentials (MDP) [1] that employs discrete counterparts of Calderon's operators. The MDP has previously been used for the simulation of both time-harmonic [2] and time-dependent waves [3]. As an extension of [3], the current work addresses exterior problems and offers high order accuracy.

A fundamental difficulty in applying boundary methods (e.g., those based on retarded potential boundary integral equations [4] or those based on Calderon's operators) to time-

dependent problems is that the boundary extends with time. To avoid the growth of cost, we employ the strong Huygens' principle that helps us truncate the ever expanding "tail" of the algorithm. It also guarantees that only outgoing waves will be present in the solution to the exterior problem. The time marching is therefore performed on a sliding window of fixed duration and only along the boundary $\partial\Omega \times [0, T]$, which has dimension (2+1) in space-time. As such, the method provides sub-linear complexity, i.e., outperforms the typical explicit schemes in long-time simulations. Moreover, changing the boundary condition (1b) incurs only a minor additional cost compared to that for a conventional volumetric time-stepping technique.

2 Method

The MDP reduces the PDE (1a) from the unbounded domain $\mathbb{R}^3 \setminus \Omega \times [0, T]$ to the operator equation at the boundary $\Gamma = \partial\Omega \times [0, T]$:

$$\mathbf{P}_\Gamma \boldsymbol{\xi}_\Gamma = \boldsymbol{\xi}_\Gamma. \quad (2)$$

In (2), \mathbf{P}_Γ is Calderon's projection for the d'Alembert operator and $\boldsymbol{\xi}_\Gamma \equiv (\xi_0, \xi_1)$ is the density of the generalized Calderon's potential:

$$\begin{aligned} \mathbf{P}_\Omega \boldsymbol{\xi}_\Gamma = & \int_\Gamma \left\{ \xi_1(\mathbf{y}, t') G(\mathbf{x} - \mathbf{y}, t - t') \right. \\ & \left. - \xi_0(\mathbf{y}, t') \frac{\partial G}{\partial \mathbf{n}}(\mathbf{x} - \mathbf{y}, t - t') \right\} dt' dS_{\mathbf{y}}. \end{aligned} \quad (3)$$

The functions ξ_0 and ξ_1 in (2), (3) are traces of the solution and its normal derivative on Γ , respectively, and $G(\mathbf{x}, t)$ in (3) is the fundamental solution of the d'Alembert operator. The projection \mathbf{P}_Γ in (2) is the vector trace of the potential (3): $\mathbf{P}_\Gamma \boldsymbol{\xi}_\Gamma = (\mathbf{P}_\Omega \boldsymbol{\xi}_\Gamma, \frac{\partial \mathbf{P}_\Omega \boldsymbol{\xi}_\Gamma}{\partial \mathbf{n}})|_\Gamma$.

The boundary equation (2), which is equivalent to (1a), is solved as a system along with the BC (1b). This can be arbitrary as long as the overall formulation (1) is well-posed. In simple cases, the BC explicitly provides one component of $\boldsymbol{\xi}_\Gamma$, e.g., ξ_0 for a Dirichlet BC and ξ_1

for a Neumann BC. The remaining component is then obtained as a solution to (2).

To discretize (2), the MDP computes the finite difference projection operator by solving a series of inhomogeneous auxiliary problems (APs) for equation (1a). The AP is originally formulated as a Cauchy problem and then truncated to a bounded domain Ω_0 of simple shape, see Figure 1, where it can be easily integrated by any appropriate finite difference scheme. The Huygens' principle combined with MDP enables a perfectly reflectionless treatment of the artificial outer boundary $\partial\Omega_0$, as in [5].

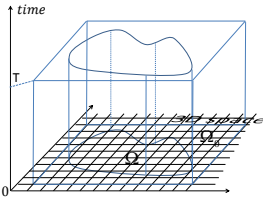


Figure 1: Computational domain for the AP.

Moreover, the Huygens' principle incorporated into our time-marching algorithm implies that for a bounded domain Ω in space, the extent of the backward dependence of the solution u to equation (1a) in time is finite and non-increasing. This property allows us to solve (2) (and thus, (1)) over long computational times $T_{\text{final}} \gg T$ sequentially, updating the density ξ_{Γ} by “chunks” of size T , see Figure 2. The solution u on Ω is computed only once, at $t = T_{\text{final}}$.

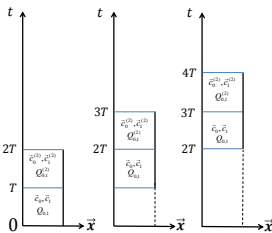


Figure 2: Time marching by “chunks” of size T .

3 Numerical demonstrations

To solve the AP, we employed a fourth order accurate compact scheme [6] (it controls the dispersion error more efficiently than the previously used lower order schemes). The test

problem is scattering of a plane wave about a sphere of radius R_0 . All computations are conducted on a Cartesian grid, for which the spherical boundary $r = R_0$ is non-conforming. Figure 3 shows the error profiles for a long-time run with $T_{\text{final}} = 4000R_0/c$ on two consecutive grids. Table 1 demonstrates that the CPU time to advance the solution over $T = R_0/c$ scales roughly as $2^3 = 8$ for the proposed boundary method versus $2^4 = 16$ for an explicit volumetric scheme.

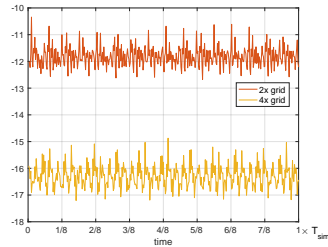


Figure 3: Fourth order convergence of the proposed boundary method with Robin BC (1b).

Grid	CPU time, sec		scaling rate	
	MDP	Volume	MDP	Volume
1x	0.0474	1.26	-	-
2x	0.421	19.8	8.87	15.7
4x	3.56	322	8.46	16.3

Table 1: Comparison of numerical performance over a fixed time interval $T = R_0/c$ of the proposed boundary method (MDP+Huygens' principle) vs. standard volumetric time marching.

Acknowledgment

Work supported by US ARO, grants W911NF-16-1-0115 and W911NF-14-C-0161, and US-Israel BSF, grant 2014048.

References

- [1] V. S. Ryaben'kii, *Method of Difference Potentials and Its Applications*, Springer-Verlag, Berlin, 2002.
- [2] M. Medvinsky, S. Tsynkov, E. Turkel, *J. Sci. Comput.*, **53** (2012), pp. 150–193.
- [3] S. Petropavlovsky, S. Tsynkov, E. Turkel, *J. Comput. Phys.*, **365** (2018), pp. 294–323.
- [4] F.-J. Sayas, *Retarded potentials and time domain boundary integral equations. A road map*, Springer, Cham, Switzerland, 2016.
- [5] S. V. Petropavlovsky, S. V. Tsynkov, *J. Comput. Phys.*, **336** (2017), pp. 1–35.
- [6] F. Smith, S. Tsynkov, E. Turkel, to appear in the *J. Sci. Comput.*, (2019).

High order transmission conditions for a Domain Decomposition Method applied to an efficient and accurate solution of EM scattering problems

Bruno Stupfel¹, Matthieu Lecouvez^{1,*}

¹CEA-Cesta, 15 avenue des sablières, 33114 Le Barp, France

*Email: matthieu.lecouvez@cea.fr

Abstract

In this paper, we present a non-overlapping *Domain Decomposition Method* (DDM) for the solution of electromagnetics problems such as the computation of the *Radar Cross Section* (RCS) of an object. As we target objects that are coated with layers of material, we restrict ourselves to non-intersecting interfaces so that no subdomain has more than two neighbours. For the sake of high accuracy, an exact radiation condition is used to close the computational domain. We investigate various high order transmission conditions, for which Sufficient Conditions for Uniqueness (SCU) can be derived, ensuring the wellposedness of the local problems. An implementation of this algorithm, using finite elements, is presented in an HPC framework and numerical results show the interest of our method.

Keywords: domain decomposition, EM scattering, GMRES, HPC

1 Introduction and model problem

We are interested here in the numerical computation of the RCS of objects coated with (possibly thin) layers of material, in open space. The governing equations for the targeted problem are the Maxwell's equations in the frequency domain. We use an electric field formulation (E is the electric field, μ and ϵ are the characteristic properties of the materials):

$$\nabla \times (\mu^{-1} \nabla \times E) - k_0^2 \epsilon E = 0. \quad (1)$$

Let S_0 be the surface of the object of interest, on which we prescribe an impedance condition

$$n \times \mu^{-1} \nabla \times E = -\frac{ik_0}{Z} E_t, \quad \text{on } S_0, \quad (2)$$

where $E_t = -n \times (n \times E)$ is the tangential field, and n is the outgoing normal. Above S_0 , several layers of materials are located, up to a surface S . Finally, the computational domain is closed by a fictive surface S_f (see Figure 1 for an illustration of the computational domain). Between S and

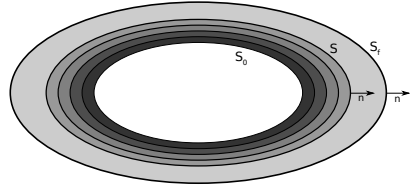


Figure 1: The computational domain: Between S_0 and S , materials are present.

S_f , we have $\mu = \epsilon = 1$. On S_f , we prescribe an integral representation [1] that links the electric field on S_f to the fields on S : $\forall x \in S_f$,

$$\begin{aligned} E(x) &= E^{inc}(x) - \mathcal{T}J(x) - \mathcal{L}K(x), \\ \mathcal{T}J(x) &= -\frac{1}{ik_0} \nabla \int_S g(x, y) \nabla \cdot J(y) dy \\ &\quad + ik_0 \int_S g(x, y) J(y) dy, \\ \mathcal{L}K(x) &= \int_S \nabla g(x, y) \times K(y) dy, \end{aligned} \quad (3)$$

where g is the usual Green kernel, $K = n \times E$, $J = n \times H$ and $H = -\frac{1}{ik_0} \mu^{-1} \nabla \times E$. Equations (1), (2) and (3) form the well-posed global problem [2]. It is discretized using classical first order Raviart-Thomas basis functions in $H(curl)$, supported by the edges of the mesh.

Considering the problem sizes that we are targeting, (up to 300 millions of unknowns), it is natural to consider a DD method.

2 Domain decomposition framework

The computational domain Ω (between S_0 and S_f) is decomposed into subdomains, that may correspond to the material layers. Traditionally, the subdomains are coupled through their interfaces thanks to *Transmission Conditions* (TCs) and the coupled problem is solved *via* a Krylov method (GMRES). It is well known that the convergence of the algorithm strongly depends on the TCs [3]. Very generically, one can write these TCs on each interface as follows

$$T_i^\pm(E_i^\pm, J_i^\pm) = T_i^\pm(E_i^\mp, J_i^\mp), \quad \text{on } S_i. \quad (4)$$

In (4), the + and - subscripts denotes quantities located above and below the interface S_i respectively, and T_i^\pm are operators acting on the tangential electric field and on the electric current. Most TCs in the literature can be written within this framework [3], in particular

- Robin-like TCs: $T^\pm(E, J) = \alpha E \pm J$
- Rational fractions of 2nd order operators

These TCs lack efficiency or robustness: Robin-like TCs may have slow convergence, Padé approximant of the square root operator may have great convergence but no proof of wellposedness of the subproblems. When these TCs are tuned in order to comply with SCU, the convergence strongly degrades.

3 High order transmission conditions

To overcome these issues, we introduce heuristic HOTC, whose general form reads

$$\begin{aligned} T_1 E_t^+ + \eta T_2 J^+ &= T_1 E_t^- + \eta T_2 J^- \\ T_1 E_t^+ - \eta T_2 J^+ &= T_1 E_t^- - \eta T_2 J^- \end{aligned} \quad (5)$$

where $T_i = 1 - (a_i L_D - b_i L_R)/k_0^2$ ($i = 1, 2$) and L_D and L_R are the divergence and the rotational part of the Hodge operator: $L_D V = \nabla_t \nabla_t \cdot V$ and $L_R = \nabla_t \times ([n \cdot (\nabla_t \times V)] n)$. By taking specific values of a_i and b_i , one can greatly simplify the analysis of the problem, in particular if one takes $a_1 = b_1 = a_2 = \alpha$ and $b_2 = 0$, it can be shown that

$$\begin{aligned} \Re e(\alpha) \geq 0, \quad \Re e(\eta) > 0 \\ \Im m(\alpha) \Im m(\eta) \leq 0 \end{aligned} \quad (6)$$

are sufficient conditions that ensure the uniqueness of the solution in each subdomain, and the equivalence to the global problem. Moreover, by noting that $L_D L_R = L_R L_D = 0$, one can simplify the TCs to get $(\Lambda_R = 1 + \alpha/k_0^2 L_R)$

$$\Lambda_R E_t^\pm \pm \eta J^\pm = \Lambda_R E_t^\mp \pm \eta J^\mp. \quad (7)$$

The implementation of these TCs does not require any additional unknowns or Padé approximant, leading to almost no extra cost compared with Robin-like TCs.

4 A numerical example

This method has been implemented in a fully parallel framework [4]. All sub-problems are solved concurrently and directly using the parallel (MPI + OpenMP) solver PaStix, the dense

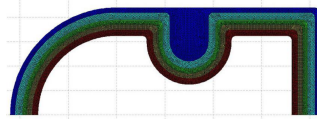


Figure 2: Geometry of the test case.

blocks arising from the integral representation are compressed in parallel (MPI + OpenMP) using the ACA algorithm and any other GMRES step is also parallelized.

The test case presented has run on 640 cores (20 nodes) of the Tera1000-1 supercomputer at CEA. The geometry corresponds to a cylinder with a hemispherical cap and a lateral groove (see Figure 2). We compare the HOTC to Després TCs and optimized Robin-like TCs. The computation is done at 1 GHz, leading to about 44.5M unknowns. We report the number of iterations and time to solution for each case.

- Després: 274 it., 5890 s
- Optimized: 207 it., 4320 s
- HOTC: 142 it., 3470 s

This example shows a clear reduction of the number of iterations (about 30%), as well as a reduced time to solution (about 20%).

References

- [1] J. Liu and J.M. Jin, A novel hybridization of higher order finite element and boundary integral methods for electromagnetic scattering and radiation problems, *IEEE Transactions on Antennas and Propagation* **49** (2001), pp. 1794–1806.
- [2] A. Jami, M. Polyzakis, A finite element solution of diffraction problems in unbounded domains, *Comput. Methods Appl. Mech. Eng.*, **29** (1981), pp. 1–18.
- [3] M. Gander, Schwarz methods over the course of time, *Electronic transactions on numerical analysis* **31** (2008).
- [4] B. Stupfel and M. Lecouvez, One-way domain decomposition method with exact radiation condition and fast GMRES solver for the solution of Maxwell’s equations, *Journal of Computational Physics* **322** (2016), pp. 882-904.

An integral equation on infinite boundaries when a global Green's function is not available

Anne-Sophie Bonnet-Ben Dhia¹, Sonia Fliss¹, Yohanes Tjandrawidjaja^{1, 2,*}

¹POEMS (CNRS - INRIA - ENSTA Paristech), Palaiseau, France

²CEA-LIST, Gif-sur-Yvette, France

*Email: yohanes.tjandrawidjaja@ensta-paristech.fr

Abstract

We are interested in time-harmonic scattering problems for configurations where the Green's function is not easily computable for the exterior domain, but different Green's functions are available in several unbounded subdomains covering the whole space. For a model problem, by using integral representations of the solution in each subdomain, we propose a formulation coupling the traces and the normal traces of the solution on infinite boundaries. The system of equations is shown to have a unique solution in the dissipative case.

Keywords: integral equations, domain decomposition

1 The model problem

We search u in $H^1(\Omega)$ which satisfies:

$$-\Delta u(\mathbf{x}) - (k(\mathbf{x}) + i\epsilon)u(\mathbf{x}) = f \text{ in } \Omega, \quad (1)$$

where k is positive, and $\Omega = \Omega_b \cup \Omega_0 \cup \Omega_1$, with $\Omega_j, j \in \{0, 1\}$ is such that the Green's functions G_j associated to the problem in Ω_j can be computed. Finally, the support of f is included in Ω_b . In Figure 1 we represent 2 examples: the junctions of 2 stratified media or 2 half-spaces of different topography. In this second case, we impose for instance a compactly supported Dirichlet condition on $\partial\Omega$.

To focus only on the originality of the method, let us suppose that u is known on the boundary of the bounded domain Ω_b :

$$u = g \text{ on } \partial\Omega_b, \quad (2)$$

with $g \in H^{1/2}(\partial\Omega_b)$ a given data.

2 The system of integral equations

The idea of this integral method is to couple several representations obtained from its traces φ_j and normal traces ψ_j on the boundary of

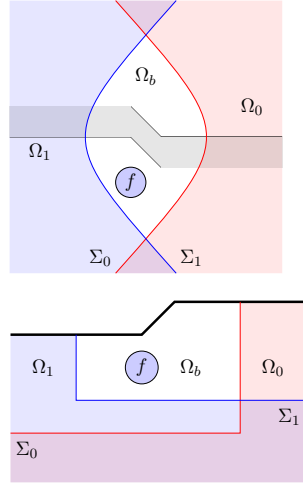


Figure 1: Multi-domain representation

each subdomain:

$$u|_{\Omega_j}(\mathbf{x}) = U_j(\varphi_j, \psi_j) \text{ in } \Omega_j \quad (3)$$

$$:= \int_{\Sigma_j} \varphi_j(\mathbf{y}) \frac{\partial G_j}{\partial \nu_j}(\mathbf{x} - \mathbf{y}) - \psi_j(\mathbf{y}) G_j(\mathbf{x} - \mathbf{y}) d\gamma_j$$

where ν_j is the exterior normal of Ω_j .

On the part of Σ_0 located in Ω_1 , we have by definition:

$$u = \varphi_0,$$

and by using the representation (3) for $j = 1$, we have

$$u = U_1(\varphi_1, \psi_1).$$

As a consequence, on this part of Σ_0 we must have $\varphi_0 = U_1(\varphi_1, \psi_1)$. Proceeding in the same manner for the normal trace ψ_0 , we obtain on $\Omega_0 \cap \Sigma_1$:

$$\varphi_0 = U_1(\varphi_1, \psi_1) \text{ and } \psi_0 = \partial_{\nu_0} U_1(\varphi_1, \psi_1).$$

The boundary condition (2) implies that

$$\varphi_0 = g \text{ on } \Sigma_0 \cap \partial\Omega_b.$$

Finally, there are several possible equations for ψ_0 on $\Sigma_0 \cap \partial\Omega_b$:

$$\varphi_0 = U_0(\varphi_0, \psi_0) \text{ or } \psi_0 = \partial_{\nu_0} U_0(\varphi_0, \psi_0).$$

In the sequel we choose the first option. Similar equations can be obtained by permuting 0 and 1. This leads to: for $j \in \{0, 1\}$,

$$\begin{cases} \varphi_{1-j} = U_j(\varphi_j, \psi_j) & \text{on } \Sigma_{1-j} \cap \Omega_j, \\ \psi_{1-j} = \partial_{\nu_{1-j}} U_j(\varphi_j, \psi_j) & \text{on } \Sigma_{1-j} \cap \Omega_j, \\ \varphi_j = g & \text{on } \Sigma_j \cap \partial\Omega_b, \\ \varphi_j = U_j(\varphi_j, \psi_j) & \text{on } \Sigma_j \cap \partial\Omega_b. \end{cases} \quad (4)$$

3 The mathematical formulation

The natural choice of functional spaces for the traces are $\varphi_j \in H_g^{1/2}(\Sigma_j) := \{\phi \in H^{1/2}(\Sigma_j), \phi = g \text{ on } \Sigma_j \cap \partial\Omega_b\}$ and $\psi_j \in H^{-1/2}(\Sigma_j)$. However, the traces involved in the system (4) are defined piece by piece, meaning that we "cut" them. To avoid this, we have to choose the test functions cleverly and not in the same space as the unknowns. To do so, we define the curves

$$\tilde{\Sigma}_j := \partial(\Omega_j \cup \Omega_b) = (\Sigma_j \cap \Omega_{1-j}) \cup (\Sigma_{1-j} \cap \partial\Omega_b).$$

We choose the test functions $\tilde{\varphi}_j^t \in H_0^{1/2}(\tilde{\Sigma}_j) := \{\phi \in H^{1/2}(\tilde{\Sigma}_j), \phi = 0 \text{ on } \tilde{\Sigma}_j \cap \partial\Omega_b\}$, and $\tilde{\psi}_j^t \in H^{-1/2}(\tilde{\Sigma}_j)$. Afterwards, we define several operators that allow us to pass functions defined on $\Sigma_0 \cup \Sigma_1$ to functions defined on $\tilde{\Sigma}_0 \cup \tilde{\Sigma}_1$:

$$\begin{cases} E_j : H_g^{1/2}(\Sigma_0) \times H_g^{1/2}(\Sigma_1) \rightarrow H_g^{1/2}(\tilde{\Sigma}_j), \\ E_j(\varphi_0, \varphi_1) = \tilde{\varphi}_j = \begin{cases} \varphi_j \text{ on } \Sigma_j \cap \Omega_{1-j}, \\ \varphi_{1-j} \text{ on } \Sigma_{1-j} \cap \partial\Omega_b, \end{cases} \end{cases}$$

$$\text{and } \tilde{E}_j : H_g^{1/2}(\tilde{\Sigma}_0) \times H_g^{1/2}(\tilde{\Sigma}_1) \rightarrow H_g^{1/2}(\Sigma_j).$$

Finally, the formulation is written as: find for $j \in \{0, 1\}$, (φ_j, ψ_j) in $H_g^{1/2}(\Sigma_j) \times H^{-1/2}(\Sigma_j)$ such that for all $(\tilde{\varphi}_j, \tilde{\psi}_j)$ in $H_0^{1/2}(\tilde{\Sigma}_j) \times H^{-1/2}(\tilde{\Sigma}_j)$,

$$\begin{cases} \langle E_0(\varphi_0, \varphi_1), \tilde{\psi}_0^t \rangle_{\tilde{\Sigma}_0} = \langle U_1(\varphi_1, \psi_1), \tilde{\psi}_0^t \rangle_{\tilde{\Sigma}_0}, \\ \langle \psi_0, \tilde{E}_0(\tilde{\varphi}_0^t, 0) \rangle_{\Sigma_0} = \langle \partial_{\nu_0} U_1(\varphi_1, \psi_1), \tilde{\varphi}_0^t \rangle_{\tilde{\Sigma}_0}, \\ \langle E_1(\varphi_0, \varphi_1), \tilde{\psi}_1^t \rangle_{\tilde{\Sigma}_1} = \langle U_0(\varphi_0, \psi_0), \tilde{\psi}_1^t \rangle_{\tilde{\Sigma}_1}, \\ \langle \psi_1, \tilde{E}_1(0, \tilde{\varphi}_1^t) \rangle_{\Sigma_1} = \langle \partial_{\nu_1} U_0(\varphi_0, \psi_0), \tilde{\varphi}_1^t \rangle_{\tilde{\Sigma}_1}. \end{cases} \quad (5)$$

Remark that the first equation of (5) combines the first and the last equations of (4).

Theorem 1 System (5) has a unique solution.

4 Numerical result

For the numerical simulation, we use 2D Lagrange finite elements to treat the volume unknown. For the trace unknowns, we truncate the curves Σ_j far enough and use 1D Lagrange finite elements for both types of traces. Finally, once we obtain the φ_j and ψ_j , we can reconstruct the solution by applying Formula (3). This method can be used to solve scattering problems in configurations like in Figure 1 bottom. In Figure 2, we represent the scattered field for a particular incident field (which has to be defined precisely). This result is obtained by using XLife++.

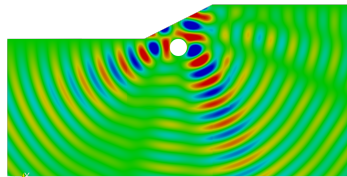


Figure 2: Numerical validation with a localized defect.

Note that although the theory is established for dissipative media, the numerical simulation work as well in the case without dissipation.

Remark 2 When the Green's function of each subdomain is not available in a closed form, we could take, instead of 2 curves, at least 3 straight lines and then use a Fourier integral representation instead of (3) (see for instance [1, 2]). It is particularly useful in the elasticity problem in locally perturbed 3D anisotropic plate, where both types of the traces are needed to represent the displacement field in each half-plate.

References

- [1] Bonnet-Ben Dhia A.-S., Fliss S., and Tonnoir A. (2018), *The halfspace matching method: a new method to solve scattering problem in infinite media*, JCAM vol. 338, pp. 44-68.
- [2] Bonnet-Ben Dhia A.-S., Fliss S., and Tjandra-dwidjaja Y. (2019), *Numerical analysis of the Half-Space Matching method with Robin traces on a convex polygonal scatterer*, in *Maxwell's Equations: Analysis and Numerics*, De Gruyter.

Non-overlapping domain decomposition algorithm for time-harmonic elastic wave problems

M. Darbas¹, C. Geuzaine², V. Mattesi²

¹University of Picardie Jules Verne, LAMFA UMR CNRS 7352, Amiens

²University of Liège, Department of Electrical Engineering and Computer Science

Abstract

We focus on the construction of an optimized non-overlapping domain decomposition method (DDM) for 2D-elastic scattering problems where the sub-domains are coupled by a new high-order Transmission Boundary Condition (TBC). These TBCs are defined in terms of an approximate local Dirichlet-to-Neumann (DtN) map. First, we explain the derivation of the new TBC in the context of a non-overlapping DDM and recall the standard low-order Lysmer-Kuhlemeyer TBC. Next, a convergence study mode-by-mode for a model problem is addressed.

Keywords: Scattering, 2D elastic waves, optimized Schwarz method, approximate DtN map

1 Mono-domain time-harmonic elastic wave problem

Let us consider $\Omega^- := \{\mathbf{x} \in \mathbb{R}^2 : |\mathbf{x}| \leq r_{int}\}$ with boundary Γ and its complementary $\Omega^+ := \mathbb{R}^2 \setminus \Omega^-$. Let us remind the second-order harmonic elastic wave equation :

$$\operatorname{div} \sigma(\mathbf{u}) + \rho \omega^2 \mathbf{u} = 0, \tag{1}$$

where $\mathbf{u} \in \Omega^+$, σ and ϵ are the stress, respectively strain tensors defined in the isotropic case by $\sigma(\mathbf{u}) = \lambda(\operatorname{div} \mathbf{u})\mathbf{I} + 2\mu\epsilon(\mathbf{u})$, $\epsilon(\mathbf{u}) = \frac{1}{2}([\nabla \mathbf{u}] + [\nabla \mathbf{u}]^T)$, with λ and μ the Lamé coefficients. When illuminated by a time-harmonic incident wave \mathbf{u}^{inc} , the scattering problem is formulated as follows: find the displacement \mathbf{u} solution to the Navier equation (1) in Ω^+ such that

$$\mathbf{u} = -\mathbf{u}^{inc}, \quad \text{on } \Gamma, \tag{2}$$

and satisfying the Kupradze radiation conditions at infinity and particularly on $\Gamma^\infty := \{\mathbf{x} \in \mathbb{R}^2 : |\mathbf{x}| = r_{ext}\}$ which delimits the studied bounded domain $\Omega := \{\mathbf{x} \in \mathbb{R}^2 : r_{int} \leq |\mathbf{x}| \leq r_{ext}\}$.

2 Domain decomposition

We split the domain Ω into N_{dom} sub-domains Ω_i without overlap. Let us denote $\Gamma_i := \Gamma \cap \Omega_i$,

$\Gamma_i^\infty := \Gamma^\infty \cap \Omega_i$ and $\Sigma_{ij} := \overline{\Omega_i \cap \Omega_j}$ the transmission boundary. At iteration $(n+1)$ for a sub-domain Ω_i , the additive Schwarz DDM leads to solve two problems:

- Find $\mathbf{u}_i^{n+1} := \mathbf{u}_{|\Omega_i}$, $i = 1, \dots, N_{dom}$ solution to

$$\begin{cases} \operatorname{div} \sigma(\mathbf{u}_i^{(n+1)}) + \rho \omega^2 \mathbf{u}_i^{(n+1)} = 0, & \text{in } \Omega_i, \\ \mathbf{u}_i^{(n+1)} = -\mathbf{u}^{inc}, & \text{on } \Gamma_i, \\ \mathcal{T}_{n_i} \mathbf{u}_i^{(n+1)} = \mathcal{B} \mathbf{u}_i^{(n+1)}, & \text{on } \Gamma_i^\infty, \\ \mathcal{T}_{n_i} \mathbf{u}_i^{(n+1)} - \mathcal{S}_{n_i} \mathbf{u}_i^{(n+1)} = \mathbf{g}_{ij}^{(n)}, & \text{on } \Sigma_{ij}, \end{cases} \tag{3}$$

where n_i is the outgoing normal to Ω_i , \mathcal{B} the operator describing boundary conditions at infinity, \mathcal{T} the traction operator, \mathcal{S} the transmission operator and $\mathbf{g}_{ij}^{(n)}$ the surface fields given by the previous iteration of the algorithm.

- Update the interface unknowns $\mathbf{g}_{ji}^{(n+1)}$ as

$$\mathbf{g}_{ji}^{(n+1)} = -\mathbf{g}_{ij}^{(n)} - (\mathcal{S}_{n_i} + \mathcal{S}_{n_j}) \mathbf{u}_i^{(n+1)}, \quad \text{on } \Sigma_{ij}, \tag{4}$$

with n_j the outgoing normal to Ω_j .

3 Transmission operator

A key point of the method remains in approximating accurately the traction operator \mathcal{T} by the transmission operator \mathcal{S} . The choice of this operator is important for the convergence rate of the iterative solver. We consider two transmission operators:

- The low-order transmission operator:

$$\mathcal{S}^0 = i(\lambda + 2\mu)\kappa_p \mathbf{I}_n + i\mu\kappa_s \mathbf{I}_\tau, \tag{5}$$

with $\kappa_{\{p,s\}}$ the wavenumbers associated to respectively the P- and S-waves, $\mathbf{I}_n = n_i \otimes n_i$ and $\mathbf{I}_\tau = \mathbf{I} - \mathbf{I}_n$.

- The high-order (HO) non-local transmission operator inspired by [1]- [2]:

$$\mathcal{S}_{1,\epsilon}^{1,\epsilon} = (\mathbf{I} + \Lambda_{2,\epsilon,n})^{-1} \Lambda_{1,\epsilon} + 2\mu \mathcal{M}_n, \tag{6}$$

with

$$\Lambda_{1,\epsilon} = i\rho\omega^2 \left[\frac{n}{\kappa_{p,\epsilon}} \left(\frac{\Delta_\Gamma}{\kappa_{p,\epsilon}^2} + \mathbf{I} \right)^{-1/2} \mathbf{I}_n + \frac{\tau}{\kappa_{s,\epsilon}} \left(\frac{\Delta_\Gamma}{\kappa_{s,\epsilon}^2} + \mathbf{I} \right)^{-1/2} \mathbf{I}_\tau \right], \tag{7}$$

$$\Lambda_{2,\epsilon,n} = -i \begin{bmatrix} \frac{\tau}{\kappa_{s,\epsilon}} \partial_s \left(\frac{\Delta_\Gamma}{\kappa_{s,\epsilon}^2} + I \right)^{-1/2} I_n \\ - \frac{n}{\kappa_{p,\epsilon}} \partial_s \left(\frac{\Delta_\Gamma}{\kappa_{p,\epsilon}^2} + I \right)^{-1/2} I_\tau \end{bmatrix}, \quad (8)$$

and \mathcal{M}_n the Günter tangential derivative given by

$$\mathcal{M}_n = \partial_s(n \cdot I_n)\tau - \partial_s(\tau \cdot I_\tau)n. \quad (9)$$

We denoted Δ_Γ the Laplace-Beltrami operator and ∂_s the curvilinear derivative.

4 Convergence analysis

In order to study the convergence of the proposed DDM with the non-local HO-TBC (6), we analyze a model problem with two sub-domains: a disk-shaped bounded sub-domain Ω_0 of radius R and an unbounded complementary domain Ω_1 . We denote by $\Gamma := \partial\Omega_1$ the boundary of Ω_1 . The convergence analysis can be developed by studying the spectral properties of the iteration operator \mathcal{A} (a matrix 4×4) defined by

$$\mathcal{A} := \begin{pmatrix} \mathbf{0}_2 & \mathcal{A}_0 \\ \mathcal{A}_1 & \mathbf{0}_2 \end{pmatrix}, \quad (10)$$

with \mathcal{A}_0 and \mathcal{A}_1 2×2 matrices satisfying

$$\begin{aligned} \mathcal{A}_0 \mathbf{g}_0^{(p)} &:= -\mathbf{g}_0^{(p)} - (\mathcal{S}_{n_0}^{1,\epsilon} + \mathcal{S}_{n_1}^{1,\epsilon}) \mathbf{u}_0^{(p+1)}, \\ \mathcal{A}_1 \mathbf{g}_1^{(p)} &:= -\mathbf{g}_1^{(p)} - (\mathcal{S}_{n_0}^{1,\epsilon} + \mathcal{S}_{n_1}^{1,\epsilon}) \mathbf{u}_1^{(p+1)}. \end{aligned} \quad (11)$$

The modal iteration matrix \mathcal{A}_m is determined through a Fourier-Hankel serie expansion of the solutions. An important result is that the spectral radius of \mathcal{A}_m vanishes for evanescent modes ($m \rightarrow \infty$).

To highlight the efficiency of the HO non-local TBC, let us choose $\kappa_p = 12\pi/\sqrt{3} \text{ m}^{-1}$, $\kappa_s = 12\pi \text{ m}^{-1}$, $\rho = 1 \text{ Kg.m}^{-3}$, $R = 1 \text{ m}$ and a maximal number of modes $m^{\max} = 140$. We report in Figure 1 the modal spectral radius $\rho(\mathcal{A}_m)$ with respect to m corresponding to the transmission operators \mathcal{S}^0 , $\mathcal{S}^{1,0}$, $\mathcal{S}^{1,\epsilon}$, where $\mathcal{S}^{1,0}$ is the non-local HO-TBC operator taking $\epsilon_p = \epsilon_s = 0$. The LO-TBC operator \mathcal{S}^0 acts on propagative modes only. As the Després condition in the Helmholtz case [3], the spectral radius of \mathcal{A}_m is equal to 1 for evanescent modes. Applying the new non-local HO-TBC without damping related to $\mathcal{S}^{1,0}$, the convergence rate is optimal for the evanescent modes and an improvement over the LO-TBC is observed. The singularities of the square-root operators in the

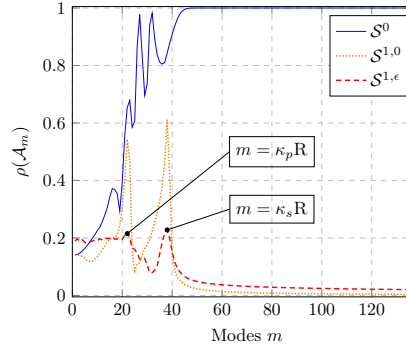


Figure 1: Spectral radius of the modal iteration matrix \mathcal{A}_m with respect to the mode m . $f = 6 \text{ Hz}$, $R = 1 \text{ m}$, $[\kappa_p] = 22 \text{ m}^{-1}$, $[\kappa_s] = 38 \text{ m}^{-1}$.

transition zone of creeping modes ($m \approx \kappa_p R$ and $m \approx \kappa_s R$) lead to two expected amplitude peaks. Finally, adding damping parameters $\epsilon_{\{p,s\}} = 0.39 \kappa_{\{p,s\}}^{1/3} R^{-2/3}$, the non-local HO-TBC leads to a smaller spectral radius for the grazing modes than without damping.

In a finite element context, a localization procedure is needed [3], which is achieved through a complex Padé approximation of the inverse of the square-root operator.

References

- [1] S. Chaillat, M. Darbas and F. Le Louer, Approximate local Dirichlet-to-Neumann map for three-dimensional time-harmonic elastic waves, *Computer Methods in Applied Mechanics and Engineering*, **297** (1) (2015), pp. 62-83.
- [2] V. Mattesi, M. Darbas and C. Geuzaine, A high-order absorbing boundary condition for 2D time-harmonic elastodynamic scattering problems, *Computers & Mathematics with Applications*, **77** (6) (2019), pp. 1703 - 1721.
- [3] Y. Boubendir, X. Antoine and C. Geuzaine, A quasi-optimal non-overlapping domain decomposition algorithm for the Helmholtz equation, *Journal of Computational Physics*, **231** (2), pp. 262 - 280.

A Preconditioner for the Electric Field Integral Equation on Screens

Ralf Hiptmair¹, Carolina Urzúa-Torres^{2,*}

¹Seminar for Applied Mathematics, ETH Zurich, Zurich, Switzerland.

²Mathematical Institute, University of Oxford, Oxford, UK

*Email: carolina.urzuatorres@maths.ox.ac.uk

Abstract

We consider the electric field integral equation (EFIE) arising from the scattering of time-harmonic electromagnetic waves by a perfectly conducting screen. When discretizing the EFIE by means of low-order Galerkin boundary element methods (BEM), one obtains linear systems that are ill-conditioned on fine meshes. This makes iterative solvers perform poorly and motivates the use of preconditioning.

This paper presents a new preconditioner for the EFIE on screens that achieves condition numbers that are bounded and independent of the meshwidth h , is robust with respect to the so-called low-frequency break-down, and works on non-uniformly refined meshes. This last property is very important as solutions to the EFIE on screens feature edge singularities.

We provide some numerical results to verify our theoretical findings.

Keywords: Electric field integral equation, preconditioning, screen problems.

1 Introduction

Let Γ be a simple Lipschitz screen, $k > 0$ a fixed wave number, and $\mathbf{g} \in (\tilde{\mathbf{H}}^{-1/2}(\text{div}_\Gamma, \Gamma))'$ be given. The corresponding EFIE variational problem reads: Seek $\boldsymbol{\xi} \in \tilde{\mathbf{H}}^{-1/2}(\text{div}_\Gamma, \Gamma)$ such that

$$\begin{aligned} a_k(\boldsymbol{\xi}, \boldsymbol{\eta}) &:= \langle \mathbf{V}_k \boldsymbol{\xi}, \boldsymbol{\eta} \rangle - \frac{1}{k^2} \langle \mathbf{V}_k \text{div}_\Gamma \boldsymbol{\xi}, \text{div}_\Gamma \boldsymbol{\eta} \rangle \\ &= \langle \mathbf{g}, \boldsymbol{\eta} \rangle, \end{aligned}$$

for all $\boldsymbol{\eta} \in \tilde{\mathbf{H}}^{-1/2}(\text{div}_\Gamma, \Gamma)$.

Here \mathbf{V}_k is the weakly singular boundary integral operator for the Helmholtz operator $(\Delta + k^2)$, and \mathbf{V}_k its extension to surface vector fields (see [4] for notation and definitions of the corresponding Sobolev spaces).

When discretizing the EFIE by means of low-order Galerkin boundary element methods (BEM), one obtains linear systems that are ill-conditioned on fine meshes. Moreover, the resulting Galerkin matrix will also suffer from the

so-called *low-frequency break-down*. These two phenomena make iterative solvers perform poorly and motivate the use of preconditioning that is robust with respect to the meshwidth h and for $k \rightarrow 0$.

Several preconditioning approaches have been proposed for the EFIE in the literature, see for example [2, Sect. 1.c] and the references therein. However, many of these strategies do not work in the case of screens, and those that do, require special treatment and do not achieve h -independent condition numbers when dealing with screens. A popular technique on closed surfaces is the so-called *Calderón preconditioning*, which builds on Calderón identities and leads to mesh independent condition numbers [1]. Unfortunately, these identities do not hold on screens. Indeed, when using them in the screen setting, one obtains condition numbers that still grow like $\log(h)$. It is worth noticing that this result is a consequence of the operators' mapping properties. Therefore, the construction of a suitable preconditioner for the EFIE on screens needs to find different identities that actually hold in the energy trace spaces involved. On the other hand, since in this case the solution features edge singularities, it is important that the preconditioner can also handle meshes refined towards the boundary of the screen.

We present a novel preconditioner for the EFIE on screens. First, we find a compact equivalent inverse of the EFIE operator. Then, we use this to construct an operator preconditioner that is stable. Furthermore, the stability of the preconditioner relies only on the stability of the scalar L^2 duality pairing, instead of the vectorial one. This approach not only offers h -independent condition numbers, but it allows for non-uniform meshes without additional computational effort.

2 Compact Equivalent inverse

Let V_0 and W_0 be the weakly and hypersingular operators arising from the Exterior Laplacian BVPs on Γ . We introduce the following

operators derived in [4]:

$$\mathbf{B}_z = \mathbf{curl}_\Gamma \circ \mathbf{W}_0^{-1} \circ (\mathbf{curl}_\Gamma)^*$$

and

$$\mathbf{B}_\perp = \mathbf{L} \circ \mathbf{V}_0^{-1} \circ \mathbf{L}^*,$$

with $\mathbf{L} : \tilde{\mathbf{H}}_*^{-1/2}(\Gamma) \rightarrow X_\perp(\Gamma)$ being a right inverse of \mathbf{div}_Γ .

For $k > 0$, we define the operator \mathbf{B}_k , mapping from $\mathbf{H}^{-1/2}(\mathbf{curl}_\Gamma, \Gamma)$ to $\mathbf{H}^{-1/2}(\mathbf{div}_\Gamma, \Gamma)$, as

$$\mathbf{B}_k = \mathbf{B}_z - k^2 \mathbf{B}_\perp. \tag{1}$$

This operator satisfies:

Theorem 1 (Theorem 3.2 in [4]) *The operator \mathbf{B}_k from (1) is continuous and satisfies*

$$\mathbf{B}_k \mathbf{A}_k = \mathbf{Id} + \mathbf{C}_k \tag{2}$$

with \mathbf{C}_k a compact operator, uniformly bounded for $k \rightarrow 0$.

From (2) we get that \mathbf{B}_k would be a suitable preconditioner for \mathbf{A}_k .

3 Preconditioner

We formulate our preconditioner from \mathbf{B}_k such that it fulfills all the requirements of operator preconditioning and its discretization is stable. In order to achieve this purpose, we resort to the following mixed variational formulations:

- ① $\mathbf{B}_z \mathbf{g}$ is obtained by finding $u \in \tilde{\mathbf{H}}^{1/2}(\Gamma)$, $\lambda \in H^{-1/2}(\Gamma)$ such that

$$\begin{aligned} \langle \mathbf{W}_0^{-1} \lambda, \phi \rangle + \langle u, \phi \rangle &= 0, \\ \langle \lambda, w \rangle &= - \langle \mathbf{g}, \mathbf{curl}_\Gamma w \rangle, \end{aligned}$$

for all $v \in \tilde{\mathbf{H}}^{1/2}(\Gamma)$, and then applying $\mathbf{curl}_\Gamma : \mathbf{B}_z \mathbf{g} := \mathbf{curl}_\Gamma u$.

- ② Let $\tilde{\mathbf{H}}_d := \tilde{\mathbf{H}}^{-1/2}(\mathbf{div}_\Gamma, \Gamma) \cap \mathbf{L}_t^2(\Gamma)$. The computation of $\mathbf{B}_\perp g$ boils down to the following two steps:

- (i) Seek $\boldsymbol{\mu} \in \tilde{\mathbf{H}}_d, u \in H_*^{1/2}(\Gamma)$ such that

$$\begin{aligned} \langle \boldsymbol{\mu}, \mathbf{j} \rangle + \langle u, \mathbf{div}_\Gamma \mathbf{j} \rangle &= \langle \mathbf{g}, \mathbf{j} \rangle, \\ \langle \mathbf{div}_\Gamma \boldsymbol{\mu}, v \rangle &= 0, \end{aligned}$$

for all $\mathbf{j} \in \tilde{\mathbf{H}}_d$ and $v \in H_*^{1/2}(\Gamma)$.

- (ii) Seek $\boldsymbol{\xi}_\perp \in \tilde{\mathbf{H}}_d, w \in H_*^{1/2}(\Gamma)$ such that:

$$\begin{aligned} \langle \boldsymbol{\xi}_\perp, \mathbf{q} \rangle + \langle w, \mathbf{div}_\Gamma \mathbf{q} \rangle &= 0, \\ \langle \mathbf{div}_\Gamma \boldsymbol{\xi}_\perp, v \rangle &= \langle \mathbf{V}_0^{-1} u, v \rangle \end{aligned}$$

for all $\mathbf{q} \in \tilde{\mathbf{H}}_d$ and $v \in H_*^{1/2}(\Gamma)$.

Then $\mathbf{B}_\perp \mathbf{g} := \boldsymbol{\xi}_\perp \in \tilde{\mathbf{H}}_d \subset \tilde{\mathbf{H}}^{-1/2}(\mathbf{div}_\Gamma, \Gamma)$.

Remark 2 *There are closed-form integral operator formulas for the inverses of the weakly and hypersingular operators on the unit disk \mathbb{D} [3]. Moreover, their associated symmetric bilinear forms are easy to incorporate into a BEM implementation.*

During the presentation, we will explain further details and report numerical experiments for different wave numbers k , both on the unit disk and on more general screens.

References

- [1] F.P. Andriulli, K. Cools, H. Bagci, F. Olyslager, A. Buffa, S. Christiansen, and E. Michielssen, A Multiplicative Calderón Preconditioner for the Electric Field Integral Equation. *IEEE Trans. Antennas and Propagation* **56** (8) (2008), pp.2398–2412.
- [2] S. Adrian, *Rapidly Converging Boundary Integral Equation Solvers in Computational Electromagnetics*, Dissertation, Technische Universität München, 2018.
- [3] R. Hiptmair, C. Jerez-Hanckes, and C. Urzúa-Torres, Closed-Form Inverses of the Weakly Singular and Hypersingular Operators On Disks. *Integral Equations and Operator Theory*, **90**:4 (2018).
- [4] R. Hiptmair and C. Urzúa-Torres, Compact Equivalent Inverse of the Electric Field Integral Operator on Screens, *submitted to Integral Equations and Operator Theory*, pre-print available in Technical Report 2018-46, Seminar for Applied Mathematics, ETH Zürich, 2018.

**Non overlapping domain decomposition methods with non local transmission conditions
for electromagnetic wave propagation**

Xavier Claeys¹, Francis Collino², Patrick Joly², Emile Parolin^{2,*}

¹Sorbonne Université, Université Paris-Diderot SPC, CNRS, INRIA, LJLL, 75005 Paris, France

²POEMS (UMR 7231 CNRS-INRIA-ENSTA ParisTech), INRIA Saclay, 91120 Palaiseau, France

*Email: emile.parolin@inria.fr

Abstract

In this work, we investigate iterative non overlapping domain decomposition methods for time harmonic Maxwell's equations. The main novelty of our approach is the use of non-local operators (integral operators) in the transmission conditions between two adjacent subdomains, in the spirit of previous works for Helmholtz equation. Under suitable assumptions on the transmission operators the algorithm converges linearly, that is to say the error decreases exponentially. In this work, we address the issue of designing well adapted integral operators. The main difficulty is to take into account the particular properties of the trace spaces of solutions of Maxwell's equations. A second difficulty is to propose an adequate finite element approximation. The main theoretical aspects of this construction process will be detailed and preliminary numerical results will be presented.

Keywords: Domain Decomposition, Impedance transmission conditions, Non-local operators.

Domain decomposition method

We consider time harmonic Maxwell's equations in a bounded domain $\Omega \subset \mathbb{R}^3$. Let $k > 0$ be the (possibly varying) wave number of the medium and $\mathbf{f} \in \mathbf{L}^2(\Omega)$, we seek $\mathbf{u} \in \mathbf{H}(\mathbf{curl}; \Omega)$ such that (we impose a first order absorbing condition on the boundary Γ , omitted here for brevity)

$$(\mathbf{curl} \mathbf{curl} - k^2) \mathbf{u} = \mathbf{f}, \quad \text{in } \Omega. \quad (1)$$

We suppose that the domain is partitioned into two non-overlapping subdomains $\bar{\Omega} = \bar{\Omega}_- \cup \bar{\Omega}_+$ with interface Σ for which the unit normal vector \mathbf{n} is oriented from Ω_- to Ω_+ . We suppose in addition that Σ does not intersect Γ . We introduce the tangential trace operators

$$\begin{aligned} \gamma^0 : \mathbf{H}(\mathbf{curl}; \Omega) &\rightarrow \mathbf{H}_t^{-1/2}(\mathbf{curl}_\Sigma), \\ \gamma^1 : \mathbf{H}(\mathbf{curl}; \Omega) &\rightarrow \mathbf{H}_t^{-1/2}(\mathbf{div}_\Sigma), \end{aligned} \quad (2)$$

respective extensions of $\gamma^0 \mathbf{u} = \mathbf{n} \times (\mathbf{u} \times \mathbf{n})$ and $\gamma^1 \mathbf{u} = \frac{1}{k} \mathbf{n} \times \mathbf{curl} \mathbf{u}$ for regular fields. The idea

consists in considering the following transmission problem, equivalent to (1), in the spirit of previous works in the acoustic setting [1, 2],

$$\begin{aligned} \text{Find } \mathbf{u}_\pm \in \mathbf{H}(\mathbf{curl}; \Omega_\pm) \text{ such that} \\ (\mathbf{curl} \mathbf{curl} - k^2) \mathbf{u}_\pm = \mathbf{f}|_{\Omega_\pm}, \quad \text{in } \Omega_\pm, \quad (3) \\ (\gamma^1 \mp i \mathbf{T} \gamma^0) \mathbf{u}_\pm = (\gamma^1 \mp i \mathbf{T} \gamma^0) \mathbf{u}_\mp, \quad \text{on } \Sigma. \end{aligned}$$

If the boundary operator

$$\mathbf{T} : \mathbf{H}_t^{-1/2}(\mathbf{curl}_\Sigma) \rightarrow \mathbf{H}_t^{-1/2}(\mathbf{div}_\Sigma) \quad (4)$$

is a positive self-adjoint isomorphism, the associated relaxed Jacobi algorithm converges linearly: there exists $\tau < 1$ and $C > 0$ such that the n -th iterates \mathbf{u}_\pm^n satisfy

$$\|\mathbf{u}_\pm^n - \mathbf{u}|_{\Omega_\pm}\| + \|\mathbf{u}_\pm^n - \mathbf{u}|_{\Omega_\mp}\| \leq C \tau^n. \quad (5)$$

Construction of \mathbf{T}

A valid candidate for \mathbf{T} is a dissipative version of the EFIE operator as proposed in [3]. In this work, we propose an alternative that lend itself to a quasi-localization process.

Our construction is guided by the Helmholtz decompositions of the two trace spaces (valid for simply connected surfaces)

$$\begin{aligned} \mathbf{H}_t^{-1/2}(\mathbf{curl}_\Sigma) &= \nabla_\Sigma H^{1/2} + \mathbf{curl}_\Sigma H^{3/2}, \\ \mathbf{H}_t^{-1/2}(\mathbf{div}_\Sigma) &= \nabla_\Sigma H^{3/2} + \mathbf{curl}_\Sigma H^{1/2}. \end{aligned} \quad (6)$$

We see that a suitable \mathbf{T} is a pseudo-differential operator of order -1 on the ∇ -part and order 1 on the \mathbf{curl} -part. Such a property cannot be realized by a local operator.

We introduce the regularizing operator (Ries potential) of order $-3/2$ which admits the following representation for regular fields $\mathbf{f} \in \mathbf{L}_t^2(\Sigma)$

$$R\mathbf{f}(\mathbf{x}) := \int_\Sigma \frac{\mathbf{f}(\mathbf{y})}{\Sigma (k|\mathbf{x} - \mathbf{y}|)^{1/2}} d\sigma(\mathbf{y}), \quad \forall \mathbf{x} \in \Sigma, \quad (7)$$

and the coercive operator

$$L := \text{Id} - k^{-2} \nabla_\Sigma \mathbf{div}_\Sigma. \quad (8)$$

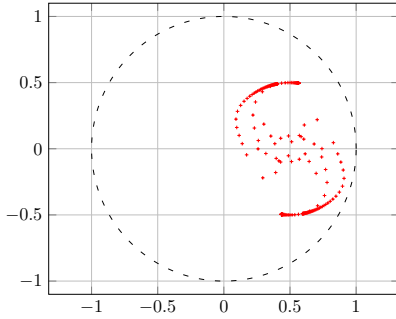


Figure 1: Eigenvalues of the iterative operator

We define

$$\mathbf{T} = \Lambda_0^* \Lambda_0 + \Lambda_c^* \Lambda_c + \Lambda_g^* \Lambda_g, \quad (9a)$$

$$\text{with } \begin{cases} \Lambda_0 = L^{-1/2} (\mathbf{i} \mathbf{n} \times \cdot), \\ \Lambda_c = \mathbf{curl}_\Sigma R \mathbf{curl}_\Sigma, \\ \Lambda_g = -L^{-1/2} (\nabla_\Sigma R \mathbf{div}_\Sigma). \end{cases} \quad (9b)$$

It is clear that such a \mathbf{T} is a positive self-adjoint operator. Furthermore, it can be shown that Λ_0 , Λ_c and Λ_g map continuously $\mathbf{H}_t^{-1/2}(\mathbf{curl}_\Sigma)$ to $\mathbf{L}_t^2(\Sigma)$ and that \mathbf{T} is an isomorphism.

The main role of the first term in (9a) will become clear in the next section. The last two terms in (9a) allow us to act selectively and independently on the two components of the decomposition of tangential fields since

$$\nabla_\Sigma H^{1/2} \subset \text{Ker } \Lambda_c, \quad \mathbf{curl}_\Sigma H^{3/2} \subset \text{Ker } \Lambda_g.$$

The relaxed Jacobi algorithm can be rewritten in the compact form

$$\mathbf{u}^{n+1} = \mathbf{A}_r \mathbf{u}^n, \quad (10)$$

where r is the relaxation parameter. In Fig. 1 we report the eigenvalues of the iteration operator $\mathbf{A}_{0.5}$ in the case where $\Omega = \mathbb{R}^3$, Σ is the unit sphere and the medium is homogeneous with $k = 10$. Note that the spectrum is strictly contained inside the unit circle.

Quasi-localization

The main advantage of \mathbf{T} given in (9a) is that it can be “quasi-localized” while retaining its positivity and self-adjointness. To do so, given

a smooth cut-off function χ defined on \mathbb{R}^+ and supported on $[0, \delta]$, we first define R_χ as in (7), except that $\mathbf{f}(\mathbf{y})$ is replaced by $\chi(|\mathbf{x} - \mathbf{y}|)\mathbf{f}(\mathbf{y})$. Then in (9a), we substitute Λ_c and Λ_g for $\Lambda_{c,\chi}$ and $\Lambda_{g,\chi}$ which are defined as in (9b) with R replaced by R_χ . Hence, the “localized” transmission operator \mathbf{T}_χ involves only local or quasi-local operators and writes in full

$$\begin{aligned} \mathbf{T}_\chi &= -\mathbf{n} \times L^{-1} (\mathbf{n} \times \cdot) \\ &+ (\mathbf{curl}_\Sigma R_\chi \mathbf{curl}_\Sigma) (\mathbf{curl}_\Sigma R_\chi \mathbf{curl}_\Sigma) \quad (11) \\ &+ (\nabla_\Sigma R_\chi \mathbf{div}_\Sigma) L^{-1} (\nabla_\Sigma R_\chi \mathbf{div}_\Sigma). \end{aligned}$$

The injectivity of \mathbf{T}_χ is secured by the first term. The surjectivity follows from the fact that R_χ is a compact perturbation of R since the singularity of the kernel in (7) is preserved.

Finite Elements approximation

The approximation of \mathbf{T}_χ in (11) using finite elements is a delicate task. Indeed, if one resorts to using standard (Nedelec or Raviart-Thomas) first order edge elements, the associated bilinear form does not satisfy a discrete inf-sup condition. We propose to use Buffa-Christiansen dual finite elements [4] to solve this issue.

Acknowledgement

This work was supported by the research Grant ANR-15-CE23-0017-01.

References

- [1] F. Collino, S. Ghanemi and P. Joly, Domain decomposition method for harmonic wave propagation: a general presentation, *CMAME*, **184** (24), pp. 171–211, 2000.
- [2] M. Lecouvez, Méthodes itératives de décomposition de domaine sans recouvrement avec convergence géométrique pour l'équation de Helmholtz, PhD Thesis, École polytechnique, 2015.
- [3] X.Claeys, B.Thierry and F.Collino, Integral equation based optimized Schwarz method for electromagnetics, P.E.Bjorstad (ed.) et al., Domain decomposition methods in science and engineering XXIV, *Lecture Notes in Computational Science and Engineering*, **125**, pp. 187–194, 2018.
- [4] A. Buffa and S. H. Christiansen, A Dual Finite Element Complex on the Barycentric Refinement, *Mathematics of Computation*, **76** (260), pp. 1743–1769, 2007.

New transmission conditions for corners and cross-points

Bruno Després¹, Anouk Nicolopoulos^{1,*}, Bertrand Thierry²

¹Laboratoire Jaques-Louis Lions, Sorbonne Université, Paris

²CNRS & LJLL, Sorbonne Université, Paris

*Email: nicolopoulos@ljl.math.upmc.fr

Abstract

We are interested in deriving transmission conditions (TC) for domain decomposition methods (DDM) with mesh constraints such as corners and cross-points. With respect to [1] where the study concerns right-angle cross-points or [2] which deals the Neumann conditions, our framework addresses Dirichlet and Neumann conditions with more general mesh features. To do so, we start by defining an absorbing boundary condition (ABC) that treats corner points, that we further adapt to define a TC. This work is illustrated by numerical simulations.

Keywords: parallel DDM, corner points, cross points, integral constraints, Helmholtz equation

Introduction. We focus on the Helmholtz equation on a polygonal domain Ω with a compactly supported source term f with classical second order absorbing boundary condition

$$\begin{cases} (-\Delta - \omega^2)u = f & \text{in } \Omega, \\ \left(1 - \frac{1}{2\omega^2}\partial_{tt}\right)\partial_{\mathbf{n}}u - i\omega u = 0 & \text{on } \partial\Omega = \overline{\cup\Gamma_k}. \end{cases}$$

In a weak formulation, because of the derivative of $\partial_{\mathbf{n}}u$ along $\partial\Omega$ which is a closed broken line, additional relations have to be prescribed at the corners $\mathbf{A}_{k\ell} = \Gamma_k \cap \Gamma_\ell$ on $\partial_{\mathbf{n}}u$.

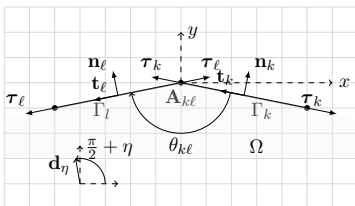


Figure 1: Geometric setting at corners of $\partial\Omega$

Geometry. We consider the geometric setting corresponding to the above figure, and for each

k we introduce the unknown

$$\varphi_k = \partial_{\mathbf{n}_k}u \in H^1(\Gamma_k).$$

For an incident plane wave $u_\eta(\mathbf{x}) = \exp(i\omega(\mathbf{d}_\eta, \mathbf{x}))$ we are able to obtain the two following quasi-continuity relations of order $O(\eta^2)$

$$\begin{cases} i\omega \cos(\theta_{k\ell}) (\varphi_k - \varphi_\ell) (\mathbf{A}_{k\ell}) \\ -\cos\left(\frac{\theta_{k\ell}}{2}\right) (\partial_{\tau_k}\varphi_k - \partial_{\tau_\ell}\varphi_\ell) (\mathbf{A}_{k\ell}) = 0, \\ -i\omega \cos\left(\frac{\theta_{k\ell}}{2}\right) (\varphi_k + \varphi_\ell) (\mathbf{A}_{k\ell}) \\ + (\partial_{\tau_k}\varphi_k + \partial_{\tau_\ell}\varphi_\ell) (\mathbf{A}_{k\ell}) = 0. \end{cases} \tag{CR}$$

Remark that these relations coincide with the continuity relations if the line is flat at $\mathbf{A}_{k\ell}$ (*i.e.* $\theta_{k\ell} = -\pi$).

The solution $\varphi = (\varphi_k)_k \in \oplus_k H^1(\Gamma_k)$ of

$$\left(1 - \frac{1}{2\omega^2}\partial_{t_k^2}\right)\varphi_k = u \quad \text{in } \Gamma_k$$

that verifies a combination of equations (CR) at corners leads to the definition of a bounded linear operator T in $L^2(\Gamma)$. Once introduced in the Helmholtz equation we obtain

$$\begin{cases} (-\Delta - \omega^2)u = f & \text{in } \Omega, \\ \partial_{\mathbf{n}}u - i\omega T(u) = 0 & \text{on } \Gamma. \end{cases}$$

DDM with 2nd order ABC. Let us now consider the DDM $\Omega = \cup\Omega_i$, and define for all k, i the segments $\Gamma_{i,k} := \partial\Omega_i \cap \Gamma_k$. $T(u)$ is a global operator on Γ , so that a DDM using the simple condition $\partial_{\mathbf{n}_i}u_i^{p+1} = i\omega T(u^{p+1})$ couples all subdomains that meet the border. Instead, an auxiliary unknown $\varphi_{i,k} \in H^1(\Gamma_{i,k})$ is introduced to replace the global $T(u)$ on each $\Gamma_{i,k}$. After initialization, the algorithm reads at iteration number $p = 0, 1, \dots$: Solve for all i

$$\begin{cases} (-\Delta - \omega^2)u_i^{p+1} = f & \text{in } \Omega_i, \\ (\partial_{\mathbf{n}_i} - i\omega)u_i^{p+1} = -(\partial_{\mathbf{n}_j} + i\omega)u_j^p & \text{on } \partial\Omega_i \cap \partial\Omega_j, \\ \partial_{\mathbf{n}_i}u_i^{p+1} = i\omega\varphi_{i,k}^{p+1} & \text{on } \Gamma_{i,k}, \end{cases}$$

coupled with, for all k

$$\left\{ \begin{array}{l} \left(1 - \frac{1}{2\omega^2} \partial_{\mathbf{t}_k}^2\right) \varphi_{i,k}^{p+1} = u_i^{p+1} \quad \text{in } \Gamma_{i,k}, \\ \left[\left(1 + \mathbf{i} \frac{\cos\left(\frac{\theta_{k\ell}}{2}\right)}{\cos\theta_{k\ell}}\right) \partial_{\tau_k} \varphi_{i,k}^{p+1} \right. \\ \quad \left. + \left(\omega - \mathbf{i}\omega \cos\left(\frac{\theta_{k\ell}}{2}\right)\right) \varphi_{i,k}^{p+1} \right] (\mathbf{A}_{k\ell}^{ij}) \\ = \left[\left(-1 + \mathbf{i} \frac{\cos\left(\frac{\theta_{k\ell}}{2}\right)}{\cos\theta_{k\ell}}\right) \partial_{\tau_\ell} \varphi_{j,\ell}^p \right. \\ \quad \left. + \left(\omega + \mathbf{i}\omega \cos\left(\frac{\theta_{k\ell}}{2}\right)\right) \varphi_{j,\ell}^p \right] (\mathbf{A}_{k\ell}^{ij}). \end{array} \right.$$

The resolution of this DDM can be done in parallel for all i by solving local problems in Ω_i with unknowns $\left(u_i^{p+1}, (\varphi_{i,k}^{p+1})_k\right)$ supported on $\Omega_i \times (\oplus_k \Gamma_{i,k})$. To show the algorithm is convergent, we focus on the vanishing source case and show the decrease of energy

$$\begin{aligned} F^p &= \sum_i \int_{\partial\Omega_i - \Gamma} |(\partial_{\mathbf{n}_i} - \mathbf{i}\omega) u_i^p|^2 d\gamma \\ &+ \sum_{\mathbf{A}_{k\ell}^{ij}} c_{\theta_{k\ell}} \left| \left(1 + \mathbf{i} \frac{\cos\left(\frac{\theta_{k\ell}}{2}\right)}{\cos\theta_{k\ell}}\right) \partial_{\tau_k} \varphi_{i,k}^p \right. \\ &\quad \left. + \left(\omega - \mathbf{i}\omega \cos\left(\frac{\theta_{k\ell}}{2}\right)\right) \varphi_{i,k}^p \right|^2 (\mathbf{A}_{k\ell}^{ij}). \end{aligned}$$

The coupling between u_i^{p+1} and $(\varphi_{i,k}^{p+1})_k$ can be removed by introducing new auxiliary unknowns $(\psi_{i,k}^{p+1})_k$ that correspond to the values of u_i^{p+1} on the segments $\Gamma_{i,k}$. The system on u_i^{p+1} is then solved as a Helmholtz boundary value problem, where the boundary conditions involve $(\varphi_{i,k}^p)_k$ and $(\psi_{i,k}^p)_k$.

2nd order TC. The main difference between ABC and TC is that an ABC is a model for a radiation condition, whereas TC are a preconditioning of

$$u_i - u_j = 0 \text{ and } \partial_{\mathbf{n}_i} u_i + \partial_{\mathbf{n}_j} u_j = 0 \text{ on } \partial\Omega_i \cap \partial\Omega_j.$$

To obtain stability when transposing the ABC into TC, we want to respect the structure of these operators. We assume here the interfaces $\partial\Omega_i \cap \partial\Omega_j$ are straight lines for the sake of simplicity, but the method generalizes to the case of broken lines. We number the corners of a subdomain Ω_i as \mathbf{C}_r^i for $r = 1$ to m_i . When two sub-domains Ω_i and Ω_j have a corner in common, we denote it

$$\mathbf{P}_{rs}^{ij} = \mathbf{C}_r^i = \mathbf{C}_s^j.$$

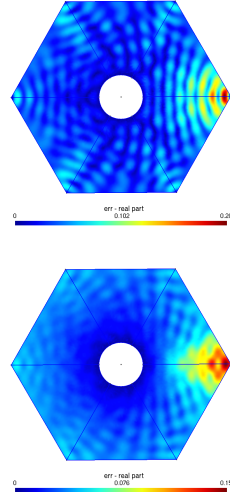


Figure 2: Error between the real parts of the analytical solution and the computed solutions without the corner treatment above, with the new corner treatment in the ABC below.

After considering a first TC based on the resolution in $H^1(\partial\Omega_i \cap \partial\Omega_j)$ of

$$\begin{cases} \left(1 - \frac{1}{2\omega^2} \partial_{\mathbf{t}^2}\right) \varphi = u & \partial\Omega_i \cap \partial\Omega_j, \\ \partial_{\mathbf{t}^i} \varphi(\mathbf{P}_{rs}^{ij}) = 0, \end{cases}$$

and noting that the value at the corners is persistent, we define a second TC with integral constraint based on the resolution $H^1(\partial\Omega_i \cap \partial\Omega_j)$ with the constraint of zero mean of

$$\int \varphi \psi + \frac{1}{2\omega^2} \partial_{\mathbf{t}^i} \varphi \partial_{\mathbf{t}^i} \psi = \int (u - \langle u \rangle_{ij}) \psi.$$

References

- [1] A. Modave, C. Geuzaine and X. Antoine, Corner treatment for high-order local absorbing boundary conditions in high-frequency acoustic scattering, hal-01925160 preprint 2018.
- [2] M. J. Gander and K. Santugini, Cross-points in domain decomposition methods with a finite element discretization in *Electronic Transactions on Numerical Analysis*, Vol. 45, pp. 219–240, 2016.

Linear isotropic elastodynamics by means of potentials: The case of transmission conditions for piecewise homogeneous media.

Jorge Albella^{1,*}, Sébastien Imperiale², Patrick Joly³, Jerónimo Rodríguez¹

¹Departamento de Matemática Aplicada, Universidade de Santiago de Compostela, Spain.

²Inria & LMS, Ecole polytechnique, CNRS, Université Paris-Saclay, France

³POEMS (CNRS-INRIA-ENSTA Paristech), Palaiseau, France

*Email: jorge.albella@usc.es

Abstract

When solving 2D linear elastodynamics equations in homogeneous isotropic media, two types of waves travel at different velocities. In many applications, a high difference on the velocities penalise the numerics. Then, the introduction of potentials helps to rewrite the problem as two scalar wave equations only interacting on boundaries and interfaces. The resultant is a problem better adapted for discretization, however some difficulties arise on the treatment of boundary and transmission conditions. In previous works, the authors addressed the cases of rigid and free boundary conditions. Here, the aim is to follow the same philosophy to treat the transmission conditions between two isotropic homogeneous media.

Keywords: Elastodynamics, Transmission problem, Potentials, Mixed formulation.

1 Motivation and basic idea

In 2D elastodynamics, the variation of the displacement field \mathbf{u} is governed by the law

$$\rho \partial_t^2 \mathbf{u} - \operatorname{div} \boldsymbol{\sigma} = \mathbf{f}, \quad \begin{array}{l} \boldsymbol{\sigma} \equiv \text{stress tensor,} \\ \rho \equiv \text{density.} \end{array}$$

For isotropic homogeneous media, this translates into (λ and μ are Lamé coefficients)

$$\boxed{\rho \partial_t^2 \mathbf{u} - (\lambda + 2\mu) \nabla \operatorname{div} \mathbf{u} + \mu \operatorname{curl} \operatorname{curl} \mathbf{u} = \mathbf{f}}$$

Two types of waves (P-waves and S-waves) propagate at different velocities $V_P > V_S$ and therefore with wavelengths $\lambda_P \sim V_P$ and $\lambda_S \sim V_S$. With standard time explicit numerical methods, the space step h is constrained by the smaller wavelength λ_S for accuracy, while the time step Δt is constrained by the higher velocity V_P for stability. In consequence, the computations are costly when $V_P \gg V_S$.

This motivates to find a formulation that decouples the two type of waves. In the whole space,

the idea is to introduce the two scalar potentials

$$\boxed{\varphi_P = V_P^2 \operatorname{div} \mathbf{u}} \quad \text{and} \quad \boxed{\varphi_S = -V_S^2 \operatorname{curl} \mathbf{u}} \quad (1)$$

These realize a Helmholtz decomposition of

$$\partial_t^2 \mathbf{u} - \mathbf{f} / \rho = \nabla \varphi_P + \operatorname{curl} \varphi_S. \quad (2)$$

Then, applying div and curl to (2), we get two decoupled scalar wave equations

$$\frac{1}{V_Q^2} \partial_t^2 \varphi_Q - \Delta \varphi_Q = \frac{1}{\rho} g_Q, \quad Q \in \{P, S\}.$$

where $g_P = -\operatorname{div} \mathbf{f}$ and $g_S = -\operatorname{curl} \mathbf{f}$.

2 Piecewise homogeneous media

We now consider a bounded domain Ω formed by two non overlapping homogeneous isotropic domains Ω_1 and Ω_2 and we denote the interface $\Gamma := \partial\Omega_1 \cap \partial\Omega_2$. Then (1, 2) only hold in each subdomain. More precisely, introducing an index $i \in \{1, 2\}$ for the related potentials, we have

$$\frac{1}{V_{Q,i}^2} \partial_t^2 \varphi_{Q,i} - \Delta \varphi_{Q,i} = \frac{1}{\rho_i} g_Q, \quad \text{in } \Omega_i. \quad (3)$$

We assume that $\partial\Omega$ is a closed loop on which $\mathbf{u} = \mathbf{0}$ is imposed. Indeed, (3) need to be completed with transmission conditions on which we focus in the following (the treatment of boundary conditions has been addressed in [1,2]).

3 Transmission conditions

Assume that Γ is a closed loop, with abscissa $s \in [0, L]$, that does not intersect $\partial\Omega$. We note \mathbf{n} and $\boldsymbol{\tau}$ the normal (outward to Ω_1) and tangential unit vector along Γ . The transmission conditions along Γ read

$$(i) [\mathbf{u}] = \mathbf{0} \quad \text{and} \quad (ii) [\boldsymbol{\sigma}(\mathbf{u})] \mathbf{n} = \mathbf{0}, \quad (4)$$

where $[\cdot]$ is the jump across Γ . Introducing the new unknown $\mathbf{u}_\Gamma := \mathbf{u}|_\Gamma$, which encodes (4)(i), one first show using (2) that, if $\operatorname{supp} \mathbf{f} \subset \Omega_1$, \mathbf{u}_Γ is related to the potentials via

$$\begin{aligned} \partial_n \varphi_{P,i} &= \partial_t^2 \mathbf{u}_\Gamma \cdot \mathbf{n} + \partial_\tau \varphi_{S,i}, \\ \partial_n \varphi_{S,i} &= \partial_t^2 \mathbf{u}_\Gamma \cdot \boldsymbol{\tau} - \partial_\tau \varphi_{P,i}. \end{aligned} \quad (5)$$

Next, introducing $\varphi = (\varphi_P, \varphi_S)^t$ defined by (1), one can show that (4)(ii) becomes

$$2[\mu]\partial_\tau u_{\Gamma,1} = [\rho\varphi] \cdot \tau, \quad 2[\mu]\partial_\tau u_{\Gamma,2} = -[\rho\varphi] \cdot \mathbf{n}.$$

In the general case $[\mu] \neq 0$, one can eliminate \mathbf{u}_Γ using $\mathcal{I}\eta(s) = \int_0^s \eta(\gamma)$:

$$\mathbf{u}_\Gamma = \frac{1}{2[\mu]} \begin{pmatrix} \mathcal{I}([\rho\varphi] \cdot \tau) \\ -\mathcal{I}([\rho\varphi] \cdot \mathbf{n}) \end{pmatrix} + \begin{pmatrix} c_1 \\ c_2 \end{pmatrix}, \quad (6)$$

with some constants (c_1, c_2) .

If $[\mu] = 0$, things become much simpler since the transmission conditions reduce to

$$[\rho\varphi] \cdot \mathbf{n} = [\rho\varphi] \cdot \tau = 0. \quad (7)$$

Note that (5, 6), (or (7)) couple (φ_P, φ_S) at the interface and that, as soon as $[\rho] \neq 0$, φ jumps across Γ , contrary to \mathbf{u} .

4 Naive variational formulations

First, notice that by (2) we seek φ in

$$\mathbf{V} = \mathbf{V}_1 \times \mathbf{V}_2, \quad \mathbf{V}_i = H(\text{div}, \Omega_i) \cap H(\text{curl}, \Omega_i).$$

In the case $[\mu] \neq 0$, we even deduce that the solution must be searched in the closed subspace

$$\mathbf{V}_0 = \{\varphi \in \mathbf{V} / \int_\Gamma [\rho\varphi] \cdot \mathbf{n} = \int_\Gamma [\rho\varphi] \cdot \tau = 0\}. \quad (8)$$

It is then easy to see that a variational formulation of (3, 5, 6) read as follows

Find $\varphi(t) : \mathbb{R}^+ \rightarrow \mathbf{V}_0$ such that

$$\partial_t^2 m(\varphi, \psi) + a(\varphi, \psi) = \ell(\psi), \quad \forall \psi \in \mathbf{V}_0 \quad (9)$$

where $\ell(\psi)$ is the source term and, if $\varphi_i = \varphi|_{\Omega_i}$,

$$a(\varphi, \psi) = \sum_{i=1,2} \rho_i \int_{\Omega_i} \begin{pmatrix} \text{div } \varphi_i \\ \text{curl } \varphi_i \end{pmatrix} \cdot \begin{pmatrix} \text{div } \psi_i \\ \text{curl } \psi_i \end{pmatrix},$$

while $m = m_\Omega + m_\Gamma$, $m_\Omega(\varphi, \psi) = \int_\Omega \frac{\rho}{V_{3,i}} \varphi \cdot \psi$ and m_Γ is the symmetric bilinear form associated to the quadratic form

$$m_\Gamma(\varphi, \varphi) = [\mu]^{-1} \int_\Gamma \mathcal{I}([\rho\varphi] \cdot \mathbf{n}) [\rho\varphi] \cdot \tau \quad (10)$$

Unfortunately, this naive formulation is not a good one by defect of positivity of m :

Lemma 1 *There exists $\psi \in \mathbf{V}_0 / m(\psi, \psi) < 0$.*

In consequence, as in the case of free boundary conditions in [2], a natural Galerkin discretization is expected to be unstable.

Remark 2 *In the special case $[\mu] = 0$ (see (7)), things are much simpler. The variational formulation is still of the form (9), however the space \mathbf{V} must be replaced by the subspace,*

$$\mathbf{V}_{0,\Gamma} = \{\varphi \in \mathbf{V} / [\rho\varphi] \cdot \mathbf{n} = [\rho\varphi] \cdot \tau = 0\}, \quad (11)$$

and, more importantly, $m = m_\Omega$, which is positive definite. As a consequence the naive formulation is, only in this case, stable.

5 Stabilization when $[\mu] \neq 0$

Using the same philosophy as in [2], the idea is to find a subspace \mathbf{V}_+ of \mathbf{V}_0 such that

- (a) $\varphi(t) \in \mathbf{V}_+$, for all $t \geq 0$, (consistency)
- (b) For all $\psi \in \mathbf{V}_+ \setminus \{0\}$, $m(\psi, \psi) > 0$,

where (b) yields well-posedness of (9) in \mathbf{V}_+ .

Lemma 3 *A space \mathbf{V}_+ satisfying (a), (b) is*

$$\mathbf{V}_+ = \{\varphi \in \mathbf{V}_0 / \forall \psi \in \mathbf{T}, m(\varphi, \psi) = 0\},$$

where $\mathbf{T} = \{\psi \in \mathbf{V}_0 / \text{div } \psi_i = \text{curl } \psi_i = 0\}$. Moreover, we have $\mathbf{V}_0 = \mathbf{V}_+ \oplus \mathbf{T}$.

The definition of \mathbf{V}_+ naturally leads to introduce a Lagrange multiplier to impose $\varphi(t) \in \mathbf{V}_+$. This leads to the stable mixed problem

Find $(\varphi, \lambda) : \mathbb{R}^+ \rightarrow \mathbf{V}_0 \times \mathbf{T}$ such that

$$\forall (\psi, \mu) \in \mathbf{V}_0 \times \mathbf{T},$$

$$\partial_t^2 m(\varphi, \psi) + a(\varphi, \psi) + m(\lambda, \psi) = \ell(\psi),$$

$$m(\varphi, \mu) = 0.$$

For numerics, we use the characterization $\mathbf{T} = \{\mathcal{E}\nu, \nu \in \mathbf{M}\}$, $\mathcal{E} \in \mathcal{L}(\mathbf{M}, \mathbf{T})$, where

$$\mathbf{M} = \{\nu = (\nu_1, \nu_2), \nu_i \in H^{-\frac{1}{2}}(\partial\Omega_i)\}$$

$$\int_{\partial\Omega_i} \nu_i = 0 \text{ and } \int_\Gamma (\nu_1 + \nu_2) = 0\},$$

with $\mathcal{E}\nu := (\nabla p_1/\rho_1, \nabla p_2/\rho_2)$, $p_i \in H^1(\Omega_i) / \mathbb{R}$ the unique solution of

$$\begin{cases} -\Delta p_i = 0, & \text{in } \Omega_i, \\ \partial_{\mathbf{n}_i} p_i = \nu_i, & \text{on } \partial\Omega_i. \end{cases}$$

References

- [1] A. Burel, S. Imperiale, P. Joly, Solving the homogeneous isotropic linear elastodynamics equations using potentials and finite elements. *Num Anal and Appl.*, (2012)
- [2] J. Albella, S. Imperiale, P. Joly, J. Rodríguez, Solving 2D linear isotropic elastodynamics by means of scalar potentials: a new challenge for finite elements, *J Sci Comput.*, (2018)

**Numerical aspects of Energetic Boundary Element Method
for 2D soft scattering in linear elastodynamics**

Alessandra Aimi¹, Giulia Di Credico^{1,*}, Mauro Diligenti¹, Chiara Guardasoni¹

¹Dept. of Mathematical, Physical and Computer Sciences, University of Parma, Parma, Italy

*Email: giulia.dicredico@unipr.it

Abstract

We consider an exterior linear elastodynamics problem with vanishing initial conditions and Dirichlet datum on the scatterer. We convert the Navier Equation, governing the wave behavior, into two space-time Boundary Integral Equations (BIEs) whose solution is approximated by the Energetic Boundary Element Method (BEM). To apply this technique, we have to set the BIEs in a weak form related to the energy of the differential problem solution at the final time instant of analysis. After the space-time discretization of the weak formulation, we have to deal with double space-time integrals, with a weakly singular kernel depending on primary and secondary wave speeds and multiplied by Heaviside functions. The main purpose of this work is the analysis of these peculiar integrals and the study of suitable quadrature schemes for their approximation.

Keywords: Elastodynamics, Energetic BEM, weakly singular kernel, numerical integration

1 Introduction

The study of elastodynamics has several applications, including mechanical and civil engineering problems, seismic risk assessment, etc. In literature, the main approach to deal with it is the Finite Element Method (FEM) (see [1] and, for a recent improvement, [2]), but this is not an optimal choice for unbounded domains. In this scenario, elastodynamics problems can be efficiently resolved using Boundary Element Method (BEM), which has already been successfully applied for electromagnetic wave propagation, computation of transient acoustic wave, fluid dynamics, achieving highly accurate results. The advantages in using BEMs lie in approximating the solution of the problem by solving a system of integral equations (BIEs) defined only on the usually bounded domain boundary, incorporating the solution behavior at infinity. Unfortunately, in time-domain framework, the standard Galerkin and collocation BEMs are nu-

merically unstable, while genuine convergence results are obtained using a weak formulation of the BIEs related to the energy of the elastodynamics problem. The consequent discretization approach, called Energetic BEM, already analyzed in case of scalar waves propagation [3], shows a long-time stability and guarantees excellent approximation accuracy; here, it is extended to elastodynamics in the context of soft scattering. Its algebraic reformulation leads to a linear system with block lower triangular Toeplitz structured matrix, useful for memory savings and for an efficient computation of linear system solution. On the other side, matrix elements are space-time double integrals with a log singular kernel, depending on primary and secondary wave speeds, multiplied by Heaviside functions and functions not regular in the first spatial derivative; hence a consistent part of this work is focused on a suitable partition of integration domain and on the study of efficient quadrature rules [3, 4] used in order to overcome the above highlighted numerical issues. Several results on benchmark problems will be discussed, too.

2 Statement of the problem and BIEs energetic weak formulation

For the vectorial wave propagation in the time interval $[0, T]$, in absence of body forces and in the 2D unbounded domain $\Omega := \mathbb{R}^2 \setminus \Gamma$ made of a linear, elastic, homogeneous and isotropic medium and exterior to the obstacle Γ represented by a non-intersecting open arc in the plane, the problem is featured by the following Navier equation:

$$(\lambda + \mu)\nabla(\nabla \cdot \mathbf{u}) + \mu\Delta\mathbf{u} = \rho\ddot{\mathbf{u}} \quad \mathbf{x} \in \Omega, t \in (0, T] \quad (1)$$

where λ and μ are the Lamè parameters and ρ is the mass density. The unknown $\mathbf{u}(\mathbf{x}, t) = (u_1, u_2)^T(\mathbf{x}, t)$ identifies the displacement field and dots indicate time differentiation. The differential equation is equipped by vanishing initial conditions and Dirichlet boundary datum $\mathbf{u}(\mathbf{x}, t) = \mathbf{g}(\mathbf{x}, t)$ assigned on $\Sigma = \Gamma \times (0, T]$.

Having set $r = \|\mathbf{x} - \boldsymbol{\xi}\|_2$ and denoted by $\boldsymbol{\phi} = (\phi_1, \phi_2)^\top$ a vectorial density function, we can consider the single-layer representation formula for the field $\mathbf{u}(\mathbf{x}, t)$ in $\Omega \times (0, T]$, i.e. for $i = 1, 2$

$$u_i(\mathbf{x}, t) = \sum_{j=1}^2 \int_0^t \int_\Gamma G_{ij}(\mathbf{x}, \boldsymbol{\xi}; t, \tau) \phi_j(\boldsymbol{\xi}, \tau) d\Gamma \xi d\tau,$$

where

$$G_{ij}(\mathbf{x}, t; \boldsymbol{\xi}, \tau) = \frac{1}{2\pi\rho} \left\{ \frac{H[c_p(t-\tau)-r]}{c_p} \left[\frac{2A_p^2-1}{\sqrt{A_p^2-1}} \left(\frac{r_{,i}r_{,j}}{r} \right) - \frac{\delta_{ij}}{r} \sqrt{A_p^2-1} \right] - \frac{H[c_s(t-\tau)-r]}{c_p} \left[\frac{2A_s^2-1}{\sqrt{A_s^2-1}} \left(\frac{r_{,i}r_{,j}}{r} \right) - \frac{\delta_{ij}}{r} \frac{A_s^2}{\sqrt{A_s^2-1}} \right] \right\},$$

with $A_\kappa = \frac{c_\kappa(t-\tau)}{r}$, $\kappa = p, s$, c_p the velocity of primary wave, defined by $c_p^2 = (\lambda + 2\mu)/\rho$, and c_s the velocity of secondary wave, defined by $c_s^2 = \mu/\rho$. Then, with a limiting process to $\mathbf{x} \in \Gamma$, using Dirichlet datum we can to obtain a system of two space-time BIEs in the unknown $\boldsymbol{\phi}$ on Σ :

$$\begin{bmatrix} V_{11} & V_{12} \\ V_{21} & V_{22} \end{bmatrix} \begin{bmatrix} \phi_1(\mathbf{x}, t) \\ \phi_2(\mathbf{x}, t) \end{bmatrix} = \begin{bmatrix} g_1(\mathbf{x}, t) \\ g_2(\mathbf{x}, t) \end{bmatrix}$$

where for $i, j = 1, 2$

$$[V_{ij}\phi_j](\mathbf{x}, t) := \int_0^t \int_\Gamma G_{ij}(\mathbf{x}, \boldsymbol{\xi}; t, \tau) \phi_j(\boldsymbol{\xi}, \tau) d\Gamma \xi d\tau.$$

At this stage, the energetic weak formulation [3] is defined as follows:

find $\phi_i \in L^2([0, T]; H^{-\frac{1}{2}}(\Gamma))$ such that for $i = 1, 2$

$$\sum_{j=1}^2 \langle [V_{ij}\phi_j], \psi_i \rangle_{L^2(\Sigma)} = \langle g_i, \psi_i \rangle_{L^2(\Sigma)} \quad (2)$$

where ψ is a suitable test function belonging to the same functional space of $\boldsymbol{\phi}$. We can write the energy identity:

$$\sum_{j,i=1}^2 \langle [V_{ij}\phi_j], \phi_i \rangle_{L^2(\Sigma)} = \mathcal{E}(\mathbf{u}, T)$$

where the right-hand side represents the energy of the solution of (1) at the final time instant of analysis.

3 Energetic BEM and integration issues

We define the time knots $t_n = n\Delta t, n = 0, \dots, N_{\Delta t}$, with time step $\Delta t = T/N_{\Delta t}$ and we denote with $\epsilon_m, m = 1, \dots, M$, the M linear elements meshing the obstacle Γ . The unknowns ϕ_i will be

approximated by a linear combination of shape functions in space and time, i.e. for $(\mathbf{x}, t) \in \Sigma$

$$\widehat{\phi}_i(\mathbf{x}, t) = \sum_{n=0}^{N_{\Delta t}-1} \sum_{m=1}^{M_{\Delta x}} \alpha_{nm}^i w_m(\mathbf{x}) v_n(t)$$

where v_n is piece-wise constant and w_m is a piece-wise polynomial function, obtained from local lagrangian basis fixed for each element ϵ_m . Due to this discretization, (2) becomes a linear system $\mathbb{E}\alpha = \beta$, where the elements of the vector α are the coefficients α_{nm}^i and \mathbb{E} is a block lower triangular Toeplitz matrix made of $N_{\Delta t}$ blocks. Each block has dimension $2M_{\Delta x}$: having set $\Delta_{\bar{n}, \bar{n}} := t_n - t_{\bar{n}}$, for fixed m, \bar{m}, i, j , its entries are linear combination of integrals of the type

$$\int_\Gamma w_{\bar{m}}(\mathbf{x}) \int_\Gamma w_m(\boldsymbol{\xi}) \nu_{ij}(\mathbf{x} - \boldsymbol{\xi}; \Delta_{\bar{n}, n}) d\Gamma \xi d\Gamma \mathbf{x} \quad (3)$$

where the kernel ν_{ij} appears after the time integration. Double space integral (3) depends strongly on the distance r and on the two phase speeds c_s and c_p . In the region where $0 \leq r \leq c_s \Delta_{\bar{n}, n}$ the kernel ν_{ij} has a $\log(r)$ singularity for $r \rightarrow 0$ and it has to be treated with a specific interpolatory quadrature rule [3]. If $c_s \Delta_{\bar{n}, n} < r < c_p \Delta_{\bar{n}, n}$ there are no space singularities but ν_{ij} depends on the argument $\sqrt{c_p^2 \Delta_{\bar{n}, n}^2 - r^2}$ that is not regular for $r \rightarrow c_p \Delta_{\bar{n}, n}$ in its first spatial derivative. In this case, to improve the efficiency of the standard Gaussian quadrature rule, we apply the correction formula in [4] that shifts the quadrature nodes closer to $r = c_p \Delta_{\bar{n}, n}$.

References

- [1] L. V. Andersen, Linear Elastodynamic Analysis, (2006).
- [2] A. Burel et al., Solving the homogeneous isotropic linear elastodynamics equations using potentials and finite elements. The case of the rigid boundary condition, *Num. An. Appl.* **5** (2012), pp. 136–143.
- [3] A. Aimi et al., An energy approach to space–time Galerkin BEM for wave propagation problems, *IJNME* **80** (2009), pp. 1196–1240.
- [4] G. Monegato, L. Scuderi, Numerical integration of functions with boundary singularities, *JCAM*, **112** (1999), pp. 201–214.

Spectral analysis of a nonhomogeneous rotating Timoshenko beam: Riesz basis property

Jean-Luc Akian^{1,*}

¹DMAS, ONERA, Université Paris Saclay F-92322 Châtillon - France

*Email: jean-luc.akian@onera.fr

Abstract

We consider a spatially nonhomogeneous Timoshenko beam mounted on the periphery of a rigid root of radius R rotating about its axis at a constant angular speed Ω . The junction between the beam and the root is assumed to be elastically restrained and damped. It is shown that under some hypotheses on the physical properties of the beam, one can find a sequence of root vectors of the unbounded operator associated to the problem which form a Riesz basis [1]. The outline of the proof is as follows. First we write a variational formulation of the problem which is transformed into a first order evolution equation. The unbounded operator of this evolution equation is the generator of a contraction semigroup so that the problem is well-posed. This operator has a compact resolvent but it is non-self-adjoint. The spectrum of this operator is studied by making a change of variable in order to reduce the problem to a first-order system asymptotically linear in the spectral parameter. By applying some results of [2], we obtain the asymptotics of the spectrum of this operator and we show that its eigenvalues are asymptotically algebraically simple. Then we show that the system of root vectors of the operator is complete and, applying a theorem from [3], that they form a Riesz basis. As a consequence of this result, one obtains an asymptotic expansion of the solution of the initial problem.

Keywords: Timoshenko beam, non-self-adjoint, Riesz basis

1 Introduction

In what follows, l is the length of the beam, A its cross-sectional area, E its Young modulus, ρ its mass density, I the moment of inertia of its cross-section, G its shear modulus, α_s its shear correction factor, w its infinitesimal transverse displacement, φ the infinitesimal rotation of its cross-section, k_w, k_φ, c_w and c_φ the corresponding spring and damping con-

stants at the junction. All the coefficients and their inverses are assumed to be in $W^{1,\infty}(0, l)$. If $\mathbf{u}_0, \mathbf{v}_0$ are given in subspaces of $[H^1(0, l)]^2$ and $[L^2(0, l)]^2$, the corresponding variational problem reads as follows: find $\mathbf{u} = {}^t(w, \varphi) \in C^1([0, +\infty[; [H^1(0, l)]^2) \cap C^2([0, +\infty[; [L^2(0, l)]^2)$ such that $\forall \delta \mathbf{u} \in [H^1(0, l)]^2$,

$$m(\dot{\mathbf{u}}, \delta \mathbf{u}) + b(\dot{\mathbf{u}}, \delta \mathbf{u}) + a(\mathbf{u}, \delta \mathbf{u}) = 0$$

and such that $\mathbf{u}(0) = \mathbf{u}_0; \dot{\mathbf{u}}(0) = \mathbf{v}_0$ (Problem (P)), where $\forall \mathbf{u}, \delta \mathbf{u} \in [H^1(0, l)]^2$,

$$a(\mathbf{u}, \delta \mathbf{u}) = \int_0^l [T w' \delta w' + EI \varphi' \delta \varphi'] dx + \int_0^l \alpha_s G_s [(w' - \varphi)(\delta w' - \delta \varphi)] dx + k_w w(0) \delta w(0) +$$

$$k_\varphi \varphi(0) \delta \varphi(0) - \Omega^2 \int_0^l \rho I \varphi \delta \varphi dx,$$

$$b(\mathbf{u}, \delta \mathbf{u}) = c_w w(0) \delta w(0) + c_\varphi \varphi(0) \delta \varphi(0),$$

and $\forall \mathbf{u}, \delta \mathbf{u} \in [L^2(0, l)]^2$,

$$m(\mathbf{u}, \delta \mathbf{u}) = \int_0^l \rho I \varphi \delta \varphi dx + \int_0^l \rho A w \delta w dx.$$

Setting $\mathbf{v} = {}^t(z, \psi), \mathbf{U} = \begin{pmatrix} \mathbf{u} \\ \mathbf{v} \end{pmatrix}, \mathbf{U}_0 = \begin{pmatrix} \mathbf{u}_0 \\ \mathbf{v}_0 - \Omega \mathbf{u}_0 \end{pmatrix}$, after replacing $\mathbf{u}(t)$ by $e^{\Omega t} \mathbf{u}(t)$, (P) boils down to

$$\dot{\mathbf{U}} = \mathcal{A} \mathbf{U}, \mathbf{U}(0) = \mathbf{U}_0,$$

where \mathcal{A} is an unbounded operator of $\mathcal{H} = [H^1(0, l)]^2 \times [L^2(0, l)]^2$ with domain $D(\mathcal{A})$. \mathcal{A}^* is an unbounded operator of \mathcal{H} with a domain $D(\mathcal{A}^*) \neq D(\mathcal{A})$ so that \mathcal{A} is non-self-adjoint. On the other hand $0 \in \rho(\mathcal{A})$ and \mathcal{A}^{-1} is a compact operator of \mathcal{H} therefore the spectrum of \mathcal{A} consists of isolated eigenvalues of finite algebraic multiplicity. \mathcal{A} is maximal-dissipative hence \mathcal{A} is the generator of a contraction semigroup on \mathcal{H} . Returning to the initial problem (P) it follows that if $\mathbf{U}_0 \in D(\mathcal{A})$, there exists a unique solution to (P) such that $\mathbf{u} \in C^0([0, +\infty); [H^2(0, l)]^2) \cap C^1([0, +\infty); [H^1(0, l)]^2) \cap C^2([0, +\infty); [L^2(0, l)]^2)$ and such that $\mathbf{U} \in C^0([0, +\infty); D(\mathcal{A}))$.

2 Spectral theory of \mathcal{A}

Setting $\alpha_1 = \sqrt{\frac{\rho A}{T + \alpha_s G A}}$, $\alpha_2 = \sqrt{\frac{\rho}{E}}$, $\tilde{\Lambda}_1 = \text{diag}(\alpha_1, \alpha_2, -\alpha_1, -\alpha_2)$ there exist matrices $T_0, \tilde{\Lambda}_0, \tilde{\Lambda}_{-1}, \tilde{B}_1, \tilde{B}_0, \tilde{C}_1, \tilde{C}_0$ such that for $\lambda \in \mathbb{C}^*$, the conditions: $\mathbf{U} \in D(\mathcal{A})$, $\mathbf{U} \neq 0$ and $(\mathcal{A} - \lambda Id)\mathbf{U} = 0$ are equivalent to the conditions: $Z \in [H^1(0, l)]^4$, $Z \neq 0$ and $T(\lambda)Z = 0$ where $Z = T_0^{-1} \begin{pmatrix} \mathbf{u} \\ \mathbf{u}'/\lambda \end{pmatrix}$, $T(\lambda) = \begin{pmatrix} T^D(\lambda) \\ T^R(\lambda) \end{pmatrix}$,

$$T^D(\lambda)Z = Z' - (\lambda \tilde{\Lambda}_1 + \tilde{\Lambda}_0 + \frac{1}{\lambda} \tilde{\Lambda}_{-1})Z,$$

$$T^R(\lambda)Z = (\tilde{B}_1 + \frac{1}{\lambda} \tilde{B}_0)T_0 Z(0) + (\tilde{C}_1 + \frac{1}{\lambda} \tilde{C}_0)T_0 Z(l).$$

Assume that there exists a constant $C > 0$ such that $|\alpha_1 - \alpha_2| \geq C > 0$ on $[0, l]$. Then from [2], Theorem 2.8.2, there exists an asymptotic fundamental matrix function of $T^D(\lambda)Z = 0$ denoted $\tilde{E}(\cdot, \lambda)$ such that for $\lambda \in \mathbb{C}^*$, the conditions: $Z \in [H^1(0, l)]^4$, $T^D(\lambda)Z = 0$ are equivalent to the condition: $\exists c(\lambda) \in \mathbb{C}^4$ with $Z(\cdot, \lambda) = \tilde{E}(\cdot, \lambda)c(\lambda)$. It follows that λ is an eigenvalue of \mathcal{A} iff $\det M(\lambda) = 0$ where $M(\lambda) = T^R(\lambda)\tilde{E}(\cdot, \lambda)$. If $c_w \neq (\alpha_1(T + \alpha_s G A))(0)$ and $c_\varphi \neq (\alpha_2 EI)(0)$ the eigenvalues of \mathcal{A} are given asymptotically by the formulas $\lambda_n^1 = \mu^1 - \Omega + \nu_n^1$, $\lambda_n^2 = \mu^2 - \Omega + \nu_n^2$ where $\mu_1, \mu_2 \leq 0$, $\nu_n^1, \nu_n^2 \in i\mathbb{R}$, $|\nu_n^1|, |\nu_n^2| \rightarrow +\infty$ when $|n| \rightarrow +\infty$. If $\mu_1 \neq \mu_2$ the zeros of $\det M(\lambda)$ are asymptotically simple and $\inf_{n \neq m} |\lambda_n - \lambda_m| > 0$.

If Ω is an open nonempty subset of \mathbb{C} , E and F are Banach spaces, $\mu \in \Omega$, $S \in H(\Omega, L(E, F))$ and $x \in H(\Omega, E)$ are holomorphic families, x is called a root function of S at μ if $x(\mu) \neq 0$ and $(Sx)(\mu) = 0$. The order of the zero of Sx at μ is called the multiplicity of x with respect to S at μ . One can also define the geometric and algebraic multiplicities of S at μ [2], Chapter I. By comparing the multiplicities of the root functions and the geometric multiplicities of the three holomorphic families $\lambda \in \mathbb{C}^* \mapsto T(\lambda) \in L([H^1(0, l)]^4, [L^2(0, l)]^4 \times \mathbb{C}^4)$, $\lambda \in \mathbb{C}^* \mapsto A(\lambda) = \mathcal{A} - \lambda Id \in L(D(\mathcal{A}), \mathcal{H})$ and $\lambda \in \mathbb{C}^* \mapsto M(\lambda) \in L(\mathbb{C}^4, \mathbb{C}^4)$ at an eigenvalue of \mathcal{A} , it can be shown that if $\mu_1 \neq \mu_2$, the eigenvalues of \mathcal{A} are asymptotically algebraically simple (in the "classical" sense). By estimating the resolvent of \mathcal{A} first on the negative real axis (comparing \mathcal{A} with the self-adjoint operator obtained by taking $c_w = c_\varphi = 0$) and then on the

right half-plane (using the Hille-Yosida Theorem) and by applying the Phragmen-Lindelöf Theorem to a certain function of exponential type, it is shown that the system of root vectors of \mathcal{A} is complete in \mathcal{H} .

Recall that a sequence $(h_n)_{n \in \mathbb{N}}$ of a Hilbert space V is a Riesz basis of V iff there exists an isomorphism U of V and a Hilbert basis $(e_n)_{n \in \mathbb{N}}$ of V such that $\forall n \in \mathbb{N}$, $h_n = Ue_n$. Applying Theorem 1.1 of [3], it follows that there exists a sequence of root vectors of \mathcal{A} which forms a Riesz basis of \mathcal{H} . The following theorem gives an expansion of the solution of (P) .

Theorem 1 Assume that $\mathbf{U}_0 \in D(\mathcal{A})$. Let $\{\lambda_k, k \in \mathbb{N}\}$ be the set of eigenvalues of \mathcal{A} . For all $k \in \mathbb{N}$, let r_k be the geometric multiplicity of λ_k , $\mathbf{U}_{k,i,j}$, $i = 1, \dots, r_k$, $j = 0, \dots, m_{k,i} - 1$ a family of root vectors corresponding to λ_k such that $(\mathcal{A} - \lambda_k Id)\mathbf{U}_{k,i,j} = \mathbf{U}_{k,i,j-1}$, $i = 1, \dots, r_k$, $j = 0, \dots, m_{k,i} - 1$ (with $\mathbf{U}_{k,i,-1} = 0$) and set $\mathbf{U}_{k,i,j} = \begin{pmatrix} \mathbf{u}_{k,i,j} \\ \mathbf{v}_{k,i,j} \end{pmatrix}$.

Then there exists a family of polynomial functions $P_{k,i,j}$ of degree $\leq m_{k,i} - 1 - j$, $k \in \mathbb{N}$, $i = 1, \dots, r_k$, $j = 0, \dots, m_{k,i} - 1$ such that if for all $n \in \mathbb{N}$ and $t \in \mathbb{R}$ we set

$$\mathbf{u}^n(t) = \sum_{k=0}^n \sum_{i=1}^{r_k} \sum_{j=0}^{m_{k,i}-1} a_{k,i,j}(t) \mathbf{u}_{k,i,j}$$

where $a_{k,i,j}(t) = e^{(\Omega + \lambda_k)t} P_{k,i,j}(t)$, then for all $T > 0$, $\mathbf{u}^n \rightarrow \mathbf{u}$ in $C^0([0, T]; [H^2(0, l)]^2) \cap C^1([0, T]; [H^1(0, l)]^2) \cap C^2([0, T]; [L^2(0, l)]^2)$.

References

- [1] J.-L. Akian. Spectral analysis of a nonhomogeneous rotating Timoshenko beam. Technical Report RT 3/28000, ONERA, February 2019.
- [2] R. Mennicken and M. Möller. *Non-Self-Adjoint Boundary Eigenvalue Problems*. North-Holland, 2003.
- [3] G.Q. Xu and S.P. Yung. The expansion of a semigroup and a Riesz basis criterion. *Journal of Differential Equations*, 210:1–24, 2005.

Galerkin boundary element methods for high-frequency sound-hard scattering problems

Fatih Ecevit^{1,*}, Akash Anand², Yassine Boubendir³, Souaad Lazergui³¹Department of Mathematics, Boğaziçi University, Istanbul, Turkey (Research supported by TÜBİTAK-1001-117F056)²Department of Mathematics and Statistics, Indian Institute of Technology Kanpur, Kanpur, India³New Jersey Institute of Technology, Department of Mathematical Sciences, Newark NJ, USA

*Email: fatih.ecevit@boun.edu.tr

Abstract

We consider two-dimensional sound-hard scattering problems in the exterior of smooth compact strictly convex obstacles. In this connection, we derive high-frequency uniform asymptotic expansions of the Dirichlet trace of the total field associated with a plane wave incidence, and obtain wavenumber explicit estimates on its derivatives. These estimates, in return, can be used to develop efficient high-frequency Galerkin approximation spaces for the solution of coercive integral equation formulations.

Keywords: high-frequency scattering, sound-hard obstacle, asymptotic expansions, Galerkin boundary element methods

1 Introduction

State-of-the-art integral equation methods for the solution of high-frequency scattering problems in the exterior of compact smooth strictly convex obstacles have been confined to sound-soft boundary conditions [1, 3–5, 7]. In this case, the scattering problem can be reduced to determination of the Neumann trace μ of the total field on the boundary, and the aforementioned algorithms are based on phase extraction $\mu(x, k) = e^{ik\alpha \cdot x} \mu^{\text{slow}}(x, k)$ (assuming for simplicity a planewave incidence $u^{\text{inc}}(x, k) = e^{ik\alpha \cdot x}$) along with the Melrose-Taylor asymptotic expansion [6, 8]

$$\mu^{\text{slow}} \sim \sum_{p, q \geq 0} k^{2/3 - 2p/3 - q} b_{p, q}(x) \Psi^{(p)}(k^{1/3} Z(x))$$

of the amplitude μ^{slow} . In sound-hard scattering problems, in contrast, the problem reduces to the determination of the Dirichlet trace η of the total field on the boundary, and here we derive the asymptotic expansion of the related amplitude over the entire boundary. We also obtain sharp wavenumber explicit estimates on its derivatives which can be used in the design and

analysis of efficient numerical methods for the solution of associated integral equations.

2 Scattering problem and asymptotic expansion of the amplitude

We consider a smooth compact strictly convex sound-hard obstacle $K \subset \mathbb{R}^2$ illuminated by a plane wave incidence $u^{\text{inc}}(x) = e^{ik\alpha \cdot x}$ with direction α ($|\alpha| = 1$ and $k > 0$). In this case, the associated scattered field u satisfies [2]

$$\begin{cases} (\Delta + k^2)u = 0 & \text{in } \mathbb{R}^2 \setminus K, \\ \partial_\nu u = -\partial_\nu u^{\text{inc}} & \text{on } \partial K, \\ \lim_{r \rightarrow \infty} \sqrt{r} \left(\frac{\partial u}{\partial r} - ik u \right) = 0, & r = |x| \end{cases} \quad (1)$$

where ν is the exterior unit normal to ∂K . The direct approach in integral equation formulations transforms problem (1) into the determination of the Dirichlet trace of the total field, say η , on ∂K since the scattered field can then be recovered through the integral [2]

$$u(x) = \int_{\partial K} \frac{\partial G(x, y)}{\partial \nu(y)} \eta(y) ds(y). \quad (2)$$

Here G is the outgoing free space Green's function for the Helmholtz equation. While η can be recovered through a variety of uniquely solvable integral equations, as in the case of sound-soft scattering problems, development of efficient boundary element methods can be based on phase extraction

$$\eta(x, k) = e^{ik\alpha \cdot x} \eta^{\text{slow}}(x, k)$$

provided the asymptotic behavior (as $k \rightarrow \infty$) of the amplitude η^{slow} is incorporated into the solution strategy.

Indeed, assuming that the boundary ∂K admits a P -periodic regular parameterization $\gamma(s)$, writing $\eta^{\text{slow}}(s, k)$ for $\eta^{\text{slow}}(\gamma(s), k)$, we have the following which extends the associated asymptotic expansion in [8] to the entire boundary ∂K .

Theorem 1 *The Dirichlet trace η of the total field associated with the Neumann and Robin boundary conditions belongs to the Hörmander class $S_{2/3,1/3}^0([0, P] \times (0, \infty))$, and admits the asymptotic expansion*

$$\eta^{\text{slow}}(s, k) \sim \sum_{\substack{p, q, r \in \mathbb{Z}_+ \\ \ell \in -\mathbb{N}}} k^{-(1+2p+3q+r+\ell)/3+(\ell+1)-} \times b_{p,q,r,\ell}(s) (\Psi^{\ell,r})^{(p)}(k^{1/3}Z(s))$$

where $t_- = \min\{t, 0\}$, where $b_{p,q,r,\ell}$ are P -periodic complex-valued C^∞ functions, Z is a P -periodic real-valued C^∞ function that is positive on the illuminated region $\{s : \alpha \cdot \nu(\gamma(s)) < 0\}$, negative on the shadow region $\{s : \alpha \cdot \nu(\gamma(s)) > 0\}$, and vanishes precisely to first order on the shadow boundary $\{s : \alpha \cdot \nu(\gamma(s)) = 0\}$. Finally, $\Psi^{\ell,r}$ are complex-valued C^∞ functions such that

$$\Psi^{\ell,r}(\tau) \sim \sum_{j \in \mathbb{Z}_+} a_{\ell,r,j} \tau^{1+\ell-2r-3j}$$

as $\tau \rightarrow +\infty$ and are rapidly decreasing in the sense of Schwarz as $\tau \rightarrow -\infty$.

3 Wavenumber explicit estimates on the derivatives of the amplitude

Theorem 1 implies that the amplitude η^{slow} admits boundary layers in neighborhoods of size $\mathcal{O}(k^{-1/3})$ around the shadow boundary points, say $\{t_1, t_2\} = \{s : \alpha \cdot \nu(\gamma(s)) = 0\}$. Numerical methods for the solution of associated integral equations can therefore preserve their efficiency throughout the entire frequency spectrum only if they resolve these boundary layers efficiently.

As in the case of sound-soft scattering problems, in regards to the design and numerical analysis of such algorithms, sharp wavenumber explicit estimates on the derivatives of the amplitude η^{slow} plays a key role. In this connection, we have the following estimates.

Theorem 2 *Given $k_0 > 1$ and $n \in \mathbb{Z}_+$, there exists a constant C independent of k such that*

$$|D_s^n \eta^{\text{slow}}(s, k)| \leq C W(s, k)^{-n}$$

holds for all $(s, k) \in [0, P] \times [k_0, \infty)$ with

$$W(s, k) = k^{-1/3} + |\omega(s)|$$

and $\omega(s) = (s - t_1)(t_2 - s)$.

As in the case of sound-soft scattering problems [4,5], these estimates can be used in the design and analysis of Galerkin boundary element methods for the solution of integral equation formulations that require an increase of only $\mathcal{O}(k^\epsilon)$ (for any $\epsilon > 0$) in the number of degrees of freedom to maintain any prescribed accuracy independent on frequency.

References

- [1] O.P. Bruno, C.A. Geuzaine, J.A. Jr. Monro, and F. Reitich, Prescribed error tolerances within fixed computational times for scattering problems of arbitrarily high frequency: the convex case, *Phil. Trans. R. Soc. Lond. Ser. A Math. Phys. Eng. Sci.* **362** (2004), pp. 629–645.
- [2] S.N. Chandler-Wilde, I.G. Graham, S. Langdon S and E.A. Spence, Numerical-asymptotic boundary integral methods in high-frequency acoustic scattering, *Acta Numer.* **21** (2012), pp. 89–305.
- [3] V. Domínguez, I.G. Graham and V.P. Smyshlyaev, A hybrid numerical-asymptotic boundary integral method for high-frequency acoustic scattering, *Numer. Math.* **106** (2007), pp. 471–510.
- [4] F. Ecevit and H.H. Eruslu, A Galerkin BEM for high-frequency scattering problems based on frequency-dependent changes of variables, *IMAJNA* **39** (2019).
- [5] F. Ecevit and H.Ç. Özen, Frequency-adapted galerkin boundary element methods for convex scattering problems, *Numer. Math.* **135** (2017), pp. 27–71.
- [6] F. Ecevit and F. Reitich, Analysis of multiple scattering iterations for high-frequency scattering problems. I. The two-dimensional case. *Numer. Math.* **114** (2009), pp. 271–354.
- [7] D. Huybrechs and S. Vandewalle, A sparse discretization for integral equation formulations of high frequency scattering problems, *SIAM J. Sci. Comput.* **29** (2007), pp. 2305–2328.
- [8] R.B. Melrose and M.E. Taylor, Near peak scattering and the corrected Kirchhoff approximation for a convex obstacle, *Adv. in Math.* **55** (1985), pp. 242–315.

Least squares collocation for a high-frequency scattering problem

Andrew Gibbs¹, David P. Hewett², Daan Huybrechs^{1,*}, Emile Parolin³¹Department of Computer Science, KU Leuven, Belgium²Department of Mathematics, University College London, UK³Unité de Mathématiques Appliquées, ENSTA ParisTech, France

*Email: daan.huybrechs@cs.kuleuven.be

Abstract

Hybrid numerical asymptotic methods for integral equations in scattering problems are based on incorporating asymptotic information about the solution at high frequencies into the discretization. However, in several cases this leads to an overcomplete set of functions, rather than to a basis, and this in turn leads to conditioning problems at small or moderately large frequencies. We show that such ill-conditioning is remedied effectively by considering a least squares collocation approach. The oversampled collocation scheme is found to be numerically stable regardless of the frequency and of the order of the discretization. Since it is based on single integrals rather than double integrals in the discretization, it is also computationally much more efficient than a Galerkin approach. We show examples for scattering by a screen.

Keywords: boundary element method, collocation, least squares, high-frequency

Introduction

High-frequency scattering problems necessitate a large number of degrees of freedom in their numerical discretization. The size of the discretization can be reduced by adding well chosen oscillatory basis functions to the approximation space, modelling for example reflected, refracted and diffracted waves. This approach leads to two distinct computational challenges:

1. The discretization of an integral operator with oscillatory kernel and oscillatory basis functions requires the evaluation of a large number of highly oscillatory integrals;
2. Function approximation by a collection of wavelike basis functions often seems ill-conditioned.

We tackle the first challenge by considering effective modern numerical methods for highly oscillatory integrals [1], noting that the collocation

approach yields single integrals only. In particular, all integrals are evaluated at a cost that is independent of the frequency. In this talk we mainly focus on the second challenge, for which the proposed remedy is to oversample. Thus, we consider a least squares collocation approach. This follows from recent results on function approximation using redundant sets [2, 3].

Scattering by a screen

We consider 2D time-harmonic acoustic scattering by a sound-soft (Dirichlet) screen $\Gamma \subset \mathbb{R}^2$. This is modelled by the Helmholtz equation,

$$\Delta u + k^2 u = 0,$$

with appropriate boundary conditions (see [5]).

We use a first kind integral equation formulation

$$S\phi = f, \quad (1)$$

in which S is the single layer potential

$$S\phi(\mathbf{x}) = \int_{\Gamma} \Phi(\mathbf{x}, \mathbf{y}) \phi(\mathbf{y}) ds(\mathbf{y}), \quad \mathbf{x} \in \Gamma \quad (2)$$

with in 2D $\Phi(x, y) = \frac{i}{4} H_0^{(1)}(k\|x - y\|)$.

The HNA ansatz

An approximation space is proposed with the generic form

$$\phi(\mathbf{x}) \approx \sum_{m=1}^d \sum_{n=1}^{N_m} c_{m,n} \psi_{m,n}(\mathbf{x}) e^{ikg_m(\mathbf{x})}. \quad (3)$$

Here, the phases g_m are chosen based on the known high frequency asymptotics. In the case of a single flat screen (see Fig. 1), $d = 2$ and the two phases represent diffracted rays emanating from the corners. The corresponding amplitudes are known to be highly peaked: this is accommodated by choosing the basis functions $\psi_{m,n}(\mathbf{x})$ to be piecewise polynomials on a graded mesh, with geometric refinement towards the respective corners.

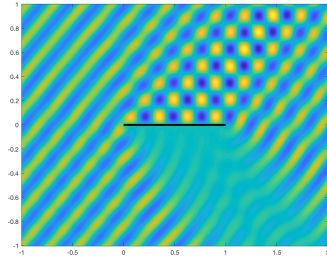


Figure 1: A typical screen scattering problem with $k = 32$.

Least squares collocation

The collocation method is described in [4] and is ongoing work by the authors of this talk. The redundancy of (3) is most evident in the limit $k \rightarrow 0$. Indeed, in that limit we have:

$$\phi(\mathbf{x}) \approx \sum_{m=1}^d \sum_{n=1}^{N_m} c_{m,n} \psi_{m,n}(\mathbf{x}). \quad (4)$$

The unknown is described by a union of piecewise polynomials defined on the same domain. A function on that domain may have several representations with wildly different coefficients: this lack of uniqueness implies that any linear system to solve for $c_{m,n}$ is necessarily extremely ill-conditioned or even singular, even without an integral operator involved.

The ansatz (3) is plugged into (1). The collocation points are chosen to be Chebyshev nodes on each of the pieces of the graded meshes involved. We employ oversampling by a factor of $C_{OS} \geq 1$. The resulting rectangular linear system is solved by a regularization technique, in our implementation using the singular value decomposition with truncation of singular values smaller than a prescribed threshold ϵ .

Numerical results

For the single screen scattering problem illustrated in Fig. 1, it is shown in Fig. 2 that the number of degrees of freedom required to achieve a given accuracy in practice improves with increasing wavenumber. Fig. 3 shows that maximal accuracy for larger values of the polynomial degree is only achieved with oversampling.

References

[1] A. Deaño, D. Huybrechs and A. Iserles, *Computing highly oscillatory integrals*,

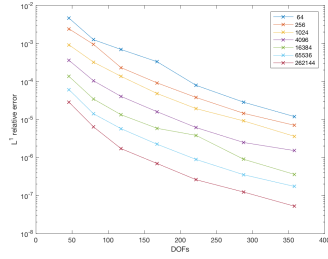


Figure 2: The number of degrees of freedom required to reach a certain accuracy for increasing values of the wavenumber.

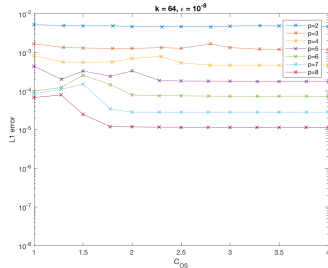


Figure 3: Accuracy as a function of the oversampling ratio C_{OS} for fixed $k = 64$ and increasing degree of the piecewise polynomials.

SIAM, Philadelphia, 2017.

[2] B. Adcock and D. Huybrechs, Frames and numerical approximation, *SIAM Review*, to appear.

[3] B. Adcock and D. Huybrechs, Frames and numerical approximation II: generalized sampling, *arXiv:1802.01950*.

[4] E. Parolin, A hybrid-numerical asymptotic boundary element method for high-frequency wave scattering, *Master's thesis*, University of Oxford, 2015.

[5] D. P. Hewett and S. Langdon and S. N. Chandler-Wilde, A frequency-independent boundary element method for scattering by two-dimensional screens and apertures, *IMA J. Numer. Anal.* **35** (2015), pp. 1698–1728.

PathFinder: a toolbox for oscillatory quadrature

Andrew Gibbs^{1,*}, Daan Huybrechs¹¹Department of Computer Science, KU Leuven, Belgium

*Email: andrew.gibbs@cs.kuleuven.be

Abstract

A range of contemporary methods exist for the efficient evaluation of highly oscillatory integrals. These methods are very effective for model integrals, but may require expertise and manual intervention for integrals with higher complexity. The *PathFinder* project aims to develop robust and fully automated numerical software for such problems. In this paper we outline the main algorithm, focusing on its approach for efficient handling of coalescing stationary points.

Keywords: Oscillatory quadrature, steepest descent, high frequency

1 Introduction

Here we consider the model integral:

$$I_\gamma^\omega[f, g] = \int_\gamma f(z) e^{i\omega g(z)} dz, \quad (1)$$

where γ is a contour in \mathbb{C} , f and g are non-oscillatory analytic functions and $\omega > 0$ is our frequency parameter. Integrals of the form (1) arise frequently in wave-based problems, however evaluation via a standard quadrature routine requires a computational cost which grows like $O(\omega)$. In contrast, oscillatory quadrature routines become more accurate as ω grows (for fixed cost), when numerically stable. PathFinder is an algorithm which in a stable manner constructs an oscillatory quadrature rule based on numerical steepest descent (NSD), requiring as inputs ω , g , g' , g'' and endpoints of γ (available at github.com/AndrewGibbs/PathFinder).

2 Numerical steepest descent

Steepest descent (SD) methods deform the path of integration γ onto a region in \mathbb{C} along which the integrand of (1) is non-oscillatory and exponentially decaying. It follows by Cauchy's Theorem that the value of the integral (1) remains unchanged after this deformation.

The asymptotic behaviour of (1) for large ω can be described by the set of *critical points* Φ . For an infinite contour γ , this is simply

$\Phi = \{z \in \mathbb{C} : g'(z) = 0\}$, the set of *stationary points*. For polynomial g , PathFinder obtains stationary points via a companion matrix. Otherwise a global bisection method based on the argument principle is used, requiring only g' and g'' . In the case where γ has one or two finite endpoints, these are also included in Φ .

The SD paths from a critical point $\xi \in \Phi$ are the solution(s) to

$$g(h_{\xi,j}(p)) = g(\xi) + ip^{r_\xi}, \quad \text{for } p \in [0, P_{\xi,j}], \quad (2)$$

for $j \in J_\xi := \{1, \dots, r_\xi\}$; $P_{\xi,j} \in [0, \infty)$ and r_ξ is the smallest natural number such that $g^{(r_\xi)}(\xi) \neq 0$ (see, e.g., [1, Prop. 5.6]). There are r_ξ solutions to (2) at each ξ , hence r_ξ possible SD paths (indexed by j). It follows from (2) that along such a path $z = h_{\xi,j}(p)$, the integrand of (1) is exponentially decaying. If g^{-1} is unavailable, we may consider the ODE

$$h'_{\xi,j}(p) = ip^{r_\xi} / g'(h_{\xi,j}(p)), \quad \text{for } p \in [0, P_{\xi,j}], \quad (3)$$

which follows by differentiating (2), and can be solved numerically for $h_{\xi,j}$ (see, e.g., [1, 5.3.1]).

We now transform the path of integration into a series of SD paths from points in Φ , to obtain $I_\gamma^\omega[f, g] =$

$$\sum_{\xi \in \Phi, j \in J_\xi} \frac{c_{\xi,j} e^{i\omega g(\xi)}}{\omega^{1/r_\xi}} \int_0^{P_{\xi,j}} f\left(h_{\xi,j}\left(\frac{p}{\omega}\right)\right) h'_{\xi,j}\left(\frac{p}{\omega}\right) e^{-p^{r_\xi}} dp + O(e^{-\omega P^*}), \quad \text{where } P^* = \max_{\xi,j} P_{\xi,j}^{r_\xi} \quad (4)$$

and $c_{\xi,j} \in \{-1, 0, 1\}$ are chosen such that the union of the SD paths in \mathbb{C} is a deformation of γ (with the endpoints unchanged). Algorithmically, PathFinder constructs a graph with nodes at $\xi \in \Phi$ and at the valleys of g , and with edges based on the SD paths. Deforming γ is equivalent to solving this shortest path problem.

Each term in (4) can be integrated by Gaussian quadrature with the appropriate exponential weight. An example is given in Fig. 1.

3 Instability for coalescing stationary poi

We say a phase g has *coalescing* stationary points if they are very close together; (equivalently) g

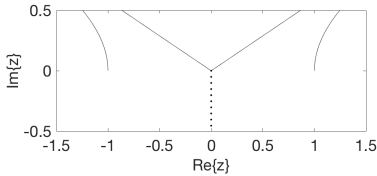


Figure 1: SD paths in \mathbb{C} for $I_{[-1,1]}^\omega[f, z^3]$. The term $c_{0,j}$ corresponding to the dotted path is 0, this path is not used when deforming $[-1, 1]$.

is only a small perturbation from a phase with fewer stationary points of higher order. An unwelcome consequence of coalescence is that the Jacobian $h'_{\xi,j}(p/\omega)$ of (4) will be nearly singular when p is small. This can lead to instabilities in the numerical solution of the ODE (3) and in the quadrature approximation of (4). To the best knowledge of the authors, PathFinder contains the first algorithm with a general and robust framework for coalescing stationary points.

4 A general and robust algorithm

Conveniently, in the region of \mathbb{C} where coalescence occurs and $h'_{\xi,j}$ is nearly singular, $\omega|g'|$ is very small and hence the integrand of (1) can be treated locally as non-oscillatory. We exploit this by partitioning \mathbb{C} into two distinct regions Ω_\pm . Loosely speaking, in the region Ω_+ , the quantity $\omega|g'|$ is bounded below, and NSD performs well. Meanwhile in Ω_- , we have that $\omega|g'|$ is small, the integrand of (1) is non-oscillatory, and standard quadrature performs well.

Formally, these regions are divided by a contour, which (assuming $g' \neq 0$) is derived from

$$\tilde{\Gamma}_\xi = \{z \in \mathbb{C} : \omega|g(z) - g(\xi)| = C\},$$

for some constant $C > 0$ (we choose $C = 1$ in §5) and a stationary point ξ . It follows by the maximum modulus principle that each $\tilde{\Gamma}_\xi$ is a finite union of closed contours. We choose Γ_ξ to be the unique closed contour of $\tilde{\Gamma}_\xi$ which contains ξ and define Ω_- as the open set enclosed by the contours $\cup_\xi \Gamma_\xi$, and $\Omega_+ := \mathbb{C} \setminus \Omega_-$. If required, in contrast to (2) and (3), PathFinder traces SD paths from the edge of the contour Γ_ξ starting at Φ^* : the set of local minima of $\text{Im}\{g|_{\Gamma_\xi \cap \Omega_+}\}$. This notation-heavy explanation is made clearer by the figure at the end of §5.

PathFinder’s approach avoids approximation of the SD paths in regions which may be numer-

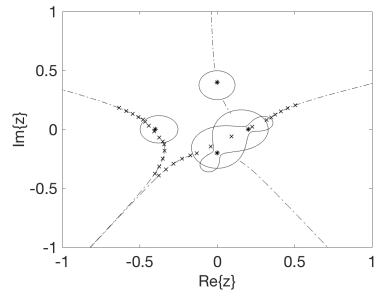
ically unstable. Fixing C and varying ω , the number of quadrature points required to accurately represent (1) is at worst $O(1)$. Fixing g , if $r_\xi \leq 2$ for all $\xi \in \Phi$, there exists some $\omega_+ > 0$ such that for all $\omega \geq \omega_+$ PathFinder is numerically robust using (3)–(4), recovering the asymptotic order of NSD: $O(\omega^{-\frac{2N+1}{2}})$ error for N quadrature points per SD path [1, Thrm 5.7].

5 Numerical experiments

Our experiments focus on cases of coalescence, which (as explained in §3) are unstable with a naive implementation of (4). Below we give errors for the approximation of $I_{[-1,1]}^\omega[1, g_\epsilon]$, where $g_\epsilon(z) := z^3/3 - \epsilon^2 z$ (which has coalescing stationary points at $\pm\epsilon$), by 50 quadrature points: PathFinder can handle any number of coalescing

$\omega \setminus \epsilon$	0.1	0.01	0.0001	0
1,000	3.4e-06	2.7e-07	2.9e-07	2.9e-07
10,000	1.1e-07	1.6e-07	1.3e-07	1.3e-07
100,000	1.4e-08	2.1e-08	9.3e-09	9.3e-09

stationary points, as is demonstrated in the figure below - which shows the topology for a phase with $g'(z) = (z + \epsilon)(z - \epsilon/2)(z + i\epsilon/2)(z - i\epsilon)$, for $\epsilon = 2/5$, with an infinite contour γ connecting $e^{9\pi i/10}$ to $e^{21\pi i/10}$. The stars mark the stationary points, the dashed lines are the SD paths, the closed contours are Γ_ξ and the crosses represent the quadrature nodes.



References

[1] A. Deaño, D. Huybrechs and A. Iserles, *Computing Highly Oscillatory Integrals*, SIAM, Pennsylvania, 2018.

Ray density transport through a mesh using a phase-space integral operator with a direction preserving discretisation

David Chappell^{1,*}, Martin Richter^{1,2}, Gregor Tanner²

¹Department of Mathematics and Physics, Nottingham Trent University, Nottingham, UK

²School of Mathematical Sciences, University of Nottingham, Nottingham, UK

*Email: david.chappell@ntu.ac.uk

Abstract

Phase-space integral operator models for transporting ray densities through complex two and three dimensional domains have recently been proposed, based on the Frobenius-Perron operator. The dependence of the density on the momentum (or equivalently direction) variable has typically been approximated using a basis expansion of orthogonal polynomials. This approach allows for the inclusion of directivity in the model, going beyond more conventional radiosity based methods. However, due to the finite basis approximation, numerical diffusion leads to an accumulation of error each time the integral operator is applied. This issue is particularly problematic for transporting densities through a mesh, since transmission from one cell to the next is modelled via successive applications of the integral operator. In this work, the possibility of a direction preserving discretisation procedure will be discussed in order to eliminate these errors.

Keywords: High frequency asymptotics, Ray tracing, Frobenius-Perron operator, Geometrical optics

1 Introduction

The transport of phase-space densities along a trajectory flow map φ^τ through time τ and space \mathbb{R}^d can be formulated in terms of the Frobenius-Perron (FP) operator (see, for example, [1]). The action of this operator on a phase-space density f may be expressed in the form

$$\mathcal{L}^\tau f(X) = \int \delta(X - \varphi^\tau(Y)) f(Y) dY, \quad (1)$$

where X and Y are phase-space coordinates in \mathbb{R}^{2d} . Solving such problems when $d > 1$ and for physically relevant systems is often considered intractable due to both high dimensionality and potentially complex geometries [2]. In this work, the FP operator is reformulated as a phase-space boundary integral operator, which

is imposed in a weak Galerkin form with a basis approximation applied in both the position and momentum variable. An efficient numerical implementation of this integral equation model on two-dimensional mesh elements was proposed in [3] and further extended to three-dimensional meshed domains in [4].

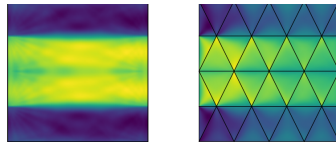


Figure 1: A density propagating horizontally inside a unit square domain. The initial density ρ_0 illuminates the central section of the left edge and both plots show numerical models with similar total numbers of degrees of freedom. The left plot is computed using a boundary integral model of the unit square, the right plot shows the effect of introducing an internal mesh and instead propagating between mesh edges, instead of the outer boundary only.

When applied to a meshed object, the FP operator transports a density from the boundary of one mesh cell to the next where the density may be reflected or transmitted, depending on the underlying physics. The finite basis approximation in momentum (i.e. direction) leads to a smoothing of the directivity pattern each time the FP operator is applied. Hence on a mesh with many cells, significant errors due to the repeated smoothing of the directivity may arise - see Fig. 1. In this work we propose a discretisation for the momentum variable which is based on a global direction set. The local basis on a particular mesh boundary is then selected as a subset from this global set, allowing in many cases for the direction to be preserved as the density is translated across the mesh.

2 Mathematical model: FP operator as a local boundary integral operator

Consider the propagation of a density f through a mesh $\mathcal{M} = \bigcup_{j=1}^N \mathcal{E}_j \subset \mathbb{R}^2$, consisting of N convex polygonal elements \mathcal{E}_j , $j = 1, \dots, N$. Let us assume that the trajectory flow is governed by Hamiltonians of the form $H_j(r, p) = c_j|p| = 1$ in \mathcal{E}_j , where c_j is the flow velocity for $r \in \mathcal{E}_j$ and the momentum coordinate p lies on a circle of radius c_j^{-1} . This Hamiltonian is associated to the Helmholtz equation with wave velocity $c(r)$.

Let the phase-space on the boundary of \mathcal{E}_j be written $Q_j = \partial\mathcal{E}_j \times (-c_j^{-1}, c_j^{-1})$. Then the associated coordinates are given by $X_j = [s_j, p_j] \in Q_j$ with $s_j \in [0, L_j)$ parameterising $\partial\mathcal{E}_j$, where L_j is the total length of the boundary of the j th element, and $p_j \in (-c_j^{-1}, c_j^{-1})$ parameterising the component of the inward momentum vector tangential to $\partial\mathcal{E}_j$. Next we define $\varphi_{ij} : Q_j \rightarrow Q_i$ to be the boundary flow map, which takes a vector in Q_j and maps it along the flow given by H_j to a vector in Q_i . The propagation of the density f along the map φ_{ij} is given by the FP operator acting on this map as follows

$$\mathcal{L}f(X_i) = \sum_j \int_{Q_j} \delta(X_i - \varphi_{ij}(X_j)) f(X_j) dX_j. \quad (2)$$

The operator \mathcal{L} describes propagation of f along a trajectory with endpoint on the boundary of element \mathcal{E}_i and start point on the boundary of each neighbouring or coincident element \mathcal{E}_j . In order to include reflection/transmission along with other physics such as dissipation we need to add a weighting factor $w_{i,j}(X_j)$ in (2).

The stationary density $\rho(X_i)$ on Q_i , $i = 1, \dots, N$, due to an initial boundary distribution ρ_0 on Q_j , $j = 1, \dots, N$ is the density accumulated in the long time (many iterate) limit. That is

$$\rho(X_i) = \sum_{n=0}^{\infty} \mathcal{L}^n \rho_0(X_i), \quad (3)$$

where \mathcal{L}^n is the n th iterate of the operator (2) including the weight factor $w_{i,j}$. For the sum (3) to converge requires the incorporation of a dissipative term within $w_{i,j}$, so that the spectral radius of \mathcal{L} is less than one.

3 Discretisation: basis choice and truncation errors

We consider a finite dimensional approximation of the stationary boundary density ρ on Q_j us-

ing a basis expansion of the form

$$\rho(s_j, p_j) = \sum_{l=1}^{N_j} \sum_{n=0}^{N_p} \rho_{(j,l,n)} b_l(s_j) P_n(p_j), \quad (4)$$

where N_j is the number of boundary elements on \mathcal{E}_j and N_p is the order of the basis expansion in the momentum coordinate p_j . We apply piecewise-constant basis functions b_l in the space coordinate s_j , with support only on the l th boundary element on \mathcal{E}_j . The role of the functions P_n is to model the dependence of the stationary density ρ on the direction of transport. In Ref. [3], P_n are chosen as Legendre polynomials and hence the Galerkin projection of a point or line source (where the directional dependence will be expressed as a Dirac δ) onto the finite dimensional basis will lead to smoothing and diffusion - see Fig. 1.

In this work we instead propose a basis of the form $P_n(p_j) = \delta(p_j - p_j^n)$ for $n = 0, 1, \dots, N_p$, where p_j^n are a set of momenta obtained from the projection of a global direction set in $[0, 2\pi)$ onto the local boundary element l on \mathcal{E}_j . In this way, a consistent direction of travel may be preserved through different mesh cells. A Petrov-Galerkin scheme will be necessary to ensure that the Galerkin projection is well defined. Piecewise constant test functions are a convenient choice and lead to orthonormality in the L^2 inner product.

References

- [1] P. Cvitanović, R. Artuso, R. Mainieri, G. Tanner, and G. Vattay, *Chaos: Classical and Quantum*. Copenhagen: Niels Bohr Institute, 2012. <http://ChaosBook.org>.
- [2] S. Siltanen, T. Lokki, S. Kiminki, and L. Savioja, The room acoustic rendering equation, *J. Acoust. Soc. Amer.* (2007) **122**: pp. 1624–1635.
- [3] D.J. Chappell, G. Tanner, N. Søndergaard and D. Löchel, Discrete flow mapping: transport of phase-space densities on triangulated surfaces, *Proceedings of the Royal Society A*, (2013) **469**: 20130153.
- [4] J. Bajars, D.J. Chappell, N. Søndergaard and G. Tanner, Transport of phase-space densities through tetrahedral meshes using discrete flow mapping, *Journal of Computational Physics*, (2017) **328**: pp. 95–108.

Convergence Properties of Transfer Operators for Billiards with a Mixed Phase-Space

Martin Richter^{2,1,*}, David J. Chappell¹, Gregor Tanner²

¹Department of Mathematics and Physics, Nottingham Trent University, Nottingham, UK

² School of Mathematical Sciences, University of Nottingham, Nottingham, UK

*Email: martin.richter@nottingham.ac.uk

Abstract

We analyse the convergence properties of a ray-tracing approach via transfer operators. The investigation focuses on a two-dimensional Hamiltonian system with a mixed-phase space, i.e. co-existing integrable and chaotic dynamics. As we focus on mid- to high-frequency regimes of the corresponding wave problem, we construct the transfer operator by means of a ray-tracing approach. We then solve the propagation problem numerically and investigate the rate of convergence. We accompany this with an investigation of the dynamics in phase space in terms of the boundary map. We compare our findings with recent rigorous proofs carried out for a circular domain and conclude with an outlook about its applicability to real-world problems.

Keywords: Transfer operator, ray tracing, billiard dynamics, mixed phase space

1 Introduction

Solving wave equations and the corresponding energy transport is a very common problem in many fields ranging from quantum mechanical transport through materials, electromagnetic settings in media or cavities to vibrational problems in structure-borne sound propagation. Despite being widely studied from a mathematical point of view, real-world problems often require numerical tools to approximate solutions for flows through complex geometries. Especially in mid- to high-frequency regimes, classical finite-element methods (FEM) fail to give good results unless the underlying meshes for describing the structure under investigation are refined accordingly, thereby increasing numerical effort and hardware requirements. On the other hand, at very high frequencies, the often complex nature of the objects allows for a statistical description of the problem, dubbed "Statistical Energy Analysis", SEA [1]. Between the two extremes, a method based on ray-tracing techniques applied to meshes called "Dynamical Energy Analysis" [2] can be used to describe, for

example, structure-borne sound.

While the approach of DEA as a ray-tracing method over FEM meshes works well in practice [3], less is known about the mathematical error bounds on its convergence behaviour. To remedy this, a recent work investigated the convergence of the algorithm on a circular billiard domain [4]. While the proven result in this example works very well, little is known for more generic systems and further investigations are necessary to understand the convergence behaviour of transfer-operator methods on complex, real-world meshes.

This work undertakes one of these necessary investigations: We focus on a deformed circle thereby taking the first logical step away from globally integrable dynamics. While not comparable with the full complexity with a real-world mesh it still is a valid and important step towards the understanding of the latter as it introduces generic properties of mixed phase-space dynamics to previously integrable dynamics. We choose the boundary from the family of Limaçon billiards [5] and present their phase-space portraits as well as a comparison of the transfer operator in a Fourier basis. In order to understand the convergence we will also study spectral properties of the operator and investigate the role of invariant subsets in phase-space introduced by the boundary deformation.

2 Transfer Operator

In the short-wavelength limit of wave problems, a description in terms of propagating rays along geodesics is a meaningful approximation. This can be used to describe the propagation of energy by means of transfer operators T . More specifically, in two-dimensional billiard problems like the one discussed here, it is feasible to use a boundary map to describe this transport [6].

Numerically, these operators T are decomposed into a orthonormal basis which is truncated at a certain order K , then we arrive at a finite-dimensional matrix representation of the

transfer operator. To calculate an element of the transfer matrix, we have to solve the flow equation and integrate

$$T_{nmkl} = \frac{(-1)^{l-m}}{2\pi^2} \int_0^{2\pi} \int_{-\pi/2}^{\pi/2} e^{i(k\varphi+2l\psi)} \times \quad (1)$$

$$\times e^{-i(n\mathcal{M}_\varphi(\varphi,\psi)+2m\mathcal{M}_\psi(\varphi,\psi))} d\psi d\varphi$$

$$= \frac{(-1)^{l-m}}{2\pi^2} \int_0^{2\pi} \int_0^{2\pi} \left| \frac{\partial\psi}{\partial\varphi'}(\varphi,\varphi') \right| \times \quad (2)$$

$$\times e^{i(k\varphi-n\varphi'+2l\psi(\varphi,\varphi')-2m\psi'(\varphi,\varphi'))} d\varphi' d\varphi$$

where \mathcal{M} is the boundary map (see for example Eq. (4)) and $\psi(\varphi,\varphi')$ denotes the outgoing angle for a trajectory connecting the points φ, φ' . Analogously, $\psi'(\varphi,\varphi')$ is the angle after the next reflection of the same trajectory. The main object of interest is the equilibrium density from a given initial density ρ_0 on the boundary via

$$\rho_\infty = \sum_{k=0}^{\infty} T^k \rho_0 = (1 - T)^{-1} \rho_0 \quad (3)$$

in dependence of the truncation of the order of the basis used to describe the above matrix.

For a perfect circle, the boundary dynamics can be solved straightforwardly. If φ is the polar angle and ψ the angle of a reflected ray with respect to the normal pointing towards the interior of the circle, then we have with $\varphi \in (0, 2\pi)$ and $\psi \in (-\pi/2, \pi/2)$.

$$(\varphi, \psi) \mapsto \mathcal{M}(\varphi, \psi) = (\varphi + \pi - 2\psi, \psi). \quad (4)$$

In order to generalise this and to introduce more complicated ray dynamics, we focus on a deformed circle from the Limaçon family given by a boundary according to

$$r(\varphi) = 1 + \delta \cdot \cos(m \cdot \varphi). \quad (5)$$

For this system, the boundary map (4) has to be solved numerically.

3 Phase-Space of a Deformed Circle

To get an overview of the ray dynamics in the deformed billiard, we can plot the sequence of points for various initial conditions and compare them to real-space orbits plotted in the (φ, ψ) plane, see Fig. 1. At this point it is important to note that depending on m the deformation parameter δ must not be too large as otherwise

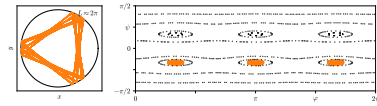


Figure 1: Boundary map and real-space orbit for the deformed circle. The deformation in Eq. (5) is $m = 3, \delta = 0.1$. Slightly larger deformations would lead to a non-convex billiard.

the billiard gets non-convex and Eq. (2) becomes more complicated as there might be no solution for $\psi(\varphi, \varphi')$ for specific values of φ and φ' .

In order to investigate the convergence we will use functions of different smoothness and different norms to describe the rate of convergence. We present properties of the transfer matrix in terms of its spectrum as well as more efficient implementations. We close the talk with a direct comparison to results known from a circular domain [4].

References

- [1] R. Lyon and R. DeJong, *Theory and Application of Statistical Energy Analysis*, Butterworth-Heinemann, Boston, 1995.
- [2] G. Tanner, Dynamical energy analysis – determining wave energy distributions in vibro-acoustical structures in the high-frequency regime, *J. Sound Vib.* **320** (2009) pp. 1023–1038.
- [3] T. Hartmann, S. Morita, G. Tanner, D. J. Chappell, High-frequency structure- and air-borne sound transmission for a tractor model using Dynamical Energy Analysis, *Wave Motion* **87** (2019) pp. 132–150.
- [4] J. Slipantschuk, M. Richter, D. J. Chappell, G. Tanner, W. Just, and O. F. Bandtlow, to be published.
- [5] H. R. Dullin and A. Bäcker, About ergodicity in the family of limaçon billiards, *Nonlinearity* **14** (2001) pp. 1673–1687.
- [6] D. J. Chappell, G. Tanner, D. Löchel, N. Søndergaard, Discrete flow mapping: transport of phase space densities on triangulated surfaces, *Proc. R. Soc. Lond. A* **469** (2013) pp. 20130153

Error estimates for Gaussian beams at a fold caustic

Olivier Lafitte^{1,*}, Olof Runborg^{2,*}

¹ LAGA, Institut Galilée, Université Paris 13, Sorbonne Paris Cité, Université Paris 8

² Department of Mathematics, KTH, Stockholm, Sweden

*Email: olofr@kth.se

Abstract

We consider approximations of high frequency solutions to the Helmholtz equation in two dimensions by Gaussian beam superpositions. We derive a new error estimate for first order beams at a fold caustic, showing a pointwise error of size $O(k^{-5/6})$, where k is the wave number.

Keywords: high frequency approximations, Gaussian beams, caustics

1 Introduction

Gaussian beam superpositions is a high frequency asymptotic model for solution of wave equations [1]. It is often used in numerical methods to simulate waves in the high frequency regime. In this paper we consider error estimates for the model in terms of the wave number k . Unlike standard geometrical optics, the Gaussian beam model does not break down at caustics, which is one of its main advantages.

Error estimates for Gaussian beams are known in a number of settings. See for instance [2, 3] and the references therein. The main result is that, in L^2 and Sobolev norms, the relative error of first order beams decays as $O(k^{-1/2})$, independently of dimension and regardless of the presence of caustics. The better rate $O(k^{-1})$ is typically observed in numerical computations and has been shown in L^2 for the Schrödinger equation, and also in L^∞ on sets strictly away from caustics. Similar estimates have been shown for higher order beams.

There are, however, no precise, pointwise, error estimates for the solution at a caustic. In particular, for first order beams it has not been shown that this error vanishes as $k \rightarrow \infty$, although there is ample numerical evidence to this effect. The purpose of this paper is to show such an error estimate for a typical fold caustic in two dimensions. More precisely, we consider the index of refraction $n(x, y)^2 = 1 - y$ and the fold caustic that this generates in the out-going solution of the Helmholtz equation with a compactly

supported source that concentrates on $y = 0$,

$$\Delta u + k^2(1 - y)u = ik\delta(y)f(x),$$

where we take

$$f(x) = \frac{1}{\xi_0}A_0(x)e^{i\eta_0 x}, \quad \xi_0 = \sqrt{1 - \eta_0^2}.$$

This represents an incoming plane wave in the direction θ with amplitude envelope $A_0(x)$, where $\eta_0 = \cos \theta$. A caustic develops along the line $y = \xi_0^2$. Fig. 1 shows a representative solution.

2 Exact solution

We let $\hat{u}(\eta, y)$ be the k -scaled Fourier transform in x of the exact solution,

$$\hat{u}(\eta, y) = \sqrt{k/2\pi} \int e^{-i\eta kx} u(x, y) dx.$$

For $y > 0$ we can derive an exact expression using Airy functions [4],

$$\hat{u}(\eta, y) = e^{-\frac{i\pi}{3}} \frac{\text{Ai}(k^{\frac{2}{3}}(y + \eta^2 - 1))}{\text{Ai}(e^{\frac{i\pi}{3}} k^{\frac{2}{3}}(1 - \eta^2))} \hat{A}_0(\eta). \quad (1)$$

In this expression, one notices that the denominator never vanishes because all the roots of the Airy function are on the negative real axis.

3 Gaussian beam approximation

The approximation is made up of a superposition of Gaussian beams,

$$u_{GB}(x, y) = \sqrt{k/2\pi} \int v(x, y; z) dz.$$

where v is the Gaussian beam starting at $x = z$,

$$v(\mathbf{x}; z) = A(s; z) \exp\left(ik[S(s; z) + (\mathbf{x} - \gamma(s; z)) \cdot \mathbf{p}(s; z) + \frac{1}{2}(\mathbf{x} - \gamma(s; z))^T M(s; z)(\mathbf{x} - \gamma(s; z))\right],$$

and $\mathbf{x} = (x, y)$. The beam parameters are the central ray position γ , the beam direction \mathbf{p} the Gaussian shape M , the initial phase S and the

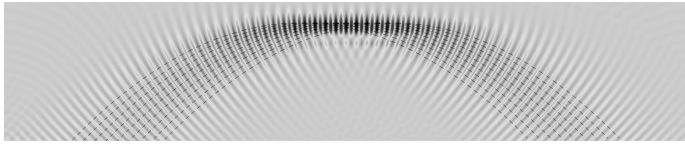


Figure 1: The fold caustic: Full solution and ray tracing picture.

amplitude A . They all satisfy known ODEs in s with initial data determined by z . In this particular case the ODEs can be solved exactly, and we can derive the following expression for the k -scaled Fourier transform of u_{GB} ,

$$\hat{u}_{GB}(\eta, y) = c_0 \hat{A}_0(\eta - \eta_0) \sqrt{\frac{k}{2\pi}} e^{ik(-2\eta_0\xi_0(\eta-\eta_0)+2\xi_0^3/3)} \times \int \frac{e^{ik\phi(y,\theta,\eta-\eta_0)}}{\sqrt{1+2(\xi_0+\theta)i - (\xi_0+\theta)^2(1+2i\xi_0)}} d\theta, \tag{2}$$

where $c_0 = \eta_0 \sqrt{4\xi_0^2 - 2i\xi_0}$ and

$$\phi(y, \theta, \eta) = -\frac{1}{3}\theta^3 + \theta(\xi_0^2 - y - 2\eta_0\eta) + \frac{1}{2}m(\xi_0 + \theta)(y - \xi_0^2 + \theta^2)^2,$$

with m being a smooth function with positive imaginary part. One deduces then, through Malgrange preparation theorem, that there exists two functions $\tilde{\rho}$, ϕ_0 and two symbols σ_0, σ_1 (see below) such that

$$\hat{u}_{GB}(\eta, y) = c_0 \hat{A}_0(\eta - \eta_0) \sqrt{2\pi} k^{\frac{1}{6}} \times [\sigma_0 \text{Ai} + ik^{-\frac{1}{3}} \sigma_1 \text{Ai}'](-k^{\frac{2}{3}} \tilde{\rho}(y, \eta)) \times e^{ik(-2\eta_0\xi_0(\eta-\eta_0)+2\xi_0^3/3+\phi_0(y,\eta))}. \tag{3}$$

4 Error estimate

The max error at a fixed y is given by the estimate,

$$\sup_x |u_{GB}(x, y) - u(x, y)| \leq \sqrt{k/2\pi} \int |\hat{u}_{GB}(\eta, y) - \hat{u}(\eta, y)| d\eta.$$

Away from the caustic ($0 \leq y < \xi_0^2$) stationary phase estimates for \hat{u}_{GB} in (2) and asymptotic estimates for large arguments of Airy functions for \hat{u} in (1) yield the expected $O(k^{-1})$ error. At the caustic where $y = \xi_0^2$, the asymptotic estimates above fail and a more precise analysis is

needed.

Comparing (1) and (3), using the principal term of $\tilde{\rho}$, ϕ_0 , σ_0 , σ_1 , the error is of the order $O(k^{-5/6})$. One notes that since the size of the solution itself grows as $O(k^{1/6})$ at the caustic [5], the relative error is then $O(k^{-1})$, the same as the L^∞ error away from caustics.

Determination of $\tilde{\rho}$ and ϕ_0 . Critical values of the phase ϕ for η small are needed. As $\partial_\theta^2 \phi(\xi_0^2, 0, 0) < 0$, let $\theta(y)$ solve (locally) $\partial_\theta^2 \phi(y, \theta(y), \eta) = 0$, hence $\theta(y) = (y - \xi_0^2)h(y)$ and the (complex) critical points are $\theta_\pm(y, \eta) = \theta(y) \pm \delta_\pm \sqrt{\partial_\theta \phi}$ for $\Re \partial_\theta \phi > 0$. Thus, for η small, two critical values arise which lead to $\tilde{\rho}$ and ϕ_0 :

$$\begin{aligned} \phi_\pm(y, \eta) &= \phi_0(y, \eta) \pm \frac{2}{3}(\tilde{\rho}(y, \eta))^{\frac{3}{2}}, \text{ with} \\ \tilde{\rho}(y, \eta) &= \partial_\theta \phi(y, \theta(y), \eta)r(y, \eta) \\ &= (\xi_0^2 - y + 2\eta\eta_0 + O((y - \xi_0^2)^2))r. \end{aligned}$$

References

- [1] J. Ralston. Gaussian beams and the propagation of singularities. In *Studies in partial differential equations*, volume 23 of *MAA Stud. Math.*, pages 206–248. Math. Assoc. America, Washington, DC, 1982.
- [2] H. Liu, O. Runborg, and N. M. Tanushev. Error estimates for Gaussian beam superpositions. *Math. Comp.*, 82:919–952, 2013.
- [3] H. Liu, O. Runborg and N. Tanushev. Sobolev and max norm error estimates for Gaussian beam superpositions. *Commun. Math. Sci.*, 14(7):2037-2072, 2016.
- [4] J. D. Benamou et al. A geometric optics based numerical method for high frequency electromagnetic fields computations near a fold caustic I. *J. Comp. Appl. Math.*, 156(1):93–125, 2003.
- [5] D. Ludwig. Uniform asymptotic expansions at a caustic. *Commun. Pur. Appl. Math.*, 19:215–250, 1966.

Calderón cavities inverse problem as a shape-from-moments problem

Alexandre Munnier¹, Karim Ramdani^{2,*}

¹Université de Lorraine (IECL), Nancy, France

²Inria (SPHINX Team), Nancy, France

*Email: karim.ramdani@inria.fr

Abstract

In this paper, we address a particular case of Calderón’s conductivity inverse problem in dimension two, namely the case of a homogeneous background containing a finite number of cavities (i.e. heterogeneities of infinitely high conductivities). We aim to recover the location and the shape of the cavities from the Dirichlet-to-Neumann (DtN) map of the problem. Our reconstruction method is non iterative and uses two main ingredients. First, we show that the so-called generalized Pólya-Szegő tensors (GPST) of the cavities can be computed from the DtN map. Secondly, we conjecture (and prove for some particular configurations) that these GPST can be related to a moment problem for an unknown measure supported in the cavity. Numerical simulations show that solving this moment problem provide an efficient reconstruction method, for quite general configurations.

Keywords: Inverse problems, integral equations, complex moments problem

1 Introduction

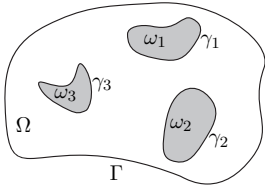


Figure 1: The domain and the unknown cavities.

Let $\Omega \subset \mathbb{R}^2$ be a simply connected open bounded set with Lipschitz boundary Γ . We suppose that Ω contains a multiply connected domain $\omega = \cup_{k=1}^N \omega_k$, where the open sets ω_k , for $k = 1, \dots, N$ are non intersecting simply connected domains with $C^{1,1}$ boundaries γ_k and $\bar{\omega} \subset \Omega$ (see Figure 1). We denote by $\gamma = \cup_{k=1}^N \gamma_k$

and by n the unit normal to $\Gamma \cup \gamma$ directed towards the exterior of $\Omega \setminus \bar{\omega}$. For every trace f in $H^{\frac{1}{2}}(\Gamma)$, let $(u^f, \mathbf{c}^f) \in H^1(\Omega \setminus \bar{\omega}) \times \mathbb{R}^N$, with $\mathbf{c}^f := (c_1^f, \dots, c_N^f)^T$, be the solution of the Dirichlet problem:

$$-\Delta u^f = 0 \quad \text{in } \Omega \setminus \bar{\omega} \tag{1a}$$

$$u^f = f \quad \text{on } \Gamma \tag{1b}$$

$$u^f = c_k^f \quad \text{on } \gamma_k, \quad k = 1, \dots, N, \tag{1c}$$

with the additional conditions:

$$\int_{\gamma_k} \partial_n u^f \, d\sigma = 0, \quad k = 1, \dots, N. \tag{1d}$$

By following the proof given in the Appendix of [3] for the case of a single cavity ($N = 1$), it can be easily shown that this elliptic problem is well-posed. Its solution can be seen as the limit solution of Calderón’s problem for a piecewise constant conductivity when the constant conductivities inside the cavities tends to infinity. The inverse problem investigated in this paper can be formally stated as follows: *Knowing the Dirichlet-to-Neumann (DtN) map $\Lambda_\gamma : f \mapsto \partial_n u^f|_\Gamma$, how to reconstruct the multiply connected cavity ω ?*

Combining an integral formulation with tools from complex analysis, the authors solve in [3] this inverse problem in the case of a single cavity (ω simply connected). This limitation is due to the crucial use of the Riemann mapping theorem in the reconstruction method. In this talk, we present an alternative reconstruction method that can handle the case of several cavities (for more details, see [4]).

2 Reconstruction method

The proposed reconstruction method uses two main ingredients. The first one is summarized in the following result, which shows that the knowledge of the DtN maps with and without the cavities allows one to compute the entries of the so-called Generalized Pólya-Szegő Tensors

(GPST) of the multiply connected cavity (see also [1]). More precisely, let Λ_γ and Λ_0 denote respectively the DtN maps with and without the cavities, and let S_Γ denote the trace of the single layer potential on the outer boundary Γ . Using the measurements, we can compute the following operator:

$$R := S_\Gamma(\Lambda_\gamma - \Lambda_0).$$

Identifying every point $x = (x_1, x_2)$ of the plane with the complex number $z = x_1 + ix_2$, let us introduce for every integer $m \geq 1$, the harmonic polynomials of degree m : $P_1^m(x) = \text{Re}(z^m)$, $P_2^m(x) = \text{Im}(z^m)$. Finally, let us define the polynomials $Q_{\ell,\Gamma}^m := P_\ell^m + c_{\ell,\Gamma}^m$, $\ell = 1, 2$, where the constants $c_{\ell,\Gamma}^m$ are chosen such that the densities $\widehat{Q}_{\ell,\Gamma}^m := S_\Gamma^{-1}Q_{\ell,\Gamma}^m$ satisfy $\langle \widehat{Q}_{\ell,\Gamma}^m, 1 \rangle_{-\frac{1}{2}, \frac{1}{2}, \Gamma} = 0$.

Theorem 1 For $m, m' \geq 1$ and $\ell, \ell' = 1, 2$, the Generalized Pólya-Szegő Tensors (GPST) of the cavity $\langle Q_{\ell,\gamma}^m, Q_{\ell',\gamma}^{m'} \rangle_{\frac{1}{2}, \gamma}$ are given by the formula

$$\langle Q_{\ell,\gamma}^m, Q_{\ell',\gamma}^{m'} \rangle_{\frac{1}{2}, \gamma} = \langle (\text{Id} + R)^{-1}RQ_{\ell,\Gamma}^m, Q_{\ell',\Gamma}^{m'} \rangle_{\frac{1}{2}, \Gamma}.$$

The second step is to recover the geometry of the cavities from the new available data, namely the real quantities $\langle Q_{\ell,\gamma}^m, Q_{\ell',\gamma}^{m'} \rangle_{\frac{1}{2}, \gamma}$, or equivalently the complex quantities $\langle Q_\gamma^m, Q_\gamma^{m'} \rangle_{\frac{1}{2}, \gamma}$, where we have set $Q_\Gamma^m := Q_{1,\Gamma}^m + iQ_{2,\Gamma}^m$. Inspired by the limit case of small cavities (see for instance [2]), we conjecture the existence of a Borel measure ν supported in the cavity ω such that (z denotes the variable in the complex plane)

$$\frac{1}{m} \langle Q_\gamma^m, Q_\gamma^1 \rangle_{\frac{1}{2}, \gamma} = \int_\omega z^{m-1} d\nu, \quad \forall m \geq 1.$$

This formula connects the complex GPST (which can be computed from the measurements thanks to Theorem 1) to the moments of the unknown measure ν supported in the cavity. We have been able to prove this conjecture in two special cases: for a simply connected cavity and in the case of two disks.

Admitting this conjecture, it is natural to seek an atomic approximation of the measure ν in the form $\sum_{i=1}^n c_i \delta_{z_i}$, for some integer n , where the weights c_i are positive and the points z_i are distinct. This leads to the following reconstruction algorithm :

1. Given $n \geq 1$, compute for $0 \leq m \leq 2n - 1$:

$$\tau_m := \int_\omega z^m d\nu = \frac{1}{m+1} \langle Q_\gamma^m, Q_\gamma^1 \rangle_{\frac{1}{2}, \gamma}.$$

2. Solve Prony's system with the $2n$ unknown (z_i) and (c_i) :

$$\sum_{i=1}^n c_i z_i^m = \tau_m, \quad \forall m = 0, \dots, 2n - 1.$$

3. Plot the disks of centers (z_i) and radii (ρ_i) , with $\rho_i = \sqrt{|c_i|/2\pi}$.

Below an example of reconstruction of a multiply connected cavity having three connected components, for $n = 21$ (i.e. using 21 disks).

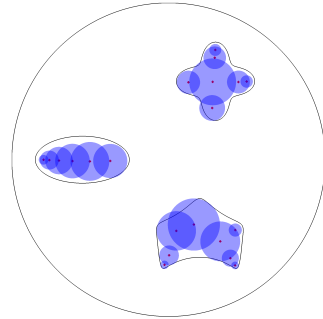


Figure 2: Reconstruction of a multiply connected cavity.

References

- [1] H. Ammari, J. Garnier, H. Kang, M. Lim and S. Yu, Generalized polarization tensors for shape description, *Numer. Math.* **126** (2014), pp. 199–224.
- [2] A. Friedman and M. Vogelius, Identification of small inhomogeneities of extreme conductivity by boundary measurements: a theorem on continuous dependence, *Arch. Rational Mech. Anal.* **105** (1989), pp. 299–326.
- [3] A. Munnier and K. Ramdani, Conformal mapping for cavity inverse problem: an explicit reconstruction formula, *Applicable Analysis* **96** (2017), pp. 108–129.
- [4] A. Munnier and K. Ramdani, Calderón cavities inverse problem as a shape-from-moments problem, *Quarterly of Applied Mathematics* **76** (2018), pp. 407–435.

On well-posedness of scattering problems in a Kirchhoff-Love infinite plate

Laurent Bourgeois^{1,*}, Christophe Hazard¹

¹Laboratoire POEMS, Ensta ParisTech, Palaiseau, France

*Email: laurent.bourgeois@ensta.fr

Abstract

We prove well-posedness of scattering problems for impenetrable obstacles in an infinite elastic Kirchhoff-Love plate in the purely bending case.

Keywords: Scattering problem, Impenetrable obstacle, Kirchhoff-Love plate

1 Introduction

Let us consider a smooth bounded open domain $D \subset \mathbb{R}^2$. The scattered field v^s satisfies in the unbounded domain $\Omega = \mathbb{R}^2 \setminus \overline{D}$ the problem

$$\begin{cases} \Delta^2 v^s - k^4 v^s = 0 & \text{in } \Omega \\ B_1(v^s + u^i) = B_2(v^s + u^i) = 0 & \text{on } \partial\Omega \\ \lim_{r \rightarrow +\infty} \int_{\partial B_r} |\partial_n v^s - ikv^s|^2 ds = 0. \end{cases} \tag{1}$$

Here $k > 0$ is the wave number, u^i is a smooth incident field which satisfies $\Delta^2 u^i - k^4 u^i = 0$ in \mathbb{R}^2 , B_r is the open disc centered at 0 and of radius r , n is the outward normal to B_r . The first line describes the motion of the plate in the frequency domain, the second one characterizes the boundary conditions on the boundary of the obstacle while the third one is the radiation condition, which specifies that only outgoing scattering waves are admissible. Concerning the surface differential operators B_1 and B_2 , we consider the four different cases:

1. $(B_1, B_2) = (I, \partial_n)$ (clamped plate)
2. $(B_1, B_2) = (I, M)$ (simply-supported plate)
3. $(B_1, B_2) = (\partial_n, N)$ (rolled-supported plate)
4. $(B_1, B_2) = (M, N)$ (free plate),

where I is the identity, n is the outward unit normal to Ω , M is the bending moment and N is the shear force. More precisely, if $x = (x_1, x_2) \in \mathbb{R}^2$, $t = n^\perp$ is the unit tangent vector and s the corresponding curvilinear abscissa, M and N are defined by

$$\begin{cases} Mu &= \nu \Delta u + (1 - \nu)M_0 u, \\ Nu &= -\partial_n \Delta u - (1 - \nu)\partial_s N_0 u, \end{cases}$$

where M_0 and N_0 are given by

$$\begin{cases} M_0 u &= \partial_1^2 u n_1^2 + 2\partial_1 \partial_2 u n_1 n_2 + \partial_2^2 u n_2^2, \\ N_0 u &= \partial_1 \partial_2 u (n_1^2 - n_2^2) - (\partial_1^2 u - \partial_2^2 u) n_1 n_2 \end{cases}$$

and $\nu \in [0, 1/2)$ is the Poisson's ratio. The main result is the following:

Theorem 1 *The problem (1) has a unique solution in $H_{\text{loc}}^2(\Omega)$*

- for any k in cases 1 (clamped), 2 (simply-supported) and 3 (rolled-supported),
- for $k \notin \mathcal{K}$ in case 4 (free), where the set \mathcal{K} is formed by a sequence of $k_n > 0$ such that $k_n \rightarrow +\infty$.

Note that such kind of existence-uniqueness theorem for diffraction problems in an infinite plate seems new, if we except [1] for a Bilaplacian perturbed by zero and first order perturbations.

Remark 2 *A crucial point is that if u satisfies $\Delta^2 u - k^4 u = 0$ in Ω , then $U := \Delta u + k^2 u$ and $V := \Delta u - k^2 u$ satisfy $\Delta U - k^2 U = 0$ and $\Delta V + k^2 V = 0$, respectively. This enables us to establish that at infinity, the solution u is an (infinite) linear combination of the four functions $H_m(kr)e^{im\theta}$, with $H_m(z) = H_m^{(1)}(z)$, $H_m^{(1)}(iz)$, $H_m^{(2)}(z)$, $H_m^{(2)}(iz)$, where $H_m^{(1)}$, $H_m^{(2)}$ are the Hankel functions of first and second kinds and order $m \in \mathbb{Z}$. Only the first two satisfy the radiation condition.*

2 Sketch of the proof

Let us introduce the exterior problem: for $(f, g) \in H^{3/2}(\Gamma_R) \times H^{1/2}(\Gamma_R)$ and $\Gamma_R = \partial B_R$, find $u \in H_{\text{loc}}^2(\mathbb{R}^2 \setminus \overline{B_R})$ such that

$$\begin{cases} \Delta^2 u - k^4 u = 0 & \text{in } \mathbb{R}^2 \setminus \overline{B_R} \\ (u, \partial_n u) = (f, g) & \text{on } \partial B_R \\ \lim_{r \rightarrow +\infty} \int_{\partial B_r} |\partial_n u - ik u|^2 ds = 0. \end{cases} \tag{2}$$

The general strategy for proving Theorem 1 is the following. In step 1 we prove uniqueness in problem (1). In step 2 we prove existence

in problem (2) by using separation of variables. This very technical step relies as in [2] on a precise analysis of the asymptotic behaviour of Hankel functions. Step 1 and step 2 imply that problem (2) is well-posed, which enables us to define a Dirichlet-To-Neumann operator or T which from $(f, g) \in H^{3/2}(\Gamma_R) \times H^{1/2}(\Gamma_R)$ associates $(Nu, Mu) \in H^{-3/2}(\Gamma_R) \times H^{-1/2}(\Gamma_R)$, where u is the solution to problem (2). We then introduce the bounded domain $\Omega_R = \Omega \cap B_R$, where $R > 0$ is such that B_R contains the obstacle D . It is easy to prove that problem (1) is equivalent to the following problem: find $u^s \in H^2(\Omega_R)$ such that

$$\begin{cases} \Delta^2 u^s - k^4 u^s = 0 & \text{in } \Omega_R \\ B_1(u^s + u^i) = B_2(u^s + u^i) = 0 & \text{on } \partial\Omega \\ \begin{pmatrix} Nu^s \\ Mu^s \end{pmatrix} = T \begin{pmatrix} u^s|_{\Gamma_R} \\ \partial_n u^s|_{\Gamma_R} \end{pmatrix} & \text{on } \Gamma_R. \end{cases} \quad (3)$$

Assume that $(f, g) \in H^{3/2}(\Gamma_R) \times H^{1/2}(\Gamma_R)$ has decomposition

$$(f, g) = \sum_{m \in \mathbb{Z}} (f_m, g_m) e^{im\theta}.$$

The operator T is then explicitly given by

$$T \begin{pmatrix} f \\ g \end{pmatrix} = \sum_{m \in \mathbb{Z}} \begin{pmatrix} T_m^{11} & T_m^{12} \\ T_m^{21} & T_m^{22} \end{pmatrix} \begin{pmatrix} f_m \\ g_m \end{pmatrix} e^{im\theta},$$

with

$$\begin{cases} T_m^{11} &= -(1 - \nu) \frac{m^2}{R^3} - 2ik^3 \frac{r_m s_m}{r_m - is_m} \\ T_m^{12} = T_m^{21} &= (1 - \nu) \frac{m^2}{R^2} + k^2 \frac{r_m + is_m}{r_m - is_m} \\ T_m^{22} &= -\frac{1 - \nu}{R} - \frac{2k}{r_m - is_m} \end{cases}$$

and

$$r_m = \frac{(H_m^{(1)})'(kR)}{H_m^{(1)}(kR)}, \quad s_m = \frac{(H_m^{(1)})'(ikR)}{H_m^{(1)}(ikR)}.$$

Step 3 consists in proving with a variational approach that the problem (3) is of Fredholm type, which relies on a sign analysis of the real part of matrices T_m for large $|m|$. Hence uniqueness implies existence. We conclude that problem (3) is well-posed, as well as (1).

3 Uniqueness

Let us give some insights into the uniqueness proof. We set $u^i = 0$ in (1) and $u = v^s$. We first

eliminate the propagating part V (see Remark 2) of u . Since u satisfies the radiation condition, we can prove that when $r \rightarrow +\infty$,

$$\|Nu - ik^3 u\|_{L^2(\partial B_r)} + \|Mu - ik\partial_n u\|_{L^2(\partial B_r)} \rightarrow 0.$$

By multiplying the first equation of (1) by \bar{u} and using an adapted Green formula in Ω_r we obtain

$$\text{Im} \left\{ \int_{\partial B_r} (Nu^s \bar{u} + Mu \partial_n \bar{u}) ds \right\} = 0.$$

The two above ingredients imply that

$$\lim_{r \rightarrow +\infty} \{ \|u\|_{L^2(\partial B_r)} + \|\partial_n u\|_{L^2(\partial B_r)} \} = 0. \quad (4)$$

We can prove that $\|U\|_{L^2(\partial B_r)} \rightarrow 0$ when $r \rightarrow +\infty$, which implies the same property for $V = U - 2k^2 u$. By the Rellich theorem for Helmholtz equation, we obtain that $V = \Delta u - k^2 u = 0$ in Ω . We have now to eliminate the evanescent part U of u . For boundary conditions 1, 2 and 3, we have either $u = 0$ or $\partial_n u = 0$ on $\partial\Omega$, which by reusing (4) implies that $u = 0$ in Ω , which completes the proof. Case 4 is more complicated. We introduce the following coupled system on the boundary $\partial\Omega$: for $\lambda > 0$, find $(\mathcal{U}, \mathcal{V}) \in H^1(\partial\Omega) \times H^1(\partial\Omega)$ such that

$$\begin{cases} \frac{d^2 \mathcal{U}}{ds^2} + \gamma \mathcal{V} - \lambda \mathcal{U} = 0, \\ \frac{d^2 \mathcal{V}}{ds^2} - \frac{d}{ds} \left(\gamma \frac{d\mathcal{U}}{ds} \right) + \lambda \mathcal{V} = 0, \end{cases} \quad (5)$$

where γ is the curvature. We obtain that the traces functions $\mathcal{U} = u|_{\Omega}$ and $\mathcal{V} = \partial_n u|_{\partial\Omega}$ satisfy problem (5) with $\lambda = k^2/(1 - \nu)$. By using a well-designed sequence (λ_m) of λ such that $\lambda_m \rightarrow +\infty$, we obtain there exists $\lambda > 0$ such that if $(\mathcal{U}, \mathcal{V}) \in H^1(\partial\Omega) \times H^1(\partial\Omega)$ satisfies the system (5) associated with λ , then $(\mathcal{U}, \mathcal{V}) = 0$. The Fredholm analytic Theorem then enables us to conclude.

Remark 3 In addition, in case 4 we prove that for convex obstacles D , uniqueness holds for any sufficiently large k (for any k if D is a disk).

References

- [1] T. Tyni and V. Serov, Scattering problems for perturbations of the multidimensional biharmonic problem, *Inverse Problems and Imaging* **12-1** (2018), pp. 205–227.
- [2] C. Hazard and M. Lenoir, Determination of scattering frequencies for an elastic floating body, *SIAM J. Math. Anal.* **24-6** (1993), pp. 1458–1514.

The Linear Sampling Method applied to Kirchhoff-Love infinite plates

Arnaud Recoquilly^{1,*}, Laurent Bourgeois²

¹CEA LIST, Gif-sur-Yvette, France

²Laboratoire POEMS ENSTA ParisTech, 828 boulevard des Maréchaux, 91120 Palaiseau, France

*Email: arnaud.recoquilly@cea.fr

Abstract

Previous works [1] showed the possibility to apply sampling methods such as the Linear Sampling Method [2] to image thick plates. In particular, images of real defects in plates were obtained when considering the plate as a 2D waveguide, that is considering it to be invariant according to one direction. The objective of this talk is to present the adaptation of the Linear Sampling Method to the case of infinite thin elastic plates, for which the wave propagation can be modeled thanks to the Kirchhoff-Love model in 2D, neglecting the plate's thickness. This method is applied to numerical data computed using a Finite Element Method coupled with a transparent boundary condition.

Keywords: inverse scattering, Linear Sampling Method, thin plate, Kirchhoff-Love model

1 Forward problem

In this talk, only impenetrable obstacles are considered. Let $D \subset \mathbb{R}^2$ be a bounded open domain of class C^3 , characterized either by a Dirichlet or a Neumann boundary condition, and $\Omega = \mathbb{R}^2 \setminus \bar{D}$. The considered forward problem is then: find $v^s \in H_{loc}^2(\Omega)$ such that

$$\begin{cases} \Delta^2 v^s - k^4 v^s = 0 & \text{in } \Omega \\ B_1(v^s + u^i) = B_2(v^s + u^i) = 0 & \text{on } \partial D \\ \lim_{r \rightarrow +\infty} \int_{\partial B_r} |\partial_n v^s - ikv^s|^2 ds = 0, \end{cases} \quad (1)$$

where $k > 0$ is the wave number, B_r is the open ball centered at 0 and of radius r , n is the outward unit normal to B_r and s is the measure on ∂B_r , whereas u^i is an incident field satisfying $\Delta^2 u^i - k^4 u^i = 0$ in a neighborhood of D . As for the surface boundary operators B_1 and B_2 , they satisfy either $(B_1, B_2) = (I, \partial_n)$ for the Dirichlet boundary condition or $(B_1, B_2) = (M, N)$ for the Neumann boundary condition, M and N being respectively the bending moment and the shear force, defined in [3]. It is shown in [3] that

Theorem 1 *The problem 1 has a unique solu-*

tion in $H_{loc}^2(\Omega)$ for any k in the Dirichlet case and except for a set \mathcal{K}_0 formed by a sequence of $k_n > 0$ such that $k_n \rightarrow +\infty$ in the Neumann case.

Consider now the bounded domain $\Omega_R = \Omega \cap B_R$, where $R > 0$ is such that B_R contains \bar{D} . Then, the problem (1) is equivalent to: find $u^s \in H^2(\Omega_R)$ such that

$$\begin{cases} \Delta^2 u^s - k^4 u^s = 0 & \text{in } \Omega_R \\ B_1(u^s + u^i) = B_2(u^s + u^i) = 0 & \text{on } \partial D \\ \begin{pmatrix} Nu^s \\ Mu^s \end{pmatrix} = T \begin{pmatrix} u^s|_{\partial B_R} \\ \partial_n u^s|_{\partial B_R} \end{pmatrix} & \text{on } \partial B_R, \end{cases} \quad (2)$$

with $T : H^{3/2}(\partial B_R) \times H^{1/2}(\partial B_R) \rightarrow H^{-3/2}(\partial B_I) \times H^{-1/2}(\partial B_R)$ a Dirichlet-to-Neumann operator defined as follows: assume that $(f, g) \in H^{3/2}(\partial B) \times H^{1/2}(\partial B_R)$ can be decomposed as

$$(f, g) = \sum_{m \in \mathbb{Z}} (f_m, g_m) \xi_m, \quad \xi_m(\theta) = e^{im\theta},$$

then

$$T \begin{pmatrix} f \\ g \end{pmatrix} = \sum_{m \in \mathbb{Z}} T_m \begin{pmatrix} f_m \\ g_m \end{pmatrix} \xi_m, \quad T_m = \begin{pmatrix} T_m^{11} & T_m^{12} \\ T_m^{12} & T_m^{22} \end{pmatrix}$$

with

$$\begin{cases} T_m^{11} = -(1 - \nu) \frac{m^2}{R^3} - 2ik^3 \frac{r_m s_m}{r_m - is_m} \\ T_m^{12} = (1 - \nu) \frac{m^2}{R^2} + k^2 \frac{r_m + is_m}{r_m - is_m} \\ T_m^{22} = -\frac{1 - \nu}{R} - \frac{2k}{r_m - is_m} \end{cases}$$

$$\text{and } r_m = \frac{H_m^{(1)'}(kr)}{H_m^{(1)}(kr)}, \quad s_m = \frac{H_m^{(1)'}(ikR)}{H_m^{(1)}(ikR)},$$

where $H_m^{(1)}$ is the Hankel function of the first kind and order m .

It is then possible to compute artificial data discretizing (2) with nonconforming finite elements such as the Morley finite element and truncating the series $(T_m)_{m \in \mathbb{Z}}$.

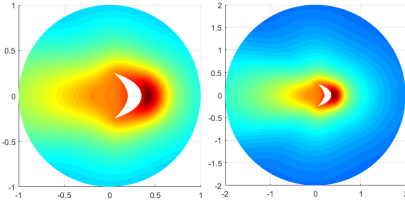


Figure 1: Computed scattered field for two values of R (same color scale)

2 Inverse problem

Let $G(\cdot, y)$ be the fundamental solution, which satisfies

$$\begin{cases} \Delta^2 G(\cdot, y) - k^4 G(\cdot, y) = \delta_y \text{ in } \mathbb{R}^2 \\ \lim_{r \rightarrow +\infty} \int_{\partial B_r} |\partial_n G(\cdot, y) - ikG(\cdot, y)|^2 ds = 0, \end{cases}$$

and is given by

$$G(x, y) = \frac{i}{8k^2} (H_0^{(1)}(k|x-y|) - H_0^{(1)}(ik|x-y|)).$$

Suppose that sources and receivers are placed all over ∂B_R . Then, let $u^s(\cdot, y)$ denote the scattered field associated to $u^i = G(\cdot, y)$ through (1) and $\tilde{u}^s(\cdot, y)$ denote the one associated to $u^i = \partial_{n_y} G(\cdot, y)$, where n_y is the outward unit normal to B_R at y . The assumption is made that, for all $y \in \partial B_R$, $u^s(\cdot, y)$ and $\tilde{u}^s(\cdot, y)$ as well as their normal derivatives are measured at all $x \in \partial B_R$. The objective of the Linear Sampling Method is to recover the obstacle D from these data. To do so, let $N : L^2(\partial B_R)^2 \rightarrow L^2(\partial B_R)^2$ be the near-field operator:

$$N \begin{pmatrix} h \\ t \end{pmatrix} = \begin{pmatrix} \int_{\partial B_R} u^s(\cdot, y) h(y) + \tilde{u}^s(\cdot, y) t(y) ds(y) \\ \partial_n \int_{\partial B_R} u^s(\cdot, y) h(y) + \tilde{u}^s(\cdot, y) t(y) ds(y) \end{pmatrix}.$$

Theorem 2 *Let \mathcal{K} be either the union of \mathcal{K}_0 and the set of the fourth roots of the Neumann eigenvalues of operator Δ^2 in D , or the fourth roots of the Dirichlet eigenvalues of Δ^2 in D . Assume that $k \notin \mathcal{K}$, for some $z \in \mathbb{R}^2$, we have*

$$\text{if } \begin{pmatrix} G(\cdot, z) \\ \partial_n G(\cdot, z) \end{pmatrix} \in \text{Range}(N), \text{ then } z \in D.$$

The converse statement is false in general, but a weaker statement exists: assume that $k \notin \mathcal{K}$, if

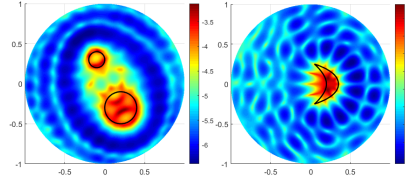


Figure 2: Reconstruction of a Dirichlet (left) and a Neumann (right) obstacle.

$z \in D$, then for all $\varepsilon > 0$ there exists a solution $(h_\varepsilon(\cdot, z), t_\varepsilon(\cdot, z))$ of the inequality

$$\left\| N \begin{pmatrix} h_\varepsilon(\cdot, z) \\ t_\varepsilon(\cdot, z) \end{pmatrix} - \begin{pmatrix} G(\cdot, z) \\ \partial_n G(\cdot, z) \end{pmatrix} \right\|_{L^2(\partial B_R)^2} \leq \varepsilon,$$

such that, for a given fixed ε , it satisfies

$$\lim_{z \rightarrow \partial D} \|(h_\varepsilon(\cdot, z), t_\varepsilon(\cdot, z))\|_{L^2(\partial B_R)^2} = +\infty.$$

The justification of the Linear Sampling Method uses the same arguments as for the Helmholtz case, a special attention being given to the considered functional spaces. In view of theorem 2, the following near-field equation is introduced:

$$N \begin{pmatrix} h \\ t \end{pmatrix} = \begin{pmatrix} G(\cdot, z) \\ \partial_n G(\cdot, z) \end{pmatrix}. \quad (3)$$

As the near-field operator N is compact, (3) is ill-posed and needs to be solved in the sense of Tikhonov. Plotting the inverse of the norm of the solution allows to image the defect, as shown figure 2 on artificial data, as this norm goes to infinity outside of the obstacle.

References

- [1] V. Baronian, L. Bourgeois, B. Chapuis and A. Recoquillay: Linear Sampling Method applied to Non Destructive Testing of an elastic waveguide: theory, numerics and experiments, in *Inverse Problems* **34** (2018)
- [2] D. Colton and A. Kirsch: A simple method for solving inverse scattering problems in the resonance region, in *Inverse Problems* **12** (1996) pp. 383-393.
- [3] L. Bourgeois and C. Hazard: On well-posedness of scattering problems in a Kirchhoff-Love infinite plate, in *Abstracts of WAVES 2019*

Crack monitoring using transmission eigenvalues with artificial backgrounds

Lorenzo Audibert¹, Lucas Chesnel², Houssem Haddar², Kevissh Napal^{2,*}

¹Prisme, EDF R&D, Chatou, France

²CMAP, École Polytechnique, Palaiseau, France

*Email: kevissh.napal@polytechnique.edu

Abstract

We propose a new method to localize cracks from far field data based on Transmission Eigenvalues (TEs) associated with a carefully chosen artificial background. It relies on scanning the probed domain with a fictitious inclusion and exploits the fact that TEs change only if the inclusion intersects the cracks. We explain how these TEs can be identified from measured far field data and validate our procedure in the case of extended cracks. The method also allows for the detection and quantification of small cracks aggregates.

Keywords: inverse scattering, crack monitoring, transmission eigenvalues.

1 Introduction

In this work, we are interested in the problem of identifying cracks embedded in some homogeneous background from far field data at multiple frequencies. We rely on the notion of Transmission Eigenvalues. For the considered inverse problem, TEs were usually presented as the frequencies one should avoid to guarantee the success of some inversion methods such as the Linear Sampling Method or the Factorization Method. Several recent works have tried to use TEs to recover quantitative information on the material properties of probed domains. In this approach, the difficulty lies in the fact that the link between TEs and the physical parameters is not straightforward. To bypass this problem, it has been proposed in the literature to work with a modified far field operator constructed from an artificial background and for which the corresponding TEs have a more direct connection to the physical parameters [1]. We shall exploit this idea for the imaging problem related to cracks. Let us recall that because the cracks have empty interior, one cannot define usual TEs if the background is homogeneous. Working with a non homogeneous artificial background, for instance containing an obstacle, we show that we can define new TEs whose values depend on the relative positions between the crack and the artificial obstacle. The numerical procedure is then as follows. First, we subtract to the measured far field F

numerically computed far field F^{num} corresponding to an artificial sound-soft obstacle located in some arbitrary domain Ω and we set $F^{rel} := F - F^{num}$. The TEs associated with the relative far field operator F^{rel} are then defined as the frequencies such that there are generalized incident fields that have the same far field both for the true reference medium and for the artificial one. In absence of crack in Ω , these TEs are simply the Dirichlet eigenvalues of Ω , otherwise they are different. These TEs can be evaluated from F^{rel} using the framework of generalized linear sampling method. Varying the position of Ω , and comparing the TEs with the Dirichlet eigenvalues of Ω , one is able to identify the cracks position. In the case of small cracks aggregates, one obtains an indicator function on the cracks density.

2 The forward scattering problem

We start by presenting the scattering problem for a crack embedded in a homogeneous medium. Let $\Gamma \subset \mathbb{R}^3$ be a portion of a non-intersecting surface that encloses a domain with smooth boundary. The scattering of the plane wave $u_i(\theta, x) := e^{ik\theta \cdot x}$ of incident direction $\theta \in \mathbb{S}^2 := \{\theta \in \mathbb{R}^3 \mid |\theta| = 1\}$ by Γ leads us to consider the problem

$$\begin{cases} \text{Find } u = u_t + u_s \text{ such that} \\ \Delta u + k^2 u = 0 & \text{in } \mathbb{R}^3 \setminus \Gamma \\ \sigma(u) = 0 & \text{on } \Gamma \\ \lim_{|x| \rightarrow +\infty} |x|(\partial_{|x|} u_s - iku_s) = 0. \end{cases} \quad (1)$$

Here $\sigma(u)$ is a generic boundary condition (Neumann, Dirichlet, ...) and $k > 0$ is the wave number. Moreover, the last line of (1) corresponds to the Sommerfeld radiation condition. The scattered field $u_s(\theta, x)$ has the expansion

$$u_s(\theta, x) = e^{ik|x||x|^{-1}} (u_s^\infty(\theta, \hat{x}) + O(1/|x|)) \quad (2)$$

as $|x| \rightarrow +\infty$, uniformly in $\hat{x} = x/|x|$, where $u_s^\infty(\theta, \hat{x}) \in \mathbb{C}$ is the far field pattern in the direction \hat{x} . The inverse problem we consider consists in reconstructing Γ from the knowledge of $u_s^\infty(\cdot, \cdot) : \mathbb{S}^2 \times \mathbb{S}^2 \rightarrow \mathbb{C}$. We define the far field operator $F : L^2(\mathbb{S}^2) \rightarrow L^2(\mathbb{S}^2)$

such that

$$(Fg)(\hat{x}) = \int_{\mathbb{S}^2} g(\theta) u_s^\infty(\theta, \hat{x}) ds(\theta). \quad (3)$$

By linearity of (1), Fg is nothing but the far field pattern of the scattered field associated with the incident field $u_i(g) := \int_{\mathbb{S}^2} g(\theta) e^{ik\theta \cdot x} ds(\theta)$ (Herglotz wave function), with $g \in L^2(\mathbb{S}^2)$.

3 The relative far field operator

Let Ω be an arbitrary bounded domain of \mathbb{R}^3 . Introduce $F^{\text{num}} : L^2(\mathbb{S}^2) \rightarrow L^2(\mathbb{S}^2)$ the far field operator defined as F in (3) replacing u_s by \tilde{u}_s , \tilde{u}_s being the solution of the exterior Dirichlet problem

$$\begin{cases} \Delta \tilde{u}_s + k^2 \tilde{u}_s = 0 & \text{in } \mathbb{R}^3 \setminus \Omega \\ \tilde{u}_s + u_i = 0 & \text{on } \partial\Omega \\ \lim_{|x| \rightarrow +\infty} |x|(\partial_{|x|} \tilde{u}_s - ik\tilde{u}_s) = 0. \end{cases} \quad (4)$$

Note that F^{num} does not depend on the data and can be computed numerically. Finally, we define the relative far field operator

$$F^{\text{rel}} := F - F^{\text{num}}.$$

One can show that F^{rel} admits a factorization $F^{\text{rel}} = G^{\text{rel}} H^{\text{rel}}$ for certain operators $G^{\text{rel}}, H^{\text{rel}}$ that we do not explicit here. The TE are then defined as the values of $k > 0$ such that F^{rel} has a non trivial kernel. Using the Rellich lemma, one can prove the following characterization.

Theorem 1 *TEs coincide with the $k > 0$ such that there is a non trivial $w \in H^1(\Omega \setminus \Gamma)$ solving*

$$\begin{cases} \Delta w + k^2 w = 0 & \text{in } \Omega \setminus \Gamma \\ w = 0 & \text{on } \partial\Omega \\ \sigma(w) = 0 & \text{on } \Gamma \cap \Omega. \end{cases} \quad (5)$$

From this proposition, we observe that when $\Gamma \cap \Omega = \emptyset$, the TEs are nothing but the eigenvalues of the Dirichlet laplacian in Ω . In the next section, we will explain how to compute TEs from F . Hence scanning the probed domain with different Ω , one can identify the cracks using TEs. In the particular case of sound-hard cracks, i.e. when $\sigma(w) = \partial_\nu w$, ν being a unit normal vector to Γ , the spectrum of (5) consists of real positive eigenvalues $0 \leq \tau_1^j \leq \tau_2^j \leq \dots$ satisfying the following min-max principle:

$$\tau_j^\Gamma = \min_{W \in \mathcal{W}_j^\Gamma} \max_{w \in W \setminus \{0\}} \frac{\|\nabla w\|_{L^2(\Omega \setminus \Gamma)}^2}{\|w\|_{L^2(\Omega \setminus \Gamma)}^2}, \quad (6)$$

where \mathcal{W}_j^Γ denotes the sets of j -dimensional subspaces of

$$V^\Gamma := \{v \in H^1(\Omega \setminus \Gamma) | v = 0 \text{ on } \partial\Omega\}.$$

Consequently, given two cracks $\Gamma_1 \subset \Gamma_2 \subset \Omega$, since $V^{\Gamma_1} \subset V^{\Gamma_2}$, we obtain that $\tau_j^{\Gamma_1} \geq \tau_j^{\Gamma_2}$ for all $j \in \mathbb{N}$. This monotonicity result, which also holds in the case of sound-soft cracks, allow us to quantify crack densities in Ω .

4 Imaging with TE's computed from far field data

The computation of TEs exploits the behaviour of the solution $g \in L^2(\mathbb{S}^2)$ of the far field equation $F^{\text{rel}} g \in \Phi_z^\infty$, where Φ_z^∞ is the far field of the fundamental solution Φ_z of the Helmholtz equation (with a Dirac source term at $z \in \mathbb{R}^3$). To state our result, we define the cost function such that, for $\alpha > 0$, $g \in L^2(\mathbb{S}^2)$,

$$J_\alpha(g) = \alpha P(g) + \|F^{\text{rel}} g - \Phi_z^\infty\|_{L^2(\mathbb{S}^2)}, \quad (7)$$

with the penalty term $P(g) = |\langle F^{\text{num}} g, g \rangle| + |\langle Fg, g \rangle|$. Let g_z^α be a minimizing sequence of J_α .

Theorem 2 *Assume that k is such that $F^{\text{rel}} : L^2(\mathbb{S}^2) \rightarrow L^2(\mathbb{S}^2)$ has dense range. Then k^2 is an eigenvalue of (5) if and only if the set of point z for which $P(g)$ is bounded as $\alpha \rightarrow 0$ is nowhere dense in Ω .*

As a consequence, the eigenvalues τ_j^Γ coincide with the peaks in the curve $k \mapsto \int_\Omega P(g_z^\alpha) dz$ for small values of α . In Figure 1, we provide a numerical result in 2D. We identify a sound-hard crack by working with a collection of artificial backgrounds with sound-soft disks. For each disk, the distance between TEs and Dirichlet eigenvalues is materialized by the contrast in the red colour. Note that when the radius of the disks tends to zero, the Dirichlet eigenvalues blow up. Therefore, to obtain a thin resolution, it is necessary to work at high frequencies with a k large band.

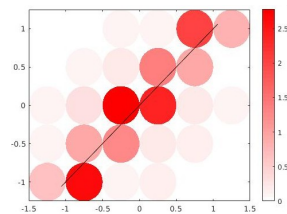


Figure 1: Detection of a sound-hard crack using TEs for artificial backgrounds with sound-soft disks.

References

- [1] L. Audibert, L. Chesnel, H. Haddar, Transmission eigenvalues with artificial background for explicit index identification, *C. R. Acad. Sci. Paris, Ser. I*, vol. 356, 6:626-631, 2018.

Near-Field Inverse Dipole Problems in Spherical Media

Nikolaos L. Tsitsas¹¹School of Informatics, Aristotle University of Thessaloniki, Thessaloniki, Greece, ntsitsas@csd.auth.gr**Abstract**

A homogeneous dielectric spherical medium excited by an internal point-dipole is utilized as a simplified benchmark model in different application domains, like e.g. medical imaging. In this work, we investigate the electromagnetic inverse source problem of the determination of the internal dipole's characteristics by using near-field measurements on the boundary of the medium. We describe a simple analytic inverse algorithm.

Keywords: electromagnetic scattering, inverse source problem, internal dipole

1 Introduction

Excitation of a spherical medium by an internal dipole constitutes a simplified realistic model for applications in medical imaging [1]. For example, in electroencephalography (EEG) the brain's spontaneous primary electrical activity is determined by means of measurements from multiple electrodes placed on the scalp [2]. Mathematical techniques for the study of brain imaging applications involving point dipoles inside spheres are overviewed in [3].

The mathematical modeling of such applications requires the formulation and solution of a near-field inverse source problem. In the context of acoustic scattering, inversion algorithms for determining the characteristics of an acoustic point-source or point-dipole, radiating inside a homogeneous sphere were developed in [4].

The purpose of the present work concerns the investigation of the pertinent electromagnetic boundary-value-problem corresponding to the excitation of a homogeneous dielectric spherical medium by an internal dipole. The location and moment of the dipole are determined analytically by using a set of measurements on the boundary of the medium. In particular, the developed algorithm exploits the information from the moments, obtained by integrating on the unit sphere the inner products of the total tangential electric field on the medium's spherical interface with the vector spherical harmonic functions.

2 Description of the Scattering Problem and Boundary Data

Consider a homogeneous spherical medium of radius a , dielectric permittivity ϵ_1 and magnetic permeability μ_1 . The sphere's exterior is assumed homogeneous with permittivity ϵ_0 and permeability μ_0 . The medium is excited by an arbitrary internal electric dipole with polarization $\mathbf{p} \in \mathbb{R}^3$ and located at $\mathbf{r}_1 = (r_1, \theta_1, \phi_1)$ (with $0 \leq r_1 < a$). The total electric field in the exterior of the spherical medium is expressed as the double series of the vector wave functions [under $\exp(-i\omega t)$ time dependence] [5]

$$\begin{aligned} \mathbf{E}^0(\mathbf{r}; \mathbf{r}_1, \mathbf{p}) = & A \sum_{n=1}^{\infty} \sum_{m=0}^n \sum_{\sigma=e,o} \frac{2n+1}{n(n+1)} \epsilon_m \\ & \frac{(n-m)!}{(n+m)!} \left[\alpha_n \mathbf{M}_{\sigma mn}^3(\mathbf{r}, k_0) (\mathbf{M}_{\sigma mn}^1(\mathbf{r}_1, k_1) \cdot \mathbf{p}) \right. \\ & \left. + \gamma_n \mathbf{N}_{\sigma mn}^3(\mathbf{r}, k_0) (\mathbf{N}_{\sigma mn}^1(\mathbf{r}_1, k_1) \cdot \mathbf{p}) \right], \quad r > a, \end{aligned} \quad (1)$$

where the field coefficients α_n and γ_n are given by (31) of [5], while $A = -\frac{\omega \mu_0 k_1}{4\pi}$.

The total surface electric field \mathbf{E}^{surf} , i.e. the total field \mathbf{E}^0 on the boundary $r = a$ of the spherical medium, is decomposed into its normal and tangential components, as

$$\begin{aligned} \mathbf{E}^{\text{surf}}(\theta, \phi; \mathbf{r}_1, \mathbf{p}) = & E_r^{\text{surf}}(\theta, \phi; \mathbf{r}_1, \mathbf{p}) \hat{\mathbf{r}} \\ & + \mathbf{E}_t^{\text{surf}}(\theta, \phi; \mathbf{r}_1, \mathbf{p}). \end{aligned} \quad (2)$$

We consider, next, the expressions of the spherical vector wave functions in terms of the vector spherical harmonics $\mathbf{B}_{\sigma mn}$ and $\mathbf{C}_{\sigma mn}$ to derive an expression of the tangential component $\mathbf{E}_t^{\text{surf}}$, which is useful in the development of the inverse source algorithm. Precisely, we obtain

$$\begin{aligned} \mathbf{E}_t^{\text{surf}}(\theta, \phi; \mathbf{r}_1, \mathbf{p}) = & A \sum_{n=1}^{\infty} \sum_{m=0}^n \sum_{\sigma=e,o} \frac{2n+1}{\sqrt{n(n+1)}} \epsilon_n \\ & \frac{(n-m)!}{(n+m)!} \left[\tilde{\alpha}_n \mathbf{C}_{\sigma mn}(\theta, \phi) (\mathbf{M}_{\sigma mn}^1(\mathbf{r}_1, k_1) \cdot \mathbf{p}) \right. \\ & \left. + \tilde{\gamma}_n \mathbf{B}_{\sigma mn}(\theta, \phi) (\mathbf{N}_{\sigma mn}^1(\mathbf{r}_1, k_1) \cdot \mathbf{p}) \right], \end{aligned} \quad (3)$$

where $\tilde{\alpha}_n = \alpha_n h_n(k_0 a)$, $\tilde{\gamma}_n = \gamma_n \tilde{h}_n(k_0 a)$, h_n are the n -th order spherical Hankel functions of the first kind, and $\tilde{h}_n(z) = [z h_n(z)]'/z$.

The boundary data of $\mathbf{E}_t^{\text{surf}}$ are exploited to determine the internal dipole's characteristics. Note that the tangential part of the electric field is continuous on $r = a$.

3 Inverse Dipole Algorithm

We consider the moments, obtained by integrating the product of $\mathbf{E}_t^{\text{surf}}$ with the vector spherical harmonic functions. Thus, for $\nu \geq 1$, $\mu = 0, \dots, \nu$ and $s = e, o$, we have

$$Q_{s\mu\nu} = q_\nu \int_{\Omega} \mathbf{E}_t^{\text{surf}}(\theta, \phi; \mathbf{r}_1, \mathbf{p}) \cdot \mathbf{B}_{s\mu\nu}(\theta, \phi) d\Omega, \quad (4)$$

$$R_{s\mu\nu} = r_\nu \int_{\Omega} \mathbf{E}_t^{\text{surf}}(\theta, \phi; \mathbf{r}_1, \mathbf{p}) \cdot \mathbf{C}_{s\mu\nu}(\theta, \phi) d\Omega, \quad (5)$$

where Ω is the unit sphere, and the quantities

$$q_\nu = \frac{\sqrt{\nu(\nu+1)}}{4\pi A \tilde{\gamma}_\nu}, \quad (6)$$

$$r_\nu = \frac{\sqrt{\nu(\nu+1)}}{4\pi A \tilde{\alpha}_\nu} \quad (7)$$

are known (for known parameters of the sphere).

Now, by using the known orthogonality properties of the vector spherical harmonic functions, we get from (4) and (5) that

$$Q_{s\mu\nu} = \mathbf{N}_{s\mu\nu}^1(\mathbf{r}_1, k_1) \cdot \mathbf{p}, \quad (8)$$

$$R_{s\mu\nu} = \mathbf{M}_{s\mu\nu}^1(\mathbf{r}_1, k_1) \cdot \mathbf{p}. \quad (9)$$

We seek to determine the six unknowns of the inverse dipole problem, namely the components of the position vector $\mathbf{r}_1 = (r_1, \theta_1, \phi_1)$ and the polarization vector $\mathbf{p} = (p_x, p_y, p_z)$ of the internal dipole. To this end, we combine the results obtained from (8) and (9) for different moments (i.e. for different values of μ and ν). Particularly, we use R_{e01} , R_{e02} , R_{e03} and R_{e04} as well as the recurrence relation of the spherical Bessel functions

$$j_{n-1}(z) + j_{n+1}(z) = \frac{2n+1}{z} j_n(z), \quad (10)$$

to get

$$\frac{1}{k_1 r_1 \cos \theta_1} + \frac{2}{5} \frac{R_{e03}}{1 - 5 \cos^2 \theta_1} = \frac{3}{5} R_{e01}, \quad (11)$$

$$\frac{14}{3} \frac{1}{k_1 r_1} \frac{R_{e03}}{1 - 5 \cos^2 \theta_1} - \frac{4R_{e04}}{3 \cos \theta_1 - 70 \cos^3 \theta_1} = -\frac{1}{3 \cos \theta_1} R_{e02}. \quad (12)$$

The last two equations lead to a third-degree polynomial for $\cos^2 \theta_1$, the coefficients of which are determined explicitly by means of the moments $R_{s\mu\nu}$. Then, the value of θ_1 is uniquely determined by using the expressions for R_{e01} and R_{e02} . The modulus r_1 of the position vector of the dipole is obtained from (11) or (12).

To determine the remaining unknown parameters ϕ_1 , p_x , p_y and p_z , we consider the equations resulting by using the higher-order moments $Q_{s1\nu}$ and $R_{s1\nu}$. Then, two distinct polynomial equations are obtained for $\sin \phi_1$ and $\cos \phi_1$ respectively; thus, ϕ_1 is uniquely determined. Finally, p_x , p_y and p_z are also found analytically.

The explicit forms of the equations leading to the analytic determination of all unknown parameters are not included here due to space limitations, and will be presented in the conference. The treatment of special cases, such as $\cos \theta_1 = 0$ (when (11) and (12) cannot be obtained), will be also analyzed in detail.

References

- [1] J. C. E. Sten, and I. V. Lindell, Electrostatic Image Theory for the Dielectric Sphere with an Internal Source, *Microw. Opt. Technol. Let.* **5** (1992), pp. 597–602.
- [2] H. Ammari, *An Introduction to Mathematics of Emerging Biomedical Imaging*, Springer, 2008.
- [3] G. Dassios and A. S. Fokas, Electromagneto-encephalography for a three-shell model: dipoles and beyond for the spherical geometry, *Inverse Probl.* **25** (2009) 035001.
- [4] N. L. Tsitsas and P. A. Martin, Finding a source inside a sphere, *Inverse Probl.* **28** (2012) 015003.
- [5] P. Prokopiou and N. L. Tsitsas, Electromagnetic Excitation of a Spherical Medium by an Arbitrary Dipole and Related Inverse Problems, *Studies Appl. Math.* **140** (2018) pp. 438–464.

Imaging small dielectric inclusions with polarization data

Patrick Bardsley¹, Maxence Cassier^{2,*}, Fernando Guevara Vasquez³¹Cirrus Logic, Salt Lake City, United States²Aix Marseille Univ, CNRS, Centrale Marseille, Institut Fresnel, Marseille, France³Mathematics Department, University of Utah, Salt Lake City, United States

*Email: maxence.cassier@fresnel.fr

Abstract

We present a method for imaging small dielectric inclusions in a homogeneous medium from polarization measurements. The problem is a generalization of phase-less imaging, with data being the coherency matrix of the electric field at an array of receivers. The data are obtained by illuminating the scatterers with a single point source with known position and polarization. The imaging consists of two steps. First we partially recover “the ideal data”, i.e. when the full scattered field is measured on the array for three independent source polarizations. Second, we use an electromagnetic version of Kirchhoff imaging. We show that for high frequencies, the images we obtain are close to the ones obtained with ideal data. Resolution estimates of the reconstructed quantities and numerical results to illustrate our method are presented. A time domain interpretation of this imaging problem is left to the talk.

Keywords: Polarization imaging, Kirchhoff migration, phaseless imaging, coherency matrix.

1 Introduction and mathematical model

We consider the problem of imaging the position and polarizability tensor of N small dielectric polarizable inclusions in an homogeneous medium (with permeability μ) by using polarization data only. This is a common assumption in optics, where it is easier to measure polarization (a statistical property of light) than the full electrical field. We assume that the medium is probed by a single electric source whose position $\mathbf{x}_s \in \mathbb{R}^3$ is known and dipole moment is $\mathbf{j}'_s(\omega) \in \mathbb{C}^3$ at the frequency ω . Furthermore, the source and the two dimensional array \mathcal{A} of receivers (within the plane $z = 0$) are supposed to be far from the inclusions. To model “white light” we assume its “rescaled dipole moment” $\mathbf{j}_s(\omega) = \mu \omega^2 \mathbf{j}'_s(\omega) \in \mathbb{C}^3$ is given at each frequency by a circular symmetric Gaussian random vector with zero mean $\langle \mathbf{j}_s(\omega) \rangle = 0$. The

covariance of this vector is assumed known and determines the polarization state of the probing wave. It is given as $\mathbf{U}_s \mathbf{J}_s(\omega) \mathbf{U}_s^*$, where $\mathbf{J}_s(\omega)$ is a 2×2 complex positive definite matrix and \mathbf{U}_s is 3×2 unitary matrix whose range $\text{Ran}(\mathbf{U}_s)$ is the cross-range of the source. This corresponds to losing the range component of the source’s polarization in the far field, where the probing wave is close to a plane wave near the inclusions [1].

At each realization, the source emits an incident wave: $\mathbf{E}_i(\mathbf{x}; \omega) = \mathbf{G}(\mathbf{x}, \mathbf{x}_s; \omega) \mathbf{j}_s(\omega)$, where $\mathbf{G}(\mathbf{x}, \mathbf{x}_s; \omega)$ denotes the standard Dyadic Green tensor [4]. As the inclusions are assumed to be small with respect to the wavelength, they can be modelled as a point-like inclusion localized at $\mathbf{y}_n \in \mathbb{R}^3$ whose scattering properties are determined by a polarizability tensor $\alpha'(\mathbf{y}_n; \omega)$ for $n = 1, \dots, N$ that is a 3×3 complex symmetric matrix. We denote by $\alpha(\mathbf{y}_n) = \mu \omega^2 \alpha'(\mathbf{y}_n; \omega)$ “the rescaled polarizability tensor”, assumed here to be frequency independent. The incident wave is then reflected and the resulting scattered field (see [4]) is given under the first Born approximation by: $\mathbf{E}_s(\mathbf{x}; \omega) = \mathbf{\Pi}(\mathbf{x}; \omega) \mathbf{j}_s(\omega)$ with

$$\mathbf{\Pi}(\mathbf{x}; \omega) = \sum_{n=1}^N \mathbf{G}(\mathbf{x}, \mathbf{y}_n; \omega) \alpha(\mathbf{y}_n) \mathbf{G}(\mathbf{y}_n, \mathbf{x}_s; \omega).$$

Finally, one records at each receiver $\mathbf{x}_r \in \mathcal{A}$ the 2×2 coherency matrix:

$$\psi(\mathbf{x}_r; \omega) = \langle [(\mathbf{E}(\mathbf{x}_r; \omega) \mathbf{E}(\mathbf{x}_r; \omega)^\top)]_{1:2, 1:2} \rangle, \quad (1)$$

that encodes the polarization of the total field $\mathbf{E} = \mathbf{E}_i + \mathbf{E}_s$ on \mathcal{A} (where $\langle \cdot \rangle$ is the expectation).

2 Kirchhoff imaging with ideal data

We consider now the case of ideal data, that is when one can measure $\mathbf{\Pi}(\mathbf{x}; \omega)$ for $\mathbf{x} \in \mathcal{A}$ or equivalently the scattered field for three independent source’s dipole moments. We use a matrix-valued electromagnetic version of the Kirchhoff imaging function [3]:

$$\mathcal{I}[\mathbf{\Pi}](\mathbf{y}; \omega) = \int_{\mathcal{A}} d\mathbf{x}_r \overline{\mathbf{G}(\mathbf{x}_r, \mathbf{y}; \omega)} \mathbf{\Pi}(\mathbf{x}_r; \omega) \overline{\mathbf{G}(\mathbf{x}_s, \mathbf{y}; \omega)}$$

We denote by $\mathbf{U}_r = [\mathbf{e}_1, \mathbf{e}_2]$ (where $(\mathbf{e}_1, \mathbf{e}_2, \mathbf{e}_3)$ is the canonical basis of \mathbb{R}^3) the 3×2 unitary matrix whose range is the cross-range of \mathcal{A} . We extract from \mathcal{I} a stable reconstruction [1, 3] of the position \mathbf{y}_n and of the 2×2 block $\tilde{\boldsymbol{\alpha}}_n = \mathbf{U}_r^* \boldsymbol{\alpha}(\mathbf{y}_n) \mathbf{U}_s$ of the polarizability tensor $\boldsymbol{\alpha}(\mathbf{y}_n)$ (up to a complex phase). The other components of $\boldsymbol{\alpha}(\mathbf{y}_n)$ are lost in this regime of propagation. In the Fraunhofer regime [1], resolution estimates for the reconstruction of these two quantities are given (as in acoustics) by the Rayleigh criterion in cross-range and by c/B in range (where the constant c is the wave propagation speed and B the frequency bandwidth of the data $\mathbf{\Pi}(\cdot, \omega)$). Moreover, one shows that

$$\mathcal{I}[\mathbf{\Pi}](\mathbf{y}; \omega) \approx \mathcal{I}[\mathbf{U}_r \tilde{\mathbf{\Pi}} \mathbf{U}_s^*](\mathbf{y}; \omega) \text{ with } \tilde{\mathbf{\Pi}} = \mathbf{U}_r^* \mathbf{\Pi} \mathbf{U}_s.$$

Thus, instead of using $\mathbf{\Pi}$, one can image as well with $\mathbf{U}_r \tilde{\mathbf{\Pi}} \mathbf{U}_s^*$, i.e. the ideal data $\mathbf{\Pi}$ projected on the left on the cross-range of the array and on the right on the cross-range of the source.

3 The Phase-less imaging method

The strategy we use for imaging generalizes the approach for scalar waves of [2]. One first pre-processes the data $\boldsymbol{\psi}(\mathbf{x}_r; \omega)$ to calculate the matrix $p(\boldsymbol{\psi}) = \mathbf{U}_r \tilde{\mathbf{\Pi}} \mathbf{U}_s^* + \text{error terms}$. It consists in particular to partially recover the data $\mathbf{U}_r \tilde{\mathbf{\Pi}} \mathbf{U}_s^*$ by eliminating the contribution of the incident field \mathbf{E}_i in (1). The remaining error terms are antilinear and sesquilinear in $\tilde{\mathbf{\Pi}}$. The key is that these terms do not affect the Kirchhoff images for high frequencies. Indeed, one shows [1] via a stationary phase argument and under mild assumptions on the geometry of the problem that the imaging functions with either $p(\boldsymbol{\psi})$ or $\mathbf{\Pi}$ data are similar, i.e. as $\omega \rightarrow \infty$ we have

$$\mathcal{I}[p(\boldsymbol{\psi})](\mathbf{y}; \omega) = \mathcal{I}[\mathbf{U}_r \tilde{\mathbf{\Pi}} \mathbf{U}_s^*](\mathbf{y}; \omega) + o(1).$$

Our method is illustrated in figure 1 where the medium contains two dipoles located at $\mathbf{y}_1 = (-6, 4, 105)\lambda_0$ and $\mathbf{y}_2 = (7, 4, 105)\lambda_0$ with λ_0 the central wavelength of B . To image the position, we use the Frobenius norm $\|\tilde{\boldsymbol{\alpha}}(\cdot)\|_F$ of the recovered polarizability tensor. To visualize the polarization tensor (up to a complex phase) we visualize $\text{Re } \tilde{\boldsymbol{\alpha}} = 1/2(\tilde{\boldsymbol{\alpha}} + \tilde{\boldsymbol{\alpha}})$ and $\text{Im } \tilde{\boldsymbol{\alpha}} = (1/2i)(\tilde{\boldsymbol{\alpha}} - \tilde{\boldsymbol{\alpha}})$, which are real non-symmetric matrices. We visualize 2×2 real matrices \mathbf{A} with the ellipse $\mathcal{E}(\mathbf{A}) = \{\mathbf{A}\mathbf{v} \mid \|\mathbf{v}\|_2 = 1\}$. To emphasize that the matrices are not symmetric,

we also display the vectors $\sigma_1 \mathbf{v}_1$ and $\sigma_2 \mathbf{v}_2$ as axes, where the σ_j are the singular values and \mathbf{v}_j the right singular vectors of \mathbf{A} .

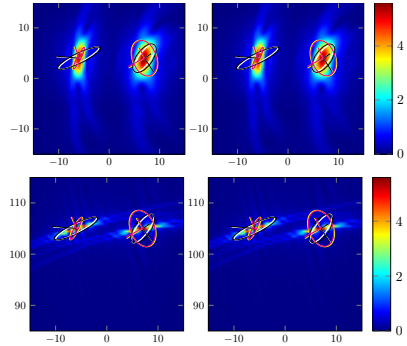


Figure 1: Cross-range (top) and range (bottom) images of $\|\tilde{\boldsymbol{\alpha}}(\cdot)\|_F$. The columns show reconstructions with $\mathbf{\Pi}$ (left) and with $p(\boldsymbol{\psi})$ (right). Here (up to a reference phase [1]) the true tensor $\text{Re } \tilde{\boldsymbol{\alpha}}$ (resp. $\text{Im } \tilde{\boldsymbol{\alpha}}$) is depicted by the white (resp. yellow) ellipses/axes, whereas the recovered tensor is depicted using black (real part) and magenta (imaginary part) ellipses/axes.

This work was partially supported by the National Science Foundation grant DMS-141157. The work of M. C. was supported by Simons Foundation grant #376319 (M. I. Weinstein).

References

- [1] P. Bardsley, M. Cassier and F. Guevara Vasquez, Imaging small polarizable scatterers with polarization data, *Inverse Problems* **34** (10) (2018), pp. 104002.
- [2] P. Bardsley and F. Guevara Vasquez, Kirchhoff migration without phases, *Inverse Problems* **32** (10) (2016), pp. 105006.
- [3] M. Cassier and F. Guevara Vasquez, Imaging polarizable dipoles, *SIAM J. Imaging Sci.* **10** (3) (2017), pp. 1381–1415.
- [4] L. Novotny and B. Hecht, *Principles of nano-optics*, Cambridge univ. press, 2012.

One-Way Operators for Time Dependent Wave Splitting and Echo Removal

Daniel Baffet¹, Marcus J. Grote¹

¹Department of Mathematics and Computer Science, University of Basel, Basel, Switzerland

Abstract

We propose a method for the separation of time-dependent wave fields given measurements of the total wave field. The method is based on classical absorbing boundary conditions (ABC); it is local in space and time, deterministic, makes no prior assumptions on the frequency spectrum and the location of sources or physical boundaries, and can be made arbitrarily accurate.

Keywords: Wave splitting, source separation, echo removal, absorbing boundary conditions, non-reflecting boundary conditions

1 Introduction

For decades absorbing boundary conditions (ABC) have been used to truncate unbounded regions for the simulation of time-dependent wave phenomena [1–3]. Typically, an ABC consists of a linear “one-way” operator, B , which eliminates outgoing waves. By imposing the boundary condition

$$B[u] = 0 \quad (1)$$

at the outer artificial boundary, (unphysical) incoming waves are set to zero while outgoing waves remain unaffected.

Here we show that one-way operators also permit to split and recover individual wave fields, given observations from a time-dependent total wave field, a problem that arises, e.g., in marine seismic exploration [4]. Our approach [5] is local in space and time and does not require deriving any new PDE.

2 Wave splitting

We consider the simple but generic set-up of source separation in free space to present the main idea underlying our approach for wave splitting. Let the total wave field u satisfy the wave equation

$$\frac{\partial^2 u}{\partial t^2} - \Delta u = F(x, y, t) \quad (2)$$

in $\mathbb{R}^2 \times (0, T)$ with homogeneous initial conditions at time $t = 0$. Suppose F is given by

$$F = F_1 + F_2, \quad (3)$$

where each F_1 and F_2 is compactly supported in $\Omega_1 = (-\infty, 0) \times \mathbb{R}$, and $\Omega_2 = (0, \infty) \times \mathbb{R}$, respectively. Then, the wave field u admits the unique (Kirchhoff) decomposition

$$u = u_1 + u_2, \quad (4)$$

where u_1 and u_2 each solve (2) in $\mathbb{R}^2 \times (0, T)$ with $F = F_1$ and $F = F_2$, respectively.

Given the time-dependent total wave field u and its normal derivative $\partial u / \partial n$ on Γ , we wish to recover u_1 and u_2 on Γ for all t . As seen from Γ , u_1 is purely rightward moving whereas u_2 is purely leftward moving; therefore, we may use one-way operators to distinguish between them.

Let B be a one-way operator such that $B[u_2] = 0$ on Γ and the corresponding initial boundary value problem (IBVP) in Ω_2 is well-posed. Applying B to u on Γ then yields

$$B[u_1] = B[u_1] + B[u_2] = B[u]. \quad (5)$$

Provided $B[u]$ can be computed from the measured total field u , (5) yields an equation for u_1 on the interface Γ of Ω_1 and Ω_2 . It is not obvious how to reconstruct u_1 itself from (5), as the equation typically involves normal derivatives of u_1 at Γ . For Γ a circle, (5) can be used to derive a hyperbolic partial differential equation for u_1 , which involves only time and tangential derivatives and thus can be solved on Γ [6].

Instead, we note that $v = u_1$ is the unique solution of the IBVP in $D_\infty = (0, \infty) \times \mathbb{R}$:

$$\frac{\partial^2 v}{\partial t^2} - \Delta v = 0 \quad \text{in } D_\infty \times (0, T) \quad (6a)$$

$$B[v] = g(y, t) \quad \text{on } \Gamma \times (0, T) \quad (6b)$$

$$v(0) = \frac{\partial v}{\partial t}(0) = 0 \quad \text{in } D_\infty, \quad (6c)$$

with $g = B[u]$. Although here D_∞ coincides with Ω_2 , this is not true in general. To recover u_1 , we simply solve numerically the IBVP (6) in D_∞ . For computations, we truncate D_∞ by a perfectly matched layer (PML) in the x direction. In principle, the truncated domain (excluding the PML) can be arbitrarily narrow and even consist only of a fixed number of mesh points in width.

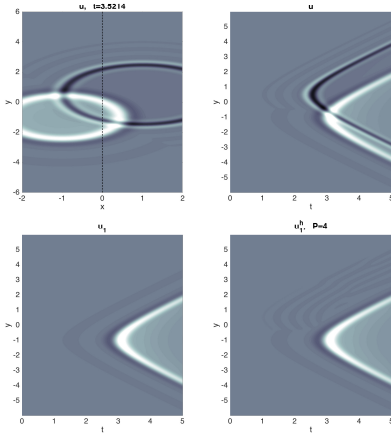


Figure 1: Source separation. Top left: snapshot of u at $t \approx 3.5$; the measurement surface Γ is marked by a dashed line. Top right: the space-time data u on Γ . Bottom left: the reference solution u_1 . Bottom right: the split data u_1^h obtained with $P = 4$.

3 Numerical results

To recover u_1 from u on Γ , we require a one-way operator B that discriminates between incoming and outgoing waves such that the IBVP (6) is well-posed. We consider the high-order ABC by Collino [2, 3] and let B equal the corresponding P -th order one-way operator, which becomes increasingly accurate with increasing P .

The top left frame of Figure 1 shows a snapshot of the total field u , whereas the top right frame shows the space-time data on Γ used for the reconstruction. In particular, we observe the emergence of two space-time cones as the leftward and rightward moving wave fronts cross Γ . The numerical solution, u_1^h , of the IBVP (6) is shown in the bottom right frame and compares remarkably well with the reference solution, u_1 , shown at the bottom left. In fact, u_1 and u_1^h essentially coincide, as shown in the left frame of Figure 2 where we compare their time evolution at a fixed location on Γ . In the right frame of Figure 2, we observe that the relative space-time global error E decays exponentially with the order of the operator P , until it saturates at the level of the discretization error.

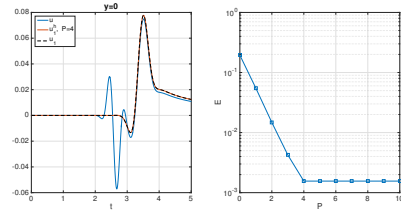


Figure 2: Source separation. Left: the numerical solution u driven by the two sources, the reference solution u_1 and the reconstructed signal u_1^h at $(x, y) = (0, 0)$. Right: the relative global error E as a function of the order P of the operator B .

References

- [1] B. Engquist and A. J. Majda, *Absorbing Boundary Conditions for the Numerical Simulation of Waves*, Math. Comp. **31** (139), pp. 629–651 (1977).
- [2] F. Collino, *High Order Absorbing Boundary Conditions for Wave Propagation Models. Straight Line Boundary and Corner Cases*, Proc. 2nd Int. Conf. on Math. & Num. Aspects of Wave Propagation (1993).
- [3] D. Givoli, *High-Order Local Non-Reflecting Boundary Conditions: A Review*, Wave Motion, 39 (2004), pp. 319-326.
- [4] J. O. A. Robertsson, L. Amundsen, *Wave Equation Processing Using Finite-Difference Propagators, Part 2: Deghosting of Marine Hydrophone Seismic Data*, Geophysics, Vol. 79 (2014), pp. T301–T312.
- [5] D. H. Baffet, M. J. Grote, *On Wave Splitting, Source Separation and Echo Removal with Absorbing Boundary Conditions*, J. Comput. Phys., Vol. 387 (2019), pp. 589–596.
- [6] M. J. Grote, M. Kray, F. Nataf and F. Assous, *Time-Dependent Wave Splitting and Source Separation*, J. Comput. Phys., 330 (2017), pp. 981–996.

How to solve inverse scattering problems without knowing the source term

Marie Graff^{1,*}, Marcus J. Grote², Frédéric Nataf³, Franck Assous⁴¹Department of Mathematics, University of Auckland, Auckland, New Zealand²Department of Mathematics and Computer Science, University of Basel, Basel, Switzerland³Laboratoire Jacques-Louis Lions, UMR 7598, Paris and INRIA Rocquencourt, Alpines, France⁴Department of Mathematics, Ariel University, Ariel, Israel

*Email: marie.graff@auckland.ac.nz

Abstract

Solving inverse scattering problems always presupposes knowledge of the incident wavefield and requires repeated computations of the forward problem, for which knowing the source term is essential. Here we present a three-step strategy to solve inverse scattering problems from total field measurements when the time signature of the source is unknown. The proposed strategy combines three recent techniques: (i) wave splitting to retrieve the incident and the scattered wavefields, (ii) time-reversed absorbing conditions for redatuming the data inside the computational domain, (iii) adaptive eigenspace inversion to solve the inverse problem.

Keywords: Inverse scattering, unknown source, redatuming, wave splitting, time reversal

1 Introduction

When solving inverse scattering problems, optimization techniques always require repeated computations of the forward problem. Therefore the knowledge of the source term is crucial to perform the reconstruction of the unknown parameter. However, some applications such as medical or seismic imaging do not always provide that information. We then need to retrieve it from the measurement data only. By judiciously combining our wave splitting approach [4] with the time-reversed absorbing conditions (*TRAC*) [1], we propose a strategy to recover the incident and the scattered wavefields on an annulus inside the computational domain that encloses the unknown parameter. Finally, we solve the resulting inverse problem, for instance by performing the adaptive eigenspace inversion (AEI) [3].

We consider an unbounded medium with velocity c whose (unknown) local variations determine a scatterer \mathcal{O} . Next, we illuminate the medium with a source f , for which we approxi-

mately know the location but not the time signature, and record the total wave field and its normal derivative on a boundary Γ enclosing both the source and the scatterer. Hence, the total field u satisfies the wave equation

$$\begin{aligned} \partial_{tt}^2 u - c^2 \Delta u &= f, & \text{in } (0, T) \times \Omega, \\ u|_{t=0} &= 0, \quad \partial_t u|_{t=0} &= 0, & \text{in } \Omega. \end{aligned}$$

From the measured data on Γ , we seek to recover the shape, location and properties of the scatterer \mathcal{O} .

2 A three-step strategy

Since the source f is unknown, we reduce the computational domain Ω to an area D_S which encloses the scatterer but does not include the source. Thus, f will not directly affect subsequent solutions of the forward problem in D_S , but only indirectly so through the incident wavefield, still to be determined in the vicinity of D_S .

As we have only recorded the total wavefield u on Γ , we now proceed in two steps to reconstruct the incident wavefield in the vicinity of D_S : First, we split u on Γ into its incident u^I and scattered u^S components; then, we back-propagate the recovered fields u^I and u^S into $\Omega \setminus D_S$ using the *TRAC* method.

The total field u admits the unique decomposition $u = u^I + u^S$. To split u into its individual components, we assume that we know the approximate location of both the source and the scatterer. Let D_I , resp. D_S , denote the circular subdomain enclosing the source, resp. the scatterer. Henceforth, the index K may refer to either I or S . Now, we consider the first order Bayliss-Turkel absorbing boundary condition

$$B_K[u] := \partial_t u + c \partial_{r_K} u + c u / 2r_K \simeq 0 \quad \text{on } \Gamma,$$

where r_K denotes the distance of any point of Γ from the center of D_K . By neglecting higher order terms and by linearity, we get

$$B_K[u] = B_K[u^I] + B_K[u^S] \quad \text{and} \quad B_K[u^K] = 0,$$

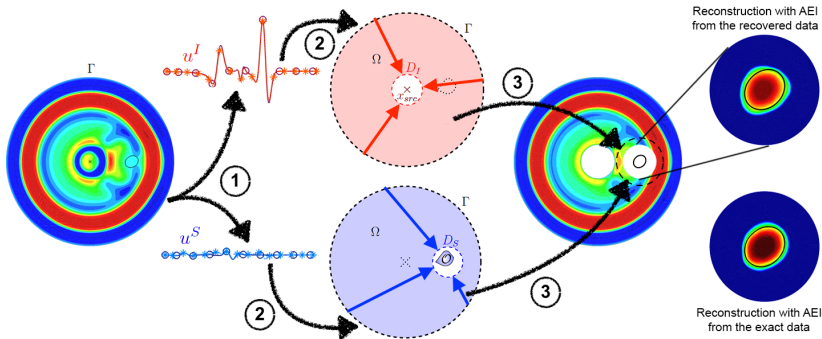


Figure 1: Schematic: (1) Wave splitting to retrieve u^I and u^S from the measurements on the boundary Γ ; (2) reconstruction of u^I and u^S individually from the split data on Γ using the *TRAC* method; (3) recovery of the scatterer in a smaller computational domain D_S from the redatumed $u = u^I + u^S$.

which yields

$$B_S[u^I] = 0 \quad \text{and} \quad B_I[u^S] = 0, \quad \text{on } \Gamma. \quad (1)$$

To solve (1) on Γ , we use the progressive wave expansion to replace normal derivatives by time and tangential derivatives. Then, we recover u^I and u^S on Γ by solving the resulting first-order hyperbolic PDE in time and tangential variables on four disjoint quarter circles – see [4].

Once u^I and u^S have been retrieved on Γ , we reconstruct u^K inside the computational domain $\Omega \setminus D_K$. This second *redatuming* step determines u^I and u^S in the vicinity of D_S – see [1, 3]. Here, we use the *TRAC* method which combines time reversal techniques with a numerical sink to avoid artifacts during the back-propagation of boundary information. Each wavefield u^K , K denoting I or S , thus solves

$$\begin{aligned} \partial_t^2 u_R^K - c^2 \Delta u_R^K &= 0, \quad \text{in } (0, T) \times \Omega \setminus D_K, \\ u_R^K|_{t=0} &= 0, \quad \partial_t u_R^K|_{t=0} = 0, \quad \text{in } \Omega \setminus D_K, \\ u_R^K &= u_R^{K,data}, \quad \text{on } (0, T) \times \Gamma, \\ \text{TRAC}_K[u_R^K] &= 0, \quad \text{on } (0, T) \times \partial D_K, \end{aligned} \quad (2)$$

where TRAC_K denotes the time-reversed B_K and $u_R^{K,data}$ is the time-reversed knowledge of u^K on Γ from wave splitting. To finally get the redatumed total field u in the vicinity of D_S , we sum u^I and u^S in $\Omega \setminus (D_I \cup D_S)$.

3 Numerical results

In Fig. 1, we illustrate our three-step strategy for an elliptic scatterer with a 3:1 contrast in the squared velocity c^2 . Once we have split the total field u and redatumed u^I and u^S using (2), resulting in a relative error of 8.0% in the vicinity of D_S , we solve the inverse problem inside D_S using AEI [3]. The recovered scatterer, shown in Fig. 1, compares remarkably well with that obtained from the exact wave fields u^I and u^S with a relative error of only 6.1%.

References

- [1] F. Assous, M. Kray, F. Nataf and E. Turkel, Time reversed absorbing condition: Application to inverse problems. *Inverse Problems* **27** (2011), pp 065003.
- [2] F. Assous, M. Kray, F. Nataf, Time reversed absorbing condition in the partial aperture case. *Wave Motion* **49** (2012), pp 617-631.
- [3] M. de Buhan and M. Kray, A new approach to solve the inverse scattering problem for waves: combining the *TRAC* and the Adaptive Inversion methods. *Inverse Problems* **29** (2013), pp 085009.
- [4] M. J. Grote, M. Kray, F. Nataf and F. Assous, Time-dependent wave splitting and source separation. *J. Comp. Physics* **330** (2017), pp. 981-996.

**Shape reconstruction of deposits inside a steam generator
using eddy current measurements**

Hugo GIRARDON^{1,*}, Housseem HADDAR², Lorenzo AUDIBERT³

¹INRIA, École Polytechnique (CMAP), Palaiseau, FRANCE

²INRIA, École Polytechnique (CMAP), Palaiseau, FRANCE

³PRISME department, EDF R&D, Chatou, FRANCE

*Email: hugo.girardon@polytechnique.edu

Abstract

Non-destructive testing is an essential tool to assess the safety of the facilities within nuclear plants. In particular, conductive deposits on U-tubes in steam generators constitute a major danger as they may block the cooling loop. To detect these deposits, eddy-current probes are introduced inside the U-tubes to generate currents and measuring back an impedance signal. Based on the work of [3], we develop a shape optimization technique with regularized gradient descent to invert these measurements and recover the deposit shape. To deal with the unknown, and possibly complex, topological nature of the latter, we propose to model it using a level set function as it is introduced in [1].

The methodology is first validated on synthetic axisymmetric configurations and fast convergence is ensured by careful adaptation of the gradient steps and regularization parameters. Using the actual domain, from which the acquisitions are made, we then consider a more realistic modeling that incorporates the support plate and the presence of imperfections on the tube interior section. We employ in particular an asymptotic model to take into account these imperfections and treat them as additional unknowns in our inverse problem. A multi-objective optimization strategy, based on the use of different operating frequencies, is then developed to solve this problem. We shall present various numerical examples with synthetic data showing the viability of our approach.

Keywords: Shape optimization, inverse problems, level set, eddy-current approximation

1 Problem modelling

Consider the 3D Maxwell equations :

$$\begin{cases} \mathbf{curl} \mathbf{H} + (i\omega\varepsilon - \sigma)\mathbf{E} = \mathbf{J} & \text{in } \mathbb{R}^3 \\ \mathbf{curl} \mathbf{E} - i\omega\mu\mathbf{H} = \mathbf{0} & \text{in } \mathbb{R}^3 \end{cases} \quad (1)$$

where the source term \mathbf{J} is supported by the coils. The material parameters σ , ε and ω are such that the **eddy current** approximation : $\sigma \gg \omega\varepsilon$ holds true. The coils inside the tube move along the vertical direction z and collect measurements at different positions.

Our goal is to invert the **impedance signal** measured by the coils varying in a given z interval. The impedance signal represents the difference of the flow of the electromagnetic field $(\mathbf{E}_k, \mathbf{H}_k)$ created by the coil k in presence of deposit and the flow $(\mathbf{E}_l^0, \mathbf{H}_l^0)$ created by the coil l , without deposit. It can be written as :

$$\Delta Z_{kl} = \frac{1}{I^2} \int_{\partial\Omega_d} (\mathbf{E}_l^0 \times \mathbf{H}_k - \mathbf{E}_k \times \mathbf{H}_l^0) \cdot \mathbf{n} \, dS \quad (2)$$

where Ω_d represents the deposit.

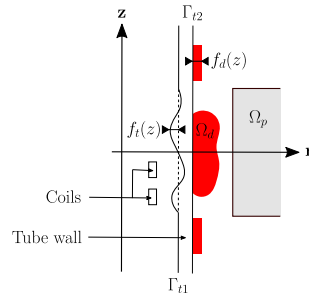


Figure 1: Axisymmetric domain

We here will concentrate on axisymmetric configurations of the domain to validate more easily the algorithm. Under the assumption \mathbf{J} axisymmetric, (1) leads to the following scalar equation verified by the azimuthal component of \mathbf{E}

$$-\operatorname{div} \left(\frac{1}{\mu r} \nabla(rE_\theta) \right) - i\omega\sigma E_\theta = i\omega J_\theta \text{ in } \mathbb{R}_+^2 \quad (3)$$

Where $\nabla := (\partial_r, \partial_z)^t$ and $\text{div} := \nabla \cdot$.

A plate, modeling the supporting grating, made out of a highly conductive ($\sigma_p = 100\sigma_{\text{tube}}$) and magnetic material is added to the domain. It can be replaced by an impedance condition on its boundary since the penetration depth $\delta = 1/\sqrt{i\omega\sigma_p\mu_p} \ll 1$:

$$\frac{1}{\mu} \partial_n(rE_\theta) = \frac{\sqrt{2}}{2\mu_p\delta} (-1 + i)(rE_\theta) \text{ on } \partial\Omega_p \quad (4)$$

Due to uncertainties in the manufacturing of the tube, its thickness is not constant and is modeled by a function $f_t(z)$ as defined in Figure 1. Moreover, thin deposits have been observed outside of the plate area, their thickness is modeled using a function $f_d(z)$. Since these fluctuations are small compared to the deposit and tube thickness, asymptotic models can be used to replace them by a transmission condition at the interface:

$$\frac{1}{\mu_t} \partial_r(rE_\pm) - i\omega\sigma_{t/d} f(z)(rE_\pm) = \frac{1}{\mu_v} \partial_r(rE_\mp) \text{ on } \Gamma_{t1/2}$$

where E_- is the solution on the left of the interface and E_+ on the right.

2 Optimization algorithm

Consider N impedance measurements on a given z interval Z_{mes} . The aim is to find the shape Ω_d^* , the tube thickness variation f_t^* and the thin deposit thickness f_d^* that corresponds to these measurements, considering that impedance signals Z can be computed for any Ω_d , f_t , f_d in some admissible class of regular and bounded parameters. In terms of optimization problem, this can be written as

Find Ω_d^* , f_t^* and f_d^* solution of :

$$\min_{\Omega_d, f_t, f_d} \int_{-z_0}^{z_0} |Z(\Omega_d, f_t, f_d; \zeta) - Z_{\text{mes}}(\zeta)|^2 d\zeta \quad (5)$$

where Z is given for different industrial pulsations ω . A gradient descent simultaneously on the three unknowns that are Ω_d , f_t , and f_d is used to solve (5). The optimization with respect to f_d and f_t is a standard vector optimization after discretizing the functions on the interfaces. The optimization with respect to Ω_d needs the introduction of the notion of shape derivative and the definition of appropriate regularized descent direction with the help of adjoint state. To handle topological changes in the shape, we choose to model it using a *level-*

set functions ψ . For a shape Ω_d , ψ is a function negative inside, zero on the boundary and positive outside Ω_d . This level-set function solves a Hamilton-Jacobi equation with velocity field equals the shape gradient. For the numerical implementation, the mesh for the level-set function is taken independently from the mesh used for the computation of the solution.

3 A numerical example

The 2D axisymmetric eddy current problem is solved with \mathbb{P}^2 finite elements, using the FE-*software FreeFem++*. On Figure 2, we consid-

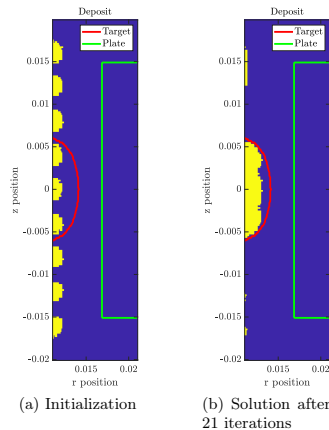


Figure 2: Example of a numerical result

ered a test case with an elliptical deposit on the tube wall (the red line), paired with an elliptical tube thickness variation. The signal to invert is given on 71 coil positions. The reconstruction algorithm is initialized with $f_t \equiv 0$ and the yellow shape on Figure 2a. After 21 iterations, Figure 2b displays in yellow the optimal shape.

References

- [1] G. Allaire, F. De Gournay, F. Jouve, A.-M. Toader, *Journal of Computational Physics* **Vol. 194, Issue 1**, (2004), pp 363-393.
- [2] M. Duruflé, H. Haddar and P. Joly, *Comptes Rendus Physique* **Vol. 7, Issue 5**, (2006), pp 533-542.
- [3] Z. Jiang, PhD thesis, École Polytechnique, 2014.

Essential spectrum generated by a negative material described by the Lorentz model

Christophe Hazard^{1,*}, Sandrine Paolantoni¹

¹POEMS, CNRS / ENSTA Paristech / INRIA, Palaiseau, France

*Email: christophe.hazard@ensta-paristech.fr

Abstract

In [2], we investigated the spectral effects of an interface between vacuum and a negative material described by the non dissipative Drude model. We showed in particular that such an interface is responsible for various resonance phenomena related to various components of an *essential spectrum*. The aim of the present work is to extend these results to the so-called Lorentz model (dissipative or not).

Keywords: metamaterials, spectral theory

1 The spectral problem

We consider here a two-dimensional scalar problem which can be derived from Maxwell’s equations in a cavity which contains an inclusion of negative material (NeM) described by the so-called Lorentz model. As shown in Figure 1, our cavity is represented by a bounded open set $\mathcal{C} \subset \mathbb{R}^2$ and the inclusion by a polygonal domain \mathcal{N} assumed for simplicity such that their respective boundaries $\partial\mathcal{C}$ and $\partial\mathcal{N}$ are disjoint. We denote by $\mathcal{V} := \mathcal{C} \setminus \overline{\mathcal{N}}$ the “vacuum” complementary domain. Our aim is to investigate the following eigenvalue problem:

Find $\omega \in \mathbb{C}$ and $\varphi \in H_0^1(\mathcal{C}) \setminus \{0\}$ such that

$$\operatorname{div} \left(\frac{1}{\kappa_\omega^{\mathcal{C}}} \operatorname{grad} \varphi \right) + \omega^2 \varphi = 0 \quad \text{in } \mathcal{C}, \quad (1)$$

where (1) is understood in the distributional sense and $\kappa_\omega^{\mathcal{C}}$ is a piecewise constant function defined by

$$\kappa_\omega^{\mathcal{C}}(x) = \begin{cases} 1 & \text{if } x \in \mathcal{V}, \\ \kappa_\omega := 1 - \frac{\omega_p^2}{\omega^2 - \omega_r^2 + i\gamma\omega} & \text{if } x \in \mathcal{N}, \end{cases}$$

where the three coefficients $\omega_p > 0$ (plasma frequency), $\omega_r > 0$ (resonance frequency) and $\gamma \geq 0$ (damping factor) characterize the Lorentz material. We see in particular that in the non-dissipative case, i.e., if $\gamma = 0$, then $\kappa_\omega < 0$ when $\omega^2 \in (\omega_r^2, \omega_r^2 + \omega_p^2)$.

Problem (1) is clearly a *nonlinear* eigenvalue problem since κ_ω is a rational function of ω .

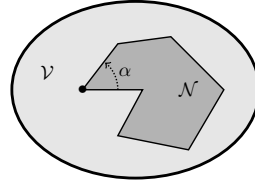


Figure 1: The cavity $\mathcal{C} = \mathcal{V} \cup \overline{\mathcal{N}}$

Thanks to the introduction of auxiliary variables, it can be written equivalently as a *linear* eigenvalue problem. The approach we present here is slightly different from that we propose in [2] for the Drude model, since the latter cannot be extended to the present problem. Denote by $\mathcal{R} : L^2(\mathcal{C}) \rightarrow L^2(\mathcal{N})$ the operator of restriction from \mathcal{C} to \mathcal{N} and by $\mathcal{R}^* : L^2(\mathcal{N}) \rightarrow L^2(\mathcal{C})$ the adjoint operator, that is, the operator of extension by 0 from \mathcal{N} to \mathcal{C} . By setting

$$\begin{aligned} p &:= \omega^{-1} (\kappa_\omega^{\mathcal{C}})^{-1} \operatorname{grad} \varphi, \\ u &:= (1 - \kappa_\omega) \mathcal{R} p, \\ v &:= \omega u, \end{aligned} \quad (2)$$

it is easy to verify that (1) is equivalent to

$$\begin{pmatrix} 0 & -\operatorname{div} & 0 & 0 \\ \operatorname{grad} & 0 & 0 & \mathcal{R}^* \\ 0 & 0 & 0 & 1 \\ 0 & \omega_p^2 \mathcal{R} & \omega_r^2 & -i\gamma \end{pmatrix} \begin{pmatrix} \varphi \\ p \\ u \\ v \end{pmatrix} = \omega \begin{pmatrix} \varphi \\ p \\ u \\ v \end{pmatrix} \quad (3)$$

provided $\omega \neq 0$, $\kappa_\omega \neq 0$ and $\kappa_\omega^{-1} \neq 0$. The block operator matrix of the left-hand side defines an unbounded operator \mathcal{A} in the Hilbert space $\mathcal{H} := L^2(\mathcal{C}) \times L^2(\mathcal{C})^2 \times L^2(\mathcal{N})^2 \times L^2(\mathcal{N})^2$ with domain

$$D(\mathcal{A}) := H_0^1(\mathcal{C}) \times H(\operatorname{div}; \mathcal{C}) \times L^2(\mathcal{N})^2 \times L^2(\mathcal{N})^2.$$

One can prove that if $\gamma = 0$, this operator is selfadjoint provided that \mathcal{H} is equipped with the following inner product, for $X := (\varphi \ p \ u \ v)^\top$ and $X' := (\varphi' \ p' \ u' \ v')^\top$:

$$\begin{aligned} (X, X')_{\mathcal{H}} &:= (\varphi, \varphi')_{\mathcal{C}} + (p, p')_{\mathcal{C}} \\ &\quad + \omega_p^{-2} \omega_r^2 (u, u')_{\mathcal{N}} + \omega_p^{-2} (v, v')_{\mathcal{N}} \end{aligned}$$

where $(\cdot, \cdot)_{\mathcal{C}}$ or $_{\mathcal{N}}$ denotes the usual inner product in $L^2(\mathcal{C})$ or \mathcal{N} .

2 The essential spectrum $\sigma_{\text{ess}}(\mathcal{A})$

We show that contrary to cavities filled by a usual material, negative contrasts κ_ω generate an essential spectrum. As in [2], the idea is to construct Weyl sequences of \mathcal{A} for values of ω which correspond to various sets of critical values of the contrast that are responsible for various resonance phenomena. In our case, the mapping $\omega \mapsto \kappa_\omega$ is easily inverted: noticing that the spectrum of \mathcal{A} is symmetric with respect to the imaginary axis, we restrict ourselves to $\text{Re } \omega \geq 0$ and define, for all $\kappa \in (-\infty, 0)$,

$$\omega_\kappa = \frac{-i\gamma + \sqrt{4(\omega_r^2 + \omega_p^2/(1 - \kappa)) - \gamma^2}}{2}$$

where we assume for simplicity that $\gamma < 2\omega_r$. Recall that a Weyl sequence associated to some $\omega \in \sigma_{\text{ess}}(\mathcal{A})$ is a sequence $(X_n) \in \text{D}(\mathcal{A})^{\mathbb{N}}$ such that $\|X_n\|_{\mathcal{H}} = 1$, $\|(\mathcal{A} - \omega)X_n\|_{\mathcal{H}} \rightarrow 0$ and $X_n \rightharpoonup 0$ in \mathcal{H} (weakly). In the following, we briefly show how to construct such sequences, more precisely the first components $(\varphi_n) \in H_0^1(\mathcal{C})^{\mathbb{N}}$ (the others follows by relations (2)).

(i) Bulk resonance: $\kappa = -\infty$. For the frequency $\omega_{-\infty} := \lim_{\kappa \rightarrow -\infty} \omega_\kappa$, the idea is simply to start from a sequence $(\varphi_n^{\mathcal{N}}) \in H_0^1(\mathcal{N})^{\mathbb{N}}$ of eigenfunctions of the Dirichlet Laplacian in \mathcal{N} , which satisfy $-\Delta \varphi_n^{\mathcal{N}} = \lambda_n \varphi_n^{\mathcal{N}}$ in \mathcal{N} with $\lambda_n \rightarrow +\infty$, and then define $\varphi_n := \mathcal{R}^* \varphi_n^{\mathcal{N}}$. Noticing that $\omega_{-\infty}$ is not an eigenvalue of \mathcal{A} , we infer that it is an accumulation point of eigenvalues of \mathcal{A} , whose associated eigenfunctions are confined in the NeM.

(ii) Surface resonance: $\kappa = -1$. This particular value of κ is known to be a critical value of the contrast which is related to the so-called *plasmonic waves* that are highly oscillating waves propagating at the boundary of a NeM. Weyl sequences for ω_{-1} are searched as plasmonic waves which are more and more localized near a given point of $\partial\mathcal{N}$ (apart from vertices). In the simple case where the NeM fills a half plane, say $x_1 > 0$, it is readily seen that for any $k > 0$, the function $\exp(ik(x_2 + ix_1))$ satisfies equation (1) with $\kappa = -1$ and the term $\omega^2 \varphi$ removed (this term acts as a small perturbation for large wavenumbers k). Any superposition of such surface waves still satisfies the same equation. By choosing proper densities of superposition, one can construct more and more confined surface waves, which yields the expected Weyl sequence using smooth cutoff functions.

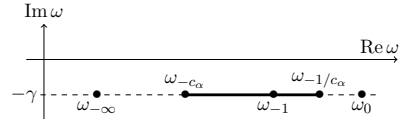


Figure 2: $\sigma_{\text{ess}}(\mathcal{A}) \cap \{\text{Re } \omega \geq 0\}$

(iii) Corner resonance: $\kappa \in K(\alpha)$ with $K(\alpha) :=]-c(\alpha), -1/c(\alpha)[\setminus \{-1\}$ where $c(\alpha) := \max((2\pi/\alpha - 1), (2\pi/\alpha - 1)^{-1})$. Contrary to the latter case, instead of one critical value, each vertex of $\partial\mathcal{N}$ is related to two critical intervals of the contrast depending on the angle α of the vertex (see Figure 1). Indeed, it is shown in [1] that if κ belongs to $K(\alpha)$, then one can construct highly oscillating solutions to (1) with the term $\omega^2 \varphi$ removed, which concentrate near the vertex and can be interpreted as *black hole waves*. Indeed their behavior in polar coordinates (r, θ) centered at the vertex is $r^{i\eta} m(\theta)$ as $r \rightarrow 0$ where $\eta \in \mathbb{R}$ and $m(\theta)$ is the angular modulation, which is L^2 but not H^1 near the vertex. Weyl sequences for the frequency ω_κ associated to some $\kappa \in K(\alpha)$ can be constructed by superpositions of black hole waves of the neighboring frequencies with densities of superposition that tend to a Dirac measure at ω_κ .

The last possible point of $\sigma_{\text{ess}}(\mathcal{A})$ correspond to $\kappa = 0$. Indeed ω_0 appears as an eigenvalue of infinite multiplicity of \mathcal{A} , which is actually an artifact of the augmented formulation (3) that is not representative of a physical phenomenon. To sum up, we have the following theorem, illustrated by Figure 2.

Theorem 1 $\sigma_{\text{ess}}(\mathcal{A})$ is composed of $\omega_0, \omega_{-1}, \omega_{-\infty}$ and, for each corner of $\partial\mathcal{N}$ of angle α , the set $\Omega(\alpha) := \{\omega_\kappa; \kappa \in \overline{K(\alpha)} \setminus \{-1\}\}$, as well as the symmetric of these components with respect to the imaginary axis.

References

- [1] A.-S. Bonnet-Ben Dhia, L. Chesnel and P. Ciarlet Jr., T-coercivity for scalar interface problems between dielectrics and metamaterials, *Math. Mod. Num. Anal.* **46** (2012), pp. 1363–1387.
- [2] C. Hazard and S. Paolantoni, Spectral analysis of polygonal cavities containing a negative-index material, hal-01626868 (2017).

Numerical study of the spectrum of cavities containing a negative-index material

Sandrine Paolantoni^{1,*}, Christophe Hazard¹

¹POEMS, CNRS / ENSTA ParisTech / INRIA, Palaiseau, France

*Email: sandrine.paolantoni@ensta-paristech.fr

Abstract

The purpose of this work is the numerical approximation of the spectrum of a cavity partially filled with a negative-index material (NIM), that is, a dispersive material whose electric permittivity and magnetic permeability become negative in some frequency range. We consider here a simple two-dimensional scalar toy problem (derived from Maxwell's equations) where the NIM is described by a non-dissipative Drude model. In [1], the spectral analysis of this problem highlighted three resonance phenomena associated to an *essential spectrum* of the cavity. We investigate here the numerical simulation of these phenomena.

Keywords: Metamaterials, spectral theory

1 The continuous spectral problem

We first recall some results obtained in [1]. We consider a circular cavity \mathcal{C} , divided into two angular sectors \mathcal{V} and \mathcal{N} defined by an angle $\alpha \in (0, 2\pi)$, as shown in Figure 1. The domains \mathcal{V} and \mathcal{N} respectively contain vacuum and a NIM described by a non dissipative Drude model. This leads us to define two functions $\varepsilon_\lambda(\theta)$ and $\mu_\lambda(\theta)$ of the polar angle $\theta \in (-\pi, \pi]$ by

$$\frac{\varepsilon_\lambda(\theta)}{\varepsilon_0} = 1 - \frac{\Lambda_e}{\lambda} \mathbf{1}_{\mathcal{N}}(\theta) \text{ and } \frac{\mu_\lambda(\theta)}{\mu_0} = 1 - \frac{\Lambda_m}{\lambda} \mathbf{1}_{\mathcal{N}}(\theta),$$

where λ is the square of the frequency, Λ_m and Λ_e are constants linked with the NIM, and $\mathbf{1}_{\mathcal{N}}$ is the indicator function of $(-\alpha/2, \alpha/2)$ (so that $\varepsilon_\lambda(\theta) = \varepsilon_0$ and $\mu_\lambda(\theta) = \mu_0$ if $|\theta| > \alpha/2$).

We consider the following eigenvalue problem : find $\lambda \in \mathbb{C}$ and $\varphi \in H_0^1(\mathcal{C}) \setminus \{0\}$ such that

$$\text{div} \left(\frac{1}{\mu_\lambda} \text{grad} \varphi \right) + \lambda \varepsilon_\lambda \varphi = 0. \quad (1)$$

This problem is clearly non-linear (with respect to λ). It can be linearized by using an ‘‘augmented formulation’’ approach which consists in introducing a new unknown u only defined in \mathcal{N} . We denote by \mathcal{R} the operator of restriction to \mathcal{N} of functions defined on the whole cavity \mathcal{C} and

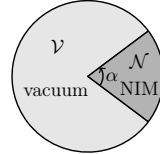


Figure 1: The cavity

by \mathcal{R}^* the operator of extension by 0 in \mathcal{V} of functions defined in \mathcal{N} . It is readily seen that if $\lambda \notin \{0, \Lambda_m\}$, problem (1) is equivalent to find $(\varphi, u) \in H_0^1(\mathcal{C}) \times L^2(\mathcal{N}) \setminus \{(0, 0)\}$ such that

$$\mathbb{A} \begin{pmatrix} \varphi \\ u \end{pmatrix} = \lambda \begin{pmatrix} \varphi \\ u \end{pmatrix} \quad (2)$$

$$\text{with } \mathbb{A} := \begin{pmatrix} -\frac{1}{\varepsilon_0 \mu_0} \Delta + \Lambda_e \mathbf{1}_{\mathcal{N}} & -\frac{1}{\varepsilon_0 \mu_0} \text{div} \mathcal{R}^* \\ \Lambda_m \mathcal{R} \text{grad} & \Lambda_m \end{pmatrix}.$$

In the Hilbert space $\mathcal{H} := L^2(\mathcal{C}) \times L^2(\mathcal{N})^2$ equipped with the inner product

$$((\varphi, u), (\psi, v))_{\mathcal{H}} := \varepsilon_0 \mu_0 \int_{\mathcal{C}} \varphi \bar{\psi} + \frac{1}{\Lambda_m} \int_{\mathcal{N}} u \cdot \bar{v},$$

\mathbb{A} appears as a non-negative self-adjoint operator with domain $D(\mathbb{A}) := \{(\varphi, u) \in H_0^1(\mathcal{C}) \times L^2(\mathcal{N})^2; \text{div}(\text{grad} \varphi + \mathcal{R}^* u) \in L^2(\mathcal{C})\}$.

In [1], we proved that the essential spectrum of \mathbb{A} is composed of 1) $\lambda = 0$, linked with a *bulk resonance* in the NIM (accumulation of eigenvalues), 2) $\lambda = \Lambda_m/2$, associated to a *surface resonance* on the interface between both media, 3) the set $\{\lambda \in \mathbb{R}; |\lambda - \Lambda_m/2| < |1 - \alpha/\pi| \Lambda_m/2\}$ related to a *corner resonance* interpreted as a ‘‘blac hole’’ phenomena, and finally 4) $\lambda = \Lambda_m$, which can be seen as an artifact of the augmented formulation.

2 The numerical spectrum

We show now some numerical results obtained by a Finite Element (FE) discretization of the eigenvalue problem (2). Note that such an approach cannot be justified by theoretical arguments: our aim is to explore the influence of

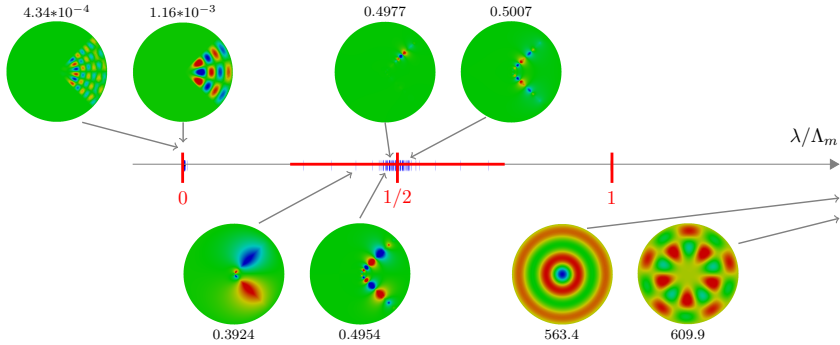


Figure 2: FE discretization of (2). On the horizontal line, red thick lines represent the essential spectrum of \mathbb{A} , whereas blue dashes are the numerical eigenvalues. Above and below are shown the real parts of the eigenvectors associated to some of them (the value of λ/Λ_m is given for each of them).

the essential spectrum of \mathbb{A} when using a standard numerical scheme. The starting point is the variational formulation of (2) which writes as

$$\int_C (\text{grad}\varphi + \mathcal{R}^*u) \cdot \overline{(\text{grad}\psi + \mathcal{R}^*v)} + \Lambda_e \varepsilon_0 \mu_0 \int_N \varphi \bar{\psi} = \lambda ((\varphi, u), (\psi, v))_{\mathcal{H}},$$

for all $(\psi, v) \in H_0^1(C) \times L^2(\mathcal{N})^2$. Choosing a FE subspace of the latter variational space leads us to solve a matrix eigenvalue problem of the form $AX = \lambda MX$. For the implementation of this problem, we used the library XLiFE++ [2] developed in POEMS. We chose respectively P1 and P0 usual FE spaces for φ and u .

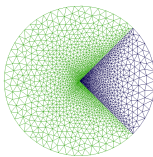


Figure 3: Example of refined mesh

Since we are interested in resonance phenomena which can be localized near the interface between both media or near the corner, we used a refined mesh as shown in figure 3. As “black hole” waves have a radial behavior like $r^{i\eta}$ (for real η , where r stands for the distance to the corner), we chose meshes whose element size decreases exponentially as $r \rightarrow 0$. For the numeri-

cal application presented in Figure 2, the values of the parameters of the problem are the following: the radius of C is 1, $\alpha = \pi/2$, $\varepsilon_0 \mu_0 = 1$, $\Lambda_m = \Lambda_e = 0.25$. Let us comment these results.

Firstly, the accumulation of eigenvalues near $\lambda = 0$ predicted by the theory is well approximated (although poorly visible here: all computed eigenvalues are very close to 0). Both displayed eigenmodes clearly confirm the bulk resonance in the NIM. Secondly, contrary to what we could expect, we did not find a large number of eigenvalues spread in the interval $\lambda/\Lambda_m \in [1/4, 3/4]$, even with an extremely refined mesh. The only concentration of eigenvalues is observed near $1/2$: it mixes “corner modes” and “interface modes”: the latters are localized outside the corner, whereas the formers are interface modes that interact at the corner. The small number of eigenvalues near the bounds of the interval $[1/4, 3/4]$ will be explained in the talk. Finally, as expected for large values of λ/Λ_m , the shapes of the modes behave as in a usual non-dispersive cavity (since the NIM behaves like vacuum).

References

[1] C. Hazard and S. Paolantoni, Spectral analysis of polygonal cavities containing a negative-index material, hal-01626868 (2017).
 [2] N. Kielbasiewicz and E. Lunéville, XLiFE++ Tutorial, <https://uma.ensta-paristech.fr/soft/XLiFE++> (2018).

Constant-intensity waves in non-Hermitian media

Andre Brandstötter^{1,*}, Konstantinos G. Makris², Etienne Rivet³, Romain Fleury⁴,
Stefan Rotter¹

¹Institute for Theoretical Physics, Vienna University of Technology (TU Wien), Vienna, Austria

²Department of Physics, University of Crete, Heraklion, Greece

³Signal Processing Laboratory 2, EPFL, Lausanne, Switzerland

⁴Laboratory of Wave Engineering, EPFL, Lausanne, Switzerland

*Email: andre.brandstotter@tuwien.ac.at

Abstract

When waves propagate through a non-uniform potential landscape their interference typically gives rise to a complex intensity pattern. Here we show how to entirely suppress these intensity variations by adding system-specific gain and loss components to the potential. The resulting constant-intensity waves are entirely free of interference-fringes and get perfectly transmitted across any such non-Hermitian scattering landscape. Quite surprisingly, these waves can be found for the paraxial equation of diffraction, the discrete and continuous nonlinear Schrödinger equation, and the scalar Helmholtz scattering wave equation. We show how to use these wave solutions to make a medium completely invisible from one side and report on a recent experimental implementation using an acoustic waveguide and a set of simple electroacoustic resonators.

Keywords: disorder scattering, non-Hermitian physics, complex media

1 Introduction

Waves play an important role in many fields of science and in all of them the plane wave solution is the one that solves the corresponding wave equation in the most straightforward way. When placing a spatially varying potential in the way of such a plane wave, however, the problem becomes immediately less trivial as potentials typically reflect and scatter the wave, leading to interference and a non-uniform wave intensity that is strongly position-dependent. Such a potential could be a non-uniform distribution of a dielectric medium for an electromagnetic wave or a wall that reflects an acoustic pressure wave. All of these cases lead to diffraction and wave interference, resulting in the highly complex variation of a wave's spatial profile that we are all very familiar with. Here we show that for

a general class of non-Hermitian potentials featuring both gain and loss, it is possible to eliminate the intensity variations in wave scattering entirely, and create constant-intensity waves.

2 Theory

Scalar wave scattering is governed by the 1D-Helmholtz equation, $[d^2/dx^2 + k^2 n^2(x)]\psi(x) = 0$ where $\psi(x)$ is the electric field, k the wavenumber in vacuum and $n(x)$ the non-Hermitian distribution of the refractive index. We now make an ansatz for the electric field traveling in positive x -direction with constant amplitude, $\psi(x) = \exp[ik \int W(x)dx]$, with an arbitrary real-valued generating function $W(x)$. The corresponding wave intensity is given by $|\psi(x)|^2 = 1$, i.e., it is constant everywhere inside the medium. By fixing the shape of $W(x)$, we can identify analytically the required non-Hermitian optical potential

$$\begin{aligned} n^2(x) &= [n_R(x) + in_I(x)]^2 \\ &= W^2(x) - \frac{i}{k} \frac{d}{dx} W(x), \end{aligned} \quad (1)$$

that supports a constant-intensity wave [1–3]. Such a scattering state is perfectly transmitted with no reflection (from left to right) and no intensity variations inside the medium despite the fact that the dielectric constant can be highly fluctuating.

3 Results

We consider now one specific example of an index distribution and study the constant-intensity waves it gives rise to. Fig. 1(a) shows the real part of a refractive index distribution $n_R(x)$ as the gray shaded area. A wave impinging on this dielectric structure composed of only $n_R(x)$ is partly reflected and features a highly oscillatory profile [see blue line in Fig. 1(a)]. Quite in contrast, when adding also the gain and loss inherent in the imaginary index component $n_I(x)$ de-

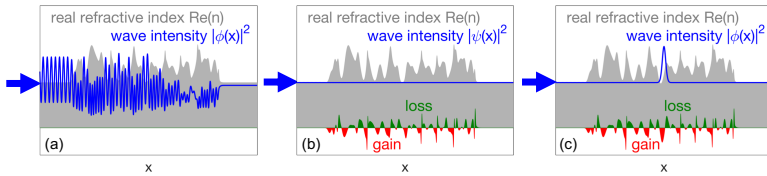


Figure 1: (a) Strongly fluctuating intensity of a wave (blue) impinging from the left on a disordered refractive index distribution $n_R(x)$ (gray). (b) Our calculations show that the wave loses all its interference fringes and gets perfectly transmitted, when a suitable combination of gain and loss is added to the disorder [see red and green for the corresponding imaginary refractive index $n_I(x)$]. (c) Moreover, by using a similar concept, we can create a wave state that shows a strong focus inside the structure.

rived from Eq. (1) [see green and red regions in Fig. 1(b)], the resulting scattering state is fully transmitted and features a constant intensity.

Choosing the generating function $W(x)$ to be complex instead of purely real, we can not only generate a wave with a constant-intensity profile but, in fact, with any arbitrary intensity pattern. Fig. 1(c) shows, for example, a wave that features a strong focus inside the structure.

In a recent work [3] we showed that by carefully choosing the generating function $W(x)$, we can even turn a structure perfectly invisible. In contrast to already existing invisibility concepts, our design principle requires neither a specific symmetry (like \mathcal{PT} -symmetry) nor periodicity and can thus be applied in a much wider context.

4 Experimental realization with an acoustic waveguide

The first experimental realization of the constant-intensity concept was carried out in acoustics where the acoustic impedance replaces the refractive index in optics [4]. Instead of a continuous system, which is difficult to implement in practice, a discrete acoustic setup was used to produce constant pressure waves inside of it. Specifically, a one-dimensional acoustic metamaterial composed of an air-filled tube was considered, loaded with a set of discrete inclusions (loudspeakers), see Fig. 2. Our measurements on this non-Hermitian acoustic metamaterial demonstrate unambiguously the creation of a wave that features the same constant pressure in front of each inclusion in this disordered structure.

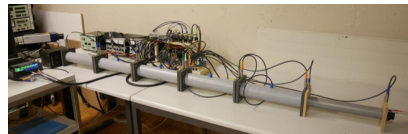


Figure 2: A one-dimensional acoustic metamaterial consisting of a waveguide loaded with actively controlled non-Hermitian acoustic inclusions supporting constant pressure waves.

References

- [1] K.G. Makris et al, Constant-intensity waves and their modulation instability in non-hermitian potentials, *Nat. Comm.* **6** (2015), p. 8257.
- [2] K.G. Makris et al, Wave propagation through disordered media without backscattering and intensity variations, *Light: Science & Applications* **6** (2017), p. e17035.
- [3] A. Brandstötter et al, Scattering-free pulse propagation through invisible non-hermitian media, *Phys. Rev. B* **99** (2019), p. 115402.
- [4] E. Rivet et al, Constant-pressure sound waves in non-hermitian disordered media, *Nat. Phys.* **14** (2018), p. 942.

Use (and Misuse) of the Method of Images

P. A. Martin^{1,*}¹Department of Applied Mathematics and Statistics, Colorado School of Mines, Golden, USA

*Email: pamartin@mines.edu

Abstract

Images are often used to replace flat boundaries. We do that in the context of antiplane elastic waves in an anisotropic half-space: the image of a singularity is not at the mirror-image point.

Keywords: images, elastic waves, anisotropy

1 Introduction

Mirror images are known to small children. Like them, we know that our image is located behind the mirror: if we place a source at a distance h from a flat mirror, the image is at a distance h behind the mirror, and the image itself is a faithful copy of the source.

This notion is used (and sometimes misused) when one wants to replace a flat boundary by appropriate images. For example, consider the Helmholtz equation $(\nabla^2 + k^2)u = 0$ in the semi-infinite region $y > -h$ with a sound-hard wall at $y = -h$ (so that $\partial u/\partial y = 0$ at $y = -h$) together with a source at the origin. Then, quoting Pierce [4, p. 208], ‘the original boundary-value problem of source plus wall is replaced by one with two sources (original source and image source) but no wall.’ Exploiting and extending this simple idea leads to useful methods for solving scattering problems when one has scatterers in the presence of flat boundaries.

2 Antiplane anisotropic elasticity

Time-harmonic antiplane motions of a homogeneous anisotropic elastic solid are governed by

$$C_{55} \frac{\partial^2 u}{\partial x^2} + 2C_{45} \frac{\partial^2 u}{\partial x \partial y} + C_{44} \frac{\partial^2 u}{\partial y^2} + \rho\omega^2 u = 0, \quad (1)$$

where $u(x, y)$ is the out-of-plane displacement, C_{55} , C_{45} and C_{44} are stiffnesses, ρ is the density and ω is the frequency. Suppose we want to solve (1) in a half-space $y > -h$ ($h > 0$) with a traction-free boundary condition at $y = -h$ and a scatterer of some kind (such as a circular cavity) within the half-space. For simplicity, assume that the origin is inside the scatterer.

The simplest case is *isotropy*. Then $C_{44} = C_{55}$, $C_{45} = 0$ and (1) reduces to the Helmholtz

equation with $k^2 = \rho\omega^2/C_{55}$. The basic singular solution is $H_0(kr)$ where $r^2 = x^2 + y^2$ and H_0 is a Hankel function. The boundary condition, $\partial u/\partial y = 0$ at $y = -h$, can be incorporated by adding an image term,

$$u(x, y) = H_0(kr) + H_0(k\hat{r}), \quad (2)$$

where $\hat{r}^2 = x^2 + (y + 2h)^2$. The extra term is singular at the image point $(x, y) = (0, -2h)$, which is the mirror image of the origin in the ‘mirror’ at $y = -h$.

A slightly more complicated case is *orthotropy*, for which $C_{44} \neq C_{55}$ and $C_{45} = 0$. Then we can reduce (1) to the Helmholtz equation by scaling x , y or both. For example, putting $x' = x/\alpha$ with $\alpha = \sqrt{C_{55}/C_{44}}$ gives $\partial^2 u/\partial x'^2 + \partial^2 u/\partial y^2 + (\alpha k)^2 u = 0$ with k as before. This scaling does not move the flat boundary at $y = -h$ but it does deform the shape of the scatterer. Alternatively, put $y' = \alpha y$ giving $\partial^2 u/\partial x^2 + \partial^2 u/\partial y'^2 + k^2 u = 0$. Stretching y is closer to what is often done in the context of anisotropic elasticity but it moves the flat boundary to $y' = -\alpha h$. Once the stretching has been done, we can reuse known solutions for the Helmholtz equation. In particular, for a solution singular at the origin, we can incorporate the boundary condition at $y = -h$ by adding an appropriate solution that is singular at the mirror-image point.

For the general *anisotropic* case, governed by (1) with $C_{45} \neq 0$, we could transform (1) into the Helmholtz equation using an appropriate scaling and rotation of coordinates, the rotation being needed so as to eliminate the mixed-derivative term in (1). The implication is that solutions involving Hankel (or Bessel) functions of certain arguments will appear. This approach is convenient for full-space problems but less so for half-space problems because the required transformation will also move the boundary of the half-space.

Instead, we first construct the full-space solutions (as has been done by others) and express them in terms of the original independent variables, x and y . We then introduce correspond-

ing solutions singular at an appropriate image point. The location of this point was found by Ting [6, §3.5]: *it is not the mirror-image point unless $C_{45} = 0$* , it is at

$$(x, y) = (2qh, -2h) \quad \text{with } q = -C_{45}/C_{44}.$$

Ting was concerned with static problems, but introducing dynamics does not change the *location* of the image point, just the kind of solutions that are to be singular at that point. Once this observation has been made, the rest is mere calculation [3]. For the simplest example, we find the fundamental solution

$$G(x, y) = H_0(kR) + H_0(k\hat{R}), \quad (3)$$

where R and \hat{R} are given by

$$\begin{aligned} R^2 &= (C_{44}x^2 - 2C_{45}xy + C_{55}y^2)/C_{44}, \\ \hat{R}^2 &= \{C_{44}x^2 - 2C_{45}xy + C_{55}(y + 2h)^2 \\ &\quad - 4h(y + h)C_{45}^2/C_{44}\}/C_{44}. \end{aligned}$$

The function G satisfies (1) everywhere in the anisotropic half-space $y > -h$ except for a logarithmic singularity at the origin, and it satisfies the traction-free boundary condition at $y = -h$. In the special case of orthotropy, (3) reduces to a formula in Kausel's book [1, eqn (5.10)]. In fact, the formula (3) itself can be found in a paper by Stevenson [5, §6]. He considers a three-dimensional (but scalar) version of (1).

Multipole solutions (with higher-order singularities) can also be constructed [3]. Note that the curve $R = \text{constant}$ is a material-dependent ellipse in the xy -plane. Consequently, infinite series of multipoles will converge in regions bounded by certain confocal ellipses (i.e., not concentric circles).

3 Discussion

Obviously, G could be used to derive boundary integral equations for scattering problems posed in an anisotropic half-space. The corresponding multipoles may also have their uses; see [3] for some discussion.

More generally, the whole subject of images and their use may be worth further investigation and systemisation. (For some examples of misuse, see references given in [2,3].) Evidently, one difficulty with (1) stems from the mixed derivative term, but that cannot be the whole story: for example, with linear water waves, the velocity potential u satisfies Laplace's equation in

the water, $y > 0$, with the boundary condition $Ku + \partial u/\partial y = 0$ on the mean free surface at $y = 0$, where K is a positive constant. The corresponding fundamental solution is known explicitly but it is quite complicated. One can say the same about plane-strain elastic waves in an isotropic half-space.

Fundamental solutions for half-space problems can often be constructed but an interesting question remains: when can the effect of a (flat) boundary be replaced by (a finite number of) image singularities? This is probably a difficult question, in general. For example, Ting [6, §8.7] shows that, for some problems involving an anisotropic elastic half-space, 9 distinct image singularities are needed!

References

- [1] E. Kausel, *Fundamental Solutions in Elastodynamics*, Cambridge University Press, 2006.
- [2] P. A. Martin, Scattering by defects in an exponentially graded layer and misuse of the method of images, *Int. J. Solids Struct.* 48 (2011) 2164–2166.
- [3] P. A. Martin, Antiplane elastic waves in an anisotropic half-space: fundamental solution, multipoles and scattering problems, *Mech. Res. Comm.* 95 (2019) 104–107.
- [4] A. D. Pierce, *Acoustics*, Acoustical Society of America, 1989.
- [5] R. C. Stevenson, Green's function for the Helmholtz equation of a scalar wave in an anisotropic halfspace, *SIAM J. Appl. Math.* 50 (1990) 199–215.
- [6] T. C. T. Ting, *Anisotropic Elasticity*, Oxford University Press, 1996.

A step towards the embedding formula for the ‘varying’ Robin half-plane diffraction

Marianti Moschou^{1,*}, Raphaël Assier¹

¹School of Mathematics, University of Manchester, Manchester, United Kingdom

*Email: marianthi.moschou@manchester.ac.uk

Abstract

A study of the acoustic diffraction by a half-plane, subject to ‘varying’ Robin boundary conditions is discussed. The problem is approached by evaluating the *diffraction coefficient*, which contains all the necessary information for the description of the far-field. The *embedding formula* gives the far-field diffraction coefficient; an important step towards the derivation of the embedding formula includes finding the *edge Green’s functions*, a special form of the usual Green’s functions. This step is achieved by using Mellin transformations, which enable us to determine the near-field asymptotics of the edge Green’s functions.

Keywords: embedding formula, diffraction coefficient, Robin boundary conditions, edge Green’s functions

1 Introduction

In this study the acoustic diffraction by a half-plane subject to ‘varying’ Robin boundary conditions will be considered. The technique used involves solving an auxiliary problem instead of the main diffraction problem with plane-wave incidence. The auxiliary problem is associated with the excitation of the field by a point source located asymptotically close to the edge of the half-plane, generating a specific form of the Green’s solution, the *edge Green’s function*. The solution of the original problem is then represented in terms of the auxiliary problem. Such a representation is called *embedding formula*.

Embedding formulae have previously been derived for several diffraction problems. Mostly, cases with perfect boundaries have been considered. The technique is well explained by Craster et al. for a general geometry [1], with various papers to follow [2, 3] which discuss the implementation and further developments of the technique.

For the derivation of the embedding formula a number of steps are considered. Firstly, the near-edge behaviour of the *edge Green’s functions* should be studied. Once the oversingu-

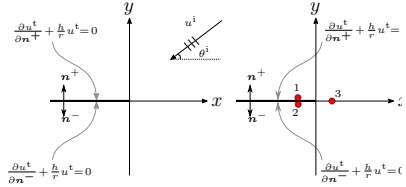


Figure 1: The geometry of the physical problem with plane-wave incidence (left) and the geometry of the auxiliary problem with source-incidence (right)

lar solution is obtained (note that the source is placed asymptotically close to the edge of the half-plane creating an unphysical field), a differential operator is introduced and applied to the physical field. Next, the reciprocity theorem is used, relating the far-field of the edge Green’s function to the near field of the physical problem. Finally, the acoustic uniqueness theorem is used.

In this talk we discuss the early step in the derivation process, that is to find the asymptotic behaviour of the edge Green’s function subject to ‘varying’ Robin boundary conditions.

2 Formulation of the problem

We assume time-harmonicity, with the suppress time-factor $e^{-i\omega t}$ and consider an incident wave of the form $u^i = e^{-ikr \cos(\theta - \theta^i)}$, where k is the wavenumber, θ^i the angle of incidence and (r, θ) the polar coordinates.

Then, the total velocity potential $u^t(r, \theta)$ satisfies the Helmholtz equation $(\nabla^2 + k^2)u^t = 0$ and the boundary condition¹ $\frac{\partial u^t}{\partial n^\pm} + h u^t = 0$, where n^+ (n^-) is the normal to the top (bottom) surface of the boundary and h is a constant associated with the acoustic impedance of the boundary. Moreover, the field satisfies the edge condition

¹In order to make our boundary conditions separable the constant h is divided by r . These are not the standard Robin boundary conditions, but a ‘varying’ version of them.

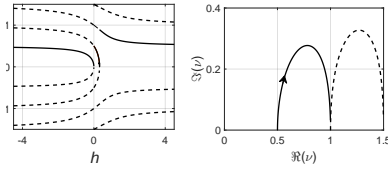


Figure 2: Graph of the set of non-zero solutions of (2), where the solid line depicts ν_1 . Left: $h \in \mathbb{R}$. Right: $h = re^{i\phi}$ as $0 < r < 100$ and $\phi = -\pi/2$.

$$u^t \sim A + \mathcal{O}(r^{\nu_1}), \quad \text{as } r \rightarrow 0. \quad (1)$$

where $\nu_1 = \nu_1(h)$ is the non-zero solution of

$$(h \sin(\pi\nu) - \nu \cos(\pi\nu))(h \cos(\pi\nu) + \nu \sin(\pi\nu)) = 0, \quad (2)$$

with the smallest positive real part (see Fig. 2). Note that (2) is obtained by separation of variables. Finally, a radiation condition at infinity is applied.

3 Edge Green's function

The auxiliary problem is introduced. This is assumed to be similarly formulated with the main difference being the source-incidence. Three sources are located at a distance ϵ from the edge; two sources at positions $(\epsilon, \pm\pi)$ with strength $\mathcal{S}_{1,2}(\epsilon)$ and one source at position $(\epsilon, 0)$ with strength $\mathcal{S}_3(\epsilon)$ (see Fig. 1). Then, the function $\hat{u}_\epsilon(r, \theta)$ satisfies the inhomogeneous Helmholtz equation

$$(\nabla^2 + k^2) \hat{u}_\epsilon = \frac{\delta(r - \epsilon)}{r} \sum_{j=1}^3 \mathcal{S}_j(\epsilon) \delta(\theta - \theta_j),$$

where $\mathcal{S}_1(\epsilon) = \mathcal{S}_2(\epsilon)$, $\theta_1 = -\theta_2 = \pi$ and $\theta_3 = 0$. Finally, the desired edge Green's function is given by \hat{u} , which is defined by $\hat{u} = \lim_{\epsilon \rightarrow 0} \hat{u}_\epsilon$.

As the behaviour of the edge Green's function needs to be determined near the edge, one can scale the space variables with a parameter η such that $k\eta \ll 1$ and solve Laplace's equation instead of Helmholtz's equation. Note that one solves three separate problems for each source and then uses the superposition principle to obtain \hat{u}_ϵ . Next, each problem is approached using Mellin transformations. Let $f(r)$ be a locally integrable function on $(0, \infty)$. The Mellin transform of f is

$$F(s) = \int_0^\infty r^{s-1} f(r) dr,$$

which converges absolutely for $-a < \Re(s) < b$, for

$$a = \sup \{ \alpha : f(r) = \mathcal{O}(r^\alpha) \text{ as } r \rightarrow 0^+ \}$$

$$b = \sup \{ \beta : f(r) = \mathcal{O}(r^{-\beta}) \text{ as } r \rightarrow \infty \}.$$

The general solution of the j^{th} transformed problem in the Mellin space can be found to be

$$\hat{U}_j(s, \theta; \theta_j) = (\epsilon/\eta)^s \mathcal{S}_j(\epsilon) \times$$

$$\frac{1}{2s} (s \cos(s(\pi \pm \theta_j)) - h \sin(s(\pi \pm \theta_j))) \times$$

$$\left(\frac{\cos(s\theta)}{h \cos(s\pi) + s \sin(s\pi)} \pm \frac{\sin(s\theta)}{s \cos(s\pi) - h \sin(s\pi)} \right)$$

where the plus (minus) sign stand for the case $\theta_j < \theta < \pi$ ($-\pi < \theta < \theta_j$). Note that the strength is carefully chosen to be $\mathcal{S}_j(\epsilon) = C_j/\epsilon^{\nu_1}$, where C_j is a constant. This choice of strength ensures the existence of the $\hat{u} = \lim_{\epsilon \rightarrow 0} \hat{u}_\epsilon$ limit and that it is non-trivial.

Then, as mentioned before, superposition of all three solutions will give the full solution. Finally, after applying the inverse Mellin formula, a residue series will be obtained, with leading order

$$\hat{u} \sim \hat{A} + \mathcal{O}(r^{-\nu_1}), \quad \text{as } r \rightarrow 0, \quad (3)$$

where ν_1 the solution of (2) with the smallest strictly positive real part.

4 Future work

Since the near-field behaviour of the edge Green's function has been determined, we are ready to move to the next step of the derivation of the embedding formula. The procedure as explained earlier in the introduction can be followed to obtain the sought-after embedding formula.

References

- [1] R.V. Craster, A.V. Shanin, E.M. Doubravsky, Embedding formulae in diffraction theory, *Proc. R. Soc. A Math. Phys. Eng. Sci.*, **459**(2038), pp. 2475–2496, 2003
- [2] R.V. Craster, A.V. Shanin, Embedding formulae for diffraction by rational wedge and angular geometries, *Proc. R. Soc. A Math. Phys. Eng. Sci.*, **461**, pp. 2227–2242, 2005
- [3] R.C. Assier, N. Peake, On the diffraction of acoustic waves by a quarter-plane, *Wave Motion*, **49**(1), pp. 64–82, 2012

Acoustic excitation of a layered scatterer by N internal point sourcesAndreas Kalogeropoulos¹, Nikolaos L. Tsitsas^{1,*}¹School of Informatics, Aristotle University of Thessaloniki, Thessaloniki, Greece

*Email: ntsitsas@csd.auth.gr

Abstract

Excitation of a layered obstacle by N acoustic internal point sources is considered. Scattering relations are derived. These involve the fields in a specific layer of the scatterer due to a source or a group of sources in any other layer. Potential applications of such problems are pointed out.

Keywords: acoustic scattering, internal point sources, scattering relations

1 Introduction

The study of scattering and radiation problems, where a layered scatterer is excited by internal point-generated waves, is motivated by interesting applications, including e.g. the excitation of the human brain by the neurons currents [1]. Particularly, the excitation of a layered medium by N internal point sources finds applications in optical diffusion, where an incident beam is replaced by multiple point sources of different strengths inside the medium [2]. Besides, having groups of sources in different layers offers additional degrees of freedom and makes feasible the determination of mean-fields variations due to stochastically distributed sources.

In this work, some preliminary scattering relations are reported concerning the acoustic excitation of a layered scatterer by N internal point sources. By adopting specific decompositions of the fields, we present certain general scattering theorems relating the fields in one layer due to all excitation fields of an other layer. Optical theorems are also given which determine the scattering cross section by means of the secondary fields at the sources locations.

2 Mathematical Formulation

A layered scatterer V of \mathbb{R}^3 contains P homogeneous layers V_p ($p = 1, \dots, P$) each with mass density ρ_p and wavenumber k_p . The core V_P is soft, hard, or penetrable. The exterior V_0 of V has parameters ρ_0 and k_0 . The scatterer V is excited by N internal point sources (of strength $A_{q,j}$) located in Q excitation layers V_q^{ex} ($q = 1, \dots, Q$). Each layer V_q^{ex} contains m_q sources

located at \mathbf{r}_q^j ($j = 1, \dots, m_q$) and generating the primary fields (under $\exp(-i\omega t)$ time dependence)

$$u_q^{\text{pr}}(\mathbf{r}; \mathbf{r}_q^j) = A_{q,j} \frac{\exp(ik_q|\mathbf{r} - \mathbf{r}_q^j|)}{|\mathbf{r} - \mathbf{r}_q^j|}, \quad \mathbf{r} \neq \mathbf{r}_q^j. \quad (1)$$

The *individual field* induced in V_q^{ex} due to the excitation by a single source at \mathbf{r}_q^j is

$$u_q^t(\mathbf{r}; \mathbf{r}_q^j) = u_q^{\text{pr}}(\mathbf{r}; \mathbf{r}_q^j) + u_q^{\text{sec}}(\mathbf{r}; \mathbf{r}_q^j), \quad (2)$$

for $\mathbf{r} \in V_q^{\text{ex}} \setminus \{\mathbf{r}_q^j\}$. The *q-excitation field* of V_q^{ex} due to excitation by all m_q sources located in the same layer is given for $\mathbf{r} \in V_q \setminus \{\mathbf{r}_q^1, \dots, \mathbf{r}_q^{m_q}\}$ by

$$u_q^t(\mathbf{r}; \mathbf{r}_q^1, \dots, \mathbf{r}_q^{m_q}) = u_q^{\text{pr}}(\mathbf{r}; \mathbf{r}_q^1, \dots, \mathbf{r}_q^{m_q}) + u_q^{\text{sec}}(\mathbf{r}; \mathbf{r}_q^1, \dots, \mathbf{r}_q^{m_q}). \quad (3)$$

Total, secondary and primary *q*-excitation fields induced in layer V_p (due to all sources in layer V_q^{ex}) are the superpositions of the corresponding total, secondary and primary individual fields induced in V_p . When $V_p \neq V_q^{\text{ex}}$, the total fields are equal with the secondary fields.

Individual (as well as *q*-excitation) fields satisfy the scalar Helmholtz equations

$$\nabla^2 u_p^t(\mathbf{r}; \mathbf{r}_q^j) + k_p^2 u_p^t(\mathbf{r}; \mathbf{r}_q^j) = 0, \quad (4)$$

in V_p , if V_p is not an excitation layer and in $V_q^{\text{ex}} \setminus \{\mathbf{r}_q^1, \dots, \mathbf{r}_q^{m_q}\}$ if V_p coincides with an excitation layer V_q^{ex} . Each individual field satisfies the transmission conditions

$$u_{p-1}^t(\mathbf{r}; \mathbf{r}_q^j) = u_p^t(\mathbf{r}; \mathbf{r}_q^j) \quad (5)$$

$$\frac{1}{\rho_{p-1}} \frac{\partial u_{p-1}^t(\mathbf{r}; \mathbf{r}_q^j)}{\partial n} = \frac{1}{\rho_p} \frac{\partial u_p^t(\mathbf{r}; \mathbf{r}_q^j)}{\partial n} \quad (6)$$

on the layers boundaries, oriented by the outward normal unit vector $\hat{\mathbf{n}}$. The *q*-excitation fields also satisfy (5) and (6). The total field in V_0 satisfies the Sommerfeld radiation condition.

Next, we define the *q-excitation cross section* due to all sources in V_q^{ex} as

$$\sigma_q = \frac{1}{k_0^2} \int_{S^2} |g_q(\hat{\mathbf{r}})|^2 ds(\hat{\mathbf{r}}), \quad (7)$$

where S^2 is the unit sphere of \mathbb{R}^3 and g_q the corresponding far-field pattern.

3 Scattering Theorems

By considering the above formulation and using Theorem 4 of [3], we get that for any two sources at $\mathbf{r}_q^j, \mathbf{r}_q^\nu$, holds

$$k_0 \rho_0 \left[\frac{\overline{iA_{q,j}}}{\rho_q} u_q^{\text{sec}}(\mathbf{r}_q^j, \mathbf{r}_q^\nu) + \frac{iA_{q,\nu}}{\rho_q} \overline{u_q^{\text{sec}}(\mathbf{r}_q^\nu, \mathbf{r}_q^j)} + \mathcal{A}(\mathbf{r}_q^j, \mathbf{r}_q^\nu) \right] = \frac{1}{2\pi} \int_{S^2} \overline{g_q^j(\hat{\mathbf{r}})} g_q^\nu(\hat{\mathbf{r}}) ds(\hat{\mathbf{r}}), \quad (8)$$

where

$$\mathcal{A}(\mathbf{r}_q^j, \mathbf{r}_q^\nu) = 2k_q \overline{A_{q,j}} A_{q,\nu} \text{sinc}(k_q |\mathbf{r}_q^j - \mathbf{r}_q^\nu|). \quad (9)$$

For constant \mathbf{r}_q^j , we get the corresponding relations of (8) for all the other sources of V_q^{ex} . In this way, we obtain the following *general scattering* theorem for the excitation layer V_q^{ex} .

Theorem 1 For the q -excitation secondary field and the individual fields induced in V_q^{ex} due to all sources radiating in the same layer, holds

$$k_0 \rho_0 \left[\frac{\overline{iA_{q,j}}}{\rho_q} u_q^{\text{sec}}(\mathbf{r}_q^j, \mathbf{r}_q^1, \dots, \mathbf{r}_q^{m_q}) + \sum_{\nu=1}^{m_q} \frac{iA_{q,\nu}}{\rho_q} u_q^{\text{sec}}(\mathbf{r}_q^\nu, \mathbf{r}_q^j) + \sum_{\nu=1}^{m_q} \mathcal{A}(\mathbf{r}_q^j, \mathbf{r}_q^\nu) \right] = \frac{1}{2\pi} \int_{S^2} \overline{g_q^j(\hat{\mathbf{r}})} g_q(\hat{\mathbf{r}}) ds(\hat{\mathbf{r}}). \quad (10)$$

Relations of the form (10) hold for all sources at $\mathbf{r}_q^j \in V_q^{\text{ex}}$. By summing for $j = 1$ to m_q , and considering the definition (7), we arrive at the following *optical theorem* for layer V_q^{ex} .

Theorem 2 The q -excitation cross section due to excitations by all sources of V_q^{ex} , is given by

$$\sigma_q = 4\pi \frac{\rho_0}{k_0} \left[\sum_{j=1}^{m_q} \text{Re} \left(\frac{\overline{iA_{q,j}}}{\rho_q} u_q^{\text{sec}}(\mathbf{r}_q^j, \mathbf{r}_q^1, \dots, \mathbf{r}_q^{m_q}) \right) + \frac{1}{2} \sum_{j=1}^{m_q} \sum_{\nu=1}^{m_q} \mathcal{A}(\mathbf{r}_q^j, \mathbf{r}_q^\nu) \right]. \quad (11)$$

Then, by using Theorem 2 of [3] and following a similar procedure to that of Theorem 1, we get the following *general scattering* theorem.

Theorem 3 The q -excitation field of V_s^{ex} and the s -excitation field of V_q^{ex} satisfy

$$k_0 \rho_0 \left[\sum_{j=1}^{m_q} \frac{\overline{iA_{q,j}}}{\rho_q} u_q^t(\mathbf{r}_q^j, \mathbf{r}_s^1, \dots, \mathbf{r}_s^{m_s}) + \sum_{\nu=1}^{m_s} \frac{iA_{s,\nu}}{\rho_s} \overline{u_s^t(\mathbf{r}_s^\nu, \mathbf{r}_q^1, \dots, \mathbf{r}_q^{m_q})} \right] = \frac{1}{2\pi} \int_{S^2} \overline{g_q(\hat{\mathbf{r}})} g_s(\hat{\mathbf{r}}) ds(\hat{\mathbf{r}}). \quad (12)$$

Considering Eqs. (12) for any pair of excitation layers and using Theorems 1 and 2, we get by summation the following *optical theorem*.

Theorem 4 The cross section σ due to excitation by all N point sources is given by

$$\sigma = 4\pi \frac{\rho_0}{k_0} \left[\sum_{q=1}^Q \sum_{j=1}^{m_q} \text{Re} \left(\frac{\overline{iA_{q,j}}}{\rho_q} u_q^{\text{sec}}(\mathbf{r}_q^j, \mathbf{r}^1, \dots, \mathbf{r}^N) \right) + \frac{1}{2} \sum_{q=1}^Q \sum_{j=1}^{m_q} \sum_{\nu=1}^{m_q} \mathcal{A}(\mathbf{r}_q^j, \mathbf{r}_q^\nu) \right], \quad (13)$$

where $u_q^{\text{sec}}(\mathbf{r}_q^j, \mathbf{r}^1, \dots, \mathbf{r}^N)$ is the secondary field of V_q^{ex} due to excitation by all N internal sources

The presented theorems quantify the relations between the individual, the q -excitation fields and the respective cross sections. Additional relations between cross sections due to individual sources and the total cross section have been worked out and will be presented at the conference. Such relations are expected to be important for the applications mentioned in the Introduction to distinguish the fields contributions generated by different sources.

References

- [1] G. Dassios, A. S. Fokas, and F. Karipourou, On the non-uniqueness of the inverse magnetoencephalography problem, *Inverse Problems* **21** (2005), pp. L1–L5.
- [2] J. L. Hollmann and L. V. Wang, Multiple-source optical diffusion approximation for a multilayer scattering medium, *Applied Optics* **46** (2007), pp. 6004–6009.
- [3] C. Athanasiadis and N. L. Tsitsas, Scattering Theorems for Acoustic Excitation of a Layered Obstacle by an Interior Point Source, *Studies in Applied Mathematics* **118** (2007), pp. 397–418.

Heterogeneous Multiscale Method for Maxwell’s Equations

Marlis Hochbruck¹, Bernhard Maier^{1,*}

¹Institute for Applied and Numerical Mathematics, Karlsruhe Institute of Technology, Karlsruhe, Germany

*Email: bernhard.maier@kit.edu

Abstract

We discuss a Heterogeneous Multiscale Method (HMM) proposed in [3] for the time-dependent linear Maxwell’s equations in first order formulation with highly oscillatory material parameters. We discretize in space using Nédélec’s edge elements. For the time integration, we investigate algebraically stable Runge–Kutta schemes, the Crank–Nicolson method, and the leapfrog scheme. By combining the uniform error analysis of non-conforming space discretizations from [2] and an error analysis of the time integration schemes, we provide an error estimate for both the semi-discrete and the fully discrete scheme. We conclude with numerical tests.

Keywords: Heterogeneous Multiscale Method, first order time-dependent Maxwell’s equations, fully discrete error analysis

Multiscale Maxwell’s equations and homogenization

Let $\Omega \subset \mathbb{R}^3$ be a bounded domain and $T > 0$. We consider the linear Maxwell’s equations with permeability $\mu^\eta(x) = \mu(x, \frac{x}{\eta})$ and permittivity $\varepsilon^\eta(x) = \varepsilon(x, \frac{x}{\eta})$ being periodic in the second argument for a characteristic microscopic length $0 < \eta \ll 1$, i.e.,

$$\begin{aligned} \mu^\eta \partial_t \mathbf{H}^\eta &= -\operatorname{curl} \mathbf{E}^\eta, \\ \varepsilon^\eta \partial_t \mathbf{E}^\eta &= \operatorname{curl} \mathbf{H}^\eta - \mathbf{J}, \end{aligned} \tag{1}$$

in $(0, T) \times \Omega$, subject to perfectly conducting boundary conditions $(n \times \mathbf{E}^\eta)|_{\partial\Omega} = 0$ and initial conditions. Here, $\mathbf{H}^\eta(t, x)$ and $\mathbf{E}^\eta(t, x)$ denote the magnetic and the electric field, respectively, and $\mathbf{J}(t, x)$ is a given electric current independent of the microscopic length η .

As η is very small in comparison to the diameter of Ω , it is very costly to resolve these fine oscillations in numerical schemes. Hence, we use results from analytical homogenization in [4] describing the qualitative macroscopic behavior as

$$\begin{aligned} \mu^{\text{eff}} \partial_t \mathbf{H}^{\text{eff}} &= -\operatorname{curl} \mathbf{E}^{\text{eff}}, \\ \varepsilon^{\text{eff}} \partial_t \mathbf{E}^{\text{eff}} &= \operatorname{curl} \mathbf{H}^{\text{eff}} - \mathbf{J}, \end{aligned} \tag{2}$$

in $(0, T) \times \Omega$. The effective material parameters $\alpha^{\text{eff}} = \mu^{\text{eff}}, \varepsilon^{\text{eff}}$ are pointwise given as

$$\alpha^{\text{eff}}(x) = \int_{Y(x)} \alpha(x, \frac{y}{\eta}) \left(I - D_y \chi_\alpha(x, \frac{y}{\eta}) \right) dy \tag{3}$$

for a periodic solution $\chi_\alpha(x, \frac{y}{\eta}) \in W_{\text{per}}^{1,2}(Y(x))$ of the local problems

$$\begin{aligned} \int_{Y(x)} \alpha(x, \frac{y}{\eta}) D_y \chi_\alpha(x, \frac{y}{\eta}) \cdot \nabla_y v(\frac{y}{\eta}) dy \\ = \int_{Y(x)} \alpha(x, \frac{y}{\eta}) \nabla_y v(\frac{y}{\eta}) dy, \end{aligned} \tag{4}$$

for all periodic functions $v \in W_{\text{per}}^{1,2}(Y(x))$, where $Y(x)$ is the unit cube with midpoint x .

Space discretization and HMM

We discretize (2) in space using Nédélec’s edge elements of order ℓ on a mesh \mathcal{T}_H of Ω with maximal edge length H . We further use the standard nodal finite elements of order k on a mesh \mathcal{T}_h of $Y(x)$ with maximal edge length h for the local problems (4). In addition, all integrals in the weak form of (2) and in the computation of the effective material parameters are replaced by quadrature rules of sufficiently high order.

The basic idea of HMM is to evaluate (3) only at the quadrature points. Therefore, every quadrature node \hat{x} of the macro mesh \mathcal{T}_H is the midpoint of a scaled unit cell $Y(\hat{x})$ with micro mesh \mathcal{T}_h , on which the local problems (4) are solved.

The approximation to (2) obtained by the HMM is then given as the solution of the system

$$\begin{aligned} \mu_H^{\text{HMM}} \partial_t \mathbf{H}_H^{\text{HMM}} &= -\operatorname{curl} \mathbf{E}_H^{\text{HMM}}, \\ \varepsilon_H^{\text{HMM}} \partial_t \mathbf{E}_H^{\text{HMM}} &= \operatorname{curl} \mathbf{H}_H^{\text{HMM}} - \mathbf{J}_H, \end{aligned} \tag{5}$$

in $(0, T) \times \Omega$, using the quadrature rules as inner product of the approximation space. We only need the values of the HMM material parameters $\mu_H^{\text{HMM}}, \varepsilon_H^{\text{HMM}}$ at the quadrature points. As the inner products of the continuous and discrete space do not coincide, (5) is a nonconforming discretization. Using [2] yields the following

error estimate for the difference between the effective solution and the approximation by the HMM.

Theorem 1 For a sufficiently smooth solution $u^{\text{eff}} = (\mathbf{H}^{\text{eff}}, \mathbf{E}^{\text{eff}})$ of (2) and the approximation $u_{H,n}^{\text{HMM}} = (\mathbf{H}_{H,n}^{\text{HMM}}, \mathbf{E}_{H,n}^{\text{HMM}})$ obtained as solution of (5), the error at time $t \in [0, T]$ is bounded by

$$\|u^{\text{eff}}(t) - u_{H,n}^{\text{HMM}}(t)\|_{L^2(\Omega)} \leq C(1+t)(H^\ell + (\frac{h}{\eta})^k).$$

Full discretization

For a fully discrete scheme, we integrate (5) in time, e.g., using algebraically stable and coercive Runge–Kutta schemes with s stages and order at least $s + 1$. Combination of the stability estimate [3] with the techniques from Theorem 1 yields the following result.

Theorem 2 For a sufficiently smooth solution $u^{\text{eff}} = (\mathbf{H}^{\text{eff}}, \mathbf{E}^{\text{eff}})$ of (2) at time $t_n \in [0, T]$ and $u_{H,n}^{\text{HMM}} = (\mathbf{H}_{H,n}^{\text{HMM}}, \mathbf{E}_{H,n}^{\text{HMM}})$ obtained by the HMM with algebraically stable Runge–Kutta schemes of order at least $s + 1$ with step size τ , the error is bounded by

$$\|u^{\text{eff}}(t_n) - u_{H,n}^{\text{HMM}}\|_{L^2(\Omega)} \leq C(\tau^{s+1} + H^\ell + (\frac{h}{\eta})^k).$$

We further consider the Crank–Nicolson method and the explicit leapfrog scheme, both being of second order. Showing that the Crank–Nicolson method is unconditionally stable and that the leapfrog scheme is stable under the standard step size restriction, we get the following result.

Theorem 3 For a sufficiently smooth solution $u^{\text{eff}} = (\mathbf{H}^{\text{eff}}, \mathbf{E}^{\text{eff}})$ of (2) at time $t_n \in [0, T]$ and the approximation $u_{H,n}^{\text{HMM}} = (\mathbf{H}_{H,n}^{\text{HMM}}, \mathbf{E}_{H,n}^{\text{HMM}})$ by the HMM with the Crank–Nicolson method, the error is bounded by

$$\|u^{\text{eff}}(t_n) - u_{H,n}^{\text{HMM}}\|_{L^2(\Omega)} \leq C(\tau^2 + H^\ell + (\frac{h}{\eta})^k).$$

The same estimate holds for the leapfrog scheme under the standard step size restriction.

Numerical examples

For the numerical tests, we consider the HMM with the leapfrog scheme for a model problem. The time step size τ is chosen sufficiently small to observe the convergence in the spatial grid parameters. Figure 1 shows the error dependent on the macroscopic edge length H (a) and the microscopic edge length h (b) for various different values of h and H , respectively. As proposed

in Theorem 3 for linear elements ($\ell = k = 1$), we get linear convergence in H and quadratic convergence in h/η .

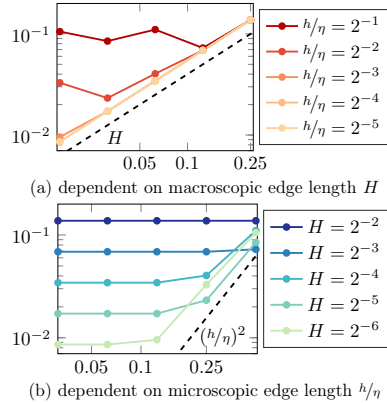


Figure 1: Error for HMM with leapfrog scheme

Our implementation of the HMM using the finite element library deal.II [1] is accessible under www.waves.kit.edu/hmm-maxwell.php including the configuration file for the model problem considered here.

Acknowledgement

We gratefully acknowledge financial support by the Deutsche Forschungsgemeinschaft (DFG) through CRC 1173.

References

- [1] W. Bangerth, R. Hartmann, and G. Kanschat, deal.II – a general-purpose object-oriented finite element library, *ACM Trans. Math. Software* **33**(4) (2007), art. 24.
- [2] D. Hipp, M. Hochbruck, and C. Stohrer, Unified error analysis for nonconforming space discretizations of wave-type equations, *IMA J. Numer. Anal.* **00** (2018), pp. 1–40.
- [3] M. Hochbruck, B. Maier, and C. Stohrer, Heterogeneous multiscale method for Maxwell’s equations, preprint, http://www.waves.kit.edu/downloads/CRC1173_Preprint_2018-54.pdf, (2018).
- [4] N. Wellander, Homogenization of the Maxwell equations. Case I. Linear theory, *Appl. Math.* **46**(1) (2001), pp. 29–51.

Fast time-explicit micro-heterogeneous wave propagation

Roland Maier^{1,*}, Daniel Peterseim¹

¹Department of Mathematics, University of Augsburg, Germany

*Email: roland.maier@math.uni-augsburg.de

Abstract

Explicit time stepping schemes are very popular in the context of wave propagation because they are relatively simple and allow for fast computations. However, the so-called CFL condition that bounds the time step size with respect to the spatial mesh size needs to be fulfilled. In case of micro-heterogeneous media where spatial finescale information have to be resolved, such a condition is very restrictive. We show that using numerical homogenization in space can reduce the complexity in space and time.

Keywords: explicit time stepping, wave equation, numerical homogenization

Problem formulation

We consider the model problem

$$\begin{aligned} \ddot{u} - \operatorname{div} A \nabla u &= f && \text{in } (0, T) \times \Omega, \\ u(0) &= u_0 && \text{in } \Omega, \\ \dot{u}(0) &= v_0 && \text{in } \Omega, \\ u|_{\partial\Omega} &= 0 && \text{in } (0, T), \end{aligned} \tag{1}$$

on a polygonal, bounded, convex Lipschitz domain $\Omega \subseteq \mathbb{R}^2$ with suitable initial conditions u_0, v_0 . We assume that the coefficient A fulfills $\alpha|\xi|^2 \leq A(x)\xi \cdot \xi$ and $|A(x)\xi| \leq \beta|\xi|$ for all $\xi \in \mathbb{R}^2$ and almost all $x \in \Omega$ for some $0 < \alpha \leq \beta < \infty$. We have in mind coefficients that vary on some small scale but without further assumptions such as (local) periodicity or scale separation.

A classical time-explicit discretization of (1) seeks $u_H^n \in V_H$, $n \geq 2$ such that

$$\begin{aligned} \tau^{-2}(u_H^{n+1} - 2u_H^n + u_H^{n-1}, v_H)_{L^2(\Omega)} \\ + (\nabla u_H^n, A \nabla v_H)_{L^2(\Omega)} = (f(n\tau), v_H)_{L^2(\Omega)} \end{aligned} \tag{2}$$

for all $v_H \in V_H$. Here, $V_H \subset H_0^1(\Omega)$ is a standard P_1 (or Q_1) finite element space based on a mesh \mathcal{T}_H of Ω with mesh size H , τ is some fixed time step, and u_H^0 and u_H^1 are appropriate initial conditions. The benefit of this approach is its simple nature and fast computations in every time step. However, the method in (2) is only

stable if the CFL condition $\tau \lesssim H$ holds. This condition is in general a severe restriction if the space V_H should resolve finescale features because in this case H , and thus τ , need to be very small. Since standard (coarse) finite element spaces lack the desired approximation properties, the idea is to add finescale information to a space V_H with parameter H that does not resolve the fine scale. This is referred to as numerical homogenization. Here, we use the Localized Orthogonal Decomposition (LOD) method introduced in [6].

Homogenization in space

The LOD method is built upon a (local) quasi-interpolation operator $I_H: H_0^1(\Omega) \rightarrow V_H$ that fulfills

$$\begin{aligned} \|H^{-1}(v - I_H v)\|_{L^2(\Omega)} \\ + \|\nabla I_H v\|_{L^2(\Omega)} \lesssim \|\nabla v\|_{L^2(\Omega)} \end{aligned}$$

and

$$\|I_H v\|_{L^2(\Omega)} \lesssim \|v\|_{L^2(\Omega)}$$

for any $v \in H_0^1(\Omega)$. With such an operator, we can define for any function $v_H \in V_H$ its *element correction* $\mathcal{C}_T^\ell v_H$ by

$$(\nabla \mathcal{C}_T^\ell v_H, A \nabla w_h)_{L^2(\mathcal{N}^\ell(T))} = (\nabla v_H, A \nabla w_h)_{L^2(T)}$$

for all $w_h \in V_h \cap \ker I_H$ and its (full) *correction* by $\mathcal{C}^\ell v_H = \sum_{T \in \mathcal{T}_H} \mathcal{C}_T^\ell v_H$. Here, V_h denotes a P_1 (or Q_1) finite element space with h small enough to resolve any relevant scales and $\mathcal{N}^\ell(T)$ is the extension of T by ℓ layers of elements, where $\ell \lesssim |\log H|$. These corrections allow to define an adapted space $\tilde{V}_H = (1 - \mathcal{C}^\ell) V_H$ that can be used in (2) instead of V_H . The new space has much better approximation properties and stability of the method is still guaranteed with time steps subject to the CFL condition $\tau \lesssim H$. Note that the element corrections are computed in parallel for a set of basis functions. This only moderately increases the computation time in the offline stage and leads to slightly denser system matrices (dependent on ℓ). Further, this approach can also be extended to higher-order

methods. For more details and an error analysis, we refer to [4]; see also [1] for the implicit and the semi-discrete case or [7] for the wave equation on adaptive meshes.

Numerical example

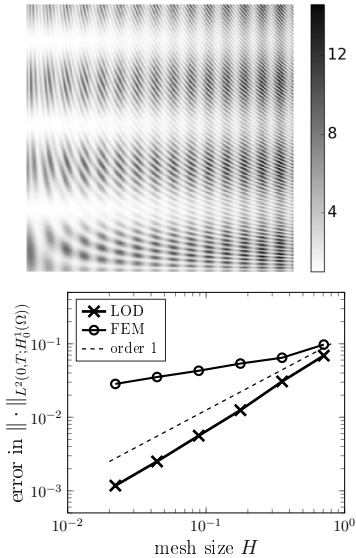


Figure 1: Coefficient A (top) and errors (bottom) for the numerical example.

The numerical example is taken from [5]. We set $\Omega = (0, 1)^2$ and $T = 1$. The reference solution is computed using standard Q_1 elements on a uniform quadrilateral mesh with parameter $h = \sqrt{2} \cdot 2^{-8}$ which is also used for the computations of the corrector problems. The time step τ is chosen small enough subject to the CFL condition, $f = 1$, $u_0 = v_0 = 0$, $\ell = 2$ and A as shown in Figure 1 (top). All computations are done based on the code from [3]. The errors in the energy norm for a standard finite element approach and one based on LOD are depicted in Figure 1 (bottom) with respect to H . The classical finite element method shows a suboptimal convergence rate because it does not account for finescale information. The method based on the LOD discretization leads to an optimal convergence rate of order one which can also be shown

theoretically, see [4].

Ongoing work: reconstruction of system matrices

Based on recent findings in [2] regarding the reconstruction of effective low-resolution models from coarse data in the elliptic setting, the next step is to tackle this problem in the context of wave propagation. We assume to be given coarse measurements of solutions corresponding to problems of the form (1) with an unknown (finescale) coefficient A . If no further information on A is given, the reconstruction of A is basically unfeasible. Thus, we want to reconstruct an effective numerical model (in the form of system matrices with a prescribed sparsity pattern in the spirit of numerical homogenization) that can reproduce the given measurements. Such a model can then for instance be used to simulate the effective behavior of other problems based on the same unknown coefficient.

References

- [1] A. Abdulle and P. Henning. Localized orthogonal decomposition method for the wave equation with a continuum of scales, *Math. Comp.*, **86**(304), 549–587 (2017).
- [2] A. Caiazzo, R. Maier, and D. Peterseim. Reconstruction of quasi-local numerical effective models from low-resolution measurements, *WIAS Preprint No. 2577* (2019).
- [3] F. Hellman. Gridlod, <https://github.com/fredrikhellman/gridlod>, GitHub repository (2017).
- [4] R. Maier and D. Peterseim. Explicit computational wave propagation in micro-heterogeneous media, *BIT Numer. Math.* (2018).
- [5] R. Maier and D. Peterseim. Fast time-explicit micro-heterogeneous wave propagation, *PAMM* **18**(1) (2018).
- [6] A. Målqvist and D. Peterseim. Localization of elliptic multiscale problems, *Math. Comp.* **83**(290), 2583–2603 (2014).
- [7] D. Peterseim and M. Schedensack. Relaxing the CFL condition for the wave equation on adaptive meshes, *J. Sci. Comput.* **72**(3), 1196–1213 (2017).

Discrete Wave Equation Upscaling in 1-D and 2-D

Cyrill Boesch^{1,*}, Dirk-Jan van Manen¹, Andreas Fichtner¹¹Department of Earth Sciences, ETH, Zurich, Switzerland

*Email: cyrill.boesch@erdw.ethz.ch

Abstract

We present a novel homogenization technique, referred to as Discrete Wave Equation Upscaling (DWEU). Its advantages are (i) the applicability to arbitrary heterogeneous and anisotropic media, (ii) the computation of effective properties directly on a coarser grid, which enables more efficient numerical solutions of the wave equation, as well as (iii) conceptual and computational simplicity that only requires Fourier transforms. We develop DWEU for the elastic wave equation in 1-D and 2-D. In addition to reproducing analytical results for simple media, we provide numerical examples, as well as an analysis of the homogenization operators in relation to the ill-posedness of the inverse problem.

Keywords: Numerical Homogenization, Elastic Wave Propagation, Inverse Theory.

1 Introduction

Homogenization is a mathematical procedure to transform a medium with sub-wavelength structure into an effective medium that is smooth compared to the shortest wavelength, while producing nearly the same deformation field as the detailed medium at sufficiently low frequencies. Homogenization reduces the computational cost of the forward problem solution, and it allows us to understand the relation between sub-wavelength structure and the ill-posedness of inverse (imaging) problems.

In contrast to scale-expansion methods (e.g. [4]), DWEU operates on the discretized wave equation on a fine, N -point grid (we assume that the medium of interest can be fully represented by a finite number of grid points N), which is transformed by Fourier projections into an effective wave equation on a coarser K -point grid ($K < N$). Thereby, effective density and elasticity properties are obtained. Using wavelets, a similar approach was suggested by [3]. The major difference of DWEU is the explicit computation of effective material properties, whereas [3] homogenize the wave operator as a whole.

2 Method

In the interest of simplicity, we outline the DWEU concept in 1-D, following [1]. For this, we start from the frequency-domain, continuous, elastic wave equation

$$-\omega^2 \rho(x)u(x, \omega) - \partial_x[\mu(x)\partial_x u(x, \omega)] = f(x, \omega), \quad (1)$$

where ρ is the density, μ the elastic parameter, ω the circular frequency, f the source and u the wavefield. Discretizing (1) on an N -point grid using a finite-difference scheme gives

$$-\omega^2 \mathbf{M}_N \mathbf{u}_N - \mathbf{D}_N \mathbf{R}_N \mathbf{D}_N \mathbf{u}_N = \mathbf{f}_N, \quad (2)$$

where $\mathbf{M}_N \in \mathbb{R}^{N \times N}$ is the mass matrix with the density $\rho_N \in \mathbb{R}^{N \times 1}$ on its diagonal, $\mathbf{R}_N \in \mathbb{R}^{N \times N}$ the elasticity matrix with the elastic modulus $\mu_N \in \mathbb{R}^{N \times 1}$ on its diagonal, $\mathbf{f}_N \in \mathbb{R}^{N \times 1}$ is the source, and $\mathbf{D}_N \in \mathbb{R}^{N \times N}$ are differential operator matrices. DWEU transforms (2) into a new, effective wave equation on a K -dimensional grid ($K < N$), given by

$$-\omega^2 \mathbf{M}_K \mathbf{u}_K - \mathbf{D}_K \mathbf{R}_K \mathbf{D}_K \mathbf{u}_K = \mathbf{f}_K. \quad (3)$$

All the matrices in (3) are now in $\mathbb{R}^{K \times K}$ and the vectors are in $\mathbb{R}^{K \times 1}$. Solutions of the effective K -point wave equation (3) approach solutions of the original N -point wave equation (2) arbitrarily closely for sufficiently low frequencies. Interestingly, the effective mass and elasticity matrices, \mathbf{M}_K and \mathbf{R}_K , are not diagonal anymore, giving rise to non-local rheologies. This implies that non-locality in a metamaterial may compensate for sub-wavelength structure. For numerical modelling, we extract the diagonals of \mathbf{M}_K and \mathbf{R}_K . In summary, the effective wave equation is derived by the following steps:

1. Project the discrete, frequency-domain wave equation on the N -D grid onto the discrete spatial Fourier domain using an N -D discrete Fourier transform.
2. Solve for the first K low-wavenumber components of the wavefield to obtain a K -D discrete wave equation in the wavenumber domain.

3. Invert to the space domain using a K -D inverse Fourier transform.

We extended the above formalism to 2-D, allowing for arbitrary heterogeneous and anisotropic elastic materials, defined by density ρ and the 2-D reduction of the fourth-order elastic tensor C_{ijkl} . In figure 1 we present a 2-D example where a layered but isotropic medium is transformed into a homogeneous but anisotropic medium, confirming analytical results [2]. In figure 2 DWEU is applied to a random medium.

3 Results

Besides the extension of the method to the most general 2D case, we performed detailed analyses in 1-D. For this, we explicitly defined the homogenization operators for density (linear), $\mathcal{H}_\rho : \rho_N \rightarrow \rho_K$ and elasticity (non-linear), $\mathcal{H}_\mu : \mu_N \rightarrow \mu_K$. Their properties (nullspace, eigenvectors, etc.) are linked to properties of the inverse problem. For instance, the nullspace of a homogenization operator contains those medium perturbations relative to a constant medium that do not affect the wavefield. Those are perturbations about which the wave does not carry any information, meaning that they are impossible to recover in an inverse problem solution. To physically test and interpret the mathematical findings and to highlight the practical applicability of our method, we performed extensive numerical wave propagation experiments.

References

- [1] A. Fichtner and S. M. Hanasoge, Discrete wave equation upscaling, *Geophysical Journal International* **44** (2017), pp. 353-357.
- [2] G. E. Backus, Long-wave elastic anisotropy produced by horizontal layering, *Journal of Geophysical Research* **44** (1962), pp. 4427-4440.
- [3] B. Engquist, P. Loetstedt, and O. Runborg, *Multiscale modeling and simulation in science*, volume 66, Springer Science and Business Media, 2009.
- [4] E. Sanchez-Palencia, Homogenization in mechanics: a survey of solved and open problems, *Rend. Sem. Mat. Univ. Politec. Torino* **44** (1986), pp. 1-45.

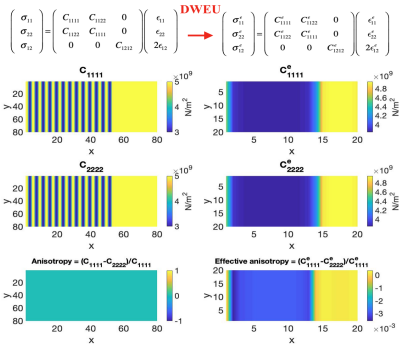


Figure 1: (Left column) Two of the elastic parameters on the fine 80×80 grid. (Right column) The effective parameters on the coarse 20×20 grid after the 2-D DWEU was applied. The fine layered, isotropic part of the medium is transformed into an anisotropic (transversely isotropic), but homogeneous medium. This is in agreement with Backus, 1962 [2]. The constant part of the medium remains constant (in fact, a constant medium is an eigenvector to the homogenization operator).

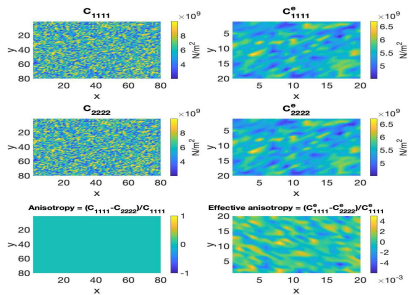


Figure 2: The same figure as figure 1 but for an originally random medium (left column). As expected, the effective medium (right column) is smoothed, however some of the random character is retained. Randomly distributed discontinuities of the original medium are converted to local anisotropies in the effective medium. This can be explained as follows: If by chance some of the heterogeneity with a similar directionality are stacked, then the wave will "see" an effective anisotropy.

A matrix-free Discontinuous Galerkin method for the time dependent Maxwell equations in open domains

Bernard Kapidani^{1,*}, Joachim Schöberl¹

¹Institute for Analysis and Scientific Computing, TU Wien, Vienna, Austria

*Email: bernard.kapidani@tuwien.ac.at

Abstract

A Discontinuous Galerkin (DG) approach for the time dependent Maxwell equations is introduced, based on the covariant projection, on each element of the mesh, of an orthogonal modal basis of $L^2(\hat{K})$ originally defined on a reference element \hat{K} . This approach leads to an explicit time stepping scheme for which the the mass matrix is at most $d \times d$ block-diagonal (in $d = 2, 3$ spatial dimensions) and other discrete bilinear forms involved in the scheme can be computed and stored only once on the reference element. Open boundaries are also handled naturally in the formulation through a complex stretching based approach.

Keywords: Discontinuous Galerkin, Maxwell, covariant transformation, PML

1 Theoretical aspects

When solving numerically time dependent wave propagation problems, discontinuous Finite Elements are an attractive choice, because they allow for a cheap inverse of the mass matrix and therefore explicit time stepping schemes on unstructured grids. These are based on introducing a triangulation \mathcal{T}_Ω of the domain Ω , and subsequently testing the solution of the equations to be solved against a basis of polynomial order p on each mesh element K . For Maxwell equations (with the usual meaning of symbols for fields and material tensors) the weak formulation reads

$$\begin{aligned} \partial_t \sum_{K \in \mathcal{T}_\Omega} \int_K \varepsilon \mathbf{e} \cdot \boldsymbol{\varphi}_{\ell j} &= \sum_{K \in \mathcal{T}_\Omega} \int_K (\nabla \times \mathbf{h}) \cdot \boldsymbol{\varphi}_{\ell j}, \\ \partial_t \sum_{K \in \mathcal{T}_\Omega} \int_K \boldsymbol{\mu} \mathbf{h} \cdot \boldsymbol{\varphi}_{\ell j} &= - \sum_{K \in \mathcal{T}_\Omega} \int_K (\nabla \times \mathbf{e}) \cdot \boldsymbol{\varphi}_{\ell j}, \end{aligned}$$

holding for all $\boldsymbol{\varphi}_{\ell j}$, $\ell \in \{1, 2, \dots, N\}$ and $j \in \{1, 2, 3\}$. These vector test functions are defined as

$$\boldsymbol{\varphi}_{\ell j}(\mathbf{x}) = \underline{J}_K^{-T} \hat{\boldsymbol{\varphi}}_{\ell j}(\hat{\mathbf{x}}) = \underline{J}_K^{-T} \hat{\boldsymbol{\varphi}}_\ell(\hat{\mathbf{x}}) \hat{\mathbf{v}}_j, \quad (1)$$

with $\hat{\mathbf{v}}_j$ being one of the three Cartesian unit vectors, and we have used the covariant transformation rule for vector fields from point $\hat{\mathbf{x}}$ on the reference element (triangle or tetrahedron) to \mathbf{x} on the *physical* finite element, i.e. the second order tensor \underline{J}_K is defined such that $\underline{J}_K^{-1} = \partial x_j / \partial \hat{x}_k$. By choosing the scalar test functions on the right-hand side of (1) among the Dubiner basis functions [1], such that $\langle \hat{\varphi}_\ell, \hat{\varphi}_{\ell'} \rangle = \delta_{\ell \ell'}$ also holds (with respect to the appropriate inner product on the reference element), it easily follows that the $\hat{\boldsymbol{\varphi}}_{\ell j}(\hat{\mathbf{x}})$ form a basis of the space $[\mathcal{P}^p(\hat{K})]^3$, i.e. $[L^2(K)]^3$ functions which are polynomials of degree at most p on \hat{K} . The solution is accordingly sought in the same finite dimensional trial space:

$$\begin{aligned} \mathbf{e}(\mathbf{x}, t) &= \sum_{\ell=1}^{\ell=N} \sum_{j=1}^{j=d} u_{\ell j}(t) \boldsymbol{\varphi}_{\ell j}(\mathbf{x}), \\ \mathbf{h}(\mathbf{x}, t) &= \sum_{\ell=1}^{\ell=N} \sum_{j=(d \bmod 3)+1}^{j=3} f_{\ell j}(t) \boldsymbol{\varphi}_{\ell j}(\mathbf{x}). \end{aligned}$$

The above definitions are used in the final weak formulation both on the r.h.s. and on the l.h.s. Take any pair of trial and test functions: for the mass matrix term associated to their inner product it holds

$$\int_K (\varepsilon \boldsymbol{\varphi}_{\ell k}) \cdot \boldsymbol{\varphi}_{\ell' k'} = \int_K \mathcal{J}_K \left(\underline{J}_K^{-1} \varepsilon \underline{J}_K^{-T} \hat{\boldsymbol{\varphi}}_{\ell k} \right) \cdot \hat{\boldsymbol{\varphi}}_{\ell' k'},$$

while for the bilinear forms on the r.h.s. it holds

$$\begin{aligned} \int_K \nabla \times \boldsymbol{\varphi}_{\ell k} \cdot \boldsymbol{\varphi}_{\ell' k'} &= \\ \int_K \mathcal{J}_K \left(\frac{1}{\mathcal{J}_K} \underline{J}_K \hat{\nabla} \times \hat{\boldsymbol{\varphi}}_{\ell k} \right) \cdot \underline{J}_K^{-T} \hat{\boldsymbol{\varphi}}_{\ell' k'}, \end{aligned} \quad (2)$$

where $\mathcal{J}_K = \det(\underline{J}_K)$ and the Piola transformation has been used to map curls of covariant vector fields. From (2) it is easy to see that all discrete bilinear forms on the r.h.s. of the equations (even after integration by parts as in common FEM practice) are independent of mesh geometry, and can thus be computed once and for

all on the reference element and re-used for all elements in the mesh.

Furthermore, when absorbing layers based on complex coordinate stretching are used as boundary conditions, identical transformation rules are employed, which keeps bilinear forms involving differential operators geometry independent [2].

2 Numerical results

We take as an example a waveguide-ring structure with four ports (P1 through P4 in Fig.2) as the one described in [3], wrapped by a layer of Cartesian PML.

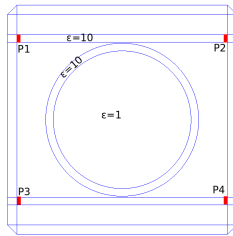


Figure 1: The test waveguide ring geometry: PML wrap-around is clearly shown.

Through Fourier analysis on a single time simulation, we can compute spectra of scattering parameters for the four port system (Fig.2).

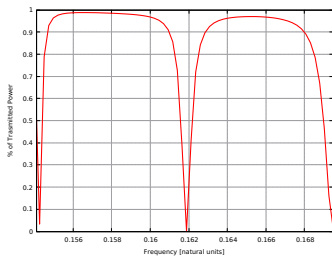


Figure 2: Ratio between power absorbed from P2 over power injected at P1, obtained by FFT.

Consequently we can validate this result by injecting a pure sine mode at the resonant frequency: in Fig.2, the energy of the sinusoidal field injected in the slab waveguide is split, through evanescent mode coupling, between the ring structure and the waveguide’s upper-right output port. After a full round-trip of the guided mode around

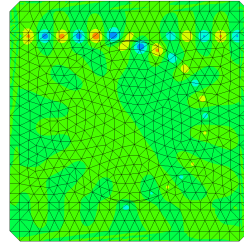


Figure 3: First few wave-fronts of the time domain simulation, polynomial order $p = 5$.

the ring structure the guided wave interacts (again through evanescent mode coupling) destructively with the continuous wave coming from the source the steady state behaviour, shown in Fig.2, comprises resonant energy stored in the ring structure, and a guided mode from the P1 to P3 clearly visible.

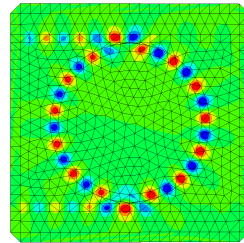


Figure 4: Steady-state fields after 400 000 time steps.

We finally remark that all results have been obtained within the FEM library NGSolve [4].

Acknowledgements

BK is supported by the Austrian FWF under project SFB 65.

References

- [1] M. Dubiner, Spectral methods on triangles and other domains, *J. Sci. Comput.*, 6(4), 1991, pp. 345–390.
- [2] A. Modave, J. Lambrechts, C. Geuzaine, Perfectly matched layers for convex truncated domains with discontinuous Galerkin time domain simulations, *Computers & Mathematics with Applications*, 73(4), 2017, pp. 684–700.
- [3] K. Busch, M. KÖnig, J. Niegemann, Discontinuous Galerkin methods in nanophotonics, *Laser & Photonics Reviews*, 5(6), 2011, pp. 773–809.
- [4] J. Schöberl et al., www.ngsolve.org.

Perturbed edge finite element method for the simulation of electromagnetic waves in magnetised plasmas

Damien Chicaud^{1,*}, Patrick Ciarlet¹, Axel Modave¹

¹Team POEMS (CNRS-INRIA-ENSTA), Palaiseau, France

*Email: damien.chicaud@ensta-paristech.fr

Abstract

Numerical simulation of electromagnetic waves in magnetised plasmas is a challenging topic. We address the finite element solution of a time-harmonic model. With the classical method, the variational formulation has a poor coercivity which leads to an ill-conditioned numerical system and numerical instabilities. We propose a perturbed formulation to improve the conditioning of the system. Promising preliminary numerical results are discussed.

Keywords: Maxwell's equations, Magnetised plasmas, Edge finite element method

1 Introduction

The study of electromagnetic waves in magnetised plasmas is a growing field, notably for its importance in the promising controlling of nuclear fusion in tokamaks. We follow the model described in [1,2]. Mathematical analyses of this model show that the problem, although well-posed, has bad properties which causes the numerical system to be ill-conditioned and hard to solve.

In [1], Back *et al.* have considered nodal finite element methods. This is made possible thanks to the regularity of the solution, as shown in [2]. However, instabilities are observed due to the poor conditioning of the system.

We present and analyse $\mathbf{H}(\mathbf{curl})$ -conforming formulations and their discretization using Nédélec's edge elements. We consider the plain formulation obtained with standard tools, as well as a perturbed version motivated by the hope of getting a better conditioning, while preserving a good approximation of the solution.

2 Model

The electric field \mathbf{E} in time-harmonic domain, in a bounded domain Ω filled with plasma as described in [1], is governed by equation

$$\mathbf{curl} \mathbf{curl} \mathbf{E} - \frac{\omega^2}{c^2} \underline{\mathbf{K}} \mathbf{E} = \mathbf{0}, \quad (1)$$

which derives from Maxwell's equations; ω is the wave angular frequency, c the light celerity, and $\underline{\mathbf{K}}$ the medium response tensor. $\underline{\mathbf{K}}$ results from two main physical phenomena: conductivity due to interactions between particles, and Landau damping.

From a mathematical point of view, the tensor $\underline{\mathbf{K}}$ is complex-valued, non-diagonal (the medium is anisotropic), and non-hermitian. Besides, we will assume $\underline{\mathbf{K}}$ to be bounded and satisfying the following property:

There exist two strictly positive constants η and ζ (possibly dependent on ω), s.t., $\forall \mathbf{v} \in \mathbf{L}^2(\Omega)$,

$$0 < \zeta \|\mathbf{v}\|_{\mathbf{L}^2}^2 \leq \Im \mathbf{m}(\underline{\mathbf{K}} \mathbf{v} | \mathbf{v}) \leq |(\underline{\mathbf{K}} \mathbf{v} | \mathbf{v})| \leq \eta \|\mathbf{v}\|_{\mathbf{L}^2}^2 \quad (2)$$

The boundary Γ of Ω is smooth, and made up of two parts: on Γ_C there holds a perfectly conducting condition. On the remaining $\Gamma_A := \Gamma \setminus \Gamma_C$ of the boundary, an antenna imposes an electric current \mathbf{j}_A , and there holds

$$\mathbf{curl} \mathbf{E} \times \mathbf{n} = i\omega\mu_0 \mathbf{j}_A. \quad (3)$$

3 Variational formulations

We consider $\mathbf{H}(\mathbf{curl})$ formulations, by contrast with [1]. We seek \mathbf{E} in the space $V := \{\mathbf{v} \in \mathbf{H}(\mathbf{curl}, \Omega), \mathbf{v} \times \mathbf{n}|_{\Gamma_C} = \mathbf{0}\}$.

3.1 Plain formulation

The natural, so-called "plain" formulation reads: Find \mathbf{E} in V s.t., $\forall \mathbf{F} \in V$,

$$(\mathbf{curl} \mathbf{E} | \mathbf{curl} \mathbf{F}) - \frac{\omega^2}{c^2} (\underline{\mathbf{K}} \mathbf{E} | \mathbf{F}) = l(\mathbf{F}), \quad (4)$$

where $l(\mathbf{F})$ contains the data of the imposed current \mathbf{j}_A .

This plain formulation is analysed in [1]. Assumption (2) ensures that it is well-posed. However, it appears to be poorly coercive (i.e. with a very small coercivity constant), which results in a numerical system that is poorly conditioned. This is not the formulation discretized in [1]. Instead, an "augmented" formulation, which leads to a nodal FE discretization, is preferred.

3.2 Perturbed formulation

Following [3], we propose a perturbation method to approach the plain formulation. The perturbed formulation reads:

Find \mathbf{E}_γ in V s.t., $\forall \mathbf{F} \in V$,

$$(\mathbf{curl} \mathbf{E}_\gamma | \mathbf{curl} \mathbf{F}) + \left(\gamma - \frac{\omega^2}{c^2} \right) (\underline{\mathbf{K}} \mathbf{E}_\gamma | \mathbf{F}) = l(\mathbf{F}) \tag{5}$$

for a small $\gamma \in \mathbb{C}$.

Under certain conditions on γ , we prove that the perturbed formulation is well-posed. Additionally, the solution of the perturbed formulation converges well to the solution of the plain formulation (*proofs not shown*). More precisely,

$$\|\mathbf{E} - \mathbf{E}_\gamma\|_{\mathbf{H}(\mathbf{curl})} = \mathcal{O}(\gamma). \tag{6}$$

4 Preliminary numerical results

To analyse the accuracy of the method, we consider the following toy problem, posed in $\Omega = [0, 1]^3$:

$$\mathbf{curl} \mathbf{curl} \mathbf{E} - \frac{\omega^2}{c^2} \underline{\mathbf{K}} \mathbf{E} = \mathbf{f}, \tag{7}$$

with the boundary condition $\mathbf{n} \times \mathbf{E} = \mathbf{0}$ on $\partial\Omega$. In the following, $\omega = c = 1$. We set as reference solution

$$\mathbf{E}_{exa} = \begin{pmatrix} 2 \cos(\pi x) \sin(\pi y) \sin(\pi z) \\ -\sin(\pi x) \cos(\pi y) \sin(\pi z) \\ -\sin(\pi x) \sin(\pi y) \cos(\pi z) \end{pmatrix} \tag{8}$$

and compute the right-hand side in consequence. The tensor $\underline{\mathbf{K}}$ is set to

$$\underline{\mathbf{K}} = \begin{pmatrix} 1 & 0 & 0 \\ 0 & 1 & 0 \\ 0 & 0 & -2 + 10^{-4}i \end{pmatrix}. \tag{9}$$

This is a first step on the road to modelling plasmas appropriately with $\underline{\mathbf{K}}$ as in [2], where extra-diagonal terms arise. Numerical results are obtained using FreeFem++, with edge finite elements (linear basis functions).

According to theory, we expect the error in $\mathbf{H}(\mathbf{curl})$ norm to be in $\mathcal{O}(h)$. On Fig.1., we observe that this convergence rate is numerically recovered.

We denote by γ_{opt} the value of $\gamma \in \mathbb{C}$ minimizing the error. For this value, we actually get a smaller error than when $\gamma = 0$. Thus, our perturbed method permits a significant decreasing of the error, without any additional cost.

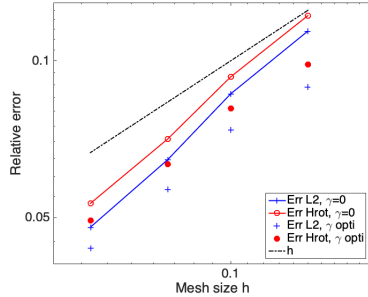


Figure 1: Convergence of the method

Numerical results are presented in Table 1. We observe that γ_{opt} , *a priori* a complex number, is *a posteriori* a negative real number. Its value varies with h . More precisely, γ_{opt} decreases in $\mathcal{O}(h^2)$, which recalls the result of [3] obtained in a different context.

Mesh size	1/8	1/10	1/12	1/15
Err $\gamma = 0$	0.1221	0.09315	0.07077	0.05325
Err γ_{opt}	0.0984	0.08106	0.06333	0.04934
Gain	19%	13%	10%	7%
γ_{opt}	-0.037	-0.023	-0.016	-0.010
$-\gamma_{opt}/h^2$	2.368	2.3	2.304	2.25

Table 1: Gain of the perturbed method

These preliminary results show the perturbed method performs well, and is quite promising compared to a more standard approach, as it permits to improve the problem conditioning and reduce the error without any additional cost. Future work will focus on a more precise numerical analysis of the method, including results on more realistic testcases.

Acknowledgement: We thank the DGA/AID for its financial support.

References

- [1] A. Back, T. Hattori, S. Labrunie, J.R. Roche, and P. Bertrand, *ESAIM: Mathematical Modelling and Numerical Analysis*, 49:1239–1260, 2015.
- [2] T. Hattori, PhD thesis, Université de Lorraine, 2014.
- [3] P. Ciarlet Jr, H. Wu, and J. Zou, *SIAM Journal on Numerical Analysis*, 52(2), 779-807, 2014.

An Inf-Sup Stable Space-Time Variational Formulation for the Scalar Second-Order Wave Equation

Marco Zank^{1,*}, Olaf Steinbach²

¹Faculty of Mathematics, University of Vienna, Vienna, Austria

²Institut für Angewandte Mathematik, TU Graz, Graz, Austria

*Email: marco.zank@univie.ac.at

Abstract

For the discretisation of time-dependent partial differential equations, usually explicit or implicit time stepping schemes are used. An alternative approach is the usage of space-time methods, where the space-time domain Q is discretised and the resulting global linear system is solved at once. In any case, the underlying space-time variational formulation plays a decisive role for space-time Galerkin methods. In this talk, space-time variational formulations for the scalar second-order wave equation, which are well-suited for space-time Galerkin methods, are investigated. A new space-time approach is introduced, where the starting point is a Hilbert space $\mathcal{H}(Q)$. Then, a completion procedure is used to define a suitable subspace $\mathcal{H}_0(Q) \subset \mathcal{H}(Q)$, where a Poincaré-Friedrichs type inequality holds. This idea leads to a uniquely solvable variational formulation in $\mathcal{H}_0(Q)$, including an isomorphic solution operator and a corresponding inf-sup condition.

Keywords: second-order wave equation, space-time methods, inf-sup condition

Variational Formulation in $H^1(Q)$

As a model problem, the homogeneous Dirichlet problem for the second-order wave equation,

$$\begin{aligned} \partial_{tt}u - \Delta_x u &= f & \text{in } Q = \Omega \times (0, T), \\ u &= 0 & \text{in } \Sigma = \partial\Omega \times [0, T], \\ u(\cdot, 0) = \partial_t u(\cdot, 0) &= 0 & \text{in } \Omega, \end{aligned}$$

where $\Omega \subset \mathbb{R}^d$, $d = 1, 2, 3$, is a bounded Lipschitz domain with boundary $\partial\Omega$, $T > 0$ is a terminal time and f is a given right-hand side, is examined. Integration by parts with respect to time and space leads to the variational formulation to find $u \in H_{0,0}^{1,1}(Q) \subset H^1(Q)$ such that

$$a_{H^1}(u, v) = \langle f, v \rangle_{L^2(Q)} \tag{1}$$

for all $v \in H_{0,0}^{1,1}(Q) \subset H^1(Q)$, where $f \in L^2(Q)$ is given. Here, the bilinear form

$$a_{H^1}(\cdot, \cdot): H_{0,0}^{1,1}(Q) \times H_{0,0}^{1,1}(Q) \rightarrow \mathbb{R}$$

is defined by

$$a_{H^1}(u, v) = -\langle \partial_t u, \partial_t v \rangle_{L^2(Q)} + \langle \nabla_x u, \nabla_x v \rangle_{L^2(Q)}$$

for $u \in H_{0,0}^{1,1}(Q)$, $v \in H_{0,0}^{1,1}(Q)$, where the standard Sobolev spaces

$$H_{0,0}^{1,1}(Q) = L^2(0, T; H_0^1(\Omega)) \cap H_{0,0}^1(0, T; L^2(\Omega)),$$

$$H_{0,0}^{1,1}(Q) = L^2(0, T; H_0^1(\Omega)) \cap H_{0,0}^1(0, T; L^2(\Omega)),$$

endowed with the norm

$$|v|_{H^1(Q)} = \sqrt{\|\partial_t v\|_{L^2(Q)}^2 + \|\nabla_x v\|_{L^2(Q)}^2},$$

fulfil the homogeneous Dirichlet condition, and the initial or terminal condition, i.e.

$$v(\cdot, 0) = 0 \text{ in } \Omega \quad \text{or} \quad v(\cdot, T) = 0 \text{ in } \Omega.$$

In addition, $\langle \cdot, \cdot \rangle_Q$ denotes the duality pairing in $[H_{0,0}^{1,1}(Q)]' \times H_{0,0}^{1,1}(Q)$ as extension of the $L^2(Q)$ inner product $\langle \cdot, \cdot \rangle_{L^2(Q)}$.

In (1), the initial condition $u(\cdot, 0) = 0$ is considered in the strong sense, whereas the initial condition $\partial_t u(\cdot, 0) = 0$ is incorporated in a weak sense. It is well known that for $f \in L^2(Q)$, there exists a unique solution $u \in H_{0,0}^{1,1}(Q)$ of the variational formulation (1), see [1, Theorem 3.2 in Chapter IV], and [2]. However, the bilinear form $a_{H^1}(\cdot, \cdot)$ does not satisfy an inf-sup condition, see [4, Subsection 4.2]. To overcome this problem, a new space-time variational formulation is introduced, see [4, Subsection 4.4] or [3] for the proofs of the statements of the next section.

New Variational Formulation in $\mathcal{H}(Q)$

To derive a new space-time variational formulation, the space

$$\begin{aligned} \mathcal{H}(Q) &= \{v|_Q: v \in L^2(Q_-), v|_{\Omega \times (-\infty, 0)} = 0, \\ &\quad \square_{Q_-} v \in [H_{0,0}^{1,1}(Q)]'\} \end{aligned}$$

with the Hilbertian norm

$$\|v\|_{\mathcal{H}(Q)} = \sqrt{\|v\|_{L^2(Q)}^2 + \|\square_{Q_-} v\|_{[H_{0;0}^{1,1}(Q)]'}^2}$$

is considered, where

$$Q_- = \Omega \times (-\infty, T) \subset \mathbb{R}^{d+1}$$

is the unbounded domain with respect to time and

$$\square_{Q_-} : \mathcal{D}'(Q_-) \rightarrow \mathcal{D}'(Q_-)$$

is the distributional wave operator for distributions $\mathcal{D}'(Q_-)$. It can be shown that the space $\mathcal{H}(Q)$ is complete, i.e. a Hilbert space.

Lemma 1 *It holds $H_{0;0}^{1,1}(Q) \subset \mathcal{H}(Q)$. Furthermore, each function $u \in H_{0;0}^{1,1}(Q)$ fulfils*

$$\langle \square_{Q_-} u, v \rangle_Q = a_H(u, v)$$

for all $v \in H_{0;0}^{1,1}(Q)$.

Since $H_{0;0}^{1,1}(Q) \subset \mathcal{H}(Q)$, one defines by completion the Hilbert space

$$\mathcal{H}_0(Q) = \overline{H_{0;0}^{1,1}(Q)}^{\|\cdot\|_{\mathcal{H}(Q)}} \subset \mathcal{H}(Q)$$

endowed with the Hilbertian norm $\|\cdot\|_{\mathcal{H}(Q)}$. A Poincaré-Friedrichs type inequality is true on this subspace $\mathcal{H}_0(Q)$.

Lemma 2 *For $u \in \mathcal{H}_0(Q)$, it holds*

$$\|\square_{Q_-} u\|_{[H_{0;0}^{1,1}(Q)]'} \geq \frac{\sqrt{2}}{T} \|u\|_{L^2(Q)}.$$

Hence, the subspace $\mathcal{H}_0(Q) \subset \mathcal{H}(Q)$, endowed with the Hilbertian norm $\|\square_{Q_-}(\cdot)\|_{[H_{0;0}^{1,1}(Q)]'}$, is a Hilbert space. The weak variational formulation for a given $f \in [H_{0;0}^{1,1}(Q)]'$ is as follows:

Find $u \in \mathcal{H}_0(Q)$ such that

$$a_W(u, v) = \langle f, v \rangle_Q \quad (2)$$

for all $v \in H_{0;0}^{1,1}(Q)$, where the bilinear form

$$a_W(\cdot, \cdot) : \mathcal{H}_0(Q) \times H_{0;0}^{1,1}(Q) \rightarrow \mathbb{R}$$

is defined by

$$a_W(u, v) = \langle \square_{Q_-} u, v \rangle_Q$$

for $u \in \mathcal{H}_0(Q)$, $v \in H_{0;0}^{1,1}(Q)$. Next, properties of the bilinear form $a_W(\cdot, \cdot)$ are given and finally, unique solvability of the weak variational formulation (2) is proven.

Lemma 3 *The bilinear form $a_W(\cdot, \cdot)$ fulfils the following properties:*

First, there holds the boundedness

$$|a_W(u, v)| \leq \|\square_{Q_-} u\|_{[H_{0;0}^{1,1}(Q)]'} |v|_{H^1(Q)}$$

for all $u \in \mathcal{H}_0(Q)$, $v \in H_{0;0}^{1,1}(Q)$.

Second, there holds the inf-sup condition

$$\sup_{0 \neq v \in H_{0;0}^{1,1}(Q)} \frac{|a_W(u, v)|}{|v|_{H^1(Q)}} = \|\square_{Q_-} u\|_{[H_{0;0}^{1,1}(Q)]'}$$

for all $u \in \mathcal{H}_0(Q)$.

Third, for each $0 \neq v \in H_{0;0}^{1,1}(Q)$, there exists an element $u \in \mathcal{H}_0(Q)$ with $a_W(u, v) \neq 0$.

A direct consequence of the last lemma is the following main result.

Theorem 4 *For each $f \in [H_{0;0}^{1,1}(Q)]'$, there exists a unique solution $u \in \mathcal{H}_0(Q)$ of the variational formulation (2). Furthermore,*

$$\mathcal{L}_W : [H_{0;0}^{1,1}(Q)]' \rightarrow \mathcal{H}_0(Q), \quad \mathcal{L}_W f = u,$$

is an isomorphism, satisfying

$$\|\square_{Q_-} \mathcal{L}_W f\|_{[H_{0;0}^{1,1}(Q)]'} = \|f\|_{[H_{0;0}^{1,1}(Q)]'}.$$

Conclusions

A new weak space-time variational formulation (2) for the scalar second-order wave equation with a homogeneous Dirichlet boundary condition and homogeneous initial conditions is introduced. Since the related bilinear form is inf-sup stable, this new framework might be used for the analysis of different approximation schemes, e.g., finite element methods or wavelets, and might be useful for deriving and analysing corresponding boundary integral equations, leading to boundary element methods.

References

- [1] O. A. Ladyzhenskaya, *The boundary value problems of mathematical physics*, Springer-Verlag, New York, 1985.
- [2] O. Steinbach and M. Zank, Coercive space-time finite element methods for initial boundary value problems, *Submitted*, 2018.
- [3] O. Steinbach and M. Zank, Inf-Sup Stable Variational Formulations for the Wave Equation, *To be submitted*, 2019.
- [4] M. Zank, *Inf-Sup Stable Space-Time Methods for Time-Dependent Partial Differential Equations*, PhD thesis, TU Graz, 2019.

On Trefftz virtual element spaces

Alexey Chernov¹, Lorenzo Mascotto^{2,*}, Ilaria Perugia², Alexander Pichler²

¹Institut für Mathematik, Carl von Ossietzky Universität, Oldenburg, Germany

²Fakultät für Mathematik, Universität Wien, Vienna, Austria

*Email: lorenzo.mascotto@univie.ac.at

Abstract

We discuss the construction of Trefftz virtual element spaces for certain classes of partial differential equations with zero right-hand side. Such spaces may asymptotically have better approximation properties in terms of the number of basis functions than other Trefftz technologies, such as Trefftz discontinuous Galerkin methods. We present here a “unified” theoretical framework, which allows for extensions to a plethora of other problems. Numerical results will be shown as well.

Keywords: Trefftz methods, virtual element methods

1 Model problems

In order to illustrate in an easy fashion the construction of Trefftz virtual element (VE) spaces, we consider a Laplace and a Helmholtz problems. More precisely, given $\Omega \subset \mathbb{R}^2$ a polygonal domain, $k > 0$ a wave number, and g_L and g_H two functions in $H^{\frac{1}{2}}(\partial\Omega)$ and $H^{-\frac{1}{2}}(\partial\Omega)$, respectively, we aim to approximate the solutions to the two following problems:

$$\begin{cases} \text{find } u \in H_{g_L}^1(\Omega) \text{ such that} \\ (\nabla u, \nabla v)_{0,\Omega} = 0 \quad \forall v \in H_0^1(\Omega), \end{cases} \quad (1)$$

and

$$\begin{cases} \text{find } u \in H^1(\Omega) \text{ such that} \\ (\nabla u, \nabla v)_{0,\Omega} - k^2(u, v)_{0,\Omega} \\ + ik(u, v)_{0,\partial\Omega} = -1/2 \langle g_H, v \rangle_{1/2} \\ \forall v \in H^1(\Omega), \end{cases} \quad (2)$$

where, for any $g \in H^{\frac{1}{2}}(\partial\Omega)$, we have set

$$H_g^1(\Omega) = \{v \in H^1(\Omega) \mid v|_{\partial\Omega} = g \text{ in } H^{\frac{1}{2}}(\partial\Omega)\}.$$

Importantly, both problems are the weak formulation of partial differential equations with zero right-hand side.

2 Local and global Trefftz virtual element spaces

Here, we construct Trefftz VE spaces for problems (1) and (2), see Sections 2.1 and 2.2, respectively.

In both cases, we construct global nonconforming spaces, since this choice allows for a general framework including various problems. We point out that for problem (1), a *conforming* Trefftz space has been introduced in [1].

Henceforth, we denote by \mathcal{T}_n a (conforming) polygonal decomposition of Ω , and \mathcal{E}_n its set of edges. Further, given a polygon $K \in \mathcal{T}_n$, we denote its set of edges by \mathcal{E}^K .

2.1 Nonconforming harmonic VE space for the Laplace problem

It is well known that harmonic polynomials have “proper” h - and p -approximation properties for harmonic functions [2]. However, employing only piecewise harmonic polynomials as an approximation space would lead to a global fully discontinuous space; we can “reduce” the discontinuity of such space by defining global spaces of the form

$$V_n = \{v_n \in L^2(\Omega) \text{ such that} \\ \int_e \llbracket v_n \rrbracket_e q_{p-1} = 0 \forall q_{p-1} \in \mathbb{P}_{p-1}(e) \forall e \in \mathcal{E}_n, \\ v_n|_K \in V_n(K) \forall K \in \mathcal{T}_n\},$$

where $\llbracket \cdot \rrbracket_e$ denotes the jump operator across the edge e , and where

$$V_n(K) = \{v_n \in H^1(K) \mid \Delta v_n = 0, \\ \partial_n v_n|_e \in \mathbb{P}_{p-1}(e) \forall e \in \mathcal{E}_n\}.$$

Thus, the local spaces $V_n(K)$ contain harmonic polynomials, guaranteeing good approximation properties, and the global space V_n contains functions that are “continuous” in an integral sense.

For the analysis of approximation properties of V_n , the construction of the method, and how the basis functions are used in practice, we refer to [3].

2.2 Nonconforming Trefftz VE spaces for the Helmholtz problem

Focusing now on a possible approximation space for the Helmholtz equation (2), we recall that plane waves have “proper” h - and p -approximation properties of functions in the kernel of the Helmholtz operator [4].

However, employing only piecewise plane waves as an approximation space would lead to a global fully discontinuous space; we can “reduce” the discontinuity of such space by defining global spaces of the form

$$V_n = \{v_n \in L^2(\Omega) \text{ such that} \\ \int_e \llbracket v_n \rrbracket_e w_p = 0 \forall w_p \in \mathbb{P}\mathbb{W}_p(e) \forall e \in \mathcal{E}_n, \\ v_n|_K \in V_n(K) \forall K \in \mathcal{T}_n\},$$

where $\llbracket \cdot \rrbracket_e$ denotes the jump operator across the edge e , where $\mathbb{P}\mathbb{W}_p(e)$ denotes the space of Dirichlet traces of p plane waves traveling along different directions, and where

$$V_n(K) = \{v_n \in H^1(K) \mid \Delta v_n + k^2 v_n = 0, \\ \partial_n v_n + ikv_n|_e \in \mathbb{P}\mathbb{W}_p(e) \forall e \in \mathcal{E}^K\}.$$

Thus, the local spaces $V_n(K)$ contain plane waves (guaranteeing approximation properties) and the global space V_n contains functions that are “continuous” in an integral sense.

For the analysis of approximation properties of V_n , the construction of the method, and how the basis functions are used in practice, we refer to [5].

3 Unified framework

The construction of the Trefftz spaces defined in Sections 2.1 and 2.2 can be generalized to partial differential equations of the form $\mathcal{L}u = 0$ endowed with certain boundary conditions, for some differential operator or \mathcal{L} , as follows.

Given $\mathcal{A}_n(K) = \{\tilde{v}_n \mid \mathcal{L}\tilde{v}_n = 0\}$ a space of *computable* functions with “proper” h - and p -approximation properties, one may introduce the local Trefftz space

$$V_n(K) = \{v_n \mid \mathcal{L}v_n = 0, \gamma(v_n)|_e = \gamma(\tilde{v}_n)|_e \\ \text{for some } \tilde{v}_n \in \mathcal{A}_n(K), \forall e \in \mathcal{E}^K\},$$

where γ denotes a “suitable” trace operator. By doing so, it is clear that $\mathcal{A}_n(K) \subseteq V_n(K)$, which entails good approximation properties of $V_n(K)$.

The construction of the global nonconforming space follows along the same lines as in Sections 2.1 and 2.2; in particular, the continuity is enforced in an integral sense by testing the jumps of functions in the global space across edges with *suitable* traces of functions in $\mathcal{A}_n(K)$.

4 Advantages and “cliff effect”

By employing Trefftz VE spaces, one can asymptotically achieve a given accuracy employing less basis functions than other Trefftz methods, such as Trefftz discontinuous Galerkin methods. In particular, it happens that, after few h - and p -refinements, the approximation error converges to zero without a real growth of the dimension of the spaces. This phenomenon, analyzed in [6], has been regarded as “cliff effect” [7].

References

- [1] A. Chernov and L. Mascotto, The harmonic virtual element method: stabilization and exponential convergence for the Laplace problem on polygonal domains, *IMA J. Numer. Anal.* doi: <https://doi.org/10.1093/imanum/dry038>, 2019.
- [2] R. Hiptmair, A. Moiola, I. Perugia and C. Schwab, Approximation by harmonic polynomials in star-shaped domains and exponential convergence of Trefftz hp -dGFEM, *ESAIM Math. Model. Numer. Anal.*, 48(3), pp. 727–752, 2014.
- [3] L. Mascotto, I. Perugia, and A. Pichler, Nonconforming harmonic virtual element method: h - and p -versions, *J. Sci. Comput.*, 77(3), pp. 1874–1908, 2018.
- [4] R. Hiptmair, A. Moiola and I. Perugia, Plane wave discontinuous Galerkin methods for the 2D Helmholtz equation: analysis of the p -version, *SIAM J. Numer. Anal.*, 49(1), pp. 264–284, 2011.
- [5] L. Mascotto, I. Perugia, and A. Pichler, A nonconforming Trefftz virtual element method for the Helmholtz problem, submitted, accepted for publication on *Math. Models Methods Appl. Sci.*, 2019.
- [6] L. Mascotto, I. Perugia, and A. Pichler, A nonconforming Trefftz virtual element method for the Helmholtz problem: numerical aspects, *Comput. Methods Appl. Mech. Engrg.*, 347, pp. 445–476, 2019.
- [7] L. M. Imbert-Gérard, Private Communication, Concepción, Chile, 2019.

A Trefftz discontinuous Galerkin method for acoustic scattering by small circular obstacles

Monique Dauge¹, Ilaria Perugia², Alexander Pichler^{2,*}

¹Institut de recherche mathématique, Université de Rennes, France

²Department of Mathematics, University of Vienna, Austria

*Email: alex.pichler@univie.ac.at

Abstract

We introduce a Trefftz discontinuous Galerkin (DG) method for the numerical approximation of solutions to acoustic scattering problems by small circular obstacles with a mesh resolving the position of the obstacles but not their size. This is achieved by employing circular waves adapted to the geometry, so that boundary conditions around each obstacle are directly embedded in the trial functions. Since the employed basis functions are Trefftz, i.e. they lie elementwise in the kernel of the Helmholtz operator, a large reduction in the required number of degrees of freedom for a given accuracy, when compared to standard finite element methods, can be obtained; see [3] for a survey.

Keywords: acoustic scattering, discontinuous Galerkin methods, Trefftz functions

1 Model problem

Let S_{ε_j} , $j = 1, \dots, N$, be a set of pairwise non-intersecting circular scatterers with radii ε_j and centers \mathbf{x}_j . Given an incident plane wave u^{inc} with wave number $k > 0$, the continuous problem for the scattered acoustic pressure field reads

$$\begin{cases} -\Delta u^{\text{sca}} - k^2 u^{\text{sca}} = 0 & \text{in } \mathbb{R}^2 \setminus S, \\ u^{\text{sca}} = -u^{\text{inc}} & \text{on } \partial S, \\ \lim_{r \rightarrow \infty} \sqrt{r} (\partial_r - ik) u^{\text{sca}} = 0, \end{cases}$$

where $S = \cup_{j=1}^N S_{\varepsilon_j}$ and $r = |\mathbf{x}|$. The total acoustic pressure field is $u := u^{\text{sca}} + u^{\text{inc}}$.

2 Trefftz-DG method

Let $\Omega \subset \mathbb{R}^2$ be a polygonal bounded domain such that $S \subset \Omega$ and $\Sigma := \partial\Omega$ is far from ∂S . We set $\Omega_S := \Omega \setminus S$. Our aim is to design a DG method with the following properties:

- the method is applicable to all kind of polygonal meshes over Ω instead of Ω_S , thus it is not necessary to resolve the size of the scatterers;

- the Sommerfeld radiation condition is directly taken into account by the method.

Both of these aspects will be achieved by the use of specifically tailored basis function that are additionally Trefftz, i.e. local solution to the homogeneous Helmholtz equation, and therefore have good approximation properties.

3 Construction in the case of one circular scatterer

The construction of a method with the above-mentioned properties for the case of one circular scatterer with radius $\varepsilon > 0$ and center \mathbf{x}_0 gives insight for the case of multiple scatterers.

Meshes. Let \mathcal{T}_h^\sharp be a polygonal mesh of Ω not resolving the scatterer. Then, by agglomeration of elements, a mesh \mathcal{T}_h containing the scatterer in exactly one element \tilde{K} can be obtained from \mathcal{T}_h^\sharp . The main idea of the method is to consider the infinite domain $K^\infty := \mathbb{R}^2 \setminus \Omega$ as a single element and then solve the Helmholtz problem over the mesh $\mathcal{T}_h \cup K^\infty$.

Trefftz functions. The following three sets of basis functions are employed: Given effective degrees $q_{\tilde{K}}, q_{K^\infty}, q_K \in \mathbb{N}$,

- $\{W_n^{r[\varepsilon]}(kr)e^{in\varphi}\}_{|n| \leq q_{\tilde{K}}}$ in \tilde{K} ,
- $\{H_n^{(1)}(kr)e^{in\varphi}\}_{|n| \leq q_{K^\infty}}$ in K^∞ ,
- $\{J_n(kr_K)e^{in\varphi_K}\}_{|n| \leq q_K}$ elsewhere,

where $n \in \mathbb{Z}$, (r, φ) and (r_K, φ_K) are the polar coordinates centered at \mathbf{x}_0 and the element barycenters, respectively, and

$$W_n^{[\varepsilon]}(kr)e^{in\varphi} := \left(J_n(kr) + \beta_n^{[\varepsilon]} Y_n(kr) \right) e^{in\varphi},$$

with $\beta_n^{[\varepsilon]} := -\frac{J_n(k\varepsilon)}{Y_n(k\varepsilon)}$. Here, J_n and Y_n denote the Bessel functions of the first and second kind, respectively, and $H_n^{(1)}$ are the Hankel functions of the first kind. By definition, $W_n^{[\varepsilon]}(kr)e^{in\varphi}$ automatically incorporate the homogeneous Dirichlet boundary condition on ∂S_ε ; see e.g. [4].

Trefftz-DG variational formulation. Following the concept of the ultra weak variational formulation [1], after introducing a circular domain B_R centered at \mathbf{x}_0 with radius $R > 0$ such that $\Omega \subset B_R$, one can design a variational formulation over the skeleton of \mathcal{T}_h for

$$\tilde{u}_p := \begin{cases} u_p & \text{in } \Omega_S, \\ u_p^{\text{sca}} & \text{in } K^R := B_R \setminus \bar{\Omega}, \end{cases}$$

where u_p represents an approximation of the total field u inside Ω_S , and u_p^{sca} approximates the scattered field u^{sca} in K^R . By taking $R \rightarrow \infty$, a formulation over \mathbb{R}^2 is obtained.

4 The case of multiple scatterers

The above process can be extended to the case of several small circular scatterers by modification of the involved basis functions. More precisely, after an agglomeration process, one can employ in each element containing a scatterer basis functions of the type $W_n^{[\epsilon]}(kr_j)e^{im\varphi_j}$ with polar coordinates (r_j, φ_j) centered at the scatterer centers. For the approximation of the scattered field u^{sca} , one can either employ sets of Fourier-Hankel functions associated to the scatterer centers ('method 1') or to a common center of gravity ('method 2').

A comparison of these methods can be carried out in terms of the farfield pattern. To this purpose, we consider a numerical example with two circular scatterers with radii $\epsilon = 0.02$ and centers in $(-d, 0)$ and $(d, 0)$, for $d = 0.1$ and $d = 0.4$, respectively. As mesh \mathcal{T}_h , we take the one depicted in Figure 1. Further, we fix $k = 15$ and the effective degrees $q = 35$ in all elements of \mathcal{T}_h . For method 1, we employ $q = 4$ as effective degrees for the two sets of Fourier-Hankel functions associated with to the two scatterers, whereas for method 2, we take $q = 9$. The obtained farfield pattern for $d = 0.1$ and $d = 0.4$ are shown in Figure 2, where we also compare them with 'method 3', which superposes the scattered solutions of the two scatterers without taking the joint backscattering into account. From the plots, we observe that backscattering plays in fact an important role. It turns out that method 2 is preferable when the scatterers are close to each other, whereas method 1 should be used when they are further away.

A full description of the method including exponential error estimates and various numerical experiments will be presented in [2].

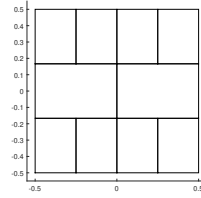


Figure 1: Mesh for the numerical example.

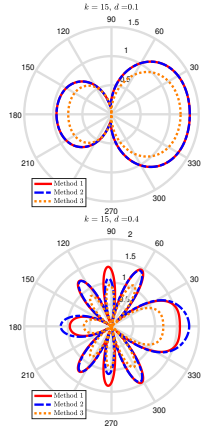


Figure 2: Farfield pattern for two scatterers centered at $(-d, 0)$ and $(d, 0)$, $d = 0.1$ and $d = 0.4$.

References

- [1] O. Cessenat and B. Després, Application of an ultra weak variational formulation of elliptic PDEs to the two-dimensional Helmholtz problem, *SIAM J. Numer. Anal.*, **35** (1998), pp. 255–299.
- [2] M. Dauge, I. Perugia and A. Pichler, in preparation, 2019.
- [3] R. Hiptmair, A. Moiola and I. Perugia, A survey of Trefftz methods for the Helmholtz equation, *LNCS*, Vol. 114, 2016, pp. 237–278, Springer.
- [4] M. Stojek, Least-squares Trefftz-type elements for the Helmholtz equation, *Int. J. Numer. Methods Eng.*, **41** (1998), pp. 831–849.

A DPG Maxwell Approach for Studying Nonlinear Thermal Effects in Active Gain Fiber Amplifiers

Stefan Henneking^{1,*}, Leszek Demkowicz¹, Jacob Grosek²

¹The University of Texas at Austin, USA

²Air Force Research Laboratory, Albuquerque, NM, USA

*Email: stefan@ices.utexas.edu

Abstract

Fiber lasers at high-power operation suffer from undesired thermal coupling effects such as transverse mode instability (TMI). Indeed, TMI is a major obstacle in power-scaling of continuous wave, weakly-guided, large mode area (LMA), active gain, silica fiber amplifiers. A better understanding of these nonlinear coupling effects is beneficial in the design of new fibers. To that end, we propose a three-dimensional discontinuous Petrov-Galerkin (DPG) finite element approach for studying a novel nonlinear full vectorial Maxwell model. The model incorporates both amplification and thermal effects via coupling with the heat equation. The high-frequency nature of this wave propagation problem requires the use of high-order discretizations to effectively counter numerical pollution. We present numerical results for this coupled system, modeling fibers with several hundred wavelengths. Our results provide new insight into the nonlinear effects of laser gain and thermal polarization in fiber amplifiers.

Keywords: High-frequency wave propagation, High-order finite element discretization, Nonlinear fiber optics, Active gain fiber amplifiers

1 Introduction

Continuous wave, weakly guided, LMA, active gain, silica fiber amplifiers can achieve high-power operation with great efficiency and provide highly coherent light sources [4]. We con-

sider a step-index fiber, core-doped with active Ytterbium (Yb) ions that lase around 1064nm very efficiently [4]. Two near-monochromatic fields are present: the signal field, seeded at 1064nm, and the pump field, at 976nm. At high power levels, thermal effects become relevant as they may severely degrade beam quality [2]. We model active gain and thermal effects within a three-dimensional Maxwell formulation coupled with the heat equation in order to investigate nonlinear phenomena in the fiber amplifier.

2 DPG Methodology

The DPG methodology [1] has been successfully applied to various complex multiphysics applications, including acoustic and electromagnetic wave propagation [3, 5]. DPG admits working with any well-posed variational formulation, and it guarantees mesh-independent discrete stability [1]. In the context of high-frequency wave propagation, the ultraweak DPG formulation has proven superior in many ways. Its built-in a-posteriori error estimator enables *hp*-adaptivity in the preasymptotic regime, which has led to state-of-the-art multilevel preconditioners applicable to wave propagation problems [5].

We apply the ultraweak DPG formulation to the full vectorial Maxwell system for two coupled time-harmonic fields. The Maxwell system is then coupled with the primal DPG formulation of the heat equation, yielding a formulation that requires the use of elements of the entire exact sequence [1].

3 Coupled Maxwell/Heat Fiber Model

We assume that no free charges are present in the dielectric silica fiber, and that magnetic polarization of the material is neglectable. Since we are dealing with two near-monochromatic fields, we may apply the time-harmonic ansatz and obtain the time-harmonic Maxwell equa-

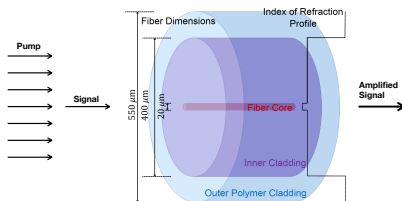


Figure 1: Fiber schematic

tions in the silica fiber:

$$\nabla \times \mathbf{E}_k = -i\omega_k \mu_0 \mathbf{H}_k \quad (1)$$

$$\nabla \times \mathbf{H}_k = i\omega_k (\varepsilon_0 \mathbf{E}_k + \mathbf{P}_k) \quad (2)$$

where $k \in \{s, p\}$ refers to either the signal (s) or pump (p) field. The electric polarization \mathbf{P} is given by,

$$\mathbf{P}_k = \mathbf{P}_k^{\text{background}} + \mathbf{P}_k^{\text{gain}} + \mathbf{P}_k^{\text{thermal}} \quad (3)$$

where the background polarization, assuming an isotropic material refractive index, is

$$\mathbf{P}_k^{\text{background}} = \varepsilon_0 (n^2 - 1) \mathbf{E}_k \quad (4)$$

The gain polarization is derived as a complex perturbation to the refractive index [3],

$$\mathbf{P}_k^{\text{gain}} = i\varepsilon_0 \frac{nc}{\omega_k} g_k (\mathbf{E}_{\{s,p\}}) \mathbf{E}_k \quad (5)$$

And the thermal polarization is induced by the thermal response of the material refractive index in the fiber,

$$\begin{aligned} n(T) &= n(T_{\text{ambient}}) + \delta n \\ &\approx n(T_{\text{ambient}}) + \frac{dn}{dT} (T_{\text{ambient}}) \delta T \end{aligned} \quad (6)$$

where T is the temperature, $\frac{dn}{dT}$ is the thermo-optic coefficient, and δT , δn are the temperature change and the induced refractive index perturbation, respectively. The gain function g_k is derived from Yb ion rate equations [4],

$$g_k \approx -\sigma_k^{\text{abs}} \mathcal{N}_{\text{total}}^{\text{Yb}} + (\sigma_k^{\text{abs}} + \sigma_k^{\text{ems}}) \mathcal{N}_{\text{excited}}^{\text{Yb}} \quad (7)$$

where σ_k^{abs} , σ_k^{ems} are effective ion absorption and emission cross-sections, respectively. The steady-state excited ion population density is,

$$\mathcal{N}_{\text{excited}}^{\text{Yb}} = \frac{\sum_{k=\{s,p\}} \frac{I_k}{h\nu_k} \sigma_k^{\text{abs}}}{\frac{1}{\tau} + \sum_{k=\{s,p\}} \frac{I_k}{h\nu_k} (\sigma_k^{\text{abs}} + \sigma_k^{\text{ems}})} \mathcal{N}_{\text{total}}^{\text{Yb}} \quad (8)$$

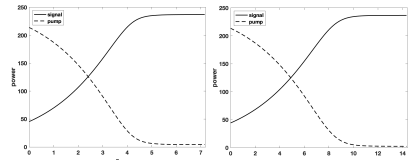
where τ is the upper level radiative lifetime, and $I_k = |\Re\{\mathbf{E}_k \times \mathbf{H}_k^*\}|$ denotes the irradiance.

The derived Maxwell system is coupled with the heat equation, where the heat source Q is dependent upon the gain and optical intensities of the fields inside the fiber core,

$$Q(I_{\{s,p\}}) = -(g_p(I_{\{s,p\}})I_p + g_s(I_{\{s,p\}})I_s) \quad (9)$$

4 Numerical Simulation

The number of wavelengths (λ) in a real length fiber is about 10^7 , which is computationally not feasible in a 3D high-order finite element discretization. To investigate gain and heating effects in a short fiber, we introduce a novel scaling for the coupled system: an artificial gain amplifier \tilde{g}_a and an anisotropic heat diffusion operator. Figure 2 presents gain scaling results by plotting the cross-sectional power along a fiber of 120 and 240 wavelengths, with different gain amplifiers, illustrating the concept of equivalent gain in a short fiber.



(a) 120λ , $\tilde{g}_a = 5.0 \cdot 10^3$ (b) 240λ , $\tilde{g}_a = 2.5 \cdot 10^3$

Figure 2: Gain scaling in short fiber

Acknowledgement

This work is partially supported by AFOSR FA9550-17-1-0090 and AFOSR 18RDCOR018.

References

- [1] C. Carstensen, L. Demkowicz, and J. Gopalakrishnan. Breaking spaces and forms for the DPG method and applications including Maxwell equations. *Comput. Math. Appl.*, 2016.
- [2] T. Eidam et al. Experimental observations of the threshold-like onset of mode instabilities in high power fiber amplifiers. *Optics express*, 19(14):13218–13224, 2011.
- [3] S. Nagaraj et al. A 3D DPG Maxwell approach to nonlinear Raman gain in fiber laser amplifiers. *ICES report (accepted in J. Comput. Phys.)*, 18–12, 2018.
- [4] H. Pask et al. Ytterbium-doped silica fiber lasers: versatile sources for the 1–1.2 μm region. *IEEE Journal of Selected Topics in Quantum Electronics*, 1(1):2–13, 1995.
- [5] S. Petrides. Adaptive multilevel solvers for the discontinuous Petrov-Galerkin method with an emphasis on high-frequency wave propagation. *Ph.D. dissertation, The University of Texas at Austin*, 2019.

A numerical algorithm to reduce the ill conditioning in meshless methods for the Helmholtz equation

Pedro R. S. Antunes¹

¹Group of Mathematical Physics - University of Lisbon

Abstract

Some meshless methods have been applied to the numerical solution of boundary value problems involving the Helmholtz equation. In this work we focus on the Method of Fundamental Solutions and the Plane Waves Method. It is well known that these methods can be highly accurate assuming smoothness of the domains and the boundary data. However, the matrices involved are often ill-conditioned and the effect of this ill conditioning may drastically reduce the accuracy. In this work, we propose a numerical algorithm to reduce the ill conditioning in both methods. The idea is to perform a suitable change of basis. This allows to obtain new basis functions that span exactly the same space as the original meshless method, but are much better conditioned.

Keywords: Helmholtz equation, method of fundamental solutions, plane waves, ill conditioning

1 The direct approaches of the Method of Fundamental Solutions (MFS) and the Plane Waves Method (PWM)

Let Ω be a smooth bounded planar domain. We consider the following boundary value problem,

$$\begin{cases} \Delta u + \kappa^2 u = 0 & \text{in } \Omega, \\ u = g & \text{on } \partial\Omega, \end{cases} \quad (1)$$

for some given function g defined on $\partial\Omega$.

We will denote by Φ_κ a fundamental solution of the Helmholtz equation,

$$\Phi_\kappa(x) = \frac{i}{4} H_0^{(1)}(\kappa|x|),$$

where $H_0^{(1)}$ is a Hankel function of the first kind of order zero. This fundamental solution is analytic, except at the origin, where it has a logarithmic type singularity. The standard approach of the Method of Fundamental Solutions, which will be called *Direct-MFS*, approximates the solution of the boundary value problem (1) by a linear combination

$$u_N^{MFS-Dir}(x) = \sum_{j=1}^N \alpha_j^{MFS-Dir} \Phi_\kappa(x - y_j). \quad (2)$$

Each basis function is a translation of the fundamental solution to some source point y_j placed on some admissible source set $\tilde{\Gamma}$ that does not intersect $\bar{\Omega}$. Thus, by construction it satisfies the PDE of the problem. The approximation of the boundary condition can be justified by density results (eg. [1]). We will assume that the source points are distributed uniformly on a circumference of radius $R > R_\Omega := \max_{x \in \partial\Omega} \|x\|$,

$$y_j = R(\cos(\gamma_j), \sin(\gamma_j)), \quad j = 1, \dots, N, \quad \gamma_j = \frac{2\pi j}{N} \quad (3)$$

The coefficients of the linear combination (2) can be determined by collocation, forcing the boundary conditions of the problem. We consider P collocation points $x_i, i = 1, 2, \dots, P$, and solve

$$\mathbf{A}^{MFS-Dir} \boldsymbol{\alpha}^{MFS-Dir} = \mathbf{G}, \quad (4)$$

where

$$\mathbf{A}^{MFS-Dir} = [\Phi_\kappa(x_i - y_j)]_{P \times N}, \quad \mathbf{G} = [g(x_i)]_P$$

and $\boldsymbol{\alpha}^{MFS-Dir}$ is a vector with all the coefficients of the *Direct-MFS* linear combination (2). In this work we took $P = 2N$ and solved (4) in the least-squares sense.

Another Trefftz type method is the PWM. In this case, for given unitary directions d_1, d_2, \dots, d_N the numerical approximation for the solution of the boundary value problem is a linear combination of plane waves,

$$u_N^{PWM-Dir}(x) = \sum_{j=1}^N \alpha_j^{PW-Dir} e^{i\kappa x \cdot d_j}. \quad (5)$$

The approximation of the boundary condition is justified by a density result, stating that if Ω is a bounded simply connected domain and κ is not an eigenfrequency of Ω , then (eg. [4])

$$L^2(\partial\Omega) = \overline{\text{span}\{e^{i\kappa x \cdot d} : d \in S^1\}}.$$

The *Direct-MFS* can be highly accurate, even with a small number of source points. For example, the method can achieve exponential convergence on analytic domains and boundary data

[3,5]. On the other hand, the linear least squares problem is often ill-conditioned, which affects the accuracy and prevents the exponential convergence to be observed in the numerical simulations.

2 New formulations - the MFS-QR and PWM-QR algorithms

We assume that the source points are given by (3), for $R > R_\Omega$. Dropping the constant $i/4$ that may be incorporated in the coefficients of the linear combination, by Graf’s addition theorem [4], each MFS basis function can be written as

$$H_0^{(1)}(\kappa|x - y_j|) = H_0^{(1)}(\kappa|y_j|)J_0(\kappa|x|) + 2 \sum_{n=1}^{\infty} H_n^{(1)}(\kappa|y_j|)J_n(\kappa|x|) \cos(n\beta),$$

where β denotes the angle between x and y_j . We will use the notation $\hat{x} = x/|x|$ and $\hat{y}_j = y_j/|y_j|$ and write $\hat{x} = (\cos(\theta), \sin(\theta))$, for some $\theta \in [0, 2\pi)$. Then,

$$\hat{x} \cdot \hat{y}_j = \cos(\theta) \cos(\gamma_j) + \sin(\theta) \sin(\gamma_j) = \cos(\theta - \gamma_j)$$

and by the law of cosines,

$$\hat{x} \cdot \hat{y}_j = |\hat{x}| |\hat{y}_j| \cos(\beta) = \cos(\beta).$$

Therefore, in polar coordinates, we have

$$\psi_j(r, \theta) := H_0^{(1)}(\kappa R)J_0(\kappa r) + 2 \sum_{n=1}^{\infty} H_n^{(1)}(\kappa R)J_n(\kappa r)[\cos(n\theta) \cos(n\gamma_j) + \sin(n\theta) \sin(n\gamma_j)].$$

Concerning the PWM we can use Jacobi-
Anger expansion [4],

$$e^{i\kappa x \cdot d} = J_0(\kappa|x|) + 2 \sum_{n=1}^{\infty} i^n J_n(\kappa|x|) \cos(n\beta), \tag{6}$$

where in this case β is the angle between x and d . Thus, writing $d_j = (\cos(\gamma_j), \sin(\gamma_j))$ each basis function is written in polar coordinates as

$$\phi_j(r, \theta) := J_0(\kappa r) + 2 \sum_{n=1}^{\infty} i^n J_n(\kappa r)[\cos(n\theta) \cos(n\gamma_j) + \sin(n\theta) \sin(n\gamma_j)].$$

We will skip the details that can be found in [2], but after truncating these expansions, we are led to the following matrix factorization

$$\Theta(r, \theta) = \mathbf{B} \mathbf{D} \mathbf{F}(r, \theta), \tag{7}$$

where $\Theta(r, \theta)$ is a vector-valued function of all the basis functions of each of the methods, the matrix \mathbf{B} is well-conditioned, even for large values of N . The ill-conditioning of the *Direct-MFS* arises essentially from the diagonal matrix \mathbf{D} . To reduce this ill-conditioning we propose an algorithm which allows to construct new basis functions. The main idea is to use the fact that if we multiply an invertible matrix from the left in (7), this procedure will change the basis functions without modifying the functional space that is generated by them. Thus, we propose a way to determine such a suitable matrix to be multiplied from the left, and instead of the basis functions defined through (7), we propose to use a new set of basis function defined by

$$\Psi(r, \theta) = \tilde{\mathbf{R}} \mathbf{F}(r, \theta), \tag{8}$$

for a convenient matrix $\tilde{\mathbf{R}}$ (see [2] for details).

References

[1] C. J. S. Alves and P. R. S. Antunes, *The method of fundamental solutions applied to some inverse eigenproblems*, SIAM J. Sci. Comp. **35** (2013), A1689–A1708.

[2] P. R. S. Antunes, A numerical algorithm to reduce the ill conditioning in meshless methods for the Helmholtz equation, *Numerical Algorithms* **79**(3), (2018), pp. 879–897.

[3] A.H. Barnett and T. Betcke, Stability and convergence of the method of fundamental solutions for Helmholtz problems on analytic domains, *J. Comput. Phys.*, **227**(14) (2008), pp. 7003–7026.

[4] D. Colton and R. Kress, *Inverse Acoustic and Electromagnetic Scattering*, 3rd ed. Springer, Berlin (2013).

[5] M. Katsurada, A mathematical study of the charge simulation method. II, *J. Fac. Sci. Univ. Tokyo Sect. IA Math.* **36** (1) (1989), pp. 135–162.

New Mass-Lumped Tetrahedral Elements for 3D Wave Propagation Modelling

S. Geevers^{1,*}**Abstract**

We present a new accuracy condition for constructing mass-lumped elements. This condition is less restrictive than the one previously used and enabled us to construct new mass-lumped tetrahedral elements for 3D wave propagation modelling. The new degree-2 and degree-3 elements require significantly fewer nodes than previous versions and mass-lumped tetrahedral elements of higher degree had not been found before. We also present a new accuracy condition for evaluating the stiffness matrix-vector product. This enabled us to obtain tailored quadrature rules for the new elements that further reduce the computational cost.

Keywords: mass lumping, tetrahedral element, spectral element, wave equation

1 Introduction

Finite element methods offer a good alternative to finite difference methods for wave propagation modelling when the geometry of objects or the topography of seismic models need to be accurately modelled. Tetrahedral elements are particularly suitable for complex 3D models due to their geometric flexibility. A major drawback of the classical finite element method, however, is that, at each time step, it requires solving a large system of equations of the form $Mx = y$, with M the stiffness matrix, which is large and sparse, but not diagonal. The high computational cost required for solving this linear problem is avoided by lumping the mass matrix into a diagonal matrix. This is accomplished by approximating the matrix using a quadrature rule and by placing the basis function nodes at the quadrature points.

For first-order elements, mass-lumping is accomplished by placing the quadrature points and nodes at the vertices. Higher-order triangular and tetrahedral mass-lumped elements are obtained by enriching the element space with higher-degree bubble functions [1–3, 5]. For tetrahe-

Table 1: Element spaces \hat{U} of mass-lumped tetrahedral elements of degree p with $\#$ nodes. Asterisks indicate new elements.

p	$\#$	\hat{U}
2*	15	$P_2 + F + I$
2	23	$P_2 + FP_1 + I$
3*	32	$P_3 + FP_1 + IP_1$
3	50	$P_3 + FP_2 + IP_2$
4*	60	$P_4 + FP_2 + I(P_2 + F)$
4*	61	$P_4 + FP_2 + I(P_2 + F + I)$
4*	65	$P_4 + F(P_2 + F) + I(P_2 + F + I)$

dra, only elements up to degree 3 [1, 5] were available. By deriving a new and less restrictive accuracy condition for the quadrature rule, we could obtain mass-lumped tetrahedral elements of degree 4 and new elements of degree 2 and 3 with significantly fewer nodes.

To further improve the efficiency of the numerical scheme, we also derived a new accuracy condition for evaluating the stiffness matrix-vector product and obtained new tailored quadrature rules with less points than rules previously available. It is known that, for higher-degree elements, computing the stiffness matrix-vector product on the fly is more efficient than using a pre-assembled matrix and recently, we showed that the new quadrature rules also outperform exact integration algorithms [4].

2 New mass-lumped elements

Previously, the accuracy condition imposed on the quadrature rule for the mass matrix was exactness for polynomials of degree $p + p' - 2$, with p the polynomial degree of the element and p' the highest polynomial degree of the enriched element space. We proved in [3] that, to obtain optimal convergence rates, it is sufficient if the quadrature rule is exact for $\hat{U} \otimes P_{p-2}$, where \hat{U} denotes the element space and P_{p-2} the poly-

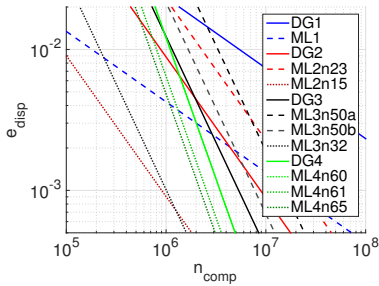


Figure 1: Dispersion error of the symmetric interior penalty DG method (solid), the former mass-lumped element method (dashed), and the new mass-lumped elements (dotted).

mials of degree at most $p - 2$.

Using this new accuracy condition, we were able to construct new mass-lumped tetrahedral elements. An overview of the different elements is given in Table 1. There, F denotes the set of degree-3 face bubble functions and I denotes the degree-4 interior bubble function.

The efficiency of the new and former mass-lumped elements, together with symmetric interior penalty discontinuous Galerkin methods, have also been compared using a dispersion analysis. The dispersion error, defined as the relative error of the numerical wave propagation speed, is computed for travelling plane waves moving through a regular tetrahedral mesh and is plotted in Figure 1 against the estimated computational cost, which is based on the size of the stiffness matrix and the number of time steps. The figure shows that the new mass-lumped methods are more efficient than the previous ones and the DG methods, especially for $p = 2$ and $p = 3$.

3 Tailored quadrature for the stiffness matrix

To obtain optimal convergence rates, it is sufficient to approximate the stiffness matrix-vector product using a quadrature rule that is exact for $D\hat{U} \otimes P_{p-1}$ [4], with $D\hat{U}$ the space of all partial derivatives of all functions in \hat{U} . With this condition, we obtained tailored quadrature rules for the new elements. A comparison with other available quadrature rules is given in Table 2.

Table 2: Number of quadrature points of the new tailored rules, order- $(p + p' - 2)$, and exact (order- $(2p' - 2)$) rules, for computing the stiffness matrix-vector product of the new n -node degree- p mass-lumped tetrahedral elements.

$p-n$	new	order- $(p + p' - 2)$	exact
2-15	14	14	24
3-32	21	24	46
4-60	51	59	127
4-61	60	79	194
4-65	60	79	194

Especially the tailored rules for the degree-4 elements have significantly less points than other rules available in the literature.

Various numerical tests also confirm the efficiency of the new mass-lumped elements.

References

- [1] M.J.S. Chin-Joe-Kong, W.A. Mulder and M. van Veldhuizen, Higher-order triangular and tetrahedral finite elements with mass lumping for solving the wave equation, *J Eng Math* **35-4** (1999), pp. 405–426.
- [2] G. Cohen, P. Joly and N. Tordjman, Higher order triangular finite elements with mass lumping for the wave equation *SIAM J Numer Anal* **38-6** (2001), pp. 2047–2078.
- [3] S. Geevers, W.A. Mulder and J.J.W. van der Vegt, New Higher-Order Mass-Lumped Tetrahedral Elements for Wave Propagation Modelling, *SIAM J Sci Comput* **40-5** (2018), pp. A2801–A2829.
- [4] S. Geevers, W.A. Mulder and J.J.W. van der Vegt, Efficient quadrature rules for computing the stiffness matrices of mass-lumped tetrahedral elements for linear wave problems, accepted for publication in *SIAM J Sci Comput*.
- [5] W.A. Mulder, A comparison between higher-order finite elements and finite differences for solving the wave equation, in *Proceedings of the 2nd ECCOMAS Conference on Numerical Methods in Engineering, Paris, France, 9-13 September 1996*, pp. 344–350.

Study of a stable hybridization method to couple FVTD/DG scheme with FDTD/FEM scheme

N. Deymier¹, S. Pernet², X. Ferrieres^{3,*}¹GERAC, 1 rond point du général Eisenhower, 31120 Toulouse, France²ONERA/DTIS-LMA2S, Université de Toulouse, F-31055 Toulouse, France³ONERA/DEM/R-LMA2S, Université de Toulouse, F-31055 Toulouse, France

*Email: xavier.Ferrieres@onera.fr

Abstract

The purpose of this paper is the study of a stable method for coupling two types of schemes using or not numerical fluxes for the resolution of Maxwell's equations in time domain. The methods considered in the hybridization process are Finite Volume (FV), Finite Element (FEM), Finite Difference (FD) and Discontinuous Galerkin (DG). We give the principle of the hybrid method and by the study of an energetic quantity, one specifies the conditions of stability of it. Finally, one example is given to validate the proposed hybrid method.

Keywords: Hybrid method, finite element scheme, Galerkin discontinuous scheme, Maxwell's equations in time domain

Introduction

Current electromagnetic problems require the processing of complex structures in which geometrical details, computational time and size of the discrete problem are important factors to consider in the simulation. To increase the performances in terms of computation time and storage memory, the use of cartesian meshes is preferred, whereas near the geometry, to guarantee the precision, it is rather necessary to use a non-structured mesh. For each type of mesh or class of problems, there are different kinds of schemes more or less appropriate to solve it. This is due to the approximations made in the scheme which induce different kinds of errors on the solution. Then, to improve the simulation, a good idea consists in dividing the computational domain into different sub-domains where we apply the most appropriate numerical method to solve the Maxwell equations. In this strategy, different numerical schemes are coupled and the difficulty lies in having a stable and consistent hybrid scheme. In this paper, we propose a stable hybrid method allowing to take into account FV, FD, FEM and DG schemes. After the presentation of the hybridization principle, by considering a leapfrog time discretization for the hybrid method, one shows that it exists a condition according to the schemes taken in the hybridization which ensures the conservation of an energetic quantity. This condition gives a stability condition of the hybrid method. Next, we give some results on the study of a propagative mode inside a wave guide to validate the proposed hybrid method.

Principle of the hybrid method

In this paper we present a hybrid method based on the coupling of some numerical schemes (FEM, DG, FD etc.) to solve the transient Maxwell equations. One of the main difficulties is to ensure the stability of the method at the space and time level. In the literature, it exists, for example, several approaches constructed from interpolation techniques which suffer from numerical instabilities. To overcome this problem, we propose to use a DG formalism in order to couple together in a stable manner the sub-domains in which different numerical methods are used. Now, we briefly explain our approach. Let $(\Omega_i)_{i=1, \dots, N}$ be a partition of the computational domain Ω , $\Sigma_{i,j} := \Omega_i \cap \Omega_j$, $n_{i,j}$ the unit normal to $\Sigma_{i,j}$ directed from Ω_i et Ω_j and $V(i)$ is the set of neighbour subdomains of Ω_i . In a first step, we write the Maxwell problem in Ω as a transmission one on the subdomains : $\forall i = 1, \dots, N$,

$$\varepsilon \frac{\partial E_i}{\partial t} - \nabla \times H_i = J \text{ in } \Omega_i \quad (1a)$$

$$\mu \frac{\partial H_i}{\partial t} + \nabla \times E_i = 0 \text{ in } \Omega_i \quad (1b)$$

$$n_{i,j} \times E_i = n_{i,j} \times E_j \text{ on } \Sigma_{i,j}, \forall j \in V(i) \quad (1c)$$

$$n_{i,j} \times H_i = n_{i,j} \times H_j \text{ on } \Sigma_{i,j}, \forall j \in V(i) \quad (1d)$$

Next, we rewrite (1) in a weak form by using a DG approach : $\forall \varphi, \psi \in H(\text{curl}, \Omega_i)$,

$$\int_{\Omega_i} \left(\varepsilon \frac{\partial E_i}{\partial t} - \nabla \times H_i \right) \cdot \varphi \, dx = \int_{\Omega_i} J \cdot \varphi \, dx + \sum_{j \in V(i)} \int_{\Sigma_{i,j}} \alpha_{i,j} (n_{i,j} \times H_i - n_{i,j} \times H_j) \cdot \varphi \, d\gamma \quad (2a)$$

$$= \int_{\Omega_i} \left(\mu \frac{\partial H_i}{\partial t} + \nabla \times E_i \right) \cdot \psi \, dx - \sum_{j \in V(i)} \int_{\Sigma_{i,j}} \gamma_{i,j} (n_{i,j} \times E_i - n_{i,j} \times E_j) \cdot \psi \, d\gamma \quad (2b)$$

To ensure the equivalence of this reformulation with the original problem, the coefficients $\alpha_{i,j}$ and $\gamma_{i,j}$ must be as follows :

$$1 - \alpha_{i,j} + \alpha_{j,i} = 0 \text{ and } 1 - \gamma_{i,j} + \gamma_{j,i} = 0 \\ \alpha_{i,j} + \gamma_{j,i} = 0 \text{ and } \alpha_{j,i} + \gamma_{j,i} = 0$$

Stability

We now use in each subdomain Ω_i an adapted spatial numerical scheme (FEM, DG, FDTD, FV) and a second order leapfrog scheme for the time discretization. To ensure the stability of the hybrid scheme, we study the evolution in time of a quantity given by $\int_{\Omega} \varepsilon E(x) \cdot E(x) dx + \int_{\Omega} \nu H(x) \cdot H(x) dx$.

More precisely, we have to prove that this quantity is maintained or decreased along the time. For example, by considering an hybridization between DG [1] and FEM [2] methods, we have [3] :

$$\Delta t \leq \frac{2}{c_0 \left[\max(A_1, A_2, A_3) \right]} \quad \text{with}$$

$$A_1 = \sqrt{\rho \left(\hat{\mathcal{M}}_1^{-\frac{1}{2}} \hat{\mathcal{R}}_1 \hat{\mathcal{M}}_1^{-\frac{1}{2}} \right) + \frac{\sqrt{\mu}}{\sqrt{\varepsilon}} \max \left(\rho \left(\hat{\mathcal{M}}_1^{-\frac{1}{2}} \hat{\mathcal{B}}_1^E \hat{\mathcal{M}}_1^{-\frac{1}{2}} \right) \right)}$$

$$A_2 = \rho \left(\hat{\mathcal{M}}_1^{-\frac{1}{2}} \hat{\mathcal{B}}_1^H \hat{\mathcal{M}}_1^{-\frac{1}{2}} \right)$$

$$A_3 = \frac{1}{\Lambda_{\mathcal{K}}} \left(\sqrt{\rho \left(\hat{\mathcal{M}}_2^{-\frac{1}{2}} \hat{\mathcal{R}}_2 \hat{\mathcal{M}}_2^{-\frac{1}{2}} \right) + \frac{\sqrt{\mu}}{\sqrt{\varepsilon}} \rho \left(\hat{\mathcal{M}}_2^{-\frac{1}{2}} \hat{\mathcal{B}}_2 \hat{\mathcal{M}}_2^{-\frac{1}{2}} \right)} \right)$$

with $\rho(A)$ the spectrum radius, c_0 the waves speed, the matrices $\hat{\mathcal{M}}_2, \hat{\mathcal{R}}_2, \hat{\mathcal{B}}_2$ the mass, stiffness and jump matrices for the DG scheme and $\hat{\mathcal{M}}_1, \hat{\mathcal{R}}_1, \hat{\mathcal{B}}_1^E, \hat{\mathcal{B}}_1^H$ the same for FEM. $\Lambda_{\mathcal{K}}$ is a coefficient which depends on the Jacobian matrix of the transformation between \mathcal{K} and the unit element for the DG scheme.

Numerical validation

To validate our hybrid method, we propose to study a propagative mode inside a curved wave guide. The guide is divided into two parts on which a hybrid FEM/DG method is applied (see Figure 1). In Figure 2, we compare the results obtained with our hybrid FEM/DG method and with a DG method applied on all the problem. We can show on this figure the good agreement between the solutions obtained by our FEM/DG and the DG methods at a test-point located inside the curved guide.

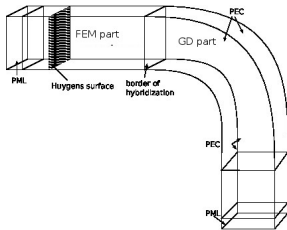


Figure 1: Curved guide geometry with the two domains for FEM/GD Hybrid method.

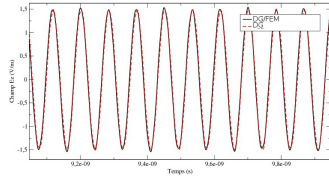


Figure 2: Comparison between FEM/DG and DG approaches.

Conclusion

In this paper, we proposed a stable hybrid method between continuous and discontinuous Galerkin scheme in order to solve the Maxwell equations in time domain. We have specified how to establish a stability condition for two combined methods and we give, as example, a stability condition for a hybrid FEM/DG method. Finally, we showed a validation of this method by comparison to a reference DG solution, based on the computation of a propagative mode inside a curved wave guide.

References

- [1] G.Cohen, X.Ferrières and S. Pernet, A spatial high order discontinuous Galerkin Method to solve Maxwell's equation in time domain, *Journal of Computational Physics* 217 (2006) 340-363.
- [2] N.Deymier, T.Volpert, X.Ferrières, V.Mouysset, B.Pecqueux, New High order FDTD method to solve EMC problem, *Advanced Electromagnetics*, vol.4, No.2, october 2015.
- [3] N.Deymier, Etude d'une méthode éléments finis d'ordre élevé et de son hybridation, *PHD université de Toulouse*, 2016.

A residual-based artificial viscosity finite difference method for scalar conservation laws

Vidar Stiernström^{1,*}, Lukas Lundgren¹, Murtazo Nazarov¹, Ken Mattsson¹

¹Department of Information Technology, Uppsala University, Uppsala, Sweden

*Email: vidar.stiernstrom@it.uu.se

Abstract

We present a residual-based artificial viscosity (AV) finite difference method (FDM) for solving scalar conservation laws. The AV is constructed such that at most first-order upwind dissipation is applied at shocks, without destroying accuracy in smooth regions. The spatial discretization uses summation-by-parts (SBP) finite difference operators and boundary conditions are imposed weakly through simultaneous approximation terms (SAT), allowing for fully explicit time integration of the resulting scheme. The method is benchmarked against the 2D advection equation and the Kurganov-Petrova-Popov (KPP) rotating wave problem.

Keywords: finite difference methods, high-order accuracy, scalar conservation laws, first-order viscosity, upwinding, shock-capturing

1 Introduction

Conservation laws govern fundamental physical processes and are of interest in many engineering applications. Developing accurate and stable solution methods for non-linear conservation laws is a challenging task which has received considerable attention in the last decades. Noted by Lax already in the 1950s, first-order convergence for non-linear hyperbolic equations is readily achieved by using the first-order upwind flux. In recent work within the finite element community (see e.g [1, 2]), non-linear stabilization methods utilizing a residual- or entropy-based AV have shown to be successful where many traditional stabilization methods converge to incorrect entropy solutions. However, in contrast to entropy-based AV, residual-based AV is proven to be convergent [1]. To our knowledge, a residual-based AV-FDM is currently lacking in the literature, and differs from the FEM setting in particular regarding treatment of boundaries. The FDM presented here is based on the SBP-SAT framework, which is a robust and well-proven high-order methodology that ensures stability of time-dependent partial differential equations. In the present work, diagonal-norm up-

wind operators derived in [3] are used to provide additional high-order dissipation, suppressing oscillations in regions away from shocks.

2 Residual-based artificial viscosity

For a conserved quantity u with flux $\mathbf{f}(u)$ defined on the domain Ω , the associated scalar conservation law is given by

$$u_t + \nabla \cdot \mathbf{f}(u) = 0, \quad \bar{x} \in \Omega, \quad t \geq 0 \quad (1)$$

Discretizing (1) in space using SBP finite difference operators, results in the semi-discrete problem

$$\bar{u}_t = -D_f(\bar{u}) + D_2^{(\varepsilon)}(\bar{u}) + SAT, \quad t \geq 0 \quad (2)$$

where D_f is a discretization of $\nabla \cdot \mathbf{f}$ and $D_2^{(\varepsilon)}$ is a variable-coefficient second-derivative operator introducing diffusion proportional to ε . Well-posed boundary conditions for (1) are imposed through the *SAT* term, allowing for a proposed linearly stable discretization. The AV is chosen as

$$\varepsilon = \min(\varepsilon_1, \varepsilon_r) \quad (3)$$

with

$$\varepsilon_1 = C_1 h |\mathbf{f}'(\bar{u})|, \quad \varepsilon_r = C_r h^2 \max_{loc} \frac{|R(\bar{u})|}{n(\bar{u})}.$$

ε_1 is the first-order upwind viscosity, where C_1 is a constant and h is the grid spacing. For instance, discretizing (2) using second-order central differences and choosing $C_1 = \frac{1}{2}$, one retains the traditional Lax-Friedrichs scheme for $\varepsilon = \varepsilon_1$. Shock detection is provided by the residual viscosity ε_r , where C_r is a constant, $R(\bar{u})$ is the residual and $n(\bar{u}) = |\bar{u} - \|\bar{u} - \text{mean}(\bar{u})\|_{L2}|$ is a normalization, with $\bar{u} = \max_{loc} \bar{u} - \min_{loc} \bar{u}$. Here \max_{loc} denotes the maximum of neighboring grid points (similarly for \min_{loc}). In the present work, $C_1 = \frac{1}{2}$, $C_r = 1$ is used. The residual $R(\bar{u})$ is calculated as

$$R(\bar{u}) = D_t(\bar{u}) + \tilde{D}_f(\bar{u}), \quad (4)$$

where $D_t(\bar{u})$ and $\tilde{D}_f(\bar{u})$ are discretizations of u_t and $\nabla \cdot \mathbf{f}(u)$, respectively. In the present work, $D_t(\bar{u})$ is computed using higher-order backward difference formulas, while $\tilde{D}_f(\bar{u})$ is discretized using SBP finite difference operators.

3 Computations

Consider the 2D advection equation

$$u_t + (\mathbf{a} \cdot \nabla)u = 0, \quad \bar{x} \in \Omega, \quad t \geq 0, \quad (5)$$

with a rotating velocity field $\mathbf{a}(x, y) = (-y, x)$ on $\Omega = [-0.5, 0.5] \times [-0.5, 0.5]$. In order to demonstrate that the AV is localized to regions with steep gradients, (5) is solved with initial data given by a slotted cylinder, a cone and a hump, as shown in Figure 1a. The solution is calculated at $t = 2\pi$ using a 5th order accurate spatial discretization on a 401×401 grid. The solution together with the AV is presented in Figures 1b - 1c. Note that the shape of the cone and the hump is preserved, while the cylinder is diffused along its edges.

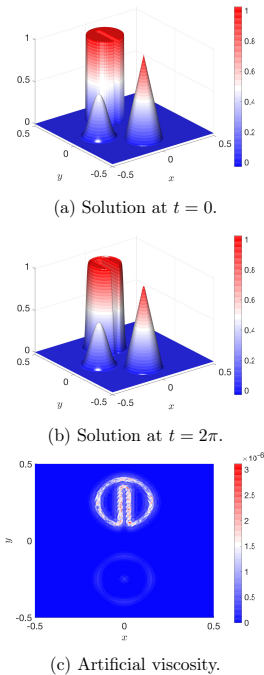


Figure 1: Advection equation.

Finally to illustrate that the method can handle non-convex fluxes, the KPP rotating wave problem given by (2) with $\mathbf{f}(u) = (\sin u, \cos u)$ is solved, using initial data as in [2]. The result

at $t = 1$ is presented in Figure 2 using a 5th order accurate spatial discretization and 401×401 grid points.

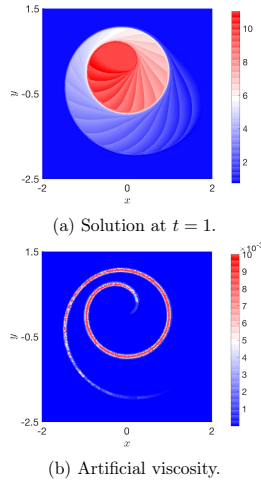


Figure 2: KPP rotating wave problem.

Although not presented here, expected first-order convergence in presence of shocks has been verified for the 2D Burgers' equation. Furthermore convergence for smooth problems has been verified for (5), where the solution converges with the accuracy of the spatial discretization. This has been tested using 3rd up to 9th order accurate SBP finite difference operators. In future work, we hope to extend the method to systems of equations and include the positivity preserving property.

References

- [1] M. Nazarov, Convergence of a residual based artificial viscosity finite element method, *Comput. Math. Appl.*, **65** (2013), pp 616–626
- [2] J.-L. Guermond, and M. Nazarov, A maximum-principle preserving C^0 finite element method for scalar conservation equations, *Comput. Methods Appl. Mech. Engrg.* **272** (2014), pp. 198–213
- [3] K. Mattsson, Diagonal-norm upwind SBP operators, *J. Comput. Phys.*, **335** (2017), pp 283 - 310

Globally Divergence-Free Discontinuous Galerkin Methods for Ideal Magnetohydrodynamics Equations

Pei Fu^{1,*}, Fengyan Li², Yan Xu³

¹Department of Information Technology, Uppsala University, Uppsala, Sweden

²Department of Mathematical Sciences, Rensselaer Polytechnic Institute, Troy, USA

³School of Mathematical Sciences, University of Science and Technology of China, Hefei, China

*Email: pei.fu@it.uu.se

Abstract

Ideal magnetohydrodynamic (MHD) equations are widely used in many areas in physics and engineering, and these equations have a divergence-free constraint on the magnetic field. In this paper, we propose a high order globally divergence-free numerical methods to solve the ideal MHD equations. The algorithms are based on discontinuous Galerkin methods in space. The induction equation is discretized separately to approximate the normal components of the magnetic field on elements interfaces, and to extract additional information about the magnetic field when higher order accuracy is desired. This is then followed by an element by element reconstruction to obtain the globally divergence-free magnetic field. In time, strong-stability-preserving Runge-Kutta methods are applied. Our methods are local and the approximated magnetic fields are globally divergence-free. Numerical examples are presented to demonstrate the accuracy and robustness of the methods.

Keywords: Globally divergence-free; Discontinuous Galerkin method; MHD equation

1 Introduction

In this paper [1], we developed globally divergence-free discontinuous Galerkin (DG) methods to numerically simulate ideal magnetohydrodynamic (MHD) equations. The main difficulties to solve MHD equations are to solve the whole nonlinear system and to handle the divergence-free constraint. Our work follows the development of exactly divergence-free central DG methods for ideal MHD equations in [2], and it is related to the exactly divergence-free DG methods for the magnetic induction equations using multi-dimensional Riemann solvers [3]. We obtain the globally divergence-free magnetic field based on the discrete space for magnetic field with exactly divergence-free space and computing locally. The main difficulty in our method is how

to approximate electric field flux in DG scheme on element interface.

2 MHD equations and DG scheme

The MHD equation in two dimension is

$$\begin{aligned} \frac{\partial \rho}{\partial t} + \nabla \cdot (\rho \mathbf{u}) &= 0, \\ \frac{\partial(\rho \mathbf{u})}{\partial t} + \nabla \cdot [\rho \mathbf{u} \mathbf{u}^T + (p + \frac{1}{2} |\mathbf{B}|^2) \mathbf{I} - \mathbf{B} \mathbf{B}^T] &= 0, \\ \frac{\partial \mathbf{B}}{\partial t} - \nabla \times (\mathbf{u} \times \mathbf{B}) &= 0, \\ \frac{\partial \mathcal{E}}{\partial t} + \nabla \cdot [(\mathcal{E} + p + \frac{1}{2} |\mathbf{B}|^2) \mathbf{u} - \mathbf{B}(\mathbf{u} \cdot \mathbf{B})] &= 0, \end{aligned}$$

with a divergence-free constraint

$$\nabla \cdot \mathbf{B} = 0.$$

We rewrite it as

$$\begin{aligned} \frac{\partial \mathbf{U}}{\partial t} + \nabla \cdot \mathbf{F}(\mathbf{U}, \mathbf{B}) &= 0, \\ \frac{\partial \mathbf{B}}{\partial t} + \widehat{\nabla} \times E_z(\mathbf{U}, \mathbf{B}) &= 0, \end{aligned}$$

where $\mathbf{U} = (\rho, \rho u_x, \rho u_y, \rho u_z, B_z, \mathcal{E})^T$, $\mathbf{B} = (B_x, E_z(\mathbf{u}, \mathbf{B}), u_y B_x - u_x B_y)^T$. The approximate spaces for DG method of MHD equation are defined as following. The discrete space for variable \mathbf{U}_h^k is

$$\mathbf{V}_h^k = \{ \mathbf{v} : \mathbf{v}|_K \in [P^k(K)]^{s-d}, \forall K \in \mathcal{T}_h \},$$

and the discrete space for magnetic field \mathbf{B}_h^k is

$$\begin{aligned} \mathcal{M}_h^k &= \{ \mathbf{v} \in H(\text{div}^0; \Omega) : \mathbf{v}|_K \in \mathcal{W}^k(K), \forall K \in \mathcal{T}_h \} \\ &= \{ \mathbf{v} : \mathbf{v}|_K \in \mathcal{W}^k(K), \nabla \cdot \mathbf{v}|_K = 0, \forall K \in \mathcal{T}_h, \\ &\quad \text{and } \mathbf{v} \cdot \mathbf{n} \text{ is continuous on element interface} \}, \end{aligned}$$

with \mathcal{W}^k defined as

$$\mathcal{W}^k = [P^k(K)]^d \oplus \text{span} \{ \widehat{\nabla} \times (x^{k+1} y), \widehat{\nabla} \times (x y^{k+1}) \}.$$

The DG methods for MHD equation are we look for $\mathbf{U}_h^{n+1} \in \mathcal{V}_h^k$, such that for any $\mathbf{w} \in \mathcal{V}_h^k$ and any element $I_{ij} \in \mathcal{T}_h$,

$$\begin{aligned} \int_{I_{ij}} \mathbf{U}_h^{n+1} \cdot \mathbf{w} dx dy &= \int_{I_{ij}} \mathbf{U}_h^n \cdot \mathbf{w} dx dy \\ - \Delta t \left(\int_{\partial I_{ij}} \mathbf{H}_e \cdot \mathbf{I}_U \cdot \mathbf{w} ds - \int_{I_{ij}} \mathbf{F}(\mathbf{U}_h^n, \mathbf{B}_h^n) \cdot \nabla \mathbf{w} dx dy \right) \end{aligned}$$

with

$$\mathbf{H}_{e,I_{ij}}(\mathbf{a}, \mathbf{b}; \mathbf{n}) = \frac{1}{2} (\mathbf{F}(\mathbf{a}) \cdot \mathbf{n} + \mathbf{F}(\mathbf{b}) \cdot \mathbf{n} - \alpha(\mathbf{b} - \mathbf{a})),$$

Next, we use the DG method to get the continuous normal component $\mathcal{B} \cdot \mathbf{n}$ of the magnetic field on element interfaces. That is to look for $b_{ij}^x(y) \in P^k([y_{j-\frac{1}{2}}, y_{j+\frac{1}{2}}])$, such that for any $\varphi(y) \in P^k([y_{j-\frac{1}{2}}, y_{j+\frac{1}{2}}])$

$$\int_{y_{j-\frac{1}{2}}}^{y_{j+\frac{1}{2}}} b_{ij}^x(y) \varphi dy = \int_{y_{j-\frac{1}{2}}}^{y_{j+\frac{1}{2}}} B_x^n(x_{i+\frac{1}{2}}, y) \varphi dy - \Delta t \left(\widehat{E}_z(x_{i+\frac{1}{2}}, y) \varphi \Big|_{y_{j-\frac{1}{2}}}^{y_{j+\frac{1}{2}}} - \int_{y_{j-\frac{1}{2}}}^{y_{j+\frac{1}{2}}} \overline{E}_z(x_{i+\frac{1}{2}}, y) \frac{\partial \varphi}{\partial y} dy \right),$$

and look for $b_{ij}^y(x) \in P^k([x_{i-\frac{1}{2}}, x_{i+\frac{1}{2}}])$, such that for any $\varphi(x) \in P^k([x_{i-\frac{1}{2}}, x_{i+\frac{1}{2}}])$

$$\int_{x_{i-\frac{1}{2}}}^{x_{i+\frac{1}{2}}} b_{ij}^y(x) \varphi(x) dx = \int_{x_{i-\frac{1}{2}}}^{x_{i+\frac{1}{2}}} B_y^n(x, y_{j+\frac{1}{2}}) \varphi dx - \Delta t \left(\widehat{\overline{E}}_z(x, y_{j+\frac{1}{2}}) \varphi \Big|_{x_{i-\frac{1}{2}}}^{x_{i+\frac{1}{2}}} - \int_{x_{i-\frac{1}{2}}}^{x_{i+\frac{1}{2}}} \overline{\overline{E}}_z(x, y_{j+\frac{1}{2}}) \frac{\partial \varphi}{\partial x} dx \right).$$

$\widehat{E}_z, -\widehat{E}_z$ and $\overline{E}_z, \overline{\overline{E}}_z$ are exact or approximate Riemann solvers to approximate the electric field flux E_z at the vertices and on the element interfaces. For $k \geq 2$, we look for $\tilde{\mathcal{B}}_h \in [P^{k-2}(I_{ij})]^2$ such that for any $\Phi \in [P^{k-2}(I_{ij})]^2$ with $\Phi = (\Phi_1, \Phi_2)^T$,

$$\int_{I_{ij}} \tilde{\mathcal{B}}_h \cdot \Phi dx dy = \int_{I_{ij}} \mathcal{B}_h^n \Phi dx dy - \Delta t \left(\int_{x_{i-\frac{1}{2}}}^{x_{i+\frac{1}{2}}} (\widetilde{E}_z \Phi_1) \Big|_{y_{j+\frac{1}{2}}} dx - \int_{x_{i-\frac{1}{2}}}^{x_{i+\frac{1}{2}}} (\widetilde{E}_z \Phi_1) \Big|_{y_{j-\frac{1}{2}}} dx + \int_{y_{j-\frac{1}{2}}}^{y_{j+\frac{1}{2}}} (\widetilde{\overline{E}}_z \Phi_2) \Big|_{x_{i+\frac{1}{2}}} dy - \int_{y_{j-\frac{1}{2}}}^{y_{j+\frac{1}{2}}} (\widetilde{\overline{E}}_z \Phi_2) \Big|_{x_{i-\frac{1}{2}}} dy - \int_{I_{ij}} \left(E_z \frac{\partial \Phi_1}{\partial y} - E_z \frac{\partial \Phi_2}{\partial x} \right) dx dy \right).$$

Here \widetilde{E}_z and $\widetilde{\overline{E}}_z$ are the numerical flux along an x -direction edge and y -direction edge.

Reconstruction: Given an element I_{ij} , the reconstruction is to obtain $\mathcal{B}_h^{n+1} |_{I_{ij}} \in \mathcal{W}^k(I_{ij})$ on I_{ij} , such that $\mathcal{B}_h^{n+1} = (B_{x,h}^{n+1}, B_{y,h}^{n+1})^T$ satisfies

R1. $\int_{y_{j-\frac{1}{2}}}^{y_{j+\frac{1}{2}}} (B_{x,h}^{n+1}(x_{l+\frac{1}{2}}, y) - b_{ij}^x(y)) \varphi(y) dy = 0$ on the y -direction edge with $l = i - 1, i$ and any $\varphi(y) \in P^k([y_{j-\frac{1}{2}}, y_{j+\frac{1}{2}}])$,

R2. $\int_{x_{i-\frac{1}{2}}}^{x_{i+\frac{1}{2}}} (B_{y,h}^{n+1}(x, y_{l+\frac{1}{2}}) - b_{ij}^y(x)) \varphi(x) dx = 0$ on the x -direction edge with $l = j - 1, j$ and any $\varphi(x) \in P^k([x_{i-\frac{1}{2}}, x_{i+\frac{1}{2}}])$,

R3. $\int_{I_{ij}} (\mathcal{B}_h^{n+1}(x, y) - \tilde{\mathcal{B}}_h(x, y)) \Phi dx dy = 0$ for any $\Phi(x, y) \in [P^{k-2}(I_{ij})]^2$ when $k \geq 2$.

Theorem 1 Under the conditions that 1) the electric field flux approximations along the same edge satisfy

$$\overline{\overline{E}}_z = -(\widetilde{\overline{E}}_z), \quad \overline{\overline{\overline{E}}_z} = -(\widetilde{\overline{\overline{E}}_z}),$$

2) and the electric field flux approximation at the same vertex is single-valued, satisfying

$$\widehat{\overline{\overline{E}}_z} = -\widehat{\overline{E}}_z,$$

then for $\forall k \geq 0$, the reconstructed $\mathcal{B}_h^{n+1}(I_{ij})$ exists uniquely in $\mathcal{W}^k(I_{ij})$ and $\nabla \cdot \mathcal{B}_h^{n+1} |_{I_{ij}} = 0$.

The choice of numerical flux is

$$\begin{aligned} \widetilde{E}_z &= \frac{E_z^{LD} + E_z^{LU}}{2} - \frac{\alpha_y}{2} (B_x^{LU} - B_x^{LD}), \\ \widetilde{\overline{E}}_z &= \frac{(-E_z^{RD} - E_z^{LD})}{2} - \frac{\alpha_x}{2} (B_y^{RD} - B_y^{LD}), \\ \widehat{E}_z &= \frac{1}{4} (E_z^{LU} + E_z^{RU} + E_z^{LD} + E_z^{RD}) \\ &\quad + \frac{\beta}{4} \left(\frac{B_x^{LU} + B_x^{RU}}{2} - \frac{B_x^{LD} + B_x^{RD}}{2} \right) \\ &\quad - \frac{\alpha}{4} \left(\frac{B_y^{RD} + B_y^{RU}}{2} - \frac{B_y^{LD} + B_y^{LU}}{2} \right). \end{aligned}$$

For more details, please see the paper [1].

References

[1] P. Fu, F. Li and Y. Xu, Globally divergence-free discontinuous Galerkin methods for ideal magnetohydrodynamic equations, *Journal of Scientific Computing* **77**(2018), pp. 1621-1659.
 [2] F. Li and L. Xu, Arbitrary order exactly divergence-free central discontinuous Galerkin methods for ideal MHD equations, *Journal of Computational Physics* **231** (2012), pp. 2655-2675.
 [3] D. Balsara and R. Käppeli, Von Neumann stability analysis of globally divergence-free RKDG schemes for the induction equation using multidimensional Riemann solvers, *Journal of Computational Physics*, **336** (2017), pp.104-127.

**Compact fourth order scheme for the elastic wave equation
in the frequency domain using a first order formulation**

Dan Gordon^{1,*}, Rachel Gordon², Eli Turkel³

¹Dept. of Computer Science, University of Haifa, Haifa, Israel

²Dept. of Aerospace Engineering, The Technion, Haifa, Israel

³Dept. of Applied Mathematics, Tel-Aviv University, Tel-Aviv, Israel

*Email: gordon@cs.haifa.ac.il

Abstract

We develop a compact fourth order scheme for the elastic wave equation in the frequency domain using a first order formulation of the equation. We use a 3D staggered grid and apply our minimalistic "Gradient Method" concept to the BGT absorbing boundary condition. The equations are solved in a partitioned domain using the block-parallel CARP-CG algorithm. The results are compared with the analytic solution.

Keywords: Elastic wave equation, frequency domain, first order formulation, compact scheme, fourth order accuracy, gradient method absorbing boundary conditions.

1 The compact fourth order scheme

The elastic wave equation in the frequency domain can be expressed as a first order system of velocities and stresses. The stresses are denoted by σ_{ij} and form a symmetric matrix, so there are only six different values of σ_{ij} . For convenience, we denote $D = \frac{\partial u}{\partial x} + \frac{\partial v}{\partial y} + \frac{\partial w}{\partial z}$. Then the system (including a forcing term) is given by the following nine equations:

$$\begin{aligned} -\rho i \omega u &= \frac{\partial \sigma_{11}}{\partial x} + \frac{\partial \sigma_{12}}{\partial y} + \frac{\partial \sigma_{13}}{\partial z} + F^u \\ -\rho i \omega v &= \frac{\partial \sigma_{12}}{\partial x} + \frac{\partial \sigma_{22}}{\partial y} + \frac{\partial \sigma_{23}}{\partial z} + F^v \\ -\rho i \omega w &= \frac{\partial \sigma_{13}}{\partial x} + \frac{\partial \sigma_{23}}{\partial y} + \frac{\partial \sigma_{33}}{\partial z} + F^w \\ -\rho i \omega \sigma_{11} &= \lambda D + 2\mu \frac{\partial u}{\partial x} \\ -\rho i \omega \sigma_{22} &= \lambda D + 2\mu \frac{\partial v}{\partial y} \\ -\rho i \omega \sigma_{33} &= \lambda D + 2\mu \frac{\partial w}{\partial z} \\ -\rho i \omega \sigma_{12} &= \mu \left(\frac{\partial u}{\partial y} + \frac{\partial v}{\partial x} \right) \\ -\rho i \omega \sigma_{13} &= \mu \left(\frac{\partial u}{\partial z} + \frac{\partial w}{\partial x} \right) \\ -\rho i \omega \sigma_{23} &= \mu \left(\frac{\partial v}{\partial z} + \frac{\partial w}{\partial y} \right) \end{aligned}$$

$u(x, y, z), v(x, y, z), w(x, y, z)$ are the displacements in the x, y, z directions, respectively, and $F(x, y, z) = (F^x, F^y, F^z)$ is the vector of displacements in the x, y, z directions at a point of the domain. Additional parameters: $\omega = 2\pi f$, where f is the frequency, λ and μ are the Lamé parameters and ρ is the density (which are all assumed to be constant). The elastic equations give rise to two wave speeds, the compression or P-wave v_p , and the shear or S-wave v_s , given by

$$v_p = \sqrt{\frac{\lambda + 2\mu}{\rho}}, \quad v_s = \sqrt{\frac{\mu}{\rho}}.$$

The wave numbers associated with the two wave speeds are $k_p = \omega/v_p$ and $k_s = \omega/v_s$.

2 Discretization

We use the standard discretization notations on a staggered grid, but we forgo the development steps of the discretization. This yields

$$u_{xxx} = -i\omega \left(\frac{\sigma_{11}}{\lambda + 2\mu} \right)_{xx} - \left(\frac{\lambda v_y}{\lambda + 2\mu} \right)_{xx} - \left(\frac{\lambda w_z}{\lambda + 2\mu} \right)_{xx}$$

with corresponding expressions for v_{yyy} and w_{zzz} . We also obtain appropriate 4th order expressions for σ_{ij} , which depend on these third order derivatives. The derivatives in the $O(h^2)$ terms are replaced by second order central differences. These can all be computed on a compact $3 \times 3 \times 3$ stencil.

3 Absorbing boundary conditions

The absorbing boundary conditions (ABC) of [1] (BGT) was originally developed for a sphere and used radial derivatives (which are also normal to the boundary direction). We made the following adaptation of BGT for the elastic case, which we call BGTE:

$$\left(\frac{\partial}{\partial r} + \frac{1}{r} - ik_p \right) \left(\frac{\partial}{\partial r} + \frac{1}{r} - ik_s \right) u = 0,$$

where r is the distance from the source and the derivatives are in the radial direction.

In [3] we developed the "Gradient Method" concept for ABCs, which is based on the principle that the directional derivatives in any ABC

should be in the direction of the *gradient* of the wavefront, without regard to the orientation of the boundary. According to this concept, BGT and BGTE can be used in any convex domain with an interior source. The advantage of this approach is that the ABCs take up just one extra grid point on each side, and this is big advantage over PMLs.

4 Preliminary results

We use a well-known example from the literature, see, for example, [5]. The domain is of size 2000^3 meters, with a source at the center, discretized by 142^3 grid points (including the extra points for the ABC). Since the Green's function of the solution is known, the source of impact was simulated by placing a small cube at the center with values of the Green's function. We made tests with the BGTE ABC and also with Dirichlet BC (with boundary values from the Green's function). The density was $\rho = 1000$ Kg/m^3 , and the frequency was $f = 10$. The acoustic case and the elastic case were tested, with parameters $v_p = 2500$ m/s, $v_s = 0$ m/s for the acoustic case, and $v_p = 5000$ m/s, $v_s = 2500$ m/s for the elastic case.

The acoustic case was solved with GMRES, with a restart of 20. For the elastic case, we used the CARP-CG algorithm [2], which has been shown to be especially useful on strongly convection-dominated PDEs and the Helmholtz equation at high frequencies. CARP-CG was used in various wave problems e.g. [3-5].

Fig. 1 shows sample plots for the acoustic and elastic cases. Each plot compares the Green's function with the solutions with the ABC and with Dirichlet boundary conditions. The acoustic case is the Helmholtz equation for the 3 stresses σ_{ii} . The good correspondence between the plots is in line with our previous Helmholtz results. The results in the elastic case are not as good, and work on improving the ABC for this case is still in progress.

References

[1] A. Bayliss, M. Gunzburger & E. Turkel. Boundary conditions for the numerical solution of elliptic equations in exterior regions. *SIAM J. Appl. Math.* 42:430-451, 1982.

[2] D. Gordon & R. Gordon. CARP-CG: a robust and efficient parallel solver for linear systems, applied to strongly convection dominated PDEs. *Parallel Computing* 36:495-515, 2010.

[3] D. Gordon, R. Gordon & E. Turkel. Compact high order schemes with gradient-direction derivatives for absorbing boundary conditions. *J. Comput. Physics* 297:295-315, 2015.

[4] Y. Li, L. Métivier, R. Brossier, B. Han & J. Virieux. 2D and 3D frequency-domain elastic wave modeling in complex media with a parallel iterative solver. *Geophysics* 80:T101-T118, 2015.

[5] Y. Li, B. Han, L. Métivier & R. Brossier. Optimal fourth-order staggered-grid finite-difference scheme for 3D frequency-domain viscoelastic wave modeling. *J. Comput. Physics* 321:1055-1078, 2016.

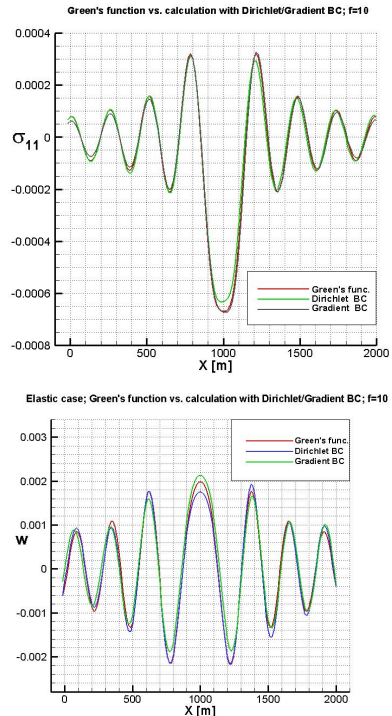


Figure 1: Comparison of the Green's function with the solutions obtained with Dirichlet boundary condition and the ABC. Top: the acoustic case. Bottom: the elastic case.

High-order finite difference methods for the time-dependent Schrödinger equation on deforming domains

Ylva Rydin^{1,*}, Ken Mattsson¹, Jonatan Werpers¹, Erik Sjöqvist²

¹Department of Information Technology, Uppsala, Sweden

²Department of Physics and Astronomy, Uppsala, Sweden

*Email: ylva.rydin@it.uu.se

Abstract

In this talk finite-difference discretization for the Schrödinger equation on domains that deform in time will be presented. This problem set-up gives rise to interesting solutions that are caused by quantum mechanical phenomena. An example of such phenomenon is Berry phases. In this study, Berry phases on deforming quantum billiards are explored numerically with provably stable high-order finite difference methods. To model the deforming quantum billiard, the Schrödinger equation is solved with Dirichlet boundary conditions on domains with moving boundaries.

Keywords: finite difference methods, quantum mechanics, high-order accuracy, stability, boundary treatment, deforming domain

Introduction

A much used model in the study of quantum chaos is particles localized in spatial domains surrounded by infinite potential walls. The energy levels of such model systems typically show a rich behaviour of avoided crossings and crossings occurring in domains that lack symmetry ('diabolical points'). The corresponding wave functions show complex structures, such as scars resembling classical periodic orbits. To capture the complex and rich behaviour of such systems, there is need for stable and accurate numerical methods. In this work, we derive a stable and accurate high-order *Summation-By-Parts* (SBP) finite-difference scheme for the 2-dimensional (2D) Schrödinger equation on deforming domains that can be used to efficiently model this type of complex quantum systems. An example on how this type of quantum systems behave is displayed in Figure 1, where the probability density of a quantum state is displayed before and after a small domain deformation.

Solutions Schrödinger equation are in general wave dominated, therefore numerical methods with low dispersion errors are needed for effi-

cient numerical solutions. It is well known that higher-order finite-difference methods are well suited for this type of problems. However, constructing stable boundary treatment for these methods is a challenging task. A technique for constructing stable high-order finite-difference methods for initial-boundary-value-problems is to combine discretization by SBP finite-difference operators with a weak method of imposing the boundary conditions *Simultaneous-Approximatiu Term* (SAT). So far, the development of the SBP-SAT technique is mainly focused on problems on fixed domains. How to extend the technique to deforming domains for first order hyperbolic systems by a time-dependent coordinate transformation is described in [1]. In this work we extend this framework to the 2-dimensic (2D) Schrödinger equation.

Continuous problem

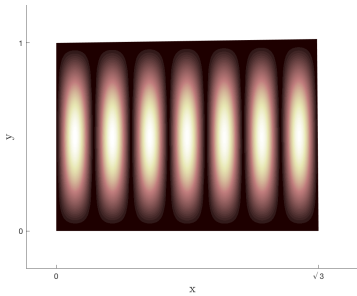
To allow efficient and stable numerical discretization, the Schrödinger equation is subjected to a time-dependent coordinate transformation. This methodology can be extended to higher dimensions, but for notational simplicity this work is restricted to the 2D-case. We consider the Schrödinger equation on the domain $\Omega(t)$, with infinite potential walls which are implemented by Dirichlet boundary conditions:

$$\begin{aligned} u_t &= i\Delta u - iV(x, y, t)u, & t > t_0, & u \in \Omega(t), \\ u &= 0, & t \geq t_0, & u \in \partial\Omega(t), \\ u &= u_0(x, y), & t = t_0, & u \in \Omega(t). \end{aligned} \quad (1)$$

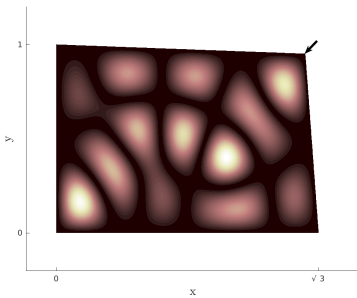
Here, $\partial\Omega(t)$ denotes the domain boundary and u_0 the initial condition. Since the positions of the physical domain boundaries are time-depend the coordinate transformation

$$\begin{aligned} x &= x(\xi, \eta, \tau), & \xi &= \xi(x, y, t), \\ y &= y(\xi, \eta, \tau), & \eta &= \eta(x, y, t), \\ t &= t(\tau), & \tau &= \tau(t), \end{aligned} \quad (2)$$

is performed in both time and space. In the new coordinates the Schrödinger equation (1) is



(a) Probability density of initial state.



(b) Probability density after moving the upper right corner adiabatically along the black arrow

Figure 1: Example of adiabatic evolution of in a quantum billiard

given by

$$u_\tau = -\mathcal{T}(u) + i\Delta u - iV(\xi, \eta, \tau, u)u, \quad (3)$$

where $\mathcal{T}(u) = \frac{1}{2J}(\gamma_1 u_\xi + (\gamma_1 u)_\xi + \gamma_2 u_\eta + (\gamma_2 u)_\eta - J_\tau u)$. Here J is the Jacobian determinant, and γ_1, γ_1 metrical coefficients derived in the transform.

Discretisation

In space, the equation is discretised by high-order SBP finite difference operators, the boundary conditions are imposed weakly by SAT. The summation-by-parts property of the operators, that mimic the continuous integration-by-part property gives a provably stable discretization that preserves the probability. The resulting

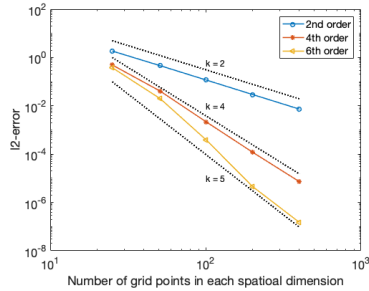


Figure 2: Convergence for the numerical scheme

ODE-system is integrated in time with a fourth order Magnus-Lacsoz integrator which is known to be a suitable choice for highly oscillating Hamiltonian systems, such as the Schrödinger equation [2].

Numerical experiments

The scheme has been verified by recreating the experiments on adiabatic deforming quantum billiard presented by Lauber et al in [3]. The numerical simulations have shown to agree well with the experimental results. Further, the convergence rate is verified for 2nd, 4th and 6th order SBP operators by a manufactured solution, see Figure 2.

References

- [1] S. Nikkar, J.Nordström, Fully discrete energy stable high order finite difference methods for hyperbolic problems in deforming domains, *Journal of Computational Physics* **106** (2015), pp. 385-395
- [2] K. Kormann, S. Holmgren and H.-O. Karlsson, Accurate time propagation for the Schrödinger equation with an explicitly time- dependent Hamiltonian Accurate time propagation for the Schrödinger equation with an explicitly time-dependent Hamiltonian *The Journal of Chemical Physics* **228** (2008)
- [3] H.-M. Lauber and P. Weidenhammer, Geometric Phases and Hidden Symmetries in Simple Resonators, *Physical Review Letter* **24** (1993), pp. 3760-3763.

Gypsilab, an open source efficient software for wave scattering simulation

François Alouges^{1,*}, Matthieu Aussal¹, Marc Bakry¹¹CMAP - Ecole polytechnique, CNRS, Institut Polytechnique de Paris, Palaiseau, France

*Email: francois.alouges@polytechnique.edu

Abstract

Gypsilab is a MATLAB suite that enables the user to solve various problems in wave scattering simulation. In particular, it contains a complete environment that allows to solve problems in FEM, or BEM in 2D or 3D. This paper focuses on the main functionalities and the concept that were used as guides for the development of the toolbox.

Keywords: Finite element method, boundary element method, \mathcal{H} -matrices, MATLAB

1 Introduction

In many wave scattering simulation problems, people often uses classical numerical methods such as the Finite Element Method (FEM) or the Boundary Element Method (BEM). Very classically both methods possess differents advantages and drawbacks that might limit its own range of application. We present a new MATLAB complete environment to do such applications, called GYPSILAB [2,3] which is open source and freely available under the GPL 3.0 license.

2 Gypsilab

Gypsilab allows to code directly the variational formulation of the problem under consideration with a syntax which is very close to the mathematical formulation in a way comparable to FREEFEM++ [9] or FENICS [5] or XLIFE++ [11]. The novelty is that the approach is generalized to variational formulations that come from the Galerkin or collocation approximations of boundary integral operators. Moreover the Green kernels used for the problem might be completely freely given by the user. A classical semi analytical regularization technique of singular integrals is also provided. Un example of the core of the computational code for the acoustic scattering by a unit sphere, that produces eventually the picture given in Fig. 2 is given afterwards. The familiar user will immediately recognize the classical discretization of the single layer equation.

% Parameters

```
N = 9e4; tol = 1e-3; X0 = [0 0 -1];
```

% Spherical mesh

```
sphere = mshSphere(N,1);
```

```
S2 = dom(sphere,3);
```

% Frequency

```
f = 3e3; k = 2*pi*f/340;
```

% Incident wave

```
PW = @(X) exp(1i*k*X*X0');
```

% Green kernel

```
Gxy = @(X,Y) ...
```

```
femGreenKernel(X,Y,'[exp(ikr)/r]',k);
```

% Finite element space

```
Vh = fem(sphere,'P1');
```

% Operator

```
LHS=1/(4*pi)*integral(S2,S2,Vh,Gxy,Vh,to
```

```
LHS=LHS+ ...
```

```
1/(4*pi)*regularize(S2,S2,Vh,'[1/r]',Vh)
```

```
% Wave trace --> \int_Sx psi(x)' pw(x) d
```

```
RHS = integral(S2,Vh,PW);
```

```
% Solve the system [-S] * lambda = - PO
```

```
lambda = LHS \ RHS;
```

3 \mathcal{H} -matrices

One of the known drawbacks of the BEM is that it usually leads to dense matrices that might not fit in the memory of usual computers. Special methods and algorithms have been designed to circumvent this problem such as the FMM [6], the SCSD [1] or the \mathcal{H} -matrices [4, 7, 8].

Developed mainly by the team of W. Hackbush since 2000, the latter theory is a format that permits to compress standard full matrices while keeping the flexibility of realizing standard operations (addition, multiplication, LU factorization, inversion, etc.).

The GYPSILAB library contains a full subset of functions, grouped inside the openHmx folder that implements, in full MATLAB, the hierarchical format. The adopted viewpoint consists of an object class containing all the algorithms for a complete algebra [4].

In openHmx, all traditional operations have been overloaded in such a way that the new format can be completely used transparently as the

classical full and sparse formats. It is therefore possible to add, subtract, multiply or invert \mathcal{H} -matrices (via the LU factorization) or even visualize their structure through the command `spy`. An output of this command is given in Fig. 1.

In GYPSILAB, this type of matrices may be freely used for the numerical solution of wave scattering problems using the BEM. Moreover, the library allows for a coupling of sparse and \mathcal{H} -matrices opening the possibility of coupling FEM and BEM discretizations.

Other functionalities, and in particular new algorithms, will be also presented that makes it possible to generalize the approach to quite large scale computations. Applications of such cases will be shown.

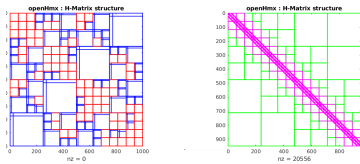


Figure 1: Two \mathcal{H} -matrices showing low rank extradiagonal blocks (left) or empty and sparse (right). The first structure is typically used in BEM applications while the second one is useful in FEM.

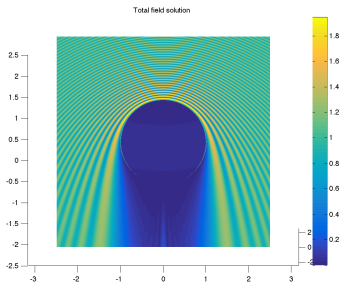


Figure 2: Magnitude of the pressure produced in the acoustic scattering by a unit sphere of a plane wave coming from above, using GYPSILAB. The sphere is discretized with $9 \cdot 10^4$ vertices and the frequency used is $3 \cdot 10^3$ Hz, and the problem is solved using the \mathcal{H} -matrix toolbox OPENHMX.

References

- [1] François Alouges and Matthieu Aussal. The sparse cardinal sine decomposition and its application for fast numerical convolution. *Numerical Algorithms*, 70(2):427–448, 2015.
- [2] F. Alouges, M. Aussal. FEM and BEM simulations with the Gypsilab framework, SMAI J. Comp. Math. 4, p. 297-318, 2018.
- [3] The library is downloadable under GPL 3.0 license at <https://github.com/matthieuaussal/gypsilab>.
- [4] S. BORM, L. GRASEDYCK et W. HACKBUSCH. *Introduction to hierarchical matrices with applications. Engineering analysis with boundary elements*, 27(5), 405-422. 2003.
- [5] Fenics is available at <https://fenicsproject.org>. [Accessed - Sept. 2018].
- [6] Leslie Greengard. *The rapid evaluation of potential fields in particle systems*. MIT press, 1988.
- [7] W. HACKBUSCH. *A sparse matrix arithmetic based on H-matrices. Part I. Introduction to H-matrices*, Computing, 1999.
- [8] W. HACKBUSCH. *Hierarchische Matrizen*, Springer, 2009.
- [9] Frédéric Hecht. New development in FreeFem++. *Journal of numerical mathematics*, 20(3-4):251–266, 2012. See also <http://www.freefem.org>.
- [10] Wojciech Śmigaj, Timo Betcke, Simon Arridge, Joel Phillips, and Martin Schweiger. Solving boundary integral problems with BEM++. *ACM Transactions on Mathematical Software (TOMS)*, 41(2):6, 2015.
- [11] Xlife++ is available at <https://uma.ensta-paristech.fr/soft/XLIFE++/>. [Accessed - Sept. 2018].

Analysis of the hp -version of a first order system least squares method for the Helmholtz equation

Maximilian Bernkopf^{1,*}, Jens Markus Melenk¹

¹Institute of Analysis and Scientific Computing, TU Wien, Vienna, Austria

*Email: maximilian.bernkopf@asc.tuwien.ac.at

Abstract

We consider a first order system least squares method (FOSLS) for the Helmholtz equation. To that end, we first derive sharp error estimates for the scalar variable for a second order elliptic model problem with emphasis on the case of limited Sobolev regularity of the data. The results rely on a careful analysis of an appropriate dual problem in conjunction with recently developed approximation operators with suitable orthogonality properties. The results are then transferred to the Helmholtz equation for which we present an error analysis for the scalar variable in a high frequency regime under certain scale resolution conditions.

Keywords: Helmholtz equation, Least Squares FEM, hp -FEM

1 Introduction

In the first part of the talk we consider a Poisson-like second order model problem written as a system of first order equations. For the numerical discretization of the vector valued and scalar variable an $\mathbf{H}(\Omega, \text{div}) \times H^1(\Omega)$ -conforming least squares formulation is employed. A least squares formulation has the major advantage that regardless of the original formulation the linear system resulting from a least squares type discretization is always positive semi-definite, making it easier to solve. Even though our model problem in its standard $H^1(\Omega)$ formulation is coercive our methods and lines of proof can most certainly be applied to other problems as well, see [1, 3] for an application to Helmholtz equation. A major drawback of a least squares formulation is that the energy norm is somewhat intractable. Deducing error estimates in other norms, e.g., the $L^2(\Omega)$ norm of the scalar variable, is more difficult. Numerical examples in our previous work [1] suggested convergence rates previous results did not cover. Closing this gap in the literature will be our main focus of the first part of the talk.

In the second part we consider the Helmholtz

equation with large wavenumber k . Extending the results of [3], we show *a priori* estimates for the least squares method that is explicit in h and p . These estimates are valid under the scale resolution condition that kh/p is sufficiently small and $p/\log k$ is sufficiently large. Our key refinement over [3] is a wavenumber explicit regularity estimate of a suitable dual problem.

2 Part 1

Let Ω denote a bounded simply connected domain in \mathbb{R}^n , $n = 2, 3$ with C^∞ boundary Γ and outward unit normal vector \mathbf{n} . For $\gamma > 0$ fixed and $f \in L^2(\Omega)$ we consider the following model problem

$$\begin{aligned} -\Delta u + \gamma u &= f & \text{in } \Omega, \\ \partial_n u &= 0 & \text{on } \Gamma. \end{aligned} \tag{1}$$

We formulate (1) as a first order system: Introducing the new variable $\varphi = -\nabla u$ we arrive at the system

$$\begin{aligned} \nabla \cdot \varphi + \gamma u &= f & \text{in } \Omega, \\ \nabla u + \varphi &= 0 & \text{in } \Omega, \\ \varphi \cdot \mathbf{n} &= 0 & \text{on } \Gamma. \end{aligned} \tag{2}$$

The corresponding least squares problem is to find $(\varphi, u) \in \mathbf{H}_0(\Omega, \text{div}) \times H^1(\Omega)$ such that

$$b((\varphi, u), (\psi, v)) = F((\psi, v)),$$

for all $(\psi, v) \in \mathbf{H}_0(\Omega, \text{div}) \times H^1(\Omega)$ with the bilinear form b and the linear functional F given by

$$\begin{aligned} b((\varphi, u), (\psi, v)) &= (\nabla \cdot \varphi + \gamma u, \nabla \cdot \psi + \gamma v)_{L^2(\Omega)} \\ &\quad + (\nabla u + \varphi, \nabla v + \psi)_{L^2(\Omega)}, \\ F((\psi, v)) &= (f, \nabla \cdot \psi + \gamma v)_{L^2(\Omega)}. \end{aligned}$$

Next we perform a duality argument for the scalar variable: For any $(\varphi, w) \in \mathbf{H}_0(\Omega, \text{div}) \times H^1(\Omega)$ there exists $(\psi, v) \in \mathbf{H}_0(\Omega, \text{div}) \times H^1(\Omega)$ such that

$$\|w\|_{L^2(\Omega)}^2 = b((\varphi, w), (\psi, v)),$$

with (ψ, v) allowing for explicit regularity estimates. Exploiting this duality argument gives the error estimate

$$\|u - u_h\|_{L^2(\Omega)} \lesssim h \|(u - u_h, \varphi - \varphi_h)\|_b,$$

which is well-known in the literature. At this point higher order convergence rates are just a question of approximation properties in the energy norm $\|(\cdot, \cdot)\|_b$. With $f \in L^2(\Omega)$ elliptic regularity immediately gives $u \in H^2(\Omega)$. Therefore u can be approximated by globally continuous piecewise polynomials of degree greater or equal to one with a rate of h^2 in the $L^2(\Omega)$ norm, which is achieved by classical FEM, due to the Aubin-Nitsche trick. In contrast, the above estimate does not give the desired rate. The norm $\|(\varphi - \varphi_h, u - u_h)\|_b$ contains a term of the form

$$\|\nabla \cdot (\varphi - \varphi_h)\|_{L^2(\Omega)} = \|f - \nabla \cdot \varphi_h\|_{L^2(\Omega)},$$

from which no further convergence rate can be extracted, since f is only in $L^2(\Omega)$.

The main result of this part will be an optimal $L^2(\Omega)$ error estimate for the scalar variable. To that end, an approximation operator \mathbf{I}_h on $\mathbf{H}_0(\Omega, \text{div})$ is constructed that satisfies

$$(\nabla \cdot (\varphi - \mathbf{I}_h \varphi), \nabla \cdot \chi_h) = 0$$

for any χ_h in the finite element space together with approximation properties in $L^2(\Omega)$. Here a crucial tool are recently developed projection based commuting diagram operators, see [4].

3 Part 2

We consider a first order least squares method for the Helmholtz equation with wavenumber k :

$$\begin{aligned} -\Delta u - k^2 u &= f & \text{in } \Omega, \\ \partial_n u - iku &= g & \text{on } \Gamma. \end{aligned} \tag{3}$$

Similar to the elliptic model problem we will first derive a least squares formulation and perform a duality argument. As in [5] a wavenumber explicit splitting of the dual solution is performed. Again these results are used to derive an error estimate in $L^2(\Omega)$ for the scalar variable under the scale resolution conditions

$$\frac{kh}{p} \text{ small and } p \gtrsim \log k.$$

We conclude this part with numerical examples which confirm our findings.

References

- [1] M. Bernkopf and J.M. Melenk, Analysis of the hp -version of a first order system least squares method for the Helmholtz equation, arXiv:1808.07825
- [2] M. Bernkopf and J.M. Melenk, Optimal convergence rates in L^2 for a first order system least squares finite element method, in preparation
- [3] H. Chen and W. Qiu A first order system least squares method for the Helmholtz equation, *Journal of Computational and Applied Mathematics* **309** (2017), pp. 145–162.
- [4] J.M. Melenk and C. Rojik, On commuting p -version projection-based interpolation on tetrahedra, arXiv:1802.00197
- [5] J.M. Melenk and S. Sauter, Wavenumber explicit convergence analysis for Galerkin discretizations of the Helmholtz equation, *SIAM J. Numer. Anal.* **49** (2011), pp. 1210–1243.

Robust adaptive hp discontinuous Galerkin finite element methods for the Helmholtz equation

Scott Congreve¹, Joscha Gedicke^{2,*}, Ilaria Perugia²

¹Faculty of Mathematics and Physics, Charles University, Praha, Czech Republic

²Faculty of Mathematics, University of Vienna, Vienna, Austria

*Email: joscha.gedicke@univie.ac.at

Abstract

This talk presents an hp a posteriori error analysis for the 2D Helmholtz equation that is robust in the polynomial degree p and the wave number k . For the discretization, we consider a discontinuous Galerkin formulation that is unconditionally well posed. The a posteriori error analysis is based on the technique of equilibrated fluxes applied to a shifted Poisson problem, with the error due to the nonconformity of the discretization controlled by a potential reconstruction. We prove that the error estimator is both reliable and efficient, under the condition that the initial mesh size and polynomial degree is chosen such that the discontinuous Galerkin formulation converges, i.e., it is out of the regime of pollution. We confirm the efficiency of an hp -adaptive refinement strategy based on the presented robust a posteriori error estimator via several numerical examples.

Keywords: a posteriori error analysis, hp discontinuous Galerkin finite element method, equilibrated fluxes, potential reconstruction

1 Introduction

In this talk, we consider the Helmholtz problem with impedance boundary condition: Find a (complex) solution u such that

$$\begin{aligned} -\Delta u - k^2 u &= f \quad \text{in } \Omega, \\ \nabla u \cdot \mathbf{n} - ik u &= g \quad \text{on } \partial\Omega, \end{aligned}$$

where $\Omega \subset \mathbb{R}^2$ is a bounded, Lipschitz domain, \mathbf{n} denotes the outer unit normal on the boundary $\partial\Omega$, $f \in L^2(\Omega)$, $g \in L^2(\partial\Omega)$, and $k > 0$ is the (constant) wavenumber.

In [2] we developed an a posteriori error estimator based on equilibrated fluxes [1, 3, 4]. Since the Helmholtz problem is highly indefinite, it is not clear how to localize it in order to obtain localized problems for the error approximation that are well posed. However, the error has two components, the interpolation error and the pollution error. While the pollution error is global

and hence cannot be estimated with local error indicators, it is possible to derive equilibrated a posteriori error estimators for the interpolation error.

We will apply the theory of equilibrated flux and potential reconstructions [3, 4] and derive the a posteriori error estimator of the form

$$\begin{aligned} \eta_{hp}^2 := & \sum_{T \in \mathcal{T}} \left(\|\mathcal{G}(u_{hp}) + \boldsymbol{\sigma}_{hp}\|_{0,T} \right. \\ & + \frac{h_T}{j_{1,1}} \|f + k^2 u_{hp} - \operatorname{div} \boldsymbol{\sigma}_{hp}\|_{0,T} \\ & + C_{tr} \sum_{E \in \mathcal{E}(T) \cap \mathcal{E}(\partial\Omega)} h_E^{1/2} \|g_{osc}\|_{0,E} \Big)^2 \\ & + \sum_{T \in \mathcal{T}} \|\mathcal{G}(u_{hp}) - \nabla s_{hp}\|_{0,T}^2, \end{aligned}$$

where $\mathcal{G}(u_{hp})$ denotes a discrete gradient, $\boldsymbol{\sigma}_{hp}$ an equilibrated flux reconstruction, s_{hp} a potential reconstruction, $g_{osc} := \boldsymbol{\sigma}_{hp} \cdot \mathbf{n} + g + ik u_{hp} - \gamma k \frac{h}{p} (g - \nabla_h u_{hp} \cdot \mathbf{n} + ik u_{hp})$, h_T and h_E are the diameter of the element T of the mesh \mathcal{T} and the edge E of T , respectively, C_{tr} is a trace inequality constant, and $j_{1,1}$ is the first positive root of the Bessel function of the first kind. We prove that the a posteriori error estimator is reliable and efficient, for suitably chosen functions $\boldsymbol{\sigma}_{hp}$ and s_{hp} , up to generic constants which are independent of the wave number, the polynomial degrees, and the element sizes.

2 A posteriori error analysis

We approach the a posteriori error estimation of the DG finite element approximation of the Helmholtz problem [5] by considering the following (shifted) Poisson problem with Neumann boundary conditions: Find a (complex) function w such that

$$\begin{aligned} -\Delta w &= F \quad \text{in } \Omega, \\ \nabla w \cdot \mathbf{n} &= G \quad \text{on } \partial\Omega, \end{aligned}$$

where $F := f + k^2 u_{hp}$, and $G := g + ik u_{hp} - \gamma k \frac{h}{p} (g - \nabla_h u_{hp} \cdot \mathbf{n} + ik u_{hp})$. Note that the boundary condition is chosen in such a way that the

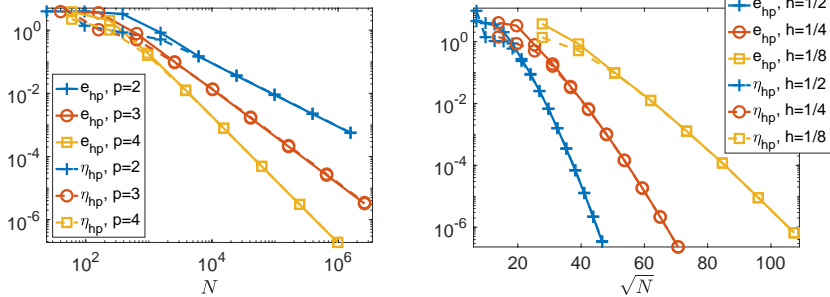


Figure 1: Algebraic convergence $\mathcal{O}(h^p)$ for the h -version (left) and exponential convergence of the p -version (right) of the error $e_{hp} = \|\nabla u - \mathcal{G}(u_{hp})\|_{0,\Omega}$ and the estimator η_{hp} for $k = 20$, cf. [2, fig. 1].

compatibility condition for the pure Neumann problem is satisfied.

Definition 1 (Flux reconstruction) For given $u_{hp} \in V_{hp}$, we define an equilibrated flux reconstruction for u_{hp} as any function $\sigma_{hp} \in H(\text{div}; \Omega)$ which satisfies

$$\int_T \text{div } \sigma_{hp} \, dx = \int_T F \, dx \quad \forall T \in \mathcal{T},$$

$$\int_E \sigma_{hp} \cdot \mathbf{n} \, ds = \int_E -G \, ds \quad \forall E \in \mathcal{E}(\partial\Omega).$$

Definition 2 (Potential reconstruction) We define a potential reconstruction as any function

$$s_{hp} \in H_*^1(\Omega) := \{v \in H^1(\Omega) : (v, 1) = 0\}.$$

Theorem 3 (Reliability) Let $u \in H^1(\Omega)$ be the weak solution of the Helmholtz problem, and $u_{hp} \in V_{hp}$ be the discrete solution. Then, for the error estimator η_{hp} , we have that

$$\|\nabla u - \mathcal{G}(u_{hp})\|_{0,\Omega} \lesssim$$

$$\eta_{hp} + k^2 \|u - u_{hp}\|_{0,\Omega} + k \|u - u_{hp}\|_{0,\partial\Omega}$$

$$+ \|\gamma k \frac{h}{p} (g - \nabla_h u_{hp} \cdot \mathbf{n} + iku_{hp})\|_{0,\partial\Omega},$$

where the hidden constant is independent of k .

Note that reliability of η_{hp} holds for any equilibrated flux and potential reconstructions under the condition that $p \approx \ln k$ and $\frac{kh}{p}$ small enough. In order to also have efficiency, we locally define equilibrated flux and potential reconstructions similar to [3, 4], for which we can

prove efficiency of the estimator with constants independently of the polynomial degree [1].

In the talk, we present extensive numerical results also for varying k .

References

- [1] D. Braess, V. Pillwein, and J. Schöberl. Equilibrated residual error estimates are p -robust. *Comput. Methods Appl. Mech. Engrg.*, 198(13-14):1189–1197, 2009.
- [2] S. Congreve, J. Gedicke, and I. Perugia. Robust adaptive hp discontinuous Galerkin finite element methods for the Helmholtz equation. *SIAM J. Sci. Comput.*, 41(2):A1121-A1147, 2019.
- [3] V. Dolejší, A. Ern, and M. Vohralík. hp-adaptation driven by polynomial-degree-robust a posteriori error estimates for elliptic problems. *SIAM J. Sci. Comput.*, 38(5):A3220–A3246, 2016.
- [4] A. Ern and M. Vohralík. Polynomial-degree-robust a posteriori estimates in a unified setting for conforming, nonconforming, discontinuous Galerkin, and mixed discretizations. *SIAM J. Numer. Anal.*, 53(2):1058–1081, 2015.
- [5] S. Sauter and J. Zech. A posteriori error estimation of hp-dG finite element methods for highly indefinite Helmholtz problems. *SIAM J. Numer. Anal.*, 53(5):2414–2440, 2015.

A discontinuous Galerkin Trefftz type method for solving the Maxwell equations

H. S. Fure¹, S. Pernet^{2,*}, S. Tordeux³

¹ ONERA/DTIS, Université fédérale de Toulouse F-31000, Toulouse France

² ONERA/DTIS, Université fédérale de Toulouse F-31000, Toulouse France

³UPPA, INRIA Magique 3D, Pau, France

*Email: Sebastien.Pernet@onera.fr

Abstract

We propose a symmetric Trefftz Discontinuous Galerkin (DG) scheme to solve the time-harmonic heterogeneous Maxwell problems. It allows to a drastic decrease of the so-called numerical pollution effect which is unacceptable when large computational domains (in term of wavelength) are considered. Moreover, this approach has a great flexibility on the construction of the DG mesh in term of shape and size of cells.

Keywords: Trefftz method, Galerkin Discontinuous, pollution effect, electromagnetism

1 Introduction

Numerical methods like the finite element method and the finite difference method are widely being used to solve electromagnetic time-harmonic wave equations. One limitation they all face is called the pollution effect. When solving for high frequency on large domains: $1 \ll L/\lambda$, where λ is the wavelength and L is a characteristic length of the physical domain of interest, numerical stability deteriorates at a high rate. High dispersion occurs, and a large number of points must be used to ensure acceptable precision. Currently, lot of research is being conducted to overcome these problems and thus to propose a general and efficient method for dealing with large wave propagation problems (acoustic, electromagnetic, seismic). An idea is to use basis functions adapted to the physical phenomena rather than "simple" polynomials. The performances of the method obviously depend on the choice of basis functions. Recently, the team Magique3D of INRIA has developed an efficient Trefftz method for acoustics [1]. Their scheme is based on the one hand on a GD formulation of the problem and on the other hand on a non-explicit approximation space constructed from local resolutions of the underlying PDE. In particular, this method allows an accurate take into account of evanescent modes which is a weakness of approaches based on plane waves.

For this talk, we will present an extension of this type of approach in the context of electromagnetism problems. In this case, we propose an approximation space parametrized from the range of an impedance trace operator defined on the edges/faces of the Trefftz cells and basis functions computed by using a high-order edge finite elements. This choice makes it possible a great flexibility on the shape and size of the cells constituting the mesh. In particular, polygonal / polyhedral cells, even non-convex, are allowed. Two-dimensional numerical examples will illustrate the relevance of the proposed method.

2 A symmetric Trefftz DG method for the Maxwell equations

We are interested in the following second order time-harmonic Maxwell system:

$$\begin{cases} \nabla \times \frac{1}{\mu} \nabla \times \mathbf{E} - \varepsilon k^2 \mathbf{E} = 0 \text{ in } \Omega \\ \gamma_{\times} \left(\frac{1}{\mu} \nabla \times \mathbf{E} \right) - Z \gamma_{\nu} \mathbf{E} = \mathbf{g}_R \text{ on } \Gamma_R \\ \gamma_{\nu} \mathbf{E} = \mathbf{g}_D \text{ on } \Gamma_D \end{cases} \quad (1)$$

where Ω is a bounded and open Lipschitz domain, $\partial\Omega = \Gamma_D \cup \Gamma_N$, \mathbf{g}_R , \mathbf{g}_D are boundary data, $Im(Z(x)) > 0$ a.e on Γ_R , k is the wavenumber in vacuum, ε , μ are the relative dielectric parameters and γ_{\times} and γ_{ν} are the tangential trace and component operators respectively.

Let \mathcal{T} be a partition of the computational domain Ω i.e $\Omega = \cup_{T \in \mathcal{T}} T$ and $\forall T \neq K \in \mathcal{T}$, $T \cap K = \emptyset$. \mathcal{F}_i and \mathcal{F}_b are the sets of interior and boundary faces respectively. We now define a space of local (Maxwell) solutions: for each Trefftz cell $T \in \mathcal{T}$,

$$\begin{aligned} X_T &= \{ \mathbf{w} \in H(\text{curl}, T); \\ &\nabla \times \frac{1}{\mu T} \nabla \times \mathbf{w} - \varepsilon T k_T^2 \mathbf{w} = 0 \text{ in } T, \\ &\gamma_{\nu} \mathbf{w}|_{\partial T}, \gamma_{\times} \left(\frac{1}{\mu} \nabla \mathbf{w} \right)|_{\partial T} \in L^2(\partial T) \} \end{aligned}$$

The Maxwell problem (1) can be rewritten in the following symmetric DG formulation: find $\mathbf{E} \in \mathcal{X}_T := \Pi_{T \in \mathcal{T}} \mathcal{X}_T$ such that $\forall \mathbf{w} \in \mathcal{X}_T$, $a(\mathbf{E}, \mathbf{w}) = \ell(\mathbf{w})$ where

$$\begin{aligned} a(\mathbf{E}, \mathbf{w}) := & \int_{\Gamma} (\{\{\mathbf{E}\}\} \cdot [\gamma \times \mu^{-1} \nabla \times \mathbf{w}] + [\gamma \times \mu^{-1} \nabla \times \mathbf{E}] \cdot \{\{\mathbf{w}\}\} \\ & - \{\{\mu^{-1} \nabla \times \mathbf{E}\}\} \cdot [\gamma \times \mathbf{w}] - \{\{\mu^{-1} \nabla \times \mathbf{w}\}\} \cdot [\gamma \times \mathbf{E}]) ds \\ & + \int_{\partial \Omega} \mathbf{E} \cdot \mathbf{n} \times (\mu^{-1} \nabla \times \mathbf{w}) + \mathbf{n} \times (\mu^{-1} \nabla \times \mathbf{E}) \cdot \mathbf{w} ds \\ & - 2 \int_{\Gamma_b} Z^{-1} (\mu^{-1} \nabla \times \mathbf{E}) (\mu^{-1} \nabla \times \mathbf{w}) ds \end{aligned}$$

and

$$\begin{aligned} \ell(\mathbf{w}) := & -2 \int_{\Gamma_b} Z^{-1} \mathbf{g}_R \cdot (\mu^{-1} \nabla \times \mathbf{w}) ds \\ & + 2 \int_{\Gamma_b} \mathbf{g}_D \cdot \mathbf{n} \times (\mu^{-1} \nabla \times \mathbf{w}) ds. \end{aligned}$$

with $[\cdot]$ and $\{\{\cdot\}\}$ are the classical jump and average operators and $\Gamma := \cup_{F \in \mathcal{F}_i} F$.

3 Discretization

Following the idea of [1], the construction of our approximation space is based on a parametrization of the spaces \mathcal{X}_T from Cauchy data. For that, we first introduce the isomorphism $\mathcal{L} : L^2(\partial T) \rightarrow \mathcal{X}_T$ defined by $\mathcal{L}(g) = \mathbf{w}$ where \mathbf{w} is the solution of

$$\begin{cases} \nabla \times \mu_T^{-1} \nabla \times \mathbf{w} - \varepsilon_T k_T^2 \mathbf{w} = 0 \text{ in } T \\ \gamma \times (\mu_T^{-1} \nabla \times \mathbf{w}) - Z_T \gamma_t \mathbf{w} = \mathbf{g} \text{ on } \partial T \end{cases} \quad (2)$$

where Z_T is an impedance operator such that $\text{Im}(Z_T) > 0$ (for example $Z_T := i\sqrt{\varepsilon_T \mu_T} k$).

For each Trefftz cell $T \in \mathcal{T}$, we first introduce two meshes $\mathcal{T}_h(\partial T)$ and $\mathcal{T}_h(T)$ of ∂T and T respectively. Next, we introduce two finite elements spaces $\mathcal{P}_h^q(\partial T)$ and $\mathcal{N}_h^p(T)$ which are respectively a space of piecewise polynomials of degree at most q defined from $\mathcal{T}_h(\partial T)$ and a high-order H-curl conforming space of order p defined from $\mathcal{T}_h(T)$.

The discretization of the problem (2) by using a finite element method on $\mathcal{N}_h^p(T)$ induces a discrete equivalent operator \mathcal{L}_h^p of \mathcal{L} . Finally, the discrete DG Trefftz formulation is : find $\mathbf{E}_h \in \Pi_{T \in \mathcal{T}} \mathcal{L}_h^p(\mathcal{P}_h^q(\partial T))$ such that

$$\forall \mathbf{w}_h \in \Pi_{T \in \mathcal{T}} \mathcal{L}_h^p(\mathcal{P}_h^q(\partial T)), \quad a(\mathbf{E}_h, \mathbf{w}_h) = \ell(\mathbf{w}_h).$$

Remark 1 The basis functions $(\mathbf{w}_i)_{i=1, \dots, N}$ are defined from a set $(\varphi_i)_{i=1, \dots, N}$ of basis functions of $\mathcal{P}_h^q(\partial T)$ by using the relation $\mathbf{w}_i := \mathcal{L}_h^p(\varphi_i)$.

4 Numerical validations

The main motivation for Trefftz DG type methods is reducing the impact of the pollution effect, by which more classical FE methods tend to be limited. One way of analyzing this is by studying long range wave propagation. For that, we consider a duct of height 1 and length L where an incoming plane wave is generated at $x = 0$, propagating freely to the right, and finally arriving at a transparent boundary condition at the right side. The figures 1 show that the pollution effect is one order of magnitude larger for the FEM than for the Trefftz method at comparable meshes and approximation orders.

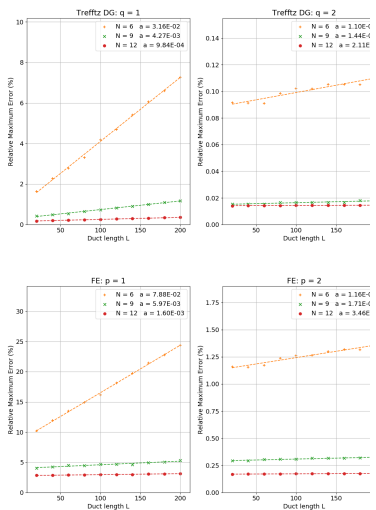


Figure 1: Relative maximum error for long range propagation using the DG Trefftz (up) and FEM (down) for different orders and meshes. N on this figure corresponds to $1/h$.

References

- [1] H. Barucq, A. Bendali, MB Fares, V. Matetsi and S. Tordeux, *A Symmetric Trefftz-DG formulation based on a local boundary element method for the solution of the Helmholtz equation*, Journal of Computational Physics, vol. 330, p. 1069–1092, 2017.

High order discretization of seismic waves-problems based upon DG-SE methods[†]Hélène Barucq¹, Henri Calandra², Aurélien Citrain^{3,1,*}, Julien Diaz¹, Christian Gout³¹Team project Magique.3D, INRIA, E2S UPPA, CNRS, Pau, France²TOTAL SA, CSTJF, Pau, France³INSA Rouen-Normandie Université, LMI EA 3226, 76000, Rouen

*Email: aurelien.citrain@insa-rouen.fr

[†]This work is dedicated to the memory of Dimitri Komatitsch.**Abstract**

Hybrid meshes comprised of hexahedras and tetrahedras are particularly interesting for representing media with local complex geometrical features like the seabed in offshore applications. We develop a coupled finite element method for solving elasto-acoustic wave equations. It combines Discontinuous Galerkin (DG) finite elements for solving elastodynamics with spectral finite elements (SE) for solving the acoustic wave equation. SE method has demonstrated very good performances in 3D with hexahedral meshes and contributes to reduce the computational burden by having less discrete unknowns than DG. The implementation of the method is performed both in 2D and 3D and it turns out that the coupling contributes to reduce the computational costs significantly: for the same time step and the same elementary mesh size, the CPU time of the coupled method is almost halved when compared to the one of a full DG method.

Keywords: Hybrid meshes, Discontinuous Galerkin method, Spectral Element method, coupling

1 Introduction

We focus on the first-order elasto-dynamic system due to space constraint. We denote by Ω a rectangular domain in 2D or a parallelepiped in 3D. We consider the system of wave equations:

$$\begin{cases} \rho(\mathbf{x}) \frac{\partial \mathbf{v}}{\partial t}(\mathbf{x}, t) &= \nabla \cdot \underline{\underline{\sigma}}(\mathbf{x}, t), \\ \frac{\partial \underline{\underline{\sigma}}}{\partial t}(\mathbf{x}, t) &= \underline{\underline{C}}(\mathbf{x}) \underline{\underline{\epsilon}}(\mathbf{v}(\mathbf{x}, t)), \end{cases} \quad (1)$$

where ρ is the density, $\underline{\underline{C}}$ the elasticity tensor and $\underline{\underline{\epsilon}}$ the deformation tensor. The space variable is $\mathbf{x} \in \mathbb{R}^d$ (with $d = 2, 3$) and $t \geq 0$ is the time variable. The two unknowns are \mathbf{v} the wavespeed and $\underline{\underline{\sigma}}$ the strain tensor. This system

can be solved by using DGm (see [1, 2]) or a SEm (see [3–5]). Our objective is to construct a variational formulation resulting from the combination of both approximations. The difficulty of such a coupling is the communication between the two different schemes.

2 Variational Formulation

Offshore geophysical exploration can be represented by a reference domain composed of a layer of water over the ocean bottom (see Fig 1). The computational domain is covered by a hybrid grid composed of hexahedra on the top and tetrahedra within the bottom. Basically, we define two areas: $\Omega_{h,1}$ composed of cartesian cells and $\Omega_{h,2}$ paved with unstructured tetrahedra capable of following the topography of the in-depth site. The transition between both areas is located inside the water. Hence, the interface $\Gamma_{1/2} = \Omega_{h,1} \cap \Omega_{h,2}$ is flat and the two regions communicate with each other through suitable fluxes. The portion $\Omega_{h,1}$ of the mesh can thus be seen as a macro-element of the DG partition. In the following, we use the subscript 1 to designate the fields computed over $\Omega_{h,1}$ while any field with subscript 2 corresponds to a quantity computed over $\Omega_{h,2}$. We introduce the pair (w, ξ) to test the continuous problem (1) and to get a variational formulation set in the whole domain Ω . For the sake of simplicity, we denote by a_j, b_j, c_j and d_j the bilinear forms defined by

$$\begin{aligned} a_j(v, w) &= \int_{\Omega_{h,j}} \rho \partial_t v \cdot w, \\ b_j(\underline{\underline{\sigma}}, w) &= - \int_{\Omega_{h,j}} \underline{\underline{\sigma}} \cdot \nabla w \\ c_j(\underline{\underline{\sigma}}, \underline{\underline{\xi}}) &= \int_{\Omega_{h,j}} \partial_t \underline{\underline{\sigma}} : \underline{\underline{\xi}}, \\ d_j(v, \underline{\underline{\xi}}) &= - \int_{\Omega_{h,j}} (\nabla(\underline{\underline{C}} \underline{\underline{\xi}})) \cdot v \end{aligned}$$

Then the global variational formulation reads as:

$$\begin{aligned}
 a_1(v_1, w_1) + a_2(v_2, w_2) &= b_1(\underline{\underline{\sigma}}_1, w_1) + b_2(\underline{\underline{\sigma}}_2, w_2) \\
 &+ \sum_{\Gamma \in \Gamma_{int}} \int_{\Gamma} \{ \{ \underline{\underline{\sigma}} \} \} [[w_2]] \cdot \mathbf{n} + \\
 &\int_{\Gamma_{1/2}} \{ \{ \underline{\underline{\sigma}} \} \} [[w]] \cdot \mathbf{n} \\
 c_1(\underline{\underline{\sigma}}_1, \underline{\underline{\xi}}_1) + c_2(\underline{\underline{\sigma}}_2, \underline{\underline{\xi}}_2) &= d_1(v_1, \underline{\underline{\xi}}_1) + d_2(v_2, \underline{\underline{\xi}}_2) \\
 &+ \sum_{\Gamma \in \Gamma_{int}} \int_{\Gamma} [[\underline{\underline{C}} \underline{\underline{\xi}}_2]] \{ \{ v_2 \} \} \cdot \mathbf{n} + \\
 &\int_{\Gamma_{1/2}} [[\underline{\underline{C}} \underline{\underline{\xi}}]] \{ \{ v \} \} \cdot \mathbf{n}
 \end{aligned}$$

where Γ_{int} stands for the set of internal boundaries limiting DG-elements. The shortage of the paper challenges us to omit to speak about external boundary conditions.

At the interface $\Gamma_{1/2}$, we define \mathbf{n} as the unitary normal vector oriented from $\Omega_{h,1}$ to $\Omega_{h,2}$. We can see how the two areas communicate through the different fluxes involving the jump and the mean value respectively defined by:

$$[[w]] = (w_{K_2} - w_{K_1}) \cdot \mathbf{n}, \{ \{ \underline{\underline{\xi}} \} \} = \frac{1}{2} (\underline{\underline{\xi}}_{K_2} + \underline{\underline{\xi}}_{K_1})$$

K_1 and K_2 are two connected DG-cells and w_{K_j} (resp. $\underline{\underline{\xi}}_{K_j}$) is the value of w (resp. $\underline{\underline{\xi}}$) in K_j .

In comparison with the implementation of a full SEM or a full DGM, we have to create new terms corresponding to the handling of $\Gamma_{1/2}$. They are written in terms of integrals mixing DG basis functions with a SE-one.

3 Numerical tests

We consider an exemple of anisotropic elastoacoustic domain depicted in Figure 1

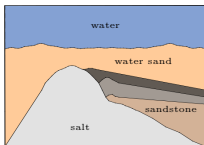


Figure 1: Propagation domain

It is a square 3000 meters paved with 74969 cells composed of 53969 unstructured triangles and 21000 structured quadrangles. The source

is a second-order Ricker point source located on the top of the layer of water. Both DGM and SEM have been validated separately in stratified media for which we dispose of analytical solutions. To assess the accuracy of the coupling, we have compared the full DG solution with the DG-SE one at order three and the results are displayed in Table 1. We compare the CPU-time at equal time-step and the relative error between these two solutions and a reference solution computed using DGM at order five. The second column shows that the DG-SEM solution has the same accuracy as the DG one. Then the third column certifies that the coupling allows to reduce the CPU time by a factor of 2. It is worth noting that we have used a global time-step and in the near future, we hope to improve our results by using local-time stepping.

	Relative error(%)	CPU-time(s)
DGM	5e-4	16317
DG_SEM	1e-3	8918

Table 1: DGM vs DG_SEM comparison.

Acknowledgments

The authors acknowledge the support of the European Union's research FEDER program under the M2NUM agreement HN0002137 and of the DIP Inria-TOTAL research project.

References

- [1] Reed, W. H. and Hill, TR., Triangular mesh methods for the neutron transport equation, 1973
- [2] Cockburn, B., Karniadakis, G. E. and, Shu, C., The development of discontinuous Galerkin methods, *Springer*, 3-50, 2000
- [3] Patera, A. T., A spectral element method for fluid dynamics: laminar flow in a channel expansion *Journal of computational Physics*, 54, 468-488, 1984
- [4] Seriani, G., Priolo, E., Carcione, J and, Padovani, E., High-order spectral element method for elastic wave modeling *Society of Exploration Geophysicists*, 1285-1288, 1992
- [5] Komatitsch, D., Méthodes spectrales et éléments spectraux pour l'équation de l'élastodynamique 2 D et 3 D en milieu hétérogène, Thèse de doctorat, 1997

Designing symmetry-protected valley-Hall networks in phononic systems

Mehul Makwana^{1,*}, Richard Craster¹, Sebastien Guenneau², Kun Tang³, Patrick Sebbah⁴, Gregory Chaplain¹

¹Department of Mathematics, Imperial College London, London SW7 2AZ, UK

²Aix–Marseille Univ, CNRS, Centrale Marseille, Institut Fresnel, Marseille, France

³Department of Physics, The Jack and Pearl Resnick Institute for Advanced Technology, Bar-Ilan University, Ramat-Gan 5290002, Israel

⁴Institut Langevin, ESPCI ParisTech CNRS UMR7587, 1 rue Jussieu, 75238 Paris cedex 05, France

*Email: mehul.makwana07@imperial.ac.uk

Abstract

Predictive theory to geometrically engineer materials in continuum systems to have desired symmetry-induced effects is developed here by bridging the gap between quantum and continuum descriptions. We emphasise a predictive approach, the strength of which is demonstrated by the ability to design well-defined broadband edge states and valley-Hall networks. The design of these valley-Hall networks is contingent upon properties specific to the underlying geometries chosen. We hope that the additional degrees of freedom afforded by our designs, in addition to the topological robustness of the modes, will result in its assimilation into practical devices.

Keywords: valley-Hall, topological, networks, elasticity, phononics

1 Introduction

Guiding waves, splitting, and redirecting them between channels, and steering waves around sharp bends in a lossless manner is of interest across many areas of engineering and physics. In particular, geometrically engineering valley-Hall phononic crystals to direct waves along interfaces in a robust tunable manner has shown much potential. Herein, we elucidate the core concepts of these effects as well as a myriad of other exotic symmetry-induced phenomena.

2 Models

We choose to illustrate our theory within the context of flexural waves upon thin structured elastic plates, by doing so we emphasise the continuum nature of the model and show the generality of the basic ideas. These displacement eigenmodes are governed by the (non-dimensionalised) Kirchhoff-Love (K-L) equation

$$(\nabla_{\mathbf{x}}^4 - \omega_{\kappa}^2) \psi_{n\kappa} = F(\mathbf{x}), \quad (1)$$

and the reaction forces at the point constraints $F(\mathbf{x})$ introduce the dependence upon the direct lattice. The simplest constraints are those of point mass-loading with the reaction forces proportional to the displacement via an impedance coefficient and thus

$$F(\mathbf{x}) = \omega_{\kappa}^2 \sum_{\mathbf{n}} \sum_{p=1}^P M_{\mathbf{n}}^{(p)} \psi_{n\kappa}(\mathbf{x}) \delta(\mathbf{x} - \mathbf{x}_{\mathbf{n}}^{(p)}). \quad (2)$$

Here \mathbf{n} labels each elementary cell, containing $p = 1 \dots P$ constraints, that periodically repeats to create the infinite physical platonic crystal. The mass in cell \mathbf{n} at point constraint p is given by $M_{\mathbf{n}}^{(p)}$. This constraint automatically encompasses the point pinn platonic crystal, as the limit $\omega_{\kappa}^2 M_{\mathbf{n}}^{(p)} \rightarrow \infty$, where the reaction forces are retained. This model has the advantage of being almost completely explicit; this leads to highly resolved solutions that enable us to interpret the results accurately.

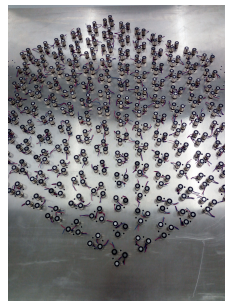


Figure 1: Underside of periodically pinned elastic plate. The displacement of the flexural waves satisfies the K-L equation where $F(\mathbf{x})$ is given by Eq. (2) in the limit $\omega_{\kappa}^2 M_{\mathbf{n}}^{(p)} \rightarrow \infty$.

3 Hexagonal valley-Hall networks

The valley Hall effect originates from the gapping of Dirac cones, resulting in nontrivial band gaps where broadband edge states are guaranteed to reside. In two-dimensional systems, there are only three symmetry sets that are guaranteed to yield Dirac cones, all of which occur on hexagonal lattices. These three cases are distinguished by their point groups at Γ in Fourier space; these are C_{6v} , C_6 , C_{3v} [1]. We demonstrate that from these edge states can be intelligently constructed that are imbued with a chiral flux that results in enhanced robustness against defects [2]. Utilising these edge states alongside tunneling phenomena, the interfacial wave networks designed contain splitters which partition energy in two, three, four, or five directions (Fig. 2). This enriches the valleytronics literature that has, so far, been limited to two-directional splitters. *Importantly*, note that only the two and four-way splitters, designed, result in outgoing leads that retain topological protection. Experimental results for a periodically pinned elastic plate (setup shown in Fig. 1) will be shown in the presentation.

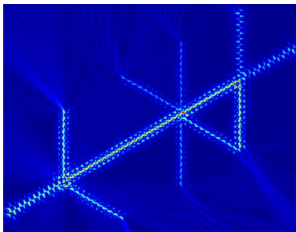


Figure 2: Valley-Hall supernetwork containing a four-way topological energy-splitter (that utilises tunneling phenomena)

4 Three-way valley-Hall beam-splitter for elasticity

Strategically combining four structured domains, Fig. 3(a), creates the first ever three-way topological energy-splitter for elasticity, Fig. 3(b) [3]; remarkably, this is only possible using a square, or rectangular, lattice, and not the hexagonal structures more commonly used in valleytronics. To achieve this effect accidental Dirac cones, that are located away from high symmetry points, are engineered. The geometrical construction of our structured medium allows for the three-way splitter to be adiabatically converted into a wave steerer around sharp bends [3].

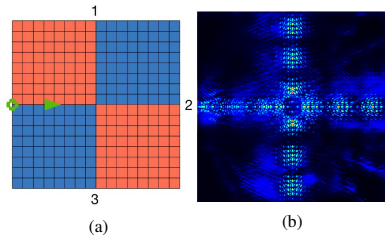


Figure 3: Panel (a): Schematic of structured domain containing four geometrically distinct regions, source located (highlighted) at beginning of leftmost interface. Panel (b): three-way valley-Hall energy-splitter for an elastic plate.

Unlike the four-way topological beam-splitter alluded to in the previous section, this three-way splitter is unreliant upon tunneling phenomena and hence the transmission along the outgoing leads is far more tunable. Dissimilar to the hexagonal case, the two interfaces of this square structure, are related by time-reversal symmetry (TRS). This subtlety is what allows for more than two-way partitioning of energy away from a well-defined nodal point without the need for tunneling.

5 Conclusion

We have geometrically engineered interfacial wave networks containing energy-splitters that partition energy in more than two directions. Due to the tunability of the energies directionality by geometry, our results have far-reaching implications for applications such as beam-splitters, switches and filters across wave physics.

References

- [1] M. Makwana and R. V. Craster, Geometrically navigating topological plate modes around gentle and sharp bends, *Physical Review B* (2018),98: 184105.
- [2] M. Makwana and R. V. Craster, Designing multidirectional energy splitters and topological valley supernetworks, *Physical Review B* (2018),98: 235125.
- [3] M. Makwana and G. J. Chaplain, Tunable three-way topological energy-splitter, *arXiv* (2019), 1901.01937v2, 2019.

Hybrid approach for modelling wave motion in a layered phononic crystal with multiple cracks and piezoelectric transducers

Mikhail V. Golub^{1,*}, Alisa N. Shpak¹, Sergey I. Fomenko¹, Olga V. Doroshenko¹,
Chuanzeng Zhang²

¹Institute for Mathematics, Mechanics and Informatics, Kuban State University, Krasnodar, Russian Federation

²Department of Civil Engineering, University of Siegen, Siegen, Germany

*Email: m_golub@inbox.ru

Abstract

A hybrid approach based on the boundary integral equation method (BIEM) and the frequency domain spectral element method (FDSEM) to simulate wave propagation in a layered phononic crystal (PnC) with multiple delaminations and a network of piezoelectric transducers mounted on its surface is presented here. The proposed hybrid approach incorporates the advantages of the BIEM and the FDSEM. Boundary conditions at the crack faces are satisfied by Bubnov-Galerkin method. In order to satisfy continuity boundary conditions at the contact area between a PnC and a piezoelectric transducer, the collocation method and Petrov-Galerkin method are applied.

Keywords: hybrid method, wave propagation, crack, periodic, phononic crystal

1 Introduction

This paper presents a hybrid approach for modelling wave phenomena in a layered PnC with multiple delaminations and a network of piezoelectric transducers. The method employs the FDSEM [1] to discretize piezoelectric structures and the BIEM [2] to simulate wave propagation in a multi-layered waveguide with a set of horizontal delaminations. The presented method extends the hybrid approach proposed in [3] to simulate dynamic interaction of perfectly bonded or partially debonded piezoelectric structures with a layered elastic waveguide. The coupling of the methods is performed in the contact area between the PnC and transducers via the introduction of unknown traction vectors.

2 Statement of the problem

Let us consider in-plane motion of a network of piezoelectric transducers (PZTs) occupying rectangular domains $\Omega^{(n)}$ and a PnC composed of M unit-cells (each is made of 2 elastic lay-

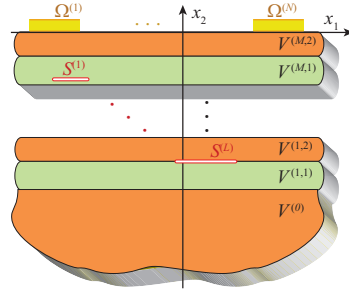


Figure 1: Geometry of the problem

ers $V^{(m,k)}$, $m = 1, 2, \dots, M$, $n = 1, 2$) on a half-space $V^{(0)}$ and L strip-like cracks with stress-free faces occupying domains $S^{(l)}$, see Figure 1. The following governing equation in terms of displacements u_i and electric potential ϕ are valid in $\Omega^{(n)}$ for the time-harmonic motion with the angular frequency ω :

$$C_{ijkl}u_{k,lj} + e_{kij}\phi_{,kj} + \rho\omega^2 u_i = 0, \quad (1)$$

$$e_{ikl}u_{k,li} - \varepsilon_{ik}\phi_{,ki} = 0. \quad (2)$$

Here C_{ijkl} , e_{kij} and ε_{ik} are elastic, piezoelectric and dielectric constants, ρ is the mass density, $u_{k,lj}$ denotes derivative of u_k with respect to x_l and x_j . Electric potentials $V_{\pm}^{(n)}$ are applied at lower $\widehat{S}_{-}^{(n)}$ and upper $\widehat{S}_{+}^{(n)}$ surfaces of PZTs $\Omega^{(n)}$:

$$\phi = V_{\pm}^{(n)}, \quad \mathbf{x} \in \widehat{S}_{\pm}^{(n)}, \quad (3)$$

At the side boundaries of the PZTs, horizontal electric displacements $D_1 = 0$. In the PnC, the governing equations (1) are employed with zero electric potential. The continuity of the displacement \mathbf{u} and the traction ($\boldsymbol{\tau} = \{\sigma_{12}, \sigma_{22}\}$) vectors is assumed at the interfaces between sublayers and at the boundaries $\widehat{S}_{-}^{(n)} = V^{(M,2)} \cap \Omega^{(n)}$. The crack faces $S^{(l)}$ are stress-free.

3 Hybrid scheme

At first, traction vector $\boldsymbol{\tau} = \mathbf{q}^{(n)}$ is introduced in the contact area $S^{(n-)}$. The solution in PZTs is constructed via the FDSEM [1], so that the state vector $\mathbf{y} = \{u_1, u_2, \phi\}$ can be approximated using Lagrange interpolation polynomials $C^I(x_1, x_2)$ at Gauss–Lobatto–Legendre points via a special index I [3]:

$$\mathbf{y}^{(n)} = \sum_I \mathbf{y}_I^{(n)} C_I(x_1, x_2), \quad (4)$$

The total wave-field in the PnC can be obtained as a sum of wave-fields $\hat{\mathbf{u}}^{(n)}$ excited by PZTs and the wave-fields $\mathbf{u}^{(n)}$ scattered by the cracks. According to the BIEM [2], displacement and traction vectors can be expressed as follows:

$$\hat{\mathbf{u}}^{(n)} = \frac{1}{2\pi} \int_{\Gamma} \mathbf{K}^{(n)}(\alpha, x_2) \mathbf{Q}^{(n)}(\alpha) e^{-i\alpha x_1} d\alpha, \quad (5)$$

$$\hat{\boldsymbol{\tau}}^{(n)} = \frac{1}{2\pi} \int_{\Gamma} \mathbf{T}^{(n)}(\alpha, x_2) \mathbf{Q}^{(n)}(\alpha) e^{-i\alpha x_1} d\alpha. \quad (6)$$

Here $\mathbf{Q}^{(n)}$, $\mathbf{K}^{(n)}$ and $\mathbf{T}^{(n)}$ are the Fourier transforms of $\mathbf{q}^{(n)}$ and corresponding Green's matrices for the PnC, while Γ is the integration contour (for more details, see [2]). Similar expressions are written for the scattered wave-fields:

$$\mathbf{u}^{(l)} = \frac{1}{2\pi} \int_{\Gamma} \mathbf{K}^{(l)}(\alpha, x_2) \mathbf{W}^{(l)}(\alpha) e^{-i\alpha x_1} d\alpha, \quad (7)$$

$$\boldsymbol{\tau}^{(l)} = \frac{1}{2\pi} \int_{\Gamma} \mathbf{T}^{(l)}(\alpha, x_2) \mathbf{W}^{(l)}(\alpha) e^{-i\alpha x_1} d\alpha. \quad (8)$$

Here $\mathbf{K}^{(l)}$, $\mathbf{T}^{(l)}$ and $\mathbf{W}^{(l)}$ are the Fourier transforms of Green's matrices and unknown crack opening displacement (COD) $\mathbf{w}^{(l)}(x_1)$ for l -th crack. In order to obtain the solution, the COD for l -th crack is expanded in terms of Chebyshev polynomials of the second kind with square-root weight $p_i^{(l)}(x_1)$

$$\mathbf{w}_k^{(l)}(x_1) = \sum_i \gamma_{ki}^{(l)} p_i^{(l)}(x_1), \quad (9)$$

while the traction vector is approximated using splines $s_J(x_1)$ based at the nodal points [3]

$$\mathbf{q}^{(n)}(x_1) = \sum_J \mathbf{q}_J^{(n)} s_J(x_1). \quad (10)$$

In accordance with the FDSEM, substitution of (4) and (10) into governing equations (1) and (2) leads to the equations

$$\mathbf{A}^{(n)} \cdot \hat{\mathbf{y}}^{(n)} + \mathbf{B}^{(n)} \cdot \hat{\mathbf{q}}^{(n)} = \boldsymbol{\phi}^{(n)}, \quad n = \overline{1, N},$$

where vectors $\hat{\mathbf{y}}^{(n)}$, $\hat{\mathbf{q}}^{(n)}$ and $\hat{\boldsymbol{\gamma}}^{(l)}$ are composed of unknown expansion coefficients, while $\boldsymbol{\phi}^{(n)}$ arises from boundary condition (3). Substitution of representations (4)–(8) into the boundary conditions of the continuity of displacements and the application of Bubnov-Galerkin method leads to the relations

$$\mathbf{C}^{(n)} \cdot \hat{\mathbf{y}}^{(n)} = \mathbf{D}^{(nk)} \cdot \hat{\mathbf{q}}^{(k)} + \mathbf{F}^{(nm)} \cdot \hat{\boldsymbol{\gamma}}^{(l)}, \quad n = \overline{1, N}.$$

Substitution of integral representations (5)–(8) into the stress-free boundary conditions at crack faces gives relations

$$\mathbf{G}^{(lk)} \cdot \hat{\mathbf{q}}^{(k)} + \mathbf{H}^{(lm)} \cdot \hat{\boldsymbol{\gamma}}^{(m)} = \mathbf{0}, \quad l = \overline{1, M},$$

which finalize the system necessary to obtain solution of the considered boundary value problem.

4 Conclusions

The proposed method is applicable to the multi-parameter analysis of the phenomena related to elastic wave excitation and scattering in multi-layered structures. In order to obtain the transient solution, the Laplace transform with respect to the frequency variable can be applied.

The research was supported by the Russian Foundation for Basic Research within the project 18-501-12069 with the German Research Foundation (DFG, Project No. ZH 15/29-1).

References

- [1] L. Shi, Y. Zhou, J.M. Wang, M. Zhuang, N. Liu and Q.H. Liu, Spectral element method for elastic and acoustic waves in frequency domain, *Journal of Computational Physics* **327** (2016), pp. 19–38.
- [2] Glushkov, E.V., Glushkova, N.V., Golub, M.V. and Zhang, C. Resonance blocking of travelling waves by a system of cracks in an elastic layer, *Acoustical Physics* **55** (2009), pp. 8–16.
- [3] M.V. Golub and A.N. Shpak, Semi-analytical hybrid approach for the simulation of layered waveguide with a partially debonded piezoelectric structure, *Applied Mathematical Modelling* **65** (2019), pp. 234–255.

Optimal Wave Fields for Micromanipulation in Complex Scattering Environments

Matthias Kühmayer^{1,*}, Michael Horodynski¹, Andre Brandstötter¹, Kevin Pichler¹, Yan V. Fyodorov², Ulrich Kuhl³, Stefan Rotter¹

¹Institute for Theoretical Physics, Vienna University of Technology (TU Wien), Austria

²Department of Mathematics, King's College London, United Kingdom

³Institut de Physique de Nice, Université Côte d'Azur, CNRS, Nice, France

*Email: matthias.kuehmayer@tuwien.ac.at

Abstract

Due to its many applications ranging from physics to biology, the field of micromanipulation has grown tremendously in recent years. Here, we introduce and experimentally demonstrate a novel approach to identify the optimal light fields for micromanipulation even in very complex environments like disordered media. Our approach is based on a generalization of the well established Wigner-Smith time-delay operator and can be used to transfer torque, to apply pressure or to create an intensity focus at any desired target. Most importantly, these optimal light fields can be created based solely on the far-field information stored in the experimentally accessible scattering matrix.

Keywords: micromanipulation, disordered systems, complex scattering

1 Introduction

Starting with the seminal work of Ashkin on optical trapping of nano-scale dielectric particles with a laser beam [1], the field of optical micromanipulation has become a research area on its own and has enabled many interesting applications like cellular manipulation, micro-robotics and tests of fundamental physics. A recent and very promising trend in this research field is to make use of the technological advances of spatial light modulators to create light fields that are tailor-made for each desired purpose [2]. The techniques developed in this context so far rely, however, mostly on iterative optimization schemes, which do not assure the convergence to the optimal wave state in the iteration, as one may get stuck in some local minimum [3, 4]. Here, we demonstrate a novel approach that allows us to obtain the optimal scattering state for micromanipulation purposes as the solution of a simple eigenvalue problem based on the scattering matrix of a system and its dependence on the target's properties.

2 Theory

To achieve the optimal field configuration for manipulating a designated target buried inside a scattering medium, we utilize a generalization of the Wigner-Smith time-delay operator $Q_\omega = -iS^{-1}dS/d\omega$ [5, 6], which is originally based on the scattering matrix S of a given system and its derivative with respect to the frequency ω . Due to this frequency derivative, the eigenvalues of Q_ω correspond to well-defined delay times associated with the scattering by a given potential, where time is the conjugate quantity to frequency. By replacing the frequency derivative with a derivative with respect to some arbitrary parameter α of the target, the eigenstates of this generalized Wigner-Smith (GWS) operator now feature eigenvalues, which correspond to a well-defined change in the conjugate quantity to α between the incoming and outgoing waves [7]. In Ref. [7] we demonstrate that choosing the parameter α as the position of the target that we want to manipulate, yields GWS-eigenstates that are optimal in terms of the momentum transfer onto the target. As we will show here analytically, numerically and experimentally, this concept can also be extended to deliver an optimal torque or radiation pressure onto the target or for focusing wave intensity inside of it.

3 Results

Using the GWS-operator $Q_\alpha = -iS^{-1}dS/d\alpha$ we show that considering α as the radius of a circular target enables us to apply a well-defined pressure to it. Similarly, we can also control the torque exerted onto a target by considering the orientation angle of a non-circular target as the parameter α . Moreover, using the refractive index of the target as the parameter α allows us to control the total intensity deposited inside the target. In addition to the analytical proofs, we confirm our theoretical find-

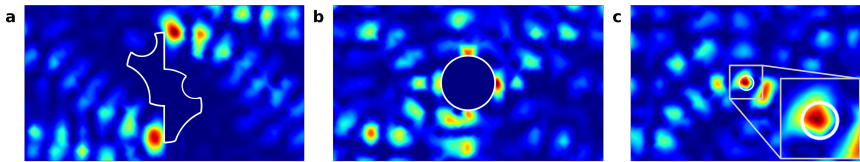


Figure 1: Measured intensity distribution for the GWS-eigenstates corresponding to the largest eigenvalue (a) for the rotation of an asymmetric metallic target inside an empty waveguide, (b) for a radius change of a metallic cylindrical target inside a disorder, and (c) for a change in the target's refractive index. In (a) the intensity builds up as far away as possible from the target's center such that the maximal torque is transferred, whereas the intensity distribution in (b) builds up on all sides of the target to produce an optimal value of the applied radiation pressure. Using the refractive index as parameter α results in GWS-eigenstates, which maximize the stored intensity inside the target as can be seen in (c).

ings by numerical simulations in which we solve the two-dimensional scalar Helmholtz equation $[\Delta + n(\vec{r})^2 k_0^2] \psi(\vec{r}) = 0$ for waveguide geometries filled with randomly placed circular scatterers of varying sizes using a finite element method [8]. Here, Δ is the Laplacian in two dimensions, $n(\vec{r})$ is the refractive index distribution dependent on the position $\vec{r} = (x, y)$, k_0 is the vacuum wavenumber and $\psi(\vec{r})$ is the z -component of the TE-polarized electric field. Since the GWS-operator is Hermitian for unitary scattering matrices its eigenbasis is complete and orthogonal with the consequence that the GWS-eigenstate featuring the largest eigenvalue corresponds to the optimal state for a given change in the conjugate quantity to α . Note that our approach is applicable to any kind of target scatterer in arbitrary environments for any kind of waves (electromagnetic, acoustic, etc.). The only requirement of our protocol is a linear wave scattering problem to which a scattering matrix can be assigned.

Finally, we implemented these ideas also experimentally with a microwave setup featuring a waveguide that contains a disordered medium with randomly placed cylindrical Teflon scatterers of varying size. In the middle of the scattering region we place target scatterers of different shapes and sizes. Since we have full control of the injected microwave field both in phase and amplitude, this setup allows us to measure the scattering matrices needed for the construction of the GWS-operator. The resulting eigenstates are then reinjected into the system and their measured electric field distributions around the

target scatterer (see Fig. 1) confirm the findings of our theoretical analysis.

References

- [1] A. Ashkin et al., Observation of a single-beam gradient force optical trap for dielectric particles, *Optics Letters* **11** (1986), p. 288.
- [2] K. Dholakia, T. Čižmár, Shaping the future of manipulation, *Nat. Photonics* **5** (2011), p. 335.
- [3] Y. E. Lee et al., Computational inverse design of non-intuitive illumination patterns to maximize optical force or torque, *Optics Express* **25** (2017), p. 6757.
- [4] M. A. Taylor et al., Enhanced optical trapping via structured scattering, *Nat. Photonics* **9** (2015), p. 669.
- [5] E. P. Wigner, Lower Limit for the Energy Derivative of the Scattering Phase Shift, *Phys. Rev.* **98** (1955), p. 145.
- [6] F. T. Smith, Lifetime Matrix in Collision Theory, *Phys. Rev.* **118** (1960), p. 349.
- [7] P. Ambichl et al., Focusing inside Disordered Media with the Generalized Wigner-Smith Operator, *Phys. Rev. Lett.* **106** (2017), p. 033903.
- [8] Netgen/NGSolve Finite Element Tool, <https://ngsolve.org/>

Analysis of topological derivative as a means for qualitative identification

Marc Bonnet^{1,*}, Fioralba Cakoni²¹POEMS (CNRS, INRIA, ENSTA), ENSTA, Palaiseau, France²Department of Mathematics, Rutgers University, Piscataway, USA

*Email: mbonnet@ensta.fr

Abstract. This work addresses the mathematical justification of topological derivative-based qualitative inverse scattering, for the case of anisotropic scatterers and background and near-field data. Our results include justification of sign heuristics and verification, in the isotropic case, of spatial decay.

Keywords: topological derivative, inverse scattering

Consider an unbounded, homogeneous reference propagation medium where a wave u satisfies

$$-\operatorname{div}(\mathbf{A} \cdot \nabla u) - \kappa^2 u = 0$$

(with $\mathbf{A} \in \mathbb{R}_{\text{sym}}^{3 \times 3}$, see [4] for scattering in anisotropic media). The medium hosts an unknown inhomogeneity with compact support $B \subset \mathbb{R}^3$ and material parameters $\tilde{\mathbf{A}} \in \mathbb{R}_{\text{sym}}^{3 \times 3}$. Both \mathbf{A} and $\tilde{\mathbf{A}}$ are positive definite. Probing excitations and measurements are supported by the respective closed surfaces Γ_s and Γ_m , which surround B and are assumed to either coincide or be nested.

Let the single-layer potential operator $S_{r\alpha} : H^{-1/2}(\Gamma_\alpha) \rightarrow H_{\text{loc}}^1(\mathbb{R}^3)$ ($\alpha = m, s$) be defined by

$$S_\alpha \varphi(\mathbf{x}) = \int_{\Gamma_\alpha} \Phi_\kappa(\mathbf{x} - \mathbf{y}) \varphi(\mathbf{y}) \, d\mathbf{y}$$

($\alpha = m, s$) where $\Phi_\kappa(\mathbf{x} - \mathbf{y})$ is the radiating fundamental solution for the background medium. Towards the identification of B , the medium is excited by source densities $g \in H^{-1/2}(\Gamma_s)$ creating incident fields $u = S_s g$, which give rise in the perturbed medium to the total field

$$u_B^g(\mathbf{x}) = \int_{\Gamma_s} u_B(\mathbf{x}; \mathbf{s}) g(\mathbf{s}) \, d\mathbf{s} \quad \mathbf{x} \in \mathbb{R}^3$$

where $u_B(\cdot; \mathbf{s})$ is the radiating solution of

$$-\operatorname{div}(\mathbf{A}_B \cdot \nabla u_B) - \kappa^2 u_B = \delta(\cdot - \mathbf{s})$$

with $\mathbf{A}_B := \mathbf{A} + (\tilde{\mathbf{A}} - \mathbf{A})\chi_B$. In the present setting (where sources and measurements are not in the far field), point sources and their superposition as potentials replace plane waves and Herglotz wave functions used in e.g. [1].

Let $\mathbf{W}_\kappa[g]$ be the volume potential defined for any density $g \in L_{\text{comp}}^2(\mathbb{R}^3; \mathbb{C}^3)$ by

$$\mathbf{W}_\kappa[g](\mathbf{x}) = \int_{\mathbb{R}^3} \nabla \Phi_\kappa(\mathbf{x} - \mathbf{y}) \cdot g(\mathbf{y}) \, d\mathbf{y}.$$

The scattered field $u_B^s(\cdot; \mathbf{s}) := u_B(\cdot; \mathbf{s}) - u(\cdot; \mathbf{s})$ is then given by $u_B^s(\cdot; \mathbf{s}) = \mathbf{W}_\kappa[\mathbf{h}_B]$, where $\mathbf{h}_B := (\tilde{\mathbf{A}} - \mathbf{A}) \cdot \nabla u_B(\cdot, \mathbf{s}) \in L^2(B; \mathbb{C}^3)$ solves the singular volume integral equation (VIE)

$$\mathbf{A}^{1/2} \mathbf{Q} [\mathbf{I} - \mathbf{Q} \mathbf{R}_\kappa] \mathbf{A}^{1/2} \mathbf{h}_B = 2\mathbf{h} \quad \text{in } B \quad (1)$$

with $\mathbf{Q} := (\tilde{\mathbf{A}} + \mathbf{A})^{-1}(\tilde{\mathbf{A}} - \mathbf{A})$ and $\mathbf{R}_\kappa := \mathbf{I} + 2\mathbf{A}^{1/2} \mathbf{W}_\kappa \mathbf{A}^{1/2}$. There exists a matrix $\mathbf{q} \in \mathbb{R}^{3 \times 3}$ and a diagonal matrix $\boldsymbol{\sigma}$ such that $\mathbf{Q} = \mathbf{q}^T \boldsymbol{\sigma} \mathbf{q}$, with the nonzero entries of $\boldsymbol{\sigma}^2$ (also diagonal) being ± 1 according to the sign of the corresponding eigenvalue of \mathbf{Q} . The VIE (1) is known to be well-posed, see [2] for details.

Cost functional We assume the knowledge on Γ_m of a measurement $u_{\text{obs}}(\cdot; \mathbf{s})$ of $u_B(\cdot; \mathbf{s})$ for each source location $\mathbf{s} \in \Gamma_s$, and idealize the situation further by considering noise-free data, i.e. $u_{\text{obs}}(\cdot; \mathbf{s}) = u_B(\cdot; \mathbf{s})$. We formulate the problem of identifying B in terms of the minimization of the cost functional

$$\mathcal{J}_E(D) := \frac{1}{2} \int_{\Gamma_s} \int_{\Gamma_s} |(Eu_D - Eu_{\text{obs}})(\mathbf{s}'; \mathbf{s})|^2 \, d\mathbf{s} \, d\mathbf{s}'$$

where D is the support of a trial inhomogeneity and the bounded linear operator $H^{1/2}(\Gamma_m) \rightarrow H^{1/2}(\Gamma_s) E$, defined by $E := (\gamma_m S_s)^* (\gamma_m S_m)^{-1}$ and acting on the first variable of u_D, u_{obs} , produces an ‘‘equivalent measurement’’ Eu_{obs} and its model prediction Eu_D that are defined on the source surface Γ_s . Crucially for our analysis, E ensures a symmetrical factorization of the measurement operator $g \mapsto u_B^g$. This symmetrization issue commonly arises for factorization methods with near field data (see e.g. [5]).

Topological derivative. The medium is ‘‘sampled’’ using trial inhomogeneities $B_\delta(\mathbf{z})$ of support $B_\delta(\mathbf{z}) = \mathbf{z} + \delta B$ and size $\delta > 0$, centered at a given point \mathbf{z} and endowed with specified material constants \mathbf{A}_z . Denoting by $u_\delta := u_{B_\delta}$ the total field for $D = B_\delta(\mathbf{z})$, we set $J(\delta) := \mathcal{J}_E(B_\delta)$. The topological derivative (TD) $\mathcal{T}(\mathbf{z})$ of J at \mathbf{z} is then defined (see e.g. [6]) through the expansion

$$J(\delta) = J(0) + \delta^3 \mathcal{T}(\mathbf{z}) + o(\delta^3).$$

The heuristic basis for identification is that $\mathcal{T}(\mathbf{z})$ is expected to take pronounced negative values in a neighborhood of B , consistently with the notion of minimizing \mathcal{J} . This heuristic involves both the magnitude and the sign of $\mathcal{T}(\mathbf{z})$.

An explicit expression of $\mathcal{T}(\mathbf{z})$ can be formulated and analysed [3], taking advantage of the form (1) of the governing VIE and using its solution operator; this yields the following result:

Theorem 1 *Given the true anisotropic scatterer (B, \mathbf{A}) , we assume that the background is isotropic $(\mathbf{A} = a\mathbf{I})$ and that the contrast has a definite sign in the sense that $\sigma^2 = \sigma^2 \mathbf{I}$ with $\sigma^2 = \pm 1$. Then, if we consider a spherical isotropic trial inhomogeneity (i.e. \mathcal{B} the unit ball and $\mathbf{A}_z = a_z \mathbf{I}$) and a wave number κ such that*

$$\|\mathbf{q} \cdot \mathbf{R}_\kappa \cdot \mathbf{q}\|_{L^2(B) \rightarrow L^2(B)} < 1, \quad (2)$$

the TD satisfies the sign condition

$$\text{sign}(\mathcal{T}(\mathbf{z})) = -\text{sign}\left(\frac{a_z - a}{a_z + a} \sigma^2\right)$$

ensuring correctness of the TD sign heuristic. When both media are anisotropic, the above result remains true if the trial contrast also has a sign (i.e. if $\sigma_z = \sigma_z \mathbf{I}$ with $\sigma_z^2 = \pm 1$).

Condition (2) restricts the justification of the sign heuristic to “moderate” scatterers. It is less restrictive than the weak scattering condition $\|\mathbf{q} \cdot \mathbf{R}_\kappa \cdot \mathbf{q}\| \ll 1$ defining the Born approximation.

Spatial decay of TD. The spatial decay of $\mathcal{T}(\mathbf{z})$ as \mathbf{z} moves away from B is the other component of the TD heuristic warranting justification. As near-field data is assumed, we need to understand how $\mathcal{T}(\mathbf{z})$ decays for \mathbf{z} “far” from B while still remaining “reasonably” distant from Γ_m . We treat this issue by means of a two-scale asymptotic calculation [3], limited to the case

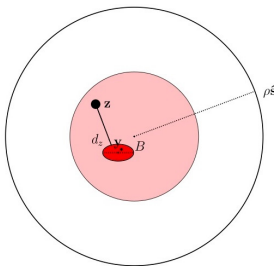


Figure 1: Two-scale asymptotics: notation.

where (i) B_δ is spherical and (ii) $\Gamma_s = \Gamma_m = \rho \hat{S}$ (with \hat{S} the unit sphere). For a fixed \mathbf{z} outside B we set the reference length as $d_z := \text{dist}(\mathbf{z}, B)$, noting that $|\mathbf{y} - \mathbf{z}|, \mathbf{y} \in B$ is $O(d_z)$. Let $\eta > 0$ be a small parameter that characterizes the ratio between the size of B and the radius ρ of $\Gamma_m = \Gamma_s$ (Fig. 1), so that $|\mathbf{y}|/|\mathbf{s}| = |\mathbf{y}|/\rho = O(\eta)$ ($\mathbf{y} \in B, \mathbf{s} \in \rho \hat{S}$). We express the facts that (a) the probing region and inhomogeneity are far from $\Gamma_s = \Gamma_m$ and (b) \mathbf{z} stays “far from” the inhomogeneity, by assuming that

$$\frac{|\mathbf{y} - \mathbf{z}|}{|\mathbf{s}|} = \frac{|\mathbf{y} - \mathbf{z}|}{\rho} = O(\eta^\alpha), \quad \frac{|\mathbf{y}|}{|\mathbf{y} - \mathbf{z}|} = O(\eta^{1-\alpha}),$$

respectively, uniformly for $\mathbf{y} \in B$ and for some constant $0 < \alpha < 1$. Loosely speaking our scaling is such that $d_z/\rho = \eta^\alpha$ and $\text{diam}(B)/d_z = \eta^{1-\alpha}$ (Fig. 1). We performed a “far field” asymptotic expansion of $\mathcal{T}(\mathbf{z})$ as $\eta \rightarrow 0$, retaining only the $O(1)$ and $O(\eta^\alpha)$ terms (the $O(1)$ terms being those appearing in the far field expansion [1]).

Theorem 2 *For an unknown isotropic inhomogeneity B and with the above definitions, we have $\mathcal{T}(\mathbf{z}) = O((\kappa \text{dist}(\mathbf{z}, B))^{-2})$ as $\eta \rightarrow 0$.*

Numerical examples. The main theoretical findings of this work are supplemented by 3D numerical examples [3]. Results (a) show that the operator E , which is important for the analysis by allowing a symmetric source-to-data factorization, affects only mildly the results in practice, and (b) verify the well-documented robustness of TD-based imaging against data noise.

References

- [1] C. Bellis, M. Bonnet and F. Cakoni, Acoustic inverse scattering using topological derivative of far-field measurements-based l^2 cost functionals. *Inverse Problems*, **29**:075012, 2013.
- [2] M. Bonnet, A modified volume integral equation for anisotropic elastic or conducting inhomogeneities. Unconditional solvability by Neumann series. *J. Integral Equ. Appl.*, **29**:271–295, 2017.
- [3] M. Bonnet and F. Cakoni, Analysis of topological derivative as a tool for qualitative identification. *Inverse Problems*, **35**(2019), in press.
- [4] G. Dassios and K. S. Karadima, Time harmonic acoustic scattering in anisotropic media. *Math. Meth. in Appl. Sc.*, **28**:1383–1401, 2005.
- [5] A. Kirsch and N. Grinberg, *The factorization method for inverse problems*. Oxford, 2008.
- [6] J. Sokolowski and A. Zochowski. On the topological derivative in shape optimization. *SIAM J. Control Optim.*, **37**:1251–1272, 1999.

Topology optimisation for cloaking of arbitrary objects

Hiroshi Isakari^{1,*}, Ryo Yamamoto¹, Kenta Nakamoto², Toru Takahashi¹, Toshiro Matsumoto¹

¹Department of Engineering, Nagoya University, Nagoya, Japan

²Fixstars Corporation, Tokyo, Japan

*Email: isakari@nuem.nagoya-u.ac.jp

Abstract

We propose a new topology optimisation for cloaking devices. In the present formulation, we explore an optimum dielectric material distribution minimising total electromagnetic field in a domain as well as far-field scattering amplitude. The dielectric distribution obtained in the present formulation works as a “material- and shape-independent cloak”. We can put any object in the area in which the electromagnetic field is minimised without disturbing the scattered field. Thus, the optimised dielectric material distribution cloaks any object regardless of its shape and material.

Keywords: cloaking, topological derivative, level-set method, boundary element method

1 Introduction

Recently, various topology optimisations have been proposed to realise so-called cloaking devices [1, 2]. Most of the existing formulations minimise scattered field in a preset bounded region (which is often set by trial and error) by a specific material of particular shape. A device obtained in such a way may not work as a cloaking for an object which has a slightly different shape or material constants from the expected ones. Also, the scattering outside the preset region is not necessarily minimised. In this study, to resolve these issues, we propose a new formulation for topology optimisation of the cloaking device which works regardless of shape or material of objects [3]. The numerical experiments show the effectiveness of the proposed formulation.

2 Electromagnetic scattering in 2D

We here consider a plane electromagnetic wave scattered by dielectric materials. We assume that the electromagnetic field is uniform in x_3 direction and is TE-polarised, i.e., the magnetic field only has an x_3 component which is denoted by u . With these settings, u is governed by the

following boundary value problem:

$$\nabla^2 u(\mathbf{x}) + k_i^2 u(\mathbf{x}) = 0 \quad \mathbf{x} \in \Omega_i, \quad (1)$$

$$[u(\mathbf{x})] = \left[\frac{1}{\varepsilon_i} \frac{\partial u(\mathbf{x})}{\partial n} \right] = 0, \quad (2)$$

$$\text{The radiation condition as } |\mathbf{x}| \rightarrow \infty, \quad (3)$$

where $k_i := \omega \sqrt{\mu_i \varepsilon_i}$, ε_i and μ_i are the wave number, relative permittivity and permeability in Ω_i , respectively, and i takes either 1 or 2. We here assume Ω_2 is a bounded domain filled with a dielectric material, and $\Omega_1 := \mathbb{R}^2 \setminus \overline{\Omega_2}$ is the host vacuum domain. ω is the angular frequency with which the time dependence of the electromagnetic fields is written as $e^{-i\omega t}$. Also, $[[\cdot]]$ in (2) denotes the jump in its argument across the boundary Γ of Ω_i , and \mathbf{n} is the unit normal on Γ directed from Ω_2 .

It is well known that the scattered field $u^{\text{sc}} = u - u^{\text{in}}$ (where u^{in} denotes a plane incident wave) admits the following far-field approximation:

$$u^{\text{sc}}(\mathbf{x}) = e^{-\frac{i\pi}{4}} \sqrt{\frac{2}{\pi k_1 |\mathbf{x}|}} e^{ik_1 |\mathbf{x}|} f(\hat{\mathbf{x}}), \quad (4)$$

in which f is the far-field pattern evaluated as

$$f(\hat{\mathbf{x}}) = -\frac{i}{4} \int_{\Gamma} \left[\frac{\partial u^{\text{sc}}(\mathbf{y})}{\partial n} + ik_1 (\hat{\mathbf{x}} \cdot \mathbf{n}(\mathbf{y})) u^{\text{sc}}(\mathbf{y}) \right] d\Gamma(\mathbf{y}), \quad (5)$$

and $\hat{\mathbf{x}} = \mathbf{x}/|\mathbf{x}|$.

3 Topology optimisation

With the far-field pattern reviewed in the previous section, our topology optimisation problem is defined as follows: For a specific incident plane wave u^{in} , find $\Omega_2 \subset D$ such that the following cost function J is minimised:

$$J = \frac{w_1}{N_1} \sum_{i=1}^{N_1} |f(\mathbf{p}_i^{\text{sc}})|^2 + \frac{w_2}{N_2} \sum_{i=1}^{N_2} |u(\mathbf{x}_i^{\text{obs}})|^2, \quad (6)$$

where D is a bounded domain (which is often called fixed design domain), \mathbf{p}^{sc} is set as

$\mathbf{x}_i^{\text{sc}} = (\cos 2\pi i/N_1, \sin 2\pi i/N_1)^T$, $\mathbf{x}_i^{\text{obs}}$ is i -th observation point at which the total magnetic intensity will be minimised. $w_1, w_2 > 0$ are preset constants. Dielectric material distribution Ω_2 minimising the cost function J achieves cloaking for arbitrary objects. In fact, Ω_2 itself is invisible since the scattering amplitudes for all the directions are reduced. Furthermore, even when an arbitrarily shaped object with arbitrary material constants is put in the region where the observation points distribute, the object does not influence the scattering field because the total field in the area is minimised.

In this study, we explore such a distribution of Ω_2 by the level-set method [4, 5], which involves the topological derivative [6, 7]. Our method [4] is an extension of [5] and uses B-spline surface as the level-set function, which enables us to reduce the number of design variables considerably. We will present at the oral presentation the explicit representation of the topological derivative for our cost function and the detailed algorithm of our level-set method.

4 Numerical examples

We here present an example of optimised cloaking device. In this numerical example, we set the fixed design domain as $D = [0, 60]^2$ in which four circular dielectric material (relative permittivity: $\varepsilon_2 = 2$) of radius eight are allocated at regular interval. We use $N_1 = 360$ directions to evaluate the scattering amplitude and put $N_2 = 151 \times 151$ observation points in $[25.5, 34.5]^2$. With these settings, we minimised the cost function J (with $w_1 = 0.1$ and $w_2 = 1.0$) for the incident plane wave of angular frequency $\omega = 0.7$ propagating along x_1 direction. In the optimisation, 31×31 B-spline functions are used to express the level-set function, and the topological derivative is evaluated by the boundary element method.

Figure 1 shows the topology optimised cloaking device as well as the corresponding magnetic field. Not only the scattered field but also the total field in the dashed rectangle is reduced. One can put any material in the dashed rectangle without disturbing the scattered field. This means that the designed cloak can make arbitrary objects invisible.

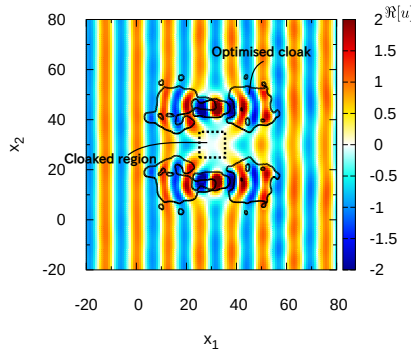


Figure 1: Topology optimised cloaking device (Solid line). The real part of the corresponding magnetic field is also plotted.

5 Concluding remarks

In this study, we have proposed a new formulation for cloaking design which can make arbitrary objects invisible.

References

- [1] J. Andkjær and O. Sigmund, *Applied Physics Letters*, **98**(2) (2011), pp. 021112.
- [2] G. Fujii, H. Watanabe, T. Yamada, T. Ueta and M. Mizuno, *Applied Physics Letters*, **102**(25) (2013), pp. 251106.
- [3] K. Nakamoto, H. Isakari, T. Takahashi and T. Matsumoto, *arXiv preprint*, (2016), arXiv:1611.08072.
- [4] H. Isakari, T. Takahashi and T. Matsumoto, *Transactions of the Japan Society for Computational Methods in Engineering*, **17** (2017), pp. 125–130.
- [5] S. Amstutz, and H. André, *Journal of Computational Physics*, **216**(2) (2006), pp. 573–588.
- [6] J. Sokolowski and A. Zochowski, *SIAM journal on control and optimization*, **37**(4) (1999), pp. 1251–1272.
- [7] M. Bonnet and B. Guzina, *International Journal for numerical methods in engineering*, **61**(13) (2004), pp. 2344–2373.

Topological optimization of periodic materials to enhance anisotropic dispersive effects

Cédric Bellis¹, Rémi Cornaggia^{1,*}, Bruno Lombard¹

¹Laboratoire de mécanique et d'acoustique, UMR 7031 AMU - CNRS - Centrale Marseille, France

*Email: cornaggia@lma.cnrs-mrs.fr

Abstract In the context of waves in periodic media, we propose an iterative algorithm that determines an optimal material distribution to reach target effective dispersive properties. It relies on an homogenized model of this medium, an update procedure based on the topological derivative concept, and on an efficient FFT-accelerated method to solve cell problems.

Keywords: Topological optimization, homogenization, dispersion

Introduction We are interested in standing waves in unbounded two-dimensional domains filled with a periodic medium, *e.g.* antiplane elastic shear waves. The material is made of cells $Y_\ell = \ell Y$, where Y is the reference unit cell and ℓ the characteristic periodicity length (Fig. 1). At circular frequency ω , the wave amplitude u_ℓ obeys the equation:

$$\nabla \cdot (\mu_\ell \nabla u_\ell) + \rho_\ell \omega^2 u_\ell = 0, \quad (1)$$

where μ_ℓ and ρ_ℓ are the Y_ℓ -periodic shear modulus and density of the medium.

In the long wavelength regime ($\lambda > \ell$), the motion can be described approximatively by the superposition of a slowly varying mean field U and higher-order (in $\varepsilon = \ell/\lambda$) oscillating correctors. Given an effective (homogenized) model satisfied by U , the effective dispersion of the medium is characterized by the variations of the phase velocity $c(k, \mathbf{d}) = \omega(k, \mathbf{d})/k$ of a plane wave $U(\mathbf{x}) = \exp(i\mathbf{k}\mathbf{d} \cdot \mathbf{x})$ when the wavenumber k and direction \mathbf{d} vary. Here we adopt the following direction-dependent dispersion indicator:

$$\gamma(\mathbf{d}) := \left. \frac{\partial^2 c^2(k, \mathbf{d})}{\partial k^2} \right|_{k=0}. \quad (2)$$

In this work, the goal is to optimize the material distribution within the unit cell Y to reach some target effective dispersive properties, in particular to maximize their anisotropy. The proposed method relies on four main components: a second-order homogenized effective model, the topological derivatives of the model's coefficients, an iterative topological optimization algorithm for the unit cell, and an efficient

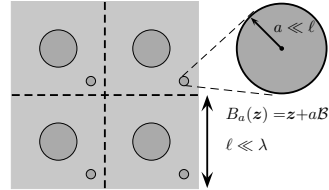


Figure 1: Periodic material and small phase change

fixed-point FFT method to evaluate these topological derivatives at each iteration. These components are now described in more details.

Second-order homogenized model The two-scale asymptotic homogenization method [1,3] is a popular way to derive an effective model from the equation (1). One obtains a fourth-order wave equation for the mean field U :

$$\begin{aligned} \mu^0 : \nabla^2 U + \omega^2 \varrho^0 U \\ + \ell^2 [\mu^2 :: \nabla^4 U + \omega^2 \varrho^2 : \nabla^2 U] = 0, \end{aligned} \quad (3)$$

where $(\mu^0, \varrho^0, \mu^2, \varrho^2)$ are constant tensors computed by solving cell problems over Y [3], “:” and “::” indicate inner products between second- and fourth-order tensors, and $\nabla^j = \nabla(\nabla^{j-1})$. Moreover, this model coincides with the one obtained by the Bloch-Floquet wave method (see [1, Sect. 3] for the case $\rho_\ell = 1$). The dispersion indicator γ defined by (2) is then simply given by:

$$\gamma(\mathbf{d}) = 2\ell^2 \left[\frac{\varrho^2 \otimes \mu^0 - \varrho^0 \mu^2}{(\varrho^0)^2} \right] :: (\mathbf{d} \otimes \mathbf{d} \otimes \mathbf{d} \otimes \mathbf{d}). \quad (4)$$

Topological optimization of the unit cell

To reach a target dispersive behavior, one first defines a cost functional to be minimized, *e.g.*

$$J(Y; \mathbf{d}_1, \mathbf{d}_2, \dots, \mathbf{d}_{N_d}) = \frac{1}{2} \left(\sum_{j=1}^{N_d} w_j [\gamma(\mathbf{d}_j)]^{\alpha_j} \right), \quad (5)$$

where each exponent α_j is fixed to 2 (resp -2) to minimize (resp. maximize) the dispersion in direction \mathbf{d}_j and the positive constants w_j are user-defined weights that balance the contribution of each term in the cost functional. This cost functional depends on the cell Y implicitly through the homogenized coefficients that intervene in the expression (4) of γ .

An iterative topological optimization algorithm, already used in microstructural optimization of static properties [2], is then adapted to the present situation. We restrain ourselves to two-phase cells, which are described thanks to a level-set function ψ . At each iteration, the update of this function is based on the concept of topological sensitivity (TS) of the cost functional to an infinitesimal phase change at point \mathbf{z} , supported by a small disc B_a of size $a \ll \ell$, as depicted in Figure 1. This TS, denoted $\mathcal{D}J$, is the leading-order coefficient of the following expansion of the perturbed cost functional J_a :

$$J_a = J + (a/\ell)^2 \mathcal{D}J(\mathbf{z}) + o((a/\ell)^2).$$

The negative minima of the map $\mathbf{z} \mapsto \mathcal{D}J(\mathbf{z})$ thus indicates the locations in Y where a small phase change would decrease J the most. Following [2], the level-set update $\psi_n \rightarrow \psi_{n+1}$ is done by partial projections of ψ_n onto the TS $\mathcal{D}J$. The algorithm stops when the optimality condition $\mathcal{D}J > 0$ is reached, indicating a local minimum of J .

Computational considerations At each iteration, the TS $\mathcal{D}J$ is computed by simple algebraic combinations of the TSs of the four coefficients $(\mu^0, \varrho^0, \mu^2, \varrho^2)$ whose evaluation requires the resolution of 12 direct and adjoint scalar potential problems on the current material configuration of the cell Y , as specified in [3].

To solve these problems, we adopted the FFT-accelerated algorithm proposed by Moulinec and Suquet in the 90's (see *e.g.* the introduction of [4]), that permits (i) a meshless representation of the unit cell as an image, (ii) a very simple implementation of the whole procedure and (iii) good computational performances.

An example of microstructure obtained with the proposed procedure is presented in Fig. 2. We also note that a similar study is conducted in [1], using the shape derivative of the homogenized coefficients rather than their topological derivative to update the level-set.

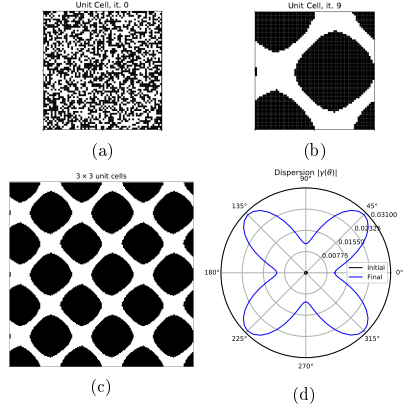


Figure 2: Microstructure optimization to maximize the dispersion in the directions $\theta = \pm\pi/4$ and minimize it in the directions $\theta = 0, \pi/2$ ($N_d = 4$ in the definition (5) of J). The unit cell is discretized into 128×128 pixels and initialized with a random distribution of materials 1 (white pixels) and 2 (black pixels). The material ratios are $\mu_2/\mu_1 = 6$ and $\rho_2/\rho_1 = 1.5$. The optimality condition was reached after 9 iterations. (a) Initial unit cell, (b) final unit cell, (c) resulting microstructure (3×3 unit cells) and (d) final dispersion indicator γ .

References

- [1] G. Allaire and T. Yamada. Optimization of dispersive coefficients in the homogenization of the wave equation in periodic structures. *Numerische Mathematik*, 2018.
- [2] S. Amstutz, S. M. Giusti, A. A. Novotny, and E. A. de Souza Neto. Topological derivative for multi-scale linear elasticity models applied to the synthesis of microstructures. *Int. J. Numer. Methods Eng.*, 2010.
- [3] M. Bonnet, R. Cornaggia, and B. Guzina. Microstructural topological sensitivities of the second-order macroscopic model for waves in periodic media. *SIAP*, 2018.
- [4] H. Moulinec, P. Suquet, and G. W. Milton. Convergence of iterative methods based on Neumann series for composite materials: Theory and practice. *Int. J. Numer. Methods Eng.*, 2018.

Efficiently optimizing inclusion rotation angle for maximal power flow

Boaz Blankrot^{1,*}, Clemens Heitzinger¹¹Institute of Analysis and Scientific Computing, TU Wien, Austria

*Email: boaz.blankrot@tuwien.ac.at

Abstract

We present an efficient method for optimizing the rotation angles of a collection of objects for maximal time-averaged electromagnetic power flow in a specified direction. This method combines a reduced-order model and multiple-scattering approach for computing the electromagnetic field with adjoint state optimization, and achieves fast and accurate results. We demonstrate our method with a numerical example that shows a dramatic increase in power flow.

Keywords: Electromagnetic scattering, Optimization, Photonics

1 Introduction

Significant research effort has been expended in recent years for the analysis, design, and optimization of dielectric optical nanostructures, as the span of their potential uses continues to grow [1]. A common subclass of these nanostructures contains devices consisting of many repetitions of a dielectric subwavelength building block which is parametrized in some way, be it by radius, height, or rotation angle, where the overall structure has unique light manipulation capacities. Researchers would benefit from the ability to choose these parameters, given arbitrary desired electromagnetic properties, in an efficient and automated way. In this work, we focus on power flow maximization, where the design parameters are the rotation angles of a set of otherwise identical inclusions, building upon our field intensity optimization approach in [2]. With this approach, the single repeated inclusion is discretized, after which all inclusions are replaced with multipole expansions that have coefficients β (see also [3]). These coefficients give rise to a multiple-scattering formalism which is both easy to solve and differentiable with respect to the rotation angles φ .

2 Formulation

We assume an arbitrary layout of smooth two-dimensional inclusions that are identical up to rotation with relative permittivity ε_r , a trans-

verse magnetic incident plane wave with wavelength λ that is represented by the multipole coefficients α , and use the multiple-scattering formulation to arrive at our system of equations

$$(\mathbf{I} - \mathbf{XT})\beta = \mathbf{X}\alpha, \quad (1)$$

where \mathbf{X} is a block diagonal scattering matrix that depends on the shape and rotation angle of each inclusion, and \mathbf{T} is a translation matrix that depends on the distances between the inclusions. The residual of this system is denoted by \mathbf{c} . Our goal is to maximize the time-averaged power flowing through a curve strictly outside the inclusions, as given by

$$P = \frac{1}{2} \Re \int (\mathbf{E} \times \mathbf{H}^*) \cdot \hat{\mathbf{n}} \, dl. \quad (2)$$

As the multipole expansion yields the representation $E_z(\mathbf{r}) = \mathbf{e}_z(\mathbf{r}) \cdot \beta$, and similar representations for H_x, H_y , we can find the derivatives of the power with respect to these coefficients, $\partial P / \partial \beta$. We can now construct the gradient g for our optimization problem using the adjoint state method. For a complex vector ζ , we define the Lagrangian

$$\Lambda = -P + 2\Re(\zeta^\top \mathbf{c}), \quad (3)$$

whose total derivative with respect to one of the rotation angles φ_i is

$$\begin{aligned} \frac{d\Lambda}{d\varphi_i} = & 2\Re \left(\left[\zeta^\top (\mathbf{I} - \mathbf{XT}) - \frac{\partial P}{\partial \beta} \right] \frac{\partial \beta}{\partial \varphi_i} \right) \\ & - 2\Re \left(\zeta^\top \frac{\partial \mathbf{X}}{\partial \varphi_i} \mathbf{X}^{-1} \beta \right). \end{aligned} \quad (4)$$

Solving the adjoint system of equations in the square brackets for ζ , which does not depend on i , means that the right-hand side of Eq. (4) can be computed for all values of i with a single system solution. On the other hand, since we are solving for $\mathbf{c} = 0$, we know that the total derivatives of Λ and $-P$ are equal. Finally, the derivatives of the scattering matrix are readily available by a multiplication of sparse and diagonal matrices. Thus both P and its gradient can be computed with the runtime complexity of 2 system solutions, which in our case are accelerated with the Fast Multipole Method.

3 Numerical results

We apply our approach to a collection of 38 rounded stars with diameter $0.6\lambda_0$ and $\varepsilon_r = 9$ that are arranged on a triangular lattice. Fig. 1(a) depicts the initial structure with rotation angle $\varphi = 0$ for each inclusion, as well as the electric field amplitude in its vicinity in response to an incident unit plane wave. This structure completely blocks the plane wave from propagating to the right. We ran our optimization procedure with the objective of maximizing the right-propagating power flow on the dotted line shown in Fig. 1. The optimized structure is presented in Fig. 1(b), where the electric field amplitude along the dotted line is substantially larger. The rotation angles do not adhere to any obvious pattern and are vertically asymmetric.

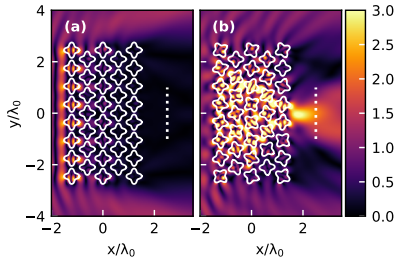


Figure 1: Electric field amplitude (a) before and (b) after the optimization process. The dotted line indicates the 50 points where power flow was maximized.

The optimization process converged with the criterion $\Delta P < 10^{-5}$ in 149 seconds and 112 iterations, and is shown in detail in Fig. 2, where P_0 denotes the power flow without the structure and $\|g\|_\infty$ is the infinity norm of the gradient. In particular, the normalized power P/P_0 increased from 9.3×10^{-3} to 2.57.

Finally, we investigate the dependence of the transmitted power on the wavelength of the incident plane wave in Fig. 3. The power flow exhibits a sharp peak at the design frequency λ_0 which rapidly drops off below P_0 , with a full width at half maximum of $0.01\lambda_0$. This is unsurprising, as we only optimized the rotation angles for a single frequency.

The code for our approach is available in the open-source Julia package ParticleScattering [4].

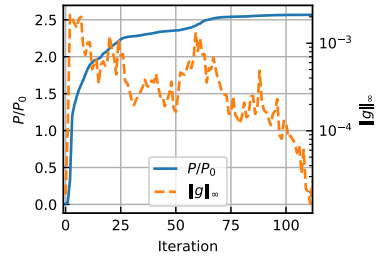


Figure 2: Convergence of the normalized power and the gradient norm.

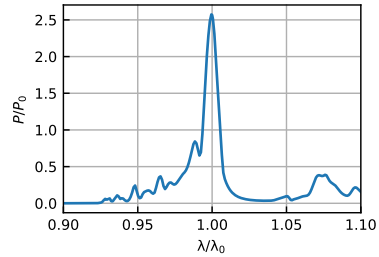


Figure 3: Right-propagating power vs. wavelength for the optimized device.

References

- [1] I. Staude and J. Schilling, Metamaterial-inspired silicon nanophotonics, *Nature Photonics* **11** (2017), pp. 274–284.
- [2] B. Blankrot and C. Heitzinger, Efficient computational design and optimization of dielectric metamaterial devices, *Submitted for publication*, pp. 1–16. Preprint at <http://arxiv.org/abs/1804.09489>
- [3] J. Lai, M. Kobayashi and A. Barnett, A fast and robust solver for the scattering from a layered periodic structure containing multi-particle inclusions, *Journal of Computational Physics* **298** (2015), pp. 194–208
- [4] B. Blankrot and C. Heitzinger, ParticleScattering: Solving and optimizing multiple-scattering problems in Julia, *Journal of Open Source Software* **3**(25) (2018), 691.

Guided modes in a hexagonal periodic graph like domain : the zigzag and the armchair cases

Berangère Delourme^{1,*}, Sonia Fliss²

¹LAGA (UMR 7539), Université Paris 13, Villetaneuse, France

²POEMS (CNRS-INRIA-ENSTA Paristech), Palaiseau, France

*Email: delourme@math.univ-paris13.fr

Abstract

In this work, we study the wave propagation in hexagonal periodic media that are close to a graph domain. By using an asymptotic analysis, we exhibit situations where the introduction of lineic defects into the geometry of the domain leads to the appearance of guided modes and we show that the direction of the defect leads to very different properties of the guided modes.

Keywords: honeycomb structure, periodic media, spectral theory, guided modes.

1 Introduction

Let us first consider a hexagonal periodic medium Ω_ε that consists of the plane \mathbb{R}^2 minus an infinite set of equi-spaced hexagonal perfect conductor obstacles. The distance between each obstacle is supposed to be small and is denoted ε (see in Figure 1 where Ω_ε lies in the grey region). Let $(\mathbf{e}_1, \mathbf{e}_2)$ be the two directions of periodicity of Ω_ε represented in Figure 1 (without loss of generality, we suppose that the period is 1 along these directions).

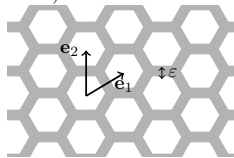


Figure 1: The hexagonal periodic medium Ω_ε

Then we introduce two types of unbounded lineic defects, the zigzag one and the armchair one, by changing the distance between two obstacles from each side of a broken line having respectively a zigzag form or an armchair one. More precisely, the lineic defect is in the vertical direction $\mathbf{v}^z = \mathbf{e}_2$ for the zigzag case and in the horizontal direction $\mathbf{v}^a = 2\mathbf{e}_1 - \mathbf{e}_2$ for the armchair case (see Figure 2). The corresponding domains are denoted respectively $\Omega_{\varepsilon,\mu}^z$ and $\Omega_{\varepsilon,\mu}^a$. Each domain $\Omega_{\varepsilon,\mu}^j$ is periodic in the direction \mathbf{v}^j , we denote $\widehat{\Omega}_{\varepsilon,\mu}^j$ one of its period. We are inter-

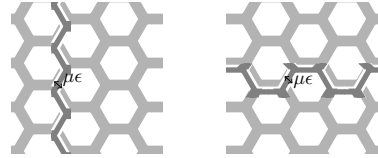


Figure 2: Two types of lineic defect: the zigzag and the armchair cases

ested in the existence of guided modes, that is to say solutions of the homogeneous wave equation propagating along the defect. In other words, for a fixed wavenumber $\beta \in \mathbb{R}$, we look for couples $(u_\varepsilon^j(\beta), \lambda_\varepsilon^j(\beta)) \in H_{\text{loc}}^1(\Omega_{\varepsilon,\mu}^j) \times \mathbb{R}^+$ satisfying for $j \in \{z, a\}$

$$\begin{cases} -\Delta u_{\varepsilon,\mu}^j = \lambda_{\varepsilon,\mu}^j u_{\varepsilon,\mu}^j, & \text{in } \Omega_{\varepsilon,\mu}^j \\ \partial_n u_{\varepsilon,\mu}^j = 0 & \text{on } \partial\Omega_{\varepsilon,\mu}^j \end{cases} \quad (1)$$

such that $u_{\varepsilon,\mu}^j|_{\widehat{\Omega}_{\varepsilon,\mu}^j} \in H^1(\widehat{\Omega}_{\varepsilon,\mu}^j)$ and

$$\forall \mathbf{x} \in \Omega_{\varepsilon,\mu}^j, \quad u_{\varepsilon,\mu}^j(\mathbf{x} + \mathbf{v}_j) = e^{2i\pi\beta} u_{\varepsilon,\mu}^j(\mathbf{x}). \quad (2)$$

This problem can be rewritten as an eigenvalue problem for a self-adjoint operator $A_{\varepsilon,\mu}^j(\beta)$ in $L^2(\widehat{\Omega}_{\varepsilon,\mu}^j)$. We want, in this work, to exhibit conditions on the perturbations which ensure existence of guided modes and we want to point out the differences between the zigzag and the armchair cases. Remark that we have performed a similar study for square lattices with a lineic perturbation [1]. The condition on the perturbation was simple: if $\mu \in (0, 1)$, for ε small enough, there exist guided modes for any β .

2 Methodology

Inspired by previous works on square lattices [1], we analyse the spectral problem and more generally the spectrum of the operator $A_{\varepsilon,\mu}^j(\beta)$ by using a standard approach of asymptotic analysis. We first identify the formal limit of the eigenvalue problem as the distance between the obstacles tends to 0. It corresponds to an eigenvalue problem for a second order differential operator defined along an hexagonal graph, obtained by taking the geometrical limit of the domain $\Omega_{\varepsilon,\mu}^j$ when the thickness tends to 0. The

differential operator $\mathcal{A}_{\varepsilon,\mu}^j(\beta)$ is the laplacian on each edge defined for continuous, β -quasi periodic (in the direction \mathbf{v}^j) functions satisfying the so-called Kirchhoff conditions at each vertex of the graph. The spectrum of this operator can be characterized explicitly. Finally, we show that the spectrum of the operator $A_{\varepsilon,\mu}^j(\beta)$ approaches in some sense the spectrum of the operator $\mathcal{A}_{\varepsilon,\mu}^j(\beta)$ as ε is small enough (see e.g. [2]).

3 Spectrum of the operators $A_{\varepsilon,\mu}^j(\beta)$

Before studying the discrete spectrum of the operators $A_{\varepsilon,\mu}^j(\beta)$, let us describe their essential spectrum. Using the Weyl’s theorem, we know that they are linked to the essential spectrum $\sigma(A_\varepsilon)$ of the unperturbed operator $A_\varepsilon = -\Delta$, $D(A_\varepsilon) = \{u \in H^1(\Omega_\varepsilon), \Delta u \in L^2(\Omega_\varepsilon), \partial_n u_\varepsilon = 0 \text{ on } \partial\Omega_\varepsilon\}$. Thanks to the Floquet Theory, we have

$$\sigma(A_\varepsilon) = \bigcup_{\mathbf{k} \in \mathbb{R}^2} \bigcup_{n \in \mathbb{N}} \mu_{\varepsilon,n}(\mathbf{k})$$

where $(\mu_{\varepsilon,n}(\mathbf{k}))_n$ is the increasing sequence of the eigenvalues of $A_\varepsilon(\mathbf{k}) = -\Delta$, $D(A_\varepsilon(\mathbf{k})) = \{u \in H^1(\Omega_\varepsilon), \Delta u \in L^2(\Omega_\varepsilon), \partial_n u_\varepsilon = 0 \text{ on } \partial\Omega_\varepsilon, u(\mathbf{x} + \mathbf{e}_j) = e^{i\mathbf{k} \cdot \mathbf{e}_j} u(\mathbf{x})\}$. Of course, the Floquet variable \mathbf{k} can be considered in the Brillouin zone, which is here also a hexagon defined thanks to the dual basis $(\mathbf{e}_1^*, \mathbf{e}_2^*)$ of $(\mathbf{e}_1, \mathbf{e}_2)$ (defined by $\mathbf{e}_i \cdot \mathbf{e}_j^* = 2\pi\delta_{ij}$). By using the same asymptotic approach than the one described in the previous section but adapted to the operator A_ε , we can show that, as in e.g. [3], because of the symmetry and the invariance by $2\pi/3$ -rotation, for ε small enough the spectrum of A_ε contains Dirac points in the Brillouin zone, i.e conical intersections between two dispersion surfaces (see a numerical computation of the spectrum in Figure 3).

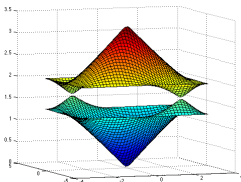


Figure 3: Dirac Points in the spectrum of A_ε . More precisely for $k^* = (-1/3, 1/3)$, let $\mu^* = \mu_{\varepsilon,0}(k^*)$, we have

$$\begin{cases} \mu_{\varepsilon,0}(\pm k^* + \eta) = \mu^* - \alpha_\varepsilon \|\eta\| + O_\varepsilon(\|\eta\|^2) \\ \mu_{\varepsilon,1}(\pm k^* + \eta) = \mu^* + \alpha_\varepsilon \|\eta\| + O_\varepsilon(\|\eta\|^2) \end{cases}$$

These Dirac points are one of the specificity of hexagonal or honeycomb structures (they do not appear in square lattices for instance) responsible for particular phenomena. We want in this work to point out one of them.

Finally, we have that for the zigzag case

$$\sigma_{\text{ess}}(A_{\varepsilon,\mu}^z(\beta)) = \bigcup_{k_1 \in \mathbb{R}} \bigcup_{n \in \mathbb{N}} \mu_n(k_1, \beta)$$

the Dirac Point being in $\sigma_{\text{ess}}(A_{\varepsilon,\mu}^z(\beta))$ for $\beta = \pm 1/3$ and for the armchair case

$$\sigma_{\text{ess}}(A_{\varepsilon,\mu}^a(\beta)) = \bigcup_{2k_1 - k_2 = \beta} \bigcup_{n \in \mathbb{N}} \mu_n(k_1, k_2)$$

the Dirac Point being in $\sigma_{\text{ess}}(A_{\varepsilon,\mu}^a(\beta))$ for $\beta = 0$. Besides, still using the asymptotic analysis, we can show the following result.

Theorem 1 *For any $\mu \neq 1$, for ε small enough, there exists $\delta > 0$ such that for all $\beta \in (-1/3 + \delta, 1/3 - \delta)$, $A_{\varepsilon,\mu}^z(\beta)$ has an eigenvalue $\lambda_{\varepsilon,\mu}^z(\beta) = \mu^* + O(\varepsilon)$.*

In other words, guided modes arise for any periodic lineic perturbation of zigzag type, this corresponds in a certain sense to a robustness result. Moreover, these guided modes have almost zero-group velocity. For the armchair case, this result does not hold : we can show that the existence of guided modes is extremely dependent on μ and β . The influence of the Dirac points on that phenomena is under investigation. We want also to study the existence of guided modes in such structure when the symmetry or the invariance by rotation is broken. We will illustrate all the theoretical results by numerical simulations.

References

- [1] DELOURME, B., FLISS, S., JOLY, P., & VASILEVSKAYA, E., *Trapped modes in thin and infinite ladder like domains. Part 1: existence results*. Asymptotic Analysis, 103(3), 103-134, 2017.
- [2] POST O., *Spectral convergence of quasi-one-dimensional spaces*. Ann. Henri Poincaré/e, 7(5) :933– 973, 2006
- [3] LEE-THORP, J. P., WEINSTEIN, M. I. AND ZHU, Y., *Elliptic operators with honeycomb symmetry: Dirac points, Edge States and Applications to Photonic Graphene*. Archive for Rational Mechanics and Analysis, 232(1), 1-63, 2019.

Reconstruction of a Local Perturbation in Inhomogeneous Periodic Layers

Alexander Kirsch ^{1,*}

¹Center for Industrial Mathematics, University of Bremen, Bremen, Germany

*Email: alexk@uni-bremen.de

Abstract

We consider the scattering problem for an inhomogeneous periodic layer in \mathbb{R}^d , $d = 2, 3$, which is locally perturbed by some bounded defect. We formulate the corresponding variational problem on an unbounded domain and show the equivalence of this problem to a family of quasiperiodic problems on a bounded domain. This allows us to prove unique existence of the scattered wave using only a classical condition for the uniqueness like local absorption of the refractive index and to introduce a numerical method to approximate the solution.

Hereafter, we address the inverse scattering problem to reconstruct the perturbation by analyzing the near field operator, proving the uniqueness of the reconstruction and applying the Newton-method for numerical examples. Moreover, we define a carefully designed far field operator for our setting and formulate the Factorization method to reconstruct the shape of the perturbation.

Keywords: non-periodic wave scattering, inverse scattering problem, numerical approximation, Bloch-Floquet transform

1 Introduction

The growing industrial interest for micro or nano-structured materials and the resulting challenge to construct an automated non-destructing testing method for the structures is one of the fundamental motivations to study perturbed periodic scattering problems. For a first study, we will consider a simplified physical model of electromagnetic scattering in TE mode. To fix the notation, we define for $R \geq 0$ the sets

$$\begin{aligned} \Omega^R &:= \mathbb{R}^{d-1} \times (0, R), & \Gamma^R &:= \mathbb{R}^{d-1} \times \{R\}, \\ \Gamma_0^R &:= (-\pi, \pi)^{d-1} \times \{R\}, & I &:= (-1/2, 1/2)^{d-1}. \end{aligned}$$

2 Direct problem

Suppose $n_p^2 \in L^\infty(\mathbb{R}_+^d)$, $d = 2, 3$, is an 2π -periodic refractive index in $\underline{x} := (x_1, \dots, x_{d-1})$, which satisfies $n_p^2 = 1$ for $x_d > R_0 > 0$ and characterizes the unperturbed scattering layer.

To simplify the notation, we assume that the local perturbation $q \in L^\infty(\mathbb{R}_+^d)$ has the support in $\Omega_0^{R_0}$, where $\Omega_0^{R_0} := (-\pi, \pi)^{d-1} \times (0, R)$ for $R > 0$, such that we consider the perturbed refractive index $n^2 := n_p^2 + q$. The scattering problem is to find the scattered field $u \in H_{0,loc}^1(\mathbb{R}_+^d) \cap H^1(\Omega^R)$ for every $R > R_0$, such that

$$\Delta u + k^2 n^2 u = -f \text{ in } \mathbb{R}_+^d, \quad u = 0 \text{ on } \Gamma^0, \quad (1)$$

for some right hand side $f \in L^2(\Omega^{R_0})$. Moreover, the scattering field is assumed to satisfy the so-called angular spectrum representation. As a consequence, we can define the exterior Dirichlet-to-Neumann map T , which is a bounded linear operator from $H^{1/2}(\Gamma^R)$ to $H^{-1/2}(\Gamma^R)$. We call the space of $H^1(\Omega^R)$ -functions with vanishing trace on Γ^0 as $\tilde{H}^1(\Omega^R)$ and consider an arbitrary function $f \in L^2(\Omega^R)$, thus, the variational formulation is to

Find a function $u \in \tilde{H}^1(\Omega^R)$, such that

$$\begin{aligned} \int_{\Omega^R} \nabla u \cdot \nabla \bar{v} - k^2 n^2 u \bar{v} \, dx \\ - \int_{\Gamma^R} T(u|_{\Gamma^R}) \bar{v} \, dS = \int_{\Omega^R} f \bar{v} \, dx \end{aligned}$$

for all $v \in \tilde{H}^1(\Omega^R)$. Since for real wave numbers k and for a real refractive index some surface waves can exist, we assume that the set $\{\text{Im } n_p^2 > 0\}$ is not empty.

Theorem 1 For $\text{Im } n_p^2 \geq 0$ and $\text{Im } q \geq 0$ and if there is an open ball contained in $\{\text{Im } n_p^2 > 0\}$, then the variational problem has a unique solution for every right hand side $f \in L^2(\Omega^R)$.

3 Inverse problem

The next step is to analyze the inverse scattering problem to reconstruct the local perturbation. For that, we consider the following measurement operator \mathcal{S} .

Definition 2 Let $\Lambda_q : L^2(\Omega^{R_0}) \rightarrow \tilde{H}^1(\Omega_0^R)$ be the solution operator for some $q \in Q := \mathcal{D}(\mathcal{S})$ and let $\gamma_{\Gamma_0^R} : \tilde{H}^1(\Omega^R) \rightarrow H^{1/2}(\Gamma_0^R)$ be the trace

operator restricted to Γ_0^R . We define the measurement operator

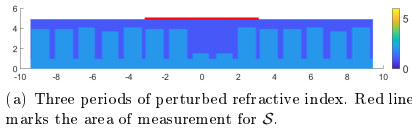
$$\mathcal{S} : Q \rightarrow \mathcal{L}(L^2(\Omega_0^{R_0}), L^2(\Gamma_0^R)), \quad q \mapsto \gamma_{\Gamma_0^R} \circ \Lambda_q,$$

which only measures the scattered field on one periodic cell of the upper boundary.

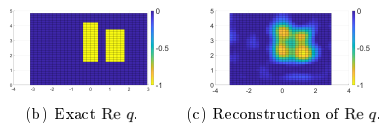
We show injectivity of \mathcal{S} by utilizing the complex geometrical optics.

Theorem 3 Consider for $d = 3$ two perturbations q_1 and $q_2 \in Q \cap C^2(\mathbb{R}_+^3)$ with compact support in \mathbb{R}_+^3 , and assume $n_p^2 \in C_p^2(\Omega_0^R)$. If we call the solution operator $\Lambda_q : L^2(\Omega_0^{R_0}) \rightarrow \tilde{H}^1(\Omega^R)$ for $q \in Q$, and define $\tilde{\mathcal{S}} : Q \rightarrow \mathcal{L}(L^2(\Omega^{R_0}), L^2(\Gamma^R))$, $q \mapsto \gamma_{\Gamma^R} \circ \Lambda_q$, where γ_{Γ^R} is the trace operator, then it holds: If $\tilde{\mathcal{S}}(q_1) = \tilde{\mathcal{S}}(q_2)$, then $q_1 = q_2$.

In the following, we will reconstruct the perturbation by CG-REGINN. For that, we prove differentiability and ill-posedness of the measurement operator \mathcal{S} . We discretize $L^2(\Omega_0^{R_0})$ in $2 \times N_f = 32$ right hand sides and add 1.1% additive relative noise to the traces of the approximated solutions vector $\mathbf{w}|_{\Gamma_0^R}$, i.e., the measurement is given by $\mathbf{v}^\varepsilon = (\mathbf{w} + \mathbf{c})|_{\Gamma_0^R}$, where $\|\mathbf{c}|_{\Gamma_0^R}\|_{L^2(\Gamma_0^R)}^{2N_f} = 0.011 \times \|\mathbf{w}|_{\Gamma_0^R}\|_{L^2(\Gamma_0^R)}^{2N_f}$.



(a) Three periods of perturbed refractive index. Red line marks the area of measurement for \mathcal{S} .



(b) Exact $\text{Re } q$. (c) Reconstruction of $\text{Re } q$.

Figure 1: Result for 1.1% noise and $k^2 = 3$.

4 Factorization method

Now we drop the homogeneous boundary condition and consider the two dimensional scattering problem

$$\Delta u^s + k^2(n_p^2 + q)u^s = -f \quad \text{in } \Omega^R, \quad (2a)$$

$$\frac{\partial}{\partial x_2} u^s = T^{\pm R} u^s \quad \text{on } \Gamma^{\pm R}, \quad (2b)$$

where Ω^R is redefined as $\Omega^R := \mathbb{R} \times (-R, R)$ and analogously Ω_0^R . The analysis of the forward problem is easily extendable to the setting of free space scattering problem. Fix some small $\eta > 0$ and consider the plane waves $u^{\text{inc}}(x, d) = e^{-ikd \cdot x}$ with some $d \in S$, where

$$S := \{d \in \mathbb{R} \times \mathbb{C} : d \cdot d = 1, |\text{Im } d_2| \leq \eta\}.$$

Set α as a function by defining $\alpha(d) := kd_1$ and let $\tilde{u}_{\text{qp}}^s(\cdot, d) + u^{\text{inc}}(\cdot, d)$ be the α -quasiperiodic total field $\tilde{u}_{\text{qp}}^s(\cdot, d)$ solving the scattering problem $\Delta \tilde{u}_{\text{qp}}^s(\cdot, d) + k^2 n_p^2 \tilde{u}_{\text{qp}}^s(\cdot, d) = 0$ in \mathbb{R}^2 .

Definition 4 We set the notation $\tilde{u}^s(\underline{x}, \pm R, d')$ $\mathcal{J}u^s(\alpha(d'), \underline{x}, \pm R)$, where \mathcal{J} is the Bloch-Floquet transform, and define the far field $u^\infty \in L^2(S)$ of the solution u^s by

$$u^\infty(d') := \left[\int_{\Gamma_0^R} - \int_{\Gamma_0^R} \right] \frac{\partial \tilde{u}^s}{\partial x_2}(\cdot, -d') u^{\text{inc}}(\cdot, d') - \tilde{u}^s(\cdot, -d') \frac{\partial u^{\text{inc}}(\cdot, d')}{\partial x_2} dS.$$

Define the far field operator $F : L^2(S) \rightarrow L^2(S)$, $Fg(d') := \int_S u^\infty(d, d')g(d) dS(d)$, where $u^\infty(d, \cdot)$ is the far field of the solution $u^s(\cdot, d)$ for $f = k^2 q \tilde{u}_{\text{qp}}^s(\cdot, d)$.

Theorem 5 Under some assumptions the operator $F_{\#} := |(\text{Re } F)| + (\text{Im } F) : L^2(S) \rightarrow L^2(S)$ is strictly positive and it holds for $z \in \mathbb{R}^2$

$$z \in \text{supp}(q) \Leftrightarrow \phi_z^\infty \in \mathcal{R}(F_{\#}^{1/2}),$$

where ϕ_z^∞ is the far field of the fundamental solution for (2) with right hand side $f = \delta_z$.

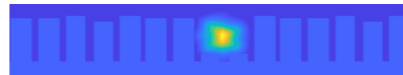


Figure 2: Result of FMM (1% rel. noise, $k^2 = 3$).

References

- [1] H. Haddar and A. Kanschin, *Factorization Method for Imaging a Local Perturbation in Inhomogeneous Periodic Layers from Far Field Measurements*, submitted (2019).
- [2] A. Kanschin and A. Lechleiter, *Reconstruction of a Local Perturbation in Inhomogeneous Periodic Layers from Partial Near Field Measurements*, Inverse Problems, <http://dx.doi.org/10.1088/1361-6420/abc166> (2019).

Modelling of acoustic waves in fluid-saturated periodic scaffolds: Bloch wave decomposition and homogenization approaches

Eduard Rohan^{1,*}, Robert Cimrman¹

¹NTIS New Technologies for Information Society, Department of mechanics, Faculty of Applied Sciences, University of West Bohemia, Pilsen, Czech Republic

*Email: rohan@kme.zcu.cz

Abstract

We consider acoustic wave propagation in periodic rigid scaffolds saturated by viscous or inviscid fluids. In a case of perfused pores, the steady flow is incompressible, while the acoustic perturbations are given by the barotropic approximation. To analyze the wave dispersion, two approaches are examined: the periodic homogenization (PH) and the Floquet-Bloch wave decomposition (FB). The PH method provides suitable approximation of the dispersion for low wave numbers, the FB method enables to capture band gap behaviour which is influenced by the scaffold geometry.

Keywords: Acoustics, periodic scaffolds, Floquet-Bloch theory, homogenization, band gaps

1 Introduction

Modelling of acoustic waves in fluid saturated porous media has been treated mostly using the homogenization theory [1], or using the phenomenological models using the theory of porous media. Here we consider waves propagating in a fluid saturating these periodic structures (scaffolds) while neglecting their compliance. To analyze wave dispersion for wave lengths comparable with the periodicity size, the Floquet-Bloch (FB) theory is employed, cf. [3]. For comparison, the lowest frequency modes are compared with the homogenization-based prediction.

Both the homogenization procedure and the Floquet-Bloch wave analysis are concerned with boundary value problems formulated in the representative pore $Y_f \subset Y \subset \mathbb{R}^3$, see Fig. 1, with $Y = \Pi_{i=1}^3]0, a_i[$, whereby on $\partial_{\#} Y_f = \partial Y_f \cap \partial Y \neq \emptyset$ periodicity conditions are prescribed for Y -periodic functions. Alternatively we consider a steady flow of the Newtonian incompressible fluid through a periodic system of scaffolds in an infinite medium; the velocity field $\bar{\mathbf{w}}$ is governed by the Navier-Stokes (N-S) equations with non-slip conditions on the pore walls $\Gamma_s = \partial Y_f \cap Y$ and assuming incompressible fluid,

$\nabla \cdot \bar{\mathbf{w}} = 0$. The acoustic waves are superimposed to the steady flow, so that the total velocity and pressure fields are $\mathbf{w} = \bar{\mathbf{w}} + \bar{\mathbf{u}}$ and $q = \bar{q} + \bar{p}$.

2 Scaffolds with inviscid static fluid

For an inviscid fluid and assuming $\bar{\mathbf{w}} = 0$, the N-S system reduces to

$$\gamma \rho_0 \frac{\partial^2 \bar{p}}{\partial t^2} = \nabla^2 \bar{p}, \quad (1)$$

with $\boldsymbol{\nu}^f \cdot \nabla \bar{p} = 0$ on Γ_s , where $\boldsymbol{\nu}^f$ denotes the unit normal vector and γ is the acoustic fluid compressibility. The FB analysis of plane waves relies on the wave decomposition (note $i^2 = -1$)

$$\begin{aligned} \bar{p}(y, t) &= p(y) e^{-i\boldsymbol{\kappa} \cdot \mathbf{y}} e^{i\omega t}, \\ \bar{\mathbf{u}}(y, t) &= \mathbf{u}(y) e^{-i\boldsymbol{\kappa} \cdot \mathbf{y}} e^{i\omega t}, \end{aligned} \quad (2)$$

where p and \mathbf{u} are Y -periodic functions, ω is the frequency, and the wave vector $\boldsymbol{\kappa} = \varkappa \mathbf{n}$ is given by the wave direction \mathbf{n} and the wave number \varkappa . This ansatz substituted in (1) leads to the eigenvalue problem: Given $\varkappa \in \mathbb{R}$, find ω_k and the Y -periodic eigenmode p^k , $k = 0, 1, \dots$ satisfying

$$\begin{aligned} -\nabla \cdot (\nabla p^k - 2i\varkappa n p^k) + \varkappa^2 p^k &= \omega_k^2 \gamma \rho_0 p \quad \text{in } Y_f \\ \boldsymbol{\nu}^f \cdot (\nabla p^k - i\varkappa n p^k) &= 0 \quad \text{on } \Gamma_s. \end{aligned} \quad (3)$$

It can be shown that $\omega_k \in \mathbb{R}$. The numerical solutions are obtained using the FE-discretization.

The periodic homogenization of the pore fluid governed by (1) considered in the frequency domain provides a modified Helmholtz equation,

$$\nabla \cdot \mathbf{A} \nabla p^0 + \frac{\omega^2}{c_f^2} \phi_f p^0 = 0, \quad (4)$$

where ϕ_f is the fluid volume fraction, $c_f = 1/\sqrt{\gamma}$ is the sound speed in the free fluid. The structural tensor $\mathbf{A} = (A_{ij})$ is computed in terms of a characteristic response of the Laplace operator in Y_f . Planar harmonic wave have no dispersion, since $\varkappa = \kappa_f \sqrt{\phi_f / \mathbf{A} : \mathbf{n} \otimes \mathbf{n}}$, where $\kappa_f = \omega / c_f$ is the free fluid wave number.

3 Viscous flow fluid in scaffolds

We assume $\bar{\mathbf{w}}$ is Y -periodic and given. The perturbed N-S system yields

$$\begin{aligned} \rho_0 \left(\frac{\partial}{\partial t} \tilde{\mathbf{u}} + \bar{\mathbf{w}} \cdot \nabla \tilde{\mathbf{u}} + \tilde{\mathbf{u}} \cdot \nabla \bar{\mathbf{w}} \right) &= \nabla \cdot \mathbb{D}e(\tilde{\mathbf{u}}) - \nabla \tilde{p}, \\ \gamma \left(\frac{\partial}{\partial t} \tilde{p} + \bar{\mathbf{w}} \cdot \nabla \tilde{p} \right) &= -\nabla \cdot \tilde{\mathbf{u}}, \end{aligned} \tag{5}$$

where tensor $\mathbb{D} = (D_{ijkl})$ with $D_{ijkl} = \eta \delta_{ij} \delta_{kl} + \mu (\delta_{ik} \delta_{jl} + \delta_{il} \delta_{jk})$ depends on the 1st and the 2nd viscosities, μ and η .

The homogenization of acoustic problem (5) leads to the extended Darcy flow model,

$$\nabla \cdot [\mathcal{K}(i\omega) \nabla p] - i\omega \gamma \phi_f p = 0,$$

in which $\mathcal{K}_{ij}(i\omega) = i\omega |Y|^{-1} \int_{Y_f} w_i^j$ is the dynamic permeability tensor, computed using the characteristic response $\mathbf{w}^j = (w_i^j)$ of the linearized N-S equation involving the incompressibility constraint and the convective acceleration given by $\bar{\mathbf{w}}$. Let us define $V_y = \{ \mathbf{v} \in \tilde{\mathbf{H}}_{\#}^1(Y_f) \mid \nabla_y \cdot \mathbf{v} = 0 \text{ in } Y_f, \mathbf{v} = \mathbf{0} \text{ on } \Gamma_s \}$, where $\tilde{\mathbf{H}}_{\#}^1(Y_f)$ is a space of Y -periodic functions. We find $\mathbf{w}^k \in V_y, k = 1, 2, 3$, satisfying

$$\begin{aligned} i\omega \int_{Y_f} \mathbf{w}^k \cdot \mathbf{v} - 2 \int_{Y_f} \bar{\mathbf{w}} \otimes \mathbf{w}^k : \mathbf{e}_y(\mathbf{v}) \\ + \bar{\nu} \int_{Y_f} \nabla_y \mathbf{w}^k : \nabla_y \mathbf{v} = -\frac{i}{\omega} \int_{Y_f} v_k, \end{aligned} \tag{6}$$

for all $\mathbf{v} \in V_y$, where $\bar{\nu} = \bar{\mu} / \rho_0$ is the kinematic viscosity. For non-vanishing $\bar{\mathbf{w}}$ the dynamic permeability is non-symmetric. For plane waves, the dispersion relationships can be computed by

$$\varkappa = \sqrt{(-i\omega \gamma \phi_f) / \mathcal{K}(i\omega) : \mathbf{n} \otimes \mathbf{n}}.$$

4 Numerical illustration and discussion

In Fig. 2, we report wave dispersion analysis computed for water-saturated porous periodic structures using the inviscid model, see Fig. 1. The eigenvalue problems were solved by the finite element method implemented in the software SfePy, see <http://sfepy.org>, using the ARPACK solver [2] through the SciPy package.

With decreasing porosity $\phi_f = |Y_f|/|Y|$ (increasing the fibres diameter) the two lowest modes separate and a band gap opens. The homogenized model provides good predictions only for very large ϕ_f , or for long waves only.

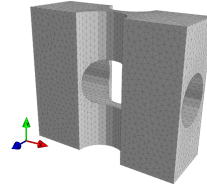


Figure 1: The fluid part Y_f of the periodic cell.

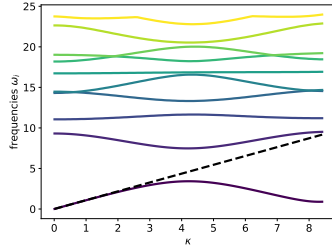


Figure 2: Dispersion curves for microstructure with fibre diameter $d = 0.23$ mm (inviscid fluid, eq. (3)). The dashed lines depict the response $\omega - \varkappa$ of the homogenized model, eq. (4).

This research was supported by project GACR 17-01618S of the Czech Scientific Foundation and by project LO 1506 of the Czech Ministry of Education, Youth and Sports.

References

- [1] D. Cioranescu, A. Damlamian, G. Griso. *The Periodic Unfolding Method: Theory and Applications to Partial Differential Problems*, Springer, 2018.
- [2] R. B. Lehoucq, D. C. Sorensen and C. Yang. *ARPACK Users Guide: Solution of Large Scale Eigenvalue Problems by Implicitly Restarted Arnoldi Methods*, SIAM, Philadelphia, PA., 1998.
- [3] M. Collet, M. Ouisse, M. Ruzzene, and M.N. Ichchou. Floquet-Bloch decomposition for the computation of dispersion of two-dimensional periodic, damped mechanical systems. *International Journal of Solids and Structures*, **48** (2011), pp. 2837–2848.

A high order numerical method for scattering from locally perturbed periodic surfaces

Ruming Zhang^{1,*}

¹Institute of Applied and Numerical mathematics, Karlsruhe Institute of Technology, Karlsruhe, Germany

*Email: ruming.zhang@kit.edu

Abstract

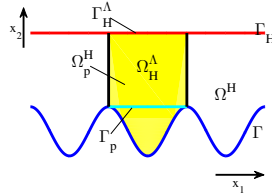
In this paper, we introduce a high order numerical method to solve the scattering problems with locally perturbed periodic surfaces in 2D spaces. For these problems, classical methods to treat quasi-periodic scattering problems no longer work, while a Bloch transform based numerical method was proposed. This numerical method converges slowly. The motivation of this paper is to improve this numerical method from the regularity results of the Bloch transform of the total field. As the set of the singularities of the total field is finite in one periodic cell, we are able to improve the numerical method by designing a proper integration contour with special conditions at the singularities. We can prove that the new numerical method converges super algebraically. This new method improves the efficiency significantly. This method could be extended to 3D cases when further conditions are satisfied.

Keywords: high order method, scattering problems, local perturbation, periodic surface, convergence rate

1 Introduction

In this paper, we propose an efficient numerical method of solving scattering problems from locally perturbed periodic surfaces with non-periodic incident fields. Different from the well-studied scattering problems with periodic background and incident fields, the classical framework no longer works. In [?], a Floquet–Bloch based numerical method was applied to solve this kind of problems. However, the convergence rate of this method is low. In this paper, the method is improved by reducing the computational complexity significantly (see [1]).

Suppose Γ is a bounded periodic surface and Γ_p is a local perturbation of Γ . In this paper, we fix the period as 2π . Let Ω (Ω_p) be the unbounded domain above Γ (Γ_p). Suppose $\Gamma_H := \mathbb{R} \times \{H\}$ be a straight line above both Γ and Γ_p , let Ω_H (Ω_p^H) be the domain between Γ



(Γ_p) and Γ_H , then the scattering problem could be modelled by the following equation:

$$\Delta u + k^2 u = 0 \quad \text{in } \Omega_p^H; \quad u = 0 \quad \text{on } \Gamma_p. \quad (1)$$

Moreover, from the radiation condition, we also put the following boundary condition on Γ_H :

$$\frac{\partial u}{\partial x_2} - T^+ u = f, \quad f \text{ is defined by the incident field} \quad (2)$$

In Chandler-Wilde *et. al.*, 2010, it is proved that when f in the weighted Sobolev space $H_r^{-1/2}$ (where $|r| < 1$), the scattering problem is unique solvable in $H_r^1(\Omega_p^H)$.

2 The Floquet-Bloch transform

The definition of the Floquet-Bloch transform is similar to a Fourier series, i.e.,

$$(\mathcal{J}\phi)(\alpha, x) := \sum_{j \in \mathbb{Z}} \phi(x_1 + 2\pi j, x_2) e^{-i2\pi\alpha j},$$

where $\alpha \in W$ ($W := (-1/2, 1/2]$) and $x \in \Omega_H^{2\pi}$ ($\Omega_H^{2\pi} := (-\pi, \pi] \times \mathbb{R} \cap \Omega_H$). It is easily checked that the transformed field is 1-periodic in α and α -quasi-periodic in x . As the transform is only defined in periodic domains, we introduce a diffeomorphism Φ that maps the periodic domain Ω_H to the locally perturbed Ω_p^H . Let

$$u_T := u \circ \Phi; \quad w(\alpha, x) := (\mathcal{J}u_T)(\alpha, x),$$

then w satisfies the following variational problem defined in $W \times \Omega_H^{2\pi}$:

$$\int_W a_\alpha(w(\alpha, \cdot), \phi(\alpha, \cdot)) d\alpha + b(w, \phi) = \langle F, \phi \rangle,$$

where $a_\alpha(\cdot, \cdot)$ is the variational form of the classic α -quasi-periodic scattering problem in $\Omega_H^{2\pi}$, and $b(\cdot, \cdot)$ is a sesquilinear form defined in the bounded domain $W \times \Omega_H^{2\pi}$, $F = \mathcal{J}f$.

In Lechleiter *et. al.*, 2017, it is proved that when $f \in H_r^{-1/2}(\Gamma_H)$, then the variational problem (2) is uniquely solvable in $H^r(W, H^1(\Omega_H^{2\pi}))$.

To apply the finite element method, we require that the surfaces are smoother and $f \in H_r^{1/2}(\Gamma_H)$ such that the solution lies in the space $H^r(W, H^2(\Omega_H^{2\pi}))$. We divide the interval W into N uniform subintervals, and generate regular and quasi-uniform meshes for the domain $\Omega_H^{2\pi}$ with the meshsize h . We formulate the finite dimensional problem by the piecewise constant basic functions on W and piecewise linear basic functions on $\Omega_H^{2\pi}$, then the finite element problem is uniquely solvable. Let $w_{N,h}$ be the finite element solution, then the L^2 -error decays with the rate $h(N^{-r} + h)$.

3 Singularity of w with respect to α

Let the finite set S be all the points $\alpha \in \overline{W}$ such that there is an $n \in \mathbb{Z}$, $|\alpha + n| = k$. Then S is a finite set with at most three elements, set $S = \{\alpha_1, \dots, \alpha_N\}$. Define Property* by:

Definition 1 (Property*) A function $\phi(\alpha, \cdot)$ with $\alpha \in W$ satisfies Property* if

$$\phi(\alpha, \cdot) = \sum_{n=1}^N \sqrt{\alpha - \alpha_n} \phi_n(\alpha, \cdot)$$

where $\phi_n(\alpha, \cdot)$ depends smoothly on $\alpha \in W$.

Inspired by the analysis in Kirsch *et. al.*, 1993, we can prove the following theorem.

Theorem 2 When $F = \mathcal{J}f$ satisfies Property*, then the solution w also satisfies Property*.

4 High order numerical method

The key point for the high order method is the inverse Bloch transform, i.e., to design a high order method for the integral

$$(\mathcal{J}^{-1}w)(x) = \int_W w(\alpha, x) d\alpha.$$

We can redefine W by $(-\alpha_0, 1 - \alpha_0)$ where α_0 is defined by k , then there are two different classes of S :

1. $S = \{-\alpha_0, 1 - \alpha_0\}$;

2. $S = \{-\alpha_0, \alpha_0, 1 - \alpha_0\}$.

Based on the two different types of S 's, we could choose two different curves for the integral. Let g be a smooth enough and monotoni-

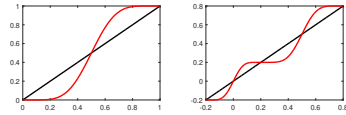


Figure 1: Two different choices of the function g .

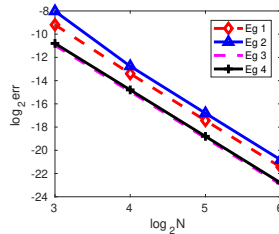
cally increasing function with any order derivative at points in S vanishes. Let α be replaced by $\alpha = g(t)$, then let $\tilde{w}(t, x) := w(g(t), x)g'(t)$, then $\tilde{w}(t, \cdot)$ depends smoothly on t . We use the same meshes and basic functions to formulate the finite dimensional problem, then we can prove the following convergence result.

Theorem 3 Let $\tilde{W}_{N,h}$ be the finite element solution, then for any $n \in \mathbb{N}$,

$$\|\tilde{W}_{N,h} - w\|_{L^2(W \times \Omega_H^{2\pi})} \leq Ch(N^{-n} + h), \quad (3)$$

where C depends on n and the incident field.

The finite element method for the high order case is carried out in the same way as introduced in Section 2. The relationship between the number of nodals in W and relative errors are shown in the following figure.



References

[1] R. Zhang, A high order numerical method for scattering from locally perturbed periodic surfaces, *SIAM J. Sci. Comput.*, **40** (2018), pp. A2286–A2314.

Near-Field Imaging of an Unbounded Elastic Rough Surface with a Direct Imaging Method

Xiaoli LIU^{1,*}, Bo Zhang², Haiwen Zhang²

¹INRIA Saclay-Ile-de-France/CMAP Ecole Polytechnique, Palaiseau, France

²NCMIS and Academy of Mathematics and Systems Science, Chinese Academy of Sciences, Beijing, China

*Email: xiaoli.liu@inria.fr

Abstract

A direct imaging method is developed to reconstruct unbounded rough surface $S := (x_1, f(x_1))$, which is supposed to be smooth enough such that $f \in BC^{1,1}(\mathbb{R})$, from the elastic scattered near-field Cauchy data generated by point sources. A Helmholtz-Kirchhoff-type identity is derived and then used to provide a theoretical analysis of the direct imaging algorithm. Numerical experiments are presented to show that the direct imaging algorithm is fast, accurate and robust with respect to noise in the data.

Keywords: inverse elastic scattering, unbounded rough surface, direct imaging method

1 Introduction

The domain above the rough surface is filled with a homogeneous and isotropic elastic medium, and the medium below the surface is assumed to be elastically rigid. See Fig. 1 for the geometry.

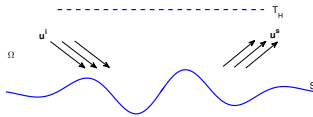


Figure 1: Problem Geometry

Compared with inverse acoustic scattering problems (see [1]), the elastic cases are more complicated due to the coexistence of the compressional and shear waves that propagate at different speeds. For bounded elastic bodies, several numerical inversion algorithms have been proposed. See also the monograph [2] for a good survey. However, as far as we know, not many results are available for inverse elastic scattering by unbounded rough surfaces.

The purpose of this paper is to develop a direct imaging method for inverse elastic scattering problems by an unbounded rigid rough surface. Motivated by the Helmholtz-Kirchhoff identity for bounded obstacles, we consider the unbounded rough surface and provide an integral identity concerning the fundamental solution of the Navier equation on an infinite line (see Lemma 1). In addition, a reciprocity relation (see Lemma 2) is proved for the elastic scattered field corresponding to the unbounded rough surface. Based on these results, the required imaging function is then proposed, which, at each sampling point, involves only the inner products of the measured data and the fundamental solution of the Navier equation in a homogeneous background medium. Numerical results are presented to show that our imaging method can provide an accurate and reliable reconstruction of the unbounded rough surface. This paper is a nontrivial extension of our recent work in [3] from the acoustic case to the elastic case since the elastic case is much more complicated than the acoustic case due to the coexistence of the compressional and shear waves that propagate at different speeds.

2 The imaging algorithm

The propagation of time-harmonic waves with circular frequency ω in an elastic solid with Lamé constants μ, λ ($\mu > 0, \lambda + \mu \geq 0$) is governed by the Navier equation

$$\mu \Delta \mathbf{u} + (\lambda + \mu) \text{grad div } \mathbf{u} + \omega^2 \mathbf{u} = 0.$$

Here, $\mathbf{u} = (u_1, u_2)^T$ denotes the elastic field.

For any $H \in \mathbb{R}$, introduce the sets

$$U_H := \{x = (x_1, x_2) \in \mathbb{R}^2 : x_2 > H\},$$

$$T_H := \{x = (x_1, x_2) \in \mathbb{R}^2 : x_2 = H\}.$$

Lemma 1 (Helmholtz-Kirchhoff-type identity)

$$\int_{T_H} \left([\Pi_{\xi, x}^{(1)}]^T \overline{\Gamma_{\xi, y}} - [\Gamma_{\xi, x}]^T \overline{\Pi_{\xi, y}^{(1)}} \right) ds(\xi) = 2i \Im \Gamma_{y, \cdot}$$

for $x, y \in \mathbb{R}^2 \setminus \bar{U}_H$, where Γ is the free-space Green's tensor for the 2-D Navier equation and $\Pi^{(1)}$ is the corresponding derivatives with the unit normal \mathbf{n} on T_H pointing into U_H .

Lemma 2 (Reciprocity relation) For $\mathbf{p}, \mathbf{q} \in \mathbb{R}^2$, let $\mathbf{u}^s(z, x, \mathbf{p})$ and $\mathbf{u}^s(z, y, \mathbf{q})$ be the scattered fields in Ω associated with the rough surface S and the incident point sources $\mathbf{u}^i(z, x, \mathbf{p}) := \Gamma(z, x)\mathbf{p}$ and $\mathbf{u}^i(z, y, \mathbf{q}) := \Gamma(z, y)\mathbf{q}$, respectively. Then

$$\mathbf{u}^s(y, x, \mathbf{p}) \cdot \mathbf{q} = \mathbf{u}^s(x, y, \mathbf{q}) \cdot \mathbf{p}, \quad x, y \in \Omega.$$

Based on the above two lemmas, we can present the following theorem which leads to the imaging function for our imaging algorithm.

Theorem 3 Define $\mathbf{U}^i(y, z, \mathbf{e}_j) := 2ie_j^T \Im \Gamma(y, z)$, $j = 1, 2$, then the scattered field generated by $\mathbf{U}^i(y, z, \mathbf{e}_j)$ is given by

$$\begin{aligned} \mathbf{U}^s(y, z, \mathbf{e}_j) &:= \int_{T_H} \left(\mathbf{T} \mathbf{u}^s(x, y, \mathbf{e}_j) \cdot \overline{\mathbf{u}^i(x, z, \mathbf{e}_j)} \right. \\ &\quad \left. - \mathbf{u}^s(x, y, \mathbf{e}_j) \cdot \overline{\mathbf{T} \mathbf{u}^i(x, z, \mathbf{e}_j)} \right) ds(x) \\ &\quad - 2ie_j \cdot \Im_- \Gamma(z, y) \mathbf{e}_j, \end{aligned}$$

where \mathbf{T} is the stress operator.

Motivated by Theorem 3, we finally give the imaging function for each sampling point z as

$$I(z) := \sum_{j=1}^2 \int_{T_H} \left| \mathbf{U}^s(y, z, \mathbf{e}_j) \right|^2 ds(y).$$

Since $\mathbf{U}^s(y, z, \mathbf{e}_j)$ is the scattered field corresponding to $\mathbf{U}^i(y, z, \mathbf{e}_j) := 2ie_j^T \Im \Gamma(y, z)$, which is related to the Bessel function J_0 , it is expected that $I(z)$ takes a large value when $z \in S$ and decays as z moves away from the rough surface S .

3 Numerical results

We now present several numerical experiments to demonstrate the effectiveness of our imaging algorithm and compare the reconstructed results under different parameters.

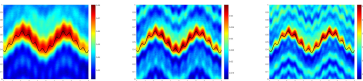


Figure 2: Reconstructed results with $w = 9, 15, 20$, respectively.

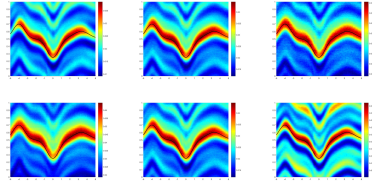


Figure 3: Different measurement places. Top row (from left to right): the Cauchy data are measured on $(x_1, 2)$ such that $|x_1| \leq 7.5$, $|x_1| \leq 10$ and $|x_1| \leq 15$, respectively. Bottom row (from left to right): the Cauchy data are measured on $(x_1, 1.2)$, $(x_1, 2)$ and $(x_1, 4)$ such that $|x_1| \leq 10$, respectively.

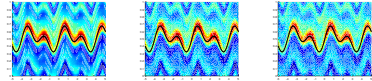


Figure 4: Reconstructed results with no noise, 20% noise and 40% noise, respectively.

Fig.2 shows that the reconstruction result is getting better with the increase of the frequency. From Fig.3, it can be seen that the reconstructed result is getting better if both the measurement line segment is getting closer to the rough surface and its length is getting longer. Finally, Fig.4 proved that our imaging method is very robust to the noise in the data.

References

- [1] D. Colton and R. Kress, *Inverse Acoustic and Electromagnetic Scattering Theory*, 3rd Edition, Springer, New York, 2013.
- [2] H. Ammari and E. Bretin, J. Garnier, H. Kang, H. Lee, A. Wahab, *Mathematical Methods in Elasticity Imaging*, Princeton University Press, 2015.
- [3] X. Liu and B. Zhang, H. Zhang, A direct imaging method for inverse scattering by unbounded rough surfaces, *SIAM J. Imaging Sci.* 11 (2018), pp. 1629-1650.

A Frequency Domain Method for Scattering Problems with Moving Boundaries

D. Gasperini^{1,2,3}, X. Antoine¹, C. Geuzaine², H. P. Beise³, U. Schroeder³

¹University of Lorraine, Institut Elie Cartan, CNRS UMR 7502, INRIA SPHINX team, Vandoeuvre-lès-Nancy, France

²University of Liège, Montéfiore Institute, Liège, Belgium

³IEE S.A., Contern, Luxembourg

Abstract

We focus on the construction of a frequency domain resolution method for the wave scattering problem in one dimension with moving boundaries. We compare the obtained results with those given while applying the fast Fourier transform to more standard space-time resolution and show that the proposed method is much more efficient.

Keywords: Scattering, 1D Acoustic Wave, Frequency Domain Resolution, Moving Boundaries.

1 Introduction

We are interested in radar detection of moving scatterers. The aim of this ongoing work is to present a method to solve in the frequency domain time-harmonic acoustic scattering problems for which the scatterer is spatially oscillating. Brute approaches may be comprised of a first space-time resolution on which one applies the fast Fourier transform. However such computations exhibit high costs since they require long time samples and are also penalized by frequency dispersion effects. Such problems have already been investigated for instance by explicit asymptotic expansion in [1], but restricted to unbounded time-shifted domain. In our approach we investigate the problem in the frequency domain, and derive how the frequency components of the solution must be coupled, and compute only the ones with significative contributions by solving coupled systems of Helmholtz-type equations. This provides an alternative which combines both accuracy and efficiency. Below we sketch a general description of this method and compare it with brute force approach.

2 Problem statement

Let us consider the bounded domain $\Omega := \{x : x \in]0, l(t)\}$ with moving boundary $l(t) := 1 + \epsilon \sin(\omega_s t)$ for $\omega_s > 0$ and $0 < \epsilon < 1$. We impose at the left boundary a source term $e^{i\omega_f t}$ and ho-

mogeneous Dirichlet boundary conditions at the moving right boundary. Other boundary conditions (for instance impedance boundary conditions) that fit with more realistic models could also be taken into account and will be presented in the extended paper. The scattering problem is formulated as follows: find the wave $u(x, t)$ in $\{(x, t) \in \mathbb{R} \times \mathbb{R}_+^+, \text{ such that } 0 < x < l(t)\}$, such that $u(0, t) = e^{i\omega_f t}$, $u(l(t), t) = 0$ and $u(x, 0) = \partial_t u(x, 0) = 0$, solution to

$$\frac{1}{c^2} \partial_{tt} u - \partial_{xx} u = 0 \quad (1)$$

3 Methodology

We apply a suitable smooth change of space variable $\tilde{x} : (x, t) \mapsto \tilde{x}(x, t)$ with $\tilde{x}(0, t) = 0$ and $\tilde{x}(l(t), t) = 1$ for all $t > 0$, while keeping the time coordinate the same in order to work in a fixed spatial domain. The previous scattering problem (1) becomes: find $\tilde{u}(\tilde{x}, t) = u(x, t)$, solution in $\tilde{\Omega} \times \mathbb{R}_+^+$ with $\tilde{\Omega} =]0, 1[$, of the equation

$$\begin{aligned} \partial_{tt} \tilde{u} - c^2 \left[\left(\frac{\partial \tilde{x}}{\partial x} \right)^2 \partial_{\tilde{x}\tilde{x}} \tilde{u} + \frac{\partial^2 \tilde{x}}{\partial x^2} \partial_{\tilde{x}} \tilde{u} \right] \\ + \left(\frac{\partial \tilde{x}}{\partial t} \right)^2 \partial_{\tilde{x}\tilde{x}} \tilde{u} + 2 \frac{\partial \tilde{x}}{\partial t} \partial_{\tilde{x}t} \tilde{u} + \frac{\partial^2 \tilde{x}}{\partial t^2} \partial_{\tilde{x}} \tilde{u} = 0 \end{aligned} \quad (2)$$

with $\tilde{u}(0, t) = e^{i\omega_f t}$, $\tilde{u}(1, t) = 0$ and $\tilde{u}(\tilde{x}, 0) = \partial_t \tilde{u}(\tilde{x}, 0) = 0$. We consider the linear change of variable

$$\tilde{x} = \frac{x}{l(t)}.$$

By linearity of \tilde{x} the term $\frac{\partial^2 \tilde{x}}{\partial x^2}$ vanishes. As in [2] the resulting equation in the fixed domain depends on the space Jacobian $\frac{\partial \tilde{x}}{\partial x}$ of \tilde{x} . If for a practical radar sensing applications, the perturbation amplitude ϵ is much smaller than the size of the domain, then the terms in (2) arising from the second order temporal derivative (second line of the previous equation) can be neglected. The following simplified problem can

be formulated: find u^* solution of the equation

$$\frac{l^2}{c^2} \partial_{tt} u^* - \partial_{\tilde{x}\tilde{x}} u^* = 0 \quad (3)$$

with the same initial and boundary conditions as before.

4 Frequency domain resolution

We assume that $t \mapsto u^*(\tilde{x}, t)$ is integrable on \mathbb{R} for all $\tilde{x} \in \Omega$ and that there exists $\varphi(t)$ integrable on \mathbb{R}_*^+ such that for all $(\tilde{x}, t) \in \Omega \times \mathbb{R}^+$, we have $|\partial_{\tilde{x}\tilde{x}} u^*| \leq \varphi(t)$, and apply a time Fourier transform on (3). Then the problem is: find \hat{u} in $\Omega \times \mathbb{R}^+$ solution of the equation

$$\begin{aligned} \partial_{\tilde{x}\tilde{x}} \hat{u} + \left[\left(\frac{2\pi\xi}{c} \right)^2 \hat{u} \right] \cdot \left[\left(1 + \frac{\epsilon^2}{2} \right) \right. \\ \left. + \frac{\epsilon}{i} \left(\tau_{\frac{\omega_s}{2\pi}} - \tau_{-\frac{\omega_s}{2\pi}} \right) - \frac{\epsilon^2}{4} \left(\tau_{\frac{\omega_s}{\pi}} + \tau_{-\frac{\omega_s}{\pi}} \right) \right] = 0 \end{aligned} \quad (4)$$

such that $\hat{u}(\tilde{x}, 0) = 0$, $\hat{u}(1, \xi) = 0$, $\hat{u}(0, \xi) = 0$ for $\xi \neq \omega_f$ and $\hat{u}(0, \omega_f) = 1$, with τ_θ the translation operator applied on the second variable. Due to the discrete spectrum of the Laplace operator in bounded domains, \hat{u} is a linear combination of the main excitation \hat{u}_{ω_f} and the contributions of the proper modes \hat{u}_{ω_i} of the system, for $i \in \mathbb{N}$. The perturbation creates around each contributing frequency ω a symmetric cluster of coupled frequencies spaced by ω_s . We write the corresponding term \hat{u}_ω as a Fourier expansion around ω with ω_s -multiple harmonics:

$$\hat{u}_\omega(\tilde{x}, \xi) = \sum_{j \in \mathbb{Z}} a_j(\tilde{x}) \delta \left(\xi - \frac{\omega + j\omega_s}{2\pi} \right).$$

For each ω , (4) leads to the following algebraic-differential coupled system, for all $j \in \mathbb{Z}$:

$$\begin{aligned} \partial_{\tilde{x}\tilde{x}} a_j + k_j^2 \left(1 + \frac{\epsilon^2}{2} \right) a_j + \frac{\epsilon}{i} [k_{j-1}^2 a_{j-1} - k_{j+1}^2 a_{j+1}] \\ - \frac{\epsilon^2}{4} [k_{j-2}^2 a_{j-2} + k_{j+2}^2 a_{j+2}] = 0 \end{aligned} \quad (5)$$

with $k_j := \frac{\omega + j\omega_s}{c}$. As the size of the domain is much larger than ϵ , we neglect the second order terms in ϵ . The coupling between the a_j 's is the consequence of the variation of l and describes how the amplitudes associated to the frequency components depend on each other. Taking either $\epsilon = 0$ or $\omega_s = 0$ leads to the standard Helmholtz equation with fixed boundaries. It is

analytically shown that there exists $J > 0$ such that for $|j| > J$, $\max_{\tilde{x}}(a_j)$ is fastly decaying to zero when $|j|$ increases. In the present method we solve (5) for $|j| \leq J$ with the same boundary conditions, assuming $a_j \equiv 0$ for $|j| > J$.

5 Preliminary numerical results

The reference is computed with the FFT applied on the FDM time resolution of (3), taking $\omega_f = 10$ Hz and $\omega_s = 1$ Hz. The multiharmonic, frequency domain system is solved with FDM for $J = [-9, 8]$. Given a spatial discretization of 100 nodes, the CPU time ratio between both methods is 350.

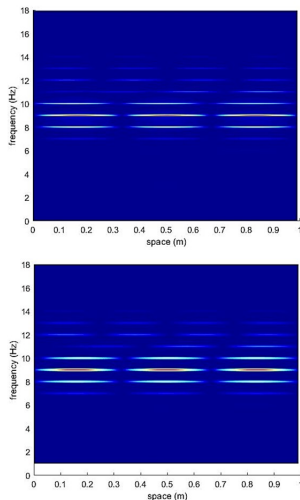


Figure 1: Comparison of the brute force solution (top) with the present method centered on ω_f (bottom).

References

- [1] I. C. Christov and C. I. Christov. On mechanical waves and doppler shifts from moving boundaries. *Mathematical Methods in the Applied Sciences*, 40(12):4481–4492, 2017.
- [2] A. Halbach and C. Geuzaine. Steady-state, nonlinear analysis of large arrays of electrically actuated micromembranes vibrating in a fluid. *Engineering with Computers*, 155(3):591–602, 2017.

Scattering for NLS with a sum of two repulsive potentials

David Lafontaine^{1,*}

¹Department of Mathematical Sciences, University of Bath, Bath, UK

*Email: d.lafontaine@bath.ac.uk

Abstract

We will present a scattering result [Laf18] for a defocusing nonlinear Schrödinger equation with a sum of two repulsive potentials with strictly convex level surfaces. We deal with this unstable-trapping framework using a concentration, compactness and rigidity approach together with new *almost-Morawetz estimates*.

Keywords: Non-linear Schrödinger equation, scattering, trapped trajectories, potential, Morawetz estimates, concentration-compactness/rigidity

1 Introduction

We are concerned with the scattering behaviour, as defined in Definition 1 below, of the following defocusing non-linear Schrödinger equation with a potential

$$i\partial_t u + \Delta u - Vu = u|u|^\alpha, \quad u(0) = \varphi \in H^1, \quad (1)$$

in arbitrary spatial dimension $d \geq 1$. Once good dispersive properties of the linear flow, such as Strichartz estimates, are established, the local well-posedness of (1) follows by usual fixed point arguments. Because of the energy conservation law,

$$E(u(t)) := \frac{1}{2} \int |\nabla u(t)|^2 + \int V|u(t)|^2 + \frac{1}{\alpha + 2} \int |u(t)|^{\alpha+2} = E(u(0)),$$

this result extends to global well-posedness. Thus, it is natural to investigate the asymptotic behaviour of solutions of (1), and, in particular, whether the non-linearity still plays a role for large times. If it is not the case, we say that the solutions scatter, in the sense that

Definition 1 A solution $u \in C(\mathbb{R}, H^1(\mathbb{R}^d))$ of (1) scatters in $H^1(\mathbb{R}^d)$ if there exists a unique couple of data $\psi_\pm \in H^1(\mathbb{R}^d)$ such that

$$\|u(t) - e^{-it\Delta}\psi_\pm\|_{H^1(\mathbb{R}^d)} \xrightarrow{t \rightarrow \pm\infty} 0.$$

In the homogeneous case $V = 0$, in the in-critical regime

$$\frac{4}{d} < \alpha < \begin{cases} +\infty & d = 1, 2, \\ \frac{4}{d-2} & d \geq 3, \end{cases} \quad (2)$$

the scattering of solutions of (1) is well-known since Nakanishi’s paper [Nak99]. The inhomogeneous setting $V \neq 0$ was investigated more recently, for example in [BV16], [Laf16], [Hon16]. However, all these scattering results rely on a non-trapping assumption, namely, that the potential is *repulsive*:

$$x \cdot \nabla V \leq 0,$$

or, as in [Car16], that its non-repulsive part is sufficiently small.

The aim of this talk is to present a first scattering result [Laf18] in a trapping situation. More precisely, we are interested in one of the simplest unstable-trapping frameworks, that is, the case where V is the sum of two positive, repulsive potentials with strictly convex level surfaces. This is the potential-analog of the homogeneous problem outside two strictly convex obstacles, subject of a work in progress [LL].

2 Statement of the result

Let V_1 and V_2 be two positive, smooth potentials and let $V = V_1 + V_2$ be the total potential. We make the following geometrical assumptions:

(G1) V_1 and V_2 are repulsive, that is, there exists a_1 and a_2 in \mathbb{R}^d such that

$$(x - a_{1,2}) \cdot \nabla V_{1,2} \leq 0.$$

Without loss of generality, we assume that $0 \in [a_1, a_2]$.

(G2) The level surfaces of V_1 and V_2 are convex, and uniformly strictly convex in the non-repulsive region: the eigenvalues of their second fundamental forms are uniformly bounded below by a strictly positive universal constant in $\{x \cdot \nabla V > 0\}$.

(G3) All the trapped trajectories of the Hamiltonian flow associated with $-\mathcal{L} V$ belong to a same line \mathcal{R} .

We will, in addition, suppose that the total potential follows the following decay assumption

$$V, \nabla V \in L^{\frac{d}{2}}(\mathbb{R}^d, (1 + |x|^\beta)dx), \quad \beta > 1. \quad (3)$$

And finally, that the pointwise dispersive estimate

$$\|e^{it(-\Delta+V)}\|_{L^1 \rightarrow L^\infty} \lesssim \frac{1}{|t|^{d/2}} \quad (4)$$

holds. This estimate gives us in particular crucial Strichartz estimates mentioned above. Note that this last assumption is automatically verified using Goldberg and Schlag's result [GS04] under the non-negativity and decay assumption with $\beta \geq 2$ in dimension $d = 3$. Our result reads

Theorem 1 *Assume that $d \geq 3$. Let V_1 and V_2 be two positive, smooth potentials, satisfying (G1)-(G2)-(G3), such that the sum $V = V_1 + V_2$ satisfies (3) and (4). Then, in the intercritical regime (2), every solution of (1) with potential V scatters in $H^1(\mathbb{R}^d)$.*

3 Outline of the proof

We use the strategy of concentration, compactness and rigidity first introduced by Kenig and Merle in [KM06]: seeking a contradiction, one assumes that there exists a finite energy above which solutions do not scatter. This assumption allows one to construct a compact-flow solution (a so-called critical solution), which is then eliminated.

Notice that in the case of a repulsive potential, this last rigidity part is immediate by classical Morawetz estimates. This is the main difficulty to overcome and the novelty of [Laf18].

The construction of a critical solution follows [Laf16], generalizing it to any spatial dimension. The difficulty in this construction is the lack of translation invariance of the equation due to the potential. The key idea to deal with it is to notice that a profile escaping to infinity does not see the potential.

Finally, we eliminate this critical solution using a family of Morawetz multipliers that almost vanish on the trapped trajectory. This almost-Morawetz multipliers family is our main idea to deal with scattering for nonlinear wave equations in unstable-trapping geometries. We believe that it could be used efficiently to treat other similar problems and geometrical frameworks.

References

- [BV16] Valeria Banica and Nicola Visciglia, *Scattering for NLS with a delta potential*, J. Differential Equations **260** (2016), no. 5, 4410–4439. MR 3437592
- [Car16] Rémi Carles, *On semi-classical limit of nonlinear quantum scattering*, Ann. Sci. Éc. Norm. Supér. (4) **49** (2016), no. 3, 711–756. MR 3503830
- [GS04] M. Goldberg and W. Schlag, *Dispersive estimates for Schrödinger operators in dimensions one and three*, Comm. Math. Phys. **251** (2004), no. 1, 157–178. MR 2096737 (2005g:81339)
- [Hon16] Younghun Hong, *Scattering for a nonlinear Schrödinger equation with a potential*, Commun. Pure Appl. Anal. **15** (2016), no. 5, 1571–1601. MR 3538870
- [KM06] Carlos E. Kenig and Frank Merle, *Global well-posedness, scattering and blow-up for the energy-critical, focusing, non-linear Schrödinger equation in the radial case*, Invent. Math. **166** (2006), no. 3, 645–675. MR 2257393 (2007g:35232)
- [Laf16] D. Lafontaine, *Scattering for NLS with a potential on the line*, Asymptot. Anal. **100** (2016), no. 1-2, 21–39. MR 3570874
- [Laf18] David Lafontaine, *Scattering for nls with a sum of two repulsive potentials*, <https://arxiv.org/abs/1812.04968> (2018).
- [LL] D. Lafontaine and C. Laurent, *Scattering for critical nonlinear waves outside some strictly convex obstacles*, Work in progress.
- [Nak99] Kenji Nakanishi, *Energy scattering for nonlinear Klein-Gordon and Schrödinger equations in spatial dimensions 1 and 2*, J. Funct. Anal. **169** (1999), no. 1, 201–225. MR 1726753 (2000m:35141)

Comparison of Full-waveform and Travel-time Inversions in Helioseismology

Majid Pourabedian^{1,*}, Laurent Gizon¹, Thorsten Hohage², Damien Fournier¹,
Chris S. Hanson³

¹Max-Planck-Institut für Sonnensystemforschung, Göttingen, Germany

²Institut für Numerische und Angewandte Mathematik, Georg-August-Universität Göttingen,
Göttingen, Germany

³Center for Space Science, NYUAD Institute, New York University Abu Dhabi, Abu Dhabi, UAE

*Email: pourabedian@mps.mpg.de

Abstract

Performing inversions in time–distance helioseismology is demanding because of the large amount of data and the high level of noise which is due to the stochastic excitation of the solar oscillations. Averaging the input data is thus pivotal to increase the signal-to-noise ratio and make the problem tractable. Here, we compare full-waveform and travel-time inversions to recover flows at a given 3D location in the solar interior. With the same noise levels, we find that averaging kernels are more localized when using the cross-covariance function in frequency domain (full-waveform inversion), rather than travel times as input data.

Keywords: helioseismology, full-waveform inversion, travel time

1 Helioseismic observables

The Sun is stochastically oscillating due to the turbulent convection. Time–distance helioseismology [1] is a method to probe the solar internal structure using the observed oscillation signals (e.g., Doppler velocities) on the solar surface. In this manner, the cross-covariance function is then defined as the product of the observed signals, denoted by ψ at angular frequency ω , at two surface locations, indexed by i , like $i = (\mathbf{r}_1, \mathbf{r}_2)$:

$$C_i(\omega) = \frac{2\pi}{T} \psi^*(\mathbf{r}_1, \omega) \psi(\mathbf{r}_2, \omega), \quad (1)$$

where T is the observation time and the star denotes the complex conjugation. One then seeks to relate the observed surface measurements d_i (e.g., cross-covariance in Eq. (1)), with the corresponding noise n_i , to the solar internal structure, e.g., flows as

$$d_i(\omega) = \int_S \mathbf{K}_i(\omega, \mathbf{r}) \cdot \mathbf{u}(\mathbf{r}) d\mathbf{r} + n_i(\omega), \quad (2)$$

where $\mathbf{u}(\mathbf{r}) = (u^r(\mathbf{r}), u^\theta(\mathbf{r}))$ is an unknown flow vector at a position \mathbf{r} . Here, \mathbf{r} denotes a 2D position at radius r and co-latitude θ in spherical coordinates and S is a half-disk of the solar radius R_\odot . The responses of the observed measurements to the local flow changes are described via the sensitivity kernels $\mathbf{K}_i = (K_i^r, K_i^\theta)$ (see Figure 1). The cross-covariance resembles a

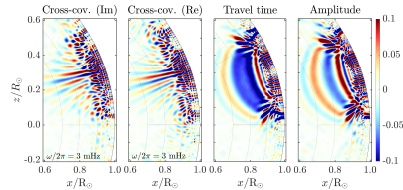


Figure 1: Sensitivity kernels $K^\theta(\mathbf{r})$ for perturbations in u^θ for cross-covariance (imaginary and real parts at 3 mHz), travel-time and amplitude measurements. The measurements correspond to a pair of points located at the latitudes 3° and 33° on the solar surface. The values of the kernels are normalized and saturated and are computed following the framework in [2].

seismogram as it contains the information about the travel times and amplitudes of the waves propagating in the solar interior. Hence, the cross-covariance is considered as the full-waveform observable. One might instead use some intermediate data products of the cross-covariance as observable (e.g., travel times of the waves). In addition to travel times, cross-covariance amplitudes may also be beneficial in helioseismology as they carry independent information of the wave field than travel times. The travel times and amplitudes are computed from the cross-covariance and they are averaged quantities over a range of frequencies [2]. Thus, the

forward problem in Eq. (2) for travel-time or amplitude observables shrinks to:

$$d_i = \int_S \mathbf{K}_i(\mathbf{r}) \cdot \mathbf{u}(\mathbf{r}) d\mathbf{r} + n_i. \quad (3)$$

Note that the sensitivity kernels for the cross-covariance measurements are frequency-dependent, while the kernels of travel times and amplitudes only depend on the observational pairs of points (see Figure 1).

So far local helioseismic inversions have been based on the computation of travel times or cross-covariance amplitudes as an intermediate step. However, such procedures neglect a substantial amount of information contained in the cross-covariance of the seismic wavefield which provides the full-waveform inversion (FWI). In this study, as the inversion procedure, we compare different choices of observables in terms of resolution and propagated errors to the solution. Note that d (see Eqs. (2) and (3)) can be any types of observables as we consider cross-covariance in frequency domain (FWI), travel-time and amplitude measurements.

2 Comparison of inversion strategies

In helioseismology, the inverse problem is mainly solved linearly. Thus, we seek to find the flow solution vector $\hat{\mathbf{u}}$ such that

$$\hat{\mathbf{u}} = W\mathbf{d}, \quad (4)$$

where the solution vector is a weighted average of the input data vector \mathbf{d} . Each row of the weight matrix W provides the optimal coefficients to compute the solution at a chosen target position $\mathbf{r}_0 = (r_0, \theta_0)$. To find the weights W in Eq. (4), we seek solutions to the discrete regularized least squares problem:

$$\hat{\mathbf{u}} = \underset{\mathbf{u}}{\operatorname{argmin}} \left\{ \|\Lambda^{-1/2}(K\mathbf{u} - \mathbf{d})\|_2^2 + \alpha \|\mathbf{u}\|_2^2 \right\}, \quad (5)$$

where \mathbf{u} is the unknown flow vector. We compute K which is the matrix of the sensitivity kernels, Λ is the noise covariance matrix of the measurements and α is a regularization parameter. Here, $\|\dots\|_2$ denotes the 2-norm. The inverse problem is a balance between resolution and propagated errors to the solution. This can be seen by computing the difference between the reconstructed and the exact flow

$$\begin{aligned} \mathbb{E} \left[\|\hat{\mathbf{u}} - \mathbf{u}\|_2^2 \right] &= \mathbb{E} \left[\|W\mathbf{d} - \mathbf{u}\|_2^2 \right] \\ &= \|(\mathcal{K} - \mathbb{I})\mathbf{u}\|_2^2 + \|W\|_2^2, \end{aligned} \quad (6)$$

where \mathbb{E} denotes the expectation value, \mathbb{I} is the identity matrix and \mathcal{K} is called averaging kernel

$$\mathcal{K} = WK. \quad (7)$$

The averaging kernels describe the resolution of the inversion and it is desirable that the averaging kernels have a peak near the target $\mathbf{r}_0 = (r_0, \theta_0)$. The localization of the averaging kernel depicts the bias of the linear estimator in Eq. (4). The last term in Eq. (6) corresponds to the variance of the estimator, i.e. the error propagation to the estimated solution in Eq. (4).

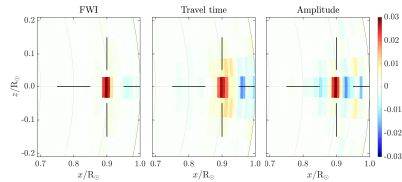


Figure 2: Averaging kernels \mathcal{K} for u^θ corresponding to the FWI (left panel), travel-time (middle panel) and amplitude (right panel) inversions for $T = 4$ years and frequencies between $[2-4]$ mHz. The crosshairs (solid lines) indicate the target location at $r_0/R_\odot = 0.9$ on the solar equator. The magnitude of the propagated error to the solutions at this chosen target is approximately 1.5 m/s for the three observables.

Considering the same propagated error to the solution at $r_0/R_\odot = 0.9$, Figure 2 shows that the cross-covariance measurements lead to a more localized averaging kernel than the travel-time and amplitude measurements. In other words, with the same noise level, the FWI gives solutions with higher resolutions in comparison to inversion results using other types of measurements such as travel times of waves. This motivates us to infer the solar meridional flow using the observational data in the next step.

References

- [1] T. L. Duvall Jr., *et al.*, Time-distance Helioseismology, *Nature* **362** (1993), pp. 430–432.
- [2] L. Gizon, *et al.*, Computational Helioseismology in the Frequency Domain: Acoustic Waves in Axisymmetric Solar Models with Flows, *A&A* **600** (2017), pp. A35.

Imaging the Solar Interior with Seismic Holography

Damien Fournier^{1,*}, Dan Yang¹, Laurent Gizon¹

¹Max-Planck-Institut für Sonnensystemforschung, Justus-von-Liebig-Weg 3, 37077 Göttingen, Germany

*Email: fournier@mps.mpg.de

Abstract

Despite 20 years of high-quality observations of Doppler velocities at the solar surface, the internal structure of the Sun still presents some mysteries. As it is impossible to treat all the data at once, some averages have to be performed a priori. These averages are based on some physical understanding or on the analysis of wave propagation in a reference solar-like background. We analyze and improve a classical method called seismic holography which aims at propagating the surface data to any location in the solar interior.

Keywords: helioseismology, holography, inverse problem

1 Introduction

Time-distance helioseismology [1] aims at recovering subsurface properties of the Sun from the observation of the Doppler velocities at the surface. Due to convection, the data are stochastic and one generally analyzes the cross-covariances of the wavefield ψ between any two points \mathbf{r}_1 and \mathbf{r}_2 at the solar surface

$$C^\omega(\mathbf{r}_1, \mathbf{r}_2) = \psi^*(\mathbf{r}_1, \omega)\psi(\mathbf{r}_2, \omega). \quad (1)$$

Here ω denotes the frequency and the product of the wavefield in frequency space corresponds to a convolution in the time domain. Every 45 s, a map of size $4\text{k} \times 4\text{k}$ pixels of Doppler velocities on the solar surface is available which lead to 10^{13} possible cross-covariance measurements at each time. The number of available frequencies is linked to the observation time (e.g. 5000 frequencies for 4 days of observations). It is thus impossible to save all measurements and some averagings in space and/or frequency have to be performed a priori. One possibility is called seismic holography which aims at propagating the wavefield from the surface to any target point in the interior based on the knowledge of the wave equation satisfied by the wavefield. Here, we analyze this method and propose some possible improvements.

2 Forward model

We suppose that the wavefield satisfies an acoustic wave equation [2]

$$-(\Delta + k^2)\psi - \frac{2i\omega}{\rho^{1/2}c}\rho\mathbf{u} \cdot \nabla \left(\frac{\psi}{\rho^{1/2}c} \right) = s, \quad (2)$$

where ρ and c are the density and sound speed taken from a standard solar model, γ is the attenuation, \mathbf{u} a flow term, and s a stochastic source of excitation. The local wavenumber k is given by

$$k^2 = \frac{(\omega^2 + 2i\omega\gamma) - \omega_c^2}{c^2}, \quad \omega_c^2 = \rho^{1/2}c^2\Delta(\rho^{-1/2}).$$

A radiation boundary condition that takes into account the exponential decay of the density close to the solar surface is used to complement Eq. 2 [3]. The wave equation is solved using high-order finite elements on a mesh adapted to the strong stratification of the Sun [4].

At first order, the perturbation to the cross-covariance with respect to a reference model is linked to perturbations in the background medium via a sensitivity kernel [4]

$$\delta C^\omega(\mathbf{r}_1, \mathbf{r}_2) = \int_V K^\omega(\mathbf{x}; \mathbf{r}_1, \mathbf{r}_2)\delta q(\mathbf{x})d\mathbf{x}, \quad (3)$$

where $q \in \{\rho, c, \gamma, \mathbf{u}\}$. The kernels K can be computed from the knowledge of the Green's function of the wave equation.

Aim: *Averaging the data δC in space and frequency in order to be as sensitive as possible to a scatterer δq at a given location \mathbf{x} in the solar interior.*

3 Seismic holography

Seismic holography is one possibility to average the data. From the knowledge of the wavefield everywhere on the observed surface A of the Sun, one can generate the hologram Φ_α^ω

$$\Phi_\alpha^\omega(\mathbf{x}) = \int_A H_\alpha^\omega(\mathbf{x}, \mathbf{r}')\psi(\mathbf{r}', \omega)d\mathbf{r}', \quad (4)$$

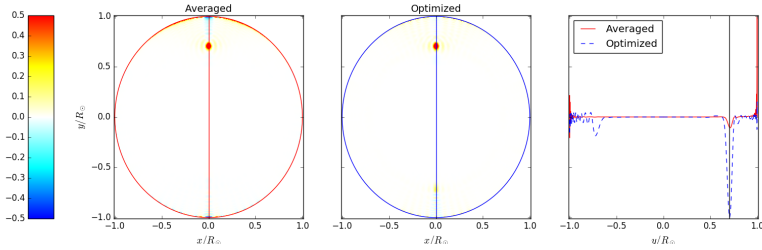


Figure 1: Sound speed sensitivity kernel $\langle \mathcal{K}_{\alpha\beta}^\omega(\mathbf{x}; \mathbf{x}_s, \mathbf{x}_s) \rangle$ for a scatterer located at a depth of $z_s = 0.7R_\odot$ along the polar axis. Left: the frequencies are directly averaged ($W = 1$), middle: optimal averaging obtained by principal component analysis, right: cut of the two kernels along the polar axis.

which aims at estimating the wavefield ψ at a target location \mathbf{x} . H_α^ω is a wave propagator, for example the Green's function associated to a wave equation, but it can be seen as a general weighting of the observations.

Similarly to the cross-covariance of the wavefield, the cross-covariance between two holograms is defined as

$$I_{\alpha\beta}^\omega(\mathbf{x}_1, \mathbf{x}_2) = \Phi_\alpha^{\omega*}(\mathbf{x}_1)\Phi_\beta^\omega(\mathbf{x}_2) = \int_A \int_A H_\alpha^{\omega*}(\mathbf{x}_1, \mathbf{r})H_\beta^\omega(\mathbf{x}_2, \mathbf{r}')C^\omega(\mathbf{r}, \mathbf{r}')d\mathbf{r}d\mathbf{r}'. \quad (5)$$

The measurement $I_{\alpha\beta}$ is thus an averaging of all the cross-covariances at the solar surface. Combining Eqs. 3 and 5, one can link the measurement $I_{\alpha\beta}^\omega$ to perturbations δq

$$\delta I_{\alpha\beta}^\omega(\mathbf{x}_1, \mathbf{x}_2) = \int_V \mathcal{K}_{\alpha\beta}^\omega(\mathbf{x}; \mathbf{x}_1, \mathbf{x}_2)\delta q(\mathbf{x})d\mathbf{x}. \quad (6)$$

By choosing properly the wave propagators, one can get sensitive to a physical parameter at a given target location in the solar interior. Ideally the averaging should lead to a kernel \mathcal{K} that is localized close to the target location \mathbf{x} .

4 Optimizing the averaging

Due to convection, the data at one frequency are extremely noisy. One needs to average frequencies using a given weighting $w(\omega)$ such that the averaged measurement is given by

$$\langle \delta I_{\alpha\beta}^\omega(\mathbf{x}_1, \mathbf{x}_2) \rangle = \sum_\omega W(\omega)\delta I_{\alpha\beta}^\omega(\mathbf{x}_1, \mathbf{x}_2). \quad (7)$$

Usually, a constant weighting in some frequency bands is used. This is not optimal as the kernel is oscillating extremely rapidly as a function

of frequency [2]. We use a principal component analysis in order to obtain the most significant averaging in the frequency domain. A representation of a sound speed kernel for constant and optimized weightings is shown in Fig. 1. One can see that the optimized version is more localized close to the target location with a way smaller contribution from the surface. This optimization is promising and will be used to improve the current capabilities of imaging the interior and farside of the Sun. Moreover, it is unclear if the holography weightings given by Eq. 5 are optimal. We will perform a similar analysis to determine the most significant averaging of the data in space depending on the type of scatterers.

References

- [1] T. L. Duvall, S. M. Jefferies, J. W. Harvey, and M. A. Pomerantz, Time-distance helioseismology *Nature*, **362** (1993), pp. 430–432.
- [2] L. Gizon, D. Fournier, D. Yang, A. C. Birch, and H. Barucq, Signal and noise in helioseismic holography, *A&A* **620** (2018), A136.
- [3] H. Barucq, J. Chabassier, M. Duruflé, L. Gizon, and M. Leguèbe, Atmospheric radiation boundary conditions for the Helmholtz equation. *M2AN*, **52** (3) (2018), pp. 945–964.
- [4] L. Gizon et al., Computational helioseismology in the frequency domain: acoustic waves in axisymmetric solar models with flows, *A&A*, **600** (2017), A35.

Low-rank representation of omnidirectional subsurface extended image volumes

Mengmeng Yang¹, Marie Graff^{2,*}, Rajiv Kumar³, and Felix J. Herrmann^{1,4}

¹School of Earth and Atmospheric Sciences, Georgia Institute of Technology, Atlanta GA, USA

²Department of Mathematics, University of Auckland, Auckland, New Zealand

³DownUnder GeoSolutions, Perth, Australia

⁴School of Computational Science and Engineering, Georgia Institute of Technology, Atlanta GA, USA

*Email: marie.graff@auckland.ac.nz, earlier known as Marie Kray

Abstract

We propose a low-rank representation of full subsurface extended image volumes, which are usually described as large dense matrices. Our approach proves to be cost-effective in the computation without explicitly calculating the adjoint wavefields, since the customary loop over sources is avoided. Moreover, storage issues are overcome thanks to the randomized SVD algorithm and probing techniques involved in the computation. Then, information of the extended image volume can be extracted using simple linear algebra tools. We illustrate the efficiency of our approach through a numerical example from seismic imaging.

Keywords: image volume, randomized SVD, low-rank factorization, seismic exploration

1 Introduction

In seismic exploration, extended image volumes (EIVs) are tools to image reflections from a coarse or blurred background velocity model of the Earth's underground, with applications in detecting deposits such as gas, oil or salt [3]. They can be defined as a cross-correlation of the forward and adjoint wavefields for non-zero space offsets, i.e.

$$\mathbf{E} = \mathbf{V}\mathbf{U}^*, \quad (1)$$

where the forward field \mathbf{U} and the adjoint field \mathbf{V} satisfy

$$\mathbf{H}(\mathbf{m})\mathbf{U} = \mathbf{P}_s^\top \mathbf{Q}, \text{ and } \mathbf{H}^*(\mathbf{m})\mathbf{V} = \mathbf{P}_r^\top \mathbf{D},$$

with \mathbf{H} the modeling operator, e.g. the monochromatic Helmholtz equation, \mathbf{m} the blurred velocity model, \mathbf{P}_s (resp. \mathbf{P}_r) the projector on the sources (resp. receivers) locations, and \mathbf{Q} and \mathbf{D} the sources and data matrices. As a result, the EIV is represented as a square matrix, which contains all available information by extracting: e.g. the reverse time migration (RTM)

image in the diagonal or the common-image point (CIP) gathers in columns. As they are quadratic and because of redundant information due to the subsurface offsets, EIVs are usually huge and dense, which makes them impossible to compute and store for real-life applications in seismic exploration.

2 Low-rank form of EIV

In [4] a cost-effective approach is proposed via probing techniques with canonical vectors and matrix-free operations to build the EIV. Whereas a single canonical vector is enough to extract a column containing CIP gathers, it is more expensive to investigate other parts of the EIV, like the diagonal to get the RTM for instance. Moreover, it is not feasible to store the resulting quadratic matrix. Therefore, each new extracted information requires to rebuild the EIV, and each computation means to solve two PDEs for each of the n_s sources, i.e. $2n_s$ PDE-solves.

As seismic data exhibits low-rank structure, [2] recently combined probing techniques with the randomized SVD algorithm [1] to judiciously deliver a storable low-rank representation of the EIV. Let r denote the estimated rank of the EIV. Using randomized SVD allows us to compute the low-rank form of the EIV in only $2r$ PDE-solves and store two $N \times r$ matrices, where N is the number of grid points, such that $r \leq n_s \ll N$ and originally the EIV is a $N \times N$ matrix of maximal rank n_s .

Algorithm 1:

Low-rank SVD algorithm [1] for EIV

1. $\mathbf{X} = \mathbf{E}^* \mathbf{W}$, here, \mathbf{W} is $(N \times r)$ Gaussian random matrix for probing
2. $[\mathbf{G}, \mathbf{R}] = \text{qr}(\mathbf{X})$
3. $\mathbf{B} = \mathbf{E} \mathbf{G} \in \mathbb{C}^{N \times r}$
4. $[\mathbf{Y}, \mathbf{S}, \mathbf{Z}] = \text{svd}(\mathbf{B})$, where svd computes the top r singular vectors of \mathbf{B}
5. $\mathbf{Z} \leftarrow \mathbf{Z} \mathbf{G}$
6. $\mathbf{L} = \mathbf{Y} \sqrt{\mathbf{S}}$ and $\mathbf{R} = \mathbf{Z} \sqrt{\mathbf{S}}$
7. $\mathbf{E} = \mathbf{L} \mathbf{R}^*$, here \mathbf{L}, \mathbf{R} are $(N \times r)$ matrices

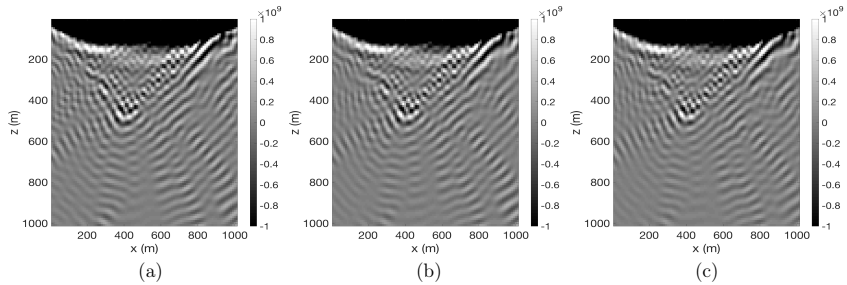


Figure 1: Diagonal extraction aka RTM image. (a) From full EIV (1). (b) Using only 15 significant singular values in the standard SVD of \mathbf{E} , energy kept at 94.4%. (c) With 15 probing vectors in Alg. 1, then using in (2) for the low-rank form \mathbf{LR}^* , energy kept at 93.5%.

3 Information extraction

The randomized SVD algorithm applied for EIV allows us to compute the thin ($N \times r$) matrices \mathbf{L} and \mathbf{R} such that $\mathbf{E} = \mathbf{LR}^*$, which we can store and use to extract elements of the EIV. For instance, to access to the RTM image, we would want to extract the main diagonal of \mathbf{E} . To do so, we consider the following formula coming from linear algebra: for \mathbf{L}_k , resp. \mathbf{R}_k , denoting the k -th column of \mathbf{L} , resp. \mathbf{R} , we get:

$$\text{diag}(\mathbf{E}) = \sum_{k=1}^r \mathbf{L}_k \odot \bar{\mathbf{R}}_k, \quad (2)$$

Clearly, we do not need to recompute the full EIV to extract its diagonal. Similarly, we can use a permutation matrix \mathbf{P} , to extract off-diagonals of the EIV, yielding information about nonzero-offsets, inaccessible to until now.

4 Numerical results

To illustrate the efficiency of our approach, we consider a $1\text{km} \times 1\text{km}$ profile \mathbf{m} extracted from the Marmousi model, with $N = 101^2 = 10201$ grid points, receivers and sources at each surface points, i.e. $n_s = 101$. For a fixed frequency, $\nu = 25\text{Hz}$, we compute the full EIV \mathbf{E} , available for this small example and we compare with the low-rank form \mathbf{LR}^* . In Fig. 1, we show the RTM image extracted from the full \mathbf{E} (left), from the 15 more significant singular values in the SVD of \mathbf{E} (middle), and when using eq. (2) on \mathbf{L} and \mathbf{R} for only $r = 15$ probing vectors (right). The resulting relative error is less than 7% for only $2r$ solutions of the Helmholtz equation.

5 Discussion

While impossible to build otherwise in the requirements specification of the geophysics society, we use a matrix-free algorithm to compute and store a low-rank representation of the EIV. This representation also allows us to consider model changes without recomputing the EIV thanks to an invariance formulation [2]. An extension to the time-domain is also in progress.

References

- [1] N. Halko, P.-G. Martinsson and J. A. Tropp, Finding structure with randomness: Probabilistic algorithms for constructing approximate matrix decompositions, *SIAM review* **53** (2011), pp. 217–288.
- [2] R. Kumar, M. Graff-Kray, T. van Leeuwen and F. J. Herrmann, Low-rank representation of extended image volumes: Applications to imaging and velocity continuation, in *SEG Technical Program Expanded Abstracts, Anaheim CA, USA, 18 October 2018*, pp. 4418–4422.
- [3] P. Sava and I. Vasconcelos, Extended imaging conditions for wave-equation migration, *Geophysical Prospecting* **59** (2011), pp. 35–55.
- [4] T. van Leeuwen, R. Kumar and F. J. Herrmann, Enabling affordable omnidirectional subsurface extended image volumes via probing, *Geophysical Prospecting* **65** (2017), pp. 385–406.

Excitation and Propagation of Whispering Gallery Waves in a Vicinity of Curvilinear Isobath in Shallow Water

Boris Katsnelson^{1,*}, Pavel Petrov²

¹Dr. Moses Strauss Department of Marine Geosciences, University of Haifa, Haifa, Israel

²Laboratory of Geophysical Hydrodynamics, V.I. Il'ichev Pacific Oceanological Institute, Vladivostok, Russia

*Email: bkat snels@univ.haifa.ac.il

Abstract

In the paper sound signals propagation in shallow water area with varying bathymetry which could be part of an underwater canyon, bay, a lagoon or a lake with bowl-like bottom relief is studied. It is shown that whispering gallery waves localized near curvilinear isobaths exist.

Keywords: whispering gallery waves, shallow-water acoustics

1 Introduction

In the paper sound propagation in a shallow-water waveguide with rotational symmetry is considered (Fig. 1). It is characterized by curvilinear (in particular circular) isobaths with the water depth increasing toward their center of curvature (i.e., toward the deeper part of bowl-like bottom). Let us consider a waveguide with

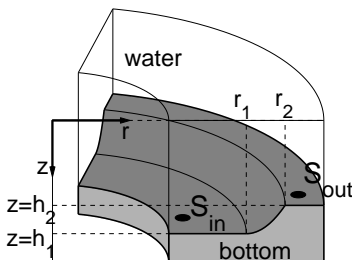


Figure 1: Shallow-water waveguide with bowl-like bottom (no vertical walls are present).

variable water depth:

$$h(r) = \begin{cases} h_1, & \text{if } r \leq r_1, \\ h_2, & \text{if } r \geq r_2. \end{cases} \quad (1)$$

and with some transitional segment $r_1 < r < r_2$. If $r_1 = r_2$ then we have step-like bathymetry.

The question we study is the possibility of formation of waves localized near circular isobaths [1], in other words whispering gallery waves (WG waves).

2 Mathematical formulation

Amplitude of the sound field $P(x, y, z)$ with the constant frequency is found in the form of decomposition over adiabatic vertical modes [2]

$$P(x, y, z) = \sum_{j=1}^{N_m} A_j(r, \theta) \phi_j(r, z), \quad (2)$$

where local (adiabatic) eigenfunctions $\phi_j(r, z)$ and the corresponding horizontal wavenumbers $q_j(r)$ can be found via solution of the Sturm-Liouville problem for each value of r [2]. Amplitudes $A_j = A_j(r, \theta)$ depending on mode number and the source frequency describe distribution of acoustic intensity in the horizontal plane and satisfy the following equation

$$\frac{1}{r} \frac{\partial}{\partial r} \left(r \frac{\partial A_j}{\partial r} \right) + \frac{1}{r^2} \frac{\partial^2 A_j}{\partial \theta^2} + q_j^2 A_j = 0. \quad (3)$$

Amplitudes $A_j(r, \theta)$ can be found in turn as a decomposition over radial modes $R_\nu(r)$

$$A_j = \sum R_{j\nu}(r) \psi_{j\nu}(\theta). \quad (4)$$

In our study a spectral problem for the radial modes $R_\nu(r)$ in the horizontal plane is obtained and studied (ν is the spectral parameter). Its solutions corresponding to WG waves can be computed by the WKB method, and the respective solutions $\nu, R_{j\nu}(r)$ are called WG modes [1].

3 Some examples

Certain radial modes with large values of the spectral parameter $\nu \sim 2500$ have specific shape with maximum in area of boundary/transition segment and correspond to the WG modes. In the Fig. 2 these modes $R_\nu(r)$ (hereafter we consider $j = 4$) are shown for step-like bathymetry

where $r_1 = r_2 = 6$ km, $h_1 = 24$ m, $h_2 = 26$ m. In this case they are expressed in terms of the Bessel functions. Note that radial modes in the Fig. 2 have only outgoing waves in area $r > r_2$, and they can be excited by the source located in the deeper part $r < r_2$ of the waveguide (S_{in} in Fig. 1). At the same time, all WG modes are

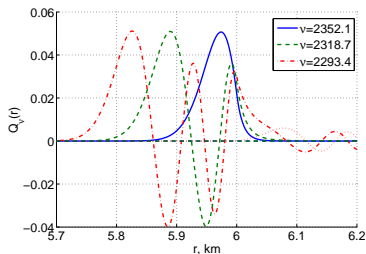


Figure 2: Radial modes localized in the vicinity of the boundary $r = r_2 = 6$ km between two areas of constant depth.

leaking (see Fig. 3), as there is no total internal reflection at a curvilinear boundary (if this situation is considered in the framework of horizontal rays and vertical modes). This corresponds to the fact that the spectral parameter ν always has a nonzero imaginary part. It can be shown however that for WG modes $\Im(\nu) \ll \Re(\nu)$.

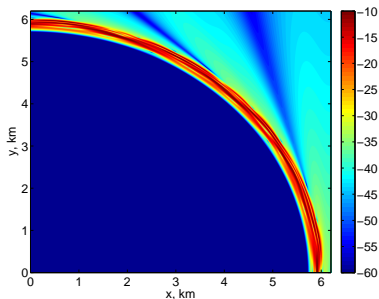


Figure 3: Sound field due to a point source located in the deeper part (S_{in}).

A rather interesting phenomenon for the considered waveguide is the possibility of excitation of WGM by the source located in the area of smaller depth $r > r_2$ (source S_{out} in the Fig. 1). It means that we can find radial modes $R_\nu(r)$,

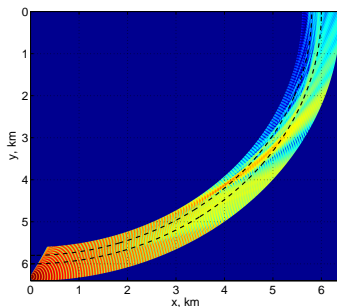


Figure 4: Sound field in the horizontal plane excited by the source S_{out} (computed by solving paraxial equation in a ring-like area).

that contain outgoing and incoming waves in the area $r > r_2$. Excitation of WG modes by the source located in the shallower part of the waveguide in Fig. 1 corresponds to the so called tunnel effect in quantum mechanics. In Fig. 4 the distribution of the sound field for this case is shown in the horizontal plane at $z = 10$ m (the point source is located at $r_s = 6.2$ km, while $r_2 = 6$ km). This distribution was obtained from the numerical solution of mode parabolic equations that can be derived from Eq. (3) in a standard way.

Acknowledgments

Work was supported by Israel Science Foundation grant No. 565/15 and the Russian Foundation for Basic Research under the contract No. 18-05-00057_a.

References

- [1] B. Katsnelson and P. Petrov, Whispering gallery waves localized near circular isobaths in shallow water, to appear in *J. Acoust. Soc. Am.*.
- [2] B. Katsnelson, V. Petnikov and J. Lynch, *Fundamentals of shallow water acoustics*, Springer, New York et al, 2012.

Implicit-explicit scheme for the elastodynamic wave equation in plates

Sonia Fliss¹, Alexandre Imperiale², Sébastien Imperiale³, Hajer Methenni^{1,2,*}

¹POEMS (CNRS-INRIA-ENSTA Paristech), Université Paris-Saclay, Palaiseau, France

²DISC, CEA-LIST, Gif-sur-Yvette, France

³INRIA — LMS (École polytechnique-CNRS), Université Paris-Saclay, Palaiseau, France

*Email: hajer.methenni@ensta-paristech.fr

Abstract

Our objective is to provide an efficient simulation tool for the propagation of elastic waves in thin plates in the context of Guided Waves based Structural Health Monitoring. A naive discretization procedure based on a Leap-frog explicit scheme can be really costly because of the small thickness of the plate. By treating implicitly the operators corresponding to derivatives through the thickness, we show by a stability analysis that the time step is less restricted by the space discretization along the thickness. The price to pay is to solve at each iteration small independent linear systems, but this strategy offers an accurate and efficient discretization of the elastic fields in all dimensions.

Keywords: Elastodynamics, Time discretization, Plate models.

1 Setting of the problem

We consider the solution, for $t > 0$, $\mathbf{u}^\delta(t) \in V \equiv H^1(\Omega^\delta)^3$ of the elastodynamic equations

$$\begin{cases} \rho \partial_t^2 \mathbf{u}^\delta - \operatorname{div} \mathbf{C} \varepsilon(\mathbf{u}^\delta) = 0 & \text{in } \Omega^\delta, \\ \mathbf{C} \varepsilon(\mathbf{u}^\delta) \mathbf{n} = \mathbf{g}^\delta & \text{on } \partial\Omega^\delta, \end{cases} \quad (1)$$

where $\Omega^\delta = \Sigma \times [-\delta, \delta]$ is a plate ($\Sigma \subset \mathbb{R}^2$) with δ , the dimensionless thickness, being a small parameter, ρ is the density, \mathbf{C} the elasticity tensor and $\varepsilon(\cdot)$ the symmetrised gradient tensor. The problem is completed with vanishing initial conditions. The term \mathbf{g}^δ , the transverse loading imposed by a thin piezoelectric patch located on the upper face of the plate, is so that

$$\operatorname{supp} \mathbf{g}^\delta \subset \Sigma \times \{\delta\}, \quad \mathbf{g}^\delta = \delta (g_1, g_2, 0)^t.$$

The term \mathbf{g}^δ is scaled by δ in order to obtain bounded solutions when δ goes to 0.

Of course, this method can be used for any other source term.

2 A rescaled problem

We introduce the rescaled displacement $\hat{\mathbf{u}}^\delta$

$$\hat{\mathbf{u}}^\delta(x_1, x_2, x_3, t) = \mathbf{u}^\delta(x_1, x_2, \delta x_3, t) \quad \text{in } \Omega$$

with $\Omega = \Sigma \times [-1, 1]$. We also introduce the following operators

$$\varepsilon_3(\mathbf{v}) = \frac{1}{2} \begin{pmatrix} 0 & 0 & \partial_3 v_1 \\ 0 & 0 & \partial_3 v_2 \\ \partial_3 v_1 & \partial_3 v_2 & 2\partial_3 v_3 \end{pmatrix},$$

and $\varepsilon_\tau(\mathbf{v}) = \varepsilon(\mathbf{v}) - \varepsilon_3(\mathbf{v})$. From Problem (1) and the notation introduced above one can deduce the following variational formulation: for all $\mathbf{v} \in V$ find $\hat{\mathbf{u}}^\delta(t) \in V$ such that

$$\frac{d^2}{dt^2} m(\hat{\mathbf{u}}^\delta(t), \mathbf{v}) + a^\delta(\hat{\mathbf{u}}^\delta(t), \mathbf{v}) = \ell(\mathbf{v}),$$

where $m(\cdot, \cdot) = \rho(\cdot, \cdot)$, (\cdot, \cdot) being the $L^2(\Omega)^3$ -scalar product. The bilinear form a^δ is defined by

$$a^\delta(\mathbf{u}, \mathbf{v}) = a_\tau(\mathbf{u}, \mathbf{v}) + \delta^{-1} a_m(\mathbf{u}, \mathbf{v}) + \delta^{-2} a_3(\mathbf{u}, \mathbf{v})$$

where a_τ stands for the bilinear form involving only in-plane differential operators, a_3 only in the thickness direction and a_m involves differential operators of mixed type: for $q \in \{\tau, 3\}$

$$a_q(\mathbf{u}, \mathbf{v}) = (\mathbf{C} \varepsilon_q(\mathbf{u}), \varepsilon_q(\mathbf{v})),$$

$$a_m(\mathbf{u}, \mathbf{v}) = (\mathbf{C} \varepsilon_\tau(\mathbf{u}), \varepsilon_3(\mathbf{v})) + (\mathbf{C} \varepsilon_3(\mathbf{u}), \varepsilon_\tau(\mathbf{v})).$$

Finally ℓ is a linear form given by

$$\ell(\mathbf{v}) = \int_{\Sigma \times \{1\}} (g_1, g_2, 0)^t \cdot \mathbf{v} \, d\gamma.$$

3 A standard discretization method

We consider first a standard discretization procedure by conforming finite elements and centered explicit finite difference in time (with time step Δt). Let V_h be finite dimensional subspaces of V . It is constructed using high order spectral finite elements with mass-lumping on an extruded mesh (see [2]), i.e., the mesh along the thickness is obtained by extrusion, with step size, ηh ($\eta > 0$) of a quasi-uniform subdivision of size h of Σ .

For $n \in \mathbb{N}$, we look for $\mathbf{u}_h^n \sim \hat{\mathbf{u}}^\delta(n\Delta t)$ solution of, for all $\mathbf{v}_h \in V_h$,

$$m_h \left(\frac{\mathbf{u}_h^{n+1} - 2\mathbf{u}_h^n + \mathbf{u}_h^{n-1}}{\Delta t^2}, \mathbf{v}_h \right) + a^\delta(\mathbf{u}_h^n, \mathbf{v}_h) = \ell(\mathbf{v}_h),$$

where we assume that m_h is an approximation of m using mass lumping techniques (yielding a diagonal mass matrix). The stability condition for this scheme is well-known

$$\Delta t^2 \leq 4 \left(\sup_{\mathbf{v}_h \in V} \frac{a^\delta(\mathbf{v}_h, \mathbf{v}_h)}{m_h(\mathbf{v}_h, \mathbf{v}_h)} \right)^{-1}.$$

In practice such condition depends on δ , indeed we can prove the following estimation

$$\Delta t^2 \lesssim h^2(1 + \delta^{-2}\eta^{-2})^{-1}. \quad (2)$$

One can see that choosing $\eta \sim \delta^{-1}$, i.e., a very coarse discretization along the thickness, would provide a satisfactory stability condition, however this is not always possible for at least two reasons: *i*) if one wants to construct reference solutions; *ii*) if the medium is varying (typically stratified) along the thickness. In these cases, (2) is severely penalising the computations.

4 An implicit-explicit method

Our objective is to obtain a numerical scheme for which the CFL condition is less restricted by δ . In [1], a θ -scheme is used locally on penalizing finite elements while in our case the θ -scheme is used only on the penalising part of the bilinear form a^δ , namely $\delta^{-2}a_3$. This gives

$$m_h \left(\frac{\mathbf{u}_h^{n+1} - 2\mathbf{u}_h^n + \mathbf{u}_h^{n-1}}{\Delta t^2}, \mathbf{v}_h \right) + a_\tau(\mathbf{u}_h^n, \mathbf{v}_h) + \delta^{-1}a_m(\mathbf{u}_h^n, \mathbf{v}_h) + \delta^{-2}a_3(\{\mathbf{u}_h^n\}_\theta, \mathbf{v}_h) = \ell(\mathbf{v}_h),$$

where $\{\mathbf{u}_h^n\}_\theta = \theta\mathbf{u}_h^{n+1} + (1-2\theta)\mathbf{u}_h^n + \theta\mathbf{u}_h^{n-1}$. The stability condition now reads, for all $\mathbf{v}_h \in V_h$,

$$m_h(\mathbf{v}_h, \mathbf{v}_h) - \frac{\Delta t^2}{4}(a_\tau + \delta^{-1}a_m)(\mathbf{v}_h, \mathbf{v}_h) + \delta^{-2} \frac{(4\theta - 1)\Delta t^2}{4}a_3(\mathbf{v}_h, \mathbf{v}_h) \geq 0.$$

If $\theta = 1/4$ then, our estimation shows that Δt^2 should be bounded by $O(h^2(1 + \delta^{-1}\eta^{-1})^{-1})$ which is already an improvement compared to (2). The bound obtained just above can be improved, by

considering $\theta > 1/4$. Indeed, for an homogeneous isotropic medium, one can show that the stability condition becomes

$$\Delta t^2 \leq 4 \left(1 + \frac{1}{4\theta - 1} \right)^{-1} \sup_{\mathbf{v}_h \in V} \left(\frac{a_\tau(\mathbf{v}_h, \mathbf{v}_h)}{m_h(\mathbf{v}_h, \mathbf{v}_h)} \right)^{-1},$$

and is independent of δ .

5 Numerical aspects

At each iteration, one needs to solve a linear system which is decoupled into several small linear systems (that can be solved efficiently in parallel) for each interpolation point on Σ . This property holds because we consider a structured mesh and since the bilinear form a_3 depends only on ∂_3 . See Figure 1 where $\theta = 1/2$.

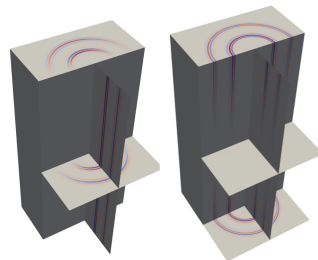


Figure 1: The x_1 and x_3 components of the displacement field in a rescaled plate.

This method can be used to compute reference solutions and verify the validity of asymptotic models such as Reissner–Mindlin model and some extensions [3] (since there exists no rigorous justifications for elastodynamic problems). Finally under some conditions on the mesh, our approach can be extended to plates with a smoothly varying thickness.

References

- [1] T. Rylander and A. Bondeson, *Stability of Explicit-Implicit Hybrid Time-Stepping Schemes for Maxwell's Equations*, *J. Comput. Phys.*, **179** (2002), pp. 426–438.
- [2] G. Cohen and P. Grob, *Mixed Higher Order Spectral Finite Elements for Reissner-Mindlin Equations in the Time Domain*, *SIAM J. Sci. Comput.*, **29** (2007), pp. 986–1005.
- [3] D. Chapelle and K.-J. Bathe, *The Finite Element Analysis of Shells - Fundamentals*, 2nd edition, Springer, 2011.

Semi-implicit time discretisation of incompressible elastodynamic equations

Federica Caforio¹, Sébastien Imperiale^{2,*}¹Computational Cardiology Laboratory, Institute of Biophysics, Medical University of Graz,

Inria & LMS, Ecole polytechnique, CNRS, Université Paris-Saclay

²Inria & LMS, Ecole polytechnique, CNRS, Université Paris-Saclay

*Email: sebastien.imperiale@inria.fr

Abstract

The principal aim of this work is to provide an adapted numerical scheme for the approximation of elastic wave propagation in nearly-incompressible solids. The simulation in such media is computationally intensive due to the severe stability condition that is imposed on the time step of explicit methods. We construct an implicit/explicit, second-order time discretisation, that, by using penalisation techniques, provides an efficient way to deal with incompressibility: at the price of solving at each time step a scalar Poisson problem (that can be performed by various, efficient algorithms), the time step restriction is independent of the incompressibility parameters.

Keywords: Elastodynamic equations, Time discretisation, Incompressibility

1 Statement of the problem

In the context of wave propagation in soft tissues (such as transient elastographic waves in living tissues), we look for the solution of the nearly-incompressible elastodynamic equation

$$\partial_t^2 \underline{y}_\lambda - \operatorname{div} \underline{\underline{C}} \underline{\underline{\varepsilon}}(\underline{y}_\lambda) - \lambda \nabla \operatorname{div} \underline{y}_\lambda = \underline{f} \quad (\Omega \times [0, T]),$$

where $\underline{y}_\lambda \in \mathcal{X} = H_0^1(\Omega)^d$ is the elastic displacement, $\underline{\underline{\varepsilon}}$ the symmetrised gradient, $\underline{\underline{C}}(\underline{x})$ a fourth-order elasticity tensor that accounts for heterogeneities and anisotropy (e.g. in fibered tissues such as muscles) and λ , the first Lamé parameter, is very large (i.e. $\lambda \gg \|\underline{\underline{C}}\|$). The problem is completed with vanishing initial conditions and we assume \underline{f} smooth.

2 A fully explicit scheme

We consider a finite-dimensional subspace of \mathcal{X} , denoted \mathcal{X}_h , and a scalar product $(\cdot, \cdot)_h$ that induces in \mathcal{X}_h a norm equivalent to the norm in $\mathcal{H} = L^2(\Omega)^d$. This scalar product accounts for quadrature formulae that are typically used for mass lumping. We set, for \underline{v}_h and \underline{w}_h in \mathcal{X}_h ,

$$(A_h \underline{v}_h, \underline{w}_h)_h = (\underline{\underline{C}}(\underline{\underline{\varepsilon}}(\underline{v}_h)), \underline{\underline{\varepsilon}}(\underline{w}_h))_{\mathcal{H}}.$$

Moreover, we define \mathcal{L} as the space of functions in $L^2(\Omega)$ with zero average and

$$(D_h \underline{v}_h, \underline{w}_h)_h = (\operatorname{div} \underline{v}_h, \operatorname{div} \underline{w}_h)_{\mathcal{L}}.$$

A straightforward space-time discretisation of our problem yields the scheme

$$[[\underline{y}_{\lambda,h}^n]] + A_h \underline{y}_{\lambda,h}^n + \lambda D_h \underline{y}_{\lambda,h}^n = \underline{f}_h^n, \quad (\text{NI})$$

where $[[z_h^n]] = (z_h^{n+1} - 2z_h^n + z_h^{n-1})/\Delta t^2$. Although fully explicit, this scheme is highly penalised by the CFL condition: if Lagrangian finite elements are used on subdivisions of Ω of size h , then one has $\Delta t \lesssim h \lambda^{-\frac{1}{2}}$. Of course, an implicit discretisation (a so-called theta scheme) would solve this problem but, in that case, a linear system on the DOFs representing the displacement field must be solved at each iteration.

3 The pure incompressible formulation

Since it is not efficient to use (NI) in practice, an alternative is to consider the limit equations for $\lambda \rightarrow +\infty$:

$$\partial_t^2 \underline{y} - \operatorname{div} \underline{\underline{C}} \underline{\underline{\varepsilon}}(\underline{y}) - \nabla p = \underline{f}, \quad \operatorname{div} \underline{y} = 0. \quad (1)$$

It can be proved that $\sup_t \|\underline{y}_\lambda - \underline{y}\|_{\mathcal{X}} \lesssim \lambda^{-1}$. The discretisation of (1) requires further notation and, in particular, we introduce a factorisation of the operator D_h . Let $\mathcal{M}_h \subset (\mathcal{L} \cap H^1(\Omega))$ be a family of finite-dimensional spaces. Following [3], we introduce the space $\mathcal{Y}_h = \nabla \mathcal{M}_h + \mathcal{X}_h \subset \mathcal{H}$ and the discrete divergence operator $C_h : \mathcal{Y}_h \rightarrow \mathcal{M}_h$ such that, for all $q_h \in \mathcal{M}_h$ and $w_h \in \mathcal{Y}_h$,

$$(C_h w_h, q_h)_{\mathcal{L}} := (w_h, C_h^T q_h)_{\mathcal{L}} := -(\nabla q_h, w_h)_{\mathcal{H}}.$$

Then, we define the embedding $i_h = \mathcal{X}_h \rightarrow \mathcal{Y}_h$ and its transpose, for all $\underline{v}_h \in \mathcal{X}_h$ and $\underline{w}_h \in \mathcal{Y}_h$,

$$(\underline{v}_h, i_h^T \underline{w}_h)_{\mathcal{H}} := (i_h \underline{v}_h, \underline{w}_h)_{\mathcal{H}} := (\underline{v}_h, \underline{w}_h)_{\mathcal{H}}.$$

Finally, we define another discrete divergence operator $B_h = C_h i_h$, and a discrete gradient operator $B_h^T = i_h^T C_h^T$. One can show that

$$D_h = B_h^T B_h = i_h^T C_h^T C_h i_h.$$

As a consequence, from Eq. (1) we deduce the following scheme: we look for $\underline{y}_h^n \in \mathcal{X}_h$ and $p_h^n \in \mathcal{M}_h$ solution of

$$[[\underline{y}_h^n]] + A_h \underline{y}_h^n + B_h^T p_h^n = \underline{f}_h^n, \quad B_h \underline{y}_h^n = 0. \quad (I)$$

The stability condition of (I) only depends on A_h . Moreover, at each iteration, one has to solve

$$B_h B_h^T p_h^n = B_h \underline{f}_h^n - B_h A_h \underline{y}_h^n$$

and, if an adequate inf-sup condition holds (e.g. \mathcal{M}_h should not be too large), then a unique solution exists. Scheme (I) is preferable compared to fully implicit schemes, since only a scalar field has to be recovered at each iteration. However, the operator $B_h B_h^T$ does not correspond to the standard Laplace operator that would be $C_h C_h^T$. In practice, this represents a crucial gain since fast methods [2] can be employed to solve the Laplace problem.

4 A penalised formulation

Our main contribution presented during the talk is described in what follows. Starting from (1), we consider the equation

$$\partial_t^2 \underline{y}_\alpha - \operatorname{div} \underline{C} \underline{\varepsilon}(\underline{y}_\alpha) - \nabla p_\alpha = \underline{f}, \quad \operatorname{div} \underline{y}_\alpha = -\alpha \Delta p_\alpha.$$

We can prove that $\sup_t \|\underline{y}_\alpha - \underline{y}\|_{\mathcal{X}} \lesssim \alpha^{\frac{1}{2}}$ and, under some assumptions on the properties of the operator $\operatorname{div} \underline{C} \underline{\varepsilon}$, we also show that

$$\|\underline{y}_\alpha - \underline{y}\|_{L^2(0,T;\mathcal{X})} \lesssim \alpha. \quad (2)$$

Hence, for small α , \underline{y}_α is an accurate approximation of \underline{y} , that is itself an accurate approximation of \underline{y}_λ . Then, we propose the following, rather straightforward, fully discrete scheme

$$\begin{cases} [[\underline{y}_{\alpha,h}^n]] + A_h \underline{y}_{\alpha,h}^n + B_h^T p_{\alpha,h}^n = \underline{f}_h^n, \\ B_h \underline{y}_{\alpha,h}^n = \alpha \Delta t^2 C_h C_h^T p_{\alpha,h}^n. \end{cases} \quad (P)$$

Note that we have replaced α by $\alpha \Delta t^2$. We have proved that the stability condition for (P) only depends on A_h , and that $\underline{y}_{\alpha,h}^n - \underline{y}_h^n$ goes to zero in the L^2 norm as Δt^2 for α fixed (see Fig. 1).

	(NI)	(I)	(P)
System to solve	—	$B_h B_h^T$	$C_h C_h^T$
$\Delta t^2 \leq$	$\frac{4}{\ A_h + \lambda B_h B_h^T\ }$	$\frac{4}{\ A_h\ }$	$\frac{4\alpha - 1}{\alpha \ A_h\ }$

Table 1: Main properties of the schemes

At each iteration one can compute $p_{\alpha,h}^n$ by inverting $C_h C_h^T$ using fast solvers for scalar Laplace equation (such as the one we have developed in [2]).

5 Numerical convergence analysis

Although we wish to solve the nearly incompressible problem, we performed a space-time convergence analysis of $\underline{y}_{\alpha,h}^n - \underline{y}_h^n$ on a rather difficult case: we considered a heterogeneous (linearly varying from top to bottom) transversely isotropic medium representing a fibered tissue. We used 7^h order spectral finite element on quadrangles for \mathcal{X}_h and 6^h order finite elements for \mathcal{M}_h . We fixed $\alpha = 1/3$, chose $\Delta t \simeq \|A_h\|^{-\frac{1}{2}}$, h and let h go to zero (hence Δt goes to 0 as well). We observed the expected behaviour: second-order convergence in Δt and a small loss of convergence in the H^1 -norm when the wave hits the boundary (as for Stokes problems – see [3] – boundary layers are expected).

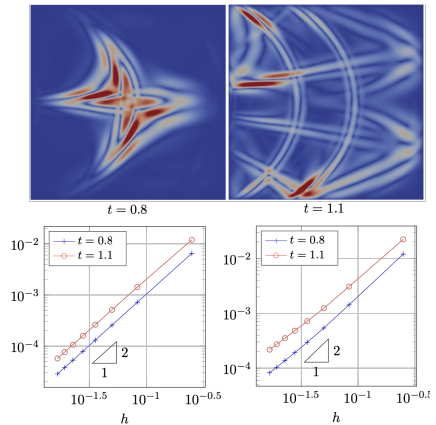


Figure 1: Top: Elastic wave propagation (absolute value) in a heterogeneous transversely isotropic medium. Bottom: $\sup_{s \in [0,t]} \|\underline{y}_\alpha - \underline{y}\|_{\mathcal{V}}$, $\mathcal{V} = \mathcal{H}$ (left) and $\mathcal{V} = \mathcal{X}$ (right).

References

- [1] F. Caforio, S. Imperiale, A conservative penalisation strategy for the semi-implicit time discretisation of incompressible elastodynamics equation, AMSES, (2018).
- [2] F. Caforio, S. Imperiale, High-order discrete Fourier transform for the solution of the Poisson equation, Under review.
- [3] J.L. Guermond, L. Quartapelle. On the approximation of the unsteady Navier-Stokes equations by finite element projection methods, Num. Math, (1998).

High-order locally implicit time schemes

Hélène Barucq¹, Marc Duruflé², Mamadou N'Diaye^{1,3,*}¹Magique-3D INRIA Bordeaux Sud-Ouest, E2S UPPA, CNRS, Pau, France²Magique-3D INRIA Bordeaux Sud-Ouest, IMB, Bordeaux, France³Department of Energy Resources Engineering, Stanford University, California, USA

*Email: mndiaye@stanford.edu

Abstract

Locally implicit time discretizations can be of great interest for accurate simulations of wave propagation in complex media like Earth subsurface. They allow to use unconditionally stable schemes in the regions of computational domain covered by small cells and explicit schemes in the remaining. The receivable values of the time step are then increased which reduces the computational costs while limiting the dispersion effects. In this work, we propose to combine optimized explicit schemes and implicit schemes to form high-order locally implicit schemes for linear ODEs, including in particular wave problems.

Keywords: Acoustic wave, implicit-explicit time schemes, Runge-Kutta (RK) and Padé schemes

1 Introduction

When solving wave equations in a complex geometry, the mesh may contain very small elements. For this reason, explicit schemes may have a highly restrictive stability condition leading to a prohibitive computational time. Using implicit time schemes allow to take a large time step, but the solution of the linear system to be solved in this approach requires a large amount of memory space, especially in 3D. In this talk, we propose high order locally implicit schemes for linear ODEs of the form

$$y'(t) = Ay(t) + F(t), \quad t \in (0, T] \quad (1)$$

where A is a given matrix, coming from a spatial discretization, and F is the source term.

Herein, the development of the locally implicit method shares the same idea as the local time stepping presented in [1]. The mesh used for the spatial discretization is divided into two parts: a coarse region where explicit time stepping is applied, and a refined region where an implicit time scheme is used [2]. For the implicit part, we use either Padé schemes or LSDIRK (Linear-Singly Diagonally Implicit RK)

schemes [3]. Padé schemes are constructed from the Padé approximation of the exponential function while LSDIRK schemes are based on the approximation of the exponential function by a fraction with a unique pole. Therefore, LSDIRK schemes usually require less memory than Padé schemes but are more demanding in computational time. Both Padé and LSDIRK schemes are unconditionally stable, they are available until order 12. For the explicit schemes, we use optimized RK schemes in order to have a large CFL number (stability condition). The optimized RK schemes are constructed, first by defining a typical profile using the spectrum of the operator A in (1), and then compute a stability function that maximize the CFL number for the typical profile as described in [4]. The coupling between these two families of scheme (explicit and implicit) is completed by ensuring the same order of accuracy as the schemes used in the refined or coarse region. Numerical experiments are performed in 2D and 3D for schemes of order 4 and order 8. We used the finite elements C++ code Montjoie. All the details about this work are presented in the PhD dissertation [5].

2 Convergence and numerical results

We consider the acoustic wave equation

$$\begin{cases} \rho \partial_t u - \operatorname{div} v = 0, & \forall (x, t) \in \Omega \times \mathbb{R}^+ \\ \mu^{-1} \partial_t v - \nabla u = 0, & \forall (x, t) \in \Omega \times \mathbb{R}^+ \\ u = f_D, & x \in \Gamma_D \end{cases} \quad (2)$$

To produce the space-time convergence curve equation (2) is solved in $\Omega = [5, 5]^2$ with $\rho = \mu = 1$ using the finite element solver Montjoie. The time step is taken as $\Delta t = \alpha \Delta x$, where α is a constant close to the CFL number of the explicit scheme and Δx is the mesh size which changes with the number N of points taken along the axes. We choose $[0, 200]$ for the time interval. We use a Gaussian source

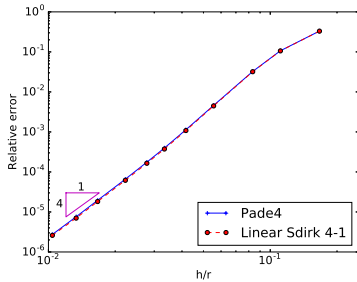


Figure 1: Space-time convergence curves of ERK4-2 combined with Padé4 and LSDIRK4-1. We used Q_3 elements in space.

in space and a Ricker source in time with initial frequency $f_0 = 1$. In Figures 1 and 2 we show the space-time convergence curves of the locally implicit schemes obtained from the optimized explicit schemes combined with Padé and Linear-SDIRK schemes of order 4 and order 8.

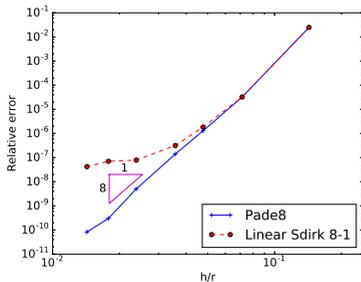


Figure 2: Space-time convergence curves of ERK8-2 combined with Padé8 and LSDIRK8-1. We used Q_7 elements in space.

To evaluate the efficiency, we solve (2) in a 2D Magnetron containing sixteen resonating cavities shown in Figure 3. In Table 1, we present the computational times needed for purely explicit, purely implicit and local implicit schemes of order 4 to reach 0.3% of relative L^2 error computed at $t = 200$ between the numerical solution and a reference solution computed with the eighth order Padé scheme with $\Delta t = 0.01$. As expected, the results show that a locally implicit scheme is a compromise in terms of computational time and memory usage compared to purely explicit and implicit schemes.

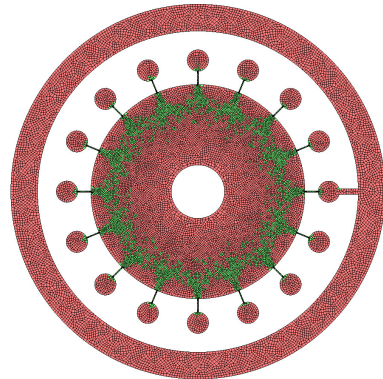


Figure 3: Cavity resonant mesh. Refined region in green, and coarse region in red. ABC is set in the outer circle and Dirichlet condition elsewhere.

Method	Time step	CPU Time	Memory
ERK4-2	$9.09e^{-4}$	8h52min	720 Mo
Local LSDIRK	0.025	54min15s	1.8 Go
LSDIRK	0.04	1h12s	3.2 Go
Local Padé	0.025	39min11s	2.3 Go
Padé	0.033	38min27s	4.8 Go

Table 1: Efficiency of ERK4-2 combined with LSDIRK4-1 and Padé4 (relative error of 0.3%).

References

- [1] M. Mehlin, T. Mitkova and M. Grote, “RK based LTS methods for wave propagation”, *SIAM J. on Scientific Computing*, 2015
- [2] S. Descombes, S. Lanteri and L. Moya, “Locally implicit time integration strategies in a dG method for Maxwell’s equations”, *SIAM J. Scientific Computing*, 2012
- [3] H. Barucq, M. Duruffé and M. N’diaye, “High-order Padé and SDIRK schemes for linear ODEs, application to wave propagation problems.”, *Num. Meth. for Part. Differential Eq.*, 2017
- [4] D. I. Ketcheson and A. J. Ahmadi, “Optimal stability polynomials for numerical integration of initial value problems”, *Comm. in Applied Math. And Comput. Sci.*, 2012
- [5] M. N’diaye, “PhD thesis - On the study and development of high-order time schemes for ODEs”, *Université de Pau et des Pays de l’Adour*, 2017

Efficient Uncertainty Quantification for Wave Propagation in Complex Geometry

Marcus J. Grote¹, Simon Michel^{1,*}¹Department of Mathematics and Computer Science, University of Basel, Switzerland

*Email: simon.michel@unibas.ch

Abstract

Monte Carlo methods are probably the most popular approach in uncertainty quantification to compute expected values of quantities of interest (QoIs). Multilevel Monte Carlo (MLMC) methods significantly reduce the computational cost by distributing the sampling across a mesh hierarchy and restricting most samples to the coarser grids [1]. Geometric constraints, however, may impede uniform coarsening thereby forcing some elements to remain small across all levels. Then, the increasingly stringent CFL stability condition on the time-step on coarser levels effectively nullifies the advantages of the multilevel approach. By adapting the time-step to the locally refined elements on each level, local time-stepping (LTS) methods [2] permit to restore the efficiency of MLMC methods even in the presence of complex geometry without sacrificing the explicitness and inherent parallelism.

Keywords: Multilevel Monte Carlo, local time-stepping, finite elements, mesh adaptivity

1 Introduction

We consider the wave equation with stochastic coefficient in a bounded domain $D \subset \mathbb{R}^d$,

$$\frac{\partial^2}{\partial t^2} u - \nabla \cdot (c^2(\mathbf{x}, \omega) \nabla u) = 0, \quad (1)$$

with appropriate (deterministic) boundary and initial conditions. Here we model the uncertainty in the wave speed $c > 0$ as a time independent random field $c : D \times \Omega \rightarrow \mathbb{R}$, where Ω is the sample space of a complete probability space. To estimate the statistics of some QoI of the solution $u = u(\mathbf{x}, t, \omega)$ [3], or alternatively the expected value of the solution $E[u] := E[u(T)] \in V$ at a fixed time $T > 0$ itself, we now consider MLMC methods.

2 Multilevel Monte Carlo methods

MLMC methods [1] provide a robust, efficient and noninvasive approach by sampling the solution on a sequence of meshes of size $H_\ell = H_0/2^\ell$ and appropriate time steps $\Delta t_\ell \leq CH_\ell$,

$\ell = 0, \dots, L$. Let u_ℓ denote the corresponding FE approximations of u on level ℓ . Then,

$$E[u_L] = E[u_0] + \sum_{\ell=1}^L E[\underbrace{u_\ell - u_{\ell-1}}_{\Delta u_\ell}],$$

which motivates the MLMC estimator of $E[u_L]$,

$$\hat{u}_h^{\text{ML}} := \sum_{\ell=0}^L \frac{1}{N_\ell} \sum_{i=1}^{N_\ell} (\Delta u_\ell(\omega^{(i)})), \quad (2)$$

where N_ℓ is the number of samples $\omega^{(i)}$ computed on level ℓ . The mean square error (MSE),

$$e(\hat{u}_h^{\text{ML}})^2 := E[\|\hat{u}_h^{\text{ML}} - E[u]\|_V^2] \quad (3)$$

splits into total variance and numerical bias:

$$e(\hat{u}_h^{\text{ML}})^2 = \sum_{\ell=0}^L N_\ell^{-1} V_\ell + \|E[u_L - u]\|_V^2, \quad (4)$$

with

$$V_\ell = E[\|\Delta u_\ell\|_V^2] - \|E[\Delta u_\ell]\|_V^2. \quad (5)$$

To bound the MSE by a given tolerance ε , one chooses N_ℓ and L such that both contributions are bounded by $\varepsilon^2/2$ – see e.g. [4].

3 Local time-stepping (LTS)

Due to geometric constraints, it may not be possible to coarsen the entire mesh uniformly. On coarser levels, standard explicit time-stepping schemes then become increasingly inefficient due to the ever more restrictive CFL condition. To overcome this bottleneck, we consider explicit local time-stepping (LTS), which use a larger time step Δt_ℓ in the coarser part and a smaller time-step $\Delta t_\ell/p_\ell$ in the finer part of the mesh with $p_\ell \simeq H_\ell/h_{\min}$ [2].

4 Computational cost

Let C_ℓ denote the computational cost of computing one sample on level ℓ . Then, the total cost of the MLMC estimator is given by

$$C[\hat{u}_h^{\text{ML}}] = \sum_{\ell=0}^L N_\ell C_\ell.$$

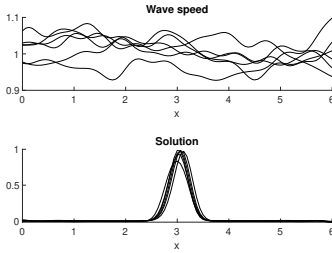


Figure 1: Overlay of realizations of wave speed $c(x, \omega^{(i)})$ (top) and FE-solutions $u_0(x, T, \omega^{(i)})$ at $T = 6$ (bottom).

In general, $C[\hat{u}_h^{\text{ML}}] = \mathcal{O}(\varepsilon^{-2})$, if $V_\ell C_\ell \rightarrow 0$ for $\ell \rightarrow \infty$, regardless of the numerical method [1].

To estimate the gain in computational cost for MLMC with leap-frog (LF) based LTS over standard LF, we compute the theoretical speed-up Q_{eff} ,

$$Q_{\text{eff}}(r, p_0, L, \{V_\ell\}) = \frac{C_{\text{LTS-LF}}[\hat{u}_h^{\text{ML}}]}{C_{\text{LF}}[\hat{u}_h^{\text{ML}}]}, \quad (6)$$

where r denotes the relative measure of the locally refined region, D_{fine} , with respect to D . The smaller D_{fine} , the smaller Q_{eff} and hence the greater the gain of using LTS. Typically, Q_{eff} reaches its minimum at moderate values of the local refinement factor or $p_0 \approx 8 - 32$.

5 Numerical Example

We consider (1) in $D = (0, 6) \subset \mathbb{R}$ with homogeneous Neumann conditions and set the initial condition to the Gaussian pulse:

$$u(0, x) = e^{-16(x-3)^2}, \quad u_t(0, x) = 0.$$

For simplicity, c is modelled here by a standard Karhunen-Loève expansion,

$$c^2(x, \omega) = 1 + \sum_{k=1}^{20} \frac{\xi_k(\omega)}{2\pi^2 k} \left(\cos\left(\frac{k\pi x}{6}\right) + \sin\left(\frac{k\pi x}{6}\right) \right),$$

where $\xi_k \sim U(-1, 1)$ are i.i.d. random variables, but clearly other choices are possible. We let the locally refined region $D_{\text{fine}} = [4.4, 4.5]$ with fixed mesh size $h = H_0/16$ across all levels.

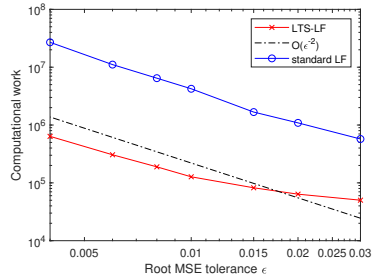


Figure 2: Computational work vs. root MSE tolerance ε with, or without, LTS.

Figure 1 shows an overlay of six particular samples $c(x, \omega^{(i)})$ and the respective FE-solutions $u_\ell(T, \omega^{(i)})$ of (1) at $T = 6$ on the coarsest level with $H_0 = 1/16$. In Figure 2, we compare the performance of MLMC using either leap-frog (LF) based LTS or the standard LF method with \mathcal{P}^1 -FE with mass-lumping. Although the total computational cost behaves inversely proportional to the MSE tolerance ε^2 in both cases, the LTS-LF based MLMC method achieves a one order of magnitude reduction in computational cost. In general, the speed-up Q_{eff} in (6) will depend on the parameters of the problem.

References

- [1] M. B. Giles, Multilevel Monte Carlo path simulation, *Operations Research* **56** (2008), pp. 607–617.
- [2] J. Diaz and M. J. Grote, Energy Conserving Explicit Local Time-stepping for Second-order Wave Equations, *SIAM J. Sci. Comp.* **31** (2009), pp. 1985–2014.
- [3] M. Motamed and D. Appelö, A multi-order discontinuous Galerkin Monte Carlo method for hyperbolic problems with stochastic parameters, *SIAM J. Numer. Anal.* **56** (2018), pp. 448–468.
- [4] K. A. Cliffe, M. B. Giles, R. Scheichl and A. L. Teckentrup, Multilevel Monte Carlo methods and applications to elliptic PDEs with random coefficients, *Comput. Visualization Sci.* **14** (2011), pp. 3–15.

Numerical methods for efficiently solving fractionally damped wave equations

Katherine Baker^{1,*}, Lehel Banjai¹

¹The Maxwell Institute for Mathematical Sciences, School of Mathematical & Computer Sciences, Heriot-Watt University, Edinburgh, UK

*Email: kb54@hw.ac.uk

Abstract

We study numerical quadrature methods that aim to improve efficiency (in particular memory efficiency) and reduce computational complexity in solving wave equations with time fractional damping. These equations include non-local fractional derivatives to incorporate the effects of acoustic attenuation of the wave, making them appropriate for modelling high intensity focused ultrasound therapy (HIFU).

Initially existence and uniqueness results of the given PDE will be discussed, then a wave equation with an additional fractional (lower order) time derivative is discretized. The non-local nature of the fractional time-derivative is treated with convolution quadrature. Recent improvements in storage requirement for convolution quadrature are employed. Paper is of topical interest for WAVES.

Keywords: Convolution quadrature, finite element method, Caputo fractional derivative

1 Fractional Wave Equation

High intensity focused ultrasound is a non-invasive and non-ionising medical treatment that is used to ablate tissue; it is used to treat a number of disorders, such as cancer [1]. The aspect of this treatment that we wish to understand is energy decay of the ultrasound waves as they propagate through tissue. It is known that this acoustic attenuation adheres to a frequency dependence defined by the power law,

$$S(\vec{x} + \Delta \vec{x}) = S(\vec{x})e^{-\gamma(\omega)|\vec{x}|}, \quad (1)$$

where S is amplitude, $\Delta \vec{x}$ is wave propagation distance, ω is frequency and $\gamma(\omega) = \gamma_0|\omega|^y$ is the term describing attenuation. This attenuation is dependent on parameters y and γ_0 which relate to the media.

To model this we consider the modified version of Szabo's convolution wave equation that is presented by Chen and Holm [3] which uses the Caputo fractional derivative as opposed to the Riemann-Liouville derivative. We aim to

find solutions to the initial boundary value problem involving this PDE in a bounded domain $\Omega \subset \mathbb{R}^d$ given by,

$$\partial_t^\alpha u - \Delta u + \partial_t^\alpha u = f, \text{ in } \Omega \times [0, T] \quad (2)$$

$$u(\cdot, 0) = u_0, \text{ in } \Omega$$

$$\partial_t u(\cdot, 0) = v_0, \text{ in } \Omega$$

$$u(\cdot, t) = 0, \text{ on } \partial\Omega \times [0, T]$$

where $\alpha = y + 1$ and remaining coefficients have been set to 1. We use this fractionally damped wave equation because its solutions obey the frequency dependence power law (1).

Theorem 1 *Given $u_0 \in H_0^1(\Omega)$, $v_0 \in L^2(\Omega)$, $f \in L^2(0, T; L^2(\Omega))$ and $\alpha \in (0, 1]$ a unique weak solution $u \in L^\infty(0, T; H_0^1(\Omega))$ exists to the IBVP with $\partial_t^\alpha u \in L^2(0, T; L^2(\Omega))$, $\partial_t^2 u \in L^2(0, T; H^{-1}(\Omega))$ and $\partial_t u \in L^\infty(0, T; L^2(\cdot))$. There also exists a unique weak solution in the case where $\alpha \in (1, 2)$ with the same regularity conditions when $v_0 = 0$.*

2 Derivation of Numerical Method

2.1 Space Discretization

To convert (2) into a discrete problem with respect to the spatial domain we use a Galerkin method. Thus, the problem becomes seeking a solution $u_h \in V_h$, where V_h is a finite dimensional subset of the original solution space $H_0^1(\Omega)$, to

$$\int_{\Omega} \partial_t^\alpha u_h \chi + \int_{\Omega} \nabla u_h \nabla \chi + a \int_{\Omega} \partial_t^\alpha u_h \chi = \int_{\Omega} f \chi \quad (3)$$

where $\chi \in V_h$. We assume solutions have the form

$$u_h = \sum_{j=0}^k U^j \phi_j(x)$$

for a set of basis functions $\{\phi_j\}_{j=0}^k$, and let the test function $\chi = \phi_i$ for $i = 0..k$. Then we are left with

$$M \partial_t^\alpha U + AU + M \partial_t^\alpha U = F$$

where \mathbf{M} and \mathbf{A} denote mass and stiffness matrices.

2.2 Time Discretization

As previously mentioned the time discretization is developed using a mix of two schemes. Initially, we use the second order Leapfrog method to discretize our standard derivatives,

$$\frac{MU_{n+1} - 2MU_n + MU_{n-1}}{\Delta t^2} + \mathbf{A}U_n + \left[(\partial_t^{\Delta t})^{\alpha-1} \mathbf{M}V \right]_n = F_n \quad (4)$$

where $V_j = \frac{U_{j+1} - U_{j-1}}{2\Delta t}$. Then apply the convolution quadrature method [4] to discretize the fractional derivative,

$$\left[(\partial_t^{\Delta t})^{\alpha-1} \mathbf{M}V \right]_n = \sum_{j=0}^{n-1} \omega_{n-j} \mathbf{M}V_j + \frac{\omega_0 \mathbf{M} (U_{n+1} - U_{n-1})}{2\Delta t} \quad (5)$$

where ω denotes the quadrature weights. These weights are defined by,

$$\left(\frac{\delta(\zeta)}{\Delta t} \right)^{\alpha-1} = \sum_{j=0}^{\infty} \omega_j \zeta^j,$$

where $\delta(\zeta)$ is the generating function of the linear multi-step method being used. When using BDF1 the weights can be calculated using a recurrence relation, but for higher order methods we derive them using a fast Fourier transform method.

3 Standard vs Fast Convolution Quadrature

As a result of the sum that arises from the convolution quadrature we need to store all previous data and process all this data at each time step. This drastically increases the schemes memory requirement and computational complexity. To resolve this we have been implementing an algorithm for improving this quadrature that was discussed in [2]. In short, this method decomposes the sum in (5) into two parts, one part is a sum up to a small n_0 where the weights are calculated in the usual sense via fast Fourier transform. The second is a sum containing the remaining terms, but the weights are calculated in such a way that fewer are required and the

sum itself can be written as a recurrence relation.

We have conducted a number of numerical experiments which show the effects of the new quadrature and its ability to retain the same degree of accuracy as the standard method with fewer weights. Table 1 shows the effectiveness of reducing the number of weights on memory consumption.

dx	Standard	Fast
0.5	0.0069	0.0095
0.25	0.0347	0.0342
0.125	0.2162	0.1364
0.0625	1.4708	0.5314
0.03125	10.7389	2.1884
0.015625	81.6034	8.7616
0.0078125	636.3872	34.781

Table 1: Memory usage (MB) of the two methods as the mesh size (dx) decreases, with $\alpha = 0.5$, $\text{tol} = 10^{-6}$ and the CQ uses BDF1.

References

- [1] Al-Bataineh.O, Jenne.J and Huber.P. Clinical and future applications of high intensity focused ultrasound in cancer. *Cancer Treatment Reviews* **38**(5) (2012), pp 346-353.
- [2] Banjai.L, López-Fernández.M. Efficient high order algorithms for the fractional integral and associated FDEs. *Numerische Mathematik* **141**(2) (2019), pp 289-317.
- [3] Chen.W and Holm.S. Modified Szabo's wave equation models for lossy media obeying frequency power law. *The Journal of the Acoustical Society of America* **114**(5) (2003), pp 2570-2574.
- [4] Lubich.C. Discretized Fractional Calculus. *SIAM Journal on Mathematical Analysis* **17**(3) (1986), pp 704-719.

Error analysis for transparent boundary conditions in fractal trees

Patrick Joly^{1,*}, Maryna Kachanovska¹

¹POEMS, ENSTA ParisTech-INRIA-CNRS, INRIA, Palaiseau, France

*Email: patrick.joly@inria.fr

Abstract

This work is dedicated to an efficient resolution of the wave equation in fractal trees (with application to wave propagation in a human lung). Thanks to self-similarity, it is possible to avoid computing the solution at deeper levels of the tree by using transparent boundary conditions. The corresponding DtN operator is defined by a functional equation for its symbol. in the frequency domain. In this work, we analyse an approximate transparent condition, cf. Waves 2017, based on rational approximation of the symbol. The error and complexity analysis relies on Weyl-like estimates of eigenvalues of the weighted Laplacian and related eigenfunctions.

Keywords: fractal tree, wave equation, rational approximations, Weyl estimates

1 Introduction

Given a compact self-similar p -adic tree \mathcal{T} consisting of a countable set of edges and vertices, we study the wave equation defined on its edges

$$\mu \partial_{tt} - \partial_x(\mu \partial_x u) = 0 \tag{1}$$

equipped with $u(M^*, t) = f(t)$ at the root vertex M^* of \mathcal{T} . The (space) function μ is constant along every edge Σ . If the length of Σ is ℓ , the length of each of its p children Σ_j , $j = 0, \dots, p-1$ is $\alpha_j \ell$ with $0 < \alpha_j < 1$. Moreover the value of μ along Σ_j is μ_j times its value along Σ , with $\mu_j > 0$. (1) is completed with vertex conditions (see also Figure 1)

$$u|_{\Sigma} = u|_{\Sigma_k}, \quad 0 \leq k \leq p-1,$$

$$\partial_x u|_{\Sigma} = \sum_{k=0}^{p-1} \mu_k \partial_x u|_{\Sigma_k}.$$

The problem (1) is equipped with Neumann or Dirichlet boundary conditions at 'infinity' (even though the tree is compact), incorporated in the variational formulation of the problem. For the Neumann case considered in this paper, this is:

$$\frac{d^2}{dt^2}(\mu u, v)_{\mathcal{T}} + (\mu \partial_x u, \partial_x v)_{\mathcal{T}} = 0, \quad \forall v \in H_{\mu}^1 \tag{2}$$

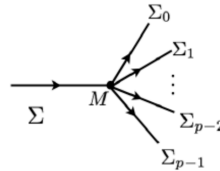


Figure 1: Edge transmission conditions

where we look for $u \in C^1(\mathbb{R}^+; L_{\mu}^2) \times C^0(\mathbb{R}^+; H_{\mu}^1)$. For a precise definition of the (weighted) spaces L_{μ}^2 and H_{μ}^1 and scalar products, see [1]. An important (non-trivial) result of [1] is that the embedding $H_{\mu}^1 \subset L_{\mu}^2$ is compact. As a consequence, setting $\alpha = (\alpha_i)$ and $\mu = (\mu_i)$, (2) can be rewritten in abstract form as

$$\frac{d^2 u}{dt^2} + A_{\alpha, \mu} u = 0. \tag{3}$$

where $A_{\alpha, \mu}$ is a positive definite self-adjoint in L_{μ}^2 which has a pure point spectrum

$$\sigma(A_{\alpha, \mu}) = \{\omega_1^2 \leq \omega_2^2 \leq \dots\}, \quad \omega_n \rightarrow +\infty, \tag{4}$$

each eigenvalue repeated with its multiplicity.

2 Transparent conditions

In order to compute the solution, we truncate the tree at a certain level using a transparent boundary condition at each end point M :

$$\partial_x u(M) = \sum_{i=0}^{p-1} \mu_i \Lambda_i(\partial_t) u(M, \cdot)$$

where $\Lambda_i(\partial_t) = \ell^{-1} \Lambda(\alpha_i \ell \partial_t)$, $\Lambda(\partial_t)$ is the DtN operator associated with a reference tree (with length 1 root edge) and ℓ the length of the edge ending at M . $\Lambda(\partial_t)$ is a convolution operator whose Fourier-Laplace symbol $\Lambda(\omega), \omega \in \mathbb{C}$, is not known explicitly but satisfies

$$\Lambda(\omega) \cos \omega - \omega \sin \omega = \left(\cos \omega + \Lambda(\omega) \frac{\sin \omega}{\omega} \right) \left(\sum_{i=0}^{p-1} \frac{\mu_i}{\alpha_i} \Lambda(\alpha_i \omega) \right). \tag{5}$$

The above equation admits a unique even meromorphic solution as soon as $\Lambda(0) = 0$, which is easily seen for the Neumann problem. Moreover, using (3, 4) for the reference tree, one shows that

$$\Lambda(\omega) = \sum_{n=1}^{+\infty} \frac{a_n \omega^2}{\omega^2 - \omega_n^2}, \quad a_n = \frac{\partial_x \varphi_n(0)^2}{\omega_n^2}, \quad (6)$$

where $A_{\alpha, \mu} \varphi_n = \omega_n^2 \varphi_n$, $\|\varphi_n\|_{L^2_\mu} = 1$ and 0 the root edge of the reference tree. An approximate transparent condition is obtained by truncating the above expansion at some order $N > 1$

$$\Lambda(\omega) \sim \Lambda_N(\omega) := \sum_{n=1}^N \frac{a_n \omega^2}{\omega^2 - \omega_n^2}. \quad (7)$$

The resulting boundary condition is local in time: at each end point M , we write an inhomogeneous Neumann condition involving N auxiliary unknowns coupled to u via ordinary differential equations (harmonic oscillators with frequencies ω_n). In practice, the (a_n, ω_n) 's are computed through the numerical solution of (5). The stability of the resulting IBVP can be shown via energy estimates. Below we address the corresponding error (and complexity) analysis.

3 Error and complexity analysis

Let us denote u_N the solution on the truncated tree issued from the approximation of $\Lambda(\partial_t)$ by $\Lambda_N(\partial_t)$ through (7) and $e_N := u - u_N$ the corresponding error. The full error analysis relies on three steps. Denoting \mathcal{T}_c the finite truncated tree, and given $T > 0$, we set

$$\begin{aligned} \|e_N\|_{c,T} &= \|e_N\|_{L^\infty(0,T;H^1_\mu(\mathcal{T}_c))} \\ &+ \|\partial_t e_N\|_{L^\infty(0,T;L^2_\mu(\mathcal{T}_c))}. \end{aligned} \quad (8)$$

Lemma 1 *For sufficiently smooth data, one has*

$$\|e_N\|_{c,T} \leq C T r_N \|\partial_t^4 \partial_x u\|_{L^1(0,T;L^2_\mu)} \quad (9)$$

with r_N the remainder of a converging series

$$r_N := \sum_{n=N}^{+\infty} \frac{a_n}{\omega_n^2} \equiv \sum_{n=N}^{+\infty} \frac{\partial_x \varphi_n(0)^2}{\omega_n^4}. \quad (10)$$

Lemma 1 is proven by energy techniques. For estimating r_N , we first get a lower bound for ω_n^2 by using min-max and Dirichlet-Neumann bracketing techniques and adapting the ideas of [2]. The result depends on two quantities

$$|\alpha| = \alpha_0 + \dots + \alpha_{p-1} \in]0, p[\quad (11)$$

$$d_\alpha > 0 \text{ unique sol. } d \text{ of } \sum_{i=0}^d \alpha_i^d = 1. \quad (12)$$

Lemma 2 *There exists $\omega_* > 0$ such that:*

If $|\alpha| < 1$, $d_\alpha < 1$ and $\omega_n^2 \geq \omega_*^2 n^2$.

If $|\alpha| = 1$, $d_\alpha = 1$ and $\omega_n^2 \geq \omega_*^2 n^2 / \log n$.

If $|\alpha| > 1$, $d_\alpha > 1$ and $\omega_n^2 \geq \omega_*^2 n^{2/d_\alpha}$.

Let us emphasize that these bounds are sharp in the sense that similar upper bounds, with $\omega_* > 0$ instead of ω_* , can be obtained.

The next step involves particular upper bounds involving the eigenfunctions φ_n . Using a theorem of [3] (that can be straightforwardly adapted to our case) we prove the (note the difference between r_N and the left hand side of (13))

Lemma 3 *There exists $C > 0$ such that,*

$$\forall M > 0, \quad \sum_{\omega_n^2 \geq M^2} \frac{\partial_x \varphi_n(0)^2}{\omega_n^4} \leq \frac{C}{M}. \quad (13)$$

Our main result is obtained by combining lemmas 1, 2 and 3.

Theorem 4 *For sufficiently smooth data, the estimate (8) holds with*

$$\begin{cases} r_N \leq C N^{-1} & \text{if } |\alpha| < 1, \\ r_N \leq C N^{-1} \log N & \text{if } |\alpha| = 1, \\ r_N \leq C N^{-(1/d_\alpha)} & \text{if } |\alpha| > 1. \end{cases} \quad (14)$$

Note that the computational complexity of the method is directly related to (14) since the cost of the boundary condition is proportional to N .

In the talk, we shall also propose some hints (suggested by the convergence proof) to improve accuracy with (almost) no additional cost.

References

- [1] P. Joly, M. Kachanovska, A. Semin : Wave propagation in fractal trees. Mathematical and numerical issues. Networks and Heterogeneous Media. To appear (2019)
- [2] J. Kigami, M.L. Lapidus : Weyl's problem for the spectral distribution of Laplacians on p.c.f. self-similar fractals. Comm. Math. Phys. 158(1), 93-125 (1993).
- [3] A.H. Barnett, S. Hassell : Boundary quasi-orthogonality and sharp inclusion bounds for large Dirichlet eigenvalues. SIAM J. Numer. Anal. 49(3), (2011).

Computation of plasmon resonances localized at corners using frequency-dependent complex scaling

Anne-Sophie Bonnet-Ben Dhia¹, Christophe Hazard¹, Florian Monteghetti^{1,*}

¹POEMS (CNRS-INRIA-ENSTA ParisTech), Palaiseau, France

*Email: florian.monteghetti@ensta-paristech.fr

Abstract

A plasmonic device with a non-smooth boundary can exhibit strongly-oscillating surface waves whose phase velocities vanish as they reach the corners. This work investigates in the quasi-static limit the existence of corner resonances, which are analogous to scattering resonances in the sense that the local behavior at each corner plays the role of the behavior at infinity. Resonant contrasts are sought as eigenvalues of the transmission problem with complex scaling applied at corners. Since the scaling function must depend upon the contrast, the corresponding eigenvalue problem is nonlinear.

Keywords: sign-changing permittivity, complex resonances, complex scaling

1 Definition of corner resonances

This work focuses on the transmission problem

$$\begin{cases} \operatorname{div}(\varepsilon(\mathbf{x})^{-1} \nabla u(\mathbf{x})) = 0 & (\mathbf{x} \in \Omega \subset \mathbb{R}^2) \\ u(\mathbf{x}) = 0 & (\mathbf{x} \in \partial\Omega), \end{cases} \quad (1)$$

where the differentiations are weak, Ω is a bounded C^∞ domain, and ε is piecewise constant

$$\varepsilon(\mathbf{x}) = \kappa \mathbb{1}_{\Omega_m}(\mathbf{x}) + \mathbb{1}_{\Omega \setminus \Omega_m}(\mathbf{x}), \quad (2)$$

where Ω_m is a piecewise-smooth domain modeling the plasmonic device, see Figure 1.

Typically, the *contrast* κ depends upon the frequency ω through a physical model; this dependency need not be introduced herein since ω does not appear explicitly in the quasi-static approximation (1).

If the contrast κ is not real, then the only solution of (1) in $H^1(\Omega)$ is $u = 0$. Let us review some results for $\kappa \in \mathbb{R}$.

If $\partial\Omega_m$ is smooth there is a sequence of *real* eigenvalues $(\kappa_n)_n$, for which (1) has a non-null solution, accumulating at -1 [3, Thm. 1]. These contrasts are associated with surface waves known as *surface plasmons*, whose energy-concentrating properties are employed in many applications.

Let $\partial\Omega_m$ have one corner \mathbf{x}_c of angle $\phi \in (0, \pi)$. If κ lies in the *critical interval* [1, Tab. 1] [4]

$$I_c := \left[\frac{\phi - 2\pi}{\phi}, -1 \right] \cup \left[-1, \frac{\phi}{\phi - 2\pi} \right] = I_c^{\text{odd}} \cup I_c^{\text{even}},$$

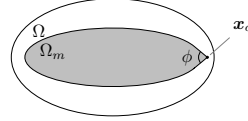


Figure 1: Transmission problem on Ω . The plasmonic inclusion Ω_m has a corner of angle ϕ .

then there is $\eta \in \mathbb{R}$, which depends implicitly on the contrast κ through the dispersion relation

$$f_\phi(\eta, \kappa) := \left[\frac{\sinh(\eta\pi)}{\sinh[\eta(\pi - \phi)]} \right]^2 - \left[\frac{1 - \kappa}{1 + \kappa} \right]^2 = 0, \quad (3)$$

such that the strongly-oscillating *black-hole* field

$$u_{\text{bh}}(r, \theta) = r^{i\eta} \Phi(\theta) \quad (\theta \in (-\pi, \pi])$$

is a solution to (1) in a neighborhood of \mathbf{x}_c . Note that $u_{\text{bh}} \in L^2(\Omega)$ but $u_{\text{bh}} \notin H^1(\Omega)$. The requirement that u_{bh} be outgoing leads to (using energy considerations or a limiting absorption principle)

$$\eta < 0 \text{ if } \kappa \in I_c^{\text{odd}}, \quad \eta > 0 \text{ if } \kappa \in I_c^{\text{even}}. \quad (4)$$

The purpose of this work is to investigate the existence of complex resonances occurring at the corners of $\partial\Omega_m$, which can be built analogously to that of usual scattering resonances. We propose here the following, somewhat imprecise, definition:

Definition 1. A *corner resonance* is a value of κ for which there is a non-trivial solution u to (1) that is outgoing at a corner $\mathbf{x}_c \in \partial\Omega_m$.

A corner resonance function is localized at a corner \mathbf{x}_c of $\partial\Omega_m$ in the sense that it blows up as

$$u(r, \theta) \underset{r \rightarrow 0^+}{\sim} r^{i\eta} \Phi(\theta) \quad (\theta \in (-\pi, \pi]), \quad (5)$$

where κ solves (3) with $\Im(\eta) \geq 0$. The multivalued nature of $\kappa \mapsto \{\eta \mid f_\phi(\eta, \kappa) = 0\}$ suggests that such resonances can exist. This seems to be corroborated by the strategy proposed in [5], which consists in perturbing a smooth $\partial\Omega_m$ with corners so that eigenvalues κ_n are perturbed into embedded eigenvalues or resonances.

2 Complex scaling for corners resonances

The principle of complex scaling is to *define* a modified transmission problem such that if κ is a corner resonance with resonance function u , then κ is an eigenvalue of the modified problem. The construction exploits the analyticity of (5) with respect to r .

To formalize this, let (r, θ) be cylindrical coordinates originating at a corner $x_c \in \partial\Omega_m$. The complex scaling technique introduced in [1] consists in analytically continuing u from $(0, R) \times (-\pi, \pi]$ to $\{r^{1/\alpha} \mid r \in (0, R)\} \times (-\pi, \pi]$, where $\alpha \in \mathbb{C}$ is the complex scaling parameter to be *chosen*. By defining $u_\alpha(r, \theta) := u(r^{1/\alpha}, \theta)$, the modified problem is

$$\varepsilon^{-1} (\alpha r \partial_r)^2 u_\alpha(r, \theta) + \partial_\theta (\varepsilon^{-1} \partial_\theta u_\alpha)(r, \theta) = 0 \quad (6)$$

on $(0, R) \times (-\pi, \pi]$, which can be discretized with a finite element method. A suitable choice of $\alpha \neq 1$ enables to turn resonances κ that belong to a given region $K_\alpha \subset \mathbb{C}$ into eigenvalues of (6). The associated eigenfunction $u_\alpha \in L^2(\Omega)$ behaves at each corner as (compare with (5))

$$u_\alpha(r, \theta) \underset{r \rightarrow 0^+}{\sim} r^{i\frac{\theta}{\alpha}} \Phi(\theta) \quad (\theta \in (-\pi, \pi]),$$

where $\alpha \in \mathbb{C}$ is chosen such that $\Im(\eta/\alpha) < 0$.

The numerical difficulty stems from the fact that (6) is nonlinear in κ , since $\arg(\alpha)$ *must* depend upon κ , echoing [6] where parameters with frequency-dependent modulus are considered. This is apparent from the outgoing condition (4), which implies

$$\arg(\alpha) < 0 \text{ if } \kappa \in I_c^{\text{odd}}, \quad \arg(\alpha) > 0 \text{ if } \kappa \in I_c^{\text{even}}.$$

Specifically, a study of the dispersion relation (3) shows that α must satisfy the stability constraint

$$\theta_{\min}(\kappa) < \arg(\alpha(\kappa)) < \theta_{\max}(\kappa) \quad (\kappa \in \mathbb{R}), \quad (7)$$

which ensures that only outgoing corner waves must be exponentially decaying (equivalently, the corner must not bring energy into the domain).

Figure 2 illustrates (7). The values of θ_{\max} for $\kappa < \frac{\phi-2\pi}{\phi}$ and θ_{\min} for $\kappa > \frac{\phi}{\phi-2\pi}$ are consequences of (4). Any κ -independent scaling parameter such as $\alpha_1 = e^{-i\pi/4}$ fails (7); $\alpha_2(\kappa) = e^{i\theta(\kappa)}$ where $\theta(\kappa)$ is a polynomial satisfying (7) for $\kappa \in [-6, 0]$.

Figure 3 plots the deformation of the essential spectrum

$$\sigma_{\text{ess}} = \{\kappa \mid \exists \eta \in \mathbb{C}^*: f_\phi(\eta, \kappa) = 0, \Im(\eta/\alpha) = 0\}$$

for $\alpha = 1$ (i.e. no complex scaling, in which case we recover I_c), for the κ -independent scaling α_1

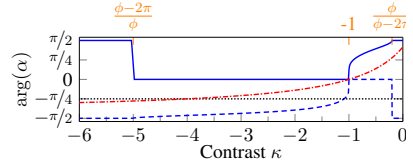


Figure 2: Illustration of condition (7) for a corner angle $\phi = \pi/3$. Stability limits: (—) θ_{\max} , (---) θ_{\min} . Complex scaling parameters: (.....) $\alpha_1 = e^{-i\pi/4}$, (-.-.-) $\alpha_2 = e^{i\theta(\kappa)}$.

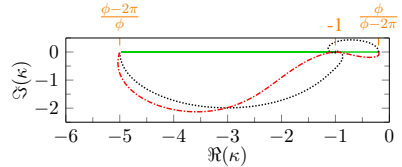


Figure 3: Essential spectrum σ_{ess} for a corner angle $\phi = \pi/3$ and various complex scaling parameters: (—) $\alpha = 1$, (.....) $\alpha_1 = e^{-i\pi/4}$, (-.-.-) $\alpha_2 = e^{i\theta(\kappa)}$.

(discussed in [2, §4.7.1]), and for the κ -dependent scaling α_2 . The region K_α where resonances can be computed is the region uncovered by the deformation of the essential spectrum.

Ongoing work focuses on the construction of a scaling function $\kappa \mapsto \alpha(\kappa)$ that maximizes $|K_\alpha|$ while still leading to a tractable nonlinear eigenvalue problem in κ .

References

- [1] A.-S. Bonnet-Ben Dhia, C. Carvalho, L. Chesnel, and P. Ciarlet. “On the use of Perfectly Matched Layers at corners for scattering problems with sign-changing coefficients.” In: *J. Comput. Phys.* 322 (2016), pp. 224–247.
- [2] C. Carvalho. “Étude mathématique et numérique de structures plasmoniques avec coins.” PhD thesis, ENSTA Paris Tech, 2015.
- [3] D. Grieser. “The plasmonic eigenvalue problem.” In: *Rev. Math. Phys.* 26.03 (2014).
- [4] C. Hazard and S. Paolantoni. “Spectral analysis of polygonal cavities containing a negative-index material.” hal-01626868, 2018.
- [5] W. Li and S. P. Shipman. “Embedded eigenvalues for the Neumann-Poincaré operator.” arXiv:1806.00950, 2019.
- [6] L. Nannen and M. Wess. “Computing scattering resonances using perfectly matched layers with frequency dependent scaling functions.” In: *BIT Numer. Math.* 58.2 (2018).

Complex Scaled Infinite Elements for Electromagnetic Problems in Open Domains

B. Auinger¹, K. Hollaus¹, M. Leumüller^{2,*}, L. Nannen², M. Wess²¹Silicon Austria Labs GmbH, Graz, Austria²Institut für Analysis und Scientific Computing, TU Wien, Vienna, Austria

*Email: michael.leumueller@tuwien.ac.at

Abstract

A popular approach for treating time-harmonic Maxwell problems in open domains is the technique of complex scaling. Thereby a complex coordinate stretching is applied leading to exponentially decreasing outgoing solutions. Usually a perfectly matched layer is generated by truncating the domain and discretizing the problem in the bounded layer with finite elements. In our work we present a method based on complex scaling that omits truncation by the use of infinite elements. These infinite elements are straightforward to use and lead to super-algebraic convergence with respect to the number of unknowns in propagation direction. Moreover, they are stable, i.e. the condition numbers of the discretization matrices are small.

Keywords: time harmonic Maxwell's equations, waveguide, infinite elements, complex scaling, transparent boundary conditions

1 Introduction

This work considers electromagnetic problems in open domains with an electromagnetic source. Such problems appear in the context of electromagnetic compatibility in electronic based systems [1, 2]. Interesting results may be the input impedance, the radiated power, etc.

The performance of the standard perfectly matched layer (PML) method depends on the thickness of the layer, the discretization and the finite element (FE) order in the layer, as well as the complex coordinate stretching. Optimizing these parameters is cumbersome. Moreover, the PML has exponential convergence with respect to the thickness of the layer, but standard FE convergence with respect to the discretization in the layer. We propose infinite elements (IE) which depend only on a damping parameter and the degrees of freedom (DoF) in the direction of propagation and lead to super-algebraic convergence with respect to the DoFs in the direction of propagation.

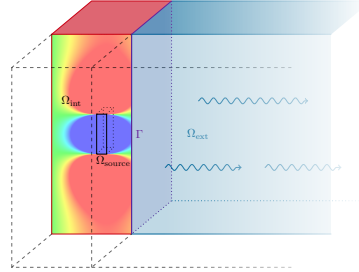


Figure 1: Longitudinal section of a waveguide.

2 Mathematical formulation

Let $\Omega \subset \mathbb{R}^3$ such that $\Omega = \Omega_{\text{int}} \cup \Gamma \cup \Omega_{\text{ext}}$ where Ω_{int} is bounded, $\Omega_{\text{ext}} = \Omega \setminus \overline{\Omega_{\text{int}}}$ is unbounded and $\Gamma = \Omega_{\text{int}} \cap \overline{\Omega_{\text{ext}}} \cap \Omega$. To simplify the explanation of the method the focus is set on waveguides (cf. Figure 1) where $\Gamma = \{0\} \times \Gamma_0$ for a suitable bounded Lipschitz domain $\Gamma_0 \subset \mathbb{R}^2$.

The goal is to solve time-harmonic Maxwell's equations in the following form

$$\text{curl } \mu^{-1} \text{curl } \mathbf{A} - \omega^2 \varepsilon \mathbf{A} = \mathbf{J}_0 \quad (1)$$

on Ω , where \mathbf{A} is the magnetic vector potential, $\omega \in \mathbb{R}_{>0}$ the angular frequency, μ the permeability, ε the permittivity and \mathbf{J}_0 the given electric current density. Moreover, boundary conditions on $\partial\Omega$ are imposed. Since Ω is unbounded, an additional radiation condition is imposed in the following way: A solution \mathbf{A} to (1) is called outgoing if the real part of its radiated power

$$S = \frac{1}{2} \int_{\Gamma} (i\omega \mathbf{A} \times \mu^{-1} \text{curl } \mathbf{A}) \cdot \mathbf{n} \, d\Gamma \quad (2)$$

is non-negative and if \mathbf{A} is bounded. Here \mathbf{n} denotes the normal vector on Γ pointing into Ω_{ext} .

3 Complex Scaling

To obtain exponentially decreasing solutions of (1) in Ω_{ext} for $|\mathbf{x}| \rightarrow \infty$ a complex coordinate

stretching is applied in Ω_{ext} . This is necessary for two reasons. It allows to derive a weak formulation of (1), and it ensures that only physically relevant outgoing solutions and exponentially decreasing evanescent modes are obtained. The scaling alters the longitudinal coordinate only and has the form

$$\mathbf{x} = (x_1, x_2, x_3)^\top \mapsto (\sigma x_1, x_2, x_3)^\top,$$

for some complex parameter σ with positive imaginary part.

4 Infinite Elements

The interior problem is discretized using a high-order FE space $\mathcal{V}_{\text{int}} \subset H_{\text{curl}}(\Omega_{\text{int}})$. The discretization of the complex scaled exterior problem is inspired by [3]. A tensor product basis $\mathcal{W} := \widetilde{\mathcal{W}} \otimes \hat{\mathcal{W}}$, with a subspace $\widetilde{\mathcal{W}} \subset H^1(\mathbb{R}_{>0})$ in longitudinal and $\hat{\mathcal{W}} \subset H^1(\Gamma)$ in transversal direction, discretizing $H^1(\Omega_{\text{ext}})$ is used. The idea is to discretize $H^1(\mathbb{R}_{>0})$ by exponentially decreasing functions imitating the behavior of the complex scaled solution in direction of propagation. The basis functions $\widetilde{\mathcal{W}}$ discretizing $H^1(\mathbb{R}_{>0})$ are

$$\xi \mapsto \exp(-\xi) p_j(\xi), \quad j = 0, \dots, N, \quad (3)$$

for certain polynomials p_j of degree j . These polynomials are closely linked to the *Laguerre polynomials* which form a complete orthogonal system for a weighted L^2 -space on $\mathbb{R}_{>0}$. The orthogonality leads to sparse system matrices.

A conforming discretization $\mathcal{V} \subset H_{\text{curl}}(\Omega_{\text{ext}})$ is derived such that it contains the gradients of basis functions of \mathcal{W} .

We choose

$$\mathcal{V} := \begin{pmatrix} \widetilde{\mathcal{W}}' \otimes \hat{\mathcal{W}} \\ \mathbf{0} \end{pmatrix} \oplus \begin{pmatrix} \mathbf{0} \\ \widetilde{\mathcal{W}} \otimes \hat{\mathcal{V}} \end{pmatrix}. \quad (4)$$

Thereby, $\widetilde{\mathcal{W}}'$ consists of the derivatives of the basis functions of $\widetilde{\mathcal{W}}$, $\hat{\mathcal{W}} \subset H^1(\Gamma)$, and $\hat{\mathcal{V}} \subset H_{\text{curl}}(\Gamma)$ is the trace space of \mathcal{V}_{int} on Γ .

5 Results

The method described above is applied to the problem introduced in Section 2. The dimensions of Ω_{int} are $0.08\text{m} \times 0.2\text{m} \times 0.2\text{m}$. The domain Ω_{source} is centered at $(-0.03\text{m}, 0.1\text{m}, 0.1\text{m})^\top$ and has the dimensions $0.01\text{m} \times 0.01\text{m} \times 0.04\text{m}$. Ω_{ext} is located at the right side of Ω_{int} with the

same depth and height and infinite length in x -direction. The shared boundary is Γ . Homogeneous Dirichlet boundary conditions are imposed on $\partial\Omega$ and as source $\mathbf{J} = (0, 0, J)^\top$ with $J = 10^8 \frac{\text{A}}{\text{m}^2}$ which is only supported in Ω_{source} has been chosen. Moreover, parameters are set to $\omega = 2\pi \cdot 10^9 \frac{\text{rad}}{\text{s}}$, $\mu = 4\pi \cdot 10^{-7} \frac{\text{Vs}}{\text{Am}}$, $\varepsilon = 8.854 \cdot 10^{-12} \frac{\text{As}}{\text{Vm}}$. A high order tensor product FE basis has been used to discretize the problem in Ω_{int} . The interior domain was split into $7 \times 10 \times 10$ sections. The FE order p varied between 2 and 4. The radiated power was evaluated on the plane $\{-0.005\text{m}\} \times [0\text{m}, 0.2\text{m}] \times [0\text{m}, 0.2\text{m}]$, with a section wise applied Gauk-Quadratur of order 8.

In Figure 2 the relative error is shown. The reference value was calculated using FE order 5 and IE with 30 DoF. Super-algebraic convergence with respect to the DoF of IE is observed. The errors are constant when the accuracy of the FE discretization of Ω_{int} is reached.

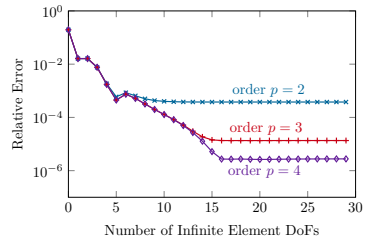


Figure 2: Relative error of the radiated power with respect to the number of DoF of IE for different FE orders.

6 Acknowledgement

This work was supported by the Austrian Science Fund (FWF) under Project P 26252.

References

- [1] H. Hackl, B. Auinger, B. Deutschmann, A. Gheonjian, The shielding effect of a multi-cable harness as function of IC output termination impedance. *IEEE EMC/APEMC* 2018, pp. 707-712.
- [2] Henry W. Ott, *Electromagnetic compatibility engineering Hoboken, N.J. John Wiley & Sons* (2009) Rev. ed.
- [3] L. Nannen, T. Hohage, A. Schädle, J. Schöberl, Exact sequences of high order Hardy space infinite elements for exterior Maxwell problems. *SIAM J. Sci. Comput.* **35** (2013), no. 2, pp. 1024-1048.

Complex Scaled Infinite Elements for Wave Equations in Heterogeneous Open Systems

L. Nannen¹, K. Tichy¹, M. Wess^{1,*}¹Institut für Analysis und Scientific Computing, TU Wien, Vienna, Austria

*Email: markus.wess@tuwien.ac.at

Abstract

The technique of *complex scaling* is a popular way to deal with the *wave equation* on unbounded domains. It is based on a complex coordinate stretching in the time harmonic regime. In our work we consider settings, where the usual cartesian or radial scalings are not applicable due to inhomogeneous exterior domains (e.g. open waveguides in non-axial directions). We apply a scaling in *normal* direction. Moreover we use *infinite elements* to discretize the complex scaled equation instead of truncating the domain to benefit from superior approximation properties and omit an additional truncation error. We present numerical experiments to illustrate our results.

Keywords: wave equation, infinite elements, complex scaling

1 Introduction

We consider numerically solving the wave equation

$$c(\mathbf{x})^2 \Delta_{\mathbf{x}} p(t, \mathbf{x}) = \frac{d^2}{dt^2} p(t, \mathbf{x}) \quad (1)$$

on $\Omega := \mathbb{R}^2$. We are interested in settings similar to the one sketched in Figure 1, where the wave speed c is constant inside and outside of a set of open waveguides respectively. More generally we assume that there exist $\Omega_{\text{int}}, \Gamma, \Omega_{\text{ext}} \subset \mathbb{R}^2$, such that $\Omega = \Omega_{\text{int}} \dot{\cup} \Gamma \dot{\cup} \Omega_{\text{ext}}$, where Ω_{int} is open, bounded, and convex, $\Gamma = \partial\Omega_{\text{int}}$ is smooth with outer normal \mathbf{n} ,

$$\Omega_{\text{ext}} = \{ \hat{\mathbf{x}} + \xi \mathbf{n}(\hat{\mathbf{x}}) : \xi \in \mathbb{R}_{>0}, \hat{\mathbf{x}} \in \Gamma \}, \quad (2)$$

such that the coordinates $\xi(\mathbf{x}), \hat{\mathbf{x}}(\mathbf{x})$ are unique for each $\mathbf{x} \in \Omega_{\text{ext}}$ and

$$c|_{\Omega_{\text{ext}}}(\mathbf{x}) = \tilde{c}(\xi(\mathbf{x})) \hat{c}(\hat{\mathbf{x}}(\mathbf{x})).$$

Since we allow inhomogeneities which are neither radial nor parallel to the axes, the frequently used cartesian or radial complex scalings are not applicable in this case.

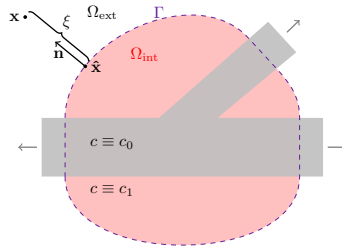


Figure 1: Example domain, where cartesian or spherical scalings would fail: Open waveguide with junction.

2 Absorbing layers for the wave equation

To construct absorbing boundary layers for the wave equation we follow the ideas presented for example in [4]. Note that the following steps are merely theoretical prerequisites to our method. The numerical method itself consists of discretizing the resulting system of equations. First, we apply a Fourier transformation. Then the technique of complex scaling is applied to the resulting *Helmholtz equation*. This technique relies on a complex coordinate stretching $\gamma: \Omega_{\text{ext}} \rightarrow \mathbb{C}^2$, which is chosen such that the outgoing solutions of the Helmholtz equation on the complex scaled domain $\gamma(\Omega_{\text{ext}})$ are exponentially decaying. We use normal scalings (cf. [1]), meaning that the complex deformation $\gamma(\mathbf{x}(\hat{\mathbf{x}}, \xi)) := x(\hat{\mathbf{x}}, s(\xi))$ for a scalar scaling function $s: \mathbb{R}_{>0} \rightarrow \mathbb{C}$, is only applied to the normal coordinate ξ . The scaling function s is of the form

$$s_{\omega}(\xi) = \frac{q_1(i\omega)}{q_2(i\omega)} \xi \quad (3)$$

with complex polynomials q_1, q_2 . While the dependency on the frequency is advantageous for resonance problems (cf. [3]) due to better approximation properties, it is essential for time domain. The wrong treatment of a subset of the present frequencies can lead to exponentially

growing and therefore unstable solutions in time. Different choices of (3) are suitable for different problem settings.

The resulting complex scaled equation is subsequently transformed back to time domain by applying the according inverse Fourier transformation. Since powers of $-i\omega$ are transformed to time derivatives, we introduce a suitable set of additional unknowns to end up with a second order system in time again.

3 Discretization in space

To discretize the system obtained in the previous section in space, usually the finite element method is applied to a truncated exterior domain which introduces an additional error. Differing from this approach we use infinite elements which are based on Hardy space infinite elements (cf. [2]) instead. To this end, we use the exterior coordinates $\xi, \hat{\mathbf{x}}$ and a tensor product ansatz space (cf. Figure 2). The first part

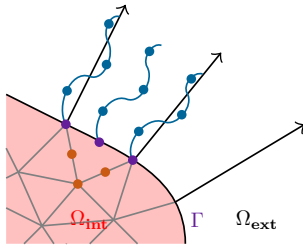


Figure 2: Sketch of the tensor product basis and some of the degrees of freedom for triangular finite elements of order 2 and infinite elements of order 3.

of this space is composed of boundary functions, which are the traces of the basis functions of the interior discretization. The second part consists of basis functions in the normal coordinate

$$\phi_j(\xi) = \exp(-\xi) p_j(\xi),$$

for certain polynomials p_j of degree j (cf. Figure 3). These polynomials are closely linked to the *Laguerre polynomials* which form a complete orthogonal system for a weighted L^2 -space on $\mathbb{R}_{>0}$.

Desirable properties of the basis functions ϕ_j include that they result in sparse, well-conditioned discretization matrices. Moreover it can

be shown that they approximate the normal components of the solution super-algebraically with respect to the number of basis functions. They are simple to evaluate and can be integrated numerically. Coupling the interior and exterior problem works in a straightforward way.

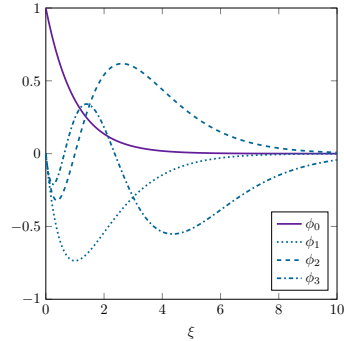


Figure 3: The first few basis functions ϕ_j . The basis function ϕ_0 couples with the interior and corresponds to the degrees of freedom on the interface Γ in Figure 2, while the remaining basis functions live purely in the exterior.

4 Time integration

After spacial discretization the resulting semi-discrete system in time is discretized using implicit time-stepping methods. A possible extension of our method would be the use of explicit time-stepping schemes to improve computational efficiency. To this end, a discontinuous Galerkin approach for the interior and interface basis functions can be used.

References

- [1] M. Lassas, E. Somersalo, Analysis of the PML equations in general convex geometry, *Proceedings of the Royal Society of Edinburgh Sec. A* **131** (2001), pp. 1183–1207.
- [2] T. Hohage, L. Nannen, Hardy space infinite elements for scattering and resonance problems, *SIAM J. Numer. Anal.* **47** (2009), pp. 972–996.
- [3] L. Nannen, M. Wess, Computing scattering resonances using perfectly matched layers with frequency dependent scaling functions, *BIT* **58** (2018), pp. 373–395.
- [4] F. Collino, P. Monk, The perfectly matched layer in curvilinear coordinates, *SIAM J. Sci. Comput.* **19** (1998), pp. 2061–2090.

Stable Perfectly Matched Layers for a Class of Anisotropic Dispersive Models

Éliane Bécache^{1,*}, Maryna Kachanovska¹¹POEMS, UMR ENSTA-INRIA-CNRS, Palaiseau, France

*Email: eliane.becache@inria.fr

Abstract

We consider wave propagation in 2D anisotropic dispersive media in an unbounded domain described by Maxwell's equations with an antisymmetric dielectric permittivity tensor and scalar magnetic permeability. Bounding the computational domain is required to obtain the solution. In order to do so, we use the perfectly matched layer (PML) technique. However, the PMLs exhibit instabilities connected to the presence of backward propagating waves. This work is dedicated to stabilizing the PMLs for this case.

Keywords: perfectly matched layers, PMLs, Laplace transform, passive metamaterials

1 Introduction

The wave propagation in the 2D dispersive media is described by the Maxwell's equations

$$\begin{aligned} \partial_t D_x &= \partial_y H_z, \\ \partial_t D_y &= -\partial_x H_z, \\ \partial_t B_z &= -\partial_x E_y + \partial_y E_x. \end{aligned} \quad (1)$$

The relations between the fields \mathbf{D} and \mathbf{E} , and B_z and H_z are written in the Laplace domain, more precisely, denoting by $\hat{u}(s)$ the Laplace transform of u , $\hat{\mathbf{D}} = \underline{\underline{\varepsilon}}(s)\hat{\mathbf{E}}$, and $\hat{B}_z = \mu(s)\hat{H}_z$, where $\underline{\underline{\varepsilon}}$ is the dielectric permittivity tensor and μ the scalar magnetic permeability. In a first step, we consider a diagonal dielectric tensor, $\underline{\underline{\varepsilon}}(s) = \text{diag}[\varepsilon_x(s), \varepsilon_y(s)]$ and we will present at the end an extension to antisymmetric dielectric tensors. This kind of tensors appears for instance for the wave propagation in magneto-optical or plasma materials.

We assume that the material has the so-called passivity property : a function $f(s)$ is passive if it is analytic in $\mathbb{C}_+ = \{s : \text{Re } s > 0\}$, and $\text{Re}(sf(s)) > 0$ for all $s \in \mathbb{C}_+$. This property is satisfied by $\mu(s)$, $\varepsilon_x(s)$, $\varepsilon_y(s)$. These conditions are consistent with physics literature and are related to stability and energy conservation.

In order to apply the PML method [2], we first rewrite (1) in the Laplace domain. Then the construction of the PMLs amounts to per-

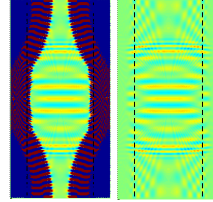


Figure 1: The field H_z for a dispersive anisotropic problem obtained with the Bérenger's PML (left) and stabilized PML (right). The boundary between the domain and the PML is marked in black.

forming the change of variables

$$x \rightarrow x + \frac{1}{s} \int_0^x \sigma(x') dx', \quad (\sigma(x) > 0),$$

and rewriting the newly obtained equations in the time domain. However, as demonstrated in [1], this change of variables may lead to instabilities in presence of backward propagating waves in the PML direction (waves with x -components of group and phase velocities of the opposite sign). In the same work it was suggested that for isotropic ($\varepsilon_x(s) = \varepsilon_y(s)$) dispersive materials a modified change of variables $x \rightarrow x + \frac{\psi(s)}{s} \int_0^x \sigma(x') dx'$ would stabilize the PMLs, provided a special choice of $\psi(s)$. We can show that this preserves the perfect matching as in the classical case. In the present work we show that the results of [1] can be extended to the cases where the dielectric tensor is either diagonal or antisymmetric; however, we base our considerations on a different kind of analysis. This abstract summarizes some of the results of [3].

2 Passivity and stability

In the Laplace domain (1) reads

$$s^2 \mu(s) \hat{H}_z - \varepsilon_x(s)^{-1} \partial_{yy} \hat{H}_z - \varepsilon_y(s)^{-1} \partial_{xx} \hat{H}_z = 0.$$

The following result on the stability holds true.

Theorem 1 Assume that $\mu, \varepsilon_x, \varepsilon_y$ are passive. Then the formulation

$$A(\hat{H}_z, v) = \langle \hat{f}, v \rangle, \quad \forall v \in H^1(\mathbb{R}^3),$$

$$A(\hat{H}_z, v) = s^2 \mu(s) (\hat{H}_z, v) + \frac{1}{\varepsilon_x(s)} (\partial_y \hat{H}_z, \partial_y v)$$

$$+ \frac{1}{\varepsilon_y(s)} (\partial_x \hat{H}_z, \partial_x v)$$

has a unique solution \hat{H}_z for all $\hat{f} \in H^{-1}(\mathbb{R}^3)$, and all $s \in \mathbb{C}_+$. If \hat{f} is a Laplace transform of a causal $C^2(\mathbb{R}, H^{-1}(\mathbb{R}^3))$ -function f , with $f^{(3)} \in L^1(\mathbb{R}, H^{-1}(\mathbb{R}^3))$, then H_z is a continuous causal function and, for some $\alpha > 0$,

$$\|H_z(t)\|_{H^1} \leq \alpha \max(t^3, 1)$$

$$\times \int_0^t \|(1 + \partial_\tau)^3 f(\tau)\|_{H^{-1}} d\tau, \quad t \geq 0.$$

We will say that the sesquilinear form $A(u, v)$, defined in the above theorem, is passive, if $\mu, \varepsilon_x, \varepsilon_y$ are passive. The above result shows that the passivity of the sesquilinear form implies well-posedness and stability (i.e. at most polynomial growth of the time domain solution provided a sufficiently fast decaying at infinity RHS data).

3 Construction of stable PMLs

Let $\sigma = \text{const} > 0$. As shown in Theorem 1, for the stability of the PML it is sufficient to ensure the passivity of the coefficients of the sesquilinear form stemming from PML. With the new change of variables $x \rightarrow x(1 + s^{-1}\sigma\psi)$, we get

$$A_\sigma(\hat{H}_z, v) = s^2 \mu(s) (\hat{H}_z, v) + \frac{1}{\varepsilon_x(s)} (\partial_y \hat{H}_z, \partial_y v)$$

$$+ \frac{1}{\varepsilon_y(s) (1 + \frac{\sigma\psi}{s})^2} (\partial_x \hat{H}_z, \partial_x v).$$

Theorem 2 Let $\psi(s) = \varepsilon_y(s)^{-1}$. Then the form $A_\sigma(\hat{H}_z, v)$ is passive.

This result allows to apply Theorem 1 to show the stability of the PML solution. However, the choice $\psi(s) = \varepsilon_y(s)^{-1}$ may be non-optimal, in the sense that it may require the introduction of many additional unknowns in the time-domain PML system. For a class of passive systems a characterization of 'stable' $\psi(s)$ is available.

4 Stable PMLs for local nondissipative materials

Assume that $\mu, \varepsilon_x, \varepsilon_y$ and ψ can be represented as $1 + \frac{p(s^2)}{q(s^2)}$, where $p(s)$ and $q(s)$ are polynomials with real coefficients that have no common

roots, and $\text{deg } p < \text{deg } q$. For this case in [1] the authors derived *necessary conditions* of the stability of the PMLs, which we can reformulate in a more convenient form. Given a function $r(s)$, we will denote $\tilde{r}(\omega) = r(-i\omega)$. Then the necessary stability conditions of the PML can be reformulated as the following two conditions:

1. $\psi(s)^{-1}$ is passive
2. For all propagative frequencies $\omega \in \mathbb{R}$ (i.e. satisfying $\tilde{\varepsilon}_x(\omega)\tilde{\mu}(\omega) > 0$ or $\tilde{\varepsilon}_y(\omega)\tilde{\mu}(\omega) > 0$), it holds: $\psi(\omega)\tilde{\varepsilon}_y(\omega) \geq 0$.

Let us introduce $\hat{A}_\sigma(\hat{H}_z, v) = \psi(s)\varepsilon_y(s)A_\sigma(\hat{H}_z, v)$

Theorem 3 Let $\psi(s)^{-1}$ be passive. Then the second necessary stability condition is equivalent to the passivity of $\hat{A}_\sigma(u, v)$.

Figure 1 confirms the above results, obtained with $\psi(s) = \varepsilon_y(s)^{-1}$.

5 Extension to antisymmetric dielectric tensors

We now consider the case where the off-diagonal entries do not vanish and satisfy $\varepsilon_{xy}(s) = -\varepsilon_{yx}(s)$. We can show that, in this case, the equation satisfied by \hat{H}_z becomes:

$$s^2 \mu(s) \hat{H}_z - \tau_x(s)^{-1} \partial_{yy} \hat{H}_z - \tau_y(s)^{-1} \partial_{xx} \hat{H}_z = 0,$$

where $\tau_x = \det \underline{\underline{\varepsilon}} / \varepsilon_y$ and $\tau_y = \det \underline{\underline{\varepsilon}} / \varepsilon_x$.

Lemma 4 Let $\underline{\underline{\varepsilon}}(s)$ be a passive tensor (in the sense $\Re(s \underline{\underline{\varepsilon}}(s)u, u) > 0, \forall u \in \mathbb{C}^2 \setminus \{0\}, \forall s \in \mathbb{C}_+$), then τ_x and τ_y are passive.

Therefore, we are in the framework of diagonal dielectric tensors and the previous results apply.

References

- [1] É. Bécache, P. Joly and V. Vinoles, On the analysis of perfectly matched layers for a class of dispersive media and application to negative index metamaterials, *Math of Comp*, vol. 87, pp. 2775–2810, nov. 2018.
- [2] J. P. Berenger, A perfectly matched layer for the absorption of electromagnetic waves, *JCP*, vol. 114, pp. 185-200, 1994.
- [3] É. Bécache, M. Kachanovska, Stable Perfectly Matched Layers for a Class of Anisotropic Dispersive Models. Part I : Necessary and Sufficient Conditions of Stability, *ESAIM: M2AN*, vol. 51, number 6, pp. 2399 - 2434, 2017.

**High Order Farfield Expansion ABC coupled with IGA and Finite Differences
Applied to Acoustic Multiple Scattering**

Vianey Villamizar^{1,*}, Jacob Badger¹, Thasin Khajah², Sebastian Acosta³

¹Department of Mathematics, Brigham Young University, Provo, Utah

²Department of Department of Mechanical Engineering, University of Texas at Tyler, Texas

³Department of Pediatrics–Cardiology, Baylor College of Medicine, Houston, Texas

*Email: vianey@mathematics.byu.edu

Abstract

We have constructed and successfully applied *high order local Farfield Expansions* absorbing boundary conditions (FEABC) for time-harmonic single acoustic scattering in two- and three-dimensions in previous works [1, 2]. We have also extended the formulation of FEABC to two and three dimensional acoustic multiple scattering in previous papers. In this work, we present some numerical results for two-dimensional multiple scattering from obstacles of arbitrary shape. We will also discuss weak formulations of these multiple scattering problems as our first step to implement general curvilinear finite element methods in the context of *Isogeometric Analysis* (IGA) for multiple scattering.

Keywords: Acoustic multiple scattering, High order local absorbing boundary conditions

1 The Local FEABC for multiple scattering

For brevity, we specialize our discussion to the two dimensional case but its extension to three dimensions follows a similar procedure [1]. We consider M disjoint obstacles each occupying a bounded domain with boundary Γ_m for $m = 1, \dots, M$. The unbounded region in the exterior of Γ_m is denoted by Ω_m . The obstacles are sufficiently separated from each other so as to enclose each one with disjoint circular artificial boundaries \mathcal{B}_m . The computational region Ω_m^- is bounded internally by the obstacle boundary Γ_m and externally by the artificial boundary \mathcal{B}_m . The unbounded region in the exterior of \mathcal{B}_m is denoted by Ω_m^+ so that \mathcal{B}_m is precisely the interface between Ω_m^- and Ω_m^+ . We also consider the following definitions:

$$\begin{aligned} \Omega &= \bigcap_{m=1}^M \Omega_m, & \Omega^- &= \bigcup_{m=1}^M \Omega_m^-, \\ \Omega^+ &= \bigcap_{m=1}^M \Omega_m^+ & \text{and } \Gamma &= \bigcup_{m=1}^M \Gamma_m. \end{aligned}$$

The scattering problem that we are considering consists of the scattering of a plane incident wave, u_{inc} , from multiple soft (Dirichlet) or hard (Neumann) obstacles embedded in the unbounded two-dimensional region Ω . As stated in our previous work, the construction of the FEABC is based on

a decomposition of the scattered field u into purely-outgoing wave fields u^m , such that $u = \sum_{m=1}^M u^m$ in Ω^+ , where each u^m is an outgoing wave radiating from the artificial boundary \mathcal{B}^m . The fundamental idea of this work is the use of a truncated expansion introduced by Karp in 1961 to represent each u^m in Ω_m^+ as

$$\begin{aligned} u^m(r^m, \theta^m) &= H_0(kr^m) \sum_{l=0}^{L-1} \frac{F_l^m(\theta^m)}{(kr^m)^l} \\ &+ H_1(kr^m) \sum_{l=0}^{L-1} \frac{G_l^m(\theta^m)}{(kr^m)^l}. \end{aligned} \quad (1)$$

The angular functions $F_l^m(\theta^m)$ and $G_l^m(\theta^m)$ are additional unknowns. They depend on the geometry of the scatterers and the properties of the domains Ω_m^- . An improved version of the formulation for the scattered field u is given by

$$\Delta u + k^2 u = 0, \quad \text{in } \Omega^-, \quad (2)$$

$$u = -u_{inc}, \text{ or } \partial_r u = -\partial_r u_{inc}, \quad \text{in } \Gamma, \quad (3)$$

$$u = \sum_{m=1}^M u^m \quad \text{on } \mathcal{B}_m, \quad (4)$$

$$\frac{\partial u}{\partial \nu^m} = \sum_{m=1}^M \frac{\partial u^m}{\partial \nu^m} \quad \text{on } \mathcal{B}_m, \quad (5)$$

$$\mathcal{H}^m[u] = \sum_{m=1}^M \mathcal{H}^m[u^m] \quad \text{on } \mathcal{B}_m, \quad (6)$$

for $m = 1, \dots, M$ in equations (4)-(6).

In (5), ν^m denotes the normal derivative on \mathcal{B}_m . The symbol \mathcal{H}^m is the Helmholtz operator in terms of the local polar coordinate system in Ω_m^- . The Eqs. (4)-(5) are the usual continuity of u and its normal derivative at the interface \mathcal{B}_m . The condition (6) establishes the continuity of the Helmholtz operator at the interface. The system is completed by adding the recurrence formulas for the angular

functions for $l = 1 \dots L - 1$, defined on B^m ,

$$2l G_l^m(\theta) = (l - 1)^2 F_{l-1}^m(\theta) + d_\theta^2 F_{l-1}^m(\theta) \quad (7)$$

$$2l F_l^m(\theta) = -l^2 G_{l-1}^m(\theta) - d_\theta^2 G_{l-1}^m(\theta). \quad (8)$$

The weak formulation for this BVP is an extension of the one found in [2] to several obstacles. For the IGA application to the BVP (3)-(8) with Dirichlet BC, we define the function spaces

$$\begin{aligned} \mathcal{S} &= \{(u, F_0^1, G_0^1, \dots, F_0^M, G_0^M, \dots, F_{L-1}^M, G_{L-1}^M) | u = \\ &= -u_{inc} \text{ on } \Gamma, u \in H^1(\Omega^-), F_l^m, G_l^m \in H^1(B_m)\} \\ \mathcal{S}_0^m &= \{v^m \in H^1(\Omega_m^-) | v^m = 0, \text{ on } \Gamma_m\}, \end{aligned}$$

for $m = 1, \dots, M$. Then, the weak formulation consists of finding $(u, F_0^1, G_0^1, \dots, F_{L-1}^M, G_{L-1}^M) \in \mathcal{S}$ such that the following equations are satisfied:

$$a(u, v^m) - \sum_{\bar{m}=1}^M (\partial u_{\bar{m}}^m, v^m)_{B_m} = 0, v^m \in \mathcal{S}_0^m,$$

$$a(u, v^m) = \int_{\Omega_m^-} (\nabla u \cdot \nabla v^m - k^2 u v^m) d\Omega_m^-,$$

$$(u, \hat{v}^m)_{B_m} - \sum_{\bar{m}=1}^M (u_{\bar{m}}^m, \hat{v}^m)_{B_m} = 0, \text{ for } \hat{v}^m \in H^1(B_m)$$

$$(\mathcal{H}^m[u^m], \hat{v}^m)_{B_m} = 0, \text{ for } \hat{v}^m \in H^1(B_m)$$

$$2l(F_l^m, \hat{v}^m)_{B_m} + l^2(G_{l-1}^m, \hat{v}^m)_{B_m} - \left((G_{l-1}^m)' , (\hat{v}^m)' \right)_{B_m}.$$

The angular function G_l^m satisfies a similar equation to this last equation.

Some of our numerical results obtained by numerically solving (2)-(8) with a second order finite difference approximation in generalized curvilinear coordinates are illustrated by Figs. 1- 3. We will present numerical results from the IGA technique at the conference.

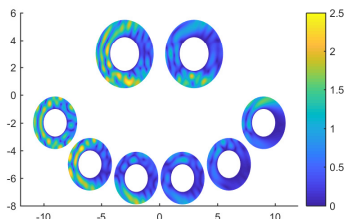


Figure 1: Total pressure field with $k = 2\pi$, for eight soft cylinders using $L = 8$ terms in the FEABC

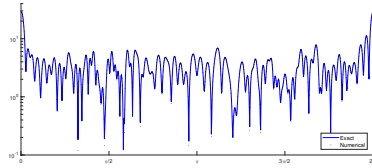


Figure 2: Comparison of exact and numerical far-field pattern for the eight cylinders of Fig. 1

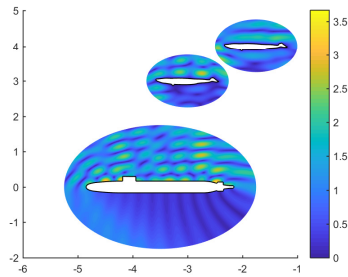


Figure 3: Scattering from a hard submarine and two soft whales with $k = 4\pi$ using $L = 12$ terms

2 Concluding remarks

In the experiments shown above, the numbers of terms, L in the FEABC was increased to achieve the best possible approximation. The overall order of convergence of the combined method for the cylindrical scatterers was two due to the second order of convergence of the numerical method used in the interior. The local nature of the FEABC is of great advantage when compared to alternative ABCs such as Dirichlet to Neumann.

References

- [1] V. Villamizar, S. Acosta, and B. Dastrup. High order local absorbing boundary conditions for acoustic waves in terms of farfield expansions. *J. Comput. Phys.*, 333:331–351, 2017.
- [2] T. Khajah and V. Villamizar. Highly accurate acoustic scattering: Isogeometric analysis coupled with local high order farfield expansion ABC. *Comput. Methods Appl. Mech. Engrg.*, 349:477–498, 2019.

A high order impedance boundary condition with uniqueness conditions to solve the time harmonic Maxwell's equations

Pierre PAYEN^{1,*}, Olivier LAFITTE², Bruno STUPFEL¹

¹CEA, DAM, CESTA, F-33114 Le Barp, France

²LAGA, Université Paris 13, F-93430 Villetaneuse, France

*Email: pierre.payen@cea.fr

Abstract

We consider the electromagnetic scattering from an object modelled by an impedance boundary condition (IBC). The originality of this paper is the exhibition of sufficient uniqueness conditions (SUC) to compute the IBC coefficients and their implementation in an integral equation code. The approximated solution is then validated on some objects of interest.

Keywords: Maxwell, impedance boundary condition, sufficient uniqueness condition, constrained optimisation, integral equation

1 Introduction

In this paper, \vec{x} is a vector and \mathbf{A} is a matrix.

Let Ω be a 3D object whose exterior boundary Γ is infinitely smooth and its outgoing normal vector is \vec{n} . The object Ω may be a coating of layers of materials on a perfectly conducting body, the layers being characterised by their thickness d , their (complex) relative permittivities ϵ and permeabilities μ , constant in each layer. The free space impedance is $\eta_0 = \sqrt{\mu_0/\epsilon_0}$.

We seek harmonic ($e^{i\omega t}$) solutions of the Maxwell's equations in \mathbb{R}^3 scattered by Ω , supplemented by a radiation condition at infinity. From ω , we define the wavenumber $k_0 = \omega\sqrt{\epsilon_0\mu_0}$.

The radiation condition (2) is expressed on a ball of a large radius whose outgoing normal vector is $\vec{\nu}$ (see [2] for the expression of \mathcal{T}):

It is proven in [1] that there exists a Calderon operator $\text{Op}(\mathcal{C})$ such that Maxwell equations on $\Omega \cup \Omega^c$ with radiation condition (2) is equivalent to (1)-(2)-(3).

$$\begin{cases} \vec{\nabla} \times \vec{E} = ik_0\mu\vec{H} & \text{in } \Omega^c \cap B(\vec{0}, R) \\ \vec{\nabla} \times \vec{H} = -ik_0\epsilon\vec{E} & \text{in } \Omega^c \cap B(\vec{0}, R) \end{cases} \quad (1)$$

$$\vec{\mathcal{T}}E_t = -\vec{\nu} \times \vec{H} \quad \text{on } \partial B(\vec{0}, R) \quad (2)$$

$$\vec{E}_t = \text{Op}(\mathcal{C}) \left(\vec{n} \times \vec{H} \right) \quad \text{on } \Gamma \quad (3)$$

The equation (3) is traditionally replaced by an approximate boundary condition denoted by IBC.

To compute a solution of (1)-(2)-(3) in $\Omega^c \cap B(\vec{0}, R)$ is impractical, and so the surface integral equation method is used on Γ (see [2]).

2 High order impedance boundary condition

We call a high order impedance boundary condition (HOIBC) an IBC that contains differential operators. Several HOIBC have been proposed (see [4, 6]). We chose the following, here named IBC3.

$$\begin{aligned} & (I + b_1\mathcal{L}_D + b_2\mathcal{L}_R)\vec{E}_t = \\ & (a_0I + a_1\mathcal{L}_D + a_2\mathcal{L}_R)\vec{n} \times \vec{H} \quad \text{on } \Gamma \quad (4) \end{aligned}$$

and we refer to [4, 6] where operators $\mathcal{L}_D, \mathcal{L}_R$ are defined.

Coefficients a_0, a_1, a_2, b_1, b_2 are complex functions of the coating and the frequency and their computation will be explained later.

3 Sufficient uniqueness conditions

Uniqueness of the solution of (1)-(2) is guaranteed when

$$\Re \left(\int_{\Gamma} \left(\vec{n} \times \vec{H} \right) \cdot \overline{\vec{E}_t} ds \right) \geq 0 \quad (5)$$

(see [1, 5]). Let $z = |a_1|^2|a_2|^2 - b_1a_0\overline{a_1}|a_2|^2 - b_2a_0\overline{a_2}|a_1|^2$. If a_1 and a_2 are non-zero and the following quantities are positive:

$$\begin{array}{ccc} \Re(\overline{a_0}z) & -\Re(\overline{a_1}z) & -\Re(\overline{a_2}z) \\ \Re(b_1\overline{a_1}) & \Re(b_2\overline{a_2}) & -\Re(a_1) \\ -\Re(b_1\overline{a_2}a_1a_0) & -\Re(b_2\overline{a_1}a_2a_0) & -\Re(a_2) \end{array} \quad (6)$$

one can prove (5), hence (6) are called sufficient uniqueness conditions (SUC) and imply uniqueness of the solution of (1)-(2)-(4).

We denote by \mathfrak{C} the subset of \mathbb{C}^5 where the SUC (6) are verified.

4 The locally planar approximation

Since Γ is infinitely smooth, we assume it is locally flat. This new boundary gives by a Fourier analysis the symbol of the Calderon operator. Thus the HOIBC coefficients are solution of the following constrained optimisation problem:

Find $\underline{x} = (a_0, a_1, a_2, b_1, b_2)^t \in \mathcal{C}$ that minimise

$$\|\mathbf{A}\underline{x} - \underline{b}\|_{L_2}^2 \quad (7)$$

where \mathbf{A} is a $n_i \times 5$ complex matrix, \underline{b} is a complex vector of size n_i , depending on the value of the symbol of the Calderon operator at some incidence of interest. The number n_i is the number of angles of incidence.

In the case of lossless material, the cost function is equal to ∞ when the incidence belongs to the set of critical values where $k_0\sqrt{\epsilon\mu - s^2}d$ is a pole of \tan , a term contained in the symbol of the Calderon operator. Our numerical method needs to avoid such points therefore other SUC have been used.

5 Surface integral equation

The system (1)-(2)-(4) is equivalent to a surface integral equation (see [2]) from which one can deduce the electromagnetic fields. This surface integral equation is approximated with the Boundary Element Method (BEM) and leads to the following basis dependent linear system:

$$\begin{bmatrix} \mathbf{S}_0 + \mathbf{Z}_{JJ} & \mathbf{S}_G - \mathbf{Z}_{JK} \\ \mathbf{S}_G - \mathbf{Z}_{KJ} & -\mathbf{S}_0 - \mathbf{Z}_{KK} \end{bmatrix} \begin{bmatrix} \underline{J} \\ \underline{K} \end{bmatrix} = \begin{bmatrix} \underline{b}_E \\ \underline{b}_H \end{bmatrix} \quad (8)$$

The unknowns \underline{J} and \underline{K} are complex vectors of size n_f where n_f is the number of degrees of freedom of the mesh. The right hand side of (8) is given and depends on the incident field.

Projecting a new set of test functions ¹ to account for the discretisation of the \mathcal{L}_R terms, one can deduce

$$\begin{aligned} \mathbf{Z}_{JJ} &= 2\pi(a_0\mathbf{M} - (a_1\mathbf{L}_D + a_2\mathbf{L}_R)) \\ \mathbf{Z}_{JK} &= 2\pi(b_1\mathbf{L}_D + b_2\mathbf{L}_R)\mathbf{P} \\ \mathbf{Z}_{KJ} &= \frac{2\pi}{a_0}(a_2\mathbf{L}_D + a_1\mathbf{L}_R)\mathbf{P} \\ \mathbf{Z}_{KK} &= \frac{2\pi}{a_0}(\mathbf{M} - (b_2\mathbf{L}_D + b_1\mathbf{L}_R)) \end{aligned} \quad (9)$$

Matrices \mathbf{S}_0 , \mathbf{S}_G , \mathbf{M} , \mathbf{P} , \mathbf{L}_D , \mathbf{L}_R are defined in [5].

¹which differs from the usual Raviart-Thomas Hddiv conforming function

6 Numerical results

We model one layer of low index material $\epsilon = 1 - i$, $\mu = 1$ of thickness $d = 0.05m$. The wavenumber is $k_0 = 4.192m^{-1}$. Figure 1 shows the bistatic radar cross section (RCS) for a spherecone of the BEM+IBC3 code to a 3D axisymmetric code, labelled as 'Exact'.

	$\frac{\ r_{pl} - r_{IBC3}\ _2^2}{\ r_{pl}\ _2^2}$
IBC3	3.80010^{-7}
IBC3 + SUC	5.56910^{-4}

Table 1: Relative L_2 error of the reflection coefficient of the infinite plane.

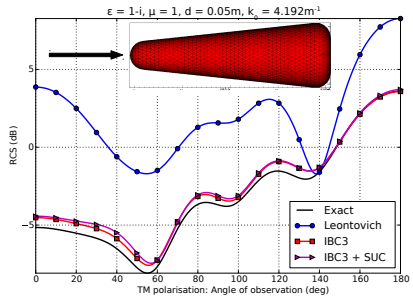


Figure 1: Bistatic RCS of the IBC3 of a spherecone illuminated on the tip

7 Conclusion

The IBC3 outperforms the Leontovich approximation and the SUC ensures the uniqueness of the solution.

References

- [1] M. Cessenat, "Mathematical Methods in Electromagnetism: Linear Theory and Applications, vol. 41". World Scientific, 1996.
- [2] J.-C. Nédélec, "Acoustic and Electromagnetic Equations: Integral Representations for Harmonic Problems", Springer Science & Business Media, 2001.
- [3] B. Stupfel and D. Poget, "Sufficient uniqueness conditions for the solution of the time harmonic Maxwell's equations associated with surface impedance boundary conditions", Journal of Computational Physics, vol. 230, n. 12, p. 4571-4587, 2011.
- [4] A. Aubakirov, "Electromagnetic scattering problem with higher order impedance boundary conditions and integral methods", Ph.D thesis, Cergy-Pontoise, 2014.
- [5] B. Stupfel, "Implementation of High-Order Impedance Boundary Conditions in Some Integral Equation Formulations", IEEE Transactions on Antennas and Propagation, vol. 63, n. 4, p. 1658-1668, 2015.
- [6] P. Soudais, "3D MoM computations with high order impedance boundary condition", in International Conference on Electromagnetics in Advanced Applications (ICEAA), 2017, p. 340-341.

Combining Dynamical Energy Analysis with Advanced Transfer Path Analysis

Gregor Tanner^{1,*}, Timo Hartmann¹, Satochi Morita², Martin Richter¹¹School of Mathematical Sciences, University of Nottingham, UK²Yanmar R&D Europe, Firenze, Italy

*Email: gregor.tanner@nottingham.ac.uk

Abstract

Dynamical Energy Analysis (DEA) is a high frequency integral method modelling structure borne sound for complex built-up structures. The method works directly on existing finite element meshes circumventing time-consuming and costly remodelling strategies. DEA has been used to calculate the structure borne sound of an assembled agricultural tractor and good agreement between measurements and DEA calculations has been shown. We propose here to integrate measurement data into DEA based on the Advanced Transfer Path Analysis (ATPA) to extract energy transmission characteristics of a structure. The proposed method is verified by comparing with measurements on a full tractor structure.

Keywords: High frequency asymptotics, transfer operator, structure borne sound, transfer path analysis

1 Introduction

Simulations of the vibro-acoustic performance of cars, trains, airplanes as well as heavy goods vehicles such as lorries and tractors are routinely carried out at various design stages. The Finite Element Method (FEM) is used for noise and vibration simulations in complex structures in the low frequency regime. It requires extremely fine meshes at high frequencies, however, to capture shorter wave lengths leading to large model sizes. Statistical representations such as the Statistical Energy Analysis (SEA) [1] have been developed, leading to relatively small and simple models in comparison with FEM. However, SEA gives results only on a relatively coarse scale and cannot deal with details of the structure [2]. We start from a ray-tracing ansatz reformulated in terms of integral equations. This leads to linear flow equations for the mean vibrational energy density and forms the basis of the Dynamical Energy Analysis (DEA) method [3]. DEA includes SEA as special case via a low order representation of the so-called transfer oper-

ator. Higher order implementations enrich the DEA model with information from the underlying ray dynamics. DEA allows for more freedom in sub-structuring the total system and variations of the energy density across sub-structures can be modelled. Hence, DEA can resolve the full geometrical complexity of the structure. An efficient implementation of DEA on meshes has been presented in [4]. DEA has been used to calculate the structure borne sound of an assembled agricultural tractor and good agreement between measurements and DEA calculations has been demonstrated [5]. It is often difficult to generate accurate FE meshes of assembled complex structures such as the gear box, the engine or the power train. For these parts, DEA is expected to work less well and we suggest here to cut out these complex parts of the structure from the DEA mesh and replace it with coupling elements derived from measurement data. We generate these new DEA coupling elements based on the so-called Advanced Transfer Path Analysis (ATPA), which generates a transfer matrix from measurements [6]. In the following, we will show some results for a real tractor structure. For a description of the DEA or the ATPA method, see [4, 5] and [6] as well as [7] for the theory behind combining these two methods.

2 Results

The DEA-ATPA approach was validated in [7] with an FE model for a simple structure made of three plates connected by beams. We assume that the middle plate represents the complicated part and is modelled as the DEA-ATPA element. Four interface points were defined at the boundaries of the connecting beams and the ATPA transfer function was calculated, here using FEM data instead of measuring a real structure. Validation is also performed doing an FE calculation of the full structure.

In this presentation, the hybrid method is extended to a real tractor structure as shown in

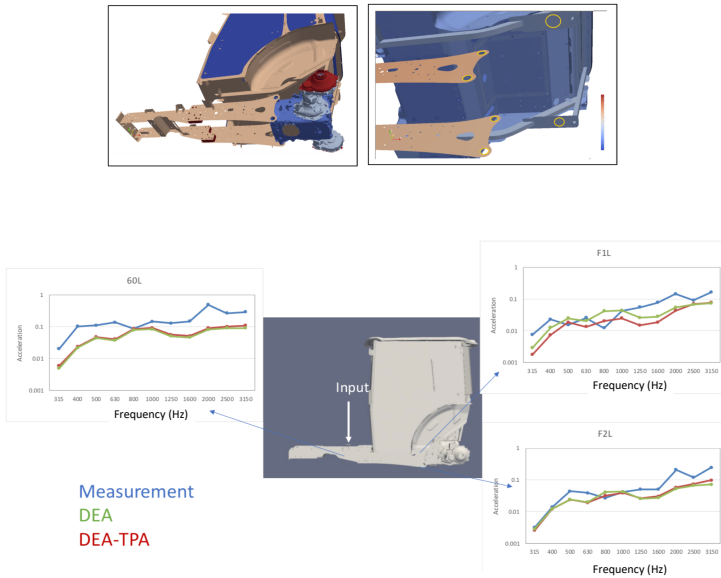


Figure 1: Upper panel: Tractor model with and without the gearbox; lower panel: results based on DEA, DEA-ATPA and measurements

the upper half of Fig. 1. The part below the cabin containing the gear-box and other complex structural elements is treated as the ATPA coupling element. The entries for the transfer function are obtained from measurements by applying shakers to the structure and measuring the response at the connection points (yellow circles in Fig. 1). The results from measurements on the full structure compare favourably with the DEA and the DEA-ATPA results as can be seen in the lower half of Fig. 1.

References

- [1] R. H. Lyon, and R. G. DeJong, *Theory and Application of Statistical Energy Analysis*, Butterworth-Heinemann, Boston, 1995.
- [2] P. J. Shorter and R. S. Langley, *Vibro-acoustic analysis of complex systems*, Journal Sound Vib., Vol. 288, 669-699, 2005.
- [3] G. Tanner, *Dynamical energy analysis - Determining wave energy distributions in vibro-acoustical structures in the high-*

frequency regime, J. Sound Vib. 320, 1023-1038, 2009.

- [4] D. J. Chappell, G. Tanner, D. Löchel and N. Søndergaard, *Discrete flow mapping: transport of phase space densities on triangulated surfaces*, Proc. R. Soc. A, 469, 20130153, 2013.
- [5] T. Hartmann, S. Morita, G. Tanner, and D. J. Chappell, *High-frequency structure-borne sound transmission for a tractor model using Dynamical Energy Analysis*, accepted for publication in Wave Motion.
- [6] O. Guasch, F. X. Magrans, *The Global Transfer Direct Transfer method applied to a finite simply supported elastic beam*, J. Sound Vib., 276, 335-359, 2004
- [7] S. Morita, T. Hartmann, G. Tanner, *Dynamical Energy Analysis Modelling by using Transfer Path Analysis*, Proc. of ISMA 2018.

Sound radiation from complex vibrating mechanical structures using Wigner transformation techniques

Mohammed, Neekar M^{1,*}, Tanner, Gregor¹, Creagh, Stephen C¹

¹School of Mathematical Sciences, University of Nottingham, United Kingdom

*Email: pmxnm3@nottingham.ac.uk

Abstract

We propose a new method to model sound radiation using the vibrational response obtained from Dynamical Energy Analysis (DEA) calculations. The link between the structural response and the acoustic field can be achieved using so-called Wigner transform (WF) techniques. The energy density from a DEA structure-borne sound calculation can be related to two-point correlations of the vibrational displacement and then used to propagate the acoustic field using Rayleigh integral methods. This integral relates the vibration of a plate to the sound pressure at a point in a half-space above the plate. In this way we compute the intensity of the sound pressure radiated from a structure, here from a flat plate. Furthermore, we present a formula of radiation efficiency in terms of the WF. This technique has the potential to be used for generic complex mechanical structures.

Keywords: Sound radiation, fluid-structure coupling, Wigner distribution functions

1 Introduction

Sound propagation in and radiation from complex vibrating mechanical built-up structures is an important research area for mechanical engineering. While standard methods such as the finite element (FEM) or boundary element method (BEM) can be used in the low frequency regime, these methods have limitations when the wavelength of the field becomes small compared to the size of the structure. Therefore, more efficient algorithms become desirable, and in particular, high frequency approximation methods become an attractive alternative. Dynamical Energy Analysis (DEA) [1] is used to model vibro-acoustic response of complex mechanical structures based on meshed shell structure models in frequency ranges where FEM or BEM models are becoming too large. In this paper, we extend DEA towards coupling structural vibration calculations with estimating acoustic radiation in the surrounding fluid; the method is

based on the Wigner transformation technique (WF). The WF technique has its origin in quantum mechanics [2], but has been intensively studied also in the context of electromagnetism such as for radio frequency (RF) radiation [3] and optics [4]. The energy density from DEA can be related to two-point correlations of the vibrational wave. We propagate the acoustic field using a Rayleigh integral method [5]. In addition, we describe how field-field correlation functions can be efficiently propagated using the propagator obtained by Fourier transforming Rayleigh's first integral. Furthermore, we derive an acoustic phase-space representation in the classical ray tracing limit.

2 Rayleigh integral and the propagator in the momentum representation

We use as a basis for our calculation the Kirchhoff-Helmholtz equation for irregularly shaped vibrating bodies, which can be further simplified, for planar structures, to the so-called Rayleigh integral [5]. The pressure p radiated by the structure is then determined by

$$p(\mathbf{r}) = -\frac{i\rho kc}{2\pi} \int_{\Omega} w(\mathbf{r}') \frac{\exp(ik|\mathbf{r} - \mathbf{r}'|)}{|\mathbf{r} - \mathbf{r}'|} d\mathbf{r}', \quad (1)$$

where $\mathbf{r} = (x, y)$, Ω is the domain of the planar structure, k denotes the acoustic wave number, $w(\mathbf{r}')$ is the normal surface velocity, c is the speed of sound in the surrounding medium and ρ is the fluid density. We take the Fourier transforms in x and y of both sides of Eq.(1) to get [3]

$$P(\mathbf{p}, z) = \rho c W(\mathbf{p}, z) \frac{e^{ikT(\mathbf{p})z}}{T(\mathbf{p})}, \quad (2)$$

where $P(\mathbf{p}, z)$, $W(\mathbf{p}, z)$ denote the momentum representation of the sound pressure and the normal surface velocity respectively, z denotes the distance above the plate and $k\mathbf{p}$ is the wave vector component in the (x, y) -plane. In this work, the normal component of the unit wave

vector is defined as

$$T(\mathbf{p}) = \begin{cases} \sqrt{1 - |\mathbf{p}|^2} & \text{for } |\mathbf{p}|^2 \leq 1, \\ i\sqrt{|\mathbf{p}|^2 - 1} & \text{for } |\mathbf{p}|^2 > 1. \end{cases}$$

In the next section we connect the structural response from DEA to the sound pressure and for that we need the acoustic correlation function.

2.1 Propagation of correlation data and Wigner transformation

The aim of this work is to predict acoustic emission from complex, nosily driven vibrating structures using methods that combine well with phase-space simulation methods such as DEA. In this setting, the vibrational and radiated acoustic fields are naturally described statistically, in the form of field-field correlation functions. Here we work with a correlation function in momentum representation, defined by

$$\hat{\Gamma}_z(\mathbf{p}_1, \mathbf{p}_2) = \langle P(\mathbf{p}_1, z), P^*(\mathbf{p}_2, z) \rangle, \quad (3)$$

where $P(\mathbf{p}, z)$ is given in Eq.(2). A phase-space representation, which combines position and momentum coordinates can be obtained from Eq.(3) through the WF. Using this, we can find the propagated acoustic WF in the form

$$W_z(\mathbf{r}, \mathbf{p}) = W_0(\mathbf{r}, \mathbf{p}) *_r g_z(\mathbf{r}, \mathbf{p}), \quad (4)$$

where $\mathbf{p} = (\mathbf{p}_1 + \mathbf{p}_2)/2$, $\mathbf{r} = (\mathbf{r}_1 + \mathbf{r}_2)/2$, $\mathbf{q} = \mathbf{p}_1 - \mathbf{p}_2$, and $*_r$ represents a convolution with respect to \mathbf{r} . W_0 is the WF of the surface normal velocity correlation function, and

$$g_z(\mathbf{r}, \mathbf{p}) = \left(\frac{k\rho c}{2\pi}\right)^2 \int \frac{1}{T(\mathbf{p} + \mathbf{q}/2)T^*(\mathbf{p} - \mathbf{q}/2)} e^{ikz[T(\mathbf{p} + \mathbf{q}/2) - T^*(\mathbf{p} - \mathbf{q}/2)]} e^{ik\mathbf{q} \cdot \mathbf{r}} d\mathbf{q}. \quad (5)$$

The kernel $g_z(\mathbf{r}, \mathbf{p})$ can be simplified through a ray-based approximation [3]. In the case of the spatial variation in the source correlation is assumed to take place on a scale larger than the wavelength, significant contributions to Eq.(5) come from small values of \mathbf{q} . This suggests using a Taylor expansion of the kernel exponent around $\mathbf{q} = \mathbf{0}$. Retaining only the leading order contribution, the Green integral operator becomes a Dirac delta function. Thus, one obtains the classical ray tracing approximation of

the acoustic WF in the form

$$W_z(\mathbf{r}, \mathbf{p}) = \frac{\rho^2 c^2}{|T(\mathbf{p})|^2} \begin{cases} W_0(\mathbf{r} - \frac{z\mathbf{p}}{\sqrt{1 - \mathbf{p}^2}}, \mathbf{p}) & \text{for } |\mathbf{p}|^2 \leq 1, \\ W_0(\mathbf{r}, \mathbf{p})e^{-2kz\sqrt{|\mathbf{p}|^2 - 1}} & \text{for } |\mathbf{p}|^2 > 1. \end{cases} \quad (6)$$

We are interested in calculating radiation efficiency in terms of the WF. From classical formulations of radiation efficiency, one can derive a formula for it in terms of the WF using Eq.(6), sampled at $z = 0$ (because total sound been radiated is independent of z). This takes the form

$$\sigma = \frac{\int_{\Omega} d\mathbf{r} \int_{\mathbb{R}^2} d\mathbf{p} W_0(\mathbf{r}, \mathbf{p}) f(\mathbf{r}, \mathbf{p})}{\int_{\Omega} d\mathbf{r} \int_{\mathbb{R}^2} d\mathbf{p} W_0(\mathbf{r}, \mathbf{p})}, \quad (7)$$

where $f(\mathbf{r}, \mathbf{p})$ is a Wigner representation of $\text{Re}(1/T(\mathbf{p}))$ projected onto the region Ω . This approach allows us to quantify acoustic radiation from noisy vibrating structures with $W_0(\mathbf{r}, \mathbf{p})$ being approximated by phase-space simulations such as DEA.

References

- [1] Tanner, G., Dynamical energy analysis - Determining wave energy distributions in vibro-acoustical structures in the high-frequency regime, *Journal of Sound and Vibration* **320** (2009), pp. 1023–1038
- [2] Hillery, M. and O’Connell, R.F., Scully, M.O. and Wigner, E.P., Distribution functions in physics: fundamentals, *Physics Reports* **106** (1984), pp. 121–167
- [3] Gradoni, G., Creagh, S.C. and Tanner, G. and Smartt, C. and Thomas, D.W.P., A phase-space approach for propagating field-field correlation functions, *New Journal of Physics* **17** (2015), pp. 093027
- [4] Alonso, M. A., Wigner functions in optics: describing beams as ray bundles and pulses as particle ensembles, *Advances in Optics and Photonics* **3** (2011), pp. 272–365
- [5] Rayleigh, L., XXXVII. On the passage of waves through apertures in Plane screens, and allied problems, *The London, Edinburgh, and Dublin Philosophical Magazine and Journal of Science* **43** (1897), pp. 259–272

3d Modeling and Simulation of a Harpsichord

Lukas Larisch¹, Babett Lemke², Gabriel Wittum³

¹lukas.larisch@kaust.edu.sa

²babett.lemke@gcsc.uni-frankfurt.de

³gabriel.wittum@kaust.edu.sa

Abstract

In our talk, we present FEM based numerical simulations of a harpsichord. We aim to capture the oscillation behavior of eigenfrequencies of its soundboard. We resolve the complicated geometry by an unstructured 3d grid and take into account the anisotropy of wood. The eigenvalue problem is solved using the preconditioned inverse iteration method (PINVIT) with an efficient multi grid preconditioner. The latter allows us to resolve the harpsichord with a high resolution grid, which is required to capture fine modes of the simulated eigenfrequencies. To verify our results, we compare them with measurement data obtained from an experimental modal analysis of the harpsichord that we have modeled. We finally investigate the impact of various aspects of the geometry on the computed eigenfrequencies.

Keywords: Eigenvalue problem, finite strain mechanics, FEM, musical instrument

1 Introduction

The mathematical characterization of the sound of a musical instrument still follows Schumann's laws [1]. According to this theory, the resonances of the instrument body, the formants, filter the oscillations of the sound generator (e.g. string) and produce the characteristic "timbre" of an instrument. This is a strong simplification of the actual situation: It applies to a point source and can be easily performed by a loudspeaker, disregarding the three dimensional structure of music instruments. To describe the effect of geometry and material of the instruments, we set up a three dimensional model and simulate it using the simulation system UG4 [2] [3].

The design of musical instruments is primary a matter of experience. Understanding the connection between geometry and material on the one hand (morphology) and the timbre of the instrument on the other hand, is still lacking quantitative insight. Modeling musical instru-

ments aims at obtaining a quantitative characterisation of the sound and timbre of musical instruments. In particular the connection between geometry, material and the characteristic sound needs investigation.

2 Modeling

In order to understand and simulate the oscillations of a soundboard, we investigate the occurring mechanical forces on the soundboard and how they deform it. We consider the soundboard an elastic body on which outer and inner forces are acting. We use a displacement-ansatz to solve the coupled system of equations

$$(1) \operatorname{div} \underline{\sigma} + \underline{f} = 0$$

$$(2) \underline{\sigma} = \underline{\epsilon} : \underline{\epsilon}$$

$$(3) \underline{\epsilon} = \frac{1}{2}(\nabla \underline{u} + (\nabla \underline{u})^T),$$

the equilibrium of forces (1), Hookes law (2) and conditions of kinematics (3), leading to the generalized eigenvalue problem

$$(4) \operatorname{div}(\underline{\epsilon} : (\frac{1}{2}(\nabla u_0 + (\nabla u_0)^T))) = -\lambda \underline{u}_0,$$

which is then discretized by FEM with quadratic ansatz functions.

We created four geometries of the soundboard corresponding to successive manufacturing stages. The complete model is a (plain) soundboard with several ribs, a bridge and a rosette.

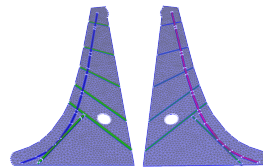


Figure 1: Complete geometry of the soundboard. Left: top view, Right: bottom view.

3 Experimental Modal Analysis

It is possible to describe properties in structural dynamics (e.g., frequencies, mode shapes) of components with help of an experimental modal analysis. We are interested in the eigenmodes of the harpsichord on the soundboard for verification of our simulations.

Basically, the measurement setup consists of an oscillation generator and a vibrometer that measures the reaction corresponding to the excitations. Because we are interested in the oscillation behavior of various excitation frequencies, the frequency generated by the oscillation generator is altered with time. The excitation force thereby remains constant.

We carried out the experiments in the laboratories of Polytec, where we used a PSV-400 Scanning Vibrometer [4]. During the experiment, the frequency of the excitation ranged from 5Hz to 2000Hz with a sampling rate of 0.5Hz. We thereby investigated the displacement of 2013 points.

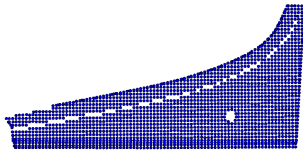


Figure 2: Grid for the experimental modal analysis.

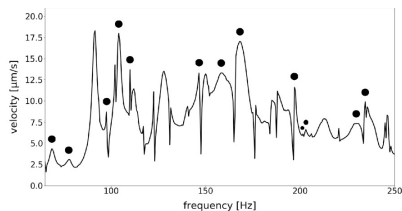


Figure 3: Response (velocity) within the experiment. Dots above peaks denote eigenmodes that are shared between simulation and experiment.

4 Results

The simulations show that the ribs and the bridge are crucial for the oscillation behavior of the

soundboard whereas the effects of the rosette are negligible. We investigated the impact of three different sets of material constants on the results of the simulation. They do not have considerable influence on mode shapes, but are sensitive on the eigenfrequencies.

We observe that all but one of 16 simulated eigenmodes can be found on our reference harpsichord that has been used for the experiments. However, the real soundboard has several eigenmodes that do not appear in the simulations, because our models cover the actual soundboard, but other parts of the harpsichord as, e.g., the case, which is oscillating as well.

References

- [1] E.K Schumann, Physik der Klangfarben, 1929, Leipzig.
- [2] Sebastian Reiter, Andreas Vogel, I Heppner, and Gabriel Wittum, A massively parallel geometric multigrid solver on hierarchically distributed grids, *Computing and Visualization in Science* 16 (2014), no. 4, pp. 151–164.
- [3] Andreas Vogel, Sebastian Reiter, Martin Rupp, Arne Nagel, and Gabriel Wittum, Ug 4: A novel flexible software system for simulating pde based models on high performance computers, *Computing and Visualization in Science* 16 (2013), no. 4, pp. 165–179.
- [4] Polytec, <http://www.polytec.com>.

Transparent boundary conditions for periodic waveguides: analysis and extensions

Sonia Fliss^{1,*}, Patrick Joly¹, Vincent Lescarret²

¹POEMS (CNRS-INRIA-ENSTA Paristech), Palaiseau, France

²LSS, UMR8506 CNRS-SUPELEC-UPS11, Gif-sur-Yvette, France

*Email: sonia.fliss@ensta-paristech.fr

Abstract

We consider the time harmonic wave equation in perturbed periodic waveguides. We justify rigorously the construction of the transparent boundary conditions based on Dirichlet-to-Neumann map and show that the problem with these transparent boundary conditions is of Fredholm type except for a countable set of frequencies. This allows to define and compute the physical solution of the problem.

Keywords: periodic media, Floquet modes, Dirichlet-to-Neumann operator.

1 Introduction

It is really delicate to define the physical solution of the time harmonic wave equation in perturbed periodic media, especially in presence of guided modes. Recent progresses have been done about the mathematical analysis of the time harmonic wave equation in (1) periodic waveguides and (2) surfaces and layers. In order to define uniquely the physical solution, radiation conditions have been proposed in [3] for perfectly periodic closed waveguide, in [2] for periodic closed half-waveguide and finally in [4] for periodic open waveguides.

From a numerical point of view, there are few methods. Some years ago, we have proposed a numerical method, based on Dirichlet-to-Neumann operators (DtN) for the time harmonic wave equation in locally perturbed periodic waveguides. This method was rigorously justified in presence of dissipation. In this work we provide a rigorous mathematical justification of this numerical method in the absence of dissipation.

2 Model problem

Let us consider a half-waveguide which is an open connected domain, unbounded in one direction and bounded in the other directions $\Omega \subset S \times]-a, +\infty[$. A generic point of Ω has coordinates (\mathbf{x}_s, x_d) where x_d is the coordinate in the infinite direction of the waveguide and

$\mathbf{x}_s \in S \subset \mathbb{R}^{d-1}$ ($d \geq 2$) is the coordinate in the transverse direction. The semi-infinite part $\Omega^+ = \Omega \cap \{x_d > 0\}$ is L -periodic ($\Omega^+ + L e_d \subset \Omega^+$). We denote \mathcal{C} the periodicity cell of Ω^+ which is defined by

$$\mathcal{C} = \Omega \cap \{0 < x_d < L\},$$

Let $\Omega^0 = \Omega \setminus \Omega^+$ be the remaining part of the propagation domain and $\Gamma^0 = \Omega \cap \{x_d = 0\}$ the interface between Ω^0 and Ω^+ . Let ν denotes the outgoing normal to Ω .

We wish to solve the Helmholtz equation

$$\begin{cases} -\nabla(A(x) \nabla u) - \omega^2 B(x) u = f & \text{in } \Omega \\ A(x) \nabla u \cdot \nu = 0 & \text{on } \partial\Omega \end{cases} \quad (1)$$

where the source term f is in $L^2(\Omega)$ and has a compact support included in Ω^0 , the characteristic of the medium A and B are L^∞ -functions, positively bounded from below, and L -periodic in Ω^+ , the frequency ω is in \mathbb{R} .

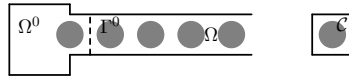


Figure 1: The domains Ω and \mathcal{C}

(1) is not always sufficient to define the physical solution of the problem. In order to characterize it, we often use the limiting absorption principle. Let u_ε be the unique solution in $H^1(\Omega)$ of (1) where ω^2 is replaced by $\omega^2 + i\varepsilon\omega$ with $\varepsilon > 0$. Then the restriction of u_ε in Ω^0 is solution of the problem set in Ω^0 with the transparent boundary conditions

$$A(x) \nabla u_\varepsilon^0 \cdot e_d + \Lambda_\varepsilon u_\varepsilon^0 = 0 \text{ on } \Gamma^0$$

where Λ_ε is the associated DtN map, defined by periodic half-waveguide problems set on Ω^+ . In [1], an algorithm to compute this operator has been proposed. We investigate here the limit of Λ_ε when ε tends to 0. Using [2], we show that,

Wave Equation in a Periodic Waveguide with a Local Perturbation

Marina Fischer^{1,*}

¹Mathematisches Institut, Heinrich-Heine-Universität, Düsseldorf, Germany

*Email: marina.fischer@uni-duesseldorf.de

Abstract

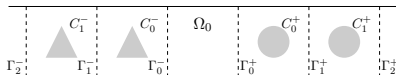
We focus on the numerical computation of the wave equation in a periodic waveguide that is locally perturbed in a bounded domain. By using the Laplace transform in time, we transfer our computations to the frequency domain and obtain a Helmholtz equation. Applying the ideas in [1, 2], we derive transparent boundary conditions on the perturbed domain by solving local problems on one periodicity cell and extend the solution to the rest of the waveguide. With the inverse Laplace transform, we then obtain transparent boundary conditions in the time domain which are now given as a convolution. On using convolution quadrature methods we are able to compute the solution of the wave equation in the perturbed domain. Besides, with the same technique the solution on the rest of the waveguide can be computed.

Keywords: periodic waveguide, transparent boundary conditions, DtN operator, convolution quadrature

1 Introduction

In contrast to theoretical considerations, periodic media in real applications usually are not perfectly periodic but contain some bounded regions where the periodic structure is perturbed. For example, this can be observed in photonic crystals. A well-known idea for the numerical computations in these regions is to take advantage of the periodicity outside.

In this contribution, we consider a periodic waveguide Ω which contains a local perturbation in the region $\Omega_0 := \Omega \cap \{-a < x < a\}$. Out-



side the region Ω_0 the waveguide Ω is periodic to the left and to the right. The periodicity cells on the periodic sub-domains are denoted by C_j^\pm , where $\Gamma_j^\pm := C_j^\pm \cap \{x = \pm a(1 + 2j)\}$ are the “vertical” boundaries.

We study the wave equation

$$\rho(x, y) \partial_t^2 u - \Delta u = f \text{ in } \Omega \times \mathbb{R}^+ \quad (1)$$

subject to the initial conditions $u(\cdot, 0) = u_0$ and $\partial_t u(\cdot, 0) = u_1$ in Ω and with quasi-periodic boundary conditions on $\partial\Omega$. In particular, we are interested in finding the transparent boundary conditions on the vertical segment $\Gamma_0^- \cup \Gamma_0^+$ that enable us to solve the wave equation in Ω_0 . We assume $\text{supp}(f(\cdot, t)) \subset \Omega_0 \forall t \in \mathbb{R}^+$ as well as $\text{supp}(u_0) \subset \Omega_0$ and $\text{supp}(u_1) \subset \Omega_0$. The function ρ is a strictly positive function of $L^\infty(\Omega)$ and periodic in x -direction outside the region Ω_0 , thus modelling the local perturbation. Under these hypotheses the wave equation (1) is well posed (c.f. [3]).

2 Transformation into frequency domain

For brevity, we now restrict our considerations to the sub-domain $\Omega^+ := \bigcup_{j=0}^\infty C_j^+$, i.e. to the construction of the boundary condition on Γ_0^+ . Because of the periodicity, it is clear that all cells C_j^+ can be identified to C_0^+ and all boundaries Γ_j^+ to Γ_0^+ .

Since we would like to apply the approach in [1–3] which benefits from this identification, we use the Laplace transform in t of (1) to transfer our computations into the frequency domain. This yields the Helmholtz equation

$$\rho(x, y) s^2 U - \Delta U = 0 \text{ in } \Omega^+ \text{ with } s \in \mathbb{C}, \quad (2)$$

where $U(x, y, s) := \mathcal{L}\{u(x, y, \cdot)\}(s)$. Imposing the boundary condition $U = \varphi$ on Γ_0^+ for $\varphi \in H^{1/2}(\Gamma_0^+)$ and using the solutions of two local problems on C_0^+ , we can compute the transparent boundary condition which is given as the DtN operator

$$\Lambda^+(s)\varphi := -\frac{\partial}{\partial x} U|_{\Gamma_0^+},$$

as well as the extension operators

$$\mathcal{P}^+(s)\varphi := U|_{\Gamma_1^+} \quad \text{and} \quad \mathcal{S}^+(s)\varphi := U|_{C_0^+}.$$

The solution U of (2) is thus characterized by $U|_{C_j^+} = \mathcal{S}^+(s) \circ (\mathcal{P}^+(s))^j \varphi$, $j = 0, \dots$ (cf. [1, 2]).

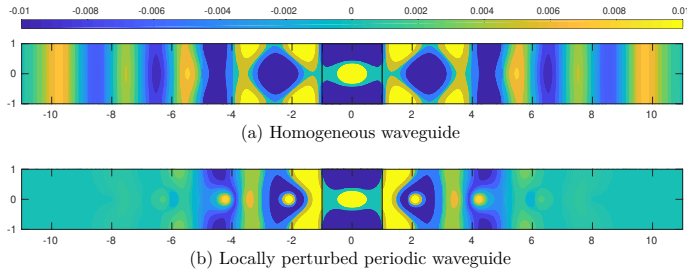


Figure 1: Solution of the wave equation (1) for $t = 10$ on a homogeneous waveguide (a) and on a periodic waveguide (b) with a local perturbation in $\Omega_0 = [-1, 1]^2$.

Analogously, we can derive the operators $\Lambda^-(s)\varphi := \frac{\partial}{\partial x} U|_{\Gamma_0^-}$, $\mathcal{P}^-(s)$ and $\mathcal{S}^-(s)$ on the periodic sub-domain $\Omega^- := \bigcup_{j=0}^{\infty} C_j^-$.

3 Transforming back into the time domain

Instead of solving the Helmholtz equation in Ω_0 subject to the exact boundary conditions on $\Gamma_0^- \cup \Gamma_0^+$, we use the inverse Laplace transform to get back to solving the wave equation (1), where the transparent boundary conditions are now given as the convolution

$$\pm \frac{\partial}{\partial x} u = \int_0^t \mathcal{L}^{-1}\{-\Lambda^\pm(\cdot)\}(t-\tau) u(\cdot, \tau) d\tau \text{ on } \Gamma_0^\pm.$$

We use the convolution quadrature presented in [4] to approximate this integral. For this method we do not have to compute the kernel but require only its Laplace transform which are the DtN operators we already know. On the boundaries Γ_0^\pm , we thus get at time $t_N = N\Delta t$, with N steps and step size Δt , the approximation

$$\pm \frac{\partial}{\partial x} u(\cdot, t_N) \approx \Delta t \sum_{n=0}^N \omega_{N-n}^\pm u(\cdot, t_n).$$

Here the convolution quadrature weights ω_n^\pm can be represented as integrals over a circle with radius ϑ , i.e.,

$$\Delta t \omega_n^\pm = \frac{1}{2\pi i} \int_{|\zeta|=\vartheta} \zeta^{-n-1} \left(-\Lambda^\pm\left(\frac{\delta(\zeta)}{\Delta t}\right)\right) d\zeta,$$

where $\delta(z)$ is the generating function of the time discretization method, e.g. $\delta(z) = 1 - z$ for the implicit Euler method. Approximating the

above integral by the trapezoidal rule yields

$$\Delta t \omega_n^\pm \approx \frac{\vartheta^{-n}}{J} \sum_{j=0}^{J-1} -\Lambda^\pm\left(\frac{\delta(\zeta_j)}{\Delta t}\right) e^{-2\pi i n j/J}$$

with $\zeta_j = \vartheta e^{2\pi i j/J}$ and $J \geq N$. The weights, thus, can be computed using fast Fourier transforms.

In the same manner as the DtN operator, the solution of equation (1) on each cell C_j^\pm can be represented as

$$u|_{C_j^\pm} = \int_0^t \mathcal{L}^{-1}\{\mathcal{S}^\pm(\cdot)(\mathcal{P}^\pm(\cdot))^j\}(t-\tau) u(\cdot, \tau)|_{\Gamma_0^\pm}$$

and, thus, also be computed using convolution quadrature.

References

- [1] P. Joly, J.-R. Li and S. Fliss, Exact Boundary Conditions for Periodic Waveguides Containing a Local Perturbation, *Commun. Comput. Phys.* **1** **6** (2006), pp. 945-973.
- [2] S. Fliss and P. Joly, Exact Boundary Conditions for Time-Harmonic Wave Propagation in Locally Perturbed Periodic Media, *Appl. Numer. Math.* **59** **9** (2009), pp. 2155-2178.
- [3] J. Coatléven, Transparent Boundary Conditions for Evolution Equations in Infinite Periodic Strips, *SIAM J. Sci. Comput.* **34** **3** (2012), pp. A1563-A1583.
- [4] Ch. Lubich, Convolution Quadrature and Discretized Operational Calculus. I, II, *Numer. Math.* **52** (1988), pp. 129-145, 413-425.

**Discrete nonlinear Schrödinger equations for periodic optical systems:
pattern formation in $\chi^{(3)}$ coupled waveguide arrays**

J. M. Christian^{1,*}, R. Fox¹

¹Joule Physics Laboratory, University of Salford, Greater Manchester M5 4WT, UK

*Email: j.christian@salford.ac.uk

Abstract

Discrete nonlinear Schrödinger equations have been used for many years to model the propagation of light in optical architectures whose refractive index profile is modulated periodically in the transverse direction. Typically, one considers a modal decomposition of the electric field where the complex amplitudes satisfy a coupled system that accommodates nearest neighbour linear interactions and a local intensity dependent term whose origin lies in the $\chi^{(3)}$ contribution to the medium's dielectric response.

In this presentation, two classic continuum configurations are discretized in ways that have received little attention in the literature: the *ring cavity* and *counterpropagating waves*. Both of these systems are defined by distinct types of boundary condition. Moreover, they are susceptible to spatial instabilities that are ultimately responsible for generating spontaneous patterns from arbitrarily small background disturbances. Good agreement between analytical predictions and simulations will be demonstrated.

Keywords: Ring cavity, counterpropagation, Turing instability

1 Introduction

In optics, discrete nonlinear Schrödinger (dNLS) equations are often used to describe the way in which electromagnetic waves propagate through structures whose dielectric properties vary periodically [1]. The archetypal waveguide array, for instance, comprises a refractive index distribution engineered in the form of a square wave with period D . Light confined to each channel in the array is coupled to that in its nearest neighbours due to evanescent fields.

While dNLS equations have been studied extensively for over thirty years, here we address two geometries that have received little attention. First, the *ring cavity* involves confining a periodic array between a set of mirrors and feeding the output back into the input. Such systems are known in dNLS contexts, but here

we relax the mean field considerations that have tended to underpin previous works. Second, the *counterpropagating waves* scenario appears to be entirely new to the dNLS realm and does not lend itself well to a mean-field theory. Both proposed dNLS models turn out to support spontaneous pattern formation through the universal mechanism discovered by Turing [2].

2 Ring cavity

In dimensionless form, the slowly-varying envelope confined within waveguide channel $n = 0, \pm 1, \pm 2, \dots$ is denoted by E_n . It follows that

$$i\partial_z E_n + cL(E_{n+1} - 2E_n + E_{n-1}) + \chi L|E_n|^2 E_n = 0, \quad (1a)$$

where $z \in [0, 1]$ denotes the (scaled) longitudinal position along an array of length L , c is a coupling constant, and χ parametrizes the intensity dependent polarization of the medium. To capture the essence of the cavity, we enforce the traditional boundary condition [3]

$$E_n(0) = tE_n + r \exp(i\delta)E_n(1). \quad (1b)$$

Here, E_n is the complex amplitude of the plane wave pump field, the transmission t and reflection r coefficients of the coupling mirror satisfy $t^2 + r^2 = 1$, and δ allows for interferometric mistuning between the pump and intracavity waves.

3 Counterpropagating waves

The continuum counterpropagating waves configuration [4] may be reformulated within a discrete framework by following much the same approach as with the cavity. The array is illuminated from both ends by plane waves travelling in exactly opposite directions down the longitudinal axis z . Channel n then supports a forward and a backward wave whose slowly-varying envelopes are denoted by $F_n \equiv F_n(z, t)$ and $B_n \equiv B_n(z, t)$, respectively. In dimensionless form, we find that F_n and B_n must satisfy

$$i(\partial_z + \partial_t) F_n + cL(F_{n+1} - 2F_n + F_{n-1}) + \chi L(|F_n|^2 + G|B_n|^2) F_n = 0, \quad (2a)$$

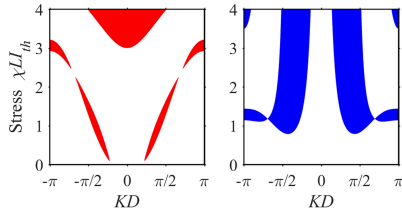


Figure 1: Typical threshold instability spectra obtained for (left) the ring cavity and (right) counterpropagating waves.

$$i(-\partial_z + \partial_t) B_n + cL(B_{n+1} - 2B_n + B_{n-1}) + \chi L(|B_n|^2 + G|F_n|^2) B_n = 0, \quad (2b)$$

where t is now the time coordinate and $1 \leq G \leq 2$ is the grating factor [4]. Equations (2a) and (2b) belong to the “1+2” class of problem [note that Eq. (1a) is the simpler “1+1” class]. They are supplemented by the plane wave pumping boundary conditions $F_n(0, t) = F_0$ and $B_n(1, t) = B_0$ for all n , where F_0 and B_0 are constants.

4 Spontaneous patterns

The uniform states of Eqs. (1a) and (2a)–(2b) can be identified, and the discrete stability analysis subsequently proceeds in a way that takes its inspiration from the corresponding continuum model [3, 4]. These states are perturbed, and one seeks solutions to the linearized problem that prescribe Fourier modes with transverse spatial frequency K and which must respect the appropriate boundary conditions. It turns out that counterpropagation is the more difficult case to analyze, involving the exponentiation of a non-diagonal 4×4 matrix.

The threshold instability spectrum has been derived for both systems, which predicts the minimum wave intensity required to drive the growth of a perturbation mode at any given K . These spectra comprise discrete sets of islands or bands whose structure is periodic in 2π along the KD axis (see Fig. 1). The most unstable frequency, denoted by K_0 , is defined to be that K with the lowest threshold and which hence possesses the highest growth rate.

In regimes with $KD \ll \mathcal{O}(1)$, the threshold conditions revert to those of their continuum counterparts [3, 4]. This type of asymptotic behaviour is required on physical grounds since

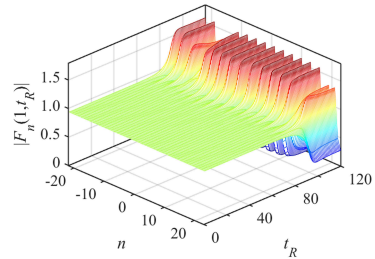


Figure 2: Emergence in time of a static pattern in the output forward wave of the counterpropagation problem. The discrete index t_R denotes the number of passes through the medium.

perturbation wavelengths $2\pi/K$ much greater than D do not ‘see’ the periodic structure.

Simulations have been performed for both systems, wherein the uniform state is initialized with a small level of (filtered) noise added to mimic a random background fluctuation. When the intensity of the uniform state *just* exceeds threshold, a simple pattern is seen to grow spontaneously after a sufficient number of transits through the medium. Such patterns appear to be static in nature and they have a dominant spatial scalelength given by $2\pi/K_0$ (see Fig. 2). The numerics have thus provided some encouraging evidence to confirm the threshold predictions of K_0 made by linear stability analysis.

References

- [1] M. J. Ablowitz and Z. H. Musslimani, Discrete spatial solitons in a diffraction-managed nonlinear waveguide array: a unified approach, *Physica D* **184** (2003), pp. 276–303.
- [2] A. M. Turing, The chemical basis of morphogenesis, *Phil. Trans. Roy. Soc. Lond. B* **237** (1952), pp. 37–72.
- [3] D. W. McLaughlin, J. V. Moloney and A. C. Newell, New class of instabilities in passive optical cavities, *Phys. Rev. Lett.* **54** (1985), pp. 681–684.
- [4] W. J. Firth and C. Paré, Transverse modulational instabilities for counterpropagating beams in Kerr media, *Opt. Lett.* **13** (1988), pp. 1096–1098.

An algorithm for the localization of exceptional points and the computation of Puiseux series with applications to acoustic waveguides

Benoit Nennig^{1,*}, Emmanuel Perrey-Debain²

¹Institut supérieur de mécanique de Paris (SUPMECA), Laboratoire Quartz EA 7393, 3 rue Fernand Hainaut, 93407 Saint-Ouen, France.

²Sorbonne universités, Université de Technologie de Compiègne, Laboratoire Roberval CNRS FRE 2012, CS 60319, 60203 Compiègne cedex, France.

*Email: benoit.nennig@supmeca.fr

Abstract

Finding the defective eigenvalues of parametric non hermitian eigenvalue problem is of particular interest due to the rich physics attached to the singular behavior at the branch point.

Here, a new algorithm is proposed to explore the parametric space and to locate exceptional point (EP). The method requires the computation of successive derivatives of two selected eigenpairs with respect to the parameter so that, after recombination, regular functions can be constructed. This algebraic manipulation permits the localization of exceptional points (EP), using standard root-finding algorithms and the computation of the associated Puiseux series up to an arbitrary order.

Practical applications dealing with dissipative acoustic waveguides are given to illustrate the efficiency and the versatility of the proposed method.

Keywords: Exceptional point, Puiseux series, defective eigenvalue, parametric eigenvalue problem, acoustic waveguides

Introduction

In presence of losses, gain or with open systems, the finite element discretization of the wave equation typically yields sparse non-hermitian eigenvalue problem depending smoothly on a single complex parameters ν

$$\mathbf{L}(\lambda(\nu), \nu)\mathbf{x}(\nu) = \mathbf{0}. \quad (1)$$

Here $\lambda(\nu)$ is the eigenvalue, $\mathbf{x}(\nu) \neq \mathbf{0}$ is the right eigenvector. In the context of duct acoustics, the description of waves is usually accomplished using mode decomposition and \mathbf{L} takes the form of a quadratic eigenvalue problem [7] and λ represents the axial wave number.

Depending on the configuration, the parameter can be, for instance, a wall impedance associated with a locally reacting liner or the effective

density of a porous material as illustrated in Fig. 1. For some specific values ν^* the matrix (1) is defective, and in the case of an isolated defective eigenvalue λ^* of algebraical multiplicity 2, we can anticipate the local behavior of the two branches of solution by using Puiseux series expansion [4]. These can be written formally as

$$\lambda_1(\nu) = \lambda^* + \sum_{k=1}^{\infty} a_k \left((\nu - \nu^*)^{\frac{1}{2}} \right)^k, \quad (2a)$$

$$\lambda_2(\nu) = \lambda^* + \sum_{k=1}^{\infty} a_k \left(-(\nu - \nu^*)^{\frac{1}{2}} \right)^k. \quad (2b)$$

As stated in [5], as long as $a_1 \neq 0$ the two branches coalesce at a branch point singularity as ν tends to ν^* . The branch point ν^* in the ν -complex plane is called an *exceptional point* [4].

In the vicinity of the EP, eigenvalues coalesce in opposite directions, and this has remarkable effects on modal attenuation [3, 7] and on stability issues like the flutter phenomenon [1]. EPs also arises in quantum mechanics [6] or in phase transition in PT-symmetric systems.

In this work, we are interested in finding ν^* as well in computing the coefficients of the Puiseux series up to a certain order.

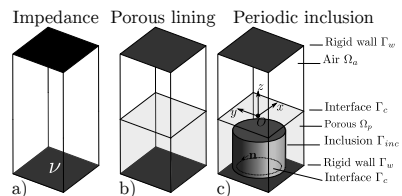


Figure 1: Examples of acoustical waveguides.

EP localization

The proposed algorithm exploits the knowledge of high order derivatives of two selected eigenvalues (λ_1, λ_2) calculated at an arbitrary value ν_0 . In order to circumvent the branch point singularity (2) two auxiliary functions are defined

$$g(\nu) = \lambda_1 + \lambda_2, \quad \text{and} \quad h(\nu) = (\lambda_1 - \lambda_2)^2. \quad (3)$$

By construction, these functions are holomorphic in the vicinity of ν^* (as this was already mentioned in [6] and in [4, p. 66]). The method consists of 3 steps:

1. Computation of the derivatives of two selected eigenpairs $(\lambda_i, \mathbf{x}_i)$ ($i = 1, 2$) following the technique presented in [2]. This serves to construct the truncated Taylor series T_g and T_h of g and h with respect to the arbitrary value ν_0 . This step is the most computationally expensive.
2. Application of standard root-finding algorithms for polynomials in order to find the zeros of T_h and locate the branch point ν^* .
3. Find the connecting coefficients between the Taylor series T_g and T_h with those given by the Puiseux series (2).

To illustrate the method, we consider a bidimensional acoustic waveguide with one treated wall (at $y = 0$). The eigenvalue problem is obtained from the discretization of the weak formulation

$$(k^2 - \lambda)\langle \psi, \phi \rangle - \langle \psi', \phi' \rangle + \frac{1}{\nu}\psi(0)\phi(0) = 0. \quad (4)$$

As illustrated in Fig. 2, the spurious roots of T_h tend to be aligned on a circle (which is known to be connected with the radius of convergence of the series) and genuine zeros corresponding to the EP located inside the circle of convergence. The computed value ν^* is a good approximation of the true value with a relative error of 0.4% for a significantly distant initial value $\nu_0 \approx 2.3\nu^*$.

References

- [1] R. O. Akinola, M. A. Freitag, and A. Spence. The computation of Jordan blocks in parameter-dependent matrices. *IMA J. Numer. Anal.*, 34(3):955–976, 2014.
- [2] A. L. Andrew, K.-W. E. Chu, and P. Lancaster. Derivatives of eigenvalues and eigenvectors of matrix functions. *SIAM J. Matrix Anal. Appl.*, 14(4):903–926, 1993.

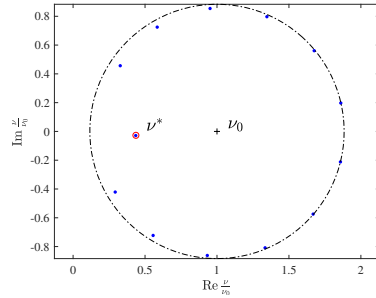


Figure 2: Roots of T_h . Example of EP localization in the case of locally reacting liner with 13 derivatives with $\nu_0 = 0.5825 - 0.6412i$. Roots of T_h (\cdot), initial value ν_0 ($+$) and Tester’s reference solution $\nu_{\text{ref}}^* = (1.6506 + 2.0599i)^{-1}$ (\circ) for the merging of the two least attenuated modes.

- [3] W. Bi and W. Pagneux. New insights into mode behaviours in waveguides with impedance boundary conditions. *arXiv:1511.05508*, 2015.
- [4] T. Kato. *Perturbation Theory for Linear Operators*, 2nd edition, page 623pp. Springer-Verlag, Berlin, Heidelberg, 1980.
- [5] A. P. Seyranian, O. N. Kirillov, and A. A. Mailybaev. Coupling of eigenvalues of complex matrices at diabolic and exceptional points. *J. Phys. A*, 38(8):1723, 2005.
- [6] R. Uzdin and R. Lefebvre. Finding and pinpointing exceptional points of an open quantum system. *J. Phys. B*, 43(23):235004, 2010.
- [7] L. Xiong, B. Nennig, Y. Aurégan, and W. Bi. Sound attenuation optimization using metamorous materials tuned on exceptional points. *J. Acoust. Soc. Am.*, 142(4):2288 – 2297, 2017.

Recovering underlying graph for networks of 1D waveguides by reflectometry and transferometry

Geoffrey Beck^{1,*}, Maxime Bonnaud², Jaume Benoit²

¹POEMS (CNRS-INRIA-ENSTA Paristech) Palaiseau, France

²CEA, LIST, 91191 Gif-sur-Yvette CEDEX, France

*Email: geoffrey.beck.poems@gmail.com

Abstract

We present a method for blind recovery of network made out of a tree of 1D homogeneous waveguides with the same physical characteristics using reflectogram and transferogram(s).

Keywords: Inverse problem, Topology recovering, Quantum graph, Reflectometry, Wire analysis

1 Introduction

We consider an unknow quantum graph \mathcal{G} (see [2]) equipped with a wave operator along its branches and some transmission conditions on its nodes connecting together the quantities evaluated on the branches. Our graph is a rooted tree graph, where all branches are oriented from a root-point Inp to end-points Out_k ($k = 1 \dots K$). We will consider a maximum of two consecutive nodes between Inp and any Out_k and at least a node in \mathcal{G} .

We will now explain how a wave V propagates along the graph \mathcal{G} :

- On each branch of \mathcal{G} the wave satisfy an homogeneous wave's equation

$$\partial_{tt}^2 V - c^2 \partial_{xx}^2 V = 0,$$

where t denotes the time and x the abscissa along the considered branch. The celerity c of the waves is supposed to be a known constant.

- Following Kirchhoff's rules, V is continuous on \mathcal{G} and at each node J

$$\partial_x V|_{\mathbf{e}_{j_0}}(J) = \sum_{j_k=J_1}^{j_K} \partial_x V|_{\mathbf{e}_{j_k}}(J),$$

where \mathbf{e}_{j_k} are the branches connected to J , with \mathbf{e}_{j_0} the branch closest to Inp .

- On Inp , we have an impedance boundary condition

$$\partial_t V(\text{Inp}, t) - c \frac{Z_u}{Z_c} \partial_x V(\text{Inp}, t) = (\partial_t u)(t)$$

where the constant Z_u and $u \in H_{\text{loc}}^1(\mathbb{R})$ are known. The unknown characteristic impedance Z_c is supposed to be constant.

- At each Out_k we have an impedance condition

$$\partial_t V + c \frac{Z_k}{Z_c} \partial_x V = 0,$$

where Z_k is an unknown constant.

2 Graph recovery problem

Reflectometry and transferometry methods can be applied to any practical electrical or acoustic network. The reflectogram is the following Steklov operator :

$$u(t) \mapsto \mathfrak{R}(t) := V(\text{Inp}, t),$$

whereas transferograms are operators for $k = 1 \dots K$:

$$u(t) \mapsto \mathfrak{T}_k(t) := V(\text{Out}_k, t).$$

We suppose that we can control u . With a known celerity c and the input load Z_u , the reflectogram and optionally some transferograms, we want to recover \mathcal{G} that is to say to determine

- the number of nodes and end-points, and their ordering (topology),
- the length ℓ_j of all branches,
- the end-points load Z_k ,
- the characteristic impedance Z_c .

3 Injectivity

There can exists several quantum graph with the same reflectogram, so we will make two hypothesis. Firstly, no scatterer (node or end-points) have the same distance from Inp , to ensure they can be dissociated. Secondly, no Z_k is equal to Z_c to ensure waves are reflected on the end-point. We will suppose that $Z_k > Z_c$ is always satisfied.

4 Scattering

We can choose the excitation signal u such that it is a peak function (sole local maximum). It propagates at celerity c along a branch until it meets a scatterer. \mathfrak{R} is the sum of attenuated u -shaped peaks, i.e. of the form $\sum_p S_p u(t - t_p)$ where each (t_p, S_p) - called echo - corresponds to the duration and the amplitude attenuation of a propagation of u in \mathcal{G} through transmissions T and reflections Γ looping on Inp. T_k is similarly generated, with propagations from Inp to Out $_k$. An echo amplitude S_p gives the nature of its contained scatterers (order for a node, load for an end-point), its abscissa the path length between the observation point (Inp for \mathfrak{R} and Out $_k$ for \mathfrak{T}_k) and the scatterer.

The algorithm presented in [1] identifies echoes in a complex reflectogram and associates them with unknown scatterers in \mathcal{G} , giving their nature and location. It runs iteratively, dispelling ambiguities from peaks overlapping and accumulated reflections.

But this method requires knowledge of Z_c and supposes that $Z_c = Z_u$ (no reflections at Inp). It can be enhanced by the use of transferograms.

5 Algorithm

5.1 Recovering Z_c

We simply recover Z_c from the reflectogram at origin where we see an echo (called mismatch echo) of amplitude $T_u = (1 - \Gamma_u)$ with $\Gamma_u = (Z_u - Z_c)/(Z_u + Z_c)$. Of course if $Z_c = Z_u$ then the mismatch peak is null.

5.2 Recovering the first node

The first echo observe in \mathfrak{R} after the mismatch echo have for abscissa $2\ell_0/c$ and for amplitude $T_u(1 + \Gamma_u)\Gamma_0$ with $\Gamma_0 = (2/m_0 - 1)$ where m_0 is the order of the first node J_0 . We thus recover ℓ_0 and m_0 .

5.3 Using the transferograms

If the amplitude of the first echo (t_1, S_1) of \mathfrak{T}_k is above $4T_u(\Gamma_0 + 1)/3$, then Out $_k$ is directly connected to J_0 . Thus we have $S_1 = T_u(2/m_0)(1 + \Gamma_k)$ with $\Gamma_k = (Z_k - Z_c)/(Z_k + Z_c)$, so we recover Z_k . The length of the J_0 to Out $_k$ branch is $(ct_1 - \ell_0)$. If S_1 is under $T_u(\Gamma_0 + 1)$, a node exists between J_0 and Out $_k$. This recovered topology

can remove branch location ambiguities for an unknown scatterer with the reflectogram.

5.4 Using the reflectogram

We use the algorithm developed in [1] to continue the analysis of \mathfrak{R} . We changed the procedure to use informations from the transferograms, and adapt to $Z_u \neq Z_c$. Indeed, we need to apply a $T_u(1 - \Gamma_u)$ factor to all \mathfrak{R} echoes amplitude and to consider reflexions on Inp when discriminating between echoes.

This method achieves an error-free topology reconstruction if some technical hypothesis on u are fulfilled. ℓ_j are retrieved with an accuracy decreasing when farther from Inp (relative error under 5% from 350 simulations), as are Z_c (under 0.1%) and Z_k (under 10%). Better determination is possible by optimizing the all lengths $\tilde{\ell}$ and all loads $\tilde{\mathbf{Z}}$ vectors such that they minimize the functional

$$J(\ell, \mathbf{Z}) = \int_0^{8\ell_{max}/c} \frac{|\mathfrak{R}(t) - \mathfrak{R}_{\ell, \mathbf{Z}}(t)|^2}{3\ell_{max}/c + t^2} dt$$

where ℓ_{max} is the maximum ℓ_j from previous steps and $\mathfrak{R}_{\ell, \mathbf{Z}}$ the simulated reflectogram using the recovered topology with ℓ and \mathbf{Z} . We look for the minimum of J with Newton's algorithm, initializing $\tilde{\ell}$ and $\tilde{\mathbf{Z}}$ with the previously recovered values.

6 Applications

This algorithm can be used for recovering unknown electrical networks, with one reflectometry device and optional transferometry transceivers on end-points. Removing the condition on Z_u makes the algorithm more resilient to real-life implementation limitations.

References

- [1] G. Beck, *Reconstruction of an unknown electrical network from their reflectogram by an iterative algorithm based on local identification of peaks and inverse scattering theory*. International Instrumentation and Measurement Technology Conference IEEE I2MTC, 2018 (to appear)
- [2] P. Kuchment, *Quantum graphs I. Some basic structures* Waves in Random Media 14, S107-S128 (2004)

Exact zero transmission during the Fano resonance phenomenon in non symmetric waveguides

Lucas Chesnel^{1,*}, Sergei A. Nazarov²

¹INRIA/CMAP, École Polytechnique, Université Paris-Saclay, Palaiseau, France

²IPME, Russian Academy of Sciences, St. Petersburg, Russia

*Email: Lucas.Chesnel@inria.fr

Abstract

We investigate a time-harmonic wave problem in a waveguide. We work at low frequency so that only one mode can propagate. It is known that the scattering matrix exhibits a rapid variation for real frequencies in a vicinity of a complex resonance located close to the real axis. This is the so-called Fano resonance phenomenon. And when the geometry presents certain properties of symmetry, there are two different real frequencies such that $R = 0$ or $T = 0$, where R, T denote the reflection and transmission coefficients. In this work, we prove that without the assumption of symmetry of the geometry, quite surprisingly, there is always one real frequency such that $T = 0$. In this case, all the energy sent in the waveguide is reflected.

Keywords: waveguides, complex resonance, zero transmission, scattering matrix

1 Setting of the problem

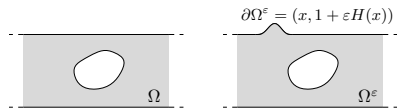


Figure 1: Original waveguide Ω (left) and perturbed geometry Ω^ϵ (right).

Let $\Omega \subset \mathbb{R}^2$ be a connected waveguide which coincides with the strip $\{(x, y) \in \mathbb{R} \times (0; 1)\}$ for $|x| \geq d$ where $d > 0$ is given (see Figure 1 left). Propagation of acoustic waves in Ω with sound hard walls leads to study the problem

$$\begin{cases} \Delta u + \lambda u = 0 & \text{in } \Omega \\ \partial_\nu u = 0 & \text{on } \partial\Omega. \end{cases} \quad (1)$$

For $\lambda \in (0; \pi^2)$, only two waves $w^\pm(x, y) = e^{\pm i\sqrt{\lambda}x}$ can propagate in Ω . The scattering of the incident rightgoing wave w^+ yields a solution of (1) admitting the expansion

$$u_+ = \begin{cases} w^+ + R w^- + \dots, & \text{for } x < -d \\ T w^+ + \dots, & \text{for } x > d. \end{cases} \quad (2)$$

Here $R \in \mathbb{C}$ is a reflection coefficient, $T \in \mathbb{C}$ is a transmission coefficient and the dots stand for terms which are exponentially decaying at infinity. Similarly, there is a solution u_- of (1) associated with the incident leftgoing wave w^- . We denote \hat{R}, \hat{T} the corresponding scattering coefficients (\hat{T} is the same for u_+ and u_-). We define the scattering matrix

$$\mathfrak{s} := \begin{pmatrix} R & T \\ T & \hat{R} \end{pmatrix} \in \mathbb{C}^{2 \times 2},$$

which is unitary ($\mathfrak{s}\bar{\mathfrak{s}}^\top = \text{Id}$). We assume that the geometry is such that the Neumann Laplacian in Ω admits a simple eigenvalue $\lambda^0 \in (0; \pi^2)$. In the sequel, we perturb a bit the geometry, so that this real eigenvalue becomes a complex resonance, and we study the behaviour of the scattering matrix for real frequencies in a neighbourhood of λ^0 .

2 Perturbation of the frequency and of the geometry

We perturb the geometry from some smooth compactly supported profile function H with amplitude $\epsilon \geq 0$ as in Figure 1 right. We denote Ω^ϵ the new waveguide and $\mathfrak{s}(\epsilon, \lambda), T(\epsilon, \lambda), R(\epsilon, \lambda), \hat{R}(\epsilon, \lambda)$ the quantities introduced above in the geometry Ω^ϵ at frequency λ . For short, we set $\mathfrak{s}^0 = \mathfrak{s}(0, \lambda^0), T^0 = T(0, \lambda^0), R^0 = R(0, \lambda^0), \hat{R}^0 = \hat{R}(0, \lambda^0)$. Decomposition in Fourier series guarantees that the eigenfunctions associated with λ^0 , the trapped modes, behave at infinity as $K_\pm e^{-\sqrt{\pi^2 - \lambda^0}|x|} \cos(\pi y) + \dots$ where $K_\pm \in \mathbb{C}$. In [1], the following theorem is proved.

Theorem 1 Assume that $(K_+, K_-) \neq (0, 0)$. There is a quantity $\ell(H) \in \mathbb{R}$, which depends linearly on H , such that when $\epsilon \rightarrow 0$,

$$\mathfrak{s}(\epsilon, \lambda^0 + \epsilon\lambda) = \mathfrak{s}^0 + O(\epsilon) \quad \text{for } \lambda' \neq \ell(H),$$

and, for any $\mu \in \mathbb{R}$,

$$\mathfrak{s}(\epsilon, \lambda^0 + \epsilon\ell(H) + \epsilon^2\mu) = \mathfrak{s}^0 + \frac{\tau^\top \tau}{i\bar{\mu} - |\tau|^2/2} + O(\epsilon).$$

In this expression $\tau = (a, b) \in \mathbb{C} \times \mathbb{C}$ depends only on Ω and $\tilde{\mu} = A\mu + B$ for some unessential real constants A, B with $A \neq 0$.

Theorem 1 shows that the mapping $\mathfrak{s}(\cdot, \cdot)$ is not continuous at $(0, \lambda^0)$ (setting where trapped modes exist). And for ε_0 small fixed, the scattering matrix $\lambda \mapsto \mathfrak{s}(\varepsilon_0, \lambda)$ exhibits a quick change in a neighbourhood of $\lambda^0 + \varepsilon_0 \ell(H)$: this is the Fano resonance phenomenon. When $(K_+, K_-) = (0, 0)$ a faster Fano resonance phenomenon occurs. In the sequel, to simplify we denote $\mathfrak{s}^\varepsilon(\mu)$, $T^\varepsilon(\mu)$, $R^\varepsilon(\mu)$, $\tilde{R}^\varepsilon(\mu)$ the values of \mathfrak{s} , T , R , \tilde{R} in Ω^ε at the frequency $\lambda = \lambda^0 + \varepsilon \ell(H) + \varepsilon^2 \mu$. When Ω^ε is symmetric with respect to an axis orthogonal to the direction of propagation of waves, one can deduce quite simply from Theorem 1 that the complex curves $\mu \mapsto T^\varepsilon(\mu)$ and $\mu \mapsto R^\varepsilon(\mu)$ pass through zero for ε small enough (see [1]). In the next section, we explain how to show that without assumption of symmetry, in Ω^ε , there is still a real frequency closed to λ^0 such that the transmission coefficient is zero. However in general $\mu \mapsto R^\varepsilon(\mu)$ does not pass through zero.

3 Exact zero transmission

Theorem 2 *Assume that $T^0 \neq 0$. Then there is $\varepsilon_0 > 0$ such that for all $\varepsilon \in (0; \varepsilon_0]$, there is $\mu \in \mathbb{R}$ such that $T^\varepsilon(\mu) = 0$.*

PROOF. Theorem 1 provides the estimate

$$|T^\varepsilon(\mu) - T^{\text{asy}}(\mu)| \leq C\varepsilon \quad (3)$$

$$\text{with } T^{\text{asy}}(\mu) = T^0 + \frac{ab}{i\tilde{\mu} - (|a|^2 + |b|^2)/2}.$$

For any compact set $I \subset \mathbb{R}$, the constant $C > 0$ in (3) can be chosen independent of $\mu \in I$.

★ First, we study the set $\{T^{\text{asy}}(\mu), \mu \in \mathbb{R}\}$. Classical results concerning the Möbius transform guarantee that $\{T^{\text{asy}}(\mu), \mu \in \mathbb{R}\}$ coincides with $\mathcal{C}^{\text{asy}} \setminus \{T^0\}$ where \mathcal{C}^{asy} is a circle passing through T^0 . Let us show that \mathcal{C}^{asy} also passes through zero. One finds that $T^{\text{asy}}(\mu) = 0$ for some $\mu \in \mathbb{R}$ if and only if there holds

$$\frac{|a|^2 + |b|^2}{2} = \Re e \left(\frac{ab}{T^0} \right). \quad (4)$$

An intermediate calculus of [1] implies $R^0 \bar{a} + T^0 \bar{b} = a$ and $T^0 \bar{a} + \tilde{R}^0 \bar{b} = b$. From this and the unitarity of \mathfrak{s}^0 which imposes $\tilde{R}^0 = -\overline{R^0 T^0 / T^0}$, we can obtain (4). Denote μ_* the value of μ

such that $T^{\text{asy}}(\mu_*) = 0$ and for $\varepsilon > 0$, define the interval $I^\varepsilon = (\mu_* - \sqrt{\varepsilon}; \mu_* + \sqrt{\varepsilon})$. From (3), for $\varepsilon > 0$ small, we know that the curve $\{T^\varepsilon(\mu), \mu \in I^\varepsilon\}$ passes close to zero. Now, using the unitary structure of $\mathfrak{s}^\varepsilon(\mu)$ as in [2], we show that this curves passes exactly through zero for ε small.

★ Assume by contradiction that for all $\varepsilon > 0$, $\mu \mapsto T^\varepsilon(\mu)$ does not pass through zero in I_ε . Since $\mathfrak{s}^\varepsilon(\mu)$ is unitary, there holds $R^\varepsilon(\mu) \overline{T^\varepsilon(\mu)} + T^\varepsilon(\mu) \overline{\tilde{R}^\varepsilon(\mu)} = 0$ and so

$$-R^\varepsilon(\mu) \overline{\tilde{R}^\varepsilon(\mu)} = T^\varepsilon(\mu) / \overline{T^\varepsilon(\mu)} \quad \forall \mu \in I^\varepsilon.$$

But if $\mu \mapsto T^\varepsilon(\mu)$ does not pass through zero on I^ε , one can verify that the point $T^\varepsilon(\mu) / \overline{T^\varepsilon(\mu)} = e^{2i \arg(T^\varepsilon(\mu))}$ must run rapidly on the unit circle for $\mu \in I_\varepsilon$ as $\varepsilon \rightarrow 0$. On the other hand, $R^\varepsilon(\mu) / \tilde{R}^\varepsilon(\mu)$ tends to a constant on I_ε as $\varepsilon \rightarrow 0$. This way we obtain a contradiction. □

Remark 3 *The fact that \mathcal{C}^{asy} passes through zero is quite mysterious. Without assumption of symmetry, we do not have physical reason to explain this miracle.*

In the geometry of Figure 2, first we find that trapped modes exist for $\varepsilon = 0$ and $\sqrt{\lambda^0} \approx 1.2395$. Then we approximate (FEM) $T(\varepsilon, \lambda)$ (×) and $R(\varepsilon, \lambda)$ (•) for $\sqrt{\lambda} \in (1.2; 1.3)$ and $\varepsilon = 0.05$. As predicted, we observe that $\lambda \mapsto T(\varepsilon, \lambda)$ passes through zero around λ^0 . Finally, we display the real part of u_+ in Ω^ε for $\varepsilon = 0.05$ and $\sqrt{\lambda} = 1.2449$. In this setting, we have $T(\varepsilon, \lambda) \approx 0$.

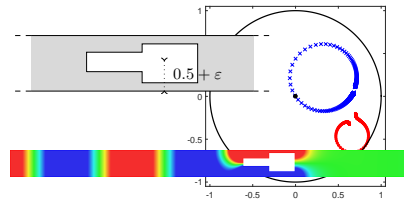


Figure 2: Zero transmission in a waveguide.

References

- [1] L. Chesnel and S.A. Nazarov, Non reflection and perfect reflection via Fano resonance in waveguides, *Comm. Math. Sci.*, vol. 16, 7:1779-1800, (2018).
- [2] H.-W. Lee, Generic transmission zeros and in-phase resonances in time-reversal symmetric single channel transport, *Phys. Rev. Lett.*, vol. 82, 11:2358, (1999).

Bound States in the Continuum for a Class of Lattice Models

Ya Yan Lu^{1,*}¹Department of Mathematics, City University of Hong Kong, Hong Kong

*Email: mayylu@cityu.edu.hk

Abstract

A general theory for bound states in the continuum (BICs) is developed for a lattice model governed by an infinite real symmetric matrix with simple tridiagonal tails. An eigenvalue problem with a finite real nonsymmetric matrix is derived for computing BICs and other modes. A condition for the existence of BICs is obtained. The robustness of BICs against structural perturbations is analyzed.

Keywords: Bound states, lattice models

1 Introduction

The concept of bound states in the continuum (BICs) was originally introduced by Von Neumann and Wigner in 1929. For classical waves, a BIC is a trapped mode with a frequency in the radiation continuum, and it corresponds to an eigenvalue embedded in the continuum spectrum. Recently, BICs have been intensively studied in optics [1–3]. When a perfect structure with a BIC is perturbed, the BIC may continue to exist or become a resonant mode with a complex frequency. Resonant modes are useful in numerous applications. To understand BICs, it is desirable to determine conditions for BICs to exist, to determine perturbations that preserve the BICs, and to analyze the resonances for perturbations that do not preserve the BICs.

The experiments of [1, 2] are performed on waveguide arrays. To analyze waveguide arrays, approximate ODE systems are widely used. The unknown functions in the ODE system are the amplitudes of guided modes propagating on individual waveguides and the independent variable is the spatial variable z along the waveguide axes. Assuming the array consists of infinite number of waveguides and with the z variable separated, the ODE system is reduced to

$$A\mathbf{x} = \lambda\mathbf{x}, \quad (1)$$

where A is an infinite real symmetric matrix and $\mathbf{x} = [\dots, x_{-1}, x_0, x_1, x_2, \dots]^T$ is an infinite vector. The above equation also appears in other applications and it will be referred to as the lattice

model. If the independent variable in the ODE system is time t , then λ is the frequency. BICs on lattice models have been studied by a number of authors [1, 2, 4], but a systematic study is not available. In the following, we study BICs for a rather general lattice model that covers those of Refs. [1, 2, 4] as special cases. Our study helps to gain physical insight, and provides guidelines for analyzing more complicated structures.

2 Theory

If the waveguide array is infinite and one dimensional with identical waveguides that couple (identically) to the nearest neighbors only, then A is an infinite tridiagonal matrix with a constant diagonal entry α and a constant non-zero off-diagonal entry β . We modify $n + 1$ waveguides (labeled by integers $0, 1, \dots, n$) and allow them to couple arbitrarily with each other, then A has an $(n+1) \times (n+1)$ diagonal block (which is a general real symmetric matrix), and the other parts of A are identical to the original infinite tridiagonal matrix. We can assume $\alpha = 0$ and $\beta = 1$, since otherwise we can redefine λ by subtracting α and dividing by β .

Since A is infinite, Eq. (1) can be an eigenvalue problem or a boundary value problem. The special block of A is for rows and columns from 0 to n . If $j < 0$ or $j > n$, the j -th row of Eq. (1) is simply $x_{j-1} + x_{j+1} = \lambda x_j$. For $\lambda \in (-2, 2)$, we have the general solution $x_j = C_1 \mu^j + C_2 \mu^{-j}$, where μ is a complex number with unit amplitude satisfying $\mu^2 + 1 = \lambda \mu$. We assume $x_j = \mu^{-j}$ is a wave that propagates in the increasing j direction. For any given $\lambda \in (-2, 2)$, we can specify an incident wave (for example $x_j^{\text{inc}} = \mu^j$) for $j > n$, and try to find the reflected wave for $j > n$ and the transmitted wave for $j < 0$. This gives rise to a boundary value problem for Eq. (1).

We are interested in eigenvalue problems of Eq. (1), where λ (the eigenvalue) is to be determined. We look for solutions satisfying

$$x_j = x_0 \mu^j, \quad j \leq 0; \quad x_j = x_n \mu^{n-j}, \quad j \geq n, \quad (2)$$

where μ satisfies $\mu^2 + 1 = \lambda \mu$. A bound state is

a solution such that $\sum |x_j|^2 < \infty$. A BIC is a bound state with $\lambda \in (-2, 2)$. A resonant mode is a solution with a complex μ such that μ^{-j} represents an outgoing wave as $j \rightarrow +\infty$.

It is possible to find solutions of (1) and (2) by solving a new eigenvalue problem with a finite matrix. We have

$$\begin{bmatrix} A_n & -J^T \\ J & \mathbf{0} \end{bmatrix} \mathbf{u} = \mu \mathbf{u}, \quad (3)$$

where A_n is the $(n+1) \times (n+1)$ block of A for rows and columns from 0 to n , $J = [\mathbf{0}, I_{n-1}, \mathbf{0}]$ is an $(n-1) \times (n+1)$ matrix, and I_{n-1} is the $(n-1) \times (n-1)$ identity matrix, and μ is the eigenvalue. A zero eigenvalue of Eq. (3) does not correspond to a ‘‘physical’’ solution. Non-zero eigenvalues of Eq. (3) include BICs, resonant modes and other modes.

It is easy to show that a BIC must be compact, that is, $x_0 = x_n = 0$. If we let

$$A_n = \begin{bmatrix} * & \mathbf{b}^T & * \\ \mathbf{b} & B & \mathbf{c} \\ * & \mathbf{c}^T & * \end{bmatrix}, \quad \mathbf{y} = \begin{bmatrix} x_1 \\ \vdots \\ x_{n-1} \end{bmatrix}.$$

then a BIC must satisfy

$$B\mathbf{y} = \lambda\mathbf{y}, \quad \mathbf{b}^T\mathbf{y} = \mathbf{c}^T\mathbf{y} = 0. \quad (4)$$

A solution of (4) is a compact mode. A BIC requires the additional condition $\lambda \in (-2, 2)$.

The BIC of [1] is symmetry-protected. We can use Eq. (4) to understand symmetry protected BICs. Let P be a real $(n-1) \times (n-1)$ matrix such that $P^2 = I$, we say the structure is symmetric if

$$PB = BP, \quad P^T\mathbf{b} = \mathbf{b}, \quad P^T\mathbf{c} = \mathbf{c}. \quad (5)$$

In that case, the eigenvectors of matrix B must satisfy either $P\mathbf{y} = \mathbf{y}$ (symmetric) or $P\mathbf{y} = -\mathbf{y}$ (anti-symmetric). An anti-symmetric mode corresponds to a symmetry protected bound state. As usual, the symmetry protected compact bound states are robust to symmetry preserving perturbations. That means, if we perturb B , \mathbf{b} and \mathbf{c} such that Eq. (5) remains valid, then we have an anti-symmetric compact bound state with a slightly different λ .

In general, a perturbation of the structure will turn a BIC to a resonant mode with a complex λ . If the strength of the perturbation is δ , the imaginary part of λ is usually $O(\delta^2)$. However, if we add two parameters depending on

δ , it is possible to preserve the BIC. More precisely, assuming the structure described by matrix B , vectors \mathbf{b} and \mathbf{c} has a BIC with eigenvector \mathbf{y} and eigenvalue $\lambda \in (-2, 2)$, and if B is perturbed to $B + \delta B_1$ where B_1 is a real symmetric matrix and \mathbf{y} is not an eigenvector of B_1 , \mathbf{b}_1 and \mathbf{c}_1 are given vectors such that $\mathbf{b}_1^T\mathbf{y} \neq 0$ and $\mathbf{c}_1^T\mathbf{y} \neq 0$, then for small but arbitrary δ , there are two small numbers β and γ depending on δ , such that the system corresponding to $B + \delta B_1$, $\mathbf{b} + \beta\mathbf{b}_1$ and $\mathbf{c} + \gamma\mathbf{c}_1$ also has a BIC. This result has some similarity with the robustness result for BICs on periodic structures [5].

3 Conclusion

For a lattice model described by an infinite symmetric matrix, we developed a general theory for computing and analyzing BICs. Formulated as a finite matrix eigenvalue problem, all modes can be easily calculated and BICs can be easily obtained. Based on the new formulation, we developed perturbation theories for BICs. In particular, special perturbations that preserve the BICs are obtained.

Acknowledgement

The work is partially supported by the Research Grants Council of Hong Kong Special Administrative Region, China (CityU 11304117).

References

- [1] Y. Plotnik *et al.*, Experimental observation of optical bound states in the continuum, *Phys. Rev. Lett.* **107** (2011), 183901.
- [2] S. Weimann *et al.*, Compact surface Fano states embedded in the continuum of waveguide arrays, *Phys. Rev. Lett.* **111** (2013), 240403.
- [3] C. W. Hsu *et al.*, Observation of trapped light within the radiation continuum, *Nature* **499**, 188 (2013).
- [4] S. Longhi, Bound states in the continuum in a single-level Fano-Anderson model, *Eur. Phys. J. B* **57** (2007), pp. 45–51.
- [5] L. Yuan and Y. Y. Lu, Bound states in the continuum on periodic structures: perturbation theory and robustness, *Opt. Lett.* **42** (2017), pp. 4490–4493.